Fraunhofer

ICT

Institut
Chemische Technologie

ENERGETIC
MATERIALS -
Technology,
Manufacturing
and Processing

DTIC QUALITY INSPECTED 4

27th International Annual Conference of ICT
June 25 - June 28, 1996
Karlsruhe, Federal Republic of Germany

Fraunhofer Institut
Chemische Technologie

ENERGETIC
MATERIALS -
Technology,
Manufacturing
and Processing

27th International Annual Conference of ICT
June 25 - June 28, 1996
Karlsruhe, Federal Republic of Germany

19970618 036

Energetic Materials -
Technology, Manufacturing and Processing

Since our last event on this theme in 1987 new topics have received special interest in the field of technology, manufacturing and processing of energetic materials. The development of new ingredients and the tailoring of explosive systems in view of LOVA requirements lead to changes in manufacturing and processing technology. Another increasing requirement to modern explosive technology is to guarantee environmental compatibility during the whole life cycle of the energetic materials.

The 27th International ICT Annual Conference centers at the discussion of the art in research and development of modern rocket propellants, explosives, gun propellants and pyrotechnics emphazising technology, manufacturing and processing.

Main topics are

- Components
- Manufacturing and Processing Techniques
- Safety Technology
- Analysis and Characterization of Energetic Materials
- Environmental Aspects

Chairman of the Conference
Dr. Thomas Keicher,
ICT, Pfinztal, D

June 25 - June 28, 1996
Karlsruhe, Congress Center
Stadthalle, Weinbrenner-Saal
Federal Republic of Germany

VORBEMERKUNG

Die Themen unserer Jahrestagung haben wieder ein breites internationales Echo gefunden. Die große Anzahl von eingegangenen Beiträgen machte, wie in den vorigen Jahren, eine Einteilung in Vorträge und Poster notwendig. Poster ermöglichen eine intensivere Diskussion und eine direkte Rückkopplung von interessierten Tagungsteilnehmern.

Der vorliegende Tagungsband erscheint zu Konferenzbeginn und enthält die schriftlichen Fassungen der Vorträge und Poster. Aus zeitlichen Gründen mußte die Drucklegung vor Eingang sämtlicher Beiträge erfolgen. Nachträglich eingegangene Manuskripte finden sich im Anhang oder wurden durch die Kurzfassung ersetzt.

PRELIMINARY REMARK

The subjects of the annual ICT-Conference have again found wide international response. The vast number of contributions necessitated - as in previous years - a division into oral presentations and posters. Posters enable an intensive discussion and direct feedback from interested conference participants.

The Conference Proceedings are published at the beginning of the conference and contain the written versions of the presentations and posters. Due to the shortage of time, printing had to commence prior to receipt of all contributions. Subsequently received manuscripts are either included in the Annex or the abstract is printed instead.

TABLE OF CONTENTS

LECTURES

V10

NON-LEADED BALLISTIC MODIFIERS FOR PLATEAU AND MESA PRODUCING SOLID
PROPELLANTS

S.B. Thompson

V11

THERMAL RESPONSE AND PARAMETRIC ANALYSIS OF ALUMINIZED AP/HTPB BASED
PROPELLANTS WITH VARYING COMPOSITION

L.F. Dimaranan, I. Lee, F.E. Hudson III

V12

A COMBUSTION MODEL FOR AN/HTPB-IPDI COMPOSITE SOLID PROPELLANTS

P. Carvalheira, J. Campos, G.M.H.J.L. Gadiot

V13

EINFLUSS DER KORNGRÖSSE DES REDUKTIONSMITTELS AUF DIE REAKTIONSPARAMETER
PYROTECHNISCHER SYSTEME
*INFLUENCE OF THE PARTICLE-SIZE ON THE REACTION PARAMETERS OF PYROTECHNIC REDOX-
SYSTEMS*

B. Berger, B. Haas, G. Reinhard

V14

SPEKTROSKOPISCHE UNTERSUCHUNG AN BORHALTIGEN FESTBRENNSTOFFEN IN EINER
STAUBRENNKAMMER
SPECTROSCOPIC INVESTIGATIONS ON BORON CONTAINING PROPELLANTS

A. Blanc, W. Liehmann, H. Ciezki, H. Feinauer

V15

THERMAL STUDIES ON DMNB, A DETECTION AGENT FOR EXPLOSIVES

D.E.G. Jones, R.A. Augsten

V16

STABILITY STUDIES OF SPHERICAL PROPELLANTS

P. Guillaume, A. Fantin, M. Rat, S. Wilker, G. Pantel

V17

EINSATZLEBENSDAUER EINIGER GASGENERATORSÄTZE BEI TEMPERATURBELASTUNG
*APPLICATION LIFE TIME OF SOME GASGENERATING PROPELLANTS AT DIFFERENT
TEMPERATURES AND CLIMATIC CONDITIONS*

M. Kaiser, E. Lissel, U. Ticmanis, P. Jacob

V18

THE CHARACTERISATION AND DEVELOPMENT OF NEW ENERGETIC MATERIALS

A.J. Sanderson

V19
DEVELOPMENT OF HIGH-EFFICIENCY ENERGETIC EXPLOSIVES

V. Pepekin

V20
DEVELOPMENT OF COMPOSITE PROPELLANTS WITH A LOW PRESSURE EXPONENT SUITABLE FOR NOZZLELESS BOOSTER MOTORS

G.J. van Zyl

V21
PROPERTIES OF AN AND PSAN/GAP-PROPELLANTS

K. Menke, J. Böhnlein-Mauß

V22
GUIDELINES TO HIGHER ENERGY GUN PROPELLANTS

R.L. Simmons

V23
NEW MOLECULES FOR HIGH ENERGETIC MATERIALS

B. Finck, H. Graindorge

V24
SYNTHESIS OF LINEAR GAP-BASED ENERGETIC THERMOPLASTIC ELASTOMERS (ETPEs) FOR USE IN HELOVA GUN PROPELLANT FORMULATIONS

G. Ampleman, F. Beaupre

V25
INVESTIGATION OF HIGH MOLECULAR WEIGHT GAP

Wang Ping, Xia Zhongjun, Zhou Yuqi, Li Changqing

V26
AN ENVIRONMENTALLY-FRIENDLY ROUTE TO NITRAMINES AND NITRATE ESTERS VIA NITRODESILYLATION CHEMISTRY USING DINITROGEN PENTOXIDE

R.W. Millar, S.P. Philbin

V27
SYNTHESIS OF THE CAGED NITRAMINE HNIW (CL-20)

R.B. Wardle, J.C. Hinshaw, P. Braithwaite, M. Rose, G. Johnstone, R. Jones, K. Poush

V28
NENA-SPRENGSTOFFE
NENA HIGH EXPLOSIVES

H.H. Licht, H. Ritter, B. Wanders

V29

A NEW SYNTHESIS OF TATB USING INEXPENSIVE STARTING MATERIALS AND MILD REACTION CONDITIONS

A.R. Mitchell, P.F. Pagoria, R.D. Schmidt

V30

NITROFURAZANYL MOIETY AS AN ALTERNATIVE TO PICRYL ONE FOR HIGH ENERGETIC MATERIAL CONSTRUCTION

A.B. Sheremetev, T.S. Pivina

V31

THE DEVELOPMENT OF AN ELEVATED TEMPERATURE FRICTION SENSITIVENESS

G. Miles, M.R. Williams, R.K. Wharton, A.W. Train

V32

CHARACTERIZATION OF THE INTERNAL QUALITY OF HMX CRYSTALS

A.E. van der Heijden, W. Duvalois

V33

ENTWICKLUNG UND EINSATZ EINES NEUEN TNT-FREIEN PLATTIERSPRENGSTOFFES
DEVELOPMENT AND APPLICATION OF A NEW TNT-FREE EXPLOSIVE FOR CLADDING PURPOSES

U. Richter

V34

EINSATZ VON HNS IN DER ERDÖLEXPLORATIONSTECHNIK
APPLICATION OF HEXANITROSTILBENE IN GAS EXPLORATION

U. Gessel, H. Zöllner

V35

METHODOLOGY OF EXAMINATION OF THE WAYS OF THE ACCIDENTAL EXPLOSIONS PREVENTION AT ENERGETIC MATERIALS PRODUCTION AND APPLICATION

B.N. Kondrikov

V36

SENSITIVITY TO PROJECTILE IMPACT OF PRE-HEATED EXPLOSIVE COMPOSITIONS

H.Cherin, D. Lemoine, L. Gautier

V37

VULNERABILITY TESTING OF HIGH EXPLOSIVES

P. Vavra

V38

HAZARD ANALYSIS OF A GAS GENERANT

K. Hara, M. Kanazawa, T. Yoshida

V39

COMPUTER MODELING OF POSSIBLE POLYMORPHIC TRANSFORMATIONS IN HNIW (CL-20) P

T.S. Pivina, E.A. Arnautova, A.V. Dzyabchenko

V40

DEMILITARIZATION FACILITY FOR THE ENVIRONMENTAL AND ACQUISITION LIFE CYCLE ANALYSIS OF EXPLOSIVES AND MUNITIONS SYSTEMS

S.R. Jeffers, J. Corley, A.F. Spencer, J.L. Clark

V41

HYPERGOLIC CHEMICAL INITIATION OF NON-DETONATIVE AUTOCATALYTIC SELF-CONSUMPTION/DESTRUCTION OF TNT, RDX, AND TNT-BASED EXPLOSIVES

A.J. Tulis, A. Snelson, J.L. Austing, R.J. Dihu, D.L. Patel, B.D. Briggs, D.C. Heberlein

V42

INITIIERGESETZ VON SPRENGLADUNGEN BEI BESCHUSS MIT PROJEKTILEN VON UNTERSCHIEDLICHEN DICHTEN
INITIATION CRITERIA OF HIGH EXPLOSIVES ATTACKED WITH PROJECTILES OF DIFFERENT DENSITIES

M. Held

V43

BEHAVIOUR OF ALUMINIUM AND TNT IN THE DETONATION WAVE OF AMMONIUM NITRATE EXPLOSIVES

A. Maranda, S. Cudzilo, W. Trzcinski, J. Nowaczewski

V44

UNDERWATER EXPLOSION PERFORMANCE OF EXPLOSIVELY DISPERSED TI-B MIXTURES

J. G. Connor, R.M. Doherty

POSTER PRESENTATIONS

P45

PROCESSING OF Mg-NaNO$_3$ BASED FUEL-RICH PROPELLANT BY POWDER COMPACTION TECHNIQUE FOR AIR-BREATHING PROPULSION SYSTEMS

H. Singh, P. Srinivasa Rao, R. Bhaskara Rao

P46

NOVEL METHODS FOR THE CHEMICAL AND BALLISTIC ASSESSMENT OF NEW GENERATION PROPELLANTS

A. Fraser, G. Gillies, C. Holmes, B. Kelso, A. Ross, I. Sharp

P47

SOLID PROPELLANTS FOR CONTROLLED ROCKET MOTORS

V.I. Petrenko, A.M. Rusak

P48

EFFECT OF ALUMINIUM CONTENT AND PARTICLE SIZE ON THE BALLISTIC AND MECHANICAL
PROPERTIES OF HTPB BASED COMPOSITE SOLID PROPELLANTS

S. Özkar, F. Pekel, F.N. Tüzün

P49

MODELING AND RHEOLOGY OF HTPB BASED SOLID PROPELLANTS

C. Erisken, A. Göcmez, F. Pekel, Ü. Yilmazer, S. Özkar

P50

INFLUENCE OF N, N'-DINITROPIPERAZINE ON CHARACTERISTICS OF COMPOSITE MODIFIED
DOUBLE BASE PROPELLANT

Pan Wenda, Chang Jingxiang

P51

PRELIMINARY STUDY OF BUNENA GUN PROPELLANTS

Lu Anfang, Bao Guan-ling, Liao Xin, Shen Qiong-hua

P52

HIGH ENERGY OXETANE/HNIW GUN PROPELLANTS

R.B. Wardle, P.C. Braithwaite, A.C. Haaland, J.A. Hartwell, R.R. Hendrickson, V. Lott,
I.A. Wallace, C.B. Zisette

P53

EFFECT OF PLASTICIZER ON PERFORMANCE OF XM-39 LOVA

R.L. Simmons

P54

PERKUSSIONS-ZÜNDELEMENT MIT SCHADSTOFFARMEM ZÜNDSATZ FÜR HANDFEUERWAFFEN
NONTOXIC PERCUSSION PRIMER WITHOUT PRIMARY EXPLOSIVES

J. Kutzli, W. Rauber, M. Tobler

P55

SOME RULES FOR THE DESIGN OF HIGH SOLID LOADING COMPOSITE SOLID PROPELLANTS
AND EXPLOSIVES

P. Carvalheira, J. Campos, G.M.H.J.L. Gadiot

P56

AQUEOUS EMULSION EXPLOSIVE WITH TNT

M. Mendonca, J. Campos, C. Moutinho

P57

PBX MANUFACTURING AND TESTING WITH MODIFIED PETN PARTICLES

C. Moutinho, J. Campos, J.C. Gois, M. Figueiredo

P58

EVALUATING THE ABILITY TO DO WORK OF PBX

Hua Pinghuan

P59

DETONATION OF MIXTURES ON BASE OF THE STRONG NITRIC ACID

V.M. Raikova, B.N. Kondrikov, G.D. Kozak

P60

ON THE NEW METHOD OF BRISANCE SPECIFICATION OF HIGH EXPLOSIVES

J. Vagenknecht, A. Vojtech, J. Psencik

P61

EIDS HIGH EXPLOSIVES FOR 1.6 MUNITIONS

A. Becuwe, A. Delclos, J. Isler

P62

ENTWICKLUNG EINES GALVANISCH LEITENDEN HOCHLEISTUNGSSPRENGSTOFFS
DEVELOPMENT OF AN ELECTRICAL CONDUCTIVE HIGH EXPLOSIVE

J. Mathieu, F. Lebet, H.R. Bircher

P63

EFFECT OF MICROSTRUCTURE ON EROSIVE COMBUSTION OF ENERGETIC MATERIALS

Y.I. Dimitrienko

P64

withdrawn

P65

PRESSABLE TPE-BASED EXPLOSIVES FOR METAL ACCELERATING APPLICATIONS

R.E. Hollands, I.E.P. Murray, T.H. Jordan, C.J. Leach

P66

DEVELOPMENT OF THE HIGH PERFORMANCE METAL ACCELERATING EXPLOSIVE PBXW-11

L.J. Montesi, K.E. Alexander

P67

MINIATURE INSENSITIVE SILVER CUTTING CORDS

T. Rogers, M. Wasko

P68

THE EFFECTS OF ADDITIVES (HNS) IN EXPLOSIVES FILLING ON THE STRUCTURAL INTEGRITY OF
TNT BASED COLUMNS AND FINALLY THE TERMINAL PERFORMANCE OF THE SHELLS

F.A. Venter, F.C. Fouche

P69

TNT-BASED INSENSITIVE MUNITIONS

F.C. Fouche, G.C. van Schalkwyk

P70

withdrawn

P71

DETONATION BEHAVIOUR OF HMX-BASED EXPLOSIVES CONTAINING MAGNESIUM AND POLYTETRAFLUOROETHYLEN

S. Cudzilo, W. Trzcinski, A. Maranda

P72

SULFURIC ACID INFLUENCE ON POLYNITROCOMPOUNDS SLOW DECOMPOSITION AND DETONATION REACTIONS

B.N. Kondrikov, G.D. Kozak, V.M. Raikova

P73

A NEW APPROACH TO DETERMINATION OF THE DANGER OF DEFLAGRATION-TO-EXPLOSION TRANSITION IN EXPLOSIVE MATERIALS

A. Sulimov, B. Ermolaev, V. Foteenkov, B. Khasainov, S. Malinin

P74

THERMAL BEHAVIOR AND REACTION MECHANISM OF SOME ENERGETIC MATERIALS WITH NYLON 6/12

Zhang Xiaoyi, Chen Xuelin, Wang Xiaochuan, Zhou Jianhua

P75

GREAT INFLUENCE OF ADDING WAY OF CARBON BLACK ON THE CATALYTIC COMBUSTION OF NITROAMINE-CMDB PROPELLANTS

Lei Liangfang, Ma Xieqi, Zhang Guodong, Sun Tiegang, Shan Wengang

P76

LOW-TOXIC BURNING RATE CATALYSTS FOR DOUBLE-BASE PROPELLANTS

A.P. Denisjuk, B.M. Balojan, J.G. Shepelev, L.A. Demidova

P77

COMBUSTION BEHAVIOUR OF RADIATION CURED ENERGETIC COMPOSITES

V.G. Dedgaonkar, P.B. Navie, P.G. Shrotri

P78

THE CHANGE OF THE COMBUSTION PERCOLATION MECHANISM BY THE ACTION OF TEMPERATURE AND CATALYSTS

V.V. Klyucharev

P79

FEATURES OF THE SOLID PROPELLANT COMBUSTION IN CONDITIONS OF VARIABLE OVERLOAD

V.I. Petrenko, V.L. Popov, A.M. Rusak

P80

INCINERATION OF EXPLOSIVES IN A FLUIDISED BED

A. Pires, J. Campos, L. Duraes, S. Almada

P81

COMBINED METHODS FOR DIAGNOSTICS OF BURNING PRODUCTS COMPOSITION IN FLAME

S. Korotkov, V. Samsonov

P82

TEMPERATURPROFILE UND ABBRANDRATEN VON POOL FIRE BRENNSTOFFEN
TEMPERATURE PROFILES AND BURNING RATES OF POOL FIRES

V. Weiser, I. Franchin, N. Eisenreich

P83

CHEMICAL KINETICS IN THE IGNITION DELAY OF AP/AN/INERT BINDER COMPOSITE PROPELLANTS

O. Frota, L. Araujo

P84

IR-EMISSIONSSPEKTROSKOPIE BEI VERBRENNUNGSVORGÄNGEN VON TREIBSTOFFEN UND ANZÜNDMITTELN
IR-EMISSION SPECTROSCOPY ON PROPELLANT AND IGNITER BURNING

A. Baier, V. Weiser, N. Eisenreich, A. Halbrock

P85

NAHINFRAROT-TRANSMISSIONSSPEKTROSKOPIE AN TREIB- UND EXPLOSIVSTOFFEN
NEAR INFRARED-TRANSMISSION SPECTROSCOPY ON PROPELLANTS AND EXPLOSIVES

T. Rohe, E. Grünblatt, N. Eisenreich

P86

POLARIZED-OPTICAL METHOD FOR ANALYSIS OF FUEL IGNITION AND COMBUSTION

V. Samsonov

P87

TEMPERATUR- UND KONZENTRATIONSMESSUNGEN MITTELS KOHÄRENTER ANTI-STOKES RAMAN-STREUUNG (CARS) AN VERBRENNUNGSPROZESSEN VON FLÜSSIGEN UND FESTEN TREIB- UND EXPLOSIVSTOFFEN
MEASUREMENT OF TEMPERATURES AND CONCENTRATIONS DURING COMBUSTION OF LIQUID AND SOLID PROPELLANTS AND EXPLOSIVES BY CARS

C. Gilles, U. Giesen, D. Brüggemann, A. Kurtz

P88

STUDY ON THE NITROLYSIS OF HEXAMETHYLENETETRAMINE BY NMR-SPECTROMETRY III. THE NMR SPECTRAL DATA OF SOME PRODUCTS AND INTERMEDIATES FROM THE NITROLYSIS OF HA

Zhijie Fang, Ju Chen, Fuping Li

P89

STUDY ON THE NITROLYSIS OF HEXAMETHYLENETETRAMINE BY NMR-SPECTROMETRY IV. A NOVEL MECHANISM OF THE FORMATION OF RDX FROM HA

Zhijie Fang, Shaofang Wang, Fuping Li

P90

CHEMISTRY OF DETONATION - EXPERIMENTAL CONFIRMATION OF EQUATIONS FOR REACTIONS GENERATING DETONATION ENERGY

L.T. Eremenko, D.A. Nesterenko

P91

THE ICT-THERMOCHEMICAL DATA BASE

F. Volk, H. Bathelt

P92

THE ICT THERMODYNAMIC CODE

F. Volk, H. Bathelt

P93

MODELLING OF THERMODYNAMICAL PROPERTIES OF PROPELLANTS

J. Petrzilek, J. Zigmund

P94

PERFORMANCES INVESTIGATION OF ADVANCED SOLID PROPELLANT FORMULATIONS BY CONVENTIONAL AND INNOVATIVE METHODOLOGIES

B. D'Andrea, F. Lillo, R. Massimi

P95

MOLECULAR MODELLING OF NOVEL ENERGETIC MATERIALS

E. Robson, J. Kendrick, W. Leeming, G.A. Leiper, A.S. Cumming, C. Leach

P96

KINETISCHE MODELLIERUNG DER STABILISATORABNAHME UND DER STABILISATORFOLGEPRODUKTE IN EINEM TREIBLADUNGSPULVER
KINETIC MODELLING OF THE STABILIZER CONSUMPTION AND THE SECONDARY STABILIZERS IN A GUN PROPELLANT

M.A. Bohn, N. Eisenreich

P107

SICHERHEITSTECHNISCHE STUDIE AN EXPLOSIVEN ORGANOMETALLVERBINDUNGEN
SAFETY TECHNOLOGY STUDY OF EXPLOSIVE METALORGANICS

T. Fischer, A. Pfeil, N. Eisenreich, S. Rushworth, A. Jones

P108

MODELLIERUNG DER STRAHLUNGSEMISSION BEIM ABBRAND CHEMISCHER ENERGIETRÄGER
UNTER SICHERHEITSTECHNISCHEN GESICHTSPUNKTEN
*MODELLING OF RADIATION EMITTED FROM PROPELLANT COMBUSTION WITH RESPECT TO
SAFETY ASPECTS*

M. Weindel, W. Eckl, N. Eisenreich

P109

ÜBER REAKTION VON TRINITROTOLUOL-ISOMEREN IN BASISCHEM MEDIUM
REACTIONS OF TRINITROTOLUENE-ISOMERES IN A BASIC MEDIUM

V.L. Zbarsky

P110

RECENT ADVANCES IN THE MOLTEN SALT TECHNOLOGY FOR THE DESTRUCTION OF
ENERGETIC MATERIALS

R. Upadhye, C. Pruneda, B. Watkins

P111

MOLTEN SALT DESTRUCTION OF HIGH EXPLOSIVES

B. Watkins, R. Upadhye, R. Behrens Jr.

P112

ENERGETIC MATERIAL TREATMENT USING MOLTEN SALT OXIDATION

J.M. Heslop, J.P. Consaga

P113

BIOLOGICAL REMEDIATION BY FUNGI OF SOILS CONTAMINATED WITH EXPLOSIVES

G. Ampleman, S. Thiboutot, J. Lei, C. Marion, C.W. Greer, D. Beaumier, D. Rho, J. Hawari,
G. Sunahara

P114

BIOTREATABILITY ASSESSMENT OF SOILS CONTAMINATED WITH RDX AND TNT

S. Thiboutot, G. Ampleman, J. Hawari, C.W. Greer, A. Jones, S. Guiot, C.F. Shen, J. Sunahara

P115

HPLC METHODE FÜR DIE ANALYTIK EHEMALIGER STANDORTE VON TREIBLADUNGSPULVER-
FABRIKEN
ENVIRONMENTAL ANALYSIS OF FORMER GUN PROPELLANT PLANTS

M. Kaiser, L. Stottmeister

P116

SORBENT ON THE BASE OF FULLERENCE C_{60} FOR HIGH PERFORMANCE LIQUID CHROMATOGRAPHY OF ENERGETIC SUBSTANCES

L.L. Gumanov, G.A. Volkov, A.V. Shastin, B.L. Korsounskii

P117

BESTIMMUNG VON DIPENTAERYTHRIT IN HANDELSÜBLICHEN PENTAERYTHRIT MITTELS HPLC
DETERMINATION OF DIPENTAERYTHRITOL IN COMMERCIAL PENTAERYTHRITOL BY MEANS OF HPLC

R. Schirra

P118

PROPAGATION OF STRESS-STRAIN WAVE IN PROPELLANT UNDER IGNITION

V. Samsonov

P119

THE MECHANICAL PERFORMANCE OF PMMA / FR BLEND BINDERS AND RDX COMPOSITIONS

Zhao Shengxiang, Li Shengying

P120

TORSIONS-DMA-GLASÜBERGANG DER BINDERELASTOMERE GAP-N100- UND HTPB-IPDI ALS FUNKTION DER ALTERUNG
GLASS TRANSITION OF THE NONAGED AND AGED BINDERS GAP-N 100 AND HTPB-IPDI MEASURED BY TORSION-DMA

M.A. Bohn, P. Elsner

P121

CHEMICAL INTERACTION OF NITRO GLYCERINE WITH PBO IN WATER

B. Lurie, I. Oganyan

P122

ENERGY OF INTERACTION IN SYSTEM NITROCELLULOSE-DIBUTYLPHTALATE

Y. N. Matyushin, T.S. Konkova

P123

PHASE STATE, STRUCTURE AND PROPERTIES OF CELLULOSE NITRATES PLASTICIZED BY NITRO COMPOUNDS

B.M. Balojan, J.M. Lotminzev

P124

THE INFLUENCE OF A PHENOLIC RESIN BARRIER COATING ON THE MIGRATION OF NITROGLYCERINE AND CAMPHOR IN SECONDARY AUGMENTING CHARGES

H. Schalkwyk, J.M. Venter, C. van Vuren

P125
EFFECTS OF KNEADING PROCESS ON RHEOLOGICAL PROPERTIES OF CASTING RDX-CMDB PROPELLANTS SLURRY

Shan Wengang, Shun Tiegang, Zhang Guodong, Lei Liangfang

P126
BENCH SCALE COOLING CRYSTALLIZATION OF RDX

J.H. ter Horst, R.M. Geertman, G.M. van Rosmalen, A.E. van der Heijden

P127
PHASENGLEICHGEWICHTSUNTERSUCHUNGEN AM SYSTEM TRINITROTOLUOL-KOHLENDIOXID
CHARACTERIZATION OF THE PHASE EQUILIBRIUM OF THE SYSTEM TRINITROTOLUENE-CARBON DIOXIDE

U. Teipel, P. Gerber, H. Krause

P128
EXTRAKTION VON EXPLOSIVSTOFFEN DURCH ÜBERKRITISCHES MODIFIZIERTES KOHLENDIOXID
EXTRACTION OF EXPLOSIVES BY SUPERCRITICAL FLUIDS

M. Niehaus, U. Teipel, H. Krause, G. Bunte

P129
A NEW SELF-BALANCING METHOD FOR OPTIMUM TEMPERATURE CONTROL OF BATCH REACTORS

Hu Shaoming, Hu Yaning, Tong Ziyi

P130
COMBUSTION WAVE GENERATED TITANIUM AS A PRECURSOR FOR REACTION BONDED TITANIUM NITRIDE CERAMICS

A. Pivkina, Y. Frolov, P.J. van der Put, J. Schoonman

P131
ELASTOMERIC POLYMERS AS POTENT ADDITIVES FOR EMULSION EXPLOSIVES

V. Mohan Rao, P.K. Ghosh

P132
ENERGETIC THERMOPLASTIC ELASTOMERS BASED ON GLYCIDYL AZIDE POLYMERS WITH INCREASED FUNCTIONALITY

G. Ampleman, S. Desilets, A. Marois

P133
SYNTHETIC STUDY OF BUNENA

Shen Qiong-hua, Bao Guan-ling, Zhang Yu-xiang, Lu An-fang

P134

3,4,5-TRINITROPHENYLFUROXANS: SYNTHESIS AND KINETICS OF HYDROLYSIS

N.N. Makhova, M.E. Epishina

P135

SYNTHESIS OF HIGH DENSITY AZIDONITRAMINES

Yan Hong, Guan Xiaopei, Chen Boren

P136

CHARACTERIZATION OF 2-OXY-4,6-DINITRAMINE-S-TRIAZINE

P. Simoes, P. Carvalheira, A. Portugal, J. Campos, L. Duraes, J. Gois

P137

KINETIC STUDIES OF ACETOLYSES OF HEXAMETHYLENETETRAMINE

G.F. Rudakov, A.V. Kobec, V.F. Zhylin

P138

EINSATZ DER RÖNTGENBEUGUNG BEI DER CHARAKTERISIERUNG UND ENTWICKLUNG VON LOVA-KOMPONENTEN
APPLICATION OF X-RAY DIFFRACTION FOR THE INVESTIGATION AND DEVELOPMENT OF LOVA COMPONENTS

M.J. Herrmann, W. Engel

P139

STRÖMUNGSVISUALISIERUNG IN SELBSTLEUCHTENDEN REAKTIONSZONEN MITTELS PIV
FLOW VISUALIZATION OF SELF-ILLUMINATED EXHAUST PLUME BY PIV

L. Deimling, A. Brock

P140

THE INFLUENCE OF THE MATRIX-FILLER-INTERACTION ON THE MECHANICAL PROPERTIES OF FILLED ELASTOMERS

M. Lohrmann, C. Hübner

P141

ON SENSITIVITY OF TATB-BASED SHOCK WAVE DAMAGED EXPLOSIVE

I.Y. Plaksin, V.F. Gerasimenko, V.I. Shutov, V.M. Gerasimov

P142

UNTERSUCHUNGEN ZUR EINKOPPLUNG ELEKTRISCHER ENERGIE IN FLÜSSIGE ENERGIETRÄGER UND DEREN VERBRENNUNGSPRODUKTE
COUPLING OF ELECTRICAL ENERGY IN LIQUID PROPELLANTS AND THEIR COMBUSTION PRODUCTS

A. Koleczko, W. Eckl, T. Rohe

P143

THERMISCHES VERHALTEN VON ADN
THERMAL BEHAVIOUR OF ADN

S. Löbbecke, H. Krause, A. Pfeil

P144

THERMISCHES VERHALTEN VON PAP-G
THERMAL BEHAVIOUR OF PAP-G

S. Löbbecke, T. Keicher, H. Krause, A. Pfeil

P145

SOLVATOCHROME INDIKATOREN ZUR UNTERSUCHUNG DER LÖSLICHKEIT ENERGETISCHER
MATERIALIEN IN ÜBERKRITISCHEM KOHLENDIOXID
*INVESTIGATIONS INTO THE SOLUBILITY OF ENERGETIC MATERIALS IN SUPERCRITICAL CARBON
DIOXIDE USING SOLVATOCHROMIC INDICATORS*

R. Eberhardt, S. Löbbecke, T. Härdle, A. Pfeil, H. Krause, B. Neidhardt

P146

ANOMALOUS COMBUSTION REGIMES OF SOLID PROPELLANTS WITH DEFECTS

N.N. Smirnov, I.D. Dimitrienko, S.I. Rumyantseva

P147

FERROCENDERIVATE: EFFIZIENTE ABBRANDMODIFIKATOREN FÜR COMPOSIT-
RAKETENTREIBSTOFFE UND GASGENERATOREN
*FERROCENES: HIGHLY EFFICIENT BURNING MODIFIERS FOR COMPOSITE ROCKET- AND
GASGENERATING PROPELLANTS*

H. Jungbluth, W. Kalischewski, K.-P. Brehler, K. Menke

P148

AN AUTOMATED AND REMOTE METHOD OF MEASURING FEEDER PERFORMANCE

F.M. Gallant

P149

CONTINUOUS PROCESSING OF COMPOSITE PROPELLANTS (CPOCP) - A JOINT PROJECT
BETWEEN SNPE AND INDIAN HEAD DIVISION NAVAL SURFACE WARFARE CENTER (IHDIV,
NSWC)

C. Murphy, E. Giraud

P150

RHEOLOGY AND SIMULATION-BASED DIE DESIGN FOR EXTRUDABLE COMPOSITE PROPELLANT

M. Michienzi, C. Murphy, S. Railkar, D. Kalyon

P151

SOLVENTLESS PROCESSING OF EXTRUDED COMPOSITE ROCKET PROPELLANT IN A TWIN
SCREW MIXER/EXTRUDER

R.S. Muscato

P152

NEW PROCESSING AID AND EMULSIFIER FOR ENERGETICS

B.M. Kosowski, R.C. Taylor

P153

ROOM-TEMPERATURE STORABLE BONDING AGENT

P.F. Aiello, R.W. Hunter, A.P. Manzara

Air Senior National Representative
Long Term Technology Project
on
Insensitive High Explosives (IHEs)

Studies of High Energy Insensitive High Explosives

Authors: (Technical Group, ASNR LTTP on IHE)
Patrick Lamy(DME/FR), Carl-Otto Leiber (BICT/GE), <u>Adam S Cumming(DRA/UK)</u>,
M Zimmer(USAF/US), et al

<u>Abstract</u>

The Technical Group (TG) of the ASNR LTTP on IHE comprises members from FR, GE, UK and US. Through successful international collaboration, the TG has developed and characterised a group of insensitive high explosive candidate formulations. The responses of these formulations to the Substance Tests prescribed for EIDS in Test Series 7 of the United Nations' "Recommendations on the Transport of Dangerous Goods" are presented. The responses observed in a sympathetic reaction hazard assessment series are also discussed.. The report details the compositions of these formulations along with their densities, detonation velocities, critical diameters and response to impact, friction, thermal stability and small scale burning tests. Conclusions regarding the collaboration, the formulations and the test methodologies are also presented.

<u>Introduction</u>

This paper summarises the accomplishments of the Technical Group (TG) during Phases 1 and 2 of the Four Power Air Senior National Representative Co-operative Long Term Technology Project on Insensitive High Explosives (ASNR LTTP on IHE). The TG of the Four Power ASNR LTTP on IHE comprises members from FR, GE, UK and US. In Phase 1 the TG has developed and characterised a group insensitive high explosive candidate formulations. TNT-based and inert (hydroxyterminatedpolybutadiene, HTPB) binder systems employing nitrotriazolone (NTO) or nitroguanidine (NQ) along with TNT, RDX or HMX were used to achieve extremely insensitive detonating substances (EIDS). In Phase 2 the TG has developed and characterised a group of formulations with a wide range of vulnerability and performance characteristics. HMX was balanced with NTO, NQ or triaminotrinitrobenzene (TATB) in a variety of HTPB and energetic binder systems to achieve formulations which have performance levels similar to Comp B, but which are significantly less sensitive than Comp B[1,2,3,4,5,6].

Objectives

Each of the nations participating in the ASNR LTTP on IHE has a need to develop an approach to insensitive munitions (IMs). Insensitive high explosives are a necessary part of any program aimed at reducing hazards, since the reduction of the hazards associated with explosives should reduce the overall vulnerability of munitions in which they are contained. The objective of the ASNR LTTP on IHE is to evaluate candidate IHEs submitted by each of the participating nations and to identify deficiencies and the need for improvements to characteristics of these IHEs.

In Phase 1 of the programme, the goal was for IHE candidates from each nation to fulfil the requirements imposed by the United Nations' (UN) "Recommendations on the Transport of Dangerous Goods" for extremely insensitive detonating substances (EIDS). Cast TNT was chosen as a reference but no specification for performance was given.

For Phase 2 of the program, the goal was for IHE candidates from each nation to have a level of performance equivalent to Comp B while remaining as insensitive as possible. No pass/fail criteria were given for Phase 2. The UK composition, RT Type A, equivalent to Comp B was chosen as reference

Methodology

IHE candidates from each nation were chosen to minimise vulnerability while maintaining performance. Spherical nitroguanidine (SNQ) and nitrotriazolone (NTO) are known to be less sensitive than HMX or RDX. Therefore, in each Phase 1 formulation, RDX and HMX were partially or completely replaced with SNQ or NTO. Minor modifications to tests prescribed by Test Series 7 were incorporated to meet program objectives. The Phase 2 formulations were designed to equal the performance of Composition B while exhibiting low vulnerability.

The participants agreed to a series of screening and hazard assessment tests. Screening tests were conducted in the nation of origin for each material according to procedures prescribed by that nation. For Phase 1 of the program, the hazard assessment test series was Test Series 7 for

substances prescribed by the Reference 1 and included determination of critical diameter. Minor modifications to tests prescribed by Test Series 7 were incorporated to meet program objectives.

For instance, only three trials of the Cap Test were performed for each IHE candidate. Also, cast Comp B donors were used in the Gap Test. The PMMA gap thickness for the Comp B system which is equivalent to the 70 mm PMMA gap for the Pentolite system is 82 mm. The thickness of the PMMA attenuator was varied to obtain a sensitivity threshold value rather than simply a GO/NOGO value at a given thickness as prescribed by the UN. Additionally, the French 3-litre model was used in place of the steel pipe for the Bullet Impact Tests. Finally, FR performed the slow cookoff test with the French 3-litre model for FR and US IHE candidates. US performed the slow cookoff test in the UN prescribed pipe for the FR and GE IHE candidates and the reference composition, TNT. The US IHE candidate and TNT were tested by the US in the SCB as well. UK Performed the test on the UK IHE candidate according to the procedures in UN Test Series 7.

In Phase 2, a multiple (3 round) Bullet Impact Test was used in lieu of the single shot prescribed by the UN. The External Fire Test was excluded from Phase 2. Instead, a Sympathetic Detonation Test series in generic hardware was performed (See Annex).

The work was distributed equitably between nations. The work share for Phase 1 of the program is provided in Table 1 below, and for Phase 2 in Table 2.

Table 1: Work Share for Phase 1 of ASNR LTTP on IHE

IHE Candidate	GE (HX-76)	FR (B-2214)	UK (CPX-305)	US (AFX-644)	TNT (Reference)
TEST					
Critical Diameter of Detonation	GE	FR	UK	US	ALL
Cap Test	GE	GE	GE	GE	GE
Gap Test	US	US	US	US	US
Susan Test	UK	UK	UK	UK	UK
Friability Test	FR	FR	FR	FR	FR
External Fire Test	FR	FR	FR	FR	FR
Slow Cook Off Test	US	FR-US	UK	FR-US	ALL
Bullet Impact Test	GE	GE	GE	GE	GE

Table 2: Work share for phase 2 of ASNR LTTP on IHE

IHE Candidate	GE (HX 310)	FR (B 2248)	UK (CPX-413)	US (ARC-8963)	Reference (RDX/TNT 60/40)
Test					
Critical Diameter of Detonation	GE	FR	UK	US	Not necessary
Cap Test (unconfined)	GE	GE	GE	GE	GE
Gap Test	US	US	US	US	US
Susan Test	UK	UK	UK	UK	UK
Friability Test	FR	FR	FR	FR	FR
Slow Cook Off Test	FR	FR	FR	FR	FR
Bullet Impact Test	GE	FR	GE	GE	GE

Results

Screening tests were performed by each participant on its own candidate IHE using the preferred national procedures. The screening test results for Phase 1 IHE candidates are summarised in Table 3 and in Table 4 for Phase 2.

Table 3: Screening test Results for ASNR LTTP on IHE Phase 1

Nation	GE	FR	UK	US	Reference
Formulation Designation	HM-76[2]	B2214[3]	CPX-305[4]	AFX-644[5]	TNT
Impact Procedure	BAM Impact Test [UN 3a(ii)]	BAM Impact Test [UN 3a(ii)]	Rotter Impact Test [UN 3a(iii)]	Bureau of Mines [UN 3a(i)]	Bureau of Mines [UN 3a(i)]
Impact Result	24.4J	>5J	79±1	200.5 cm(5 kg)	54.5 cm (5 kg)
Impact Acceptance	>2J	>2J	≥80	>10.16 cm (3.63 kg)	>10.16 cm (3.63 kg)
Friction Procedure	BAM Friction Test [UN 3b(i)]	BAM Friction Test [UN 3b(i)]	Rotary Friction Test [UN 3b(ii)]	BAM Friction Test [UN 3b(i)]	BAM Friction Test [UN 3b(i)]
Friction Result	353 N	20% @ 353 N	Out of Range	6.3 kg	3.6 kg
Friction Acceptance Criteria	>80 N	>80 N	.3.0	>3.6 kg	Standard
Thermal Stability Procedure	Stability @ 100°C	Stability @ 75°C	Vacuum Test @ 120°C	Vacuum Test @ 100°C	Vacuum Test @ 100°C
Thermal Stability Result	0.1 cm^3/g	Delta T = 1°C (Stable)	0.2 cm^3/g	0.37 cm^3/g	0.16 cm^3/g
Thermal Stability Acceptance Criteria		Delta T <3°C	<2 cm^3/g	<2 $c,^3$/g	<2 cm^3/g
Small Scale Burning Procedure		UN 3d(ii)	RARDE Burning	UN 3d(ii)	UN 3d(ii)
Small Scale Burning Result		Mild Burning	Mild Burning	Mild Burning	Mild Burning
Small Scale Burning Acceptance Criteria		No Explosion or Detonation	No Violent Reaction	No Explosion or Detonation	No Explosion or Detonation

Table 4: Screening Test Results for ASNR LTTP on IHE Phase 2

Nation	GE	FR	UK	US	Reference
Formulation Designation	HX-310[2]	B2248[3]	CPX-413[4]	ARC 8963[5]	RDX/TNT RT60/40
Impact Procedure	BAM Impact Test [UN 3a(ii)]	30 kg fall hammer	Rotter Impact Test [UK 3a(iii)]	Bureau of Mines [UN 3a(i)]	Rotte Impact Test [UN 3a(iii)]
Impact Result	30J	No Propagation > 4m No Reaction @ 2.75m	88	396.5 kg-cm	120
Friction Procedure	BAM Friction Test [UN 3b(i)]	BAM Friction Test [UN 3b(i)]	Rotary Friction Test [N 3b(ii)]	BAM Friction Test [UN 3b(i)]	Rotary Friction Test [UN 3b(ii)]
Friction Result	360 N	353 N	>6	16.8 kg f	>6
Thermal Stability Procedure	Vacuum Stability @ 100°C	Stability @ 75°C UN 3 c	Vacuum Stability @ 100°C	Differential Scanning Calorimetry/ Thermogravimetric Analysis	Vacuum Stability @ 120°C
Thermal Stability Result	0.47 cm³/g	Stable	0.52 cm³/g	See Notes 1 & 2 Below	<0.2 cm³/g
Small Scale Burning Procedure	Not Performed	UN 3d(ii)	Not Performed	Not Performed	Not Performed
Small Scale Burning Result	Not Performed	Mild Burning	Not Performed	Not Performed	Not Performed

Notes on Table 4.

Note 1: DSC; Exotherm @ 319.8°C/Onset @ 302.9°C for Heat Flow of 20.44 cal/g
Exotherm @ 371.5°C/Onset @ 357.5°C for Heat Flow of 130.5 cal/g
Note 2: TGA (10°C/min), N$_2$ Flow-60 cm³,
15.23% Weight Loss @ 193°C, 69.29% Weight Loss @ 312°C

The hazard assessment results for Phase 1 are summarised in Table 5. In Phase 1, IHE candidates from all participating nations achieved the criteria for EIDS. The vulnerability characteristics of the Phase 1 IHE candidates were significantly improved in comparison with the reference composition, TNT.

The hazard assessment results for Phase 2 are summarised in Table 3. The IHE candidates from all four participants met the performance requirement (broadly equivalent to that of Composition B-RDX/TNT 60/40) while exhibiting greatly improved vulnerability characteristics. IHE candidates from FR and UK achieved all EIDS criteria, while IHE candidates from GE and US achieved all EIDS criteria with the exception of the Gap Test. However, even the most sensitive and most energetic (as determined by relative detonation pressure calculated from Density x D²/4) Phase 2 IHE candidate (US) did not propagate the detonation of the donor item during sympathetic detonation testing in the configuration shown the Annex.

DISCUSSION/CONCLUSION

General

The results of the ASNR LTTP on IHE show it is now possible to rebalance the equation between performance and vulnerability[1,2,3,4,5,6]. The candidates chosen illustrate different ways of matching the requirement. A suite of formulation types with a variety of performance levels has been characterised and evaluated. This illustrated the choices available to the formulator as a result of the developments in the last few years. Where once only TATB was available, now NTO and new grades of NQ make the design function easier.

The test series conducted allow differences in sensitivity of the IHE candidates to be observed. Vulnerability of the IHE candidates is significantly less than that of the reference compositions, TNT and RDX/TNT--60/40. Performance levels are not necessarily compromised.

The aims of the technical group were met. All nations produced candidate formulations which achieved the UN criteria for Extremely Insensitive Detonating Substances (EIDS). Munitions containing any of the four compositions will be safer than those with existing compositions with comparable performance.

Test Methodologies

Regarding the test methodologies employed, for the Cap Test, it is imperative that the critical diameter of IHE candidates be determined for results to be meaningful. IHE candidates with critical diameters much greater than the diameter of the detonation cap do not yield meaningful results in the Cap Test.

In the Gap Test, peak pressures have been calibrated as a function of gap thickness for various donor systems as shown in Table 7. However, the impulse imparted by each donor system as a function of gap thickness is not known. Translation of the results determined with one donor system cannot be necessarily simply applied to those of another donor system. The relative sensitivities should remain the same. Also, the TG of the ASNR LTTP on IHE noted that the preferred method is to determine the PMMA thickness threshold value rather than simply a NO/NOGO result at a gap thickness of 70 mm as prescribed by the UN. This aids in establishing a safety margin for IHE candidate in sympathetic detonation scenarios.

Table 5: Phase 1 Hazard Assessment Results

Nation	GE	FR	UK	US	Reference
Formulation Designation	HX 76	B2214	CPX305	AFX-644	TNT
Composition	SNQ/RDX/HTPB	HMX/NTO/HTPB	RDX/SNQ/Al/ HTPB	TNT/NTO/ D2 Wax/Al	TNT
Weight %	55/30/15	12/72/16	30/35/20/15	30/40/10/20	100
Density (kg/m^3)	1550	1630	1650	1770	1600
Detonation Velocity (m/s)	7420	7440	7000	6800	6770
Critical Diameter (mm)	40	60<d<65	142<d<47	<40	40<d<45
Cap Test	No Reaction	No Reaction	No Reaction	No Reaction	No Reaction
Gap Test-Go/No Go Thickness (mm PMMA)	73.1/76.2	33.2/35.0	74.6/76.2	50.8/52.3	111.1/114.3
Susan Test (kPa)	7.9	4.9	11.1	17.1	17.7
Friability (MPa/ms)	0.2	0.2	0.2	0.3	8.0
Slow Cookoff		Overpressure Burst x 3--166°C		Overpressure Burst and Combustion x 2 --179°C	Explosion/Detonation x 2, Overpressure burst x 1--190°C
Bullet Impact	Burning x 4	No Reaction x 3, Burning x 1	Burning x 4	No Reaction x 4	Deflagration x 4
Overall Results	EIDS	EIDS	EIDS	EIDS	NO EIDS

Table 6: Phase 2 Hazard Assessment Results

Nation	GE	FR	UK	US	Reference
Formulation Designation	HX 310	B 2248	CPX 413	8963	RDX/TNT--60/40
Composition	HMX/NTO/NQ/ HTPB 47/25/10/18	NTO/HMX/HTPB 46/42/12	NTO/HMX/ Energetic Binder 45/35/20	HMX/TATB/ Energetic Binder 35/40/25	RDX/TNT/Wax 60/40/1
Density (kg/m)	1570	1700	1740	1760	1720
Detonation Velocity (km/s)	7.75	8.13	7.99	8.14	7.91
Critical Diameter (mm)	≤10	11	10	<3	<2
Density x $D^2/4$ (GPa/Relative Detonation Pressure	23.6/0.91	28.1/1.08	27.8/1.07	29.2/1.12	26.0/1.00
Plate Dent (Relative Depth of Crater)	0.84	0.90	0.91	0.98	1.00
Cap Test	No Reaction	No Reaction	No Reaction	No Reaction	Detonation
Gap Test-Go/No Go Thickness (mm PMMA)	92/94	72/73	73/74	95/99	135/137
Gap Test-Go/No Go Pressure (x 10^9 Pa)	2.65/2.54	4.38/4.35	4.32/4.27	2.42/2.21	1.67/1.62
Susan Test (kPa)	11.01	8.51	14.33	9.29	27.1
Friability (MPa/ms)	1.3	1.5	3.5	not performed	30
Slow Cookoff	Overpressure Burst x 3--155°C	Ovepressure Burst x 2--174°C	Overpressure Burst x 3--156°C	Overpressure Burst x 3--143°C	Detonation x 3-- 180°C
Bullet Impact (3 Round Burst/0/50 Cal AP @ 850 m/sec)	Burning x 2/Overpressure Burst x 1	Burning x 3	Burning x 2/No Reaction x 1	Burning x 1/Overpressure Burst x 1/No Reaction x 1	Detonation x 3
SD 90min Diameter/6mm Wall/50m Air Gap	Not Tested	Detonation	Not Tested	Detonation	Detonation
SD 90mm Diameter/6 mm Wall/125mm Air-- 25mm Wood Gap	No Detonation	No Detonation	No Detonation	No Detonation	No Detonation but Reaction
SD 176mm Diameter/127mm Wall/125mm Air-- 25mm Wood Gap	Not Tested	No Detonation	Not Tested	No Detonation	Detonation

Table 7: Gap Thickness Corresponding to a PMMA Gap Pressure of 3.5×10^9 Pa

Donor	PMMA Thickness (for 3.5×10^9 Pa)
50/50 Pentolite	70 mm
95/5 RDX/Wax	76 mm
Comp B	82 mm

The Susan Test was considered by the TG of the ASNR LTTP on IHE to be a discriminating test with quantifiable results. Results appeared to be influenced by the mechanical properties of the IHE being evaluated. Shots at higher velocities should be considered to fully characterise IHE compositions.

The TG of the ASNR LTTP on IHE considered the friability test to be useful for determining the reactivity of damaged energetic materials. It should not be considered as directly equivalent to the Susan Test as implied in Test Series 7 of Reference 1. The results appear to parallel more closely those from the Bullet Impact Test.[3]

Regarding performance, ranking the formulations from most energetic to least energetic as measured by relative detonation pressure, the order is US>FR≥UK>Reference CompB>GE. Ranking the formulations in terms of relative depth of crater in the Plate Dent Test, the order is Reference Comp B>US>UK≥FR>GE. Although the results appear to contradict, it is possible that the 40 mm diameter test piece for the IHE candidates in the Plate Dent Test is too small and that the test is not sufficient for comparing IHE with traditional materials. However, disregarding the results for the Reference composition, both methods of performance assessment provided the same order of performance for the IHE candidates, with the FR and UK candidates roughly equivalent. A more appropriate method of performance assessment would be to use larger samples, perhaps measuring fragment velocity from generic warheads filled with the candidates. The observations made during the Plate Dent Test illustrate the difficulties in assessing IHEs with traditional test methods. However, the Phase 2 candidates showed significant performance enhancement over those from Phase 1 (30%).

Sympathetic Detonation (SD) testing was viewed as necessary in Phase 2, since the implications of the extremely insensitivity to hazardous stimuli as observed in the generic UN subscale tests for response in actual munitions is uncertain. The TG of the ASNR LTTP on IHE decided a demonstration of the compositions in a sympathetic detonation test series would provide evidence that the generic tests prescribed by UN Test Series 7 are suitable for characterising and selecting IHE candidates.

Two of the Phase 2 candidates, the most shock sensitive (US) and the least shock sensitive (FR), as determined in the Gap Test, were selected for comprehensive sympathetic detonation testing in steel tubes simulating small diameter and large diameter missile warheads. The responses of both IHE candidates were nearly identical to each other but substantially less severe than that of the reference composition (RDX/TNT--60/40). The results illustrate that package design is critical to surviving sympathetic detonation. Also, the balance of energy to sensitivity is crucial as shown in Table 5. The probability of the FR candidate surviving SD is greater than that of the US candidate. However, there remains a substantial margin of sensitivity between the US candidate and the reference composition.

While the GE formulation contained the smallest percentage of energetic material for any of the candidates, it contained the largest percentage of HMX and the smallest percentage of less sensitive material (ie NTO, NQ, TATB). It should also be noted that while the energy obtained from the US candidate approximated that determined for the Reference Comp B, the US candidate was not very much less sensitive than the Reference Comb B. Still, the results of sympathetic detonation testing were markedly different. The sensitivity and energy results for the FR and UK candidates were nearly identical. The probability of the FR candidate surviving Sympathetic detonation is greater than that of the US candidate. However, there remains a substantial margin between the US candidate and the Reference Comp B. The responses of the UK and GE composition and their relative margin of safety can be predicted as shown in Table 8.

Table 8: Energy to Sensitivity Ratios for Phase 2 IHE Candidates and Reference

IHE Candidate	Energy to Sensitivity Ratio (Plate Dent Depth/NOGO Pressure in Gap Test)
Reference (RDX/TNT-60/40)	0.47
US Phase 2 Candidate	0.34
FR Phase 2 Candidate	0.17
UK Phase 2 Candidate	0.18
GE Phase 2 Candidate	0.30

Conclusion

All four nations have benefited from the opportunity to examine each others' approach and test philosophy. this can only provide added confidence in the compositions and in assessing future developments. This collaboration enabled a wider range of materials to be studied than could have been examined by any of the nations alone. Although difficult to quantify, the program has also, by cost sharing, achieved significant savings for the participating nations.

Acknowledgements

The authors would like to express their appreciation for the contributions of other members of the ASNR LTTP on IHE TG and associated participants. These include Jean Isler (SNPE, FR), Alain Delclos (SNPE, FR), Alain Becuwe (SNPE, FR), Prof Dr Hiltmar Schubert (ICT, GE), Dr Fritz Schedlbauer (ICT, GE), Dr Chris Leach (DRA, UK), John Corley (WL, US) and Sally Gaulter (DRA, UK).

References

1.   'Recommendations on the Transport of Dangerous Goods (Tests and Criteria), Revision 1' United Nations, February 1989.

2.   Schubert, H and Schedlbauer, F ; 'ASNR-Langzeit Technologieprogramm uber unempfindliche Sprengstoffe (IHE) Ergeßnisbericht der 1 und 2'; Proc 18. Sprengstoffgesprach, Lünen, 4./6. 10. 1995, p 315/336. FIZBw FBWT-96-01, 1996, Bonn.

3.   Becuwe, A et al ; 'EIDS High Explosives for 1.6 Munitions'; ADPA Energetic Materials Technology Symposium, September 1995.

4.   Cumming A et al ; 'Insensitive High Explosives and Propellants - The UK Approach';
      ADPA Insensitive Munitions Technology Symposium, June 1992.

5.   Corley, J., et al, 'Fuzed Insensitive General Purpose Bomb Containing AFX-645'
      Final Report, WL-TR-95-7019, May 1995.

6.   Gaulter, S et al; 'The Formulation of an Insensitive HE based on HMX, NTO and
      PolyNIMMO'; ADPA Insensitive Munitions Technology Symposium, June 1994
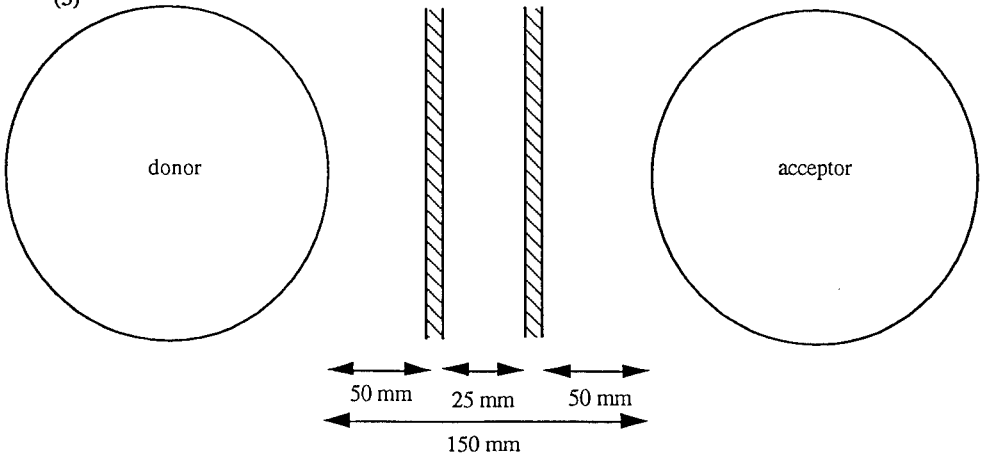
Test set up :

(1)
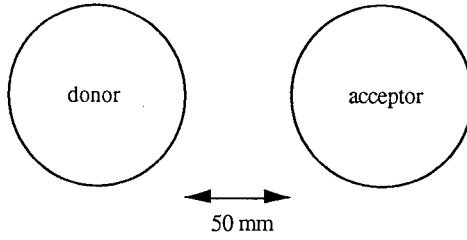
(2)
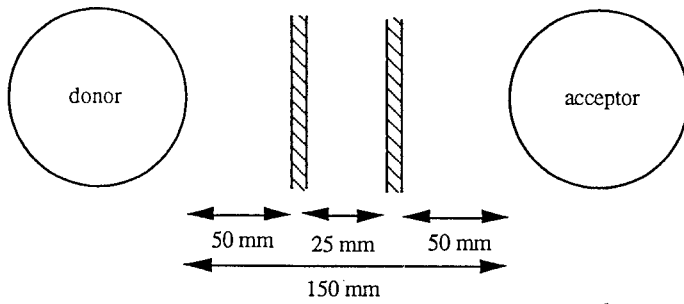
screens $\left\{ \begin{array}{l} \text{type wood (pine tree)} \\ \text{thickness 12.5 mm} \end{array} \right.$

(3)

screens $\left\{ \begin{array}{l} \text{type wood (pine tree)} \\ \text{thickness 12.5 mm} \end{array} \right.$

Verfahrenstechnik zur

Herstellung von PBX Sprengladungen

Möglichkeiten und Grenzen

Dr. Paul Wanninger
TDW
86523 Schrobenhausen

PBX Ladungen werden entwickelt und hergestellt um zwei nur scheinbar gegensätzliche Eigenschaften von Sprengladungen zu vereinigen: Höchste Leistung mit größter Unempfindlichkeit gegenüber äußeren nicht vorhersehbaren Einflüssen, wie z.B. Feuer und Beschuß (Bild 1).

Nach den unterschiedlichen Wirkmechanismen kann man die Ladungen grob in Hohlladungen, Splitterladungen und Unterwasserladungen einteilen (Bild 2).

1. Rohstoffe für PBX Ladungen

Je nach ausgewähltem Fertigungsverfahren haben die Rohstoffparameter insbesondere die des Hauptrohstoffes Sprengstoff unterschiedliches Gewicht für den Herstellprozeß.

Bei einem gegossenen PBX ist der Feinanteil stark limitiert, die Kornform und spezifische Oberfläche spielt eine große Rolle, während diese Parameter für Pressen und Extrudieren andere Wertigkeiten ergeben. Durch entsprechende Verfahrensschritte werden die gewünschten Eigenschaften des Rohstoffes Sprengstoff erreicht (Bild 3, 4).

2.   Gegossene PBX Sprengladungen

Der Herstell- und Gießprozeß der PBX Ladungen entspricht dem der Composite Propellants und wird seit den 70er Jahren nahezu unverändert durchgeführt (Bild 5).

Das zentrale Gerät ist ein Planetenmischer mit 2 oder 3 Mischflügeln, die ungefähre maximale Mischung ist im Bild 6 dargestellt, bei einer angenommenen typischen Dichte der Sprengladung von 1,7 [g/cm^3].

3.   Gepreßte PBX Sprengladungen

Solche Ladungen enthalten in der Regel zwar die gleichen Sprengstoffe RDX und HMX wie bei gegossenen Ladungen, die Anforderungen an diese Rohstoffe unterscheiden sich durch den in der Regel hohen Füllgrad solcher Ladungen (92 - 96%) und durch völlig andere hoch phlegmatisierend wirkende Binder-Systeme. Für gepreßte Ladungen wird zuerst ein Zwischenprodukt, das später zu verpressende Granulat hergestellt, dann gewichts- oder volumendosiert in einer CNC gesteuerten Presse möglichst auf Endmaß verpreßt (Bild 7, 8). Der nötige hohe Druck (2000 bis 2500 bar) begrenzt die Größe der Ladungen, mit einer 800 to-Presse kann man gerade noch 200 mm Ladungen von guter Qualität herstellen (Bild 9).

Einen Sonderfall stellen isostatische Preßverfahren dar, die zwar sehr geringe Dichtegradienten innerhalb der gefertigten Sprengladung garantieren, aber wegen sehr langer Taktzeiten und erheblicher Nacharbeit aus Kostengründen für eine größere Serie nicht akzeptabel sind.

4. Extrudierte PBX Sprengladungen

Dieser modernste und einzige kontinuierliche Prozeß zur Herstellung von Sprengladungen wird derzeit weltweit erprobt (Bild 10, 11). Es zeigen sich dabei eine Reihe von Vorteilen wie kurze Mischzeiten, Verwendung von feinstem Sprengstoff sowie automatischer Dosierung.

Die nötigen Bindergehalte liegen im gleichen Bereich wie bei gegossenen Sprengladungen (Bild 12). Eine im Mehrschichtbetrieb arbeitende Maschine kann ohne große Gefahr, da die in der Mischzone befindliche Sprengladung relativ klein ist, beachtliche Mengen produzieren (Bild 13).

Für die Herstellung von Preßgranulaten wird derzeit hauptsächlich der Planetenmischer, seltener der Slurryprozeß und noch seltener der Extruder verwendet. Die Vorteile für eine Produktion von Granulat mit dem Extruder sind durch den kontinuierlichen, automatischen Prozeß gegeben, der einzige Nachteil besteht in der notwendigen Verwendung von Lösungsmitteln und deren Rückgewinnung und Reinigung bei der Herstellung von hochgefüllten (92 - 96 %) Granulaten (Bild 14, 15).

5. Produktion von Ladungen

5.1 Herstellung von Hohlladungen

Hohlladungen haben üblicherweise ein Kaliber von 20 bis 150 mm max. 200 mm. Größere Hohlladungen werden nur in Torpedos verwendet. Zur Herstellung von Hohlladungen bietet sich das Preßverfahren als nahezu ideal an. Mit einer modernen Presse kann man mit automatischer Zuführung des Granulats hohe Stückzahlen pro Zeiteinheit erreichen. Der einzige Nachteil besteht im limitierten

Durchmesser, dieser Nachteil wiegt aber nicht sehr schwer, da von großen Hohlladungen immer nur geringe Stückzahlen benötigt werden (Bild 16).

5.2 Herstellung von Splitterladungen

Splitterladungen werden gegen unterschiedlichste Ziele eingesetzt und haben damit die verschiedensten Größen und Geometrien. Für kleine Ladungen bietet sich als Verfahren das automatische Pressen auf Endmaß an. Bei größeren Ladungen ab ca. 3 kg Ladungsgewicht hängt die Auswahl der Fertigungsverfahrens stark von den zu produzierenden Einheiten ab. Bei großen Stückzahlen ist der Extruder das ideale Produktionsmittel (Bild 17).

5.3 Herstellung von Unterwasserladungen

Solche Ladungen können wegen ihrer Größe 100 - 800 kg nur im Gieß- oder Extruderverfahren hergestellt werden. Wie bei den Splitterladungen ist der Extruder das ideale Produktionsmittel bei hohen Stückzahlen (Bidl 18).

6. Bewertung der Produktionsverfahren

Das Hauptkriterium zur Auswahl des geeigneten Herstellverfahren ist sicherlich die Größe der herzustellenden Ladung. Einschränkend können noch ausgefallene Geometrien sein, die z.B. statt Pressen, Gießen oder Extrudieren einer kleinen Sprengladung nötig machen. Eine Ladung wird oft nur spezifikationsgerecht konstruiert und nicht optimiert im Hinblick auf eine Fertigung (Bild 19, 20).

Die Belastung der Umwelt muß einer Fertigung so gering wie möglich gehalten werden. Deshalb sind Fertigungsverfahren zu bevorzugen die wenig oder gar keine Nebenprodukte oder Abfall erzeugen. Optimal stellt sich dabei das Preßverfahren dar. Bei der Aufbereitung des Granulats wird kein Lösungsmittel oder nur sehr

geringe Mengen davon verwendet, beim Pressen auf Endmaß entsteht kein Abfall, bei der sorgfältigen Auswahl der Binder entstehen keine Toxiotizitätsprobleme während der Verarbeitung oder bei der Demilitarisierung.

Gegossene Ladungen erfordern bei der Herstellung bedingt durch den Batchprozeß Reinigungsschritte mit anfallendem Lösungsmittel und Sprengladungsabfall. Als kontinuierliches Verfahren hat das Extruderverfahren nur sehr wenige Reinigungsschritte, bei der Aufbereitung von Preßgranulat muß allerdings Lösungsmittel verwendet werden, welches jedoch quantitativ zurückgewonnen und aufbereitet werden kann (Bild 21).
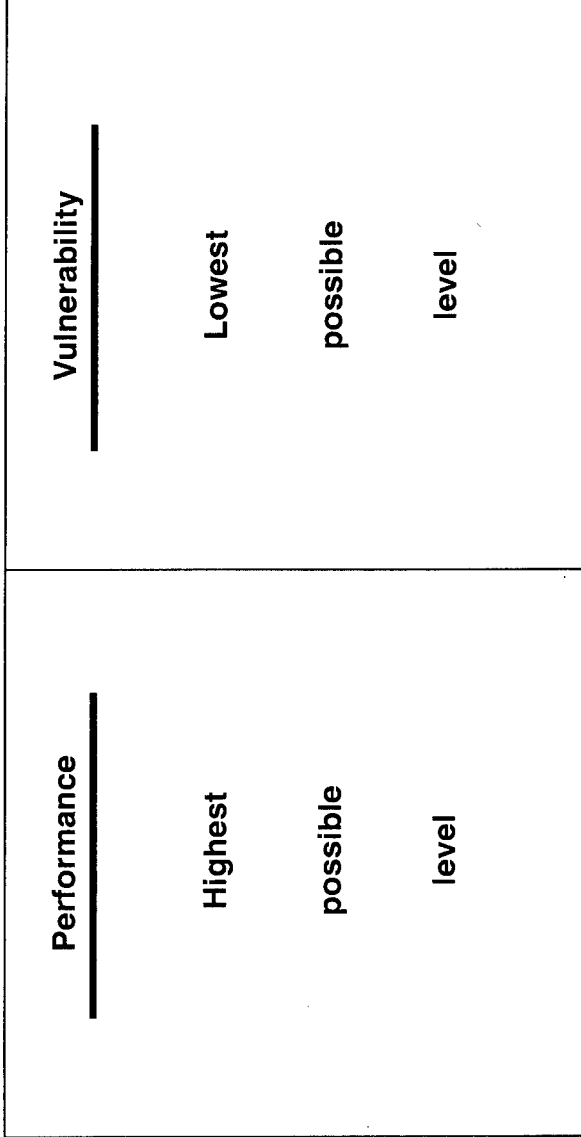
Insgesamt ist die Umweltbelastung bei PBX Ladungen sehr gering; verglichen mit alter TNT-Technologie wo nahezu 100 % der Ladung als Abfall erzeugt wurde (Bild 22).

7.   Zusammenfassung

Den unterschiedlichen Anforderungen an Sprengladungen können nur verschiedene Herstellverfahren gerecht werden. Während bei einer Hohlladung der nahezu alles bestimmende Parameter die Durchschlagsleistung ist, muß bei einer großen Ladung verstärkt auf machbare und bezahlbare Entsorgung Wert gelegt werden. Eine große Ladung stellt eine größere Gefahr dar und muß daher besonders unempfindlich gegen äußere Stimuli sein. Nur durch die rechtzeitige Einbeziehung der Parameter die im Umfeld des Produktionsprozesses liegen, die aber diesen entscheidend beeinflussen können, insbesondere die Sicherheit, Umwelt und damit auch die Produktionskosten, kann eine problemlose Fertigung über lange Zeit verifiziert werden (Bild 23, 24).
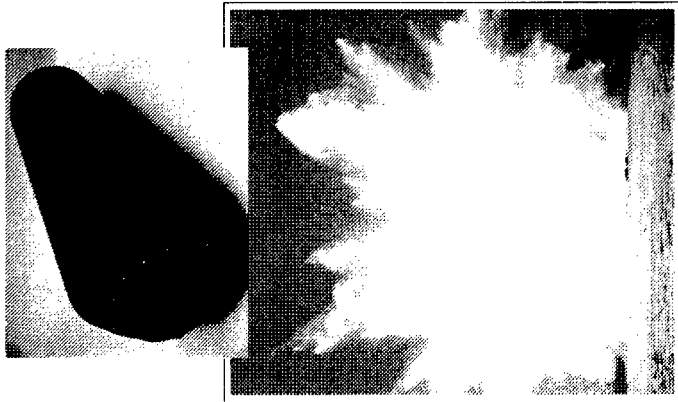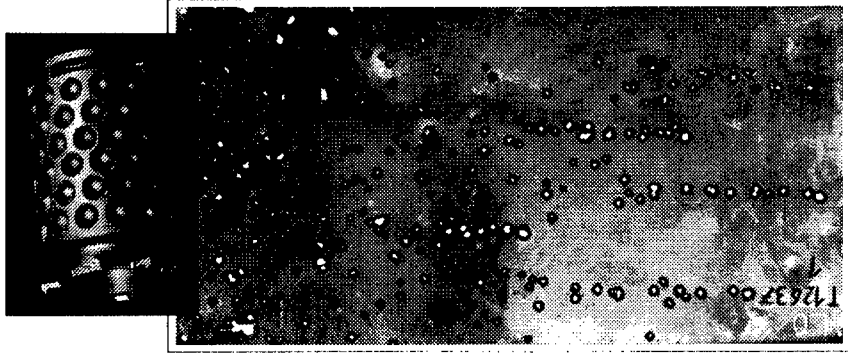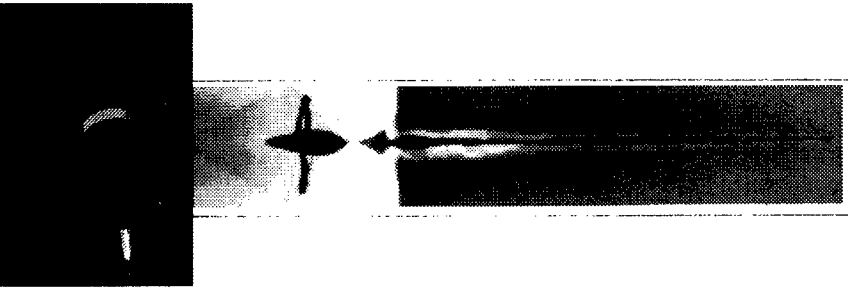
Bild 1

Production of PBX Charges

Requirements

Performance	Vulnerability
Highest possible level	Lowest possible level

TDW

04/96

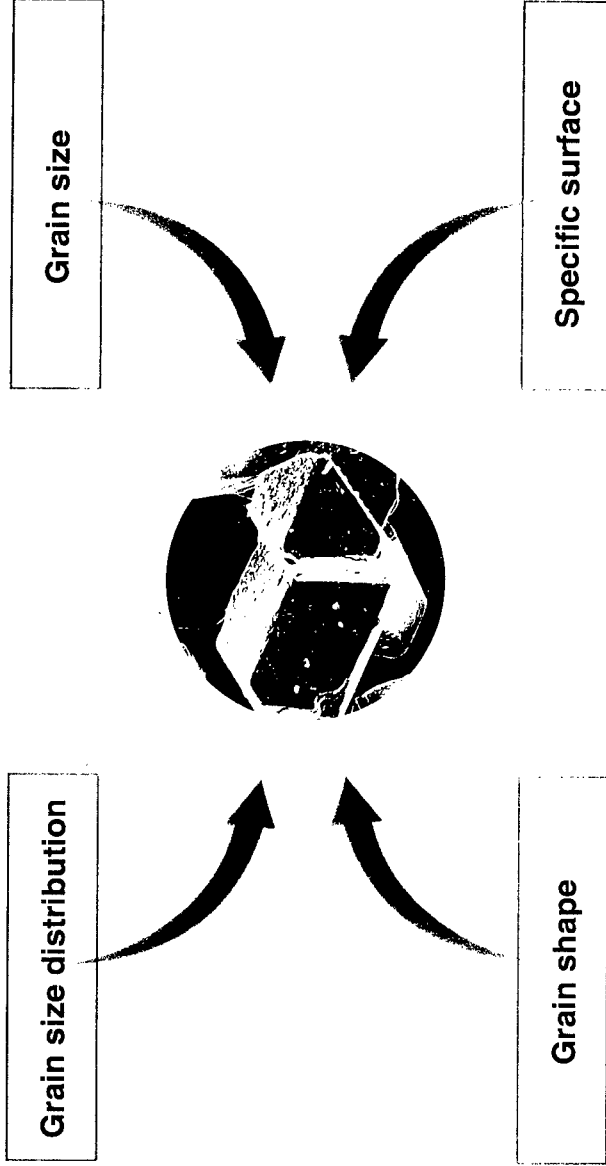# Production of PBX Charges

Charges

Production of PBX Charges

Determining Parameters

Grain size

Specific surface

Grain size distribution

Grain shape

TDW

04/96

Production of PBX Charges

Raw Material

Cristallisation

Coating

Blending

Grinding

▼TDW

Bild 5
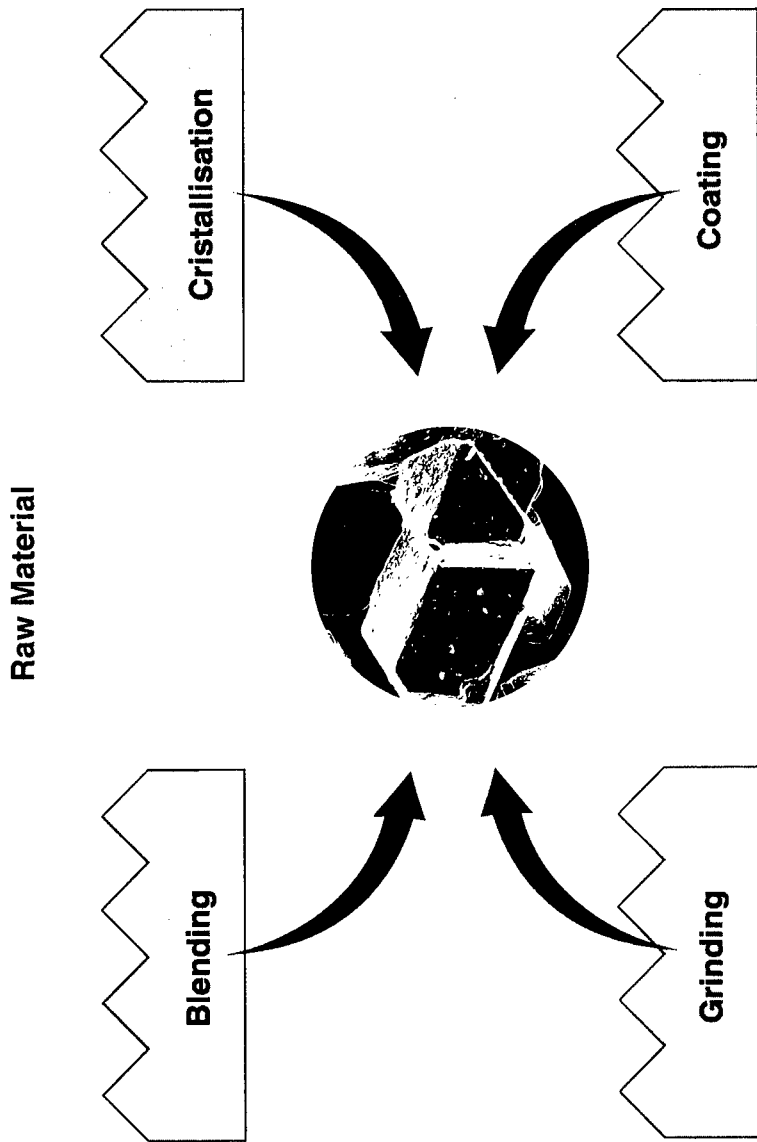
Production of PBX Charges

Casting of PBX - Detailed Process

RDX, HMX raw
NTO, AP
Al

H_2O

Grinding

Filter

H_2O

Exhaust

Hot Air

Drying

RDX
HMX
Powder

Binder

Mixing

Curing
Agent
Catalyst

Vacuum

Casting or Injection Molding

Curing

Machining

Assembling

TDW

03-96

Production of PBX Charges

Mixer Capacity

Volume of the Kettle [l] (y-axis: 0, 1, 10, 100, 1000)

Max Loading of the mixing bowl [kg] (x-axis: 1, 10, 100, 1000)

TDW

04/96
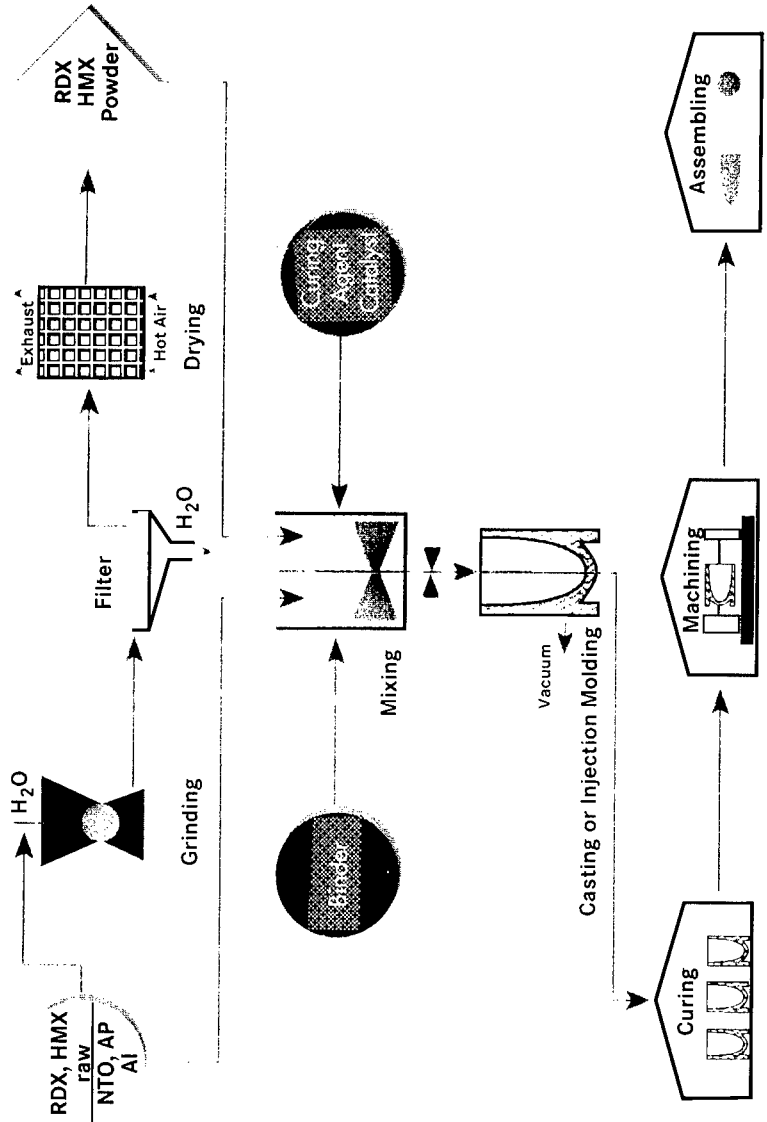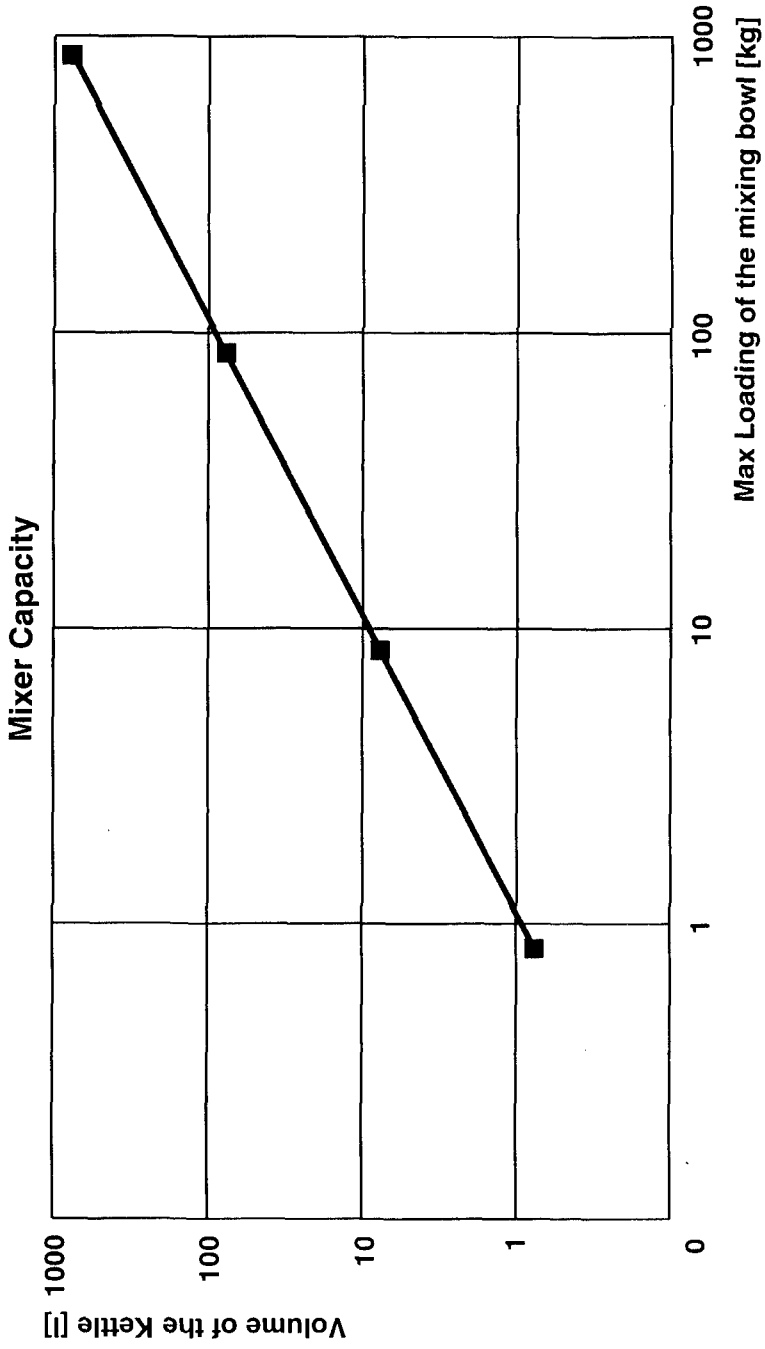
Production of PBX Charges

Pressed Charges

H.E. (e.g. HMX / RDX)	Binder
High solid content > 95 %	Low Young's modulus
High percentage of fine particles	High elongation
Low specific surface	Pressing at low temperature → Less internal stresses
Recyclable	Phlegmatising - maximal coating of the particles

TDW

Production of PBX Charges

Pressed Charges

RDX, HMX
PETN, HNS

Binder

Solvent

Planetary Mixer

phlegmatized
HE granules

Press

Charge

TDW

04/96

Bild 9
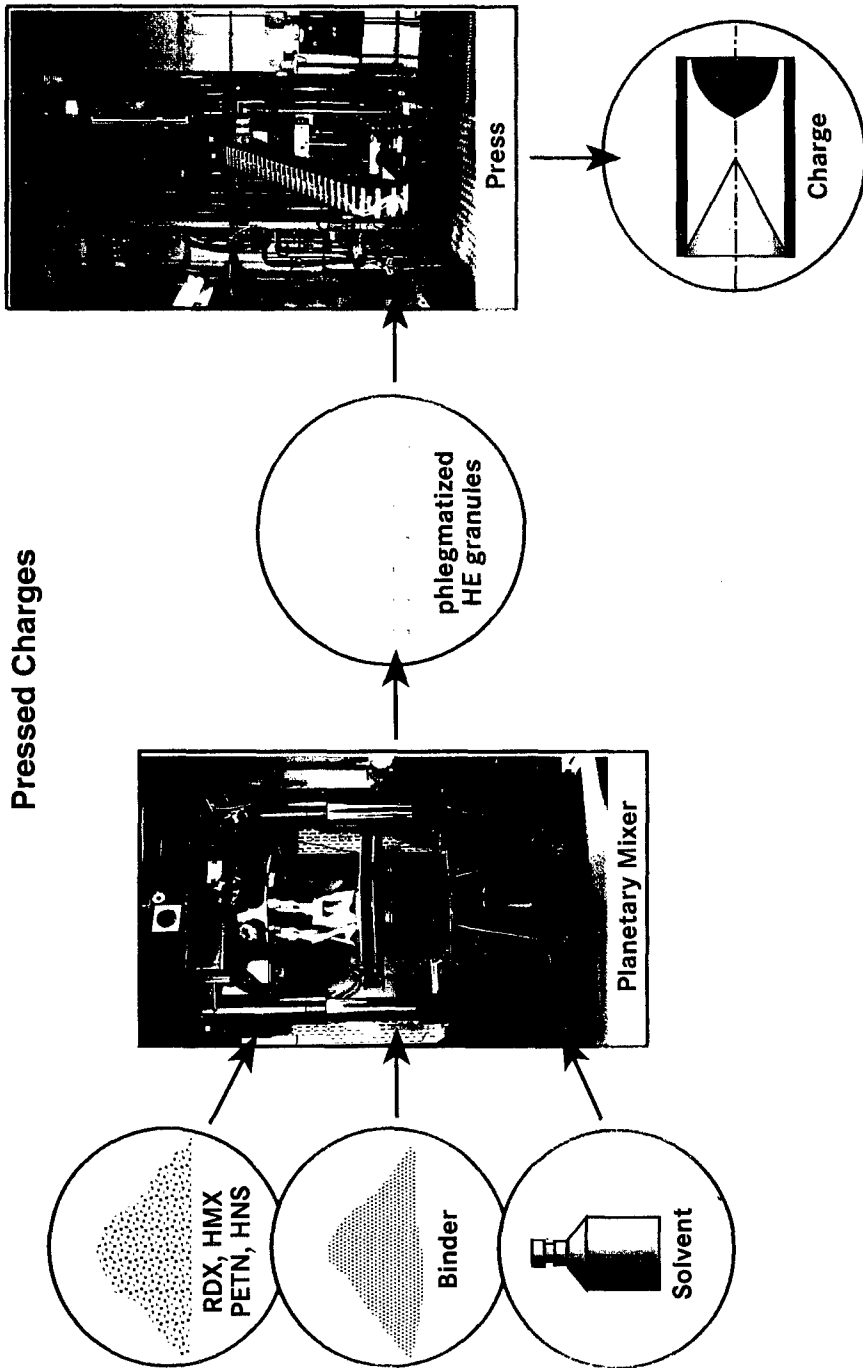
Production of PBX Charges

Pressure as a Function of Force and Diameter [mm]

▲TDW

04/96

Production of PBX Charges

Extruder

TDW
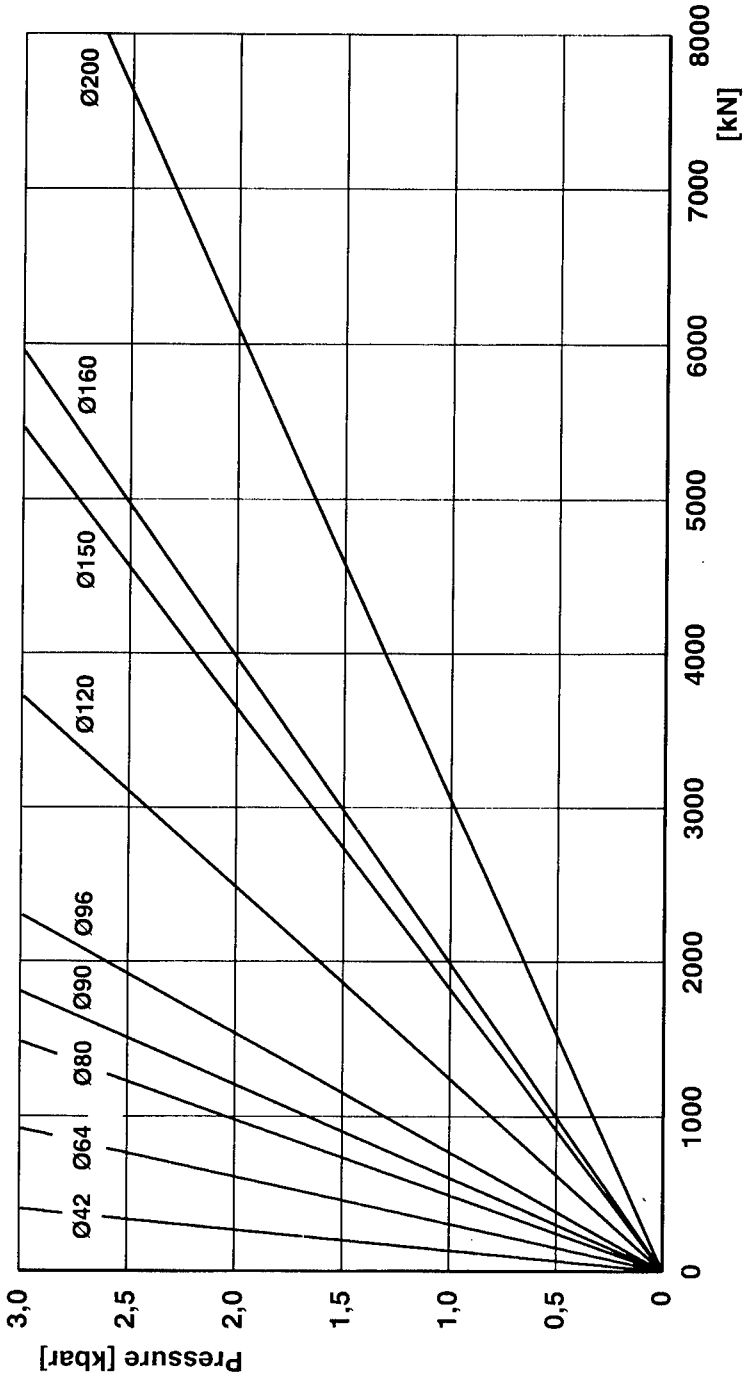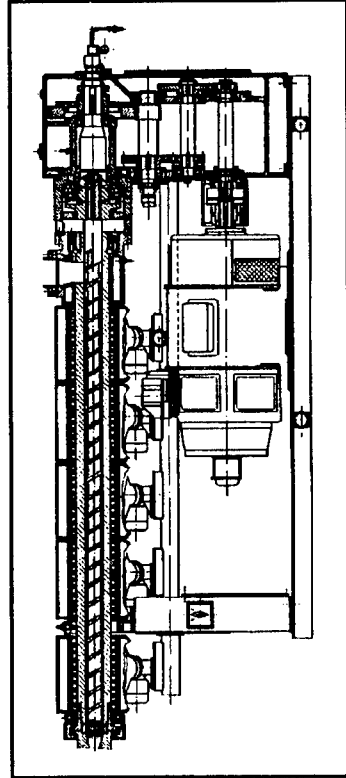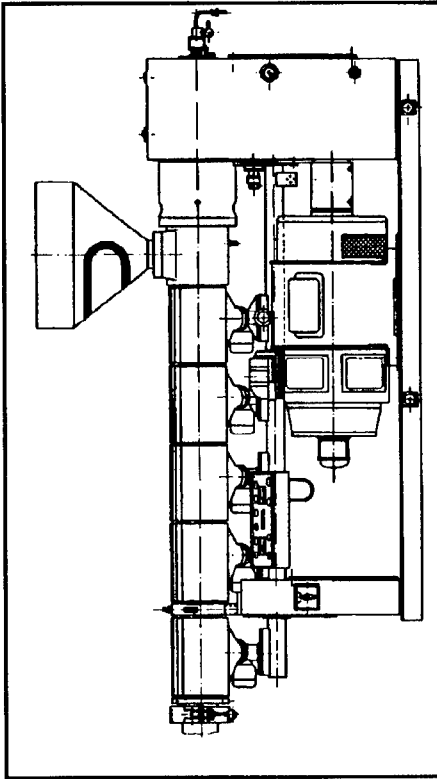
Production of PBX Charges

Extruder in action

TDW

04.96

Production of PBX Charges

Determining Parameters
Performance Criteria

Cast

90
85

Extruded

85

Pressed

96

☐ Binder
■ Solid content

◢TDW

04 96

Bild 13

Production of PBX Charges

Twin screw Extruder Capacity

Dia of the Screw [mm] (vertical axis: 100, 80, 60, 40, 20, 0)

Production [kg/h] (horizontal axis: 0, 50, 100, 150, 200, 250, 300, 350, 400, 450, 500, 550, 600, 650)

▷TDW

04.96

Bild 14
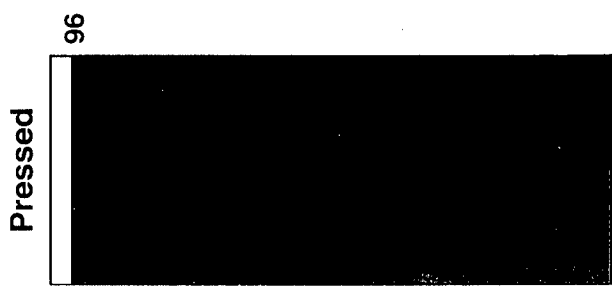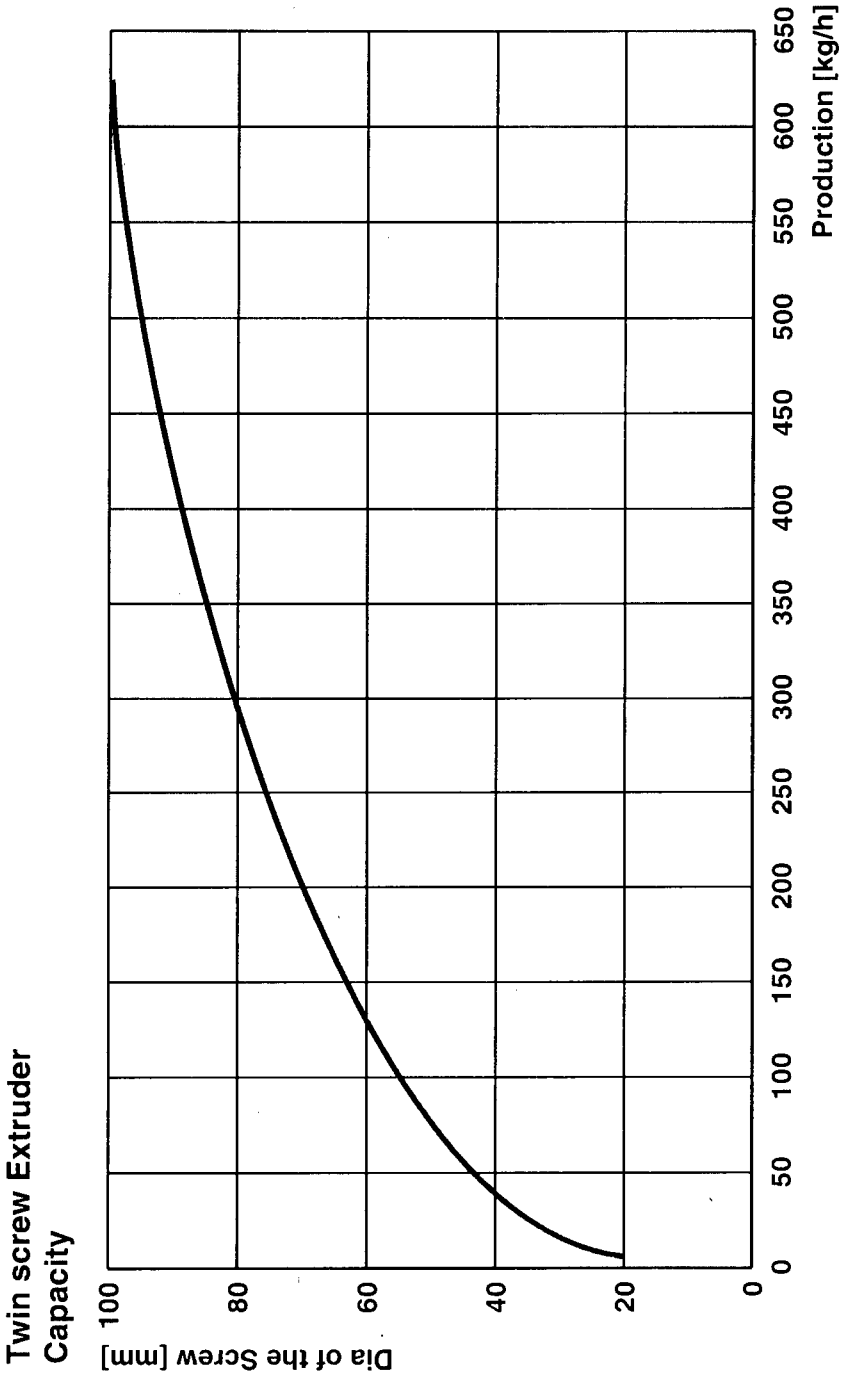
Production of PBX Charges

Granules for Pressed Charges

Planetary Mixer

Slurry Process

Extruder

◤TDW

04-96

Bild 15
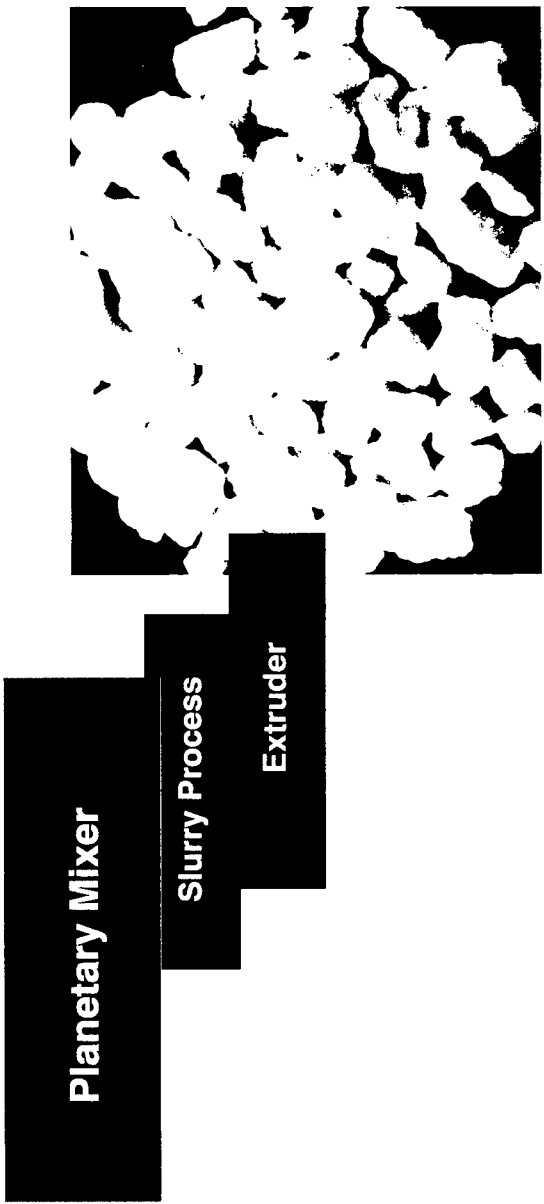
Production of PBX Charges

Production of Granules for pressed charges

Mixer

Batch process
Limited quantities
no or less solvent
necessery

Extruder
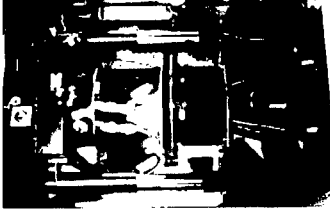
Continous process
Unlimited quantities
Solvent necessery

TDW

Production of PBX Charges

Shaped Charges

Pressed   Cast
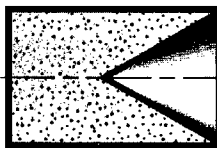
- Unlimited Diameter
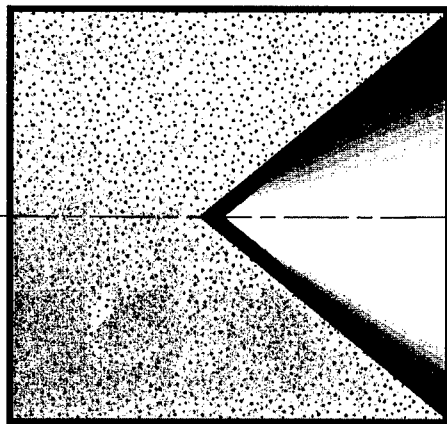
Advantage:
- Easy storing of granules
- Automotive feeding
- High production rate
- No machining
- Highest level of performance

Disadvantage:
- Limited Diameter

- Reduced level of performance
- Batch process machining necessary

⊠TDW

04/96

Production of PBX Charges

Fragmenting Charges
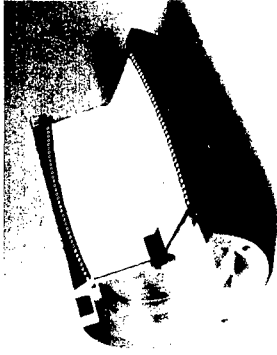
	Pressed	Cast	Extruded
Advantage:	High production rate	Every geometry possible Case bended	Every geometry possible Case bended
Disadvantage:	Only small charges Limited diameter Limited by geometry	Batch process Lower production rate	High production rate necessery

◥TDW

04-96

Production of PBX Charges

Underwater Charges

Cast

Extruded

Advantage:

Easy feeding
Easy controlling of the formulation

Automotive feeding
No cleaning during production

Disadvantage:

Batch process
Cleaning

High production rate necessary

◤TDW

Bild 19

Production of PBX Charges

Typical Production spectrum

Pressed
Shaped charges
Small mines

Cast
Fragmenting charges
Underwater charges
- Mines
- Torpedos

Extruded
Granules
Fragmenting charges
Underwater charges

◥TDW

04.96

Production of PBX Charges

Determining Parameters
Size of the charges

Pressed
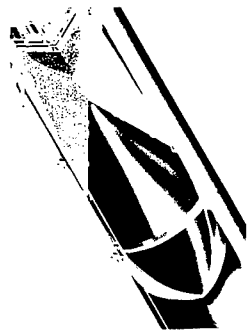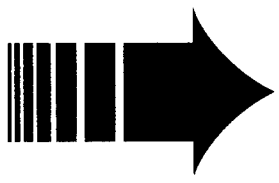
0,02 - 4 kg

Cast
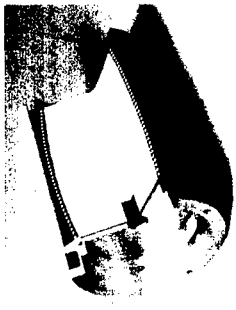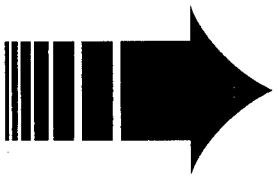
1 - 600 kg

Extruded

5 - 600 kg

TDW

04-96
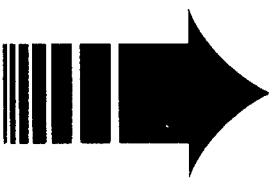
Production of PBX Charges

Environment

Problems	Pressed	Cast	Extruded
Solvent	-	(+)	(+)
Waste	-	+	+
Toxicity during production	-	+	-
Demilitarisation	-	-	-

TDW

04/96

Production of PBX Charges

Header
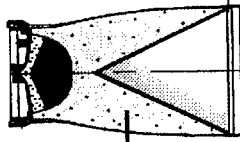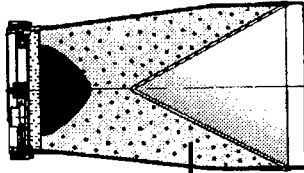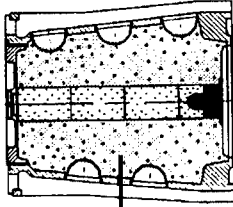
2.8 kg

2.8 kg

1.7 kg

3.2 kg
RDX/TNT

ROLAND 60D

4.2 kg
HMX/TNT

HOT

1.8 kg
HMX/TNT

MI-
LAN

Weight Header [%]   94   67   88

TDW

04/96

Bild 23

Production of PBX Charges

Requirements

Pressed Charges

Cast Charges
Extruded Charges

04/96

TDW
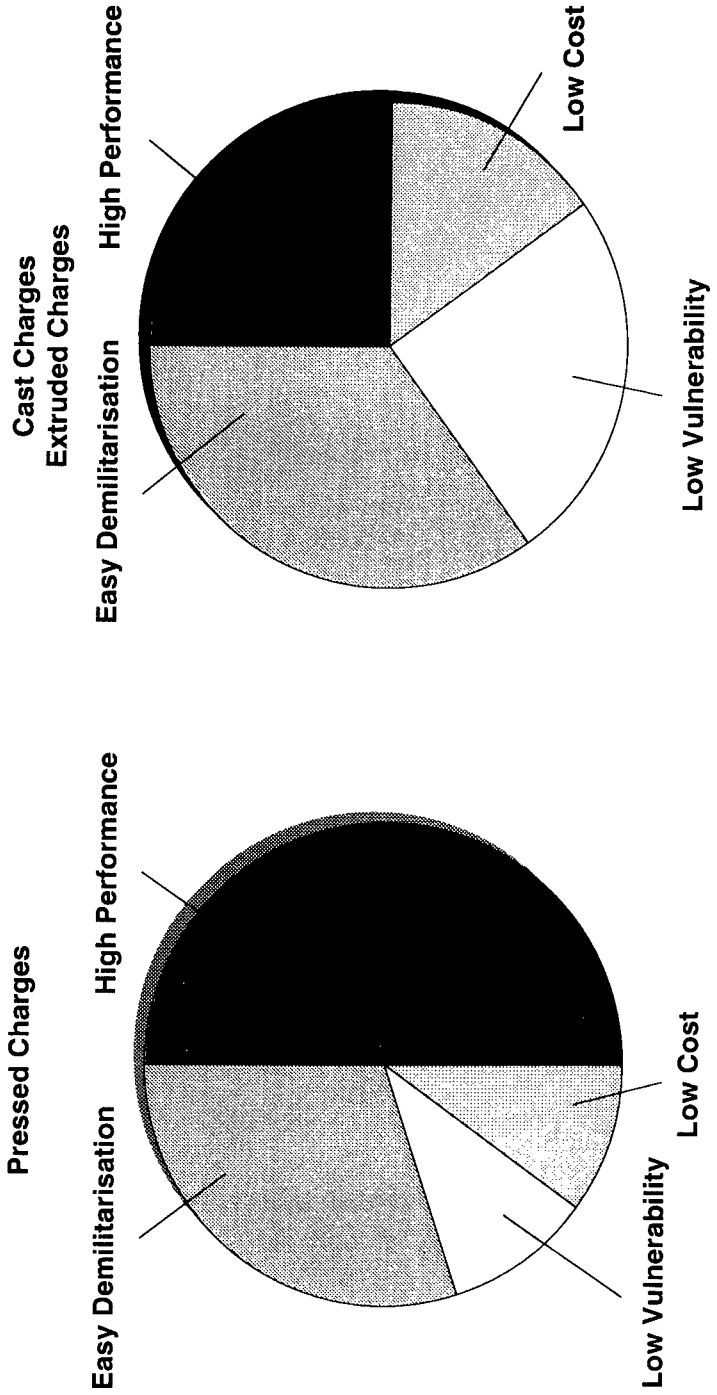
Production of PBX Charges

Process Engineering

TDW

04/96
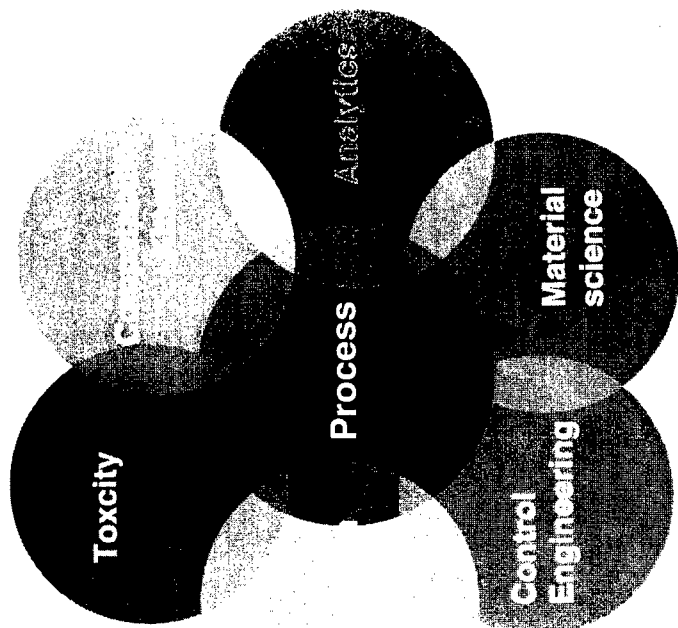
THE APPLICATION OF RHEOLOGICAL EQUIPMENT FOR IMPROVED PROCESSING OF HTPB BASED PBXES

Hordijk, A.C., Sabel, H.W.R., Schonewille, L., Meulenbrugge, J.J.

TNO-Prins Maurits Laboratory, Pyrotechnics and Energetic Materials
P.O. Box 45, 2280 AA Rijswijk
The Netherlands

Rheological equipment such as a Rotaviscometer and a Rheometer (Haake RT 10) was used to monitor the cure of HTPB binders. The effect of some catalysts (type and level), of precure with various amounts of isocyanates and of chain extenders on the cure behavoir were determined. Conclusions are drawn about pot life and cure rate.

This knowledge was applied to the casting of some unusual types of PBXes. For a specific study a number of monomodal and bimodal HTPB based PBXes with a 65 % solid loading had to be made. For such a loading the larger particle sizes tend to settle, which can be prevented by the formation of a more viscous binder at the moment of casting.

The first approach is by the use of a catalyst and prolonged mixing times (method 1). A combination of catalyst level, mixing temperature and time was selected using rheological data.

The second method is based on the precure of the binder. An optimum combination of precure NCO/OH ratio (from 0.1 to 0.5), precure temperature and time was determined by rheological monitoring.

A third method is by introducing more fines.

It appeared that the use of a binder with some pseudoplastic behavior as obtained by precure (method 2) prevents settling more effectivily than applying method 1.

The mechanical properties of the resulting castings were determined and will be presented

1. INTRODUCTION

This paper deals with HTPB binders, unfilled and filled with RDX. The final goal is to investigate the influence of the RDX mean particle size in an HTPB based PBX on the shock sensitivity [1, 2]. The rheological measurements reported here were necessary to investigate the conditions leading to an improvement of the PBX processing. The following mean diameters were used: 5, 47, 230 and 525 micron as determined by a Malvern particle sizer and coded F1, F2, C1 and C2 respectivily. For F2 a solid loading of 65 w% was obtained; to avoid variations in the shock sensitivity caused by differences in the solid load, a 65 w% solid loading was also used for the other monomodal PBXes.

The particle size C1 showed some but acceptable settling, so special measures had to be taken to obtain a homogeneous product. Later on also bimodal mixtures were made with F1C1 and F1C2 in two different ratios with 65 % solid loading. Because of the improved packing of bimodal mixtures, settling is bound to occur.

To prevent settling three ways are available:

1. increase of the percentage of fine RDX
2. increase of the end-of-mix viscosity by catalysis and prolonged mixing time
3. and increase of the viscosity by precure of the binder system

Whether settling occurs may be checked

- by using optical microscopy; surfaces are checked with respect to the relative presence of coarse particles - if there are more coarse particles at the bottom than at the top layer, settling has occurred
- by determination of the density over the length of a cast item - settling results in a higher density at the bottom.

Both methods were used.

The mechanical properties of the final products were determined as well.

Rheological measurements may be carried out with a relatively simple rotational device, such as the Rheology International Viscometer RI:2:M, which is well suited to measure fluid properties, such as the viscosity of binder systems and binders with a low solid filling.

For the measurement of visco-elastic properties more complicated devices such as the HAAKE RT 10 are needed. An oscillatory stress loading enables one to discriminate between viscous (fluid) and elastic (solid) behavior which is needed to study binder systems with high solid loadings and cure processes.

2.   RHEOLOGY

Unfilled HTPB behaves as a Newtonian fluid. In filling the HTPB prepolymer, pseudoplastic fluid behavior showes up; the stress to be applied is no longer proportional to the shear rate as for a Newtonian fluid [3]. A time dependent behavior (thixotropy) and in some cases a yield point (a relative large stress has to be applied before the mix will flow) are measured [4]. The extent of these effects increases with increasing solid load.

The addition of an isocyanate starts the chain extension and crosslinking of the prepolymer with a rate which depends on the type of isocyanate (in this case IPDI). In some cases a curing catalyst is used such as DBTD or a DBTD/TPB combination.

2.1   Rheologic approach.

For filled and unfilled binder systems, the following rheological aspects are normally determined:

- the flowcurve-which gives information about the behavior when the sample is subjected to a shear ramp. Because of the shear thinning effect [5] the viscosity at a shear rate of 1.25 s^{-1} ($\eta_{1.25}$) is used for comparison,
- the extent of thixotropy [4]
- oscillation time curve-which gives information about the visco-elastic properties and the cure behavior;

1. the complex viscosity (η^*), which takes into account the visco-elastic response, while the rotation flowcurve derived viscosity only incorporates the viscous part

2. the change with time of the viscous or loss modulus (G") and of the elastic or storage modulus (G')

3. the phase shift angle (δ), which is 90 ° for a pure viscous response and 0 ° for a pure elastic response. Delta is 45 ° when G'= G".
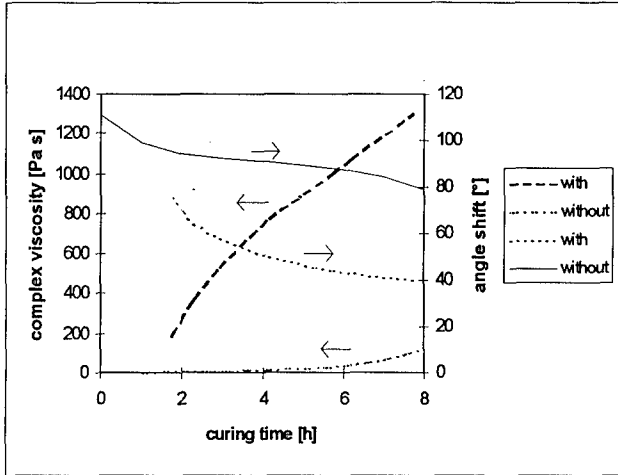
Figure 1.   Complex viscosity of a catalysed (with) and non-catalysed (without) HTPB/IPDI binder.

Figure 1 shows the result of oscillation measurements on an unfilled HTPB binder system. The cure behavior of HTPB/IPDI and the accelerated (with 0.05 % DBTD) cure of the same system at 60 °C are presented. This Figure clearly demonstrates the strong influence of the cure catalyst DBTD on complex viscosity and the phase shift angle δ. The potlife is reduced by a factor of about 5.

A typical example of an oscillation curve for a filled system is given in Figure 2. In the first stage of the curing process the viscous response increases, while the elastic response remains about the same. As a consequence δ increases from about 75 ° to about 85 °; in other words the mix behaves more as a fluid although the complex viscosity continuously increases. This is probably due to the fact that in the first cure stage chain extension is favoured over cross linking. After about 12 hours crosslinking starts and the elastic response increases very fast and the phase shift angle, δ, decreases.

The relation between the viscosity (by rotation) and the complex one (by oscillation) depends amongst others on the measuring parameters. When an oscillation frequency of 0.1 Hz and a stress of 100 Pa are applied, $\eta_{1.25} > \eta^*$ (about a factor 2). During the potlife, the time in which casting is possible, G" is about 10xG', so that η^* is determined predominantly by the viscous response. We found that for $170 < \eta^* < 200$ Pa.s the castability limit is reached.
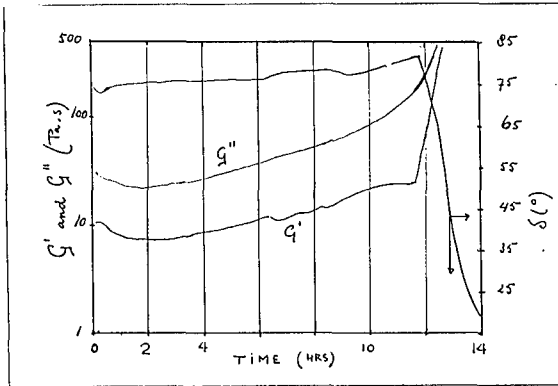
Figure 2.   A typical example of the curing of a filled system (T=20 °C, freq. = 0.1 Hz, stress = 100 Pa).

In practice this complex behavior is overcome by a larger casting mass or by casting under pressure. The cast moulds must be vibrated under vacuo to completely fill the space available and to obtain a bubble free product.

3.   THE FILLED BINDER - MONOMODAL

3.1   Binder composition and normal mixing procedure

The binder used has the composition as given in Table 1.

Table 1.   The HTPB binder composition

Compound		
HTPB	(%)	21.14
IPDI	(%)	2.64
IDP	(%)	10.45
Anti-oxidant - Flexzone 6H	(%)	0.024
Bonding agent - Dantocol DHE	(%)	0.23
Flow improver - Lecithine	(%)	0.47
Total		35.00
Density	(g/cc)	0.91
Mc (network density)	(g/crosslink)	9200
NCO/OH ratio	(-)	1.2

This is a usual composition for an HTPB binder exception for the percentage of Lecithine; this is chosen rather high. Such a high percentage will increase the end-of-mix viscosity and the thixotropic behavior. Generally settling of the larger particles is thus prevented more, but the maximum obtainable solid load decreases.

The mixing procedure is as follows. First the binder without IPDI is introduced into the mixer (5 liter with vertical mixing blades) at 60 °C and then half the amount of the solids. This composition is mixed for 10 minutes under normal pressure. Then the second half of the solids is added, mixed for 10 minutes under normal pressure and for 2 hours under vacuo.

Finally the curing agent is added and mixed for 45 minutes under vacuo after which the mix is ready for casting. The cast batches are allowed to cure for 7 days at 60 °C.

3.2 Monomodal batches (settling preventing method 1)

The tap density values for F2, C1 and C2 suggest that a solid loading of 70 % can be obtained, but a small scale mixing test showed that the F2 mix was to dry to cast, so that the choice was made for a 65 % solid loading. The F1 and F2-batch proceeded succesfully. However, the C1-batch showed some, but acceptable, settling after cure. Therefore several small scale tests with the C2-mix were performed to develop a modified procedure.

The influence of several modifications in the mixing procedure were as follows:

1) the use of 0.05 % DBTD - the effect of this catalyst was already demonstrated in Figure 1

2) the mixing temperature - at 22 and at 40 °C the cure rate was too low, even in the presence of DBTD. At 50 °C the cure rate and potlife were acceptable

3) the addition sequence of the compounds - because of the relative large potlife, the IPDI was introduced prior to the addition of the solids. The mixing proceeds until a viscosity of about 150 Pa.s is reached after which the mix is cast into the moulds.

In Figure 3 the viscosity change with time of the C2-batch is presented. From this information the optimum temperature and percentage DBTD were determined. Figure 3 showes that

- the end-of-mix viscosity without prolonged mixing is too low to prevent settling

- the viscosity tripled in about 2 hours starting from 50 Pa.s

- in the presence of 0.05 % DBTD the potlife is about 5 hours at 50 °C

- the results of the small scale mixer (IKA- RU 89-2 and 89-3) agree well with the larger scale one (HKV 5 - RU 89-4)

This modified procedure was relatively succesful; settling was not completely prevented, but only a small density change over the length of a cast item was observed.

4.   THE FILLED BINDER - BIMODAL

4.1   The use of more fines (settling preventing method 2)

Bimodal mixes of F1C1 and F2C2 in the ratio fine/coarse of 33/67 were made without isocyanate and the viscosity was measured at different solid loadings. The initial solid load was 60 w% and additions of bimodal RDX (2 to 5 % increase in solid load) were introduced, mixed after which the viscosity was measured. In Figure 4 the logarithm of the measured viscosity is given as a function of the solid loading. From this Figure it can be concluded that the solid loading for this fine/coarse ratio needs to be in between the 80 and 85 % in order to prevent settling.

It was estimated that the use of about 70 % fines in a 65 w% solid load using 0.05 % DBTD would result in time in a sufficiently high viscosity to prevent settling of the coarse particles. One small batch, also without isocyanate (RU 94-1) was made and the viscosity was measured for several solid loadings from 65 to 75 %.

The first F1C1 (70/30) batch - RU 99-1- was manufactured using the procedure modified for the C2-batch. In this case a relatively dry mix was obtained; the potlife was considerably shorter than for the C2-batch. The final batches RU 99-2 (F1C1 70/30) and RU 100-2 (F1C2 70/30) were produced with the usual processing procedure.

The cured products showed no settling.
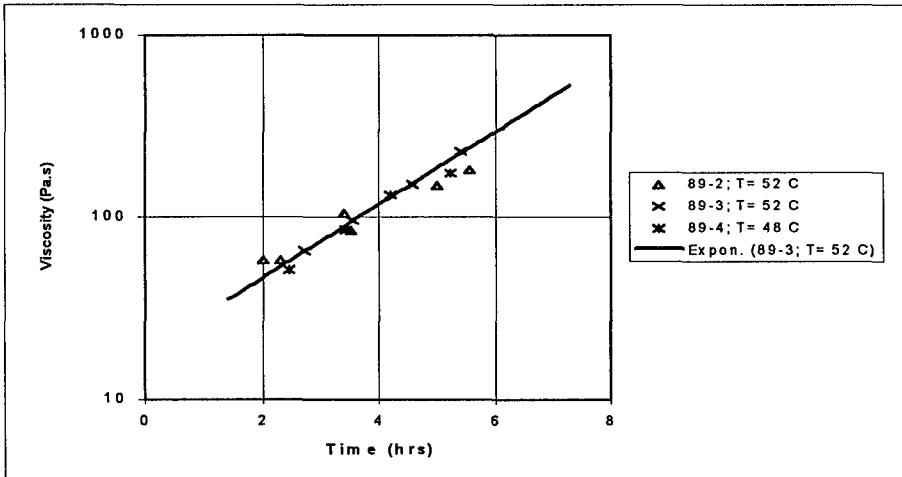
Figure 3.   Viscosity of C2-batch as function of mix-temperature and time.
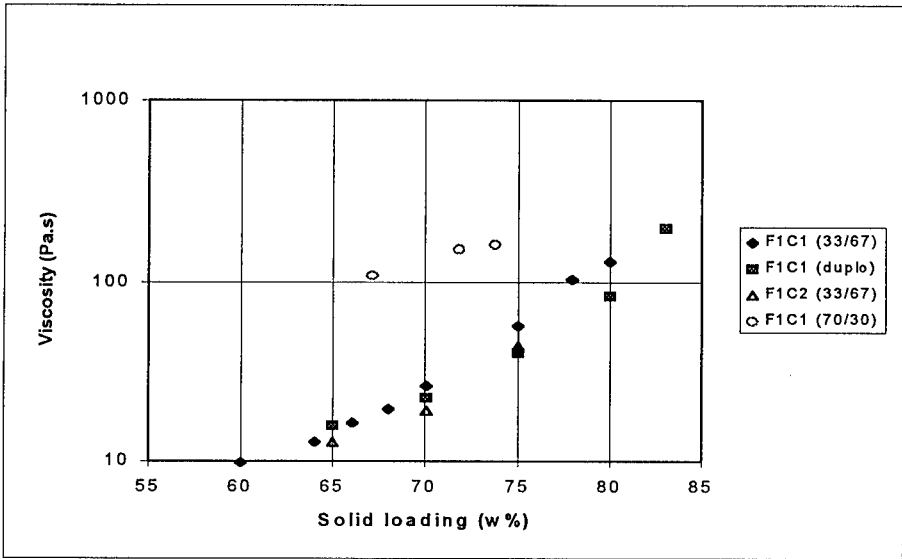
Fig. 4. Effect of change of fine concentration on viscosity.

From Figure 4 it may be concluded that

- the end-of-mix viscosity is much higher in the presence of more fines,
- the reproducibility of the processing and viscosity measurement is about 10 %
- the influence of the coarse particles (C1 and C2) on the viscosity of the 33/67 mix with F1 is only limited
- the solid load dependancy of viscosity is lower for the 70/30 than for the 33/67 fine/coarse ratio. This may be due to mixing inefficiency

The potlife is about two hours, which is in our case just sufficient for casting.

4.2 The effect of precure (settling preventing method 3)

The precure experiments with the binder were carried out at 80 °C in a flask equipped with a stirrer. IPDI was introduced in an amount corresponding with an NCO/OH ratio of 0.1 to 0.5 in steps of 0.1. The cure reaction was allowed to proceed for about 20 hours after which the viscosity was determined at 60 °C at a shear rate of 1.25 s^{-1}. In Figure 5 the measured viscosity of the precured HTPB is given as a function of the NCO/OH ratio.

A number of small scale batches were made to find out the appropriate degree of precure. For the F1C2 (33/67) mix four small scale batches with various precure NCO/OH ratios were made before the final batch could be made. In Table 3 the variations and their results are presented.
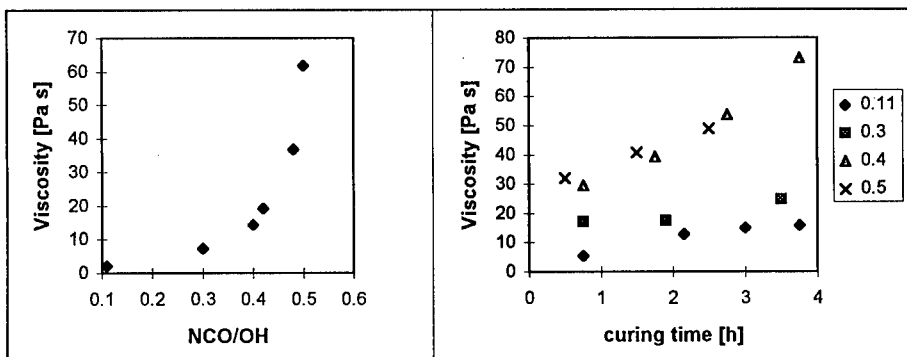
Fig. 5   Effect of NCO/OH ratio on the viscosity at 60 °C after 20 hours at 80 °C
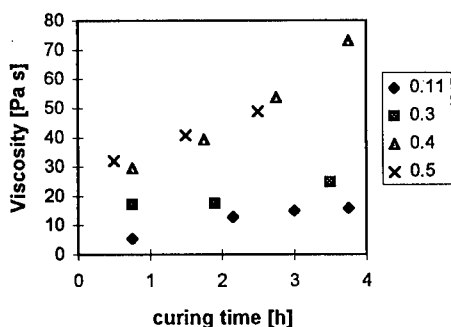
Fig. 6   Effect of time on viscosity at 60 °C of the precured PBXes (see Table 3)

Figure 5 demonstrates the strong influence of precure NCO/OH ratio on viscosity. Figure 6 clearly shows the effect of solid loading on the end-of-mix viscosity and on the viscosity change with time. The precure NCO/OH of 0.5 has been plasticised beforehand to maintain the fluidity. Probably therefore the viscosity changed somewhat different with time.

Table 3.   Various batches to determine the proper precure NCO/OH ratio for F1C2. Normal mixing procedure at a mixing temperature of 60 °C .

Batch no	RU-Code	Comment	Precure NCO/OH ratio	precured HTPB visc.	end-of-mix viscosity	remarks/settling
1		solid load 80.5 %	0	–	130	castable
2		84 %	0	–	205	still castable
3	95-1	65 %	0.11	2.2	5	settling
4	96-1		0.30	7.3	17	settling
5	97-1		0.40	20	40	to a slight degree
6	101-1		0.50	60	88	no settling
	101-2	final batch	0.50	–	90	no settling

Batch no 1, the results of which are in part presented in Figure 4, indicated that settling was inevitable in case the solid loading is reduced to 65 %. For the precured HTPB was observed that the increase in viscosity as a result of the introduction of 65 % solids is much smaller than expected; even at a precure NCO/OH ratio of 0.4 settling occurred. Only the precured HTPB (NCO/OH=0.5),

which was so sticky that a part of the plasticiser (IDP) had to be added beforehand in to the precure mix in order to guarantee the fluidity, resulted in no settling.

The cured products of F1C1 and F1C2 at the fine/coarse ratio of 33/67 showed no settling.

In Figure 7 the viscosity change with time of the monomodal batch C2 (RU 89-4) is compared with the bimodal batches in which C2 is added to F1; RU 101 (F1C2 (33/67)) and RU 100-2 (F1C2 (70/30)).
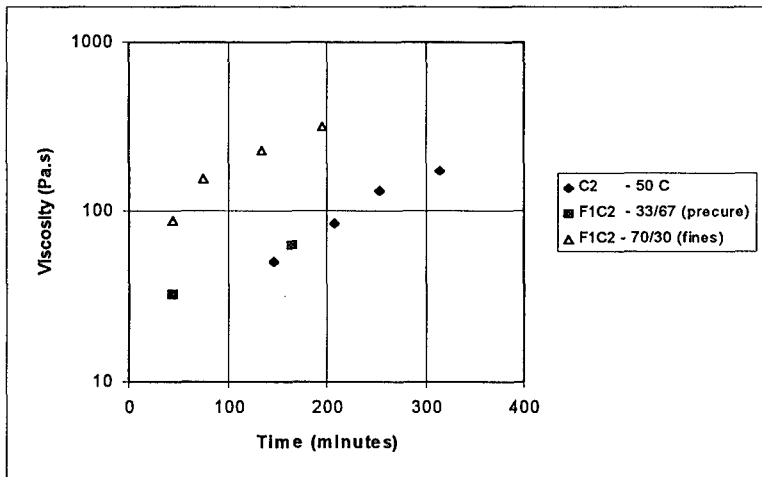
Fig 7.   The comparison of the viscosity change with time of the batches which contain C2. For C2 - batch at 50 °C and the other two at 60 °C

The conclusion is drawn that

• settling is prevented at different viscosity values
• the rate of viscosity change is about the same for the three batches

5.   MECHANICAL PROPERTIES

The mechanical properties of the various batches were determined using a tensile tester with JANNAF tensile samples. The samples were tested 3 days after the end of cure, so 10 days after casting, with a rate of 50 mm/min at 20 °C. The results are presented in Table 4.

Table 4   Mechanical properties of monomodal and bimodal PBXes (solid load is 65 w%).
            The properties of a standard PBX, 85 % solid load are included for comparison.

RU code	code	Particle size	E (MPa)	σ_m (MPa)	ε_m (%)	ε_b (%)
87-1	F1	4.7	3.9	0.71	57	65
84-1	F2	47	4.1	0.43	35	56
85-1	C1	230	5	0.24	16	40
89-4	C2	525	6	0.27	12	20
		fine/coarse				
99-2	F1C1	70/30	3.0	0.63	93	100
109-1	F1C1	33/67	5.2	0.54	23	44
100-2	F1C2	70/30	2.9	0.54	79	98
101-2	F1C2	33/67	3.9	0.42	23	42
		solid load				
ref. 81-5	standard	85 %	8.2	0.68	16.1	22

From the results in this Table it can be concluded that the mechanical properties are greatly influenced by the particle size; the larger the mean diameter the smaller the strength and strain up to about 200 to 300 micron at which this effect levels off.

The introduction of C1 to F1 to a 30 % level, as for the bimodal F1C1, increases the strain with only a limited loss in strength. Even at 67 % C1 in the F1C1 combination the mechanical properties, strength and strain, are much better than for the monomodal C1 batch.

The effect of solid loading is an increase in stiffness (E-modulus) and a considerable decrease in strain at about the same value for the strength.

CONCLUSIONS

The following conclusions may be drawn.

- Rheological equipment is absolutely needed to study the effect of changes in processing and compositions on castability and potlife

- More complicated instruments enabling oscillatory measurements give more insight in the cure processes and indicate whether results obtained with rotational measurements are valid and to what extent. The complex viscosity, which takes visco-elasticity into account may be very different from the viscosity incorporating only the viscous part

- The effect of fines on the viscosity is, that the initial viscosity (end-of-mix) increases and that the viscosity increase with time is larger as well, resulting in a decreased potlife

- The three ways to prevent settling in a low solid load system worked well. The best results were obtained using 'more fines' and 'by precure'. The method using a catalyst and mixing until the viscosity is large enough to prevent settling, needed a higher end-of-mix viscosity than the chosen 150 Pa.s for these very coarse particles.

- Mechanical properties of monomodal PBXes are strongly influenced by the particle size; the smallest sizes give the highest strength and strain.

- Mechanical properties of bimodal PBXes of 5 micron RDX combined with coarse or very coarse particles in the ratios 70/30 and 33/67 (fine/coarse) are in all cases better than the PBXes containing monomodal coarse /very coarse particles.

LITERATURE.

[1]	Ham, N. van	Less sensitive explosives
	Steen, A.C. v/d	AGARD conference proceedings 551,
	Meulenbrugge, J.J.	Oct 1991
[2]	Steen, A. van der	Crystal quality and shock sensitivity of RDX based PBXes
	et al	Paper no 168, 10 th Symposium (International) on Detonation, 1993
[3]	Schramm, G.	A practical approach to Rheology and Rheometry
		Gebr. HAAKE GmbH, 1994.
[4]	Muthiah, R.M.	Rheology of HTPB propellant.
	Krishnamurthy, V.N.	I. Effect of solid loading, oxidiser particle size and aluminum content
	Gupta, B.R.	J. of Applied Polymer Science, Vol 44, 2043-2052 (1992)
[5]	Miller, R.R.	Rheology of solid propellant dispersions
	Lee, E.	J. Rheology 35 (5), July 1991

NEUERES INDUSTRIELLES VERFAHREN ZUR HERSTELLUNG VON HOCHLEISTUNGSHOHLLADUNGEN

Dr. Jürg Meister, Rudolf Kaeser

SM Schweizerische Munitionsunternehmung
GE Hohlladungssysteme und Antriebe
Allmenstrasse 74
CH-3602   Thun

Zusammenfassung

Die Leistungsanforderungen an moderne Hohlladungen wachsen ständig. Mit leichteren oder bestenfalls gleich schweren Gefechtskopfmassen müssen immer schwierigere Zielkonfigurationen durchschlagen werden können. Dies setzt in der Regel voraus, dass eine Ladung auch bei sehr grossen Sprengabständen noch eine grosse Bohrleisung zu erbringen vermag. Diesbezüglich sind hohe Zielsetzungen möglich, wenn bei einer konstruktiv optimalen Auslegung der Ladung auch das zur Verfügung stehende Herstellverfahren so weit verbessert ist, dass die bekannten Mängel der zur Zeit industriell üblichen Giess- und Pressverfahren nicht mehr auftreten. Im Lichte dieser Erkenntnis hat die SM Schweizerische Munitionsunternehmung ein Sprengstoffpressverfahren auf isostatischer Basis und eine Zusammenbaumethode durch Schrumpfen zur industriellen Reife entwickelt. Das Verfahren ergibt eine maximal mögliche Rotationssymmetrie der Hohlladung, insbesondere verhindert es prinzipiell Zwischenräume (Spalte, Risse) im Sprengstoffbereich innerhalb des üblicherweise geforderten Temperaturbereichs.
Auf Grund der Erfahrung von zwei Seriefabrikationen sind folgende Aussagen zulässig:
- Grosse Bohrleistungen auch bei 20 Kaliber Sprengabstand. In allen vergleichenden Sprengungen besser als die gegossene oder konventionell gepresste Version
- Stark reduzierte Leistungsstreuung
- Leistungsinvarianz in einem weiten Temperaturbereich (zB von - 35 bis + 63 Grad C)
- Hohe Fabrikationssicherheit
- Herstellverfahren wirtschaftlich realisierbar

Abstract

The requirements of performance for modern shaped charges increase permanently. Often more demanding target configurations have to be penetrated with an unchanged or even reduced warhead mass. Generally this

requires that the charge has an excellent penetration at very large stand off. Relevant to this, high performance can be achieved, when in addition to an optimum design of the charge also the production procedure is improved, so that the known deficiencies of the actual industrial casting and pressing methods are eliminated. In the light of this finding, SM Swiss Munition Enterprise has brought to industrial maturity a pressing method for high explosives on the basis of an isostatic principle and an assembly procedure by shrinking. Resulting from this process of pressing and assembling, highest possible axisymmetry of the shaped charges is obtained, particularly any types of gaps and cracks are avoided by principle within the usually required temperatur range. Based on the experience of two series productions, the following statements can be made:

- Large penetrations even at 20 CD stand off. In all competing tests better than the cast or axially pressed version
- Significantly reduced deviations of penetration
- Performance invariancy in the range of - 35 to + 63 degrees C
- Increased production safety
- Industrial production can be economically realized

1. Ausgangslage

Die zZ gängigsten Verfahren der Sprengstoffverarbeitung im Hinblick auf die Fertigung von Hohlladungen sind das Giessen und das axiale Pressen. Beide Verfahren weisen nebst ihren spezifischen Vorteilen auch bedeutende Nachteile auf, die man nicht mehr alle in Kauf nehmen kann, da die Leistungsanforderungen an geformte Ladungen in den letzten Jahren enorm gestiegen sind.

Einer der gewichtigsten Schwachpunkte einer gegossenen Hohlladung ist etwa deren ungenügende Leistung bei tiefen Temperaturen, insbesondere nach Temperaturpendelungen gemäss MIL-Standard Programm.

Gepresste Ladungen anderseits weisen oft eine ungenügende Homogenität und Masshaltigkeit auf, was dann immer wieder zu unerwartet starken Leistungseinbussen führt. Erfahrungsgemäss besteht zudem beim Pressprozess ein nicht vernachlässigbares Fabrikationsrisiko für Ereignisse mit sehr hohen Kostenfolgen.

Grundlegende Verbesserungen der beiden Verfahren (axiales Pressen und Giessen) in Bezug auf Bohrleistung und deren Streuung sind nur noch schwer realisierbar. Diese Erkenntnis gründet auf jahrzehntelanger Erfahrung der SM Schweizerische Munitionsunternehmung, die beide Verfahren aus mehreren Serie-fertigungen kennt.

Ein grösseres Ereignis in Thun anlässlich eines Pressvorganges vor mehr als 10 Jahren verstärkte den Wunsch nach einem alternativen Verfahren. Dieses sollte sicherer sein, die durchschnittliche Bohrleistung der Hohlladungen anheben und die Streuung reduzieren.

2. Neuheit des Verfahrens

Bei der neuen Methode der Sprengstoffverarbeitung im Rahmen der Hohlladungsfabrikation handelt es sich um ein Pressverfahren auf isostatischer Basis. Dieses Pressprinzip wird in vielen Industriezweigen, wo granulat- oder pulverförmige Substanzen zu festen Körpern verarbeitet werden (Kunststoffverarbeitung, Pulvermetallurgie), schon lange angewendet. In der Munitionsindustrie ist das isostatische Spreng- stoffverpressen ebenfalls seit längerer Zeit bekannt, hat jedoch die Laborstufe nie überschritten.
Die Neuheit der nachstehend beschriebenen isostatischen Pressmethode besteht in deren Industrialisierung, dh der Entwicklung eines Laborverfahrens zu einer wirtschaftlichen Seriefabrikation.

Ein perfekter Sprengkörper in einer Hohlladung garantiert allerdings noch keine gute Bohrleistung. U.a. ist auch dessen Einbau in die übrige, meist metallische, Struktur von grosser Bedeutung. Gefechtsköpfe müssen bekanntlich in einem sehr grossen Temperaturbereich, beispielsweise von - 35 bis + 63 Grad C, sämtliche Anforderungen, insbesondere die leistungsbezogenen, erfüllen. In diesem ganzen Temperaturbereich dürfen weder Risse im Sprengkörper noch Spalten zu den anliegenden Strukturteilen entstehen, da diese die Strahlbildung empfindlich zu stören vermögen. Eine Schrumpfmontage bei tiefer Temperatur verhindert das Auftreten solcher Zwischenräume.

Die industrielle Verfahrensneuheit umfasst also ein verbessertes Pressverfahren und eine neue Einbaumethode zum Zusammenbau von geformten Ladungen.

3. Pressprinzip

Das auf isostatischer Basis funktionierende Prinzip ist aus den bekannten Nachteilen des konventionellen Pressens hervorgegangen. Die gewonnenen Vorzüge lassen sich deshalb am einfachsten durch eine vergleichende Beschreibung beider Verfahren darlegen.

Klassisches (axiales) Pressprinzip:

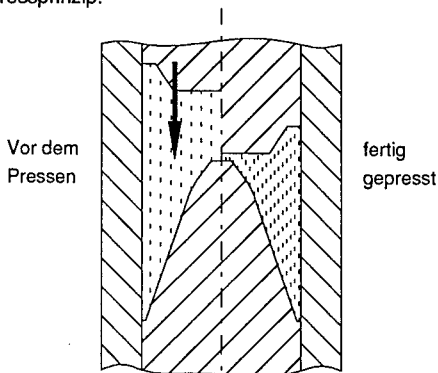Vor dem Pressen   fertig gepresst

Fig.1

Zwei Stempel im Inneren eines Zylinders komprimieren das eingefüllte Sprengstoffgranulat längs eines axialen Kompressionsweges auf ca. das halbe Volumen. Die aktive Kraft wird von einem oder beiden Stempeln aufgebracht. An den übrigen Berührungsflächen wirken Reaktions- und Wandreibungskräfte von jeweils unterschiedlicher Grösse. Bei nicht idealem Fliessverhalten des zu pressenden Materials, was in der Regel auf Sprengstoffgranulat zutrifft, entsteht im Pressling eine wenig homogene Dichteverteilung. An einigen neuralgischen Stellen wird das Material überverdichtet (Region zwischen den Stempeln in Achsnähe mit hoher relativer Kompression), an andern unterverdichtet (periphere Randzonen mit geringer relativer Kompression). Es besteht zudem kein Zwang zur Rotationssymmetrie, dh die Dichte kann mit dem Azimut variieren.

Eine weiteres Negativum ist das nicht zu vernachlässigende Sicherheitsrisiko, da der Sprengstoff grundsätzlich zwischen zwei sich gegeneinander bewegenden metallischen Bauteilen eingeschlossen ist. Entsprechende Ereignisstatistiken belegen dies.

Die nachteiligen Eigenschaften des klassischen Prinzips lassen sich im wesentlichen auf einen Umstand zurückführen: die erforderliche Volumenreduktion erfolgt mittels einer kleinen, geometrisch starren Fläche längs eines grossen Kompressionsweges. Ideal wäre dabei gerade das Umgekehrte: grosse Fläche, kurzer Kompressionsweg. Dies führt zur Idee des neuen Pressprinzips.

Prinzip des "Isopressens"

Das vollständige Presswerkzeug (Fig. 2) besteht aus einer metallischen Innenform, deren obere Kontur derjenigen der Einlage der Hohlladung entspricht, sowie einer elastischen Aussenhülle, die zB aus Gummi besteht. Das Granulat wird in die auf die Innenform aufgesetzte Hülle eingefüllt, anschliessend in einer besonderen Kammer auf Vorvakuum evakuiert . Das luft- und wasserdicht abgeschlossene System wird darauf in einen vorzugsweise mit Wasser gefüllten Autoklaven gelegt und einem zeitlichen Druckprogramm unterworfen. Die Verdichtung des Granulats geschieht über die Hülle von aussen nach innen, sowie durch eine axiale Gegenbewegung (der obere Teil des Granulats bewegt sich nach unten, der untere, durch die Hülle zwar etwas gebremst, nach oben).

Diese Pressmethode hat folgende charakteristische Merkmale:

– Die Pressbewegung ist 3-dimensional und es bewegt sich wie gewünscht eine grosse Fläche längs jeweils kurzer Kompressionswege
– Innenseitig wirken lediglich Reaktionskräfte der Innenform auf den Sprengstoff. Es ist daher streng genommen ein quasiisostatischer Pressvorgang, jedoch wegen der kurzen Kompressionswege von gleicher Pressqualität wie ein rein isostatischer
– Die Innenseite des Sprengstoffkörpers lässt sich in einfacheren Fällen bereits auf Endmass pressen. Die Aussenkontur muss immer mechanisch bearbeitet werden

**Situation vor
Evakuieren und
Pressen**

**Situation nach
dem Pressen**

Autoklav

Einfüll- und
Evakuierungs-
stutzen

Wasser
max.5000 bar

Granulat

Hüllenklemmung
(luft- und
 wasserdicht)

Sprengkörper
(Rohling)

Endform

Elastische
Hülle
(Gummi)

Innenform
(metallisch)

Hüllenklemmung
(luft- und
 wasserdicht
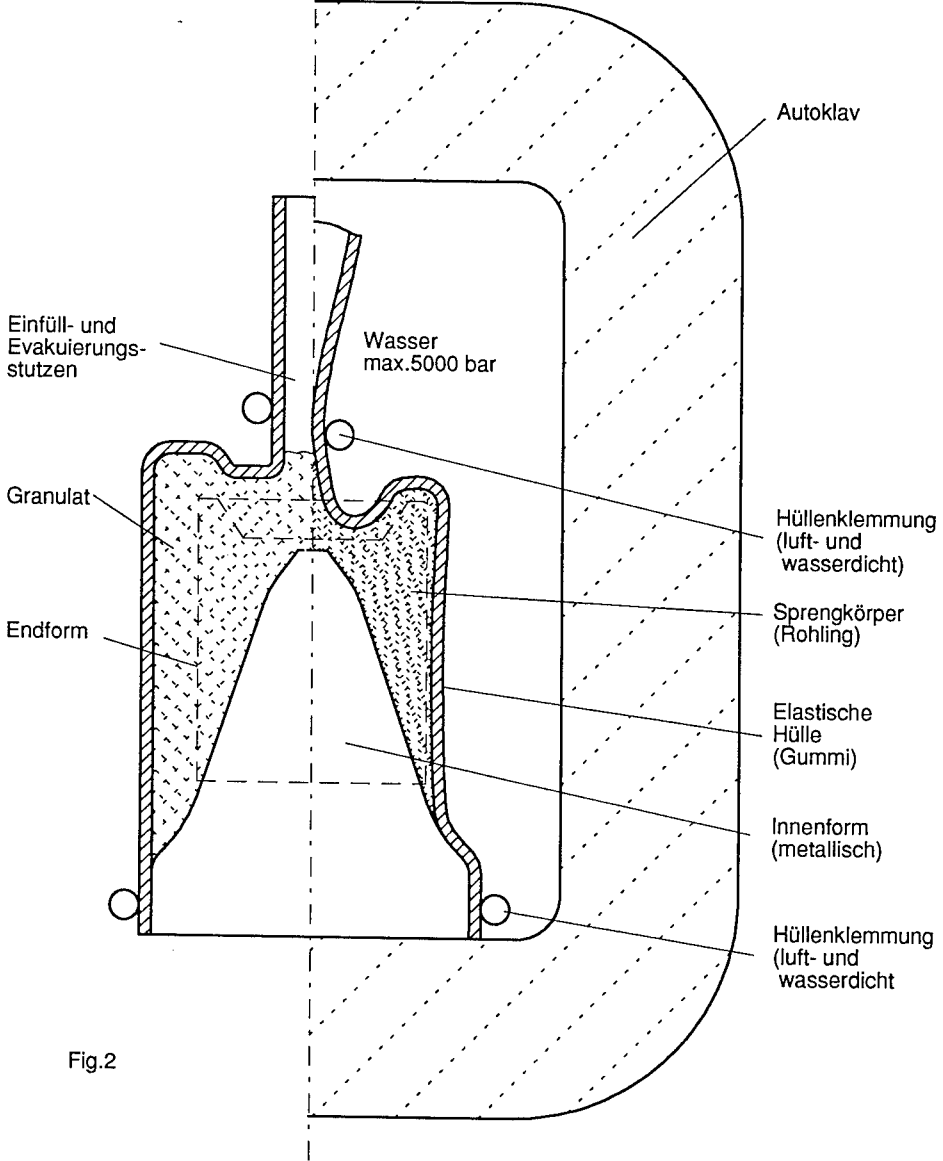
Fig.2

4. Sprengstoffarten

Bis zum heutigen Zeitpunkt haben wir folgende Sprengstoffgranulate mit Erfolg verpresst:

HMX: Octastit 4, Octastit 8, LX 14, PBXN 5
RDX: graphitiert und ungraphitiert
TNT
Insensitiver Sprengstoff: PBXN 9 (noch in Versuchsphase)

5. Presstemperaturen

Die Pressmethode lässt unterschiedslos die Verarbeitung von kalt- und warmverpressbarem Granulat zu. Beispiel einer Warmpressung: LX 14, ca 110 Grad C. Die Temperaturleitzahl des Sprengstoffs und besonders des Granulats ist niedrig genug, um das Temperaturniveau während längerer Zeit aufrecht erhalten zu können. Im Falle einer Warmverpressung muss der verdichtete Sprengstoff zu dessen chemischer Verfestigung einem Abkühlverfahren unterzogen werden. Dies geschieht noch in der elastischen Form, wobei mit unterstützenden Massnahmen dafür gesorgt wird, dass der Wärmestrom nur über die Innenform abfliesst. Die Verfestigung verläuft dadurch weitgehend spannungsfrei von innen nach aussen. Riss- und Lunkerbildung sind ausgeschlossen.

6. Mechanische Bearbeitung

Fig. 3 veranschaulicht den spanabhebenden Bearbeitungsvorgang, der in der Folge etwas näher beschrieben wird.

Arbeitsvorgänge Seriefabrikaion: 1x schruppen, 1x schlichten

Bearbeitungsweise: trocken

Entfernung der Drehabfälle: Quellabsaugung, Zwischenlagerung in einem
                                        Nassabscheider

Sicherheitsmassnahmen: Betonzelle mit Ausblasefenster
                                        Schutzstufe CNC-Maschine >=IP 54
                                        Sprinkleranlage mit UV-Sensor
                                        Fernbedienung mit TV-Ueberwachung
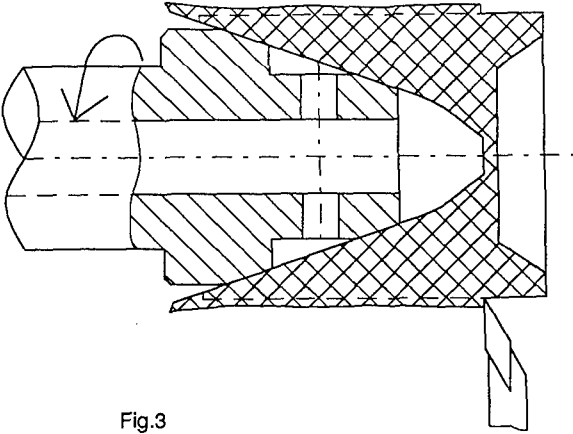
Fig.3

7. Verfahrensbedingte Vorzüge

1. Nahezu konstante und sehr hohe Dichte im ganzen Sprengstoffvolumen. Daher grösstmögliche Rotations-symmetrie gewährleistet.

2. Keine Störungen wie Risse, Lunker, "totgepresste" Zonen

3. Auch grosskalibrige Sprengstoffkörper herstellbar

4. Grosse Freiheit bezüglich Einlagegeometrie und Wandstärkeverlauf des Sprengstoffkörpers

5. Einfache und verhältnismässig billige Werkzeuge

6. Sehr rasche und kostengünstige Herstellung von Sprengstoffkörpern besonders für Entwicklungen und Versuche

7. Geringes Sicherheitsrisiko

8. Nachteile

− Eine mechanische Bearbeitung der Sprengstoffrohlinge ist unumgänglich. Der anfallende Sprengstoffabfall muss entsorgt werden. Es existiert kein kostengünstiges Recycling. Bei einer optimierten Form beträgt er etwa 25 % der eingefüllten Menge

− Die im Sicherheitsbereich erforderlichen Investitionen sind beträchtlich

9. Zusammenbau der Hohlladung

Der Zusammenbau der Hohlladung und die rechnerische Bestimmung der Sprengkörperkontur ist der zweite Teil der gesamten Verfahrensverbesserung. Er bezweckt, das Auftreten jeglicher Zwischenräume des Sprengkörpers zur Ummantelung bzw zur Einlage zu vermeiden.

Die Ursache für das Auftreten von Zwischenräumen liegt in den unterschiedlichen Wärmeausdehnungs-koeffizienten der verwendeten Materialien, zB Cu oder Molybdän für die Einlage, HMX für den Sprengkörper und Alu oder Stahl für die Ummantelung. Der Arbeitsbereich einer HL kann über 100 Grad C betragen wie dies im Extrembereich von - 53 bis +63 Grad der Fall ist (Forderung USA). Wird der Sprengkörper einfach gemäss den Zeichnungsabmessungen hergestellt und montiert, so sind Zwischenräume bei tiefen Temperaturen unvermeidlich wie Fig. 4 veranschaulicht.
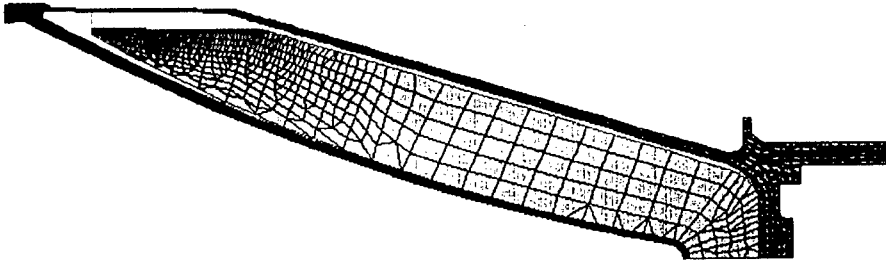
Fig. 4   FE-Auswertung in überhöhter Darstellung

Es geht also darum, eine Kontur des Sprengkörpers zu finden, die im geforderten Temperaturbereich die umgebenden Komponenten (Einlage, Ummantelung) vollständig zu berühren vermag. Für eine rationelle Seriefabrikation ist es notwendig, die kleinstmögliche Kontur zu ermitteln, damit der Einbau möglichst leicht vonstatten geht. Das Auffinden geschieht mittels einer FE-Analyse, die auch die temperaturbedingten Verformungen aller Komponenten mitberücksichtigt. In Fig. 5 ist das Resultat einer solchen Analyse für die Fertigungstemperatur von 20 Grad dargestellt. Man erkennt, dass der Sprengkörper das vorhandene Einbauvolumen übersteigt. Weil dieser von allen Komponenten den grössten Wärmeausdehnungskoeffizienten besitzt, müssen Sprengkörper und Einlage bei einer Temperatur unterhalb des geforderten Bereichs in den Mantel eingebracht werden.
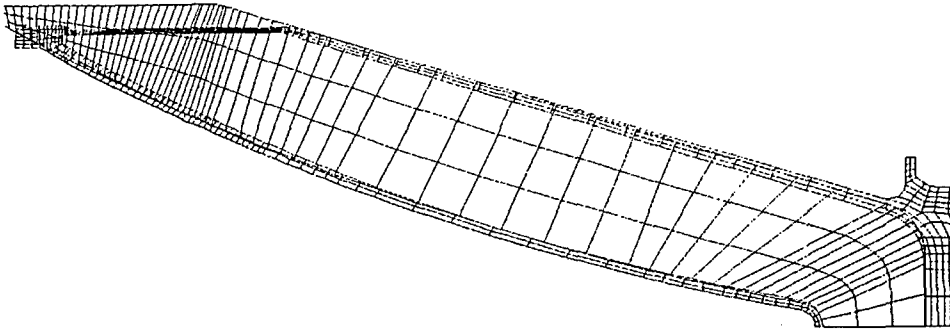
Fig. 5   Berechnete Kontur des Sprengstoffkörpers

Die Bohrleistungen einer nach dieser Methode montierten Ladung sind weitgehend temperaturunabhängig, wie experimentelle Nachweise in einer Vielzahl von Fällen zeigen.

Bemerkung:

In diesem Zusammenhang ist es angebracht, auf die grundsätzliche Problematik beim herkömmlichen Giessen hinzuweisen. Im Moment der Verfestigung, in der Regel bei + 80 Grad C, liegt noch eine allseitige Berührung vor. Der Arbeitsbereich einer Hohlladung liegt jedoch teilweise mehr als 100 Grad C tiefer. Wegen des grösseren Wärmeausdehnungskoeffizienten "fehlt" dann einfach Sprengstoffvolumen analog zu Fig.4, dh es müssen Spalte und/oder Risse entstanden sein.

10. Leistungsvergleiche

Für den Leistungsvergleich werden drei bestehende Ladungen herangezogen. Zwei davon sind gegossen (Octol 80/20), die dritte klassisch gepresst und der Sprengkörper bei Raumtemperatur eingeklebt. Vergleichsbasis ist die Stand off Kurve bei Normaltemperatur.

Vergleich mit dem Giessverfahren

Beilage 1 oben:

Es handelt sich hierbei um eine leichtgewichtige Ladung von gleichmässig ausgelegtem Wandstärkenverlauf des Sprengkörpers, eine Formgebung also, wie sie für die giesstechnische Herstellung optimal ist. Das Kaliber beträgt 120 mm. Bis zu einem Stand off von 5 Kalibern ist die Bohrleistung bei beiden Ladungen nahezu identisch. Die isogepresste Ladung erreicht das Leistungsmaximum von etwa 1000 mm bei einem Sprengpunktsabstand von 7 CD und fällt nachher nur mässig ab. Bei 20 CD liegt die Bohrleistung immer noch über 700 mm.

Die gegossene, sonst aber identische Ladung erreicht ihr Maximum bei einem etwas kürzeren Sprengpunktsabstand. Bei zunehmenden Abständen ist der Leistungsabfall viel ausgeprägter, so zB 15 % bei 10 CD oder über 50 % bei 20 CD.

Beilage 1 unten:

Der Oeffnungswinkel der Einlage dieser Ladung ist grösser, die Wandstärke des Sprengkörpers von der Basis gegen den Apex also stärker zunehmend (s. kleine Skizze auf Beilage). Der Design ist bezüglich giesstechnischer Herstellung weniger günstig. Die Ueberlegenheit der isogepressten Ladung kommt in diesem Fall noch deutlicher zum Ausdruckt, da nun auch die Maximalwerte stark differieren.

Vergleich mit dem konventionellen Pressen

Beilage 2:

Die Ladung verfügt über eine Ringzündung. Das entsprechende Bauteil weist in presstechnischer Hinsicht keine optimale Formgebung auf und verursacht möglicherweise bei den konventionell gepressten Ladungen die nach heutigen Massstäben atypische konkave Stand off Kurve.
Die isogepressten, kalt eingeschrumpften Ladungen anderseits zeigen das gewohnte Bild, nämlich nach dem Maximum zwischen 7 und 9 Kaliber Sprengpunktsabststand bleibt der Leistungsabfall begrenzt. Die Unterschiede betragen ca 30% am Ort des Maximums resp ca 70% bei 20 CD.

Relativierende Bemerkung:

Diese Unterschiede sind beträchtlich. Tatsächlich handelt es sich aber nicht um identische Ladungen. Bei den konventionell gepressten Ladungen ist graphitiertes Hexastit, bei den isogepressten Octastit 8 verwendet worden. Man darf aber annehmen, dass dies nur einen kleinen Anteil der Minderleistung ausmacht. Hätte man bei den isogepressten Ladungen gleichfalls RDX eingesetzt, so wäre lediglich das Niveau generell etwas niedriger ausgefallen, die grundsätzlich vorteilhaftere Leistungscharakteristik wäre aber geblieben.

11. Leistungen bei tiefen Temperaturen

Nachstehende Tabelle zeigt die Bohrleistung einer isogepressten, kalt schrumpfmontierten Ladung über den ganzen Temperaturbereich für einen Sprengpunktsabstand von 10 Kalibern. Sprengstoff LX 14, Kaliber Sprengstoff 146 mm, älterer Design.

-35	ca 20	+63 Grad C
1023, 1052	1110,1069	1044,1024 mm
$\bar{x}=1038$	$\bar{x}=1038$	$\bar{x}=1034$ mm

Es ist keine Abnahme der Bohrleistung beim tiefen Temperaturniveau zu beobachten.

12. Schlussbemerkung

Das Prinzip des quasiisostatischen Pressens auf Innenform ist denkbar einfach. Es liess sich aber erst wirtschaftlich in der Seriefertigung einsetzen, nachdem auf dem Markt die dafür notwendigen Betriebsmittel isostatische Presse, Drehbank und Messmaschine mit den heutzutage üblichen CNC-Steuerungen erhältlich waren.

12. Beilagen   (2)

Vergleich: Giess- mit "Isopress"-Technologie
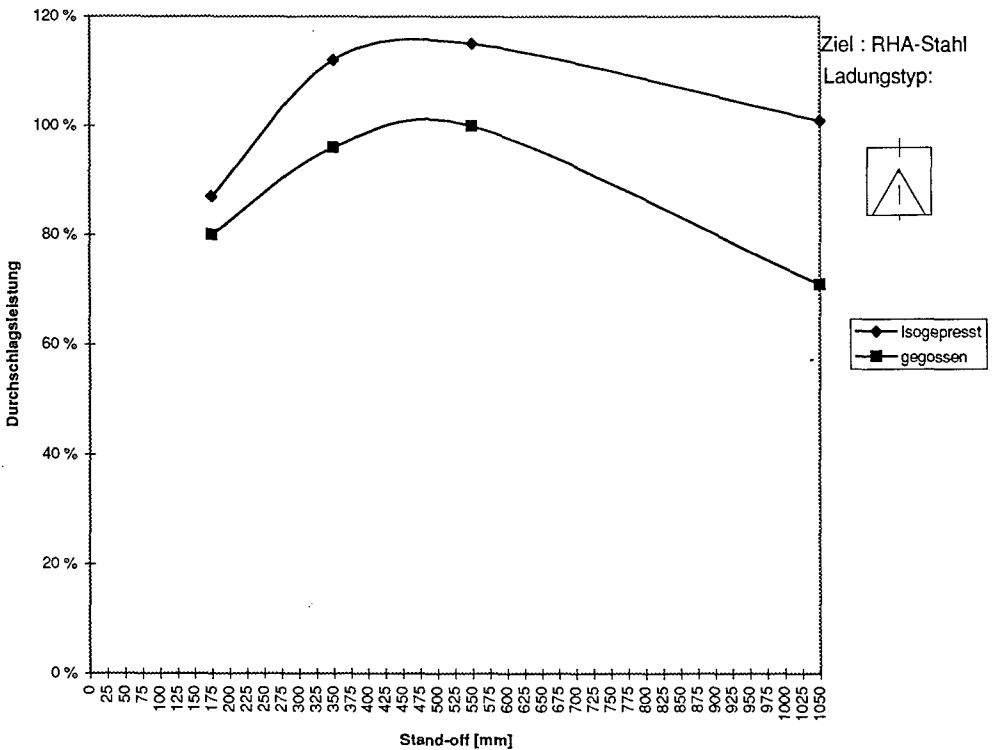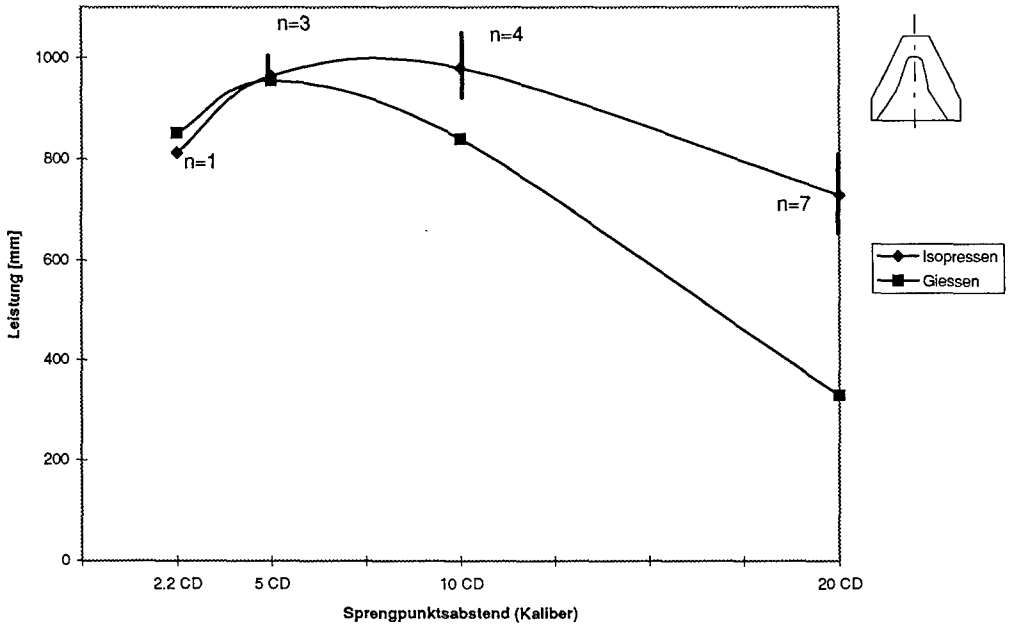
Ziel : RHA-Stahl
Ladungstyp:

Vergleich Giess- mit "Isopress"-Technologie

Ziel : RHA-Stahl

Ladungstyp:

Legend:
- Isogepresst
- konv.gepresst, Initiierung Typ 1
- konv.gepresst, Initiierung Typ 2

Y-axis: Penetration in [mm]

X-axis: Stand-off (2.2, 5, 10, 20)

CHARACTERIZATION OF MIXING PROCESSES FOR POLYMERIC ENERGETIC MATERIALS

Charles Dubois[1], Francis Thibault[2], Philippe A. Tanguy[2], Abdellatif Aït-Kadi[3]

[1]Defence Research Establishment Valcartier, PO Box 8800, Courcelette, Québec, G0A 1R0; Canada, [2]URPEI/NSERC-Paprican Chair, Department of Chemical Engineering, Ecole Polytechnique, PO Box 6079, Stn Centre-ville, Montreal, H3C 3A7, Canada; [3]Department of Chemical Engineering, Laval University, Quebec, G1K 7P4, Canada

Many modern energetic materials are composite formulations based on a polymeric binder. The processing of such materials involves different types of mixing equipment like vertical and horizontal batch mixers or twin screw extruders. Since the task of homogenizing a multicomponent mixture appears to be simple, the consequences of an inappropriate mixing cycle are often overlooked. Hence, defects like voids, sedimentation or segregated physical properties are likely to be observed. This paper describes how advanced characterization techniques can be used to optimize the selection and the operation of high-viscosity-fluid mixers. Because of the continuing development of new formulations, parameters defining the propellant processing cycle often have to be adjusted to different reaction rates and polymer properties. Given an appropriate chemorheological model, an optimized mixing cycle can be sketched if the mixer operational characteristics are known. Such a characterization was performed in a twin intermeshing conical helical mixer. From torque measurements, the power draw was determined by using Newtonian fluids in laminar flow conditions. Moreover, the existence of segregated zones was investigated with neutrally buoyant particles under different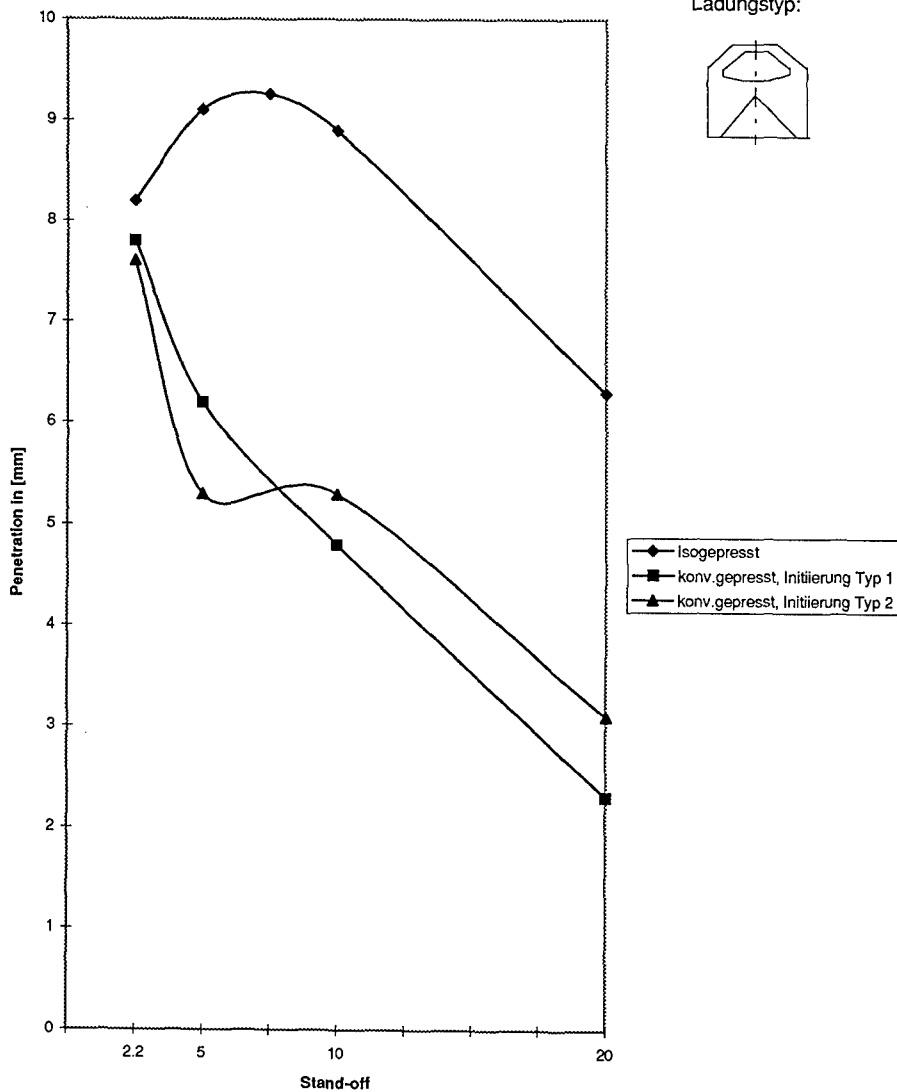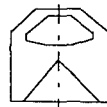 operating conditions. In addition to this experimental study, numerical simulations using the virtual finite element method were carried out. The predictions of power consumption were found to be in good agreement with experimental values and the importance of rotational speed for dispersion efficiency was also determined.

Keywords: viscous mixing, computational fluid dynamics, power consumption

Introduction

As an answer to continuously changing requirements in terms of fire-power, operational or environmental safety, the development of new energetic materials has been pursued since the end of WWII [1]. Nowadays, a considerable fraction of explosives and rocket or gun propellants are composite formulations bound by a thermoset polymeric matrix. At some stage of the formulation development, the question of processing the new material into the desired end-product has to be addressed. Since most formulations involve a fairly large number of components, the processing cycle will normally include some kind of mixing operation. The viscosity of the mixture, together with its chemical reactivity, are important factors that constrain the mixing cycle [2]. Under particular conditions, promising materials may prove to be unsuitable

for processing into a defect-free product. Accordingly, the developers must make provision for this processing characterization within their development schedule.

Over the years few improvements have been suggested to reduce the time and capital costs associated with this task. In most cases, the researchers' own experience and many series of bench-scale mixes are the common sources of information. In this paper, we would like to evaluate the ability of numerical simulation based on an advanced finite element method (FEM) for the estimation of new composite material processability. This can only be acheived if the simulation method correctly accounts for the complex flow patterns within the mixer, and also if accurate time-dependent rheological models are available. For the latter issue, more flexible models have been found but will not be reported here. We have dealt with the former issue by studying the operation of a twin intermeshing conical helical mixer formerly manufactured by Atlantic Research Corporation (USA) under the generic name of CV Helicone mixer. This unit, now sold by Design Integrated Technology Inc. (VA, USA), consists of two helical ribbons rotating inside a double conical housing. The numerical simulation results were compared to those from an experimental program carried out in order to evaluate the axial flow as well as the power consumption of a small CV unit.

Mixer Geometry
The mixer used for this study was a 4CV (bench-scale) unit with a nominal capacity of 1 US gal. This mixer was driven by a 0.75 HP motor that provided, after gear reduction, a blade speed range from 0 to 70 rpm. Two gear boxes were installed between the motor and the blades. The first one (blades side) was located just before the blades and it reduced the speed from the driving shaft to the blades by a factor of ten, while the second gear box (motor side) was variable in order to provide some speed control. The mixer helical blades rotate within a twin embedded conical assembly, as shown in Figure 1. Both blades were mounted at a small angle with respect to the vertical plane, in such a way that they converged toward the bottom of the mixer. The blades were built from two twisted ribbons joining at both ends. As also detailed in Figure 1, each ribbon spirals over one complete pitch. Torque measurements were obtained with a LEBOW on-line torque sensor, model 1804-K coupled to a LEBOW 7540 strain gage transducer with a range of 0-89 N $\cdot$ m, +/- 1% precision. The torquemeter was mounted between the two speed reducers, since

it would have been impractical to fit it directly before the blades. The speed measurement was ensured by an electromagnetic pulse counting device. Thermocouples were installed at the inner mixer surface.
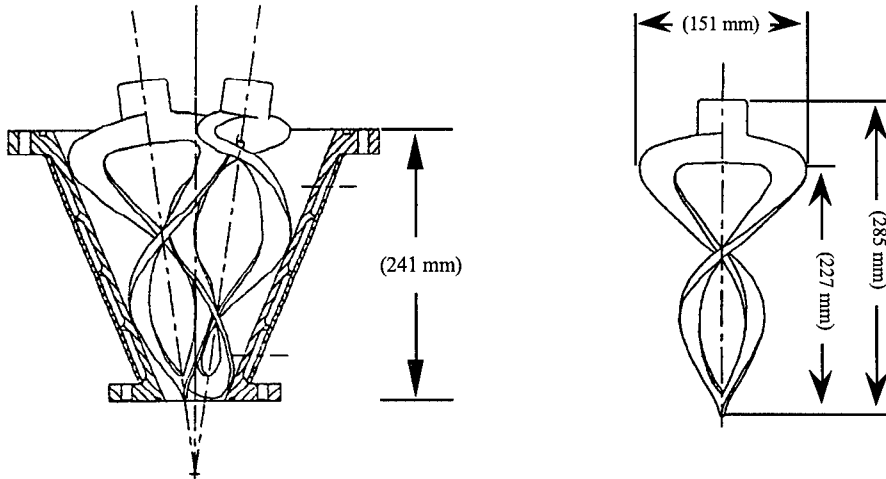
Figure 1: 4CV mixer assembly and details of a single blade

Experimental

Materials

Corn syrup and maple toffee obtained from commercial sources were used as Newtonian fluids for the power consumption studies. The experiments on axial flow were performed with two liquid polymers: a polypropylene glycol (PPG), ARCO P3025 with a nominal number-average molecular weight of 3000, was partially reacted with hexamethylene diisocyanate, Desmodur H from Bayer, and an unreacted R-45M (ARCO) hydroxy-terminated polybutadiene. Red particles made of Noryl polymer from GE Plastics acted as neutrally buoyant tracers.

Power consumption

The power consumption experiment consisted in measuring the torque on the drive as a function of blade rotational speed and fluid viscosity. The power draw was evaluated for fluid volumes of one and two liters. A total of eight isothermal experiments were conducted at temperatures

ranging from -10°C to 20°C. For each isothermal test, torque measurements were obtained by increasing the mixer speed from 10 to 60 rpm, by increments of 10 rpm, and then by returning the mixer to its initial speed with similar decreasing steps. The experiments with two liters of fluid used pure corn syrup, while one-liter tests were performed with maple toffee because of its higher viscosity.

.

Axial flow estimation

The second series of experiments were aimed at evaluating the amount of axial pumping in the 4CV mixer. Since the mixer was completely built from stainless steel, the usual visualization procedure was hardly applicable. Instead, simpler tests were carried out where neutrally buoyant particles (one to two hundred Noryl particles per test) were added to a moderately viscous fluid at the top or at the bottom of the mixer. The two fluids used had a Newtonian behavior with a viscosity around 15 Pa • s at the temperatures at which the tests were conducted. The mixer was always filled with two liters of fluid. For each experiment, the blades were activated at constant speed for a period of one to ten minutes. After each mixing sequence, the mixer was drained and two volume fractions, separated at the fluid mid-height, were collected. The number of particles within each fraction was evaluated. Rotational speeds of 20, 30 and 40 rpm were considered.

Numerical Modelling

The fluid flow generated in the conical vertical mixer is governed by the classical momentum and mass conservation principles. As there is no special symmetry that can be used to simplify the flow equations and boundary conditions, the classical Eulerian description (laboratory viewpoint) is adopted. In this viewpoint, the equations of change read as:

$$\rho\left(\frac{\partial v}{\partial t} + v\,\mathrm{grad}\,v\right) = -\,\mathrm{grad}\,p + \mathrm{div}(\mu\dot{\gamma}) \tag{1}$$

$$\mathrm{div}\,v = 0 \tag{2}$$

where

$$\dot{\gamma} = \left[grad\,v + \left(grad\,v\right)^{T} \right] \tag{3}$$

The mixer dimensions are given in Figure 1. The boundary conditions (Figure 2) are as follows:

- no-slip conditions at the vessel wall and bottom, $V = 0$
- blade velocities at each impeller i, $V_0 = \pi N_i D_i$

- no normal velocity at the free surface, $V_z = 0$

where N_i and D_i are the rotational speed and the diameter of impeller i respectively.

The above equations were resolved with a standard three-dimensional Galerkin finite element method combined with an augmented Lagrangian approach to deal with the incompressibility constraints as established by Fortin and Glowinski [3]. The weak variational form of these equations is

$$m(v,\psi) + a(v,\psi) - b(\psi,p) + c(v,\psi) = 0 \qquad \forall \psi \in \left[H_0^1(\Omega)\right]^3 \qquad (4)$$

$$b(v,\phi) = 0 \qquad \forall \phi \in L_0^2(\Omega) \qquad (5)$$

where:

$$m(v,\psi) = \int_\Omega \frac{\partial v}{\partial t}\psi d\Omega \qquad (6)$$

$$a(v,\psi) = \int_\Omega \mu\dot{\gamma}(v)\dot{\gamma}(\psi)d\Omega \qquad (7)$$

$$b(v,\phi) = \int_\Omega \phi(\mathrm{div}\,v)d\Omega \qquad (8)$$

$$c(v,\psi) = \int_\Omega \psi\,v\,\mathrm{grad}\,v\,d\Omega \qquad (9)$$

In the augmented Lagrangian method, the linear form $b(v,\phi)$, which is a constraint of the Navier-Stokes equation, is dealt with using Lagrange multipliers and a penalty method.

The discretisation of the velocity and the pressure was performed with enriched linear tetrahedral elements (Figure 3) developed by Bertrand et al [4]. This element (enriched linear velocity, discontinuous constant pressure) is particularly well-suited for irregular or curved topologies and presents all the necessary conditions of numerical stability and convergence.
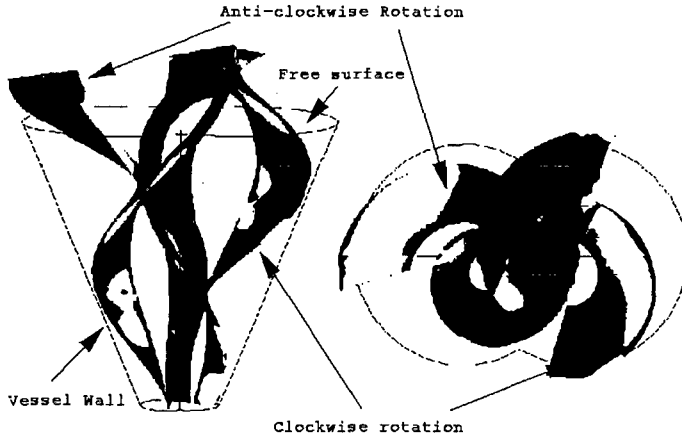
Figure 2: Mixer solid model and boundary conditions
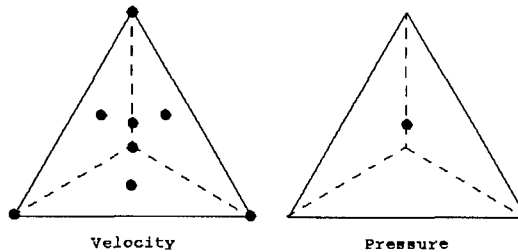
Figure 3: Tetrahedral finite elements used for velocity and pressure fields

A special approach was developed to deal with the complex kinematics of the two impellers. Indeed, due to the time evolving topology, the finite element solution cannot be obtained with a single finite element mesh and some sort of remeshing or adaptive gridding is required at each time step. Considering the number of time steps necessary to describe with reasonable accuracy the kinematics in the vertical mixer, the computational burden becomes unmanageable. To address this issue, a new method was used. This method that we developed over the last three years is particularly well-suited for multiple-impeller mixing simulations (Bertrand et al [5]). Termed as the virtual finite element method, the basic principle of this approach is to represent each impeller by a series of control points located on its surface and to regulate the rotational speed by means of velocity constraints. From a practical standpoint, the constraints are formulated directly into

the equations of change and dealt with using Lagrange multipliers and penalty techniques, as mentioned before for the incompressibility constraint [3]. One advantage of this approach is its simplicity. There is absolutely no requirement to have the velocity constraints coinciding with finite element nodes. The total number of control nodes to depict accurately the impeller is a function of the mesh. The finer the mesh, the better the description. The reader is referred to Bertrand et al [5,6] for a thorough description of the algorithms and mathematics of the method.

In terms of the actual meshing task, only the vessel needs to be meshed, which is a straightforward task. The control points are generated separately from a CAD file representing the blade surface and the knowledge of blade displacement with time. In the present work, two different meshes have been made for the 1-l and 2-l tank volumes. We used 16632 elements (102375 velocity degrees of freedom) and 15151 elements (92401 velocity degrees of freedom) for the 1-l and 2-l vessels respectively, and approximately 3835 pointwise constraints for the two impellers. A graphical representation of the surface mesh is shown in Figure 4.
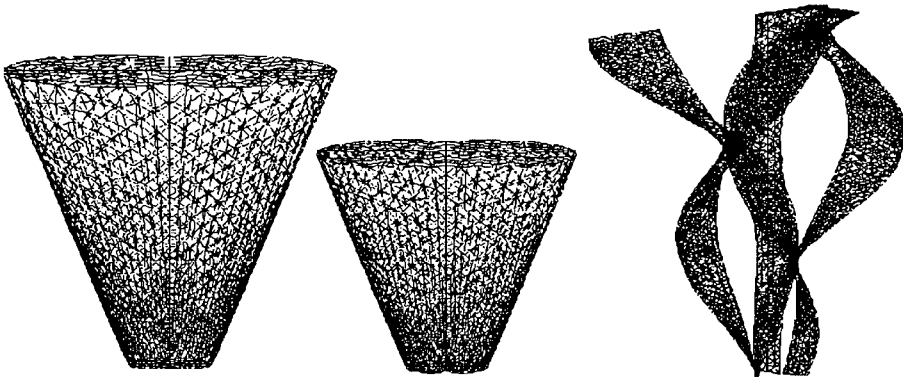
Figure 4: Finite element meshes for the two fluid volumes and the blades

Simulations

The method previously described was used to assess the power consumption of the mixer by carrying out simulations for different sets of fluid viscosity, fluid volume and mixer speed. The axial pumping was estimated in a similar fashion as in the experimental work. Knowing the velocity field in each fluid volume for different operating conditions, a first series of

computations consisted in distributing 50 massless particles in a 1-cm radius circular plan, 3 mm over the vessel bottom, and monitoring the trajectories of these particles over a period of 1 to 5 minutes. The second series of simulations used the same number of particles in a similar circular plan, 5 mm below the fluid free surface.

Results and Discussion

Analysis of power consumption

The determination of the power draw for the 4CV mixer was based on the classical dimensional analysis which states that for viscous Newtonian fluids (Metzner et al [7]):

$$N_p Re = K_p \tag{10}$$

where the dimensionless numbers are given by:

$$N_p = \frac{P}{\rho N^3 D^5} \quad (11) \quad \text{and} \quad Re = \frac{\rho N D^2}{\mu} \quad (12)$$

These relations require a proper definition of the characteristic diameter of the mixer and, accordingly, a consistent rotational speed. Because of its peculiar geometry, no such simple diameter exists for the 4CV. For the purpose of this work, we used a diameter based on the equivalent cylindrical volume displaced by the wet portion of one blade. The height of this cylinder is assume to be the actual height of fluid within the mixer. With such a choice, the rotational speed included in the correlation was simply the speed of one impeller. The symmetry of the mixer geometry justified this approach, since the total measured power was (by design) equally divided between the two helical ribbons.

The experimental procedure established to evaluate K_p consisted in changing the value of Re by varying the viscosity of the Newtonian fluid. This was easily achieved for a sugar solution like corn syrup by controlling the temperature of the fluid. For experiments with the maple toffee, its viscosity was found to be 174 Pa·s at 11°C, the temperature at which the low-volume torque measurements were conducted. The value of K_p obtained from CFD simulations was estimated by five simulations. These simulations cover a range of Re running over three decades, which is

quite similar to the experimental window. From these simulations, only one was performed with the one-liter mesh. The experimental and numerical results on the power consumption are presented in Figure 5, while details of K_p calculations are reported in Table 1 .
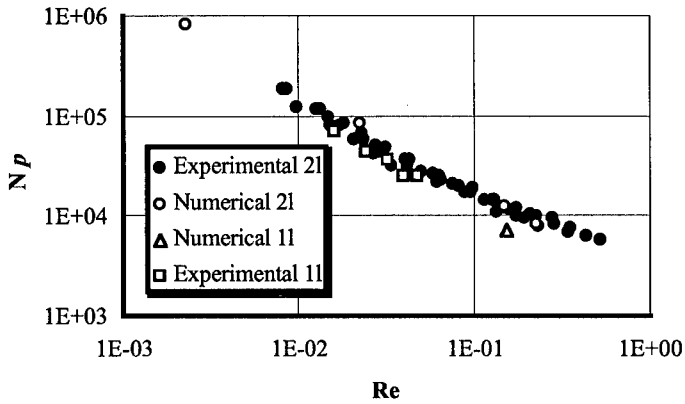
Figure 5: Experimental and calculated power consumption of the 4CV mixer

Table 1: K_p evaluation from power consumption and geometrical data

| | Volume | | | | | |
| | 1 l | | | 2 l | | |
	h (m)	D_e (m)	K_p	h (m)	D_e (m)	K_p
Experimental	0.134	0.0689	1140 ± 142	0.186	0.0827	1844 ± 131
Numerical	0.139	0.0677	1110	0.189	0.0821	1900 ± 5

An excellent agreement is found between the two sets of data. From an experimental point of view, the log-log plot of N_p against Re exhibits a good linearity with a slope of -1.04 for measurements made on the 2-l volume. A careful examination of the experimental curve shows a deviation from linearity for $Re > 0.2$, indicating the beginning of transition from the laminar regime. Unfortunately, the limitation of the torquemeter sensitivity prevented measurements at higher Re, a range that could only be reached by lowering the fluid viscosity, since the speed could

not be increased beyond the normal mixer specification. The comparison of experimental and calculated values of K_p demonstrates the superiority of the virtual FEM to quantitatively characterize a complex mixer configuration.

The most important observation related to the power consumption measurements may be that the power constants obtained at 1 l and 2 l are not directly scaleable by their volume ratio. So, on a volume-free basis, the power draw of the mixer is higher for low levels of fluid. This could be expected since the ratio of blades surface to displaced volume increases as the fluid level decreases. In order to be extended to other fluid heights, the actual K_p estimations must be correlated with this phenomenon. The key parameter to achieve this correlation turned out to be the equivalent diameter used for the calculation of N_p and Re. Hence, we found that:

$$\frac{K_p D_e}{V} = 77000 \pm 2000 \text{ m}^{-2} \tag{13}$$

Accordingly, the value of K_p for any practical volume of fluid within the 4CV mixer can be estimated from equation (13) since D_e is volume-dependent (and can be estimated from geometrical relations). Moreover, this relation should also be applicable for larger CV mixers like the 8CV or the 10CV, given that their geometrical aspect remains the same. Even if the Couette analogy used for the definition of D_e cannot fully describe the flow patterns behind this intermeshed impeller configuration (as for shear rate estimation purposes), it appears to be sufficient for power draw considerations.

The second important aspect of the presented work was to obtain a qualitative estimation of the magnitude of the axial pumping flow, as well as the dispersion capability, within the mixer. The strategy used was threefold: dipersion as a function of time at constant speed, dispersion as a function of the overall number of blade rotations, and finally dispersion as a function of volume at constant time and speed. The experiments and numerical results for the first task are summarized in Table 2. Some numerical data are missing due to difficulties with particles tracking close to the free surface. In light of the inherent incertainty associated with both of these experimental

Table 2: Particle count (%) for segregation evaluation by experimental and numerical techniques

		Initial position: top surface				Initial position: bottom			
		Top volume		Bottom volume		Top volume		Bottom volume	
Speed	time (min)	Exp.	Num.	Exp.	Num.	Exp.	Num.	Exp.	Num.
20 rpm	0	100	100	0	0	0	0	100	100
	1	82	-	18	-	0	10	100	90
	3	76	-	24	-	20	26	80	74
	5	61	-	39	-	29	30	71	70
30 rpm	0	100	100	0	0	0	0	100	100
	1	94	94.5	6	5.5	3	4	97	96
	5	82	91	18	9	16	12	84	88
	10	61	-	39	-	42	-	58	-
40 rpm	0	100	100	0	0	0	0	100	100
	1	58	-	42	-	37	12	63	88
	3	55	-	45	-	56	36	44	64
	5	36	-	64	-	49	38	51	62
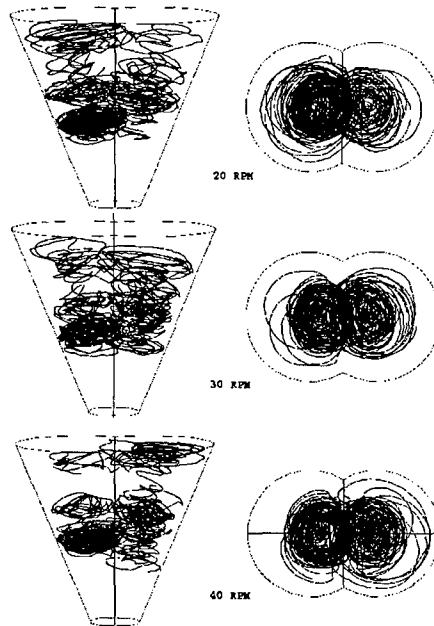
Figure 6: Dispersion for 20 blade rotations, at different speeds

and numerical procedures, the agreement between the two sources of data is rather good. An global appreciation of these results shows that the pumping action between the upper and the lower volume of the mixer is lower than expected for speeds of 20 and 30 rpm. On the other hand, at 40 rpm, the homogenization of particle concentration is acheived after one minute. The estimation of dispersion efficiency, as a number of blade rotations, is reported in Figure 6. Unexpectedly, a qualitative analysis shows the higher speed does not imply a with better particle distribution within the mixer volume. In fact, the optimal speed appears to be 30 rpm, while the 20 rpm regime offers less efficient agitation. Finally, when the effect of volume is studied, Figure 7 demonstrates that at constant speed, the smaller volume undergoes a more significant mixing process. This is consistent with the power constant results and, again, can be attributed to the larger agitation surface to volume ratio of this configuration.
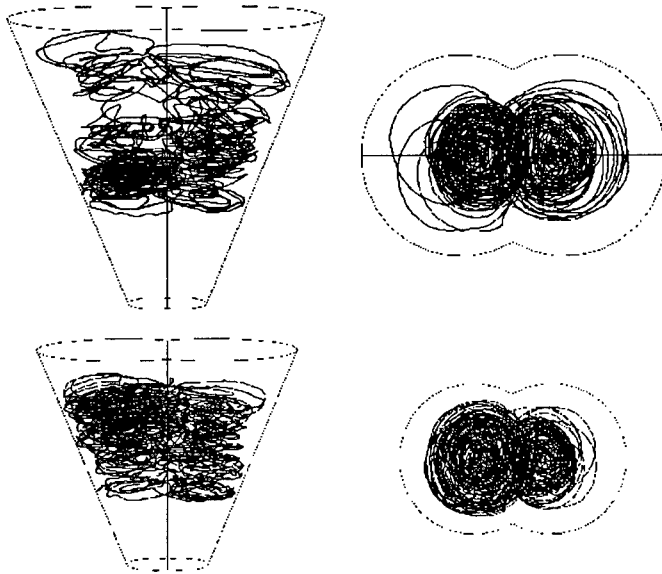
Figure 7: Effect of volume on the dispersion of massless particles at 30 rpm

Conclusion

This paper attempted to demonstrate the usefulness of experimental and numerical techniques in the design of mixing processes of highly viscous fluids. An immediate conclusion is that advanced numerical analysis was found to be a reliable tool to characterize mixing processes, even for complex configurations involving periodical movements such as those encountered with the CV family of mixers.

With respect to the specific mixer analyzed, the power draw was estimated by a dimensionless number treatment with a special adaptation for the conical geometry. This strategy allows the estimation of the mixer power constant, regardless of the volume of fluid used. The relation should hold for other CV mixers but further investigation by numerical simulations will be needed to confirm this approach. Moreover, the utility of the virtual FEM technique was also demonstrated in the evaluation of the dispersion forces within the mixer. The simulations were sensitive enough to exhibit the effect of volume, injection point and rotation speed. With this new tool and appropriate knowledge of the formulation rheology, the optimization of the processing cycle of energetic materials with minimal real-life runs is no longer out of reach.

Symbols

D_e	equivalent impeller diameter	m
K_p	power proportionality constant	-
N	impeller speed	rev/s
N_p	dimensionless power number	-
Re	Reynolds number	-
P	power	W
p	pressure	Pa
T	fluid temperature in the mixer	K
v	fluid speed	m/s
$\dot{\gamma}$	shear rate	s^{-1}
μ	viscosity	Pa·s
ρ	density	kg/m^3

References

1. Advisory Group for Aerospace Research and Development (AGARD), Environmental Aspects of Rocket and Gun Propulsion, <u>AGARD Confrence Proceedings 559</u>, 1995, NATO publication, France.

2.   Uhl, V. W. and Gray J. B., Mixing: Theory and Practice, 1967, Academic Press, New York.

3.   Fortin, M. and Glowinski, R., 1982, Méthodes de lagrangien augmenté, Dunod, Paris.

4.   Bertrand, F., Gadbois, M. and Tanguy, P. A., 1992, Tetrahedral Elements for Fluid Flow, Int. J. Num. Meth. Engineering, 33, 1251-1257.

5.   Bertrand, F., 1995, Modélisation tridimensionnelle du procédé de malaxage à mouvement planétaire de fluides visqueux rhéologiquement complexes, Ph.D. Thesis, INPL, France.

6.   Bertrand, F., Tanguy, P. A. and F. Thibault, 1996, A 3D Fictitious Domain Method for Incompressible Fluid Flow Problems in Enclosures, submitted to Int. J. Num. Meth. Fluids (28 pages).

7.   Metzner, A. B., Feehs, R. H., Ramos, H. L., Otto, R. E., Tuthill, J. D., 1961, Agitation of Viscous Newtonian and Non-Newtonian fluids, A. I. Ch. E. Journal, 7: 3 .

Herstellung von Explosivstoffpartikeln unter Anwendung überkritischer Fluide

Formation of particles of explosives with supercritical fluids

U. Teipel, P. Gerber, U. Förter-Barth, M. Niehaus, H. Krause

Fraunhofer Institut für Chemische Technologie (ICT)
Postfach 1240, D - 76318 Pfinztal, Germany

Abstract

Für Komponenten von Festtreib- und Explosivstoffen sind Partikeleigenschaften wie z.B. die Partikelgröße, die Partikelgrößenverteilung und die Partikelform von besonderer Bedeutung. Insbesondere im Hinblick auf unempfindliche Explosivstoffe ist die Herstellung fehlstellenarmer Kristalle, d.h. möglichst keine Kristallfehlstellen in Form von Lösungsmitteleinschlüssen, von großem Interesse. Möglichkeiten zur Modifikation bzw. Beeinflussung dieser Eigenschaften bieten neue Verfahren zur Herstellung von Partikeln, die die besonderen Eigenschaften hochkomprimierter bzw. überkritischer Fluide nutzen.

Beim RESS (Rapid Expansion of Supercritical Solutions) - Prozeß erfolgt die Partikelherstellung durch schnelle Expansion eines beladenen, überkritischen Fluids. Durch die Entspannung der überkritischen Lösung werden sehr hohe lokale Übersättigungen erzielt, die spontane Keimbildung und somit die Herstellung feiner Partikel mit enger Korngrößenverteilung bewirken.

Eine andere Anwendungsmöglichkeit verdichteter Gase ist ihr Einsatz als Anti-Solvent. Beim GAS (Gas Anti-Solvent) - Prozeß wird der Feststoff in einem Primärlösungsmittel gelöst, und durch Zugabe eines komprimierten Gases als Anti-Solvent erfolgt eine volumetrische Expansion der Lösung und eine Rekristallisation des Wertstoffes.

In diesem Beitrag werden die Verfahren zur Herstellung von Explosivstoffen unter Anwendung überkritischer Fluide näher erläutert und erste Ergebnisse vorgestellt.

1. Einleitung

Die Anwendung überkritischer Fluide hat in den letzten Jahren insbesondere im Bereich der Stofftrennung Einzug gefunden. Im großtechnischen Maßstab konnte sich die überkritische Extraktion zur Entcoffeinierung von Rohkaffee und die Gewinnung von Hopfenextrakten mit Kohlendioxid als Lösungsmittel etablieren.

Ein neues Anwendungsgebiet überkritischer Fluide ist die Herstellung von Mikropartikeln (Submikronbereich) mit enger Korngrößenverteilung. Hierzu stehen unterschiedliche Verfahren bzw. Verfahrensvarianten zur Verfügung.

Beim sogenannten RESS (Rapid Expansion of Supercritical Solutions) - Prozeß erfolgt in einem ersten Prozeßschritt eine überkritische Extraktion des Feststoffes und anschließend die Entspannung der beladenen, überkritischen Lösung über eine Düse. Durch den Expansionsvorgang kommt es zu einer lokalen, sehr hohen Übersättigung und zur Keimbildung im Freistrahl.

Eine weitere Anwendung von überkritischen Fluiden ist ihr Einsatz als Anti-Solvent. Beim sogenannten GAS (Gas Anti-Solvent) - Prozeß wird ein Wertstoff in einem Primärlösungsmittel gelöst, und durch Zugabe eines komprimierten Gases als Anti-Solvent erfolgt eine volumetrische Expansion des Lösungsmittels und ein Rekristallisation des Wertstoffes.

Für Festtreib- und Explosivstoffe ist die Größe, Form und Verteilung der Füllstoffpartikel, insbesondere im Hinblick auf unempfindliche Explosivstoffe, von großem Interesse.

Die oben erwähnten Verfahren bieten für die Partikelherstellung von empfindlichen Substanzen wie Explosivstoffkomponenten wesentliche Vorteile, da sich z.B. das Lösevermögen von verdichtetem Kohlendioxid sehr rapide durch Variation der Prozeßparameter verändern läßt. Nach dem Expansionsvorgang des RESS - Prozeßes hat CO_2 keine Lösungsmitteleigenschaften mehr, was besonders für die Herstellung fehlstellenarmer Explosivstoffkristalle, d.h. möglichst keine Kristallfehlstellen in Form von Lösungsmitteleinschlüssen, von Bedeutung ist.

2. Eigenschaften überkritischer Fuide

Wird ein Gas oder eine Flüssigkeit über den kritischen Druck p_C komprimiert und über die kritische Temperatur T_C erhitzt, so befindet sich das Fluid im überkritischen Zustand. Abbildung 1 zeigt schematisch das Druck - Temperatur (p,T) Diagramm von Kohlendioxid, einem in technischen Prozessen sehr häufig eingesetzten Fluid.
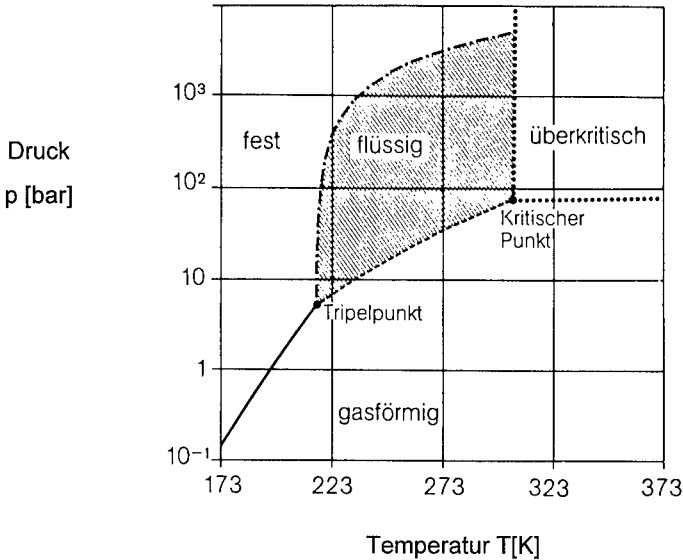
Abb. 1: Druck- Temperatur Diagramm für CO_2 /1/

Nach Überschreitung der kritischen Parameter durch Verdichtung und Temperaturerhöhung ergeben sich einige günstige Eigenschaften der Fluide. Trotz der im Vergleich zu Flüssigkeiten nur geringfügig niedrigeren Dichte überkritischer Fluide entspricht die dynamische Viskosität dem Wert von Gasen bei Normalbedingungen. Der Diffusionskoeffizient in verdichteten Gasen ist in der Nähe des kritischen Punktes um mehr als das zehnfache größer als der in Flüssigkeiten (siehe Abb.2). Hieraus resultiert ein schnelles Massentransportverhalten in überkritischen Fluiden, so daß sich überkritische Fluide sehr gut als Lösungsmittel eignen bzw einen Ersatz für die klassischen Lösungsmittel darstellen.

	ρ [kg/m^3]	η [Pas $\cdot$ 10^3]	D* [m^2/s]
Gase bei 1 bar, $\vartheta = 25\,^\circ$C	0,6 – 2,0	0,01 – 0,03	1 – 4 $\cdot$ 10^{-5}
überkritische Fluide	200 – 500	0,01 – 0,03	7 $\cdot$ 10^{-8}
Flüssigkeiten bei $\vartheta = 25\,^\circ$C	600 – 1600	0,2 – 3,0	0,2 – 2 $\cdot$ 10^{-9}

* Selbstdiffusion für Gase und verdichtete Gase, binäre Mischungen für Flüssigkeiten

Abb.2: Größenordnungsvergleich physikalischer Daten von Gasen, verdichteten Gasen und Flüssigkeiten /2/

Für die Anwendung eines überkritischen Fluids als Lösungsmittel ist es von Vorteil, wenn das Fluid niedrige kritische Parameter (Druck, Temperatur) aufweist und trotzdem über eine hinreichend hohe Löslichkeit hinsichtlich des Extraktes gegeben ist. Abbildung 3 zeigt eine Übersicht der kritischen Temperaturen und Drücke verschiedener Fluide.

Fluid	ϑ_C [$^\circ$C]	p_C [bar]
n - Pentan	196,5	33,7
n - Butan	152,0	38,0
Propan	96,8	42,5
Methan	-82,8	46,0
Ethylen	9,2	50,4
Kohlendioxid	**30,9**	**73,7**
Toluol	320,8	41,6
Methanol	239,4	80,9
Ammoniak	132,3	113,5

Abb.3: Kritische Parameter verschiedener Fluide /3/

Niedrige kritische Parameter eines Fluids sind nicht nur für die Dimensionierung der Anlage und somit für die Investitionskosten von Vorteil, sondern auch für die Anlagen- und Prozeßsicherheit. Als weitere Auswahlkriterien sollten die Toxizität, die Verfügbarkeit, die Materialkosten, die Entflammbarkeit, die Korrosivität etc. berücksichtigt werden.

Unter Berücksichtigung dieser Kriterien stellt Kohlendioxid für viele Anwendungsfälle ein geeignetes Lösungsmittel dar. Durch Zugabe eines Schleppmittels kann die Lösungskapazität von überkritischen Fluiden wesentlich gesteigert werden /4/.

Ein besonderer Vorteil von überkritischem Kohlendioxid als Lösungsmittel ist für viele technische Anwendungen, insbesondere bei der Herstellung von Partikeln mittels überkritischer Fluide, die einfache Separierbarkeit des Lösungsmittels vom Wertstoff.

3. Partikelherstellung

Bei der Herstellung feiner, möglichst engverteilter Partikeln mit Hilfe von überkritischen Fluiden sind zwei Prozeßvarianten zu unterscheiden:

- **RESS** - Prozeß (**R**apid **E**xpansion of **S**upercritical **S**olutions)

- **GAS** - Prozeß (**G**as **A**nti - **S**olvent)

3.1 Der RESS - Prozeß

Bei diesem Verfahren erfolgt in einem ersten Verfahrensschritt die überkritische Extraktion des Feststoffes und anschließend die Entspannung der beladenen, überkritischen Lösung über eine Düse. Die schnelle Expansion bewirkt eine rapide Druck- und Temperaturabsenkung, wodurch das Lösevermögen des Fluides drastisch vermindert wird. Aufgrund des Expansionsvorganges kommt es zu einer lokalen Übersättigung und zur Keimbildung im Freistrahl, so daß der gelöste Feststoff nach der

Entspannung in kristalliner Form vorliegt. Bedingt durch den Vorgang der schnellen Expansion in der Düse ist das primäre Einsatzgebiet dieses Prozeßes die Herstellung feiner engverteilter Partikel.

Ein wesentlicher Vorteil dieses Prozeßes ist es, daß keine klassischen Lösungsmittel zum Einsatz kommen und somit Kristallfehler durch Lösungsmitteleinschlüsse vermieden werden können.

Abbildung 4 zeigt die Hochdruck-Kristallisationsanlage. Diese Pilotanlage ist für einen maximalen Betriebsdruck von 300 bar und eine maximale Betriebstemperatur von 200 °C ausgelegt.

Abb. 4: Hochdruck-Kristallisationsanlage

Beim RESS - Prozeß gelangt flüssiges CO_2 aus einer Vorratsflasche in die Anlage, das im Wärmetauscher (W1) kondensiert und im Flüssigkeitsspeicher (FL) zwischengespeichert wird. Zur Vermeidung von Kavitation wird Lösemittel im Wärmetauscher (W2) unterkühlt und anschließend mit der Flüssigkeitspumpe (P) auf den Extraktionsdruck verdichtet. Im Wärmetauscher (W3) wird das Fluid auf die gewünschte Extraktionstemperatur erhitzt, so daß sich ein überkritischer Zustand einstellt. Im Extraktor (B1) wird der zu lösende Stoff extrahiert. Die beladene fluide Lösung wird mittels eines weiteren Wärmetauschers aufgeheizt und anschließend über

eine Düse in die Kolonne (B3) entspannt, wo der zuvor gelöste Feststoff auskristalli-siert und dann in der Form von Feststoffpartikeln vorliegt. Die erzeugten Partikel verbleiben in der Kolonne, während das CO_2 gasförmig zurück in den Kreislauf ge-langt.

In Abbildung 5 ist der schematische Aufbau dieser Versuchsanlage dargestellt.
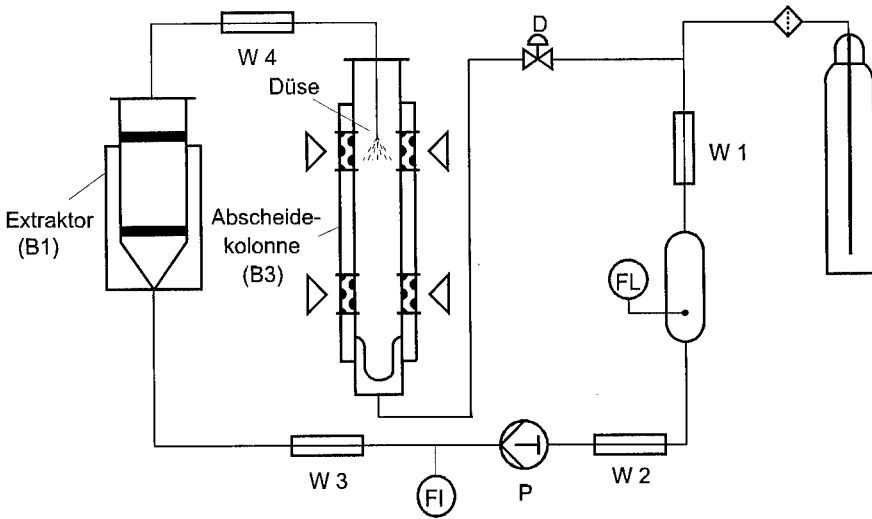
(W 1-4)	Wärmeübertrager	(FI)	Massenstrombestimmung
(FL)	Flüssigkeitsspeicher	(D)	Druckregelung
(P)	Hochdruckpumpe		

Abb. 5: Schematischer Versuchsaufbau des RESS-Prozeßes

Abbildung 6 zeigt den Verlauf des idealen RESS - Prozeßes für unbeladenes Koh-lendioxid in einem Druck - Enthalpie (p - h) Diagramm. Bei dem realen Prozeß müs-sen jedoch Reibungs- und Druckverluste, sowie Verluste durch Wärmestrahlung be-rücksichtigt werden.

Druck
p [bar]

Enthalpie h [kJ/kg]
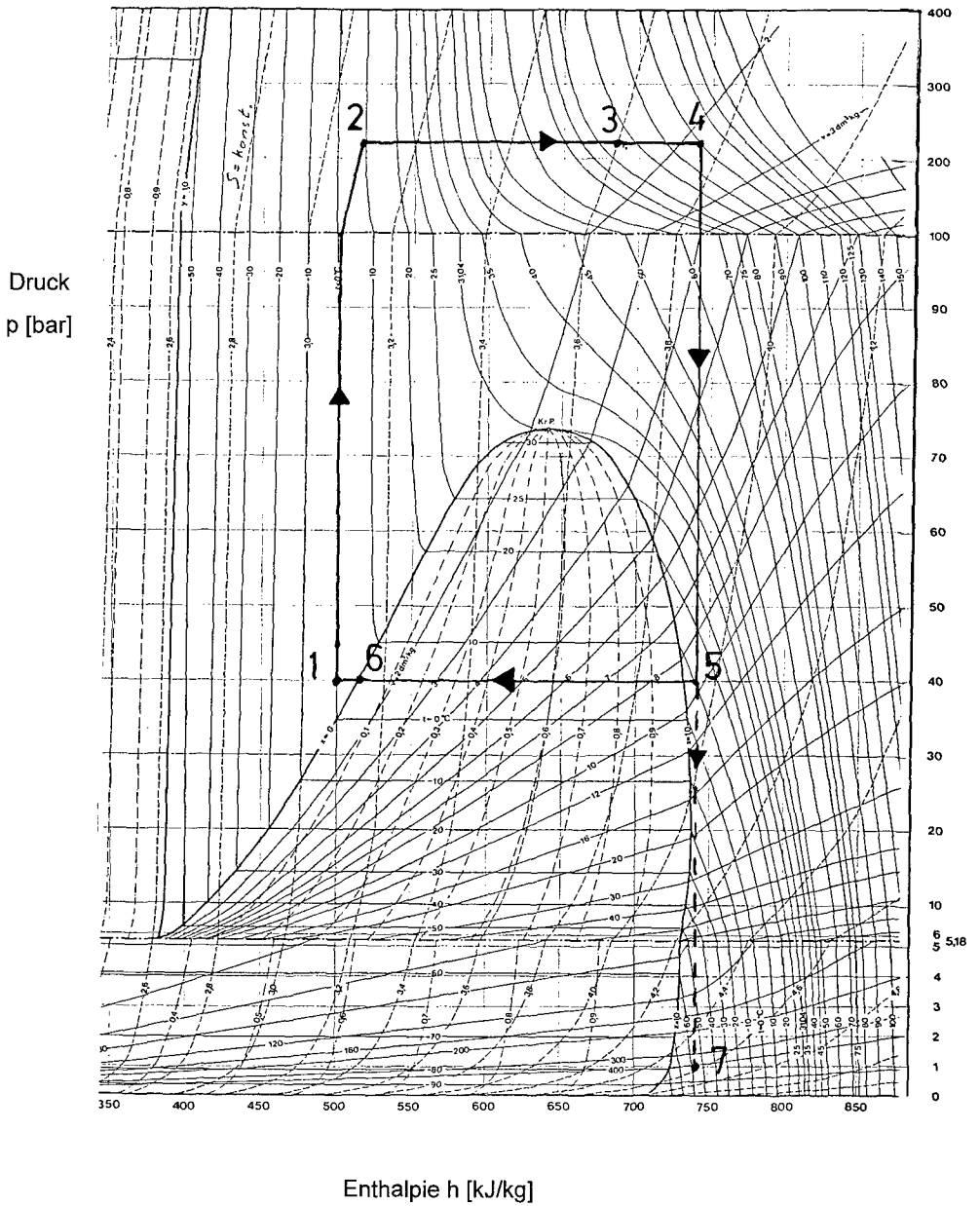
Abb. 6: Schematische Darstellung des RESS - Prozeßes im p - h Diagramm

Der ideale RESS - Prozeß läßt sich durch folgende Zustandsänderungen beschreiben:

1 - 2	isentrope Kompression		5 - 6	isobare Kondensation
2 - 3	isobare Wärmezuführung		5 - 7	irreversible Entspannung im Separator
3	Zustand im Extraktor			
3 - 4	isobare Wärmezuführung			
4 - 5	irreversible Entspannung in der Düse			
5 -	Zustand in der Kolonne			

3.1.1 Düsenströmung

Da durch den Entspannungsvorgang in der Düse sehr hohe lokale Übersättigungen erzielt werden, die spontane Phasenübergänge und somit die Bildung feiner Partikel bewirken, ist die Düse, die zur Entspannung der überkritischen Lösung eingesetzt wird, ein zentrales Bauteil der RESS - Anlage.

Die Strömung läßt sich in zwei unterschiedliche Bereiche aufteilen, in eine **isentrope Düsenströmung** und eine **nicht-isentrope Freistrahlexpansion mit Verdichtungsstößen** im Überschallbereich.
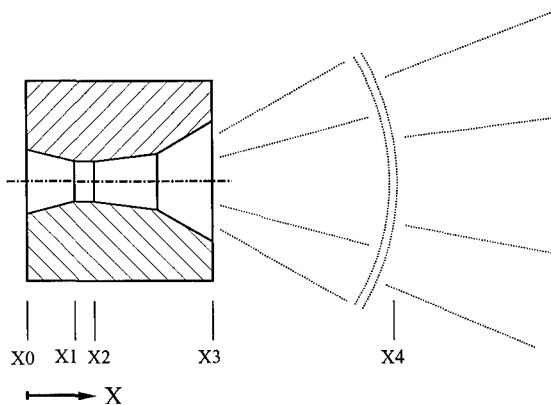
Abb. 7: Expansionsdüse

Vor dem Eintritt in die Düse befindet sich das beladene Fluid, welches durch die Ruhetemperatur T_0 ,den Massenstrom $\dot{m}_0$,den Druck $p=p_0$ gekennzeichnet ist, im überkritischen Zustand. Nach der Düse liegt das CO_2 gasförmig und der zuvor gelöste Feststoff in kristalliner Form vor. Für die im folgenden betrachtete Strömung werden vom Düsenanfang stromabwärts folgende Annahmen getroffen:

- Druck und Temperatur ändern sich <u>nur</u> in x-Richtung, die Strömung wird näherungsweise als eindimensionale Strömung betrachtet.
- Die Expansion in der Düse erfolgt aufgrund der kurzen Aufenthaltszeit adiabatisch.
- Der Druckunterschied in der Düse ist ausreichend groß, um das Fluid im engsten Querschnitt auf Schallgeschwindigkeit zu beschleunigen.
- Die Strömung ist stationär.

Als Grundlage für die Berechnung im Bereich $x_0 < x_4$ gelten folgende integrale Erhaltungssätze:

Massenerhaltung $\qquad\qquad \dot{m}_0 = \rho\, u\, A \qquad\qquad$ (1)

Energieerhaltung $\qquad\qquad h_0 = h + u^2/2 \qquad\qquad$ (2)

Die Zustansänderung wird als isentrop angenommen, so daß gilt :

$$s = s_0 = konstant.$$

Zunächst wird mit einer Zustandsgleichung (Peng Robinson, Bender o.ä.) zum vorgegebenen Ausgangszustand „o" die Dichte iterativ ermittelt und mit bekannten thermodynamischen Beziehungen die Ausgangsentropie s_0 bestimmt. Die Temperatur wird nun schrittweise abgesenkt und für jeden Schnittpunkt zwischen Isentrope und Isotherme die Dichte ρ, der Druck p und die spezifische Enthalpie h berechnet. Mit der Beziehung (2) -Energieerhaltung- ergibt sich die gesuchte Geschwindigkeit. Anhand von bekannten thermodynamischen Beziehungen, läßt sich für eine gege-

bene Temperatur und Dichte die Schallgeschwindigkeit und somit die Machzahl bestimmen. Näheres siehe /5/

Bei $x = x_2$ ist die Strömungsgeschwindigkeit gleich der Schallgeschwindigkeit.

$$M = u / a = 1 \qquad\qquad (3)$$

Bei $x > x_4$ ändern sich die Zustandsgrößen aufgrund eines Verdichtungsstoßes unstetig. Aus der Überschallströmung wird bei $x = x_4$ eine Unterschallströmung.

Durch Geometrie und Form der Düse (Laval- oder Freistrahldüse) können die strömungstechnischen Paramter des Expansionsvorgangs gesteuert werden, so daß hierdurch auch die Keimbildung beeinflußt wird.

Abbildung 8 zeigt eine Rasterelektronenmikroskopie - Aufnahme der für die Versuche eingesetzten Düse. Diese Düse ist 1,5 mm lang und hat am engsten Querschnitt einen Durchmesser von 100 μm.
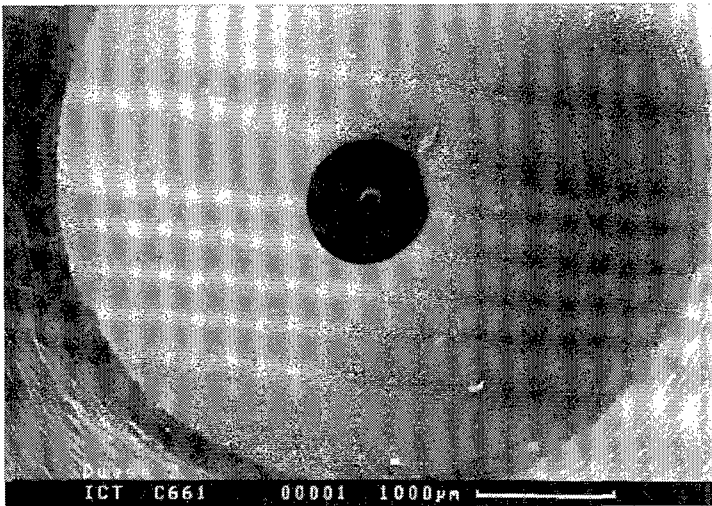
Abb. 8 : REM - Aufnahme der Lavaldüse (Öffnungsdurchmesser 100 μm)

3.1.2 Versuchsergebnisse

Zur Charakterisierung des RESS-Prozeßes wurden vor der Herstellung von Explosivstoffpartikeln Parameterstudien mit dem Dummy-Material Anthracen durchgeführt.

Folgende Einflußparameter sind beim RESS-Prozeß von besonderer Bedeutung: Druck, Temperatur, Düsengeometrie und Massenstrom. Die Zielgröße ist die Partikelgröße bzw. die Partikelgrößenverteilung, welche mittels Laserbeugungsspektrometrie (off-line) ermittelt wird. Beispielhaft ist in Abbildung 9 die Partikelgrößenverteilung von Anthracenpartikeln, die mit folgenden Prozeßparametern hergestellt wurden, dargestellt:

- Düsendurchmesser, $d = 100\ \mu m$ - Temperatur der Kolonne $T_{Kol.} = 20\ ^{\circ}C$
- Massenstrom CO_2, $\dot{m} = 6{,}5\ kg/h$ - Extraktionsdruck $p_{Extr.} = 220\ bar$
- Extraktionstemperatur $T_{Extr.} = 80\ ^{\circ}C$ - Druck in der Kolonne $p_{Kol.} = 20\ bar$
- Temperatur vor der Düse $T_{Dü.} = 110\ ^{\circ}C$

Partikeldurchmesser x [μm]
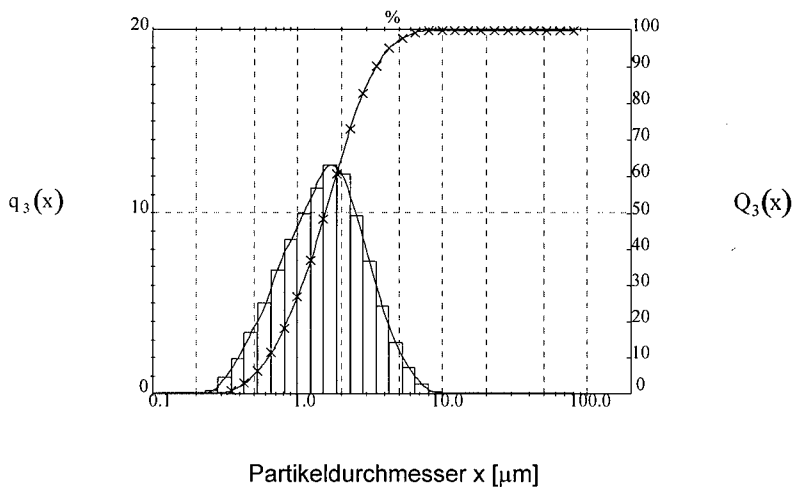
Abb. 9: Volumensummen- $Q_3(x)$ und Volumendichteverteilung $q_3(x)$
    – Anthracen, RESS-Prozeß

Die mittlere Partikelgröße beträgt $x_{50,3} = 1{,}5\ \mu m$. Die Breite der Verteilung stellt sich wie folgt dar: $x_{10,3} = 0{,}6\ \mu m$; $x_{90,3} = 3{,}5\ \mu m$.

Die Herstellung von Trinitrotuluol (TNT) - Partikeln ergab z. B. unter folgenden Versuchsbedingungen

- Düsendurchmesser, $d = 100\ \mu m$ -   Temperatur der Kolonne $T_{Kol.} = 30\ ^{o}C$
- Massenstrom CO_2, $\dot{m} = 6,5\ kg/h$ - Extraktionsdruck $p_{Extr.} = 220\ bar$
- Extraktionstemperatur $T_{Extr.} = 75\ ^{o}C$ -   Druck in der Kolonne $p_{Kol.} = 1\ bar$
- Temperatur vor der Düse $T_{Dü.} = 115\ ^{o}C$

die in Abbildung 10 dargestellte Partikelgrößenverteilung.

Partikeldurchmesser x [µm]
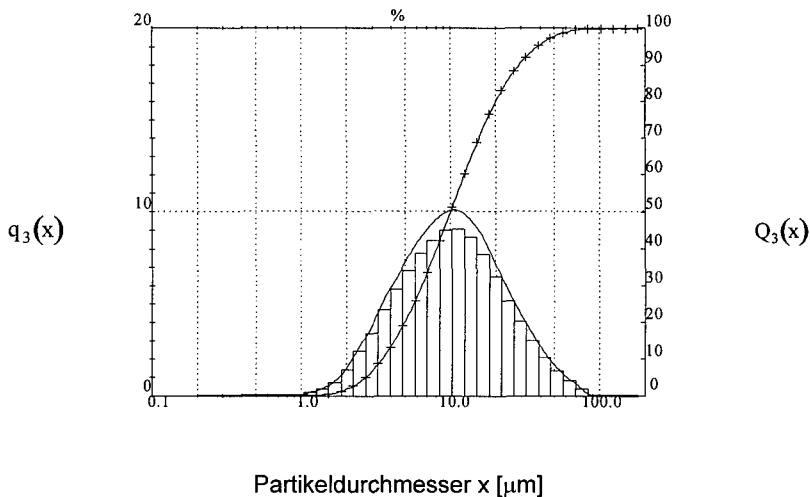
Abb. 10:   Volumensummen- $Q_3(x)$ und Volumendichteverteilung $q_3(x)$
                – TNT - Partikel, RESS-Prozeß

Die mittlere Partikelgröße beträgt $x_{50,3} = 10$ µm, die Verteilungsbreite $x_{10,3} = 3,5$ µm und $x_{90,3} = 28,8$ µm.

3.2 Der GAS - Prozeß

Während beim RESS - Verfahren ein überkritisches Fluid als Lösungsmittel einge-
setzt wird, wird beim Gas Anti-Solvent (GAS) - Verfahren ein verdichtetes Gas als
Anti-Solvent verwendet, um einen gelösten Feststoff aus einem klassischen Lö-
sungsmittel zu rekristallisieren. Dieses Verfahren wird für die Kristallisation von
Wertstoffen genutzt, die sich nicht oder nur schwer in überkritischen Fluiden lösen.

Viele organische Lösungsmittel sind zumindest partiell mit verdichteten Gasen
mischbar. Die Absorption des Gases im Lösungsmittel führt zur Expansion der flüssi-
gen Phase. Die Zunahme des spezifischen Volumens v der Lösung, d.h. die Ab-
nahme der Dichte ρ, bewirkt eine Verminderung des Lösevermögens des Lö-
sungsmittels, so daß Feststoffpartikel auskristallisieren /13/.

Die Kristallisation mittels verdichteter Gase als Anti-Solvent läßt sich technisch auf
zwei Arten realisieren:

- Die Lösung wird in einem Kristallisationsbehälter vorgelegt und das verdichtete
  Gas zugeführt.

- Die Lösung und das verdichtete Gas werden gleichzeitig, vorzugsweise im Ge-
  genstrom in die Kristallisationskolonne eingedüst. Dieses Verfahren wird PCA -
  Verfahren (Precipitation with a Compressed Fluid Anti-Solvent) genannt. Es
  handelt sich dabei um den semi - kontinuierlichen Prozeß.

3.2.1 Batch - Prozeß

Abbildung 11 zeigt das Fließbild für den Batch - Prozeß (Vorlegen der Lösung und
Einspritzen des Gases). Das Gas aus der Vorratsflasche wird im Wärmetauscher
(W1) verflüssigt und gelangt in den Vorratsbehälter. Der Vorratsbehälter hat die Auf-
gabe, für eine gleichmäßige Zuführung des Gases in den Kristallisationsbehälter zu
sorgen, ohne daß größere Druckschwankungen auftreten. Im Wärmetauscher (W2)
wird das Gas unterkühlt, um in der Pumpe Kavitation zu vermeiden. In einem dritten
Wärmetauscher (W3) wird das Gas auf Prozeßtemperatur erhitzt. Durch den Einsatz
eines Rührers wird im Kristallisationsbehälter eine gute Durchmischung von

Lösung und verdichtetem Gas erzielt. Nach der Kristallisation wird das beladene Lösungsmittel dem Separator zugeführt, wo die Trennung von Lösungsmittel und Gas erfolgt /12/.
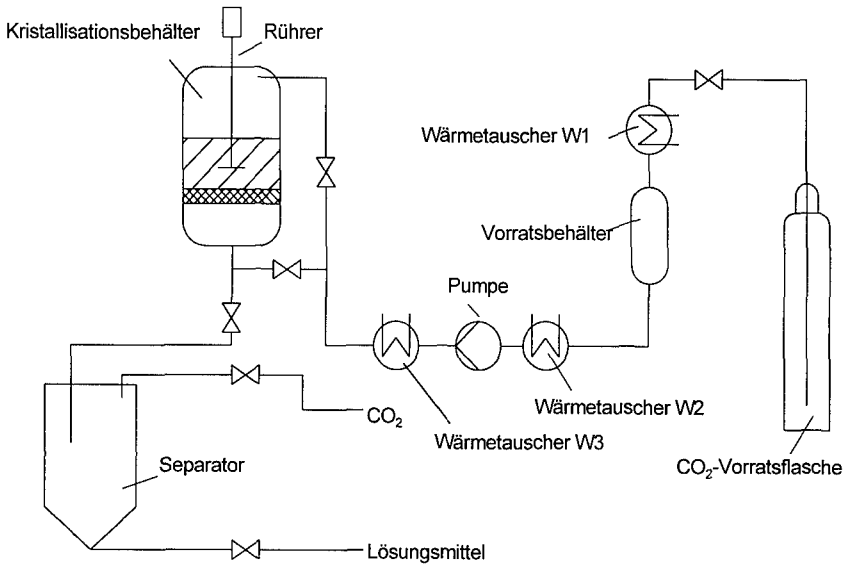
Abb. 11: Fließbild einer GAS - Anlage – **Batch - Prozeß**

3.2.2 PCA - Prozeß

Das Fließbild für den PCA - Prozeß (gleichzeitiges Eindüsen von Lösung und Gas im Gegenstrom) ist in Abbildung 12 dargestellt. Bei diesem Prozeß wird die Lösung über den Kopf der Kristallisationskolonne mittels Düse fein zerstäubt und das verdichtete Gas im Gegenstrom zugeführt. Diese Fahrweise ermöglicht eine schnelle Diffusion des Gases in die Lösung, und somit das Auskristallisieren sehr feiner Feststoffpartikel /14/.
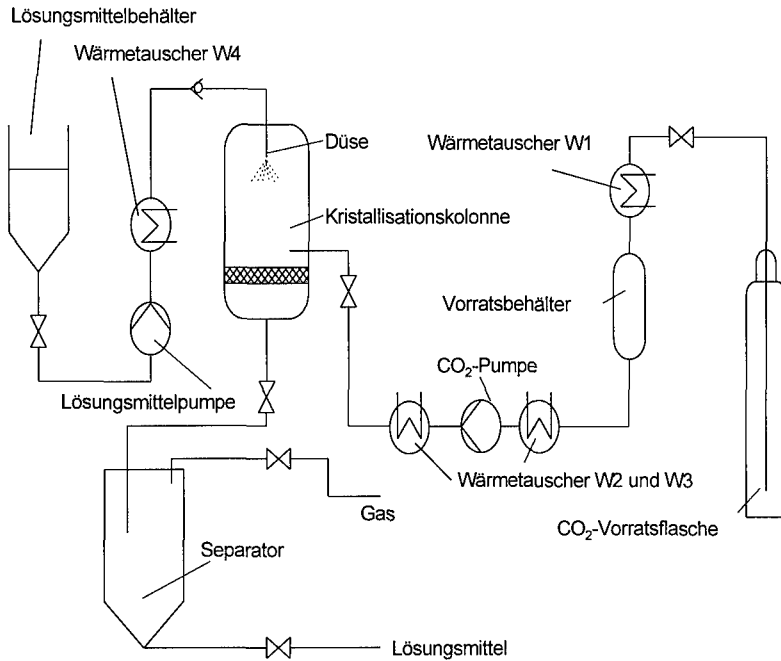
Abb. 12: Fließbild einer GAS - Anlage – **semi - kontinuierlicher Prozeß**

3.2.3 Prozeßparameter

Die volumetrische Expansion des Lösungsmittels wird durch die drei Parameter Temperatur T, Druck p und die Zeit t, die für den Druckaufbau im Kristallisationsbehälter benötigt wird, entscheidend beeinflußt.

Die Löslichkeit verschiedener Feststoffe ist in Abbildung 13 als Funktion des Druckes p bei konstanter Temparatur T für die Mischung Toluol - CO_2 dargestellt. Es ist zu erkennen, daß berechnete Werte sehr gut mit den experimentellen Ergebnissen übereinstimmen /15, 16, 17/.
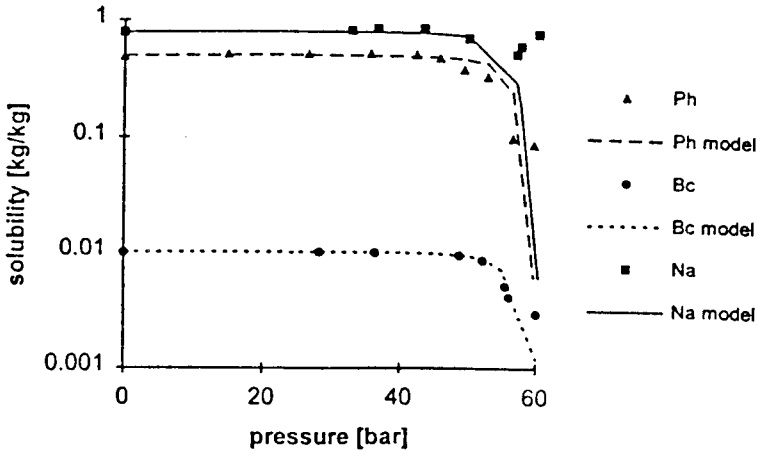
Abb. 13: Löslichkeit in der Mischung Toluol - CO_2 für Phenantren, Naphtalin und β - Carotin als Funktion des Druckes bei 25 °C /15/

Die Löslichkeit von Phenantren und β - Carotin nimmt ab einem bestimmten Druck schlagartig ab, während sie für Naphtalin nach Durchlaufen eines Minimums sogar zunimmt, was darauf schließen läßt, daß eine Rekristallisation von Naphtalin aus Toluol mit CO_2 als Anti-Solvent nicht sinnvoll ist.

Eine andere Möglichkeit der Darstellung ist die Auftragung der volumetrischen Expansion als Funktion des Druckes bei verschiedenen Temperaturen, in Abbildung 14 beispielhaft für das System Cyclohexan - CO_2 dargestellt. Mit Cyclohexan als Lösungsmittel und CO_2 als Anti-Solvent kann z:B. RDX auskristallisiert werden. Es ist sehr gut zu erkennen, daß bei höheren Temperaturen höhere Drücke notwendig sind, um die gleiche volumetrische Expansion des Lösungsmittels zu erzielen /18/.

Die hier getroffenen Aussagen gelten qualitativ für verschiedene Systeme von Lösungsmittel - gelöster Feststoff - Anti-Solvent.
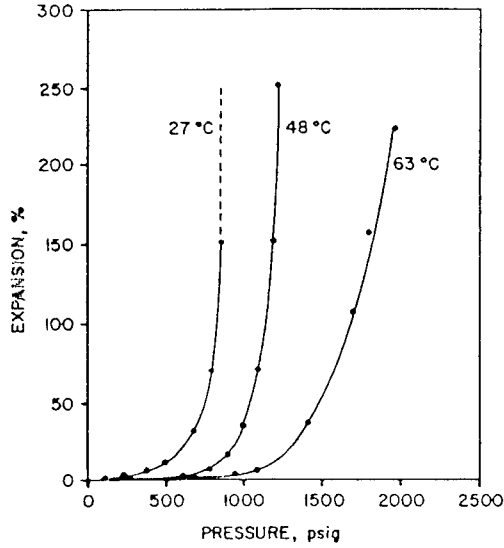
Abb. 14: Volumetrische Expansion von Cyclohexan durch CO_2 bei verschiedenen Temperaturen /18/

Die volumetrische Expansion, die mindestens zur Kristallkeimbildung erreicht werden muß, wird von der Feststoffkonzentration in der Lösung bestimmt. Bei hoher Feststoffkonzentration ist eine geringe volumetrische Expansion notwendig, um das Maß an Übersättigung zu erzielen, daß Keimbildung auftritt. Abbildung 15 zeigt dies am Beispiel einer RDX - Cyclohexan - Lösung /13, 18/.
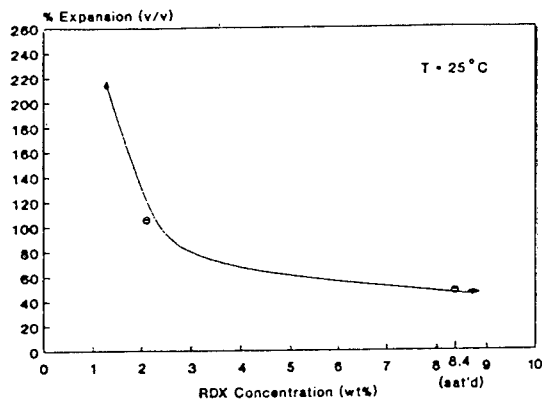
Abb. 15: Benötigte Expansion zur Kristallkeimbildung in Abhängigkeit der Feststoffkonzentration bei 25 °C /13/

Es ist bemerkenswert, daß für das hier gezeigte System RDX - Cyclohexan eine bei 25 °C gesättigte Lösung um ca. 40 % expandiert werden muß, damit Keimbildung auftritt.

Wie bereits erwähnt, ist zur Expansion der Lösung, so daß Keimbildung stattfindet, bei einer bestimmten Temperatur ein Druck notwendig, der in der Literatur als THP = Threshold Pressure bezeichnet wird. Der THP ist definiert als der Druck, bei dem erste Partikel für das bloße Auge sichtbar auskristallisieren /18/.

Die Partikelgröße und die Partikelform können beim GAS - Prozeß über zwei verschiedene Prozeßzeiten gesteuert werden, zum einen über die Zeit des Druckaufbaus im Behälter, und zum anderen über die Partikelverweilzeit (Abbildung 16).
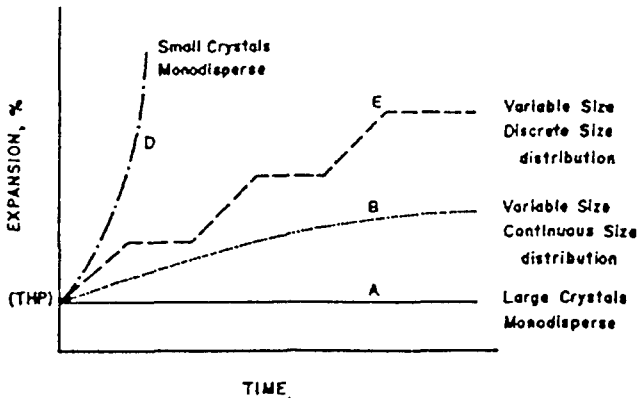
Abb. 16: Expansion einer RDX - Cyclohexan - Lösung durch Zugabe von CO_2 über der Zeit /18/

Am Beispiel des Systems RDX - Cyclohexan und CO_2 als Anti-Solvent ist ersichtlich, daß bei schneller Zuführung des CO_2 feine, engverteilte Feststoffpartikel auskristallisieren, während bei langsamer Zuführung und geringer Übersättigung, so daß gerade Keimbildung erfolgt, große, monodisperse Kristalle entstehen /18/.

4 Literatur

/1/ *Eigenschaften der Kohlensäure*, Fachverband Kohlensäure - Industrie e. V., 1992

/2/ Stahl E., Quirin K. W., Gerard D.: *Verdichtete Gase zur Extraktion und Raffination*, Springer - Verlag, Berlin, 1987

/3/ Span R.: *Eine neue Fundamentalgleichung für das fluide Zustandsgebiet von Kohlendioxid bei Temperaturen bis zu 1100 K und Drücken bis zu 800 M Pa.*, Fortschr. Ber. VDI Reihe 6 Nr. 285, Düsseldorf 1993

/4/ Niehaus M., Teipel U, Krause H., Bunte G.: *Extraktion von Explosivstoffen durch überkritisches modifiziertes Kohlendioxid*, ICT - Bericht 3/95

/5/ Theis Gerhard: *Spontankondensation in übersättigten Dampfströmungen von Kohlendioxid und von Difluordichlormethan*, Dissertation, Universität Karlsruhe, 1985

/6/ Debenedetti P. G., Tom J. W., Kwauk X.: *Rapid Expansion of Supercritical Solutions (RESS): Fundamentals and Applications*, Fluid Phase Equilibria, 82 (1993) 311 - 321, Amsterdam

/7/ Krukonis V.J.: *Processing of Polymers with Supercritical Fluids*, Polymer News, 1985, Vol. 11, pp 7 - 16

/8/ Matson D.W., Petersen R. C., Smith R. D.: *Production of powder and films by the rapid expansion of supercritical solutions*, Journal of Material Science, (1987) 1919 - 1928

/9/ McHugh M.A., Krukonis V.J.: *Supercritical Fluid Extraction, Principles and Practice*, Butterworth Publisher, 1986

/10/ Mohamed R.S. et. al.: *Solids Formation After the Expansion of Supercritical Mixtures*, ACS Symp. Serie 406, Am. Chem. Soc. (1989 b)

/11/ Tom J. W., Debenedetti P. G.: *Particle Formation with Supercritical Fluids - A Review*, J. Aerosol Sc., Vol 22, No. 5 , pp 555 - 584, 1991

/12/ Berends Edwin M.: *Supercritical Crystallization: The RESS-Process and The GAS-Process*, PhD-Thesis, University of Delft, 1994

/13/ Gallagher Paula M., Coffey M. P., Krukonis V. J.: *Gas Anti-Solvent Recrystallization of RDX: Formation of Ultra-fine Particles of a Difficult-to-Comminute Explosive*, The Journal of Supercritical Fluids, 1992, 5, 130 - 142

/14/ Yeo Sang-Do, Lim Gio-Bin, Debenedetti Pablo G., Bernstein Howard: *Formation of Microparticulate Protein Powders Using a Supercritical Fluid Anti-Solvent*, Biotechnology and Bioengineering, Vol. 42 (1993), No. 3, 341 - 346

/15/ Berends E. M., Bruinsma O. S. L., de Graauw J., van Rosmalen G. M.: *Crystallization of Phenantrene from Toluene with Carbon Dioxide by the GAS-Process*, AIChE Journal, Vol. 42 (1996), No. 2, 431 - 439

/16/ Dixon David J., Johnston Keith P.: *Molecular Thermodynamics of Solubilities in Gas Anti-Solvent Crystallization*, AIChE Journal, Vol. 37 (1991), No. 10, 1441 - 1449

/17/ Chang C. J., Randolph, A. D.: *Separartion of β-Carotene Mixtures Precipitated from Liquid Solvents with High-Pressure CO_2* , Biotechnol. Prog., Vol. 7 (1991), No. 3, 275 - 278

/18/ Gallagher P. M., Coffey M. P., Krukonis V. J., Klasutis N.: *Gas Anti-Solvent Recrystallization: A New Process to Recrystallize Compounds Insoluble in Supercritical Fluids*, In: Johnston K. P., Penninger J. M. L.: *Supercritical Fluid Science and Technology*. ACS Symposium Series 406, American Chemical Society, Washington DC, 1989, Chapter 22

THERMAL DECOMPOSITION OF DIFLUOROAMINES

V.N. Grebennikov, G.B. Manelis, G.M. Nazin

Institute of Chemical Physics in Chernogolovka, Russian Academy of Sciences, Chernogolovka, Moscow Region 142432 RUSSIA
Fax: (096) 515 35 88

Thermal decomposition of organic difluoroamines which are energetic compounds by their nature has not been adequately studied.Quantitative kinetic data for the gas phase have been obtained just for some polyfunctional difluoroamines, in particular, for $C(NF_2)_4$, $FC(NF_2)_3$ and $F_2C(NF_2)_2$ [1,2]. It has been shown that, decomposition of these substances starts with cleavage of the C-N bond. Composition of gaseous products of 1,2- and 2,2-bis(difluoroamino)propane thermal decomposition[2,3] also testifies that C-N bond cleavage takes place first. Three types of difluoroamines were included in this study for thermal decomposition investigation: *gem*-bis(difluoroamino)compounds, compounds with solitary NF_2-groups and α-polynitro(difluoroamino)alkanes. The work aimes to determine the influence of molecular structure and substance aggregate state on decomposition parameters. Reaction kinetics was studied under the static conditions by the manometric method. Correctness of the latter was checked by the GLC method.
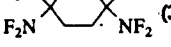
GEM-BIS(DIFLUOROAMINES)

The compounds investigated are presented in Table 1 (**1-4**). The gas-phase decomposition of **1-3** compounds takes place homogeneously and monomolecularly (the initial pressure p_o varied from 20 to 150 torr, S/V ratio of a vessel changed from 0.6 to 20 cm^{-1}). The decomposition of **4** vapors at $p_o > 20$ torr and S/V> 0.6 cm^{-1} occurs on the surface. The liquid-phase decomposition of **2-4** proceeds with self-acceleration. The degree of the latter depends on pressure of gaseous products and decreases with increasing temperature.

The kinetic parameters of both the gaseous first-order reactions and initial noncatalytic stages in the melt are given in Table 1. They are compared with the data for similarly structured polynitrocompounds. Compounds **1-3** have very close rates of decomposition in the gas phase. The reactions are characterized with the activation energy of 192-197 kJ/mol and high value of pre-exponential

factor ($\approx 10^{16}$ c^{-1}). These parameters are preserved in the liquid phase. Evidently, **1-3** have the same mechanism identical in the gas and liquid phase. The values of E and A agree with cleavage of the C-NF$_2$ bond.

Table 1. Kinetic parameters of the decompasition of *gem*-bis(difluoroamino)compounds

Compound	State	Interval T/°C	E_a /kJ mol^{-1}	log A/s^{-1}	ω*	Ref.
(CH$_3$)$_2$C(NF$_2$)$_2$ **(1)**	gas	220 - 260	196.0	15.60	1.00	This work
NF$_2$ NF$_2$ **(2)**	»	210 - 230	200.7	16.42	2.85	»
	liquid	140 - 165	196.5	16.15	3.57	»
F$_2$N NF$_2$ F$_2$N NF$_2$ **(3)**	gas	210 - 260	193.1	15.85	3.72	»
	liquid	150 - 180	197.3	16.0	4.27	»
PhCH(NF$_2$)$_2$ **(4)**	»	110 - 150	109.1	8.30	1.4×10^2	»
C(NF)$_4$	gas	190 - 460	169.6	16.4	6×10^3	[1]
C(NO$_2$)$_4$	»	86 - 177	160.4	16.3	4×10^4	[4]
FC(NF$_2$)$_3$	»	190 - 460	202.8	16.45	1.3	[1]
	»	225 - 250	192.3	15.73	2.6	[2]
FC(NO$_2$)$_3$	»	178 - 236	175.9	15.40	2.3×10^2	[4]
F$_2$C(NF$_2$)$_2$	»	372 - 457	225.1	15.75	9×10^{-4}	[1]
F$_2$C(NO$_2$)$_2$	»	235 - 270	199.0	15.58	9×10^{-1}	[4]
(CH$_3$)$_2$C(NO$_2$)$_2$	»	175 - 210	199.4	17.11	1.3×10^{-3}	[4]

* Relative rate at 200 °C

A comparison between difluoroamines and polynitroalkanes shows that D(C-N) in difluoroamines is 12-16 kJ/mol more than that in similarly structured nitroalkanes. However, it decreases at the introduction of each following NF$_2$-group into α-position similarly to nitrocompounds (20-28 kJ/mol). Alkyl groups as α-substituents do not have a noticeable effect on D(C-N).

Hence difluoroamines and nitrocompounds are very similar in relation to C-N bond cleavage, as it was mentioned in [1] .Owing to the higher activation energy and somewhat less pre-exponential factor alkyl-substituted difluoroamines should be always more stable than nitrocompounds.

Absolutely different mechanism is realized in a liquid-phase decomposition of **4** containing terminal group -CH(NF$_2$)$_2$ .The presence of α-hydrogen

drastically changes the decomposition rate. In this case decomposition evidently takes place through HF elimination.

COMPOUNDS WITH SOLITARY NF₂- GROUPS

All mono- or poly-NF_2-derivatives which do not have in α-position to NF_2 another NF_2 group or some other elecronegative substituent belong to this type. It involves the majority of synthesized difluoroamines.

Typical structures and kinetic parameters of initial stages of liquid-phase decomposition are represented in Table 2. Vaporous decomposition of these compounds is strongly complicated by heterogeneous reactions on the surface similarly to **4**. A homogeneous gas-phase decomposition at T>280 °C, p_o=30-300 torr and S/V < 1 cm⁻¹ is observed only for the most volatile compounds such as N-benzyldifluoroamines (**5**).

Table 2. Kinetic parameters of the decomposition of difluoroamines in the liquid state

Compound	ΔV_{ω} /cm³ g⁻¹	Interval T/°C	E_a /kJ mol⁻¹	$\log A$ /s⁻¹	$\omega^{\bullet}$
5 $C_6H_5CH_2NF_2$	266	110−145	110.2	8.33	1.0
6 $(C_6H_5)_2CHNF_2$	122	110−150	118.2	9.55	1.3
4 $C_6H_5CH(NF_2)_2$	315	110−150	109.1	8.30	1.3
7 $C_6H_5CH(NF_2)CN$	160	110−150	108.9	8.50	2.1
8 $CH_3CH(NF_2)CH=CHCH_2NF_2$	303	110−145	100.8	6.88	0.7
9 $C_6H_5CH(NF_2)CH_2NF_2$	280	90−140	116.1	9.30	1.4
10 $F_2NCH(CH_2)_4CHNF_2$	334	100−145	112.7	8.55	0.8
11 $[F_2NCH_2CH(NF_2)CH_2-]_2$	310	100−140	119.8	9.35	0.5
12 $F_2NCH_2CH(NF_2)CH_2OOCC(CH_3)(NF_2)CH_2NF_2$	268	110−150	100.6	6.80	0.7
13 $F_2NCH_2(CHNF_2)_3CH_3$	332	107−157	106.4	8.00	1.6
14 $F_2NCH_2C(CH_3)(NF_2)CH(NF_2)CH_2NF_2$	211	107−157	111.5	8.60	1.2
15 $(CH_3)_2CHC(CH_3)(NF_2)CH_2NF_2$	268	90−140	128.2	9.80	0.1
16 $[F_2NCH_2C(CH_3)(NF_2)COOCH_2-]_2$	248	110−160	119.8	8.73	0.1
17 $CH_3COOC(CH_3)(NF_2)CH_2C(CH_3)(COOCH_3)CH_2NF_2$	180	110−160	129.4	9.60	0.05
18 $(CH_3)_2C(NF_2)-C(NF_2)(CH_3)_2$	238	110−160	125.7	9.38	0.1

* Relative rate at 100 °C

PhCN, SiF_4 and H_2O were detected among the products of the homogeneous decomposition of **1**. The final gas evolution is poorly reproducible

and varies over the range from 1.45 to 1.97 mol. A brown film of condensed products is deposited on the walls of the vessel.

Decomposition of 2% solutions of compound **5** (the solvents are listed in Table 3) occurs according to a first-order reaction up to a substantial degree of conversion. Arrhenius parameters for the decomposition of **5** are given in Table 2. The rate constant depends on the polarity of the medium. From the data of Table 2 for 132 °C, the following linear relationship was established:

$$\log k = -4.644 - 3.22/D$$

where D is the dielectric constant of the medium

Table 3. Kinetic parameters of the decomposition of *N*-benzyl-difluoroamine

Medium	Interval $T/°C$	E_a /kJ mol^{-1}	lg(A/c)	$k \cdot 10^6/s^{-1}$ at 132 °C
Gas phase	280—300	178.1	11.78	$6.96 \cdot 10^{-6}$
Liquid phase	110—145	110.2	8.33	1.37
Solution in				
CCl$_4$	170—190	106.4	7.61	0.78
C$_6$H$_6$	170—190	107.2	7.90	1.21
CHCl$_3$	132	—	—	5.20
CH$_3$CN	132	—	—	18.00
CH$_3$NO$_2$	132	—	—	22.00

The results obtained imply that the homogeneous gas-phase decomposition of **5** occurs through elimination of HF. The activation energy coincides with that (176 kJ/mol^{-1}) for thermal abstraction of HF from CH$_3$NF$_2$ estimated from experiments with chemically activated CH$_3$NF$_2$ (see ref. [5]). Cleavage of the C-N bond in **5** may be excluded on the basis of the products composition and the bond dissociation energy, D(C-N) = 214 kJ/mol^{-1} (see ref. [6]). The pre-exponential

factor for C-N bond cleavage must be about $10^{14.5}$ s^{-1}. Therefore, this process would compete with elimination of HF at temperatures above 400 ^{0}C.

The products formed in the first stage, PhCH=NF and HF, do not affect the rate of decomposition due to their rapid decay: HF reacts with glass to give SiF$_4$ and H$_2$O, while PhCH=NF quickly decomposes to yeild PhCN and HF and partly polymerizes on the surface. Due to polymerization, the total gas evolution (1.9 mol) is less than that following from the overall reaction.

$$1 \rightarrow PhCN + H_2O + 0.5 \ SiF_4$$
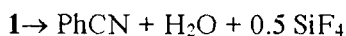
The decomposition rate of compound **5** in the liquid phase is higher than that in the gas phase by 6 orders of magnitude. This attests to a change in the mechanism and accounts for a significant degree of the heterogeneous reaction in the decomposition of difluoroamine: in the layers adsorbed on the surface, rapid decomposition occurs, which is governed by liquid-phase laws, and the contribution of this process increases with the increse in the p_o/p_s ratio, where p_s is the saturated vapor pressure at the temperature of the experiment.

The decomposition rate of **1** in solution depends on the dielectric constant of the medium which attests to the strongly polar character of the transition state.

The decomposition rates of compounds **4-11** in the liquid phase are practically identical. Undoubtedly, the decomposition mechanism of all of these compounds is the same. Small pre-exponential factors are not consistent with any of the homolytic monomolecular mechanisms and are characteristic of El-type ionic processes. The absence of electronic and resonance effects of the substituents on the reaction rate indicates that they are remote from the reaction site, *i.e.*, the latter may be located at the N atom rather than at the C atom. This is also supported by the fact that the rate does not depend on the polarity of the C-H bond, as can be seen from a comparison of compound **5** with compounds **6** and **4**.

All of these facts can be unambiguously explained by assuming that the liquid-phase decomposition of fluoroamines occurs through ionic dissociation of the N-F bond according to the following scheme:

$$RCH_2NF_2 \underset{k_2}{\overset{k_1}{\rightleftharpoons}} [RCH_2NF^+|F^-] \overset{k_3}{\longrightarrow} RCH=NF + HF$$
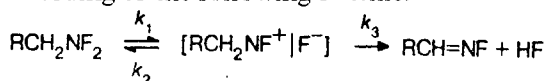
The observed rate constants and activation energies are $k_o = k_1k_3/k_2$ and $E_o = E_1 + E_3 - E_2$.

Compounds **15-18** having chain branching at α- and β-carbon atoms decompose slower than the other compounds by an order of magnitude. This is also explained by steric hindrance to solvation of the ion pair from the side of bulky substituents.

Decomposition of the NF_2 group at a tertiary carbon atom occurs with the same rate as decomposition of $R_3CCH_2NF_2$ groups sterically shielded from the side of the β-atom. Thus, in multifunctional compounds the presence of an α-hydrogen atom is not a necessary condition for decomposition, in contrast to the case of *gem*-bis(difluoroamino)compounds[5] . It is likely that the cationic constituent of the ion pair containing a tertiary carbon atom undergoes rearrangement, which ends in the abstraction of H^+ :

$$(CH_3)_2\overset{+}{C}-\overset{|}{N}F \longrightarrow CH_3\overset{+}{\underset{|}{C}}-N(CH_3)F \longrightarrow H_2C=\underset{|}{C}-N(CH_3)F + H^+,$$
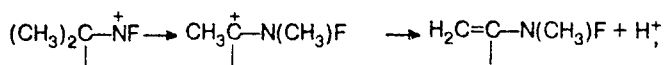
but in this case k_3 is smaller and E_3 is greater than those for direct elimination of H^+ from R_2CHN^+F.

The decomposition of *gem*-bis(difluoroamino)compounds does not involve abstraction of HF if no hydrogen atom exists in the α-position. Apparently, the rearrangement of the cation

$$CH_3(NF_2)\underset{|}{C}-\overset{+}{N}F \longrightarrow (NF_2)\overset{+}{\underset{|}{C}}-NF(CH_3)$$
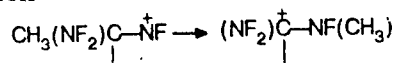
does not occur, since the electron-withdrawing NF_2 group destabilizes the positive charge at the α-carbon atom.

α-(DIFLUOROAMINO)POLYNITROALKANES

α-(Difluoroamino)polynitroalkanes. $RC(NO_2)_2NF_2$, represent a new class of high-energy compounds[1-7]. Determination of these compounds stability and investigation of the mechanism of their thermal decomposition are of interest. The following simplest compounds of this class were studied: $C(NO_2)_3NF_2$ (**19**), $FC(NO_2)_2NF_2$ (**20**) and $MeC(NO_2)_2NF_2$ (**21**) in the gas phase, and **19** and **21** also in the liquid phase. Arrhenius parameters of the first-order decomposition reaction of compounds **19-21** are listed in Table 4. For comparison, the data for pure nitro-analogs of **19-21** are given.

Table 4.. The kinetic parameters of thermal decomposition of α-(difluoroamino)polynitroalkanes and their nitro analogs[*]

Compound	State	$T/°C$	$E/$ kJ mol^{-1}	log(A/s)	k/s^{-1} (100°C)
$F_2NC(NO_2)_3$	Gas	110—175	161.3	16.00	$2.7 \cdot 10^{-7}$
	Liquid	80—90	162.1	16.40	$5.2 \cdot 10^{-7}$
$FC(NO_2)_2NF_2$	Gas	170—220	180.2	16.20	$1.0 \cdot 10^{-9}$
$MeC(NO_2)_2NF_2$	Gas	170—190	168.4	16.00	$2.7 \cdot 10^{-8}$
	Liquid	120—140	168.4	16.00	$2.7 \cdot 10^{-8}$
$C(NO_2)_4$	Gas		160.0	16.30	$8.1 \cdot 10^{-7}$
	Liquid	80—110	156.7	15.50	$3.8 \cdot 10^{-7}$
$FC(NO_2)_3$	Gas	178—236	175.6	15.40	$6.9 \cdot 10^{-10}$
$MeC(NO_2)_3$	Gas	160—210	181.0	17.11	$6.2 \cdot 10^{-9}$
	Liquid	100—140	178.5	16.93	$9.1 \cdot 10^{-9}$

[*] For the data on polynitroalkanes, see Ref. **8**

First-order kinetics of these reactions, rate constants not depending on p_o, S/V and inhibitors, as well as similar gas- and liquid-phase rates of decomposition imply that the decomposition is a homolytic monomolecular reaction. Great magnitudes of the pre-exponential factor agree with a mechanism that involves dissociation of the molecule into two large moieties,

i.e., cleavage of the $C-NO_2$ or $C-NF_2$ bond. The energies of $C-NF_2$ bonds dissociation for compounds **19-21** are 188.1, 199.9, and 208.2 kJ/mol[-1], respectively [7], *i.e.*, they are much greater than the activation energies observed. On the other hand, the kinetic parameters and absolute decomposition rates of compounds **1-3** do not differ from those of their nitro-analogs $RC(NO_2)_3$ within the limits of the experimental error (the accuracy for the activation energy was 6 kJ/mol[-1]) (see Table 4). Therefore, it may be concluded that decomposition of compounds **19-21** occurs via cleavage of the $C-NO_2$ bond, rather than the $C-NF_2$ bond. The effect of an $\alpha-NF_2$ group on the strength of a $C-NO_2$ bond is equivalent to that of a nitro-group. In other words, the replacement of one nitro-group in $RC(NO_2)_3$ by NF_2 does not result in a change of the mechanism or the rate of decomposition. This fact can be used for prediction of decomposition rates in α-(difluoroamino)polynitrocompounds using the available data for nitrocompounds studied in detail.

REFERENCES

[1] Sullivan J.M., Axworthy A.E., Hauser T.J., *J.Phys.Chem.* Vol.74, 1970, pp. 2611-2620.

[2] Neuvar E.W. *Ind. and Eng. Chem. Prod. res. and Develop.,* Vol.8, No 3, 1969, pp.319-320.

[3] Ross D.S., Mill T., Hill M.E., *J. Amer.Chem.Soc.,* Vol.94, No 25, 1972, pp.8776-8778.

[4] Nazin G.M., Manelis G.B., *Izv.Akad.Nauk SSSR, ser. Khim.,* No 4, 1972, pp. 811-816.

[5] Ross D.S., and Shaw R., *J.Phys.Chem.,* Vol.75, 1971, p.1170.

[6] Pepekin V.I., Lebedev Yu.A., Rozantsev G.G., Fainzilberg A.A., and Apin A.Ya., *Izv.Akad.Nauk SSSR, ser.Khim.,* 1962, p.452.

[7] Pepekin V.I., *Chem. Physics,* Vol.13, 1994, p.42.

[8] Nazin G.M., Manelis G.B., *Uspekhi Khimii,* Vol.63, 1994, p.327.

NON-LEADED BALLISTIC MODIFIERS FOR PLATEAU AND MESA PRODUCING SOLID PROPELLANTS

Stephen B. Thompson
Naval Surface Warfare Center
101 Strauss Ave.
Indian Head, MD USA 20640-1524

ABSTRACT:

The work presented describes the effort to develop a lead-free ballistic modifier system for a double-base propellant. The work was funded to investigate the possibility of directly replacing a standard lead-containing double-base propellant used in U.S. Navy aircrew escape propulsion systems with a lead-free formulation.

Several formulations possessing a burning rate which is insensitive to initial pressure were developed. Strand burning rate versus pressure data show that a zero slope curve (plateau) and a negative slope curve (mesa) were produced. All of the ballistic modifiers investigated lost their effectiveness at pressures greater than 27.59 MPa. The ballistic modification is a synergistic effect between the individual modifier compounds, and the removal of or large changes to the ratios of the ingredients will remove burning rate response.

Several formulations and their ballistic effects are presented in the form of strand burning rate versus pressure curves. There are some unique formulations which produce a plateau only and others which produce a plateau at lower pressures and a mesa at higher pressures. Carbon black was added to the formulation and this resulted in a broader range of pressure within which the modified ballistics were evident.

Most of the propellant formulations were tested at -54°C and 74°C to determine the sensitivity of the burning rate to initial temperature. Certain lead compounds will make the propellant extremely temperature insensitive, however the lead-free formulations investigated do not have the same feature.

This work also investigated the effect of energy level, as measured by heat of explosion (HOE), on the ballistic modification. The propellant HOE altered the steepness of the negative slope for the mesa region, while high HOE's produced no mesa at all. The curves shifted up, as a whole, with increasing HOE.

INTRODUCTION:

For more than fifty years, double-base propellants have been employed in many tactical and non-tactical systems around the world. As the state of the art in solid propellant propulsion has advanced over that period of time, higher impulse and higher density alternative propellant types have emerged. While the newer formulations have replaced double-base in some applications, the older propellant type has remained as a significant active member of the solid propellant community. The reason for the longevity of double-base propellants is centered on several beneficial characteristics not found in newer technologies. Double-base propellants produce no flash, a minimum smoke signature, a minimum amount of hazardous exhaust species and a burning rate that can be insensitive to changes in rocket motor chamber pressure and ambient temperature. This last benefit is the focus of this work.

In the 1940's it was discovered that, for unknown reasons, a double-base propellant exhibited a steady burning rate with increasing pressure. One experimental lot made in 1947

without the extrusion aid, lead stearate, resulted in a typical linearly proportional burning rate - pressure relationship, thereby removing any ballistic modification.[1] Lead stearate thus became the first ballistic modifier for double-base propellants. Since that time many other lead compounds, mostly organic salts, have been used as ballistic modifiers. Ballistic modification of double-base propellants has been almost exclusively achieved through lead compounds, which are, by far, the most effective materials.

In the mid 1970's copper ß-resorcylate (copper 2,4-di-hydroxy benzoate) was used in propellants successfully as a single modifier ingredient. This and other copper compounds have also been mixed with lead compounds to obtain more beneficial ballistic results. The copper and lead compound mixtures were soon replaced by synthesized complexes of the compounds. The complexes incorporate the lead, copper and each of the organic ligands, which allows for easier propellant processing. All of the ballistic modifiers used are water insoluble and possess a very small particle size.

Modified double-base propellants, tend to exhibit not only insensitivity to pressure variance, but insensitivity to temperature variance as well, which both prove beneficial when designing a rocket motor. The propellant burning rate is related to the chamber pressure by the Vieille equation,

$$r = aP^n \qquad \text{(Equation 1)}$$

where
r = the propellant burning rate (cm/s)
P = the chamber pressure (MPa)
a = the burning rate constant
n = the pressure exponent

As can be seen from Equation 1, an un-modified propellant, with $n = 0.8$, the rate increases exponentially with increasing pressure. For a modified propellant which has an insensitive burning rate to pressure changes, n must be approaching zero. If n is nearly 0, then r remains constant for any value of P. This effect is termed a "plateau". If $n < 0$, a decreasing burning rate with increasing pressure would result, which is defined as a "mesa". When applied to a rocket motor, a propellant with a value of n greater than zero will be susceptible to over-pressurization if there are cracks in the propellant grain or an instantaneous nozzle blockage. An increase in propellant surface area due to cracks will result in a higher burning rate which leads to a higher pressure, leading to a higher burning rate and so on. An instantaneous blockage of the nozzle will lead to a similar effect, creating an over-pressurization. A modified propellant with a value of n equal or less than zero will be much less susceptible to an over-pressurization in either of the above two cases. An increase in pressure will not affect the burning rate, whereas in the case of a mesa, the burning rate will decrease with the increase in pressure. the modified propellant allows for thinner walls in the rocket motor because of the ability to closely control the anticipated operating pressure.

The burning rate insensitivity to initial bulk temperature is another highly beneficial aspect of modified double-base propellants. This effect is primarily observed in a region of mesa burning. Because it renders the need for rocket motor performance calculations based on ambient temperatures unnecessary, modified double-base propellants are very system and user friendly. A typical lead-modified propellant shows little burning rate change within a temperature range of -54°C and 74°C, and therefore the rocket shows little change in action time over the same range of temperatures.

Over the past several years, one drawback of modified double-base propellants has received more attention, namely the toxicity of the lead in the modifiers. The potential for exposure of personnel and the environment to lead through the manufacture, testing, fleet use and disposal of the propellant and rocket motors has become a major concern. This concern over lead exposure has been the driving force to develop alternative ballistic modifiers.

This program was funded by the U.S. Naval Air Systems Command to replace the current lead-modified propellant used in U.S. Navy aircrew escape systems. The work was performed at the Naval Surface Warfare Center, Indian Head Division. The objective was to develop a lead-free double-base propellant which could directly replace the current formulation without changes to the aircrew escape system.

EXPERIMENTAL:

The double-base propellants investigated in this work are processed by a solventless method and are composed of nitroglycerin, nitrocellulose, di-propyl adipate, 2-nitro di-phenyl amine and ballistic modifiers. The first four ingredients listed are added to water and slurried together. This slurry is filtered and the resulting propellant "paste" is aged and oven dried to a moisture content of about 14% - 16% by weight. The ballistic modifiers are then blended into the paste using a horizontal, sigma-blade mixer. This modified paste is then processed on a differential speed rolling mill operating at about 85°C, which de-wets and plasticizes the paste into a sheet. The sheet is further worked on an even speed rolling mill at 71°C, until a fully plasticized sheet is obtained.

Samples of each propellant formulation are cut from the sheet in a lengthwise direction. From this sample, strands are cut with approximate dimensions of 0.64 cm x 0.25 cm x 15.25 cm, which are inhibited on all surfaces. The strands are burned in a chamber under conditions of controlled initial pressure and initial temperature. The strand burner is a modified Crawford bomb which measures the burning times for a pre-determined strand length. The burning times are then converted to burning rates (cm/s).

FIGURE 1
STRAND BURNING RATE vs PRESSURE
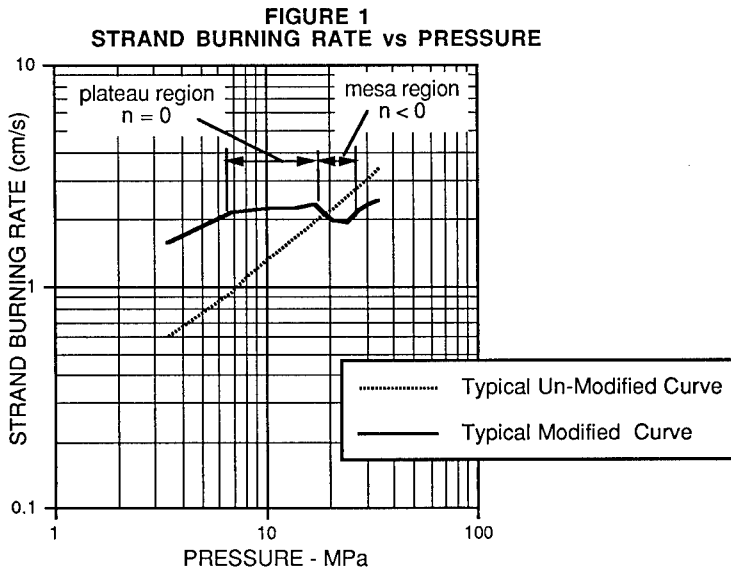
The strands, typically conditioned to temperatures of -54°C, 25°C or 74°C, are placed in the bomb chamber where a nitrogen atmosphere is introduced to a specific pressure. Upon reaching

the desired temperature and pressure, the strands are ignited, with at least three burned for each pressure and temperature.
In the interest of analyzing the data, Equation 1 is converted to the following:

$$\log(r) = (n) \log(P) + \log(a) \qquad \text{(Equation 2)}$$

The strand burning rate, in cm/s, is plotted versus the initial bomb pressure, in MPa, on a log-log scale (see Figure 1), where the slope of the curve is equal to n and the y-intercept is equal to a. Figure 1 shows a typical un-modified propellant burning rate vs. pressure curve with a slope of about 0.800 and a typical modified double-base curve with a plateau and mesa.

The line encompassing all data points for a given temperature is called an isotherm and therefore represents the relationship between the pressure and burning rate for a certain temperature. A propellant with a low sensitivity of burning rate to temperature will have hot and cold isotherms very close together, possibly having them overlap in some areas. For this work a plateau is defined as the pressure range where n is less than or equal to 0.300 and a mesa is defined as the pressure range where n is negative.

In the interest of saving time and money, initial formulations were screened by testing at 25°C and within a limited pressure range. If a formulation showed a promising ballistic effect, further testing was conducted at the cold (-54°C) and hot (74°C) temperatures and over a wider pressure range. Formulations of particular interest to the project were always duplicated to verify results.

Propellant pastes of varying energy content were made in order to determine the effects of this on the modified ballistics. The energy content of the paste is changed by varying the nitrocellulose, nitroglycerin and di-propyl adipate percentages. The propellant energy level is determined through the heat of explosion, which is reported in calories per gram (cal/g). It is well

FIGURE 2
STRAND BURNING RATE vs PRESSURE
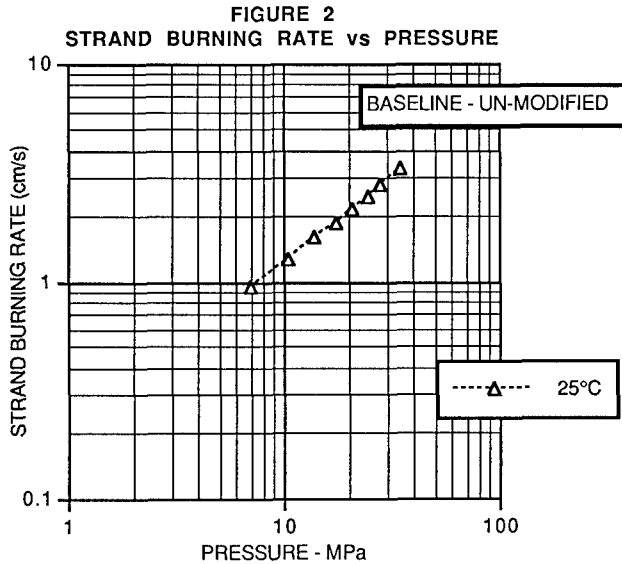
understood that the burning rate isotherms move, as a whole, up or down in rate proportionally to changes in energy. However, the placement and strength of plateaus and mesas are also dependent upon the propellant energy level, and this relationship must be established because it is formulation specific.

BASELINES:

A baseline propellant without ballistic modifiers was processed and tested, (Figure 2), to compare with the subsequent experimental, modified formulations. The specific slope and burning rates of this un-modified propellant is used to determine the degree of modification of the burning rate by the various ingredient additions. The propellant baseline, used for most of the formulations in this work, has a nearly constant slope of 0.800 at 25°C.

A second baseline propellant formulation was made to verify the processing and testing techniques which were employed throughout the study. Copper ß-resorcylate, at a level of 0.70% by weight, was added to the propellant paste, processed and then tested at -54°C and 74°C and a series of pressures. This formulation and it's ballistics are well established and specific burning rate curves were anticipated. Figure 3 shows the expected plateau and slight mesa over the entire pressure range tested, representing a plateau. The results serve to verify the propellant processing techniques and the testing techniques used for this work.

FIGURE 3
STRAND BURNING RATE vs PRESSURE
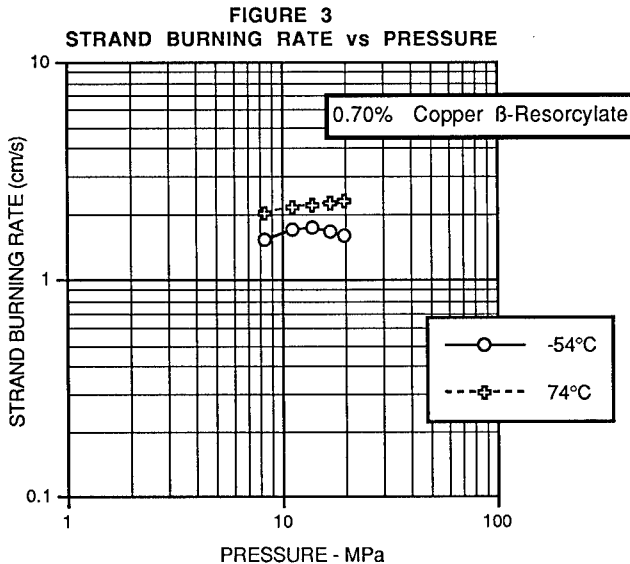
INITIAL FORMULATIONS:

Out of a variety of organic and inorganic salts of bismuth, cobalt, copper, silver, tin and zinc used both singly and in many combinations, a couple of promising candidate formulations showed marginal success. Due to a pending U.S. patent on the propellant formulations involved in this work, specific ballistic modifiers will be referred to as compound 'A', compound 'B', etc. To make

the presented data as useful as possible, the designations will remain ingredient-specific throughout this paper.

FIGURE 4
STRAND BURNING RATE vs PRESSURE
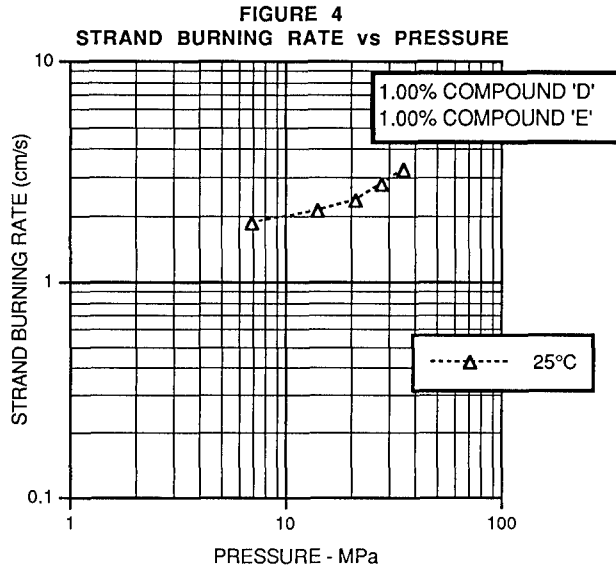
The first unique formulation investigated which produced a significant ballistic modification of interest is shown in Figure 4. The slope of 0.235 between 6.90 MPa and 20.69 MPa is, by our definition, a plateau although it does not meet the program requirements. This curve shows an acceleration of the burning rate over the un-modified propellant in the lower pressure range. The acceleration effect is lost as the pressure increases, thereby producing a low slope value in the modified burning area.

Two examples of formulations with a single modifier ingredient, one with compound 'A' only and one with compound 'B' only, are shown in Figure 5. When comparing the curves of Figure 5 to that of Figure 2, it appears, by the similarity of the slopes and burning rates, that the single ingredients are ineffective in producing a modified ballistic effect. There exists no accelerated burning rate in the lower pressure range and no decelerated rate in the higher pressure range.

Now consider the case where compound 'A' and compound 'B' are combined in one propellant formulation. The combination of ingredients used in Figure 6 are at the same percentages with which they were used individually. The results show, most notably, a plateau, whereas the same ingredients used separately produce a slope of 0.700 to 0.800. The combination also reveals an accelerated burning rate at lower pressures and a decelerated burning rate at higher pressures, both relative to the curves in Figure 5. The resulting plateau ballistics illustrate an important point observed in this investigation. In all cases, with copper ß-resorcylate being the single exception, the ballistic modifier ingredients tested show no significant useful effects alone. There is, however, a synergistic effect between certain combinations of two or three compounds. Removing or greatly changing the percentage of any one compound will result in the disappearance of the ballistic modification. The formulation of Figure 6 is encouraging, although

FIGURE 5
STRAND BURNING RATE vs PRESSURE
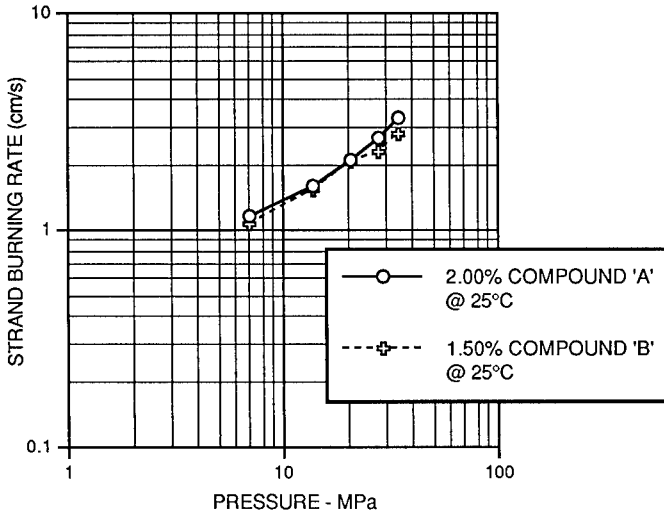
FIGURE 6
STRAND BURNING RATE vs PRESSURE
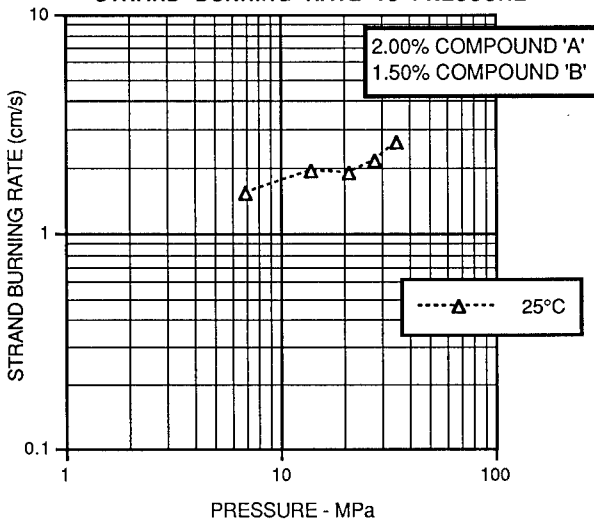
from an application point of view, the burning rates in the plateau region remain too low for the program's objectives.

It should also be noted that both modified propellant formulations shown thus far show the modification only through a pressure range of 20.69 MPa. Above this pressure, the low slope burning rate is lost and the curve returns to the shape of the un-modified propellant. As will be observed in later formulations, this trend back to the un-modified curve is typical although it takes place at higher pressures

CANDIDATE FORMULATIONS:

In order to make the ballistics of Figure 6 more useful for our application, another synergistic ingredient must be added to the formulation. Compound 'C' was added at 0.50% by weight as indicated in Figure 7, and this formulation was tested at -54°C and 74°C. Although it is difficult to observe due to the different test temperatures, the burning rate curves of Figure 7 are accelerated across the modification pressure range as compared to Figure 6. Relative to an un-modified propellant, this formulation has an accelerated burning rate in the low pressure region, including a plateau. This propellant's burning rate curves differ from that of Figure 6 in the area where the decelerated burning occurs. While Figure 6 shows a plateau, this formulation provides a greater decrease in burning rate over an un-modified propellant, resulting in a mesa. The negative slope occurs between 20.69 MPa and 27.59 MPa on the cold isotherm and between 13.79 MPa and 20.69 MPa on the hot isotherm. For both temperatures, all ballistic modification is lost after a pressure of 27.59 MPa is surpassed. The addition of compound 'C' has served to increase the burning rates over the range of ballistic modification, broaden this same range and create lower slopes.

FIGURE 7
STRAND BURNING RATE vs PRESSURE
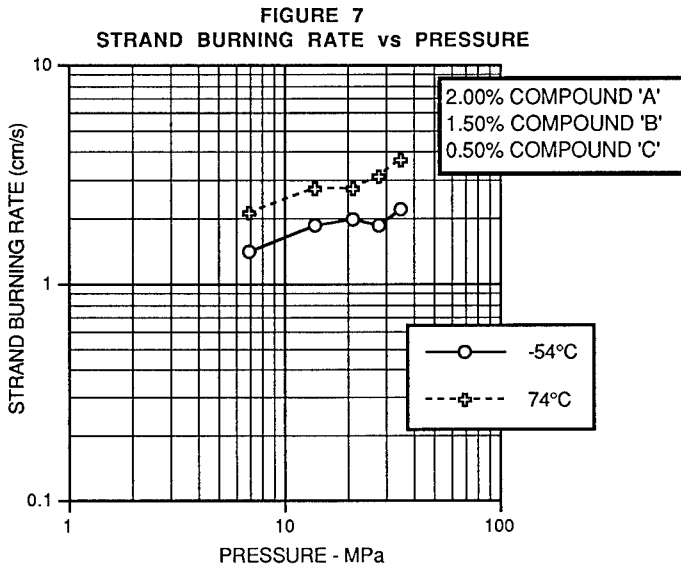
FIGURE 8
STRAND BURNING RATE vs PRESSURE

2.00% COMPOUND 'A'
1.50% COMPOUND 'B'
0.50% COMPOUND 'C'
0.10% CARBON BLACK

—O— -54°C

---+--- 74°C

STRAND BURNING RATE (cm/s)

PRESSURE - MPa

FIGURE 9
STRAND BURNING RATE vs PRESSURE

1.50% COMPOUND 'A'
1.00% COMPOUND 'B'
0.70% COMPOUND 'D'
0.10% CARBON BLACK

—O— -45.6°C

---+--- 65.6°C

STRAND BURNING RATE (cm/s)

PRESSURE - MPa

To further enhance the ballistic modification of the three compound formulation, a small amount of carbon black was added. Carbon black is well known for its ability to shift not only the pressure range over which modified burning rates occur, but it also changes the burning rate at which the plateau and/or mesa resides.[2] The test results of a formulation containing 0.10% carbon black are shown in Figure 8. Take note that the data points are taken at slightly different pressures as compared with the previous curves. At the cold isotherm, the slope is negative from 13.79 MPa to 27.59 MPa, the specific slope value being -1.244 between 24.14 MPa and 27.59 MPa. The hot isotherm is basically flat from 10.34 MPa through 27.59 MPa, with a negative dip beginning at 20.69 MPa. The addition of carbon black has helped to enlarge the pressure range over which the modified burning rate occurs and it has made the mesa much more pronounced. By comparing Figures 7 and 8, it appears that the carbon black has had the effect of lowering the burning rate at the higher pressures and hot temperatures. Another carbon black study showing similar results will be discussed later.

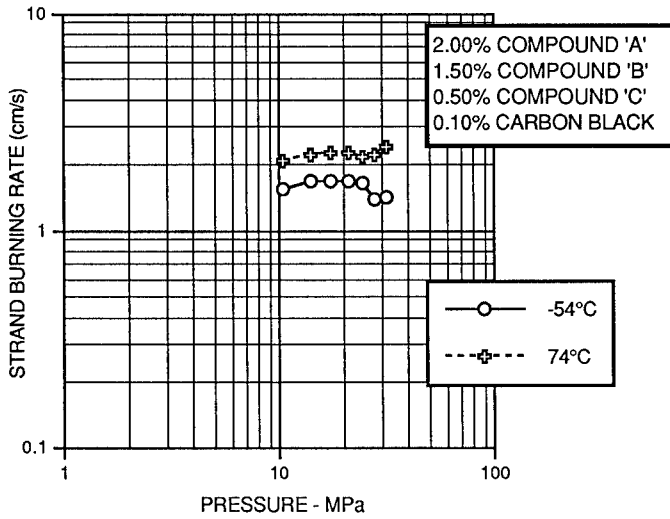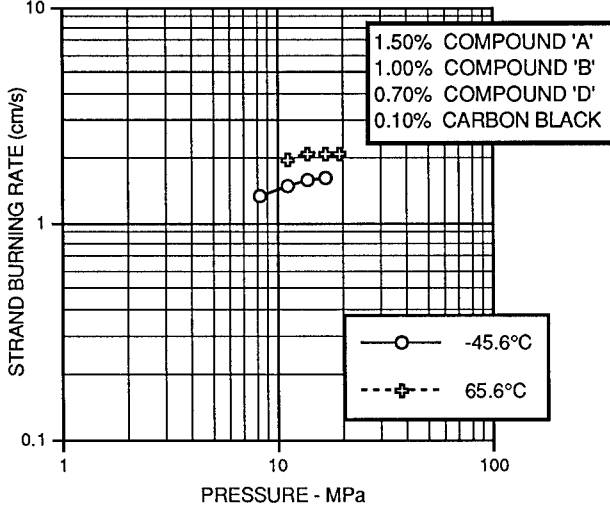Another formulation of interest that was investigated is shown in Figure 9, with compound 'D' used in lieu of compound 'C'. The results, tested at less extreme temperatures of -45.6°C and 65.6°C, show a plateau effect. On the hot isotherm, the plateau extends from 11.03 MPa to 22.06 MPa, while the cold isotherm has a slightly shorter region. The data indicate a slower burning propellant than the previous example, with a relatively long plateau region.

There remains one benefit of lead-modified double-base propellants which this work has been unable to duplicate with a lead-free formulation. Many lead-based ballistic modifiers provide propellant burning rates which are virtually temperature insensitive within rocket motor operating pressures. All of the formulations described by this work possess a higher degree of burning rate variation to the initial propellant temperature at a given pressure. This relationship can be observed as the space between the hot and cold isotherms on the burning rate versus pressure plots. A lead-modified propellant will often have hot and cold isotherms which overlap, usually in a mesa region. While the temperature sensitivity of the formulations described here are much better than those of other propellant types, difficulties must be expected when attempting to substitute them for a lead-modified propellant.

Many trials were run to determine each ingredient's role in the overall ballistic modification effect as seen in Figure 8. As stated before, the ingredients act synergistically to create a burning rate modification, and the removal of one compound will cause the effect to vanish. A normalization technique was used to help determine the small responses of the burning rate to changes in formulation. The burning rate of the test formulation is divided by that of the control formulation, which shows the burning rate response. A value greater than 1 means an accelerated burning rate and a value less than 1 denotes a delerated burning rate. By this method the contributions of each ingredient was determined. It was found that compound 'C' acts mainly to accelerate the burning rate in the lower pressure region and to shift the isotherms, as a whole, up in rate. Compound 'B' is responsible for producing a low slope in the middle pressure ranges and decelerating the burning rate in the higher pressure ranges. Compound 'A' contributes a general beneficial effect over the entire modification region, creating the mesa and broadening the plateau range. Finally, carbon black has the effect of broadening the modification area as well, while it deepens the mesa region as observed in Figure 8.

Two formulations were processed at the same time, one similar to that of Figure 8 with carbon black, (the test lot), and one the same without carbon black, (the control lot). The burning rate data for the test lot was divided by the data for the control lot to produce the normalized curves in Figure 10. The data indicates that the carbon black, as discussed before, has the effect of lowering the burning rate of the hot isotherm slightly. Also the dip below 1 on the right side of the curve indicates that the carbon black decelerated the burning rate of the control formulation, and because there is a mesa in this pressure range, Figure 7, the effect is a deeper (more negative) mesa.

FIGURE 10
FORMULATION WITH CARBON BLACK NORMALIZED
TO FORMULATION WITHOUT CARBON BLACK
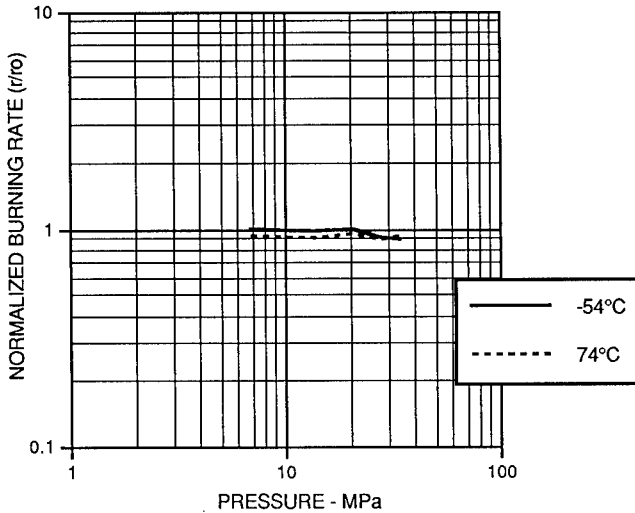
It is well understood that as the energy level of the propellant changes, as measured by the heat of explosion (HOE), the propellant burning rate will change in a directly proportional way. If the HOE change is not too large, the burning rate isotherms will simply move uniformly, maintaining the same basic shape. If the HOE change is large, in either direction, the burning rate modification effect may be lost. The HOE range within which a particular modifier system is effective is a function of the modifier ingredients themselves. The relationship between the burning rate and HOE of the following formulation was investigated:

$$2.00\% \quad \text{Compound 'A'}$$
$$1.50\% \quad \text{Compound 'B'}$$
$$0.50\% \quad \text{Compound 'C'}$$
$$0.10\% \quad \text{Carbon Black}$$

The results are plotted in Figures 11 and 12 which represent the HOE effect on the cold burning rates and hot burning rates, respectively. As is expected, the burning rate isotherms increase, in general, with increasing HOE. It is interesting that the cold burning rate isotherm is basically unchanged between 890 cal/g and 955 cal/g, (Figure 11), and this is the energy range which produces the deepest mesa values. An increase of only 20 cal/g, from 955 to 975, removes the negative slope entirely. Figure 12 shows a similar relationship between the propellant energy level and the hot burning rate isotherm. An increase in HOE above 955 cal/g is responsible for the absence of the negative slope. It should also be noted that there is an inversion of the 930 cal/g and 890 cal/g hot isotherms. This is possibly due to variations in the strand burning tests, processing or the HOE test.

FIGURE 11
HOE EFFECT ON -54°C BURNING RATE
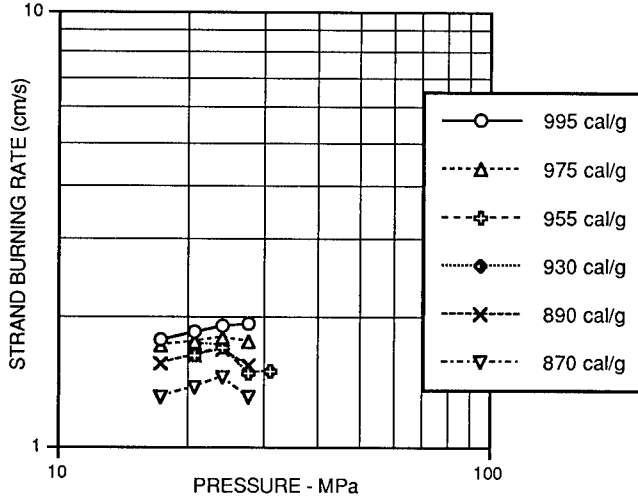
FIGURE 12
HOE EFFECT ON 74°C BURNING RATE
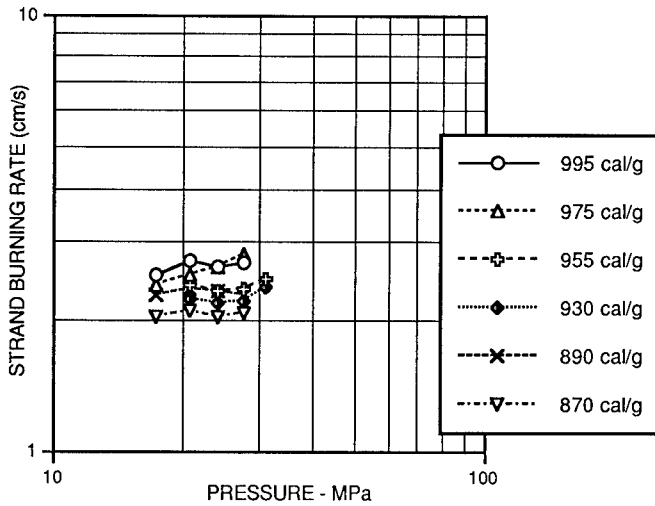
CONCLUSIONS:

A lead-free ballistic modified propellant has been developed to replace the current lead-modified double-base used in U.S. Navy aircrew escape ejection systems. The propellant formulation, (Figure 8), provides plateau (zero slope) and mesa (negative slope) burning rates with respect to pressure. The burning rate insensitivity to pressure characteristics of this propellant type allows for a greater ease in designing and using a rocket motor.

The formulations described in this work will, no doubt, lead to a family of similar lead-free propellants which address the personnel and environmental safety concerns of the conventional double-bases. Variations of the formulations described here will provide plateau and mesa ballistics at different burning rates and pressures for a variety of applications. This is especially true because the contribution of each compound to the overall modification effect is well understood.

There remains more work to be done before the lead-free formulations are considered complete. The inability of the propellants described to produce a temperature insensitivity on the order of the lead-modified propellants is a concern. The goal of future work with the lead-free compounds investigated, and other materials as well, is to make the strand burning rate isotherms as close as possible, preferably having them overlap. If this could be done with similar ballistics to Figure 8, the resulting propellant would be irresistible for many applications.

ACKNOWLEDGEMENT:

BIBLIOGRAPHY

1. Camp, A. T., et al., *A Decade of Progress in the Understanding of Certain Ballistic Properties in Double-Base Propellants*, NAVORD Report 5824, NOTS 1914, January 1958.

2. Preckel, R. F., *Plateau Ballsitics in Nitrocellulose Propellants*, AIAA Journal, **3**, No. 2, pg 346 347, February 1965.

THERMAL RESPONSE AND PARAMETRIC ANALYSIS OF ALUMINIZED
AP/HTPB BASED PROPELLANTS WITH VARYING COMPOSITION

Liza F. Dimaranan, Ilzoo Lee, Frank E. Hudson III
Research and Technology Division
Naval Air Warfare Center Weapons Division, Code 474330D
China Lake, California USA

ABSTRACT

Thermal response and decomposition kinetics of ABL 4863 commercial ammonium perchlorate (AP) and various formulations of Aluminized (Al)/AP/Hydroxy terminated polybutadiene (HTPB) based propellants have been studied for parametric analysis of cookoff behavior. This study was a coordinated experimental and modeling effort. The experimental techniques used for the thermal study involves a differential thermal analyzer (DTA), thermal expansion, and thermal diffusivity experiments. An intermediate scale differential thermal analyzer (ISDTA) using one gram samples was also designed and modeled to determine the size effects on decomposition kinetic parameters.

Reaction kinetic parameters were obtained from the change of the DTA thermograms with various heating rates for both the small scale and intermediate scale sample sizes. The small scale DTA thermogram of AP was characterized by two exotherms. Kinetic analysis showed that the first exotherm can be interpreted as a single reaction while the second exotherm involved multiple reactions. All propellants studied showed a single exotherm at approximately 340°C. In comparison to the small scale DTA results, the ISDTA experiment showed that the propellants decomposed at lower temperatures and yielded lower kinetic parameters. For both the DTA and ISDTA experiments, the kinetic parameters also varied with AP particle size and the presence of a catalyst.

In conjunction with the ISDTA experiment, computational analyses were performed using the thermal code COYOTE II. The kinetic parameters from the small scale DTA were used in the model to compare time to reaction results from the ISDTA experiment. It was found that matching the reaction time for the slowest heating rate in the thermal model was the most difficult. The modeling results also showed thermal gradients in the propellant at the highest heating rate typically found in large scale samples.

1.0   INTRODUCTION

The prediction of the cookoff response of a weapon system is an important need to the United States Department of Defense and Department of Energy communities. Advancing this predictive model to not only calculate time to reaction but also the violence of the cookoff event is an important goal. The modeling tools currently available can predict reaction time reasonably well, but predicting violence is not yet available. Before any advancements in the computer model to have the predictive capability in

calculating cookoff violence, fundamental thermal responses of the energetic material are needed as a function of temperature. Some basic questions that may be answered by various experiments include: 1) How an energetic material's properties change as it is thermally degraded (heated), 2) What is the mechanical response of the energetic material as it is heated, and 3) How does increases in size (from milligrams to hundreds of grams) affect the properties currently being used in the models.

In this study, thermal analyses of pure AP and AP/HTPB/Al based propellants with varying particle size of AP, solid content, and sample size were performed. Thermal responses of propellants from DTA were interpreted in terms of the compositional changes of propellants. Also, the kinetic parameters were calculated for the reaction where the Arrhenius type of reaction can be assumed. This study includes 1) small scale tests using milligram sample sizes such as DTA, expansion, and diffusivity measurements and 2) an intermediates scale DTA test using one gram samples.

The ISDTA experiment was designed to look at what happens to the kinetic parameters of an energetic material when it is increased in size from milligrams to one gram. This was intended as a first step in bridging the gap between using data with milligram size samples, for use in modeling large hundreds of grams in weapons systems. The same series of AP/HTPB/Al were used in this experiment and the ISDTA was set up to directly compare these propellants' kinetic parameters to the small scale DTA experiments. It was intended that by analyzing the results from both tests, it could be determined what effects increasing sample sizes has on the kinetic parameter results.

2.0 EXPERIMENTAL

2.1 Ammonium Perchlorate (AP) and Propellant Samples

Ammonium perchlorate (AP) studied in this work is commercially available ABL 4863 AP with 200μm particle size. Propellants are aluminized AP/HTPB based propellants with varying particle size of AP and solid content. Table I summarizes propellant samples and compares ingredients of propellant formulation.

TABLE I. Propellant samples and comparison of the ingredients of propellant formulation.

	% Solid	AP (μm)	Plasticizer	Catalyst
A	88	200	DOS	-
B	90	200	DOS	-
C	90	400	DOS	-
D	90	200	DOS/IDP*	-
E	90	200	DOS	1.2% Fe_2O_3

* 4% IDP (isodecyl pelagonate) instead of 2% DOS (Dioctyl sebaccate)

2.2 Thermal Analysis Using Milligram Size Samples

Differential thermal analysis (DTA, TA 2930) were performed with samples weighing about 6-7 mg under nitrogen, flushed at 80 ml/min. The DTA was equipped with residual gas analyzer (RGA) for evolved gas analysis from DTA. The evolved gases from DTA were introduced to RGA through capillary tube with

bypass inlet system in such a way that signal response time of RGA was reduced to an order of second. The capillary tube was heated to 80°C to prevent gas condensation to tube wall during gas transport. In order to determine the kinetic parameters of AP and propellants, sample heating rate of DTA were varied from 5°C/min. to 15°C/min.

2.3 Differential Thermal Analysis Using Gram Size Samples

Figure 1 shows a picture of the ISDTA with two cups for the sample and reference material (Al_2O_3). These cups were placed at the center of the furnace using alumina rods to minimize temperature gradients between the sample and reference material. The oven used in the ISDTA is a commercially available box furnace (Thermolyne type 1400) controlled using a digital temperature controller (Eurotherm Corporation model 808). Voltage outputs from the controller were fed into the computer for real time analysis. Type K thermocouples were placed at the bottom of both the sample and reference cups.
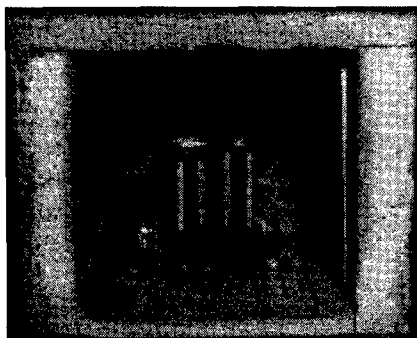
FIGURE 1. Intermediate Scale Differential Thermal Analyzer Setup.

The dimensions of the aluminum sample cups were 1.954 cm diameter, 0.0102 cm thick, and 0.432 cm height. The aluminum foil which covered the sample container was 0.00254 cm thick. The propellant sample was cut from a large block to ensure the surface chemical homogeneity. The sample weight was 1.00±0.05 grams and its dimensions were approximately 1.715 cm in diameter, 0.33 cm thick.

The oven was calibrated before testing the oven with any propellants with 200 µm diameter ammonium perchlorate (AP) particles with 0.2% TCP anti-caking inhibitor. The calibration tests were conducted at five heating rates at 3, 5, 7, 8, and 10 °C/min. The results of the linear curve fit for the ISDTA is shown in Table II. This table also shows a comparison of the kinetic parameters between the ISDTA and the small scale DTA. There was approximately a 6% difference for the kinetic parameters between the two tests. Due to stability problems for the second exotherm, ISDTA kinetic parameter results were unattainable at the same heating rates.

TABLE II. Kinetic Parameter Comparison Between DTA and ISDTA Experiments.

	E (kcal/mol)	A (1/s)
DTA	25.4	3.6×10^{10}
ISDTA	27.0	1.6×10^{11}

2.4   Thermal Expansion and Diffusivity Measurements

Linear dimensional changes of propellants were examined from room temperature to 200°C using thermomechanical analyzer (TMA, TA 2940). Thermal diffusivity measurements of propellants were obtained by using a technique developed by Parr [1] and the description of technique can be found in elsewhere [2].

3.0   RESULTS AND DISCUSSION

Differential thermal analysis of ABL 4863 AP (200μm dia.) revealed that AP has one endothermic at 242°C (T_{tr}) and two exothermic peaks at about 300 °C (T_1) and 460 °C (T_2). These results are in good agreement with the reported by K. J. Kraeutle [3]. Figure 2 shows our DTA thermogram and NH_3 gas ion intensity with respect to temperature. The first endothermic peak at 242°C signifies the reversible transition from the orthorhombic to the cubic modification which is attributed to the onset of free rotation of perchlorate anions. The first exotherm was a result of partial decomposition of AP and the second exotherms was associated with irreversible decomposition. The presence of NH_3 peaks at both the first and the second exotherms indicate that sublimation of AP concurred with each decomposition process. It can also be noticed that the occurrences of NH_3 ion peaks from RGA are slightly shifted to higher temperature from the temperatures where the exothermic peaks are found. This was probably due to the delay in response time of RGA. It also shows that the amount of temperature shift of the 2nd ion peak from T_2 was reduced compared to the amount of temperature shift of the 1st peak from T_1, indicating fast transport of hot gas through capillary tube.

The heating rate had a pronounced effect on the size and location of the large exotherms. They appeared at appreciably higher temperatures as the heating rate increased. As a result, the low temperature and the high temperature exotherms moved away from each other (Figure 3). Opposite effects were observed from the effect of pressure [3]. The exotherms appeared at appreciably lower temperature while the higher and lower exotherm moved closer together as the pressure increased. This suggests that the effect of heating rate on the sublimation and diffusion rates and hence on the rate of exothermically reacting NH_3 and $HClO_4$ was responsible for the observed change of the T_2-T_1 in Figure 3.
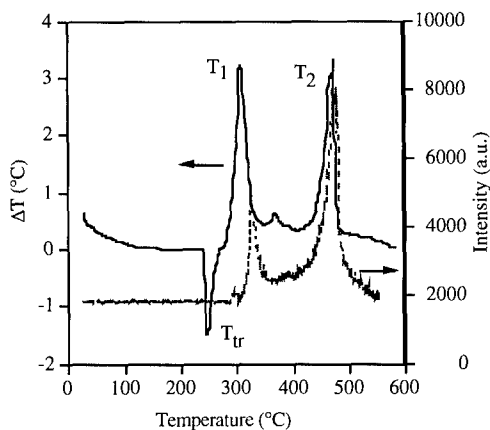
FIGURE 2. DTA thermogram of ABL 4863 AP and evolved NH_3 gas trace from RGA.
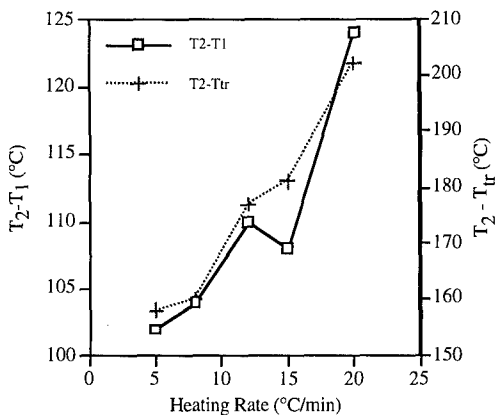
FIGURE 3. Temperature isotherm as a function of heating rate.

Assuming that the temperatures of the sublimation and decomposition are defined as the temperatures of the maximum of the peaks in each heating thermogram, are related to the heating rate by an Arrhenius type equation, the activation energy can be calculated:

$$\ln k = \ln k_o - (E/R)(1/T) \tag{1}$$

where k_o is pre-exponential factor. Figure 4 shows a plot of the experimental values of ln(heating rate) vs. $1/T_1$, the inverse of the temperature of either sublimation or decomposition temperature. From the slope of the best fit straight line, the activation energy and pre-exponential factor of 22 kcal/mol and $2.6 \times 10^9 sec^1$, respectively, were obtained. However, introducing T_2 in the equation (1), the Arrhenius-type

plot can be fitted to two straight lines that intersect at 2.25 which corresponds to a heating rate of 9.5°C/min. The different slopes are related to two different mechanisms, and activation energy values of 79 and 17 kcal/mol were respectively found for heating rates faster and lower than 9.5°C/min. Table III summarizes the results of kinetic parameters from both the first and the second exotherms.
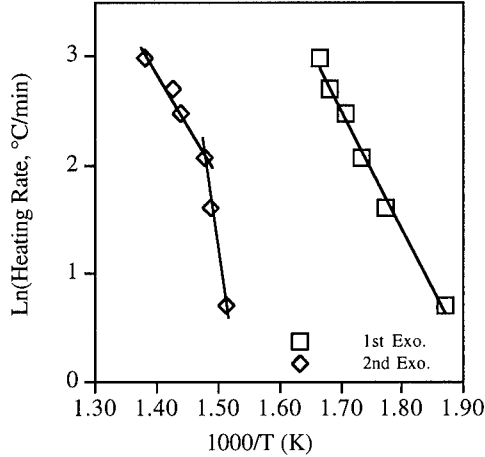
FIGURE 4. Ln(heating rate) vs. 1/T plot for AP from 1st and 2nd exothermic peaks.

TABLE III. Kinetic parameters for ABL4863 AP particles.

	E (kcal/mol)	A(1/sec)
1st exotherm.	22	2.6×10^{9}
2nd exotherm.	79, 17	1.5×10^{26}, 2.2×10^{6}

Figure 5 shows a thermograms of a series of AP/HTPB/Al based propellants with varying composition. All thermograms showed an endothermic peak at 242°C due to AP phase transition and an exothermic peak for decomposition at higher temperature. It can be seen that the decomposition of propellant E containing Fe_2O_3 showed extreme violent reaction and decomposed at significantly lower temperature than others. The results agree quite well with the work reported by Kishore et. al. [4] who postulated that transition metal oxides such as Fe_2O_3, Cr_2O_3, and MnO_2 promotes the electron transfer process during AP based propellant decomposition and affects the reaction rate in a similar fashion. Several reaction mechanisms have been proposed for the effects of catalysts on the decomposition of AP based composite propellants. However, analysis of reaction mechanisms on decomposition of the catalyzed propellants was beyond the scope of this work and the summary of the catalyst effects on the decomposition can be found in elsewhere [5].
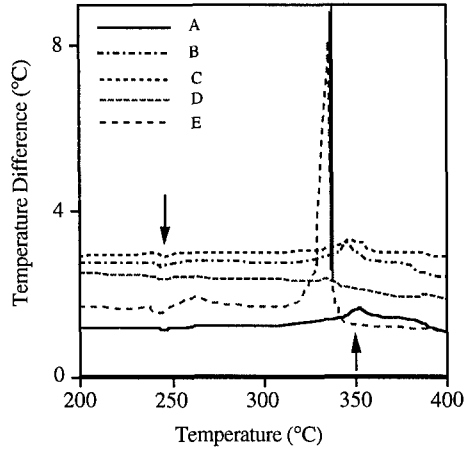
FIGURE 5. DTA thermograms of propellants.

Figure 6 shows ln(heating rate) vs. 1/T plot and kinetic parameters are summarized in Table IV. Low activation energy was observed for the propellant formulations with larger particle size of AP (propellant C) and propellant D which has 4% IDP as a plasticizer instead of 2% DOS compared to propellant A. Although the differences in kinetic parameters were observed for each propellant, present data do not strongly support the direct relationship between the differences in kinetic parameter and the differences in propellant concentration and particle size of AP.

Table IV. Kinetic parameters of AP/HTPB/Al propellants.

Propellants	E (kcal/mol)	A (1/sec)
A	45.2	9.2×10^{16}
B	44.5	6.1×10^{16}
C	38.8	9.4×10^{14}
D	40.7	8.2×10^{15}
E	51.9	9.8×10^{19}
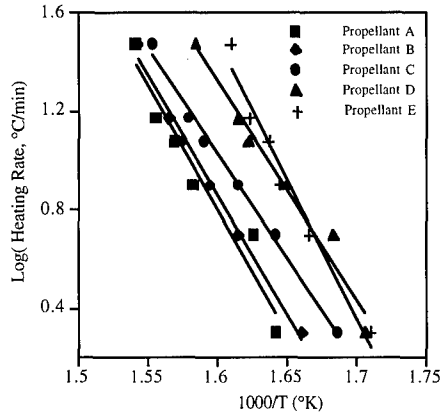
FIGURE 6. Ln(heating rate) vs. 1/T plot of AP/HTPB/Al propellants.

Figure 7 compares the ln (heating rates) versus 1/T for propellant B from both the ISDTA (One gram sample size) and the DTA (milligram sample size). This graph typifies the results for the AP/HTPB/Al propellant series. At three different heating rates (5-, 8-, 10°C/min.) the data from both tests shows a good fit to a straight line. The ISDTA propellant samples showed an earlier time to reaction temperature for each heating rate compared to the small scale test. When evaluating the kinetic parameters, the ISDTA gives a lower activation energy and with the exception of propellant A, a lower value for frequency factor. These results indicate that even using a one gram wafer sample has surface effects that must be taken into consideration before any kinetic parameters can be used from it. A milligram sample can be heated homogeneously, but as shown in the modeling section, the thermal model shows that at the 10°C/min. heating rate, there can be as much as 3°C gradient in a sample 0.33 cm thick.
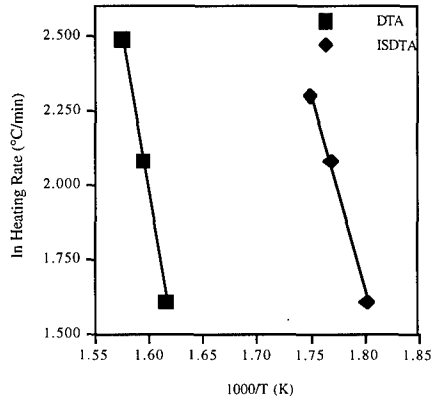
FIGURE 7. Ln (heating rate) vs. 1/T for the small scale DTA and ISDTA.

In addition to DTA analyses, other tests were conducted with the AP/HTPB/Al series of propellants for added test parameters. Figure 8 shows the thermal expansion behavior of propellants studied. All samples showed dimensional changes <1% up to 100°C except that propellant B showed pronounced shrinkage.
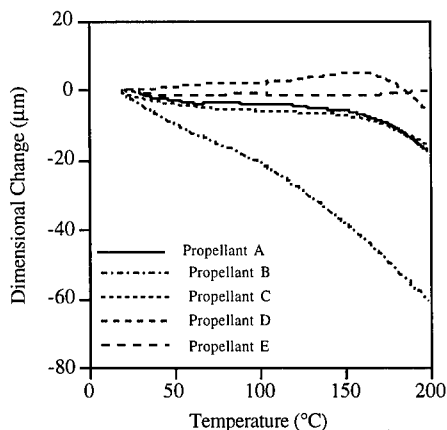
Figure 8. Thermal expansion behavior of propellants.

Table V summarizes the thermal diffusivity verses temperature data for the propellants. The thermal diffusivity decreases as temperature goes up and the value decreases in the order propellant B>E>C>A>D.

Table V. Thermal diffusivity (α x 10^{-3} cm²/sec) of AP and 5 propellants as a function of temperature.

A		B		C		D		E		AP	
T(°C)	α	T(°C)	α	T(°C)	α	T(°C)	α	T(°C)	α	T(°C)	α
27	2.6	26	3.1	24	3.1	24	2.6	25		24	1.3
49	2.7	49	3.0	47	2.9	49	2.6	51	3.1	38	1.2
74	2.6	75	2.9	74	2.6	74	2.4	75	2.9	55	1.1
91	2.5	89	3.0	87	2.6	87	2.0	86	2.7	70	1.1

The thermal diffusivity of propellants measured in this study also showed 2 to 3 times larger than AP. This increased diffusivity can possibly be attributed to the aluminum and porous structure of propellants as it was thermally reacted.

4.0 MODELING OF THE DIFFERENTIAL THERMAL ANALYZER USING ONE GRAM SAMPLES

The approach of this analysis emphasizes a coupled experimental and modeling methodology. The current thermal model of the ISDTA configuration uses the COYOTE II software developed by Sandia National Labs. COYOTE II [6,7] is a finite element computer program designed with built in chemical kinetics subroutine which accepts the chemical kinetic properties of the propellant. For the ISDTA experiment, a 2-dimensional model using first order reaction kinetics was used.

The COYOTE II model of the ISDTA experiment consists of the aluminum sample cup, propellant, and aluminum foil using both a coarse and fine grid. Figure 9 shows the configuration of the model where the right half of the picture shows the coarse grid (20 by 10 elements) of the propellant sample. The fine grid consists of doubling the number of elements (40 by 20). The coarse grid model used all five propellant samples heated at 2°C/min. and 10°C/min. heating rates while the fine grid model focused on propellant B heated at 2-, 5-, 8-, 10 °C/min. In order to conserve computational time, an axisymmetric geometry using this right half of the model was used. The dimensions of the model are the same dimensions described in the experimental section.
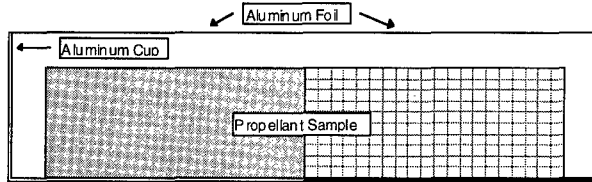
FIGURE 9. COYOTE II Model of Propellant Sample Cup.

The boundary conditions of any thermal model is a very important factor in computing accurate time to reaction results. The boundary conditions on the sample cup includes convection and radiation on all the outside surfaces as well as an enclosure radiation inside the sample cup. The same boundary conditions were applied to each of the propellants and each heating rate. Any difference in reaction time was due to the changes in the kinetic parameters, thermal conductivities, and densities of the propellant as well as the number of elements used. Figures 10 and 11 shows the temperature profiles at the reaction time of the right half of the model using propellant B heated at 10°C/min. and 2 °C/min. respectively.
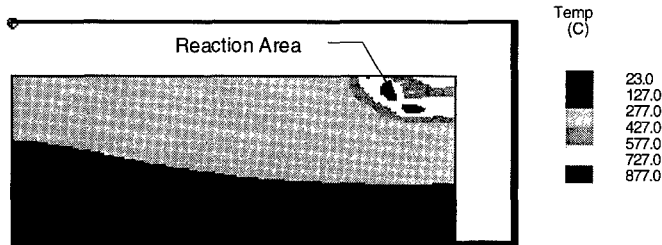
FIGURE 10. Temperature Profile of Propellant B at Time to Reaction. Heating Rate 10 °C/min.
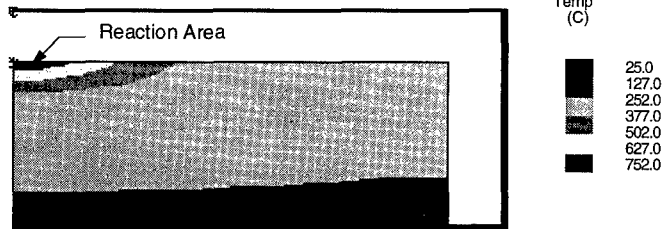
FIGURE 11. Temperature Profile of Propellant B at Time to Reaction. Heating Rate 2 °C/min.

As was stated in the experimental section, surface effects seemed to play a large part in affecting the kinetic parameters calculated in the ISDTA experiment. The results of the model also seems to verify this result. For both the 10 and 2°C/min. heating rate, the reaction occurs at or very close to the top surface of the propellant sample. Propellant B shows the typical temperature profile at the reaction time for all five propellants. At the highest heating rate, the reaction occurs at or near the surface of the propellant near the right hand corner. For the slowest heating rate, the reaction occurs closer to the center of the sample but again at the top surface.

Figure 12 shows the temperature gradient of propellant B heated at 10°C/minute. An approximate 3°C temperature gradient in the propellant was seen at this heating rate. The result shown here was typical for all five propellants being heated at 10°C/min. before any reaction occurs.
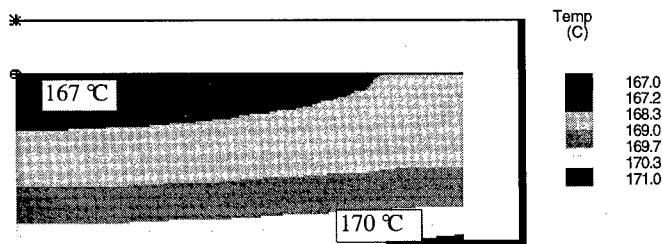
FIGURE 12. Temperature Gradient of Propellant B at 10 °C/min. heating rate.

At the current stage of model development, time to reaction is the primary computational output. The time to reaction results for the 10°C/min. and 2°C/min. heating rates for each propellant are compared to experimental values in Table VI.

TABLE VI. Coarse Grid Time to Reaction Comparison Results for 2- and 10°C/min.

| | Time to Reaction (min.) | | | |
| Propellant | 2 °C/min. | | 10 °C/min. | |
	Model	Experiment	Model	Experiment
A	99.0	not available	34.0	30.0
B	98.1	137.0	34.0	30.0
C	85.2	129.0	31.5	31.0
D	89.3	132.0	31.5	32.0
E	101.2	105.0	34.5	27.0

The results of the computer model showed that at the higher heating rate, the time to reaction calculated by COYOTE II was slightly overestimated and at the slowest heating rate, with the same boundary conditions, the calculated reaction time is greatly underestimated (with the exception of propellant E with the catalyst). At the slowest heating rate, a large number of calculations are required in determining time to reaction. This can incur round off or truncation errors. To check whether these errors greatly affected the calculated reaction time, modified COYOTE II models were conducted. These computer runs only increased the reaction time less than 10 minutes, indicating that other factors affecting the reaction time must be considered. These factors include a chemical kinetics model that is too simplified and boundary conditions that need to be modified due to the slowed heating rate.

The results between the coarse and fine grid models found that for every heating rate, refining the grid narrows the temperature range of the propellant sample at reaction time. For example, Figure 13 shows the temperature profile of the propellant with the coarse grid, while Figure 14 shows the temperature profile of the sample with the fine grid. Both pictures have the same temperature boundaries and were heated at the same rate - 8°C/min. As shown in the figures, the refined grid shows that a smaller portion of the propellant was at the same temperature compared to the propellant with the coarse grid.

Temp
(C)

347.0
427.0
507.0
587.0
667.0
747.0
827.0
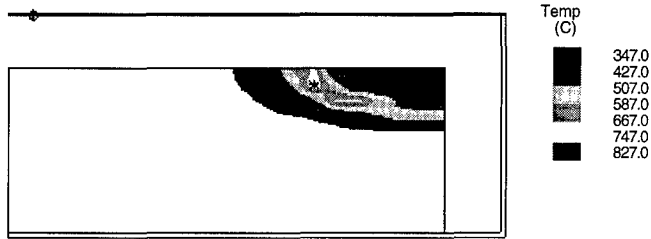
FIGURE 13. Temperature Profile of Sample Heated at 8°C/min. Using Coarse Grid

Temp
(C)

347.0
427.0
507.0
587.0
667.0
747.0
827.0
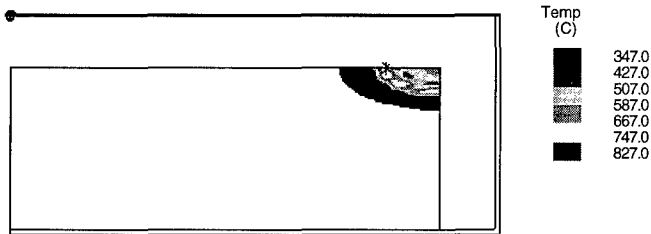
FIGURE 14. Temperature Profile of Sample Heated at 8°C/min. Using Fine Grid.

The time to reaction results for every heating rate and both grids are compared to experimental results in Table VII. Better reaction time predictions (3-10% error difference) were calculated at more intermediate heating rates (5 and 8°C/min.) for the fine grid. Similar results were found for the small scale DTA modeling effort which also found that these particular heating rates matched the experimental results the best. As with the first analysis at 2 and 10 °C, introducing a fine grid did not produce much better prediction times. Round off errors, especially for the slowest heating rate and finer grid, may continue to be a factor affecting the reaction time prediction. Because of the similarity in the results between the two different grids, these errors are most likely built into both models. Another factor when considering the differences in experimental reaction time and the models' predictions was the actual experimental setup of the test itself. The experiment had the thermocouple recording the changes in temperature at the bottom of the aluminum cup not on the sample. These temperature readings may be recording a later time compared to when the propellant was actually reacting.

TABLE VII. Comparison of Reaction Times Between Coarse and Fine Grids Using Propellant B.

Heating Rate (°C/min.)	Time to Reaction (min.)		
	Coarse Grid (20 X10 elements)	Fine Grid (40 X20 elements)	Experiment
2	99.8	99.6	137.0
5	53.6	55.2	57.0
8	33.1	34.3	38.0
10	34.4	34.7	30.0

Further analysis of this model will require modifications to the code. These modifications will enable an analysis of the temperature profiles of the propellant in the last few time steps leading up to the reaction. This will show how these profiles change in the sample until a decision is made that a reaction should occur.

5.0 SUMMARY AND CONCLUSIONS

Kinetic analysis of AP using DTA revealed that the first exotherm associated with partial decomposition of propellant yielded single reaction mechanism while the second exotherm associated with irreversible decomposition yielded two different reaction mechanisms. The decomposition behavior of propellants with varying concentration were characterized with single exotherm and decomposition occurred at about 340°C. The propellant with 400µm AP showed the lowest activation energy and the propellant with 1.2% Fe_2O_3 catalyst showed the highest activation energy among others by as much as 13 kcal/mol.

The results of the ISDTA experiments showed that the time to reaction at each heating rate occurs earlier compared to the small scale test. When kinetic parameters were derived from the ISDTA, it was found that for each propellant, the values were lower than the small scale DTA results. A few reasons for these results include that surface effects affected the one gram wafer sample or the sample was not heated homogeneously, causing the propellants to react earlier. These reasons made any comparisons between the small scale and intermediate scale test difficult because the tests were not similar enough for direct comparison of the data.

The ISDTA experiment was modeled using the thermal analysis code COYOTE II. The model showed that at the higher heating rates, there were thermal gradients in the propellant sample which supports the conclusions from the experimental results. The model used the small scale DTA kinetics to match time to reactions. The coarse grid modeling results showed close approximations for the highest heating rate (10°C/min.) but for the slowest heating rate (2°C/min.), the model greatly underestimates the reaction times. Comparisons between the coarse and fine grid models found that at the 5- and 8 °C/min. heating rates, the fine grid matched time to reaction closer to experimental results.

REFERENCES

1. D. M. Parr and T. P. Parr, "Condensed Phase Temperature Profiles in Deflagrating HMX", 20th JANNAF Combustion Meeting , CPIA Pub. 383, Vol. I, pp. 281-291, 1988.
2. I. Lee, F. E. Hudson and J. Covino, "Thermal Characterization of Solid Propellant Formulation," 1993 JANNAF Propulsion Systems Hazards Subcommittee Meeting, CPIA Publication 599, pp. 425-444, May 1993.
3. K. J. Kraeutle, "The Response of Ammonium Perchlorate to Thermal Stimulus," NAWCWPNS TP 7053, Naval Air Warfare Center, China Lake, Calif., 1990.
4   K. Kishore and M. R. Sunitha, "Effect of Transition Metal Oxides on Decomposition and Deflagration on Composite Solid Propellant Systems: A Survey," AIAA Journal, Vol. 17, pp. 1118-1125, Oct. 1979.
5   K. Kishore and V. Gayathri, "Chemistry of Ignition and Combustion of Ammonium-Perchlorate-Based Propellants," in Fundamentals of Solid-Propellant Combustion, edited by K. K. Kuo and M. Summerfield, Progress in Astronautics and Aeronautics, Vol. 90, p. 53, 1984.
6   David K. Gartling, Roy E. Hogan. "Coyote II - A Finite Element Computer Program for Nonlinear Heat Conduction Problems, Part I - Theoretical Background," SAND94-1173, Sandia National Laboratories, Albuquerque, New Mexico, October 1994.
7   David K. Gartling, Roy E. Hogan. "Coyote II - A Finite Element Computer Program for Nonlinear Heat Conduction Problems, Part II - User's Manual," SAND94-1179, Sandia National Laboratories, Albuquerque, New Mexico, October 1994.

A COMBUSTION MODEL FOR AN/HTPB-IPDI COMPOSITE SOLID PROPELLANTS

P. Carvalheira and J. Campos
Laboratório de Energética e Detónica, Departamento de Engenharia Mecânica, Faculdade de Ciências e Tecnologia da Universidade de Coimbra, Pólo II, Pinhal de Marrocos, P-3030 Coimbra, Portugal

G. M. H. J. L. Gadiot
TNO Prins Maurits Laboratorium, Lange Kleiweg 137, Postbus 45, 2280 AA Rijswijk, The Netherlands

ABSTRACT

A combustion model for solid composite propellants based in ammonium nitrate (AN) and hydroxyl terminated polybutadiene-isophorone diisocyanate (HTPB-IPDI) is presented. The model applies to propellants with unimodal spherical oxidizer particles. It is based on the classical concepts of multiple competitive flames and separate surface temperatures (SST). A new concept taking into account radiative heat transfer from the various flames and combustion products to the surface of oxidizer particles and binder of the propellant is applied. Radiative heat transfer is evaluated through consideration of the geometry and temperature of each flame, individual surface temperature, reflectivity of the oxidizer particles and fuel binder and emissivity of each flame. The preexponential factor of Arrhenius law, describing the kinetics of the monopropellant ammonium nitrate flame, is determined from experimental measurements of the monopropellant flame stand off distance at 7.0 MPa, using microthermocouples. A computer program based on this physical model was developed and allows to predict the effect of combustion chamber pressure, oxidizer particle size, oxidizer mass fraction and initial temperature of the propellant on burning rate. The model shows clearly the problems associated with partial combustion because the program attains no convergence for the pressure range when the propellant studied experimentally presents a large amount of tar in the strand burner nozzle exit after a test proving that the binder was not fully pyrolyzed. This is because in the model it is assumed that all the binder is pyrolyzed. The results of the combustion model are compared with experimental measurements of burning rates of AN/HTPB-IPDI (75.00/23.08-1.92 wt.%) and (80.00/18.46-1.54 wt.%) compositions, containing AN with an average particle size of 140 μm, and measured in a nitrogen vented strand burner in the pressure range 2-10 MPa. The AN used was phase stabilised with 1.0 wt.% NiO. The predicted results show a good agreement with the experimental measurements.

1. Introduction

This paper deals with the development of a combustion model for composite solid propellants based on ammonium nitrate (AN) and hydroxyl terminated polybutadiene (HTPB) cured with isophorone diisocyanate (IPDI) and of the results obtained. This model applies concepts introduced in previous combustion models for composite solid propellants and introduces a new concept. The most important classical concepts are the multiple competitive flames (MCF) concept introduced in the BDP model, (*vd.* Beckstead *et al.*, 1970), and the separate surface temperatures (SST) concept introduced by Andersen, (*vd.* Andersen *et al.*, 1959), and both applied by Beckstead in his SST combustion model, (*vd.* Beckstead, 1989).

The combustion model presented here takes into account the phenomena associated with radiative heat transfer from propellant flames and combustion products to the surface of the two main propellant ingredients, as a function of geometry and temperature of the flames and of propellant surface. This model is based on experimental data taken from a limited number of experimental measurements of burning rates in the range 2-10 MPa and temperature waves in AN/HTPB-IPDI propellants at 7.0 MPa. These measurements allowed to measure surface temperature of ammonium nitrate and AN flame stand-off distance.

2. Multiple competitive flames

The global equivalence ratio of the propellant is larger than one. In fact, for this type of propellants stoichiometry is obtained when the fuel binder mass fraction is about 5.8 %. AN/HTPB-IPDI composite solid propellants obtained in practice have a mass fraction of fuel binder in the range 17-30 %. Consequently, all the diffusion flames are fuel rich.

Three types of flames are considered. The first flame is a diffusion flame between the decomposition products of the oxidizer and the pyrolysis products of the fuel binder, *vd.* Fig. 1, called the primary flame. The second flame is the monopropellant flame of the ammonium nitrate oxidizer that results from the reaction among the decomposition products of ammonium nitrate. The third flame is a diffusion flame between the products of the monopropellant flame and the pyrolysis products of the fuel binder, called the final flame. The final flame only exists when the monopropellant flame of the oxidizer is present.
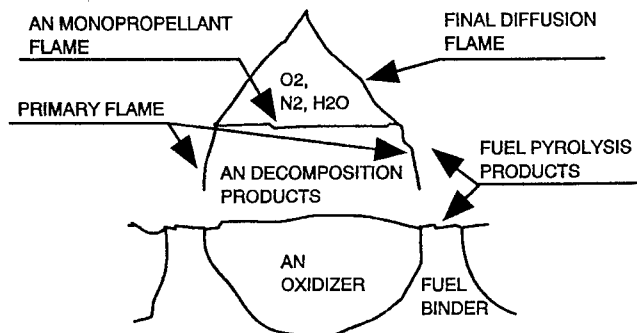
Figure 1. Multiple flames typical of the combustion of a composite solid propellant.

3. Propellant burning rate

In this model the burning rate is calculated considering the mass conservation equation in the form of Eq. (1) where r is the propellant burning rate

$$m_T = r\rho_P = m_{ox}(S_{ox} / S_0) + m_f(S_f / S_0) \tag{1}$$

In this model it is admitted that the geometry of the surface of the propellant is flat because we have no precise information regarding the shape of the surface of the oxidizer and of the binder and the flat surface assumption is the simplest, consequently Eqs. (2) and (3) apply.

$$\frac{S_{ox}}{S_0} = \zeta_{ox} \tag{2}$$

$$\frac{S_f}{S_0} = 1 - \zeta_{ox} \tag{3}$$

It is considered that the combustion of these propellants is controlled by the oxidizer due to the fact that fast thermolysis studies of ammonium nitrate in an Argon atmosphere revealed that the endotherm present at about 310 °C is replaced by an exotherm for pressures higher than 200 psi (1.36 MPa) (vd. Russel and Brill, 1989) while the pyrolysis of the fuel binder is endothermic. The mass flow rate per unit surface area of the oxidizer and of the fuel binder are given respectively by Eq. (4) and Eq. (5).

$$m_{ox} = A_{ox} \exp\left(-\frac{E_{ox}}{RT_{s,ox}}\right) \tag{4}$$

$$m_f = A_f \exp\left(-\frac{E_f}{RT_{s,f}}\right) \tag{5}$$

The surface temperature of the oxidizer is determined applying the principle of energy conservation to ammonium nitrate considering that there is no heat transfer to the fuel binder and is given by Eq. (6).

$$T_{s,ox} = T_0 + \frac{Q_{ox} + Q_{phc}\big|_{T_0}^{T_{s,ox}}}{c_{p,ox}} + \frac{(q_{c,ox} + q_{r,ox})}{c_{p,ox}m_{ox}} \tag{6}$$

The surface temperature of the fuel binder is obtained by a global energetic balance applied to a control volume that contains the propellant surface and extends to the inside of the propellant containing all the thermal affected zone of the propellant and is given by Eq. (7).

$$T_{s,f} = T_0 + \frac{Y_{ox}c_{p,ox}(T_0 - T_{s,ox}) + Q_{phc}\big|_{T_0}^{T_{s,ox}}}{Y_f c_{p,f}} + \frac{(q_{c,ox} + q_{r,ox})\zeta_{ox} + (q_{c,f} + q_{r,f})(1 - \zeta_{ox})}{\rho_P r Y_f c_{p,f}}$$
$$+ \frac{Q_{ox}Y_{ox} + Q_f Y_f}{Y_f c_{p,f}} \tag{7}$$

4. Heat release in the ammonium nitrate surface

The value assumed for this parameter is the enthalpy of reaction (8) at the temperature of the surface of the oxidizer.

$$NH_4NO_3 \rightarrow 2\ H_2O + NO + 1/2\ N_2 \tag{8}$$
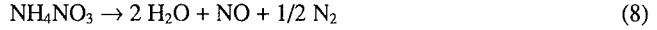
$$Q_{ox} = Q_{AN} = -\ \Delta H_R(T_{s,ox}) = -\ [H_p(T_{s,ox}) - H_r(T_{s,ox})] \tag{9}$$

which is given by Eq. (10)

$$Q_{AN}\ /(J/kg) = 333559 + (549.81\ .\ (T_{s,ox}/K)) \qquad 442.8\ K < T_{s,ox} < 550\ K \tag{10}$$

5. Heat of pyrolysis of the fuel binder surface

According to the bibliographic survey we have made the heat of pyrolysis of inert fuel binders of the type of HTPB are in the range 0 to -200 cal/g (0 to -836.8 kJ/kg), (vd. Beckstead et al., 1970). The value we found in the bibliography we gave more credit was an experimental measurement specifically for HTPB which value is -433 kJ/kg, (vd. Beck, 1987).

Later we verified that the enthalpy of vaporisation at 298.15 K, $\Delta_{vap}H(298.15\ K)$, of a very broad range of hydrocarbons with H/C in the range 1.25 < H/C < 1.75 was falling in the relatively narrow range of 382 kJ/kg < $\Delta_{vap}H(298.15\ K)$ < 408 kJ/kg, vd. Table 1. Because we are more interested in the value of $\Delta_{vap}H$ at the temperature of surface of the fuel binder we decided to verify if there was a correlation between the enthalpy of vaporisation at the boiling temperature of these hydrocarbons $\Delta_{vap}H(T_b)$ and the boiling temperature of these hydrocarbons. The hydrocarbons presented in Table 1 where chosen from a large list, (vd. Lide, 1991), with the sole criterion of having a H/C ratio as close to 1.5 as possible, which is the value of H/C for polybutadiene. For these hydrocarbons we found an excellent correlation between $\Delta_{vap}H(T_b)$ and T_b, which is represented by Eq. (11). In consequence, we considered that the value of the heat of pyrolysis of HTPB/IPDI fuel binder at the temperature of surface of the fuel binder in pyrolysis during combustion of the propellant, $Q_{p,f}$, is given by Eq. (12).

Table 1.
Enthalpy of vaporisation of selected hydrocarbons with H/C close to 1.5.

Molecular Formula	Name	Molecular weight (g/mol)	T_b /K	$\Delta_{vap}H(T_b)$ /(kJ/kg)	$\Delta_{vap}H(298.15\ K)$ /(kJ/kg)
C_4H_6	1,3-Butadiene	54.092	268.8	415.4	385.6
C_5H_8	Spiropentane	68.119	312.2	392.8	403.6
C_6H_{10}	Cyclohexene	82.145	356.3	370.8	407.4
C_8H_{10}	Ethylbenzene	106.17	409.3	335.04	397.9
C_8H_{14}	1-Octyne	110.20	399.5	325.14	383.9
$C_{10}H_{14}$	Butylbenzene	134.22	456.5	289.6	382.7

$$\Delta H_{vap}(T_b)/(kJ/kg) = 601.4 - 0.6709\ .\ (T_b/K) \tag{11}$$

$$Q_{p,f} = -\Delta H_{p,f}(T_{s,f})/(kJ/kg) = -601.4 + 0.6709\ .\ (T_{s,f}/K) \tag{12}$$
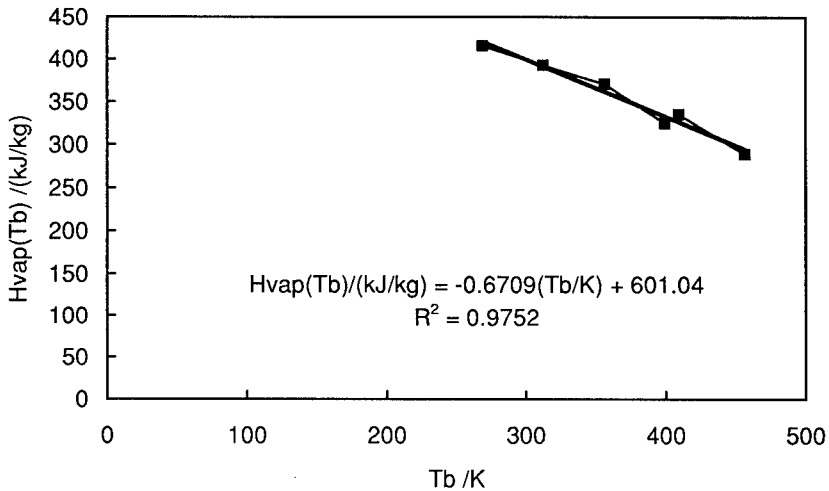
Fig. 2. Enthalpy of vaporisation at the boiling temperature of selected hydrocarbons with H/C close to 1.5.

6. Heat absorbed to heat up the ammonium nitrate from the initial temperature to the surface temperature.

The heat absorbed to heat up ammonium nitrate from the initial temperature to the surface temperature is composed of two parts. The first part is the sensible heat, $Q_{AN,sh}$. The second part is the heat absorbed in phase changes of ammonium nitrate, Q_{phc}. Table 2 presents the different phases of ammonium nitrate, without phase stabilising agents, respective values of c_p and density, in the temperature range from 233 K (- 40 °C) to 550 K (277 °C), (*vd.* Hendricks *et al.*, 1932; Feick, 1954; Fedoroff, 1960; Kolaczkowski, 1980; Grayson and Eckroth, 1983).

6.1. Sensible heat

Considering T_0 varying in the range 233.15 K (-40 °C) to 333.15 K (60 °C) we have:

$$Q_{AN,sh} = \left(\sum_{i=1}^{m} c_{p,i}(T_{u,i} - T_{lo,i}) \right) + c_{p,m+1}(T_{u,m+1} - T_0) + c_{p,l}(T_{s,ox} - T_{u,1}) \tag{13}$$

Refer to Table 2 and to the values of m given below.

$m = 4$ if 233.15 K $< T_0 <$ 255.15 K;
$m = 3$ if 255.15 K $< T_0 <$ 305.25 K;
$m = 2$ if 305.25 K $< T_0 <$ 333.15 K.

Table 2.
Ammonium nitrate phases

Phase	i	T /K	c_p /(J/kg.K)	ρ /(kg/m^3)
V	5	lower than 255.15	1523	1710
IV	4	255.15 - 305.25	1756	1725
III	3	305.25 - 357.35	1485	1661
II	2	357.35 - 398.35	1782	1666
I	1	398.35 - 442.75	2384	1594
liquid		higher than 442.75	2012	1381
Ref.		Grayson and Eckroth, 1983	Fedoroff, 1960	(Fedoroff, 1960), (Kolaczkowski, 1980)

The value of $c_{p,ox}$ used in Eqs. (6) and (7) is an average value of c_p and is calculated with Eq. (14).

$$c_{p,ox} = \frac{Q_{AN,sh}}{(T_{s,ox} - T_0)} \qquad (14)$$

6.2. Heat of phase changes

The heat absorbed in ammonium nitrate phase changes between T_0 and $T_{s,ox}$ is given by Eq. (15).

$$Q_{phc}\Big|_{T_0}^{T_{s,ox}} = \sum_{j=1}^{n} Q_{phc,j} \qquad (15)$$

Referring to Table 3 the values for n are the following:

$n = 5$ if 233.15 K $< T_0 <$ 255.15 K;
$n = 4$ if 255.15 K $< T_0 <$ 305.25 K;
$n = 3$ if 305.25 K $< T_0 <$ 333.15 K.

Table 3 presents the temperature and enthalpy of each phase change of ammonium nitrate, (*vd.* Hendricks, 1932; Fedoroff, 1960).

Table 3.
Phase changes of ammonium nitrate

Phase	j	T /K	Q_{phc} /(kJ/kg)	Ref.
V → IV	5	255.15	6.69	(Hendricks, 1932)
IV → III	4	305.25	19.86	(Fedoroff, 1960)
III → II	3	357.35	16.73	(Fedoroff, 1960)
II → I	2	398.35	52.79	(Fedoroff, 1960)
I → liquid	1	442.75	67.96	(Fedoroff, 1960)

7. Heat absorbed to heat up the fuel binder from the initial temperature to the surface temperature

The heat absorbed to heat up the fuel binder from the initial temperature to the surface temperature is given by Eq. (16).

$$Q_{f,hs} = c_{p,f}(T_{m,f}) \ (T_{s,b} - T_0) \tag{16}$$

where $c_{p,f}(T) = 6.742 \ T$ from data in (Brandrup and Immergut, 1975)   (17)

$$T_{m,f} = (T_{s,f} + T_0)/2 \tag{18}$$

8. Ammonium nitrate monopropellant flame

8.1. Flame temperature

The temperature of the monopropellant flame of ammonium nitrate depends on pressure and its value was calculated using an equilibrium thermodynamic code in isobaric adiabatic thermodynamic equilibrium with equation of state H9 (*vd.* Heuzé, 1985). Afterwards, a polynomial interpolation was performed to the temperatures obtained as a function of pressure whose equation is valid in the range 0.1-100 MPa.

$$T_{FAN}[K] = 1266.3 - 3.1190 \times 10^{-1} p[bar] + 1.4240 \times 10^{-4} p[bar]^2 - 4.7422 \times 10^{-8} p[bar]^3$$
$$r^2 = 0.99999 \tag{19}$$

8.2. Ammonium nitrate monopropellant flame distance

In the monopropellant flame the total distance of the flame to the surface of ammonium nitrate surface is only the kinetic reacting distance. This distance, x_{FAN}, is given by Eq. (20). It is assumed $\delta = 2.0$ because it is admitted that the reaction is a second order reaction

$$x_{FAN} = \frac{m_{AN}}{P^\delta \ A_{FAN} \ \exp\left(-\dfrac{E_{FAN}}{RT_{FAN}}\right)} \tag{20}$$

$$k_{FAN} = A_{FAN} \ \exp\left(-\frac{E_{FAN}}{RT_{FAN}}\right) \tag{21}$$

For the monopropellant AN flame the activation energy was considered to be $E_{FAN} = 104.6$ kJ/mol (25 kcal/mol), (*vd.* Beckstead, 1989). The preexponential factor, A_{FAN} , was calculated based in the flame stand-off distance measured experimentally for the monopropellant flame at known combustion pressure, burning rate, initial temperature of propellant, oxidizer particle size, oxidizer solid loading and with no burning rate modifier included in the composition, *vd.* Fig. 3.
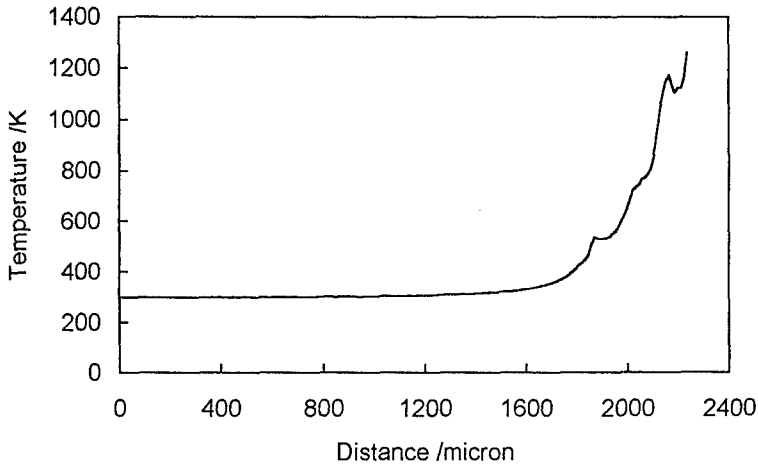
Fig. 3. Temperature wave profile of a burning PSAN/HTPB-IPDI(75.00/23.08-1.92 wt.%) propellant at 7.0 MPa, measured with a 12.7 μm in diameter K type microthermocouple with 25 μm bead diameter used to determine x_{FAN}. $T_0 = 298$ K and for PSAN $d_{50} = 140$ μm.

9. Primary and final diffusion flames

It is admitted that at the elevated heating rates of the fuel binder surface as those typical of the combustion of propellants, all the fuel binder decomposes in 1,3-butadiene (C_4H_6) according to: the tendency observed in the bibliography for the thermal decomposition of polybutadiene between low heating rates (10 K/min) and high heating rates (100 K/min) (vd. Brazier and Scwartz, 1978); the results of SMATCH/FTIR spectroscopy of HTPB and HTPB-IPDI at 250-350 ºC/s heating rate, where the IR spectrum of the gases liberated from the polymer film reveals that only butadiene, vinylcyclohexene, CH_2O, an isocyanate, and CO_2 are formed on rapid thermolysis (vd. Chen and Brill, 1991).

Thermodynamic calculations we made indicate that in the temperature range 625-1054 K, in the primary diffusion flame, in the side of AN the composition of the gases is: H_2O mole fraction is 2/3 and N_2O mole fraction is 1/3. This is the composition of the gases we assumed representative in the primary diffusion flame in the side of AN.

9.1. Flame temperature

9.1.1. Temperature of primary diffusion flame

This flame results from the reaction between the decomposition products of ammonium nitrate before reacting in the monopropellant flame and the pyrolysis products of the fuel binder. It is admitted that in this flame there is not enough time for the formation of CO_2 (vd. Beckstead, 1989) and the flame temperature was calculated suppressing the formation of CO_2.

The maximum temperature of the primary flame with CO_2 formation suppressed depends on pressure and is verified for an equivalence ratio different from 1.0. The variation in maximum temperature with pressure is small. Its value was calculated using an equilibrium thermodynamic computer code with equation of state H9, (*vd.* Heuzé, 1985). Afterwards, a polynomial interpolation was made for the temperatures obtained as a function of pressure, valid for the pressure range 1-10 MPa, viz.:

$$T_{PF}[K] = 2092.3 + 4.6470 \times 10^{-1} p[bar] - 7.6305 \times 10^{-3} p[bar]^2 + 3.5640 \times 10^{-5} p[bar]^3$$
$$r^2 = 0.97345 \tag{22}$$

The maximum temperature for this flame falls in the range 2096 K to 2100 K for the pressure range 1 to 10 MPa and corresponds to an equivalence ratio in the range 1.194 to 1.191. This temperature is different from the temperature of 2000 K for this flame, calculated by other authors (*vd.* Beckstead, 1989).

9.1.2. Temperature of final diffusion flame

This flame results from the reaction between the products of the monopropellant flame of ammonium nitrate and the pyrolysis products of the fuel binder. It is assumed on fact that in this flame there is enough time for the formation of CO_2 (*vd.* Beckstead, 1989) and the flame temperature was calculated as the thermodynamic equilibrium temperature. The maximum temperature for this flame is about 2350 K in the pressure range 1 to 10 MPa which corresponds to an equivalence ratio of 1.00. This temperature is the same as calculated by other authors (*vd.* Beckstead, 1989).

9.2. Flame distances

In the primary flame the total distance of the flame to the surface of ammonium nitrate is the sum of the kinetic distance of reaction, $x_{PF,k}$, with the diffusion distance, $x_{PF,d}$. The kinetic distance of reaction, $x_{PF,k}$ is understood in this model as the distance that the products of decomposition of the oxidizer and the products of pyrolysis of the fuel that already began to diffuse into one another along their interface, need to ignite. From that point the combustion process is limited by diffusion processes. The diffusion distance of the flame will account for the influence of combustion on the total flame distance. A kinetic distance is not considered for the final flame because when this flame is formed the gases are already burning and no ignition is needed. The only height considered for this flame is the diffusion distance.

9.2.1. Primary flame reacting kinetic distance

The kinetic distance of reaction, $x_{PF,k}$ is calculated using the concept of ignition delay, τ, of a mixture hydrocarbon-air according to the work of Spadaccini and TeVelde, (*vd.* Spadaccini and TeVelde, 1982). We will use the results of their measurements in a steady flow reactor with uniform mixture and flow, with Diesel fuel No.2, in the temperature range 650-900 K, pressure range 10-30 atm and fuel/air equivalence ratio ϕ varied from 0.3 to 1.0. The expression that Spadaccini and TeVelde obtained for the ignition delay is equivalent to Eq. (23) in SI units.

$$\tau = \left[A\, p^n \exp\left(-\frac{E_A}{RT} \right) \right]^{-1} \tag{23}$$

with $n = 2$, $A = 40.08$ Pa^2/s, $\dfrac{E_A}{R} = 20915$ K, p in Pa, T in K, τ in s

Because the temperature of the gases is increasing when the gases resulting from the decomposition of ammonium nitrate and from the pyrolysis of the fuel binder leave and move away from the propellant surface, we used the following calculation procedure to determine the ignition distance from the surface and the ignition temperature.

First of all we assumed that the temperature of the gases diffusing into one another at the interface between the decomposition gases of ammonium nitrate and the pyrolysis products of the fuel binder was increasing linearly with the distance from the surface of ammonium nitrate according to Eq. (24).

$$T_g(x) = T_{s,AN} + \frac{(T_{FAN} - T_{s,AN})}{x_{FAN}} x \tag{24}$$

The velocity of the gases, v, at certain distance from the surface of ammonium nitrate, x, is obtained from continuity and the perfect gas law and is given by Eq. (25).

$$v(x) = \frac{m_{AN}\, R_u\, T_g(x)}{p W_g} \tag{25} \qquad \text{where} \qquad W_g = \frac{W_{AN}}{\left(\dfrac{n_p}{n_r} \right)} \tag{26}$$

The temperature of the gases of decomposition of ammonium nitrate between the surface and the point of ignition of the primary flame is in the range 500-900 K, consequently according to reaction (8) $(n_p/n_r) = 3.0$.

The distance from the flame to the surface of ammonium nitrate, x_{FAN}, was then divided in small increments, dx_{FAN}, vd. Eq. (27). In the computer program we have chosen $n = 1000$ to have an increment in distance that is small enough because it is equal to 0.1 % of the ammonium nitrate monopropellant flame distance.

$$dx_{FAN} = \frac{x_{FAN}}{n} \tag{27}$$

When the gases are moving along this small increment $x_{k,i}$ is calculated, which is the distance that the gases would need to move in order to ignite at the local temperature and pressure and a nondimensional advance of reaction, $x_{b,i}$, is calculated according to Eq. (29). The same is made for the next following increments, dx_{FAN}.

$$x_{k,i} = v_i\, \tau_i \tag{28} \qquad\qquad\qquad x_{b,i} = \frac{dx_{FAN}}{x_{k,i}} \tag{29}$$

$$b_k = \sum_{i=1}^{k} x_{b,i} \text{ with } k \leq n \tag{30}$$

When the sum of the nondimensional advances of reaction, b_k, equals 1.0 we consider ignition to have occurred and the corresponding distance, x_{ign}, and gas temperature, T_{ign}, are respectively the ignition distance and the ignition temperature.

$$x_{ign} = k.dx_{FAN} \qquad (31) \qquad\qquad T_{ign} = T_{s,AN} + \frac{(T_{FAN} - T_{s,AN})}{x_{FAN}} x_{ign} \qquad (32)$$

The kinetic distance of the primary flame, $x_{PF,k}$, is equal to this ignition distance x_{ign}.

$$x_{PF,k} = x_{ign} \tag{33}$$

9.2.2. Final flame reacting kinetic distance

According to equations presented in paragraph 9.2.1 at the temperature of the primary flame this distance is so small that it has no physical meaning. Physically this corresponds to the situation that at the temperature of the primary flame in the edge between the primary flame, the ammonium nitrate monopropellant flame and the final flame, the flame already exists so there is no need for ignition.

9.2.3. Primary flame and final flame diffusion distances

The height of the primary flame includes two terms. The first term is the kinetic height and is the distance that the reactant gases displace to ignite. The second term is the diffusion height and is the distance that the reactant gases displace to diffuse completely into each other at the initial temperature of the reactants. For the final flame only the diffusion height is considered for the total height of the final flame because ignition has already occurred. The geometry of the primary and final diffusion flames is determined according to the analysis of diffusion flames of Burke-Schumann, (*vd.* Burke and Schumann, 1928; Kuo, 1986), with some adaptations to the particularities of the structure of this diffusion flame. One of the modifications done to the classical approach of the problem is related to the fact that in the classical approach always a central fuel gaseous jet is surrounded by an annular gaseous jet of oxidizer, while in our problem we have a central jet of oxidising gas species resultant from the decomposition of ammonium nitrate surrounded by a annular jet of fuel gas resulting from the pyrolysis of the fuel binder. In consequence, in the expression of v obtained by the classical approach we interchanged the terms related to the oxidizer with the terms related with the fuel. Eq.(38). The equations of the development of Burke and Schumann used in the calculation of the diffusion flame geometry are presented in the following. First we introduce the dimensionless coordinates.

The dimensionless flame radius is given by Eq. (34). The dimensionless flame height is given by Eq. (35).

$$\xi = \frac{r}{r_s} \qquad (34) \qquad\qquad\qquad \eta = \frac{z\mathcal{D}}{v_z r_s} \qquad (35)$$

The geometric locus of the points that define the flame surface $\eta = f(\xi)$ is given by Eq. (36) when we make $\gamma = 0$, (vd. Kuo, 1986).

$$\gamma = (1+\nu)C^2 - \nu + 2(1+\nu)C \sum_{n=1}^{\infty} \frac{1}{\phi_n} \frac{J_1(C\phi_1)}{[J_0(\phi_n)]^2} J_0(\phi_n \xi) \exp(-\phi_n^2 \eta) \tag{36}$$

where ϕ_n represents successive roots of the equation $J_1(\phi) = 0$, with ordering convention $\phi_n > \phi_{n-1}$, $\phi_0 = 0$, (vd. Kuo, 1986). J_0 and J_1 are the Bessel functions of first kind respectively of order 0 and order 1 (vd. Lide 1991). r_j is the radius of the internal jet (oxidizer) for $z = 0$, r_s is the radius of the external jet (fuel) for $z = 0$

$$C = \frac{r_j}{r_s} \tag{37}$$

$$\nu = \frac{(Y_F)_{z=0} W_O \nu'_O}{(Y_O)_{z=0} W_F \nu'_F} \tag{38}$$

For the primary flame it was considered

$$C = \left(1 + \frac{1-\zeta}{\zeta}\right)^{-\frac{1}{2}} \tag{39}$$

$$r_j = \frac{D}{2} \tag{40}$$

$$D = \sqrt{\frac{2}{3}} D_0 \tag{41}$$

There are two possible solutions for Eq. (36). The first solution corresponds to the situation where the flame closes over the oxidizer particle and the second solution to the situation where the flame closes over the fuel binder. These conditions correspond to the fuel rich and oxygen rich conditions, respectively. The flame that closes over the oxidizer particle is the flame that suits the type of propellants that interests us because AN/HTPB-IPDI propellants are fuel rich when the fuel binder content is larger that 5.8 wt.% and in unimodal propellants with spherical particles of oxidizer the fuel binder content is larger than or equal to 16 wt.% for AN/HTPB-IPDI propellants. To determine for which condition to solve the term (42) included in Eq. (36) is examined, (vd. Blomshield, 1989).

$$\frac{\nu - (1+\nu)C^2}{2(1+\nu)} \tag{42}$$

If this term is positive Eq. (36) can only be solved if $\xi = 0$, the flame closes over the oxidizer particle. If this term is negative Eq. (36) can only be solved if $\xi = 1$, the flame closes over the fuel binder. Whatever is the case the solution of the equation is iterative in nature and terms in the series are used until they become very small (vd. Blomshield, 1989). In our program we retained the terms until $n = 6$, included.

To determine the primary flame diffusion height Eq. (36) is solved for $\xi = 0$ and the η obtained is applied in Eq. (43), with $\mathcal{D} = \mathcal{D}_{N_2OC_4H_6}$, calculated at the temperature of surface of ammonium nitrate and combustion pressure, to obtain the primary flame diffusion height, $x_{PF_d} = z$.

$$z = \frac{\eta \, v_z r_s}{\mathcal{D}} \tag{43}$$

To determine D_{FAN} Eq. (36) is solved for $\eta = \eta_{FAN}$, vd. Eq. (44), to obtain $\xi = \xi_{FAN}$ from which D_{FAN} is obtained by Eq. (45).

$$\eta_{FAN} = \frac{(x_{FAN} - x_{PF,k})\mathcal{D}}{v_z r_s} \tag{44}$$

$$D_{FAN} = \xi_{FAN} \frac{D}{C} \tag{45}$$

To determine the final flame diffusion height Eq. (36) is solved for $\xi = 0$ and the η obtained is applied in Eq. (43), with $\mathcal{D} = \mathcal{D}_{O_2 C_4 H_6}$, calculated at the temperature of the ammonium nitrate monopropellant flame and the combustion pressure, to obtain the final flame diffusion height, x_{FFD}, which is also the final flame total height, x_{FF}, $x_{FF,d} = x_{FF} = z$.

According to several authors, (vd. Kuo, 1986; Burke and Schumann, 1928), the flame height obtained by Burke and Schumann are surprisingly in good agreement with experimental results given the drastic character of some of the assumptions made in the modelling.

9.2.3.1. Molecular interdiffusion coefficients

The molecular interdiffusion coefficients between two non polar molecular species A and B are calculated according to the ordinary diffusion theory for gases at low density using Eq. (46), (vd. Kuo, 1986). This equation allows to calculate these coefficients with a maximum error of 5 %, according to the kinetic theory of gases, (vd. Kuo, 1986).

$$\mathcal{D}_{AB} = \frac{2}{3} \left(\frac{K^3}{\pi^3} \right)^{1/2} \left(\frac{1}{2m_A} + \frac{1}{2m_B} \right)^{1/2} \frac{T^{3/2}}{p\left(\frac{d_A + d_B}{2} \right)^2} \tag{46}$$

$$m_i = \frac{M_i}{N_A} \tag{47} \qquad\qquad d_i = \sqrt[3]{\frac{b}{N_A}} \tag{48}$$

$m_{O_2} = 5.3135E\text{-}26$ kg, using Eq. (47), $d_{O_2} = 3.50E\text{-}10$ m, (vd. Mahan 1975).

$m_{N_2O} = 7.3085E\text{-}26$ kg, using Eq. (47); $d_{N_2O} = 4.188E\text{-}10$ m, calculated from the value of the van der Waals co-volume of NO_2, $b = 4.424E\text{-}05$ m³/mol, (vd. Lide, 1991), using Eq. (48).

$m_{C_4 H_6} = 8.9823E\text{-}26$ kg, using Eq. (49); $d_{C_4 H_6} = 5.883E\text{-}10$ m, calculated from the value of the van der Waals co-volume of n-butane, $C_4 H_{10}$, $b = 1.226E\text{-}04$ m³/mol, (vd. Lide, 1991), that was admitted equal to that of butadiene, $C_4 H_6$, using Eq. (48).

Using Eqs. (46) to (48) the following molecular interdiffusion coefficients are obtained taking into account the composition admitted for the reactants in each flame.

$$\mathcal{D}_{N_2OC_4H_6} = 8.5328\text{E-05}\ \frac{T^{3/2}}{p} \qquad (49) \qquad \mathcal{D}_{O_2C_4H_6} = 1.0800\text{E-04}\ \frac{T^{3/2}}{p} \qquad (50)$$

10. Criterion for the competition of flames

The criterion for the existence of one or three flames are the following. When x_{PF} is smaller than x_{FAN} we have only primary flame. When the opposite is verified we will have primary flame, monopropellant flame of ammonium nitrate and final flame. The parameter, β_F, is defined now, that first appeared in the original BDP model, related to the competition between flames that represents the mass fraction of the oxidizer that is consumed in the primary flame. Obviously, when only the primary flame exists $\beta_F = 1.0$. β_F is defined by Eq. (51) when the three flames exist simultaneously.

$$\beta_F = \frac{D^2 - D_{FAN}{}^2}{D^2} \qquad (51)$$

11. Conductive heat transfer

11.1. Heat transferred by conduction to the oxidizer

The heat flux from the primary flame to the surface of the oxidizer is given by Eq. (52).

$$q_{c,PF,ox} = \beta_F\ \frac{2\lambda_{g,ox,PF}\ (T_{PF} - T_{s,ox})}{(x_{PF} + x_{PFK})} \qquad (52)$$

$$\lambda_{g,ox,PF} = \lambda_{g,ox}(T)\ \text{ with } T = T_{s,\,ox} \qquad (53)$$

The heat flux from the monopropellant flame of the oxidizer to the surface of the oxidizer is given by Eq. (54).

$$q_{c,FAN,ox} = (1 - \beta_F)\ \frac{\lambda_{g,ox,FAN}\ (T_{FAN} - T_{s,ox})}{x_{FAN}} \qquad (54)$$

$$\lambda_{g,ox,FAN} = \lambda_{g,ox}(T)\ \text{ with } T = T_{s,\,ox} \qquad (55)$$

11.2. Heat transferred by conduction to the fuel binder

Heat flux from the primary flame to the surface of the fuel binder is given by Eq. (57) for the case that only the primary flame exists.

$$q_{c,PF,f} = \frac{2\lambda_{g,f,PF}\ (T_{PF} - T_{s,f})}{(x_{PF} + x_{PFK})} \qquad (57)$$

Heat flux from the primary flame to the surface of the fuel binder is given by Eq. (58) for the case that the three flames exists.

$$q_{c,PF,f} = \frac{2\lambda_{g,f,PF}(T_{PF} - T_{s,f})}{(x_{FAN} + x_{PFK})} \tag{58}$$

$$\lambda_{g,f,PF} = \lambda_{g,f}(T) \text{ with } T = T_{s,f} \tag{59}$$

Obviously, in the combustion conditions where there is neither the formation of the monopropellant ammonium nitrate flame neither the formation of the final flame that develops from the previous flame, the conductive heat transfer terms from these flames are zero.

12. Radiative heat transfer

For these propellants radiative heat transfer does dependend, among other factors, on the emmissivity of flames. The emmissivity of flames is mainly dependent on the temperature of gases and on the size and concentration of the solid particles dispersed in the gas, *e.g.* soot, burning rate modifier micrometric particles, (*vd.* Siegel and Howell, 1972). In the following, the procedure for the calculation of the flame emissivity was not yet included. Calculations made until now indicate that the most important contribution is from the final products of combustion of the propellant.

The radiative heat flux from the primary flame to the surface of the oxidizer is given by Eq. (60).

$$q_{r,PF,ox} = (1 - \rho_{ox})\varepsilon_{PF,ox}F_{ox,PF}\sigma(T_{PF}^4 - T_{s,ox}^4) \tag{60}$$

The radiative heat flux from the monopropellant flame of the oxidizer to the surface of the oxidizer is given by Eq. (61).

$$q_{r,FAN,ox} = (1 - \rho_{ox})\varepsilon_{FAN,ox}F_{ox,FAN}\sigma(T_{FAN}^4 - T_{s,ox}^4) \tag{61}$$

The radiative heat flux from the flame of the propellant to the oxidizer surface is given by Eq. (62).

$$q_{r,FP,ox} = (1 - \rho_{ox})\varepsilon_{FP,ox}F_{ox,FP}\sigma(T_{FP}^4 - T_{s,ox}^4) \tag{62}$$

The total radiative heat flux to the oxidizer surface is given by Eq. (63).

$$q_{r,ox} = q_{r,PF,ox} + q_{r,FAN,ox} + q_{r,FP,ox} \tag{63}$$

The radiative heat flux from the primary flame to the surface of the fuel binder is given by Eq. (64).

$$q_{r,PF,f} = (1-\rho_f)\varepsilon_{PF,f} F_{f,PF} \sigma (T_{PF}^4 - T_{s,f}^4) \qquad (64)$$

The radiative heat flux from the flame of the propellant to the surface of the fuel binder is given by Eq. (65).

$$q_{r,FP,f} = (1-\rho_f)\varepsilon_{FP,f} F_{f,FP} \sigma (T_{FP}^4 - T_{s,f}^4) \qquad (65)$$

The total radiative heat flux to the surface of the fuel binder is given by Eq. (66).

$$q_{r,f} = q_{r,PF,f} + q_{r,FP,f} \qquad (66)$$

Obviously, in the combustion conditions where there is neither the formation of the monopropellant flame of ammonium nitrate nor the formation of the final flame that develops from the previous flame, the terms relative to the radiative and conductive heat fluxes from these flames are zero.

13. View factors of radiative heat transfer

The view factor of a disk 1 to a disk 2 parallel with centers along the same normal and separated by a distance h is given by Eq. 67, (vd. Siegel and Howell, 1972).

$$F_{1-2} = \frac{1}{2}\left[X - \sqrt{X^2 - 4\left(\frac{R_2}{R_1}\right)^2} \right] \qquad (67)$$

$$R_1 = \frac{r_1}{h} \qquad (68) \qquad\qquad R_2 = \frac{r_2}{h} \qquad (69) \qquad\qquad X = 1 + \frac{1+R_2^2}{R_1^2} \qquad (70)$$

The following expressions were used to calculate the view factors.

I) existing only primary flame

The view factor from the surface of the oxidizer to the own primary flame, $F_{ox,PF}$, is given by Eq. (67) with $h = x_{PF,k}$, $r_1 = D/2$ and $r_2 = D/2$.
The view factor from the surface of the oxidizer to the flame of the propellant is given by Eq. (71). D_f is the equivalent diameter of the fuel binder and is given by Eq. (72).

$$F_{ox,FP} = 1 - F_{ox,PF} \qquad (71) \qquad\qquad\qquad D_f = D\left(\frac{\zeta_f}{\zeta_{ox}}\right)^{1/2} \qquad (72)$$

The view factor from the surface of the fuel binder to the propellant flame of the propellant, $F_{f,FP}$, is given by Eq. (67) with $h = x_{PF,k}$, $r_1 = D_f/2$ and $r_2 = D_f/2$.
The view factor from the surface of the fuel binder to the primary flame, $F_{f,PF}$, is given by Eq. (73).

$$F_{f,PF} = 1 - F_{f,FP} \qquad (73)$$

II) existing primary flame, ammonium nitrate monopropellant flame and final flame.

Due to the facts that according to the work of Spadaccini and TeVelde the ignition of a hydrocarbon in air has a very high activation energy (173898 J/mol), that it occurs in the range 600-900 K, that we have verified in our modelization that it occurs in general at about 800 K, which is shown by the shape of the temperature wave measurement of the burning propellant at 7.0 MPa in Figure 2, and because either the primary flame temperature (about 2100 K) and the ammonium nitrate monopropellant flame temperature (about 1250 K) are much larger than 800 K it is highly improbable physically that $x_{FAN} \leq x_{PF,k}$, hence, this situation will not be considered in the following analysis.

It will always be considered in the following analysis that $x_{FAN} > x_{PF,k}$

View factor from the oxidizer surface to the monopropellant flame of ammonium nitrate, $F_{ox,FAN}$, is given by Eq. (67) with $h = x_{FAN}$, $r_1 = D/2$ and $r_2 = D_{FAN}/2$.

View factor from the oxidizer surface to the primary flame, $F_{ox,PF}$, is given by Eq. (74), where $F_{ox,PF+FAN}$, is given by Eq. (67) with $h = x_{PF,k}$, $r_1 = D/2$ and $r_2 = D/2$.

$$F_{ox,PF} = F_{ox,PF+FAN} - F_{ox,FAN} \qquad (74)$$

View factor from the oxidizer surface to the flame of the propellant, $F_{ox,FP}$

$$F_{ox,FP} = 1 - F_{ox,FAN} - F_{ox,PF} \qquad (75)$$

View factor from the fuel binder surface to the flame of the propellant, $F_{f,FP}$, is given by Eq. (67) with $h = x_{PF,k}$, $r_1 = D_f/2$ and $r_2 = D_f/2$.

View factor from the fuel binder surface to the primary flame, $F_{f,PF}$, is given by Eq. (76).

$$F_{f,PF} = 1 - F_{f,FP} \qquad (76)$$

14. Reflectivity of the surfaces of propellant components

14.1. Surface reflectivity of ammonium nitrate

For ammonium nitrate without any phase stabilising agent we assumed a reflectivity $\rho_{AN} = 0.83$. For ammonium nitrate with NiO we assumed that the reflectivity decreased linearly to 0.285 with the increase in mass percentage of NiO when the amount of NiO in ammonium nitrate was 1.75 wt.%. For amount of NiO larger than 1.75 % we assumed $\rho_{AN} = 0.285$.

14.2. Surface reflectivity of the fuel binder

The common material more similar to the fuel binder used is rubber, whose emissivity is in the range 0.86-0.95, (vd. Lide, 1991). Admitting that rubber is an opaque and gray surface we have $\rho = 1 - \varepsilon$, (vd. Incropera, 1981), from which adopting for the emissivity of rubber the value 0.95 we obtain for the reflectivity the value 0.05.

15. Thermal conductivity of gases in the surface

15.1. Products of ammonium nitrate decomposition

It is assumed that the gaseous products of decomposition of ammonium nitrate are those given by reaction (8), which means the H_2O molar fraction is 2/3 and the N_2O molar fraction is 1/3. We considered the thermal conductivity of the gaseous products of decomposition of ammonium nitrate as being given by Eq. (77) taken from Bird, Stewart and Lightfoot (1960) and simplified.

$$\lambda_{g,ox} = \sum_{i=1}^{n} x_i \lambda_{g,i} \tag{77}$$

We applied a linear interpolation to the thermal conductivity data available in the bibliography, (vd. Lide, 1991; Incropera, 1981). The equations obtained were always used inside the temperature range of available data for these two gases.

$$\lambda_{g,H_2O} \, /(\text{W}/(\text{m.K})) \, (T) = 2.8338\text{E-}02 + 5.1101\text{E-}09 \, . \, (p \, /\text{Pa}) \tag{78}$$
corr = 0.99825, (460-600 K), because T_R is in the range 0.7-0.9

$$\lambda_{g,N_2O} \, /(\text{W}/(\text{m.K})) \, (T) = -6.76\text{E-}03 + 8.13 \, \text{E-}05 \, . \, (T \, /\text{K}) \tag{79}$$
corr = 0.9997, (300-600 K), because T_R is in the range 1.5-1.9

15.2. Pyrolysis products of the fuel binder

It is assumed that the only pyrolysis product of the fuel binder is the butadiene (C_4H_6). In the references no information was found on the thermal conductivity of this gas. It is known from the kinetic theory of gases that the thermal conductivity of a gas depends strongly and mainly on the molecular mass and temperature of the gas and only very slightly on pressure, because of this it was decided to use for the thermal conductivity of butadiene the values for the most similar molecule structure to butadiene and with the closest molecular mass for which available data exists in the literature. The chosen molecule was the n-butane and we used the data available in the temperature range 300-600 K to which we applied a linear interpolation, Eq. 82, that was used in the range of the available data. We considered the thermal conductivity of the n-butane equal to the thermal conductivity of the butadiene.

$$\lambda_{g,f} \, /(\text{W}/(\text{m.K})) \, (T) = -2.749\text{E-}03 + 1.427 \, \text{E-}04 \, . \, (T \, /\text{K}) \tag{80}$$
corr = 0.9979, (300-600 K)

16. Parameters used in the model

The standard parameters used in this model are presented in Table 4. The results obtained with the combustion model assuming the emmissivity of all flames equal to 0.1 is presented in Fig. 4.

Table 4
Parameters used in the model

Propellant data	Primary flame	Ammonium nitrate data	Fuel binder data
$Y_{ox} = 0.7425$	$\delta_{PF} = 2.0$	$A_{AN} = 1155.67$ m/s	$A_f = 1.897$ m/s
$Y_{NiO} = 0.0075$	$A_{PF} = 40.08$ Pa^2/s	$E_{AN} = 58576$ J/mol	$E_f = 47279$ J/mol
$Y_f = 0.2500$	$E_{PF} = 173898$ J/mol	$\rho_{ox} = 1725$ kg/m^3	$\rho_f = 921$ kg/m^3
$T_0 = 288$ K	$T_{PF} = 2107$ K	$c_{p,AN} = \sim 1920$ J/kg.K	$c_{p,f}$ /(J/kg.K) = 6.742 $(T_{m,f}/K)$
Final flame	**Monopropellant flame**	Q_{AN} /(J/kg) = 333559 + (549.81 . $(T_{s,ox}/K)$)	Q_f /(kJ/kg) = -601.4 + 0.6709 . $(T_{s,f}/K)$
$T_{FF} = 2350$ K	$\delta_{FAN} = 2.0$	$\varepsilon_{AN} = 0.53$	$\varepsilon_f = 0.95$
	$A_{FAN} = 47000$	$D_0 = 140$ μm	
	$E_{FAN} = 104600$ J/mol		
	$T_{FAN} = 1234$ K		

It is considered that the thermal decomposition of the solid oxidizer and fuel binder in the propellant are essentially independent from one another.

17. Discussion of results

The results of the model give lower burning rate than experimental for propellant PSAN/HTPB-IPDI (75/25 wt.%) and higher burning rate than experimental for propellant PSAN/HTPB-IPDI (80/20 wt.%).
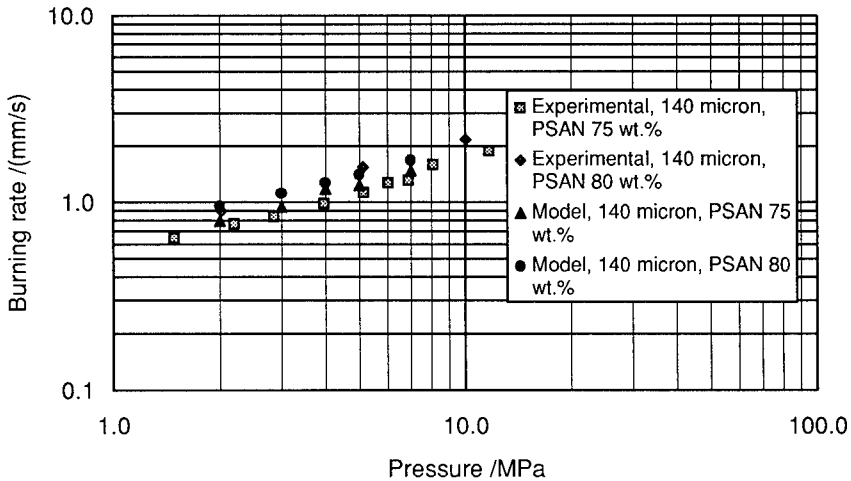
Fig. 4. Results of the combustion model for propellants AN/HTPB-IPDI (75/25 wt.%) and (80/20 wt. %) with AN unimodal particle diameter of 140 μm at 288 K, and experimental measurements for propellants PSAN/HTPB-IPDI (75/25 wt.%) and (80/20 wt. %) with PSAN particle size distribution with $d_{50} = 140$ μm, at 288 K.

18. Conclusions

A model was developed for the combustion of AN/HTPB-IPDI composite solid propellant with unimodal spherical oxidizer particles. The model uses the classical concepts of multiple flames, separate surface temperature. A new concept was introduced and applied that takes into account radiation heat transfer from the flames of the propellant surface through consideration of geometry of the flames and surface to determine radiation view factors, temperature of the flames and surface of propellant components and radiative properties of flames and propellant components. The geometry of diffusion flames was determined using the classical analysis of Burke and Schumann. It was derived correlations for the heat of pyrolysis of as a function of the surface temperature in pyrolysis of the fuel binder and for the heat released in the surface of ammonium nitrate at the surface temperature of the burning ammonium nitrate. The thermal conductivity of the gases was calculated based on the assumed composition and the diffusivity the gases for the calculation of the geometry of the diffusion flames was calculated based on assumed composition of the gases and on their molecular mass and molecular size.

The results obtained with the model are in good agreement with the experimental measurements of burning rate made by the authors and published (*vd.* Carvalheira, Campos and Gadiot, 1995), of propellants PSAN/HTPB-IPDI (75.00/23.08-1.92 wt.%) and (80.00/18.46-1.54 wt.%) with PSAN $d_{50} = 140$ μm, in the pressure range 2.0-10 MPa, at $T_0 = 288$ K.

REFERENCES

1. Beckstead, M. W., Derr, R. L., and Price, C. F., "A Model of Composite Solid-Propellant Combustion Based on Multiple Flames", *AIAA Journal*, 8 (12): 2200-2207, 1970.

2. Andersen, W. H., Bills, K. W., Mishuck, E., Moe, G., and Schultz R. D., "A Model Describing Combustion of Solid Composite Propellants Containing Ammonium Nitrate", *Combustion and Flame*, 3: 301-317, 1959.

3. Beckstead, M. W., "Burn Rate Mechanisms Study, Volume 2, A Model for Ammonium Nitrate Composite Propellant Combustion", AFAL-TR-89-016, Astronautics Laboratory, Air Force Space Technology Center, Space Division, Air Force Systems Command, Edwards Air Force Base, California 93523-5000, June 1989.

4. Russel, T. P., and Brill, T. B., "Thermal Decomposition of Energetic Materials 31 - Fast Thermolysis of Ammonium Nitrate, Ethylenediammonium Dinitrate and Hydrazinium Nitrate and Relationship to the Burning Rate", *Combustion and Flame*, 76: 393-401, 1989.

5. Beck, W. H., "Pyrolysis Studies of Polymeric Materials Used as Binders in Composite Propellants: A Review", *Combustion and Flame*, 70: 171-190, 1987.

6. Lide, David R., (Ed.), *CRC Handbook of Chemistry and Physics*, 72nd Edition, 1991-1992, CRC Press, Boca Raton.

7. Hendricks, S. B., Posnjak, E., and Kracek, F. C., "Molecular Rotation in the Solid State. The Variation of the Crystal Structure of Ammonium Nitrate with Temperature", *Journal of the American Chemical Society*, 54: 2766-2786, 1932.

8. Feick,.G., "The Dissociation Pressure and Free Energy of Formation of Ammonium Nitrate", *J. Am. Chem. Soc.*, 76: 5858-5860, 1954.

9. Kolaczkowski, Andrzej, "Spontaneous Decomposition of Ammonium Nitrate", Scientific Papers of the Institute of Inorganic Technology and Mineral Fertilizers of Wroclaw Technical University, No. 18, Monograph No.6, 1980.

10. Grayson, M., and Eckroth, D., Ed., *Kirk-Othmer Encyclopedia of Chemical Technology*, Third Edition, John Wiley and Sons, 1983.

11. Fedoroff, B. T., *Encyclopedia of Explosives and Related Items*, Picatinny Arsenal, NJ, 1960.

12. Keenan, A. G., "The Cryoscopic Heat of Fusion of Ammonium Nitrate", *J. Am. Chem. Soc.*, 60: 1356-1361, 1956.

13. Brandrup, J. and Immergut, E. H., (Ed.), *Polymer Handbook*, John Wiley and Sons, New York, 1975.

14. Heuzé, O., "Contribution au Calcul des Caractéristiques de Détonation de Substances Explosives Gazeuses ou Condensés", Thése presenté à L'U.E.R. - E.N.S.M.A., pour Obtenir le Grade de Docteur de l'Université de Poitiers, 24 Juin 1985.

15. Brazier, D. W., and Schwartz, N. V., "The Effect of Heating Rate on the Thermal Degradation of Polybutadiene", *J. Appl. Polym. Sci.*, 22:113-124, 1978.

16. Chen, J. K., Brill, T. B., "Chemistry and Kinetics of Hydroxyl-terminated Polybutadiene (HTPB) and Diisocyanate-HTPB Polymers during Slow Decomposition and Combustion-like Conditions", *Combustion and Flame*, 87: 217-232, 1991.

17. Spadaccini, L. J., and TeVelde, J. A., "Autoignition Characteristics of Aircraft-Type Fuels.", *Combustion and Flame*, 46: 283-300, 1982.

18. Burke, S. P., and Schumann, T. E. W., "Diffusion Flames", Industrial and Engineering Chemistry, 20 (10): 998-1004, 1928.

19. Kuo, Kenneth K., *Principles of Combustion*, John Wiley & Sons, New York, 1986.

20. Blomshield, F. S., "Nitramine Composite Solid Propellant Modelling", NWC TP 6992, Naval Weapons Center, China Lake, CA 93555-6001, July 1989.

21. Mahan, Bruce H., *University Chemistry*, Addison - Wesley Publishing Company, 1965.

22. Siegel, R. and Howell, J. R., *Thermal Radiation Heat Transfer*, McGraw-Hill Book Company, New York, 1972.

23. Incropera, Frank P., and DeWitt, David P., *Fundamentals of Heat Transfer*, John Wiley & Sons, New York, 1981.

24. Ishihara, A., Brewster, M. Q., Sheridan, T. A., and Krier, H. "The Influence of Radiative Heat Feedback on Burning Rate in Aluminized Propellants", *Combustion and Flame*, 84: 141-153, 1991.

25. Hydroxyl Terminated Poly Bd Resins Functional Liquid Polymers in Urethane Elastomers, Atochem, Elf Aquitaine, October 1990.

26. Strecker, R. A. H., and Linde, D., "Gas Generator Propellants for Air-to-Air Missiles". AGARD CP-259, April 1979.

27. Korting, P. A. O. G., Zee, F. W. M., Meulenbrugge, J. J., "Performance of No Chlorine Containing Composite Propellants with Low Flame Temperatures", AIAA-87-1803, *AIAA/SAE/ASME/ASEE 23rd Joint Propulsion Conference*, June 29-July 2, 1987, San Diego, California.

28. Brewster, M. Q., Sheridan, T. A., Ishihara, A., "Ammonium Nitrate-Magnesium Propellant Combustion and Heat Transfer Mechanisms", *Journal of Propulsion and Power*, 8 (4): 760-769, 1992.

29. Carvalheira, P., Gadiot, G.M.H.J.L. and de Klerk, W.P.C., "Mechanism of Catalytic Effects on PSAN/HTPB Composite Solid Propellants Burning Rates", 25th International Annual Conference of ICT, Karlsruhe, Federal Republic of Germany, pp. 65-1, 1994.

30. Carvalheira, P., Campos, J., Gadiot, G.M.H.J.L. "Burning Rate Modifiers for AN/HTPB-IPDI Composite Solid Propellants for Gas Generators", 26th International Annual Conference of ICT, Karlsruhe, Germany, pp. 69-1, 1995.

31. Bird, B. R., Stewart, W. E., and Lightfoot, E. N., *Transport Phenomena*, John Wiley and Sons, New York, 1960.

EINFLUSS DER KORNGRÖSSE DES REDUKTIONSMITTELS AUF DIE REAKTIONSPARAMETER PYROTECHNISCHER SYSTEME

B. Berger, B. Haas, G. Reinhard

Gruppe Rüstung
Fachabteilung Waffensysteme und Munition
Feuerwerkerstr. 39
3600 Thun 2 / Schweiz

Zusammenfassung

Am Beispiel des Redoxsystems Titan / Kaliumperchlorat wurde an Mischungen mit unterschiedlicher Sauerstoffbilanz der Einfluss der Korngrösse des Reduktionsmittels auf die in der Pyrotechnik relevanten Reaktionsparameter sowie auf die Sicherheitskenndaten untersucht. Die Resultate zeigen, dass unterschiedliche Korngrössen bzw. spezifische Oberflächen des Reduktionsmittels die Umsetzungsgeschwindigkeit, die Brisanz, die Reibempfindlichkeit sowie die Empfindlichkeit gegenüber elektrostatischen Entladungen wesentlich beeinflussen.

Abstract

The influence of the particle size of the reducing agent on several reaction parameters as well as on the safety data was investigated on mixtures with different oxygen balance of the pyrotechnic redox-system Titanium / Potassium Perchlorate. The results show, that the burning rate, the brisance, the sensitivity to friction and the sensitivity to electrostatic discharges are widely influenced by different particle sizes and specific surfaces respectively of the reducing agent Titanium.

1. Einleitung

Im Rahmen von IM - Untersuchungen (Insensitive Munition) wird nach chemischen Redoxsystemen gesucht, deren Output genügend gross ist um LOVA Treibmittel sicher anfeuern zu können, dh. die bei gleichbleibender bzw. geringerer Empfindlichkeit gegenüber äusseren Einflüssen eine höhere Ausgangsleistung als herkömmliche Anfeuerungssysteme aufweisen. Die anlässlich der Charakterisierung des Redoxsystems Titan Typ S / Kaliumperchlorat gemessenen Leistungsdaten haben gezeigt, dass dieses System den diesbezüglichen Anforderungen teilweise genügen würde [1]. Hingegen beträgt die maximale Abbrandgeschwindigkeit dieses Redoxsystems nur 0.3 m/s und ist somit kleiner als die Maximalwerte herkömmlicher Anfeuerungssysteme auf der Basis von Bor / Kaliumnitrat (0.45 m/s) bzw. Schwarpulver (0.5 m/s). Auf Grund verschiedener Arbeiten ist bekannt, dass die Umsetzungsgeschwindigkeit pyrotechnischer Systeme mittels der Korngrösse ihrer Komponenten gesteuert werden kann [2].
Die Resultate früherer Untersuchungen [3, 4 ,5] wiesen in diesem Fall darauf hin, dass bei pyrotechnischen Redoxsystemen, die als Oxidationsmittel Kaliumperchlorat enthalten, die Korngrösse des Reduktionsmittels der umsetzungsgeschwindigkeitsbestimmende Faktor ist. Es war deshalb naheliegend, durch die Verwendung von Titanpulver mit kleinerem Korndurchmesser die Umsetzungsgeschwindigkeit des vorliegenden Systems zu erhöhen.

2. Ziel der Untersuchung

Die Untersuchung sollte zeigen, in welchem Bereich die Umsetzungsgeschwindigkeit pyrotechnischer Systeme durch die Verwendung von feinkörnigerem Reduktionsmittel gesteigert werden kann, welche Zusammenhänge zwischen Korngrösse, Kornform, Umsetzungsgeschwindigkeit, Reaktionswärme, Brisanz, Gasdruck, thermischem Verhalten und Sicherheitskenndaten bestehen und ob solche Zusammenhänge durch Modelle erklärt werden können.

3. Experimenteller Teil

3.1 Verwendete Ausganskomponenten

Reduktionsmittel : **- Titanmetallpulver (Ti) Typ S,** Hersteller Chemetall

Mittlere Korngrösse gemäss der Spezifikation des
Herstellers, gemessen nach der Methode von Blaine:
$9 \pm 1.5 \mu$.
Mittlere Korngrösse des für die Untersuchung ver-
wendeten Materials, gemessen nach der Methode
von Malvern: 20 μ; Spezifische Oberfläche: 0.42 m²/cc.
Reinheitsanalyse:
Total Titangehalt: 98.5 %
Metallisches Titan: 96.5 %

- **Titanmetallpulver (Ti) Typ E,** Hersteller Chemetall
Mittlere Korngrösse gemäss der Spezifikation des
Herstellers, gemessen nach der Methode von Blaine:
$3 \pm 0.5 \mu$.
Mittlere Korngrösse des für die Untersuchung
verwendeten Materials, gemessen nach der Methode
von Malvern: 9.5 μ; Spezifische Oberfläche: 1.2 m²/cc.
Die Abweichung der mittleren Korngrössen sind auf
unterschiedliche Messverfahren zurückzuführen.
Reinheitsanalyse:
Total Titangehalt: 93.3 %
Metallisches Titan: 83.3 %

Oxidationsmittel :   - **Kaliumperchlorat (KCIO₄),** Hersteller Nobel Industrie /
Elektrochemie
Mittlere Korngrösse des für die Untersuchung
verwendeten Materials, gemessen nach der Methode
von Malvern: 38 μ; Spezifische Oberfläche: 0.33 m²/cc.

Binder :   - **Nitrocellulose (NC),** Hersteller Gurit-Worbla
Der Sickstoffgehalt der verwendeten Nitrocellulose
beträgt 12.6 %.

3.2 Herstellung der Mischungen

Das Titanmetallpulver und das Kaliumperchlorat wurden in einem Turbula-
mischer gemischt. Anschliessend erfolgte die Zugabe der in Ethanol / Aceton
gelösten Nitrocellulose, worauf die vorgetrocknete Masse mittels eines Siebes
der Maschenweite 0.5 mm granuliert und in einem Vakuumschrank bei 60 °C die
noch vorhandenen Lösungsmittelreste entfernt wurden.

3.3 Hergestellte Mischungen

Tab. 1 Mischungen mit dem Reduktionsmittel Titan Typ S

Komponenten	Zusammensetzung [Gew.%]							
Ti	35	40	45	50	55	70	80	90
$KClO_4$	64	59	54	49	44	29	19	9
NC	1	1	1	1	1	1	1	1

Tab. 2 Mischungen mit dem Reduktionsmittel Titan Typ E

Komponenten	Zusammensetzung [Gew.%]						
Ti	35	40	45	55	70	80	90
$KClO_4$	64	59	54	44	29	19	9
NC	1	1	1	1	1	1	1

4. Resultate

Die allgemeine chemische Reaktionsgleichung für das System lautet:

$$2\,Ti \;+\; KClO_4 \;\rightarrow\; 2\,TiO_2 \;+\; KCl$$
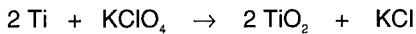
Gemäss dieser Gleichung enthält die Mischung mit ausgeglichener Sauerstoff-
bilanz 40 Gew.% Titan.
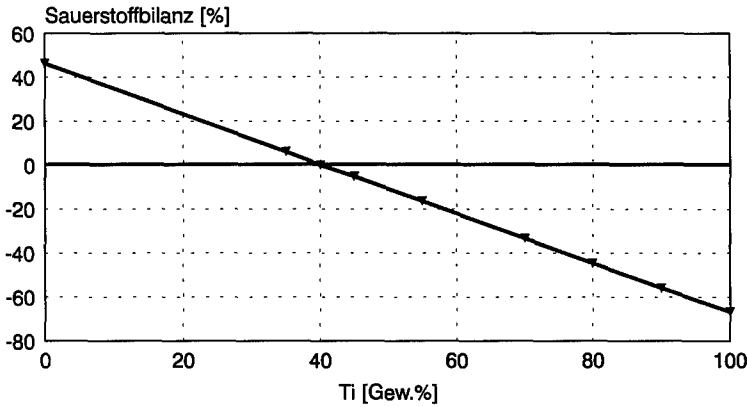
Bild 1 Sauerstoffbilanz des Redoxsystems

4.1 Umsetzungsgeschwindigkeit

Wie sich die unterschiedlichen mittleren Korngrössen des Titanmetallpulvers auf die gemessenen Umsetzungsgeschwindigkeiten der verschiedenen Mischungen des Redoxsystems auswirken, zeigt die nachfolgende Tabelle. Die aufgeführten Werte sind Mittelwerte aus mindestens drei Messungen.

Tab. 4 Gemessene Umsetzungsgeschwindigkeiten

Reduktionsmittel [Gew.%]	Umsetzungsgeschw. 1 [m/s] , Kornϕ 9.5 μ	Umsetzungsgeschw. 2 [m/s] , Kornϕ 20 μ	F (v_{u1} / v_{u2})
35	0.37	0.09	4.1
40	0.48	0.13	3.7
45	0.53	0.15	3.5
55	1.00	0.27	3.7
70	1.33	0.30	4.4
80	1.00	0.16	6.2
90	0.24	0.09	2.7
			F_m 4.0

In Bild 2 sind die Messwerte graphisch dargestellt. Die beiden Umsetzungsge-schwindigkeitskurven zeigen, dass die jeweilige Mischung mit einem Titanmetall-pulveranteil von 70 Gew.% (Reduktionsmittel) die grösste Umsetzungsge-

schwindigkeit aufweist. Diese Tatsache steht im Widerspruch zu der Zusammen-
setzung mit ausgeglichener Sauerstoffbilanz gemäss der oben zitierten klassi-
schen Reaktionsgleichung, nach der die Mischung mit 40 Gew.% Titanmetall-
pulver die grösste Umsetzungsgeschwindigkeit zeigen sollte. Diese Ungereimt-
heit ist auf die, bei diesem Redoxsystem ausgeprägt stattfindende, stufenweise
Oxidation des Reduktionsmittels zurückzuführen [6].
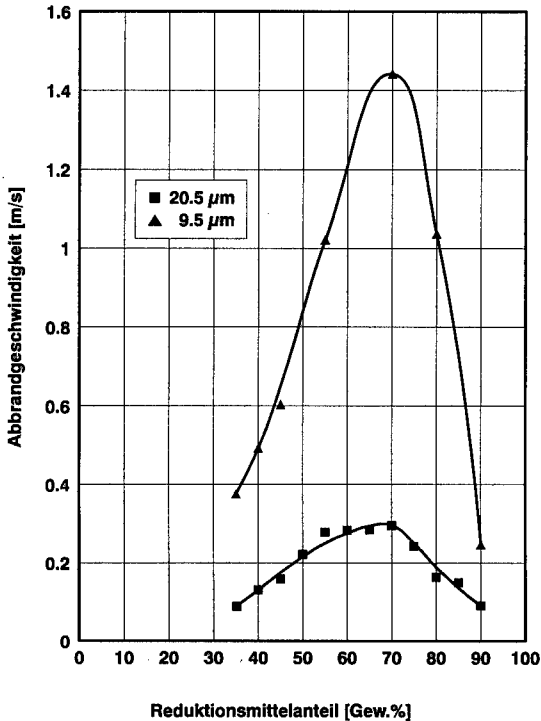
Bild 2 Umsetzungsgeschwindigkeiten von Ti / KClO4 -Mischungen unterschied-
licher Zusammensetzung, wobei das Reduktionsmittel Titan verschiedene
mittlere Korndurchmesser aufweist.

Da ein direkter Zusammenhang zwischen der Oberfläche des Reduktionsmittels
und der Umsetzungsgeschwindigkeit von Redoxsystemen besteht, sind in der
nachfolgenden Tabelle die Beschaffenheitsparameter des verwendeten Reduk-
tionsmittels zusammengestellt.

<u>Tab. 5</u> Daten der Titankörner

Komponenten	Titan Typ E	Titan Typ S	Faktor
Mittlere Korngrösse [μ]	9.5	20	2.1
Spez. Oberfläche gem. [m^2/cc]	1.26	0.42	3.0
Spez. Oberfläche ber. [1] [m^2/cc]	0.32	0.16	2.0

[1] Die Berechnung der spezifischen Oberfläche erfolgte unter der Annahme, dass die Titankörner in Kugelform vorliegen, dass alle Körner den gleichen Durchmesser aufweisen und dass eine definierte Kugelpackung vorliegt.

Die verwendeten Titanmetallpulver weisen in etwa eine Korngrössenverteilung in Form einer Gauss'schen Glockenkurve mit den in Tabelle 5 erwähnten mittleren Korndurchmessern auf. Deshalb und weil sie nicht in Kugelform vorliegen, stimmen die berechneten und die gemessenen spezifischen Oberflächen nicht überein. Der Vergleich der Umsetzungsgeschwindigkeitsfaktoren mit dem Faktor der gemessenen spezifischen Oberfläche zeigt jedoch einen signifikanten Zusammenhang zwischen der Oberfläche des Reduktionsmittels und der Umsetzungsgeschwindigkeit.

4.2 Reaktionswärme

Zur Abschätzung der Verwendungsmöglichkeit von Redoxsystemen als Pyrotechnika ist die während der Redoxreaktion entstehende Wärme ein wichtiger Parameter. Mischungen mit variierenden Anteilen an Reduktions-/ Oxidationsmittel eines Redoxsystems erzeugen unterschiedliche Reaktionswärmemengen. Diese können sowohl gemessen wie auch mittels Thermodynamik-Programmen berechnet werden.
Die für das Redoxsystem Titan / Kaliumperchlorat gemessenen und berechneten Reaktionswärmen sind in der folgenden Graphik dargestellt. Die Resultate zeigen, dass die gemessenen Höchstwerte bei der Verwendung von Titan Typ S ca. 6 % und bei der Verwendung von **Titan Typ E** ca. 15 % tiefer sind als der be-

rechnete Höchstwert. Zusätzlich fällt auf, dass die Reaktionswärmemaxima je nach Titantyp bei unterschiedlichen Zusammensetzungen gemessen werden, die ebenfalls nicht mit der Zusammensetzung der Mischung mit dem berechneten Höchstwert übereinstimmen. Dieser Effekt lässt sich durch die verschiedenen Reinheitsgehalte der verwendeten Titanpulver erklären. Es ist jedoch ersichtlich, dass die Reaktionswärme durch die Korngrösse kaum direkt beeinflusst wird. Bei kleineren Korndurchmessern ist aber der Anteil an bereits oxidierter Oberfläche grösser und entsprechend der reaktionsfähige (metallische) Anteil vom Gesamttitangehalt des Titanpulvers kleiner.
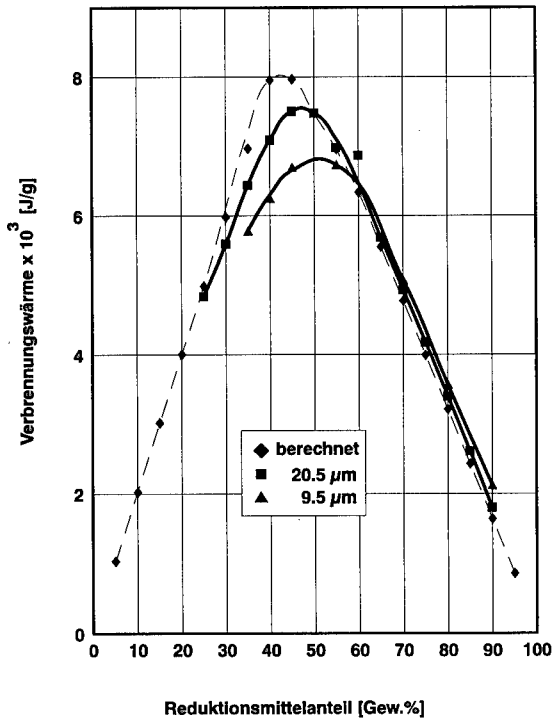
Bild 3 Gemessene und berechnete Reaktionswärmen in Abhängigkeit von Anteil und Korngrösse des Reduktionsmittels

4.3 Gasdruck

Eine weitere, für pyrotechnische Mischungen wichtige Kenngrösse ist der bei der Umsetzungsreaktion in einem geschlossenen Behältnis auftretende Gasdruck.

Die gemessenen Werte für das vorliegende Redoxsystem sind in der nachfol-
genden Graphik dargestellt. Es handelt sich um die Mittelwerte aus 4 bis 6 Ein-
zelmessungen.

Wie erwartet, zeigen die Messwerte, dass unterschiedliche mittlere Korndurch-
messer des Titanpulvers keinen signifikanten Einfluss auf den Gasdruck der ver-
schiedenen Mischungen ausüben.
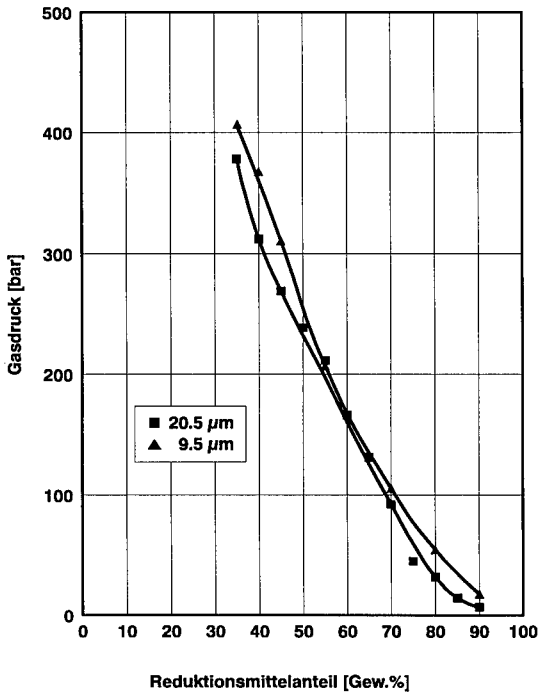
Bild 4 Gemessene Gasdrücke verschiedener Mischungen des Redoxsystems
Titan / Kaliumperchlorat. Variablen sind die Zusammensetzung und der
mittlere Korndurchmesser des Titans

4.4 Brisanz

Die Brisanz einer pyrotechnischen Mischung ist definiert als der Anstieg des
Gasdruckes pro Zeiteinheit. Demzufolge besteht zwischen der Brisanz und der
Umsetzungsgeschwindigkeit eine direkte Beziehung. Die gemessenen Brisanz-
werte der verschiedenen Mischungen des untersuchten Redoxsystems sind in

der nachfolgenden Graphik als Mittelwerte von 4 bis 6 Einzelmessungen dargestellt.

Die Graphik zeigt eindrücklich, wie die Brisanz durch die beiden unterschiedlichen mittleren Korndurchmesser des Reduktionsmittel beeinflusst wird. Am deutlichsten wirkt sich dieser Einfluss bei Mischungen mit einem kleinen Reduktionsmittelanteil, d.h. unter 50 Gew.% aus.

Achsenbeschriftung: Brisanz [bar/ms] (y-Achse), Reduktionsmittelanteil [Gew.%] (x-Achse)

Legende: ■ 20.5 µm   ▲ 9.5 µm
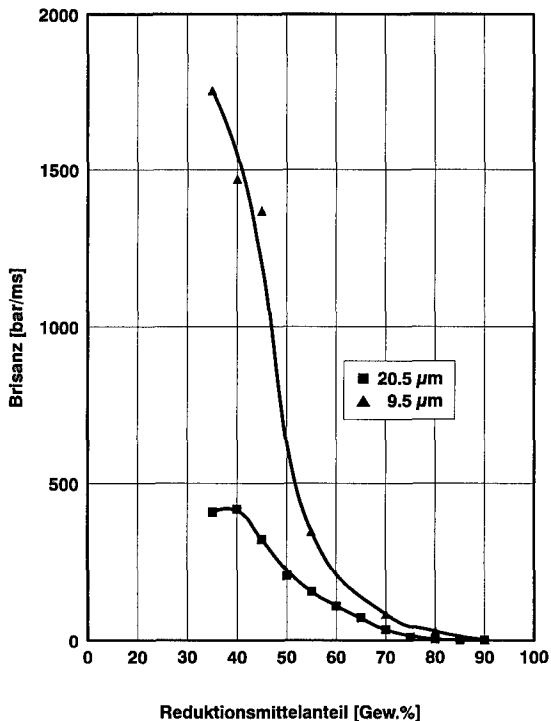
Bild 5 Gemessene Brisanzwerte verschiedener Mischungen des Redoxsystems Titan / Kaliumperchlorat mit variierender Zusammensetzung und unterschiedlichen Korndurchmessern des Reduktionsmittels

4.5 Thermisches Verhalten

Der Einfluss der unterschiedlichen Korngrössen des Titanpulvers auf das thermische Verhalten der Mischungen wurde mittels Differential - Scanning - Calorimetry (Mettler System 4000) untersucht. Die Temperaturen der maximalen Energieabgabe der Mischungen die Titan Typ E ($\varnothing$ 9.5µ) als Reduktionsmittel

enthielten, sind im Vergleich zu den äquivalenten Mischungen mit Titan Typ S ($\varnothing$ 20μ) 7 bis 25 °C tiefer (wie aus der Tabelle ersichtlich). Diese Temperaturverschiebungen sind jedoch bei Peaktemperaturen im Bereich von 500 °C bis 600 °C nicht mehr relevant.

Da es sich bei der Reaktion von Titan mit Sauerstoff um eine Mehrstufenoxidationsreaktion handelt, sind bezüglich des Auftretens der verschiedenen Reaktionsstufen noch viele Fragen ungeklärt.

<u>Tab 5</u> Peak -Temperaturen der maximalen Energieabgabe

Anteil Ti [Gew.%]	Peak Temp. [°C] Ti Typ E, $\varnothing$ 9.5μ	Peak Temp. [°C] Ti Typ S, $\varnothing$ 20μ	Δ Peak Temp. [° C]
35	584	591	7
40	577	589	12
45	572	587	15
55	558	576	18
70	542	567	25
80	519	530	11
90	510	523	13

Die Extrapolation der Peakmaxima ergibt für reines Kaliumperchlorat einen Temperaturwert von ca. 620 °C. Die Schmelztemperatur von Kaliumperchlorat wird in der Literatur mit 610 + 20°C angegeben [7].

Die DSC-Aufzeichnungen zeigen deutlich, dass mit zunehmendem Titananteil sowie mit grösserer Oberfläche des Titanpulvers die „solid-solid state reaction" zwischen Reduktions- und Oxidationsmittel zunimmt. Dies hat zur Folge, dass gemäss der Zersetzungsreaktionsgleichung von Kaliumperchlorat

$$KClO_4 \xrightarrow{\Delta T} KCl + 2 O_2$$
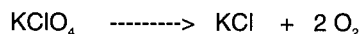
mehr Kaliumchlorid entsteht. Dieses bildet mit Kaliumperchlorat zusammen ein eutektisches Gemisch, das eine wesentlich tiefere Schmelz- bzw. Zersetzungstemperatur als reines Kaliumperchlorat aufweist.

4.6 Sicherheitskenndaten

Die in der Tabelle zusammengestellten Werte sind diejenigen Kräfte bzw. Energien, bei denen mindestens eine von 6 untersuchten Proben eine Reaktion zeigte.

<u>Tab. 6</u> Sicherheitskenndaten des Redoxsystems Ti / $KClO_4$ unter Berücksichtigung der 2 unterschiedlichen mittleren Korndurchmesser des Ti

Anteil Reduktions mittel	Empfindlichkeit gegenüber elektrostat. Entladungen [mJ]		Reibempfindlich-keit [N]		Schlagempfindlich-keit [J]	
Ti [Gew.%]	Ti Typ E ∅ 9.5µ	Ti Typ S ∅ 20µ	Ti Typ E ∅ 9.5µ	Ti Typ S ∅ 20µ	Ti Typ E ∅ 9.5µ	Ti Typ S ∅ 20µ
35	3.2	56	96	> 360	> 20	> 20
40	5.6	18	80	> 360	> 20	> 20
45	0.56	10	60	288	> 20	> 20
55	1.0	1.8	40	144	> 20	> 20
70	1.0	3.2	20	144	> 20	> 20
80	0.56	5.6	40	144	> 20	> 20
90	3.2	10	> 360	> 360	> 20	> 20

Die Werte zeigen, dass im Messbereich der Fallhammermethode die Korngrösse des Reduktionsmittels keinen Einfluss auf die Empfindlichkeit der verschiedenen Mischungen gegenüber Schlageinwirkung hat. Hingegen werden bei der Verwendung von feinkörnigerem Reduktionsmittel die meisten Mischungen um ca. einen Faktor 4 empfindlicher gegenüber Reibung und bis zu einem Faktor 18 empfindlicher bezüglich elektrostatischen Entladungen. Trotz dieser Empfindlichkeitszunahme können die Mischungen dieses Redoxsystems im Vergleich zu aedequaten, zur Zeit in der militärischen Pyrotechnik verwendeten Redoxsysteme, als wenig empfindlich betrachtet werden.

5. Zusammenfassung / Folgerungen

Am Beispiel des Redoxsystems Titan / Kaliumperchlorat wurde an Mischungen mit unterschiedlicher Sauerstoffbilanz der Einfluss der Korngrösse des Reduktions- mittels auf die in der Pyrotechnik relevanten Reaktionsparameter sowie auf die Sicherheitskenndaten untersucht.

Durch die Verwendung von Reduktionsmittel mit einem um den Faktor 2 kleineren mittleren Korndurchmesser lässt sich die Umsetzungsgeschwindigkeit der unter- suchten Mischungen durchschnittlich um einen Faktor 4 steigern. Die Brisanz von Mischungen mit positiver Sauerstoffbilanz wird durch die Korngrösse beeinflusst. Es besteht ein direkter Zusammenhang zwischen der Korngrösse des Redukti- onsmittels und der Temperatur der maximalen Energieabgabe der exothermen Umsetzungsreaktion.

Nur geringe bis keine Auswirkungen sind bei der Reaktionswärme und beim Gasdruck feststellbar.

Die Schlagempfindlichkeit wird im Messbereich der Methode durch die unter- schiedlichen Korndurchmesser des Titanpulvers nicht beeinflusst Die Reib- empfindlichkeit und die Empfindlichkeit gegenüber elektrostatischen Entla- dungen werden bei der Verwendung von Titanpuver mit kleinerem Korndurch- messer jedoch erhöht (Reibempfindlichkeit um einen Faktor 4).

Die Untersuchung zeigt, dass relevante pyrotechnische Parameter wie die Um- setzungsgeschwindigkeit und die Brisanz von Redoxsystemen, die als Oxidati- onsmittel Kaliumperchlorat enthalten, durch die Korngrösse bzw. die spezifische Oberfläche des Reduktionsmittels gesteuert werden können. Dadurch lassen sich optimal dimensionierte pyrotechnische Elemente mit geringerem Aufwand entwickeln.

6. Literatur

[1] Berger B. , Haas B. , Reinhard G.
„Charakterisierung des Anfeuerungssystems Ti / KClO4"
GRD, FA 26, FO-Bericht, 1994

[2] Hedger J. T.
„Factors Influencing the Pyrotechnic Reaction of Silicon and Red Lead"
ICI Australia Ltd, Melbourne, AUS, 1983

[3] van Ham N. H. A.

„Deflagration of Gasless Pyrotechnic Mixtures"

TNO, Prins Maurits Laboratory, 1990, NL

[4] Berger B. , Charsley E. L. , Warrington S. B.
„ Characterisation of the Zirconium-Potassium Perchlorate-Nitrocellulose

Pyrotechnic System by Simultaneous Thermogravimetry-Differential Thermal

Analysis-Mass Spectroscopy"

Propellants, Explosives, Pyrotechnics, 20, We4inheim, 1995

[5] Berger B. , Charsley E. L. , Warrington S. B. , Rooney J. J.
„ Quantitative Studies on the Zirconium-Potassium Perchlorate-Nitrocellulose

Pyrotechnic System using Differential-Scanning-Calorimetry and Chemical

Analysis"

Thermo Chimica Acta, 255, Amsterdam, 1995

[6] Ellern H.

„Military and Civilian Pyrotechnics"

Chemical Publishing Compagny, New York, 1968

[7] Handbook of Chemistry and Physics, 53rd, B-212

7. Anhang

Rasterelektronenmikroskopische Aufnahmen der Ausgangskomponenten
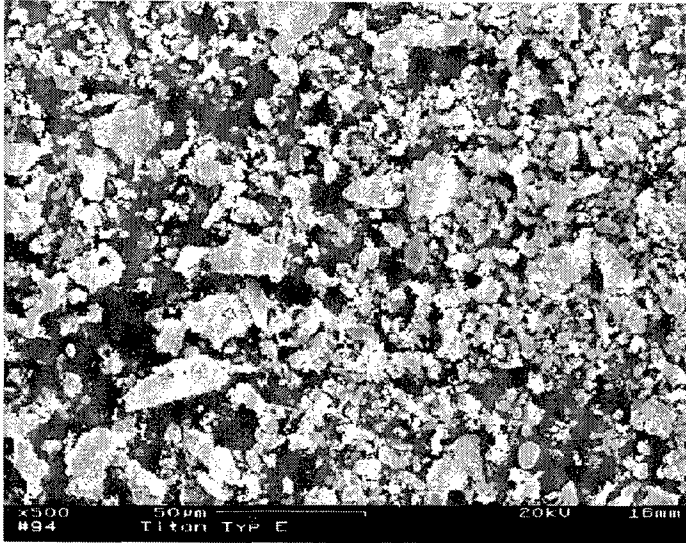
Bild 7 REM-Aufnahme von Titankörnern, Typ E
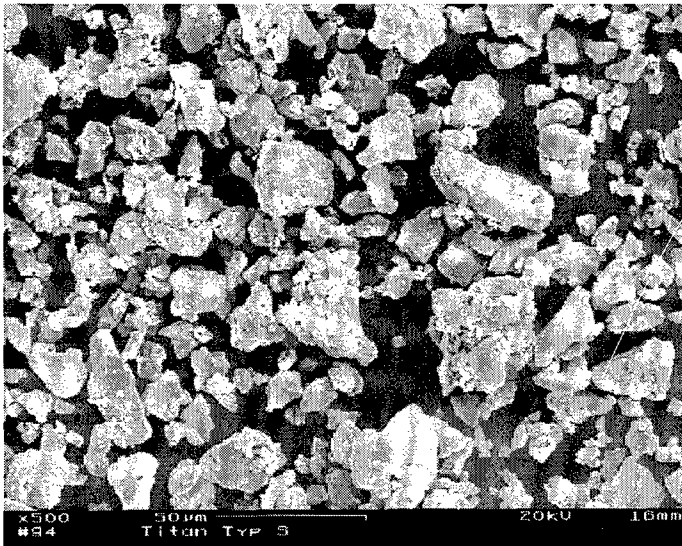
Bild 8 REM-Aufnahme von Titankörnern, Typ S
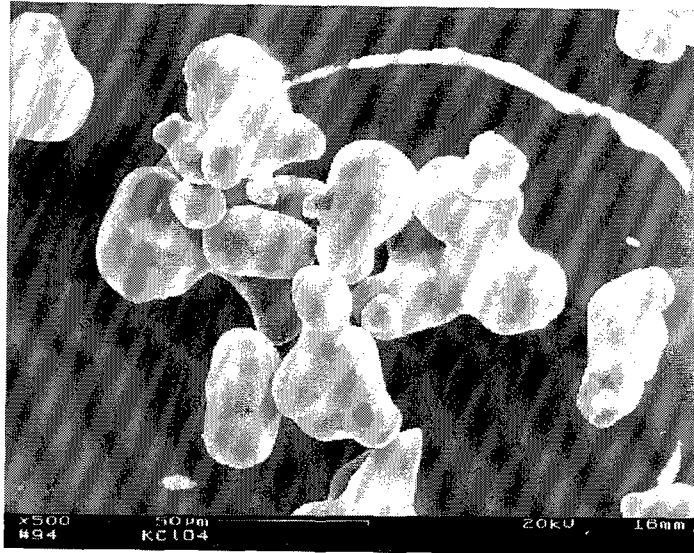
Bild 9 REM-Aufnahme von Kaliumperchlorat-Körnern

Spektroskopische Untersuchung an borhaltigen Festbrennstoffen in einer Staubrennkammer

A. Blanc*, H. Ciezki[‡], H. Feinauer[‡], W. Liehmann*

[‡]Deutsche Forschungsanstalt für Luft- und Raumfahrt

D-74238 Lampoldshausen , F.R.G.

*Fraunhofer Institut Chemische Technologie

D-76318 Pfinztal 1(Berghausen), F.R.G.

Abstract

Solid fueled ramjet test facilities and investigations on internal flow characterisation in ram combustors include one part of the DLR activities. The developement of solid propellants is a major topic at ICT.

For the purpose of getting more insight into the combustion behaviour of solid propellants in ducted rocket motors some new spectroscopic and pyrometric diagnostic systems were built up. For the detection of radiation in the IR-region three spectrometers are available ranging from 1.2 to 14.5µm with a wavelength resolution of about 1% and a scanning rate of 10ms per spectrum. The time resolution of the two colour pyrometer ranges from DC up to 50 kHz and detects fast particles with temperatures above 900K. In this paper these methods of investigation are described and the results of an application at the DLR in a direct connected ramburner with variabel optical devices are discussed.

1. Zusammenfassung

Sowohl die DLR als auch das ICT beschäftigen sich mit der Entwicklung von luftatmenden Staustrahlantrieben mit Festbrennstoff. Mit Hilfe am ICT entwickelter spektroskopischer und pyrometrischer Aufzeichnungssysteme im NIR wurden Untersuchungen zum Abbrandverhalten borhaltiger Brennstoffplatten in einer Stufenbrennkammer bei der DLR durchgeführt. Die Versuchsanordnung und die Diagnosesysteme werden vorgestellt. Die unterschiedlichen Meßergebnisse werden anhand der gewählten Treibstoffzusammensetzungen diskutiert.

2. Einleitung

Bei chemischen Antrieben entstehen bei der Verbrennung entsprechend der Treibstoffzusammensetzung Gase und kondensierte Produkte, welche eine molekülspezifische Banden- und Kontinuumsstrahlung aufweisen. Mit Hilfe von Spektrometer- und Pyrometersystemen können bei optischem Zugang zur Brennkammer Verbrennungsabläufe örtlich als auch zeitlich aufgelöst analysiert werden. Sowohl die Verbrennungstemperatur als auch die Reaktionsspezies können somit während des Abbrandes ermittelt und mit thermodynamisch berechneten Daten verglichen werden.

Die zu untersuchenden Brennstoffe enthielten als energieerhöhenden Zusatz Bor, dessen Oxid bekanntlich erst oberhalb 2300K in die Gasphase übergeht. Daneben wurde mit GAP ein neuer Binder eingesetzt, der höhere Abbrandraten der Brennstoffplatten ermöglicht.

Ein Hauptziel der gemeinsamen Meßkampagne war die Erarbeitung von Basisdaten sowie der Nachweis der Funktionalität der Meßsysteme bei geringem Abstand zur Stufenbrennkammer.

3. Meßsysteme

3.1 Infrarot-Spektrometer

Herkömmliche, hochauflösende FTIR-Spektrometer sind aufgrund langer Zykluszeiten bzw. hohem technischen Aufwand und empfindlicher Technik für solche Meßzwecke nur begrenzt einsatzfähig.

Das am ICT entwickelte Filterradspektrometer zeichnet sich hingegen durch seine hohe spektrale Zerlegungsgesschwindigkeit und seine Robustheit unter harten Betriebsbedingungen aus. Es arbeitet auf der Basis rotierender Verlaufsfilterscheiben, die je nach Bestückung einen Spektralbereich von 1 - 14μm abdecken /1/. Die einfallende Strahlung wird mittels Spiegeloptiken durch einen mit Blenden eingegrenzten schmalen Winkelbereich des rotierenden Filterrades gelenkt und anschließend auf einen Sandwichdetektor gerichtet. Die Strahlung wird dadurch in Abhängigkeit von der Winkelposition des Filterrades wellen-

längenselektiv zerlegt. Die Zeitauflösung wird über die Drehzahl des Filterades vorgegeben. Diese ist auf 100 Spektren pro Sekunde begrenzt, entsprechend einer Scanrate von 10ms pro Spektrum. Die Wellenlängenauflösung liegt bei 1% der betreffenden Wellenlänge.

3.2 Zweifarben-Quotienten-Pyrometer

Zur kontinuierlichen und ortsaufgelösten Temperaturbestimmung der in einem Verbrennungsvorgang enthaltenen festen Partikel können wegen der teilweise hohen Strömungsgeschwindigkeiten und kleinen Partikelgrößen nur schnelle strahlungspyrometrische Meßsysteme eingesetzt werden. Voraussetzung für richtige Messung ist die Emission von grauer Strahlung mit zumindest annähernd Planck'scher Strahlungsverteilung im selektierten Wellenlängenbereich. Der Emissionsgrad sollte dabei im betrachteten Wellenlängenintervall als konstant angenommen werden können.

Das hier eingesetzte, schnelle Zweifarben-Pyrometer arbeitet zwischen 0.9 und 1.3µm. Der Frequenzgang der Elektronik erlaubt Abtastraten bis 50µs pro Punkt und muß bei diesen Scanzeiten über synchrone sample & hold Stufen eingelesen werden. Es können damit Partikeltemperaturen im Bereich von 900 bis 3000K gemessen werden.

4. Versuchsaufbau

Die für die Untersuchungen eingesetzte ebene Stufenbrennkammer ist in Abb. 1 dargestellt. Ein H_2/O_2-Brenner heizt den Luftstrom, der zur Brennkammer führt, bis auf 500°C auf. Die Breite der Kammer beträgt 150mm, die Höhe 45mm und die Stufenhöhe 20mm. Die Brennstoffplatten von 198mm Länge und 100mm Breite wurden oberflächenbündig in den Boden eingesetzt. Seitlich versetzbare Quarz- bzw. CaF_2-Fenster erlauben den Einblick in die Kammer für die Beobachtung mittels Videokamera, Pyrometer und Spektrometer. Letztere waren gegenüber angeordnet, um auf denselben Meßfleck ausgerichtet zu sein. Für die hier vorgestellte Untersuchung waren die Fenster so montiert, daß Brenn-

stoffplattenoberseite und Fensterunterseite eine Ebene bildeten. Zur Vermeidung von Ruß- und Borpartikelbelegung der Fenster wurden diese mit einem Stickstoffstrom gespült. Unterhalb der Stufe ist ein weiterer Brenner montiert, dessen Flamme durch einen Schlitz kurzfristig auf die Plattenoberfläche gelenkt wird, um diese zu zünden.

Zum Einsatz kamen folgende Treibstoffe: (Zusammensetzung in Gew.%)

a] 64,1% HTPB, 5,9% IPDI, 30% Bor

b] 79,8% GAP, 10,2% N100, 10% Bor

Borpartikel amorph, mittlere Korngröße $\leq 2\mu m$

Die Lufteintrittstemperatur T_L betrug im Mittel $510^\circ C$. Die Treibstoffe wurden unter Atmosphärendruck verbrannt. Die Ermittlung des Luftmassenstroms ergab 0,155kg/s mit einem Sauerstoffanteil von ca. 21% und einem Wasseranteil von 1%. Die mittlere Brennzeit für Treibstoff a] lag bei 90 sec, die von b] bei 25 sec.

Das Filterradspektrometer wurde mit einer CaF_2 Vorsatzlinse von 125mm Brennweite betrieben. Somit ergab sich ein recht geringer Abstand zur Brennkammermitte von nur 420mm zum Eingangsspalt des Spektrometers. Dies war erforderlich, da die Flammenzone optisch dicht erschien und somit nur eine kleine Emissionsfläche zur Verfügung stand. Die Drehfrequenz wurde auf 50Rps eingestellt. Im Gegensatz dazu waren die Signale für das Zweifarbenpyrometer intensiv genug, um das in 0.8m entfernte System in dieser Position zu belassen.

Die Aufzeichnung der beiden Meßsysteme erfolgte synchron mittels PC und schneller Datenerfassungskarte (4 Kanal, 1MHz Summenabtastrate).

5. Diskussion der Ergebnisse

Es wurden von Treibstoff a] und b] je fünf Platten abgebrannt. Die ausgewerteten Spektren und Pyrometersignale zeigen gute Reproduzierbarkeit der Ergebnisse, sodaß sich die Diskussion auf die quantitativ unterschiedlichen Meßwerte konzentrieren kann.

Abb. 3 und 4 repräsentieren die Temperaturauswertung von Treibstoff a] respektive b]. Der HTPB Treibstoff mit 30% Boranteil zeigt höhere Partikeltemperaturen als GAP mit 10% Bor. Offensichtlich ist der Energieeintrag des Bors in der Reaktionszone oberhalb der Pyrolyseschicht maßgeblich für das dortige Temperaturniveau verantwortlich. Ein Vergleich der Verbrennungswärmen der reinen Bindersubstanzen würde gleichermaßen eine etwas höhere Verbrennungstemperatur der HTPB Formulierung erwarten lassen. Die thermodynamische Berechnung der adiabatischen Flammentemperatur ergibt für a] einen Wert um 2600K {2000K} und für b] 2580K {1870K}. Im Vergleich dazu die gemessenen Werte der Partikeltemperatur in Klammer. Um die hohe Zeitauflösung des Zweifarben-Pyrometers zu verdeutlichen wurden in den Abbildungen 3 und 4 die Zeitachsen in den unteren Bildausschnitten nochmals gespreizt.

Die Auswertung der Aufzeichnungen in Abb. 2 zeigt typische, für Treibstoff a] und b] gemessene, IR-Spektren mit den Hauptbanden des Wassers und CO_2 . Die absolute Strahlungsintensität ist beim Treibstoff mit GAP um den Faktor vier größer, was durch den in der gleichen Größenordnung erhöhten Massenstrom erklärt werden kann. In den Spektren des Treibstoffs a] ist im Bereich der Wasserbande bei 2,8μm eine Verbreiterung erkennbar, die auf HBO_2 Bande zurückzuführen ist. In allen IR-Spektren ist kein B_2O_3 erkennbar. Diese sollte bei 4,8μm auftreten, sofern die Verbrennungstemperatur in der Reaktionszone ausreichend hoch ist, um die weitere Umsetzung des HBO_2 in B_2O_3 zu fördern /2/. Mit Hilfe eines Computercodes, der die Banden des Wassers und des CO_2 modelliert, wurden für beide Treibstofftypen die Spektren in Form eines Parameterfits nachgerechnet. Die Ergebnisse sind in den Abb. 5 und 6 dargestellt.

6. Literatur

/1/   A. Blanc , Schnelle optische Analysesysteme für reaktionskinetische
       Untersuchungen, T/RF 11 / M 0001 / M 1100, ICT Eigenverlag, 1992

/2/   D. Meinköhn , The Ignition of Boron Particles , Combustion of Boron Based
       Slurries in a Ramburner, 22nd Int. Annual Conf. of ICT Karlsruhe 1991
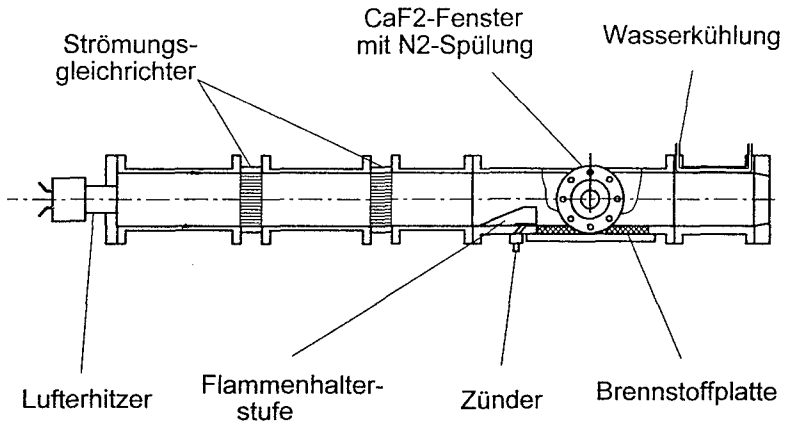
Abb. 1 Skizze der Stufenbrennkammer mit CaF_2 - Fenster
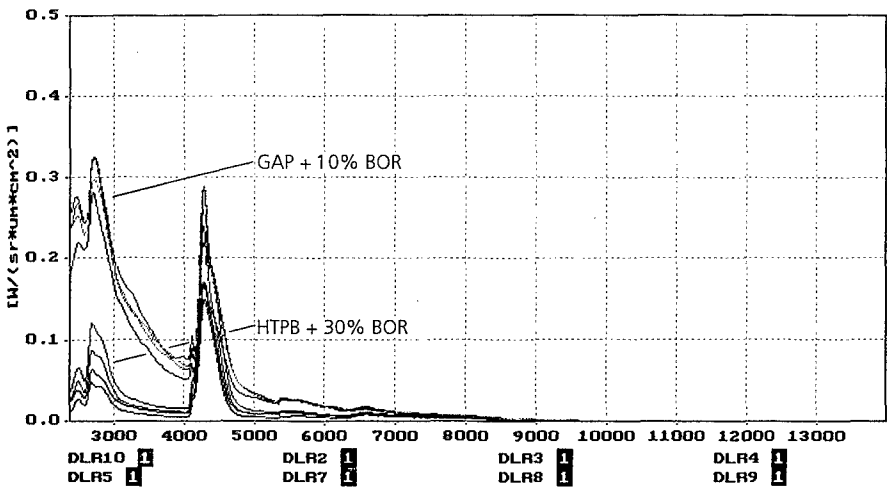
Abb. 2 Typische NIR - Spektren der beiden Versuchsreihen

DATA: C:\RAK\DLR4.DMA   16-10-1995
CAL :   C:\PYRO2\12DLR95.CAL   5-1-1996

T [K]

[ms]

DATA: C:\RAK\DLR4.DMA   16-10-1995
CAL :   C:\PYRO2\12DLR95.CAL   5-1-1996

T [K]

[ms]
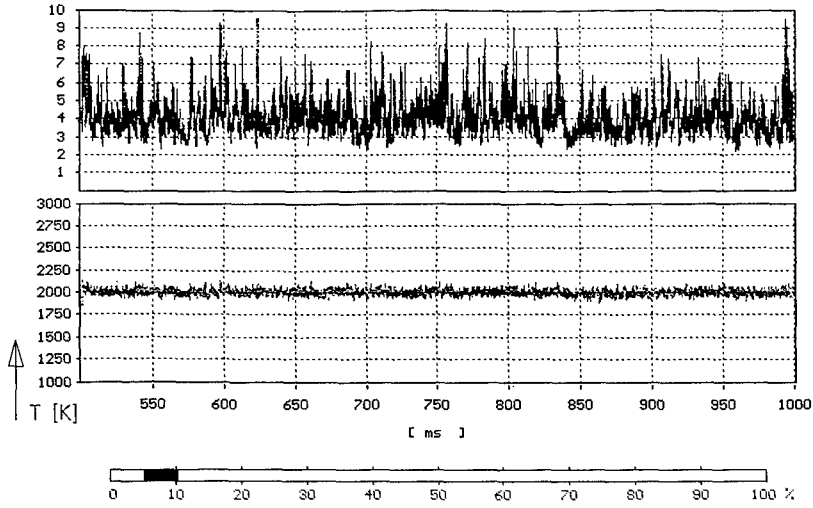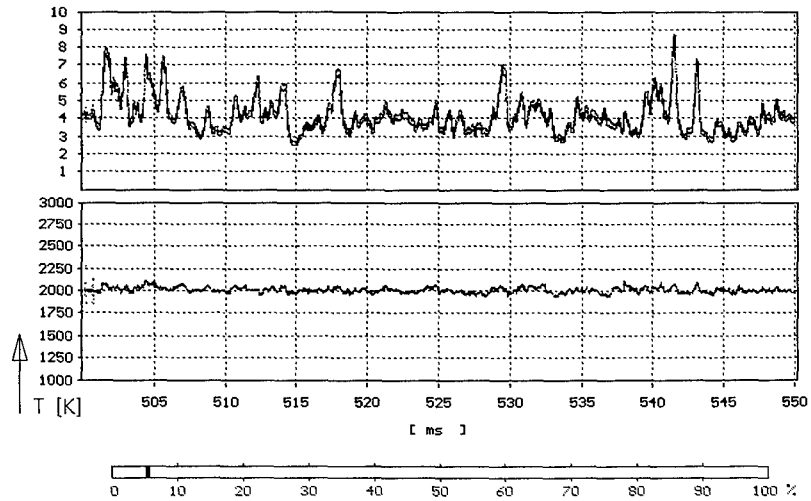
Abb. 3 Pyrometersignale und Temperaturauswertung   HTPB+30% Bor
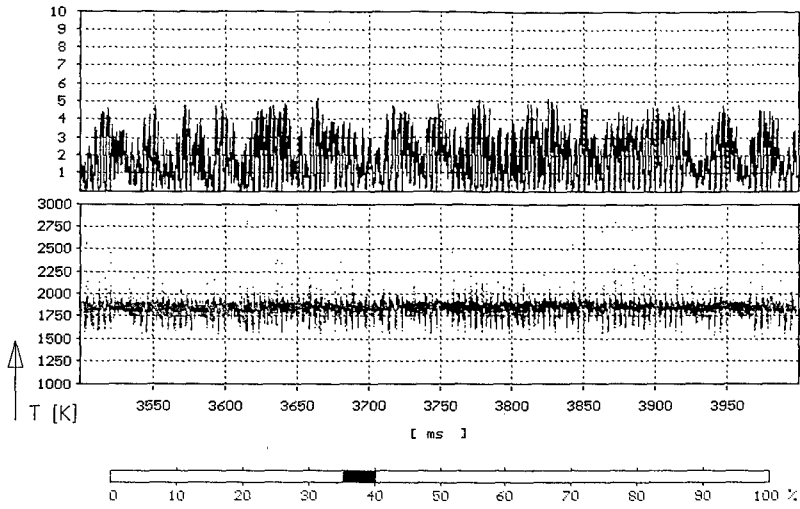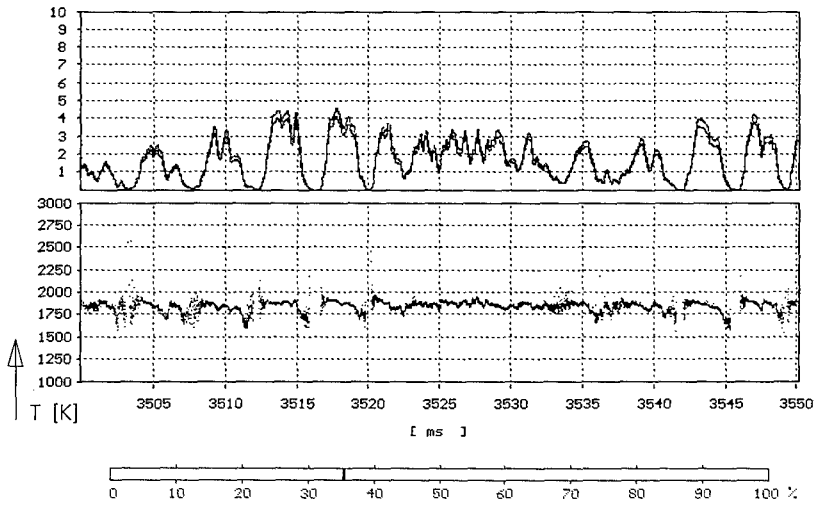
Abb. 4 Pyrometersignale und Temperaturauswertung GAP+10% Bor
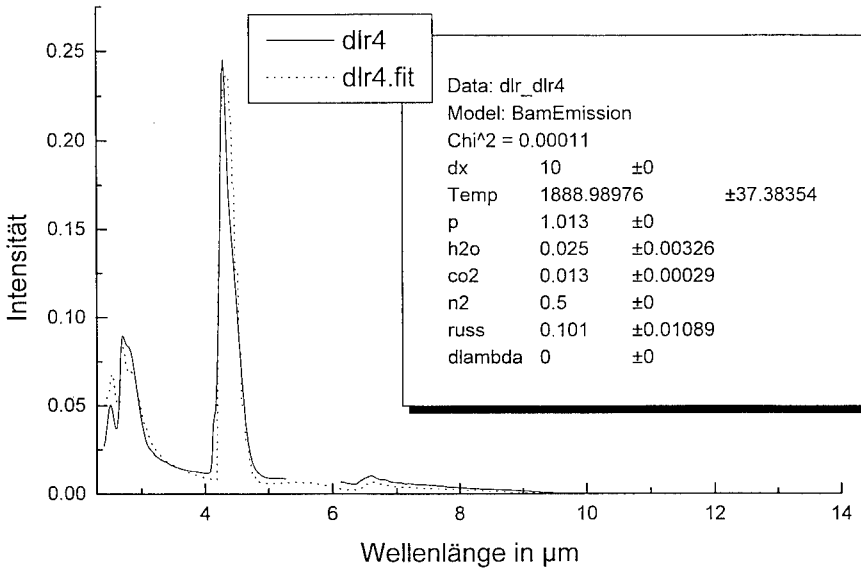
Abb. 5 Temperaturabschätzung mittels Molekülbandenmodellierung
Treibstoff HTPB + 30% Bor
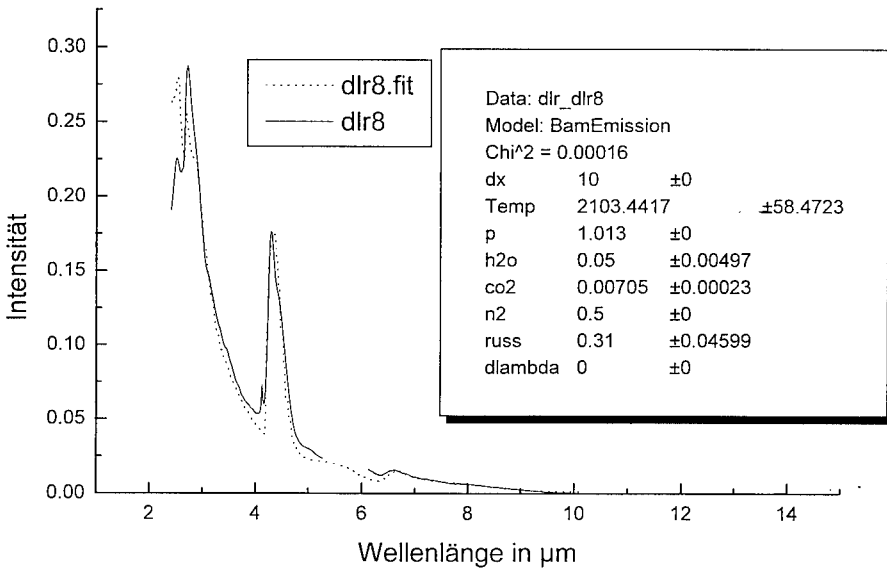
Abb. 6 Temperaturabschätzung mittels Molekülbandenmodellierung
Treibstoff GAP + 10% Bor

THERMAL STUDIES ON DMNB, A DETECTION AGENT FOR EXPLOSIVES

David E.G. Jones and Rainer A. Augsten
Canadian Explosives Research Laboratory
Natural Resources Canada
555 Booth Street
Ottawa, Ontario   K1A 0G1
CANADA

Abstract

Detection agents are incorporated into plastic explosives at the point of manufacture as a security measure. This practice has evolved as a result of efforts under the auspices of the International Civil Aviation Organization (ICAO) to combat terrorism. DMNB (2,3-dimethyl-2,3-dinitrobutane) has been selected as the most suitable of four potential detection agents for this purpose. Over the past four years, our laboratory has determined thermal and mechanical properties of the detection agents and their mixtures with various explosives. This work has been directed toward assessing the compatibility of the detection agents with the explosive in question. A continuing, international effort is underway aimed at determination of the properties of DMNB. As part of that effort, we have studied the thermal properties of DMNB in both the solid and solution phase. This paper describes the results of DSC studies, using both isothermal and nonisothermal techniques principally to determine the kinetic parameters for the decomposition of DMNB. Additionally, the results of ARC measurements are outlined and the data are analyzed to estimate kinetic parameters. The parameters determined from the DSC and ARC measurements are compared and the results for the solid and solution measurements discussed in terms of an expected mechanism for decomposition.

Introduction

International counter terrorism activities have accelerated as a result of the Air India and Pan Am (Lockerbie) incidents. The International Civil Aviation Organization (ICAO) has recently sponsored a program [1] for addition of volatile detection agents to plastic explosives in order to control illegal transport of these explosives. One particular detection agent , DMNB (2,3-dimethyl-2,3-dinitrobutane) has been identified as the most suitable of the four possible agents, for this purpose.

Extensive studies have been conducted on the detection agents and their mixtures with a variety of explosives. In particular, we have reported [2] the results of DSC (differential scanning calorimetry) studies on mixtures of the detection agents with tetryl. Additionally, DMNB per se has been characterized by DSC and NMR studies [3]. In this latter work, the various transitions observed in the DSC curve were analyzed in detail, and the kinetic parameters for the decomposition process were determined. In this paper, we report the results of further analysis of the DSC data, vapour pressure results in the temperature range of 400 to 500 K and ARC (accelerating rate calorimetry) measurements on pure DMNB. Additionally, kinetic parameters were obtained from solution studies of DMNB in mesitylene using both DSC and ARC, since overlap of the fusion endotherm and decomposition exotherm observed in the DSC measurements on the pure material poses a potential problem.

Experimental

Materials

DMNB was acquired from Aldrich Chemical Co. and was stated to be at least 98 mol % pure. Samples of DMNB purified by sublimation or recrystallization showed no discernible difference in the DSC from those untreated. Mesitylene, listed as 99 mol % pure, was obtained from Aldrich Chemical Co. and was used without further purification. No thermal events were detected for mesitylene between 323 and 623 K in a DSC experiment.

Sample Preparation

DSC measurements were conducted on solutions of DMNB in mesitylene loaded into sealed glass microampoules, similar to those described in the literature [4]. The inner wall of glass capillary of 1.0 ± 0.1 mm ID and wall thickness 0.35 ± 0.05 mm (Kimble Products Inc.) was pretreated with HF to reduce liquid surface creep and subsequently, the capillary was sealed at one end. The appropriate amounts of each of DMNB and mesitylene were loaded into the sealed capillary by mass and the inner walls were carefully cleaned.

The microampoules containing sample were constructed by sealing the capillary with an oxyacetylene flame, while maintaining the end containing the sample at about 233 K by means of a specially designed holder cooled by a thermoelectric device. The microampoule could be

manufactured in any size from 5 to 10 mm in length (limited by the size of the platform in the DSC cell chamber).

For all the measurements done in this study, an effort was made to make the microampoules of uniform length and therefore of uniform volume, namely about 5 mm^3.

After sealing, each microampoule was examined under a microscope for any sign of a flawed seal or of premature decomposition of sample. The microampoule was reweighed to check for sample loss and/or decomposition. Consistency of results obtained for analysis of both standards and DMNB provides additional evidence for the integrity of the sealing technique.

DSC Measurements

A DSC 910-TA 2100 System (TA Instruments) with an oxygen-free purge gas at a flow rate of 50 cm^3 min^{-1} was used for all measurements. The instrument was calibrated with respect to temperature and heat flow using an appropriate pair selected from the standards indium, tin, zinc or lead. Calibration was checked by using another standard from the above list, with an intermediate melting temperature. Identical experimental conditions, eg. heating rate and sample container, to those used in subsequent experiments were used in the calibration procedure.

In the vapour pressure measurements done on pure DMNB, the sample was placed in a hermetic pan having a lid with a laser-produced pinhole of about 100 μm in diameter. The procedure recommended by ASTM E 37.01.05 was closely followed, sample sizes of about 5 mg and a heating rate of 5 K min^{-1} were used.

In the kinetic studies following ASTM E 698 [5] heating rates, β from 6 to 14 K min^{-1} were used. In the verification procedure described in ASTM E 698, samples were aged at 483 K for a period of 1 h, quenched, and subsequently subjected to a heating rate of 10 K min^{-1} for determination of the ΔH for decomposition of the remaining DMNB. Isothermal DSC results at temperatures from 500 to 520 K were analyzed using the Isothermal Kinetics software supplied by TA Instruments.

ARC Measurements

An accelerating rate calorimeter was used to test the thermal stability of DMNB. In all cases, 0.5 g of DMNB was used and, for the measurements in solution, sufficient mesitylene was added to make solutions of 20, 30 and 40 mass % DMNB. Most experiments were conducted in spherical titanium bombs using a nitrogen atmosphere but some additional studies were done using Hastalloy bombs or an air atmosphere.

The ARC is an automated instrument from which experimental results may be determined for an exothermic process occurring in an adiabatic environment. It has been used to estimate the hazard potential of energetic material, including explosives.

A description of the thermokinetic information available from the ARC has been published previously [6]. A complete description of the experimental procedure and some specific applications to thermal hazard evaluation have been presented elsewhere [7].

To operate the ARC, equilibration at a starting temperature is followed by an iterative "heat-wait-search" technique until the appearance of a self-heating rate above a preset threshold limit, selected as 0.04 K min^{-1} in these experiments. The temperature at which this occurs is referred to as the onset temperature. When an exotherm is detected, time, temperature, rate of temperature increase and pressure are monitored continuously until the condition of the preset limit is no longer met. At this point, the exothermic process is considered complete.

Results and Discussion

Pure DMNB

Figure 1 shows a typical DSC curve for DMNB at a heating rate of 5 K min^{-1}. The low temperature endotherm is reported to be a result of an intermolecular transformation, in which there is rotation about the central C-C bond, resulting in a change from a molecule with NO_2 groups in the gauche position to one with groups in the trans position [8]. It is indicated that a significantly larger fraction of the DMNB is in the gauche conformation in the solid phase, because of intermolecular packing considerations. The endotherm at 387 K characterizes a crystalline phase transformation from triclinic to body centered cube, and this has been

confirmed by both X-ray [9] and NMR [3] data. In concert with the large exotherm

representing the decomposition of DMNB, there is a small endotherm resulting from the fusion of

DMNB. The DSC results suggest a slow decomposition in the solid phase but clearly, enhanced

decomposition of DMNB is prompted by the presence of the liquid phase. However, the overlap

of these two peaks prevents direct determination of $\Delta_{fus}H$ with any degree of accuracy from the

DSC data. In fact, the observed $\Delta_{fus}H$ is heating rate dependent but not entirely separable from

the decomposition exotherm even at 50 K min^{-1}. Table 1 lists thermodynamic data for DMNB,

including a value of $\Delta_{fus}H$ obtained by numerical deconvolution of the DSC data. Additionally, it

is known [10] that the overlap of the fusion endotherm and decomposition exotherm introduces

some uncertainty into the kinetic parameter results.

Further, there is a substantial vapour pressure of DMNB prior to the decomposition

exotherm (estimated as about 30 kPa at 473 K), hence, it is apparent that all three phases of

DMNB are present in the region of the observed exotherm.

The results of vapour pressure measurements using the DSC are shown in Figure 2.

The value of $\Delta_{sub}H$ obtained from these data is significantly different from that obtained from gas

chromatographic data of Elias [11] up to 323 K, the latter study done for the purpose of

evaluating the utility of DMNB as a detection agent. There is a significant difference in the

temperature ranges and, additionally, DMNB is in a different crystalline state in each of these

temperature ranges. Thus, a difference in $\Delta_{sub}H$ values is not unexpected. The DSC technique

is not suitable for measurements in the intermediate temperature range from 323 to 400 K.

Further, at pressures above about 40 kPa there is overlap of the sublimation and fusion

endotherms.

The results from a typical ARC experiment, using 0.5 g of DMNB, are shown in Figure 3.

Since R_m > 10 K min^{-1} , adiabatic conditions were not maintained in the ARC experiments,

hence no further analysis of the data was warranted. It is noted that the onset temperature of

456 ± 3 K occurs prior to fusion, indicating that substantial decomposition occurs in the solid

and/or gas phase.

Mesitylene Solutions of DMNB

A series of DSC experiments at different values of β provided the information required to determine the kinetic parameters in accordance with the ASTM E 698 procedure [5]. The results of this analysis are depicted in Figure 4 and the kinetic parameters are summarized in Table 2. The isothermal aging test described in the ASTM E 698 procedure yielded a ΔH value within 8 % of the calculated value, assuming a first order model applies.

The ΔH value recorded in Table 2 is independent of both β and solution concentration, but is significantly less exothermic than that determined for pure DMNB, which suggests differences in the final products for the two cases. Kinetic parameters determined for the solution phase studies are compared with those for pure DMNB taken from the earlier publication [3] in Table 2. The apparent first order rate constants indicate that decomposition proceeds substantially faster in pure DMNB than in solution. While there is evidence [3] for a one-step mechanism involving a five centered transition state for decomposition in pure DMNB, the results obtained here suggest that a two-step process involving homolytic C-N bond cleavage might be operative in solution.

Additionally, some DSC experiments were conducted at 10 K min^{-1} using mesitylene solutions with 30 and 50 mass % DMNB. No variation in the ΔH value was observed but the peak temperatures were found to be concentration dependent, as shown in Figure 5. Since the peak temperature is inversely proportional to the rate, it is clear that the rate increases with concentration of DMNB.

A series of isothermal DSC experiments were conducted on a 20.0 mass % solution of DMNB in mesitylene. The nature of the isothermal curve, as exemplified in Figure 6, appears to rule out an autocatalytic process. An Arrhenius plot of the rate constants derived from these experiments is shown in Figure 7. The kinetic parameters estimated from these data are listed in Table 2. Considerable variation in the order of reaction, n, was obtained from the analysis of these results but it appears that $n \approx 0.2$.

Solutions of 20.0, 30.0 and 40.0 mass % DMNB in mesitylene were studied using the "heat-wait-search" technique in the ARC. The results obtained for a 20.0 mass % solution in a titanium bomb in both nitrogen and in air are compared in Figure 8, as well as those for the same solution in a Hastalloy container. It is clear that the experimental results are not significantly dependent on the environment in the bomb. It seemed important to test this behaviour since there is considerable free space above the sample. Further, differences between the results for the titanium and Hastalloy bombs can be accounted for by the difference in masses, 10 g and 20 g, respectively, and hence the thermal inertia factor. It should be noted that the onset temperature did not vary significantly in these experiments.

Typical results for a 20.0 mass % solution are shown in Figures 9 and 10. The onset temperature of 457 $\pm$ 3 K is independent of concentration and is in excellent agreement with the onset temperature observed for solid DMNB in the ARC. This observation confirms the indication of early decomposition seen in the DSC curve for solid DMNB.

The maximum rate is concentration dependent as shown in Figure 5. The activation energy quoted in Table 2 for the ARC measurements was obtained by isolating the linear portion in a plot of ln R against 1/T for all the solution data. Preliminary attempts to analyze the data by methods described in [7] led to inconsistent results. It did not seem profitable to attempt further analysis at this stage without incorporating the effect of thermal inertia and/or examining the effect of concentration on the various models.

Conclusions

Significant improvements and additions to the fundamental thermodynamic data for DMNB have been made, although attempts to precisely determine the enthalpy of fusion have been thwarted. Use of an eutectic mixture may provide a mechanism for obtaining this result. A DSC technique has provided a route to a precise value of the enthalpy of sublimation for the cubic structure of DMNB but the crystalline phase transitions interfere with this method at lower temperatures. This technique is useful for estimation of the partial pressure of DMNB in solution measurements.

Results of solution measurements suggest decomposition by a different mechanism and at a slower rate than for the solid. The onset temperature, as determined in the ARC measurements, is independent of the state of DMNB and its concentration in solution. This temperature is significantly lower than the apparent fusion temperature, indicating that decomposition starts prior to fusion. It appears that decomposition is accelerated by the presence of the liquid phase in the measurements on pure DMNB. Further analysis of the ARC results for DMNB solutions seems to be warranted.

References

1.   Doc. 9571, ICAO Convention, International Civil Aviation Organization, Montreal, March 1, 1991.

2.   D.E.G. Jones, R.A. Augsten, and K.K. Feng, J. Thermal Analysis, 44 (1995) 533.

3.   D.E.G. Jones, R.A. Augsten, K.P. Murnaghan, Y.P. Handa and C.I. Ratcliffe, J. Thermal Analysis, 44 (1995) 547.

4.   L.F. Whiting, M.S. Labean and S.S. Eadie, Thermochim. Acta, 136 (1988) 231.

5.   ASTM E 698-79 (Reapproved 1993), Arrhenius Kinetic Constants for Thermally Unstable Materials, American Society for Testing Materials, Philadelphia, PA, USA.

6.   D.I. Townsend and J.C. Tou, Thermochim. Acta, 37 (1980) 1.

7.   R.A. Augsten, K.J. Mintz and D.E.G. Jones, EXP 95-04, March 1995.

8.   B.G. Tan, L.H.L. Chia, H.H. Huang, M.H. Kuok and S.H. Tang, J. Chem. Soc. Perkins Trans II (1984) 1407.

9.   T. Nishizaka, F. Katuragawa, K. Sawada, T. Oda and T. Koide, Chem. Express, 2 (1987) 257.

10.   R.N. Rogers, Thermochim. Acta, 3 (1972) 437.

11.   L. Elias, private communication.

Table 1

Thermodynamic Data for Phase Transformations in DMNB

Phase Change	Method	T/K	$\Delta H/kJ\ mol^{-1}$
Sublimation	vapour pressure g.c.	≤ 323	94 ± 1
	DSC + vapour pressure	413 to 503	63.5 ± 0.7
Fusion	ΔH_f data	298	15 ± 3
	solubility	≤ 308	29 ± 6
	DSC + deconvolution	473	8.8 ± 0.5
Vapourization	$\Delta_{sub} H - \Delta_{fus} H$	298	79 ± 4
		308	65 ± 7
		473	55 ± 1
I - II	DSC	322	1.14 ± 0.05
II - III	DSC	387	17.7 ± 0.5

Table 2

Decomposition Results for DMNB, Pure and in Mesitylene Solution

Method	Parameter	Pure	Solution
	$\Delta H/kJ\ mol^{-1}$	540 ± 25	436 ± 12
DSC constant β	$E/kJ\ mol^{-1}$	160 ± 8	133 ± 14
	$\ln (Z/min^{-1})*$	35.5 ± 2.1	29.02 ± 0.11
	$E/kJ\ mol^{-1}$	155 ± 7	133 ± 5
DSC isothermal			
	$\ln (Z/ min^{-1})$	34.43 ± 0.07	28.54 ± 0.03
ARC	$E/kJ\ mol^{-1}$	____	121 ± 10

*assuming first order reaction

Figure 1
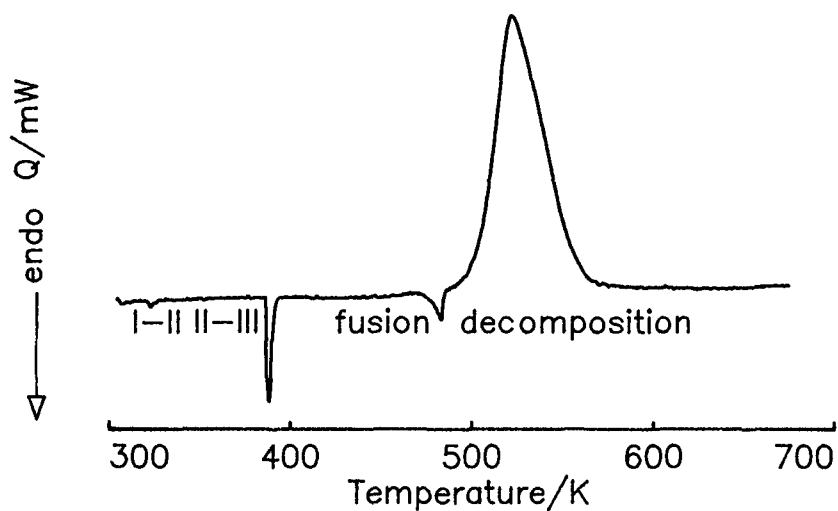
Figure 2
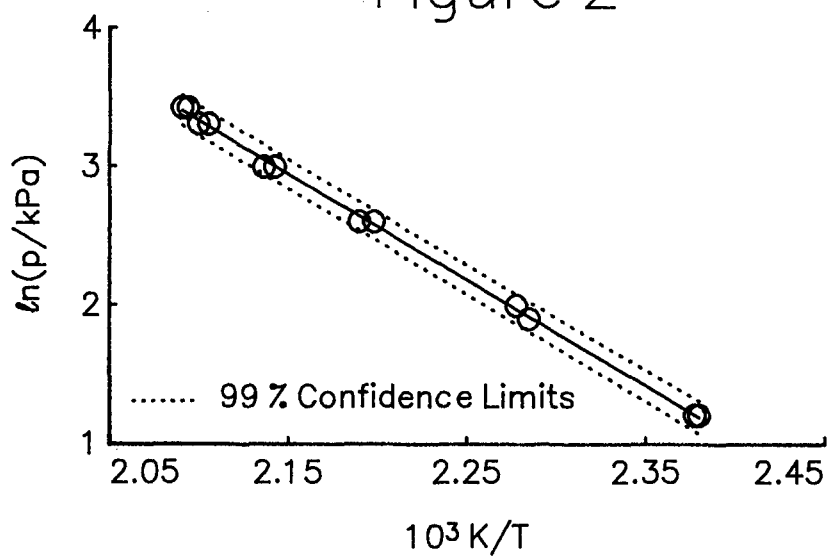
Figure 3
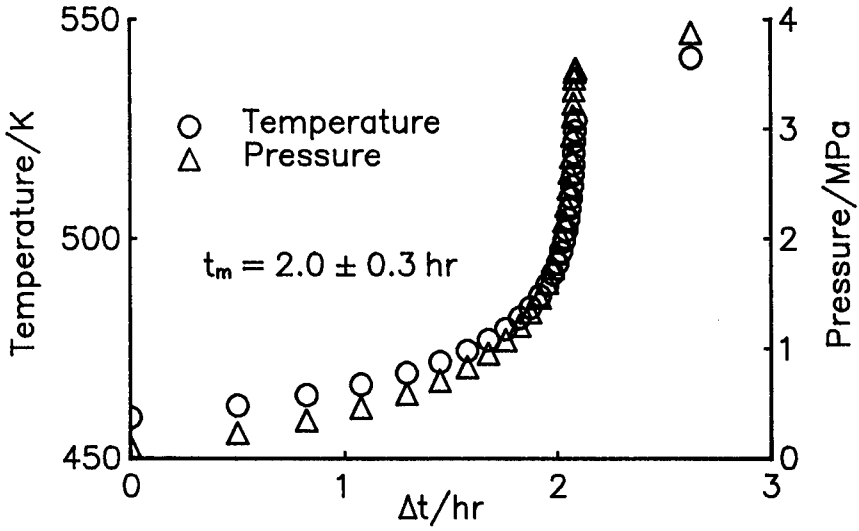
Figure 4
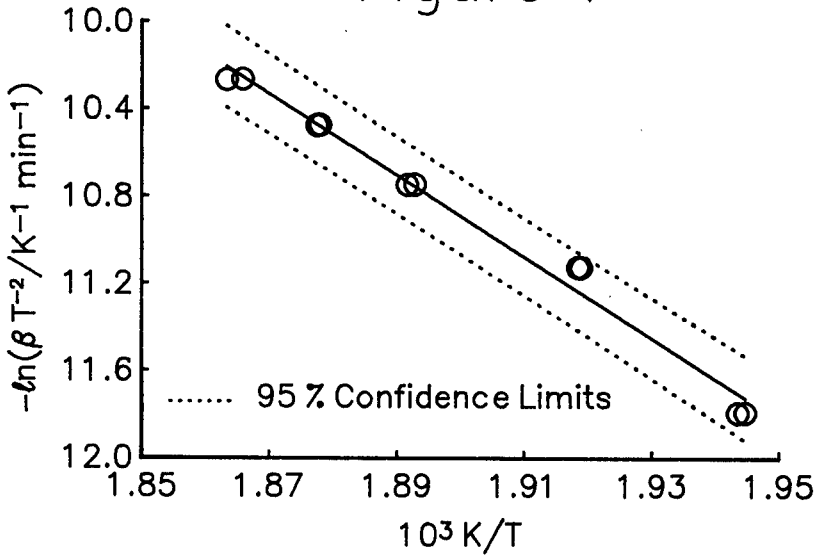
Figure 5
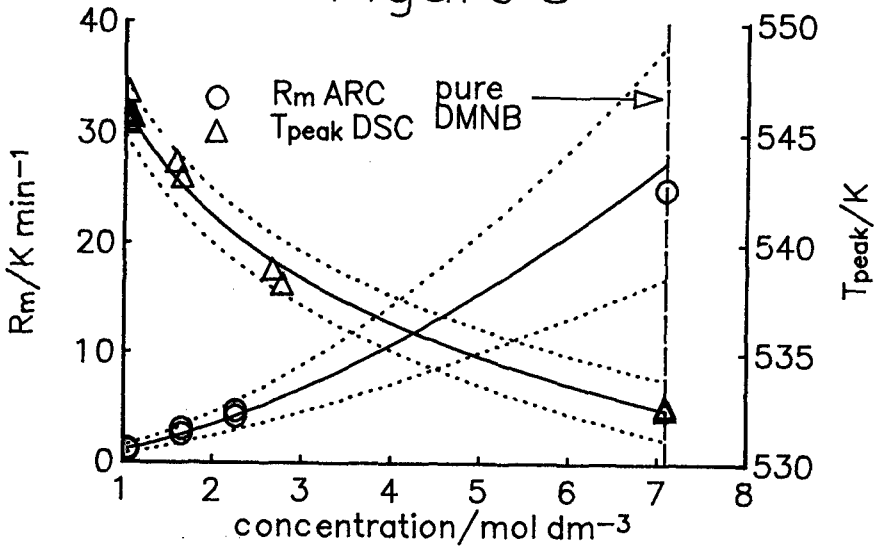
Figure 6
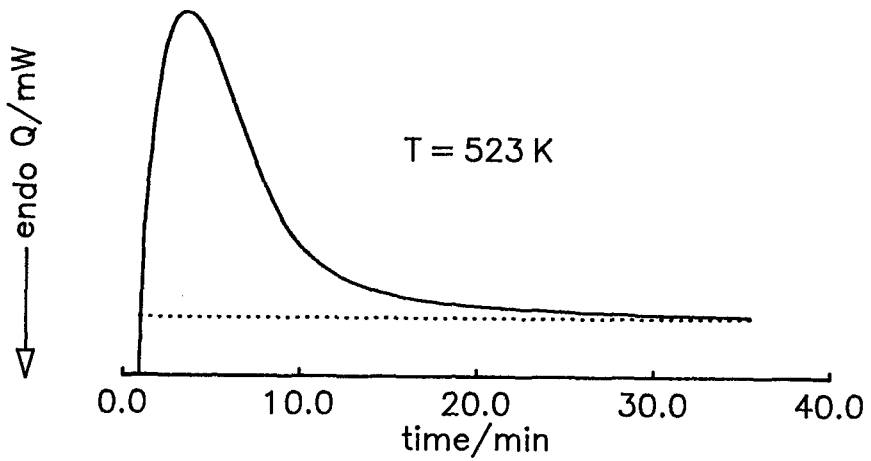
Figure 7
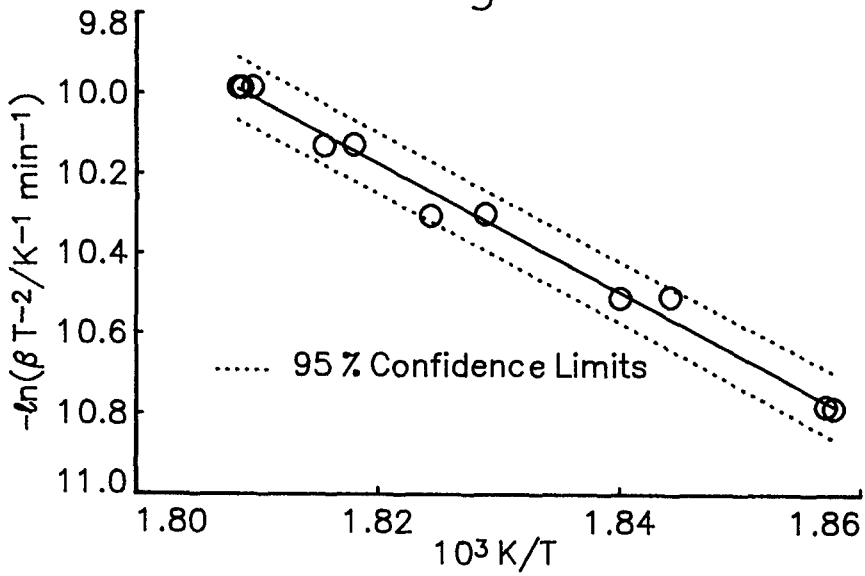
Figure 8
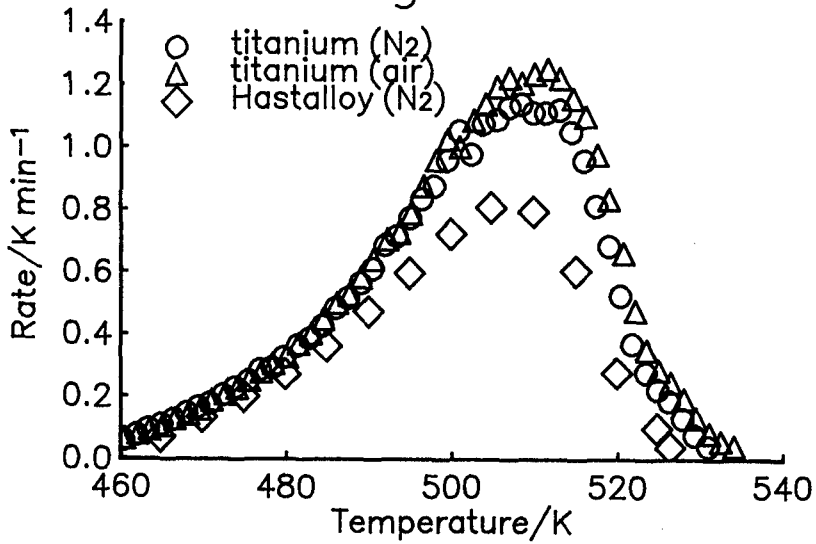
Figure 9
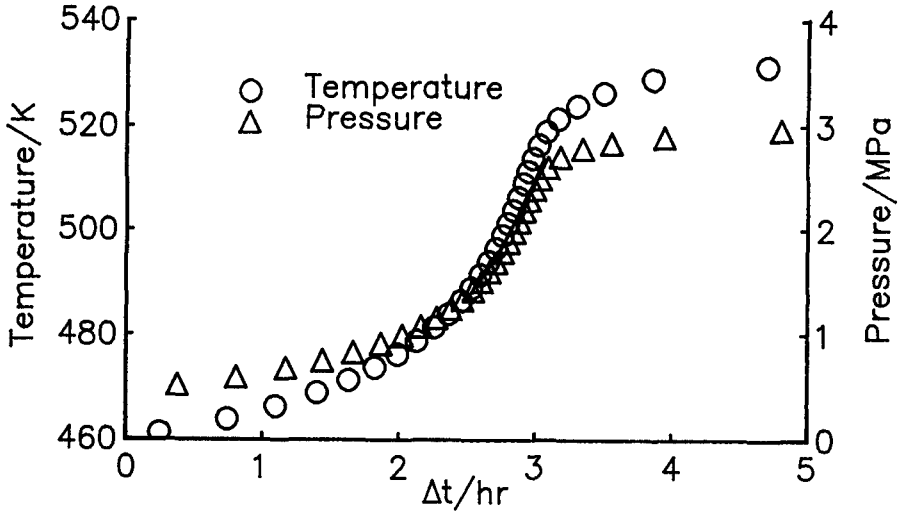
Figure 10
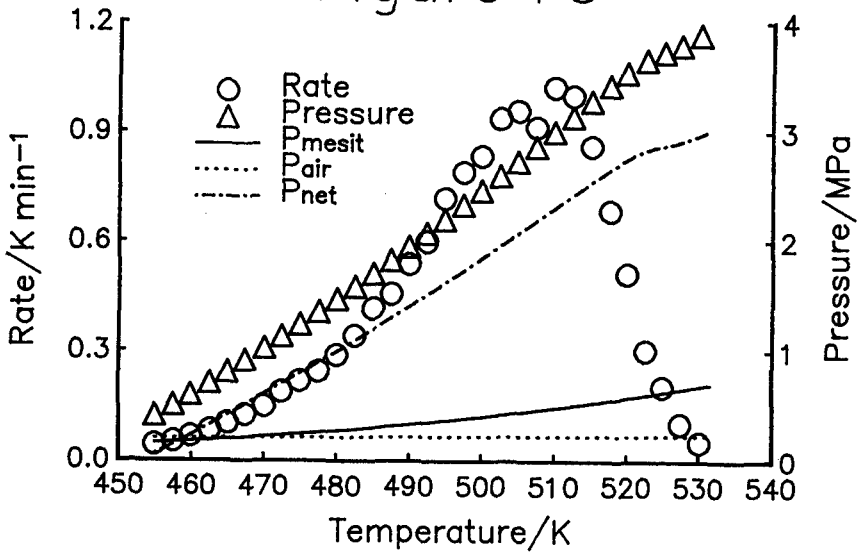
STABILITY STUDIES OF SPHERICAL PROPELLANTS

Pierre GUILLAUME*, André FANTIN*, Mauricette RAT**,
Stephan WILKER***, Gabriele PANTEL***

* P.B. Clermont S.A., Rue de Clermont 176, B-4480 ENGIS (Belgium)

**SNPE, Centre de Recherche du Bouchet, Rue Lavoisier, LE BOUCHET - BP N°2, F-91710 VERT-LE-PETIT (FRANCE)

***Bundesinstitut für chemisch-technische Untersuchungen beim BWB (BICT), Großes Cent, D-53913 SWISTTAL (GERMANY)

ABSTRACT

Different kinds of spherical propellants were investigated by various techniques.

In the first part, we discuss the influence of ingredients on the classical stability tests (Holland test, Bergmann-Junk test, Weight loss at 90°C).

In the second part, Heat flow microcalorimetry and stabiliser consumption results are compared to classical tests.

It can be summarised that the classical tests are not always reliable in concern to the stability of the propellant but depends on the way the test is conducted and on the chemical composition of the propellant. On the other hand, Heat flow microcalorimetry in combination with stabiliser consumption is a far better method to assess the chemical stability of the propellants.

1. INTRODUCTION

From the beginning of the manufacturing of smokeless propellants, the stability of the powders has been assessed through high temperature tests.

Two topics are involved with the results of those tests:

1.The useful service life of the propellant

2.The possibility of self ignition

The two aspects are the consequences of the exothermic decomposition to which the propellant is subject even at normal storage temperature [1 - 4].

The different high temperature tests are mainly based on the weight loss like for Holland test or gas evolution chemically recorded like in the Bergmann-Junk test. All those tests are performed at temperatures between 90°C and 134°C.

Moreover, extrapolations performed from those high temperature tests tend to overestimate the shelf life of the propellants at ambient temperature [5].

Finally, most of the acceptance testing values for the classical tests are grown historically by transferring the data from one propellant to a newer one of close composition.

Therefore most of the classical tests can lead to a yes/no acceptance without giving any information on a realistic chemical life of the propellant.

During the last 30 years, the tremendous development of analytical techniques has given more powerful tools to assess the service life of the propellants from lower temperature measurements. Among those techniques , we have:

-High pressure liquid chromatography (HPLC) has lead to allow the measurement of the consumption of the stabiliser and of its derivatives [6], [7].

-The Gel Permeation Chromatography (GPC) permits to follow the molecular mass depletion of the nitro-cellulose [8], [9].

-The Chemiluminescence detects the primary decomposition products (Nox) in dependence of the temperature of the samples and the atmosphere around it [10], [11].

-Heat Flow microcalorimetry (HFC) records all chemical and physical reactions which produce or consume heat during the whole measuring time [12 - 15].

The application of those techniques is possible at temperatures much lower than the classical tests, generally between 40 and 80°C. This allows to determine the kinetics of degradation of the propellant and to assess a more realistic useful service life of the propellants.

In this study, we have investigated different kinds of spherical propellants by the various techniques.

The spherical propellants, in appearance, consist of small spherical or flattened spherical grains that may undergo different surface treatments giving the required ballistic characteristics and reducing both barrel erosion and muzzle flash at the end of the production line.

To our knowledge, among the double base propellants, the spherical one's are the only stabilised only by diphenylamine (DPA). During the manufacturing of the powder and its normal ageing, the diphenylamine undergoes the same reaction scheme as other nitro-cellulose based propellants, the first derivative being the N-NO-DPA which is a stabiliser as efficient as diphenylamine [16].

Nevertheless, some spherical propellants fail to meet the specifications of high temperature classical tests [17].

For that reason, we have undertaken a more detailed investigation on the reactions that can take place in or at the surface of the grains. This study includes results from classical tests as well as from more recent tests like Heat Flow Microcalorimetry or Stabiliser Consumption in order to investigate the pertinence of the different tests to assess the chemical stability of the spherical propellants.

2. EXPERIMENTAL RESULTS

2.1 SAMPLES FORMULATIONS

For the purpose of this study, the double base spherical propellant K6210-13 was chosen, this propellant being generally at the edge of the accepted values for the classical tests. Special samples containing different amounts of surface agents were prepared. All samples contain 4.5% of dibutylphtalate which is used as a burn rate modifier. The samples'description and initial analysis are given in table I.

Samples were all made with the same raw materials . All samples were produced using 13.1% nitrogen nitro-cellulose.

2.2 CLASSICAL HIGH TEMPERATURES TEST

2.2.1 HOLLAND TEST AT 105°C

The principle of this test is the measurement of the weight loss at 105°C. The test is performed

in a stoppered glass-vessel within 72 hours [18]. The amount of propellant is 4g. The weight loss is determined by subtracting the first eight hours 'weight loss from the total weight loss. The results for the different samples are given in table II.

2.2.2 BERGMANN-JUNK TEST

The sample is heated to 115°C for 16 hours and the nitrogen oxides evolved are dissolved in an hydrogen peroxide solution and afterwards determined by titration
with sodium hydroxide n/100 [19]. The results are expressed as ml n/100 NaOH/g in table II.

2.2.3 WEIGHT LOSS TEST AT 90°C

The sample is heated at 90°C and weighted every 2 days [20] . The test is stopped when autocatalysis is occurring. The results are given in days for a 3% weight loss in table II and in figure 1.

TABLE I

SAMPLE	% SURFACE AGENT ADDED			COMPOSITION OF THE SAMPLES (%)				
	DPA	N-NO-DPA	KNO$_3$	NGL	DPA	N-NO-DPA	KNO$_3$	H$_2$O
A	0	0	0	18.2	0.68	0.48	0.0	0.76
B	0	0	0.5	17.5	0.63	0.46	0.37	0.32
L	0	0	1.0	17.8	0.61	0.45	0.82	0.39
H	0.1	0	0.5	17.7	0.67	0.45	0.46	0.42
G	0.3	0	0.5	17.5	0.82	0.46	0.46	0.43
F	0.5	0	0.5	17.7	0.94	0.46	0.42	0.42
E	0.7	0	0.5	17.5	1.04	0.47	0.33	0.49
I	0.3	0	0.1	17.9	0.78	0.45	0.17	0.47
J	0.3	0	0.3	17.8	0.81	0.45	0.26	0.42
M	0.2	0	0.0	19.1	0.60	0.62	0.0	0.30
N	0.2	0	0.5	19.0	0.54	0.64	0.72	0.37
O	0	0.2	0.0	19.2	0.45	0.74	0.0	0.43
P	0	0.2	0.5	19.1	0.46	0.76	0.40	0.30

TABLE II : RESULTS OF CLASSICAL TESTS

SAMPLE	A	B	L	H	G	F	E	I	J	M	N	O	P
HOLLAND TEST	0.47	0.59	0.58	0.65	0.74	0.75	0.69	0.55	0.74	0.59	2.0	1.1	1.4
BERGMANN-JUNK	10.4	11.0	10.0	10.5	13.5	14.0	15.5	12.1	14.2	8.2	12.5	7.3	8.0
90°C TEST	19	12	15	12	14	14	14	21	18	44	15	20	22
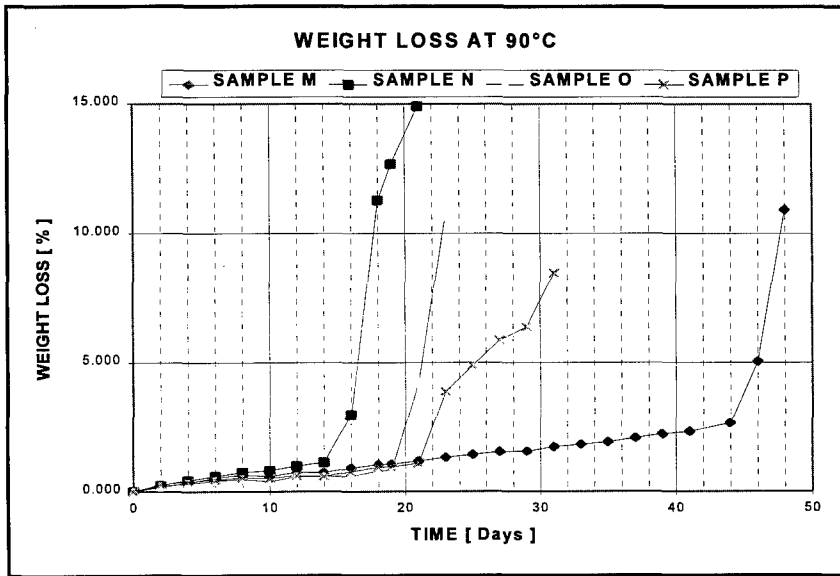
FIGURE 1 : 90°C TESTS RESULTS OF SELECTED SAMPLES

2.3 HEAT FLOW CALORIMETRY

The heat flux produced by all the physical and chemical reactions is measured at different temperatures (between 80°C and 30°C) on 3 grams of propellant sealed in a 4 ml glass ampoule. The instrument is a TAM microcalorimeter. The basic principle has already been described in various studies [13],[15]. No preliminary conditioning of the samples was applied and the measurements were recorded as soon as the samples were introduced into the microcalorimeter. At least double measurements were recorded on each sample.

Measurements were recorded on the same samples in the BICT and in P.B.CLERMONT with an excellent agreement of the results. Standard deviation is around 10%.

The figures 2 and 3 show the results recorded at 80°C for some samples.

For the evaluation of the data, we used constant heat flow values at the end of each measurement. The results of the investigation for samples M to P are collected in table III.
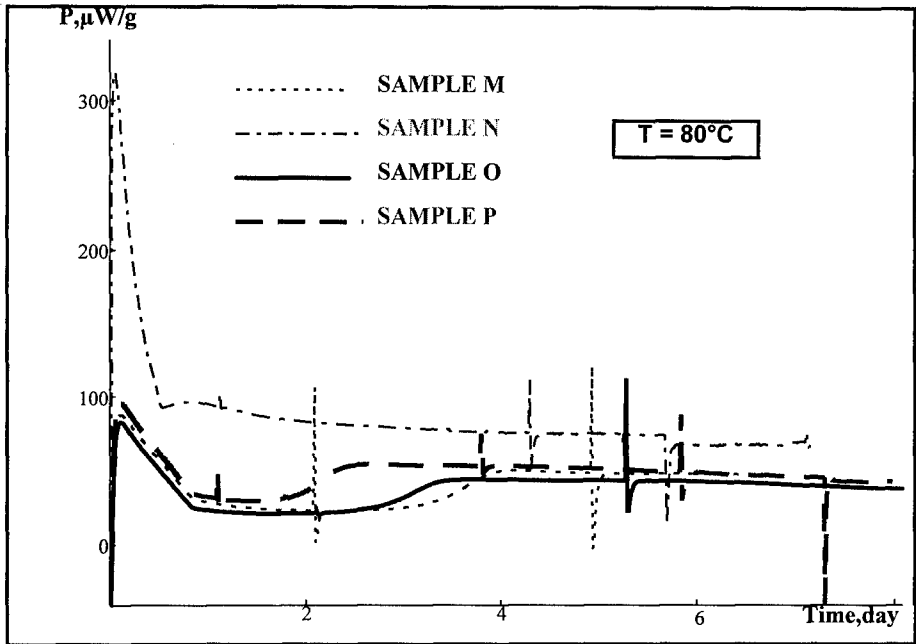
FIGURE 2 : HFC MEASUREMENTS AT 80°C
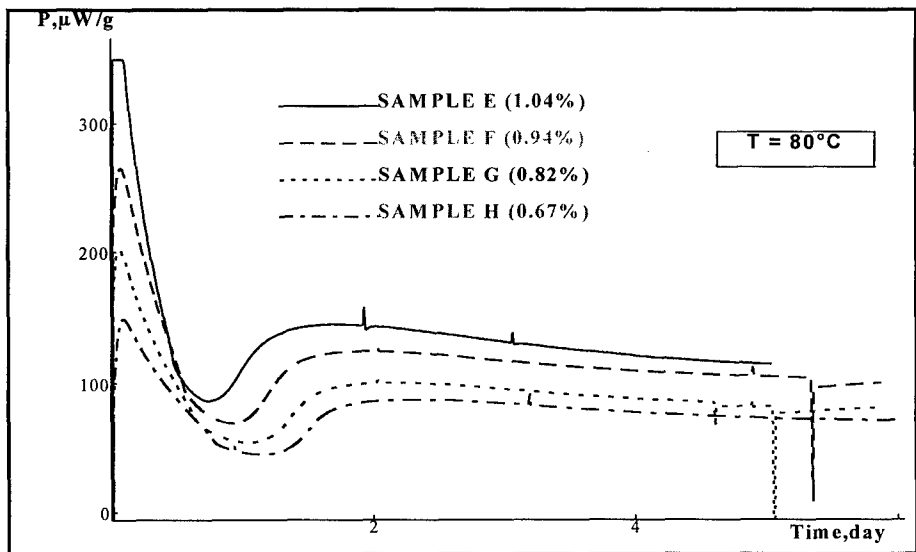
FIGURE 3 :DEPENDENCE OF HFC MEASUREMENTS ON DPA CONTENT (KNO$_3$ CONSTANT)

TABLE III :CONSTANT HEAT PRODUCTION RATE OF SAMPLES M TO P (μW/g)

T(°C)	SAMPLE M	SAMPLE N	SAMPLE O	SAMPLE P
80	44/43/46/46	68/66/73/44	30/31	42/43
70	11.9/12.3	21.4/9.6	10.4/10.6	14/6.5
60	3.8/3.4	3.5/a)	3.4/2.9	1.9/3.7
50	1.9/1.8	2.5/2.4	1.68/0.81	a)/a)
40	0.9/0.61/0.58/0.57	0.73/0.71/0.87	0.65/0.48	0.51/0.86
30	0.23/0.24	0.28/0.27	*/*	*/*

a)no evaluation of data possible

*)not determined

2.4 STABILISER CONSUMPTION

The propellant is heated for a period of time at temperatures between 50°C and 80°C in sealed ampoules like in the microcalorimetry tests. The stabiliser consumption [21] is measured by HPLC and recorded as a function of time.

2.5 GPC MEASUREMENTS

The GPC measurements show a decrease of the average molecular weight during the ageing of the samples but don't allow to make any conclusion on the stability of the propellants.

2.6 CHEMILUMINESCENCE

The preliminary chemiluminescence results show a significant increase of NOx emission when both DPA and KNO_3 are added to the propellant. More results will be presented at the conference.

3. DISCUSSION

3.1 CLASSICAL TESTS

The results of Bergmann-Junk tests show a remarkable dependence on the DPA content in the propellant, while it seems to be no effects of the KNO_3 content. This can not be explained without the HFC and stabiliser consumption experiments. One would indeed expects that the

higher content of DPA would absorb more NOx. Thus an increase in DPA content should result in a decrease of the Bergmann-Junk but in fact opposite is observed (Figure 4).
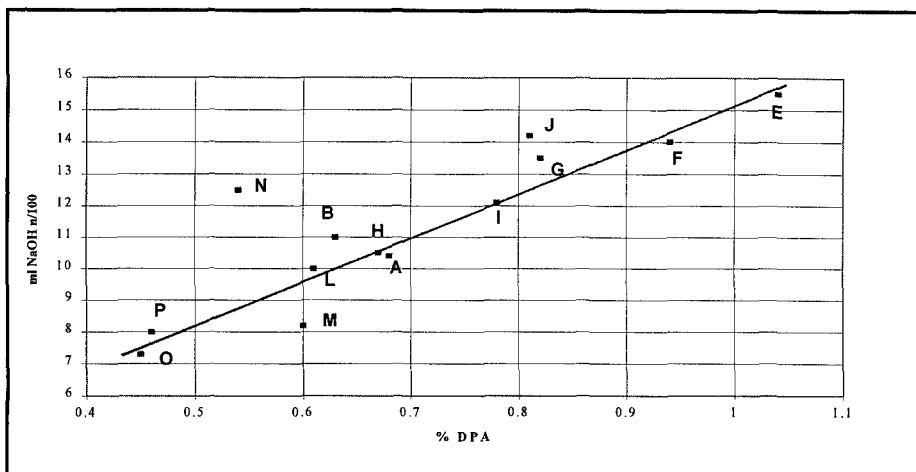
FIGURE 4 : CORRELATION BETWEEN BERGMANN-JUNK AND DPA CONTENT

The Holland test is independent of the kind of surface treatment while the 90°C test shows a dependence on the KNO_3 content when DPA is added at the surface . An exact explanation of this can not be forwarded. This might be due to the strong interaction between the operating method and the results.

In conclusion, those 3 tests show 3 different trends for the same propellants.

3.2 HEAT FLOW MICROCALORIMETRY

As shown in figure 3, there is a strong dependence of the HFC results and the DPA content. With increasing DPA content, the first maximum is higher, the valley is also higher and shortened, and the final value is also higher.

The same dependence can be observed with the KNO_3 content of the propellant (compare entries M and N in figure 2). When the total amount of KNO_3 is over 0.7%, the shape is different i.e. the valley is missing. The results of HFC are collected in table IV. Entries O and P (fig 2) show that the behaviour of KNO_3 with N-NODPA is less sensitive than with DPA because the 2 curves show the same shape and comparable values of heat production.

TABLE IV

KNO$_3$ CONSTANT (0.5%)				DPA CONSTANT (0.3%)			
DPA	A	B	C	KNO$_3$	A	B	C
0%	100	35	1.5	0%	87	25	3.5
0.1%	143	44	2.3	0.1%	112	37	3
0.3%	210	55	1.5	0.3%	136	40	2.5
0.5%	266	70	1.2	0.5%	210	55	1.5
0.7%	440	90	1.0	1.0%	1000	200	0

A : FIRST MAXIMUM (μW/g)
B : MINIMUM (μW/g)
C : SECOND MAXIMUM (days)

3.3 STABILISER CONSUMPTION

We compare the time when 50% of DPA content and 50% DPA + N-NODPA has been consumed. Without KNO$_3$ added, the samples M and O behave in the same manner. When KNO$_3$ is added, we have a different result for DPA and N-NODPA: DPA reacts much more rapidly with KNO$_3$ and N-NODPA shows no significant effect.

When DPA is increased with KNO$_3$ constant, the acceleration of stabiliser consumption is observed (see table V). Also there is an acceleration for stabiliser consumption when KNO$_3$ is added with constant DPA content. With increasing KNO$_3$, the formation of 2,2'DNDPA is favoured over the other dinitro derivatives.

TABLE V : TIME FOR 50% DPA CONSUMPTION AT 80°C (h)

KNO$_3$	DPA	0%	0.1%	0.2%	0.3%	0.5%	0.7%
0%		72		56			
0.1%					18		
0.3%							
0.5%			14		12	11	10
1%		9					

3.4 CORRELATION BETWEEN HFC AND STABILISER CONSUMPTION

We analysed the stabiliser consumption at different stages of HFC. At the minimum, most of the DPA has been converted into N-NODPA. When value is constant at the end, only N-NODPA is present besides small amounts of 2-N-DPA (see table VI and figure 5). The same correlation can be applied to the other samples. The effect of KNO$_3$ can be seen in figure 6: there is a rapid decrease of the DPA in correlation with the first peak. When all DPA is consumed, the heat generation is more or less constant which implies a constant stabiliser consumption.

TABLE VI: STABILISER CONSUMPTION AT DIFFERENT STAGES OF HEAT FLOW CALORIMETRY

Sample	Nr.	DPA	N-NO-DPA	2-N-DPA	4-N-DPA	2,2'-DN-DPA
		[%]	[%]	[%]	[%]	[%]
Before	0	45.9	48.7	2.7	2.7	0.0
1. Maximum	1	32.4	61.9	3.0	2.7	0.0
1. Minimum	2	4.1	89.6	3.5	2.8	0.0
2. Maximum	3	0.6	96.8	1.8	0.8	0.0
End of meas.	4	0.0	97.1	0.0	1.4	1.5
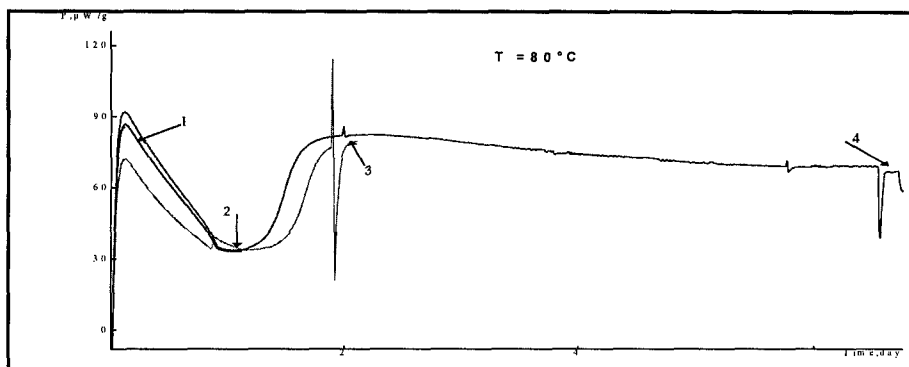
FIGURE 5
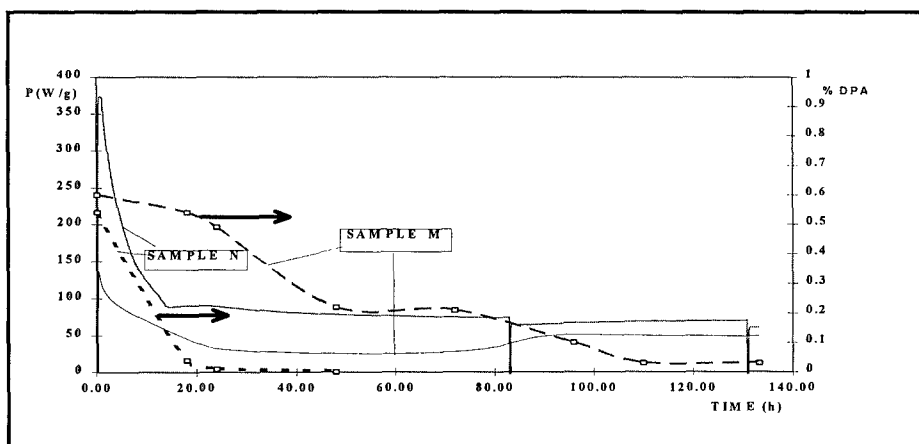
FIGURE 6 : COMPARISON OF HFC CURVES AND DPA CONSUMPTION FOR SAMPLES M AND N

3.5 LIFETIME CALCULATION FROM HFC

Kinetics parameters of the decomposition reactions has been calculated[1] for samples M, N, O and P. The results are collected in table VII. The Arrhenius plot is presented in figure 7.

TABLE VII : KINETICS DATA AND SERVICE LIFE FOR SAMPLES M, N, O AND P

SAMPLE	PREEXPONENTIAL FACTOR (W / kg)		ACTIVATION ENERGY (kJ / mol)		LIFETIME (years)	
	80-60	60 - 40	80 - 60	60 - 40	80 - 60	60 - 40
	TEMPERATURE RANGE (°C)					
M	$9,8 \cdot 10^{14}$	$1,3 \cdot 10^{10}$	124	80	94	17
N	$5,6 \cdot 10^{19}$	$1,2 \cdot 10^{9}$	142	73	183	12
O	$8,7 \cdot 10^{14}$	$1,6 \cdot 10^{9}$	111	75	65	19
P	$4,5 \cdot 10^{18}$	$1,2 \cdot 10^{6}$	136	60	195	13
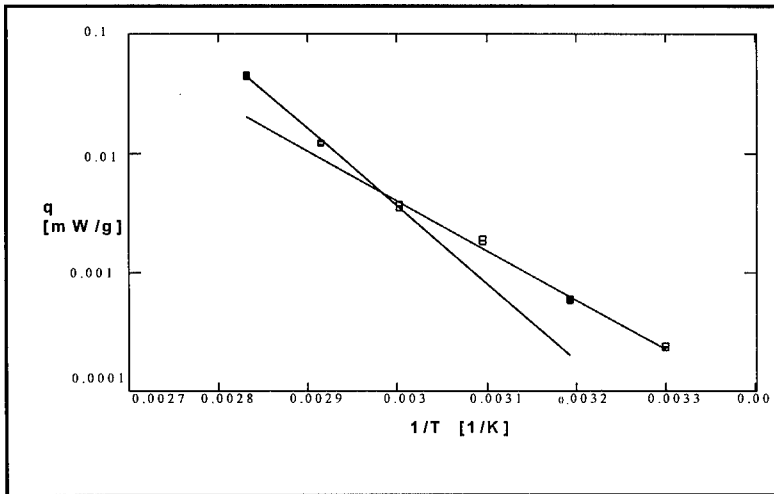
FIGURE 7 : ARRHENIUS PLOT FOR SAMPLE M

For the calculation of the service life time of the K6210-13 propellant it is necessary to use a specific heat flow measuring program. This e.g. should specify the number of days which have to be measured at 80°C to get a constant value of heat flow. Only with this small

---

[1] The life time of the propellant is calculated for a 3 % energy loss at 30°C [22]

degradation of the propellant (all DPA is converted into N-NO-DPA) a good and reproduceable measurement can be made at lower temperatures.

As it can be viewed in figure 7, there is a break in the kinetics at about 60°C. The importance of this break can lead to a wrong life time calculation if one takes into account only high temperature measurements for extrapolation at low temperature (see table VII).

These results show also that the reaction taking place in the early stage of the ageing leads to some degradation of the propellant and this will reduce its lifetime.

Those reactions involve the DPA and the KNO_3 but no detailed mechanisms can be forwarded at the present stage of this study.

4. CONCLUSIONS

From the data derived from our investigation, it can be said that the classical tests don't give enough information on the service/ballistic life time because

      a)only measurements at a single temperature are done

      b)additional initial effects depending on the surface agent used cover the « normal »
      decomposition reaction of the nitro-cellulose.

For this reason, the Holland-, Bergmann-Junk- and 90°C-test can only differentiate between « good « and « bad » propellant according to historically accepted values. (« bad » not meaning a propellant close to autocatalysis but which shows high primary effect e.g. between KNO_3 and DPA).

Although these three tests do show a trend (compare table II and III) of the rate of the degradation reaction, they are not able to give useful information for the determination of the stability of double base spherical propellant, if they are the only test used. It is much better to use combined methods like heat flow calorimetry and stabiliser consumption, because here the whole initial degradation process can be followed.

Although the influence of the KNO_3 content on the surface of the propellant and its interaction with DPA is not fully understood , it can be seen that the influence on the service life-time (see table VII) is not as big as it could be expected from the classical tests where samples with KNO_3 and additional DPA at the surface do not fulfil some or any of the admitted limit

values. The reason for this might be that all the DPA in the propellant is consumed within the first 3 days (see table V) and so big initial effects (the reaction between KNO_3 and DPA) govern the classical tests while HFC method deals with a propellant having reached a constant degradation process.

For the calculation of the service life time of the K6210-13 propellant ,it is also necessary to use the values from below 60°C for the life-time calculation, because a change in the kinetics occurs below this temperature.
It is still unknown what the service life-time would be if a not pre-aged sample is used for HFC experiments at lower temperatures. But as here initial effects (which **must** be excluded from the calculations) would last three weeks or longer at 60°C, it is impossible to do HFC measurements within an acceptable time frame at temperatures lower than 60°C with unaged samples. The same problem of far too long experimental times arises when stabiliser consumption or molecular mass depletion experiments are conducted below 60°C.

As a conclusion it can be said that classical tests can roughly give an impression about the chemical stability but only modern low temperature methods are efficient for the prediction of the life-time of double base propellants although the whole decomposition processes are not fully understood.

5. REFERENCES

[1]   I.L.C. van Geel, « Self-Ignition Hazard on Nitrate ester propellant » Dissertation TH Delft (1969).

[2]   B. Vogelsanger, R. Sopranetti, « Sicherheits-, Stabilitäts- und Lebendaueruntersuchungen im Lebenszyklus von Treiladungspulvern », Vortrag Mikrokalorimetrie-/Thermoanalyse-Workshop BICT,p.27-43 (1995)

[3]   Bohn M.A, Volk F., « Aging Behavior of Propellants Investigated by Heat Generation, Stabilizer Consumption and Molar Mass Degradation » Propellants, Explosives, Pyrotechnics **17**,171-178 (1992)

[4]   J. Tranchant, « Internal mechanism of the chemical evolution of nitrocellulose propellants: Hypotheses and consequences », Symp.Chem.Probl.Conn.Stabil.Explos. **6**, 1-20 (1982)

[5]   E.R. Bixon, D.Robertson, « Lifetime Predictions for Single Base Propellant Based on the Arrhenius Equation » 5th Int. Gun Propellant & Propulsion Symp. ,460 - 466 (1991)

[6]   G.Holl, S.Wilker, M. Kaiser, P.Guillaume, «Former and modern methods of the determination of the service life of propellants »,Proc. 87th AGARD Conference on Service Life of Solid Propellant Systems, Athens 1996, p.18-1 - 18-13

[7]   J.M. Bellerby, M.H. Sammour « Stabilizer Reactions in Cast Double Base Rocket Propellants », Propellants, Explosives, Pyrotechnics **16,** 235-239 (1991); **16,** 273 - 278(1991); **18,** 46-50 (1993); **18,** 223-229 (1993); **19,** 82-86 (1994)

[8]   F. Volk, K.M. Bucerius, G.Wunsch, «Ermittlung von Einflußgrößen auf die Genauigkeit von GPC-Messungen, Symp.Chem.Probl.Conn.Stabil.Explos. **7,** 197-216 (1985)

[9]   M.Marx-Figini, O.Soubelet, »Size Exclusion Chromatography of Cellulose Nitrate », Polymer Bull. **11,** 281-286 (1984)

[10]   H.N.Volltrauer, A.Fontijn, « Low-Temperature Pyrolysis Studies by Chemiluminescence Techniques Real-Time Nitrocellulose and PBX 9404 Decomposition » Combustion and Flame **41,** 313-324 (1981)

[11]   Y.Longevialle, M.Rat « Application de la chimiluminescence à l'étude de la stabilité des poudres » Symp.Chem.Probl.Conn.Stabil.Explos.**7,** 43- (1985)

[12]   M. Frey, « Mikrokalorimetrische Messungen an Treibstoffen unter verschiedenen Lagerbedingungen und bei Temperaturen im Bereich zwischen 30 und 90°C », Symp.Chem.Probl.Conn.Stabil.Explos, **6** 247 - 261 (1982)

[13]   C.J. Elmqvist, P.E. Lagerkvist, L.G. Svensson, « Stability and compatibility Testing Using A microcalorimetric Method » J.Haz.Mat. **7,** 281-285 (1983)

[14]   M.Rat « Application de la microcalorimetrie isotherme à l'étude de la stabilité des poudres pour armes » Symp.Chem.Probl.Conn.Stabil.Explos 361-380 (1979)

[15]   S.Wilker, G.Pantel, U.Ticmanis, « Wärmeflußkalorimetrische Untersuchungen an Anzündhütchen » Proc.Int.Conf.ICT **26,** 84 (1995)

[16]   E.L.Lilliott Sr,W.D.Mrazek,T.A.Murray « Comparative studies of the stabilizing effect of DPA and N-NODPA in single and double base experimental BALL POWDER® propellants », Comp. of Plastics and other Mat., 332-338 (1991)

[17]   E.L.Lilliott Sr,W.D.Mrazek,T.A.Murray,M.J.Posey, «Stability Evaluation of Ball Powder® Propellants relative to Nato Stanag 4117 » 5th Int. Gun Propellant &Propulsion Symp. 474-480 (1991)

[18]   TL 1376-0600, Method 2.21.1, p27 (1976)

[19]   TL 1376-0600, Method 2.22.1, p28 (1976)

[20]   TL 1376-0600, Method 2.31.1, p29 (1976)

[21]   N.J.Curtis, « Isomer Distribution of Nitro Derivatives of DPA in Gun propellants : Nitrosamine Chemistry » Propellants,Explosives,Pyrotechnics **15,** 222-230 (1990)

[22]   TL 1376-0600 , 2.5.1 « Bestimmung der chemischen Stabilitât mittels Wärmeflußkalorimetrie » (1991)

Einsatzlebensdauer einiger Gasgeneratorsätze bei Temperaturbelastung

Eckhard Lissel [1], Manfred Kaiser [1], Uldis Ticmanis[1], Peter Jacob [2]

[1] Bundesinstitut für chemisch-technische Untersuchungen beim BWB,
  Großes Cent, D-53913 Swisttal
[2] Bayern-Chemie, Aschau, Postfach 1131, D-84544 Aschau a. Inn

Abstract

For the use in fire extinguishers new azide free, but yet thermally stable gas generating mixtures - based on energetic fuels and inorganic oxidators - have been developed. Three different formulations were investigated by TGA and heat flow calorimetry in the temperature range from 70 to 160°C. A correlation of mass and energy loss was established by burning fresh and thermally stressed samples in a calorimetric bomb. The gained kinetics allow to calculate the long term storage behaviour of the mixtures. For a ten year service life time tolerable storage temperatures from 48 to 78°C were calculated.

Zusammenfassung

Im Rahmen der Entwicklung neuer azidfreier, aber dennoch thermisch stabiler Gasgeneratorsätze für Brandlöschanlagen wurden drei Rezepturen - auf der Basis energiereicher organischer Brennstoffe und anorganischer Oxidatoren - mittels Mikro-TG im Temperaturbereich zwischen 90 und 160°C untersucht. Die dabei erhaltenen kinetischen Parameter wurden durch Wärmeflußmessungen bei 70 und 80°C überprüft. Die Korrelation zwischen Massen- und Energieverlust wurde durch Abbrand unbelasteter und thermisch belasteter Proben in der kalorimetrischen Bombe ermittelt. Die Gebrauchslebensdauer wird als Temperaturfunktion dargestellt. Danach liegen die maximal tolerierbaren Temperaturen einer hypothetischen 10-jährigen Isothermlagerung zwischen 48 und 78°C. Zwei der drei untersuchten Gemische sind als bemerkenswert stabil einzuschätzen.

1 Einleitung

Für den Einsatz in Feuerlöschanlagen in Motorfahrzeugen der Bundeswehr wurden drei verschiedene Rezepturen von Gassätzen vorgestellt, die der erhöhten Wärmebelastung am vorgesehenen Einsatzort standhalten sollten. Ziel der Entwicklung war es, den verfügbaren, thermisch außerordentlich stabilen, jedoch relativ feuchteempfindlichen Airbag-Satz zu ersetzen, bei dessen hydrolytischer Spaltung die toxische Stickstoffwasserstoffsäure HN_3 freigesetzt wird. Basis der Rezepturen, die auf Wunsch der Hersteller vertraulich behandelt werden, sind energiereiche organische Brennstoffe, anorganische Oxidatoren und z.T. zusätzlich Verschlackungsmittel und Stabilisatoren. Eine Übersicht der in Gassätzen verwendeten Stoffklassen und der Optimierungsparameter geben Bucerius und Schmid [1].
In dieser Arbeit wurde der wichtigste Einsatzaspekt, die thermische Langzeitstabilität der Sätze, untersucht.

2 Wahl eines Referenzpunktes

In einer ersten Meßserie wurden die Sätze auf einer Mikrowaage über einen Zeitraum von mehreren Tagen isotherm zersetzt (Gerät: TG 439 der Fa. Netzsch; Probenmengen: 50-100 mg; Probengefäß: Aluminiumoxidtiegel mit lose aufgelegtem Deckel). Die Messungen sind in den Abb.1 bis 3 dargestellt und in Tabelle 1 zusammengefaßt.
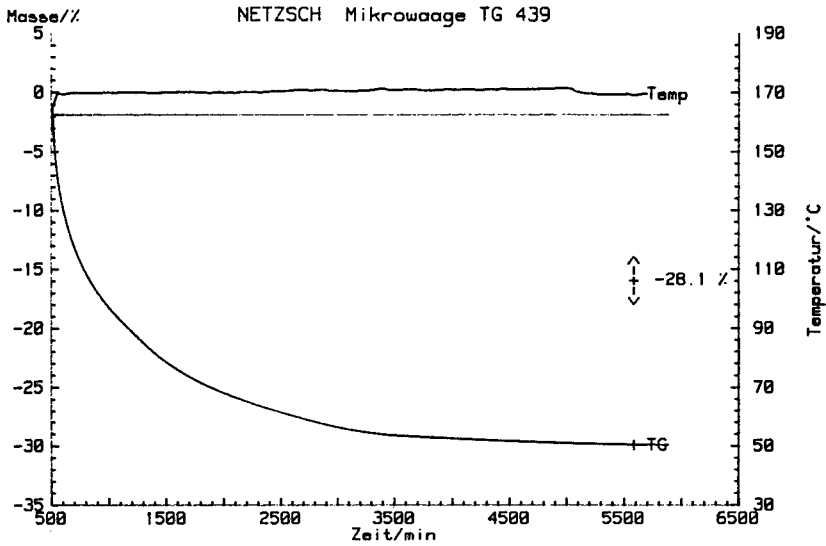
Abb. 1: Satz 1: Isotherm-TG
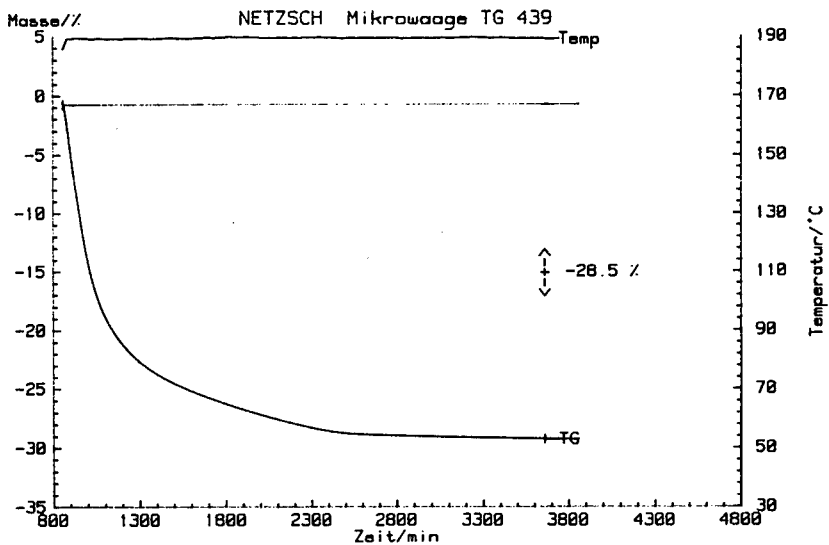
Abb. 2: Satz 2: Isotherm-TG
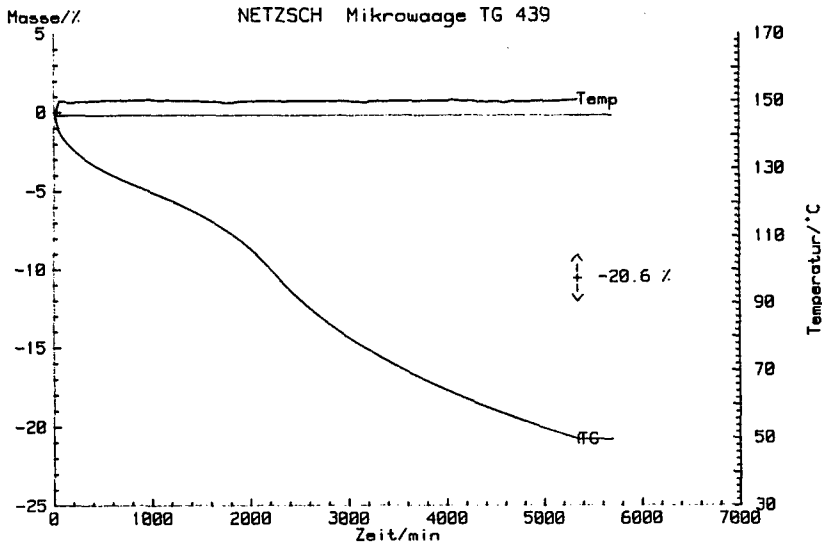
Abb.3: Satz 3; Isotherm-TG

Tabelle 1: Isotherme Zersetzung der Gassätze

Satz	Meßtemperatur [°C]	totaler Massenverlust M_{tot} [%]	zersetzte Komponente
1	170,2	28,1	Brennstoff
2	189,3	28,5	Brennstoff
3	149,9	20.6	größtenteils Oxidator

Die Erkenntnisse der letzten Spalte resultierten aus Einzelmessungen an den Komponenten.

Da Funktionsprüfungen in Feuerlöschern nicht durchführbar waren, wurde als Arbeitshypothese unterstellt, daß ein 5%iger Energieverlust noch tolerierbar ist und dieser Wert angenähert auch einer Zersetzung von 5 % der gesamten TG-Stufe entspricht. Zur Überprüfung dieser Hypothese wurden die Gemische, soweit ausreichende Mengen verfügbar waren, auf einer (Makro)Thermowaage zu 4-5 % Massenverlust, bezogen auf die TG-Stufe (= 100 %), zersetzt und im Vergleich zu unbelasteten Proben in der kalorimetrischen Bombe abgebrannt (Volumen: 25 cm^3; Einwaage: 1 g). Die Werte sind in Tabelle 2 aufgelistet.

Tabelle 2: Massenverlust und Explosionswärme

Satz	Explosionswärme [J/g]	rel. Massenverlust [%] [1]	rel. Wärmeverlust [%] [2]
1	2835	4,9	3,6
2	3134	4,3	3,2

1) bezogen auf die TG-Stufe
2) nach Korrektur der tatsächlichen Einwaage von 1 g auf die Usprungsmenge vor der
   thermischen Belastung

Der Energieverlust war stets geringer als der Massenverlust; dies mag mit der unvollständigen
Vergasung der Komponenten in der TG und Teil-Verbrennbarkeit der verbleibenden konden-
sierten Reaktionsprodukte zusammenhängen. Ein relativer Massenverlust von 5 % entspricht
im Mittel etwa 3,7 % Energieverlust, er bedeutet jedoch eine noch tolerierbare und angenähert
äquivalente Zersetzung der Sätze und ist daher als Referenzpunkt für Vergleiche der Stabilität
geeignet.

3 Versuchsführung und -auswertung

Durchgehende isotherme Messungen an mehreren Proben erfordern - will man den nötigen
Temperaturbereich von mindestens 30°C überstreichen - sehr lange Meßzeiten. Ein weniger
zeitaufwendiges Verfahren ist die Messung in isothermen Stufen [2], wie dies in den Abb.4
(Gesamtmessung) und 5 (Ausschnitt) am Beispiel des Satzes 2 dargestellt ist.
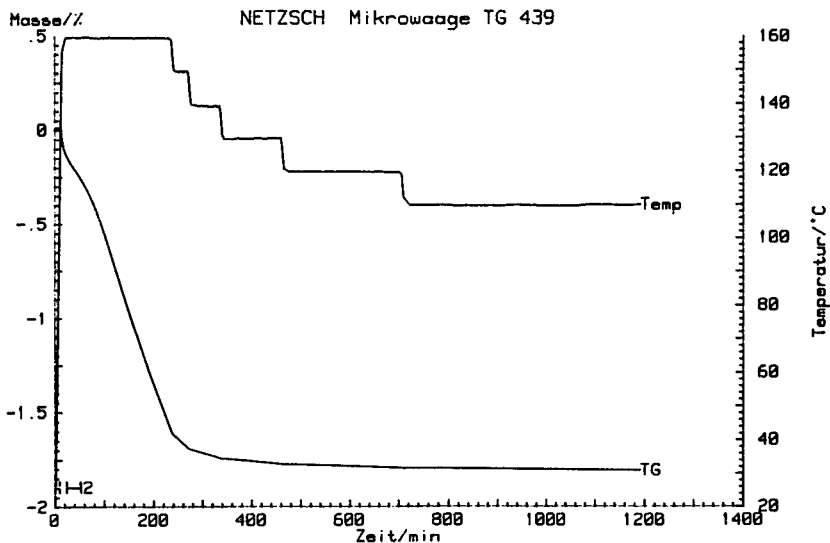
Abb. 4: Satz 2; TG in isothermen Stufen (Gesamtmessung)
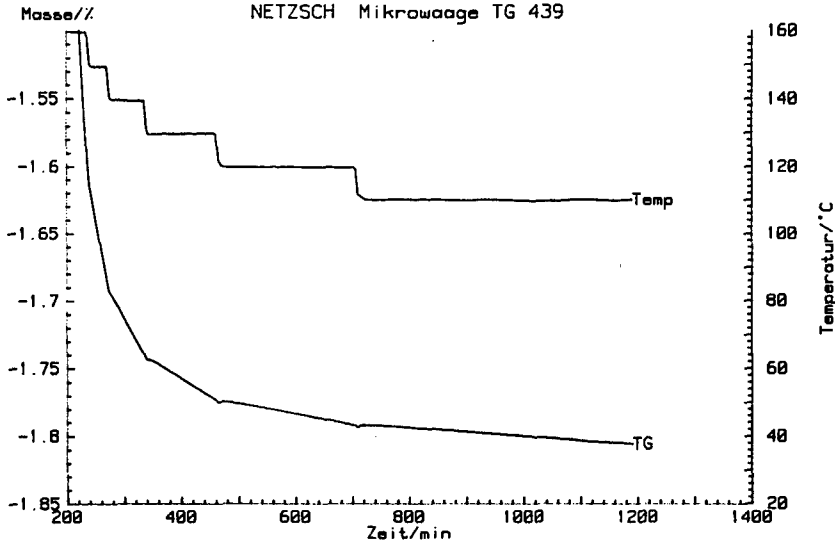
Abb.5: Satz 2; TG in isothermen Stufen (Ausschnitt)

Verläuft eine Reaktion nach der allgemeinen Gleichung (1),

$$d\alpha/dt = f(\alpha)\cdot A\cdot e^{-E/RT} \tag{1}$$

α	=	Umsatzgrad
$f(\alpha)$	=	Umsatzfunktion (Reaktionsmodell RM)
$d\alpha/dt$	=	Reaktionsrate
T	=	Reaktionstemperatur
A	=	Frequenzfaktor
E	=	Aktivierungsenergie
R	=	Gaskonstante

so ist eine relativ häufig verwendete [2, 3, 4] modellfreie (von der Kenntnis des Reaktionsmodells unabhängige) Folgerung die Beziehung (2)

$$t = t_r * e^{\frac{E}{R}*(\frac{1}{T} - \frac{1}{T_r})} \tag{2}$$

mit der aus Referenztemperaturen T_r und -zeiten t_r, die Zeit t für das Erreichen des Referenzumsatzes α_r (hier 5 % der TG-Stufe) für andere isotherme Lagertemperaturen T berechnet werden kann. Neben T_r und t_r, die direkt aus der ersten Meßperiode entnommen werden können, muß nur die Aktivierungsenergie ermittelt werden. Diese kann aus iso-α-Punkten (Punkte gleichen Umsatzgrades z.B. α_r) bei verschiedenen Temperaturen durch lineare Regression der logarithmierten Form der Gleichung (1) bestimmt werden.

$$\ln (d\alpha/dt) = \ln [f(\alpha_r)\cdot A] - E/RT \tag{3}$$

Verwendet man den Massenverlust M als Reaktionsmaß, hat Gleichung (3) die Form

$$\ln (dM/dt) = \ln A' - E/RT \qquad\qquad (4)$$

worin $A' = A \cdot M_{tot} \cdot f(M_r/M_{tot})$

Die erste (höchste) Meßtemperatur T_r der Stufen-TG wird so gewählt, daß der gewünschte Referenzumsatz in 2 bis 8 Stunden erreicht wird. Um iso-α-Bedingungen möglichst gut anzunähern, ist der Umsatz (und somit die Änderung der Umsatzfunktion) in den folgenden Meßperioden möglichst klein zu halten. Dies wird mit dem in Tabelle 3 aufgelisteten Meßprogramm recht gut realisiert (s. auch Abb.5)

Tabelle 3: Meßprogramm der Stufen TG

Meßperiode	Temperatur	Dauer (h)
1	T_r	2-8
2	$T_r - \Delta T$	0,5
3	$T_r - 2\Delta T$	1
4	$T_r - 3\Delta T$	2
5	$T_r - 4\Delta T$	4
6	$T_r - 5\Delta T$	8

Für die Temperaturdifferenz ΔT zwischen den Meßperioden wurden 6 bis 12 K gewählt. Die Referenzzeit t_r (vom Periodenbeginn an gerechnet) wird aus der 1. Periode bestimmt (Abb. 6). Die Massenverlustrate $\Delta M/\Delta t$ (der Anstieg der TG-Kurve) ist in dieser längeren Periode nicht über den ganzen Bereich konstant. In diesem Fall wird der Wert aus dem letzten, pseudokonstanten Bereich ermittelt (Abb. 7). In den folgenden Perioden sind die Verlustraten in der Regel im Rahmen der Meßgenauigkeit konstant (vgl. Abb. 8 bis 11).
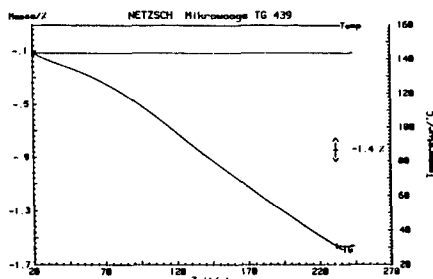
Abb. 6: Satz 2; 1. Periode
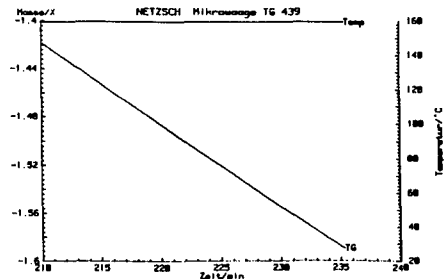
Abb. 7: Satz 2; 1. Periode, Endbereich
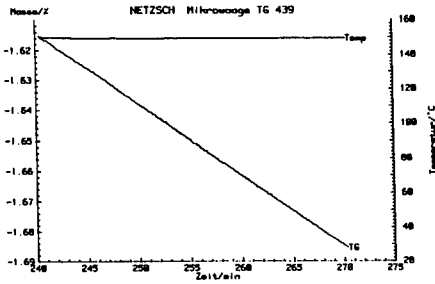
Abb. 8: Satz 2; 2. Periode
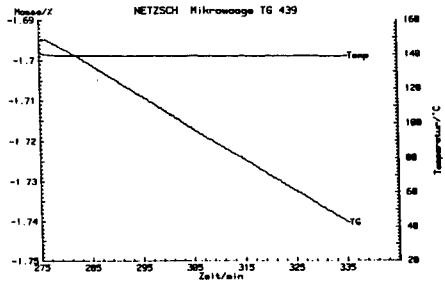
Abb. 9: Satz 2; 3. Periode
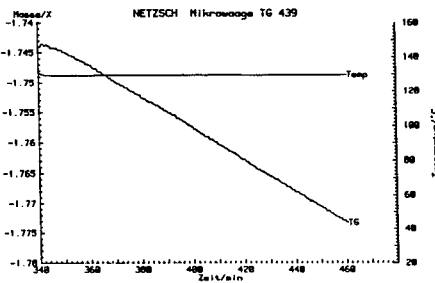
Abb. 10: Satz 2; 4. Periode
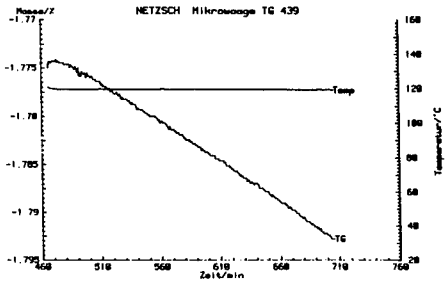
Abb. 11: Satz 2; 5. Periode

4 Ergebnisse

Die Regression der Daten nach Gleichung 4 („Arrhenius-Plot") ist in den Abb. 12 bis 14 dargestellt. Als Einheit der Massenverlustrate wurde dort µg/g·min gewählt. Die Hypothese einer einheitlichen Aktivierungsenergie ist im untersuchten Temperaturbereich offentsichtlich recht gut erfüllt. Die Ergebnisse sind in Tabelle 4 zusammengestellt.

Tabelle 4: kinetische Parameter

Satz	Temperatur-bereich	rel. Standard-abweichung	ln A'	E	T_r	t_r
	[°C]	[%][1]	A' in µg/g·min	[kJ/mol]	[°C]	[min]
1	140-90	8,0	40,706	125,19	139,5	163,3
2	160-120	1,9	47,797	156,80	159,4	213,3
3	140-110	0,6	57,591	185,60	140,1	106,7

[1] Bezogen auf die experimentellen und die nach Gl. (4) berechneten Massenverlustraten
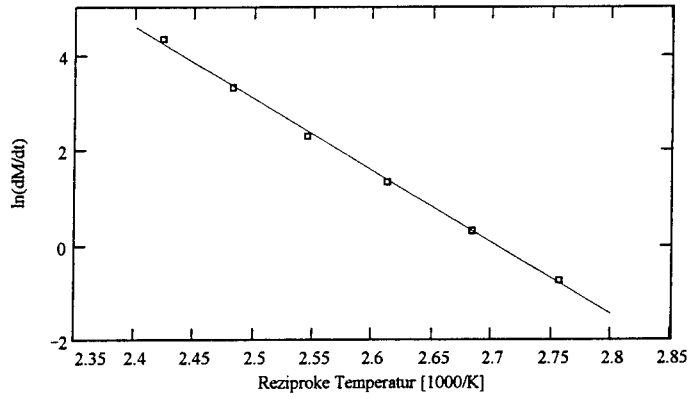
Abb. 12: Satz 1; Arrhenius-Plot
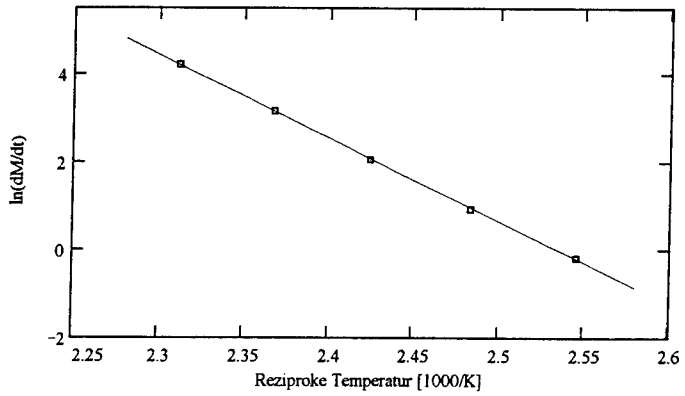
Abb. 13: Satz 2; Arrhenius-Plot
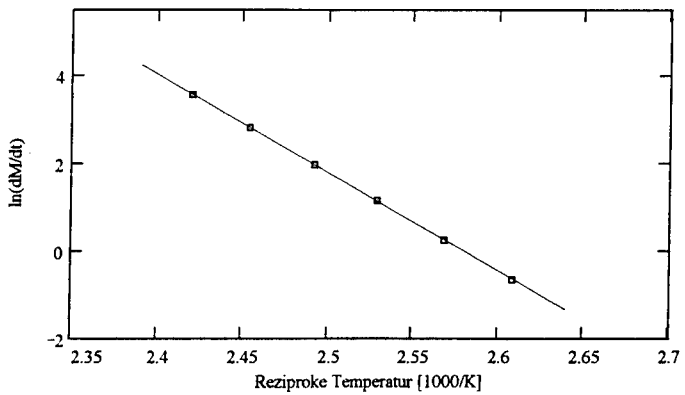
Abb.14: Satz 3; Arrhenius-Plot

Zur Überprüfung der Gültigkeit der ermittelten Aktivierungsenergien bei niedrigeren Temperaturen wurden Messungen im Wärmeflußkalorimeter bei 80 und 70°C vorgenommen. Die Proben (2-3 g) wurden vorher mittels TG auf den Referenzumsatzgrad zersetzt. Die Messungen erfolgten in Probengefäßen, in deren Deckel ein kleines Loch gestochen wurde. Die Resultate sind in der Tabelle 5 zusammengestellt. Sie bestätigen die thermogravimetrisch gefundene Stabilitätsreihenfolge. Die Werte der Aktivierungsenergie liegen allerdings mit 119 (Satz 1) und 71 kJ/mol (Satz 2) beträchtlich unter den mit TG gefundenen Werten. Die letzteren können jedoch aufgrund der Abstützung auf mehr Meßpunkte als zuverlässiger gelten. Sie werden daher für die folgenden Rechnungen verwendet.

Tabelle 5: Ergebnisse der Wärmeflußmessungen

Satz	q_{80} [μW/g]	q_{70} [μW/g]
1	14,3	4,39
2	3,04	1,50

5 Berechnung der Lebensdauer

Löst man Gleichung (2) nach der Temperatur T auf, so läßt sich die noch tolerierbare Lagertemperatur als Funktion der gewünschten Einsatzdauer berechnen. Die Prognose für die thermische Alterung der Gassätze bei solchen Langzeit-Isothermlagerungen sind in Abb.15 dargestellt.
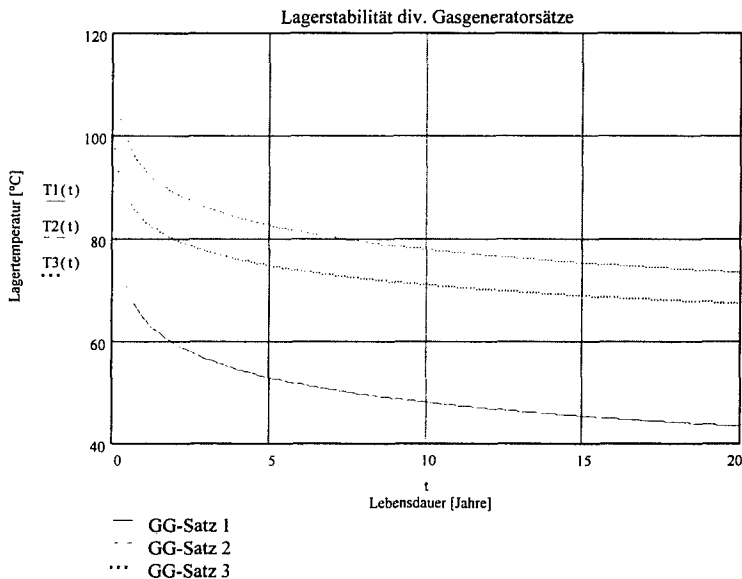
Abb. 15: Einsatzlebensdauer bei Isothermlagerung

Danach lägen z.B. für eine 10-jährige Einsatzdauer die zulässigen Lagertemperaturen zwischen 48°C (Satz 1) und 78°C (Satz 2). Für Temperaturschwankungen in geringen Grenzen können diese Werte auch als mittlere Temperaturen einer realen Lagerung interpretiert werden.

Auch unter Berücksichtigung der extremen Extrapolation (Meßzeit in Relation zur Prognosezeit) und der damit verbundenen Fehlerquellen können die Gassätze 2 und 3 mit Sicherheit als bemerkenswert stabil betrachtet werden. Die Aussage bezieht sich ausschließlich auf die thermische, nicht die klimatische Stabilität, die im Rahmen dieser Arbeit nicht untersucht wurde.

6 Literatur

[1]   K.M. Bucerius, H. Schmid, ICT-Bericht 19/92

[2]   U. Ticmanis, 10th Symposium on Chemical Problems Connected with the Stability of Explosives, Margaretetorp, Schweden, 1995

[3]   STANAG 4527, Explosives, Chemical Stability, Nitrocellulose based Propellants, Procedure for Assessment of Chemical Life and Temperature Dependence of Stabiliser Consumption Rates

[4]   W. Scheunemann, U. Ticmanis, BICT-Bericht 330/11993/92

THE CHARACTERISATION AND DEVELOPMENT OF NEW ENERGETIC MATERIALS

by Dr Andrew Sanderson, NATO Insensitive Munitions Information Centre (NIMIC), NATO HQ, B1110 Brussels, Belgium

ABSTRACT

There have clearly been significant progress in the synthesis and development of new energetic compounds for use in explosives and propellants in recent years. New compounds offer the possibility of designing munitions having both increased performance <u>and</u> reduced vulnerability. However, making the transition from the initial synthesis of new compounds to their incorporation in munitions seems to have been rather an ad hoc and inefficient process. In the present situation with many new candidate ingredients and shrinking budgets more efficient transitioning is required.

Some of the problems experienced in past transition efforts can be shown to arise from there having rarely been a systematic approach to the necessary characterisation of new materials. Reasons for this lack of characterisation include:

- a lack of understanding of how ingredient properties affect the properties of mixtures of ingredients in formulations;
- a lack of detailed understanding of how small scale characterisation data relates to desirable qualities of large charges in munitions;
- consequent difficulty in knowing what initial characterisation is required to decide whether a new energetic compound will be useful.

NIMIC is seeking to improve the current situation in two ways. First by compiling in one document all available information on new material characteristics and making this information readily available for EM designers and users from NIMIC member nations. Secondly by developing a method to relate desirable properties of complete munitions to the characteristics required of energetic compounds they contain. In this paper a report of NIMIC's activities in these areas will be made with some implications for the development and future of new energetic compounds.

Die Charakterisierung und die Entwicklung der neuen Energieträger

ZUSAMMENFASSUNG

Es gab sicher wichtige Fortschritte in der Synthese und in der Entwicklung von neuen energetischen Ingredienzen für die Benutzung in Explosiv- und Treibstoffe in den letzten Jahren. Neue Ingredienzen ermöglichen Munitionsdesign mit besser Leistung und niedriger Verwundbarkeit. Aber der Weg von der ersten Synthese der neuen Ingredienzen bis ihrer Nutzung in Munitionen sieht wie ein ad hoc und unwirksam Prozess aus. In der heutigen Lage, wo es viele neue Ingredienzen als Kandidate und senkende Haushaltpläne gibt, ein bessere Übergang wird gebraucht.

Einige Probleme, die in der vergangenen Übergangsphase auftraten, kamen auf, weil es selten eine systematische Methode gab, um neue Ingredienzen zu charakterisieren. Einige Gründe fur diese schlechte Charakterisierung sind:
- ein Mangel an Verständnis in Bezug wie die Ingredieznneigetüme edie Eigentüme der Mischungen von Ingredienzen in der Formulierungen beeinflüssen
- ein Mangel an Verständnis in Bezug auf beschreibende Daten, die aus Kleinsversuchen ermittelt werden und daraus Schlüsse zu ziehen auf die erwünschte Eigenshaft von großen Munitionsladungen
- und natürlich die Schwierigkeit , um zu wissen, welche anfängliche Charakterisierung notig ist, um zu entscheiden, ob ein neuer energetischer Ingredienz nützlich sein wird.

NIMIC will die heutige Lage in zwei Richtungen verbessern. Erstens, sammeln in einem Dokument alle verfugbaren Informationen in Bezug auf Daten über neue Energieträger, und zu verbessern ihre Verfügbarkeit in den NIMIC Ländern. Zweitens, eine Methode zu entwickeln, die die Eigentüme der ganzen Munitionen mit den gebrauchten Charakteristieken der energetischen Ingredienzen, die sie enthalten, verbinden soll. In diesem Text werden ein Zusammenfassung der Aktivitäten von NIMIC in diesen Gebieten mit den Schlüssen für die Entwicklung und die Zukunft von neuen energetischen Ingredienzen präsentiert.

INFORMATION REQUIREMENTS FOR ENERGETIC MATERIAL DESIGN AND DEVELOPMENT

Despite the efforts of those involved in synthetic chemistry and subsequent formulation design, the path to utilization of new Energetic Materials (EM) in munitions is prone to inefficiency, duplication of effort, errors and delays. Ample evidence for this is shown by the time it has taken between discovery and utilisation for every compound currently in service and the time it is taking to develop recently made compounds still not in service. For instance, TNT was first made in 1863 but accepted into widespread service in Germany only at the turn of the 20th century, likewise RDX was first made in 1899 and only developed as an explosive in the 20's and 30's. Of "new" materials not yet in service, polyglycidyl nitrate has been known since at least 1966, GAP since the mid '70s, and HNIW since the mid '80s.

Although as pointed out by Flanigan[1] what makes a useable new EM is whether or not it meets the requirements, the real requirements for EM are nowhere explicitly stated and are not always obvious. For instance, to be useful, a material that appears promising in the laboratory must be available to a definable specification within which it always meets processing, and stability requirements. For some materials (e.g. GAP, NTO and HNF) this is not a trivial problem. To make use of any new material, its properties and characteristics and how they may vary need to be known. Although good characterisation work is done, it is rarely compiled in such a way that a material's real potential can be assessed. Therefore the NATO Insensitive Munitions Information Centre (NIMIC) undertook the task of collecting and compiling the data needed by those involved in analysis, formulation design, processing, composite material modelling, and material assessment in order to aid new material development.

This resulted in two projects, first the publication of a compilation of characteristics of some of the most promising new materials[2], and secondly a workshop to try to define what is really needed from new energetic materials[3]. These projects are ongoing. As a result of

Figure 1 Some EM under development

the workshop, much new characterisation data was received, and a second and very significantly improved edition of the characterisation compendium is in preparation. In fact since the first edition was produced, the number of useful source documents for new material characterisation held by NIMIC has

A logic tree for the development of new energetic materials for military use
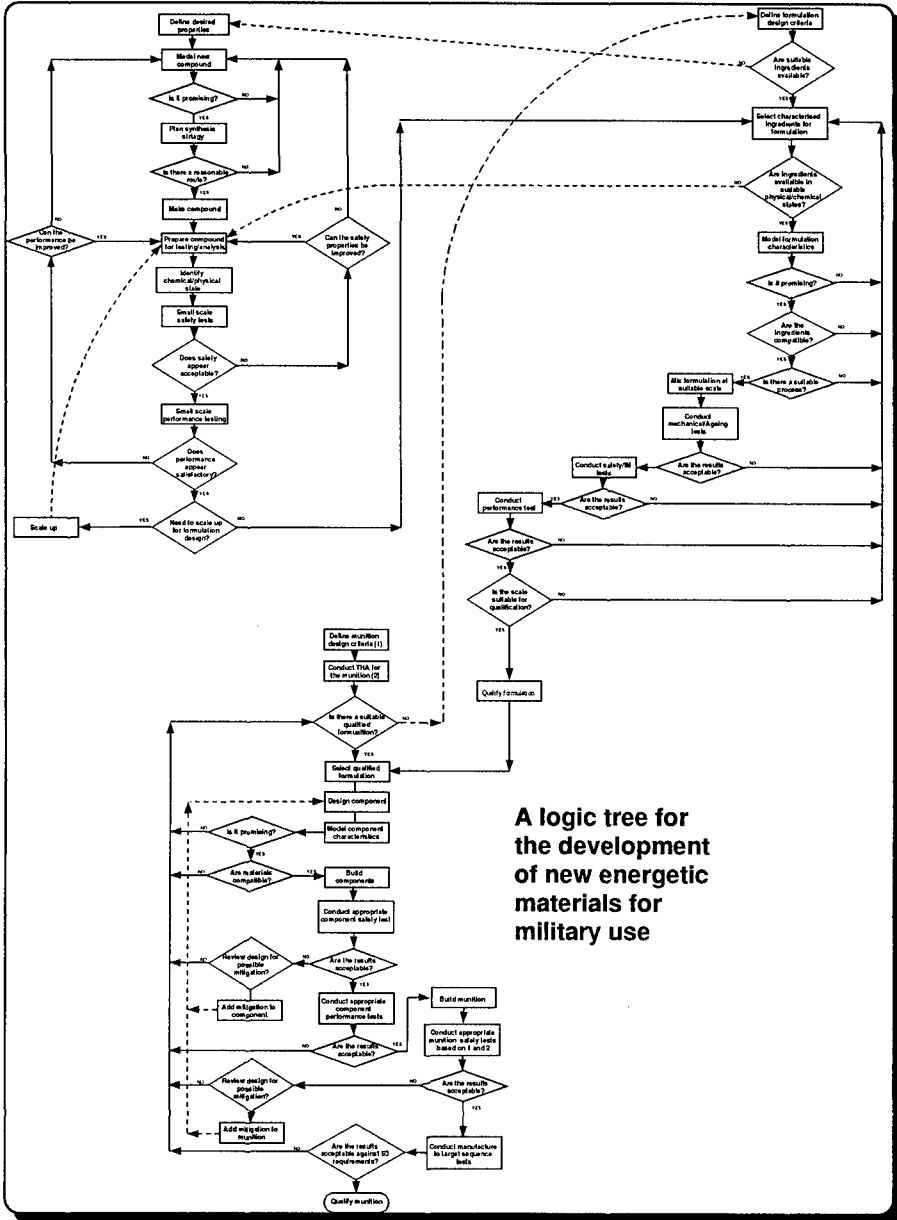
Figure 2 The energetic material flow chart from the NIMIC workshop

increased by more than an order of magnitude.

CRUCIAL PROPERTIES OF ENERGETIC MATERIALS

A number of areas were studied in the NIMIC workshop on what makes a useable new EM. For this paper, two areas of particular interest are, what is it that you really need to know, and can you predict if a EM will meet potential users requirements very early in its development (or in fact before it has ever been made)?

An excellent review of EM requirements, development and test methods for rocket propellants was written by Boggs et al[4]. From the approach of Boggs together with additional considerations for explosives and gun propellants, an outline flow chart was written for all the steps that need to be taken in EM development (figure 2). For the sake of clarity, this was broken down and studied as three connected flow charts dealing successively with ingredient design and development, formulation design development and qualification, and component design to system qualification. These flow charts together with their accompanying explanations have been used

to try to define as closely as possible what is needed to be known about EMs for them to be used in service. A complete description of the derivation of the flow chart and subsequent modifications can be found in the NIMIC workshop report.
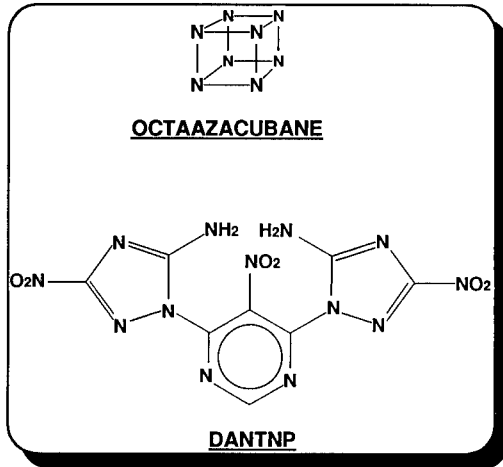
Figure 3 Examples of molecules where property prediction has been undertaken.

A challenging area related to the EM development flow charts was also develop-ed at the work-shop. It was based on the idea that not all of the necessary knowledge was required by all of those with a stake in the life cycles of EM. Different stake-holders and their needs were identified, and the picture that this study gave is proving useful in identifying the optimum route in the EM development. One of the problems in the development of new EM that this highlights is that there are conflicting requirements on the EM during its development. During early development, performance is an almost over-riding driver, during other stages, cost, stability, safety, material sourcing, processability can be the primary concern. The problem arises when much development happens before it is realised that one or other of these concerns will prevent the material from being used extensively. For instance, much work has been done on NTO (fig 1) and it appears attractive for many applications, but it is

rarely noted that its pKa presents severe compatibility and ageing problems that will always limit its utility. The question then arises, what of the materials currently under serious investigation? What questions are not being asked early in their development that may ultimately result in effort and scarce resources being wasted. Another example is polyglycidyl nitrate (figure 1). Although first made in the '60s, it has only recently come to light that although the prepolymer is stable, the material as usually prepared has a very poor stability characteristics when cured with isocyanate curatives due to an intramolecular reaction[5]. In this instance the problem can be solved by end group modification, but if this had not been the case it would have meant that only after nearly thirty years of research effort would the material have been found not to be useable. A related issue is that as performance is so important to justification of early development, there is a tendency to look only at the best performer and not those that offer lower performance but better characteristics in other areas. Also there is a tendency to drop the development of a material if another becomes available with higher performance almost regardless of other characteristics.

PREDICTION OF EM PROPERTIES

With a list of what needs to be known, there are two obvious further questions. How do you obtain the information, and better still, can you predict what it will be? Both of these were addressed at the NIMIC workshop. With regard to prediction of

energetic compound properties it emerged that there are two quite different schools of thought. One view is that for prediction of properties of new compounds it is necessary to have more reliable computer models than yet exist. The other view is that the best contemporary modelling plus empirical relationships are sufficient and in fact necessary to point the way to new useful materials.

From inspection of recent developments, it appears that both views can be right. For instance, a number of papers have been published on the theoretically possible but as yet unmade compound octaazacubane[6], N_8 (figure 3). These highlight the potentially huge increase in performance this compound has over currently used materials such as HMX (figure 4). However, even with the most complex ab

	Octaazacubane (calc.)	HMX
Hf (kcal/mol)	530	18
Density (g/ml)	2.65	1.90
Dcj (km/s)	14.75	9.1
Pcj (kbar)	1370	390

The predicted properties of N_8 vs HMX according to Stine[5].

Figure 4 An example of prediction perhaps stretched to its limit.

initio molecular structure calculations it is clear that the performance estimates are very tentative, and other important parameters (stability, sensitivity etc. are not even amenable to guesses). The reason for

the uncertainty is that N_g is completely different to any known compound and predictions highlight the fact that even the best estimates rely on inference from analogy and some extrapolation from known trends. Commonly used semi-empirical and purely empirical models can be used to give many interesting results for significant material properties. For
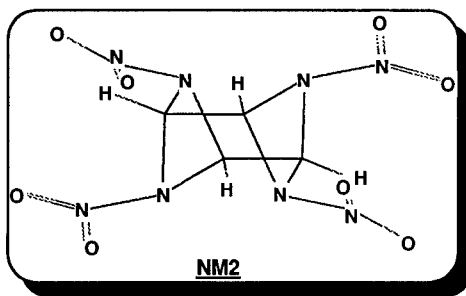
Figure 5 A MOPAC structure of a theoretical analogue of both cubane and HNIW

property relations can be used. However, whilst appearing attractive one cannot have sufficient confidence in these results for such new compounds to justify significant development work. The predictions do work if you stay close to known materials, and this is witnessed by the success of the work at CEA on DANTNP and related compounds[7] (figure 3).

instance, the structure of the molecule NM2 (figure 5) can be modelled using MOPAC or similar codes. The density can be predicted using Ammon's MOLPAK code, and the detonation parameters calculated using Cheetah (figure 6). Alternatively, more empirical structure

	"Predicted" properties of NM2	Properties of HMX (LASL)
Density	1.97 (Stine) 2.00 (Ammon)	1.90
Hf	342 kJ/mol (Stine) 380 kJ/mol (Mopac gas phase +Ammon lattice energy)	47 kJ/mol
Dcj	9.33 km/s Rothstein @1.97 g/ml 9.99 km/s Cheetah @ 2.00 g/ml	9.11 km/s @ 1.89 g/ml
Pcj	427 kbar (Kamlet) @ 1.97 g/ml 474 kbar (Cheetah) @ 2.00 g/ml	395 kbar @ 1.90 g/ml
Sensitivity	H50% = 14cm Kamlet)	H50% = 26cm (PETN = 12cm)

Stine - a) Prediction of crystal densities of organic explosives by group additivity, Los Alamos report LA-8920, 1991. b) Estimation of heats of formation and the development of chemical databases useful for energetic materials, JANNAF paper, CPIA-PUB-529-VOL-2, p53, 1989.
Ammon - MOLPAK, Ammon et al, J. Comput. Chem. 14, 422-437, 1993.
Rothstein - L R Rothstein and R Petersen, Propellants and Explosives, 4, p56, 1979.
Cheetah - Cheetah (an improved version of the Tiger thermochemical code) L R Fried, Lawrence Livermore report UCRL-MA-117541 Rev. 2, 1995.
Kamlet - The relationship of impact sensitivity with structure of organic high explosives, J M Kamlet, 6th Symposium on Detonation, 1976.
LASL - LASL Explosive property data, T R Gibbs and A Popolato, University of California Press, 1980.

Figure 6 Calculated properties for the novel theoretical molecule NM2

PREDICTION OF THE SAFETY PROPERTIES OF WHOLE MUNITION SYSTEMS

Further to the work of predicting molecular properties of new materials is the prediction of system properties (especially

IM characteristics) knowing only the design details.

The current method of IM assessment using a very limited amount of very expensive, unreliable, and uninformative destructive testing of finished weapon systems is hard to justify. Recent studies in NIMIC have focussed on the prediction of IM test resuts from small scale testing and material properties. Using a methodology called CRIMES (Critical Reaction Initiation Mechanisms), it has been shown with several examples that it is possible with a combination of modelling, testing and analytical relationships to provide more information about a weapon systems IM behaviour than can be obtained from all-up-round testing[8]. In figure 7 is shown the summarised results of an assessment made with the CRIMES approach on a generic 500lb bomb. Note that not only does this summary of the analysis give the most likely response in IM tests, but it also shows whether other responses are possible.

IM Test	Reaction type and estimated probability
SCJ	I - 100%
Fragment Impact	I (>80%) II and III (up to 20%)
Bullet impact	I, II and III (mostly I/II)
Fast Cook Off	I, II, III and IV (predominantly II and III)
Slow Cook-off	I, II and III (mostly I/II)
Sympathetic detonation	I - 100%

Figure 7 The summarised results of a CRIMES based IM assessment on a generic 500lb CompB filled bomb

Work is onging at NIMIC in this area to show how the probabilities of different responses can be predicted. In this work it has already been found that essential to this type of assessment and analysis is a knowledge of the characteristics of what must be the most important but often most neglected part of any munition system, the energetic materials it contains.

REFERENCES

1. Flanigan, D., Keynote address at ADPA Symposium on Energetic Materials Technology, Phoenix, Arizona, Sep, 1995.

2. Sanderson, A., "The NIMIC coordinated characterisation programme: a program and data for the characterisation of new ingredients for energetic materials", NIMIC technical report, NIMIC-L-06, 1994.

3. Sanderson, A., et al, "What Makes a Useable New Energetic Material?", The Proceedings of the 1994 NIMIC Workshop held at NATO HQ, Brussels, Belgium, June 22-24, 1994.

4. Boggs, T.; Chan, M.; Atwood, A.; Braun, J.; Carpenter, P.; Pakulak, M.; Hunt-Kramer, R., "Propellant Development: from idea to motor", Naval Weapons Center, China Lake, Technical

report, 1991.

5. a) Bunyan, P., "A study on the thermal decomposition of polyglyn", ADPA Symposium on Energetic materials Technology, Phoenix, Arizona, Sep, 1995. b) Paul, N., Desai, H., Leeming, B., and Bull, H., "An improved polyGLYN binder through end group modification", ADPA Symposium on Energetic materials Technology, Phoenix, Arizona, Sep. 1995.

6. Stine, J. R., and Engelke, R., "Is N_8 Cubane Stable", J. Phys. Chem., 94, 5689-5694, 1990.

7. Charrue, P.; Wartenberg, Ch.; Lugadet, F.; Laval, F., "Development of composite explosives based on 3-amino-5-nitro 1,2,4- triazole (ANT)", 5e Congrès International de Pyrotechnie du GTPS, Europyro 93, Strasbourg, June, 1993.

8. Sanderson, A., "A New approach to assessment and design of insensitive munitions by analysis of critical response mechanisms to unplanned stimuli", ADPA/NIMIC Symposium on Insensitive Munitions Technology, San Diego, March 1996.

DEVELOPMENT OF HIGH EFFICIENCY
ENERGETIC EXPLOSIVES

Vitaly Pepekin
N. Semenov Institute of Chemical Physics,
Russian Academy of Sciences,
Moscow, Russia

Experimental data on the heats of explosion, detonation veloci-
ties, and acceleration of metal plates for explosive oxidi-
zer-fuel additive systems. Three types of the additives were
used: (a) explosive-based fuel (HMX and benzotrifuroxane), (b)
nonexplosive fuels (carbon and ultra fine diamond), (c) inorga-
nic material (fine aluminum powder). It is shown that the addi-
tives enhance the detonation parameters and the metal accelera-
tion ability of the composite explosives.

Explosives of the oxidizer-fuel type are promising systems that
enable one to achieve considerable enhancement of the power properties
of well-known high explosives (HE) due to the chemical reactions bet-
ween the decomposition products of the components of the system.

This non-traditional approach o development of explosive systems
is essentially based on enhancement of the power properties not by
increasing the detonation parameters directly (synthesis of more po-
werful individual HE) but by releasing the additional energy in the CJ
zone, providing more complete reaction in the detonation wave utiliza-
tion of the energy released to perform useful forms of the explosion
work. The authors of [1] have demonstrated that this approach to deve-
loping explosive systems is very promising using as an example detona-
tion of a benzotrifuroxane-hexanitroethane mixture with a stoichiomet-
ric oxidizer content (balanced to produce CO_2). The following detona-
tion characteristics are reported in [1] for this explosive system of
density $\rho=2.05$ g/cm^3: the detonation velocity D=9.44 km/s and pressure
P=44.9 GPa, which appreciably exceeds the detonation parameters of
each of the individual HE forming the mixture.

To estimate the prospects of this approach to development of exp-

losive systems in the present work we studied some fuel-oxidizer systems experimentally. The well-known HE, bis(2,2,2-trinitro-ethyl)nitramine, $C_4H_4N_8O_{14}$ (BTEN), and little-known, bis-(2-difluora-mine-2,2-dinitroethyl)nitramine, $C_4H_4N_8O_{10}F_4$ with a positive oxygen balance was selected as oxidizer.

Oxidizer-bis(2-difluoramino-2,2-dinitroethyl)nitramine has an exceptionally high density $\rho = 2.045$ g/cm^3. As an X-ray structural analysis shows, the packing coefficient of this material is 0.85, which value is apparently the highest among the known molecular crystals. By its density, this compound surpasses not only its trinitromethyl analog but the overwhelming majority of organic energetic materials as well.

Kinetic studies of thermal decomposition of α-(difluoramine)polynitro-compounds have demonstrated that their thermal stability is no worse or even better, than that of polynitrocompounds of a similar structure. Thus, bis (2-difluoramine-2,2-dinitroethyl)nitramine oxidizer is thermally more stable than bis(2,2,2-trinitroethyl)nitramine and, moreover, is less subjected to hydrolysis; whereas, bis(2,2,2-dinitroethyl)nitramine gradually degrades in aqueous media, its fluorinated analog is stable in hot water [3]. Three types of fuels were chosen for the explosive mixtures: a) HMX, $C_4H_8N_8O_8$ and benzotrifuroxane, $C_6N_6O_6$ (BTF); b) inert organic fuel: carbon black and ultra-fine diamond; c) inorganic fuel: fine aluminum powder of the particle size 4-10 μm.

We determined experimentally the heats of explosion, the metal acceleration ability, and detonation velocity of the above composite systems. The explosion heats were measured calorimetrically and the detonation velocities, by using electronic contact gauges and electronic chronometers. The charge diameters in detonation velocity measurements was 20 mm, and the error in the velocity was ~100 m/c.

The projection velocity of a steel plate 40 mm in diameter and 4 mm thick at 40 mm from the end of a 40 x 40-mm cylindrical charge placed in a thick-walled steel enclosure was chosen as criterion of the metal acceleration ability of HE. It should be noted that the electric circuit used for recording enabled us to determine the plate velocities to within ~1.0 %.

Table 1

Detonation Parameters and Metal Acceleration Ability
of the Composite Explosives (Experiment)

Explosive system	ρ_{exp}, g/cm^3	Q, kcal/mol	Plate velocity m/s	Metal acceleration ability.%	D, km/s
$C_4H_8N_8O_8$	1.875	1350	2185	100.0	9.05
$C_4H_4N_8O_{14}$	1.92	1250	2084	95.4	8.78
$C_4H_4N_8O_{14}$	1.844	1250	2028	92.8	8.46
BTEN/HMX (30/70)	1.910	1460	2251	103.0	9.02
BTEN/BTF (60/40)	1.861	1610	2242	102.6	8.70
BTEN/C (93/7)	1.883	1505	2185	100.0	-
BTEN/diamond(93/7)	1.982	1510	2222	101.7	-
BTEN/Al (90/10)	1.946	1650	2178	99.7	-
BTEN/Al (85/15)	1.947	1820	2170	99.3	-
$C_4H_4N_8O_{10}F_4$	2.033	1534	2342	107.2	9.10
$C_4H_4N_8O_{10}F_4$/HMX (60/40)	1.973	1567	2421	110.8	-
$C_4H_4N_8O_{10}F_4$/Al (85/15)	2.111	1304	2386	109.0	-

RESULTS AND DISCUSSION

We consider the experimental data for the BTEN/HMX and BTEN/BTF systems. The heats of explosion for these systems are much higher than those for the individual HE constituting the explosive system. This experimental fact can be ascribed to chemical interaction between the decomposition products of individual HE in the mixture, i.e. to oxidation by the free oxygen contained in the oxidizing HE of the products of incomplete carbon oxidation (C and CO) formed upon explosive decomposition of HMX and benzotrifuroxane to produce carbon dioxide. These reactions are apparently completed upstream of the Chapman-Jouguet plane. The increase in the detonation velocity of the binary systems compared to its values for the individual HE at the same charge densi-

ty confirms this conclusion. It is noteworthy that calculations of the detonation velocity by the model suggested in [2] yield for the BTEN/HMX system: D=9.27 km/s at ρ=1.91 g/cm^3 and 8.8 km/s at ρ=1.861 g/cm^3 for the BTEN/BTF composition. The experimental detonation velocity of the BTEN/BTF composition is 250 m/s lower than the calculated one. The difference between the calculations and experiment is ascribed to the heterogeneous nature of the system and large size of the HMX used (60-200 μm), which prevents a close contact between fuel and oxidizer. Heterogeneous systems have a broad chemical reaction zone, and this leads to large energy losses in diffusion processes. In this connection, we should note that the high energy release in fuel-oxidizer systems is not yet fully realized. One should substantially reduce the length of the chemical reaction zone by controlling the particle size of the components in the mixture providing thereby a contact between fuel and oxidizer on a nearly molecular level.

Optimization of the chemical composition of the mixture, its oxygen balance, and the possibility of attaining the maximum charge density are also important for increasing the efficiency of the energy utilization.

Feasibility of enhancing the power characteristics by optimizing fuel-oxidizer compositions is also supported by the experimental data on the velocity of the projected steel plates (see Table 1). Thus, for the BTEN/HMX and BTEN/BTF systems the velocity of the projected plates is about 60 m/s higher than they obtained with HMX charges of 1.875-g/cm^3 density, and the relative metal acceleration ability of these mixtures significantly exceeds that of HMX of the same density. It should be noted that in the experiments in which the velocity of the projecting plate has been measured the particle size effect is less important than in detonation velocity measurements, because of the difference in the characteristic times of the processes.

The experimental data for the BTEN/carbon black and BTEN/diamond mixtures demonstrate that addition of carbon black and ultra-fine diamond to the oxidizing HE increases by more than 250 kcal/kg the heats of explosion for the system compared with that of the oxidizing HE, which is evidence of complete combustion of the carbon and ultra-fine diamond in the detonation wave. The velocity of the accelerated plate is higher by more than 100 m/s for the BTEN/carbon black system and by 140 m/s for the BTEN/diamond mixture than that attained when the plate

is launched by detonating the oxidizer HE. The relative acceleration ability of these compositions is also appreciably higher, by 5 and 7%, respectively. A comparison of the experimental data on the plate velocities and relative acceleration abilities of the BTEN/carbon black and BTEN/diamond compositions indicates that introduction of ultra-fine diamond provides a higher power and detonation characteristics of the mixture. For the plate velocity this surplus is 40 m/s and for the acceleration ability it is 1.7%. Two factors are responsible for this experimental observation. Introduction of ultra-fine diamond increases the initial density of the composition and adds the heat of diamond-graphite phase transition. This raises the acceleration ability of the charge.

It should be noted that development of composite explosives with additives undergoing exothermic phase transitions in the detonation wave is a poorly studied problem and attracts attention as one of the possible approaches to raising the power of explosive systems.

Detonation velocity calculations by model [2] yield 8.7 and 9.04 km/s, respectively, for the BTEN carbon black at $\rho=1.883$ g/cm^3 and BTEN/diamond at $\rho=1.982$ g/cm^3. A surprising result was obtained in studies of impact sensitivity of the BTEN/diamond composition. The sensitivity of this composition was found to be at a level quite acceptable for practical purposes, although diamond is an abrasive material.

Now we consider the experimental data pertaining to the BTEN/Al (90/10) and BTEN/Al (85/15) compositions. It is commonly recognized that introduction of metals into high explosives does not increase the detonation velocity, but at the same time it enhances their performance compared to the individual HE forming the explosive composition.

The experimental results on the velocity of the projected plates and relative acceleration ability demonstrate that introduction of aluminum increases these parameters by 90 m/s and 4-5%, respectively, above their values measured for oxidizer HE charges. Hence, introduction of the metal improves the acceleration efficiency of the composition but does not increase its detonation velocity. This is because introduction of the metal in the explosive composition provides a slow decay of the peak pressure in the wave, which in turn, increases the duration of the high-pressure pulse acting on the projecting plate and, hence, enhances the accelerating performance of the composition.

The metal additive has no time to completely react within the time allotted in the exploding device and, therefore, the chemical energy stored in the system is not effectively used. This part of the energy can be released only in the later stage of expansion of the detonation products. the chief reason of the incomplete energy release in charges with the powdered metal is the large particle size. As a rule, the particle size ranges between 15 and 60 μm, which results in large energy waste for compression and heating of the particles within the chemical reaction zone. The metal burns releasing the energy downstream of the CJ plane and, therefore, has no effect on the parameters of the detonation wave (velocity and pressure).

We consider the experimental data for the second oxidizer bis(2-difluoramine-2,2-dinitroethyl)nitramine. The oxidizer is plastic and can be easily pressed, It is compatible with conventional high explosives (TNT, RDX and HMX). Compositions of the oxidizer with these high explosives accelerate metal plates than pure explosives. Thus, the bis(2-difluoramino-2,2-dinitroethyl)- nitramine – HMX composition accelerates plates to velocities 10% higher than does HMX. Mixtures of this oxidizer with metal powders exhibit even higher projecting ability, e.g., for aluminum mixtures it is 9.0% higher than for pure HMX. As far as we know, this the highest value among the available energetic materials.

The performance of metal-containing compositions can be improved by using ultra-fine metal powders with a particle size of the order of hundreds of angstroms. This intensifies the metal burning process and raises the efficiency of energy utilization due to a shorter chemical reaction zone.

The use of ultra-fine metal powders reduces the porosity of the system and thereby increases the power and detonation wave parameters. Of importance in these studies is optimizing the metal content in the charges.

In conclusion we would like to emphasize the high potentiality of explosive fuel-oxidizer compositions in obtaining better detonation and power performance of HE. Practical applications of these mixtures would require optimization of their composition and implies, in the first place, seeking for oxidizer HE with an acceptable set of properties.

REFERENCES

1. M.Finger, E.Lee, B.Heyes, et al., *Detonatsiya i Vzryvchatye Veshchstva* (Detonation and High Explosives, Collection of Translations) (Mir Publ., Moscow, 1981).
2. S.A.Gubin, V.V.Odintsov and V.I.Pepekin, *Khim. Fiz.*, **10**, No.6, 848 (1991).
3. B.V.Litvinov, S.P.Smirnov, V.I.Pepekin, et,al. *Dokl.Acad.Nauk, USSR.*, **336**, No1, 67 (1994).

DEVELOPMENT OF A COMPOSITE PROPELLANT WITH A LOW PRESSURE EXPONENT SUITABLE FOR NOZZLELESS BOOSTER MOTORS

Gideon Jacobus van Zyl* and Roderick Keyser**
Somchem, Division of Denel (Pty)Ltd, P.O. Box 187, Somerset West, 7129, South Africa

Abstract

The pressure exponent of composite propellants plays an important role in the design of solid rocket motors. The nozzleless booster motor is a propulsion system in which the pressure exponent is one of the major design variables. In this paper the results of a screening investigation, to find a suitable ballistic additive for the composite propellant of a nozzleless booster motor, is reported. A burning rate catalyst like Fe_2O_3, increases the magnitude of the pressure exponent, while Catocene and Prussian Blue have a decreasing effect. When the ballistic additive Al_2O_3 is used in combination with the afore-mentioned burning rate catalysts, a small effect on the ballistic properties is observed. When amorphous boron powder is used in combination with some of the previously mentioned burning rate catalysts, a more dramatic effect on the ballistic properties is observed. In addition to their effect on the ballistic properties, the effects of the different burning rate catalysts and ballistic modifiers on the mechanical, processing and hazard properties of the propellant are also reported. Results of test firings of nozzleless booster motors indicated that the lower the pressure exponent of the propellant, the higher the delivered specific impulse and the shorter the burn time of the motor.

* Senior Scientist, Propellant Development

** Senior Engineer, Propulsion Systems

1. Introduction

The burning rate of a propellant can be represented by an analytical expression that defines burning rate as a function of pressure at a given temperature. The analytical expression most frequently used to describe the burning rate of composite propellants and the one preferred by most propellant investigators is the de Saint Robert's burning rate law[1].

$$r = aP_c^n$$

where

r = propellant burning rate

a = coefficient of pressure

P_c = chamber pressure

n = pressure exponent

Controlling the pressure dependency of composite propellants has been the subject of concern to the designers of solid rocket propulsion systems for decades. Most propellant systems are formulated to meet specific ballistic requirements of burning rate and performance. Binder systems are formulated and optimized to produce mechanical properties necessary for particular applications. In contrast, the pressure exponent is a parameter which normally receives little attention in this design and formulation effort. Various factors have an influence on the pressure exponent and a number of different methods and approaches have been used in controlling this property. This includes the effect of[2]:

(a) oxidizer size, type and concentration

(b) metal type

(c) burning rate modifiers

(d) ballistic additives

(e) oxidizer coatings

(f) binder effects

Normally the desire is to have a pressure exponent as low as possible, so that a more optimum motor design can be achieved. A low pressure exponent results in a low motor temperature sensitivity and therefore reduces variability of both pressure and thrust over the operational temperature range. This in turn narrows the performance envelope and provides a more uniform performance under all conditions. Since the operating pressure range is

reduced, lighter motor hardware can be used. This reduces inert weight, thus increasing missile performance by increasing the propellant mass fraction.

In nozzleless rocket motors the pressure exponent is one of the major design variables. The effect of a reduction in the pressure exponent of the propellant on the performance of a nozzleless booster motor is reported by Procinsky and McHale[3]. The pressure-time and thrust-time curves depicted in this paper show that the ignition pressure decreases and thereby structural loading and maximum operating pressure limits are reduced. It also shows that the pressure and operating efficiency during approximately the last half of the burn time increases, resulting in a higher average operating pressure, more impulse and a thrust output close to neutral. In the example reported, a reduction in the pressure exponent from 0.48 to 0.28 in a booster with a length of 2.21 m and a diameter of 0.4 m, increased the total impulse by 3% and lowered the maximum pressure by 7%.

The need for high burning rate composite propellants with low pressure exponents was initiated by the design and development of a nozzleless rocket booster at Somchem. Some of the work that was done during the screening process of different burning rate catalysts and ballistic modifiers is presented in this paper.

2. Experimental

A propellant with good processing and reasonable mechanical properties was chosen as baseline for this investigation. The general propellant composition that has been used, is shown in Table 1. The binder system HTPB was used, while Fe_2O_3, Prussian Blue and Catocene were evaluated as burning rate catalysts. Al_2O_3 and amorphous boron powder were evaluated as ballistic modifiers.

Table 1 Baseline high burn rate propellant composition.

Component	Concentration (m/m %)
HTPB-binder	15.0
Al	15.0
AP	67.5 - 68.0
Burning rate catalyst	2.0
Ballistic modifier	0.0 - 0.5

Pilot plant mixes of 6 kg each were mixed from which ballistic test motor grains and various other test samples were cast. Ballistic properties of the propellant at 21 °C were determined from ballistic evaluation test motors. Mechanical properties at 21 °C were determined from JANNAF samples on a tensile test apparatus. End-of-mix viscosities at 60 °C were determined on a Brookfield viscometer. Impact and friction sensitivities were determined according to standard procedures[4].

3. Results and Discussion

3.1 Ballistic Properties

Because time available for the screening program was limited, it was decided to rely on past experience and concentrate the effort on three burning rate catalysts: two solid catalysts, Fe_2O_3 (superfine grade) and Prussian Blue, as well as the liquid ferrocenium catalyst, Catocene. Two ballistic modifiers were evaluated. Munson et.al.[5] reports that the combination of Catocene with small amounts of superfine Al_2O_3, causes a large increase in burning rate. This increase in burning rate is caused by an increase in both the values of the pressure exponent "n" and pressure coefficient "a". In this investigation it was decided to evaluate the combination of Al_2O_3 with the three chosen burning rate catalysts. Another ballistic modifier reported by Sellas[2], which decreases the pressure exponent, is amorphous boron powder. This was also evaluated during the screening process. The ballistic properties of propellants with different combinations of burning rate catalysts and ballistic modifiers are listed in Table 2.

Table 2. Ballistic properties of high burn rate composite propellant compositions

Burning rate catalyst	%	Ballistic Modifier	%	a (mm/s)	n	r_{10} (mm/s)
Catocene	2.0	-	-	16.4	0.30	32.6
Catocene	2.0	Al_2O_3	0.5	14.3	0.35	32.0
Catocene	2.0	B	0.5	16.4	0.26	29.5
Fe_2O_3	2.0	-	-	8.2	0.70	40.6
Fe_2O_3	2.0	Al_2O_3	0.5	8.2	0.66	37.9
Fe_2O_3	2.0	B	0.5	12.6	0.47	37.0
Prussian Blue	2.0	-	-	12.5	0.38	29.5
Prussian Blue	2.0	Al_2O_3	0.5	10.0	0.46	29.2
Prussian Blue	2.0	B	0.5	11.9	0.32	25.1

The effect of the different burning rate catalysts on the ballistic properties of the propellant can be summarised as follow:

- The trend observed in the pressure exponent, n, for the three burning rate catalysts are, from low to high values:

  Catocene < Prussian Blue < Fe_2O_3

- The trend observed in the pressure coefficient, a, for the three burning rate catalysts are, from high to low values:

  Catocene > Prussian Blue > Fe_2O_3

From these results it is obvious that the ballistic properties produced by Catocene, would be the most suitable for the nozzleless booster motor.

The results from this study showed that the combination of Al_2O_3 with Fe_2O_3 and Prussian Blue, have a negligible effect on the ballistic properties of the propellant. The synergistic effect which was reported by Munson et.al.[5] for the combination of Al_2O_3 and Catocene, was observed to a much lesser extent. The value of the pressure exponent of this propellant composition increased slightly, while the pressure coefficient decreased slightly. No explanation could be found, why the large synergistic effect, reported by Munson, was not observed in this investigation.

The effect of amorphous boron powder as ballistic additive, was much more dramatic. The combination of boron with Catocene caused a decrease in the pressure exponent while the pressure coefficient was unaffected. This similar trend was also observed in the combination of boron with Prussian Blue. The biggest effect however was observed with the combination of boron with Fe_2O_3. The value of the pressure exponent decreased significantly from 0.70 to 0.47, while the value of the pressure coefficient increased significantly from 8.2 to 12.6 mm/s. This means that the pressure exponent of Fe_2O_3-containing propellants can be reduced by the incorporation of a small amount of boron powder. The inclusion of a small amount of boron powder would not have any detrimental effect on the energetic properties of the propellant, but would have the added advantage of decreasing the pressure exponent to a suitable level.

3.2 Evaluation of different burn rate catalysts in a nozzleless booster motor

Although the advantages of propellants with low pressure exponents in nozzleless booster motors are well known, these effects had to be quantified for the locally developed nozzleless booster motor. It was decided to evaluate the three different burning rate catalysts in ϕ180 mm nozzleless booster motor test firings. The ballistic properties and some performance parameters of three propellant compositions that have been tailored for the nozzleless booster motor are tabulated in Table 3[6]. The normalised pressure-time and thrust-time curves of these test firings are shown in Figures 1 and 2 respectively[6].

Table 3 Properties and performance parameters of three different high burning rate propellant compositions in ϕ180 mm nozzleless booster motor firings[6].

Property/Performance parameter	Catocene	Prussian Blue	Fe$_2$O$_3$
a (mm/s)	17.9	11.1	9.1
n	0.26	0.35	0.43
Max. Pressure (MPa)	9.40	5.84	5.31
Normalised Burn Time	0.50	0.80	1.00
Normalised Specific Impulse	1.086	1.048	1.000
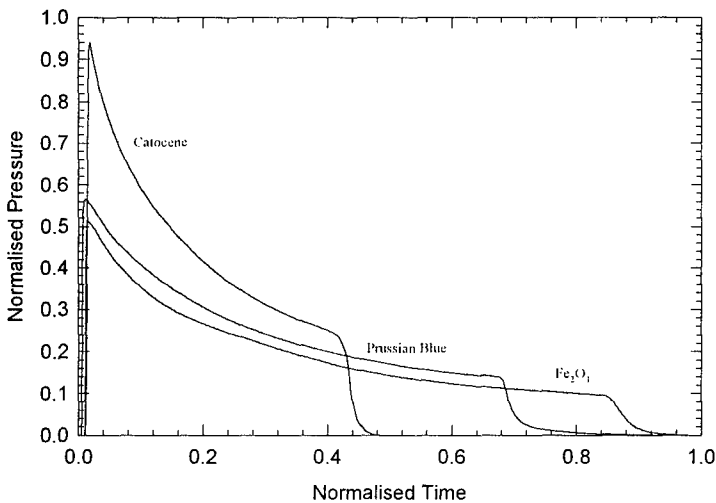
Figure 1. Pressure-time curves for ϕ180 mm nozzleless booster motors with different propellant compositions[6]

Figure 2. Thrust-time curves for ⏀180 mm nozzleless booster motors with different propellant compositions[6]

The advantages offered to the rocket propulsion designer by a propellant composition with a low pressure exponent, can clearly be seen from Table 3 and Figures 1 and 2. The burn time of the nozzleless booster is reduced by 50 % by the inclusion of Catocene instead of Fe_2O_3 as burning rate catalyst. At the same time the specific impulse increases by 8.6 %. The maximum pressure in the motor increased from 5.31 to 9.40 MPa. The benefit of using Catocene-containing propellant in the locally developed nozzleless booster motor is clearly demonstrated in these results.

3.3 Processing and Mechanical Properties

The processing properties of the propellant compositions that were investigated are defined in terms of their end of mix viscosities. In Table 4 these viscosities are tabulated, together with the mechanical properties. It must be pointed out that the reported mechanical properties were not tailored and could be improved to a certain extent, if so desired. The reported values merely represent the influence of the different burning rate catalysts and ballistic modifiers on the mechanical properties of the propellant, before tailoring of these properties would commence.

Table 4 Mechanical properties and EOM viscosities of high burn rate propellant compositions

Burning rate catalyst	%	Ballistic Modifier	%	Stress. (MPa)	Strain (%)	EOMV (kP)
Catocene	2.0	-	-	1.13	56	2.7
Catocene	2.0	Al_2O_3	0.5	0.73	59	2.5
Catocene	2.0	B	0.5	0.63	65	5.0
Fe_2O_3	2.0	-	-	0.87	41	7.5
Fe_2O_3	2.0	Al_2O_3	0.5	0.95	43	7.7
Fe_2O_3	2.0	B	0.5	0.99	42	10.5
Prussian Blue	2.0	-	-	1.08	31	7.7
Prussian Blue	2.0	Al_2O_3	0.5	1.60	22	22.3
Prussian Blue	2.0	B	0.5	1.38	31	21.3

The NCO/OH-ratios of the Prussian Blue and Fe_2O_3 propellant compositions were kept constant at 0.95. The NCO/OH ratios of the Catocene compositions were increased from 0.95 to 1.00 to increase the stress values. The mechanical properties of the Catocene and Fe_2O_3 compositions are representative of general composite propellants. The Prussian Blue composition however has a much lower strain value. Subsequent efforts to increase the strain values of Prussian Blue propellants were unsuccessful. No satisfactory explanation could be found for the low strain values observed in Prussian Blue propellants.

The combination of the ballistic modifiers with the different burning rate catalysts do not have similar effects on the mechanical properties of their respective propellant compositions. In most of the combinations, with the exception of the Prussian Blue-Al_2O_3-combination, the mechanical properties of the propellant are not detrimentally affected and could easily be tailored to suit requirements.

Processing of the different propellant compositions measured in terms of their EOM viscosities did not reveal any unexpected behavior. The lowest EOM viscosity of 2.7 kP was encountered with the liquid burning rate catalyst, Catocene, while the viscosities of the two solid catalysts, Prussian Blue and Fe_2O_3, were higher and almost of the same magnitude. The incorporation of amorphous boron powder generally led to an increase in viscosity and can be ascribed to the larger surface area that has to be wetted by the binder ingredients. The incorporation of Al_2O_3 did not influence the viscosity of the Catocene and Fe_2O_3 compositions, but the viscosity of the Prussian Blue composition increased substantially.

3.4 Hazard properties

It is important to handle high burning rate composite propellants with special care. This is especially important for propellants with low pressure exponents and high pressure coefficients. The mass flow rate of these propellants produced by combustion at atmospheric pressure, are very high and therefore represents a much bigger hazard than "general" propellant types. Hazard properties that are important during processing and handling of these type of propellants are impact and friction sensitivities. Friction and impact sensitivities of the investigated high burning rate compositions are tabulated in Table 5.

Table 5. Impact and friction sensitivities of high burning rate propellant compositions

Burning rate catalyst	%	Ballistic Modifier	%	Impact Sensitivity (kgm)	Friction Sensitivity (kg)	
					No reaction	Detonation
Catocene	2.0	-	-	1.13	21.6	25.2
Catocene	2.0	Al_2O_3	0.5	0.73	25.2	28.8
Catocene	2.0	B	0.5	0.63	28.8	32.4
Fe_2O_3	2.0	-	-	0.87	28.8	32.4
Fe_2O_3	2.0	Al_2O_3	0.5	0.95	32.4	36.0
Fe_2O_3	2.0	B	0.5	0.99	36.0	-
Prussian Blue	2.0	-	-	1.08	36.0	-
Prussian Blue	2.0	Al_2O_3	0.5	1.60	36.0	-
Prussian Blue	2.0	B	0.5	1.38	36.0	-

From the results in Table 5 is it clear that the Catocene containing compositions are more hazardous to process and handle than the Fe_2O_3 containing compositions. The Prussian Blue-containing compositions are significantly less hazardous than the afore-mentioned two types of propellant.

4. Conclusions

During this screening process, a few high burning rate propellant compositions with low pressure exponents were identified and characterized. The ferrocenium burning rate catalyst, Catocene, produces the lowest pressure exponent and good mechanical properties, but also produces more hazardous propellants. Fe_2O_3 compositions have the highest pressure exponents and good mechanical properties. The pressure exponents of the Prussian Blue compositions are intermediate between that of the Fe_2O_3 and Catocene compositions. Prussian Blue causes a unexplainable decrease in the strain capability of the propellant. The effect of the ballistic modifier, Al_2O_3, in combination with the different burning rate catalysts were disappointing. The large synergistic effect reported by Munson[3] for the combination

of Catocene and Al_2O_3 was not observed. The incorporation of the other ballistic modifier, boron, showed promising results. This is especially true for Fe_2O_3-containing compositions, where the pressure exponent can be decreased significantly by the inclusion of boron.

The goal of this investigation, namely identifying suitable propellant compositions with low pressure exponents for a nozzleless booster motor was reached. Test firings of ϕ180 mm nozzleless booster motors, proved that the best results in terms of burn time and specific impulse, can be obtained with Catocene propellant. This propellant also had the lowest pressure exponent and highest pressure coefficient.

Symbols and Abbreviations

AP	=	Ammonium perchlorate
B	=	Amorphous boron powder
Catocene	=	2,2-Bis-(ethylferrocenyl)propane
Al	=	Aluminium
HTPB	=	Hydroxy-terminated polybutadiene
Prussian Blue	=	Ferric ferrocyanide
EOMV	=	End of mix viscosity
n	=	Pressure exponent
a	=	Pressure coefficient
r_{10}	=	Burn rate at 10 Mpa
kP	=	Kilopoise

5. References

1. F.A. Warren, *"Rocket Propellants"*, Reinhold Publishing Corp. (1958).
2. J.T. Sellas, " *A review of the parameters affecting the pressure exponent in composite propellants"*, ICT 21-1 (1981).

3. I.M. Procinsky and C.A. McHale, *"Nozzleless boosters for integral-rocket ramjet missile systems"*, J. Spacecraft Rockets **18**, 193 (1981).

4. *"Hazards of chemical rockets and propellants handbook"*, Volume II, AD 870258 (1972).

5. W.O. Munson, L.R. McGee and R.B. Walker, *"Burning rate modifier effects on a high rate tactical propellant"*, AIAA Paper 77-928 (1977).

6. R Keyser, *"Somchem Internal Report (Classified)"*, 03982-000000-725130 (1996).

Acknowledgment

Beitrag zur 27. ICT-Jahrestagung 1996

Properties of AN and PSAN/GAP-Propellants

Klaus Menke, Jutta Böhnlein-Mauß

Fraunhofer-Institut für Chemische Technologie - ICT -
Joseph-von-Fraunhofer-Straße 7
76327 Pfinztal/Berghausen

1.   Abstract

Although many expectations have not been fulfilled, propellant formulations based on ammonium nitrate and GAP were developed to meet applicational profiles of less sensitive, minimum smoke rocket propellants during the last years.

Some of the characteristic properties of the more energetic formulations with nitric ester plasticizers are exhibited in this contribution. Performance, combustion behaviour and chemical stability reveal critical problems for application. These problems are connected to the ingredients, especially to AN, its numerous phase changes, its hygroscopicity, low energy and low reactivity. But also GAP and nitric ester plasticizers demonstrate incompatibility with many other chemical ingredients used for propellant formulation.

To overcome these problems formulations of four different kinds of pure and phase stabilized ammonium nitrate were compared to each other. Satisfying solutions have been found for combustion behaviour and chemical stability, if pure AN (SCAN), spray atomized from the melt and equipped with a significant low water content, was applied together with new burn rate modifiers based on mixed molybdenum/vanadium oxides.

Zusammenfassung

Obwohl sich viele Erwartungen nicht erfüllt haben, wurden Treibstofformulierungen auf der Basis von Ammoniumnitrat und GAP in den letzten Jahren für Anwendungen im Bereich wenig empfindlicher, signaturarmer Raketentreibstoffe weiter entwickelt.

Einige der charakteristischen Eigenschaften höher energetischer Formulierungen mit Nitratesterweichmachern werden in diesem Beitrag beschrieben. Die Bestimmungen der maximal möglichen thermodynamischen Leistungen, das Abbrandverhalten und die chemische Stabilität der Treibstoffe zeigen kritische Probleme für die Anwendung auf. Diese Probleme werden durch die chemischen Eigenschaften der Komponenten, insbesondere durch das Ammoniumnitrat, seine vielfältigen Phasenübergänge, seine Hygroskopizität, geringe Energie und Reaktivität verursacht. Aber auch GAP und Nitratesterweichmacher zeigen Unverträglichkeit mit vielen anderen chemischen Inhaltsstoffen, die für Treibstofformulierungen gebraucht werden.

Um diesen Problemen zu begegnen, wurden Treibstofformulierungen von vier Arten von reinem und phasenstabilisiertem Ammoniumnitrat miteinander verglichen. Für Abbrandverhalten und chemische Stabilität der Treibstoffe wurden zufriedenstellende Lösungen gefunden, wenn reines AN (SCAN), das durch Sprühkristallisation aus der Schmelze mit sehr geringen Wassergehalt ausgestattet ist, zusammen mit gemischten Molybdän/Vanadiumoxyden als Abbrandmodifikatoren eingesetzt wurde.

2.   List of Symbols

$I_{sp} \cdot \rho$	volumetric specific impulse	I_{sp}	specific impulse
ρ	density		
GAP	Glycidyl azido polymer	GAPA	Glycidylazidopolymerazide
AN	Ammonium nitrate		
SCAN	Spray crystalized AN		
PSAN	Phase stabilized AN		
Ni-,Cu-,Zn-	with NiO, CuO, ZnO phase		
PSAN	stabilized AN		
TCP	Tricalciumphosphate		
PI	Plasticizer	NE	Nitrate ester plasticizer
TMETN	Trimethylolethane trinitrate		
BTTN	1,2,4-Butanetriol trinitrate		
BDNPF/A	Bisdinitropropylformal/ acetal		
RDX	Cyclo-1,3,5-trimethylene-2,4,6-trinitramine (Hexogen)		
PMMA	Polymethacrylmethacrylate		
DPA	Diphenylamine		
NDPA	Nitrodiphenyl amine		
MNA	Methylnitroaniline		
CuPc	Copperphthalocyanate		
MOVO	Molybdenum/Vanadium oxide	mps	mean particlesize

3.   Introduction and Objective

A lot of work has been done on the development of AN propellants, on metallized[1], as well as on smokeless formulations.[2] The smokeless variants of propellant systems consisting of AN and energetic binders have been provided for high energy, less sensitive minimum smoke propellants to be used for tactical missile applications. They should have higher energy, better elasticity, lower freezing point and lower sensitivity to sympathetic detonation as well as to other hazards like bullet impact, fast and slow cook off.

Formulations work has been published on Ni-PSAN/GAP-propellants with BDNPF/A[3], nitric acid esters and azido plasticizers[4], which mostly demonstrated for the propellants to have either low performance, problematical stability and a bad combustion behaviour. The same handicaps, but a slightly higher performance have been observed for PSAN-propellants with nitramine binders.[5]

Nevertheless, the AN/GAP-system incorporates the potential for high energetic non polluting propellants which are really less sensitive and exhibit smokeless burning.

The objective of this work was to overcome the problems of combustion and stability and to develop the characteristic features and properties of AN/GAP formulations to fulfill the requirements of tactical missile propellant application.

4.   Ingredients

ICT has developed a process for the manufacturing of AN and different types of phase stabilized ammonium nitrate by spray atomization from the melt. The AN and PSAN products are characterized by small particle sizes, spherical shape and low water content. The species and properties which are available are

$$
\begin{array}{lll}
\text{AN pure} & = & \text{SCAN} \\
\text{Ni-PSAN} & = & \text{AN} + 1 - 7 \text{ \% } Ni_2O_3 \\
\text{Cu-PSAN} & = & \text{AN} + 1 - 7 \text{ \% } CuO \\
\text{Zn-PSAN} & = & \text{AN} + 1 - 7 \text{ \% } ZnO \\
\text{AN/}KNO_3 & = & \text{AN} + 1 - 7 \text{ \% } KNO_3 \\
\text{AN/}CsNO_3 & = & \text{AN} + 1 - 12 \text{ \% } CsNO_3
\end{array}
$$

All types are manufactured by a spray atomization process from the melt. They exhibit spherical particle shape and are available with mean particle sizes of:

160 μm, 55 μm and 20 - 25 μm.

If pure AN, AN/KNO_3 and AN/$CsNO_3$ have been sprayed from the melt their particles have a water content of 0,02 % to 0,04 %. For Ni-, Cu- and Zn-PSAN it is 0,1 % - 0,2 %. To prevent caking the particles are coated with 0,5 % Aerosil (SiO_2), TCP or Petro (sodiumlaurylsulfonate).

In the case of SCAN = spray crystallized ammonium nitrate the absence of water prevents the AN from undertaking the deteriorating crystal transition to phase III between 30 °C and 40 °C [6].

Table 1: Density of AN and PSAN samples which were spray atomized from the melt, coated with 0,5% Aerosil in g/cm.

mean particle size (μm)	SCAN	NiPSAN 1% NiO	NiPSAN 3% NiO	CuPSAN 3% CuO	ZnPSAN 3% ZnO	PSAN 7%KNO₃
160	1.688		1.732	1.742	1.709	
55	1.697					1.660
60		1.726				
53			1.740			
52				1.746		
50					1.706	

The densities of SCAN- and PSAN-types are outlined in table 1. Due to a higher density of Ni- and Cu-PSAN, propellants with these PSAN-types can be processed to higher solid loadings. With an appropriate particle size distribution, solid loadings up to 75 % are

possible for Ni-PSAN and Cu-PSAN / GAP / TMETN propellants including 5 % - 10 % RDX with 5 µm medium particle size. For SCAN and Zn-PSAN propellants only 70 % - 72 % solids loading are possible in this case.

The 3 % level of metal oxide phase stabilizer seems to be the optimum between phase stabilizing effect[6] and performance loss, connected to the partial replacement of AN by metal complex. SCAN, Ni-PSAN with 3 % Ni_2O_3, Cu-PSAN with 3 % CuO and Zn-PSAN with 3 % ZnO have been involved in the development of propellants, mostly with the two mean particle sizes of 160 µm and 55 µm.

GAP was purchased from SNPE. OH-di- and trifunctional versions with an equivalent weight of 1200 - 1330 were used. It was cured with the trifunctional isocyanate N100 from Bayer AG and with mixtures of N100 and IPDI from Hüls. BTTN was received from Wasag Sythen, GAPA from Rocketdyne. RDX 5 µm was made by precipitation crystallization, the molybdenum/vanadium oxide (MOVO) burning modifer was made by sintering and grinding rom the pure oxides.

5.   Thermochemical Performance Calculations

Thermochemical calculations were performed with two largely realistic high energetic propellant systems based on:

		I	II
AN	:	50 - 80 %	50 - 80 %
GAP/N100 (9:1)	:	10 - 50 %	10 - 50 %
BTTN/TMETN (4:1)	:	0 - 40 %	-
TMETN/GAPA (4:1)	:	-	0 - 40 %

From literature [3,4] and comparative calculations it was known that high values for the specific impulse of AN/GAP propellants are only achievable with nitrate ester plasticizers and BTTN/TMETN to be those with the highest energy and compatibility with GAP. The values calculated for the specific impulse and volumetric specific impulse with a 70:1 expansion ratio are outlined in fig. 1 to fig. 4. The corners of the triangles represent compositions of:

*   60 % GAP/N100, 40 % AN,
     0 % plasticizer

*   100 % AN, 0 % GAP,
     0 % plasticizer

*   60 % plasticizer, 40 % AN,
     0 % GAP

The lines mark 5 % concentration steps in each direction.

For both propellant systems high values of the specific and volumetric specific impulse are only obtained for compositions with a high plasticizer content. Due to the higher

energy and oxygen balance of BTTN/TMETN compared to TMETN/GAPA the maximum I_{sp} values are lower for formulation II.

The highest I_{sp} values for formulation I are connected with the highest plasticizer level. Due to the higher density of AN the maximum value for the volumetric specific impulse is located at 70 % AN, 10 % GAP and 20 % BTTN/TMETN with 3810 Ns/dm^3. For TMETN/GAPA the maximum values of I_{sp} and of the volumetric I_{sp} *ρ fall on the formulation with 80 % AN, 10 % GAP and 10 % TMETN/GAPA. Although there is a lower heat of formation on this point (-870 kcal/kg), a more improved oxygen balance is responsible for a higher I_{sp} .

The maximum I_{sp} values for the propellants with TMETN/GAPA plastivizer are not as high and above 240 s = 2356 Ns/kg as they are for the BTTN containing system. I_{sp} and volumetric I_{sp} * ρ values for propellants with 70 % solids loading including 3 % burn rate modifier with increasing amount of BTTN/TMETN plasticizer are exhibited in fig. 5.

Including stabilizers and burn rate modifiers and without nitramines the maximum I_{sp} of practicable propellant formulations will not exceed 235 s for BTTN/TMETN and 228 s for TMETN/GAPA-plasticizers.

6.   Combustion behaviour

Regarding literature desirable combustion properties like high burning rates and low pressure exponents never have been developed for minimum smoke AN-propellants with energetic binders[3-5]. In fact the first burn rate versus pressure curves for AN and PSAN/GAP/TMETN-propellants exhibited low burn rates and high pressure exponents (n > 0,6).

Cu- and Ni-PSAN showed a more profitable burn rate enhancing effect compared to AN- and Zn-PSAN in these formulations.[7] Both, however, cause a deteriorating effect on the stability (s.b.), Cu-PSAN shortens the pot life of propellant formulations dramatically and Ni-PSAN originates toxic combustion products. Besides their promotion effect on the combustion behaviour appeared not be sufficient for formulations with a high content of nitrate ester plasticizers. Without any other burn rate modifier it was not possible to suppress the pressure exponent below 0,6 simply by using Ni- or Cu-PSAN.

For this reason a new burn rate modifier has been developed, which has its origin in environmental chemistry. The modifier is a mixed compound of molydenum- and vanadiumoxides (MoO_3 and V_2O_5) which is from now called MOVO-catalyst[8]. With it the NOx removal from waste gases is achieved by the ammonia nitrogen oxide conversion reaction[9]:

$$4NH_3 + 6NO \rightarrow 5N_2 + 6H_2O$$
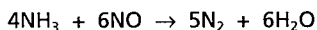
The MOVO burning modifier proves to be effective for all AN and PSAN/GAP-formulations. This is illustrated in fig. 6 and fig.7. All propellants exhibit pressure exponents below 0,6. The most remarkable effect is seen with Cu-PSAN (n = 0,49).
The burn rates of Ni- and Cu-PSAN propellants exceed 8 mm/s at 7 MPa those of Zn-PSAN and SCAN-propellants are between 7 and 8 mm/s at 7 MPa. The burn rate enhancing effects of the Ni- and Cu-PSAN-oxidants are clearly to be seen in these formulations. Due to a GAP/plasticizer ratio of 1 : 1 the specific impulse of these propellants is between 224 and 227 s at 70 : 1 expansion ratio.

For propellants with a higher plasticizer content and higher performance the effectivity of the MOVO burn rate modifier decreases. Like Cu-PSAN copper ions and complexes show a synergistic effect with MOVO compounds. For this reason it was tried to achieve an improvement by using copperphthalocyanate in combination with MOVO catalyst. The burning behaviour of such a propellant is outlined in fig. 8. Propellant AN 163 with CuPc/MOVO modifying system exhibits enhanced burn rates and reduced pressure exponents. The stability of such a formulation is, however, not sufficient.

In fig. 9 the burning behaviour of the two propellant systems with TMETN/GAPA and BTTN/TMETN plasticizer containing 2,0% MOVO catalyst and 0,4 % carbon black is compared to each other. Although it has a lower specific impulse, and a lower combustion temperatur, the propellant with the TMETN/GAPA plasticizer showed higher burn rates and lower pressure exponents than the higher energetic one with BTTN/TMETN plasticizer. The higher combustion temperature of the BTTN/TMETN formulation (2640 K compared to 2460 K) might be part of the reason for the decreasing effectivity of the MOVO system. The MOVO catalysed NH_3/NO_x conversion reaction also has been found to be temperature dependent[9].

Fortunately grinding of the MOVO catalyst improves the efficency for combustion modification. This is shown in fig. 10 with two burn rate pressure curves of propellants with 2% MOVO catalysts with 53 and 4 μm mean particle sizes. From 53 to 4 μm a considerable improvement in the enhancement of burn rates and decrease of pressure exponents can be observed even for high contents of nitrate ester plasticizers. By this way AN/GAP propellants with a specific impulse from 230-235 s (70:1), burn rates between 7-8 mm/s at 7 Mpa and pressure exponents from 0,50 to 0,58 can be successfully formulated.

7.   Chemical Stability

Stability of the AN/GAP-propellant system is expected to be a crucial property because all the main components may originate gas evolution and decomposition effects.[3,10,11] For this reason a lot of stabilizing agents have been tested in SCAN and Ni PSAN/GAP/TMETN formulations. The most important results are pointed out in table 2.

For the Dutch test the percent weight loss from 8-72 h storage at 105°C should not exceed the 3% level. For vacuum stability the gas evolution from a 2,5 g sample for 40 h at 100°C should not exceed 5 ml or 0,5 - 1 ml at 80°C respectively.

From the results in table 2 it is clearly to be seen that pure AN = SCAN exhibits the best stability with GAP and TMETN. It is the only one to fulfill the vacuum stability requirements at 100°C. Maybe due to a starting decomposition reaction of the phase stabilizing metal complexes, stability of the Ni- and Zn PSAN/GAP/TMETN formulations is within the limit at 80°C but not at 100°C. CuPSAN originates more instability, caused by incompatability with the azido groups of GAP.

DPA or MNA and 2NDPA have been found to be suitable stabilizers for the AN/GAP/TMETN system. DPA seems to have the highest stabilizing efficiency regarding these short running preliminary tests.

AN/GAP-propellants with MOVO catalysts mostly fulfill the requirements of dutch test and vacuum stability which is pointed out in table 2. A slight incompatibility however is observed, if BTTN is incorporated in the system. In this case the MNA/2NDPA stabilizer

system has an advantage against DPA. The reason might be the lower degree of basicidity of MNA.

The cube crack test may be regarded as a test to be more close to application than the values for dutch test and vacuum stability. In fig. 11 the results of a 80°C storage test for 50 mm cubes are pointed out including AN = SCAN and PSAN/GAP/TMETN propellants formulations with the MOVO and CuPc/MOVO catalyst system. The end of each bar marks the specified storage time, after that cracks occurred in the cubes. In comparison of the formulations CuPSAN, CuPc and NiPSAN appear to be responsible for crack formation after a short storage time. As it is seen in the shortrunning lab tests Cu-ions originate the highest instability, but NiPSAN/GAP/TMETN formulations are not stable too. Only formulations of SCAN/GAP/TMETN with DPA stabilizer including MOVO catalyst are stable within the whole storage time.

8.   Conclusion

The main features of AN/GAP propellants have been developed to meet the objectives of low sensitivity, smokeless combustion, non polluting combustion products and medium to high performance.
For stability reasons pure AN in the form of spray crystallized ammonium nitrate (SCAN) has been preferred for other phase stabilized AN products. CuPSAN, NiPSAN and even ZnPSAN/GAP/NE formulations do not achieve sufficient stability to meet applicational requirements. BTTN which is needed for a high specific impulse has a worse effect on stability, too which can be compensated however by using MNA stabilizer systems.

The combustion behaviour of PSAN/GAP formulations is improved by Ni and CuPSAN. It is however not possible to make use of it because the stability of these formulations is not sufficient.
A worthwhile inprovement even for high energy formulations with high amounts of BTTN/TMETN plasticizer is obtained by using a new catalyst system based on molydenum/vanadium oxides, called MOVO catalyst further on. By using this catalyst system burn rates of 7-8 mm/s and pressure exponents from 0,50 to 0,55 are achieved for high energy formulations. Stability of MOVO-containing formulations has been proved in 50 mm cube crack tests. Their combustion products are non toxic and non polluting. With 2,0% MOVO catalyst the limit for AA classification according to an AGARD PEP-coefficient of 0,35 is fulfilled.[12]

The performance limit for these formulations corresponds to an I_{sp} = 235 s at 7 Mpa (1015 psi) for AN/GAP propellants with BTTN/TMETN plasticizers and 228 s for those with TMETN/GAPA. Higher values are possible by the incorporation of high energetic nitramines, but RDX and HMX appear to have negative influence on the detonation sensitivity of these propellants[7].

Further explorations and developments are necessary in this field to reach the goal of a minimum smoke propellant with a specific impulse above 240 s at 1000psi and the desired low detonation sensitivity.

LITERATURE, REFERENCES

1) P.W. Doll, G.K. Lund;
High performance, low cost solid propellant compositions producing halogen free exhaust
US Patent 5, 076,868 (1991)

2) A.M. Helmy;
GAP propellant for gas generator application
23rd AIAA J. Prop. Conf., San Diego (1987)

3) P. Lessard et al.;
Development of a Minimum Smoke Propellant based on GAP and AN
AGARD-CP 511, 78th Spec. Meeting, Bonn (1991)

4) Y. Longevialle et.al.
Low Vulnerability Minimum Smoke Rocket Propellants
ADPA-Conf. on Energetic Mat. Techn. Meeting 680, p. 125ff
Phoenix/Arizona (1995)

5) R.L. Bivin et al.;
Development of a Class 1.3 Minimum Smoke Propellant
28th AIAA J. Prop. Conf., Nashville (1992)

6) W. Engel et al.;
Ammonium Nitrate a Less Polluting Oxidizer
24th Intern. ICT-Conf., 3.1 bis 3.9 (1993)

7) K. Menke, J. Böhnlein-Mauß, K.-P. Brehler;
Development of Less Polluting Propellants
AGARD-CP-559 84th PEP-Symp., Alesund (1994)

8) V. Weiser et. al.
Thermal Degration of AN/GAP-Blends
P. 86, 26th Int. Ann. Conf. ICT, Karlsruhe (1995)

9) M. Inomata, A. Miyamoto, Y. Murakami
J. Phys Chem 85 (1981) S. 2372

10) J.M. Bellerby, M.H. Sammour;
Stabilizer Reactions in cast Double Base Rocket Propellants
Prop., Explos., Pyr. 16, 273-278 (1991)

11) J.C. Oxley et al.;
Thermal stability and compatibility of AN explosives on a small and large scale
Thermochim. Acta 212, 77-85 (1992)

12) P.A. Kessel
in AGARD-LS-188
Rocket Motor Plume Technology, p. 3-1 to 3-9
Neubiberg (1993)

Table 2: Results of dutch test, flash point and vacuum stability for AN/GAP/NE and PSAN/GAP/NE formulations

SCAN (%)	PSAN NiO (%)	PSAN CuO (%)	PSAN ZnO (%)	GAP N100 (%)	TMETN (%)	BTTN (%)	RDX (%)	MOVO Cat. (%)	Stabilizer	%	flash point 20°C/min (°C)	dutch test 8-72h/105° (%W.loss)	vac. stab. 40h/80°C (ml/2.5g)	vac. stab. 40h/100°C (ml/2.5g)	remarks
70				30							212	1.33	0.80	3.26	stable
	70			30							208	2.52	2.23	16.2	--
		70		30							206	1.77	2.39	10.1	--
			70	30							209	1.74	2.47	11.4	--
50				19	30				NDPA	1	186	3.22	0.68	6.39	--
50				19	30				DPA	1	182	2.76	0.36	3.71	stable
	50			19	30				NDPA	1	184	2.73	0.86	15.6	--
	50			19	30				MNA	1	181	5.59	0.37	12.7	--
	50			19	30				DPA	1	181	3.30	0.35	9.67	--
	50			18.5	30				MNA NDPA	1 0.5	179	3.00	0.36	6.47	--
60				19.5	10		10		DPA	0.5	184	0.37		1.54	stable
		60		19.5	10		10		DPA	0.5	181	3.00	2.01	16.2	--
			60	19.5	10		10		DPA	0.5	186	2.09	0.57	13.6	--
64				13	20			2.0	DPA	0.6	184	2.86		2.82	stable
65				13.5	9.5	9.5		2.4	DPA	0.5	183	4.70	0.22	5.41	--
65				13.5	19			2.4	DPA	0.5	182	3.05		1.86	stable
64				11	11	11		2.0	MNA NDPA	0.5 0.5	180	3.62		2.63	stable
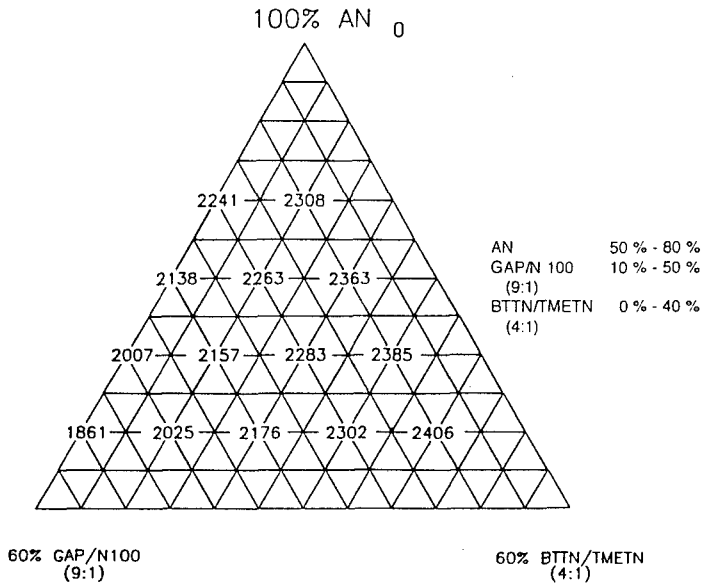
Fig. 1: Thermodynamically calculated values of the specific impulse I_{SP} (Ns/kg) at 70:1 expansion ratio for AN/GAP/BTTN/TMETN formulations

Fig. 2: Thermodynamically calculated values of the volumetric specific impulse $I_{SP} * \rho$ (Ns/dm^3) at 70:1 expansion ratio for AN/GAP/BTTN/TMETN formulations

100% AN

AN	50 % - 80 %
GAP/N 100	10 % - 50 %
(9:1)	
TMETN/GAP-A	0 % - 40 %
(4:1)	

2241 — 2313

2138 — 2227 — 2304

2007 — 2113 — 2207 — 2291

1861 — 1972 — 2085 — 2185 — 2272

60% GAP/N100
(9:1)

60% TMETN/GAP—A
(4:1)

Fig. 3: Thermodynamically calculated values of the specific impulse I_{SP} (Ns/kg) at 70:1
expansion ratio for AN/GAP/TMETN/GAPA formulations

100% AN

AN	50 % - 80 %
GAP/N 100	10 % - 50 %
(9:1)	
TMETN/GAP-A	0 % - 40 %
(4:1)	

3610 — 3779

3333 — 3521 — 3696

3033 — 3235 — 3427 — 3608

2726 — 2928 — 3138 — 3334 — 3515

60% GAP/N100
(9:1)
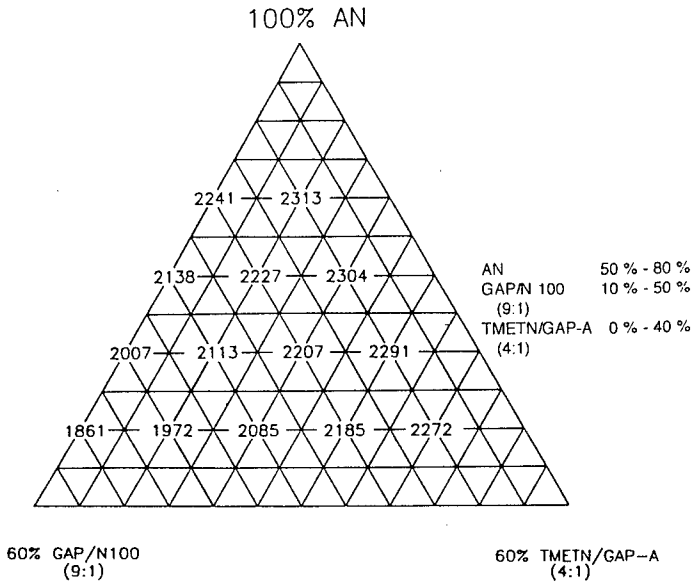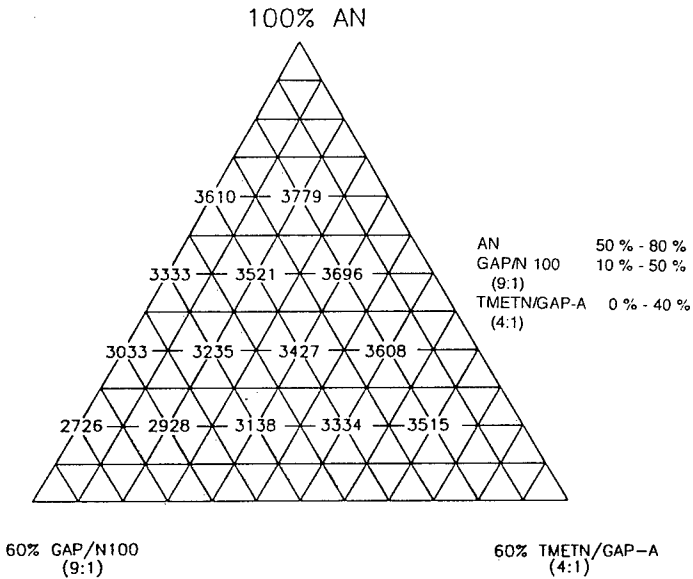
60% TMETN/GAP—A
(4:1)

Fig. 4: Thermodynamically calculated values of the volumetric specific impulse $I_{SP} * \rho$
(Ns/dm^3) at 70:1 expansion ratio for AN/GAP/TMETN/GAPA formulations
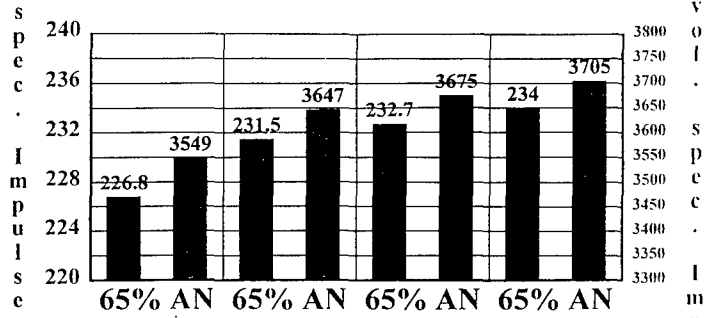
GAP/Plasticizer	1:1	1:1.5	1:1.75	1:2.15
Plast. 1	50% TMETN	50% TMETN	50% TMETN	50% TMETN
Plast. 2	50% BTTN	50% BTTN	50% BTTN	50% BTTN

■ Spec. Impuls (s)		▓ Vol. spec. Imp. (Ns/dm³)	

Fig. 5: Thermodynamically calculated values of I_{SP} (Ns/kg) and $I_{SP} * \rho$ (Ns/dm^3) at 70:1 expansion ratio for AN/GAP-formulations with 3 % burn rate modifier and increasing amounts of BTTN/TMETN
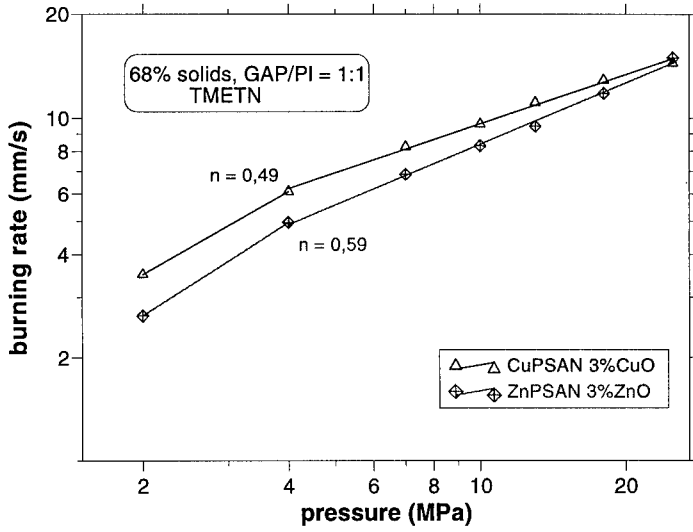
fig. 6: Burnrate vers. pressure curves for CuPSAN and ZnPSAN/GAP propellants with 10% RDX and 2,5% MOVO burnrate modifier, $I_{SP,EQ}$ = 224-227 s (70:1)
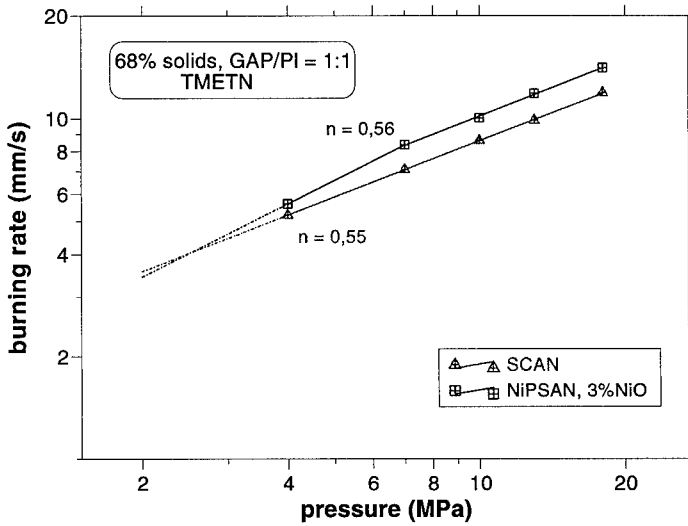
Fig. 7: Burnrate vers. pressure curves for NiPSAN and SCAN/GAP propellants with 10% RDX and 2,5% MOVO burnrate modifier, $I_{SP,EQ}$ = 224-227 s (70:1)
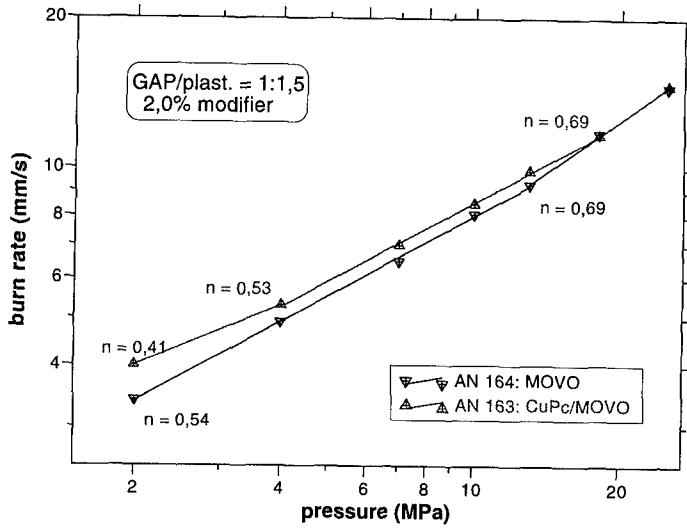
fig . 8: Burnrate vers. pressure curves for high energetic AN/GAP/BTTN/TMETN propellants with 2% MOVO and 2% CuPc/MOVO burnrate modifiers
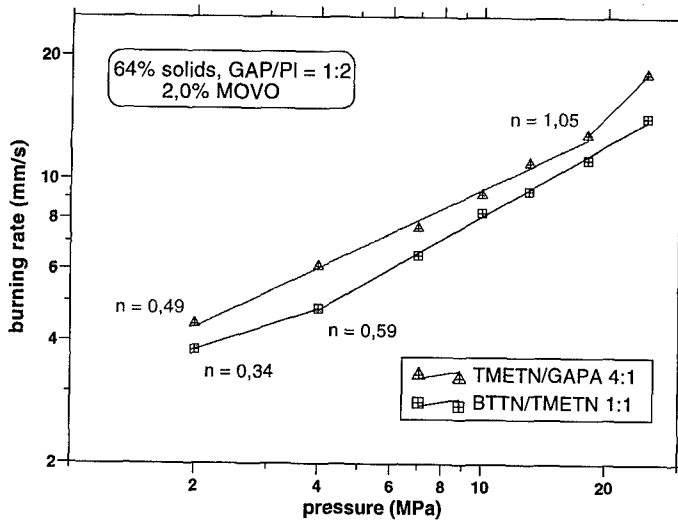
Fig. 9: Burnrate vers. pressure curves for high energetic AN/GAP/BTTN/TMETN and AN/GAP/TMETN/GAPA propellants with 2% MOVO burnrate modifier
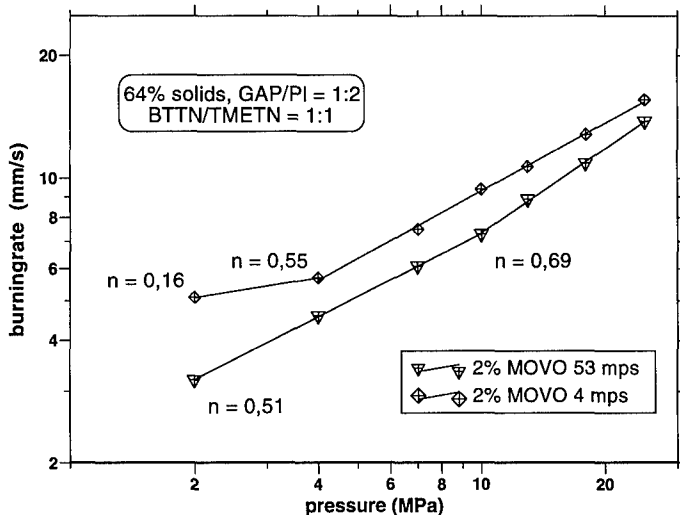
Fig. 10: Burnrate vers. pressure curves for high energetic AN/GAP/BTTN/TMETN propellants including 2% MOVO burnrate modifiers of decreasing particle sizes

Cube-Crack-Test

Lagerdauer bis zum Auftreten von Rissen im Kubus

x: nach 15 d Lagerung noch keine
Rißbildung
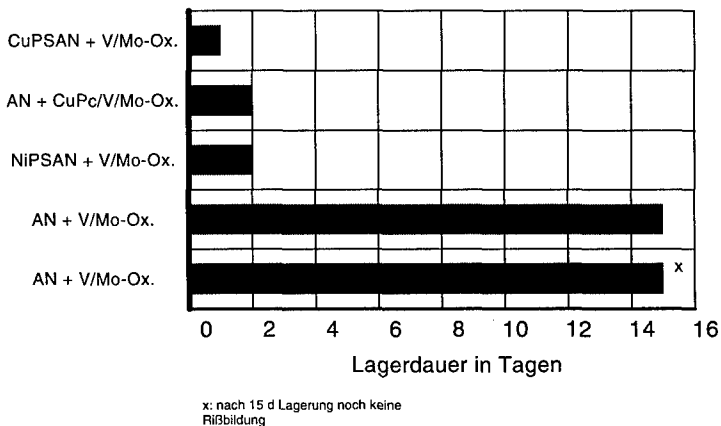
Fig. 11: Results of Cube Crack 80°C storage tests for AN and PSAN/GAP/TMETN-propellants with MOVO and CuPc/MOVO burnrate modifiers

GUIDELINES TO HIGHER ENERGY GUN PROPELLANTS

R. L. Simmons
Naval Surface Warfare Center - Indian Head Division
Indian Head, MD 20640
301-743-4635
FAX 301-743-4683

Abstract

New energetic ingredients emerging from research ... polymeric binders, plasticizers, and solid oxidizers ... will form the basis for the next generation of solid gun propellants, where impetus values > 1400 joules/gram will be possible at flame temperatures ≈ 3500°K. If flame temperature were not a constraint, impetus values above 1500 joules/g are within our grasp. Other possibilities include the development of propellants with gas MW = 18 and impetus ≈ 1200-1300 joules/g ... and a new regime where gas MW < 17. Key to these developments are the little known diazido nitramine ingredients DANP, DANPE, DATH, DADNH, and DADZP ... in addition to CL-20, TNAZ, and ADN currently being researched.

Introduction

There are new energetic propellant ingredients emerging from research in laboratories all over the world which will form the basis for the next generation of gun propellants. These new ingredients include polymeric binders, plasticizers, and solid oxidizers which will provide not only a jump in ballistic performance, but will likely have features not encountered previously in gun propellants.

In evaluating the theoretical performance of gun propellants, mass impetus (or the older term force constant) traditionally is used as an index of performance, as defined by the following (ideal gas equation of state):

$$F = nRTv = RTv/M \qquad (1)$$

where F = impetus in joules/gram, R = universal gas constant of 8.3143 joules/gram/degree, Tv = isochoric (constant volume) flame temperature (°K), n = moles of gas evolved/gram upon combustion, and M = average combustion gas molecular weight (MW).

From equation (1), it is clear there are two routes to higher impetus: increase the flame temperature (Tv), and/or decrease the combustion gas molecular weight, i.e., increase the gas output. Current NC-based gun propellants (both military and commercial) have impetus values about 1000 joules/gram, with Tv about 3000°K, and gas MW about 25.

In the past, propellant chemists simply increased the concentration of nitroglycerin in NC-based propellants (or added RDX) to achieve higher impetus. However, this practice will not work for the next generation of gun propellants where it is necessary to increase the impetus by about 40% (to 1400 joules/gram) in order to substantially increase the muzzle velocity. If there is no change in combustion gas MW, as the impetus increases to 1400 joules/gram, Tv will increase to about 4000°K -- which is intolerable in most gun systems. Current barrel metals will not withstand temperatures this high. However, if the gas MW is reduced to 18, Tv will remain constant at 3000°K, and barrel heating will remain unchanged from current levels.

There is another reason for striving for low gas MW --- the sonic velocity in the combustion gases should be as high as possible to minimize the pressure gradient between the chamber pressure and the pressure on the base of the accelerating projectile, i.e., there is always an undesirable pressure drop at the projectile base, which is inversely proportional to the local velocity of sound in the gases. The gases are both propelling the projectile and trying to "keep up with it" at the same time. This pressure gradient can be minimized by increasing the sonic velocity, which is defined as:

$$Vel^2 = k \, R \, Tv/M = k \, F \qquad\qquad (2)$$

where k = gamma = Cp/Cv (ratio of heat capacities), R = universal gas constant, Tv = isochoric flame temperature, M = gas MW, and F = impetus. From equation (2), it is clear that gamma should be high and gas MW low. The significance of high sonic velocity and low MW gases is perhaps best recognized in light gas guns where hydrogen (with MW = 2) and helium (with MW=4) are used as the working fluid to attain projectile velocities above 3000-4000 meters/second. Therefore, there are two strongly compelling reasons for wanting gun propellants which generate low MW gases: high impetus (at low Tv) and high sonic velocity.

Reducing the combustion gas MW as a route to high impetus has not been widely recognized or appreciated except by a few in the propulsion community. In the early 1950s, the Navy pursued high nitrogen compounds (such as azides, guanidine derivatives, and tetrazoles) to achieve lower flame temperatures (and flash-free behavior) in NC-based propellants with no impetus penalty. In the early 1960s, the Army (with AF funding) pursued hydrazine bisborane (and hydrazine azide) as a source of hydrogen and low gas MW for hypervelocities above 2500 meters/second. Callery Chemical Company and Esso Research & Engineering Company were also involved. Though these research programs only lasted a few years, they provided an in-sight into the types of compounds that would be beneficial in yielding low MW gases.

In the 1970s and 1980s, the Air Force (at Eglin AFB) was the leader in promoting low gas MW propellants, where the interest was high rate-of-fire and hypervelocities above 2000 meters/second (for short time-of-flight to target). High rates-of-fire meant the flame temperature could not be appreciably above 3000°K, and hypervelocities dictated that gas MW should be less than 20 (as much as possible). Based on the AF efforts, several advanced gun propellants (containing RDX, TAGN, and cool-burning aliphatic nitramines) were developed which had gas MW near 19, but none ever attained as low as 18 with reasonable impetus values --- which represents a formidable challenge in propellant chemistry today.

General Discussion

In formulating combinations of ingredients for low MW gases, one should strive for stoichiometry yielding the following gases:

H_2	MW = 2
CH_4	16
NH_3	17
H_2O	18
N_2	28

Nitrogen is preferable over carbon, even though the MW of N_2 is the same as CO (MW = 28) --- the water-gas equilibrium will allow the formation of some CO_2 (with a very high MW = 44) whenever CO is present. Also, the formation of N_2 over CO favors a flash-free muzzle blast. In general, the amount of carbon should be minimized to avoid the formation of: C(s), CO, O_2, and CO_2, even though some CH_4 (MW = 16) is desirable.

In Figure 1, where impetus is plotted versus flame temperature Tv, it can be seen that if one wants to achieve an impetus of 1400 or more and a gas MW near 18, it is not possible by simply varying the proportion of NC + NG --- ingredients of dramatically different thermochemistry must be used.

A number of ingredients of current interest to the propulsion community (and combinations thereof) were examined to determine the limits of performance possible --- in terms of low gas MW, Tv, and impetus. Polymers considered were NC, HTPB, GAP, AMMO/BAMO, poly NIMMO, and poly GLYN, while plasticizers were GAP, DANP, DANPE, and four NENAs (methyl, ethyl, propyl and butyl). Solid oxidizers examined were RDX, CL-20, TNAZ, ADN, two TAG salts (TAGAZ and TAGN), NQ, and three energetic diazido nitramines (DATH, DADNH, and DADZP).

Most of these compounds are well known throughout the propulsion community (both gun and rocket) except perhaps TAGAZ (triaminoguanidine azide) and the aliphatic diazido nitramines DANP, DATH, DADNH, and DADZP). DANP is a liquid, while the other four are solids. All five have been synthesized and known for at least several decades, they are extremely energetic, but not well characterized. However, because of their energy potential, they were excellent candidates for this screening effort.

All of these compounds are listed in Table 1 according to their oxygen/carbon ratio (O/C). Oxidizers are shown in descending O/C ratio (oxidizing ability), and fuels in ascending O/C ratio. Names for these ingredients are given in the glossary, while empirical formulas and heat of formation (ΔHf) values are shown in Table 2. The latter two parameters are the only ones needed in order to calculate the necessary ballistic performance.

While it is recognized that density is important in determining the overall volumetric performance of a propellant, it has not been considered in these performance calculations, primarily because the density of some of the compounds is either uncertain or unknown. Densities of the solids are thought to range from 1.60 to 2.0 g/cc. Though most of the thermochemical computer codes in use today yield essentially the same answer (within 1%), the Blake code (at a constant loading density of 0.20 g/cc) was used for the calculations in this paper.

Performance of some of the neat ingredients of interest is shown in Figure 2, where it can be seen that the only ones approaching the goal of gas MW = 18 are the NENAs and TAGN, and at relatively low impetus values (below 1150 joules/gram). The neat diazido nitramines DANP, DADZP, DADNH, and DATH give impressively high impetus values (higher than RDX, CL-20, and TNAZ), but only at high flame temperatures above 3700°K. As can be seen by the results summarized in Table 3, the highest impetus values (in joules/gram) are 1761 for DANP, 1650 for DADZP, 1504 for DADNH, and 1481 for DATH. All other neat ingredients are considerablly less energetic.

Several hundred calculations were made of various combinations (largely binary combinations) of the ingredients shown in Table 1 to determine the performance behavior. In many cases, ingredients of high O/C ratio (oxidizers) were matched with ones of low O/C (fuels) to obtain balanced mixtures -- though these did not always give the maximum performance. In other cases, combinations of oxidizers of various O/C ratios were examined. In general, condensed phases (typically solid carbon) begins to appear when the O/C < 0.9, therefore, nearly all of the calculations involved O/C ratios of unity or greater. Figure 3 showing behavior of NC + additives illustrates the typical behavior noted in most calculations.

Systems Offering Gas MW ≤ 18

A large number of systems were examined looking for gas MW ≤ 18 and impetus ≥ 1400 joules/g --- and none were found. Obviously, it is an extremely challenging goal. Only a very few (nine total) systems offered gas MW values ≤ 18 --- and all had Tv below 3000°K, with most below 2700°K (see Table 4) --- meaning the impetus levels were not very high. These systems represent only eight different ingrèdients (other than NC) --- GAP, TAGN, MeNENA, BuNENA, ADN, DANP, TAGAZ, and DANP. While it is not claimed that all possible binary combinations of ingredients were examined, those most likely to yield low gas MW values (and high impetus) were examined.

The highest impetus found with gas MW ≤ 18, was in the ADN-TAGAZ and ADN-TAGAZ-DANP systems. The ADN-TAGAZ system is unusual in that ADN has no carbon and TAGAZ has no oxygen. At a gas MW = 18, the impetus was 1378 and Tv = 2987°K for ADN-TAGAZ-DANP. It is doubtful that a more energetic system will be found, while keeping the gas MW at 18 --- unless ingredients of greater positive ΔHf can be found.

One of the unusual features noted for several of these systems, was that gas MW values below 17 are possible (albeit at low Tv and low impetus values). For example, a mixture of 40% TAGN and 60% TAGAZ gives the following:

$$
\begin{array}{ll}
\text{Impetus} = & 1106 \text{ joules/g} \\
\text{Tv} = & 2250°K \\
\text{Gas MW} = & 16.92 \\
\text{Gamma} = & 1.282
\end{array}
$$

The addition of a small amount of polymeric binder would undoubtedly lower the gas MW (and Tv) even more. For specialized applications where low gas MW is more important than high impetus, such a propellant may be quite useful --- and offers an opportunity to explore the rare and unusual field of propellants with gas MW < 17.

It should be realized that many of the systems examined did not contain binder. The goal was to determine the potential of various combinations of ingredients -- the effect of adding a small amount of binder would be done later.

To achieve a significant increase in impetus, it is obvious that the Tv limit needs to be raised to include JA-2 at 3450°K -- the current propellant in 120mm tank ammunition and also probably the hottest propellant in wide use.

Systems Of High Impetus with Tv Near 3500°K

Increasing Tv to 3500°K in the search for 1400 joules/g also means the maximum gas MW permitted will increase to 20.8 according to equation (1). With the increased Tv limit, sixteen combinations of ingredients were identified that will reach 1400 joules/g at 3500°K. A listing of those systems above 1400 joules/g are shown in Table 5. A common link exists in that all sixteen contain at least one diazido nitramine in the form of DANP, DANPE, DADNH, DADZP, or DATH. The most energetic system seen (at Tv near 3500°K) is 55% DANP + 45% EtNENA, where the impetus is 1484 joules/g and gas MW = 19.87. Since some of these are all liquid systems, it raises the possibility that a blend of these liquids might make for a highly interesting new energetic plasticizer.

It is realized that there is much interest and research in many laboratories around the world looking into TNAZ, CL-20, and ADN in various polymeric binders including AMMO/BAMO. However, no binary combination of RDX, TNAZ, CL-20, or ADN in HTPB, GAP, AMMO/BAMO, poly NIMMO, poly GLYN, or NC achieved an impetus of 1400 joules/g at 3500°K. Each of these systems showed increasing impetus with increased solids loading (as expected) --- with peak impetus values all occurring above 3500°K --- as noted in the following listing of peak impetus values for a 1:1 AMMO/BAMO binder:

	% Solids	Impetus	Tv - °K	Gas MW
TNAZ	88	1428	4094	23.84
CL-20	86	1402	4126	24.47
RDX	96	1393	3950	23.58
ADN	76	1358	3729	22.84

The best system near 3500°K was 76% TNAZ + 24% AMMO/BAMO at 1375 joules/g where the gas MW = 21.46. It should be borne in mind that when density is taken into account, the CL-20 system may well have the highest volumetric energy of these four.

Conclusions

In spite of several hundred (estimated to be > 600) calculations made examining more than 20 ingredients currently of interest to the propulsion community, none were found to offer gas MW ≤ 18 and impetus ≥ 1400 joules/g. This regime remains to be an extremely challenging and formidable one for future high energy gun propellants.

Only a few combinations of ingredients were found to yield a gas MW ≤ 18, regardless of impetus or flame temperature Tv constraints. The best of these involved ADN + TAGAZ, reaching an impetus of 1378 joules/g at Tv= 2987°K when DANP was added.

The lowest gas MW seen (16.9) was obtained with TAGN + TAGAZ, indicating that there may be other ingredients of similar stoichiometry that could yield even lower gas MW values. The possibility of developing a gun propellant with gas MW below 17 appears to be possible (albeit not at high impetus) --- a regime rarely encountered in gun propellants.

There are a number of combinations of ingredients that offer an impetus $\geq$ 1400 joules/g at Tv $\approx$ 3500 °K. The most promising ingredients are the diazido nitramines DANP, DADNH, and DADZP, which are extremely energetic and have neat impetus values significantly higher than the oxidizers CL-20, TNAZ, or ADN currently of keen interest to the propulsion community. If Tv were not a constraint, large increases in impetus (above 1500 joules/g) are within our grasp --- which was not thought to be possible previously. The key attribute of these diazido nitramines is a high positive ΔHf value in combination with high hydrogen and nitrogen content.

One interesting facet uncovered was the possibility of formulating new plasticizers by combining liquids such as DANP with the NENAs (methyl, ethyl, or propyl) to yield new "mixed" plasticizers that would substantially surpass the energy of current plasticizers.

It is recommended that additional research in low gas MW propellants (and for ingredients of high hydrogen content) be pursued --- with special emphasis on compounds with azide, nitramine, triaminoguanidine, and hydrazine-like moieties. Such fundamental research will be essential for hypervelocity guns of the future where ballisticians are striving to reach and exceed 2500-3000 meters/second without resorting to rather unconventional methods of propulsion.

Acknowledgments

Bibliography

1. M. E. Levy and E. D. Grossmann, *"Hypervelocity Solid Gun Propellants"*, FA Report R-1718 (AD 352535), Frankford Arsenal, May 1964, Philadelphia, PA.

2. F. Volk and H. Bathelt, *"Influence of Energetic Materials on the Energy Output of Gun Propellants"*, ADPA International Symposium on Energetic Materials Technology, September 24-27, 1995, Phoenix, AZ.

3. F. Volk and H. Bathelt, *"ICT Thermochemical Data Base"*, 26th Annual Conference of ICT, July 4-7, 1995, Karlsruhe, Germany.

4. S. T. Peters, R. B. Wardle, I. A Wallace, and A. C. Haaland, *"The Selection, Processing and Characterization of a Set of Gun Propellants Utilizing Novel Ingredients"*, ADPA International Symposium on Energetic Materials Technology, September 24-27, 1995, Phoenix, AZ.

5. Y. Longvialle, G. Berteleau, M. Golfier, and H. Mace, *"Low Vulnerability Minimum Smoke Rocket Propellants"*, ADPA International Symposium on Energetic Materials Technology, September 24-27, 1995, Phoenix, AZ.

6. F. Beaupre, G. Ampleman and E. Ahad, *"Application of GAP-based Binders to Low Vulnerability Gun Propellant Formulations"*, ADPA Sixth International Gun Propellant Symposium, November 14-17, 1994, Parsippany, NJ.

7. M. Stinecipher Campbell, K. Y. Lee, and M. A. Hiskey, *"New High-Nitrogen Energetic Materials for Gas Generators in Space Ordnance"*, 31st AIAA/ASME/SAE/ASEE Joint Propulsion Conference, July 10-12, 1995, San Diego, CA.

8. S. Moy, T. Manning, J. Prezelski, and B. Strauss, *"New Propellant Developments"*, 1995 DEA-A-76-G-1218 Meeting on Energetic Materials for Munitions, July 10-14, 1995, ICT/Karlsruhe, Diehl/Rothenbach and DASA/Schrobenhausen, Germany,

9. F.Schedlbauer, *"RDX/GAP LOVA Gun Propellants"*, International Ballistics Symposium, Quebec, Canada, October 1993.

Glossary of Ingredients

Term	Definition
ADN	Ammonium dinitramide
AMMO	3-azido methyl-3-methyl oxetane
BAMO	3,3-bis(azido methyl) oxetane
BuNENA	Butyl nitrato ethyl nitramine
CL-20	Hexanitro hexaaza isowurtzitane
DADNH	1,6-diazido-2,5-dinitrazahexane
DADZP	1,5-diazido-2,4-dintrazapentane
DANP	1,3-diazido-2-nitrazapropane
DANPE	1,5-diazido-3-nitrazapentane (also known as DIANP)
DATH	1,7-diazido-2,4,6-trinitrazaheptane
DB	Double-base; usually NC + NG
EtNENA	Ethyl nitrato ethyl nitramine
GAP	Glycidyl azide plasticizer/polymer
HTPB	Hydroxyl-terminated polybutadiene
MeNENA	Methyl nitrato ethyl nitramine
NENA	Alkyl nitrato ethyl nitramine
NC	Nitrocellulose
NG	Nitroglycerin
NQ	Nitroguanidine
Poly GLYN	Poly glycidyl nitrate
Poly NIMMO	Poly 3-nitrato methyl-3-methyl oxetane
ProNENA	Propyl nitrato ethyl nitramine
RDX	Cyclo trimethylene trinitramine
TAGAZ	Triaminoguanidine azide
TAGN	Triaminoguanidine nitrate
TNAZ	1,3,3-trinitroazetidine

Table 1

Ingredients Considered

Oxidizers (O/C ≥ 1)		Fuels (O/C < 1)	
ADN	no carbon	TAGAZ	no oxygen
TAGN	O/C = 3.00	HTPB	O/C = 0.008
CL-20	2.00	AMMO	0.200
TNAZ	2.00	BAMO	0.200
RDX	2.00	GAP	0.333
NQ	2.00	DANPE	0.500
MeNENA	1.67	Poly NIMMO	0.800
NC	1.65	BuNENA	0.800
DATH	1.50		
DADZP	1.33		
Poly GLYN	1.33		
EtNENA	1.25		
DADNH	1.00		
DANP	1.00		

Table 2

Ingredient Thermochemical Data

Ingredient	Formula	ΔHf - cal/mole
ADN	H4 O4 N4	-35,800
AMMO	C5 H9 O N3	+43,000
BAMO	C5 H8 O N6	+124,000
BuNENA	C6 H13 O5 N3	-46,000
CL-20	C6 H6 O12 N12	+81,650
DADNH	C4 H8 O4 N10	+172,270
DADZP	C3 H6 O4 N10	+179,587
DANP	C2 H4 O2 N8	+177,978
DANPE	C4 H8 O2 N8	+163,316
DATH	C4 H8 O6 N12	+146,500
EtNENA	C4 H9 O5 N3	-39,204
GAP	C3 H5 O N3	+33,000
HTPB	C7.332 H10.962 O.058	-2,970
MeNENA	C3 H7 O5 N3	-35,800
NG	C3 H5 O9 N3	-88,600
NQ	C H4 O2 N4	-22,140
Poly GLYN	C3 H5 O4 N	-68,000
Poly NIMMO	C5 H9 O4 N	-94,000
ProNENA	C5 H11 O5 N3	-42,603
RDX	C3 H6 O6 N6	+14,690
TAGAZ	C H9 N9	+105,650
TAGN	C H9 O3 N7	-11,500
TNAZ	C2 H4 O4 N4	+8,700

Table 3

Performance of Selected Neat Ingredients
(listed by increasing impetus)

Ingredient	NQ	ProNENA	NC	EtNENA
Impetus - joules/g	934	973	1041	1119
Tv - °K	2347	2122	3100	2461
Gas MW	22.90	18.14	24.75	18.28
Gamma	1.270	1.265	1.234	1.275

Ingredient	TAGN	MeNENA	CL-20	RDX
Impetus - joules/g	1160	1298	1347	1394
Tv - °K	2602	3225	4531	4086
Gas MW	18.65	20.65	27.97	24.37
Gamma	1.263	1.246	1.224	1.230

Ingredient	TNAZ	DATH	DADNH	DADZP
Impetus - joules/g	1399	1481	1504	1650
Tv - °K	4466	4050	3689	4403
Gas MW	26.53	22.74	20.39	22.19
Gamma	1.220	1.252	1.268	1.257

Ingredient	DANP
Impetus - joules/g	1761
Tv - °K	4582
Gas MW	21.64
Gamma	1.264

Table 4

Systems with Gas MW ≤ 18
(listed by increasing impetus)

	30% NC 70% TAGAZ	15% GAP 85% TAGN	30% ADN 70% BuNENA
Impetus - joules/g	1066	1073	1085
Tv - °K	2300	2325	2349
Gas MW	17.94	18.01	18.00
Gamma	1.277	1.278	1.276
O/C	0.96	1.74	1.31

	15% TAGAZ 85% TAGN	40% TAGAZ 60% MeNENA	40% DANPE 60% TAGN
Impetus - joules/g	1148	1220	1223
Tv - °K	2485	2646	2655
Gas MW	18.01	18.02	18.05
Gamma	1.271	1.275	1.277
O/C	2.50	1.33	1.28

	20% MeNENA 22% ADN 58% TAGAZ	33% ADN 67% TAGAZ	25% DANP 18% ADN 57% TAGAZ
Impetus - joules/g	1273	1298	1378
Tv - °K	2746	2797	2987
Gas MW	17.94	17.92	18.01
Gamma	1.272	1.270	1.275
O/C	1.74	2.34	1.26

Table 5

Systems with Impetus ≥ 1400 Joules/g and Tv ≈ 3500°K
(listed by decreasing impetus)

Ingredients		Impetus	Tv - °K	Gas MW
DANP + EtNENA	55/45	1484	3546	19.87
DANP + ProNENA	65/35	1480	3503	19.68
DANP + ADN + TAGAZ	30/30/40	1477	3500	19.70
ADN + DANPE		1470	3500	19.80
TAGN + DANP	50/50	1464	3515	19.96
TAGN + DADNH	15/85	1463	3510	19.95
EtNENA + DADNH	15/85	1452	3484	19.95
EtNENA + DADZP	42/58	1443	3525	20.31
GAP + MeNENA + DADNH		1446	3489	20.06
TNAZ + DANPE	40/60	1439	3490	20.16
MeNENA + DADNH	40/60	1430	3495	20.32
DATH + DANPE	60/40	1427	3497	20.38
RDX + DANPE	55/45	1425	3497	20.40
TAGN + DADZP		1420	3500	20.49
CL-20 + DANPE	40/60	1419	3527	20.67
DANP + MeNENA		1410	3534	20.84

Figure 1
Energetic Ingredients

Impetus - joules/g

Flame Temp Tv - °K
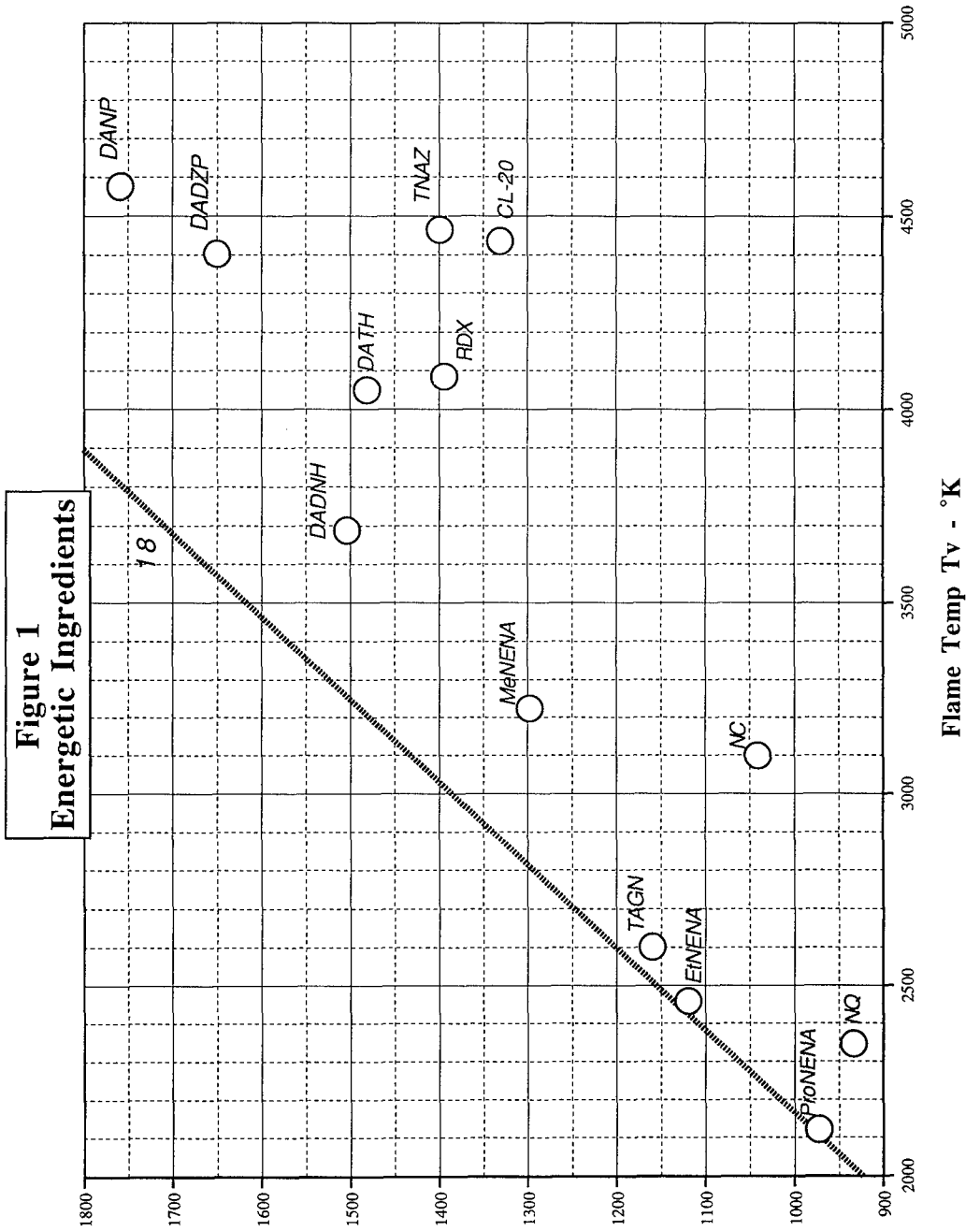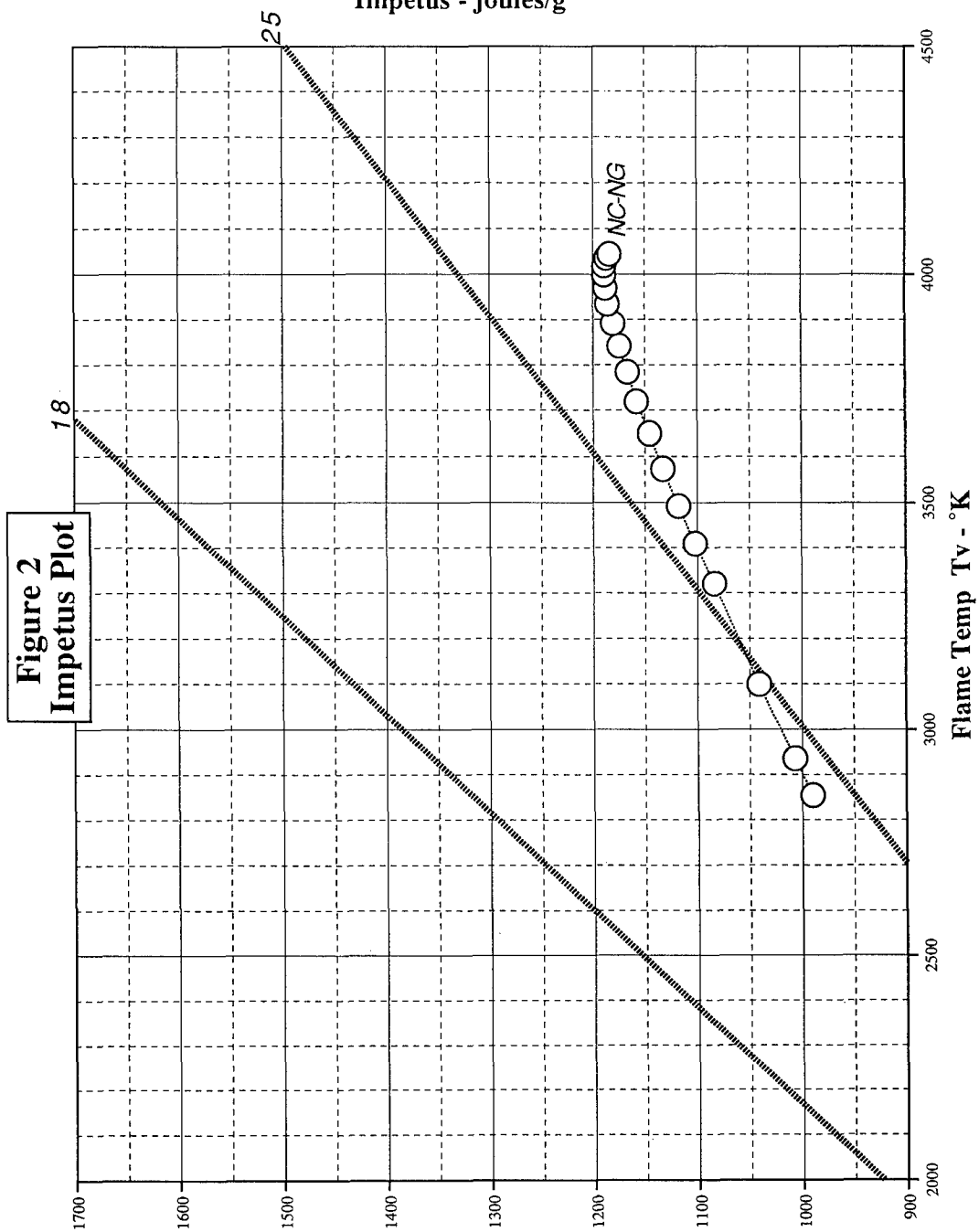
Figure 2
Impetus Plot

Figure 3
NC Binder

Impetus - joules/g

Flame Temp Tv - °K
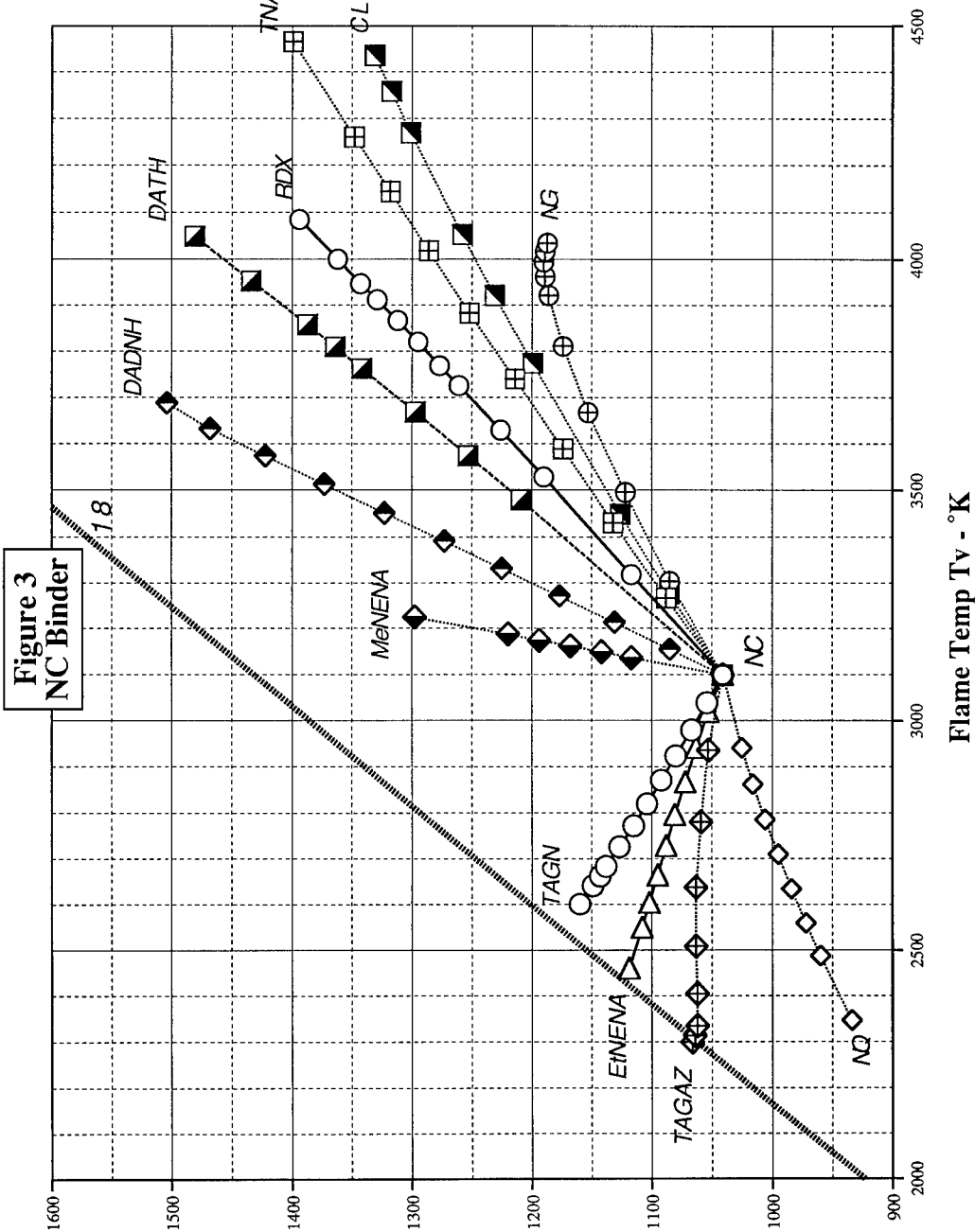
NEW MOLECULES FOR HIGH ENERGETIC MATERIALS

Bernard FINCK - Hervé GRAINDORGE

SNPE/DFP

Centre de Recherches du Bouchet
B.P N°2
91710 VERT LE PETIT
France

Abstract :

High energetic materials have wide applications in rocket propulsion, gun propellants, high explosives and pyrotechnics.

Today they are based on a limited number of molecules, sometimes synthesized a long time ago, whose potential has been systematically implemented, for example : AP, HMX, RDX, NC, NG.

New needs such as reduction of the vulnerability of combat platforms, stealth characteristics, increase of the energetic, burning and mechanical performances, and environment issues have oriented the research of new basic molecules.

This paper describes the characteristics of the new ingredients developed at SNPE and presents the main properties gained when used in energetic materials.

Some examples :

* Inert prepolymer and burning rate catalyst : BUTACENE[R] a ferrocene bonded HTPB.
* Energetic prepolymers and plasticizers : GAP DIOL, GAP TRIOL, GAPA whose properties are based on azido groups.
* Solid oxidizers : CL 2089 a caged high energy nitramine, NTO a low sensitive high explosive.

1 - INTRODUCTION

SNPE has always been involved in the synthesis and in the production of ingredients, inert and energetic molecules for Defense and Space performant materials.

The company already manufactures ammonium perchlorate with a capacity of several thousand tons, HMX, RDX at a several hundred tons level. All these energetic solids are available in different particle sizes running from ultra fine (2 to 3 μm) to coarse shapes up to 500 μm.

Different grades of nitrocellulose are produced at an industrial scale either for civilian non pyrotechnic application or for Defense and Space where the upper high nitrogen based products are requested. Nitroglycerine is also made on a continuous industrial way.

All these ingredients are largely used in the today's energetic materials for rocket and gun propellants, for explosives and pyrotechnics. Their potential has been systematically implemented and is still explored.

New needs appeard these last ten years. They are related to the final systems, for example the reduction of the vulnerability of combat platforms, the improvement of the stealth characteristics. The energetic performance enhance still remains an objective for every kinds of rockets, guns and explosives. The tailoring of the burning and mechanical properties will be a way to enlarge the applications of the systems. The environmental issues have also to be taken into account especially for large space boosters where the chlorine release is inconvenient (1).

The main objectives are summarized in chart 1.

CHART 1 : OBJECTIVES FOR ENERGETIC MATERIALS.

Development from the lab to the industrial plant of new molecules for new energetic materials with improved properties

Applications
Rocket and gun propellants, explosives, pyrotechnics

➤ *Low vulnerability*
➤ *Energetic performances increase*
➤ *Low signature (propellants)*
➤ *Burning rate extension (rocket, gun propellants)*
➤ *Thermal stability, mechanical properties increase*
➤ *Environment clean*
➤ *Low cost*

In order to achieve these requirements new molecules have been synthesized and scaled up to demonstrate the requested characteristics and properties.
They belong to the new oxidizers family as well as to prepolymers, plasticizers, additives for burning rate modification and bonding agents.

2 - METHODOLOGY TO SYNTHESIZE NEW MOLECULES

The molecules have to meet the above mentioned objectives. These are expressed in terms of final systems or energetic materials properties and have to be translated into individual molecule structures and compositions. (2)

While the knowledge and the experience gained on the formulation of all kinds of energetic materials still remain helpfull, the trend is to shift to prediction calculations before starting the synthesis. This is now made with codes which permit the prediction of the heat of formation and the density in order to calculate the a priori energetic performances of rocket and gun propellants (specific, volumetric impulse, force...) and explosives (detonation velocity and pressure).

These methods allow a previous selection of the most appropriate molecules which meet the energetic properties. Burning and mechanical properties are much more difficult to predict. Prediction methods are also carried out to know the safety behavior (3).

The whole methodology developed at SNPE to synthesize, evaluate and select new molecules is given in chart 2 which also shows the role played by the safety and compatibility issues as well as the preliminary formulation results.

CHART 2 : NEW MOLECULES DEVELOPMENT.
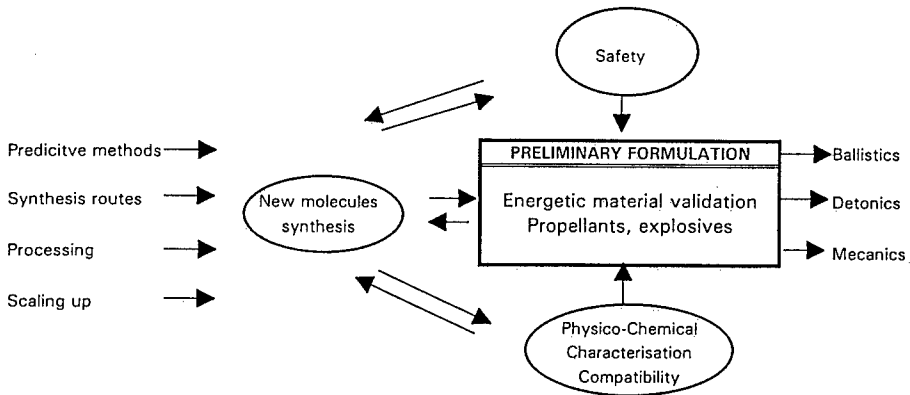
After passing these first steps the molecules are scaled up (pilot plant for example): and the assessments are conducted on larger motors, warheads or munitions.

Some example are now given which describe the characteristics of the new ingredients developed at SNPE and present the main properties gained when used in energetic materials.

3 - HIGH BURNING RATE BUTACENE⁽ᴿ⁾ BASED ROCKET PROPELLANTS

In order to achieve high burning rate AP based rocket propellants many ways have been explored, for example the UF iron oxide developed by MACH 1

The liquid ferrocenic burning rate catalysts have the advantage to combine high burning rates (higher than 30 mm/s at 7 MPa), high total solids due to the liquid state of the catalyst and low pressure exponents (lower than 0,5 over a wide pressure range), so they are very efficient for rocket motor propellants, especially rocket boosters (4).

In order to prevent the ability of the migration of the current ferrocenic burning rate catalysts SNPE has developed BUTACENE⁽ᴿ⁾ a ferrocene grafted HTPB (see chart 3).

CHART 3 : BUTACENE⁽ᴿ⁾ FORMULA AND PROPERTIES
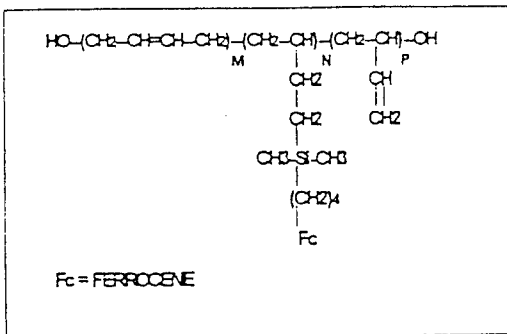
Aspect	Viscous liquid
Viscosity 25°C	< 1000 Poises
Iron (wt %)	8 +/- 0,5
OH value (equ/kg)	0.32 +/- 0,03
Volatile (wt %)	< 0,5
Tg (°C)	< -55
Density	1.00 +/- 0.02
Functionality	2,3
Antioxidant (%)	1 +/- 0.2

Since the ferrocene is bonded to the binder through the HTPB network, it cannot migrate during the aging either towards the liner or the surface of the propellant which in case of migration becomes very sensitive and reacts violently due to the high level of the degraded iron compounds.

The BUTACENE[R] and AP based composite propellants exhibit burning rates up to 70 to 80 mm/s (at 7 MPa). They keep the HTPB based mechanical properties with very good values at lower temperature (chart 4)

CHART 4 : TYPICAL PROPERTIES OF BUTACENE[R] BASED PROPELLANTS.

PROPELLANT	TOTAL SOLIDS	VISCOSITY (KP)	MECHANICAL PROPERTIES			B.R. (mm/s) 7 MPa	DENSITY	I.S. Stand. (s)
			T (°C)	σm (MPa)	em (%)			
ALUMINIZED	88	< 10	+ 20 - 50	0.8 3.2	33 12	20-50	1.82	265
REDUCED SMOKE	86	< 10	+ 20 - 50	1.3 4.4	35 32	20-75	1.72	252.5
REFERENCE ALUMIN.	88	< 10	+ 20 - 50	0.8 3.8	30/35 14	10	1.82	265.4

An unexpected property was found related to the vulnerability issues. When performing COOK OFF tests, BUTACENE[R] based propellants do not show any violent reactions. This was observed on isothermal COOK OFF tests. The specimen were compared to copper chromite and iron oxide based propellants (chart 5).

CHART 5 : ISOTHERMAL COOK OFF BEHAVIOR FOR DIFFERENT COMPOSITE AP BASED PROPELLANTS (BR = 1 INCH/S)
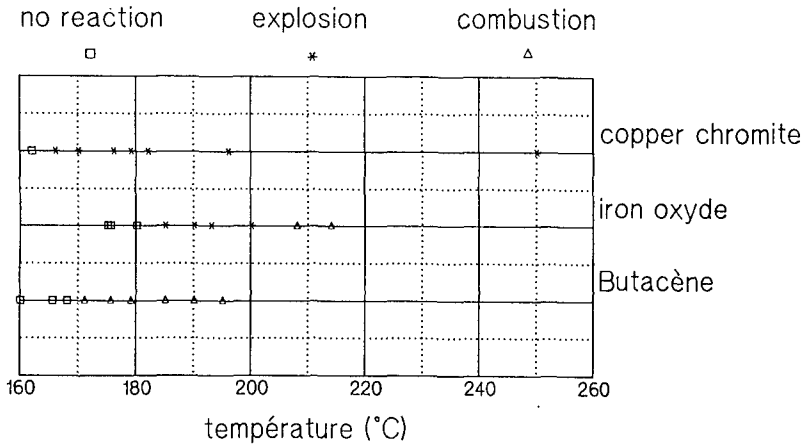
BUTACENE[R] is scaled up to a several tons/year production. Motors as large as 100 kg have been aged and then successfully fired (5).

4 - HIGH ENERGETIC GAP BASED ROCKET AND GUN PROPELLANTS

Among the different energetic prepolymers developed in the world, ICI's and THIOKOL's POLYNIMMO, POLYGLYN and POLY BAMMO/NIMMO, SNPE has chosen to produce the azido based prepolymers and plasticizers and has got now a more than ten years old experience on that compounds. The properties of the produced ingredients are given in chart 6.

CHART 6 : AZIDO BASED PREPOLYMERS AND PLASTICIZERS

GAP DIOL		GAP TRIOL	
$R-[-O-CH_2-CH-]_x-(OH)_n$ with CH_2N_3 ; $n = 2$; $X \sim 20$		$R-[-O-CH_2-CH-]_x-(OH)_n$ with CH_2N_3 ; $n = 3$; $X \geq 10$	
ΔHf cal/g	+ 280	+ 280	
Density	1.29	1.29	
Color	light yellow liquid	light yellow liquid	
Mn	1700 ± 300	≥ 900	
Mp	2000 ± 300	≥ 1000	
I	≤ 1.3	≤ 1.3	
Eq. weight	1200 ± 200	≥ 400	
Functionality	2.0	2.5 - 3.0	
Thermal Stab VT 100 °C (cm3) 200 h	≥ 3	≥ 3	
Tg °C	- 45	- 45	

GAPA

$$N_3CH_2CH_2O[CH_2-CH-O-]_nCH_2CHN_3$$
$$\qquad\qquad\quad CH_2N_3 \qquad\quad CH_2N_3$$
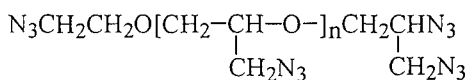
ΔHF	+ 550 cal/g
Density	1.27
Color	light yellow
Mn	700 - 900
Mp	800 - 1000
Thermal stab. VT 100°C (cm3)	≤ 3
Tg°C	≤ -56
Eq. weight	> 30 000

The GAP based derivatives exhibit different interesting properties :

- high heat of formation due to the -N3 group
- high density
- effectiveness in the burning rate enhance due the -N3 group, when combined with AP as well as with HMX, RDX, AN, CL20

The energy gained when using these compounds has led to the following application :

Rocket propellants : reduced smoke AP based, minimum smoke HMX, RDX based with increased burning rate, minimum smoke MURAT *** or IM based on AN, chlorine free space boosters applications.

Gun propellants : LOVA or MURAT type gun propellants based on GAP binder and RDX. Some examples are given in Chart 7

CHART 7 : GAP BASED ROCKET AND GUN PROPELLANTS

ROCKET PROPELLANTS

COMPOSITION	IS (s) Calc. Standard	DENSITY	VOLUM. IS (sg/cm^3)
PGA * Binder	233	1.603	373.5
GAP Binder	240.5	1.615	388.5
Δ(GAIN)	+ 7.5	+ 0.012	+ 15

GUN PROPELLANTS

BINDER FILLER	NC -	NC/NGI RDX/58 %	POLYETHER/20 RDX/80	GAP/20 RDX/80
F (MJ/kg)	1.036	1.321	1.158	1.390
ρ	1.601	1.711	1.569	1.675
F.ρ (MJ/dm^3)	1.658	2.260	1.817	2.328
T (K)	2919	3905	2558	3377

Since GAP is classified 1.3 it does not increase the detonability of the materials. GAP is compatible with GAP based plasticizers as well as nitrato esters like BTTN and TMETN which are less vulnerable than NG.

In 1990 SNPE got a license from ROCKETDYNE to manufacture and sell GAP and GAP derivatives in EUROPE. More than 2 tons of GAP and GAP derivatives have been produced at batch sizes of 150 kg in a pilot plant located in SNPE's SORGUES facility near AVIGNON.

5 - NEW ENERGETIC OXIDIZERS

SNPE develops energetic chlorine free oxidizers

Among the potential candidates : HNF (developed by TNO/APP in the Netherlands), CL20 (first developed on the USA by the NAVY and THIOKOL), ADN (first synthesized by the RUSSIANS and SRI in the USA), SNPE has chosen to put the efforts on CL20 and ADN.

```
* CL20 based propellants and explosives
```

The first synthesis of hexanitrohexaazaisowurtzitane called CL2089 at SNPE was made at SNPE's Research Center in 1989.

It is now produced in the SORGUES plant at pilot scale of 25 kg/batch. The different polymorphs have been identified and carefully analyzed. The most attractive is the ε one with a density of 2.04 and a heat of formation of + 220 cal/g.

Fig.1 shows different CL2089 ε particle sizes obtained at SNPE.

FIG. 1 DIFFERENT CL2089 ε PARTICLE SIZE
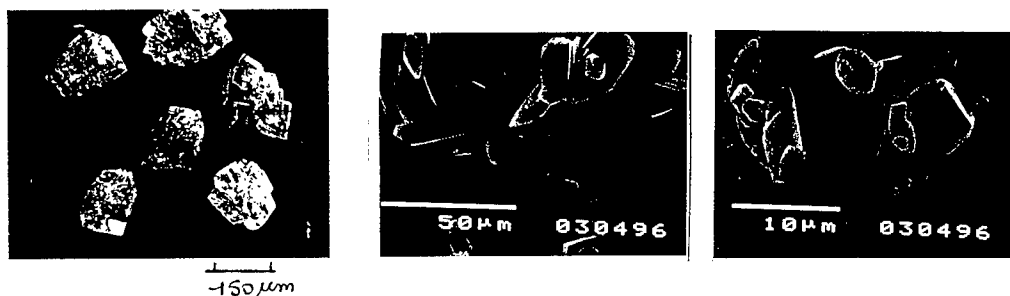
The today's work is done to improve the cristals and the particle shape. Impact sensitivity which appears to be somewhat scattered becomes good attention in order to ensure a better control by acting on the chemical and polymorph purity, the cristal quality and the grinding process. When controlling all those parameters, a CL2089 no more sensitive than HMX or RDX is obtained.

In fact when incorporated in a composite propellant or explosive the sensitivy of the final energetic material is quite acceptable (no more sentitive than HMX or RDX based materials).

Propellants and explosives have been made showing a good feasability and confirming energetic properties higher than RDX and HMX (chart. 8).

CL20 is also usefull in the burning rate increase. Combined whith GAP as binder it leads to the most powerfull and high burning rate XLDB propellant (20 mm/s at 7 MPa when catalyzed) which is feasable and can be scaled up. (chart. 9).

CHART 8 : CL2089 BASED PLASTIC BONDED
EXPLOSIVES (TOTAL SOLIDS : 66,8 % volume)

	DENSITY	DETONICS	
		Velocity (m/s)	Pressure (GPa)
HMX	1,575	8038	25,4
CL2089	1,648	8330	28,6

CHART 9 : CL2089 BASED XLDB PROPELLANTS
(ENERGETIC SOLIDS : 60 % weight)

COMPOSITION PROPERTIES	PGA / HMX binder	PGA / CL2089 binder	GAP / CL2089 binder
Is (s) stand.	242,4	250,8	257,6
Density	1.66	1.72	1.73
Burning rate mm/s 7 MPa	4.5	11.5	13.4 20.0 (when catalyzed)
Impact sensitivity (J)	8 - 20	10 - 19	8 - 19
Friction sensitivity (N.)	180	85 - 120	60 - 85

* ADN based propellants

The RUSSIAN experience (6) has revealed a large potential development for this molecule. The work has been emphasized in the synthesis of this molecule by the USA (SRI, THIOKOL) - SNPE is now pushing its efforts on that molecule which is already made at the lab scale using different synthesis routes.
The interest of this molecule can be explained by a high level of Oxygen and Hydrogen in the structure leading to low molecular weight exhausts after combustion, while the Nitrogen content can be usefull to limit the detonability of that compound.

The theoretical performances are given in chart 10 for a space booster application.

CHART 10 : THEORETICAL PERFORMANCE OF ADN

COMPOSITION	Is (s) Pc/Pe = 70/1 bar	Density	Is (s) x density	Gain in payload LEO (kg) *
HTPB/AP/Al 12 / 68 / 20	264,5	1,766	467	ref.
GAP / ADN / Al binder 25 / 55 /20	274,2	1,791	491	+1968

* LEO : Low Earth Orbital

The characteristics of SNPE's synthesized product are given in chart 11

CHART 11 : ADN CHARACTERISTICS

Melting point	92,9° C
Impact sensitivity	3,7 J
Friction sensitivity	> 353 N
ESD	> 726 mJ
Thermal stability DSC decomp.	134°C
Vacuum Test 80°C cm3	1.0
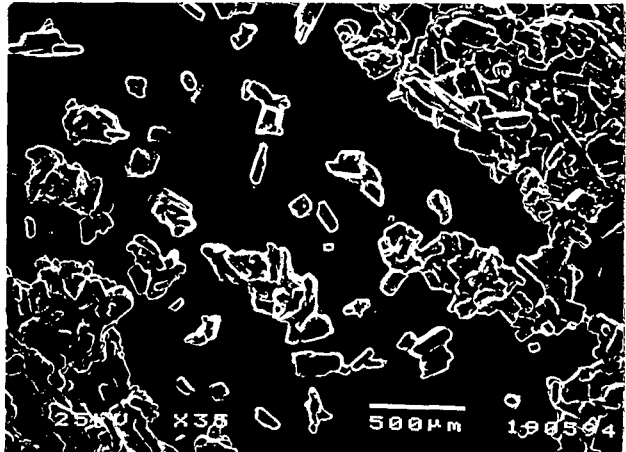
ADN crystals obtained at SNPE

Some precautions have to be taken during the storage since the material can be damaged when submitted to the light and humidity during several weeks.

6 - NTO BASED HIGH EXPLOSIVES

NTO is produced at SNPE at an industrial scale, with particle sizes running from 400 μm to micronic material.

It is used in insensitive high explosives (7) .

The chart 12 shows a better behavior in terms of vulnerability of NTO based plastic bonded explosives when compared to melt cast explosives or plasted bonded ones without NTO (7)

CHART 12

COMPARED SENSITIVITY AND VULNERABILITY OF NTO HIGH EXPLOSIVES

TEST	HEXOL 60/40 (B)	ORA 86 HMX	B2214 HMX, NTO
FUEL FIRE (FAST COOK OFF)		NO DETONATION - ONLY BURST 2 mn	
BULLET IMPACT	DETONATION	NO DETONATION ONLY BURST	NO DETONATION NO BURST
CARD GAP TEST (Cards)	200	160	25
HEAVY FRAGMENT (m/s)	$\geqslant$ 1300	$\geqslant$ 1990	$>$ 2200
FLYER PLATE TEST (Kb)	23 (1.5 μs)	40 (1.5 μs)	150 (1.5 μs)
SHAPED CHARGE TEST	DETONATION		NO DETONATION
SYMPATHETIC DETONATION	DETONATION	DEFLAGRATION	NO REACTION

CONCLUSION

SNPE is developing different families of new molecules which meet the requirements of the new energetic materials. They belong to the binder systems (prepolymers, plasticizers) to the fillers and to additives.

Some of the developed molecules like GAP, GAP derivatives and CL2089 are usable in manyfold materials like gun, rocket propellants explosives and pyrotechnics.

The combination of energetic binders and oxidizers like GAP and CL2089 lead to the most powerfull existing energetic materials.

Some new molecules like GAP, GAP derivatives, CL2089 are usefull for the burning rate improvement.

Molecules have been scaled up to SNPE's pilot or industrial facilities :

BUTACENE a ferrocenic HTPB prepolymer for high burning rate AP based propellants : the production capacity can reach 5 tons/year.

GAP DIOL, TRIOL, GAP PLASTICIZERS : the production can reach several tons/year.

NTO, molecule for insensitive high explosives ; the production is industrial : several hundreds tons/year.

CL2089 a high energetic filler : the scaling up to 25 to 50 kg/batch is now achieved.

In the field of additives SNPE produces Me BAPO a bonding agent for AP based propellants (without ammonia release) and a lead free burning rate catalyst for double base and XLDB propellants.

REFERENCES

(1)   C. PERUT, V. BODART, B.CHRISTOFOLI, "Propergols Solides pour Lanceurs Spaciaux générant peu ou pas d'Acide Chlorhydrique" AGARD Conférence Proceedings 559, 84 th Symposium, 29 August - 2 September 1994, 4-1 to 4-12

(2)   A. DAVENAS, B. FINCK "Les nouveaux matériaux énergétiques" Revue scientifique et technique de la Défense - Numéro 17 - Page 145, 1992

(3)   A. DELPUECH, J. CHERVILLE "Relation entre la structure électronique et la sensibilité au choc des explosifs secondaires nitrés. Critère moléculaire de sensibilité. Cas des esters nitriques" Prop. and Explo" - vol 4- Page 121, 1979

(4)   B. FINCK, J.C. MONDET, J. BRUNET "Non-migrating high burning rate composite propellants - ADPA 1989 - Virginia Beach (USA)

(5)   G. FONBLANC, B. HERRAN, "The maturity of BUTACENE$^{(R)}$ based composite propellants AIAA 94-3194, June 27 - 29, 1994 - Indianapolis (USA)

(6)   Z. PAK "Some ways to higher environmental safety of solid rocket propellant application" AIAA Paper 93-1755, June 1993

(7)   A. BECUWE, A. DELCLOS "L"oxinitrotriazole et son utilisation en tant qu'explosif insensible " Proceedings of the 18 th International Annual Conference of ICT, July 1987, Karlsruhe (Allemagne)

SYNTHESIS OF LINEAR GAP-BASED ENERGETIC THERMOPLASTIC ELASTOMERS FOR USE IN HELOVA GUN PROPELLANT FORMULATIONS

G. Ampleman and F. Beaupré

DEFENCE RESEARCH ESTABLISHMENT VALCARTIER

Department of National Defence, Canada

2459, Pie XI Blvd, North, (P.O. Box 8800)

Courcelette, Quebec, Canada, G0A 1R0

ABSTRACT

For the last few years, DREV has been involved in the synthesis of energetic thermoplastic elastomers (ETPEs) based on linear glycidyl azide polymer (GAP). These ETPEs are usually copolymers of type ABA or AB where A is the hard segment capable of crystallization or strong physical interactions and thus giving the thermoplastic behaviour to the copolymer, and B is the soft segment which is amorphous and responsible for the elastomeric behaviour of the copolymer. These polymers are physically-crosslinked rubbery materials which can be solubilized and recycled. Also, they could represent a new generation of binders for introduction to future formulations of propellants and explosives. Since ETPEs are recyclable, it will be easy to manage the life cycle of these new formulations from cradle to grave.

During the same time, DREV has also been active in the development of high energy low vulnerability ammunition (HELOVA) gun propellant formulations that would offer low vulnerability, good mechanical properties and a high impetus level. Moreover, it would be very interesting to develop a gun propellant formulation that could be recyclable. The incorporation of thermoplastic elastomers (TPEs) has achieved these goals and has given an appreciable improvement over the mechanical properties, but more energy is still desirable. Recently,

development at DREV of ETPEs has led to a series of three candidates suitable for incorporation in gun propellant formulations. These three different ETPEs are copolymers of type AB and are obtained by macropolymerization from GAPs having molecular weights of 500, 1000 and 2000 with a monomer A. These ETPEs are soluble in ethyl acetate and therefore could be recuperated, leading to a recyclable gun propellant. Prototypes of these ETPEs have been incorporated in HELOVA formulations and provided good impetus levels. Moreover, the formulations containing the prototypes were easily processed using the current processing technique.

At the moment, an ETPE based on GAP-1000 seems the most promising candidate. The gun propellant grains obtained from these formulations were submitted to mechanical and ballistic evaluation. This paper describes mainly the synthesis and the characterization of these new ETPEs and presents results obtained so far with gun propellant formulations in which they were incorporated.

1.0 INTRODUCTION

High-energy solid compositions, such as propellants, plastic-bonded explosives or the like, are comprised of an elastomeric binder in which are dispersed particulate solids such as oxidizers, particulate fuel material or crystalline explosives. Glycidyl azide polymer (GAP) serves as an energetic binder and is reacted with a curing agent to form a chemically crosslinked matrix for ammonium nitrate in new insensitive low smoke propellant formulations, and for RDX in new insensitive plastic-bonded explosives (Refs. 1-4). To produce this chemically crosslinked matrix, a triol or a triisocyanate, or both, or a polymer having a functionality greater than two reacting with a diisocyanate, must be used to ensure the reticulation (Refs. 5,6). In such systems, different mechanical properties of the binder can be obtained by adjusting the parameters of the curing reaction and the component concentrations, which results in varying the crosslink density of the matrix.

On the other hand, it could be desirable to introduce GAP into LOVA-type formulations in order to obtain higher energy HELOVA formulations. However, GAP must be reacted with a curing agent to form a matrix leading to good mechanical properties. With the current

processing technique used in Canada for propellants, a suitable curing reaction is hard to achieved. Moreover, such a gun propellant would not be recyclable because the crosslinks are covalent chemical bonds and thus irreversible as for explosives and rocket propellants. The use of thermoplastic elastomers (TPE) avoids a process that involves curing reactions and hence leads to recyclable LOVA-type gun propellant formulations. DREV has been active in the development of LOVA gun propellant formulations using TPEs, and the incorporation of these polymers as binders has resulted in good mechanical properties, but more energy is still desirable (Ref. 7). The use of a GAP-based TPE in HELOVA gun propellant formulations led to propellants showing good mechanical properties, low vulnerability and a high impetus. Furthermore, it allowed easier processing of a gun propellant formulation (Refs. 8-10).

Development at DREV of ETPEs based on glycidyl azide polymer led to a series of three candidates suitable for incorporation in HELOVA gun propellant formulations. These three different ETPEs are copolymers of type AB and were obtained by macropolymerization from GAPs having molecular weights of 500, 1000 and 2000 with the monomer A. This paper describes the synthesis and characterization of these ETPEs, and presents the results obtained to date with gun propellant formulations in which they have been incorporated.

2.0 THEORY

Thermoplastic elastomers are copolymers of type ABA or AB, where A and B are respectively the hard segment and the soft segment (Ref. 11). The hard segment is capable of crystallization or association and gives the thermoplastic behaviour to the copolymer, whereas the soft segment gives the elastomeric behaviour to the copolymer. The thermoplastic behaviour is the result of crystalline domain formation by chain associations due to reversible interactions such as dipole-dipole interactions, hydrogen bonding, etc. In practice, at room temperature, a thermoplastic elastomer behaves like a rubber because it is crosslinked in the same fashion as a conventional elastomer, but with reversible physical crosslinks. Since the physical crosslinks are reversible, the TPE can be melted or dissolved in a solvent and then mixed with other components of a formulation and processed. A gun or rocket propellant or a composite explosive is obtained upon cooling or evaporating the solvent. Cooling or evaporating the solvent lets the broken physical crosslinks re-form and the elastomeric properties are recovered. This also means

that obsolete material can be melted or dissolved before the separation of the components, leading to a recyclable composition.

Thermoplastic elastomer copolymers of type ABA are usually obtained by polymerization of a difunctional homopolymer B followed by the addition of monomers of the homopolymer A which is crystallizable. To achieve that type of copolymerization, monomers of both types should have a similar reactivity and most of the time the polymerization is a living one. This technology leads to a copolymer of controlled structure with suitable adjustable mechanical properties. On the other hand, copolymers of type AB are usually obtained by mixing monomers of both types having reactive compatible ending groups and represents a simpler technology. For industries, copolymers of type AB are more attractive since the process is often more simple than for copolymers of type ABA.

GAPs having a functionality of two or less can be used as a macromonomer and be polymerized with a suitable monomer which gives the thermoplastic behavior to the resulting linear copolymer not being chemically crosslinked by covalent bonds. This is only obtained under highly-controlled conditions. The stoechiometry of the reaction must be respected to avoid chemical crosslinking between the chains. In this copolymer, the elastomeric B segment is provided by the amorphous GAP, and the thermoplastic A segment is provided by the group formed during the polymerization. Each thermoplastic group within the copolymer is capable of forming hydrogen bonds. By doing so, physical crosslinks are created between the chains and as a result, a thermoplastic elastomer is obtained.

Linear copolymers having this type of hard segment melt in the region of 200°C when the thermoplastic content is about 20 to 50% by weight; this is when there are enough hard segments to induce crystallinity. Copolymers with GAP can not be melted because the decomposition of GAP occurs near 200°C. However, they can be dissolved in a solvent and used solvated in a gun propellant formulation. Using the copolymer thermoplastic elastomer based on GAP in a gun propellant formulation is therefore an elegant way to introduce an energetic binder without the problems associated with conventional cured binders. Moreover, such a formulation could be recuperated and recycled.

According to this, GAPs of different molecular weights having a functionality of two or less were reacted with a stoechiometric amount of monomer A to yield a thermoplastic elastomer copolymer which was used as a binder in HELOVA gun propellant formulations. This copolymer was solvated and mixed with the other components of gun propellant formulations using a solvent-type process. After evaporation of the solvent, extrusion, cutting and drying, a suitable gun propellant resulted.

3.0 RESULTS AND DISCUSSION

GAPs having a functionality of two or less and molecular weights of 500, 1000 and 2000 were reacted stoechiometrically with the monomer A in order to obtain three different linear copolymer thermoplastic elastomers. According to this process, hydrogen bonds were formed between the hard segments of the thermoplastic elastomer and therefore a thermoplastic behavior was observed. All the copolymers synthesized were rubber like materials which were dissolved in ethyl acetate prior their inclusion in the gun propellant formulations.

The molecular weights of the resulting copolymers were determined by gel permeation chromatography (GPC) in tetrahydrofuran at 28 °C at an elution speed of 1 mL/min using a Waters chromatograph (Waters 712 WISP). The calibration was performed with polystyrene standards on ultrastyragel columns. Copolymers based on GAP 2000 have number average molecular weights $M_N = $ 35,000 to 37,000, while those obtained from GAPs 1000 and 500 have M_N of 27,000 and 22,000 respectively. This could be explained by the fact that viscosity increases more rapidly when more hard segments are included in the copolymer. When the molecular weight of the macromonomer is small, the content of hard segments increases, leading to a greater viscosity and giving a copolymer of smaller molecular weight.

Infrared spectroscopy revealed for all copolymer samples that the groups within the hard segments formed hydrogen bonds, since a strong band at 3300 cm^{-1} corresponding to a H-bond was observed. ^{13}C-NMR and ^{1}H-NMR spectroscopy confirmed the structure of the copolymers without the presence of chemical crosslinks formed during the polymerization.

Differential scanning calorimetry measurements were conducted with a DSC 2910 apparatus from Dupont Instruments equipped with Dupont Thermal Analyst 2100. The calibration was done with indium (156.6 °C) and biphenyl (69.3 °C), and the scan rate was fixed at 10 deg/min. The glass transition temperatures for the copolymers made with GAP 2000, 1000 and 500 were respectively -28, -15 and -4 °C. No melting endotherm was observed below 200 °C, the temperature at which GAP decomposes. Nevertheless, all the copolymers obtained using this process were rubbery materials soluble in ethyl acetate. Removal of the solvent yields back the original material showing identical properties.

Once the ETPE was solvated in ethyl acetate, it was processed with an energetic nitrate ester plasticizer and the other ingredients of a HELOVA gun propellant formulation in a sigma blade mixer according to the technique presented in Ref. 12. For all formulations, the processing technique used was similar to the one for the reference formulation (LOVA) or one containing an inert TPE (Refs. 7, 12). This aspect is important since a modification of the processing would imply an increased amount of effort.

A ballistic evaluation was done for the most promising formulations. The results obtained from 700-cm^3 closed bomb vessel experiments are reported in Table I. A tourmaline gauge was used in every case. A loading density of 0.15 g/cm^3 was selected and used. Three experiments were done in all cases.

As shown in Table I, the formulations containing ETPEs have the highest relative force when compared to the reference formulation and to #36 which contains an inert TPE. Although the formulations containing GAP-1000 and GAP-500-based ETPEs still give interesting values, their impetus level is less. Theoretical thermodynamic data are not reported here but would confirm what is reported in this table. Lussier *et al.* (Ref. 13) also state that care should be taken when comparing data from thermodynamic computer codes and that the rank suggested by the ballistic data should prevail. In cases where formulations would give the same relative force, a preference will be given to those having the best mechanical properties. Since erosion is also an important issue, the less erosive formulations will also be preferred. A setup to measure and compare the erosivity of various gun propellant formulations is presently being installed at DREV and should be operational soon.

The mechanical properties of the formulations is a very important factor to be considered when developing low vulnerability gun propellants. The main purpose of adding a TPE in a formulation is to obtain gun propellant grains with a more elastic behavior. When incorporating energetic TPEs, it is expected that this will still be the case. Preliminary results obtained with a Drop Weight Mechanical Properties Tester (DWMPT) according to the testing method described in Ref. 14 have shown that these ETPE formulations were soft. The results for the most promising formulations are reported in Table II.

From Table II, it is showed that the formulations containing GAP-based ETPEs are softer than the reference. This is mostly observed by the brittleness which is much lower for these formulations than for the reference. Instead of breaking into small pieces, the formulations containing ETPEs deform into a pancake-shape which is a more desirable behaviour. When looking at the maximum stress values (σ_m), one will obseve that the values are higher, around 30MPa for the formulations having an ETPE based on GAP-1000 or GAP-500 . The difference between the different binders is more evident at a temperature of -20°C. All formulations containing the ETPEs have a better mechanical behaviour then the reference. However, improvements are still desirable and could be obtained by optimisation of the formulations.

4.0 CONCLUSIONS

It has been demonstrated that energetic thermoplastic elastomers could easily be obtained by synthesizing copolymers based on GAP. Three different molecular weights of GAP were used as macromonomers to yield three different ETPEs, which were incorporated in HELOVA gun propellant formulations using the current processing technique. Infrared and nuclear magnetic resonance spectroscopy confirmed that the copolymer is produced without chemical crosslinking. The promising results obtained from processing studies, ballistic and mechanical experiments have demonstrated that the use of ETPEs in HELOVA gun propellant formulations is an improvement over the reference formulation.

5.0 REFERENCES

1. Lessard, P., Druet, L., Villeneuve, S., Thiboutot, S., Benchabane, M. and Alexander, D., "Development of a Minimum Smoke Propellant Based on Glycidyl Azide Polymer and Ammonium Nitrate", NATO Advisory Group for Aerospace Research and Development, Conference Proceedings AGARD-CP-511 on Insensitive Munitions, Bonn (Germany), 21-23 October 1991, UNCLASSIFIED.

2. Hooton, I., Bélanger, C. and Pelletier, P., "Preliminary Studies of Energetic Binder Based PBXs", DREV Memorandum 2996/89, August 1989, CONFIDENTIAL.

3. Hooton, I. and Bélanger, C., "Improvements in GAP-Based Plastic Bonded Explosive Formulations", DREV Memorandum 3154/93, October 1993, CONFIDENTIAL.

4. Villeneuve, S. and Carignan, P., "Binders for Rocket Propellant Formulations Based on Glycidyl Azide Polymers", DREV Report 4631/91, February 1991, UNCLASSIFIED.

5. Ampleman, G., Lee, A.K., Lavigne, J., "The Curing of GAP with Diisocyanates", DREV M-3023/90, May 1990, CONFIDENTIAL.

6. Hepburn, C., "Polyurethane Elastomers", Applied Science Publishers, London, 1982.

7. Beaupré, F. and McIntosh, G., "Improvement in Mechanical Properties of LOVA-Type Gun Propellants", Proceedings of the 16th Meeting of TTCP WTP-4, China Lake, April 1991, UNCLASSIFIED.

8. Beaupré, F., Ahad, E. and Ampleman, G., "Preliminary Studies of HELOVA-type Gun Propellant Containing Energetic Binders"; Proceedings of the American Defense Preparedness Association (ADPA) International Symposium on Energetic Materials Technology, Meeting 450, Orlando, Florida, March 1994.

9.   Beaupré, F., Ahad, E. and Ampleman, G., "The Use of GAP-Based Binders in HELOVA Gun Propellant Formulations", Proceedings of the 19th TTCP WTP-4 Meeting on New Materials and Processing, DREV, May 1994.

10.   Beaupré, F., Ampleman, G. et Ahad, E., "Application of GAP-based Binders to Low Vulnerability Gun Propellant Formulations", 6th International Gun Propellant Symposium, ADPA, Event 599, Parsipanny, New Jersey, November 1994.

11.   West, J.C. and Cooper, S.L., "Thermoplastic Elastomers", Science and Technology of Rubbers, Academic Press, Chapter 13, pp. 531-567, 1978.

12.   Beaupré, F. and Durand, R., "Processing Studies of LOVA-type Gun Propellants", DREV R-4603, October 1990, UNCLASSIFIED.

13.   Lussier, L.S., Beaupré, F. and Lavigne, J., "The Use of Thermodynamic Codes for Comparison of Propellant Performance", ADPA 5th International Gun Propellant and Propulsion Symposium, 19-21 November 1991, Dover, N.J., USA.

14.   Varga, L., "DREV Drop Weight Mechanical Property Tester: A Testing Method for LOVA Gun Propellants", DREV R-4586/90, April 1990, UNCLASSIFIED.

TABLE I: Ballistic evaluation of gun propellant formulations
containing linear GAP-based ETPEs

FORMULATION	BINDER	P$_{MAX}$ MPa(psi)	RELATIVE FORCE
REFERENCE	CAB	188 (27320)	1.00
#36	INERT TPE	205 (29685)	1.09
#75	GAP-2000 BASED	226 (32789)	1.20
#76	GAP-2000 BASED	223 (32371)	1.18
#114	GAP-500 BASED	219 (31747)	1.16
#121	GAP-1000 BASED	223 (32366)	1.18
#122	GAP-1000 BASED	220 (31887)	1.17
#123	GAP-500 BASED	218 (31549)	1.15

TABLE II: DWMPT results for formulations containing linear GAP-based ETPEs

FORMULATION	BINDER	σ_m (MPa)		ε_m (%)
REFERENCE	CAB	+20	98.0	2.6
		-20	131.0	2.5
#75	GAP-2000 BASED	+20	23.0	6.2
		-20	64.7	6.0
#76	GAP-2000 BASED	+20	24.6	5.4
		-20	62.2	6.7
#114	GAP-500 BASED	+20	29.6	4.5
		-20	80.3	4.2
#121	GAP-1000 BASED	+20	29.0	4.5
		-20	82.0	4.2
#122	GAP-1000 BASED	+20	30.0	3.7
		-20	74.3	4.1
#123	GAP-500 BASED	+20	28.5	4.3
		-20	68.6	4.5

INVESTIGATION OF
HIGH MOLECULAR WEIGHT GAP[①]

Wang Ping, Xia Zhongjun, Zhou Yuqi, Li Changqing

Institute of Chemical Materials, CAEP

P. O. Box 513, Chengdu 610003, China

ABSTRACT

An elastomeric glycidyl azide polymer (H-GAP) with average molecular weight $\bar{M}_w > 1.4 \times 10^5$ was synthesized and characterized. The purpose of this work is to provide an energetic binder for more powerful polymer-bonded explosives (PBXs) and propellants. In most practical applications, the traditional method is to mix the liquid GAP prepolymer of average molecular weight less than 3000 with diisocyanates (DI) to form a high molecular polyurethane (PU). In some cases, the coupling agents like trimethanol propane (TMP) is used to make the PU well-cured. But the energy output of PBXs or propellants will be significantly decreased because of the inert properties of DI and TMP. In order to keep both high energy density and improved mechanical properties of H-GAP based PBXs or propellants, multi-hydroxy-functional branched — GAP (B—GAP) could be used to modify the surface characteristics of oxidizer crystals. The experimental results and some related problems are discussed herein.

KEYWORDS   elastomeric glycidyl azide polymer (H-GAP),

multi-hydroxy-functional branched GAP (B-GAP)

low vulnerable ammunition (LOVA)

1. INTRODUCTION

Along with the increasing modernization of the weaponry vehicle and launching systems, the requirements to their safety and survivability are more important than it used to be. That is why it is necessary to develop LOVA. The safety of LOVA is generally obtained by using a rubbery polymer as a binder containing, in most cases, plasticizers. When a projectile or warhead, flying with a velocity up to $2\sim4$ Mach, hits

the target, or it is required to detonate after penetrating the hard obstacles, it will be subjected to very high a overload. In order to guarantee the required tactical function and survivability, the binder content in PBXs or propellants must be more than 10%[1]. If the binder is an inert one, the more it involves, the more energy output will be cut down. While the efficiency to accelerate the metal flyers is one of the critical requirements for most warheads. Therefore, under the prerequisite to meet the necessary safety and survivalbility, it is still an important effort to enhance the energy of PBXs and propellants. That is the goal towards the high performance LOVA.

There are three possible ways to reach this goal:

- Synthesizing high energy density organic oxidizers with low sensitivity;
- Intermolecular explosives;
- Energetic polymer — bonded oxidizers.

Analyzing the said ways from the points of thermodynamic and reactionkinetics, the application of energetic binder is a more promising method to formulate high performance LOVA, because the chemistry of polymer synthesis is relative mature and it is not too difficult to transplant energetic groups into the given polymers' backbone or side chains.

2. HIGH ENERGY DENSITY BINDER-GAP

Compared to the inert polymers, energetic binders can increase energy and the energy utilization efficiency of PBXs and propellants, or under the same energy criteria the sensitivity can significantly be decreased by increasing the binder content[2].

In present ten years, GAP has been recognized as a promising energetic binder with satisfactory safety[3,4,5]. The experimental results of Schedlbauer[6]indicated that the safety and mechanical properties of RDX/GAP 86. 4/13. 6 are nearly the same as those of the typical LOVA formulation of RDX/HTPB 86. 4/13. 6.

We experimentaly evaluated the energy contribution of GAP to the power output of HMX/GAP 88/12 in detonation[7]. In electrothermal chemical propellant GAP can compensate the poor oxigen balance in some extent[8]. All of these results show that GAP is a prospective binder candidate for developing high performance LOVA.

3. THE PROBLEMS TO BE SOLVED

The advatageous properties of GAP are well known, but it is not perfect in all

aspects. The first is that its mechanical property at low temperature is not satifactory, because the stereo-blockage of the rigid conjugated -N_3 reduces the flexibility of the main chain.

The more sereous problem is the gas evolution when GAP is cured with diisocyanate (DI), because the water-susceptible isocyanyl group -$N=C=0$ react rapidly with H_2O to release CO_2 and form a large quantity of voids in the cured explosive or propellant charges, resulting in decrease of loading density, mechanicalstrength, performance and safety.

$$R\text{-}N=C=O + H_2O \longrightarrow R\text{-}NH_2 + CO_2 \uparrow$$
$$R\text{-}N=C=O + R\text{-}NH_2 \longrightarrow R\text{-}NH\text{-}CO\text{-}NH\text{-}R$$
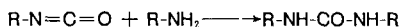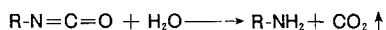
Reed, Jr. reported[9], the composite catalyst of triphenyl bismuth (TPB) and dibutyltin dilaurate (T-12) could be used to suppress the CO_2 formation andpromote the crosslink process. As a result the void-free propellant grains were obtained. But he recognized that it was impossible to thoroughly dispel the water residue embodied in GAP because of the water-affinity of its hydroxy terminals. He had not confirmed if the TPB and T-12 could be used to make large-sized void-free propellant charges. Another trouble of this method is that the 3-4days' curing period is too long to raise the work efficiency.

In order to overcome the abovesaid disadvantages and raise the energy output of GAP bonded explosive or propellant, we propose to give up the traditional diisocyanate curing method but use the elastomeric high molecular weight GAP (H-GAP), plasticized by multi-hydroxy-functional branched GAP (B-GAP)[10], to reach the following goals:

· Eliminate the origin of gassing to increase the loading density;

· Discard the inert binder to raise the energy density;

· Modify the surface characteristics of crystalline oxidizers to suppress dis-

bonding of the binder, improving the mechanical and environmental properties.

Since the binder, H-GAP, and the plasticizer, B-GAP, have the same structural units in their molecules, they can, therefore, form a homogeneous and well-compatible solution in both liquid and solid state. Moreover, the multi-hydroxy-functionality of B-GAP would be more affinitive to -NO_2 in nitramine molecules, and hence to more satisfactorily wet the explosive crystals and obtain well covered grains by the binder, The X-ray photoelectron spectrum (XPS) analysis showed[11], there is an obvious

interaction between B—GAP and TATB crystals, improving the coverage of a fluoro-rubber F on TATB (Table 1).

Table 1. Coverage of F on B-GAP Modified TATB Crystals

Sample	Coupling agent	Content (‰)	Specific area (F/N)	Coverage (%)
TF*	/	/	2.79	73.6
TF/B-GAP	B-GAP	0.5	5.27	84.1
TF/6"	6"	3.0	7.95	88.8
TF/502	502	5.0	3.59	78.2

* TF—TATB/F

Table 2. Chemical Shift of 1s Electrons in TATB and F

Sample	N_{1s} -NH$_2$	N_{1s} -NO$_2$	N_{1s} -NO$_2$	C_{1s} -CF$_2$-	F_{1s}	C_{1s}
TATB	398.8	405.2	532.0			
TF			293.8	690.6	204.1	
TF	399.4	405.7	532.1	293.9	688.8	202.4
	(0.6)	(0.5)	(0.1)	(-1.9)	(-0.8)	(-1.1)
TATB/B-GAP	400.3	405.4	533.4			
	(1.5)	(0.2)	(1.6)			
TF/B-GAP	401.3	406.9	533.9	293.5	690.6	203.4
	(1.8)	(1.2)	(1.8)	(1.6)	(1.8)	(1.0)
TATB/6"	399.4	405.0	532.2			
	(0.6)	(-0.2)	(0.3)			
TF/6"	401.3	406.6	533.5	293.5	690.4	204.1
	(1.5)	(2.4)	(0.4)	(1.6)	(1.6)	(1.7)

* The unit of chemical shift is eV, the value outside the ( ) is the original bonding energy of the 1s electron in the related atom; the value in ( ) is the potential increment after interaction of the related atom pair.

5. SYNTHESIS OF H-GAP

There is not any further report about the synthesis of H-GAP since Vandenberg patented his "Polyethers Containing Azidomethyl Side Chains" as USP 3,645,917 in 1972[12]. The most investigations of GAP, including synthesis and application, are focused on its prepolymer with molecular weight about 2000—3000. Vandenberg claimed in his patent that the chloromethyl units in polyepichorohydrin (PECH) could be substituted by azidomethyl groups from 0.2 to 100%, but he had not described the detail. He only reported the GAP containing -CH$_2$N$_3$ unit 2.1 to 15.5%.

We find from the experiments that it is not too easy to preparate H-GAP with molecular weight more than 5×10^5, because the reaction is influenced by a series of factors, including the reaction time and temperature, ratio of reactants, stabilizers and catalysts etc. shown as follows.

Table 3. Influence of Stabilizers on GAP Molecular Weight

stabilizer*	reaction time (h.)	reaction temp. (℃)	$\overline{M}_w \times 10^5$
A	100	3	5.4335
K	100	3	5.3156
A	80	5	6.6260
K	80	5	6.1338
A + B	70	9	14.7909

* A—— 1,1,3-tris(2-methyl-4-hydroxy-5-tert-butyl-phenyl)butane

B—— catalyst DLTP

K——antioxidizer KY-7910

Table 4. Catalytic Effect of LiCl on Azidation of PECH

catalyst	reaction time (h)	reaction temp. (℃)	-N$_3$ (%)
/	15	100	99.70
LiCl	3	100	99.77
LiCl	2	100	99.00

Table 5. Influence of NaN$_3$/PECH (mole) on $\overline{M}_w$ and -N$_3$(%)

NaN$_3$/PECH	reaction temp. (℃)	reaction time(h)	$\overline{M}_w \times 10^5$	-N$_3$(%)
3:1	100	1	7. 0855	93. 57
2:1	100	1	7. 7687	84. 00
3:1	100	2	5. 7637	99. 00
2:1	100	2	5. 9732	99. 16

Table 6. Influence of Reaction Temp. on $\overline{M}_w$ and N$_3$

reaction temp. (℃)	reaction time(h)	$\overline{M}_w \times 10_5$	-N$_3$(%)
60	14	18. 4220	46. 60
70	8	15. 3175	62. 00
80	5	6. 1382	91. 14
100	2	5. 7637	99. 00

Table 7. Influence of Reaction Time on $\overline{M}_w$ and -N$_3$%

reaction time(h)	reaction temp. (℃)	$\overline{M}_w \times 10^5$	-N$_3$(%)	dispersity
9	70	14. 7909	99. 66	1. 89
10	70	3. 9611	99. 69	2. 01
12	70	12. 5977	99. 80	2. 23

Despite the fact that all the above reactions were carried out under protection of antioxidizer or stabilizer and bubbled with pure nitrogen to dispel the possible by-products which would result in the precursor cleavage, but when the reaction time lasts too long, the average molecular weight of GAP is apparently reduced and its dispersity is also broadened as shown in Table 7. These results indicate that it is needed to carefully tailor all the factors saidabove to meet a optimum co-ordination for synthesizing satisfactory H-GAP.

6. AN INTERESTING PHENOMENON IN PECH AZIDATION

In synthesis of pentaerythrityl tetrazide (PETA) we found[13] that no matter how to stoichiometrically reduce the mole ratio of toluenesulfonyl chloride or sodium azide to pentaerythritol, we had never remained any hydroxy groups in the azidized product except PETA with lower yield.

In azidizing PECH we found the same phenomenon. As shown in Table 6, we obtained a H-GAP with 62% (mole) -N_3 in the azidized products. According to the general concept, there must be in average 62% -N_3 and 38% -Cl in one H-GAP molecule. While after separating the product, we surprisingly found that it was a mixture of pure H-GAP and non-azidized PECH as show in the infrared spectrum (Fig. 1 and 2). The pure H-GAP is an amber-colored elastomer and can vigorously burn, giving out a bright flame, while the residual product is a white one and not easy to ignite.

We guess this focused attack of N_3^- on PECH molecule one by one might be related to the factors of energy compensation and the energy of transition state in the reaction system. Azidation is a typical nucleophilic substitution(SN). When the first -N_3 is linked in the PECH molecule, the energy state in the system is also changed. Although the -N_3 is not at the β-position of the next -CH_2Cl and can not play the role of typical "ortho-group participation", while the strong π-electron and negative charge in R-N_3 would make it possible to go forward the intermolecular SN2 reaction under a proper configuration, and, perhaps, existing some unstable intermediate as follows:
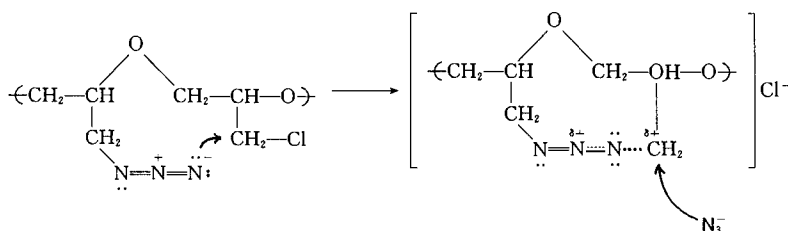
Of course, this is a reaction model we suggested. It is necessary to make more simulated experiments and identified by means of reaction kinetics and other advanced methods.
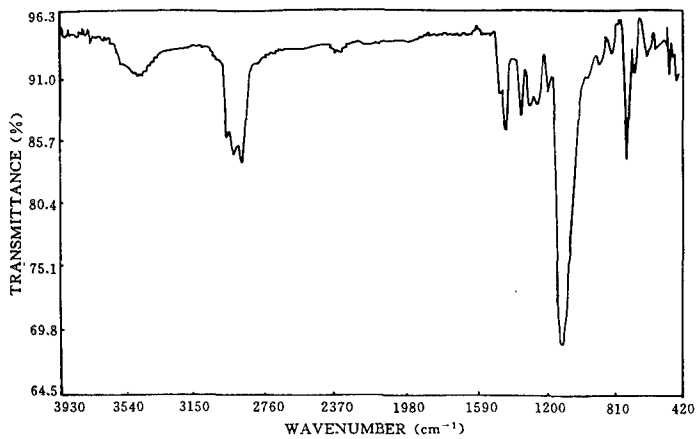
Fig. 1   Infrared spectrum of PECH
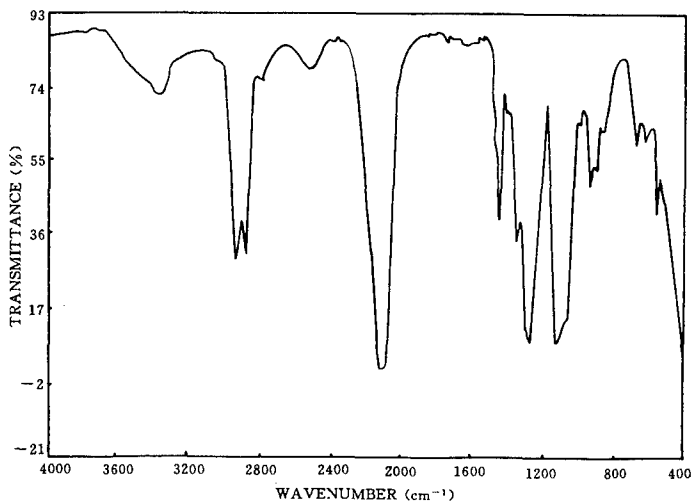
Fig. 2   Infrared spectrum of H-GAP

7. CONCLUSION

Glycidyl azide polymer with average molecular weight more than 14×10^5 was synthesized. Experimental results indicated that the extent of azidation and PECH-chain cleavage depend on a series of factors, including reaction time, temperature, reactant ratio, catalyst, stabilizer or antioxidizer and nitrogen atmosphere protection etc. It is necessary to tailor all these factors to get an optmum coordination for synthesis of H-GAP with more higher molecular weight.

The particular phenomenon of N_3^- focus-attacking one PECH molecule is supposedly discussed by means of the nucleophilic substitution.

ACKNOWLEDGEMENT

REFERENCES

1. Stacar R. G. and Husband D. M. Ideal Molecular Structure of Solid Propellants. Propellants, Explosives, Pyrotechnics, **16**:167~176,**1991**.

2. Rothstein L R. Plastic Bonded Explosives—— Past, Present and Future. Proceedings of The 13th Annual Conference of ICT, **245~265**,**1982**.

3. 张春海，叠氮缩水甘油醚聚合物（GAP）——90 年代的高性能推进剂. 国外兵器动态，**805:1**

4. US DoD Critical Technology Plan, **17**. High Energy Density Materials. AD — A234900, **1991**.

5. 田村昌三，冈本圭史等，GAP 的安全性评价. 工业火药（日），（4）:**222**

6. Schedlbauer F, LOVA Gun Propellant with GAP Binder. Propellants, Explosives, Pyrotechnics,**17**:**164~171**,**1992**.

7. Li Changqing, Wang Ping, Huang Yue et al. Investigation of Glycidyl Azide Polymer. Proceedings of The 17th International Pyrotechnics Seminar Combined with The 2nd Beijing International Symposium on Pyrotechnics and Explosives. 451

8. Huang Yue, Xia Zhongjun and Li Changqing, Preliminary Study on Electrothermal Chemical Propellant. Internaternational Symposium on Energetic Materials, Xiangfan City, Hubei Province, China, 1885.

9. Reed, Jr. Propellants Binders Cure Catalyst. USP 4,379,903, 1983.

10. Ahad E. Branched Hydroxy Terminated Azido Polymers. Proceedings of The 21st International Annual Conference of ICT. 5~1,1990.

11. Liao Hongming, Li Changqing et al. GAP Bonded TATB or HMX. A Work Sponsored by The Science Foundation of China Academy of Engineering Physics, 1995.

12. Vandenberg E J. Polymers Containing Azidomethyl Side Chains. USP 3,645,917, 1972.

13. Wang Ping, Wang Xiaochuan, Huang Yue and Li Changqing. Investigation of Pentaerythrityl Tetrazide. Proceedings of The 26th International ICT — Annual Conference, 1995.

14. A Private Communication. 1995.

AN ENVIRONMENTALLY-FRIENDLY ROUTE TO NITRAMINES AND NITRATE ESTERS VIA NITRODESILYLATION CHEMISTRY USING DINITROGEN PENTOXIDE

ROSS W. MILLAR AND SIMON P. PHILBIN

Defence Research Agency, Fort Halstead, Sevenoaks, Kent TN14 7BP, U.K.

Abstract
Nitramines and nitrate esters are synthesised conventionally using strongly acidic nitration media such as sulphuric-nitric acid mixtures, and the resulting spent liquors from these nitrations are difficult to dispose of without damage to the environment. The novel method described here dispenses with the need for strong acids as the reaction medium and instead uses dinitrogen pentoxide (N_2O_5) in an inert solvent as the nitrating agent. The N_2O_5 cleaves heteroatom-silicon bonds, in silylamines and silyl ethers respectively, to yield the desired energetic groupings (nitramines or nitrate esters respectively) without liberation of acids which would occur with conventional substrates (amines or alcohols). These nitrodesilylation reactions proceed cleanly and in good yield, and furthermore the co-product, a silyl nitrate, can be used to effect further nitrations, hence eliminating the need for disposal.

The scope of the reaction will be illustrated by 25 examples, some of which produce high energy compounds, notably plasticisers and an energetic polymer precursor, whilst in others novel energetic functions such as N-nitro-aziridines can be accessed directly for the first time. When taken in conjunction with the current advances in N_2O_5 chemistry in other fields, which have made this reagent available on large scale at reasonable cost, the use of clean routes to energetic materials such as those described here constitutes a powerful reason for changing the methods of manufacture of energetic materials in the next century.

Introduction

Nitramines and nitrate esters are classes of compounds which find widespread application in propellant and explosive technology[1-3]. Nitrate esters also find use in medicine as vasodilators[4,5]. The chemistry of each class of compound has been reviewed[6,7], and their methods of preparation by traditional routes will first be considered before describing the chemistry involved in the novel desilylative routes. Finally the advantages in the novel chemistry will be assessed, particularly from the environmental point of view.

Nitramines

Nitramines are commonly prepared by the reaction of secondary amides with nitric acid in dehydrating media such as acetic anhydride[8], although other routes are possible, for instance by the addition of nitrate salts of secondary amines to acetic anhydride in the presence of a catalyst, e.g. chloride ion[9], by direct interaction of an amine with dinitrogen pentoxide, N_2O_5[10], or by nitrolysis of gem-diamines with nitric acid-acetic anhydride[11,12]. More recently developed methods include the reaction of N,N-dialkyl-amides with nitronium tetrafluoroborate[13], the reaction of *tert.*-butylamines with nitric acid or N_2O_5[14], and the action of nitric acid-acetic anhydride on *tert.* amines with *in situ* oxidation of the resulting

nitrosamines with peracetic acid[15]. (Routes involving oxidation of <u>isolated</u> nitrosamines have been disregarded owing to the high toxicity of these compounds.)

Many of these routes have disadvantages such as contamination of the product by nitrosamines which are awkward to remove[16], the use of reagents which are not available cheaply on an industrial scale (e.g. NO_2BF_4), or the production of co-products which are difficult to dispose of, notably acyl nitrates. Further problems may arise from inaccessibility of substrates, for instance in the direct nitration of amines[10], certain categories of amine either do not form the nitramine (particularly highly basic amines), or may not be preparable in their unsubstituted form (e.g. hexahydropyrimidines - see later). Such shortcomings limit the scope and utility of existing routes for the synthesis of nitramines.

The problems outlined above are exemplified in one of the most commonly used routes for nitramine synthesis, namely the reaction of secondary amides with nitric acid under dehydrating conditions (eqn 1), where the cleavage of the N-acyl bond results in formation of the desired nitramine (I), but an acyl nitrate co-product (II) is also formed during the reaction (termed a nitrolysis[8]). The disposal of these acyl nitrates is awkward and also poses safety

[Reagents:- a) acylating agent (eg R"COCl)

b) nitrating agent, esp. pure HNO_3, $NO_2{}^+BF_4{}^-$ or N_2O_5] ----------- 1
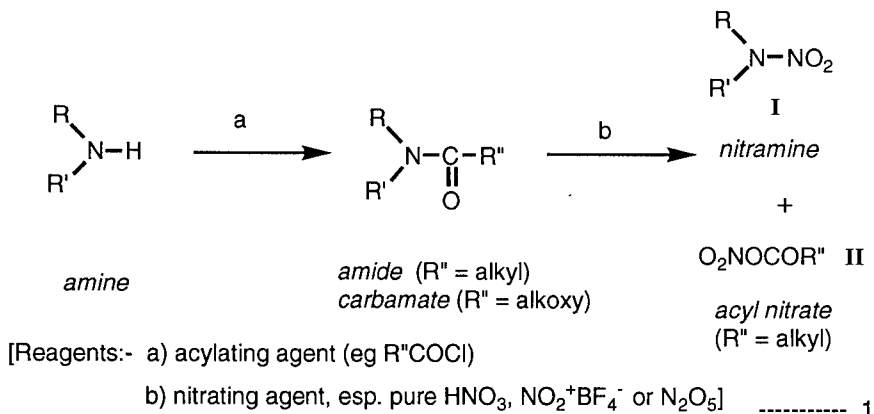
problems in certain circumstances, for instance in the synthesis of HMX from DADN[17]. A further drawback of the nitrolysis of acylamines is that cleavage of N-C bonds *other* than the acyl linkage may occur, resulting in competing reaction pathways and hence lower yields and product contamination, and in extreme cases little of the desired product may be formed (e.g. N,N-dimethylurethane (III) yields ethoxy N-methyl-N-nitrocarbamate (IV) instead of N,N-dimethylnitramine[18]). Finally, some acyl derivatives of polycyclic polyamines (e.g. the precursor of bicyclo-HMX, V) are completely inert to nitrolysis[19].

Nitrate esters

The majority of the methods reported for the synthesis of this class of compounds has relied on the use of mixed acids (HNO_3-H_2SO_4) or pure nitric acid, both of which media

$$
\begin{array}{ccc}
\textbf{III} & \textbf{IV} & \textbf{V}
\end{array}
$$
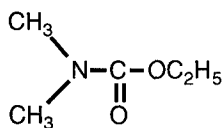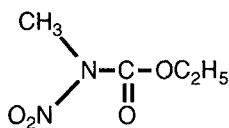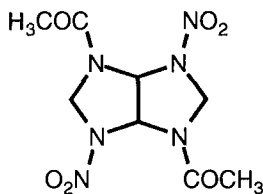
suffer from disposal problems of spent liquors which are unfriendly to the environment. Some methods utilising transfer nitrating agents[7b,7c] would appear to offer an escape from these problems until it is realised that nitronium tetrafluoroborate (NO_2BF_4), a chemical which requires aggressive reagents for its synthesis, is required for the preparation of these reactants, whilst more recent methods utilising either silver salts[20] or Lewis acids (e.g. BF_3)[21] can be ruled out on grounds of hazard and expense.

Discussion

Nitramines

In an attempt to overcome the twin problems of controlling the direction of nitrolysis reactions and forming more easily handlable co-products, the replacement of acyl functions by other readily nitrolysable groups was considered. It was felt that these problems stemmed largely from the inertness of the nitrogen atom towards electrophilic attack as a result of the electron-withdrawing acyl function, and therefore employment of substituents with the opposite inductive effect, i.e. electron-*donating* substituents, would be beneficial. With this rationale in mind, obvious candidate elements for consideration would be the group IV metalloids, and it was already known that stannylamines could be nitrolysed to yield nitramines[22]. Furthermore, publications in the mid-1980s had indicated that C-silyl compounds could be cleaved by reagents such as nitronium tetrafluoroborate to yield C-nitro compounds[23]. However, as no reports were known of the nitrolysis of the corresponding N-silyl compounds, silylamines (**VI**), this therefore seemed an obvious class of compound to examine.

In the subsequent discussion, the N-silyl substrates are divided into two categories - i) dialkylsilylamines and ii) cycloalkyl silylamines, with thirteen examples in all. The nitrodesilylation reactions of twelve silyl ethers are described later.

i) Dialkylsilylamines

The silylamines (**VI**) were derived from the corresponding secondary amines, formed *in situ* where necessary (e.g. **VIm**). Reaction with dinitrogen pentoxide (N_2O_5) in halogenated solvents such as dichloromethane generated the nitramines (**I**) cleanly and in good to excellent yield (eqn. 2 and Table 1). The reaction was found to be general for a

range of alkyl substituents both on nitrogen (R & R') and silicon (R"), with the highest yields being obtained with trimethylsilyl derivatives (R = CH$_3$, see Table 1). The reaction is
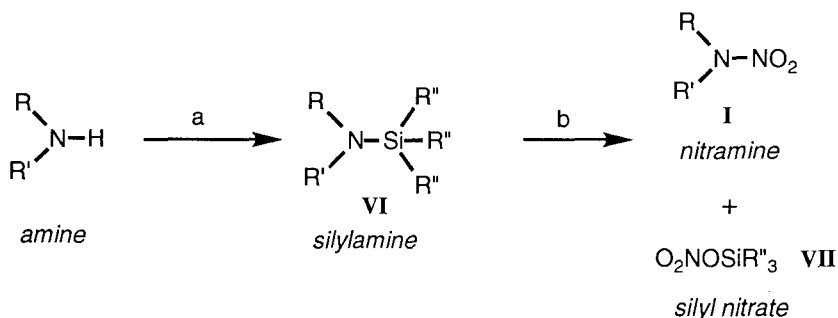
[Reagents:- a) silylating agent (R"$_3$SiX where X is a leaving
group such as halogen, dialkylamino etc)
b) nitrating agent, esp. N$_2$O$_5$, also NO$_2$BF$_4$]   ---------- 2

applicable to cases which have proved troublesome in the past, for instance sterically hindered nitramines such as **If**, and yields were in many cases improved, sometimes markedly, upon those hitherto obtained.

ii) Disilylamines and Silylaziridines

Cyclic dinitramines (**Il** & **Im**) were likewise preparable without difficulty from the corresponding disilyl precursors. It is notable that the precursor to **Im**, N,N'-bis-(trimethylsilyl)hexahydropyrimidine (**IIm**, Table 1) is derived from an unstable diamine (hexahydropyrimidine, **VIII**) and highlights an intrinsic advantage of the novel nitration over other methods which require the use of the free amine, which may be unavailable. Furthermore, the dinitramine product (**Im**), which contains a geminal dinitramine moiety which is a substructural fragment found in the RDX and HMX molecules, is preparable in a

VIII   IX
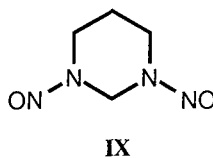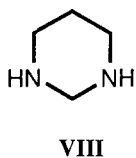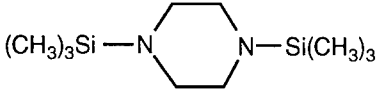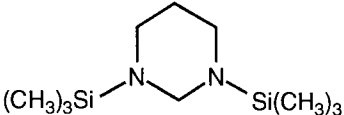
yield (69%) twice that reported in the hitherto best method (by nitro-denitrosation of the N,N'-dinitroso compound **IX**[24]). This hints at the potential of this reaction, and its viability is subject only to the availability of suitable silylated precursors; in this respect, few limitations have been encountered, one of the few groups which is incompatible with silylating agents being the nitrile group.

Table 1: Reactions of Silylamines with N_2O_5

1. Monosilylamines $\quad R^1R^2N\text{-}Si(R^3)_2R^4$

No. VI	R^1	R^2	R^3	R^4	Rn. Time (hr)	Rn. Temp. (°C)	Yield of Nitramine (%)
a	-(CH$_2$)$_2$O(CH$_2$)$_2$-		CH$_3$	CH$_3$	2	0±2	80
b	-(CH$_2$)$_5$-		"	"	0.75	-5±2	81
c	-(CH$_2$)$_4$-		"	"	0.5	-7 to -1	76
d	CH$_3$	CH$_3$	"	"	0.75	-5±2	78
e	C$_2$H$_5$	C$_2$H$_5$	"	"	0.75	-5±2	84
f	i-C$_4$H$_9$ †	i-C$_4$H$_9$	"	"	0.75	-5 to 0	87
g	-(CH$_2$)$_2$O(CH$_2$)$_2$-		"	t-C$_4$H$_9$	2.25 / 6	0 to +5 / +5 to +10	37 / 40*
h	"		n-C$_4$H$_9$	n-C$_4$H$_9$	1.5	-5 to +5	39
i	"		C$_2$H$_5$	C$_2$H$_5$	0.75	0 to +5	61*
j	i-C$_4$H$_9$ †	i-C$_4$H$_9$	"	"	1	0 to +5	70
k	-CH$_2$-CH(CH$_3$)-		CH$_3$	CH$_3$	10 min.	0±5	‡

2. Disilylamines

l	(CH$_3$)$_3$Si—N⬡N—Si(CH$_3$)$_3$	1	-8 to 0	91

m	(structure with (CH$_3$)$_3$Si and Si(CH$_3$)$_3$)	1	-5 to +5	69**

<u>Key to Table 1</u>

     * Larger excesses of N_2O_5 (50 and 100% resp.) used
    ** Mode of addition reversed (N_2O_5 added to silylamine)
    † i-C_4H_9 = $(CH_3)_2CHCH_2$-
    ‡ N-Nitroaziridine not isolated - reacted further *in situ* (see text)
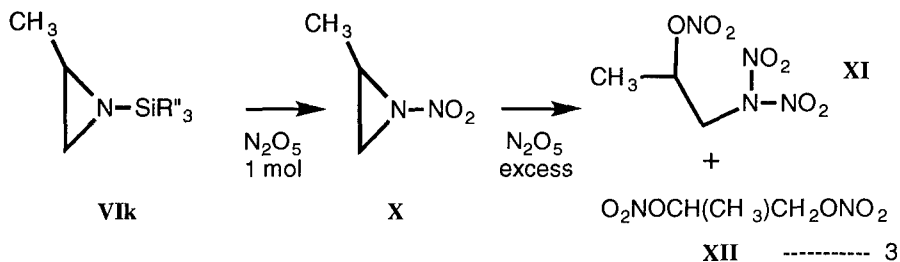
The behaviour of one substrate, the N-trimethylsilylaziridine **VIk**[25] was notable. Upon reaction with 1 mol N_2O_5 the N-nitroaziridine **X** was formed *in situ* in *ca* 80% yield, and further reaction with excess of the reagent resulted in the formation of the N,N-dinitramine-nitrate **XI** (Eqn 3), which was characterised spectroscopically, the nitramine asymmetric stretching band in the i.r. being observed at 1607 cm^{-1}, in line with previous findings[26]. The formation of the N-nitroaziridine **X** constitutes the second reported synthesis of this class of compound[27] and the first by direct electrophilic substitution, although a N-nitroaziridine intermediate was postulated in earlier work on the nitration of propyleneimine by N_2O_5[28]. Also, the N,N-dinitramine-nitrate **XI** was contaminated with some propane-1,2-diol dinitrate (**XII**); such compounds are known to be decomposition products of N,N-dinitramines[29]. Therefore the behaviour of this silylamine opens the door to some novel chemistry by affording classes of compounds which are only otherwise obtainable with extreme difficulty, and furthermore by the ring-opening nitration yields high-energy compounds such as **XI** which possesses a similar oxygen balance to nitroglycerine.

Nitrate Esters

    It was considered that O-silyl compounds, i.e. trialkylsilyl ethers (**XIII**), might behave analogously to N-silyl compounds and yield nitrate ester products (**XIV**), gaining similar advantages to those realised in the nitramine syntheses (Eqn. 4).
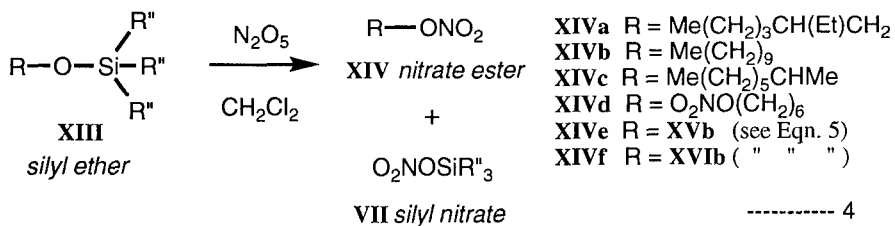
i) Acyclic silyl ethers

These silyl ethers, which share the common feature that the silicon atom bears only one O-substituent, were prepared from the corresponding alcohols by literature methods[30]. In the case of trimethylsilyl ethers, hexamethyldisilazane was used (Eqn. 5) and this was applied to both monohydric (**a** - **c**, **f**) as well as dihydric (**d** & **e**) examples. Derivatives with longer alkyl chains were prepared from the corresponding silyl chlorides in the presence of an auxiliary base and a catalyst (4-(dimethylamino)pyridine, DMAP; Eqn. 6). Preparative

Table 2: Reactions of Silyl Ethers with N_2O_5

Entry	Silyl Ether	N_2O_5 used (mol)	Rn. Temp. °C	Rn. Time h	Nitrate Ester	Yield %
i)	2-ethylhexanol TMS (**XIIIa**)	1.1	-5 to +8	1.5	**XIVa**	92
ii)	n-decanol TMS (**XIIIb**)	1.1	-5 to +8	1.5	**XIVb**	87*
iii)	2-octanol TMS (**XIIIc**)	1.1	-5 to +15	5†	**XIVc**	88
iv)	hexane-1,6-diol bis-TMS (**XIIId**)	2.2	-5 to +3	0.75	**XIVd**	83
v)	2,2-(pentamethylene)-propane-1,3-diol bis-TMS (**XIIIe**)	5.5**	-20 to +10	1.5	**XIVe**	**
vi)	3,3-bis(TMSoxymethyl)oxetane (**XIIIf**)	2.2	-5	2.0	**XIVf**	35
vii)	2-aziridineethanol TMS (**XIIIg**)	2.2	-10 to +5	1.5	**XVIII**	56††
viii)	2-ethylhexanol TBDMS (**XIIIh**)	1.15	-5 to +5	18	**XIVa**	<5
viii)a	" " "	2.0	-5	18	"	35
ix)	2-ethylhexanol tri(n-butyl) (**XIIIi**)	1.1	-5	18	**XIVa**	87
ix)a	" " "	2.0	-5	18	"	94
x)	2-ethylhexanol tri(isopropyl)(**XIIIj**)	1.1	-5	18	**XIVa**	29
x)a	" "	2.0	-5	18	"	53
xi)	2,2-dimethylpropane-1,3-diol cyclic DMS (**XIX**)	2.2	-10 to +3	1.5	**XXII**	‡
xii)	butane-1,2-diol cyclic DMS (**XX**)	5.0	-5	24	**XXIII**	66

Notes

*   The organic extract floated on brine.
†   Reaction was incomplete after 2.5 h (nmr).
** Impure product obtained, also with lower mol ratios of N_2O_5.
††   Nitramine-nitrate prepared, but impure.
‡   Main product obtained is silyl nitrate (for structure see text)

$$(Me_3Si)_2NH$$

$$R-OH \xrightarrow[\text{Me}_3\text{SiCl } 0.1 \text{ mol}]{} R-O-\overset{\overset{\displaystyle Me}{|}}{\underset{\underset{\displaystyle Me}{|}}{Si}}-Me$$

XIIIa R = Me(CH$_2$)$_3$CH(Et)CH$_2$
XIIIb R = Me(CH$_2$)$_9$
XIIIc R = Me(CH$_2$)$_5$CHMe
XIIId R = Me$_3$SiO(CH$_2$)$_6$
XIIIe R = XVa
XIIIf R = XVIa
XIIIg R = XVII

R-CH$_2$ CH$_2$—

R-CH$_2$ CH$_2$—

$$\triangleright N-(CH_2)_2-$$

---------- 5
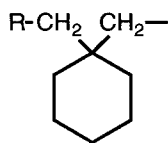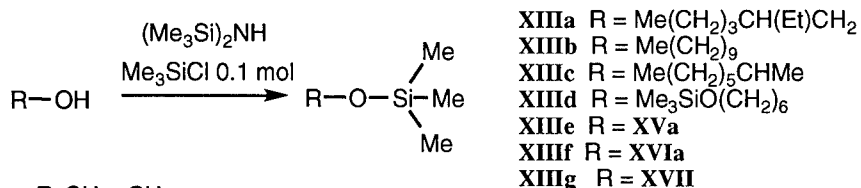
XVa R = Me$_3$SiO
XVb R = O$_2$NO
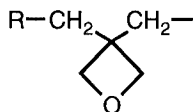
XVIa R = Me$_3$SiO
XVIb R = O$_2$NO

XVII

$$Me(CH_2)_3CH(Et)CH_2OH \xrightarrow[\text{DMAP}]{\overset{R''(R')_2SiCl}{Et_3N \text{ or } C_5H_5N}} Me(CH_2)_3CH(Et)CH_2-O-\overset{\overset{\displaystyle R'}{|}}{\underset{\underset{\displaystyle R''}{|}}{Si}}-R'$$

XIIIh R' = Me, R" = Bu^t
XIIIi R' = R" = Bu^n
XIIIj R' = R" = Pr^i

---------- 6
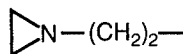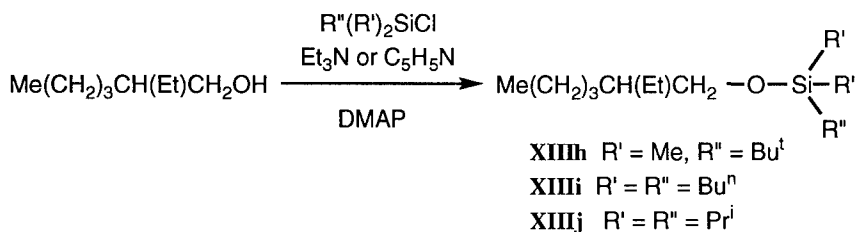
yields were generally in the range 75 to 93%. In one case (**XIIIg**) a second functionality (an aziridine ring) was present in the molecule, offering the possibility of introducing further energetic moieties by ring-opening nitration[31].

When the simple trimethylsilyl ethers **XIIIa-d** were treated with a small excess of N$_2$O$_5$ in dichloromethane, the corresponding nitrate esters **XIVa-d** were obtained cleanly and in high (83-92%) yield (see Eqn. 4 and Table 2, entries i) - vi)). The secondary example (**XIIIc**) reacted more slowly but the ultimate yield of nitrate ester **XIVc** (after 5 h at near ambient temperature) was in line with the other examples. The difunctional trimethylsilyl ethers **XIIIe-f** gave much lower yields owing to the neopentyl situation of the silyl ether functions, which gives rise to much reduced reactivity because of steric hindrance. The remaining trimethylsilyl ether, **XIIIg**, was treated with 2 mol N$_2$O$_5$ to enable reaction to occur on the aziridine function as well as the silyl ether, and a moderate (56%) yield of the known nitramine-nitrate (DINA, **XVIII**) was obtained (Eqn. 7).

$$\triangleright N-(CH_2)_2OSiMe_3 \xrightarrow[\text{CH}_2\text{Cl}_2]{N_2O_5 \text{ (2 mol)}} (O_2NOCH_2CH_2)_2NNO_2$$

XIIIg   **XVIII** ---------- 7
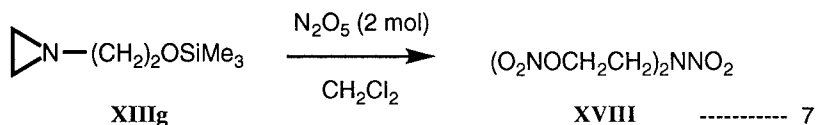
The remaining acyclic silyl ethers **XIIIh-j** (Table 2, entries viii) - x)), which bore longer alkyl chains (up to C_4) on the silicon atom (the alcohol chain, R, was in all cases 2-ethylhexyl), in general reacted more slowly with N_2O_5, mirroring the trends found in the silylamine reactions (see above). In particular, those with branched alkyl substituents were the least reactive, and with *tert.*-butyldimethyl substitution on Si a maximum yield of **XIVa** of only 35% was attained, even under forcing conditions (100 molar % excess of N_2O_5 for 18 h). These findings indicate that if, for instance, it were necessary to use a *tert.*-butyldimethylsilyl ether in a synthetic strategy (e.g. as a blocking group) then the nitrate ester could not be generated efficiently by direct reaction with N_2O_5, and alternative strategies might have to be sought. Completing the reactivity comparison of compounds **XIIIh-j**, it is apparent that the tri(n-butyl) derivative is the most reactive towards N_2O_5, giving similar yields to the trimethylsilyl examples (although with substantially longer reaction times), whilst the tri-(isopropyl) derivative displays an intermediate reactivity, yielding up to 53% nitrate ester **XIVa**.

ii) Cyclic silyl ethers

XIX R = H, n = 1
XX R = Et, n = 0

R = H, n = 1; N_2O_5 (2 mol)

R = Et, n = 0; N_2O_5 (5 mol)

XXII

(+ some 2,2-dimethylpropanediol dinitrate, **XXI**)

XXIII

---------- 8
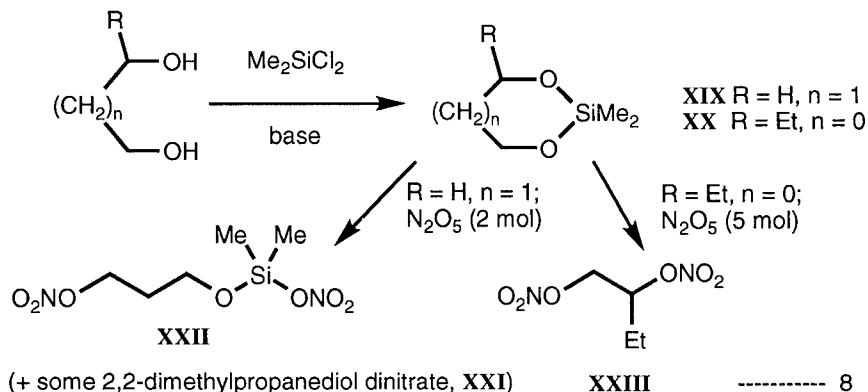
Two compounds in this class were studied: **XIX** and **XX**. They were prepared (Eqn. 8) from the corresponding 1,2- or 1,3-diols by reaction with dichlorodimethylsilane according to the literature[32]. The products obtained upon treatment with N_2O_5 were strongly dependent on the conditions. Thus with **XIX**, use of a small excess of N_2O_5 and a short reaction time resulted in the isolation of very little of the desired dinitrate **XXI**, and the major product was the partially cleaved silyl nitrate **XXII**. This compound belongs to a class of compounds, the silyl nitrates, which have received scant attention in the literature[33]. It showed interesting spectral properties whereby unusual nitrate ester bands at 1263 (symm. NO_2 stretch) and 808 (ONO_2 group) cm^{-1} were observed, which were at lower frequencies than those of C-nitrates by some 15 and 60 cm^{-1} respectively, presumably on account of the attachment of the heavier silicon atom in place of carbon.

On the other hand, when silyl ether **XX** was treated with a large (150%) excess of N_2O_5 and allowed to react for a protracted period, the dinitrate **XXIII** was obtained in useful (66%) yield (Eqn. 8). Presumably **XIX** would also give a substantial yield of **XXI** under similar conditions, but insufficient sample remained to test this hypothesis.

Conclusions

Therefore nitrodesilylations of silylamines and silyl ethers by N_2O_5 afford the corresponding nitro compounds, nitramines and nitrate esters respectively, generally in good to excellent yields. With the silylamines the reaction[34] is of wide applicability, and products bearing 1,3-bis-(N-nitro) functions are accessible such as **Im**. The success of the method in this case is significant and augurs well for the extension to polynitramines. The conditions necessary to effect the cleavage of the N-Si bond are much milder than, for instance, those required to cleave N-acyl substrates (i.e. amides) and suggest applications in those areas where cleavage of acetamides have failed to yield nitramine products, e.g. polycyclic nitramines such as bicyclo-HMX[19].

The by-product from the nitration reaction, the volatile silyl nitrate $(CH_3)_3SiONO_2$ (**VII**, R" = CH_3, Eqn 2), is a nitrating agent in its own right[35] and could easily be collected by distillation and used profitably to carry out other nitrations, such as toluene to dinitrotoluene. The formation of silyl nitrates such as **VII** is also preferable to the acidic by-products (viz. BF_3 or HBF_4) which would arise from the corresponding reactions with NO_2BF_4. Another advantage is the non-acidic nature of the reaction medium which suggests applications involving acid-sensitive substrates hitherto precluded from study in conventional nitration media.

Likewise the reaction of silyl ethers with N_2O_5 is a viable means of synthesising nitrate esters, particularly when the alkyl silicon substituents possess short or unbranched chains (particularly methyl), and yields in excess of 90% can be realised. When these substituents are branched chains the yields are lower, and with *tert.*-butyl derivatives the yield is only acceptable under forcing conditions. The short chain derivatives have the added advantage that the silyl nitrate by-product is more volatile, resulting in easier separation and purification of the nitrate ester product; hence the use of the longer chain derivatives should only be entertained if other considerations dictate that their usage is essential, e.g. protecting group strategies.

With cyclic silyl ethers, although only two cases were studied, it became apparent that more forcing conditions are necessary for the satisfactory preparation of dinitrates from these substrates. This may cause some problems if these functions are to be used in a protecting group capacity, since excesses of N_2O_5 necessary for their complete removal may interfere with functional groups elsewhere in the molecule. In this respect the silyl ethers differ from the silylamines investigated earlier, where reactivities were in general higher, even on

electron-deficient functions such as amides. Such reactivity trends are to be expected owing to the well-established difference in basicity of these elements resulting from the relative availability of the electrons in their respective lone pairs to participate in bonding. Thus the nitrogen lone pair is loosely bound and hence can readily form a sigma bond on approach of an electrophile such as the nitronium ion (which exists in N_2O_5 solutions under laboratory conditions[36]). On the other hand, the more tightly bound lone pairs on oxygen are more reluctant to do so, resulting in lower reactivities with this class of compound, in agreement with experimental observation.

Finally, it should be emphasised that this approach to nitramines and nitrate esters comprises a novel alternative to methods employing strong mineral acids, and will overcome many of the problems inherent in the latter concerning the disposal of waste acid liquors. These liquors are in some cases quite hazardous owing to the solubility of some nitrate esters in them (e.g. triethyleneglycol dinitrate shows *ca* 9% vol./vol. solubility in spent HNO_3-H_2SO_4[37]), and care is required in their handling and disposal. Furthermore, the solubility of certain nitrate esters in water can be problematic (e.g. ethyleneglycol dinitrate shows *ca* 4% wt./vol. solubility in water[38], a high figure for a covalent ester) and the necessity of water washing in conventional processes can be a distinct disadvantage. All of these factors must be taken into consideration when designing environmentally-friendly processes for the manufacture of energetic materials, such as will have to be employed next century in order to meet new legislation[39]. Nitrodesilylation methodologies such as those described here are well placed to meet such requirements, and offer the opportunity to solve many of the problems inherent in the clean manufacture of energetic ingredients for munitions applications.

Acknowledgements

Experimental

Silylamine Preparations and Their Reactions with N_2O_5.
Details have been presented elsewhere[40].

Silyl Ethers
The following trimethylsilyl ethers were prepared[30] by treatment of the corresponding alcohol with hexamethyldisilazane [HMDS] with a trace of chlorotrimethylsilane [CTMS] as follows:-
2-Ethylhexanol, n-decanol and 2-octanol: A mixture of the alcohol (0.2 mol) and HMDS (0.11 mol), to which a few drops of CTMS had been added, was heated with stirring in an oil bath in a RB flask equipped with an air condenser, initially at 60 to 65°C. The temperature was raised progressively to 150°C over 2-3 h (evolution of ammonia noted - moist indicator

paper check) and the reaction was held at this temperature overnight, or until no further ammonia could be detected. The product was then distilled, either bulb-to-bulb on a Büchi Kugelrohr GKR 50 (#) or by fractionation (Fisher Spaltrohr HMS 300 (§) or 10 cm Vigreux column (¶)), to give the pure silyl ether. Thus prepared were:- i) 2-ethylhexanol trimethylsilyl ether (**XIIIa**), b.pt.(¶) 88-89°C/ 20 mm (85%); ^{1}H nmr, δ: 0.20(s,9); 1.00(t,6); 1.35(m,8); 3.5(m,2); v_{max} (liq. film): 2959(s), 2930(s), 2867(s), 1462(m), 1382(m), 1251(s), 1092(s), 878(s), 841(s), 746(m) cm^{-1}; ii) n-decanol trimethylsilyl ether (**XIIIb**), b.pt. (#) 164°C/ 90 mm (75%); ^{1}H nmr, δ: 0.20(s,9; 0.95(t,3); 1.32(brs,16); 3.60(t,2); v_{max} (liq. film): 2956(s), 2926(s), 2855(s), 1467(m), 1384(m), 1250(s), 1100(s), 841(s), 746(m) cm^{-1}; iii) 2-octanol trimethylsilyl ether (**XIIIc**), b.pt. (¶) 95-99°C/ 30 mm (74%); ^{1}H nmr, δ: 0.15(s,9); 0.85(m,3); 1.00(d,3); 1.2(m,10); 3.65(m,1); v_{max} (liq. film): 2958(s), 2928(s), 2859(s), 1459(m), 1374(m), 1250(s), 1084(m), 841(s), 747(m) cm^{-1}. Hexane-1,6-diol, 2,2-(pentamethylene)propane-1,3-diol[41] and 3,3-bis(hydroxymethyl)oxetane[42] were treated as above, but using 0.10 mol diol and 0.11 mol HMDS (with CTMS). Thus prepared were iv) hexane-1,6-diol bis(trimethylsilyl) ether (**XIIId**), b.pt. (#) 165-170°C/ 15 mm (93%); ^{1}H nmr, δ: 0.15(s,18); 1.45(m,8); 3.60(t,4); v_{max} (liq. film): 2938(s), 2861(s), 1385(m), 1251(s), 1096(s), 1036(m), 873(s), 841(s), 747(m) cm^{-1}; v) 2,2-(pentamethylene)propane-1,3-diol bis(trimethylsilyl) ether (**XIIIe**), b.pt. (§) 103.5-104°C/ 4.5 mm (85%); purity (by ^{1}H nmr) *ca* 90%; ^{1}H nmr, δ: 0.0(s,18); 1.3(brs,10); 3.30(s,4); v_{max} (liq. film): 2955(s), 2930(s), 2859(s), 1460(m), 1250(s),1086(s), 885(s), 841(s), 747(m) cm^{-1}; and vi) 3,3-bis(trimethylsilyloxy-methyl)oxetane (**XIIIf**), b.pt. (#) 135-150°C/ 10 mm (60%); ^{1}H nmr, δ: 0.30(s,18); 3.85(s,4); 4.50(s,4); v_{max} (liq. film): 1252(s), 1085(s), 870(s), 841(s) cm^{-1}.

Long-chain silyl ethers[30]: 2-ethylhexanol *tert*-butyldimethylsilyl ether (**XIIIh**), b.pt. (#) 120°C/ 8mm (89%); ^{1}H nmr, δ: -0.05(s,6); 0.75(brs,5); 0.80(s,9); 1.2(brs, 10); 3.40(brs,2); v_{max} (liq. film): 2958(s), 2929(s), 2858(s), 1472(m), 1463(m), 1384(m), 1255(s), 1095(s), 850(s), 836(s), 774(s) cm^{-1}; 2-ethylhexanol tri-(n-butyl)silyl ether (**XIIIi**): b.pt. (#) 160-180°C/ 0.5 mm; ^{1}H nmr, δ: 0.5-1.6(m,42); 3.5(br.s,2); v_{max} (liq. film): 1092 cm^{-1}; 2-ethylhexanol tri-(isopropyl)silyl ether (**XIIIj**): b.pt. (#) 160-180°C/ 0.5 mm; ^{1}H nmr, δ: 1.0-1.7(m,36); 3.5(br.s,2).

Nitrolyses

The silyl ether (20 mmol) dissolved in dry dichloromethane (*ca* 10 ml) was added dropwise over 10-15 min. to a solution of N_2O_5[43] in the same solvent (20-25 ml). Quantities of N_2O_5 used, and temperatures and times of reactions are shown in Table 1. After the appropriate reaction time, the mixture was worked up by washing with saturated sodium hydrogen carbonate solution (*ca* 50 ml), with addition of further solid sodium hydrogen carbonate if necessary, followed by washing with saturated brine. The organic extract (washed out with further dichloromethane (15-20 ml)) was then dried over anhydrous magnesium sulphate, and finally the solvent was removed on a Rotavapor to yield the nitrate ester product, which was characterised spectroscopically and, in some cases, by HPLC.

The HPLC analyses employed an internal standard method based on the response of the nitrate ester *vs* di-(n-pentyl)phthalate. A calibration curve was produced from three different concentrations of an authentic sample of the nitrate ester, and using quadratic curve fitting it was possible to calculate sample purities and hence percentage yields based on the HPLC analyses.

Thus prepared were: 2-ethylhexanol nitrate (**XIVa**); ^{1}H nmr, δ: 0.90(t,6); 1.3(m,8); 4.30(d,2); v_{max} (liq. film) 1632(NO_2 as.), 1279(NO_2 s.), 867 (ONO_2 gp.) cm^{-1}; n-decanol nitrate (**XIVb**); ^{1}H nmr, δ: 0.90(t,3); 1.3(brs,16); 4.45(t,2); v_{max} (liq. film) 1632(NO_2 as.),

1280(NO_2 s.), 864 (ONO_2 gp.) cm^{-1}; 2-octanol nitrate (**XIVc**); ^{1}H nmr, δ: 0.80(m,3); 1.35(m,13); 5.05(qr,1); ν_{max} (liq. film) 1625(NO_2 as.), 1279(NO_2 s.), 876(ONO_2 gp.) cm^{-1}; hexane-1,6-diol dinitrate (**XIVd**); ^{1}H nmr, δ: 0.15(s,18); 1.45(m,8); 3.60(t,4); ν_{max} (liq. film) 1632(NO_2 as.), 1280(NO_2 s.), 872 (ONO_2 gp.) cm^{-1}; 2,2-(pentamethylene)propane-1,3-diol dinitrate (**XIVe**); ^{1}H nmr, δ: 1.53(br.s,10); 4.43(s,4); ν_{max} (liq. film) 1638(NO_2 as.), 1277 (NO_2 s.), 867(ONO_2 gp.) cm^{-1}; 3,3-bis(nitratomethyl)oxetane (**XIVf**); ^{1}H nmr, δ: 4.65(s,4); 4.85(s,4); ν_{max} (liq. film) 1644, 1278, 867 cm^{-1}; DINA (**XVIII**); ^{1}H nmr, δ: 4.13(t,4); 4.76(t,4); ν_{max} (mull) 1638(NO_2 as., n.ester), 1523(NO_2 as., nitramine), 1283(NO_2 s.) cm^{-1}; 2,2-dimethylpropane-1,3-diol dinitrate (**XXI**); ^{1}H nmr, δ: 1.10(s,6); 4.28(s,4); ν_{max} (liq. film) 1636(NO_2 as.), 1278(NO_2 s.), 866(ONO_2 gp.) cm^{-1}; (**XXII**); ^{1}H nmr, δ: 0.05(s,6); 0.95(s,6); 3.40(d,2); 4.28(d,2); ν_{max} (liq. film) 1632(NO_2 as.), 1279(NO_2 s.);1263(NO_2 s.), 872, 808 (ONO_2 gp.) cm^{-1}; butane-1,2-diol dinitrate (**XXIII**); ^{1}H nmr, δ: 0.5-0.8(m,2); 1.0(m,3); 4.3(m,2); 4.5(m,1); ν_{max} (liq. film) 1640(NO_2 as.), 1270(NO_2 s.) cm^{-1}.

References and Notes

1. T. Urbanski, "Chemistry and Technology of Explosives", Vol. 3, Oxford: Pergamon Press 1967.
2. See ref. 1, Vol. 2.
3. M. Grayson (Ed.), *Kirk-Othmer Encyclopedia of Chemical Technology, 3rd Edit.*, Vol. 9, pp. 572-581. New York: Wiley Interscience 1980.
4. As ref. 3, Vol. 11, p. 929.
5. M. Shiratsuchi, K Kawamura, T. Akashi, M. Fujii, H. Ishihama & Y. Uchida, *Chem. Pharm. Bull.* 35 632-641 (1987) and refs. contained therein.
6. a) G. F. Wright, "Methods of Formation of the Nitramino Group, its Properties and Reactions" in *The Chemistry of the Nitro and Nitroso Groups*, ed. H. Feuer (The Chemistry of Functional Groups Series, Series ed. S. Patai), Part 1, ch. 9. New York: Interscience 1969; b) P. A. S. Smith, "Open Chain Nitrogen Compounds", Vol. 2, Chapter 15, New York: Benjamin 1966; c) R. G. Coombes, "Nitration" in Comprehensive Organic Chemistry (Series Eds. D. Barton & W. D.Ollis), Vol. 2 (Ed. I. O. Sutherland), Oxford: Pergamon 1979; d) J. W. Fischer, "The Chemistry of Dinitrogen Pentoxide" in *Nitro Compounds: Recent Advances in Synthesis & Chemistry* (Organic Nitro Chemistry Series, ed. H. Feuer & A. T. Nielsen), ch. 3, pp 338-346. New York: VCH 1990.
7. a) R. Boschan, R. T. Merrow & R. W. van Dolah, *Chem. Rev.* 55 485-510 (1955); b) G. A. Olah, R. Malhotra & S. C. Narang, "Nitration, Methods and Mechanisms" (Organic Nitro Chemistry Series, Ed. H. Feuer), pp 269-275. New York: VCH 1989; c) G. A. Olah, "Methods for Preparing Energetic Nitrocompounds" in *Chemistry of Energetic Materials* (Ed. G. A. Olah & D. R. Squire), Ch. 7, pp 186-191. San Diego & London: Academic Press 1991. See also ref. 6b and ref. 6d, pp 327-330.
8. See ref. 1, pp. 8-13.
9. W. J. Chute, K. G. Herring, L. E. Tombs and G. F. Wright, *Canad. J Res.,* 26B, 89-103 (1948).
10. W. D. Emmons, A. S. Pagano and T. E. Stevens, *J Org. Chem.*, 23, 311-3 (1958); see also ref. 6d.
11. F. Chapman, *J Chem. Soc.* 1631 (1949).
12. For further details, see a) ref. 1, b) ref. 6c.
13. S. A. Andreev, L. A. Novik, B. A. Lebedeev, I. V. Tselinskii and B. V. Gidaspov, *J. Org. Chem. USSR*, 14(2), 221-4 (1978).
14. D. A. Cichra and H. G. Adolph, *J Org. Chem.*, 47(12), 2474-6 (1982).
15. J. H. Boyer, T. P. Pillai and V. T. Ramakrishnan, *Synthesis,* 677-9 (1985).

16. For detailed discussion of this problem see: J. C. Bottaro, R. J. Schmitt and C. D. Bedford, *J. Org. Chem.*, 52(11) 2292-4 (1987).

17. V. I. Siele, M. Warman, J. Leccacorvi, R. W. Hutchinson, R. Motto, E. E. Gilbert, T. M. Benzinger, M. D. Coburn, R. K. Rohwer & R. K. Davey, *Propellants & Explosives* 6, 67-73 (1981).

18. See ref. 6c, p 371.

19. W. M. Koppes, M. Chaykovsky and H. G. Adolph, *J Org. Chem.*, 52(6), 1113-9 (1987).

20. L. Castedo, C. F. Marcos, M. Monteagudo & G. Tojo, *Synth. Commun.* 22(5) 677-681 (1992).

21. G. A. Olah, Q. Wang, X. Li & G. K. S. Prakash, *Synthesis* 1993(2) 207-208.

22. A. T. Nielsen, personal communication.

23. a) R. J. Schmitt, J. C. Bottaro, R. Malhotra and C. D. Bedford, *J Org. Chem.*, 52(11), 2294-7 (1987); b) G. A. Olah & C. Rochin, *J. Org. Chem.*, 52 701-702 (1987); c) ref. 7b, Ch.4.

24. R. L. Willer & R. L. Atkins, *J Org. Chem.*, 49, 5147-50 (1984).

25. O. J. Scherer & M. Schmidt, *Chem. Ber.*, 98 2243 (1965).

26. Aerojet-General Corp., Brit. Pat. 1126591(6/9/63).

27. First synthesised in 1977: M. J. Haire & G. A. Boswell, *J Org. Chem.*, 42, 4251-6 (1977); M. J. Haire & R. L. Harlow, *J Org. Chem.*, 45, 2264-5 (1980).

28. P. Golding, R. W. Millar, N. C. Paul and D. H. Richards, *Tet. Letts.* 32(37), 4985 (1991).

29. C. L. Coon, personal communication.

30. E. W. Colvin, *Silicon Reagents in Organic Synthesis*, p. 91. London: Academic Press 1988.

31. P. Golding, R. W. Millar, N. C. Paul & D. H. Richards, *Tetrahedron* 49(32) 7063-7076 (1993).

32. M. G. Voronkov & P. Romadane, *Khim. Geterot. Soed.* 1966(6), 879-91; *Chem. Abs.* 67 32775f (1967).

33. S. A. Hardinger & N. Wijaya, *Tet. Letts.* 34(24) 3821-3824 (1993).

34. During the course of this work the nitrodesilylation of a few aliphatic secondary silylamines by nitronium tetrafluoroborate was noted [i) ref. 7c, ch. 7, p.197; ii) P. R. Dave, F. Farhad, T. Axenrod, C. D. Bedford, M. Chaykovsky, M.-K. Rho, R. Gilardi & C. George, *Phosphorus, Sulfur, Silicon Relat. Elem.* 90(1-4) 175-184 (1994)], but the necessity of using nitronium tetrafluoroborate reduces the scale-up potential of these reactions. Concerning the novelty of nitrodesilylations of N-silyl compounds, although some mention has been made of the formation of N-nitroheteroaromatics by the reaction of the corresponding N-silyl compounds with NO_2BF_4 (R. S. Glass et al, *Canad. J. Chem.*, 50, 3472-7 (1972)) the products are principally of use as transfer nitrating reagents. Additionally, a limited investigation of the reactions of some simple silylamines with N_2O_5 was reported but did not result in a general nitramine synthesis (H. Schultheiss and E. Fluck, *Z. Anorg. Allg. Chem.*, 445, 20-26 (1978)). Hence it is concluded that the formation of N-nitro derivatives of dialkyl- and cycloalkylamines, as a general reaction using N_2O_5 constitutes a novel synthesis of these classes of compounds.

35. See ref. 7b, p. 42.

36. R. B. Moodie, University of Exeter, personal communication.

37. See ref. 2, p. 155.

38. N. C. Paul, DRA, personal communication.

39. E.g. see C. J. Suckling, P. J. Halling, R. C. Kirkwood & G. Bell, "Clean Synthesis of Effect Chemicals". Swindon, Wilts.: AFRC-SERC Clean Technology Unit, Jan. 1992 (ISBN 1 870669 92 4).

40. R. W. Millar ,"A New Route to Nitramines in Non-Acidic Media", in "Nitration", eds. L. F. Albright, R. V. Carr & R. J. Schmit, ACS Symp. Ser. 1996 in press.

41. H. J. Backer & H. J. Winter, *Rec. Trav. Chim. Pays-Bas* 56 492-509 (1937).

42. D. B. Pattison, *J Am. Chem. Soc.* 79 3455 (1957).

43. A. D. Harris, J. C. Trebellas & H. B. Jonassen, *Inorg. Synth.* 9 83-88 (1967).

SYNTHESIS OF THE CAGED NITRAMINE HNIW (CL-20)

Robert B. Wardle, Jerald C. Hinshaw, Paul Braithwaite, Michael Rose
Thiokol Corporation, P.O. Box 707, Brigham City, Utah 84302-0707, U.S.A.

Gene Johnston, Randy Jones, Ken Poush
Thiokol Corporation, Marshall, Texas 75671 U.S.A.

INTRODUCTION:

A strategy for meeting the need for increased performance in specific impulse, ballistics, and density in several broad classes of propellants is the use of high energy/density ingredients such as hexanitrohexaaza-isowurtzitane (HNIW or CL-20). This material is predicted, based on experimentally determined physical properties, to significantly enhance performance in the areas of specific impulse and/or density in propellants and in detonation velocity and pressure in explosives. As with the vast majority of emerging technologies, this material has required considerable research and development prior to being mature enough for use in advanced development, demonstration or production systems. Thiokol Corporation, with funding from several U.S. Department of Defense organizations, has brought the synthesis of HNIW to the pilot scale. Critical attention was paid to the safety properties of the HNIW. Crystal quality has been found to significantly affect safety and processing properties.

RESULTS AND DISCUSSION:

HNIW is the most celebrated product of many years of Office of Naval Research sponsored research at the Naval Air Warfare Center by Arnold Nielsen and coworkers into the synthesis of novel nitramines and related energetic materials. The structure of HNIW (shown below) suggests even to the most casual observer that this compound should be chemically similar to the much better known mono-cyclic nitramines, HMX and RDX. The cage structure
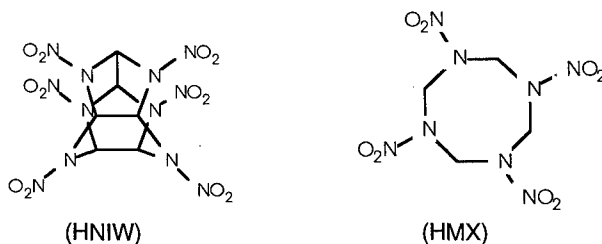
Figure 1. The structures of HNIW and HMX are shown for comparison.

has four distinct effects on the chemical characteristics of HNIW. First, the cage structure imparts greater density to the molecule. Second, the heat of formation is increased because of the ring strain from the cage. Thirdly, the oxygen-to-fuel ratio is altered due to the more highly branched structure of HNIW. Finally, the thermal decomposition is altered because of a combination of altered geometry in the cage and the three foregoing factors. Also similar to HMX, HNIW has shown several different polymorphic forms with slightly different densities.

Thermal Characteristics:

A description of the thermal stability of the various polymorphs of HNIW has been made.[1] Thermal analysis of the various polymorphs as measured by differential scanning calorimetry (DSC) demonstrates the good thermal stability of HNIW (Table 1) as does thermal gravimetric analysis (TGA, Figure 2).

Table 1. HNIW Thermal Stability Comparison

	Onset (°C)	Maximum (°C)
α-HNIW	220	250
ß-HNIW	220	240
ε-HNIW	240	253

Table 1. DSC at 10°C per minute heating rate for several HNIW polymorphs.
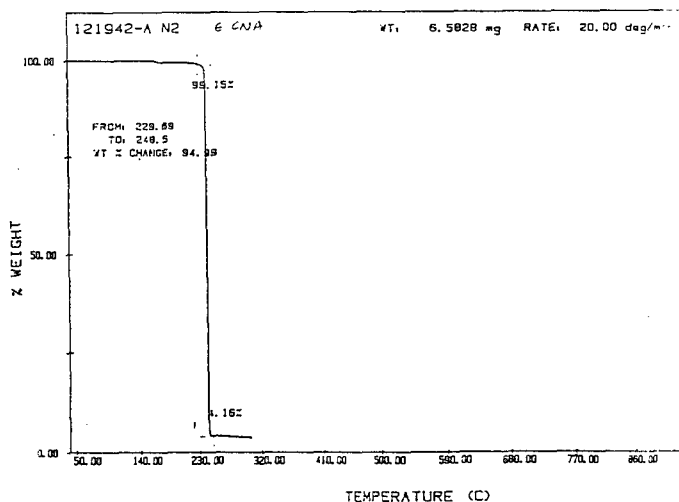
Figure 2. TGA of ε-HNIW.

Synthesis:

The first example of the hexaazaisowurtzitane family of molecules to be reported[2,3] was the hexabenzyl derivative (HBIW). From this material, HNIW is prepared (Figure 3). To date, very little has been published on the conversion of HBIW to HNIW. A report by Bellamy[4] identified a conversion of HBIW to the partially reduced intermediate, TADB. No description was given of the conversion of this material to HNIW. This work is similar to that reported by Nielsen as early as 1986.[5] A recent patent by Kodama[6] reports the synthesis of HNIW through HBIW via a silylurethane. While intellectually interesting, this route has no practical use unless a simpler chloroformate can be found to use in the replacement of the benzyl groups. The lack of extensive literature on the synthesis should soon be rectified with a relaxing of the distribution of data on CL-20 synthesis within the U.S. The original synthesis by Nielsen has been released for public distribution but does is not the current state-of-the-art and has no more bearing on future work than does the silylchloroformate route. At Thiokol, a modification of the route originally discovered by Nielsen has been aggressively scaled-up to produce larger quantities of HNIW at reasonable cost for a developmental material. In pursuing this work, care was taken at each step to carefully
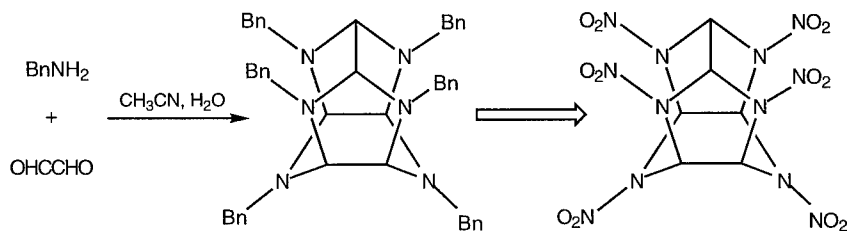
Figure 3. HBIW is prepared from benzyl amine and glyoxal. HBIW is further elaborated to HNIW.

review all aspects of the synthetic route and implication of running a given reaction at a larger scale. Particular concern was paid to: safety considerations, difficulty in executing the procedure as configured (including time and handling), yield, cost of materials (including recycling and waste disposal), and product purity (effectiveness in next reaction). The largest scale of reaction for each of the steps executed today are listed below (Table 2).

Table 2. Scale of Reactions

Step	Reactor (liters)	Product (kg)
Condensation	5700	250
Conversion to nitration substrate	1900	100
Nitration	3800	225
Crystallization	3800	450

Table 2. Approximate scale of reactions used in the stepwise transition of the HNIW synthesis from the laboratory to the pilot plant. Reactor is the size of vessel used for the reaction in liters and product is the weight of material in kilograms obtained from the given reactor. Differences in scale of the condensation and final step are chosen based on safety and equipment considerations.

Crystallization and Particle Size Control

Initial crystallization development at Thiokol focused on consistent preparation of the highest density polymorph (epsilon). Description of analytical methods and other preparation of the epsilon polymorph has been made elsewhere.[7,8] Particle size distribution was typically broad and often exhibited two or more distinct modes (figure 4). The HNIW was often polycrystalline with sharp corners and some microscopically visible defects (figure 5).
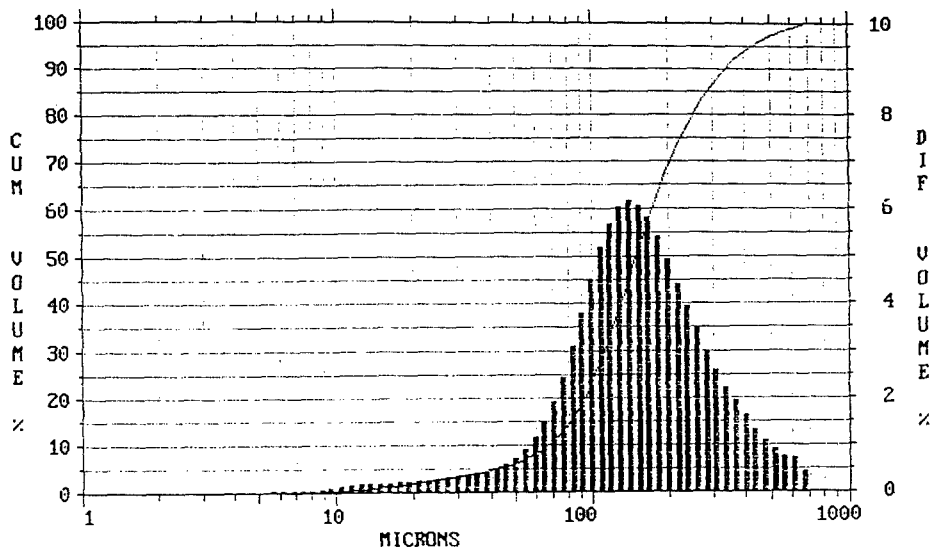
Figure 4. Particle size distribution of CL-20. The broad distribution of particle sizes typically obtained using the original two solvent crystallization method are shown above.

Figure 5. CL-20 crystals. Clearly visible in the photographs shown above is the poly-crystalline character of CL-20 produced by early crystallization techniques. Also visible are potential defects within the crystals.

Numerous alternate procedures were examined to address these three concerns without compromising the most important features of the current crystallization. Most significant among these are the reproducibility of forming ε-CL-20 and the careful removal of all acid species which dramatically affect sensitivity. The improved process has been demonstrated to afford the desired epsilon polymorph on a pilot scale. These modifications to the crystallization process also dramatically improved the particle shape of the HNIW prepared. Material prepared using an improved crystallization processes is not polycrystalline and has rounded edges (figure 6).
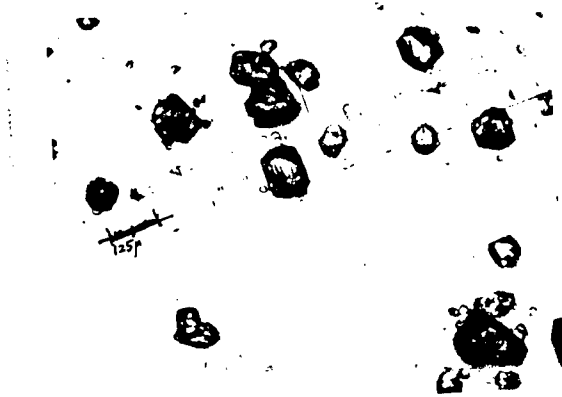
Figure 6. CL-20 crystals. Clearly visible in the photographs shown above is the improved crystal shape obtained in the current crystallization. This is in contrast to the polycrystalline nature of earlier crystals (figure 5).

Effective processing and formulating of CL-20 requires a variety of particle sizes as is the case with all other solid materials used as a significant percentage of solids in propellant, explosive and pyrotechnic formulations. Some control of particle size is possible during the crystallization process. To date, these processes have not been sufficiently reproducible to be viable pilot plant procedures. Nitramines such as HMX and RDX which are chemically and functionally similar to CL-20 are typically ground using fluid energy milling. Another common procedure includes particle size classification by sieving. In representative work done to achieve desired particle sizes, material was divided into large and small particle sizes.[a] Due to concerns with the impact and ESD sensitivity of CL-20, the processes were done with aqueous slurries of CL-20 rather than with dry material.

Two particle sizes were desired beside the "as prepared" from the crystallization: 1) a coarse fraction and 2) a fine fraction. The coarse fraction of CL-20 was obtained by mechanically separating the coarse particles mechanically. This was completed by a classification process which used an agitated screening set-up (SWECO). A single 100 mesh screen (149 microns) was used. The ε–CL-20 was slurried in water in a feed pot using a mechanical stirrer. It was fed to the screening system using a peristaltic pump. A coarse fraction typically has an average particle size of greater than 200 microns. A typical distribution is reproduced in figure 7.
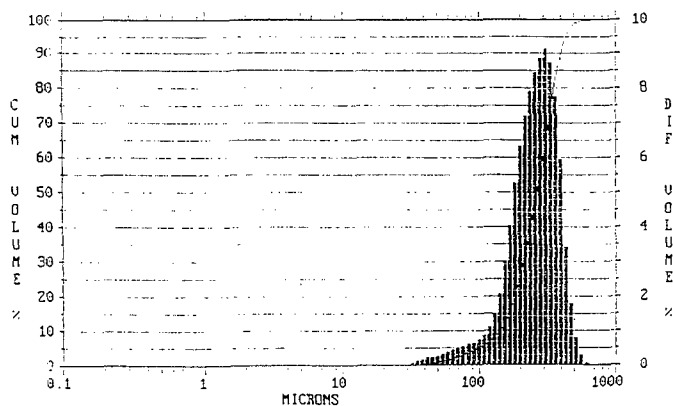
Figure 7. ε-CL-20 coarse fraction. Depicted above is the microtrac particle size distribution for the coarse fraction of CL-20 obtained by sieving. This distribution should be compared to a parent distribution presented in figure 4.

The material which passed through the screen was obviously considerably finer than the parent feedstock but with a typical average particle size of 35-50 microns was larger than desired for the fine fraction. Previous work at Thiokol had demonstrated that nitramines could be successfully ground in a standard fluid energy mill when water wet. This has been extended to CL-20.

As in the sieving, material was slurried in a feed pot and fed by a peristaltic pump into the fluid energy mill. The resulting ground material was largely collected in a collection pot although a dust collector was attached to catch any material which does not drop out of the air stream. Variations in the process can afford material from roughly 15 microns down to about 2-3 microns average particle size (figure 8). This size range adequately meets requirements for formulating.
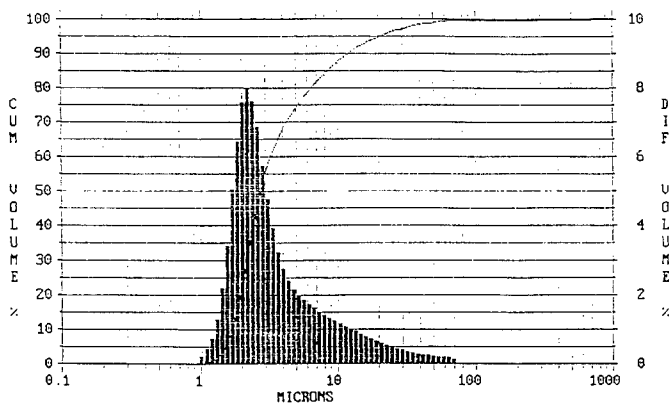
Figure 8. ε-CL-20 fine fraction. Depicted above is the microtrac particle size distribution for the fine fraction of CL-20 obtained by sieving. This distribution should be compared to the parent and coarse distributions presented in figures 4 and 7 respectively.

Safety Properties:

Comparison of standard safety test results for CL-20 which was polycrystalline and more recent rounded material shows small but consistent advantages in this material. The expected payoff will come with the material in formulation and in processing and shock sensitivity. These data are given in Table 3.

Table 3. CL-20 Sensitivity

	ε-CL-20 (polycrystalline)	ε-CL-20 (rounded)	HMX (20 micron)
Impact (in., 50%)	19.40	36.6	26.80
ABL Impact (cm, t.i.l.)	1.1-1.8	3.5	1.8
ABL Friction (lbs/@ ft/sec)	100 @ 4	100 @ 4	50-100 @ 4
ESD (J, 50%)	0.68	0.50	0.57

Perhaps more intriguing than the simple improvements in the measured safety properties are measurement of the bulk density of crystals prepared by the various crystallization methods. The bulk density of explosives has been correlated to the shock sensitivity of an explosive.[9] A method very similar to that described in the referenced paper was used to very accurately determine the effective bulk density. These data are given in Table X. It is of particular note to recognize the close correlation of the bulk density of the rounded material to the theoretical maximum (X-ray) crystal density. This demonstrates that very little further improvement in particle quality is possible since a bulk density of over 99.5% of X-ray measured crystal density has been achieved! This is an improvement compared to those cited for typical HMX and RDX as measured and reported recently.[9] This effectively explains the relative safety properties obtained in table 4.

Table 4. Bulk density measurements[10]

	Bulk Density (measured, g/ml)	Density (X-ray, g/ml)	% theoretical density
RDX	1.794-1.797	1.82	98.6-98.7
β-HMX	1.894-1.901	1.96	96.6-97.0
ε-CL-20	2.036	2.044	99.6

Initial Formulation:

HNIW compatibility with other propellant and explosive ingredients was tested by DSC of mixtures of ingredients to be tested. HNIW appears to be compatible with a wide range of standard ingredients including other nitramines, nitrate esters, azido polymers, PEG, HTPB, AP, AN, and standard curatives and catalysts. We have observed, however, an unexplained incompatibility with PBAN (CTPB has not been tested by us). Based on these initial compatibility results, formulation work was begun in both propellant (rocket and gun) and explosive applications. The general results have shown that the safety characteristics of the formulations prepared with HNIW are extremely similar to the baseline formulations but with the predicted

increase in energy content or ballistic performance. An example of the data obtained from a representative explosive formulation are given below (Table 5).

Table 5. Explosive Formulation

Composition	Nitramine (%)	Density(g/ml)	% TMD	Card Gap (in)	Pressure (kbar)
HMX/estane	93	1.75	96.0	+2.16/-2.19	17.5
CL-20/binder	93	1.93	97.2	+2.25/-2.31	15.3

Table 5. Test data for a representative explosive formulation compared to an HMX analog. The pressure listed is that required to initiate the CL-20 explosive as derived from the card gap value.

CONCLUSIONS

The caged nitramine HNIW first prepared by Nielsen has been produced on a pilot scale at Thiokol corporation at over 200 kg per batch. The material can be produced with relative ease at the pilot plant scale. Initial test results have shown that HNIW can be manipulated safely when proper precautions similar to those for other crystalline nitramines are taken. Formulation is also possible without undue risk. Ranges of performance are consistent with that predicted based on the chemical and physical characteristics of HNIW.

ACKNOWLEDGEMENTS

REFERENCES

1. a. Foltz, M.F., *Propellants, Explosives and Pyrotechnics,* **1994**, *19 (2)*, 63-69.
b. Foltz, M.F.; Coon, C.L.; Garcia, F.; Nichols, A.L. *Propellants, Explosives and Pyrotechnics,* **1994**, *19 (3)*, 133-44.

2. Nielsen, A.T.; Nissan, R.A.; Vanderah, D.J.; Coon, C.L.; Gilardi, R.D.; George, C.F.; Flippen-Anderson, J. *J. Org. Chem.*, **1990**, *55*, 1459.

3. Crampton, M.R.; Hamid, J.; Millar, R.; Ferguson, G. *J. Chem. Soc. Perkin Trans. 2*, **1993**, 923.

4. Bellamy, A.J. *Tetrahedron Letters*, **1995**, *51 (16)*, 4711-22.

5. Nielsen, A.T. "Synthesis of Polynitropolyaza Caged Nitramines," presented at the Office of Naval Research Workshop on Crystalline Energetic Materials Synthesis, 3-5 November 1986, printed in Chemical Propulsion Information Agency publication # 473, December 1987.

6. Kodama, Tomatsu *Japanese Patent 06,321,962*; 14 May 1993.

7. v. Holtz, E.; Ornellas, D.; Foltz, M.F.; Clarkson, J.E. *Propellants, Explosives and Pyrotechnics*, **1994**, *19 (4)*, 206-212.

8. Ostmark, H.; Bergmann, H,; Sjoberg, P. "Sensitivity and Spectroscopic Properties of the β- and ε-polymorphs of HNIW," presented at the ADPA International Symposium on Energetic Materials, Phoenix, Arizona, U.S.A., September 1995.

9. Borne, L. "Microstructure Effect on the Shock Sensitivity of Cast Plastic Bonded Explosives," presented at Europyro 95, 6th Congres International de Pyrotechnie du "Groupe de Travail de Pyrotechnie."

10. Values for X-ray densities were taken from "Explosives, 2nd Edition" by R. Meyer, Verlag Chemie, Weinheim, 1981. The measured values for HMX and RDX were taken from reference 9. The CL-20 value is from Richard Gilardi at the U.S. Naval Research Lab.

NENA-SPRENGSTOFFE

Hans-Heinrich Licht, Helmut Ritter und Bernd Wanders

| Institut Franco Allemand | **I.S.L.** | Deutsch-Französisches |
| de Recherches de Saint Louis | | Forschungsinstitut Saint Louis |

Postfach 1260, D-79574 Weil am Rhein 1

Zusammenfassung:

Zur Gruppe der Nitrato-ethyl-nitramine (NENA) gehören eine Reihe von brisanten Sprengstoffen. Der wichtigste und am besten untersuchte Vertreter dürfte DINA sein. NENA-Verbindungen mit niedrigem Schmelzpunkt - z.B. bei Raumtemperatur flüssige Stoffe - sind anwendungstechnisch interessante energetische Weichmacher. Allerdings ergeben sich daraus gewisse ungewöhnliche Eigenschaften von sicherheitstechnischer Bedeutung.
Wir haben neue NENA-Verbindungen mit heterocyclischem Grundkörper synthetisiert und erläutern den chemischen Hintergrund und die analytische Charakterisierung.
Schließlich werden gemessene Explosivstoff-Eigenschaften und Leistungsdaten verschiedener NENA-Verbindungen besprochen und mit Modellrechnungen verglichen.

Abstract:

Among the nitrato-ethyl-nitramines (NENA) are compounds with high explosive properties. An important and thoroughly tested NENA compound is DINA. Linear NENA molecules often have a low melting point or are liquid at ambient temperature. This fact makes this group interesting for an application as energetic plasticizers but is also responsable for an unusual behaviour under certain mechanical stress.
We have prepared new NENA compounds with heterocyclic structure. We explain the chemical background and describe the analytical characterization of these materials and their intermediates.
Finally we compare model calculations with measured explosive properties and performance data of several NENA compounds.

1. Einleitung

NENA-Verbindungen (Nitratoethylnitramine) sind durch die allgemeine Struktur-
formel $R-N(NO_2)-CH_2CH_2-O-NO_2$ gekennzeichnet, wobei die verbreitetsten
Vertreter Methyl-, Ethyl- und Butyl-NENA ebenso wie das durch seinen Energie-
inhalt besonders interessante DINA (das Dinitrat des Diethanolnitramins) eine
lineare Struktur aufweisen.

Diese Kombination aus Nitramin- und Salpetersäureestergruppen läßt ausgeprägte
Explosivstoff-Eigenschaften erwarten. Dabei wirkt sich die Nitratgruppe zwar
günstig auf die Sauerstoffbilanz aus, ist jedoch auch für die meist begrenzte
Temperaturstabilität dieser Verbindungen verantwortlich.

2. Synthese von NENA-Verbindungen

NENA-Verbindungen werden üblicherweise durch die Nitrierung von hydroxyethyl-
substituierten Aminoverbindungen hergestellt. So wird aus Diethanolamin **1** in
einem Reaktionsschritt durch die Einführung von drei Nitrogruppen das DINA **2**
erhalten /1/, und aus dem aus Formaldehyd und Aminoethanol zugänglichen Triazin-
derivat **3** /2/ entsteht durch Nitrierung unter teilweisem Ringabbau das N,N′-Bis(2-
nitratoethyl)-methylendinitramin BNE-MEDINA **4** /3/. Auch das 1,3-Bis(2-
hydroxyethylamino)-2,4,6-trinitrobenzol **5** läßt sich in eine NENA-Verbindung
umwandeln, wenngleich in Verbindung **6** noch eine nicht nitrierte N-H-Funktion
vorliegt /4/.
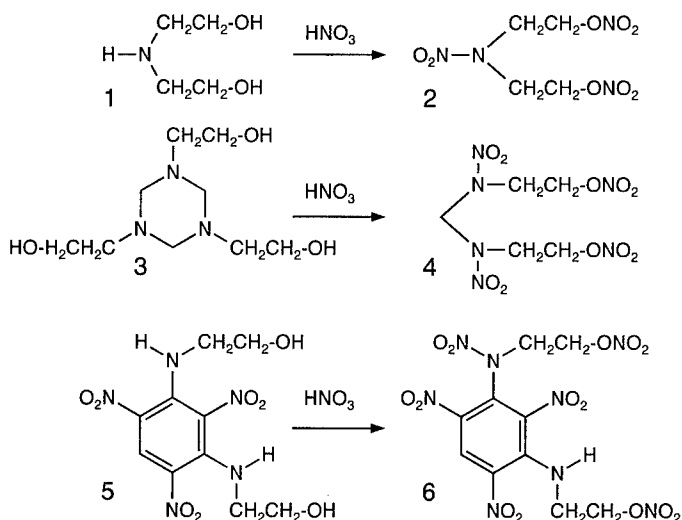
Ein alternatives Verfahren ist die Synthese von NENA-Verbindungen durch Addition von Distickstoffpentoxid N$_2$O$_5$ an substituierte Aziridine. So ergibt Cyanurchlorid **7** mit Aziridin das Tris(aziridyl)-triazin **8**, aus dem durch Umsetzung mit N$_2$O$_5$ das hochnitrierte Triazinderivat **9** entsteht /5/. Der Vorteil dieser Methode besteht in der Vermeidung von Teilnitrierungen wie im Falle des Trinitro-benzolderivats **6**.
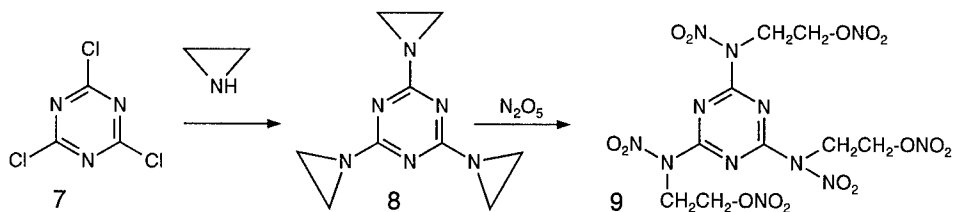
Wir wollten mit der Synthese neuer NENA-Verbindungen aus <u>Nitroheterocyclen</u> einige grundsätzliche Fragen zu Stabilität und Empfindlichkeit dieser Stoffklasse klären.

Durch die Umsetzung von 2-Chlor-3,5-dinitropyridin mit Aminoethanol wurde das Zwischenprodukt **10** erhalten, welches mit konz. Salpetersäure den Nitratester **11** ergab, während die Nitrierung unter Acetanhydrid-Zusatz zur NENA-Verbindung **12**, dem 2-(2-Nitratoethylnitramino)-3,5-dinitropyridin, führte.
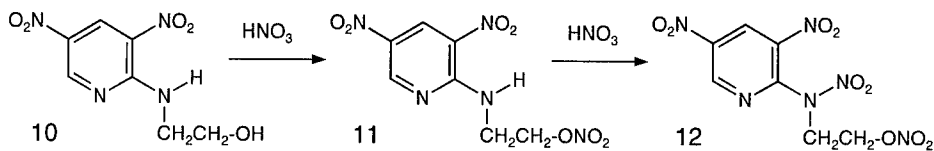
4,6-Dichlor-5-nitropyrimidin **13** ließ sich mit Aminoethanol bzw. Aziridin zu den Zwischenverbindungen **14** und **15** umsetzen. Dabei konnte das Diol **14** mit Salpetersäure nicht nitriert werden, ergab jedoch mit Distickstoffpentoxid N$_2$O$_5$ über die Zwischenstufe des Dinitrats **16** schließlich die gesuchte NENA-Verbindung **17**, das 4,6-Bis(2-nitratoethylnitramino)-5-nitropyrimidin. Auch durch Nitrierung des Diaziridyl-Derivats **15** mit N$_2$O$_5$ wurde Verbindung **17** erhalten.

O₂N — Cl / Cl — pyrimidine — **13** → O₂N — with aziridine groups — **15** ⟶ N₂O₅

13 → H,N–CH₂CH₂-OH / O₂N / H,N–CH₂CH₂-OH pyrimidine **14** — N₂O₅ → H,N–CH₂CH₂-ONO₂ / O₂N / H,N–CH₂CH₂-ONO₂ **16** — N₂O₅ → O₂N,N–CH₂CH₂-ONO₂ / O₂N / O₂N,N–CH₂CH₂-ONO₂ **17**
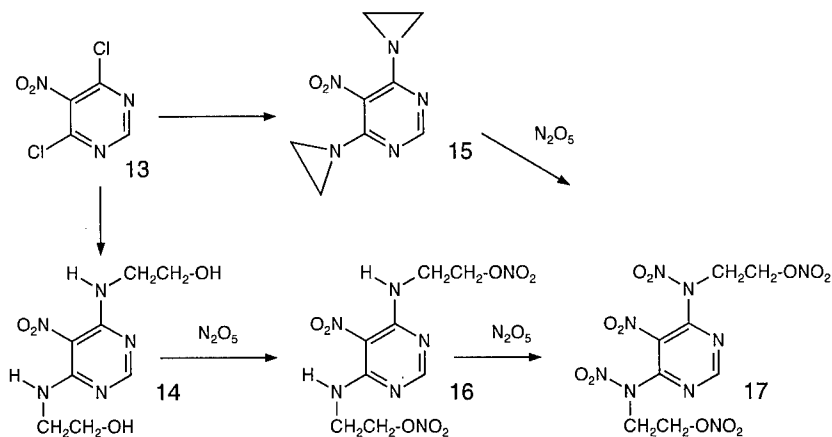
3. Spektroskopische Untersuchungen und Thermostabilität.

Die als Vorstufe zu NENA-Verbindungen anfallenden Hydroxyethylamino- und Nitratoethylamino-Verbindungen erlauben einige interessante Beobachtungen. Einerseits ergibt sich bei der Untersuchung der physikalischen Eigenschaften, daß allein das Vorhandensein von Nitratgruppen die thermische Stabilität noch nicht einschränkt. Erst das gleichzeitige Vorliegen von Nitrat- und Nitraminogruppen bewirkt eine Erniedrigung der exothermen Zersetzungstemperatur. Die Schmelz-punkte der heteroaromatischen Nitratoethylaminoverbindungen **11** und **16** erreichen allerdings nicht die bei analogen Benzolderivaten wie z.B. **6** gefundenen überraschend hohen Werte /4/.

Tab. 1: Schmelz- und Zersetzungspunkte von NENA-Verbindungen und Vorprodukten

VERBINDUNG	Schmelz-punkt (°C)	Zersetzungs-punkt (°C)
2-Hydroxyethylamino-3,5-dinitropyridin **10**	108	287
2-Nitratoethylamino-3,5-dinitropyridin **11**	73	193
2-Nitratoethylnitramino-3,5-dinitropyridin **12**	99	164
4,6-Bis(2-hydroxyethylamino)-5-nitro-pyrimidin **14**	170	257
4,6-Bis(2-nitratoethylamino)-5-nitro-pyrimidin **16**	---	162
4,6-Bis(2-nitratoethylnitramino)-5-nitro-pyrimidin **17**	87	154

In der ¹H-NMR-Spektroskopie zeigen die Hydroxyethylamino- und Nitratoethyl-amino-Verbindungen **10**, **11**, **14** und **16** ein interessantes Verhalten: Im Lösungsmittel d₆-Dimethylsulfoxid, das Austauschvorgänge von NH- und OH-Protonen verlangsamt, war stets die Wechselwirkung der CH₂CH₂-Gruppe mit

benachbarten NH- oder OH-Protonen zu erkennen, die sich in der Aufspaltung der NH- bzw. OH-Signale zu Tripletts und der CH$_2$-Signale zu Quadrupletts äußerte. Die Ausbildung einer H-Brücke zwischen der Nitrogruppe und einer Aminogruppe war bei dem Pyrimidinderivat **16** bei Raumtemperatur zu beobachten, ein Phänomen, das wir bereits bei einer Reihe von Aminodinitropyridinen beschrieben hatten /6/ und das zur Stabilität derartiger Verbindungen beiträgt.

4. Explosive Eigenschaften.
4.1 Mechanische Empfindlichkeit

Verglichen mit den klassischen Sprengölen Nitroglycerin Ngl und Diglykoldinitrat DEGN, die wegen ihrer Schlagempfindlichkeit als heikel gelten, machen die flüssigen NENA-Verbindungen Ethyl-NENA und Butyl-NENA einen gutartigen Eindruck: Sie sind nicht reibempfindlich, und unter dem Fallhammer sind sie meist weniger empfindlich als Hexogen (Tab. 2).

Tab. 2: Mechanische Empfindlichkeit von NENA-Sprengstoffen

Explosivstoff	Reib-Empfindlichkeit (kp)	Schlag-Empfindlichkeit (J)
Me-NENA		10
Et-NENA		10 (Zers.)
DINA	> 36	7.5
DEGN		0.2
Ngl	> 36	0.2
RDX	16	6.0

Ihr thermisches Verhalten ist ungewöhnlich: Obwohl sie sich beim Versuch einer Destillation kontinuierlich zersetzen, müssen die damit hergestellten Formulierungen nicht als thermisch instabil eingestuft werden. In Mischungen mit Nitrocellulose (NC) sind sie als Treibladungspulver stabil bis 200°C - wie RDX.

Diese Aussagen gelten auch für die bei Raumtemperatur kristallinen Vertreter Methyl-NENA und DINA. Hier muß allerdings eine Einschränkung gemacht werden. Beim Verpressen von DINA hatten wir einen Zwischenfall: Es trat dabei eine Detonation mit Zerlegung der Form auf. Eine Nachprüfung der Schlag-empfindlichkeit erbrachte ein ungewöhnliches Ergebnis.

Bei der Untersuchung mit dem Fallhammer werden unterschiedliche Resultate für DINA gefunden, wenn die Probe auf die Prüfrolle (Walze) des Fallhammer-Probenhalters zentriert oder am Rand verteilt eingebracht wurde :

normal | am Rand | zentriert
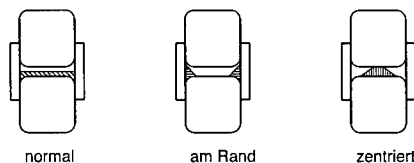
Die Anwendung dieser Prüfung auf andere Sprengstoffen ergibt eine überraschende Serie: Man beobachtet zwei verschiedene Klassen von Explosivstoffen: Eine Gruppe, die bei Probeneinbringung am Rand empfindlicher ist, und eine zweite, die die größere Schlagempfindlichkeit bei zentrierter Plazierung aufweist. Die wesentliche Eigenschaft, die die beiden Gruppen unterscheidet, ist, wie wir vermutet hatten und durch diese Versuchsreihe zeigen wollten, der niedrige Schmelzpunkt der einen und der "normale" der anderen Gruppe. Wir glauben heute, daß niedrig schmelzende Explosivstoffe beim Verpressen schmelzen können, dabei in den Spalt zwischen Stempel und Formrand gedrückt und so extremen - zur Detonation führenden - Scherbeanspruchungen unterworfen werden (s. Anhang).

Zur Verbesserung der Handhabbarkeit im Falle des DINA bot es sich an, unsere Erfahrungen der Verarbeitung des DINA in Treibladungspulvern (TLP) zu berücksichtigen: NC vermag große Mengen an DINA zu einem Gel mit - wie bei TLP üblich - reduzierter Detonierbarkeit zu binden. Eine Menge von 2.5 % NC und 2.5 % Et-NENA reichte, um die Eigenschaften dieses "DINA-Dynamits" drastisch zu verändern: Es hatte nicht nur eine geringere Schlagempfindlichkeit; es zeigte auch das Verhalten eines "hoch" schmelzenden Explosivstoffs, indem es jetzt nicht mehr bei Einbringung am Rand empfindlicher reagierte als bei zentrierter Probenanordnung

Hier sei auf ähnliche Untersuchungen an flüssigen Sprengstoffen hingewiesen, die französische Kollegen im Rahmen dieser Konferenz 1994 vorgestellt hatten /7/.

Mit einem Gaspyknometer wurde die Kristalldichte ρ und aus kalorimetrischen Messungen der Verbrennungswärmen die Standardbildungsenthalpie $\Delta H_f°$ ermittelt. Die thermische Stabilität wurde aus der DTA/TG-Registrierung bei linearer Aufheizung (6°C/min) als Verpuffungstemperatur beschrieben. Bei der Reib- und Schlagempfindlichkeit wird der Wert angegeben, der zur ersten Reaktion des Stoffs führt (Tab. 3).

Tab. 3: Physikalische Daten von NENA-Verbindungen

Verbindung	ρ (g/cm^3)	$\Delta H_f°$ (kcal/mol)	Schmelz-punkt (°C)	T_{ex} (°C)	Reibapparat (kp)	Fallhammer (N m)
Py-NENA	1.74	- 1.5	99	164	> 36	6.0
Pm-NENA	1.81	- 1.99	87	154	> 36	2.5
BNE-MEDINA	1.72	- 59.95	92	201	> 36	4.0

Es ist festzustellen, daß die hochnitrierten heterocyclischen Verbindungen - besonders die Pyrimidin-Verbindung - vergleichsweise recht empfindlich und, was nicht überraschen kann, nur begrenzt thermisch stabil sind.

4.2 Leistung der NENA-Sprengstoffe.

Eine Leistungsabschätzung der hier behandelten Explosivstoffe wurde mit den Modellen von ROTHSTEIN /8/ bzw. KAMLET & JACOBS /9/ vorgenommen. Die erhaltenen Werte für Detonationsgeschwindigkeit D, GURNEY-Energie $\sqrt{2}E_G$ und Chapman-Jouguet-Druck P_{CJ} sind in Tabelle 4 angegeben.

Tab. 4 : Berechnete Leistungsdaten von NENA-Verbindungen

Verbindung	ρ (g/cm^3)	D /8/ (m/s)	D /9/ (m/s)	$\sqrt{2}E_G$ /9/ (mm/µs)	P_{CJ} /9/ (kbar)
Py-NENA 12	1.74	7985	7973	2.68	276
Pm-NENA 17	1.81	8364	8423	2.80	316
DINA 2	1.67	7936	8282	2.82	291
DINA 2	1.61		8078	2.78	270
BNE-MEDINA 4	1.72	8266	8451	2.85	308

Nach dem ROTHSTEIN-Modell wird Pm-NENA 17, nach KAMLET & JACOBS BNE-MEDINA 2 als brisantester Sprengstoff vorhergesagt.

Die gute Zugänglichkeit des DINA erlaubte es, zylindrische Ladungen des Durchmessers 16 mm herzustellen und daran Detonationsgeschwindigkeit D und GURNEY-Energie $\sqrt{2}E_G$ zu messen.

Tab. 5: Gemessene Leistungsdaten von DINA 2

Formulierung	Δ (g/cm^3)	D (m/s)	$\sqrt{2}E_G$ (mm/µs)
DINA 95 / NC 2.5 / Et-NENA 2.5 %.	1.61	7665	2.83

Die Resultate übertreffen hinsichtlich der ballistischen Leistung (Gurney-Konstante) noch die Berechnung. Das überrascht, da die Detonationsgeschwindigkeit - auch bei Berücksichtigung der vergleichsweise niedrigen Ladedichte Δ - hinter den Erwartungen zurückbleibt.

5. Verwendung von NENA-Verbindungen als Weichmacher

Der niedrige Schmelzpunkt aliphatischer NENA-Verbindungen erlaubt ihre Verwendung als energetische Lösungsmittel und energetische Weichmacher. Nach Auflösung eines Kunststoffs in einer flüssigen NENA-Verbindung erhält man die Grundmasse für einen plastischen Sprengstoff. Ein energetischer NENA-Weichmacher vermag NC zu gelatinieren und damit die Sprengöle Nitroglycerin und Diglykoldinitrat in TLP zu ersetzen. Das Ergebnis sind alternative zweibasige Treibladungspulver. Über diese Arbeiten haben wir an anderer Stelle berichtet /10/.

Hier seien noch unsere Versuche, NENA-Sprengstoffe als Weichmacher in Formulierungen für gießbare PBX einzusetzen, erwähnt. In der Rezeptur für einen kunststoffgebundenen Sprengstoff aus Oktogen, Polybutadien mit Hydroxyl-Endgruppen und Isophorondiisocyanat (HMX / HTPB / IPDI) hatten wir den klassischen Weichmacher Dioctylphthalat (DOP) gegen eine Mischung aus Me-NENA und DINA 1/1 ausgetauscht. Trotz des scheinbar geringfügigen Anteils von nur 3 % sollte sich diese Veränderung nach einer theoretischen Abschätzung in einer durchaus meßbaren Erhöhung der Detonationsgeschwindigkeit von mehr als 200 m/s auswirken (Tab. 6)

Tab. 6 :   Leistungsdaten für kunststoffgebundene Sprengstoffe

Sprengstoff	Detonationsgeschwindigkeit - berechnet - (Ladedichte)	Detonationsgeschwindigkeit - gemessen - (Ladedichte)
Formulierung A HMX 85, HTPB 11, IPDI 1, DOP 3	**7989 m/s** (1.56 g/cm³)	**7831 m/s** (1.56 g/cm³)
Formulierung B HMX 85, HTPB 11, IPDI 1, Me-NENA 1.5, DINA 1.5	**8213m/s** (1.56 g/cm³)	**7847 m/s** (1.39 g/cm³)

Die mit den NENA-Weichmachern hergestellte Ladung bestätigte diese Abschätzung insofern, als die gleiche Detonationsgeschwindigkeit wie für die Referenz-Formulierung bei einer (wegen hoher Porosität) deutlich niedrigeren Ladungsdichte gemessen wurde.

6. Literatur

/1/ G. DESSEIGNE, Mém.Poudres **XXXII**, 117 (1950)

/2/ P.A. LAURENT, Bull.Soc.Chim.France **1967**, 571

/3/ A.N.GAFAROV, L.N.PUNEGOVA, G.A.MARCHENKO, S.S.NOVIKOV, Russ.J.Org.Chem. **15**, 1181 (1979)

/4/ M. SITZMANN, US-Patent **5, 081, 255** (1992)

/5/ R.W. MILLAR, N.C.PANE, D.H.RICHARDS, P.BUNYAN, P.GOLDING, J.A.ROWLEY, Prop.Expl.Pyrotechn. **18**, 55 (1993)

/6/ H. RITTER, M. KAISER , Magn.Res.Chem. **31**, 364 (1993)

/7/ D. LEMOINE, H. CHERIN, P. JOLIBOIS, Proc. 25th Internat.Ann.Conf. of ICT **1994**, 81-1

/8/ L.R. ROTHSTEIN, R. PETERSEN, Prop.Expl..**4**, 56 (1979)

/9/ M.J. KAMLET, S.J. JACOBS, J.Chem.Phys. **48**, 23 (1968)

/10/ H.H. LICHT, H. RITTER, 6e Congrès Internat. de Pyrotechnie **1995**, Tours (EUROPYRO 95), 39

7. Anhang

Schlagempfindlichkeit von Explosivstoffen (J) beim Fallhammertest

- Einfluß der Anordnung
  der Proben

normal   am Rand   zentriert
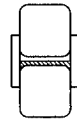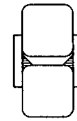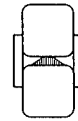
		normal	am Rand	zentriert
Nitromethan (NM) **Schmp.: - 29°**	*1.Reaktion* *50 %*	> 25.0	6.0 6.44 ± 0.10	> 25.0
Methyl-NENA (Me-NENA) **Schmp.: 36°**	*1.Reaktion* *50 %*	25.0	22.5 24.6	> 25.0
Trinitroethylbenzol (TNEB) **Schmp.: 38°**	*1.Reaktion*	> 25.0	25.0	> 25.0
DINA **Schmp.: 52°**	*1.Reaktion* *50 %*	7.0	3.0 3.9 ± 0.12	6.5 6.9 ± 0.11
DINA-Dynamit (DINA/NC)	*1.Reaktion* *50 %*	7.0	7.5 10.7 ± 0.66	10.0 10.9 ± 0.46
Erythrittetranitrat (ETN) **Schmp.: 61°**	*1.Reaktion* *50 %*		2.5 3.6 ± 0.16	4.5 5.0 ± 0.14
TNT **Schmp.: 81°**	*1.Reaktion* *50 %*		22.5 24.4 ± 0.41	15.0 21.1 ± 0.91
Tetryl **Schmp.: 130°**	*1.Reaktion* *50 %*		5.5 7.85 ± 0.65	17.5 19.2 ± 0.93
PETN, 50-200µ **Schmp.: 141°**	*1.Reaktion* *50 %*	5.0	5.5 11.9 ± 0.81	4.5 5.3 ± 0.13
Hexogen, 150-200µm (RDX) **Schmp.: 203°**	*1.Reaktion* *50 %*		22.5 23.75 ± 1.25	7.5 10.5 ± 0.73
Oktogen,<100µm (HMX)	*1.Reaktion* *50 %*		7.5 10.0 ± 0.47	5.0 6.2 ± 0.3
Oktogen,< 40µm (HMX)	*1.Reaktion* *50 %*	3.5 4.0		

A NEW SYNTHESIS OF TATB USING INEXPENSIVE STARTING MATERIALS AND MILD REACTION CONDITIONS*

Alexander R. Mitchell, Philip F. Pagoria and Robert D. Schmidt
Lawrence Livermore National Laboratory, Energetic Materials Center,
Livermore, California 94550, USA

Abstract

1,3,5-Triamino-2,4,6-trinitrobenzene (TATB) is currently manufactured in the USA by nitration of the relatively expensive and domestically unavailable 1,3,5-trichlorobenzene (TCB) to give 2,4,6-trichloro-1,3,5-trinitrobenzene (TCTNB) which is then aminated to yield TATB. Elevated temperatures (150 °C) are required for both reactions. There is a need for a more economical synthesis of TATB that also addresses current environmental issues. We have recently discovered that 1,1,1-trimethylhydrazinium iodide (TMHI) allows the amination of nitroarenes at ambient temperature via Vicarious Nucleophilic Substitution (VNS) of hydrogen. TMHI reacts with 2,4,6-trinitroaniline (picramide) in the presence of strong base (NaOMe or t-BuOK) to give TATB in over 95% yield. TMHI and picramide can be obtained from either inexpensive starting materials or surplus energetic materials available from demilitarization activities. TMHI, for example, is obtained from the reaction of methyl iodide with 1,1-dimethylhydrazine (unsymmetrical dimethylhydrazine, UDMH). UDMH (30,000 metric tons) is currently available in the former Soviet Union as a surplus rocket propellant. Transition of the new TATB synthesis from the laboratory to the pilot plant is projected.

Introduction

The objective of this program is to provide a convenient and relatively inexpensive preparation of 1,3,5-triamino-2,4,6-trinitrobenzene (TATB). TATB is a reasonably powerful high explosive whose thermal and shock stability is considerably greater than that of any other known material of comparable energy.[1] It is used in military applications because of its significant insensitivity to thermal and shock environments. There is also interest in employing TATB in the civilian sector for deep oil well explorations where heat-insensitive explosives are required. TATB had been priced at $20 to $50 per pound when it was being produced on an industrial scale in the U.S. TATB is currently available to customers outside of the Department of Energy (DOE) for $100 per pound.[2] This paper describes a new synthesis of TATB developed at Lawrence Livermore National Laboratory (LLNL) that utilizes inexpensive starting materials and mild reaction conditions.

Current Preparation of TATB

TATB is produced in the USA by nitration of the relatively expensive and domestically unavailable 1,3,5-trichlorobenzene (TCB) to give 2,4,6-trichloro-1,3,5-trinitrobenzene (TCTNB) which is then aminated to yield TATB (Scheme 1).[3] Elevated temperatures (150 °C) are required for both reactions. The major impurity encountered in this process is ammonium chloride. The inclusion of
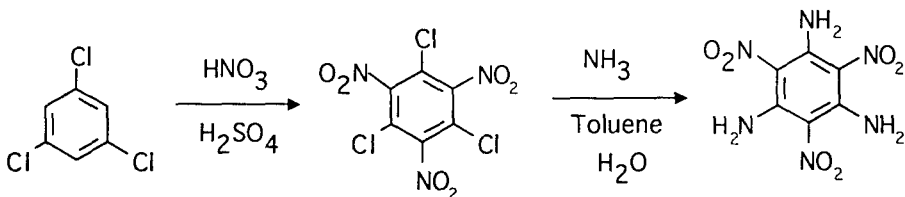
Scheme 1. Current synthesis of TATB.

2.5% water during the amination step significantly reduces the ammonium chloride content of the TATB.[4] Low levels of chlorinated organic impurities have also been identified. These impurities include 2,4,6-trichloro-1,3,5-

trinitrobenzene (TCTNB), 1,3-dinitro-2,4,5,6-tetrachlorobenzene, 1,3-dinitro-2,4,6-trichlorobenzene and their partially aminated products.[5]   A synthesis of TATB that replaces TCTNB with a non-chlorinated starting material is clearly desirable.

Vicarious Nucleophilic Substitution of Hydrogen

Vicarious nucleophilic substitution (VNS) of hydrogen is a well-established procedure for the introduction of carbon nucleophiles into electrophilic aromatic rings.[6,7] The reaction involves the addition of a carbanion bearing a leaving group (X) to an electrophilic aromatic ring and subsequent rearomatization by loss of the leaving group through elimination as HX (Scheme 2, Z=CH_2). This reaction has been applied to a wide variety of nitroarenes and nitro-substituted heterocycles.[7]

$Z = CH_2, NH$
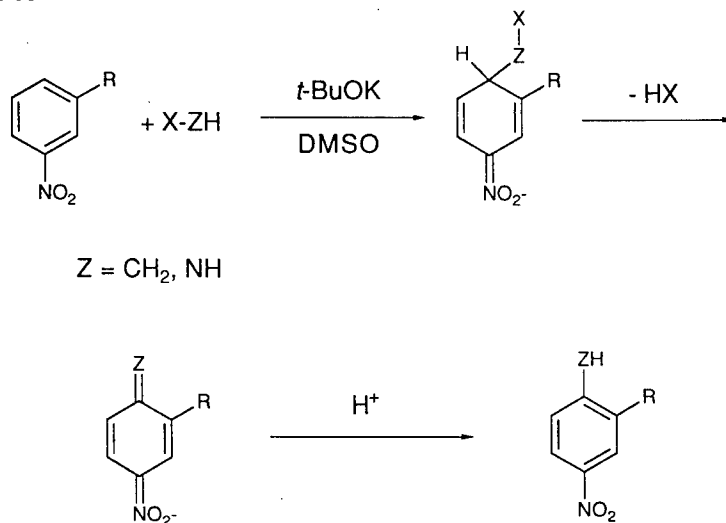
Scheme 2. Vicarious nucleophilic substitution of hydrogen.

By analogy, VNS reactions can also take place with amine nucleophiles. Such reagents are of the common form X-NH_2, where X is an auxiliary group capable of stabilizing a negative charge, thus driving rearomatization of the σ-

intermediate adduct (Scheme 2, Z=NH). One of the first examples of amination by VNS of hydrogen was provided by Meisenheimer and Patzig who reacted 1,3-dinitrobenzene with hydroxylamine in the presence of strong base to yield 2,4-dinitrophenylene-1,3-diamine.[8] Recently, a number of more active aminating reagents such as 4-amino-1,2,4-triazole[9] and substituted sulfenamides[10] have been developed. These reagents were designed to be good nucleophiles that easily add to electrophilic aromatic rings and also possess good leaving groups (Scheme 2, X)

Use of 1,1,1-Trimethylhydrazinium Iodide as a VNS Reagent

Although quaternary hydrazinium compounds have been known for over one hundred years,[11,12] they have not been employed as VNS reagents. We examined 1,1,1-trimethylhydrazinium iodide (TMHI)[13] [$(CH_3)_3N^+-NH_2$ I^-] for use as a VNS reagent. We reasoned that TMHI would be sufficiently nucleophilic to substitute into nitro-substituted aromatic rings but would be superior to the previous examples because the leaving group would be the neutral trimethylamine instead of a stabilized anionic species. In addition, there is a possibility that the hydrazinium halide would react with base to form the neutral ylide species, [$(CH_3)_3N^+-NH^-$], which may be the reactive species in the amination process. Indeed, when TMHI was reacted with various nitro-substituted aromatics the amino functionality was introduced in good to excellent yields. We found that the number of amino-groups which may be added to the electrophilic aromatic ring is equal to the number of nitro groups present on the ring.

A study of product yields and distribution of various 3-substituted nitrobenzene derivatives was performed using TMHI (Scheme 3) (Table 1).[14] The results of our study were compared with the findings reported for 4-amino-1,2,4-triazole (ATZ).[9] ATZ was found to be regioselective, giving substitution exclusively para-to the nitro group. TMHI gave all possible product isomers thereby showing no selectivity but presumably greater reactivity. There was a general tendency for TMHI to yield products in which the amine substitution occurs ortho- to the nitro group as the major components although some exceptions were noted. We are
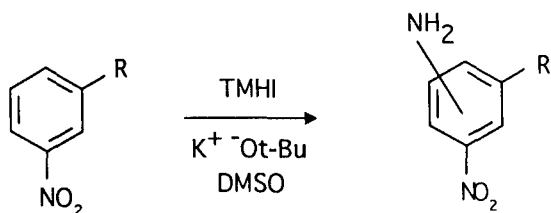
Scheme 3. Amination of 3-substituted nitroaromatics.

currently investigating the use of more sterically crowded 1,1,1-trialkylhydrazinium halides derived from UDMH in an attempt to influence the regioselectivity of the aminating reagent.

Table I. Amination of 3-Substituted Nitrobenzenes

R	Total Yield (%)	position of NH_2[a]	% isomer
H	85	2	61
		4	39
CH_3	84	2	38
		4	35
		6	27
Cl	82	2	32
		4	49
		6	19
COOH	95	4	71
		6	29
OCH_3	66	2	90
		4	10
F	84	2	45
		4	47
		6	8
I	76	2	45
		4	38
		6	17
CN	41	2	20
		4	44
		6	36

[a] Relative to NO_2

Starting Materials for TATB Synthesis

This project originally began as part of demilitarization activities related to the chemical conversion of energetic materials into higher value products.[15,16] Consequently, our synthesis of TATB has been designed so that either surplus energetic materials or inexpensive, commercially available chemicals can be used to make the necessary starting materials. Several million pounds of ammonium picrate (Explosive D) are available for disposal in the USA. Ammonium picrate can be converted to 2,4,6-trinitroaniline (picramide) by the pathways shown in Scheme 4. The reaction of picric acid with urea at elevated temperature (173 $^{\circ}$C) has been reported to provide picramide in 88% yield.[17] The analogous reaction of Explosive D with urea to directly provide picramide has not been reported. Picramide is also readily accessible from nitration of the commercially available and relatively inexpensive 4-nitroaniline[18].
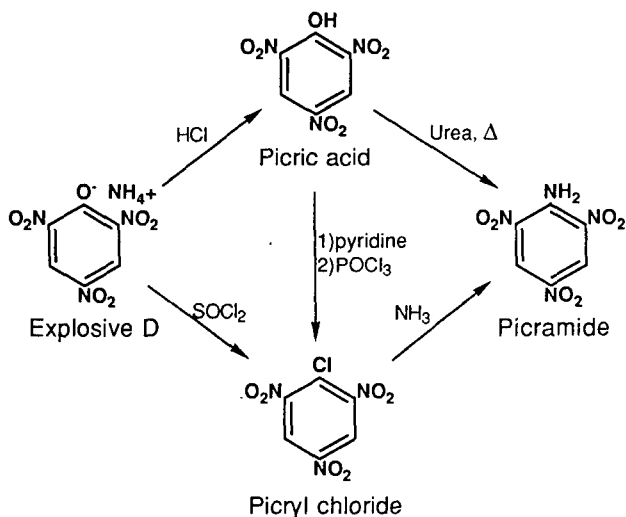
Scheme 4. Synthesis of picramide from Explosive D.

1,1-Dimethylhydrazine (unsymmetrical dimethylhydrazine, UDMH) has been used as a liquid rocket propellant. Thirty thousand metric tons of UDMH in Russia are available for disposal in a safe and environmentally responsible manner.[19] 1,1,1-trimethylhydrazinium iodide (TMHI), our VNS reagent of choice,

is readily prepared through the alkylation of UDMH by methyl iodide.[20] Alternatively, TMHI can be prepared directly from hydrazine and methyl iodide.[13]

Amination of Picramide by Hydroxylamine Derivatives

We initially explored the conversion of picramide to DATB and TATB using hydroxylamine (Scheme 5, R = H) and aqueous base as reported for the conversion of 4,6-dinitrobenzofuroxan (DNBF) to give 5,7-diamino-4,6-dinitrobenzofuroxan (CL-14).[21] DATB was obtained in a low yield (16%) after removal of unreacted picramide.

| Picramide | DATB | TATB |
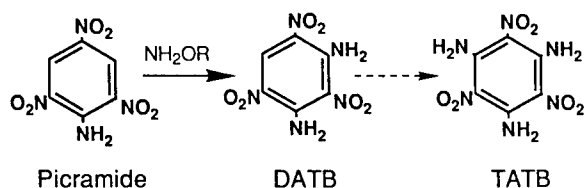
Scheme 5. Reaction of picramide with NH_2OR (R = H, CH_3, $C_6H_5CH_2$)

The replacement of aqueous base with sodium methoxide in anhydrous methanol or DMSO raised the yield of DATB from 16% to over 50%. The use of alkoxy derivatives (R = CH_3, $C_6H_5CH_2$) gave exclusively DATB in 87-91% crude yields. The reaction of picramide with hydroxylamine or its O-alkyl derivatives never yielded more than trace quantities of TATB.

Amination of Picramide by ATZ

Picramide reacts with 4-amino-1,2,4-triazole (ATZ) in dimethylsulfoxide in the presence of strong base (NaOMe or KOt-Bu) at room temperature (24 h) to yield, depending on the quantity of ATZ used, either DATB or TATB and 1,2,4-triazole (TZ) (Scheme 6).
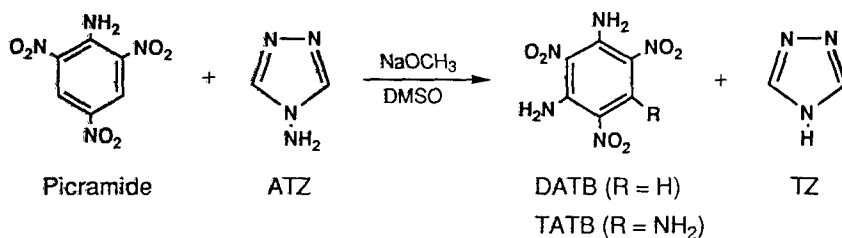
Scheme 6. Reaction of picramide with ATZ.

Amination of Picramide by TMHI

When TMHI replaces ATZ in the reaction with picramide, the reaction is complete in 3 h to yield DATB (70-80%) or TATB (95-98%) and trimethylamine (TMA) (Scheme 7).
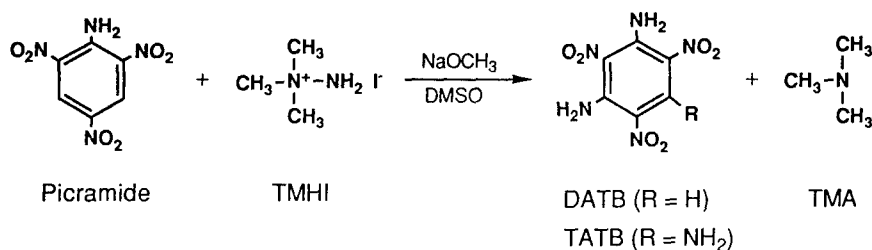
Scheme 7. Reaction of picramide with TMHI.

The TMA released can be used to regenerate the TMHI that is consumed during the reaction. The reaction of TMA with chloramine ($ClNH_2$) yields trimethylhydrazinium chloride (TMHCl) which is treated with hydroiodic acid to yield TMHI (Scheme 8).[22]
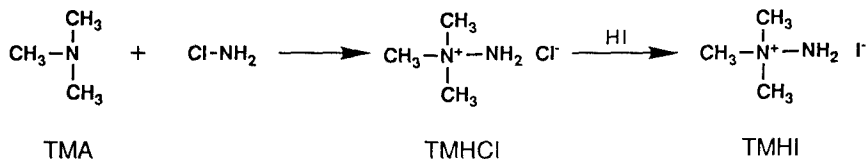
Scheme 8. Conversion of TMA to TMHI.

The use of TMHCl for nucleophilic aminations of nitroarenes is under investigation.

Summary

The new synthesis of TATB that we intend to scale up from the laboratory bench to pilot plant is outlined in Scheme 9. The starting materials are relatively inexpensive and can be obtained from demilitarization programs (Explosive D, UDMH) or commercial sources (4-nitroaniline, hydrazine). We have eliminated
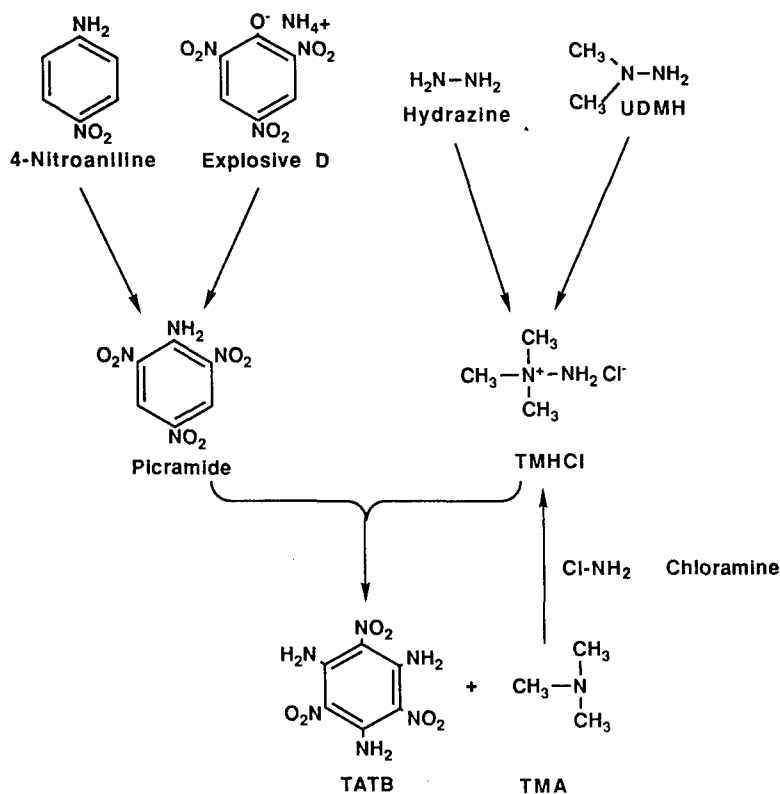
Scheme 9. Synthesis of TATB from inexpensive starting materials.

the use of chlorinated arenes in response to environmental concerns and will recycle solvents and materials whenever possible.[23] Trimethylamine, a noxious and moderately toxic gas (bp 3 °C) released during the VNS reaction, will be reacted with chloramine to regenerate the TMHCl consumed in the synthesis of TATB.

References

1. S. F. Rice and R. L. Simpson, "The Unusual Stability of TATB: A Review of the Scientific Literature", Lawrence Livermore National Laboratory, Livermore, CA, Report UCRL-LR-103683 (July, 1990).

2. R. L. Simpson, Energetic Materials Center, Lawrence Livermore National Laboratory, personal communication.

3. T. M. Benziger, "Manufacture of Triaminotrinitrobenzene," in *Chemical and Mechanical Technologies of Propellants and Explosives, Proc. 1981 Intl. Annual Conference of ICT*, Karlsruhe, Germany, 1981, p. 491.

4. T. M. Benziger, *Method for the Production of High-Purity Triaminotrinitrobenzene*, U. S. Patent No. 4,032,377 (1977).

5. S. K. Yasuda, "Identification of 1,3,5-Triamino-2,4,6-Trinitrobenzene Impurities by Two-Dimensional Thin-Layer Chromatography," *J. Chromatogr.*, **71**, 481 (1972).

6. M. Makosza and J. Winiarski, "Vicarious Nucleophilic Substitution of Hydrogen," *Acc. Chem. Res.*, **20**, 282 (1987).

7. O. N. Chupakhin, V. N. Charushin and H. C. van der Plas, *Nucleophilic Aromatic Substitution of Hydrogen*, Academic Press, San Diego, CA, 1994, pp. 59-66.

8. J. Meisenheimer and E. Patzig, "Directe Einführung von Aminogruppen in den Kern aromatischer Körper", *Ber.*, **39**, 2533 (1906).

9. A. R. Katritzky and K. S. Laurenzo, "Direct Amination of Nitrobenzenes by Vicarious Nucleophilic Substitution," *J. Org. Chem.*, **51**, 5039 (1986).

10. M. Makosza and M. Bialecki, "Amination of Nitroarenes with Sulfenamides via Vicarious Nucleophilic Substitution of Hydrogen," *J. Org. Chem.*, **57**, 4784 (1992).

11. E. Fischer, "Über aromatische Hydrazinverbidungen," *Ber.*, **9**, 880 (1876).

12. H. H. Sisler and G. Omietanski, "The Chemistry of Quaternized Hydrazine Compounds," *Chem. Rev.*, **57**, 1021 (1957).

13. C. Harries and T. Haga, "Über die Methylirung des Hydrazinhydrats," *Ber.*, **31**, 56 (1898).

14. P. F. Pagoria, A. R. Mitchell and R. D. Schmidt, "1,1,1-Trimethylhydrazinium Iodide (TMHI): A Novel, Highly Reactive Reagent for Aromatic Amination via Vicarious Nucleophilic Substitution (VNS)", *J. Org. Chem.*, in press.

15. C. O. Pruneda, A. R. Mitchell, and J. Humphrey, "Reusing the High Explosives from Dismantled Nuclear Weapons," *Energy and Technology Review*, LLNL, Livermore, CA, UCRL-52000-93-11·12 (1993), p.19.

16. A. R. Mitchell and R. D. Sanner, "Chemical Conversion of Energetic Materials to Higher Value Products," in *Energetic Materials- Insensitivity and Environmental Awareness, Proc. 24th Intl. Annual Conference of ICT*, H. Ebeling, Ed., Karlsruhe, Germany, 1993, p. 38.

17. E. Y. Spencer and G. F. Wright, "Preparation of Picramide," *Can. J. Research*, **24B**, 204 (1946).

18. A. F. Holleman, "1,3,4,5-Tetranitrobenzene," *Rec. trav. chim.*, **49**, 112 (1930).

19. *Chemical and Engineering News*, p.21 (May 8,1995).

20. O. Westphal, "Über die Alkylierung des Hydrazins," *Ber.*, **74**, 759 (1941).

21. W. P. Norris and A. P. Chafin, "CL-14, A New Dense, Insensitive, High Explosive," Naval Weapons Center, China Lake, CA, NWC TP 6597 (publication UNCLASSIFIED), May 1985.

22. G. M. Omietanski and H. H. Sisler, "The Reaction of Chloramine with Tertiary Amines. 1,1, 1-Trisubstituted Hydrazinium Salts," *J. Am. Chem. Soc.*, **78**, 1211 (1956).

23. T. E. Graedel and B. R. Allenby, *Industrial Ecology*, Prentice Hall, Englewood Cliffs, NJ, 1995.

Nitrofurazanyl Moiety as an Alternative to Picryl One for High Energetic Material Construction

Aleksei B. Sheremetev and Tatyana S. Pivina

ND Zelinsky Institute of Organic Chemistry, Russian Academy of Sciences,
47, Leninsky Prosp, Moscow 117913, RUSSIA
Fax*: +7 095 135 5328;* ***E-mail****: shab@nmr1.ioc.ac.ru*

In the field of energetic materials the compounds possessing picryl (**Pic**) moiety are well-known. Evident advantages of these compounds are comparable high energy content, molecular crystal density and thermal stability. To prepare more powerful compounds a search for high effective building blocks in construction of target structures is required.

This study has been aimed at synthesis and investigation of some physico-chemical properties for the set of compounds containing nitrofurazanyl (**Nif**) moiety in place of picryl one. Estimation of advantages and shortages of the new series of compounds as opposed to picryl analogs has been carried out.

The results of the study have indicated that compounds contained the **Nif** moiety possess more high energy and molecular crystal density than their **Pic** analogs, that provide more high values of detonation velocity and some other detonation and combustion characteristics of nitrofurazans (**NF**). Novel assemblage of properties inherent for **NF** makes the family of compounds attractive subject for comprehensive investigation.

INTRODUCTION

The path is thorny and complicated from design of new high energetic material (**HEM**) to its manufacture. It involves variety of steps and requires large expenditures. The first and very likely the central point of the process is screening - a systematical "sifting" of chemical compounds through "sieve" of special tests. As usual such work is aimed at the search for more powerful and stable compounds.

Explosive performance has been known to depend upon a number of molecular parameters.[1] The basic parameters are density d, the heat of formation ΔH_f, "oxidant balance" OB_{100}, and nitrogen content $N\%$. Thus, detonation velocity D_v and Chapman-Jouget (detonation) pressure P_{CJ} depend upon d and ΔH_f, and impact sensitivities of energetic materials to a certain extent center around OB_{100}. One of ways to raise the power of **HEM** is increasing heat of detonation Q_{ex} and improvement of detonation product compositions. Both a positive heat of formation and high-nitrogen content of energetic materials are very favorable for the purpose. It should be noted that nitrogen is to some extend "the ideal working body" in high temperature processes being low-molecular-weight gas not dissociating while burning and explosion.

Only very small part of the screening compounds turns out to be valuable so the desire to learn to construct **HEM** is quite plainly, namely to search the compounds rationally minimizing the trial-and-error method. The basis for **HEM** construction is combination of experimental theoretical, and empirical knowledge about different group and moiety influences on the properties of compound involving them.

Utilized methods of computer molecular design and screening of structures with desired set of properties plays a significant role in optimizing extremely prolonged and expensive stage of high-volume synthesis and experimental property determination of new compounds. From the set of database it is possible to reveal structure-property relationships, to obtain corresponding models determining these relationships and allowing hereinafter to estimate the perspective of the structures previous to their preparation.

As part of our program on the synthesis and structure of compounds containing furazan ring,[2] we tried to reveal analogies and varieties between two series of compounds, namely picryl derivatives (**Pic-R**) and their nitrofurazanyl (**Nif-R**) analogs.
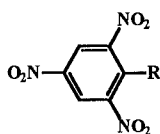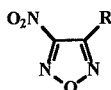
Pic-R   **Nif-R**

We report these results here including the calculated data of some predicted molecules.

WHY THE FURAZAN?

The furazan ring as key building block was used in this work not accidentally. At first, aromaticity of the ring induce increased thermal stability to its derivatives, and planarity of the ring usually provides higher density to them. Secondly, in contrast to other oxygen heterocycles furazan possesses "working" oxygen atom, i.e. not bonded with carbon or with hydrogen, and therefore able to oxidize these atoms while combustion or explosive degradation of the compounds. Finally, given below data on heat of formation (in gas phase) of four isomeric oxadiazoles, namely 3,4-dinitrofurazan (**1**), 3,5-dinitro-1,2,4-oxadiazole (**2**), 2,5-dinitro-1,3,4-oxadiazole (**3**), and 4,5-dinitro-1,2,3-oxadiazole (**4**), clearly demonstrate the advantages of furazan derivatives as well.
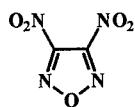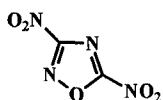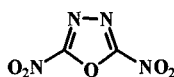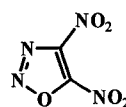
1	2	3	4
76kcal/mol	43kcal/mol	25kcal/mol	12kcal/mol

Really, these rings have the same number and type of heteroatoms; however, the energetic potency is about 2 times greater for **1** than for **2**, for **2** than for **3**, and for **3** than for **4**.

CHEMISTRY

Our efforts to optimize explosive performance led to the synthesis of a number of such novel derivatives of furazans, which would be like "twins" to the famous picryl prototypes.

The target compounds, **Nif-R**, were synthesized by using two reasonable methodology (Scheme I):[2-5] (1) by the oxidation of corresponding aminofurazans (**AF**) with hydrogen peroxide in the presence of varied additions (Route A) and (2) by nucleophilic displacement of an activated heteroaromatic (furazanic) halogen or other leaving group (Route B).

AF   **NF**
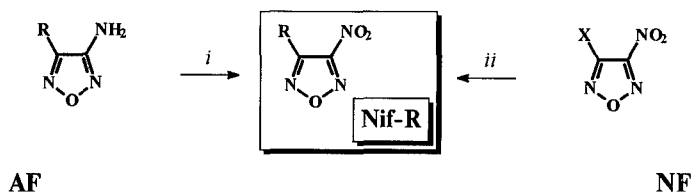
Scheme I. *Reagents and conditions: i -* Route A, H_2O_2, H^+ (H_2SO_4, AcOH, CF_3CO_2H and *et.al.*), Cat (Na_2WO_4, Na_2MoO_4, and so on), -10 ÷ 80°C; *ii -* Route B, Nu, organic solvent, -30 ÷ 60°C [X = Hal, NO_2, OSO_2R', $N(NO_2)R'$, RN=N(O)]

It cannot be too highly stressed that **AF** were the key starting substances, as they were utilized not only over route A, but were with rare exception the precursors in the synthesis of nitrofurazans **NF** representing a base for route B as well. The starting **AF** were synthesized from the appropriate available compounds as outlined in Scheme II.

Wide variety of potential precursors makes possible to obtain **AF** practically with any desirable R. The ability to prepare these amines on a multigram scale has prompted a new approach to the conversion of **AF** into the desired **Nif-R.**
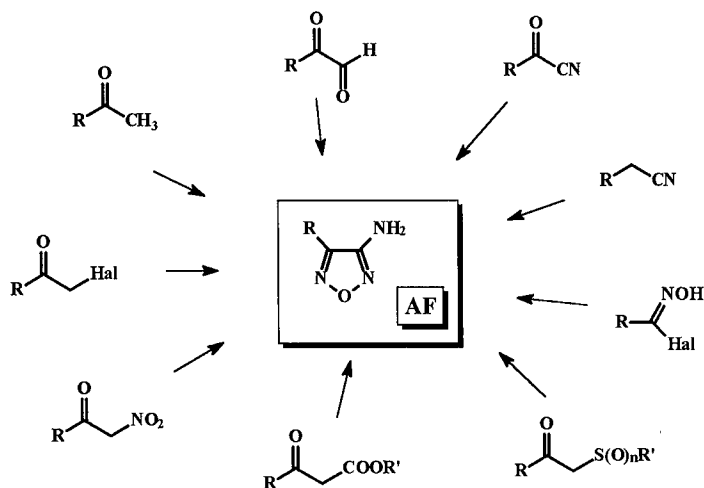
Scheme II. *Pathways to* **AF**.

Overall, as regards methods of preparation it should be noted that in contrary to **Pic-R**, there is no need for nitration reaction in the synthesis of **Nif-R**. This fact provides more favorable ecological situation during their manufacture.

Nif INSTEAD OF Pic

To our knowledge, a relatively small number of **Nif-R** have been reported as energetic materials. This probably stems from the existing until recently difficulties in the synthesis of both the **AF** and the **NF**. The first reported synthesis of a nitofurazan analog (**6**) of a classical *Hexyl* (**5**) was by Coburn.[6]

Combining structural features of **5** with nirtofurazan, a before unknown explosophore, hybrid **6** was generated. It emerged as the most potent heteroaromatic analog with alluring properties.
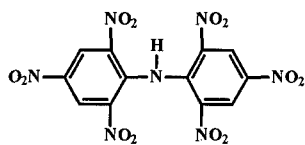
5, $C_{12}H_5N_7O_{12}$
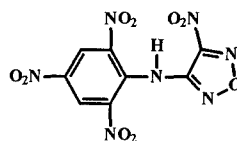
6, $C_8H_3N_7O_9$

5		6
439.21	M.w.	341.15
-1.14	OB_{100}	-0.29
22.33	$N\%$	28.74
249	mp.(°C)	180
1.64	d (g/cm^3)	1.81
18	ΔH_f (kcal/kg)	128
7.15	D_v (mm/µs)	7.75
269	P_{CJ} (kbar)	287
985	Q_{ex} (kcal/kg)	1033

From a high energetic perspective, our attention was focused on chemical modification of picryl family. We have investigated a number of compounds including from one to four nirtofurazan subunits. We will demonstrate the revealed tendencies in property conversions by the example of bridged compounds, involving two **Pic** or **Nif** moieties linked *via* bridge **A**.
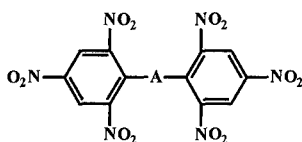
Pic-A-Pic
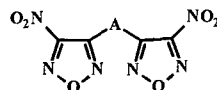
Nif-A-Nif

Fig. 1-4 given below show the comparison of the m.p., density, heats of formation, and detonation velocity of these sets.

An examination of the result comparisons for **Pic-R** and **Nif-R** series revealed the following trends:

(1) The incorporation of **Nif** in place of **Pic** on the molecule decreased *melting point* on 50-200°C.
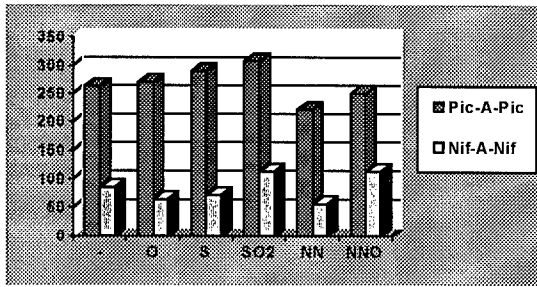
Fig. 1. Melting points (C°)
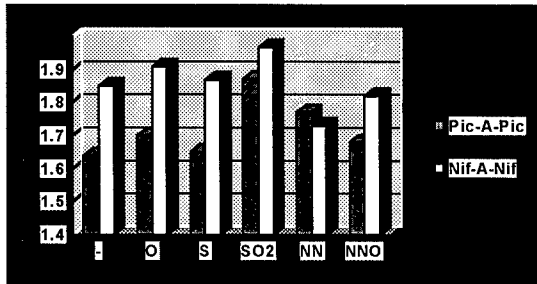
Fig. 2. Density d (g/cm^3)
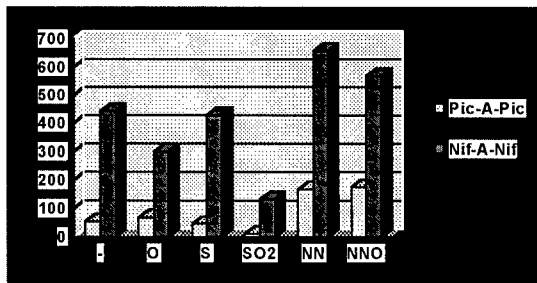
Fig. 3. Heat of formation ΔH_f (kcal/kg)
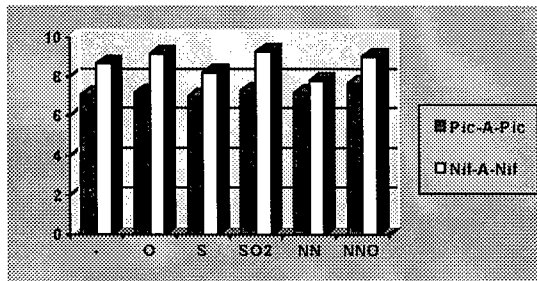
Fig. 4. Detonation velocity D_v (mm/μs)

(2) The *density* of **Nif** , as a rule, was 0.1 - 0.2 g/cm^3 greater than for **Pic** analogs.

(3) All studied **Nif** compounds possessed high positive *heat of formation*. **Pic** analogs ranked below them in the parameter from 100 to 500 kcal/kg.

Hereinafter, earlier created by us database on energetic materials, which in particular involved a wide range of physico-chemical and explosive characteristics of the compounds possessing **Pic** moiety,[1,7-9] was now expanded by the nitrofurazan properties.

CALCULATION

In earlier studies, a quantitative structure-properties relationships (QSPR) of furazanic compounds, including the nitrofurazans, were described.[10,11] In this study, a correlation between several structural features of **Pic** and **Nif** derivatives with ΔH_f and d was observed, resulting in a model with a high predictive capacity. However, the importance of these parameters provoked us to search the new prediction ways. We evaluated ΔH_f and d using the original approach for the search of structure-property relationships. Now calculations were performed using *Approximation Method of Structure-Properties Relationship by the Fourier Series* which recently was discussed in the literature.[12-14] The main idea of this approach is as follows.

Within the framework of the additive approach, the function f describing some physico-chemical characteristic is expressed as

$$f = \sum_i f_i x_i \qquad\qquad (Eq.1)$$

where f_i is the contribution of the i-th functional group, and x_i is the number of such groups in the molecule.

Eq. (1) may be considered as the linear part in the expansion of the f function by the power series. If we want to improve the accuracy of the estimation of the property f, it would be logical to take higher-order terms into account. However, if a function is to be expanded by the power series,

it must be analytical within the whole range of expansion (whereas even the continuity of the function is doubtful for many physico-chemical values). In addition, within the whole range of expansion by the power series, the approximate values of the function depend on its properties at the center of the expansion. Therefore, the empirical constants of expansion turn out to be dependent on the choice of this center. Finally, when the power of the expansion is fixed, the error in the calculations depends on the argument and increases with increasing distance between this argument and the center of the expansion.

These disadvantages significantly reduce the applicability of power series for approximation of various physico-chemical values. However, they were fairly successfully used for calculations of H,C,N,O-compounds density.[12] In the same study, it was stated that the Fourier series may be used successfully instead of power series. Moreover, the Fourier series are free from the aforementioned disadvantages: the only requirement to the expanded function is that it should be integrable within the whole range of expansion. Fourier series were used to approximate d and ΔH_f for H,C,N,O-compounds.[13,14]

Herein we used this method for estimating d and ΔH_f for **Pic** derivatives and **Nif** analogs (for example, see Table I). The arguments of the required Fourier series

$$f = a_o / 2 + \sum_n \sum_k (a_n^k \cos ny^k + b_n^k \sin ny^k)$$

were obtained with the use of the expression

$$y_k = th[\lg(1 + q_{i,j})]$$

where $q_{i,j}$ is the number of atoms of type j (element i) in the molecule. The index values at the argument y_k vary for *carbon atom* $k = j$; for *hydrogen atom*, $k = j+4$; for *nitrogen atom*, $k = j+6$; and for *oxygen atom*, $k = j+11$. The constants of the expansion a_0, a_i, b_i were calculated with the use of regression analysis, successive inclusion of variables, and least-squares technique.

The optimum set of molecular structural descriptors was selected for our experimental database on the energy content and molecular crystal

Table I. The Structures and Calculated Properties of Some **Nif** Derivatives.

NN	Structure Formula	Empirical Formula and M.w.	d, g/cm^3	ΔH_f, kcal/kg	D_v,* mm/μs	P_{cj},* kbar	Q_{ex},# J/g	T,# °K	P,# bar	Es,# J/g
7		$C_3H_4N_4O_6$ 192.09	1.84	44.2	8690	364	6339	4262	1515	1352
8		$C_9H_6N_6O_{10}$ 358.18	1.78	32.0	7922	294	4328	3469	1373	1210
9		$C_5H_4N_6O_7$ 260.12	1.95	133.7	8602	375	4934	4081	1490	1325
10		$C_5H_4N_8O_9$ 320.13	1.97	132.5	8686	385	5824	4286	1441	1289
11		$C_5H_4N_8O_8$ 304.14	1.97	294.2	8759	395	5860	4447	1566	1396
12		$C_5H_3N_7O_9$ 305.12	2.02	119.7	8732	399	6028	4347	1414	1266
13		$C_6H_3N_7O_{11}$ 349.13	1.88	57.6	8258	339	6199	4351	1377	1235

* - calculated using the TIGER-Code,[15] # - calculated with the ICT-Thermochemical Code[16] (loaing density 0.1 g/cm^3).

density of **HEM**. As a result of this choice, a set of descriptors was suggested; it includes various atom types as structural elements.

Some detonation characteristics (D_v, Q_{ex} and P_{cJ}) as well as combustion parameters (the isochoric flame temperature T, pressure P, specific energy Es) were also calculated (Table I).

Wide variety of **HEM**, both common and hypothetic, where **Pic** and/or **Nif** moieties were installed to the other explosophoric blocks has been calculated. One such set, originated from TNAZ (**7**), is in Table. The result, listed in Table I, clearly showed that the corresponding **Nif** derivatives (**9 - 13**) exhibited good properties, compared to **7**, with the degree and pattern of improvement depending on the structure of the bridge moiety as well as substitution position. Compounds bearing the **Pic** moiety, as **8** in this case, were the less interested in every series.

CONCLUSION

The results presented herein demonstrate that nitrofurazans have emerged as the leading candidates for energetic material chemistry. This particular series of heterocycles was chosen for the study since the nitrofurazans possess the desired degree of chemical and physical stability. The study has indicated that compounds containing the nitrofurazanyl moiety are low-melting and possess more high energy and molecu.   al density than their picryl analogs, that provide more high values of detonation velocity and some other detonation and combustion characteristics. Some **Nif-R** may be important candidates for further study and potential military and space applications.

The starting compounds and reagents for these reactions are readily available and relatively inexpensive, and the experimental procedures are straightforward. Even without optimization of the reaction conditions, the product yields are acceptable. These make the convergent approach highly appealing and very practical. We are currently investigating the generality of this process for the target-oriented construction of new **HEM**. By appropriate modification of the well-known **HEM** by application of

nitrofurazanyl moiety, novel **HEM** may be synthesized which displayed good calculated properties.

ACKNOWLEDGMENT

REFERENCES

1. Kohler, J. and Meyer, R. *Explosives.* - 4ed. - Weinheim: VCH, **1993**.
2. Sheremetev, A. B.; Kulagina, V. O.; Aleksandrova, N. S.; Novikova, T. S. and Khmelnitskii, L. I. "Aminofurazans as Key Synthons for Construction of High Energetic Materials". *3th (Beijing) International Symposium on Pyrotechnics and Explosives.* November 6-9, **1995**, Beijing, China.
3. Novikova, T. S.; Melnikova, T. M.; Kharitonova, O. V.; Kulagina, V. O.; Aleksandrova, N. S.; Sheremetev, A. B.; Pivina, T. S.; Khmel'nitskii, L. I. and Novikov, S. S. "Effective Method for Oxidation of Aminofurazans to Nitrofurazans". *Mendeleev Commun.*, **1994**, 138-140.
4. Sheremetev A. B.; Mantseva, E. V.; Aleksandrova, N. S.; Kuzmin, V. S. and Khmel'nitskii, L. I. "Reaction of Nitrofurazans with Sulfur Nucleophiles". *Mendeleev Commun.*, **1995**, 25-27.
5. Sheremetev, A. B.; Kharitonova, O. V.; Melnikova, T. M.; Novikova, T. S.; Kuzmin, V. S. and Khmelnitskii, L. I. "Synthesis of Symmetrical Difurazanyl Ethers". *in press.*
6. Coburn, M. D., "Picrylamino-substituted Heterocycles. II. Furazans". *J. Heterocycl. Chem.*, **1968**, 5, 83.

7. Хмельницкий, Л. И. *Справочник по взрывчатым веществам.* Часть II, Москва, **1961**. 842c. (L. I. Khmelnitskii, *Handbook on Explosives. Part II.* - Moscow, **1961**, 842p., in Russian).

8. Орлова, Е. Ю. *Химия и технология бризантных взрывчатых веществ.* Наука, Ленинград, **1981**. (E. Yu. Orlova, *Chemistry and Technology of High Explosives.* Nauka, Leningrad, **1981**).

9. Coburn, M. D.; Harris, B. W.; Lee, K.-Y.; Stinecipher, M. M. and Hayden, H. H. "Explosives Synthesis at Los Alamos". *Ind. Eng. Chem. Prod. Res. Dev.*, **1986**, *25*, 68-72.

10. Pivina, T. S. "Hierarchy of Calculation Methods for Evaluating and Predicting the Formation Enthalpy of High Energy Materials: From Chemical Intuition to Computer Chemistry Methods". *Proc. 24th Int. Annual Conf. ICT*, Karlsruhe, Germany, June 29 - July 2, **1993**, 91(1-16).

11. Pivina, T. S.; Sukhachev, D. V.; Evtushenko, A. V. and Khmelnitskii, L. I. "Comparative Characteristic of Energy Content Calculating Methods for the Furazan Series as an Example of Energetic Materials". *Propellants, Explos., Pyrotech.*, **1995**, *20*, 5-10.

12. Evtushenko, A. V.; Smirnov, B. B. and Shlyapochnikov, V. A. "A New Approach to Estimation of the Compound Density". *Izv. Akad. Nauk, Ser. Khim.*, **1993**, 685.

13. Evtushenko, A. V. and Smirnov, B. B. "Fourier Series Approximation of Substances Density". *Izv. Akad. Nauk, Ser. Khim.*, **1995**, 22-24.

14. Evtushenko, A. V. and Smirnov, B. B. "Approximation of Enthalpy of Formation by Fourier's Series". *Izv.Akad. Nauk, Ser. Khim.*, **1994**, 1389-90.

15. Cowperthwaite, M. and Zwisler, W.H. "TIGER Computer Program Documentation", *SRI Publication No. Z106*, (January **1973**).

16. ICT-Thermochemical Code, **1995**.

The Development of an Elevated Temperature Friction Sensitiveness Apparatus

Glenn Miles [†]   **Mike R. Williams** [†]

Roland K. Wharton [‡] **Andrew W. Train** [*]

ABSTRACT

Friction sensitiveness testing is an integral part of the safety assessment of energetic materials.

The test methods available for measuring friction sensitiveness include the BAM Friction Test (the UN recommended method for transport), the Rotary Friction Test and the ABL Test. All are room temperature units and are limited to this temperature because of their design.

The above methods are adequate for the assessment of safety in transport, where it is reasonable to assume that the temperature of the energetic material will remain at, or near, room temperature. However, during processing it is possible that energetic materials will be subjected to elevated temperatures either deliberately or accidentally as the result of mechanical wear or failure. Currently no methods exist to enable the in-process hazards from friction sensitiveness to be evaluated at temperatures other than room temperature.

The paper reports work currently in progress at Cranfield University (RMCS Shrivenham) to develop and commission a test unit to enable friction sensitiveness at temperatures up to 100°C to be measured.

INTRODUCTION

Unpackaged energetic materials are often processed using equipment, such as extruders or drying ovens, in which there will inevitably be a risk of the material coming into contact with solid surfaces which are moving across each other. The frictional energy produced can

[†] Environmental and Chemical Systems Department, Royal Military College of Science, Shrivenham, Swindon, Wiltshire SN6 8LA UK.
[‡] Health and Safety Laboratory, Harpur Hill, Buxton, Derbyshire SK17 9JN UK.
[*] Chemical and Hazardous Installations Division, Health and Safety Executive, Magdalen House, Stanley Precinct, Bootle, Liverpool L20 3QZ UK.

be transferred to the energetic material and it is known that a number of accidental initiations have occurred in this manner [1]. In addition, where a process is run at above room temperature, the likelihood of accidental initiation by friction at such a temperature must be considered as part of the risk assessment for that process. Current methods of measuring friction sensitiveness, however, are limited to determinations at room temperature [2,3].

At present, the only commonly used methods of assessing the susceptibility of energetic materials to accidental initiation at elevated temperatures are the measurement of their Temperature of Ignition [3] or Deflagration Point [4]. These properties are measured by heating a small amount of the energetic material in the absence of any mechanical stimulus.

Under current health and safety legislation, employers and the self-employed, are required to make a suitable and sufficient assessment of the risks associated with their work activities. Where those activities involve the handling of energetic materials at elevated temperatures, such assessments clearly need to consider any enhanced risk of a decomposition or explosion caused by, for instance, impact and friction under those operating conditions. Yet, relatively little is known about the effect of working temperatures other than room temperature on the mechanical sensitiveness of energetic materials [5]. Current impact and friction sensitiveness test methods are only used at room temperature. This limitation has been recognised by the UK Health and Safety Executive (HSE), which has commissioned research into the effect of temperature on sensitiveness. This work includes the development, at HSE's Health and Safety Laboratory, of an apparatus to measure impact sensitiveness at elevated temperatures, and, at Cranfield University (RMCS Shrivenham), an apparatus to measure friction sensitiveness at elevated temperatures. Both of these projects are sponsored by the HSE's Explosives Inspectorate.

This paper will describe the apparatus which has been developed by Cranfield University (RMCS Shrivenham). The key requirements governing the design of this machine were that:-

1. The temperature of the sample and friction surfaces would be stable and could be controlled to any level between room temperature and 100°C with a tolerance of ±2°C.

2. The machine would contain as few moving parts as possible and be relatively compact.

3. The energetic material would be subjected to friction between surfaces.
4. The frictional stimulus could be controlled in terms of measurable quantities, such as the speed of and the loading applied to the surfaces.
5. The identification of "an event" should not be reliant on operator judgement, if possible.
6. With operator safety in mind, the apparatus should be capable of being used in most existing ducted fume cupboards to contain fumes and blast fragments.
7. The results of friction sensitiveness tests using the machine at room temperature should be in line with previous studies using established test methods.

The aim of the work was to produce information on the effect of temperature on friction sensitiveness for a wide range of energetic materials. This paper describes the current status of the machine, the validation of the machine at room temperature and its use with a number of energetic materials at other temperatures.

TEST APPARATUS

Design Principles

Table 1 [6,7] summarises the main design parameters of some existing friction sensitiveness test methods and Table 2 presents an assessment of how easily each method could meet the design/performance requirements listed above.

Of the current test methods, only the BAM test would satisfy all of the criteria but since its reliability has recently been questioned by Le Roux [8], it was decided to develop a new test.

The advantage of this approach was that the test apparatus could be engineered to meet specific criteria which, in addition to those given above, included:

•   A small sample size (to produce a more uniform temperature gradient in the sample).

•   A small rubbing area to maximise the stimulus level per unit load, improve the efficiency of heating and the accuracy of remote temperature measurement.

The importance of these factors is discussed in the next section.

Mechanical Design

The RMCS friction sensitiveness test apparatus is designed to be capable of operation from room temperature up to 100°C. The friction surfaces and the energetic material are heated in situ to a stable and controllable temperature, thus minimising the exposure of the operator to potential hazards from accidental initiation associated with the handling of energetic materials at elevated temperatures. To minimise energy requirements and reduce the heating time (and hence the effects of thermal ageing on the sensitiveness of the materials) the machine was designed to be compact and well insulated.

A schematic diagram of the prototype currently being developed at Cranfield University (RMCS Shrivenham) is given in Figure 1 [9]. Because of the need for compactness, the contact area is loaded via a cantilever arm (as in the BAM method except that the load is applied to the static surface). To allow both the velocity and load to be varied it was also decided to use a static (non-rotating) loaded wheel and a moving plate or anvil, as in the ABL method. The general design is very adaptable. The geometry of the consumables has been kept simple, a wheel and a rectangular plate, both of which could be manufactured from a wide range of engineering materials.

Part of the research effort has been directed towards finding suitable materials for the frictional surfaces. The system chosen is simple and inexpensive and friction surfaces are easily produced from common abrasives.

A large variation in the principal stimulus variables (load and speed) has been allowed for, although it is thought that in practice, the speed will be held constant and the load varied. A high instantaneous speed (of up to 5 m s^{-1}) is imparted to the trolley, and hence the plate, by the impact of a ram attached to a piston (driven by a compressed gas system connected to a supply regulated at 2 bar). The use of a pendulum, or a flywheel arrangement, was rejected on the grounds of size.

The internal volume of the apparatus that needs to be heated is 2 litres and the apparatus takes 10 minutes to warm to 100°C from room temperature. Tests have shown that the plate takes a further 10 minutes to heat to 100°C after fixing in place.

The friction wheel stops in situ (merely being indexed onto a new part of the rim after each test) and can be lowered onto the plate remotely.

Test Methodology

In the course of a friction test, the input of energy to the energetic material can arise from two mechanisms:

1.   Mechanical friction forces acting on or within the energetic material.

2.   Heat input to the energetic material from the rise in temperature of the rubbing surfaces as the test proceeds.

It was felt that the test we were developing should assess the susceptibility of the material to initiation through mechanism 1., but not through mechanism 2.

To do otherwise would be to merely study the frictional heat-producing properties of two surfaces (made from materials which might not be found in any processing application) in relation to the temperature of ignition of the explosive.   To this end it was thought desirable for the movement that produces friction to act in one direction only, with the energetic material between the friction surfaces, so that:-

1.   The chance of bringing surfaces which have been remotely frictionally heated into contact with the energetic material is minimised.

2.   The energetic material is either carried with the moving part of the friction surface or left behind on a surface which has been heated by friction but which experiences no further frictional work.

The frictional energy should be quantifiable (in terms of the load and/or speed of motion). The apparatus should be capable of interfacing with event sensing equipment (light emission and gas monitoring). It should be possible to operate the unit so that there is no risk to the operator in terms of exposure to the products of reaction [10] and so that the risk associated with handling energetic materials is no greater than in current equipments. The fact that powdered explosives could be involved limits the type of heating that can be applied.   The hot air system has the flow arranged to avoid disturbing the test sample and producing a cloud of explosive dust.

TEST PROCEDURE

The sample is loaded onto the plate and the plate mounted beneath the wheel. The temperature is monitored by a surface thermocouple on the plate (withdrawn just before the plate is struck). If heat is required the enclosure is heated by the gentle flow of warm air, heated remote to the system and not recirculated. It is hoped that waste air can be vented to a ducted fume cupboard (or that the whole developed apparatus will prove small enough to fit inside a fume cupboard), so that the operator will not come into contact with combustion products. The piston strikes against the plate and events may or may not occur due to the relative motion of the plate and the wheel. The initial speed is kept constant and the load is varied from test to test to alter the stimulus level.

Event Classification

There are several means by which the occurrence of an event in the test may be indicated e.g., evolution of reaction products, generation of light, and generation of sound.

Of these, the generation of reaction products has been chosen as the principal method of event classification. This is because certain materials will not necessarily produce sound and/or light when they react. Reaction products are monitored by means of an array of electrochemical gas sensors - NO_2, CO, and SO_2. During testing, a sample of the atmosphere inside the rig is being drawn over three remote gas sensors via a long, inert tube. This gives the gases time to cool, so that the sensors are not affected by the gas temperature. An event is marked by the detectable production of any of these gases, above the background level.

It is possible to further categorise the event by using the amount of combustion products and/or rate at which these products are produced. The difference between a decomposition and a rapid event such a detonation is indicated by an increase of several orders of magnitude in the rate of and volume of gas production.

Data Collection

The system used for data collection has two stages. The first stage is to locate the 50% event frequency level using a 25-shot Bruceton up-and-down technique. This is then expanded with further trials to produce a probit plot. At present a constant plate velocity of approximately 4 m s^{-1} is used and the load varied.

In general, the response gained from a series of tests at varying levels of a shock stimulus such as friction or impact is *sigmoidal*. A probit plot is a straight line generated from this sigmoid by transforming the event frequencies using a logarithmic function.

The probit is generated from the event frequencies gained from tests at several set stimulus levels. Each test is made up from 12 identical trials under a particular set of circumstances.

RESULTS

Validation of Consumable Production

A 25-step Bruceton test was performed on HMX using consumables produced by three different operators following the same written procedure. The results of this comparison are given in Table 3 as the 50% event frequency, calculated as being the mid-point between the mean load at which a reaction occurs and at which no reaction occurs.

Room Temperature Assessment

Probit plots for three energetic materials tested at room temperature are given in Figure 2. This indicates a general usefulness of the probit approach in analysing the data from sensitiveness tests since it enables the probability of reaction to be evaluated at a range of stimulus levels.

A series of energetic materials has previously been used by Wharton and Harding to compare three friction sensitiveness tests [11]. The same energetic materials were tested using the RMCS prototype test and Table 4 summarises the data obtained. These results are compared with those previously reported [11] from the Rotary, BAM and Mallet friction tests in Table 5; it can be seen that all four methods rank the explosives similarly in terms of friction sensitiveness.

Elevated Temperature Results

Initial work on the elevated temperature testing of two materials has indicated that there can be a significant increase in the sensitiveness with temperature. Figure 3 shows the changes in sensitiveness of PETN and a pyrotechnic composition (tested at constant load and constant speed) due to changes in temperature. In addition it was noted that there was a visible and audible change in the vigour of the reaction process as the test temperature increased. For PETN there was a transition from a low energy deflagration to a detonation/fast decomposition (see Table 6).

CONCLUSIONS

At room temperature, it has been demonstrated that the RMCS prototype ranks materials with a range of sensitiveness in a manner that correlates well with established methods. Consumables made by different operators have been found to give the same performance. HMX is consistently distinguishable from RDX using a short (25-shot) Bruceton test and consumables prepared by three different operators.

PETN has been found to have increased sensitiveness at elevated temperatures, in terms of an increase in event frequency at a constant stimulus level. There was also an observed increase in the vigour of the positive events.

It is more realistic to define sensitiveness by studying the entire frequency range by means of a probit analysis. The incorporation of a short Bruceton test preceding the probit analysis allows a basic ranking to be made in the first instance, and gives an idea of the midpoint of the probit and the range over which the probit should be plotted. The Bruceton data can be reused as part of the probit, extra data being generated to fill in the gaps at high and low event frequencies.

ACKNOWLEDGEMENTS

1. Bailey, A.; Chapman, D.; Williams, M. R.; Wharton, R. K..
   "The Handling and Processing of Explosives", Proceedings of the Eighteenth International Pyrotechnics Seminar, Breckenridge, Colorado, July 1992, p. 33.
2. Recommendations on the Transport of Dangerous Goods, Manual of Tests and Criteria, second revised edition ST/SG/AC.10/11/Rev.2, United Nations, New York and Geneva, 1995.
3. Sensitiveness Collaboration Committee (SCC) Manual of Tests (ed. NP1 Division), Defence Research Agency (formerly Royal Armament Research and Development Establishment (RARDE)), Fort Halstead, Kent, October 1988, p. 3-1 (and diags).
4. Köhler, J; Meyer, R..
   Explosives, fourth revised and extended edition, VCH Publishers, New York, 1993, p. 76.
5. Niimi, M..
   "A Study of the Sensitivity and Mechanism of Initiation of Explosives", J. Japan. Soc. Ordnance and Explosives, v. 32, n. 5, 1938, p. 396. Translation available from DRIC (quote DRIC-T-10086).
6. Recommendations on the Transport of Dangerous Goods, Manual of Tests and Criteria, second edition ST/SG/AC.10/11/Rev.1, United Nations, New York, 1990, p. 108.
7. Fordham, S..
   High Explosives and Propellants, second revised edition, Pergamon Press, Oxford, 1980, p. 70.
8. Le Roux, J. J. J. P. A..
   "The Dependence of Friction Sensitivity of Primary Explosives upon Rubbing Surface Roughness", Propellants, Explosives, Pyrotechnics, v. 15, 1990, p. 243.
9. Miles, G..
   "The Development of an Elevated Temperature Friction Sensitiveness Test", Explosives Engineering, in press, 1996.
10. Harding, J. A.; Wharton R. K..
    "The Application and Development of Sensitiveness Test Methods for Explosives", Proceedings of the 25th International Conference of the ICT, Karlsrühe, Germany, 1994, p. 6.
11. Wharton, R. K.; Harding, J. A..
    "An Experimental Comparison of Three Documented Test Methods for the Evaluation of Friction Sensitiveness", J. Energetic Mat., v. 11, n. 1, March 1993, p.51.

Figure 1. Schematic of Shrivenham Prototype
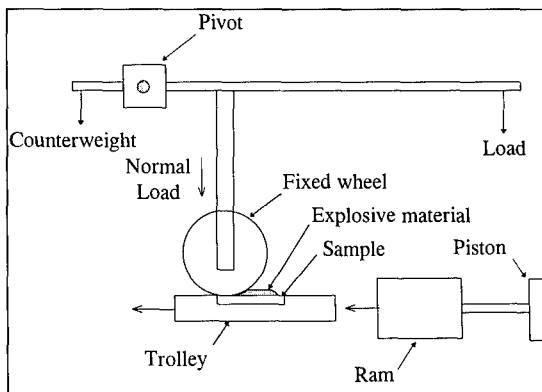
Figure 2. Room temperature probit plots for three energetic materials
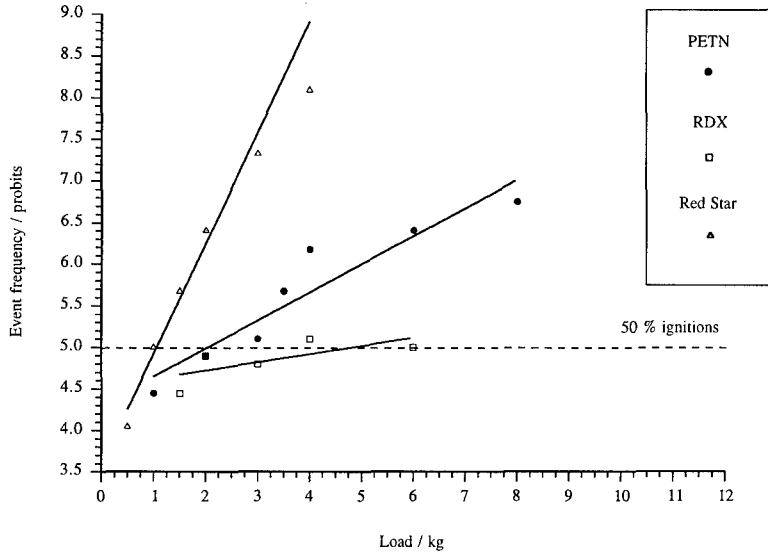
Figure 3.
The change in sensitiveness of PETN (at 3 kg stimulus level) and Red Star pyrotechnic
composition (1 kg) due to an increase in ambient temperature
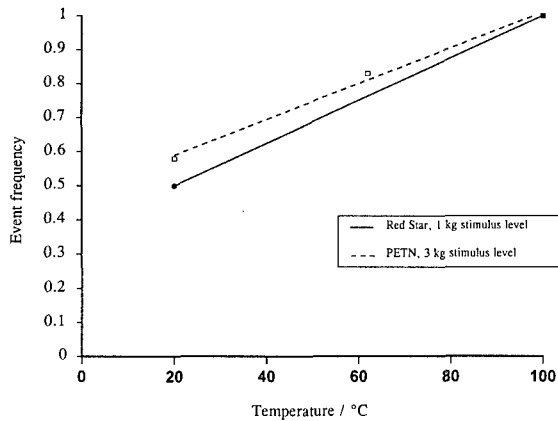
Table 1.

The main factors of some current room temperature friction sensitiveness test methods

Test Method	Contact geometry[a]	Contact surface materials	Typical speed[b] / m s^{-1}	Typical normal load pressure[c] / MPa	Typical test duration	Sensor	Recommended statistical treatment	Reference Transport criterion[d]
BAM Friction	Tangent	Porcelain	0.03	160	< 1 s	Operator	Load at 1/6	80 N
Modified BAM[e]	Tangent	Emery paper	0.03	30	< 1 s	Operator	Load at 1/10	-
Rotary Friction	Tangent	Mild Steel	0.4	0.276	ms	Operator	Speed Bruceton	RDX
Friction Sensitivity[f]	Tangent	Bearing Steel	?	500	ms	Operator	Pressure at 1/25	200 MPa
ABL Friction[e]	Tangent	MGR Steel	0.9	800	ms	Operator/ remote	Load at 1/20	PETN (dry)
Emery Paper Friction	Flat	Emery paper	2.0	0.5	ms	Operator	Speed Bruceton or range /20	-
RARDE Sliding Block	Flat	Steel	5.0	0.5	ms	Operator	none	-
Torpedo Friction [7]	Tangent	Steel	1.0[g]	-	ms	Operator	Drop height	-
Mallet Friction	Tangent	varies[h]	3.0	unknown	ms	Operator	Out of 10 Surface dependent	-

[a] Tangent represents a curved surface and a flat surface. Flat represents two flat surfaces.

[b] Unless stated in the test procedure, this value is estimated from the test description (if possible).

[c] Unless stated in the test procedure, this value is estimated from a mid-range load and the load-bearing area of the test (if possible).

[d] This criterion is that which is published in the UN Recommendations on the Transport of Dangerous Goods. It represents the highest sensitiveness that can be transported safely.

[e] A modified method was used by *Le Roux*[8].

[f] The Friction Sensitivity test (Russian) has replaced the ABL test (USA) in the UN Recommendations on the Transport of Dangerous Goods, eight edition.

[g] This is the component of the impact speed that creates a shear friction force.

[h] The Mallet Friction test is a qualitative test based on the ability of materials such as steel, wood and stone to cause initiation under nominally identical trials.

Table 2.

Consideration of adaptation of existing test method for elevated temperature testing

	Compact	Temperature control feasible	Possibility of remote sensing	Reliable	Applicability to a range of energetic materials
BAM Friction	Y	Y	Y	?	Y
Modified BAM	Y	Y	Y	Y	N
Rotary Friction	N	N	Y	?	Y
Friction Sensitivity	N	Y	Y	?	Y
ABL Friction	N	?	Y	Y	Y
Emery Paper Friction	N	Y	Y	?	N
RARDE Sliding Block	N	Y	Y	?	?
Torpedo Friction	N	N	Y	?	Y
Mallet Friction	Y	N	Y (but difficult)	Y	Y
RMCS prototype	Y	Y	Y	Y	Y

Table 3.
Comparison of consumables produced by different operators, when used to test
HMX at room temperature

Consumable set	Mean Reaction load / N	Standard deviation	Mean No Reaction Load / N	Standard deviation	50 % Initiations level / N	Span
A	35.2	5.6	28.9	6.1	32.1	6.5
B	36.9	4.8	33.5	5.7	35.2	3.4
C	36.9	6.6	32.0	7.1	34.4	4.9

Table 4.
Sensitivenesses of some energetic materials at room temperature measured by the RMCS
prototype.

Material	Load for 50% initiations / kg
LDNR	<0.5
PETN	2.0 [†]
HMX	3.5 *
RDX[‡]	4.7 [†]
Tetryl	-
RDX/TNT	-
TNT	>12

* Calculated from Bruceton method
[†] Calculated from probit plot
[‡] Nominal 850 μm grain size

Table 5.

Comparison of sensitiveness rankings of friction sensitiveness tests

Material	Rotary Friction Test [9]	BAM Friction Test [9]	Mallet Friction Test [9]	RMCS Prototype
LDNR	1	1	1	1
PETN	2	2	=2	2
HMX	3	3	=2	3
RDX	4	4	=2	4
Tetryl	5	=5	=5	-
RDX/TNT	=6	=5	=5	-
TNT	=6	=5	=5	5

Table 6.

Change in reaction behaviour of PETN during friction sensitiveness testing

with the RMCS prototype.

Test temperature	Light emission	Sound emission
20°C (Room temperature)	Shower of orange/yellow sparks	Little or none
60°C	Concentrated white/yellow flash	A sharp crack
100°C	Dark, possibly no flash	A very loud crack

CHARACTERIZATION OF THE INTERNAL QUALITY OF HMX CRYSTALS

A.E. van der Heijden[°] and W. Duvalois[*]

TNO Prins Maurits Laboratory, [°] Pyrotechnics and Energetic Materials, [*] Analysis of Toxic and Energetic Materials, P.O. Box 45, 2280 AA Rijswijk, The Netherlands

Abstract

Cooling crystallization experiments on a 2 liter scale under different experimental conditions have been carried out in order to produce HMX crystals with an averaged internal crystal quality which varies depending on the operating conditions applied during crystallization. The HMX crystals have been characterized with respect to their internal quality by means of optical microscopy and X-ray Laue diffraction. Additionally, the purity, density, size distribution, shape, surface characteristics and impact/friction sensitivity of the HMX crystals were determined. The characterization of the internal crystal quality shows that the crystals which contain a high visible amount of inclusions, show a lower degree of averaged crystal perfection in the Laue diffraction patterns and *v.v.* The Laue method is sensitive to all kind of structural defects including microscopic defects that cannot be detected by means of optical microscopy since this technique only reveals macroscopic defects, like (macro-)inclusions and cracks. Therefore, this X-ray diffraction technique can be applied as an additional tool to characterize the internal quality of crystals. The degree of perfection can be quantified with the so-called mosaic spread which can be calculated from the radial spot extension in the Laue X-ray diffraction patterns: the higher the mosaic spread, the lower the internal crystal quality.

Introduction

Recrystallization of energetic materials, like RDX and HMX, is required to obtain the desired crystal size distribution (CSD) of the product. Additionally, the purity of the materials is usually increased compared to the synthesized raw materials. Besides the product CSD, also the shape of the crystal, its surface structure and its internal perfection are important product specifications. The influence of the shape and the surface structure of *e.g.* RDX particles on the shock sensitivity were studied and reported earlier [1,2]. These investigations showed that an HTPB binder containing spherodized and additionally smoothed RDX particles, was less sensitive than a similar PBX in which the particles were applied directly, so without any post-treatment. The final objective of the current investigations is to assess the influence of the internal crystal quality on the shock sensitivity of a PBX incorporating HMX particles.

This paper describes the production of several HMX batches in an attempt to relate the product specifications with the process conditions applied during crystallization. Several techniques are used to characterize the product crystals with respect to their mean size, size distribution, density, purity, shape, surface characteristics, internal quality and impact/friction sensitivity. In particular, attention is paid to a specific X-ray diffraction technique (Laue diffraction) with which the internal quality of the crystals can be characterized.

Crystal defects and their characterization

During the mass production of crystals generally both microscopic and macroscopic crystal defects will be present in the crystals. These defects consist of (*i*) point defects, such as vacancies within the crystal structure, substitution of solute molecules *e.g.* by solvent or impurity molecules or interstitial incorporation of other molecules, (*ii*) dislocations, (*iii*) grain boundaries (networks of dislocations), (*iv*) inclusions, (*v*) strained areas and (*vi*) cracks. These defects are introduced during the crystallization process as a result of growth of the crystals combined with collisions among the crystals themselves and between crystals and moving parts within the crystallizer vessel, *e.g.* the impeller blades [3]. Due to these collisions a crystal will be damaged, in particular its edges and corners, as becomes clear from scanning electron microscopic observations [4]. Since the crystals are suspended in a supersaturated solution, the damaged parts will "heal" again. This healing process usually leads to the formation of inclusions [4] and, on a microscopic scale, generally also to dislocations and point defects [5].

The qualitative characterization of macroscopic defects usually appearing as inclusions and cracks, is done by means of optical microscopy: the crystals are submerged in a non-solvent with a refractive index that matches the (mean) refractive index of the solid particles [4,6]. The purity of the

crystals can be studied by means of GC, HPLC, NMR *etc.*, depending on the nature of the impurities. For crystals larger than ~ 1 cm, X-ray Lang topography can be used to characterize the dislocations within the crystals; also slight etching of certain crystal faces is used to characterize dislocations and slip systems [5,7–11]. The investigations by Bhat *et al.* [5] have shown that after the regrowth of intentionally damaged parts of a crystal, existing dislocations terminate while new dislocations are formed at the interface at which regrowth took place. Also inclusions turn out to be sources of (bundles of) dislocations. This implies that by reducing the inclusion content, the dislocation content will be reduced as well, in this way increasing the crystal perfection.

Mass crystallization processes generally produce crystals with a mean size in the range of 100 to 1000 μm and such crystals are too small to be characterized with Lang topography. For such crystals, Laue X-ray diffraction might be used to characterize the internal quality, since this technique is in particular sensitive to crystal lattice deformations and to slight misorientations between constituent crystallites within a single crystal [12–14]. For a crystallographically perfect crystal, the spots in the Laue diffraction pattern should be small and circular. However, crystals containing structural defects of any kind, will cause these spots to be elongated both radially and – to a minor extent – tangentially. This spot extension R is related to the misorientation or mosaic spread, η, which is a measure of the overall disorder within a crystal, according to:

$$R = 2\, \eta\, D/\cos^2 2\,\theta,$$

where D is the sample-to-film distance and θ the reflection angle [12,14]. Each spot on the diffraction pattern corresponds to a certain reflection angle according to the following relationship:

$$\text{tg } 2\,\theta = L/D,$$

where L is the distance from the origin of the Laue diffraction pattern to the centre of the spot. Values of η up to ~ 0.5° are commonly regarded as good quality crystals [14].

Experimental

HMX has been crystallized by means of cooling crystallization from a 1:1 molar mixture of acetone and γ-butyrolactone saturated at 65 °C in a 2 liter crystallizer. The experimental set-up comprises a jacketed vessel, a thermostat oil bath (Julabo FP50) and a temperature controller (Midilab A1562) with which a temperature profile can be applied. Two temperature profiles have been used: (*i*) cooling at a rate of ~ 55 °C/hr in the first half hour of the experiment, followed by a period of again half an hour during which the temperature decreased at a rate of ~ 30 °C/hr; after that the suspension temperature slowly dropped to 10 °C; (*ii*) cooling at a constant rate of ~ 18 °C/hr. An anchor type stirrer has been used with stirrer rotation rates in the range of 175 to 360 rpm. The

temperature of the oil within the thermostat and at the inflow into the jacket as well as the suspension temperature were recorded. The initiation of the crystallization process was either achieved by seeding of the solution with HMX particles, ground to a mean size of ~ 6 µm, or by addition of a certain amount of non-solvent (water) which provokes nucleation. The addition of the seeds or the non-solvent took place at a temperature of 55 °C, so 10 °C below the saturation temperature of the solution. By changing the cooling curve, the seeding method and the stirrer rotation rate, it was expected that HMX crystals could be produced with a varying internal quality. Finally, the product is filtered, washed with water and vacuum dried at 30 °C.

After the production, the HMX was characterized with respect to its density (liquid pycnometry), mean size and size distribution (forward light scattering), shape and surface structure (SEM, optical microscopy), inclusion content (optical microscopy), purity (GC), impact and friction sensitivity and internal quality (Laue X-ray diffraction). The wavelength λ of the X-ray beam used for the Laue diffraction measurements is effectively in the range of ~ $0.2 - 7$ Å. The sample-to-film distance D is 40 mm.

Results and Discussion

Table 1 lists the process conditions applied during the crystallization of HMX batches which were characterized in detail afterwards. Table 2 shows the results of the characterization tests. Powder X-ray diffraction measurements showed that the β-modification of HMX was formed.

In figure 1 optical microscopic photographs of crystals taken from the batches 22 and 28 are depicted. The crystals are either rod- or tabular-shaped. Also twinned crystals can be observed. These twins consist of two intergrown rod-shaped crystals with a specific mutual orientation. In the centre of these twinned crystals, cracks can be observed due to the fact that there is obviously some mismatch between the two crystallographic orientations which meet at the twin plane, leading to stressed regions at this twin plane. It is believed that a twinned crystal can develop into a tabular shape, which appears to be a single crystal. Only from the cracks in the centre of such crystals one is able to judge that it is a twinned crystal. The twinning of HMX will be further studied with help of the molecular modelling package Cerius^2 [15]. The photographs further show that the amount of visible inclusions in the crystals taken from batch 22 is lower than that of batch 28. This observation is in contradiction with the density measurements, which resulted in a lower density for batch 22 compared to batch 28. An explanation might be that the lower density crystals contain a large number of small inclusions which sizes are below the detection limit of the optical technique used. However, as will become clear later on, this assumption is not sustained by the results of the X-ray Laue diffraction characterization technique.
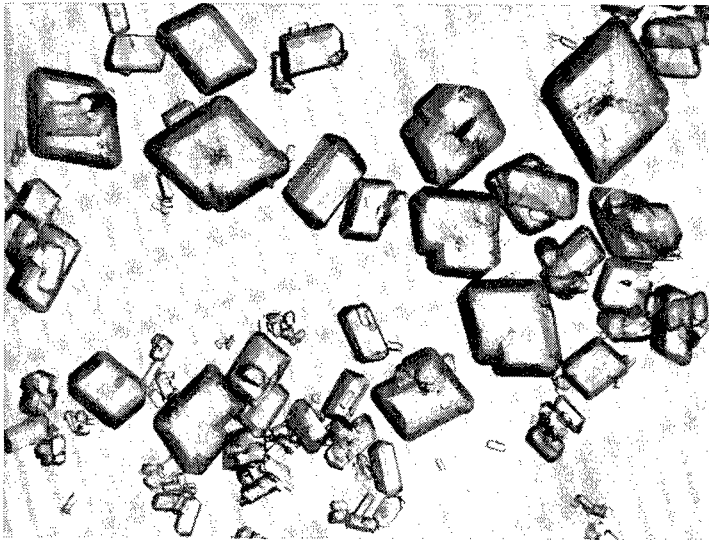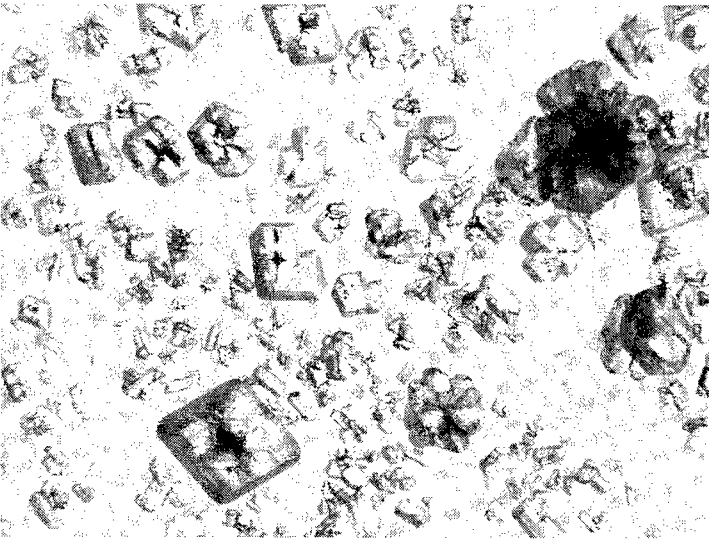
Figure 1: Optical microscopic pictures of HMX crystals taken from (*a*) batch 22 and (*b*) batch 28. The crystals are either rod- or tabular-shaped. Also twinned crystals have been formed during the crystallization process, which finally grow out to the tabular-shaped crystals. Clearly inclusions and cracks can be observed. In particular in the centre of the tabular crystals, cracks can be discerned with a certain preferential crystallographic orientation. Very likely, these cracks are oriented along the twin plane.

Table 1: Process conditions during the crystallization of HMX from a 1:1 molar ratio acetone/γ-butyrolactone mixture.

batch code	seeding method	stirrer speed [rpm]	cooling rate [°C/hr]	residence time [min]
HMX-THP-22	non-solvent	270	18	130
HMX-THP-27	non-solvent	175	18	120
HMX-THP-28	seeds	360	55 [a]	180

[a] This is the cooling rate within the first half hour of the total residence time; within the next half hour the cooling rate is 30 °C/hr; during the remaining period the suspension temperature slowly drops to 10 °C.

Figure 2 shows scanning electron microscopic (SEM) pictures of the batches 22 and 28. Concerning the shape of the crystals, the SEM observations are similar to the optical microscopic pictures. The SEM photographs further show that the crystals have smooth surfaces. The crystals from batch 28 are generally much more agglomerated and intergrown than the crystals taken from batch 22. This might be caused by the fact that seed crystals were used to initiate the crystallization process of batch 28. Since these seed crystals were added dry to the clear solution, it cannot be excluded that the seed crystals were agglomerated at the time of their addition. In case such an agglomerated seed particle starts to grow, the different crystallographic orientations of the separate crystals building up the seed particle will grow, eventually leading to the intergrown particles as shown in figure 2 (*b*).

The purity of the HMX batches, as determined with GC, is high: in practically all cases the acetone and γ-butyrolactone level is below the detection limit of 0.2 and 0.03 wt%, respectively. These results also imply that the inclusions hardly contain any solvent, *i.e.* during drying the amounts of solvent initially trapped by the inclusions almost completely disappear. Also from the high contrast of the inclusions observed by means of the optical microscope, it can be concluded that the inclusions do not contain any solvent anymore. If the inclusions would still contain solvent, the refractive index difference between the solid HMX and the inclusion content would be much less and hence a rather low contrast would be expected, which is not the case.

The impact and friction sensitivity of the HMX crystals is the same for both batch 22 and 28 (see table 2). The literature values of the impact and friction sensitivity of HMX are 7.4 Nm and 120 N, respectively [16]. This method seems to be too rough to be used as a technique to discriminate between batches comprising crystals with a varying internal quality per batch.
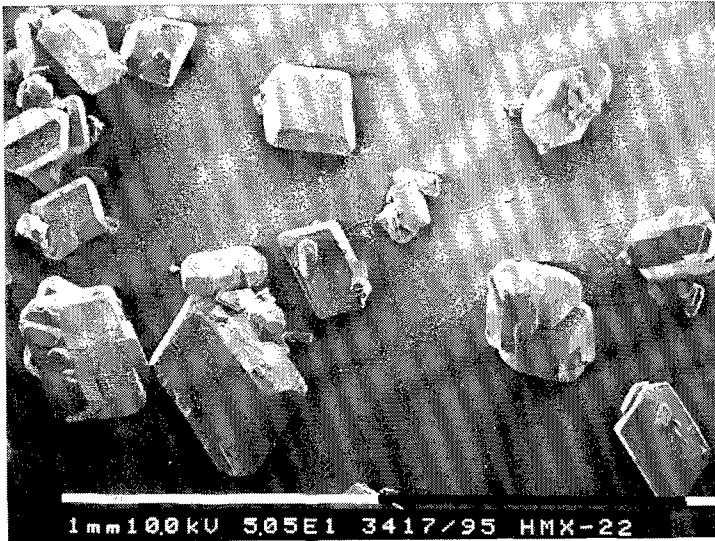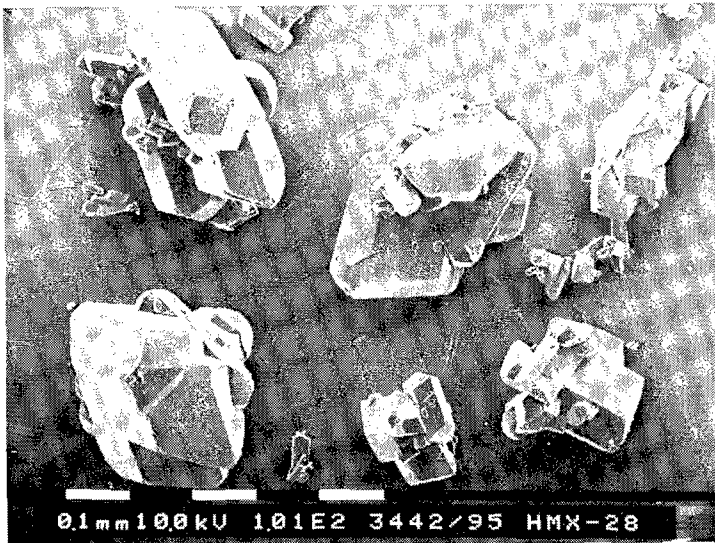
Figure 2: SEM pictures of HMX crystals taken from (*a*) batch 22 and (*b*) batch 28. Note that the crystals from batch 28 are much more agglomerated than those of batch 22.

Figures 3 and 4 show the X-ray Laue diffraction patterns of a collection of crystals taken from the batches 22 and 28, respectively. Per batch, three different samples were taken and subjected to the X-ray beam (exposure times 30 min). The radial elongation of the diffraction spots is a measure for the overall disorder within the crystals, *i.e.* the larger the radial spot extension, the higher the overall disorder. The Laue patterns recorded from the crystals of batch 22 (figure 3) show only a minor radial spot extension, pointing at a relatively high average degree of crystal perfection. However, the spot elongation in the Laue patterns of the crystals taken from batch 28 (figure 4) is much more severe, implying that these crystals have a much higher degree of disorder than the crystals from batch 22. Using the above given equation for the radial spot extension R, with $D = 40$ mm, a range of η values can be calculated for each batch (see table 2). For batch 22, $\eta \sim 0.1° - 0.7°$, which points at a high average degree of perfection of the crystals. For batch 28, a much higher mosaic spread in the range of $\sim 0.8° - 4.1°$ is found, indicating that the internal quality of these crystals is much less compared to batch 22. Batch 27 ($\eta \sim 0.3° - 2.5°$) is of an intermediate quality.

Table 2: Analytical results of the characterization of the batches listed in teble 1 (n.d. = not determined).

batch code	density [a] $[g/cm^3]$	d_{50} $[\mu m]$	purity [b] $[wt\%]$	impact sens. $[Nm]$	friction sens. $[N]$	mosaic spread $[°]$
HMX-THP-22	1.893	296	acetone: < 0.2 γ-but.: 0.03	7.5	108	0.1° – 0.7°
HMX-THP-27	1.901	304	acetone: < 0.2 γ-but.: < 0.03	n.d.	n.d.	0.3° – 2.5°
HMX-THP-28	1.901	378	acetone: < 0.2 γ-but.: < 0.03	7.5	108	0.8° – 4.1°

[a] The density of pure HMX is 1.903 g/cm^3.
[b] Detection limit for acetone 0.2 wt%, for γ-butyrolactone 0.03 wt%.

The X-ray Laue observations are in line with the optical microscopic results: the higher the visible amount of inclusions, the larger the radial spot extension in the Laue X-ray diffraction patterns. They are, however, not in-line with the density results. Since, in principle, any kind of structural defect contributes to the radial spot extension in the Laue diffraction patterns, it is expected that in case the crystals of batch 22 would contain a large number of relatively small inclusions, in order to explain the lower density of these crystals, also the spot extension would be more severe. This is, however, not the case and therefore it still remains unclear why the density results of the batches 22 and 28 are not in-line with the optical microscopy and Laue diffraction results.
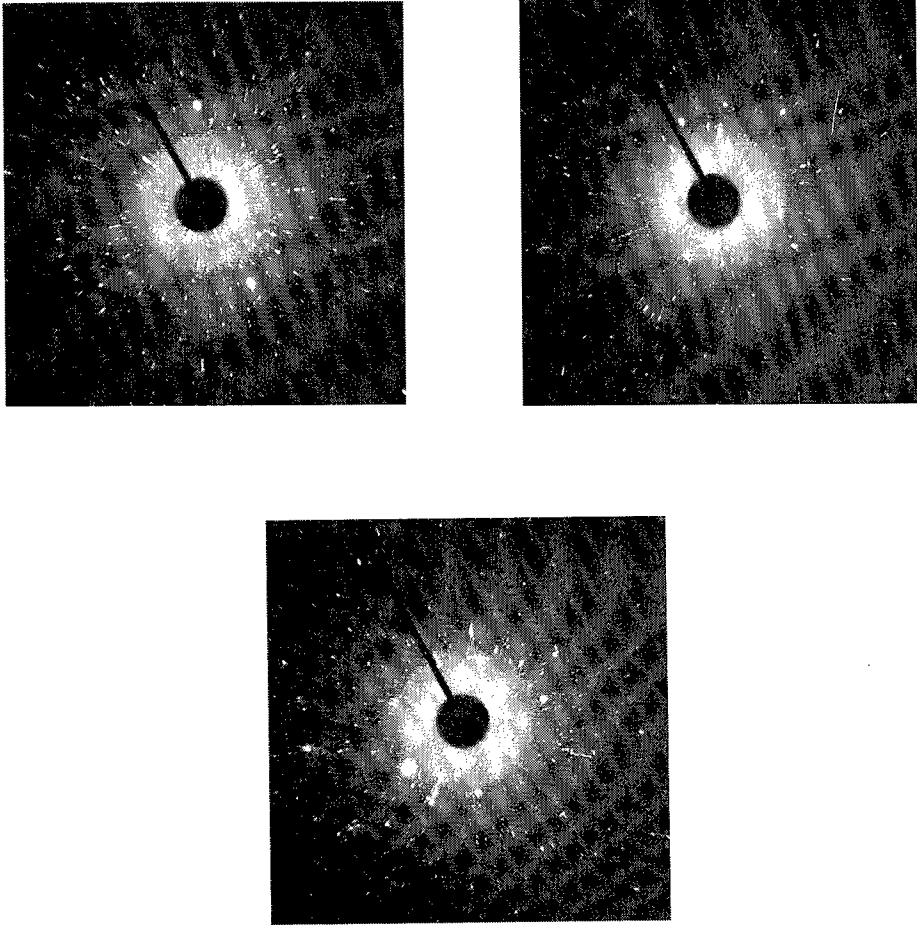
Figure 3: X-ray Laue diffraction pictures of a collection of HMX crystals from batch 22. The diffraction patterns were recorded in triplo with different samples. The diffraction spots are quite sharp and circular, implying that the averaged crystal perfection is good. The mosaic spread as determined from these pictures, is within the range of ~ 0.1° – 0.7°.
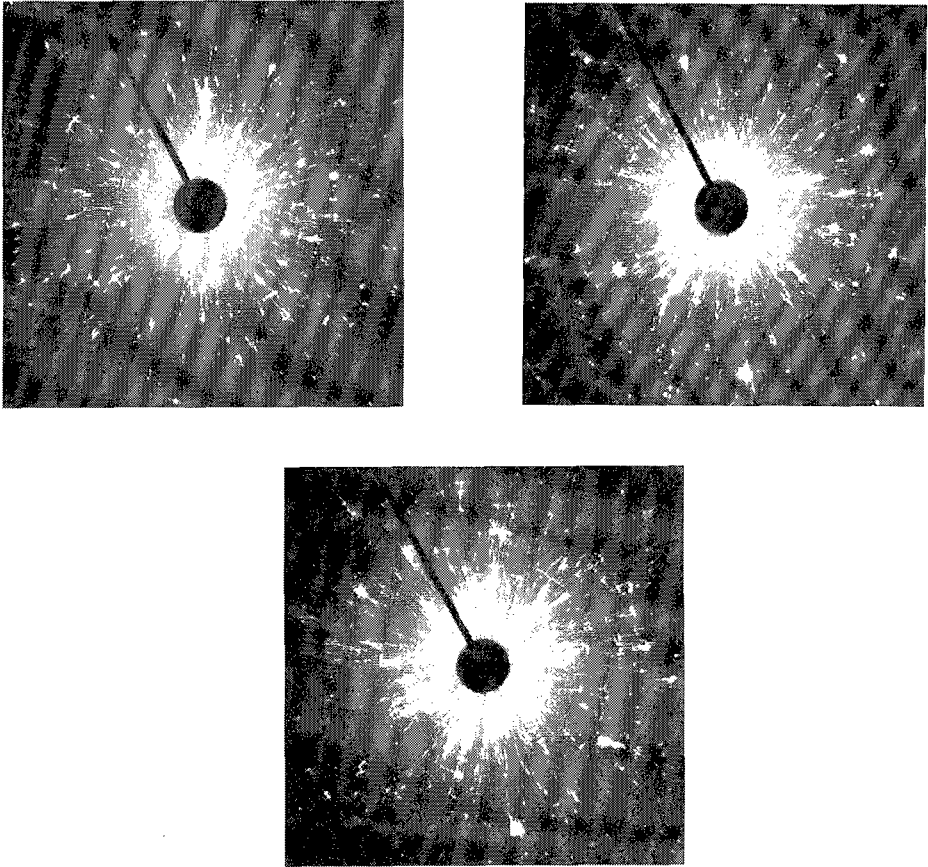
Figure 4: X-ray Laue diffraction pictures of a collection of HMX crystals from batch 28. Again, the diffraction patterns were recorded in triplo with different samples. Obviously, the diffraction spots are elongated and smeared out, indicating a much lower internal quality of the crystals compared to those of batch 22. The mosaic spread as calculated from these pictures, ranges from ~ 0.8° to ~ 4.1°.

Conclusions

The characterization of HMX crystals produced by cooling crystallization from a 1:1 molar ratio acetone/γ-butyrolactone mixture by means of X-ray Laue diffraction has shown that crystals which contain a relatively large amount of visible inclusions also exhibit a large radial extension of the spots in the Laue diffraction patterns. This points at a relatively high degree of overall disorder within the crystals, quantified by the so-called mosaic spread, η. In principle, any kind of structural defect within a crystal will contribute to the mosaic spread, whereas optical microscopy only reveals the macroscopic defects, like inclusions and cracks. This limits the information obtained on the internal

crystal quality by means of optical microscopy. Despite the fact that no detailed information is gained on the specific nature of the defects causing this mosaic spread, the X-ray Laue Diffraction technique can be used as an additional tool to characterize the degree of perfection of crystals since it includes the microscopic defects as well.

Acknowledgements

List of abbreviations

CSD	Crystal Size Distribution
GC	Gas Chromatography
HMX	$C_4H_8N_8O_8$
HTPB	Hydroxy-Terminated PolyButadiene
PBX	Plastic Bonded eXplosive
RDX	$C_3H_6N_6O_6$
SEM	Scanning Electron Microscopy

References

[1] A.C. van der Steen, W. Duvalois and A.C. Hordijk, *Crystal quality and less sensitive eplosives*, presented at the *Insensitive Munitions Technology Symposium*, 16 – 18 June 1992, Williamsburg VA, USA

[2] N.H.A. van Ham, A.C. van der Steen and J.J. Meulenbrugge, *Less sensitive explosives*, AGARD Conference Proceedings 511, 21 – 23 October 1991, Bonn, FRG

[3] A.E. van der Heijden and G.M. van Rosmalen, in: *Handbook of Crystal Growth*, chapter 7, ed. D.T.J. Hurle (Elsevier Science Publishers, Amsterdam, 1994)

[4] R.S. ÓMeadhra, *Modelling of the kinetics of suspension crystallizers. A new model for secondary nucleation*, PhD Thesis, Delft University of Technology, 1995

[5] H.L. Bhat, J.N. Sherwood and T.S. Shripathi, Chem. Eng. Sci. **42** (1987) 609

[6] L. Borne, in: *Proceedings of the 5th Congrès International de Pyrotechnie*, EUROPYRO 93 (6 – 11 June 1993, Strasbourg, France), p155

[7] P.J. Halfpenny, K.J. Roberts and J.N. Sherwood, J. Crystal Growth **65** (1983) 524

[8] P.J. Halfpenny, K.J. Roberts and J.N. Sherwood, J. Crystal Growth **69** (1984) 73

[9] P.J. Halfpenny, K.J. Roberts and J.N. Sherwood, J. Material Science **19** (1984) 1629

[10] P.J. Halfpenny, K.J. Roberts and J.N. Sherwood, Phil Mag. **A53** (1986) 531

[11] H.G. Gallagher, P.J. Halfpenny, J.C. Miller and J.N. Sherwood, Phil. Trans. R. Soc. Lond. **A339** (1992) 293

[12] R.I. Ristic, J.N. Sherwood and K. Wojciechowski, J. Crystal Growth **91** (1988) 163

[13] M.M. Mitrovic, R.I. Ristic and I. Ciric, Appl. Phys. **A51** (1990) 374

[14] M.M. Harding, R.J. Rule, R.J. Oldman and R.J. Davey, J. Crystal Growth **123** (1992) 373

[15] J.H. ter Horst, work in progress

[16] J. Köhler and R. Meyer, in: *Explosivstoffe* (7th edition, Spandel-Druck, Nürnberg, FRG, 1991)

Vortrag: Entwicklung und Einsatz eines neuen TNT-freien Plattiersprengstoffes

Dr. Ulf Richter

Sprengplattieren ist die flächige Verschweißung von zwei Metallblechen durch die Detonationsenergie einer aufliegenden Sprengstoffladung.

An die Plattiersprengstoffe werden besondere Anforderungen gestellt:
+ Detonationsgeschwindigkeit im Bereich 1500 - 3500 m/s
+ Gleichmäßige Detonation des Sprengstoffs in relativ geringer Schichtdicke (15 - 60 mm) und unverdämmt auf einer großen Fläche (bis zu 20 m²)
+ Möglichkeit der gleichmäßigen Verteilung über die Plattierfläche ohne örtliche Dicken- oder Dichteschwankungen.

Die bisher eingesetzten pulverförmigen Sprengstoffe enthielten meist Ammoniumnitrat und TNT als Grundbestandteile.   Um die Herstellung zu vereinfachen, wurden Überlegungen über die Verwendbarkeit eines TNT-freien Plattiersprengstoffes angestellt .

Ein neu entwickelter Plattiersprengstoff auf der Basis Ammonnitrat-Mineralöl erfüllt die oben genannten Anforderungen . Nach verschiedenen Testreihen konnte er inzwischen in die Sprengplattier-Produktion eingeführt werden.

Development and Application of a new TNT free Explosive
for Cladding Purposes.

Explosive cladding is a solid state metal-joinig process that
uses explosive force to create a metallurgical bond between
two metal sheets.

The explosives used for eplosive cladding must meet the following
demands:
+ low detonation velocity in the range 1500 - 3500 m/s
+ detonation must be uniform in relatively thin layers (15 - 60 mm)
  without confinement over large areas (up to 20 m^2)
+ possibility of distribution over the cladding area with uniform
  layer thickness and density.

Most cladding explosives are powderous mixtures of TNT and ammonium
nitrate with inert ingredients. A new developed cladding explosive
of the ammonium nitrate - fuel oil type contains glass microballoons
to improve the detonation sensibility in thin layers.

Dynamit Nobel	Entwicklung u. Einsatz eines neuen TNT - freien Plattiersprengstoffes	Dynamit Nobel GmbH Explosivstoff-und Systemtechnik Werk Würgendorf Plattierbetrieb Würgendorf, 30. April 1996 Seite 1 von 5

Einleitung

Sprengplattieren oder „Explosive Cladding" ist ein Verfahren zur flächigen Verschweißung von zwei unterschiedlichen Metallen mit Hilfe der Detonationsenergie einer Spengstoffladung. Vorwiegend wird es eingesetzt, um auf großflächige Stahlbleche eine korrosionsbeständige Schicht aus rostfreiem Stahl, Kupfer- oder Nickellegierung, Titan, Tantal, Silber usw. aufzubringen. Dazu wird das Blech aus dem korrosionsbeständigen Werkstoff in gleichbleibendem Abstand über dem geschliffenen Stahlblech angeordnet und seine Oberseite mit einer Sprengstoffschicht belegt. Bei Detonation des Sprengstoffs bewirkt die durchlaufende Detonationsfront, daß das darunterliegende Blech abknickt und mit hoher Geschwindigkeit unter einem kleinen Winkel (2°-25°) gegen das Stahlblech geschleudert wird. Unter diesen Bedingungen tritt in der Kollisionsfront der beiden Metalle eine Druckverschweißung ein. (Lit 1 u. 2)

Anforderungen an den Plattiersprengstoff

Um eine optimale Verschweißung zu gewährleisten und eine Rißbildung in den zu verschweißenden Metallen zu vermeiden, muß die Detonationsgeschwindigkeit des verwendeten Sprengstoffs unter der Schallgeschwindigkeit der Metalle liegen. In der technischen Praxis verwendet man vorzugsweise niedrige Detonationsgeschwindigkeiten zwischen 1500 und 3500 m/s, abhängig von der Werkstoffkombination, um auch die Änderung der mechanischen Eigenschaften der plattierten Werkstoffe (Härte, Streckgrenze, Zugfestigkeit, Dehnung, Kerb-

schlagzähigkeit) während des Durchgangs der Stoßwelle möglichst gering zu halten (Lit. 3 u. 4).

Aus Gründen der günstigen Handhabung und der Wirtschaftlichkeit setzt man für das Explosivplattieren fast ausschließlich pulverförmige Sprengstoffe ein. Rund um die Ränder des aufzuplattierenden Bleches wird ein Rahmen zur Aufnahme des Sprengstoffs aufgebracht, der aus Streifen von Pappe, Holz oder Metall bestehen kann. In den dadurch entstehenden flachen Kasten wird möglichst gleichmäßig der Sprengstoff eingefüllt. Seine Schichthöhe muß für jede Plattierkombination berechnet werden aus Dicke, Dichte und Festigkeit der zu verschweißenden Werkstoffe und den spezifischen Daten des verwendeten Sprengstoffs. Die benötigten Mengen liegen zwischen 15 und 150 kg Sprengstoff pro Quadratmeter. Die in einem Schuß zu plattierenden Flächen können größer als 20 m² sein.

An den Plattiersprengstoff werden hohe Anforderungen gestellt.

Er muß auf großen Flächen und in relativ geringer Schichtdicke (von 15 mm aufwärts) unverdämmt mit gleichbleibender Geschwindigkeit durchdetonieren. Da bei pulverförmigen Sprengstoffen die Detonationsgeschwindigkeit sowohl mit der Schichthöhe wie auch mit der Schüttdichte ansteigt, muß großes Augenmerk gelegt werden auf eine gleichmäßige Verteilung des Sprengstoffs über die Plattierfläche, ohne örtliche Dicken- oder Dichteschwankungen, die sonst zu Ungleichmäßigkeiten in der Plattierqualität führen könnten, (Lit. 5).

TNT - haltige Plattiersprengstoffe

Die am häufigsten eingesetzten Plattiersprengstoffe haben TNT und Ammoniumnitrat als wirksame Hauptbestandteile. Die Mischung kann bei höherer Temperatur geschehen, wobei sich jedes Ammonnitratteilchen mit einem Film aus flüssigem TNT überzieht, („Amatol"), oder bei

Normaltemperatur, wobei jedoch zur Einhaltung der oben genannten Anforderungen großes Augenmerk auf die richtige Kornverteilung im TNT sowie im Ammonnitrat gelegt werden muß. Um die benötigte niedrige Detonationsgeschwindigkeit zu erreichen, ist entweder eine Verdünnung mit einem Inertstoff nötig (z.B. Kochsalz; auch Sand ist eingesetzt worden) oder eine erhebliche Dichteerniedrigung (Verwendung von vakuumverdüstem Ammonnitrat; Einmischen von Aerosil, Perlite usw.) Verschiedene technologische Zusätze verbessern die Rieselfähigkeit des Pulversprengstoffs.

Die TNT- haltigen Plattiersprengstoffe haben gewisse Nachteile. Die Mischung bei erhöhter Temperatur ist sehr teuer, und die nach dem zweiten Verfahren hergestellten Mischungen neigen stark zur Staubentwicklung, was zu erhöhtem Arbeitsschutzaufwand bei der Herstellung und Verwendung führt.

Es wurden auch schon Sprengstoffe auf ANFO -Basis (94% Ammonnitrat - 6% Dieselöl) für das Sprengplattieren verwendet. Diese sind jedoch nur einsetzbar bei höheren Schichtdicken, da sie sonst nicht mehr gleichmäßig durchdetonieren, und neigen zur unregelmäßigen Verdichtung beim Auftragen auf die Blechoberfläche.

TNT - freier Plattiersprengstoff

Da aus Gründen der Arbeitssicherheit ein TNT-freier Sprengstoff vorzuziehen ist, wurden Versuche durchgeführt, einen Sprengstoff auf der Basis Ammonnitrat-Minerallöl soweit zu modifizieren, daß er die oben genannten Anforderungen an einen Plattiersprengstoff erfüllt.

Die vom Hersteller bezogenen Ammonnitrat-Prills wurden so gemahlen, daß eine bestimmte, immer gleichbleibende Kornverteilung eingehalten werden konnte. Der Anteil an Dieselöl mußte herabgesetzt werden, um die Riesel-

fähigkeit zu verbessern, und statt dessen Pflanzenmehle als Kohlenstoffträger eingemischt. Zur Herabsetzung der Detonationsgeschwindigkeit diente auch hier ein Zusatz von Inertstoff. Dadurch wurde jedoch die Detonationsfähigkeit so gemindert, daß der Sprengstoff für den vorgesehenen Zweck nicht einsetzbar war. Durch Einmischen von Mikroglashohlkugeln, wie sie auch in Emulsionssprengstoffen verwendet werden, konnte jedoch die Empfindlichkeit des Sprengstoffs so weit gesteigert werden, daß ein Durchdetonieren schon in einer 15 mm dicken Schicht in offener Schüttung stattfand. Diese Empfindlichkeitssteigerung des Sprengstoffs durch die Mikroglashohlkugeln erklärt sich durch die Bildung sogenannter „hot spots", die die Detonationsfront ideal weiterleiten.

Ein Beispiel einer solchen TNT-freien Plattiersprengstoffmischung gibt die folgende Rezeptur:

Ammoniumnitrat	68,0 Gew. %
Mineralöl	1,5 Gew. %
Mikroglashohlkugeln	2,2 Gew. %
Kochsalz	24,0 Gew. %
Pflanzenmehl und technologische Zusätze	4,3 Gew. %

Durch Änderung des Anteils des Verdünnungsmittels (z.B. Kochsalz) und der Mikroglashohlkugeln können die für die verschiedenen Plattierkombinationen benötigten Detonationsgeschwindigkeiten zwischen 1500 und 3000 m/s eingestellt werden. Auf die neue Plattiersprengstoff-Zusammensetzung wurde das deutsche Patent DE 4340577 C 1 erteilt.

Diese Sprengstoffe sind kapselempfindlich, weisen Dichten zwischen 0,65 und 0,90 g/cm³ auf und sind für den Transport als Sprengstoff Typ B der Klasse 1.1 D Ziffer 4, UN-Nr. 0082 klassifiziert. Sie werden seit 2 Jahren erfolgreich für die Sprengplattierung einer großen Zahl von Metallkombinationen eingesetzt, darunter auch so kritische wie Titan/Stahl, Tantal/Stahl oder Aluminium/Kupfer.

Literatur

1) Richter, U.:

   Sprengplattierungen im Chemie-Apparatebau

   Chemie - Technik 12 (1983) 4, S. 63 - 71

2) Prümmer, R.:

   Grundsätzliche Untersuchungen zum Explosivplattieren

   ICT - Jahrestagung 1976, S. 175 - 193

3) Richter, U.:

   Einfluß der Sprengplattierung auf die mechanischen Eigenschaften des Grundwerkstoffs

   ICT - Jahrestagung 1976, S. 195 - 210

4) Banker, J.G., Reineke, E.G.: :

   Explosive Welding

   ASTM Handbook Vol. 6, 1993 S. 303 - 305

5) Linse, V.D.

   Procedure Development and Process Considerations for Explosive Welding

   ASTM Handbook Vol. 6, 1993 S. 896 - 900

EINSATZ VON HNS IN DER ERDÖLEXPLORATIONSTECHNIK

Uwe Gessel, Helmut Zöllner

Dynamit Nobel GmbH
Explosivstoff- und Systemtechnik
53839 Troisdorf, FRG

Zusammenfassung

Explosivstoffhaltige Komponenten für die Erdölexplorationstechnik sind in der Anwendung extremen Temperaturen und Drücken ausgesetzt. Die Spitzenbelastungen liegen derzeit bei 260°C und 150 MPa. Als Sprengstoffe werden unter diesen Bedingungen vorzugsweise HNS und PYX eingesetzt.

Im Rahmen dieses Vortrages werden die Eigenschaften eines speziell für die Explorationstechnik optimierten HNS vorgestellt. Es wird insbesondere auf die Empfindlichkeit und die Stabilität verschiedener HNS-Typen eingegangen.

Abstract

Detonating devices for application in oilfield exploration technology are exposed to extreme high temperature and to high pressure. These maximum demands at present are 260°C and 150 MPa. Under these conditions HNS and PYX are mainly used.

The scope of this presentation is to present the characteristics of an optimized HNS for exploration technology. In particular the sensitivity and the stability of different types of HNS are discussed.

1 Einleitung

In den letzten 30 Jahren sind zahlreiche Veröffentlichungen zu dem Thema HNS erschienen, die sich sowohl mit neuen Herstellverfahren als auch mit neuen Einsatzgebieten beschäftigen. Besondere Bedeutung erlangte das HNS Anfang der Siebziger, als bei der schwedischen Firma Bofors entdeckt wurde, daß geschmolzenes TNT durch Zugabe von HNS feinkristallin erstarrt. In der Zündmitteltechnik spielt HNS seit der Entwicklung von EFI-Zündern eine wichtige Rolle. Der kleine kritische Durchmesser, die relativ geringe Empfindlichkeit und die gute Initiierbarkeit durch kurze Druckimpulse, wie sie in EFI-Systemen erzeugt werden, ermöglichen bei Verzicht auf Initialsprengstoffe die Fertigung von In-Line-Zündketten /1/.

Desweiteren wird HNS auch in der Luft-und Raumfahrttechnik (z.B. MDF - Mild Detonating Fuse) eingesetzt. Die hohe Temperaturbeständigkeit macht HNS ebenso für den Einsatz in der Erdölexplorationstechnik interessant. Während im unteren Temperaturbereich bis ca. 180°C vorzugsweise RDX und HMX zum Einsatz kommen, wird oberhalb dieser Grenze bis ca. 250°C zunehmend HNS in den explosivstoffhaltigen Komponenten eingesetzt. Neben den hohen Temperaturen ist das HNS bei diesen Anwendungen auch extremen Drücken ausgesetzt. Bei Bohrlochtiefen bis 7000 m können Druckwerte von 140 MPa überschritten werden.

Die Verwendung von HNS ist zunehmend bei allen Komponenten für die Explorationstechnik üblich. Trotz seiner geringen Ausgangsleistung und seiner niedrigen Detonationsgeschwindigkeit kommt HNS sowohl bei den Zündmitteln Sprengzünder, Sprengschnur sowie Booster als auch bei den Wirkkomponenten Perforatoren oder Schneidladungen zum Einsatz. Bei der Auslegung von HNS-haltigen Komponenten sind diese Nachteile besonders zu berücksichtigen.

Im folgenden werden einige wichtige Aspekte der Herstellung und Aufbereitung von HNS für den speziellen Einsatz im Bereich der Erdölexplorationstechnik vorgestellt. Dabei steht die Optimierung des HNS hinsichtlich leichter Verarbeitbarkeit, guter Temperaturbeständigkeit, hinreichender Empfindlichkeit bei Verwendung in Zündmitteln und hoher Ausgangsleistung bei Einsatz in Perforatoren im Mittelpunkt.

2 HNS und seine Eigenschaften

2.1 Herstellung

Hexanitrostilben wurde erstmals 1964 von K.G. Shipp /2,3/ im Rahmen eines Programms zur Entwicklung hochtemperaturbeständiger Sprengstoffe hergestellt. Die Synthese erfolgte seinerseits durch Oxidation von TNT mittels einer alkalischen NaOCl-Lösung in einer Ausbeute von 40-45%. Aufgrund seines hohen Schmelzpunktes von 320°C ist HNS ein sehr interessanter Sprengstoff. In den folgenden Jahren beschäftigten sich daher zahlreiche Arbeitsgruppen mit der HNS-Herstellung. Primär handelte es sich hierbei jedoch um Modifikationen des sogenannten Shipp-Prozesses. Aber auch neue Synthesemethoden wurden entwickelt, wobei in erster Linie andere Oxidationsmittel zum Einsatz kamen. Dennoch haben alle Verfahren eines gemeinsam: Als Ausgangskomponente wird TNT oder eine bei dieser Umsetzung auftretende Zwischenstufe wie HNBB (Hexanitrobibenzyl bzw. Dipikrylethan) oder Trinitrobenzylchlorid eingesetzt. Im vorliegenden Vortrag wird allerdings weder auf den Chemismus dieser Reaktionen eingegangen noch werden die anderen Herstellprozesse genau erläutert.

Dynamit Nobel befaßt sich ebenfalls seit mehr als zwei Jahrzehnten mit der Herstellung und der Verarbeitung von HNS. Vor allem durch die neue Produktlinie der Zündmittel zur Gewinnung von Erdöl und Erdgas - Zünder, Sprengschnüre, Booster und Perforatoren - hat das Interesse an diesem Hochtemperatursprengstoff stark zugenommen.

2.2 Umkristallisation

Das bei der Synthese von HNS anfallende Rohprodukt ist für den Einsatz im Hochtemperaturbereich nicht geeignet. Bedingt durch die Bildung von Nebenprodukten, insbesondere HNBB, muß das Material umkristallisiert werden. Ansonsten neigt das HNS bei den extrem hohen Anwendungstemperaturen von bis zu 250°C zur Instabilität und vorzeitiger Zersetzung. Um die Verunreinigungen zu entfernen, gibt es verschiedene Methoden:

- Organische Lösungsmittelmethode

- Chemische Methode /4/

Bei der Lösungsmittelmethode wird das Rohprodukt in einem organischen Lösungsmittel umkristallisiert. Aufgrund der geringen Löslichkeit von HNS - es lösen sich in DMF bei 100°C nur etwa 6% - fällt das Produkt beim Abkühlen wieder aus und die Beiprodukte bleiben in Lösung.

Die chemische Methode verwendet Salpetersäure als Reinigungsmedium. Hierbei wird das Roh-HNS in die entsprechende Säure eingetragen und unter Rückfluß der HNO_3 werden die Verunreinigungen zersetzt.

Beide Methoden führen zu HNS-Kristallisaten, die sich nach Literaturangaben in der thermischen Stabilität unterscheiden. Untersuchungen von Mild Detonating Fuses ergaben, daß bei Verwendung von HNS, das aus einem organischen Lösungsmittel umkristallisiert wurde, eine Funktion nach Temperaturbelastung von 225°C über einen Zeitraum von 16 h nicht mehr gewährleistet ist /5/. Setzt man dagegen ein in HNO_3 gereinigtes HNS ein, so detonieren diese Spezialsprengschnüre unter gleicher Temperaturanwendung noch nach 64 h einwandfrei durch. Andere Autoren wiederum erwähnen, daß die thermische Stabilität von HNS besser ist, wenn der Explosivstoff aus einem organischen Lösungsmittel umkristallisiert wird. Offenbar führen die Untersuchungen nicht zu einem einheitlichen Ergebnis.

Die Kristallform des HNS und die damit verbundene Rieselfähigkeit wird primär durch die Bedingung bei der Umkristallisation bestimmt. Wird DMF eingesetzt, so kristallisiert das HNS in Nadeln aus, die sich aufgrund der niedrigen Schüttdichte nicht zum Verarbeiten in Zündmitteln eignen. Um ein fließfähiges Produkt zu erhalten, sind mehrere Verfahren entwickelt worden, die sowohl organische Lösungsmittelgemische /6/ als auch Salpetersäure verwenden. Das nach diesen Verfahren hergestellte Produkt wird als HNS II bezeichnet und besitzt eine orthorhomische Kristallstruktur. HNS II hat eine Schüttdichte von größer 0,5 g/cm^3 und einen Schmelzpunkt von min. 319°C.

Neben HNS II existieren noch zwei weitere HNS-Typen. Ein HNS I mit einer Schüttdichte kleiner 0,5 g/cm^3 und ein HNS IV mit einer sehr hohen spezifischen Oberfläche von 5 bis 25 m^2/g. Die Herstellung von HNS IV erfolgt in einem speziellen Fällprozeß /7/. Hierbei wird HNS II in DMF gelöst und unter besonderen Bedingungen in einem Nichtlöser, wie z.B. H_2O oder Xylol, wieder ausgefällt. Verwendung findet dieses extrem feine Material in EFI-Detonatoren.

Untersuchungen unsererseits haben ergeben, daß ein aus Salpetersäure umkristallisiertes HNS II mit einer Schüttdichte von 0,87 g/cm^3 und einer mittleren Korngröße von 400 µm eine hervorragende Rieselfähigkeit besitzt und sich somit gut verarbeiten läßt. Bedingt durch das relativ grobe Korn, nimmt aber die Empfindlichkeit gegenüber einem Detonationsstoß deutlich ab.

Ein Maß für die Empfindlichkeit von Sekundärsprengstoffen ist der sogenannte Grenzinitialtest /8/. In diesem Test erfolgt die Bestimmung der Bleiazidmenge, die notwendig ist, um den Sekundärsprengstoff einwandfrei zu zünden (Grenzinitial). Hierzu wird der zu prüfende Sprengstoff, eine variable Menge Bleiazid und ein Friktionssatz in eine kleine Aluminiumhülse eingebracht. Die Zündung des Friktionssatzes bewirkt eine Initiierung des Bleiazids. Je nach Empfindlichkeit des Sekundärsprengstoffes wird zur Initiierung mehr oder weniger Bleiazid benötigt. In einem Probit-Test kann somit das Grenzinitial ermittelt werden.
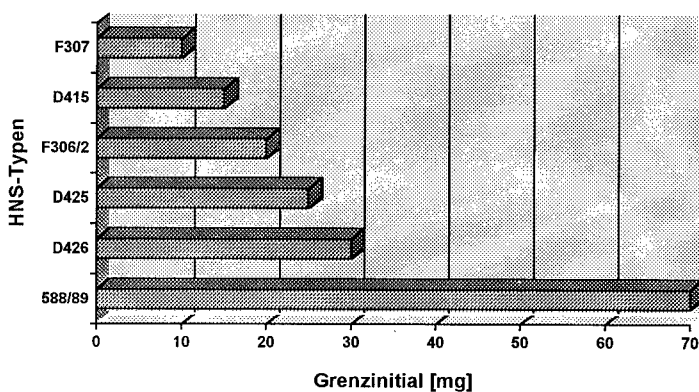
Abbildung 1: Grenzinitial verschiedener HNS-Typen

Abbildung 1 zeigt einen Vergleich der Grenzinitiale verschiedener HNS-Typen. Das Spektrum reicht von 70 mg (höher als HMX) bis hin zu 10 mg ähnlich PETN. Für die sichere Initiierung der Type 588/89 - das aus Salpetersäure umkristallisierte HNS - ist im Gegensatz zu den anderen Typen, die aus einem organischen Lösemittel umkristallisiert wurden, 70 mg Bleiazid notwendig. Die relativ hohe Unempfindlichkeit macht dieses HNS für den Einsatz in den entsprechenden Zündmitteln nur bedingt einsetzbar. Untersuchungen, speziell von DW-Zündern und Sprengschnüren, haben ergeben, daß es bei Verwendung diesen HNS-Typs nach Temperatur- und Druckbelastung immer wieder Probleme mit der Funktion gab. Entweder ließen sich die Zündmittel nicht mehr initiieren oder detonierten nicht einwandfrei durch. Die Grenzinitialwerte der aus einem organischen Lösemittel umkristallisierten HNS-Proben liegen mit 10-30 mg deutlich niedriger. Allerdings läßt sich dieses Material aufgrund der bereits erwähnten nadelförmigen Kristalle nicht verarbeiten. Daher wurde bei Dynamit Nobel ein Verfahren entwickelt, um das HNS unter Beibehaltung der Empfindlichkeit so in eine Form zu überführen, die sich einerseits gut in Zündmitteln verladen läßt und andererseits die Funktion auch unter Druck- und Temperaturbelastung gewährleistet.

2.3 Dynamit Nobel Verfahren

Zunächst wird das beim Herstellprozeß anfallende Roh-HNS in DMF umkristallisiert. Die Größe des Primärkorns und damit die Empfindlichkeit des HNS läßt sich durch die Abkühlgeschwindigkeit der Lösung beeinflussen. In Abbildung 2 ist die Abhängigkeit des Grenzinitials als Funktion der Korngröße dargestellt. Deutlich ist ein Anstieg des Grenzinitialwertes mit der Zunahme der Korngröße zu erkennen. Bei einer mittleren Korngröße von 10 μm werden zur sicheren Initiierung nur 10 mg Bleiazid benötigt und dieser Wert steigt bei einer mittleren Korngröße von 80 μm auf 30 mg Azid an.
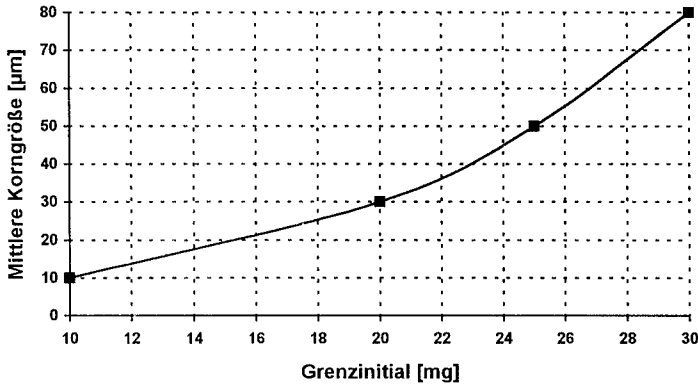
Abbildung 2: Grenzinitial als Funktion der mittleren Korngröße

Um das HNS in eine „handhabbare" Form zu überführen, wird das umkristallisierte Material in einem weiteren Verfahrensschritt gekörnt. Die Empfindlichkeit des gekörnten Materials nimmt gegenüber dem ungekörnten HNS aber nicht ab. Wie Abbildung 3 zeigt, sind die Grenzinitial-werte beider HNS Typen nahezu identisch.
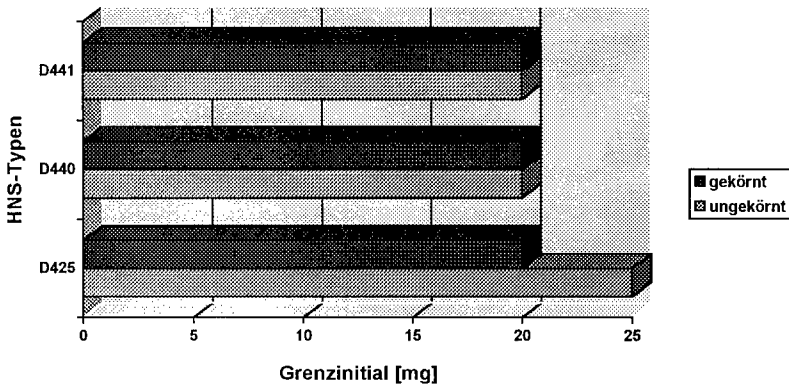
Abbildung 3: Grenzinitial von gekörnten und ungekörnten HNS-Typen

Das Körnverfahren ermöglicht Schüttdichten von bis zu 0,85 g/cm³. Bedingt durch die hohe Dichte und die gute Festigkeit der einzelnen Granulate, läßt sich dieses Material einerseits her-vorragend verarbeiten und andererseits können Zündmittel für die Explorationstechnik mit gu-ten Leistungswerten hergestellt werden. Somit ermöglichte dieses HNS die Entwicklung einer kunststoffummantelten HNS-Sprengschnur mit einer Detonationsgeschwindigkeit von nahezu 6500 m/s. Diese Sprengschnur kann 1 h bei Temperaturen bis zu 250°C eingesetzt werden. Die maximale Einsatzdauer bei 230°C, also nur 20°C niedriger, beträgt sogar 200 h. An diesen Werten läßt sich erkennen, welchen extremen Bedingungen HNS-haltige Komponenten wäh-rend einer Perforation ausgesetzt sind.

Die Einsatztemperaturen von 250°C bzw. 230°C zeigen aber auch, daß ein aus DMF umkristallisiertes HNS eine sehr gute Thermostabilität aufweist. Vergleichende Untersuchungen mittels DSC lassen zwischen diesem HNS und dem in Salpetersäure umkristallisierten HNS hinsichtlich der thermischen Beständigkeit keine Unterschiede erkennen. Der Schmelzpunkt beider HNS-Typen liegt bei einer Aufheizrate von 20K/min zwischen 321 und 323°C und der Zersetzungspunkt zwischen 361 und 365°C.

2.4 Gap-Test

Neben dem Grenzinitial wurde an den verschiedenen HNS-Typen auch die reine Stoßwellenempfindlichkeit mit Hilfe des BICT-Gap-Testes /9/ ermittelt. Als Geberladung fungiert bei dieser Methode ein Hexogen-Preßling mit einem Durchmesser von 21 mm. Die Abschwächung der Stoßwelle erfolgt durch ein variables Wasser-Gap. Die Ergebnisse sind in Abbildung 4 zusammengestellt.
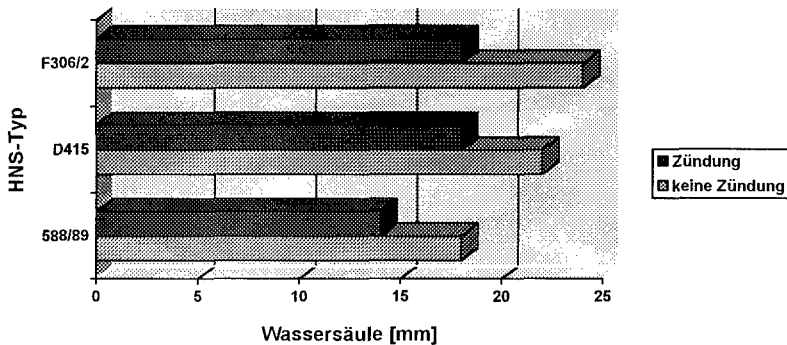
Abbildung 4: Gap-Test-Resultate verschiedener HNS-Typen

Analog zum Grenzinitialtest zeigt sich auch im Gap-Test, daß das mit HNO_3 behandelte HNS, Typ 588/89, unempfindlicher ist als die aus organischen Lösungsmitteln umkristallisierten HNS-Sorten. Während bei Typ 588/89 zur Zündung die Wassersäule auf 14 mm reduziert werden muß, ist bei D415 und F306/2 auch bei 18 mm Gap-Dicke noch eine Initiierung zu beobachten. Die Werte 14 und 18 mm entsprechen einem Stoßwellendruck von 3 bzw. 2 GPa /9/. Bei den Typen D415 und F306/2 handelt es sich jeweils um ein gekörntes Material.

3 Zusammenfassung

HNS ist ein Sprengstoff, der in den letzten Jahren immer mehr an Bedeutung gewonnen hat. Besonders in der Explorationstechnik werden bei Temperaturen von bis zu 250°C vermehrt HNS-haltige Zündmittel eingesetzt. Die besonderen Bedingungen stellen somit hohe Anforderungen an die Thermostabilität, die Zuverlässigkeit und die Leistung aller Komponenten.

Für den Einsatz in diesen Zündmitteln wurde ein spezielles HNS-Granulat mit sehr guter Rieselfähigkeit entwickelt. Die Empfindlichkeit des gekörnten Material ist gegenüber einem HNS mit einer mittleren Korngröße von 400 μm wesentlich höher und nimmt im Vergleich zum Primärkorn nicht ab, wie die entsprechenden Grenzinitialwerte verdeutlichen. Diese Unterschiede zeigen sich auch bei der Bestimmung der Stoßwellenempfindlichkeit mit Hilfe des BICT-Gap-

Testes. Bei der thermischen Stabilität wurden allerdings keine Unterschiede zwischen einem aus Salpetersäure oder einem aus DMF umkristallisierten HNS festgestellt.

Die HNS-haltigen Komponenten sind bei den Perforationen nicht nur der Temperatur, sondern teilweise auch dem hydrostatischen Druck ausgesetzt. Es gibt dabei einige Hinweise, daß die Thermostabilität des HNS insbesondere unter Druckbeanspruchung abnimmt. Weiterhin erscheinen Wechselwirkungen zwischen dem Initialsprengstoff Bleiazid und HNS bei hohen Temperaturen (> 200°C) wahrscheinlich. Diese Eigenschaften sollen in weiteren Versuchen nach Schaffung der apparativen Voraussetzungen näher untersucht werden.

4 Literatur

/1/ Stroud, J.R., „A New Kind of Detonator - The Slapper", UCRL-77639, 1976

/2/ Shipp, K.G., Kaplan, L.A., „Reactions of α-Substituted Polynitrotoluenes, J. Org. Chem., 29 (1964) 2620-23

/3/ Shipp, K.G., „Explosive Hexanitrostilbene", US Patent 3.505.413, 07.04.1970

/4/ Balwant, S., Harinder, S., Def. Sci. J., 31 (1981), 305-8

/5/ Gould, D.J., „The Thermal Stability of Hexanitrostilbene as Determined by Precise Measurements of Detonation Velocity", Compat. Plast. other Mater. Explos., Propellants, Pyrotecn., Symp. II-F, 1976, pp 1-21

/6/ Syrop, L.J., „Process for Recrystallizing Hexanitrostilbene", US Patent 3.699.176; Chem. Abstr., 78 (1973), 32252K

/7/ Feairheller, W.R., Donaldson, T.A., Thorpe, R., „Recrystallization of HNS for the Preparation of Detonator Grade Explosive Material", Monsanto Research Corporation, Miamisburg, Ohio, USA, Bericht MLM-3499 (OP), April 1988

/8/ Jobelius, H., Zöllner, H., „Empfindlichkeitsprüfung von Sekundärsprengstoffen für Zündmittel", in 22th International Annual Conference of ICT, Karlsruhe, 1991

/9/ Bartels, H., „Ein modifizierter Gap-Test zur Bestimmung der Empfindlichkeit von Zünd- und Anzündstoffen gegenüber Stoßwellen", Explosivstoffe, 20, 143-150, 1972

METHODOLOGY OF EXAMINATION OF THE WAYS OF THE ACCIDENTAL EXPLOSIONS PREVENTION AT ENERGETIC MATERIALS PRODUCTION AND APPLICATION

Boris N.Kondrikov

Mendeleev University of Chemical Technology

9 Miusskaya Sq., Moscow 125047, Russia

Fax:(095)200-4204, e-mail:kondrikov@mhti.msk.su

Abstract

During the last decade the methodology of investigations aimed to prevent the accidental explosions in the energetic materials industry was developed in this Laboratory. As one of the results the algorithms of these works planning and realization were specifically proposed. The general approach includes

(1) The detailed analysis of the material production and (or) application technology, inspection of the causes and consequences of the accidental explosions taken place in this and related branches of industry. Separation of the most dangerous stage(s) of the process.

(2) Thermodynamic and kinetic study of chemical reactions responsible for heat evolution in conjunction with physical, mechanical, and reo-hydrodynamical processes involved. Creation, if possible, the mathematical model of the heat evolution process.

(3) Ignition, or selfignition possibility prediction. Spreading of flame in the system, burning instability and possible transition phenomena examination. The main criteria describing the level of the system danger evaluation.

(4) Comparison of the results of the experimental work and theoretical predictions with the real accidents circumstances.

(5) Formulation of recommendations for the technology modification resulting in its efficiency and safety level enhancement.

The general approach described here in outlines was implemented at investigations of the causes of the accidental explosions, and corresponding modification of technology of TNT, RDX, double base rocket propellants; at elucidation of the possible ways of accidental explosions at RDX drying, at transportation of RDX and HMX; at investigations of the premature explosions of the artillery projectiles; at inspection of explosions happened during the fires in the high explosives industry; at examination of the ways of efficiency and safety of the ammunition dismantlement technologies augmentation.

.

Introduction

Production, transportation, storage and application of energetic materials (EM) is connected indissoluble with the danger of the accidental explosion of these materials. The circumstances at which the explosion, especially the catastrophic explosion is initiated usually may be considered as a result of coinciding of a row of technology shortcomings, and employees mistakes grounded very often on the overall inconsistency of the technological system as a whole. Several very heavy accidents had taken place in 80-th in the industry of EM of the former Soviet Union as forerunners of the general collapse destroying all this construction it seemed such a carefully built and intensively functioning. We do not speak here about Chernobyl or Tomsk-9, only accidents at EM, mostly high explosives, production, storage, etc. will be described.

Arsamas

One of the most catastrophic explosions in the high explosives history had taken place at the outskirts of the town of Arsamas in the very middle of the European part of Russia during the railway transportation of RDX and HMX . The author of the paper was the expert at this case investigation, and here the version of his own of the event is presented. Three 60-tons freight cars two of which were loaded by the bags of RDX and HMX (partly phlegmatized, partly dry "white powder", the third car contained ammonite and some pressed items of explosives) just behind the locomotive, were going from the town of Dzerzhinsk, and had reached Arsamas at about 9.30 in the morning, June 4, 1988. It was Sunday. A lot of people were around this place, in their houses, in cars, at the barriers of the railway level crossing, in the vegetable gardens at the low ground. Some of them were happy to survive and then they described in detail all the visible circumstances of the case . At the same place, 15-20 m apart of the level crossing the embankment of the railway was crossed also by the underground gas pipe 150 mm diameter transporting the natural

gas at low, about 3 atm, pressure to some place in suburb. The crossing was constructed about 15 years before the events described, and (as it was stated at the inspection) with the essential violations of the regulations. The tube of 280 mm dia used as a jacket of the basic gas pipe under the embankment was broken when the crossing had been built and the upper part of the destroyed jacket tube was only about 60 cm (instead of 1.5 m as it is foreseen by the regulations) under the railway bed surface. One of the joints of the basic pipe was welded also with the great infringement of the rules, and some time before the accident it was partly destroyed. The natural gas flowed out the slit, moved along the pipe in the gap between the pipe and compressed ground, got to the jacket and through the slot in the upper part of the jacket and after that through the porous bed of the railroad embankment went out to surroundings. The concentration of the gas into the air near this place was presumably not very high, but inhabitants of the area felt it and had made complaints some of which were kept at the inquiry volumes.

Of course the very important moment of the case was the usage of the bags (the paper bag inside the jute bag) as containers for the extremely dangerous high explosives without any water or some other kind of desensitization employment. The granulated high explosive pouring out from the bag obviously could not be prevented, and in fact the traces of RDX were detected by the experts along all the way of its usual railway transportation.

Presumably one or several of the bags in the case investigated also were torn, and some quantity of explosive was poured out on the floor of the car. The slits under the door of the freight car is the quite usual thing, and when the gas under the floor in space between the car and the bed was occasionally ignited, the flame had penetrated into the car, and inflamed the explosive powder. The big fire had arisen suddenly. The flame had grew over the carriage roof. Immediately after that the catastrophic explosion, about 140 tons in TNT equivalent, had happened.

All the houses in the radius of several hundred meters were blown off, the cars near the level crossing were fully destroyed, the broken parts of all the three freight cars were found at the distance of about 1 km from the site of explosion. About a hundred people were killed. The full sum total of the losses was estimated to be

approximately $ 105 million.

The very expensive experiments were performed to determine the conditions of RDX and HMX to explode in the cars as the result of an accidental ignition. The explosives had been ignited in the truck containers, and in the freight cars, at the mass of explosive in every run from 100 to 10,000 kg, at ignition of EM inside the stack of bags, and outside it, directly by the hot wire, or through a quantity of black powder. In no one case, of about twenty trials, the DDT conditions might be reproduced.

However, the same fall, RDX was occasionally ignited after a train crash on the city of Sverdlovsk railway station, and again exploded (fortunately no one was injured, but the severe damages had taken place).

Criteria of the accidental explosion danger

The probable character of the accidental explosion, the necessity of coinciding of many probable circumstances as the essential moment of the catastrophic accident is absolutely obvious. To reflect this important feature of the phenomenon the very simple characteristic of the every accidental quick, explosion-like evolution of energy was introduced recently [1]. It is the criteria of the accidental explosion danger

$$K_d = E \ \Sigma(f_i/e_i) \qquad (1)$$

where E is energy which can be evolved at this individual kind of the accidents; e_i is the energy of the specific kind of impulse, which is necessary to spend to bring about the energy E evolution; f_i is the probability of the given kind of initiation. The E value can be specified as energy of EM, or compressed gas, or superheated liquid, the nuclear reactor potential energy, the energy of the flying plane, or the moving train, or car, etc. The difference in the energy content of the object may reach on ten orders of magnitude.

It is not the objective of this paper to develop the general safety problem, but it would be necessary to note that the significant difference between EM and most of the other potential sources of the destructive energy consists mainly in the fact that usually e_i is

close on the order to E, and correspondingly it is proportional to E in some degree, sometimes in the degree equals to unity. On the contrary the value of e_i for EM as a rule is connected with E very weakly: to explode a charge of 100 g of high explosive ($E \approx 0.4$ MJ), and the stack of it by the mass of 100 tons ($E \approx 400$ GJ) the same initiating cap ($e_i \approx 4$kJ) can be used. Moreover, the small mass of explosive may not detonate when ignited by the weak heat source. It just burns out. The big mass of the same explosive, as we could see above, at inflammation by the very weak energy source (asymptotically it can be~1J) after some period of burning detonates. Correspondingly, the big masses of explosives without development of the special complex of measures aimed to increase the value of e_i are characterized by the very big value of accidental explosion danger criteria K_d. Still more sophisticated part of the equation (1) f_i is introduced specially to reflect the probable character of the initiation by the energy impulse e_i. The important task of every work in the field of methodology of the technological safety insuring consists in estimation of e_i and f_i.

Bowden chain of initiation and growth of explosion

The natural base for the methodological approach allowing the accidental explosions causes and consequences to elucidate, and the algorithms of the investigations aimed to prevent the accidents at energetic materials production and (or) application to create is the well known consequence of self-sustaining processes of explosive transformation discovered by Professor F.P.Bowden about fifty years ago in Cambridge, England.

This consequence (Fig.1) includes several main stages forming so called Bowden initiation and growth of explosion chain. Most of the accidental explosions initiated by the weak external or internal stimuli, which are located at the upper row of the Fig.1 are forced to go through all the consequence from up to bottom usually giving a chance to broke the chain at one of the sufficiently weak links, during the corresponding process propagation or on the bridge between the individual processes.

One of the objectives of this presentation is to bring life to this dry scheme and to show how in the real circumstances one can find out the most weak link of the chain and broke it to prevent

propagation of the explosive transformation along the chain from point one to point seven (or, more often, to explain why, unfortunately, the propagation in this particular case could not be prevented).

Stage 1

Of course the absolutely dependable way the accidental explosion to prevent consists in elimination of the Stage 1, at least in such an extent to avoid appearance of the Stage 2. Unfortunately it is the very expensive method of the higher level of safety achievement. It is used however in some cases, for instance at operations with primary explosives where all the subsequent stages of the Bowden scheme follow one after another very promptly, at pressing of the sensitive high explosives charges, at designing of the artillery shells construction and technology that would be able to preclude the premature explosions of the shells at the gun shot, at elaboration of the technique for transportation of liquid high explosives, where burning instability and DDT (4 and 5) Stages are developed after ignition very easily. It should be noted also that the every point of the Stage 1 has its own character, and includes at the real practical conditions a row of intricate physical, mechanical, hydro- and reodynamic processes leading to heat liberation and the evolved heat to EM transmission.

The first three points of the Stage 1, 1.1-1.3, are essentially very close to each other, they include the stage of the relatively "ineıt" heating of the full mass of EM or the big part of it to the critical temperature, after which the heat evolution in the course of the chemical reaction begins to dominate, resulting in selfignition of EM. The chemical reaction kinetic and thermodynamic properties in general define the heat explosion development. It would be necessary to note the very small contribution of pressure as the parameter of state of the system into the energetic characteristics of the process initiation.

The next three points (1.4-1.6) are connected usually with ignition, i.e. with heating of the very small part of the EM charge, forming the very thin preheated layer, or the very small hot spot. They also connected one to another very closely (the types of the connections for different methods of EM sensitivity testing are shown for instance in [2]). As opposed to the previous case pressure plays

the very significant role at initiation: in fact the process is determined predominantly by the burning rate of EM at pressure of ignition.

The last two points of this Stage: 1.7 and 1.8 can be considered as probably the most complicated forms of EM heating and initiation. Very small time between ignition and detonation, and the strong dependence of the detailed mechanism of initiation on the bullet or fragment velocity and on the shock wave amplitude make these points of the Stage 1 the most difficult sections of the theory of sensitivity.

Everyone experienced in EM production and application can recall a lot of examples when the different stages of the scheme (Fig. 1) were responsible preferably for accidental explosion growth, and when the corresponding influence could avert the explosion. I would like to enumerate some of them which had taken place in Russia during last one-two decades bearing in mind that the Western scientists practically are not familiar with the events.

Premature explosion problem

Among the problems solution of which turns on the Stage 1 probably the most important is a problem of prevention of the premature explosions of the artillery shells at the gun shot. The premature explosion danger consists not only in demolition of the gun and hitting the soldiers. Employment of all the shells of this type, sometimes several million items, becomes impossible: a gunner can not level a gun if he aims at himself. The algorithm of the problem solution was developed by the author of the paper during his visit to MRCI, Xian, China last fall. As the experimental ground of this approach a method of the fast compression of gas intrusions in a charge of explosive was chosen. Such a technique was developed in different laboratories (see, for instance, the comprehensive work [3]). The best method fitted to the type of the shells and charges under consideration was elaborated, and the results of the experiments were compared with the regular shot results at the proving ground testing of the shells. The data will be reported elsewhere. It should be noted that this type of accidents differs from many others by the rather definite conditions of the mechanical stimulus. The dangerous dimensions of the intrusions necessary for explosion. also can be estimated rather exactly.

Burning Heat Instability Role
(Stages 2 and 3)

The very productive phenomenon, as to the Stages 2 and 3 growth and extinction is concerned, relates to burning heat instability which was especially intensively studied for the case of the rocket propellants application [4].

At increasing of the heat flux q the energy content in the preheated layer sufficient for ignition Q decreases approximately proportionally q^{-1} till the critical flux value q_* is reached. After that Q quickly rises up, or even sharply turns to infinity: ignition and steady state burning are possible only at external fluxes q < q_*. The value of q_* depends mostly on pressure ($q_* \sim$ p). This phenomenon is connected with the different fields of EM technology. At turning, milling or sawing of the charges of EM, or the different kinds of ammunition containing EM we have two limiting velocities of machining confining the region of the especial danger both from below and from above: the usual low limit stipulated by the heat exchange with surrounding, and the upper limit specified by the heat instability. At melting off the explosives from ammunition two limiting heat fluxes from the heat carrier to the surface of explosive exist. About the same should be observed at bullet or fragment attack. All the features of the phenomenon as applied to the problem of ammunition dismantlement are described in the work [5].

Viscosity Influence on Stage 4

The example of the Stage 4 elimination with the corresponding significant safety increase is very well known. It is A.Nobel invention, the double-base propellant. The strong increase of the viscosity of nitroglycerin, on the one hand, and elimination of porosity of nitrocellulose, on the other hand, at mixing them one to another rules out the possibility of convective burning both NG and NC which are characterized separately by the very strong tendency of

transition to this burning regime . It is interesting to note that the
bridge between Stages 2 and 3 in this case can not be used as an
obstacle on the way of the process development: all the propellants
are constructed in such a manner that the level of burning heat
instability of them is low enough, at least it is much lower than that
of all the high explosives industrially used (meanwhile, the theory of
burning instability was created first of all for the double-base
propellants). Another remark to the problem of viscosity influence:
quite recently we have discovered that viscosity augmentation by means
of addition of the small quantity of NC to DGDN, the nitric ester of
the same group as NG, may increase noticeably the detonation ability,
one of the factors defining the safety level.

Sulfuric Acid Influence on Stages 5 and 6

Two catastrophic explosions had happened in Russia in 80-th
during TNT manufacture at the explosives producing plant. Both of them
were dictated by the proposal to increase productivity of the
manufactory using sulfuric acid of higher concentration. If the
continuous process were interrupted by the prolonged, 1-3 hours,
intermissions, the concentrations of H_2SO_4, HNO_3 and DNT in the
apparatuses of the middle part of the system becomes so high that the
very quick heat evolution resulting in selfignition may proceed. The
inflammation of the reaction mass itself is obviously unpleasant but
virtually not dangerous event. We really had previously some cases of
inflammation at TNT production (jet of flame from the hatch of
reactor) without any explosion. Moreover, at RDX production some 15-20
years ago burning of hexamethylenetetramine was the usual phenomenon
with frequency of about once a month almost at the every RDX producing
plant (explosions also had happened but still much more infrequently).

As we might expect employment of sulfuric acid of higher
concentration is connected with enormous augmentation of detonation
ability of the mixture. It was the absolutely new aspect of the
problem. Up to now all the specialists in the field of TNT production
are confident that sulfuric acid is the inert solvent, admixture of
which may only decrease the explosive characteristics of the reaction
mass. We have studied this problem carefully bearing in mind our old
results of very strong acceleration the detonation reaction in some

nitrocompounds at addition of the very small quantities of the strong mineral acids [6].

We obtained the truly threatening result: the failure diameter of $TNT/H_2SO_4/H_2S_2O_7$ mixture can be 30 times less than the failure diameter of the neat liquid TNT. DNT does not detonate in the liquid homogeneous state. Mixture $DNT/H_2SO_4/H_2S_2O_7$ is able to detonate. The detonation of aerated porous liquid systems of this sort was also investigated. It was demonstrated that the courses of the explosions are connected not only with the Stage 1, but mostly with the Stages 5 and 6 intensification. As a result of this work the courses, the way of development, and unusually heavy consequences of the explosions were elucidated, and the necessary recommendations to the industry were proposed. The detailed description of this work is presented here in form of the posters [7,8].

Explosions at Fires

Several heavy accidents, except these described in the very beginning of the paper, had happened at fires during transportation and storage of high explosives. In 1984 the magazine containing about 100 tons of flaked TNT after approximately half of hour burning exploded together with the freight car (about 40 tons of TNT) standing near the magazine. The team of firemen fought the fire without any success. Fortunately they understood in time that their efforts are in vain (as a matter of fact they were harmful) and escaped as quickly as they may. After explosion the neighboring magazine containing about 200 tons of granulated TNT was partly destroyed and TNT was ignited and began to burn, but quite naturally nobody tried to fight with the fire, and it burned out, as far as possible quietly and gently.

In 1988 the freight car loaded by TNT, inside the territory of the big ammunition plant caught a fire in the process of unloading due to a driver of truck which the freight had been transferred to did not cut the truck engine which accidentally was not equipped by the spark arrester (actually it did not have even the noise suppresser). Several teams of firemen took part in fighting with the fire. Again they felt the time to retreat came (the loaders felt it much earlier: they just jumped into the track with the engine working as only they sow the first traces of flame). Only one of the firemen who had retreated not

fast enough was killed. After the explosion had occurred about seventy hotbeds of fire arose on the territory of the plant initiated by the red-hot parts of the car thrown away. Two of the hotbeds are related to the manufactories for alumotol (15/85) and grammonite (TNT/ granulated AN) production. The technological schemes of both materials production were characterized by the presence of the systems of the long steel tubes and some other strongly confined volumes where DDT may occur. In spite of nobody was busy in those circumstances to put out the fires both of the manufactories exploded after 7-10 minutes of burning. All the workers escaped after the first explosion, when the freight car burst, and no one was killed or injured.

All the cases listed clearly demonstrate the necessity to foresee. the Stage 5 dangerous development possibility in the case of accidental fire to prevent this if it were possible on the step of designing and construction of the technological process.

References

1. Kondrikov B.N. Explosive Materials and Pyrotechnics, CNIINTIKPK, Moscow, 1994, N 9-10 (240-241), pp.3-5

2. Kondrikov B.N. ibid., 1994, N 7-8 (238-239), pp.12-30, Combustion, Explosion & Shock Waves, 1995, Vol.31, N2, pp.80-90

3. Starkenberg J. 7-th Symposium (Int.) on Detonation, NSWC MP82-334, 1991,pp.1-16

4. Novozhilov B.V. Unstable Burning of Rocket Propellants, Moscow, Nauka, 1973

5. Kondrikov B.N. to be presented in Propellants, Explosives, Pyrotechnics, 1995

6. Kondrikov B.N., Kozak G.D., Raikova V.M., Starshinov A.V. Dokl. Akad. Nauk SSSR, 1997, Vol.233, pp.402-405

7. Raikova V.M., Kondrikov B.N. Energetic Materials - Technology, Manufacturing, and Processing, 27 Int. Annual Conf. of ICT, Karlsruhe, June 25-June 28, 1996

8. Kondrikov B.N., Raikova V.M., Kozak G.D., ibid.

1. Sources of Heat

| Chemical Selfheating 1.1 | Visco-Plastic Flow 1.2 | Long Friction 1.3 | Hot Surface Hot Gas 1.4 | Impact Friction 1.5 | Adiabatic Compression of Gas Bubbles 1.6 | Bullet or Fragment Attack 1.7 | Shock Wave 1.8 |

2. Inflammation

Extinction
Heat Exchange
Burning Heat Instability

3. Steady State Burning
Hydrodynamic Instability

4. Convective Burning
Gasdynamic Instability

5. D D T

| At Fires 5.1 | At Full Confinement Filling 5.2 | In Partly Confinement Filled Tubes 5.3 |

Limited Explosion Process Failure
Confinement conditions

6. Detonation
(p_+, d_+) Values Reaching

7. Damages
Protection Systems

SENSITIVITY TO PROJECTILE IMPACT OF PRE-HEATED EXPLOSIVE COMPOSITIONS

H. CHERIN, D. LEMOINE, L. GAUTIER

Commissariat à l'Energie Atomique
Centre d'Etudes du RIPAULT
B. P. n° 16

1. INTRODUCTION

In the context of safety of weapons and ammunitions, the sensitivity of explosive compositions to projectiles impacts has been widely studied. Depending on the nature of the explosive, of the confinement, and of the characteristics of the projectile, this kind of stimulus can lead to a SDT (shock-to-detonation transition) phenomenon.

The objective of the work presented here is to study the sensitivity of our explosives for combined stimuli, that is to say for projectiles impacts on pre-heated explosives. The data obtained, introduced in a specialized pyrotechnic safety code (OCAPY) allow us to assess the sensitivity of an explosive composition for a whole range of combined stimuli.

Moreover, this work shows that thermally aged explosive compositions are very more sensitive to mechanical stimuli. The mechanisms leading to this sensitization could be a partial decomposition during heating, and/or an increase of the porosity, due to material expansion.

2. EXPERIMENTAL SET-UP

The main parameters of the experiments are :

- the pre-heating temperature,
- the velocity of the projectiles.

The experimental set-up is presented on figure 1. A system of optic barriers, separated by 50 cm is used to measure the velocity of the projectile. The experiments are filmed with an S-VHS camera, and recorded on a VCR.

The explosive samples are heated during one hour in a pulsed oven, removed just before the shot. The dimensions of the cylindrical samples are 90 mm diameter and 30 mm length. The temperature of the explosive is controlled by a thermocouple.
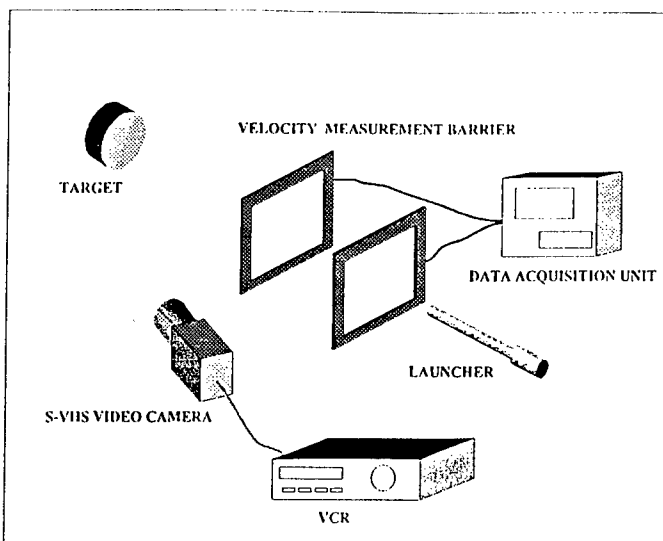
Figure 1

3. RESULTS

The studied explosive is a TATB based composition, with a few per cent of a polymeric binder, called T1. The projectiles are cylinders by 18.3 mm diameter, including a steel impacter (5 mm length) and a polymeric saddle (30 mm length). The pre-heating temperature is by 250°C.

For the T1 explosive, at 20°C, projectiles impacts up to 1270 m/s (maximum possible velocity with our launcher) do not lead to a pyrotechnic reaction. In order to help us to choose the velocity range leading to a shock-to-detonation transition at 250°C, we have used the results of the calculations made with the pyrotechnic safety code OCAPY [1]. This software has been developed in order to predict the pyrotechnic behaviour of explosive structures submitted to thermal, mechanical or combined stimuli. We have implemented in this code several analytical models of shock-to-detonation transition. Among all these models, L.R. GREEN's one [2] is particularly well suited for the impacts of cylindrical projectiles. This model enables a critical transition curve to be plotted on a velocity-diameter graph for the considered projectiles. Any impact located at a point below the critical curve will not initiate a detonation. If the point is above the curve, a SDT will be obtained. On figure 2, we have plotted the critical curves for T1 and X1 (HMX based composition) at 20°C, and for T1 at 250°C.
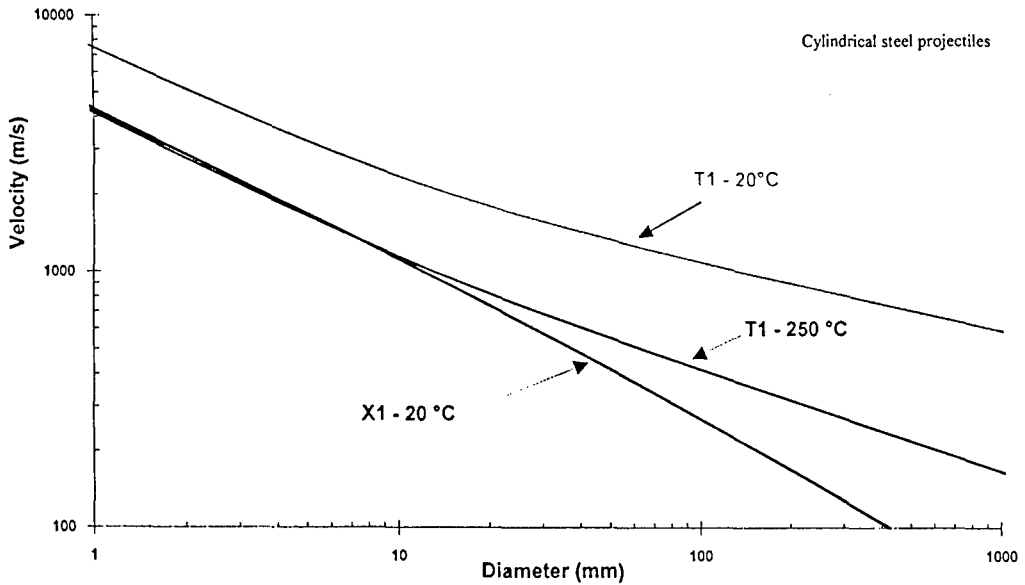
Figure 2

On this figure, it can be observed that a TATB based composition, heated to 250°C, can be as sensitive as an HMX composition at ambient temperature, for a whole range of impact velocities. For the impact of a 18.3 mm diameter steel bar, the velocity thresholds for a SDT, given by the OCAPY calculations, are as follows :

- 800 m/s for X1 at 20°C,
- 900 m/s for T1 at 250°C,
- 2000 m/s for T1 at 20°C.

The range of impact velocities to be studied for T1 at 250°C has then be fixed between 800 and 1000 m/s. The experimental results of the shots are as follows :

Temperature (0°C)	Impact velocity (m/s)	Pyrotechnic reaction
250	1021	YES
253	1021	YES
255	793	NO
254	1006	YES
253	888	NO
254	1000	YES
253	900	NO
250	974	YES

The SDT velocity threshold for this kind of projectile is in the range by 900-974 m/s, which is in good agreement with the OCAPY calculations : on figure 3, it can be seen that the calculated values are very closed to experimental data. We can say that OCAPY calculations are predictive and reliable for this kind of combined stimuli.
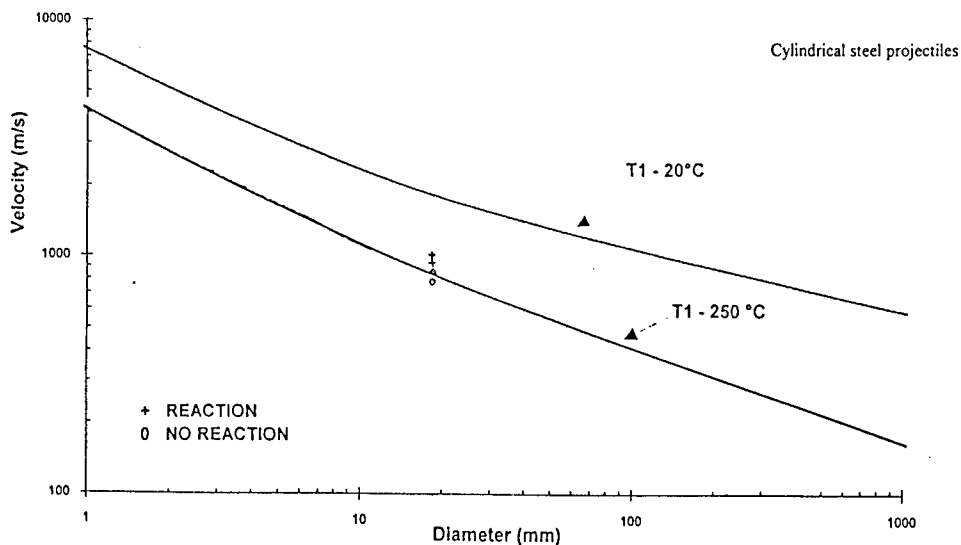
Figure 3

4. SENSITIZATION MECHANISMS

The preheating of T1 explosive leads to a sharp increase of sensitivity for projectile impacts. The threshold impact velocity leading to a SDT is reduced by about 1000 m/s between 20 and 250°C. Two kinds of mechanisms can be involved in this sensitization phenomenon :

- increase of the number and of the size of microstructural defects, due to the the material expansion at the studied temperature ;
- partial decomposition of TATB molecules during heating.

Whatever the mechanism, the heated explosive, cooled down to the ambient temperature, should be more sensitive than the fresh material. In order to verify this hypothesis, we have carried out the following experiments.

4.1 Impact sensitivity

We have first observed the result of an impact at 1000 m/s on the fresh material. The ceramic holding device is undamaged, the explosive is totally dispersed, and the recovered fragments represent about 90 % of the initial mass of the target.

We have then heated the explosive at 250°C during one hour, and cooled it down slowly to avoid damaging of the material. The result of the impact at 1000 m/s is a violent pyrotechnic reaction : the holding device is cracked, the recovered fragments exhibit large decomposition areas, and represent only 10 % of the initial mass.

4.2 Drop weight hammer test

The shock sensitivity is characterized using the drop weight hammer test. The height H_{50}, corresponding to a pyrotechnic reaction probability of 50 %, has been measured on fresh and thermally aged samples. The following results have been obtained :

- fresh explosive : H_{50} = 122.4 cm
- heated explosive, after cooling : H_{50} = 113.9 cm.

The thermally aged material is clearly more sensitive to mechanical stimuli than the fresh one.

4.3 Thermal expansion

The explosive, submitted to high temperatures, undergoes a thermal expansion, leading to an increase of the size and of the number of microstructural defects. According with the hot spot theory, this phenomenon can explain the sensitivity of the explosive for an impact at 250°C, but also the reactivity of the cooled material if we assume that the microstructural changes are remanent. This hypothesis has been verified by measuring the volume expansion of thermally aged samples, after cooling down. The results show a volume expansion of :

- 2.5 % for samples heated at 250°C during six hours,
- 3.5 % after heating at 280°C during one hour.

We have also performed dilatometry experiments, between 20°C and 250°C for studying the influence of the rise time to 250°C. We present on figure 4 the dilatometry apparatus, and on figure 5 a typical curve (relative dilatation versus temperature). The maximum relative dilatation reached is about 2,5 % for a temperature of 250°C. The residual dilatation after cooling down is closed to 0,7 %, which is important in term of micro-defects and hot spots generation. There is no influence of rise time to 250°C on the maximum relative dilatation.

4.4. Thermal damage

For a better understanding of sensitization mechanisms, we have carried out a thermal damage study on pure pressed TATB. For this purpose, we have used the experimental set-up called Thermomechanical Limit Test (TLT) [3]. The device has been modified in order to be able to analyze the gazeous and solid decomposition products (figure 6).
We measure the bulk temperature of the material during a constant temperature phase. After an induction time, the bulk temperature begins to grow up, indicating that an exothermic kinetic is started (figure 7). For different values of the bulk temperature, we have stopped the experiments by taking out gazeous decomposition products and cooling down the mold. On figure 8, we have reported all the employed analysis technics.

On figure 9, we have reported the analyzed gazeous products, for different temperatures.

Using scanning electron microscopy, we have observed modifications of the TATB initial porosity, due to the coalescence of the defects or increase of their size.

By HPLC on the solid phase in solution, we have detected, for the temperatures of 267°C and 270°C, two decomposition products that we are trying to identify.

These experiments clearly show that both phenomenons, chemical decomposition and structural modifications, are involved in the senzitization of preheated material.

displacement transducer   **push rod**   **sample diam. 5 mm length : 50 mm**

thermocouple   **sample support**   **annular furnace**
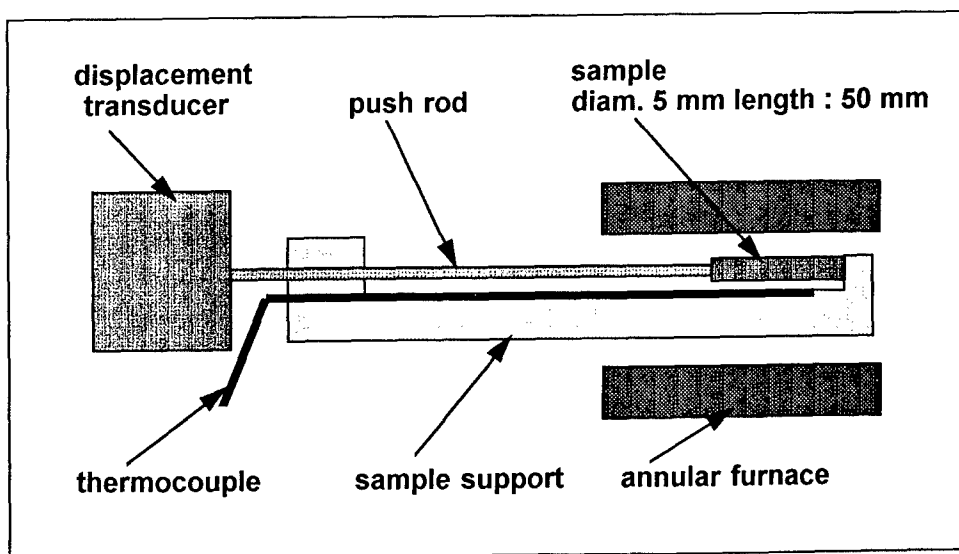
Figure 4

T1 DILATATION
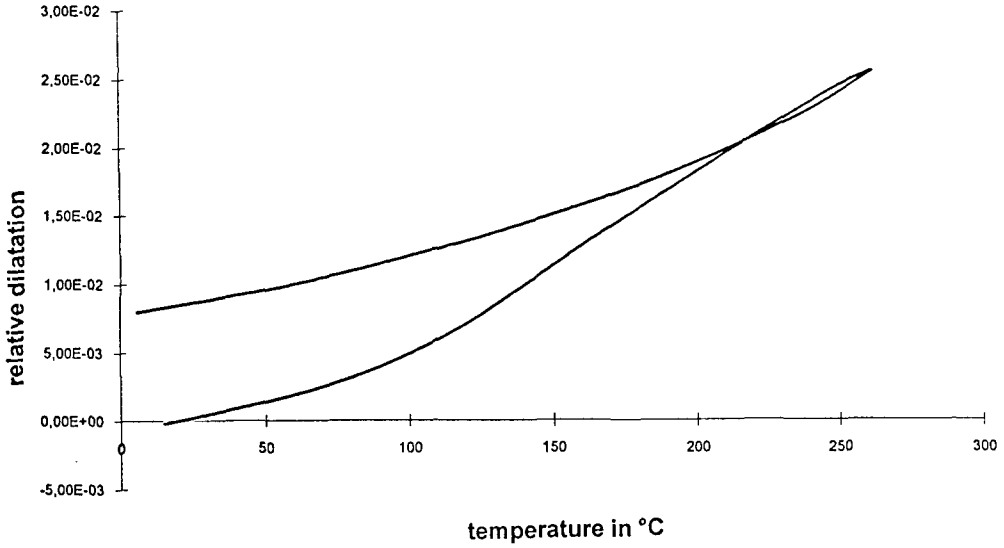
Figure 5
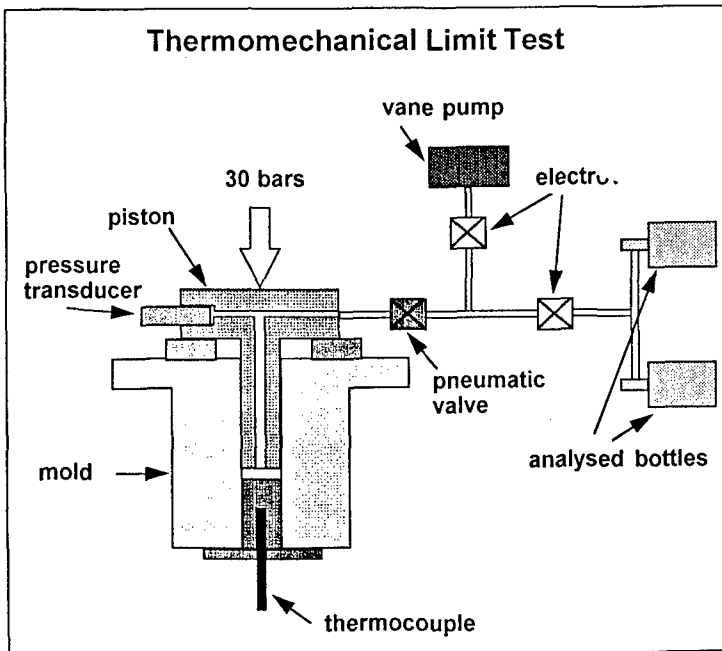
Figure 6
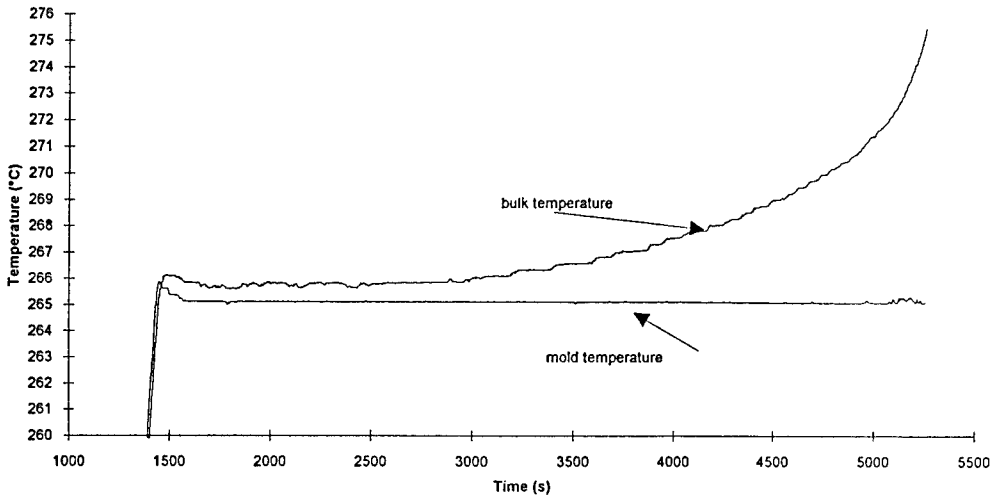
Figure 7

	High Performance Liquid Chromatography	Infra Red Spectrometry	Scanning Electron Microscopy	Mass Spectrometry
gazeous products		▓▓▓		▓▓▓
solid phase	▓▓▓	▓▓▓	▓▓▓	▓▓▓
solid phase in solution	▓▓▓	▓▓▓		▓▓▓

Figure 8

	267°C	270°C	275°C	275°C	280°C
MS	CO_2 H_2O N_2O NH_3	CO_2 H_2O N_2O NH_3	CO_2 H_2O N_2O NH_3	CO_2 H_2O N_2O NH_3	CO_2 H_2O HCN CO N_2 N_2O C_2H_2
IRS	CO_2 H_2O N_2O NH_3	CO_2 H_2O N_2O NH_3	CO_2 H_2O N_2O NH_3	CO_2 H_2O N_2O NH_3	CO_2 H_2O N_2O NH_3 CO NO C_2H_2

Figure 9

5. CONCLUSIONS

The results of this study show that a TATB based explosive composition undergoes a sharp increase of impact sensitivity when heated at 250°C : the threshold velocity of a cylindrical steel projectile leading to a SDT is quite the same as an HMX composition one at 20°C. Another important result is that the explosive can be thermally damaged : after heating and cooling down, the material is more sensitive than the fresh material. Two mechanisms can be invoked for this sensitization : partial decomposition, and appearance or growth of microstructural defects during heating.

Future works in this field will be concerned with :

- the study of the mechanisms leading to the sensitization,
- the effects of thermal aging (time, temperature) on the resulting sensitivity to mechanical or thermal stimuli.

REFERENCES :

[1] OCAPY : a computer code for safety assessment.
T. CHELIUS, H. CHERIN, F. CORDELLE, R. BELMAS.
Twentieth International Pyrotechnics Seminar, July 25-29, 1994 - COLORADO SPRINGS.

[2] Shock initiation of explosives by the impact of small diameter cylindrical projectiles.
L.R. GREEN.
VIIth Symposium (International) on Detonation, 1981 - ANNAPOLIS.

[3] Reactivity of stronly granular explosives submitted to slow heating.
D. LEMOINE, H. CHERIN, R. LETREMY, J. RIDEAU
25th International Annual Conference of ICT, June 28-July 1, 1994 - KARLSRUHE.

VULNERABILITY TESTING OF HIGH EXPLOSIVES

Petr Mošťák, Pavel Vávra

SYNTHESIA a.s.
Research Institute of Industrial Chemistry
532 17 Pardubice-Semtín
Czech Republic

ABSTRACT

The possibility of use of standard methods developed for the evaluation of sensitivity and stability of explosives for predictionary of vulnerability of ammunition was studied.

Results obtained indicate that explosive properties obtained in the gap test, DTA and vacuum stability test and also fall hammer test, performance measurement can be used as the first screen in looking for explosives with lower sensitivity.

The full scale testing using the standard methods for insensitive munition can be used in further step. Substantial economy can be achieved by this procedure.

INTRODUCTION

Parallel to the research of LOVA explosives the requirement arises to test properties of substances and their mixtures from the vulnerability point of view.

Requirements for insensitive munition and its testing are known[1] but it would be very expensive and unpractical to use them researching energetic components for explosive charges of ammunition (HE,propellants). This is the reason why various tests were designed[2,3] that should simulate behaviour of these materials when testing vulnerability of ammunition.From the research view-point it is necessary to consider the extent and number of various tests   because testing of a great number

of samples and the extensiveness of the tests make the research time consuming and expensive especially in such cases where the price of some components of energetic compositions is still quite high. The necessary quantity of sample that should be sufficient for a proper simulation of the future charge in ammunition is of great importance as well.

As well known[4,5], at some sensitivity tests the resulting values are influenced by the shape and size of particles, density of samples, technology of preparation and other circumstances. Similar situation occurs when performing heat tests.

In order to accelerate the research work and reduce the costs of the vulnerability assessment we have tried to select as far as possible simple and quick tests that should be, however, of sufficient capability to simulate behaviour of substances in real conditions.

SELECTION OF TESTS

1. Preliminary testing

In samples of explosives that are in most cases a mixture of both, energetic and inactive components we are usually able to assess quite well their performance parameters[6]. For this purpose we use the knowledge of composition, heat of formation and theoretical maximum density (TMD).

The samples are prepared in various ways: by pressing, casting (sometimes in vacuum and under vibration), extrusion etc.. These various procedures directly affect both, physical properties and explosive parameters (sensitivity, performance). That is why we have selected for the first evaluation of important properties the following tests:
- determination of density
- differential thermal analysis (DTA)
- vacuum test (VT)

The density of the real sample and its difference from TMD characterises the porosity which is usually important for the of explosive sensitivity to some external impacts. The ratio of achieved density to TMD can indicate also the degree of filler - binder physical compatibility, possible compressibility and effects the performance of the explosive as well.For these reasons attaining of as high density as possible appears to be an important requirement.

The results of DTA give us the first information concerning the sample behaviour at increased temperatures; primarily the changes of physical state, chemical compatibility and decomposition reactions. The results of tests are, of course, compared with DTA records of the individual components.

To study the informatively chemical compatibility of the components we use also vacuum stability test performed at $140^{\circ}C$ for 20 hours. Examples of both tests are given in the Table I.

Table I - Comparison of DTA and vacuum test

Sample	DTA exo onset, °C	Vacuum test 140°C, 20 hours, ml
RDX/NTO/binder 1 70/18/12	201	0,21
RDX/NTO/binder 1 53/35/12	201	0,16
RDX/binder 2 50/50	181	8,18

As we can see, at the sample No 3 in Table I both tests are showing chemical incompatibility due to unsuitable binder.

In case that the sample shows good parameters in the first group of tests it is subject to fall hammer test. The results of this test inform us about the sensitivity to impact which is important primarily for technology and handling. However, from

the view-point of reduction of vulnerability these results appear to be questionable. The sensitivity estimeted by the fall hammer test is sometimes not in correlation with other tests, for instance with results of the gap test. Some examples can be seen in the table II.

Table II - Sensitivity estimated by fall hammer test and gap test

Sample	fall hammer $E_{min.}$ (J)	small gap test $P_{inic.}$ (GPa)
TNT	35	2,5
RDX/wax 95/5	27	2,75
RDX/TNT 50/50	28	3,8
RDX/NTO/binder 1 70/18/12	32	5,6
RDX/binder 2 50/50	16	9,25

The results of these two tests should be assessed very carefully as far as the methology of the test is concerned (quantity of the sample used in the test,its geometry etc.).

As the additional tests, hardness test (Shore) and in case of elastic composites bending strength test are used. The results of tests give us certain idea of physical properties of the sample e.g. compressibility, elasticity, filer matrix physicalinteraction , " memory " of binder etc. All above mentioned tests require small quantities of the sample (tens of grams at the most) are quick and enable to perform the first selection of the perspective compositions for further testing.

2. Second group of tests

The next group of tests consists of
- small-scale gap test

- Koenen test
- burning to detonation transition test
- vacuum stability test

Assessing the results of small-scale gap test (Fig. 1a) we are to consider that the low vulnerability explosives should meet Class 1.6 of UN Standard[7] and therefore it is quite possible that the critical diameter of the material will exceed 21 mm. In this case it is necessary to use further methods of testing.

At Koenen test we suppose the evaluation of decomposition rate of the substance simulating fast cook-off. Similarly, at burning to detonation transition test (Fig. 2) we evaluate both, pre-detonation zone and resulting destruction of the tube. The vacuum stability test is carried out using standard method (120°C, 48 hours).

The quantity of the sample needed for these tests amounts hundreds of grams and the time consumption is not very large. The final samples that have showed the lowest sensitivity to the above mentioned tests are subjected to further testing.

3. Third group of tests

The next group of tests consists of
- large-scale gap test (Fig.1b)
- shape charge impact test (Fig.3)
- bullet impact test

These tests require several kg sample and increased time consumption.

So far we have not managed in developing simple and quick tests serving to good simulation of cook-off, sympathetic deto-nation and fragmentation tests.

It is necessary to say that criteria concerning technology of preparation of the investigated composition, performance parameters of energetic material, accelerated test of shelflife and preliminary economic evaluation can be used as further views for choice of samples in different phases of testing.

CONCLUSIONS

For the purposes of research of low vulnerability explosives it is possible to utilize accessible, quick and simple tests arranged to steps according to the following hierarchy:

- determination of density, DTA, vacuum test ($140^{O}C$, 20 hours), fall hammer test, hardness and elasticity
- small-scale gap test, Koenen test, burning to detonation transition test , vacuum stability test ($120^{O}C$, 48 hours)
- large-scale gap test, shaped charge impact test, bullet impact test
- slow cook-off test, fragmentation test, sympathetic detonation test

This last group of tests can be also performed in simulation mode according to the presumed utilization in ammunition. Using this procedure it is possible to reduce the time period of research and development, the costs of this process and to achieve satisfactory probability for good results of tests of munition.

However, the preliminary conclusions obtained are necessary to be verified in the development phase of the specific munition system using standard tests e.g. according to MIL STD 2105B or STANAG tests for insensitive munition.

REFERENCES

1. Hazard assessment tests for non-nuclear munitions, MIL-STD – 2105B, 1994

2. Becuwe, A., Delclos, A., Isler, J.: EIDC High Explosives for 1.6 Munitions, ADPA Energetic Materials Symposium, Phoenix, Sept. 1995

3. Langer, G., Schedlbauer, F., Ebeling, H.: Sensitivity Tests for Energetic Materials, Proc. 18th Conference of ICT, Karlsruhe 1988

4. Belmas, R., Plotard, J.-P.: Physical Origin of Hot Spots in Pressed Explosive Compositions, J. de Physique IV., Colloque C4, suppl. J. de Phys. III., Vol. 5, mai 1995

5. Baer, M.R. et al: Modeling Thermal/Chemical/Mechanical Response of Energetic Materials, Proc. 26th Conference of ICT, Karlsruhe 1995

6. Stine, J.R.: Molecular Structure and Performance of High Explosives, in: Mater. Res. Soc. Symposium Proc., Vol. 296, Pittsburgh, Penn. 1993

7. UN Recommendations on the Transport of Dangerous Goods, Tests and Criteria ST/SG/AC 10/11, 1990

Igniter

Booster

Donor

PMMA - Gap

Acceptor

Witness Plate

∅ 21 mm

21 mm

∅ 68 mm

30 mm

Large - Scale Gap Test

Fig. 1b

Igniter

Donor

PMMA - Gap

Acceptor

Witness Plate

∅ 16 mm

24 mm

∅ 21 mm

21 mm
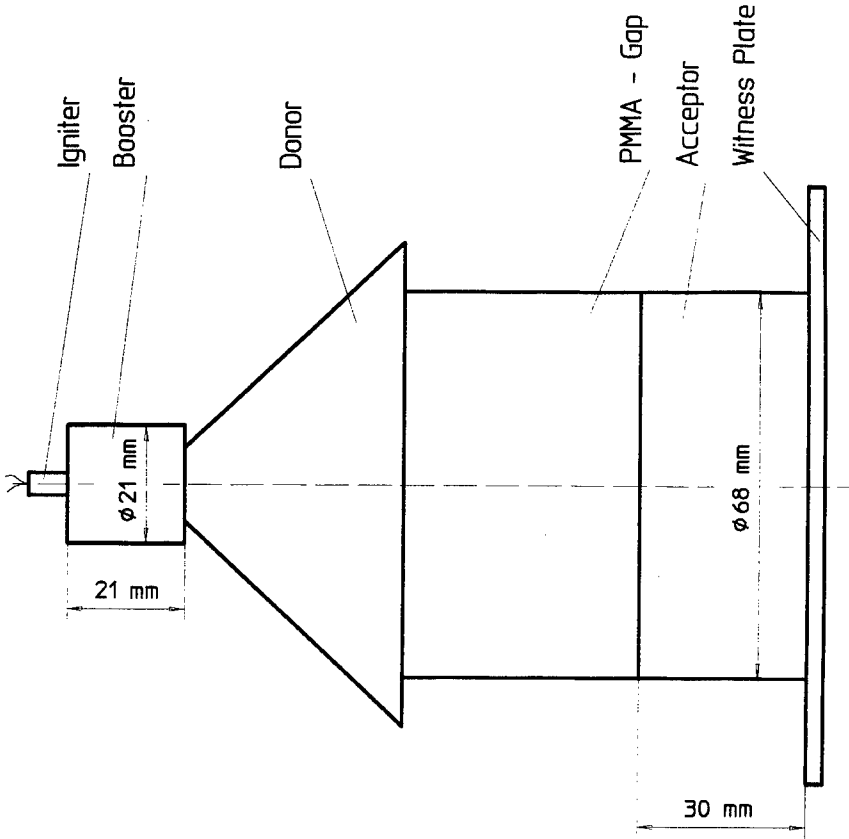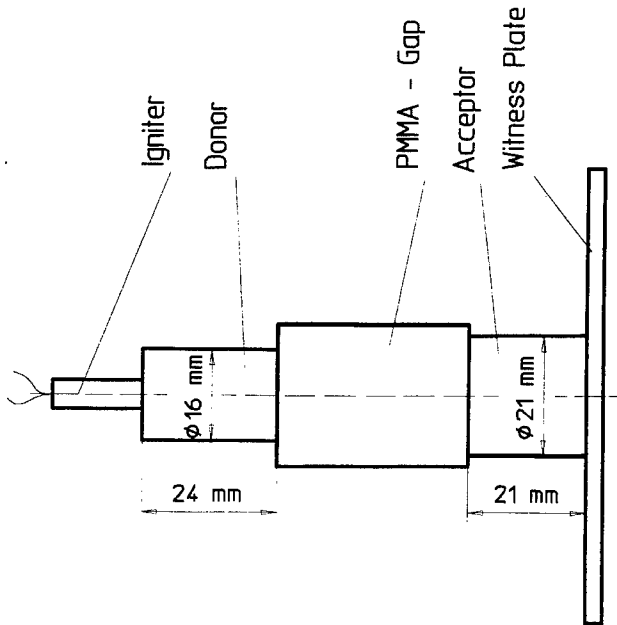
Small - Scale Gap Test

Fig. 1a
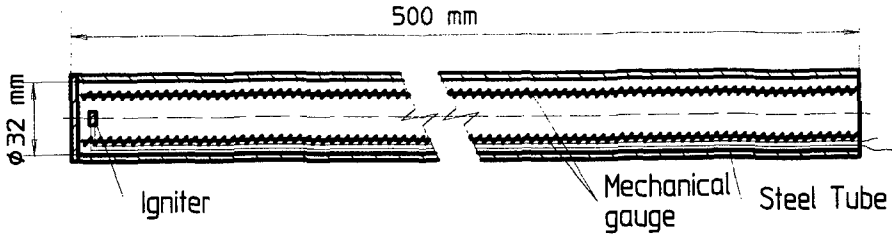
BDT Test

Fig. 2
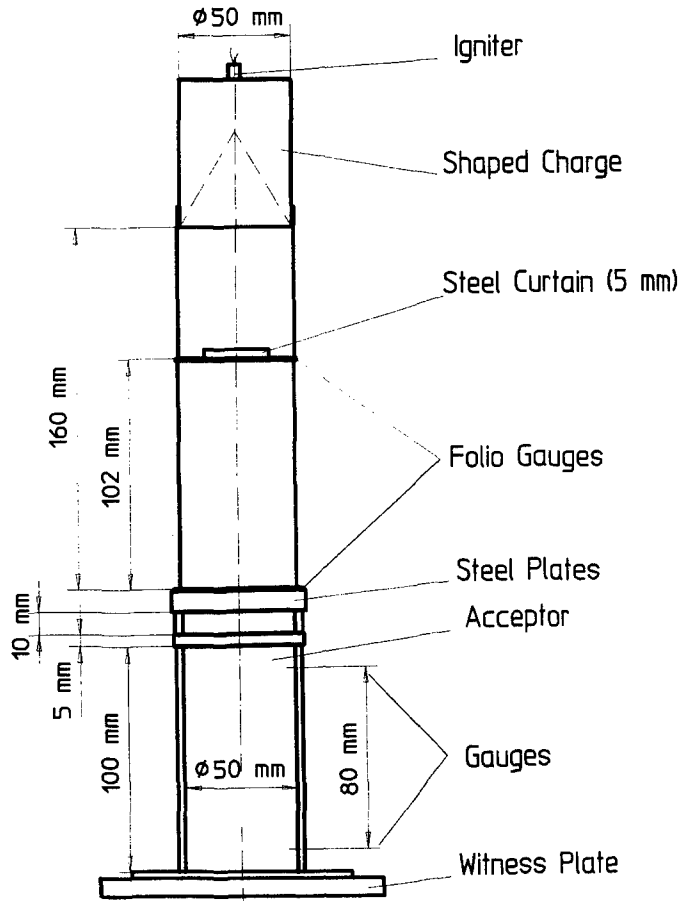
Shaped Charge Impact (50 mm)

Fig. 3

HAZARD ANALYSIS OF MANUFACTURE OF GAS GENERANTS

by

Kazuo HARA, Mitsuhiro KANAZAWA, Takayuki HASEGAWA and Tadao YOSHIDA

College of Engineering, Hosei University

3−7−2 Kajino−cho, Koganei−shi, Tokyo 184, Japan

ABSTRACT

Hazard evaluation and analysis were conducted for the manufacture of potential gas generants for airbag inflators. The compositions examined are two typical compositions including $KClO_4$ and KNO_3, and a composition including an oxidizer X. The fuel used is urazole. The experimental hazard evaluation of three compositions and their components was carried out and the results were used in the Yoshida hazard analysis(YHA). The sensitivities and the violence of combustion of these materials were categorized to four ranks, and the risk of each operation in the manufacturing process was plotted on the risk profile for normal, deviated or corrected operation. Finally, the risk profiles for corrected and deviated operations were used for promoting the safety in the manufacture of the gas generant.

1. INTRODUCTION

Automotive airbags are getting more popular in the modern car society and the sodium azide−based compositions have been almost exclusively used as gas generant for airbag inflators. The azide−based gas generant has such good performances as good burning velocity, exclusive N_2 gas effluent, low combustion temperature, low particulates and so on. However, sodium azide has some problems such as toxicity, incompatibility with acids and formation of sensitive heavy metal azide with Cu or Pb. Therefore, nonazide−based gas generants have been looked for.

Originally, the AK(ADCA/$KClO_4$) gas generant for automotive airbag inflators was developed by the auther's group to replace the azide−based gas generant [1]. The so called UX(i.e. Urazole/oxidizer X) gas generant was then developed as an improved system. The UX gas generant is more stable, has a lower combustion temperature and gives less particulates than the AK gas generant. The qualities of stability, lower combustion temperature and less particulates are advantageous for the safety and

performance of gas generant.

In developing the new gas generant system, the fire and explosion hazards of the composition as well as of the raw materials were evaluated and the results were used in the Yoshida hazard analysis(YHA) for the manufacturing process for the new gas generant. The methods for evaluating the hazards of the compositions and raw materials are similar to those described in a previous paper [2]. The hazard analysis technique used is similar to that carried out for the manufacturing process for the AK gas generant [3]. The Process Safety Management(PSM) of the Occupational Safety and Health Administration(OSHA) [4], the Zurich Hazard Analysis(ZHA) of the Zurich Insurance Company [5] and the United States Military Standard [6] were referred to in developing the YHA.

2. EXPERIMENTAL

2.1 Materials

Materials used are listed in Table 1.

Table 1   Materials used

Name	Symbol	Size	Supplier
Urazole	U	$20\mu m$	Otsuka Chemical Co., Ltd.
$KClO_4$	K	$21.9\mu m$	Japan Carlit Co., Ltd.
KNO_3	N	$60\mu m$	Otsuka Chemical Co., Ltd.
Oxidizer X	X	$30\mu m$	Otsuka Chemical Co., Ltd.
Cellulose acetate	CA		Wako Pure Chemical Co., Ltd.
Acetone	AC		Wako Pure Chemical Co., Ltd.
U/K(38/60)	UK		
U/N(41/57)	UN		
U/X	UX		

Potassium perchlorate($KClO_4$) and potassium nitrate(KNO_3) were used as typical reactive and less reactive oxidizers, respectively.

2.2 Test Methods for Evaluating Hazards

Following tests were used for evaluating fire and explosion hazards of materials and compositions used in the manufacture of the UK, UN and UX gas generants:

(1) Impact and Shock Sensitivity, and Explosion Propagation

Impact and shock sensitivity and explosion propagation were determined using (a) the JIS drop hammer test [7], (b) the shock ignitability test [8], (c) VP30 PVC initiation test [9] [10] and (d) the United Nations gap test [11].

(2) Friction Sensitivity

Friction sensitivity was evaluated using the BAM friction test [12] .

(3) Electric Spark Sensitivity

Electric spark sensitivity was determined with the electric spark test for medium-sensitive materials [13] .

(4) Ignitability by Hot Objects and Burning Rate

Ignitability by hot objects and burning rate were determined using (a) the VP30 PVC tube burning test [15] , (b) ϕ 30 steel tube burning test and (c) the conical pile burning test [15] . As the igniter, a hot Ni-Cr wire or an igniting composition was used.

(5) Thermal Stability

Thermal stability was evaluated using the SC-DSC [16] measurements.

2.3 Test Results

(1) Impact and Shock Sensitivity, and Explosion Propagation.

Test results of impact and shock sensitivity and explosion propagation are listed in Table 2.

Table 2　Results of Impact and Shock Initiation Tests

Sample	Test	Result	Explosion Propagation
U	Drop hammer	E_{50}=21J	
	Shock ignitability	No explosion by	
		an inserted No.0 D with a lid	
	VP30 initiation	Material remained	No explosion propagated
	UN gap	Material remained	No explosion propagated
UK	Drop hammer	E_{50}=17J	
	Shock ignitability	Deflagration by	
		an inserted No.0 D with a lid	
	VP30 initiation	Material remained	No explosion propagated
	UN gap	The tube fragmented	Detonation propagated
UN	Drop hammer	E_{50}=12J	
	Shock ignitability	No explosion by	
		an inserted No.0 D with a lid	
	VP30 initiation	Material remained	No explosion propagated
	UN gap	Material remained	No explosion propagated
UX	Drop hammer		
	Shock ignitability	No explosion by	
		an inserted No.0 D with a lid	
	VP30 initiation	Material remained	No explosion propagated
	UN gap	Material remained	No explosion propagated

Above results showed that the sensitivity of the UX composition is similar to the UN but not to UK. The UX composition was not sensitive to impact or shock.

(2) Friction Sensitivity

Test results of the friction sensitivity of materials used in the process are listed in Table 3.

Table 3   Results of Friction Sensitivity

Sample	Test	Result	Note
U	BAM friction	1/10(36kg)	noize
UK	BAM friction	1/10(32.4kg)	reaction without noize
UN	BAM friction	1/10(36kg)	noize
UX	BAM friction		

(3) Electric Spark Sensitivity

Results of the electric spark sensitivity test are listed in Table 4.

Table 4   Result of Electric Spark Sensitivity Test

Sample	Test	Result	Note
U	For medium sens.	3/10(51J)	
UK	For medium sens.	$E_{50}=25J$	
UN	For medium sens.	$E_{50}=38J$	
UX	For medium sens.		

(4) Ignitability by Hot Objects and Burning Rate

Test results of ignitability by hot objects and burning rate are listed in Table 5.

Table 5   Test Results of Ignitability and Burning rate

Sampl	Test	Ignitability	Burning rate
U	ϕ30 Steel	None	−
	VP30 PVC	None	−
	Conical pile	None	−
UK	ϕ30 Steel	None	−
	VP30 PVC	Ignitable	0.72mm/sec
	Conical pile	None	−
UN	ϕ30 Steel	None	−
	VP30 PVC	Ignitable	0.51mm/sec
	Conical pile	None	−
UX	ϕ30 Steel	Ignitable	0.51mm/sec
	VP30 PVC	Ignitable	0.52mm/sec
	Conical pile	Ignitable	25g/70sec

(5) Thermal Stability

Results of SC−DSC is listed in Table 6.

Table 6   Results of SC−DSC

Sample	$T_{DSC}(℃)$			$Q_{DSC}(J/g)$	
	Endo therm	Exotherm(1)	Exotherm(2)	Exotherm(1)	Exotherm(2)
U	245	284		669	
U/K	231	241		1324	
U/N	206	225	434	408	507
U/X/CA	217	240	415	358	491

3. YOSHIDA HAZARD ANALYSIS FOR ENERGETIC MATERIALS(YHA)

3.1 Outline of the YHA

The YHA is a method for preventing accidents caused by energetic materials during their manufacturing and handling. The YHA consists of a risk evaluation which uses experimental data on energetic materials and three risk profiles: one for nomal operations, one for operations deviating from normal, and one for corrected operations. For these purposes, risk is defined as follows:

Risk = (probability of occurrence) × (severity of damage)

The following items are evaluated in the YHA:

(1) the scope of the project

(2) diagrams of the process, the flow of materials and the equipment

(3) material safety information

(4) process technology information

(5) hazard identification and risk catalog

(6) risk profiles

(7) safety measures

(8) prevention of deviation from normal operation and corrected risk profile

(9) conclusions

3.2 Probability of the Occurrence of Fire and Explosion

It is assumed that the probability of occurrence of fire and explosion is a function of the sensitivity and mode of handling of hazardous materials including pyrotechnic compositions, intermediates and raw materials. Expressed symbolically,

$P = f(S, H)$

where P is the probability of occurrence of fire and explosion, S is the sensitivity of the materials, and H is the mode of handling of materials. The sensitivity of materials is divided into four categories corresponding to the probability of the occurrence of an event:

Level	Probability	Sensitivity
A	frequent	high
B	occasional	medium
C	remote	low
D	impossible	none

3.3 Criteria of Sensitivity

A high−sensitive material may be ignited frequently during ordinary handling. A medium−sensitive one requires a strong stimulus. A low−sensitive material will not be ignited nor initiated without very high friction, high impact, shock, electric spark, contact with a hot object or high temperature. After many experiments [7]~[16] , criteria for sensitivity have been determined for explosives, propellants and pyrotechnic compositions(Table 7 ～ 11).

Table 7   Criteria for Impact and Shock Sensitivity

Level	Sensitivity	Test	Criterion	Ref.
A	High	Drop Ball(Direct Impact)	$l_{50} < 5mm$	16)
		Shock Ignitability(No.0 D)	$E_{50} > 1.0J$	8)
B	Medium	Shock Ignitability(No.0 D)	$l_{50} < 5mm$	8)
		VP30 PVC Tube(No.6 D)	Propagation	10)
C	Low	VP30 PVC Tube(No.6 D)	No Propagation	10)
		UN Gap(160g Booster)	Propagation	11)
D	None	UN Gap(160g Booster)	No Propagation	11)

Table 8   Criteria for Friction Sensitivity [12]

Level	Sensitivity	Test	Criterion
A	High	BAM Friction	$M_{50} < 1kg$
B	Medium	BAM Friction	$1kg < M_{50} < 10kg$
C	Low	BAM Friction	$10kg < M_{50} < 36kg$
D	None	BAM Friction	$36kg < M_{50}$

Table 9   Criteria for Electric Spark Sensitivity [13]

Level	Sensitivity	Test	Criterion
A	High	For High-Sensitivity	$E_{50} < 1.0J$
B	Medium	For High-Sensitivity	$1.0J < E_{50}$
		For Medium-Sensitivity	$E_{50} < 10J$
C	Low	For Medium-Sensitivity	$10J < E_{50}$
			$E_{50} < 100J$
D	None	For Medium-Sensitivity	$100J < E_{50}$

Table 10 Criteria for Ignition by Contact with Hot Objects

Level	Sensitivity	Test	Criterion	Ref.
A	High	Cerium-Iron Spark	Ignition	14)
B	Medium	Cerium-Iron Spark	No Ignition	14)
		Conical pile(Ni-Cr)	Ignition	15)
C	Low	Conical pile(Ni-Cr)	No Ignition	15)
		VP30 PVC Tube(5g Ignitor)	Ignition	15)
D	None	VP30 PVC Tube(5g Ignitor)	No Ignition	15)

Table 11 Criteria for Thermal Stability [17]

Level	Sensitivity	Test	Criterion
A	High	SC-DSC	$T_{DSC} < 100°C$
B	Medium	SC-DSC	$100°C < T_{DSC} < 200°C$
C	Low	SC-DSC	$200°C < T_{DSC} < 450°C$
D	None	SC-DSC	$450°C < T_{DSC}$

3.4 Effect of an Event: Degree of Damage

The degree of damage caused by fires or explosions of hazardous materials is assumed to be a function of the violence of the fire or explosion, the amount of material involved and environmental conditions. Symbolically,

$$D = g(V, M, E)$$

where D is the degree of damage; V, the violence of the event; M, the amount of hazardous material involved, and E, the environmental conditions.

To assign materials to hazard ranks according to the violence of fire or explosion and the amount of material involved, materials are classified as follows:

(1) primary explosives, which show a deflagration to detonation transiton upon ignition
(2) semi−primary explosives, which show a deflagration to detonation transition under some conditions after ignition
(3) detonating explosives, which explode after initiation with a No.6 detonator
(4) deflagrating explosives, which burn with high speed without a shock wave when ignited or initiated by shock, or which detonate by strong initiation under tight confinement
(5) combustible materials, which burn with low speed after ignition
(6) poorly combustible materials, which burn only when an external fire is involved
(7) non−combustible materials

The range of quantities of materials corresponding to the classification and damage ranking is listed in Table 12. The effect of environmental conditions will be taken into consideration when the YHA is applied to an actual process.

Table 12 Damage ranks, degree of damage and ranges of amounts(m) of materials

Rank	Damage	Amount of Materials		
		Primary Explosives	Semi-Primary Explosives	Detonating Explosives
I	Catastorophic	100g≦m	1kg≦m	10kg≦m
II	Critical	10g≦m<100g	100g≦m<1kg	1.0kg≦m<10kg
III	Marginal	1.0g≦m<10g	10g≦m<100g	100g≦m<1.0kg
IV	Negligible	m<1.0g	m<10g	m<100g
Rank	Deflagrating Explosives	Combustible Materials	Poorly-Combustible Materials	Non-Combustible Materials
I	100kg≦m	m=∞	m=∞	m=∞
II	10kg≦m<100kg	1.0t≦m	m=∞	m=∞
III	1.0kg≦m<10kg	100kg≦m<1.0t	m=∞	m=∞
IV	m<1.0kg	m≦100kg	m=∞	m=∞

3.5 Risk Profile and Acceptable Levels

The risk profile and acceptable levels are shown in Fig.1. In this case, two acceptable levels are defined. One is acceptable without review; the second is acceptable under some restrictions with strict reviewing.

In the YHA, three risk profiles are used. The first is an expected or preliminary profile made with the assumption that the process operates normally. The second is made by assuming the worst case of deviation from normal operation. After the second profile is made, safety measures are examined. Finally, a corrected risk profile is made and the measures for preventing hazardous deviations from normal operations are shown. This assessment is especially useful for preventing human error.
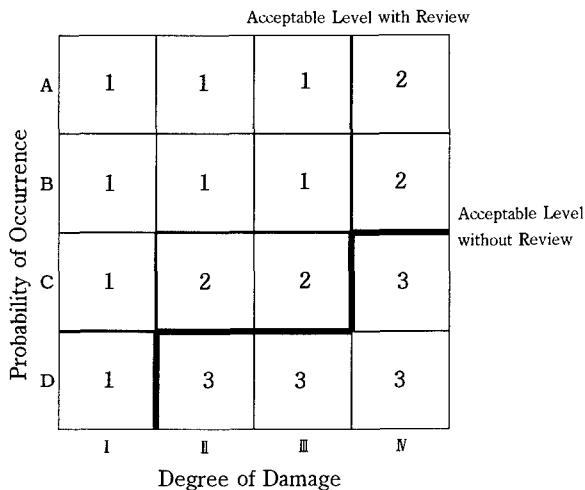
Fig.1 Risk profile and acceptable level

4. DIAGRAMS OF PROCESS AND MATERIAL FLOW AND THE EQUIPMENT

4.1 Flow Diagram of Process

The flow diagram of the process for the manufacture of a urazole gas generant is shown in Fig.2.
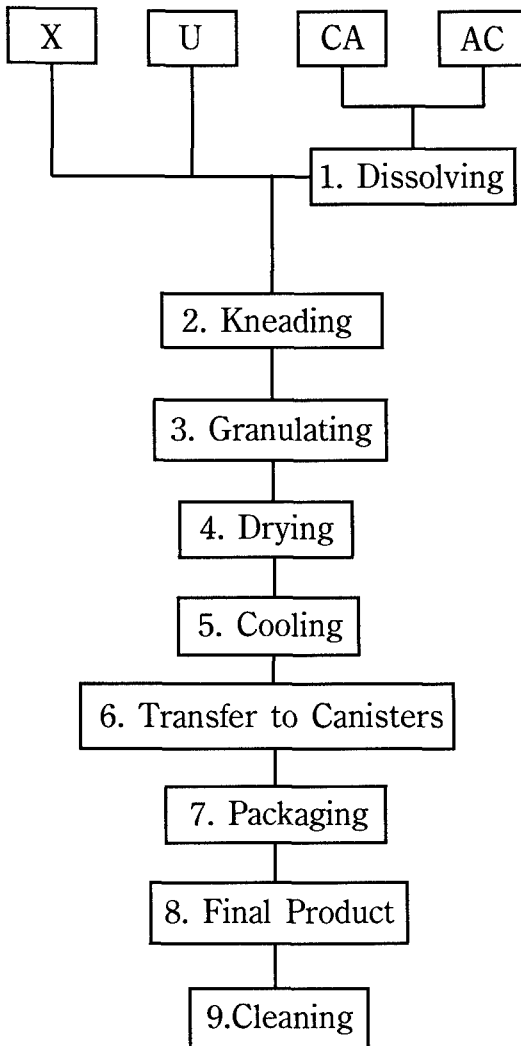
Fig.2   Flow Diagram for Manufacturing a Urazole Gas Generant

4.2 Flow Diagram for Materials

The flow diagram for materials used in the process is shown in Fig.3. The raw materials are urazole(U), oxidizer X(X), cellulose acetate(CA), acetone(AC) and other additives. The intermediates are the mixture of urazole and oxidizer X, the hot solution of cellulose acetate in acetone, the wet mixture of U, X, CA and AC, the wet granules, the dried granules in bulk, and the dried granules in bottles. The final products are the packages containing the granules in bottles.
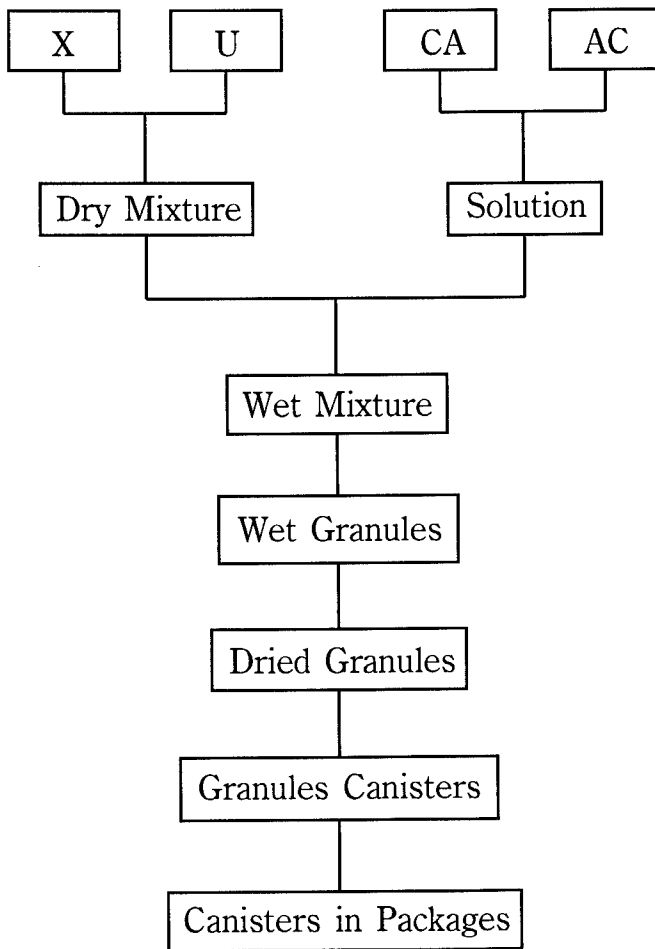
Fig.3 Materials Flow Diagram for Manufacturing a Urazole Gas Generant

4.3 Equipment

The primary equipments used in the manufacturing process are shown in Fig.4. The dissolving vessel for the cellulose acetate has a capacity of approximately 20 liters. It is made of stainless steel. The mixer is a kneading mixer. The dry urazole and oxidizer X are fed into the mixer and are preliminarily mixed. The cellulose acetate solution is added and mixed thoroughly. The granulator is an extruder at the moment tentatively. The composition in the granulator is wet with acetone.

The drying oven is a warm nitrogen gas circulating oven equipped with a safety device to prevent overheating. The drying operation is the most hazardous among all the unit operations because the possibility exists that dry granules in bulk will ignite in the oven. The cooler, the filling machine and the packaging machine are not fixed at the moment.
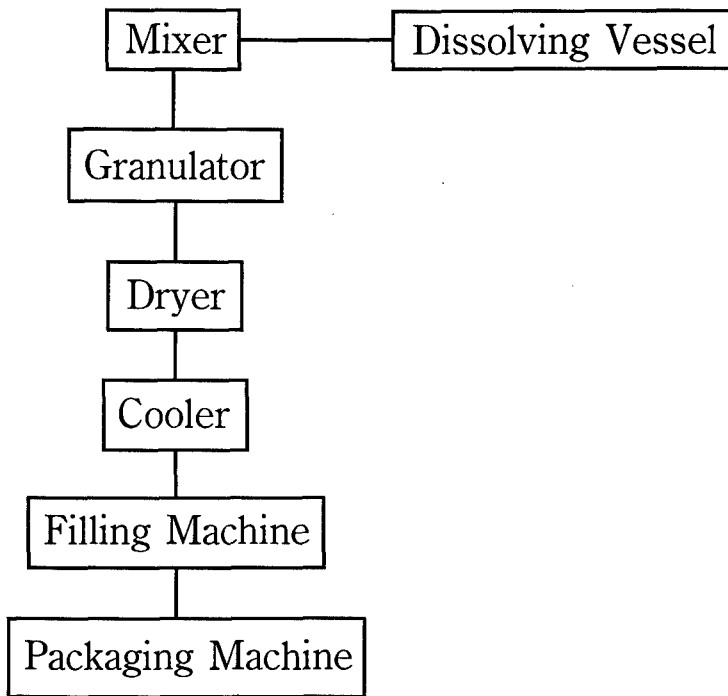
Fig.4   Equipment used in the Process

5. MATERIAL SAFETY INFORMATION

5.1 Sensitivity of Materials

The sensitivity determinations were carried out, and the sensitivity criteria based on this as well as previous works are listed in Table 7 ~ 11. The sensitivity levels of the raw materials, intermediates and product of the UX gas generant are listed in Table 12.

The thermal stability level of urazole is ranked "C" because the exothermic onset temperature, $T_{DSC} = 240\ °C$, is considered safe under normal handling conditions. When a material with that $T_{DSC} = 240\ °C$ is involved in a fire or is contacted by a hot object over 200 °C in temperature for long periods, the material may become hazardous. However, all raw materials used in this process are safe at room temperature.

Insufficient control of the oven's temperature and deficiencies in cleaning the drying oven in addition to changing the composition of the mixture without assessing the stability of new ingredients may contribute to an accident. The granules described present no problem if they are handled normally.

Table 12   Sensitivity Levels of Materials used in the Process

No.	Material	Impact Shock	Friction	Spark	Hot Object	Thermal Stability	Note
1	U	D	C	C	D	C	Raw Mat.
2	X	D	D	D	D	D	Raw Mat.
3	CA	D	D	D	C	D	Raw Mat.
4	AC	–	–	*	*	–	Raw Mat.
5	U/X	D	C	C	C	C	Intermediate
6	U/X/CA/AC	D	D	*	*	C	Intermediate
7	U/X/CA/AC(Gr)[1]	D	D	*	*	C	Intermediate
8	U/X/CA(Gr)[1]	D	C	C	C	C	Intermediate
9	U/X/CA(Gr, C)[2]	D	D	D	D	C	Intermediate
10	U/X/CA(C, P)[3]	D	D	D	D	C	Product

* Acetone(AC) is flammable with electric spark and hot object in the air.

1) Gr: Granules   2) Granules in canisters   3) Canisters in packages

5.2 Combustion Categories, Amounts and Damage Levels of Materials in the Manufacturing Process

The combustible or explosive materials used in the process are dry and wet granules in bulk:

poorly—combustible materials: urazole, cellulose acetate, the mixture of urazole and oxidizer X and canisters in packages;

combustible materials: dry and wet granules in bulk and granules in canisters.

An inventory amount corresponding to one batch from the process is assumed to consist of less than 100kg at the stage of mixing and less than 20kg in the drying operation. The combustibility categories, inventory amounts and damage levels for materials in the process are listed in Table 13.

Table 13   Combustibility Categories, Inventory Amounts and
Damage Levels of Materials in the Process

No.	Materials	Combustion Categories	Max Batch Inventory	Damage Level
1	U	Poorly-Combustible	50kg	IV
2	X	Non-Combustible	50kg	IV
3	CA	Poorly-Combustible	5kg	IV
4	AC	Combustible	20kg	III
5	U/X	Combustible	100kg	III
6	U/X/CA/AC	Combustible	100kg	III
7	U/X/CA/AC(G)	Combustible	100kg	III
8	U/X/CA(G)	Combustible	100kg	III
9	U/X/CA(G, C)	Combustible	100kg	III
10	U/X/CA(C, P)	Poorly-Combustible	100kg	IV

5.3 Effect of Materials on Health and Environment

Information on the effect of materials used in the process on the health of people in the work place and on the environment was collected. The 50% lethal dose(LD_{50}) and the time weighted average−threshold limit value(TLW−TWA) of only acetone was available among all raw materials. LD50 and TLW−TWA of acetone are 5.3g/kg, inhalation by mouse, and 750ppm, respectively. The health hazards of acetone are following: The vapor may cause dizziness or suffocation and the contact may irritate or burn skin and eyes.

6. PROCESS TECHNOLOGY INFORMATION

The process information is described according to the OSHA standard as follows:

6.1 Flow Diagram for Process

This was presented in Fig.2.

6.2 Process Chemistry

No chemical reaction takes place during the manufacturing process.

6.3 Maximum Intended Inventory

A maximum intended inventory of 100kg per batch is expected. In drying operations, a 20kg batch is assumed.

6.4 Safety Limits of the Operation

(a) Temperature (T)

$45°C < T < 55°C$ for drying the granules

$0°C < T < 40°C$ for other operations

(b) Pressure

Materials are pressurized in the granulating operation. The safety limits for these operation have not yet been set.

(c) Flow rate

In the granulating operation, the flow rate of materials are important factors for considerations of operability as well as hazard. The safety limit for flow rate has not yet been set.

(d) Composition

Changing the composition of the gas generant affects the safety and performance of the process. The composition may vary by a maximum of 5% from the normal composition.

6.5 Evaluation of Consequences of Deviations from Normal Operation

(a) Deviations in the composition

A change in the oxygen balance affects the concentrations of CO and NOx in the effluent gas. A deviation in the amounts of cellulose acetate affects the toughness of the granules. If the acetone content of the mixture deviates, the granulating process becomes more difficult to operate.

(b) Deviations in the operating conditions

When the operation of the granulating machine deviates from normal, the toughness and density of the formed granules changes, and as a result the properties of their combustion are affected.

(c) Deviation in the amount of material

Overloading the drying oven causes granules to spill, which may in turn cause accidental ignition. If a large amount of dry granules is ignited accidentally, the fire is hazardous and may damage individuals and property. If the amount of such materials is limited, any resultant fire can be easily extinguished with a water spray.

(d) Deviation in pressure

The drying oven should be designed such that the pressure does not increase when an accidental fire occurs. The burning speed of a small amount of granules of the UX gas generant is slow under atmospheric pressure, but a large amount burns quickly if under high pressure.

(e) Deviation in temperature

If the temperature in the drying oven rises too high, dry granules or dust may ignite. If dust is allowed to accumulate on the over-heated surfaces in the oven, it may ignite.

7. HAZARD IDENTIFICATION AND RISK CATALOG

The potential hazards in the manufacturing process for the UX gas generant were identified and ranked by the sensitivity, the combustibility and the amount of material used in the process. Using the results of the hazard identification and ranking, a risk catalog was made for the process as listed in Table 14.

Table 14   Risk Catalog for Operations in the Process

No.	Operation	Normal Deviation	Haz. Mat.	Risk Rank	Note
1	Dissolving	Normal	Acetone	IV D	No Problem
		Deviation	Acetone	III C	Spill and Ignition
2	Kneading	Normal	Wet Mixture	III D	Few Problem
		Deviation	Wet Mixture	II B	Bad Maintenance
3	Granulating	Normal	Wet Mixture	IV D	No Problem
		Deviation	Wet Mixture	III C	Bad Maintenance
4	Drying	Normal	Granules	III C	Few Problem
		Deviation	Granules	I B	Overheating and Ignition
5	Cooling	Normal	Granules	IV D	No Problem
		Deviation	Granules	IV D	No Problem
6	Filling	Normal	Granules	IV D	No Problem
		Deviation	Granules	IV D*	
7	Packaging	Normal	Canister	IV D	No Problem
		Deviation	Canister	IV D	No Problem
8	Cleaning	Normal	All Haz. Mat.	IV D	No Problem
		Deviation	All Haz. Mat.	II C	Over-Inventory and Ignition

* Hermestic sealing of the canister is important for preventing deteriolation of the gas generant during storage.

8. RISK PROFILES FOR NORMAL OPERATIONS AND DEVIATIONS

The risk profiles for normal operations and deviations are shown in Fig.4 (a) and (b), respectively. All normal operations fall within the acceptable level with review, and only the drying operation is outside the acceptable level in the absence of review.
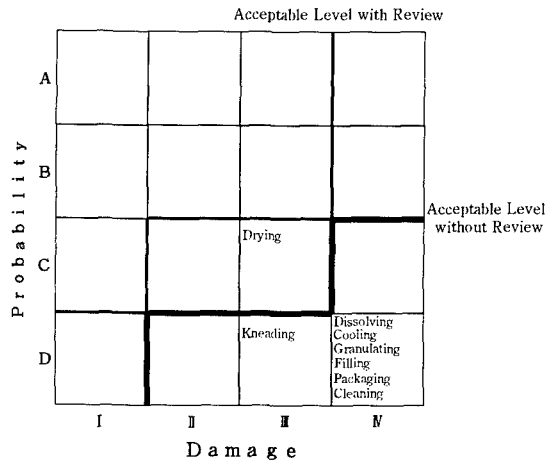
(a) Risk under normal operations
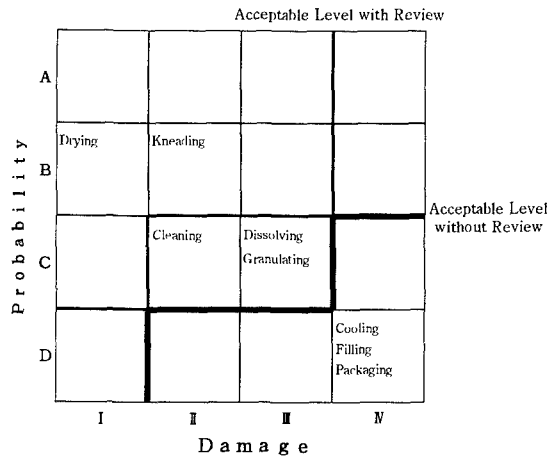
(b) Risk when handling deviates from normal

Fig.4 Risk Profiles for Manufacturing a UX Gas Generant

Many case histories are known involving hazards in the drying operations of energetic materials. Although the UX composition is stable because of its high exothermic onset temperature and few possibilities of of ignition are expected in normal drying operations, ignitions are still possible in the drying oven. One possibility is that the oven overheats the UX granules. A second possibility occurs if dust from the composition accumulates on the hot surfaces of the oven and ignites. Of course, it is also always possible that the composition may ignite from some unidentified source.

Small quantities of UX granules burn slowly under atomospheric pressure. If the drying oven is well designed, the damage level for granules is ranked at level III .

Dissolving cellulose acetate, mixing and kneading the raw materials, granulating the mixture and the amounts of materials involved should not cause accidents if operations are carried out normally.

Among the risks associated with operations that deviate from normal, the highest are associated with the drying operation. The causes of ignition include the use of an incorrectly designed oven, modification of the composition to an unstable one, contaminations, and accumulation of dust on the hot surfaces of the oven.

If the oven is maintained improperly, the oven may overheat and the UX composition may ignite. If the inside of the oven is not kept clean, dust from the composition accumulates on hot surfaces and may ignite. If the composition is contaminated with a material which catalyzes a reaction, it may become unstable. If a component of the composition is modified, a safety assessment must be done on the new formulation to establish its stability. These types of deviation from normal operation must be prevented.

The filling of canisters with UN granules and the packaging of the canisters into containers has no risk other than that of external fire. The packaging will not promate fire.

If too high an inventory of the UX powders or granules is maintained, these materials become a hazard because of their rapid combustion. This is known for the AK gas generant as well [14] . This is especially the case if the generants are sealed tightly in a container. One should avoid both over–inventory and the use of sealed vessels in processing.

If the kneading operation is done in the air environment the possibility of ignition of acetone exists, and burning the mixture may blow the cover off the mixing machine. The damage will be more severe if a machine with tight seals is used. The nitrogen environment of the kneader and dryer are useful for decreasing the probability of ignition.

The granulating machine may become heated if the acetone content of the composition is inadequate. The acetone content of the mixture must be controlled and the machinery must be regularly maintained to insure safe operation.

9. PREVENTION OF DEVIATIONS FROM NORMAL OPERATION AND CORRECTED RISK PROFILE

From the consideration of the risk catalog and profiles of the normal operation and deviations from it, we suggest measures for preventing deviations and for promoting safety of operations at acceptable levels.

9.1 Safety Measures for Drying Operations

Two measures for preventing accidents during the drying operation have been identified. One is preventing the occurrence of ignition in the oven as follows:

(1) select an oven with good temperature control

(2) select an oven without hot, exposed surfaces

(3) prevent the accumulation of dust in the oven

(4) use a composition of known stability

(5) use nitrogen gas for preventing ignition of acetone

(6) prevent contamination which makes the composition unstable

A second is to prevent damage when ignition accidentally occurs:

(1) use an oven without a tight seal

(2) limit the amount of granules in the oven

(3) use an oven with a safe door

(4) prevent anyone from approaching the safety relief opening of the oven when the drying operation is in progress

9.2 Safety Measures for Inventory

It is important to let involved people know the consequences of deviations in the amount of materials on hand and the necessity of keeping a fixed inventory.

9.3 Safety Mesures for the Granulating Operation

In the normal operation, granulating is safe because it is carried out on a mixture wet with acetone. However, the material in the machine may be subjected to excess pressure, friction or high temperature if the amount of acetone present is inadequate. It is important for appropriate personnel to be aware of these factors and to keep the machine in optimum condition to carry out the granulating operation safely.

9.4 Safety Measures for the Kneading Machine

The inert environment with N_2 is very useful for preventing ignition of acetone vapor in the machine. The workers must be educated thoroughly in this regard. The kneader sometimes heats up during operation. Excess heating indicates a deviation from normal operations, and it is essential that the cause be determined and removed.

9.5 Corrected Risk Profile

A corrected risk profile for the manufacturing process of a UX gas generant was produced according to the suggestions in this paper, but is the same as that shown in Fig.4 (a) in this case.

10. CONCLUSION

A hazard analysis has been carried out for the manufacture of a UX gas generant in a batch 100kg in size. The following conclusions were reached:

(1) The UX gas generant can be manufactured safety if the appropriate people have information on the hazards associated with the materials and the normal operations used in the process and avoid deviations from normal operating procedures.

(2) The drying operation has the highest associated risk among the operations in the process. The design of the oven, its use, use of inert N2 environment and the thermal stability of the formulation are also important.

(3) Good maintenance of the granulating machine is crucial.

REFERENCES

1) K. Hara, T. Hasegawa, S. Iyoshi, T. Yokoyama, T. Kazumi, M. Hayashi and T. Yoshida, "Concept and Performance of a Non–Azide Propellant for Automotive Airbag Inflator", The 19th International Pyrotechnics Seminar, 20–25 February, 1994, Christchurch, New Zealand

2) T. Kazumi, K. Hara, Y. Yu, Y. Yamato, T. Takahori, Y. Shimizu and T. Yoshida, "Safety Aspects of a Non–Azide Propellant for Automotive Inflators", The 19th International Pyrotechnics Seminar, 20–25 February, 1994, Christchurch, New Zealand

3) K. Hara, Y. Shimizu, Y. Higashi, T. Nojima, T. Hasegawa and T. Yoshida, "Hazard Analysis of Manufacture of Non–Azide Propellant for Automotive Airbag Inflators", Proceedings of the 20th International Pyrotechnics Seminar, Colorado Springs, USA, 25–29 July, 1994, pp.381

4) OSHA, US Department of Labor, "Process Safety Management of Highly Hazardous Chemicals, Explosives and Blasting Agents", 29 CFR Part 1910, RIN1218–AB20, Federal Register, 57(36), Feb.24, 1992

5) H. A. Zogg, "Zurich Hazard Analysis", Zurich Insurance Group, Risk Engine ̄7

6) US Department of Defence, "Military Standard. System Safety Program Requirement", MIL–STD–882C 1991

7) T. Yoshida, "Safety of Reactive Chemicals", Elsevier, Amsterdam, 1987, pp.287

8) K. Aoki, T. Yoshida, et al., Proc. "Shock Ignitability Test for Medium–Sensitive Pyrotechnic Compositions", Proceedings of the 18th IPS, Beckenridge, USA, 12–17 July, 1992, p.1

9) Y. Wada, T. Yoshida, et al., "Shock Sensitivity Test of Blasting Explosive Cartsides", J. Energetic Materials, 9, 105(1991)

10) T. Okitsu, T. Yoshida, et al., "Shock Sensitivity Tests for Commercial Explosives and Low–Sensitive Explosive Materials", Margretetorp, Aug. 23–27, 1992, p.107

11) United Nations, "Recommendation on the Transport of Dangerous Goods. Manual of Tests and Criteria", 1995

12) K. Show, "Friction Sensitivity of Energetic Materials", Bachelor theisis, Hosei University, 1994

13) S. Amari, F. Hosoya, Y. Mizushima and T. Yoshida, "Electrostatic Spark Ignitability of Energetic Materials", Proceedings of the 21th International Pyrotechnics Seminar, Moscow, Russia, 11−15 September, 1995, pp.13

14) H. Koenen, K. I. Ide and K. H. Swart, "Sicherheits Technische Kenndaten Explosionsfahigen Stoffe", Explosivstoffe, 9, 4, 30(1961)

15) D. Dayu, Unpublished results

16) T. Yoshida, Y. Wada and N. Foster, "Safety of Reactive Chemicals and Pyrotechnics", Elsevier, Amsterdom, 1995, pp.75 and 86

17) Y. Otsuka, E. Kawashima, Y. Yu, K. Hasegawa, K. Hara, Y. Shimizu and T. Yoshida, "Evaluation of Thermal Stability of Energetic Materials", The 10th Symposium on Chemical Problems Connected with the Stability of Explosives, 29 May−2 June, 1995, Margretetorp, Sweden

Computer Modeling of Possible Polymorphic Transformations in HNIW (CL-20)

Tatyana S. Pivina and Elena A. Arnautova

N.D.Zelinsky Institute of Organic Chemistry
Russian Academy of Sciences, Leninskii prospect 47, Moscow, 117913
R U S S I A

Alexander V. Dzyabchenko

L.Ya.Karpov Institute of Physical Chemistry, Obukha 10, Moscow 103064
R U S S I A

ABSTRACT

An approach to the *ab initio* prediction of crystal structures (by optimization of packings) and to the consideration of possible polymorphic transformations was developed for organic compounds. The principal features of the search method were the use of statistical data on organic crystal structural classes for the selection of the typical space groups and site symmetries for further search; consideration of the symmetry of the energy hypersurface with the aim of determining a unique search region; the use of an automated similarity-search procedure for the recognition of non-unique minima and determination of the symmetry of optimized packings.

This method was used to predict the possible crystal structures for six crystalline polymorphs of HNIW (2,4,6,8,10,12-hexanitrohexaazaizowurtzitane, CL-20). As a result, the energy-minimized structures with the densities close to 2.1 g cm^{-3} were predicted. Since the interaction between the conformational and packing forces raises the total energy to some extent, at the expense of a loss (at least partial) in molecular symmetry, the predicted densities of two previously unknown polymorphic variations are expected to be the lower estimates of the actual ones.

The possible conformational and crystal-structure transformations were calculated for these different polymorphic forms of CL-20.

INTRODUCTION

Several polymorphic modifications of a substance may be formed in the process of crystallization. These modifications may have different physicochemical properties. The differences in the properties of polymorphs, which result from variations in the conformations of their molecules (conformational polymorphism), were investigated by Bernstain [1].

In general, the problem of polymorphic transitions in molecular crystals formed by components of propellants and explosive mixtures is of principal importance for the creation, safety of production, and application of energetic

materials. This fact is easy to understand, since, as a rule, *a priori* calculations of physicochemical characteristics for these compounds are oriented at "knowing" the exact molecular crystal density for molecular crystals of this or another substance. However, during the production or practical use of these compounds, changes in the pressure and temperature conditions make this "knowledge" completely insufficient: a change in the production or operation conditions often results in a change of the molecular crystal density because of polymorphic transitions. Such well-known high-energy compound as 1,3,5,7-tetranitrotetraazacyclooctane (octogen, HMX) is a good example of this phenomenon.

However, if some (although scarce) experimental studies of polymorphic transitions are going on for HMX, virtually no attempts at theoretical analysis of this fundamental problem have been undertaken.

THE OBJECTIVE OF THE STUDY

(1) Computer structural modeling for chemical compounds from the nitroamine class and comparison of these results with experimental X-ray data for refining the optimum parameters of atom-atom potentials, which will be used in calculations for different polymorphic forms within the nitroamine class.

(2) The consideration of four octogen polymorphs as an example for studying the applicability of the atom-atom potential functions method (AAPF) for the prediction of the structure of HMX polymorphs on the basis of model energy calculations.

(3) Structural calculations for polymorphic forms of CL-20 and the routes of its polymorphic transformations.

(4) Estimation of minimum-energy routes for different forms of CL-20 and barrier heights for its structural transitions.

THEORETICAL BASIS

The usual technique of predicting a molecular crystal structure is numerical minimization of the unit cell energy in the AAPF approximation under the conditions of a given structural class. To predict polymorphic structures, one has to reveal all the deepest minima at the potential energy surface of the molecular crystal (some of these minima will correspond to polymorphic structures). For this purpose, one must explore the space of structural parameters (including the unit cell parameters, coordinates of the molecular centers and the Eulerian angles, which characterize the orientation of molecules) using a rather "small-cell" grid, and then successively use each junction of this grid as the starting point for energy minimization. Moreover, it is necessary to examine all structural classes. This examination may be reduced by confinement to triclinic structural classes with a number of symmetrically independent molecules. In this case, new elements of symmetry come out automatically.

As the basic method for theoretical description of the structural aspects characterizing the four experimentally found octogen polymorphs (α-, β-, γ-, δ-HMX), as well as for subsequent calculation of their interconversions, we suggest the method of atom-atom potential functions (AAPF). This method allows one to calculate molecular crystal densities and, in principle, to carry out calculations for polymorphs.

MODELING OF THE HMX POLYMORPHISM

HMX (1,3,5,7-tetranitro-1,3,5,7-tetraazacyclooctane, $C_4H_8N_8O_8$), an effective explosive, is known to have three possible polymorphic modifications (α, β and δ) with the crystal structures determined by X-ray diffraction and described in literature [2-4] (here, we omit γ-HMX, which contains a solvent molecule). There are two principal conformations for the eight-atom cycle of the HMX molecule: the centrosymmetrical chair-like conformation found in β-HMX, and the basket-like conformation of site symmetry 2, which is characteristic for the α- and δ-polymorphs.

In the paper [5], we considered HMX with the aim of testing our method in more detail as to its ability to predict crystal structures of organic nitramines. In particular, preliminary optimization of the HMX molecule for both conformations was performed, as implied by the *ab initio* methodology. Secondly, we tested a different (compared to the one used before) model of the interaction potential, which includes the Coulomb interactions.

Table 1. Comparison of the observed[a] and optimized molecular geometries for HMX[b]

	Observed	Optimized	Observed	Optimized
Conformation		Chair		Basket
Symmetry	$\bar{1}$	$\bar{1}$	2	$mm2$
Bond lengths (Å):				
C-N	1.453	1.467	1.461	1.467
C-H	1.099	1.080	1.080	1.080
N-N	1.364	1.391	1.362	1.391
N-O	1.217	1.217	1.225	1.217
Bond angles (deg.):				
C-N-C	123.1	114.4	120.5	113.7
N-C-N	111.9	114.5	111.7	112.5
C-N-N	117.3	112.8	119.1	123.1
N-N-O	116.9	117.3	117.6	117.6
O-N-O	126.3	125.1	124.6	124.7
Torsion angles (deg.):				
N-C-N-C	117.1	121.9	102.4	110.0
	18.1	15.9	69.7	68.4
C-N-C-N	101.7	97.5	101.2	108.4
	43.3	57.8	69.7	69.6
N-C-N-N	112.3	118.6	125.8	107.9
	88.0	80.3	76.1	67.4
C-N-N-O	-.9	-1.6	-3.9	-2.3
	-10.7	-.1	-2.9	2.5
	1.3	1.2	8.5	-2.9
	-21.7	-2.8	-10.7	2.7

[a] Averaged over different polymorphs.
[b] Calculated with the standard force-field parametrization [6], except for the equilibrium bond lengths d(O-N)=1.217 A and d(N-N)=1.380 A and equilibrium valence angles $\angle$(O-N-O)=125.49°, $\angle$(N-N-O)=113.20°, and $\angle$(C-N-C)=109.29°, which were adjusted in this work to reproduce the X-ray geometry of HMX conformers in the best way.

The two principal HMX conformers were optimized by the MMX molecular-mechanical program [6] with the use of the observed geometries as the starting point. In this calculation, the force-field constants of the nitramine fragment were adjusted in advance to improve the agreement between the

optimized and observed geometries. The final optimized geometrical parameters are compared with the observed ones in Table 1; the force-field constants that change the standard parametrization [6] are also shown. As is seen from this comparison, the geometry of the chair conformer is reproduced much better than that of the basket one. This difference is due to the fact that the optimized basket conformer adopts a higher symmetry — $mm2$ (C_{2v}) — than its actual symmetry in the crystal.

In order to distinguish the purely molecular and crystal-packing effects on the density of a molecular compound, we used the molecular density function
$$D_{mol} = M/V_{mol}, \qquad\qquad (1)$$
derived from the molecular volume V_{mol} and molecular weight M. V_{mol} was computed by the CALCVOL program [7], with the van der Waals radii assumed to be 1.16 Å for hydrogen, 1.71 Å for carbon, 1.50 Å for nitrogen, and 1.29 Å for oxygen.

For each conformer, D_{mol} showed a tendency to become greater if calculated for the optimized geometry in comparison with the observed one (Table 2). Both conformers were found to have identical D_{mol} values after optimization of geometry, thus indicating that molecular conformation has no effect on the density in this particular case.

As the first step, optimizations of packings were performed locally, starting from the three polymorphic structures. Both the observed and the MMX-optimized molecular geometry were used. The results presented in Table 2 show reasonably good agreement between the calculated and observed packing characteristics. In particular, deviations in the structural parameters and densities of crystals are not too significant (β-HMX exhibits the best agreement in the structural parameters, but the difference between the lattice energy E_{min} and the observed sublimation enthalpy ΔH_{sub} is the greatest here compared to the other two polymorphs). There are no abnormally short interatomic distances in energy-minimized structures. Note that these distances are, in the average, somewhat longer than the experimental values, in accordance with the fact that the predicted density is lower than the observed one. Passing from the observed molecular geometries to the optimized ones, we see that the agreement between the predicted and experimental parameters of the packings is deteriorated to some extent. This is understandable if we assume that the major reason for the difference between the two geometries is due to crystal packing rather than to the inadequacy of the molecular force field. At the same time, the α- and δ-polymorphs tend to assume lower stability and smaller density in the case of optimized geometry, while the β-polymorph displays the opposite effect. This behavior may be attributed to the fact that the optimized basket conformation adopts the $mm2$ symmetry, which is not very suitable for the low-symmetrical crystal environment in the former two polymorphs.

The predictions of lattice energies for the three polymorphs are not quite satisfactory from our point of view: firstly, because they are systematically less (by the absolute value) than the corresponding observed sublimation enthalpies; secondly, they are inconsistent with the fact that β-HMX is the most stable polymorph. The possible reason for this disagreement is overestimation of the Coulomb energy (at the expense of the van der Waals energy), which is much lower for the β-form (24$\%$ of the total energy) compared to the α- and δ-forms (45$\%$).

Table 2. Comparison of the observed and calculated structures of the HMX polymorphs

Structural class	I. beta-Form (chair) $P2_1/c$, $Z=2(\bar{1})$			II. alpha-Form (basket) $Fdd2$, $Z=8(2)$			III. delta-Form (basket) $P6_1$, $Z=6(1)$		
	Obsvd	C1x[a]	C1	Obsvd	B1x[a]	B1	Obsvd	B2x[a]	B2
Structural model		$\bar{1}$	$\bar{1}$		mm2	mm2		mm2	mm2
Molecular symmetry									
$-E_{pack}$[c] (ΔH_{subl}[d])	(41.9)	36.33	36.79	(39.3)	37.83	37.39	(38.0)	37.74	36.68
$-E_c$[e]	-	8.83	9.42	-	14.39	14.85	-	15.07	15.50
Crystal density[b]	1.90	1.899	1.862	1.85	1.780	1.739	1.78	1.701	1.672
C_p[f]	0.669	0.669	0.663	0.653	0.628	0.620	0.631	0.603	0.596
Unit cell constants:									
a[g]	6.54	6.48	6.52	15.14	14.86	15.16	7.71	7.73	7.68
b	11.05	10.99	10.94	23.89	24.23	23.67	7.71	7.73	7.68
c	8.70	9.02	9.12	5.91	6.14	6.30	32.55	33.49	34.58
α[h]	90	90	90	90	90	90	90	90	90
β	124.4	126.3	125.7	90	90	90	90	90	90
γ	90	90	90	90	90	90	120	120	120
Rigid-body parameters:									
u[i]	0	0	0	0	0	0	0.296	0.298	0.307
v	0	0	0	0	0	0	0.780	0.759	0.768
w	0	0	0	0	0	0	0	0	0
ϕ[h]	170.4	171.6	170.7	0	0	0	-21.0	-22.4	-23.7
θ	16.2	15.4	11.4	0	0	0	24.6	26.9	23.5
ψ	-5.5	-8.5	-6.0	11.0	11.2	8.1	-105.1	-103.7	-102.5
Shortest contacts[g]:									
H...O	2.37	2.57	2.64	2.39	2.50	2.55	2.32	2.46	2.52
C...O	3.13	3.12	3.12	3.05	3.09	3.28	2.89	3.05	3.10
N...O	3.05	3.00	3.01	2.83	2.94	2.90	3.10	3.18	3.07
Deviation parameters of the molecule:									
Shift of origin[i]	-	0	0	-	0	0	-	.020	.016
Turn angle[h]	-	3.33	4.84	-	20	2.90	-	3.03	3.91

[a] Computed with the molecular geometry as observed in the X-ray experiment. [b] In g/cm³. [c] Packing energy, kcal/mol. [d] Enthalpy of sublimation (Ref. [8]), kcal/mol. [e] Coulombic energy contributing to E_{pack}. [f] Packing coefficient [9]. [g] In Angstroms. [h] In degrees. [i] In fractions of the cell edges.

The global search for other crystal packings of HMX (in addition to the observed ones) was performed with optimized molecular geometry. The most likely structural classes listed in Table 3 were tested. The site-symmetry groups selected for the search were trivial (denoted as 1) for each conformer, centrosymmetrical ($\overline{1}$) for the chair conformer, and two-fold axial (2) for the basket conformer.

Table 3. The searched structural classes

Site symmetry	Space groups	Total occurrence ($\%$)[a]
1 (C_1)	$P2_1/c$, $P2_12_12_1$, $P\overline{1}$, $Pbca$	76.7
$\overline{1}$ (C_i)	$P2_1/c$, $Pbca$, $P\overline{1}$, $C2/c$	97.6
2 (C_2)	$C2/c$, $Pbcn$, $Fdd2$, $P2_12_12$	75.4
m (C_s)	$P2_1/m$, $Pnma$	73.5

[a] Sum of the occurrences of the listed structural classes (deduces from Table 2 of [10]).

As a result of this search, various energy minima were located; those corresponding to highest density are reported in Table 4. None of the new packings had greater density than the value predicted above for β-HMX. On the other hand, some possible packings, like B3, exhibit greater cohesion energy. The latter observation, however, is hardly an acceptable piece of evidence confirming the existence of yet-unknown polymorphs, because the accuracy of energy predictions was insufficient. It is interesting to note that some possible packings of the basket conformer acquire higher crystal symmetries than those assumed during the search. This higher symmetry is possible because of the exactly $mm2$-symmetrical geometry of the molecule with its principal axes directed along the crystallographic axes.

Table 4. Other possible packings of HMX found by global search[a].

Conformation	Chair			Basket	
Minimum	C2	C3	B3	B4	B5
Space group	$Pbca$	$P2_1/c$	$P2_1/m$	$Cmcm$	$Cmcm$
Z, site symmetry	4($\overline{1}$)	2($\overline{1}$)	2(m)	4($mm2$)	4($m2m$)
$-E_{pack}$	35.54	35.25	38.09	35.45	37.39
$-E_c$	8.69	8.19	13.01	8.90	12.48
Density	1.838	1.845	1.807	1.856	1.795
C_p	0.655	0.657	0.644	0.662	0.640
a	10.61	7.57	7.45	11.05	10.07
b	11.39	8.69	11.09	9.40	9.80
c	8.88	10.74	13.18	10.21	11.10
α	90	90	90	90	90
β	90	131.0	92.1	90	90
γ	90	90	90	90	90
u	0	0	0.295	0	0
v	0	0	1/4	0.338	0.351
w	0	0	0.313	1/4	1/4
φ	8.8	82.1	0	0	0
θ	8.9	11.3	-48.7	90	0
ψ	-7.2	87.3	0	0	0

[a] For symbols and units, see footnotes to Table 2.

So, we conducted a computational study of octogen polymorphism in order to test the sets of semiempirical atom-atom potentials available with regard for their ability to reproduce the four known octogen structures. Then, we used this methodology for studying the phenomenon of conformational polymorphism in CL-20.

A Priori Construction of Hypothetical Packing Models for CL-20 and Computer Modeling of Their Polymorphic Transformations.

Unfortunately, no X-ray data for CL-20 is available. Therefore, we had to perform, so to say, *ab initio* computer modeling for the possible polymorphic forms of CL-20 and their possible transformations.

Global search for dense packings of CL-20 molecules in 5 conformational forms (Fig.1) (three of them are known: the α-, β-, and ε-forms have been prepared and studied crystallographically; the α-form, studied as a hydrate, falls into the *Pbca* structural class [11]) showed [12] that the predicted δ- and ξ-forms correspond to deeper minima at the potential energy surface (-43.10 and 43.20 kcal/mol) than the other forms (-36.20, -35.90, and -32.40 for the α-, β-, and ε-forms, respectively). Probably this difference is due to higher electrostatic energy of the former two polymorphic modifications.
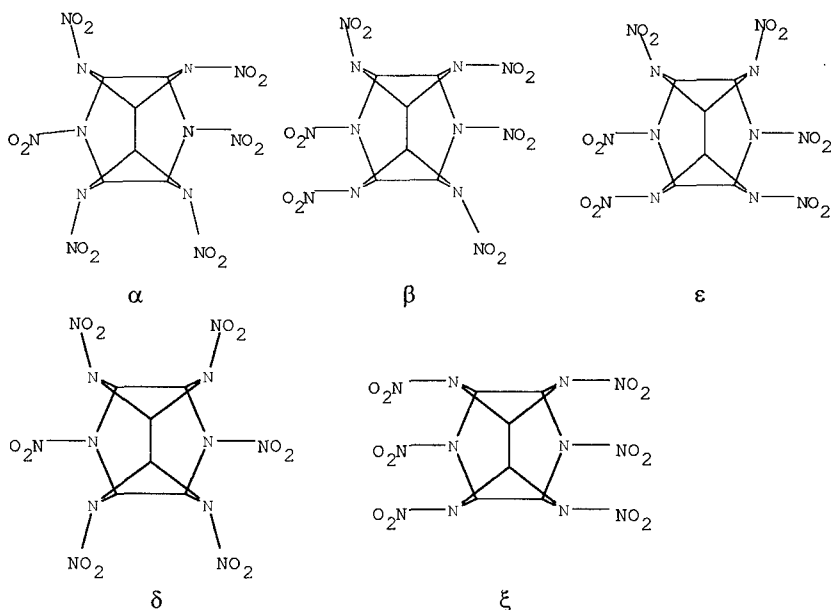
However, calculations of strain energies for CL-20 conformers indicate that the most strained framework among the studied ones is the ξ-framework. Therefore, we should not expect that the corresponding polymorphic form will be stable, even with allowance made for the aforementioned strong intermolecular electrostatic interactions in its crystal.

In connection with these results, we thought it worthwhile to study the possible polymorphic transformations ($\alpha \rightarrow \beta$ and $\alpha \rightarrow \varepsilon$) between the three most stable experimentally studied crystalline forms of CL-20. In our calculations we did not consider electrostatic interactions.

Polymorphic transformations were modeled by successive variation of several molecular parameters (namely, the orientation of nitro groups was changed). The range of the change in these parameters was divided into several parts (ten for the $\alpha \rightarrow \beta$ transition and twelve for the $\alpha \rightarrow \varepsilon$ transition). Each of these parts corresponded to a molecular structure, *i.e.*, to some intermediate model between the α and β (or α and ε) forms (conformers), respectively. In both cases, the starting point in the space of structural crystallographic parameters was one of the most dense packings in the *Pbca* (Z=8) structural class. Then, using the starting packing and removing all symmetry operations, we proceeded to the $P1$ structural class with eight independent molecules in an elementary cell, in which the molecular packings were optimized. Then, we selected the deepest minimum that was found by optimization of such a molecular packing, "placed" the next configuration of the CL-20 molecule (with the geometrical parameters from the selected range) in this minimum and optimized the crystallographic parameters again. Thus, successively considering different intermediate molecular models between the α- and β- (or α- and ε-) forms and "placing" them into the deepest minimum (obtained at the previous step of molecular packing optimization) in the space of structural parameters, we scanned the whole given range of values for the conformational transformations of the studied polymorphic forms.

To determine the symmetry elements for the class that is obtained as a result of such a transition, we used the CRYCOM computer program. As was noted by several authors [13, 14], recognition of similar crystal packings (with the aim of selecting the unique solutions) is the most difficult part in the whole procedure of global search because of the aforementioned multiple-description problem. To overcome a problem of this kind, we suggested the use of the CRYCOM (*i.e.*, CRYstal COMparison) program [15] with the algorithm (in its most principal part) implementing the ideas of [16] concerning hypersurface symmetry. For two crystal structures described by their cell constants and rigid-body parameters, CRYCOM searches over all equivalent descriptions of one structure, to match them against the description of the second structure. The second problem concerns the crystal symmetry characterization of the computed structure. It turns out that the symmetry-search problem is actually a particular case of the previous similarity-search task. Therefore, CRYCOM may be used its solution, if applied to one and the same crystal structure. Indeed, if we find all transformations of a crystal structure that match it against itself, we get the list of space-group symmetry operators whenever they occur for a given crystal [15].

Using the CRYCOM technique, we made an attempt to reveal the structural classes that were obtained by computer modeling of the CL-20 polymorphic transformations from the α-form. For any two possible descriptions representing a structure with N molecules within elementary cell we introduced following set of $2N+6$ parameters that define the deviations between the structural ones of these descriptions:
- six unit-cell parameter differences (taken by absolute value) to characterize similarity of the unit cells;

- *N* dimensionless fragment-origin distances to characterize similarity of the fragment positions;
- *N* fragment turn angles Ω to characterize similarity of fragment rotations in the two structures.

At fhe first stage we noted the maximum cell parameters deviations equal to 1.5 Å for *a*, *b*, *c* and 30^0 for α, β, γ and maximum molecular displacement and rotation equal to 0.5 and 10^0, respectively. As a result, we found that the transition to the structural class $Pb2_1a$, $Z=8(1,1)$ took place for $\alpha \rightarrow \varepsilon$ transformation and to $P112_1/a$, $Z=8(1,1)$ in case $\alpha \rightarrow \beta$ transformation. Then we gradually increased values of maximum structural parameter deviations to find other possible simmetry operations for the crystal structures. For ε-form any additional symmetry operations are absent exeptly the operations of $Pb2_1a$ structural class, while for β-form we recognized the operations corresponding to $Pbca$, $Z=8(1)$. The resultant parameters of elementary cells are given in Table 5 and the transformations are illustrated by Figs. 2.

Table 5. Structural parameters for α, β, ε-forms as a result of computer modeling of polymorphic transformations.

Polymorph	α	β			ε	
Space group	$Pbca$	$P112_1/a$		$Pbca$	$Pb2_1a$[a]	
-E$_{pack}$[b]	28.89	27.04		24.36	27.88	
Unit cell constant:						
a[c]	14.19	13.99		13.88	13.17	
b	17.02	17.11		17.50	17.72	
c	13.22	13.65		14.02	13.79	
γ[d]	90.00	86.10		90.00	90.00	
Rigid-body parameters:		moll	mol2		moll	mol2
u[e]	.2394	.2424	.2322	.2472	.1752	.2688
v	.0701	.0467	-.4472	.0531	.0701	.4775
w	-.0651	-.1098	-.1313	-.0543	.1860	-.3173
ϕ[d]	19.63	-2.83	-175.55	-11.82	8.74	175.80
θ	.37	-6.54	2.05	-11.01	5.55	-7.99
ψ	-19.42	-13.78	-40.96	-21.21	6.31	-176.20

[a] Unit cell contains two independent molecules. [b] Packing energy, kcal/mol. [c] In Angstroms. [d] In degrees. [e] In fractions of the cell edges.

It can be noted that the packing energies of β-form after additional optimization in structural classes $P112_1/a$ and $Pbca$ are different from each other (-27.04 and -24.36 kcal/mol, correspondingly), as well as from $P1$, $Z=8(1)$ packing energy (-25.37 kcal/mol).

As follows from the calculations, the polymorphic transition of the α-form (structural class $Pbca$, $Z = 8$) to the ε-form (structural class $Pb2_1a$) is associated with the difference between the lattice energies for these forms amounts to 1.03 kcal/mol; with the α-form being more stable.

The difference between the crystal lattice energies of the α- and β-forms amounts to 3.62 kcal/mol in favor of the first form, which is more stable.

DISCUSSION

The differences between the physical properties of different CL-20 polymorphs are intriguing. One of the possible reasons for these differences is,

Fig. 2. Modeling of the Pathways for PolymorphicTransitions in
CL-20 ($\alpha \to \beta$, $\alpha \to \varepsilon$).

Pbca (α) $\to$ *P112$_1$a* or *Pbca* (β)

Pbca (α) $\to$ *Pb2$_1$a* (ε)
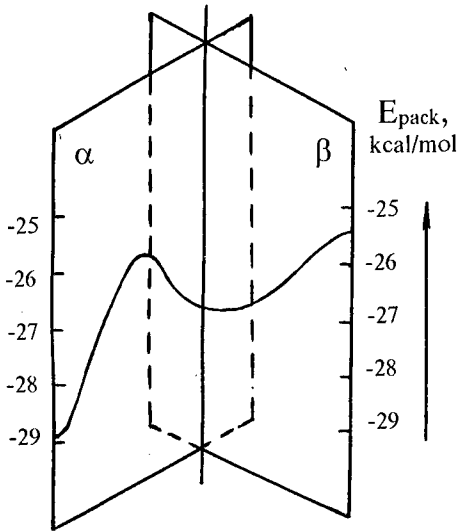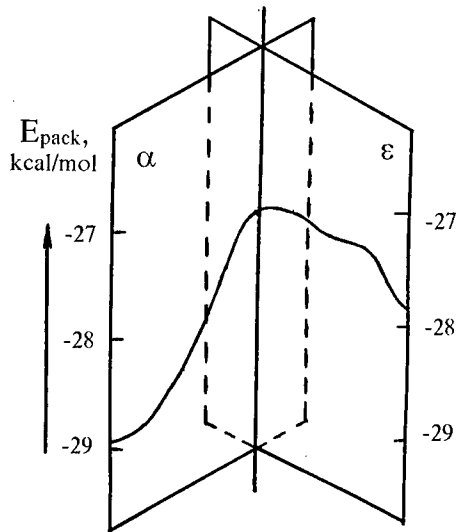
for example, the mechanism of the retention of the original crystal structure in solution. It is clear that this mechanism may also lead us towards the understanding of the "memory" phenomenon in solutions. As the first explanation of the visual differences, it would be reasonable to assume that aggregates or their fragments are thermodynamically stable. These aggregates are likely to exist even after the dissolution of a crystal.

Another reason for the "structure memory" in solutions may be the kinetic inertness of solvated complexes. Different packing of molecules in crystals of different polymorphic modifications inevitably results in the situation when solvent molecules become combined with different active sites of dissolving molecules. Further formation of the second, third, and other solvated shells results in the fixation of complexes that are formed by solvent molecules. Hence, different solvate complexes remain in solution for a long time.

We studied the possible polymorphic transformations of CL-20 only on the basis of the structural aspects that are determined by the existence of different molecular packings for the possible conformationally stable forms of this compound. In this study, we did not deal with the thermodynamic questions associated with such transitions, because we believed that the absence of an experimental basis would not let us evaluate the correctness of our calculations. Therefore, it is too early to model such complex processes in full volume.

As to the structural aspects, the results of our calculations indicate the presence of least five conformationally stable forms for CL-20 molecules. Computer search for optimum molecular packings corresponding to these five conformations showed that the most stable among them are the molecular packings that are known in literature as the α-, β- and ϵ-forms. At the same time, as to the stability of conformations, the most stable is the CL-20 molecule in the conformation that corresponds to the ϵ-form, and the least stable is the conformation that corresponds to the α-form.

Evidently, the stability of polymorphic states as a whole depends both on the stability of molecular conformations and on the energy of molecular lattices in the corresponding polymorphic forms.

Computer modeling of the structural aspects of the $\alpha \rightarrow \beta$ and $\alpha \rightarrow \epsilon$ polymorphic transitions showed that the energy differences for such transitions is determined only by molecular transformations of frameworks in molecules and by differences in the orientation of nitroamino groups.

REFERENCES

1. Bernstain J., In "Organic solid state chemistry", Ed. by G.R.Desiraju, Vol. 32, p. 471, 1987. Amsterdam: Elsevier.)
2. H.H.Cady,A.C.Larson,D.T.Cromer. Acta Crystallogr., 16 (1963) 617.
3. C.J. Choi, H.P.Boutin. Acta Cryst., B26 (1970) 1235.
4. R.E.Cobbledick, R.W.A.Small. Acta Cryst., B30 (1974) 1918.
5. A.V. Dzyabchenko, T.S. Pivina, E.A. Arnautova. J. Mol. Struct. In press.
6. U.Burkert, N.L.Allinger. "Molecular mechanics". ACS Monograph, v.177. American Chemical Society. Washington DC, 1982.
7. V.I.Shilnikov., V.S.Kuz'min., Yu.T.Struchkov. Zh.Struct.Chem., 34(3) (1993) 99.
8. J.W.Taylor, R.J.Crookes, J.Chem.Soc. Faraday Trans. Part 1, 72(3) (1976) 723

9. A.I.Kitaigorodsky, Organic Chemical Crystallography, Consultants Bureau, New York, 1961.

10. N.Yu.Chernikova, V.K. Belsky, P.M.Zorkii. Zh.Strukt.Khim., 31(4) (1990), 148.

11. P. Politzer, J.S. Murray, P. Lane, J.M. Seminario, M.E.Grice. The report, ONR contract #N00014-85-K-0217 UNO, US.

12. E.A. Arnautova, T.S. Pivina, A.V. Dzyabchenko. Proc. of 22nd IPS, Jule 1996, Colorado U.S.A.

13. A.Gavezzotti, J.Amer.Chem.Soc., 113 (1991) 4622.

14. H.R.Karfunkel, R.J.Gdanitz. J.Comp.Chem., 13(10) (1992) 1171.

15. A.V.Dzyabchenko. Acta Cryst. B50(4) (1994) 414.

16. A.V.Dzyabchenko. Acta Cryst., A39 (1983) 941.

DEMILITARIZATION FACILITY FOR THE ENVIRONMENTAL AND ACQUISITION LIFE CYCLE ANALYSIS OF EXPLOSIVES AND MUNITIONS SYSTEMS

1Lt Scott R. Jeffers, Mr. John D. Corley, Mr. Arthur F. Spencer, 2Lt Julie L. Clark
Energetic Materials Branch (WL/MNME)
2306 Perimeter Road, Suite 9
Eglin Air Force Base, Florida, USA 32542-5910
(904) 882-9532
FAX: (904) 882-3540

Abstract

The United States Air Force Wright Laboratory Armament Directorate, in accepting environmental responsibility for the life cycle of its explosives and munitions systems, has launched an aggressive pilot scale demilitarization program to recover, recycle, reuse, or dispose of the explosives and munitions systems it develops. The facility associated with this program will allow for the analysis of the environmental life cycle so that technologies can be developed with pollution prevention built into each phase of the munitions acquisition life cycle: conception, test and evaluation, production, and demil/disposal. Technologies developed at the facility will transition to industry or government agencies tasked to execute demil of production weapons systems.

Hazardous waste management is a key element of life cycle management for energetic materials. The concurrent development of advanced energetic materials for munitions applications and recovery/treatment/disposal technologies for these materials is essential if they are to be incorporated into inventory systems. This demilitarization facility provides the Energetic Materials Branch of the Armament Directorate this capability. The facility will also be available to research organizations world wide as a site for proving test concepts that have been demonstrated in laboratory environments.

The technologies employed in this pilot scale program are: High Pressure Water Washout for the removal of the bulk explosive from the munition containers; High Pressure Water Maceration for the size reduction of the bulk material for further processing and for the recovery of water soluble materials; Hydrolysis used in a unique way to remove the left over explosive residue from the sides of the munition allowing for container recovery and reuse; Molten Salt Destruction for an environmentally compatible way to completely destroy and dispose of the unrecoverable materials; and Non-Thermal Discharge (NTD) Plasma Processing as a supplement to Molten Salt Destruction for controlling any acid gas formation.

INTRODUCTION

The U.S. Air Force Wright Laboratory, Armament Directorate is currently conducting an in-house/contractor supported demilitarization demonstration program. The program objective is to provide a research and development (R&D) facility for exploring and demonstrating demilitarization, recovery, and treatment technologies for munitions systems, energetic materials, and associated waste streams. This project will contribute to advances in the "state-of-the-art" for demilitarization technologies and it will allow the High Explosive Research and Development (HERD) facility the ability to incorporate demilitarization techniques into the development of new Air Force explosives and munitions. This life cycle approach to the development of energetic materials must become commonplace within the R&D community. As new formulations and munitions systems are being developed, techniques to recover, reuse, or dispose of their constituents will be developed at the HERD facility. As a pilot-scale operation, the facility will be available to research organizations worldwide as a site for proving technology concepts which have been demonstrated in laboratory-scale environments.

From a practical viewpoint, the facility will provide a means for disposing of energetic material wastes for the HERD facility as well as an opportunity to recover valuable hardware and explosives for program offices refining their development technologies. This will posture the HERD facility for autonomous future operations. Treatment and/or reuse of recovered energetic materials will minimize the requirements for storing and disposing of hazardous wastes. Soil contamination and toxic air emissions resulting from open burning/open detonation (OB/OD) of these explosive wastes will also be minimized. Once demonstrated in pilot-scale, the technologies for treatment, recovery and disposal will be transitioned to production demilitarization facilities within the Department of Defense (DoD) using contractors and the Production Base Modernization Agency.

APPROACH

This program will provide a facility which will allow for the integration of demilitarization technologies to research and develop methods to recover, purify, recycle and/or dispose of explosives and munitions. Emphasis will be placed on pollution prevention as well as reclamation, recycling, and reuse (R^3) methodologies. Initially, we will target high volume production explosives such as TNT, RDX and HMX. We will also focus on high cost and R&D materials such as TNAZ, CL-20 and NTO. High pressure water washout will be used to remove explosive materials from munitions hardware. High pressure water maceration for the size reduction of the energetic materials and recovery of water soluble components is planned. Conversion of energetics to inerts through base hydrolysis will be investigated. Recovery of valuable non-water soluble materials using solvolysis will also be attempted. Ultimate disposal through molten salt destruction will be incorporated as well. Customization of analytical

techniques for detection and monitoring of residual effluent streams will be employed using existing HERD facility assets.

RELATED TECHNOLOGY EFFORTS

Research is being directed for explosive waste management throughout the explosives research, development, load-assembly-pack, and operational communities worldwide. Methods for analyzing, treating, recovering, recycling and responsibly disposing of these wastes, and systems contaminated with these wastes, are being developed. The HERD facility's R&D demilitarization system will utilize technology development already accomplished on a bench-scale and will integrate these specific technologies into a pilot-scale R&D system.

The University of Missouri - Rolla and the U.S. Navy have been instrumental in the development of high pressure water washout as a viable removal technique for certain energetic material applications. It is currently the method of choice for many full-scale demil facilities. The HERD facility will utilize the existing knowledge of this technology for the washout of the MK-series munitions and other BLU/GBU type munitions. One of the challenging aspects of this venture will be washing out around the conduit of these munitions.

Los Alamos National Laboratory (LANL) has researched base hydrolysis in depth for the last five years. The base hydrolysis technology is currently being utilized as a de-energization technique by the Large Rocket Motor Demil Program in the United States, and is being used as an ultimate disposal technology by United Technologies - Chemical Systems Division in San Jose, California since they are no longer allowed to open burn/open detonate (OB/OD).

Lawrence Livermore National Laboratory (LLNL) has demonstrated on a bench-scale that molten salt destruction is an effective method for disposing of energetic materials and other organic hazardous wastes. There is a growing interest in the pilot scale development of this technology since OB/OD has already been banned in certain areas of the United States. The HERD facility, along with LLNL, will be responsible for the pilot-scale characterization of the molten salt destruction technology.

MISSION IMPORTANCE

The HERD facility generates approximately 1000 lbs of explosive waste per month. Explosive wastes, contaminated hardware, and personal protective equipment are currently disposed of on the Eglin ranges using OB/OD. Waste streams of explosively contaminated water from machining operations are separated by gravity using sedimentation basins. The overflow stream is sewered to the Eglin waste water treatment facility. Demilitarization and treatment to recover valuable explosives and hardware is not accomplished by the R&D community in the USAF. The HERD facility relies upon

other contractor and DoD/DoE organizations for demilitarization and recovery of hardware. Explosive treatment, reclamation and recycling are not accomplished.

Hazardous waste management is a key element of life cycle management for energetic materials. The concurrent development of advanced energetic materials for munitions applications and treatment/disposal technologies for these materials is essential if they are to be incorporated into inventory systems. The cost for storing and handling excess munitions may dictate their dismantling as smaller defense budgets mandate smaller munitions stockpiles. The recovery of costly energetic materials (some priced as high as $1000s per pound) and R&D hardware (averaging $5000 to $10,000 per unit) must become standard procedure. Environmental regulations are disallowing OB/OD of hazardous wastes in some areas. Proactive response to such legislation could ensure the HERD facility remains operational by responsibly recovering, reusing, and disposing of its process byproducts.

ACCOMPLISHMENTS TO DATE

In FY94, extensive training in civil engineering/environmental technologies including waste water treatment, air pollution control, solid waste management and environmental law was accomplished. Site visits had been completed to: 1) GenCorp's, Aerojet Propulsion Division at Sacramento, CA to learn about their Resource Recovery System, 2) McAlester Army Ammunition Plant at McAlester, OK to see their pinkwater treatment facility (the availability of excess carbon filters for treating streams from machining operations was uncovered during this visit, 3) Lawrence Livermore National Laboratory (LLNL) in Livermore, CA to discuss their research in Molten Salt Destruction, 4) Los Alamos National Laboratory (LANL) in Los Alamos, NM to discuss their research in Base Hydrolysis, and 5) the University of Missouri at Rolla, MO to discuss their research in high pressure water washout technology. The training and site visits were used to select technologies appropriate for the HERD facility's requirements.

The Environmental Impact Assessment (EIA) was completed and a finding of no significant impact (FONSI) was granted in mid 1994. In early 1995, the architecture and engineering (A&E) was completed and the contract to build the demil facility was granted to a local contractor. In February, 1996 the 2500 square foot facility was completed. The demilitarization team is now in the process of installing the R&D equipment.

Joint activities with the national labs has also become an essential component to this program. Because of a joint program with Lawrence Livermore National Lab on the research of molten salt destruction, the HERD facility will receive a pilot scale molten salt destruction reactor in June, 1996. This joint effort has saved time and money for both players. Collaboration with Los Alamos National Laboratory has also resulted in an unofficial joint program to study the hydrolysis of energetic materials.

Finally, in November, 1995 the HERD facility awarded a contract for the design, fabrication, and installation of the equipment to support the demilitarization operation. The high pressure water washout equipment, the high pressure water maceration equipment, the hydrolysis equipment, the equipment to support the closed-loop water treatment system, the holding tanks, and all of the integration and remote control equipment is planned for completion during the spring of 1997.

CONCLUSIONS

The two main objectives of the HERD demilitarization facility are; 1) to allow for the capability to recover, recycle, reuse or dispose of energetic wastes produced by the HERD, and 2) to allow for the analysis of the environmental life cycle so that technologies can be developed with pollution prevention built into each phase of the munitions acquisition life cycle: conception, test and evaluation, production, and demil/disposal. This concurrent development of advanced energetic materials for munitions applications and treatment/disposal technologies for these materials is essential if they are to be incorporated into inventory systems. Technologies developed at this facility will transition to industry and/or government agencies tasked to execute demil of production weapons systems.

Special thanks to: Environmental and Safety Engineering (EASE), Inc.
                       - Ms. Sarah Winkler, Mr. Carl Christianson, and Dr. Hamid Adib
                  Lawrence Livermore National Laboratory
                       - Dr. Ravindra Upadhye and Dr. Bruce Watkins
                  Los Alamos National Laboratory
                       - Dr. Cary Skidmore and Mr. Robert Bishop

AHN — ADJUSTABLE HAND NOZZLE
BF — BAG FILTER
CAM — CAMERA
F — FAN
FE — FLOW ELEMENT
FI — FLOW INDICATOR
FT — FLOW TRANSMITTER
HPWP — HIGH PRESSURE WATER PUMP
LAH — LIQUID LEVEL ALARM (HIGH)
LAL — LIQUID LEVEL ALARM (LOW)
LCB — LOCAL CONTROL BOX
LCV — LEVEL CONTROL (FLOAT VALVE)
LE — LIQUID LEVEL ELEMENT
LI — LIQUID LEVEL INDICATOR
LT — LIQUID LEVEL TRANSMITTER
OCU — OIL CIRCULATING UNIT
P — PUMP
PCV — PRESSURE CONTROL VALVE
RC — REMOTE CONTROL
S — STRAINER
SS — SOFT START
T — TANK
TI — TEMPERATURE INDICATOR
⋈ — BALL VALVE
⋈ — GATE VALVE
⋈ — 3 WAY BALL VALVE

Demil Facility Layout

Mezzanine 7' high

Dotted-Line is second floor mezzanine 14' high (to hold 1 ton crane)

Molten Salt Destruction Unit

full stairs (36" wide)

straight ladder

gate

75 degree angle stairs (30" wide)

Forklift & Egress Path

Macerator

Slurry Holding Tank

Base Hydrolysis System

Hot-Oil Circulator

Air Compressor

Mezzanine 12' High

Stairs

Control Panel

CE Room

Munition

Shroud

Separator

X-Y-Z Table & Lance

Water Storage Tank

High Pressure Water Pump

Local Control Room

HYPERGOLIC CHEMICAL INITIATION OF NON-DETONATIVE AUTOCATALYTIC SELF-CONSUMPTION/DESTRUCTION OF TNT, RDX, AND TNT-BASED EXPLOSIVES

Allen J. Tulis, Alan Snelson, James L. Austing, and Remon J. Dihu
IIT Research Institute
Chicago, Illinois, 60616, U.S.A.
and
Divyakant L. Patel, Beverly D. Briggs, and David C. Heberlein
U.S. Army CECOM
Fort Belvoir, Virginia 22060, U.S.A.

ABSTRACT

The initiation of highly exothermic, autocatalytic self-consumption/destruction of military high explosives without transition to detonation has been demonstrated and is under development. The explosives under investigation are TNT, RDX, and Composition B. The methodology involves the use of small amounts of chemical reagents that are highly hypergolic with the explosives and induce a deflagrative, highly intense autocatalytic self-destruction of the explosives. Three categories of chemical reagents were investigated and demonstrated to be effective: (1) amines, (2) metal alkyls, and (3) interhalogens. Numerous candidates in each category were evaluated, in particular at low temperatures. Laboratory experiments demonstrated that the effectiveness of hypergolic initiation depended upon the form of the explosive; a solid casting requires extremely long induction times and unless adiabaticity is maintained, autocatalytic initiation is generally precluded, whereas fine explosive powders react effectively within milliseconds at ambient temperatures and within seconds, with diethylzinc, at temperatures as low as -30°C. Major large-scale field experiments involved diethylene triamine, diethylzinc, and bromine trifluoride as the selected candidates from the three categories of chemical reagents. As little as 5 to 10 mL of chemical reagent is effective at temperatures at or below 0°C when delivered in a manner such that the explosive, if a casting, is fractured to create sufficient surface area for hypergolic reaction with the chemical reagent. The induced highly-exothermic autocatalytic decomposition, once initiated, proceeds to completion and is independent of air, so that it is effective for buried as well as underwater explosives. Although in some autocatalytic decompositions of TNT profuse smoke (carbon) is liberated, often with larger castings, and always in the case of Composition B or RDX, a white-hot, smokeless and vaporless plume results, leaving no residue of the explosive.

INTRODUCTION

The indiscriminate proliferation of landmines, in particular anti-personnel (AP) mines (estimated at over 100 million in about sixty countries) continues to plague innocent civilians, killing or disabling 26,000 people worldwide each year [Ref 1]. This work is part of an ongoing major humanitarian demining program being conducted by the Countermine Directorate of the U.S. Army CECOM for implementation into the Demining Assistance Program, established by the United States, to address the problem of the tremendous amount of AP landmines that have already been implanted worldwide. This paper describes novel techniques for the chemical neutralization of TNT and TNT-based explosives typically encountered in AP landmines. This technology provides a viable means of achieving the non-detonative, autocatalytic self-consumption of the explosive, by using small amounts of appropriate chemical reagents with which the explosives are highly hypergolic and react with extensive exothermicity.

The main explosive charge in landmines is typically TNT or Composition B (Comp B), a cast composition of TNT and RDX. In a few instances the main explosive charge is also RDX. These explosives are highly energetic metastable CHNO compounds that release tremendous amounts of exothermic energy upon dissociation into stable products, typically CO_2, H_2O, CO, and N_2, as well as solid carbon in the case of very fuel-rich explosives such as TNT, all of which are essentially innocuous compounds in respect to the environment. However, it should be noted that the actual product species involve numerous other molecular and free-radical species, to a usually much lesser degree, but dependent upon the specific dissociation mode as well as extrinsic factors. These metastable compounds can dissociate by both intra- and inter-molecular mechanisms, which may involve detonation, deflagration, and autocatalytic mechanisms, by self-sustained chemical reactions which, once initiated, generally go to completion.

Furthermore, because molecular explosives such as TNT and RDX contain considerable oxygen within the metastable molecules, they do not need air in order for exothermic dissociation to occur; i.e., they will detonate, deflagrate, or dissociate by autocatalytic decomposition even when buried or under water, or in a vacuum. On the other hand, in the presence of oxygen from

the air many molecular explosives will burn (air combustion), especially the very fuel-rich explosives such as TNT. Hence, if TNT were to burn in air to stoichiometric completion it would release in excess of three times as much exothermic energy as in detonation [Ref 2]. However, since these explosives are contained in landmines, access to sufficient oxygen from the air for combustion to be sustained is generally not achievable, even in the case of surface-emplaced landmines, and whether neutralized by detonation, deflagration, or autocatalytic decomposition.

Most explosives can dissociate by alternative mechanisms, and dissociation by detonation often involves an entirely different mechanism from autocatalytic dissociation/decomposition; in fact, in some instances (even with highly sensitive nitroglycerine) the autocatalytic mechanism is preferential to the detonation mechanism, if the stimulus involved initiates the former mechanism [Ref 3]. In such cases, unless extrinsic factors are involved; e.g., heavy confinement or excessive thermal energy penetration beyond the reacting plane, the detonation mechanism is precluded. For example, TNT, and even nitroglycerine, will burn fiercely but without transition to detonation under the appropriate conditions. Hence, if a stimulus means such as a chemical hypergol or radiant-energy laser is capable of "directing" the dissociation mechanism into autocatalytic decomposition in lieu of detonation, it is likely that detonation will be precluded.

Alternatively, since these explosives are chemically synthesized from innocuous materials, then it is reasonable that they can be chemically transformed back to non-hazardous products. Basic compounds such as amines and alkoxides can neutralize the explosive properties of TNT and RDX, whereas sulfuric acid will decompose RDX into CH_2O, N_2O, NH_4, and NO_2, and other non-explosive compounds. However, in these stoichiometric reactions sufficient neutralization reagents would be required in order to effectively neutralize all of the explosive compound, and factors such as mixing and realization of reaction completion would be required and not always ascertained. In contrast, the initiation of spontaneous autocatalytic self-decomposition using very small amounts of hypergolic reagent or other effective stimulus can be expected to drive the decomposition reactions to completion. This work is based on technology developed in the 1970's for non-detonative neutralization of explosives.

BACKGROUND

In the 1970's IITRI conducted a number of programs for CECOM (at that time MERADCOM) which involved both (1) a solvation/reaction process whereby an appropriate solvent/reactant liquid mixture simultaneously dissolved and chemically decomposed TNT in a nearly isothermal manner [Ref 4,5] and (2) the chemical neutralization of TNT by direct heterogeneous liquid/solid hypergolic reaction of a liquid chemical reagent with the solid explosive to achieve initiation of an autocatalytic self-sustained exothermic decomposition, or self-consumption, of the TNT [Ref 6,7,8]. However, since the requirement at that time was for breaching a minefield, chemical neutralization, which did not involve detonation of the landmines, was deemed too slow. Because time restriction is not a factor in demining operations, and detonation is generally not desired, chemical neutralization technologies are most appropriate for demining operations. At this time, approach (2) is under development and the following three categories of chemical reagents demonstrated to be hypergolic with TNT are described.

(1) The low molecular weight metal alkyls are spontaneously flammable in air, combusting to CO_2, H_2O, and the metal oxide. They have been used effectively even when dissolved in a hydrocarbon dilutant to preclude their pyrophoric characteristics with respect to air, yet retaining their effectiveness in the hypergolic initiation of autocatalytic decomposition of TNT upon contact.

(2) The organic amines are generally strong bases with varying volatilities and usually an objectionable smell. They can be dissolved in a suitable solvent for application to explosive neutralization; neither the amines nor their products with explosives will persist at the reaction site for any extended period of time and will degrade so as to pose little environmental concern.

(3) The interhalogens, dependent upon type, are effective in reacting with explosives, but in different and not entirely known mechanisms, which in most cases lead to detonation, induced by either chemical and/or associated thermal exothermic energies. From an environmental point-of-view, the interhalogens will not persist in the atmosphere and will degrade rapidly with moisture and disperse readily.

PREVIOUS RESULTS

Figure 1 illustrates a device used in the early IITRI work to assess the induction times of candidate hypergolic reagents with TNT. It should be noted that the term hypergolic reaction implies a flame response not associated with combustion in air. These experiments were conducted under an atmosphere of dry argon. The objective was to obtain the induction times from contact of the TNT sample (powder) with a drop of hypergolic reagent, as a function of temperature (temperatures from 75°C to as low as -30°C were investigated). Results with both pyrrolidine and diethylzinc are illustrated in Figure 2. In the case of the pyrrolidine, the induction times were in the range of seconds down to 0°C, but hypergolic reaction failed at -30°C. Extrapolation of the Arrhenius plot to this low temperature would indicate an induction time in the range of several minutes; this instrumentation was not capable of evaluating very long induction times because of the sample size and non-adiabatic conditions at long times. In the case of the diethylzinc, induction times were in the range of milliseconds at ambient temperatures, and hypergolic reaction was maintained down to -30°C, the latter requiring induction times of about 10 seconds. In this previous work hypergolic reactions between the interhalogens and TNT were not observed, although in the case of bromine trifluoride an exothermic reaction did occur but did not induce a flame response.

CURRENT LABORATORY INVESTIGATION

This current investigation also involved the metal alkyls, aliphatic amines, and interhalogens, as well as Comp B and pure RDX in addition to TNT, with emphasis on field-test demonstrations of chemical neutralization of landmines. Preliminary laboratory screening experiments were sufficient to identify and/or corroborate candidate hypergol reagents at ambient temperatures. However, because of the potential failure of hypergolic chemical neutralization at low temperatures, considerable laboratory experiments were conducted to evaluate the hypergolicity of some amines and metal alkyls at low temperatures with respect to all three types of explosives. The major emphasis was on diethylzinc, which proved to be very effective even at -30°C in the earlier work. For practical considerations 0°C was selected as the test temperature for these experiments.
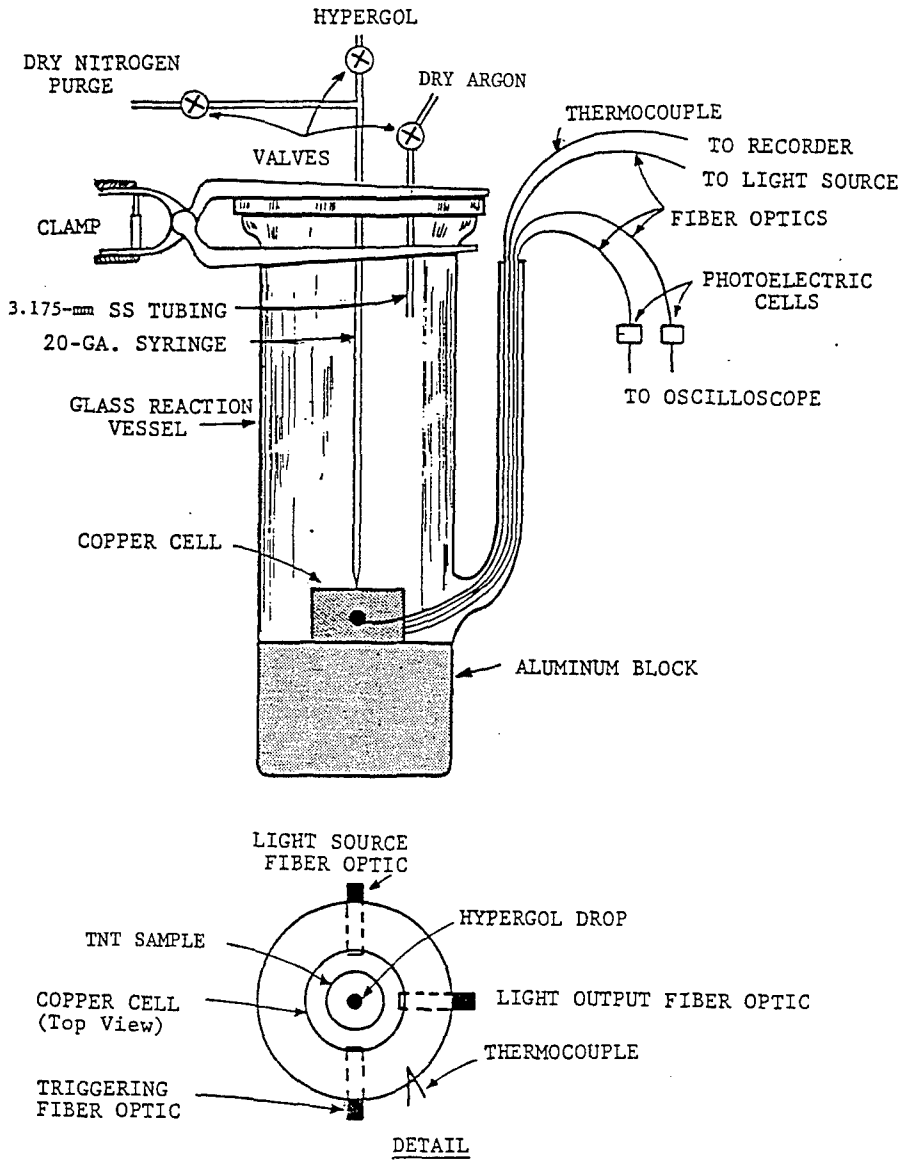
Figure 1. Inert-Atmosphere Apparatus for Evaluating the Hypergolic Ignition of TNT with Hypergolic Reagents as a Function of Temperature.
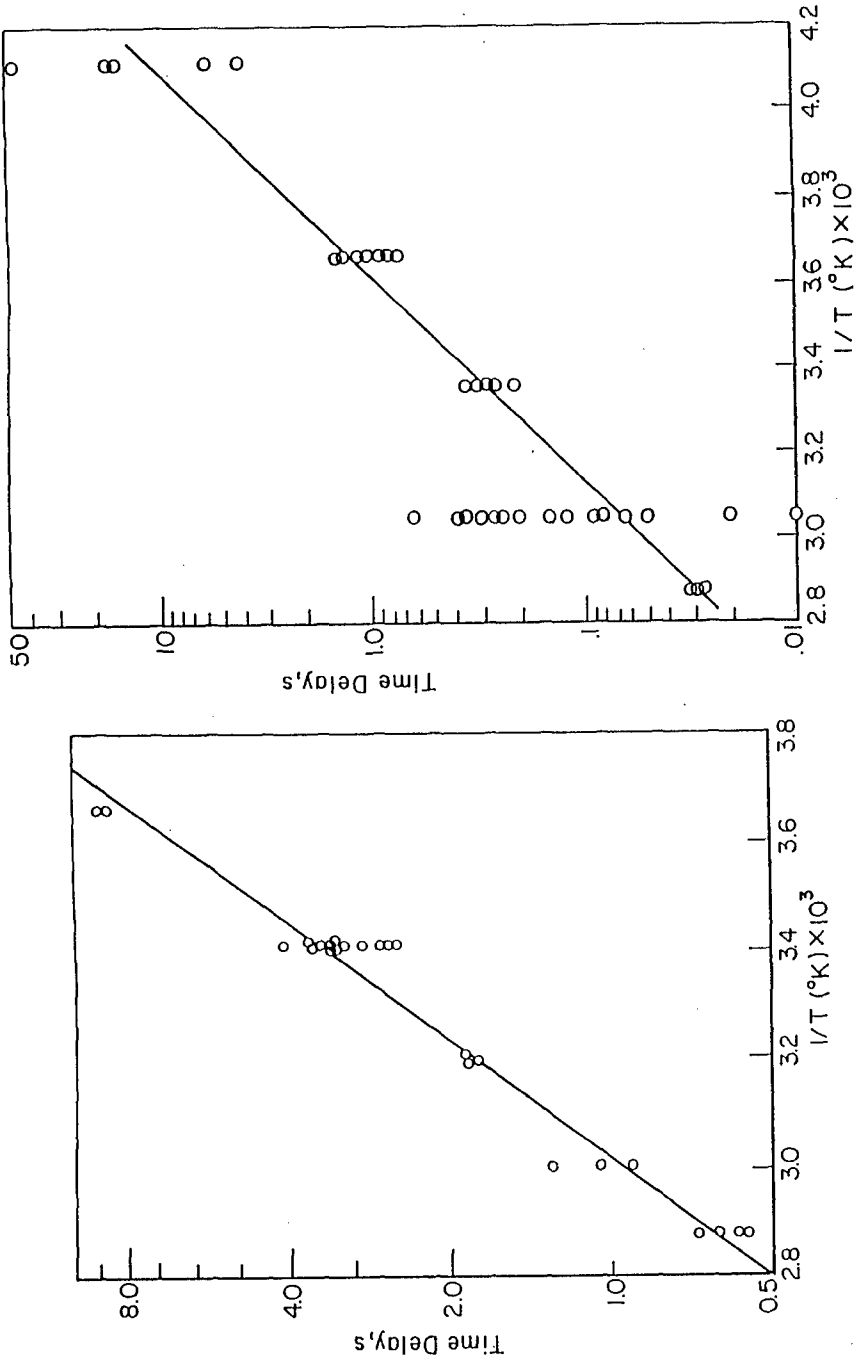
Figure 2.   Ignition Delay as a Function of Temperature for TNT-Pyrrolidine (left) and TNT-Diethylzinc (right).

Figure 3 illustrates the simple trident-shaped Pyrex reactor used for conducting 0°C experiments in the absence of oxygen. A small quantity, i.e., 0.2-0.25 g of subject explosive, was placed into the detachable lower limb of the reactor, which was then evacuated to approximately 10^{-6} mm Hg. Zero grade nitrogen was then admitted to slightly-above-atmospheric pressure at which time the ball valve on the reactor exit limb was opened and a continuous flow of nitrogen was established for the remainder of the experiment. After about 10 minutes of this zero nitrogen purging, a syringe was used to introduce about 0.25-0.5 mL of metal alkyl into the upper limb of the trident-shaped reactor below the ball valve. The reactor was then immersed in an ice bath so that both the explosive and the metal alkyl were cooled to 0°C. When the requisite temperature was achieved, the reactor was tilted to transfer the metal alkyl onto the explosive sample. When no reaction occurred, the ice bath was removed and the temperature allowed to warm to ambient with continuous monitoring of the temperature.

In these experiments the form of the explosive was as follows: the TNT was in the form of flakes, the Comp B as irregular shaped millimeter-sized particles, and the RDX was a moderately-coarse grade powder of about 450 μm. The results of these experiments were at variance with those of the previous work at 0°C in that hypergolic reactions were not obtained. It is surmised that due to the intensive evacuation in these latter experiments, surface-adsorbed water and oxygen were removed, which may have been influential in initiating hypergolic reaction at low temperatures in the earlier work. Interestingly, at near-ambient temperatures TNT and RDX reacted, respectively, with diethylzinc and triethylaluminum in an extremely exothermic reaction indicative of instant hypergolic reaction between the explosive and the respective metal alkyl.

RESULTS AGAINST LANDMINES

Field-test experiments were conducted using two candidate dynamic delivery systems against both surrogate and actual landmines. Results are discussed here only briefly; comprehensive descriptions and discussions of these tests will be presented in a future publication. Both surrogate and real AP landmines were tested. The surrogate landmines were fabricated using wood, plastic, and metal casings, with the amount of explosive fill ranging between
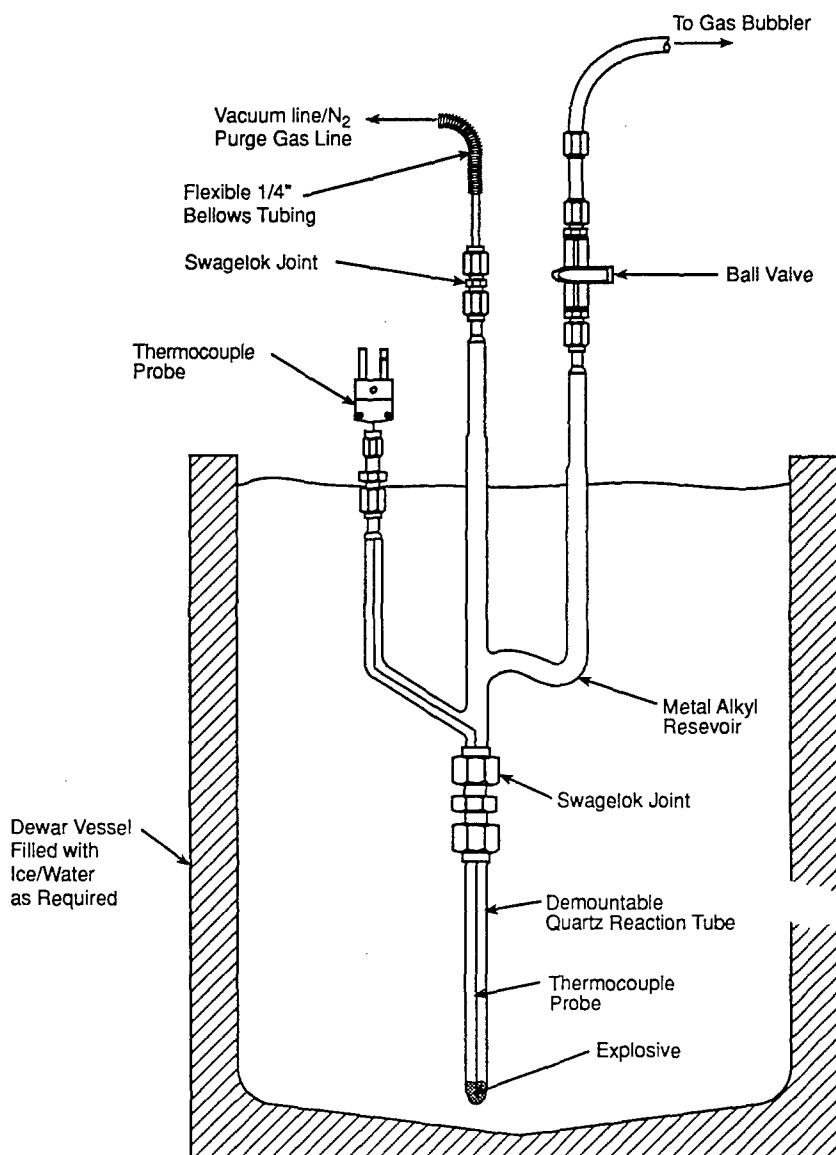
Figure 3. Simple Quartz Reactor System Used to Investigate Temperature Dependence of Explosive Reactivity with Metal Alkyls at Ambient and Ice Temperatures.

170 and 700 g, depending on the type of AP landmine being simulated. In the case of both the surrogate and the actual landmine tests, the mines were surface-emplaced; however, with the actual landmines both fuzed and unfuzed mines were tested.

Preliminary experiments were conducted utilizing several improvised dynamic delivery systems, one of which is schematically illustrated in Figure 4, depicting the sequence of events. The objective was to provide a system wherein the hypergolic candidate would be introduced into the landmine simultaneously with the penetration of the landmine casing to allow intimate contact with the hypergolic candidate reagent and the explosive. With this system, about 60 mL of amine hypergolic reagent was used, which was known to be more than ample, but the amount of the amine that actually penetrated into the mine was considerably less. In the case of the interhalogens and the metal alkyls, 3 to 10 mL amounts were used very effectively. Several of both the amine and metal alkyl hypergol reagents used were effective against all three explosives; however, in the case of RDX, bromine trifluoride caused detonation in many instances with the surrogate mines. Sufficient definitive experiments were not conducted to establish the criteria that led to detonation.

In the case of TNT and Comp B, both cast explosives, an additional benefit was derived in that the dynamic penetration of the landmine also caused fragmentation/pulverization of the explosive, which is believed to play an important role in achieving spontaneous, nearly instantaneous autocatalytic decomposition of these explosives. In the case of the surrogate plastic-cased RDX-fill landmines, in which the RDX was in the form of a compressed powder, a number of metal alkyls were found effective in causing deflagrative-type decomposition. Regarding the interhalogens, results were mixed and evidently depended on factors other than simple chemical reaction; e.g., purity of the RDX. Hence, although bromine trifluoride was effective in chemical neutralization of the surrogate pure RDX-fill landmines (causing detonation generally), it was not effective for achieving chemical neutralization of actual RDX-type landmines, in which the RDX includes a binder.

These preliminary experiments demonstrated that all three types of explosive-filled landmines could be potentially chemically neutralized with one or more
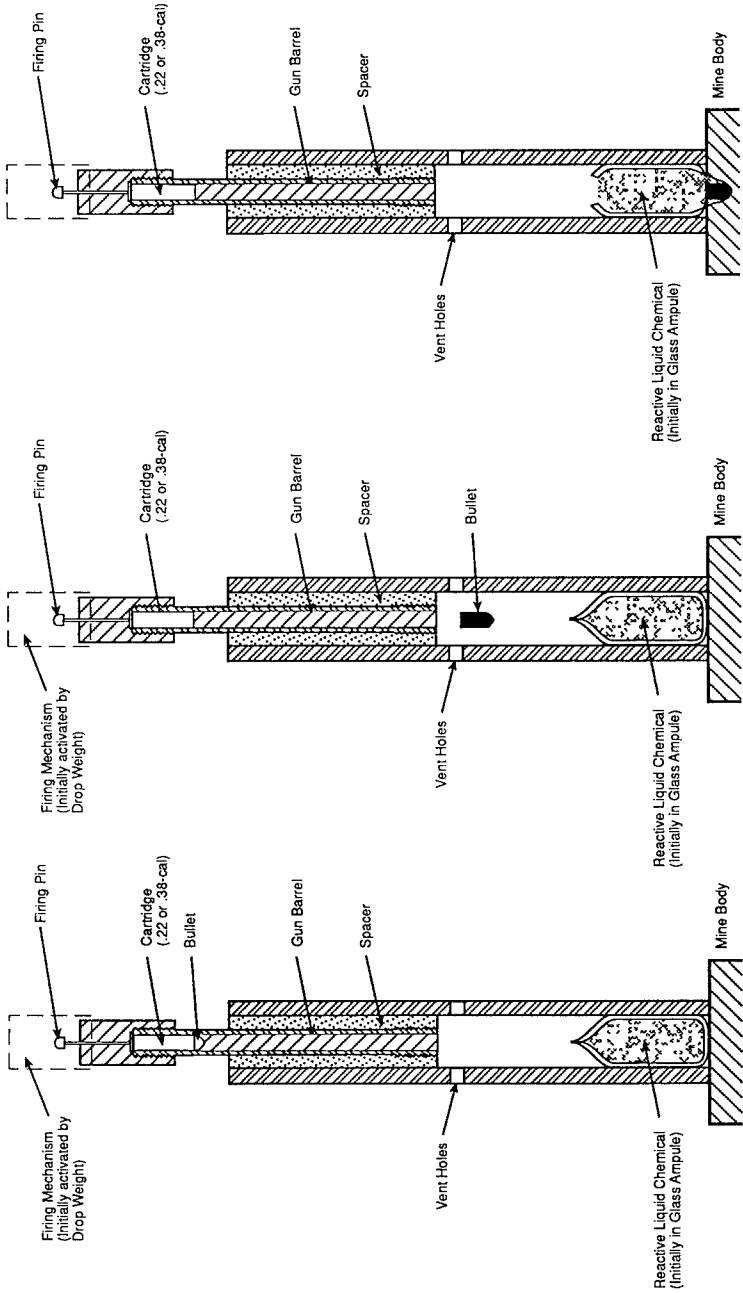
Figure 4. Schematic Representation of the Sequence of Events in the Use of the Gun Barrel Assembly.

hypergolic amine, metal alkyl, and interhalogen reagents. However, under variable dynamic delivery techniques, often one type of hypergolic reagent was found to be more effective than another against one type of explosive or another, with sometimes the reverse being the case against another explosive; the same was true regarding the dynamic delivery systems. In general, this initial investigation demonstrated that ethylenediamine, diethylenetriamine, and pyrrolidine were effective against TNT and Comp B; diethylzinc, triethylaluminum, and diethylaluminum chloride against all three explosives; and bromine trifluoride and chlorine trifluoride against all three, but not to the same extent, as observed in both the laboratory and field-test experiments.

Figure 5 illustrates an alternative delivery system, wherein the hypergolic reagent was an integral component of the bullet; i.e., the bullet was in fact a neutralization chemical-filled "capsule" that would simultaneously penetrate the mine casing (as well as overburden in the case of buried mines or underwater applications) and rupture in such fashion that the hypergolic reagent would be discharged into the penetrated mine and explosive fill. This system has a much greater viability, including firing from a distance, but is subject to much greater design criteria. Nevertheless, this delivery system was tested successfully against both surrogate and real landmines, with about 4 mL of diethylzinc diluted with 20 percent toluene (to mitigate its pyrophoricity).

Both delivery systems were tested against actual landmines, both fuzed and unfuzed, with excellent results leading to complete, non-detonative autocatalytic decomposition in a matter of minutes. At present no direct effort has been made to optimize any particular system or to select/quantify candidate hypergolic reagents for the multitude of landmines, explosive, and field conditions encountered in the real world. Further work is presently continuing.

ACKNOWLEDGMENT
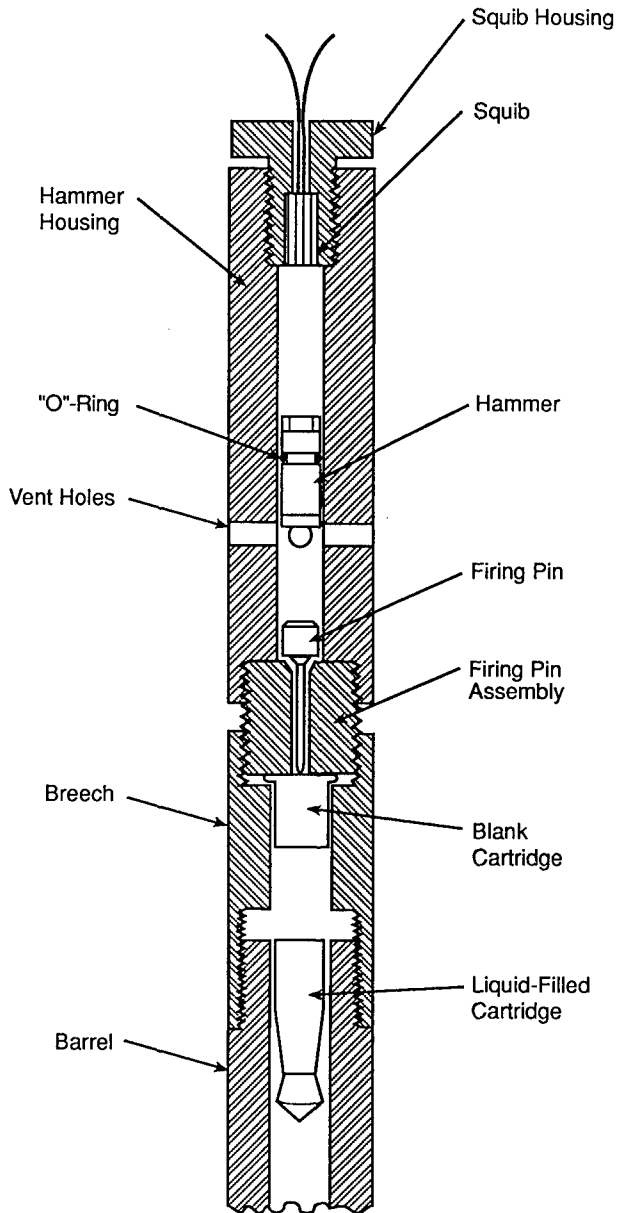
Figure 5. Chemical Neutralization System for the Hypergol-Filled Cartridge Case Projectile "Bullet" for Initiation of Autocatalytic Decomposition of Landmine Explosives.

REFERENCES

1. *The Global Landmine Crisis*, prepared by the Office of International Security and Peacekeeping Operation, Department of State Publication 10225, December 1994.

2. A.J. Tulis, R.J. Dihu, J.L. Austing, A. Snelson, D.C. Heberlein, and H. Egghart, *Oxidizer Enhancement of Detonation in Fuel-Rich Explosives,* Proc. EUROPYRO93, Strasbourg, France, June 6-11, 1993.

3. A.J. Tulis and C.K. Hersh, *Decoupling of Physical and Chemical Mechanisms in Explosive Reactions*, Astronautica Acta, 17(4-5), pp. 435-444, 1973.

4. J.N. Keith, A.J. Tulis, W.K. Sumida, and D.C. Heberlein, D.C., *Chemical Neutralization of Explosives*, Proc. Eighth Symp. on Explosives and Pyrotechnics, pp. 35.1-35.6, Los Angeles, Cal., Feb. 5-7, 1974.

5. A.J. Tulis, J.N. Keith, W.K. Sumida, and D.C. Heberlein, *Application of the Unreacted Core Model to the Chemical Neutralization of TNT in Solvent/Amine Systems*, Sixth (Int) Congress of Chemical Engineering, Caracas, Venezuela, July 13-16, 1975.

6. A.J. Tulis, J.N. Keith, W.K. Sumida, and D.C. Heberlein, *Non-Explosive Destruction of TNT with Hypergols*, Proc. Fourth (Int) Pyrotechnics Seminar, pp. 17.1-17.32, Steamboat Springs, Col., July 1974. Also available NTIS AD A057599.

7. T.C. Beverage, D.C. Heberlein, A.J. Tulis, J.N. Keith, and W.K. Sumida, *Chemical Neutralization of Land Mines*, Proceedings Fifth (Int) Pyrotechnics Seminar, pp. 21-38, Vail, Col., July 12-16, 1976. Also available NTIS AD A087513.

8. A.J. Tulis, T.J. Labus, W.K. Sumida, J.N. Keith, T.C. Beverage, and D.C. Heberlein, *Hypergolic Fluid-Jet Destruction of land Mines*, Proc. Ninth Symp on Explosives and Pyrotechnics, pp. 29.1-29.12, Philadelphia, Penn., Sept. 15-16, 1976.

Initiation Criteria of High Explosives, Attacked with Projectiles of Different Densities

Initiiergesetz von Sprengladungen bei Beschuß mit Projektilen von unterschiedlichen Dichten

Manfred Held

TDW, 86523 Schrobenhausen, Germany

Kurzfassung

Die eindimensionale Initiiergrenze für Sprengladungen wird ohne Zweifel gut mit dem p^2t-Kriterium (Walker/Wasley-Kriterium) beschrieben, wobei p der eingeleitete Stoßwellendruck und t die Einwirkdauer sind. Bei zweidimensionaler Belastung bzw. kleinen Flächenbelastungen gilt für die Initiierung von Sprengladungen das v^2d-Kriterium (Held-Kriterium) mit v als Auftreffgeschwindigkeit und d als Durchmesser des Projektiles/Stachels. Die Frage nach dem Einfluß der Dichte des Projektiles bzw. Hohlladungsstachels auf die Sprengladungsinitiierung wurden von verschiedenen Stellen unterschiedlich angegeben. Mader gab ein $\rho_p \cdot v^2d$ vor. Chick und Hatt gaben aufgrund von Experimenten ein $\sqrt{\rho_p} \cdot v^2d$ an, während Held ein u^2d vorgab, was dem Staudruck am Kratergrund entspricht. u ist dabei die Kratergrundgeschwindigkeit in der Sprengladung. Bei hydrodynamischem Eindringen ist dies gleichbedeutend mit $v^2d/(1 + \sqrt{\rho_{HE}/\rho_p})^2$ mit ρ_{HE} bzw. ρ_p den Sprengladungs- bzw. Projektil- oder Stacheldichten.

In Experimenten mit sowohl sehr leichten Projektilen, wie Lexankugeln mit der Dichte 1,2 g/cm^3, als auch Wolframkugeln mit der Dichte von 17,77 g/cm^3 wurde das u^2d-Kriterium nach Held experimentell eindeutig bestätigt.

Im Vortrag werden bei unterschiedlichen Dichten des Projektils oder des Stachels neben der allgemeinen Einleitung der verschiedenen Initiierkriterien und des experimentellen Nachweises für das u^2d-Kriterium die Folgen für die optimale Projektil- bzw. Stachelauslegung bei unterschiedlichen Abdeckungen bzw. Vorschaltungen aufgezeigt.

Abstract

The one-dimensional initiation threshold for high explosives is very well described with the p^2t-criterium by Walker/Wasley, where p is the introduced shock pressure and t the duration of the shock. At two-dimensional load, respectively small loaded areas the initiation of high explosive can be described with the v^2d-criterium by Held, where v is the impact velocity and d the diameter of the projectile or shaped charge jet. The question arises what will be the influence of the density of the projectile or the shaped charge jet on the threshold velocity. Mader used a linear function $\rho_p \cdot v^2 d$. Chick and Hatt fitted experimental results with $\sqrt{\rho_p} \cdot v^2 d$, while Held defined u^2d which corresponds to the stagnation pressure at the crater bottom, where u is the cratering velocity in the high explosive charge. If the penetration is hydrodynamical u^2d is equal to $v^2d/(1 + \sqrt{\rho_{HE}/\rho_p})^2$ where ρ_{HE} resp. ρ_p are the densities of the high explosive charge resp. projectile or jet.

In experiments with low density projectiles, as Lexan spheres with a density of 1,2 g/cm^3 and high density tungsten spheres with 17,7 g/cm^3 the u^2d criterium of Held was fully confirmed.

This paper will describe the optimum projectile or jet lay out with resp. to densities, areal mass and fixed mass for initiation of high explosive charges under different covers, beside the introduction in the different initiation criteria.

Introduction

The initiation criterea of high explosive charges with projectiles or shaped charge jets can be very well described with the v^2d-criterion which was the first time described for shaped charge jets by the author in 1968 <1>. A summary of results which confirm this criterion for a large number of high explosive charges and load conditions - shaped charge jets, projectiles, flying foils with a L/D larger than 0.2 and numerical calculations - are published in <2>. All these tests have been generally done with copper jets and with steel fragments, therefore with similar densities.

The question arises how this formula has to be modified if the density of the projectile is strongly changed. Mader has used in his numerical calculations a $\rho v^2 d$-criterium where ρ is the projectile density (<3> and <4>). Chick et al. <5> have given a relation of $\sqrt{\rho} \cdot v^2 d$ from experimental results with copper and aluminium jets. The author has considered in <6> as a rough rule the stagnation pressure for the initiation of high explosive charges and has used a u^2d criterion where u is the cratering velocity in the high explosive charge.

Recently test results of the initiation of Composition B by tungsten spheres of different diameters and plastic spheres with 76 mm diameter were published <7>. These initiation tests have used a

magnitude of different projectile densities from tungsten with 17.77 g/cm^3 to the plastic - Lexan - with the density of 1.2 g/cm^3. With these results it can be very well proved the influence of the density ρ of the projectiles on the initiation criteria of high explosives. The reaction behaviour was also modelled in detail in <7> by numerical calculation with the ignition and growth model.

Defining the threshold constant

Fig. 1, a direct copy of Fig. 4.07 of Reference <7>, shows the results of the initiation tests with cast Composition B of 1.63 g/cm^3 density with tungsten balls of 9, 14, 18 and 25 mm diameter and the density of 17.77 g/cm^3, resp. with the Lexan sphere of 76 mm diameter and a density of 1.2 g/cm^3. The tests were conducted by the Naval Research Laboratory (NRL) and are described in Reference <7> in detail.
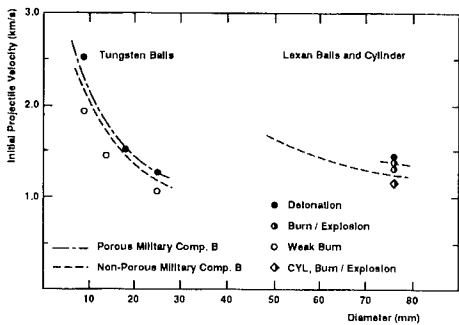
Fig. 1 Experimental detonation threshold velocities and calculated data <7>

Calculations have been made with this type of Comp. B with a density of 1.63 g/cm^3 (porous Military Comp. B) and a pressed material with higher density (1.712 g/cm^3) which is called "Non-Porous Military Comp. B". According to the standards Comp. B should be cast, never pressed. But in experiments not so well educated theoretical people often give "new definitions".

All the experimental results with the large variety of diameters, ranging from 9 mm to 76 mm, and densities, ranging from 1.2 g/cm^3 to 17.77 g/cm^3 can be very well described by the Held-equation <6>

$$I_{Cr} = u^2 d = 23 \text{ mm}^3/\mu s^2 \tag{1}$$

The cratering velocity is given by the Bernoulli-equation <8> to

$$u = v/(1 + \sqrt{\rho_t/\rho_p}). \tag{2}$$

This gives

$$I_{Cr} = u^2 d = \frac{v_{Cr}^2}{(1 + \sqrt{\rho_t/\rho_p})^2} \, d \tag{3}$$

The projectile velocity v_{Cr} can now be calculated if the above equation is solved to v_{Cr}

$$v_{Cr} = \sqrt{I_{Cr}/d} \cdot (1 + \sqrt{\rho_t/\rho_p}) \tag{4}$$

For the tungsten spheres with the density 17.77 g/cm^3, resp. Lexan spheres with the density 1.20 g/cm^3 and the "target" density = HE density of 1.70 g/cm^3 one get the following equations for the critical velocities with respect to the diameter d

$$v_W = 1,309 \cdot \sqrt{23/d} = 6.28/\sqrt{d} \quad \text{resp.} \tag{5}$$

$$v_{Le} = 2,190 \cdot \sqrt{23/d} = 10.50/\sqrt{d} \tag{6}$$

With the initiation threshold value of 23 $mm^3/\mu s^2$ all the experiments in <7> can be very well fitted resp. predicted (Fig. 2).
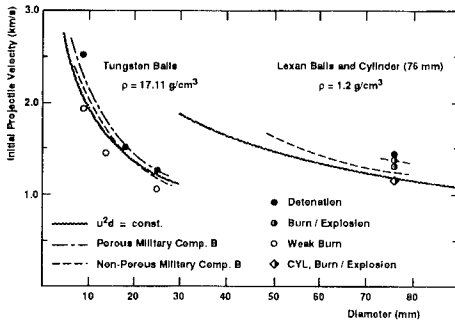
The numerically calculated detonation threshold velocities (dashed lines) for the tungsten balls are also very well represented. There is maybe a small difference in the trend for the smaller diameters between the theoretical prediction to the u^2d criterion for the Lexan balls, but this is marginal.

Fig. 2. Comparison of values with $u^2d = 23$ $mm^3/\mu s^2$ with the detonation threshold velocities of Fig. 1

By using 23 $mm^3/\mu s^2$ as the threshold value for a copper projectile or jet one get the equation

$$v_{Cu} = 1,437 \cdot \sqrt{23/d} = 6.89/\sqrt{d} \tag{7}$$

By comparing the constants for the critical velocities of tungsten and copper projectiles, resp. jets it is very remarkable, that they are nearly equal. The value of tungsten with 6.28 is only 10 % smaller than copper with 6.89.

If we use this equation in the v^2d-diagram of Reference <2> we get the stronger marked line in the log-log-diagram (Fig. 3). This confirms fully the Comp. B data of Chick & Hatt <5> where the high explosive charge was covered. All the tests under <7> are made under covered conditions.
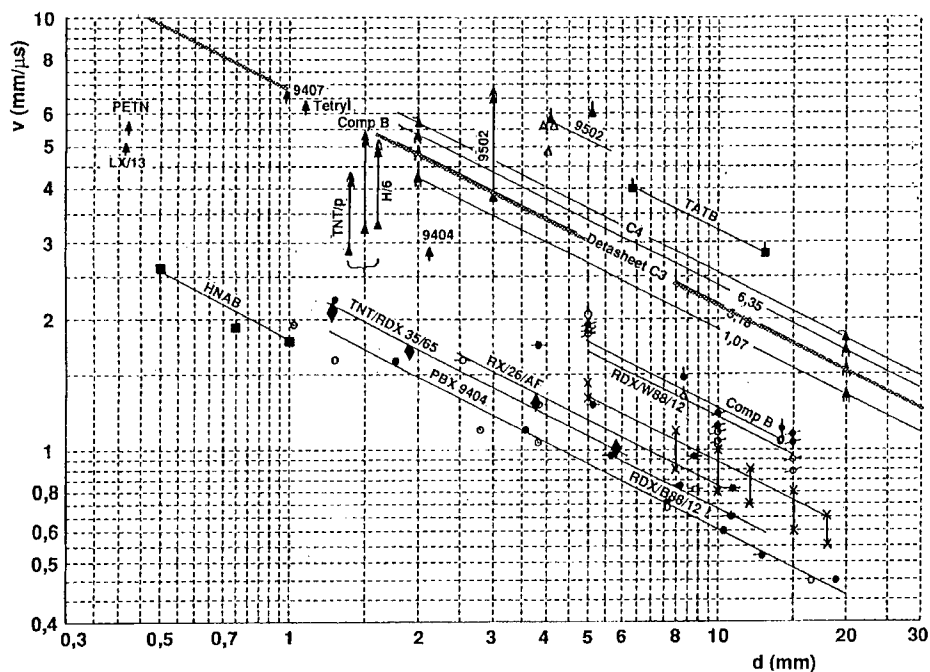
Fig. 3. $u^2d = 23$ mm^3/us resp. $v_{cu} = 6.85/\sqrt{d}$ for a copper projectile or jet for covered composition B

Obviously the equations of Chick et all. $<5>$ or Mader ($<3>$ and $<4>$) give strongly different constants of the initiation threshold values for the investigated two projectile materials. The following table shows clearly that constant values are only given by the u^2d-criterion and not by the square root $\sqrt{\rho} \cdot v^2 d$ from Chick et all. $<5>$ and the least by $\rho \cdot v^2 \cdot d$ from Mader ($<3>$ and $<4>$). With this analytical equation the influence of the densities of projectiles or shaped charge jets can be analysed with regard to the threshold velocity under different conditions, as

- constant diameter
- constant projectile mass
- constant areal mass.

This topic will be highlighted in the next chapters.

Table

Projectiles				Initiation Criteria $u^2 \cdot d = \dfrac{v^2}{(1 + \sqrt{\rho_t / \rho_p})^2} \cdot d$	$\sqrt{\rho} \cdot v^2 \cdot d$	$\rho \cdot v^2 \cdot d$
				Held (1987)	Chick (1986)	Mader (1983 / 1986)
Material	ρ (g/cm³)	d (mm)	v (km/s)	mm³ / μs²	$\sqrt{\text{g/cm}^3} \cdot$ mm³/μs²	(g/cm³) · mm³/μs²
Lexan	1,20	76	1,19	23	118	129
Tungsten	17,77	25	1,25	23	165	694

Constant projectile or jet diameter

Using this simple analytical equation (4) the trends for uncovered or slightly covered high explosive charges can be investigated with the threshold velocities as a function of projectile or jet density with the projectile resp. jet diameter as parameter (Fig. 4).

$$v_P = (1 + \sqrt{1.7/\rho_P}) \cdot \sqrt{23/d} \qquad (4.1)$$

For this a high explosive charge density of 1.7 g/cm³ and an initiation criterium $u^2 d = 23$ mm³/μs² are used. Surprisingly the threshold value is not really changing dramatically with the densities also if they are changing for more than one magnitude. Using copper as a standard material for shaped charge jets the velocity for aluminum jet by the "same diameter" has only to increase for 25 % and for a tungsten jet with the same diameter the velocity is reduced only for 10 % (Fig. 5). This is definitely a little surprising and not a really expected result.
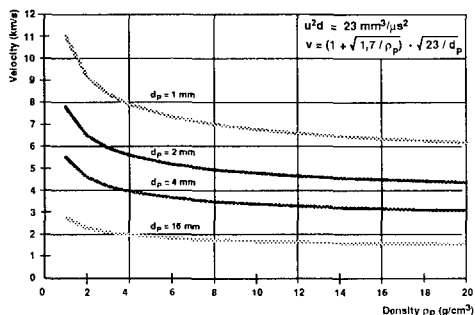
Fig. 4

Threshold initiation velocities as a
function of density with the projectile
resp. jet diameter as parameter
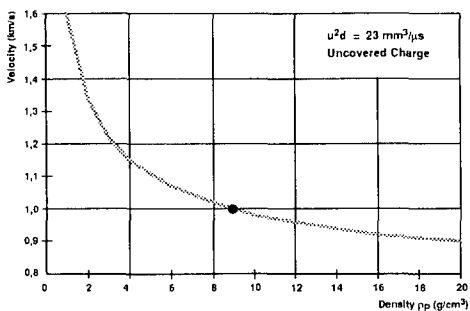
Fig. 5

Change of threshold initiation velocity
as a function of density with copper as
a reference value

Constant fragment mass

As an example it should be calculated the threshold velocity of a projectile with a constant mass
of m = 7 g and a constant length to diameter ratio of one (L/D = 1).

The threshold value for this condition can be calculated by the following equation

$$v_p = (1 + \sqrt{1.7/\rho_p}) \cdot \sqrt{23} \cdot \sqrt{10 \cdot (4 \ m/\rho_p \cdot \pi)}^{1/3} \qquad (8)$$

which includes a HE-density of 1.7 g/cm^3, threshold initiation value of 23 $mm^3/\mu s^2$, the
fragment mass m and the projectile density ρ_p as a variant. The change in velocity is nearly
negligible if the projectile density varies for one magnitude. The increasing diameter is just
compensating the loss in cratering velocity resp. pressure with the lower density projectiles
(Fig. 6).

This result is only true for uncovered or slightly covered high explosive charges. If the fragment
has first to perforate as an example a 10 mm armour steel plate before it starts to penetrate the
high explosive charge, a reduction of the velocity must be taken into account. For the reduction
of velocity the Thor-equations <9> were used. Behind the coverplate the total projectile mass
was taken into account. The reason for this is, that the explosive charge is in direct contact to the
coverplate and all the fragments are not dispersing from the original trajectory at zero distance.
The threshold values are now much more drastically changing from much higher values at low
densities to lower values at high densities (Fig. 7). The reason for this behavior is that heavy

metal fragments are able to perforate coverplates with much higher residual velocities compared to materials with lower densities then also the diameter or punched out target material volume is reduced. The values for uncovered high explosive charges are also given for comparison in Fig. 7.
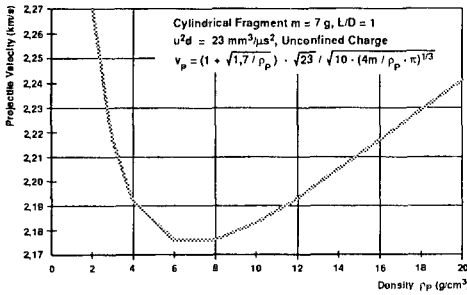
Fig. 6

Threshold value is nearly constant if a fragment of constant mass with L/D = 1 is applied
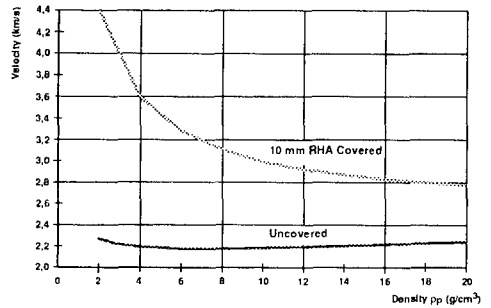
Fig. 7

Initiation threshold velocities as a function of density for constant fragment masses against uncovered or 10 mm RHA covered high explosive charge

Constant areal mass

In the case of shaped charge jets the question is not arising what will be the initiation threshold velocities with constant masses of the total jet. Here arises the question what will be the threshold velocities with constant masses across the jet area, called constant areal masses.

As discussed above the projectile has generally to perforate first shielding and cover plates. The question was also what will be the necessary jet velocity if the jet has first to perforate different barrier thicknesses.

As an example, a copper jet with a density of 8.9 g/cm^3 with 2 mm diameter and a threshold value of 23 mm^3/μs^2 and a high explosive density of 1.7 g/cm^3 were used as reference.

This gives the equation

$$v_j = (1 + \sqrt{1{,}7/\rho_x}) \cdot \sqrt{23}/(8{,}9 \cdot 2^2/\rho_p)^{1/4} \tag{9}$$

This equation gives the threshold velocity as a function of jet density with zero barrier thickness. It is surprising that the threshold velocity starts at 4.8 mm/μs for a water jet (density 1,0 g/cm^3) and 5,3 mm/μs for a tungsten jet (density 18 g/cm^3) with the same area densities A$\cdot\rho_p$ (Fig. 8).

The residual jet velocity was calculated with the following equation (equ. 22 of <8>).
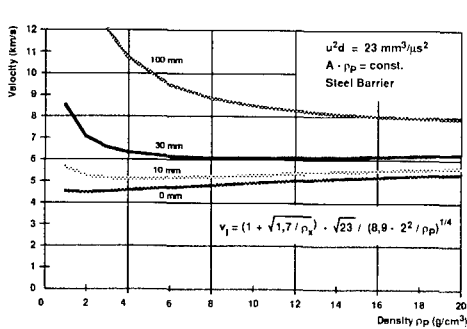
$$v_j = v_{jo} \cdot (\frac{Z_o}{Z_o + P}) \qquad (10)$$

A jet with higher density is less consumed by perforating a 10 mm or thicker barrier and therefore the trend of threshold initiation velocity first is decreasing with increasing density and then changing to increase for a constant areal mass.

Fig. 8
Initiation threshold velocity for constant areal masses A$\cdot\rho_j$ of a jet as a function of density with different steel barriers as parameter

Conclusion

The experimental as well as numerical results of the initiation treshold values of tungsten spheres with different diameters and plastic spheres - Lexan - with extremely different densities can be very well described with the Held-criterion u^{2}d where u is the cratering velocity and d the diameter of the projectile. The test results for Comp. B gives 23 mm^3/us^2 and this value is in full agreement with shaped charge jet results, obtained with covered charges.

With this analytical equation very useful trend analysis for projectiles or shaped charge jets can be made with different densities. Generally speaking, the densities of projectiles or shaped charge jets for initiation have remarkably little influence on uncovered high explosive charges. The perforation capabilities of heavy metal fragments resp. shaped charge jets with heavy metal liners are more favorable against covered charges.

References

<1> M. Held, "Initiierung von Sprengstoffen, ein vielschichtiges Problem der Detonationsphysik" Explosivstoffe, 5 2-17, 1968

<2> M. Held, "Initiation Phenomena with Shaped Charge Jets", 9th Int. Symposium on Detonation, Vol. II 1416-1426, 1989

<3> C. L. Mader and G. H. Pimbley, "Jet Initiation and Penetration of Explosives", Journal of Energetic Materials 1, 3-44, 1983

<4> C. L. Mader, "Recent Advances in Numerical Modelling of Detonations", Propellants, Explosives, Pyrotechniques, 11, 163-166, 1986

<5> M. C. Chick, T. Bussell, R. B. Frey and G. Boyce, "Initiation of Munitions by Shaped Charge Jets", 9th Int. Symposium on Ballistics, 421-430, 1986

<6> M. Held, "Discussion of the Experimental Findings from the Initiation of Covered but Unconfined High Explosive Charges with Shaped Charge Jets", Propellants, Explosives, Pyrotechniques 12, 167-174, 1987

<7> M. J. Murphy, E. L. Lee, A. M. Weston and A. E. Williams, "Composition B Shock Initiation Report (U), UCRL-ID-118300, 1994

<8> M. Held, "Hydrodynamic Theory of Shaped Charge Jet Penetration" Journal of Explosive and Propellants - R.O.C. - Taiwan, 7, 9-24, 1991

<9> Handbuch der Munitionsbewertung BWB WM VI 2, 203-314-0325200, 1979

BEHAVIOUR OF ALUMINIUM AND TNT IN THE DETONATION WAVE OF AMMONIUM NITRATE EXPLOSIVES

Andrzej Maranda, Stanisław Cudziło, Waldemar Trzciński, and Jerzy Nowaczewski

Military University of Technology

Kaliskiego 2, 00-908 Warsaw, POLAND

Abstract

Detonation of ammonium nitrate explosives containing powdered aluminium or TNT was investigated. Content and grain size of the additives were changed during experiments. For particular explosives, an extrapolated detonation velocity to infinite diameter was determined and the process of driving a copper tube by the detonation products was recorded using X-ray photography. Detonation velocity was estimated theoretically assuming an equilibrium state in the detonation products. Numerical analysis of the problem of driving a copper cylinder by the products of detonation was also performed. Correlation between experimental and calculated results was established. The results obtained enable us to draw inferences concerning chemical reaction rates in the detonation wave and in the rarefaction wave. An effective isentropic exponent for the detonation product of the non-ideal explosive tested is also determined from the cylinder test data.

1. Introduction

A chemical reaction is a basal process which contributes to propagation of a detonation wave in explosive. In the case of monomolecular explosives this reaction proceeds inside a single molecule. However, in non-ideal explosive mixtures, particularly in oxidizer-fuel compositions, the chemical reactions occur between atoms from different molecules. Thus, the diffusion process besides the reaction kinetics plays an important role in the chemical reaction and it influences the reaction rate. This means that the reaction rate depends implicitly upon reactivity of explosive components and physical structure of the mixture. Both above factors decide if particular components of the explosive mixture take part or not in chemical reactions proceeding inside the reaction zone of the detonation wave and in a rarefaction wave. Although the initiation and propagation of the detonation wave in non-ideal explosives have been explored by many authors [1-9] the problem of intermolecular reactions in the detonation wave has not been fully explained yet.

In this paper, the detonation behaviour of components in ammonium nitrate explosives with TNT and aluminium is investigated. The dependence of the detonation velocity on the charge diameter is studied. An extrapolated detonation velocity to infinite diameter is established and it is compared with that obtained from thermochemical calculations. X-ray recording of a process of driving a copper tube by the detonation products is also performed for the explosive tested. Comparison of X-ray records

with the results of numerical modelling of this process enables us to find an effective exponent of an isentrope for the detonation products.

2. Experimental

2.1. Detonation velocity

Detonation velocities of explosive mixtures containing ammonium nitrate (AN), TNT, and aluminium (Al) were measured. To prepare the AN/TNT or the AN/TNT/Al mixtures crystalline AN (size of grains less than 0.8 mm), fine-grained TNT (size below 0.8 mm), coarse TNT (1.2-2.5 mm size), flaked aluminium (11000 cm^2/g specific surface, size of grains less than 0.16 mm), and aluminium powder (size of grains less than 0.3 mm) were used. Table 1 contains data for composition of the explosive tested and their symbols used in further part of the paper.

Table 1. Composition of the explosive tested

Explosive ρ_0 =1050 kg/m^3	AN wt%	Fine TNT wt%	Coarse TNT wt%	Flaked Al wt%	Powdered Al wt%
AN/TNT-1	80	20	-	-	-
AN/TNT-2	80	-	20	-	-
AN/TNT/Al-1	80	10	-	10	-
AN/TNT/Al-2	80	10	-	-	10

Explosive were confined in polyvinyl chloride tubes with inner diameter of 36, 45, 80, or 100 mm. Wall thickness of the tubes was 5% of inner diameter and their length was 500 mm. The mean density of the charges prepared was approximately the same 1050 kg/m^3. Detonation was initiated by using 100 g charge of plastic explosive. The detonation velocity was measured by short-circuit sensors located in second part of the charge. The mean velocity was obtained from three measurement courses of about 80 mm length.

2.2. Cylinder test

The explosive mixtures tested were placed in copper tubes (25 mm inside diameter, 250 mm length) having 1.5 mm thick walls. The diagram of the set-up is shown in Fig. 1.

The registration of the copper tube driven by the detonation products was performed by X-ray SCANDIFLASH apparatus XR450 model. The X-ray photograph was made at the moment, when the detonation wave short-circuited sensor 4 located 30 mm from the end of the charge. This sensor was connected with a delay generator of X-ray apparatus. Simultaneously with the X-ray registration the measurement of the detonation velocity was made by using sensors 5.
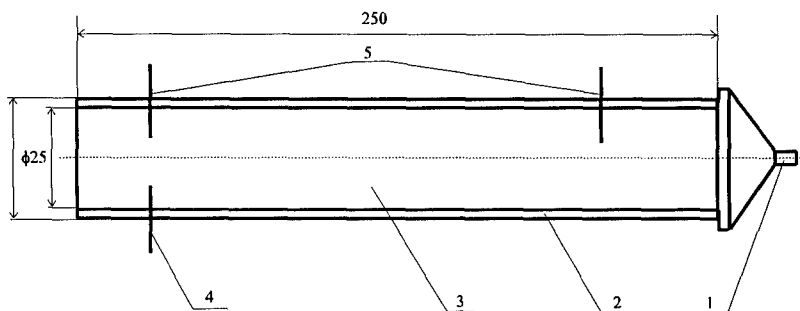
Fig. 1. Diagram of the system for X-ray recording of the process of driving a tube: 1- detonator, 2 - copper tube, 3 - charge of the explosive tested, 4, 5 - short-circuit sensors.

3. Results and discussion

3.1. Detonation velocity

The mean values of the detonation velocity, D, for the ammonium nitrate explosives containing TNT and Al are shown in Table 2. Detonation velocity was plotted against the reciprocal charge diameter (1/d) in Fig. 2

Table 2. Mean values of the detonation velocity for the explosive mixture tested

Charge diameter d [mm]	D [m/s]			
	AN/TNT-1	AN/TNT-2	AN/TNT/Al-1	AN/TNT/Al-2
36	3350 ± 80	1830 ± 80	3640 ± 40	3200 ± 40
45	3830 ± 40	3070 ± 40	3830 ± 50	3670 ± 40
80	4510 ± 120	4080 ± 40	4170 ± 100	4140 ± 50
100	4720 ± 90	4380 ± 60	4230 ± 90	4350 ± 150

The experimental results for each explosive mixture were fitted by linear relationships and represented by

$$D = D_i \left(1 - \frac{a}{d}\right)$$ (1)

where D_i is an extrapolated detonation velocity to infinite diameter and a is a constant. According to Eyring [10], a is proportional to the thickness of the reaction zone. Fig. 2 shows that the fitting by Eq. 1 is quite satisfactory excepting the result for the ammonium nitrate containing coarse TNT loaded in the charge of the smallest diameter.

Table 3 shows the summary of D_i and a for four explosive tested.
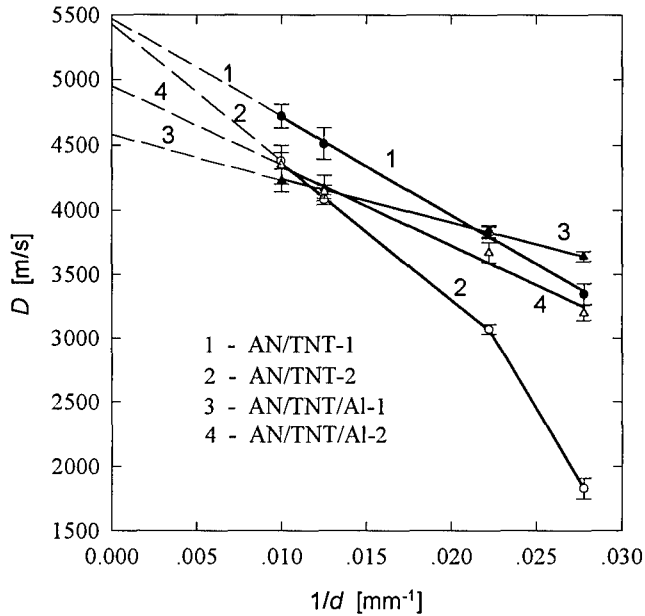
Fig. 2. Detonation velocity (D) of ammonium nitrate explosives versus reciprocal charge diameter ($1/d$)

Table 3. Experimental and theoretical values of an ideal velocity of the detonation wave

Explosive	D_i [m/s]	a [mm]	D_i^R [m/s]	D_i^S [m/s]
AN/TNT-1	5470	13.8	6060	5370
AN/TNT-2	5430	19.6	6060	5370
AN/TNT/Al-1	4580	7.4	5790	5170
AN/TNT/Al-2	4950	12.4	5790	5170

The detonation velocity of the mixtures investigated were evaluated by means of the program for thermochemical calculations TIGER - [11]. Two sets of values of the parameters α, β, κ, and θ were assumed for the BKW equation of state, one of them being taken from Ref. [12] (BKWR: $\alpha = 0.50$, $\beta = 0.176$, $\kappa = 11.80$, $\theta = 1850$) and the other from Ref. [13] (BKWS: $\alpha = 0.50$, $\beta = 0.298$, $\kappa = 10.50$, $\theta = 6620$). The latest was recommended to calculation of the detonation parameters for aluminized explosives. The detonation velocities of the explosive mixture were obtained by assuming chemical activity of all components. The calculation results for both sets of BKW parameters are given in Table 3 (D_i^R and D_i^S denote the detonation velocities for BKWR and BKWS sets, respectively).

From comparison of the experimental and theoretical data from Table 3 it follows that an agreement between the extrapolated detonation velocity D_i and the calculated velocity, obtained by assum-

ing the equilibrium state of mixture components, is better when the set of BKWS parameters is used. However, even in this case the extrapolated detonation velocities to infinite diameter for the AN/TNT/Al mixtures are considerably lower than those calculated. This fact brings a conclusion that most of aluminium behaves as inert addition in the reaction zone even for charges of large diameter ($d \to \infty$). The discrepancy between D_i and D_i^S for the mixture with flaked aluminium is greater than that for the mixture containing granular aluminium. A negative influence of aluminium having larger specific surface on the detonation velocity indicates that the heat exchange between grains of aluminium and the explosion products affected significantly the detonation process.

The detonation velocity falls off quickly with the reciprocal charge diameter for the mixtures containing coarser components (AN/TNT-2, AN/TNT/Al-2; Fig. 2). Also the thickness of the reaction zone is larger for these explosives - Table 3. This fact can be attributed to the lower degree of physical homogeneity of the mixtures containing coarser TNT and Al. Larger thickness of the reaction zone causes that a penetration of the lateral rarefaction waves into the reactive mixture is deeper. Thus, the detonation parameters are weakened, especially for small diameter charges.

On the other hand, higher degree of physical homogeneity of the mixture containing fine additions leads to the slight dependence of the detonation velocity on the reciprocal diameter and to the shorter thickness of the reaction zone (Fig. 2, Table 3). This means that influence of the lateral waves decreases. This phenomena may be connected with growing number of ignition points at the wave front in the mixtures containing the fine additives.

The diameter effect relationships for the ammonium nitrate explosives containing different kinds of TNT (AN/TNT-1, AN/TNT-2) approximately cross together in D vs. $1/d$ plane (Fig. 2). This means that the decomposition and reaction degree between AN and TNT in both the mixtures is similar for infinite diameter charges. The reaction degree falls off quicker with decreasing the charge diameter in the case of the mixture containing coarser TNT.

According to the conclusion given earlier an aluminium additive, independently of its fineness degree, does not fully react with the decomposition products of AN and TNT in the detonation wave in the charges of infinite diameter. For coarser aluminium in the mixture the energy losses in the decomposition products due to the heat transport into the additive are smaller. Thus, the value of D_i for AN/TNT/Al-2 mixture is greater than that for AN/TNT/Al-1. From Fig. 2 it is evident however that the diameter effect relationships for the mixtures containing different kinds of aluminium cross each other for some value of the reciprocal diameter and greater detonation velocities are obtained for the AN/TNT/Al-1 mixture for small diameter charges. In this case the fineness degree of the aluminium additive results in an occurrence of greater number of ignition points at the front of the detonation wave, which contribute to the decomposition of larger quantity of the mixture. Thus, fine aluminium should be used in the AN explosives for small diameter charges.

3.2. Cylinder test

The values of the detonation velocity, D_e, measured in the cylinder test are presented in Table 4. Typical X-ray photograph of a copper tube driven by the detonation products is shown in Fig. 3. The

results of registration of the motion of copper tubes for all mixtures tested are presented in Fig. 4 in the form of shapes of the external boundary of tubes .

Table 4. Detonation velocity for charges used in a copper tube

Explosive	ρ_0 [kg/m^3]	D_e [m/s]
AN/TNT-1	1050	4140 ± 60
AN/TNT-2	1050	3380 ± 40
AN/TNT/Al-1	980	3880 ± 50
AN/TNT/Al-2	1050	3900 ± 50
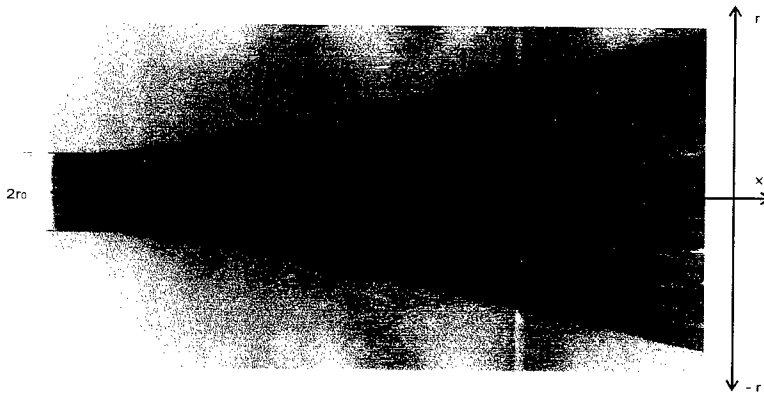
Fig. 3. Typical X-ray photograph of a copper tube.

Theoretical model proposed in Ref. [14] is used for numerical simulation of the process of driving a copper cylinder. It is assumed in this model that the time of propagation of the detonation wave is enough to neglect the influence of an initial condition. Then the motion of the detonation products may be treated as stationary in a reference frame connected with the detonation wave. It is assumed that the equation of state of the polytropic gas with the exponent of isentrope, γ, describes a behaviour of the detonation products. The material of the tube is treated as incompressible. Comparison of experimental results from the cylinder test with those of computer simulation of the driving process enable us to determine the effective exponent of an isentrope of the detonation products [15].

The calculated profiles of the copper tube and the values of effective exponent obtained are presented in Figs. 5 and 6. The dashed lines denote the diagrams obtained from modelling the process of driving the tube by the products being characterised by the constant polytropic exponent γ. The range of axis co-ordinate used in the appraisal of the value of γ is fixed by the dashed line apart from the AN/TNT/Al-2 mixture, for which the exponent value was estimated in the range of x from 0 to 80 mm. The experimental diagrams of radius position of the external boundary of tubes are also shown by the solid lines.
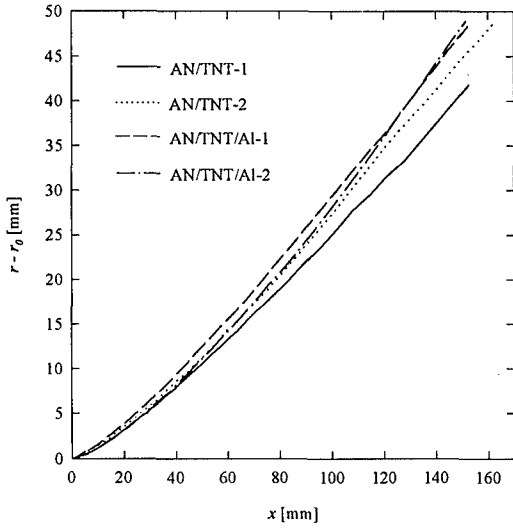
Fig. 4. Shapes of the external surface of copper tubes.
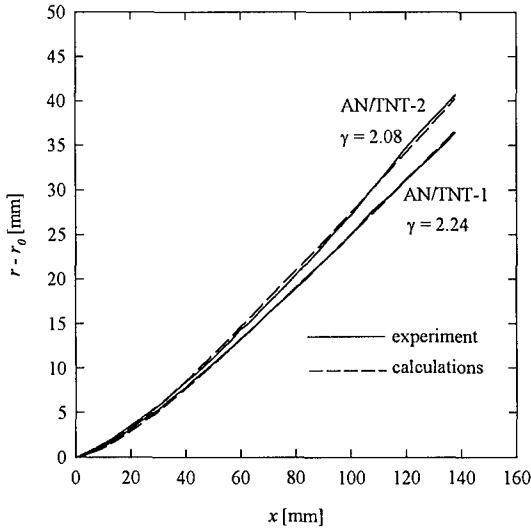
Fig. 5. Experimental and calculated profiles of the external surface of copper tubes driven by the detonation products of AN/TNT mixtures.
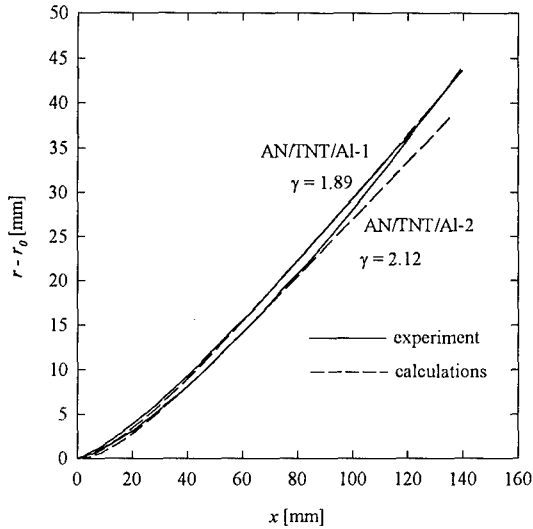
Fig. 6. Experimental and calculated profiles of the external surface of copper tubes driven by the detonation products of AN/TNT/Al mixtures.

From the Table 4 it follows that the mixture with fine TNT (AN/TNT-1) has higher detonation velocity than that with coarse TNT (AN/TNT-2). It has been mentioned earlier that this fact can be connected with producing greater number of hot points by the wave front propagating in the mixture containing fine TNT. In Fig. 5 the experimental profile of the copper tube driven by the products of the AN/TNT-1 mixture lies closely to the calculated one obtained by assuming a constant value of γ. A constant isentropic exponent means that the composition of the detonation products changes in an insignificant degree and an additional heat release does not take place during the expansion process.

Contrary to fine TNT the products of coarse TNT react to a considerable degree with the decomposition products of ammonium nitrate behind the reaction zone. This conclusion can be inferred from the experimental profile of the tube driven by the products of the AN/TNT-2 mixture. Moreover, the lower value of the isentropic exponent of the detonation products of this mixture means that the fall of a pressure in the explosion gases behind the detonation wave is smaller as compared with the AN/TNT-1 explosive due to the additional moles of gases producing or the energy releasing. This indicates that the acceleration metal ability of the detonation products of the AN/TNT-2 mixture increases.

Despite of the fact that the AN/TNT/Al mixtures used in the cylinder test have different densities, the detonation velocities measured in a copper tube are approximately equal each other. Because the mixture with fine aluminium has lower density it means that the greater amount of aluminium reacts with AN inside the reaction zone. From comparison of the experimental and theoretical profiles of the copper tubes (Fig. 6) it is evident that the remaining part of aluminium grains burns just behind this

zone. Further expansion of the detonation products of the AN/TNT/Al-1 mixture is similar to that of the polytropic gas with a constant exponent of an isentrope.

The coarse aluminium being present in the AN/TNT/Al-2 mixture behaves like an inert additive in the first stage of the expansion of the detonation products. Taking into account the initial part of the profile (Fig. 6) we obtained the effective isentropic exponent for the detonation products of the AN/TNT/Al-2 mixture only inconsiderable lower than that for the AN/TNT mixture containing also fine TNT. This means the similar metal acceleration ability of both the mixtures as well. However, in the further stage of the driving process the experimental tube profile in the case of the AN/TNT/Al-2 mixture bends up as regards the theoretical one obtained by assuming the constant value of γ and it crosses the experimental tube profile obtained for the AN/TNT/Al-1 mixture with fine aluminium. This means that at some distance behind the detonation wave the acceleration metal ability of the detonation products of this mixture increases due to the additional moles of gases occurring or the energy releasing. In the case of the Al additive only the latter influences the expansion work of the detonation products because the main reaction product of Al, aluminium oxide, is solid.

4. Summary

1. The extrapolated detonation velocities to infinite diameter for the AN/TNT/Al mixtures are considerably lower than those for the AN/TNT mixtures. The two AN/TNT explosives tested have the same value of the extrapolated velocities, independently from the type of TNT admixture. But those velocities for the two AN/TNT/Al explosives containing fine or coarse aluminium are different.

2. Coarse TNT in the AN/TNT mixture results in an decrease of the detonation velocity in finite diameter charges as compared with the fine-grained TNT admixture. Shapes of the copper tubes driven by the detonation products of the AN/TNT mixtures and the values of the isentropic exponents estimated show that coarse TNT reacts in a significant degree with the decomposition products of AN behind the reaction zone.

3. Most of aluminium grains in the mixtures tested behave like an inert additive in the reaction zone. But a comparison of the experimental and calculated profiles of tubes driven by the detonation products of the mixtures containing aluminium indicates that an energy from aluminium reaction converts to an expansion work behind the zone.

4. The diameter effect relationships for the AN explosive containing different kind of aluminium cross each other for some value of the reciprocal diameter. For large diameters of charges higher detonation velocities are obtained for the AN/TNT mixture with coarse aluminium and in the case of small charge diameters higher detonation velocity are given by the mixture with fine aluminium.

Literature

[1]   M. A. Cook, E. B. Mayfield, W. B. Partridge, *Reaction rates of ammonium nitrate in detonation*, J. Phys. Chem., **58**, 8, 1955.

[2]   A. C. van der Steen, H. H. Kodde, *Detonation velocities of the non-ideal explosive ammonium nitrate*, Prop. Expl. Pyrot., **15**, 2, 1990.

[3]   M. A. Cook, A. S. Filler, R. T. Keyes, W. S. Partidga, W. A. Ursenbach, *Aluminized explosives*, J. Phys. Chem., **67**, 2, 1957.

[4]   A. Maranda, *Investigation of an influence of organic fuel on detonation parameters of ammonium nitrate explosives* (in Russian), Fiz. Gor. Vzr., **27**, 1, 1991.

[5]   A. Maranda, *Research on the process of detonation of explosive mixtures of oxidizer-fuel type containing aluminium powder*, Prop. Expl. Pyrot., 15, 4, 1990.

[6]   K. K. Shvedov, *Some questions of detonation of explosive mixtures* (in Russian), Tchernogolovka, 1981.

[7]   J. B. Akst, *Intermolecular explosives*, Proceedings Eighth Symposium (International) on Detonation, Albuquerque, 1985.

[8]   S. Cudziło, A. Maranda, J. Nowaczewski, W. Trzciński, *Shock initiation studies of ammonium nitrate explosives*, Combustion and Flame, **102**, 1995.

[9]   S. Cudziło, A. Maranda, J. Nowaczewski, W. Trzciński, *Shock initiation of ammonium nitrate explosives,* Proceedings 25th International Annual Conference of ICT, Karlsruhe, 1994.

[10]   H. Eyring, R. E. Powell, G. H. Duffy, R. B. Parlin, *The stability of detonation*, Chem. Rev. **45**, 69, 1949.

[11]   Ch. L. Mader, *Numerical modelling of detonations*, University of California Press, 1979.

[12]   P. Crawford, *Getting started with TIGER*, Lawrence Livermore National Laboratory, 1986.

[13]   M. L. Hobbs, M. R. Baer, *Calibration of BKW-EOS and application to aluminized composite explosives*, EUROPYRO'93, Strasbourg, 1993.

[14]   Trębiński R., Trzciński W., Włodarczyk E., *Theoretical analysis of the process of driving a cylindrical liner by the products of grazing detonation*, J. Tech. Phys., **29**, 3-4, 1988.

[15]   R. Trębiński, W. Trzciński, *A method for determining an effective exponent of isentrope for the detonation products of condensed explosives* (in Polish), Biul. WAT, **45**, 3, 1996.

ABSTRACT

Underwater Explosion Performance of Explosively Dispersed Ti-B Mixtures

Joseph G. Connor, Jr. and Ruth M. Doherty
Naval Surface Warfare Center
Indian Head Division
Silver Spring, MD 20903-5000

Underwater explosion performance tests were conducted to determine whether the energy released by the reaction of titanium and boron to form the intermetallic TiB_2 (and possibly through subsequent reaction with the surrounding water to form oxides of titanium and boron) could be released in a sufficiently short time to create an oscillating explosion gas bubble such as those created by high explosives detonated underwater. Photographic coverage, both underwater and on the surface, and piezoelectric gauges to measure the pressure-time history in the water were used to record the results of the ignition and dispersal of Ti-B mixtures in water. Two active dispersal techniques, in which explosives were employed to disperse the reacting material into the water, and one passive technique, in which the expansion of the gases present in the porous Ti-B mixture dispersed the material, were tested. Baseline data on the performance of pentolite and Composition C-4 were collected for comparison.

The bubble phenomena associated with the intermetallic reaction were qualitatively very different from those of the conventional explosives. The appearance was more that of a very large number of independent bubbles than of a single coherent bubble such as is seen with conventional high explosives. The bubbles from the Ti-B mixture were smaller in diameter at the maximum and had a much shorted period of oscillation than an equal volume of pentolite. The surface phenomena were also different. The plume did not rise as high, nor did it have as great a horizontal extent as those created by high explosives.

PROCESSING OF Mg-NaNO$_3$ BASED FUEL-RICH PROPELLANT BY POWDER COMPACTION TECHNIQUE FOR AIR-BREATHING PROPULSION SYSTEMS

HARIHAR SINGH, P. SRINIVASA RAO and R.BHASKARA RAO

High Energy Materials Research Lab. Detachment (CDB Facility), Hyderabad - 500 058 (INDIA)

ABSTRACT

Study of Mg-NaNO$_3$ based formulations have shown a great interest in the recent past as fuel-rich propellants for advanced air-breathing propulsion systems due to their high heat potential. Mg-NaNO$_3$ propellant containing solid hydro-carbon as a binder was found to possess good combustion characteristics and high combustion efficiency. Wide burning rate spectrum of the propellant could be achieved by varying the particle size of the fuel and oxidiser without varying the fuel-richness. High burning rate of the propellant, a pre-requisite for the higher performance of the air-breathing system, could be achieved by "powder compaction technique" which otherwise is extremely difficult to realise by slurry cast technique.

Powder compaction technique for Mg-NaNO$_3$ based compositions, where all the ingredients are in dry powder form and are of highly hazardous nature, is more complex when compared to conventional powder metallurgy and standard pyrotechnic mixtures. Development of powder compaction technique involved : (i) small scale experimentation and testing to establish the process parameters for achieving the required ballistic performance; (ii) an exhaustive safety analysis using advanced techniques to establish personnel and equipment safety; (iii) incorporation of the results of the predictive hazard analyses into the design of the process, tooling, and equipment while scaling up of the process and (iv) development of inhibition technique.

A semi-automatic remote controlled high capacity hydraulic press was designed and developed incorporating a number of interlocks for the process safety. The tooling consisted of a high capacity hydraulic die-clamp, integrated with the main press, to contain the transmitted pressure which was observed to be as high as 70% of the applied pressure; a base plate providing the necessary initial large burning surface; a split die and a plunger containing non-metallic tip, air-escape paths and increment-bonding grooves. Compaction was carried out in an environment of controlled humidity and temperature. Certain parameters like critical density and critical inverse rate of pressure rise were found to be very important in solving the safety problems arising due to adiabatic heating of the entrapped air and dust cloud formation.

Material stress gradient, increasing towards the base, was observed during in-situ compaction method and hence was not used. Incremental pressing method, where the grain was compacted in split-die, inhibited externally and finally case bonded with the motor, was adopted.

Technological problems concerning structural rigidity, dimensional stability, and sensitivity to impact and frictional heating were resolved. Static test results of the grains processed by this technique have shown good reliability and reproducibility both in primary mode and ramjet mode.

- x -

NOVEL METHODS FOR THE CHEMICAL AND BALLISTIC ASSESSMENT OF NEW GENERATION PROPELLANTS

by

A Fraser, G Gillies, C Holmes, B Kelso, A Ross* and I Sharp*

DRA Bishopton
Scotland

The new high energy LOVA propellants present a range of problems for the propellant chemist.

The intractable nature of the material makes conventional chemical analysis unfeasible for qualification and routine periodic inspection; and the high energies now attained in gun and rocket systems render the ballistic performance assessment methods used prior to the development of these materials unsuitable.

DRA Bishopton (part of Weapons System Sector) have been investigating the use of novel techniques to tackle problems associated with the chemical analysis of these materials and with development of novel methods of ballistic assessment which can be applied to the new high energy propellants.

Supercritical Fluid Extraction has been evaluated as a means for extraction of the organic constituents i.e. RDX, energetic plasticisers, antioxidents stabilisers, residual monomer, oligomer etc. from the highly crosslinked LOVA propellants. This technique has been compared with a number of conventional techniques.

FTIR spectrometry, using chemometric data analysis, has been applied to the problem. The use of reflectance techniques for spectral recording has been investigated and multicomponent analysis methods have been applied to the results in order to assess their suitability for the characterisation and analysis of these propellants.

Ballistic assessment of gun propellant at pressures up to 600 MPa has been performed in a newly acquired high pressure 700cc Peters Vessel and a novel high pressure vessel designed by RMCS under contract to DRA. This unique vessel also has the capability to fire liquid propellants.

A newly developed mathematical model has been used to convert mass burning rate data obtained from firing rocket propellant in a Vented Vessel to linear burning rate data. This will reduce the cost of linear burning rate determination by replacing the currently used strand rate burning method with the cheaper vented vessel method. This is particularly important because of the high cost and limited availability of LOVA propellant during the development programme and also the nature of the material which makes production of strands difficult.
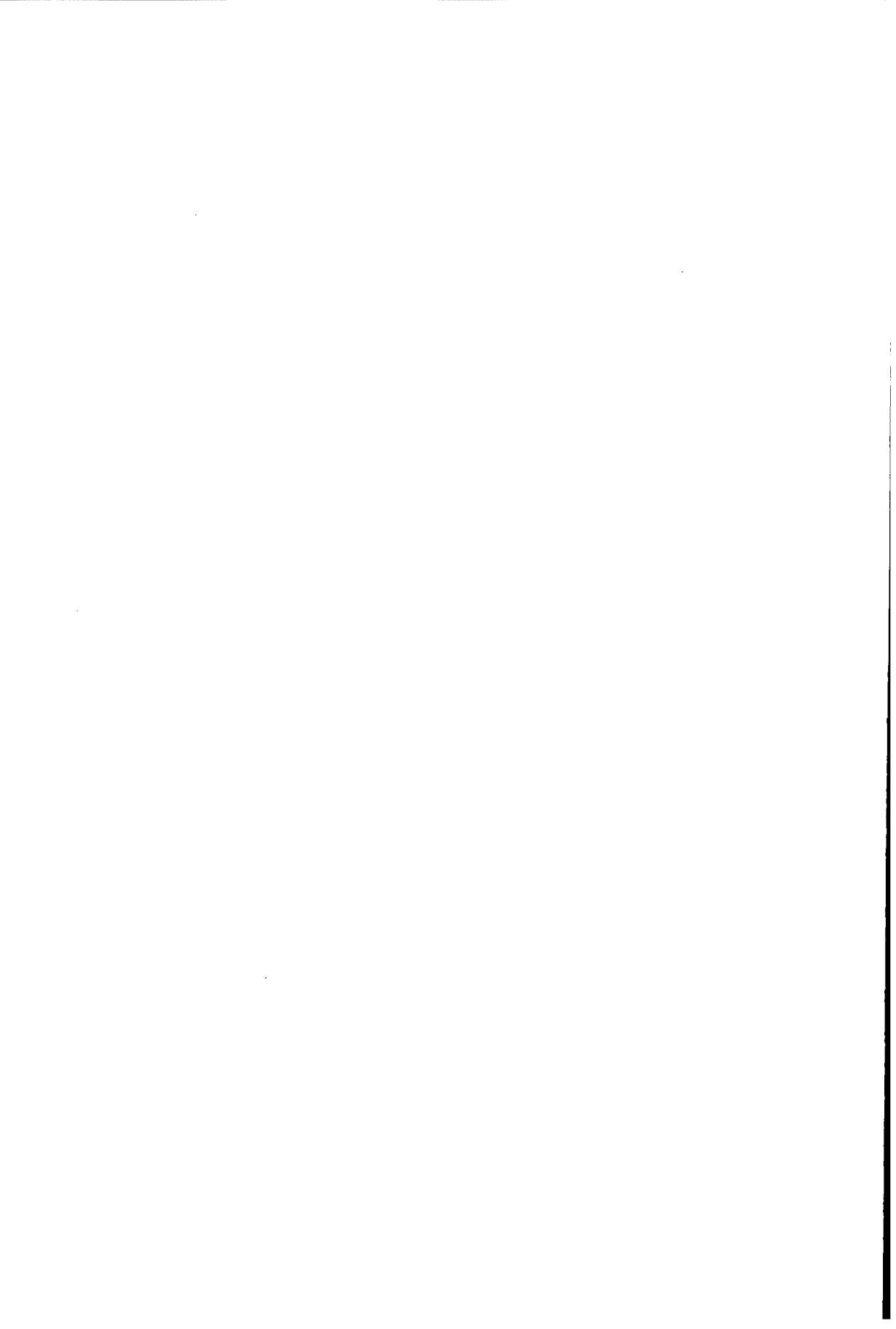
SOLID PROPELLANTS FOR CONTROLLED ROCKET MOTORS.

Dr. Prof. Vladimir I. Petrenko.
Technical University, Perm, Russia.

Dr-ing. Prof. Anatoly M. Rusak.
Aviation Technical University, Ufa,Russia.

Rocket and space technology improving is connected with the appe-
arance of multi-functional SPRM with the complex diagram of thrust mo-
dule variation. Absense of propellant supply systems, simplicity of
construction, compactness are very attractive factors for desig-
ners,who consider this type of engine to be more progressive in compa-
rison with one with a liquid propellant, that can ensure the control
on the stabilisation channels and the march regime.
It is known, that variation of the trust module may be received
by changing the following factors:
    -power characteristics of solid propellant, that may be changed,
  by launching chemically active additional mass into the
combustion chamber.
    -the products of combustion consumption by means of launching the
secondary mass to the combustion chamber.
    -changing combustion speed by means of chemical
influence on the reaction speed at the combustion zone, additional
supply of heat to the propellant combustion zone,and so on.
    -changing of the combustion surface by means of so
called "heat knife","hydraulic control",ets.
    -changing the area of the throat in presence of high enough sen-
sitivity of the combustion speed of chamber pressure,for exam,
using solid propellants with negative degree in the law of the combus-
tion propellant.
 Each of these methods appends its limitations on physical and chemical
characteristics of solid propellants, so the choice of the necessary
propellant type is multi-factor task.
 Five types of controlled SPRM are described in the report, the condi-
tions of solid propellant function are analysed for each case, experi-
mental data and calculations are available.

EFFECT OF ALUMINUM CONTENT AND PARTICLE SIZE ON THE BALLISTIC AND MECHANICAL PROPERTIES OF HTPB BASED COMPOSITE SOLID PROPELLANTS

Saim Özkar,[a] Fikret Pekel,[b] F.Nihal Tüzün [b]

[a] : Department of Chemistry, Middle East Technical University, 06531 Ankara, TURKEY

[b] : Defense Industries Research and Development Institute, TÜBİTAK, P.K. 16 Mamak, 06261 Ankara, TURKEY

Abstract

The effect of aluminum content and particle size on the ballistic and mechanical properties of the HTPB based composite propellants containing 85.5 weight percent solids was investigated for ten different aluminum contents (0, 5, 9, 11, 12, 13, 14, 16, 18 and 20%) and three different types of aluminum (ALCAN-TOYO, spherical 7.9μ; STAN CHEM, 10μ; and BDH, irregular shape 25μ). The burning rate, heat of explosion, density, and mechanical properties of the propellant samples were measured by using a Crawford Bomb testing system at 25°C under variable pressure (20-140 kg/cm^2), a bomb calorimeter under constant pressure, a stereopycnometer, and INSTRON tester, respectively. Variations in ballistic properties of the compositions were estimated by using a modified version of the computer program for calculation of complex chemical equilibrium compositions. It was found that the burning rate and pressure exponent decrease with the increasing aluminum content of the propellant whereas the density, adiabatic flame temperature, specific impulse, and heat of explosion of the propellants increase. The only deviation from this general trend is observed for the specific impulse, and heat of explosion of the sample with 20 % aluminum. The samples with the aluminum content in the range of 11-16 percent show mechanical properties acceptable for the rocket applications. The effect of three types of aluminum was studied by preparing samples of propellants with 5 % aluminum content. The use of three types of aluminum was found to have no adverse effect on the ballistic and mechanical properties of the propellant.

Introduction

Aluminum is commonly used as fuel in solid rocket propellants and increases the chemical energy of the propellant as a result of the exothermic reaction with the oxidizer. Although, use of aluminum produces a large increase in specific impulse of the propellant, the efficient conversion of the chemical energy to the propulsive force belated by its combustion product, aluminum oxide. Compared to the gaseous products, high boiling aluminum oxides release their heat more slowly and have a reduced acceleration during the expansion process in the nozzle.[1] As the aluminum replaces the oxidizer in the composite solid propellants to keep its solid content at a constant level, the aluminum concentration is anticipated to affect the burning rate of the solid propellant. However, this effect has been barely investigated and the results are rather astonishing because the effect of the added aluminum powder on the burning rate of the solid propellant has been reported to be small and furthermore to be either positive or negative.[2] The effect of aluminum particle size on the burning rate has been reported to depend on the burning rate modifier in the propellant.[3] For instance, the burning rates of propellants containing catocene and ferrocene derivatives as burning rate modifiers have been found to increase with the decreasing aluminum particle size, while the particle size of aluminum had no effect on the burning rates of the propellants containing iron(III) oxide or copper chromite as promoter.

Here we report the results of a study on the effect of aluminum content and particle size on the ballistic and mechanical properties of a well characterized HTPB/AP composite propellant containing 85.5 weight percent solids. Samples having ten different aluminum contents (0, 5, 9, 11, 12, 13, 14, 16, 18 and 20%) and three different types of aluminum (ALCAN-TOYO, spherical 7.9μ; STAN CHEM, spherical 10μ; and BDH, irregular shape 25μ) were prepared and their burning rate, heat of explosion, density, and mechanical properties were measured by using a Crawford Bomb testing system at 25°C under variable pressure (20-140 kg/cm^2), a bomb calorimeter under constant pressure, a stereopycnometer, and an INSTRON tester, respectively. In order to avoid the interfering influence of the burning rate promoter samples of HTPB/AP composite propellants were prepared by using iron(III) oxide as burning rate modifier in a fixed percentage (0.5 % Fe$_2$O$_3$).

Experimental

The samples tested were prepared by using an aluminized HTPB/AP composite propellant with a constant solid content of 85.5 % by weight. The binder percentage of the propellant was kept constant throughout the study. The amount of iron(III) oxide (Merck, Darmstadt/Germany) used as burning rate promoter was kept constant at 0.5 % as well. The distribution of AP was bimodal with a constant ratio

between the coarse and fine particles. The coarse particles were 200 μm, and the fine particles were in the range 5-7 μm in size. The fine particles were prepared by grinding the coarse particles and measured in size. The only parameter varied was the amount of metallic fuel, aluminum, which is the most important parameter affecting the specific impulse. The aluminum content replaced for the equal amount of AP in the propellant samples. Three different types of aluminum were used: ALCAN-TOYO spherical particles of 7.9 μ size, BDH irregular shape particles of 25 μ size, and STAN CHEMICAL spherical particles of 10 μ size.

The aluminum content of the propellant was varied in the range of 0-20 % by weight. Samples of propellants with ten different aluminum content (0, 5, 9, 11, 12, 13, 14, 16, 18 and 20 %) and with 5 % aluminum content of three different types were prepared by mixing AP, binder, aluminum, and the other additives in batches (sigma blade mixer with a capacity of one gallon) followed by casting into the samples of $14 \times 10 \times 2$ cm dimensions and curing at 65°C for 7 days.

The viscosity measurements of the propellant samples were carried out at 65°C after the addition of curing agent by a Brookfield viscometer with spindle Nr. 7 at 10 rpm.

The burning rates of the propellant were measured by using a strand burner Crawford Bomb testing system at 25°C under variable pressure (20 - 140 kg/cm^2).

The cured samples were tested for their mechanical properties at room temperature and with a cross-head speed of 50 mm/min by using a conventional uniaxial testing system (Hawlett Packard-85 type INSTRON) which directly gives the calculated elastic modulus.

Particle sizes of the used powders were determined by using Malvern Mastersizer Model MSX 64 with dry powder feeder and He-Ne Laser (633 nm) transmitter.

Heat of explosion of propellants was measured by using a 1261 Parr isoperibol calorimeter under constant pressure (450 psig) of nitrogen as inert gas.

Densities of propellants were determined by using a stereopycnometer of Quanta Chrom under inert helium atmosphere.

Variations in ballistic properties of the compositions were estimated by using a modified version of the computer program for calculation of complex chemical equilibrium compositions, referred to as OPHELIE.[4]

Results and Discussion

Samples of HTPB/AP composite propellants having ten different aluminum contents (0, 5, 9, 11, 12, 13, 14, 16, 18 and 20%) and three different types of aluminum were prepared and tested for their mechanical and ballistic properties. The results of the burning rate measurement are given in Figure 1 for the samples with ten different aluminum contents. All the values of the burning rates were fitted by the method of least-square to an exponential function defined by the Vielle's equation,[5] $r = aP^n$, where r is the burning rate in cm/s, P is the pressure in bar, and n is the pressure exponent. Inspection of the burning rate versus pressure curves (Figure 1) shows that the burning rate decreases with the increasing aluminum content of the solid propellant. This effect is nicely seen from the comparision of the burning rate of the propellant samples with the different aluminum content at 100 bar (Table 1). The burning rate at 100 bar is decreased from 1.461 cm/s for a non aluminized sample to 1.194 cm/s for 20% Al propellant (Table 1). This is a significant amount of decrease in the burning rate, in contrast to the previously reported values.[6] The noticeable change in the burning rate of the propellants can be attributed to the decrease in the amount of ammonium perchlorate (AP) rather than to the increase in the aluminum content. It has been already established that the burning rate of solid propellants increases with the increasing concentration of the oxidizer.[1] The addition of aluminum to the propellant by keeping the solid content constant concomitantly reduces the AP concentration, and thus the burning rate. A parallel decrease is also observed in the pressure exponent with the increasing aluminum content (Table 1).

The burning rate of the propellant samples with 5% aluminum of three different types shows that the particle size of aluminum has a not-insignificant influence on the burning rate (Table 2 and Figure 2). The sample with spherical aluminum particles of 8 and 10 μ has a burning rate of ca. 1.44 cm/s while the burning rate of the sample with irregular shape aluminum particles of 25 μ is 1.39 cm/s. This observation parallels the

previously reported results showing that the burning rate of the solid propellants decreases with the increasing particle size of aluminum powder.[7]

The samples of solid propellants were also tested for their other ballistic and mechanical properties. The results of measurements are listed in Table 1. Density of propellants increases with the increasing aluminum content as expected.[8]

The heat of explosion of the solid propellant samples increases with the increasing aluminum content up to the 20 % (Table 1 and Figure 3). However, at this composition one observes a sharp decrease in the heat of explosion of the propellant. The main cause of this abrupt change might be the insufficient amount of oxygen as a result of decreasing ammonium perchlorate content in the propellant. The calculation by using OPHELIE program shows an incomplete combustion which can be attributed to the insufficient amount of oxygen due the replacement of AP by aluminum (Table 3). Another indication for the insufficient amount of oxygen in the propellant is the increase in the amount of carbon monoxide and the decrease in the amount of carbon dioxide in the exhaust gases due the incomplete combustion. A concomitant decrease is also observed in the formation of water.

The increase in the amount of discharged free aluminum in the combustion products is indicative of the oxygen insufficiency. The great effect in the discharged free aluminum was especially sensitized on the heat of explosion, theoretical specific impulse, and energy of the propellant. All these three properties show an abrupt decrease at 20 % Al.

In general, the most important mechanical property requested in a solid propellant is elongation with high stress. This property is required to prevent the rocket motor and propellant separation due to the differences between thermal expansion coefficients. Tensile strength and elastic modulus of the propellant may be low. The unique restriction is to keep those properties above the limiting values. Because, in this situation, the load applied to the propellant can change the grain configuration. Most of the composite solid propellants used successfully in large rocket applications give 20-30 % elongation, around 0.07-0.34 kg/mm^2 tensile strength and about 0.34 - 1.36

kg/mm^2 elastic modulus changes. In this study, changes in stress at peak load, elongation and elastic modulus values were determined in the propellant samples with the increasing aluminum content (Table 1). At first glance, the nonaluminized propellant (0 % Al) sample possesses mechanical properties which are not acceptable for propellant manufacture. The samples containing aluminum in the range of 5 - 16 % have acceptable mechanical properties.

Conclusion

It was found that burning rate and pressure exponent decrease with the increasing aluminum content of the propellant whereas density, specific impulse and heat of explosion of propellants increase. The only deviation from this general trend was observed for specific impulse and heat of explosion of the sample with 20 % aluminum. The samples with the aluminum content in the range of 5-16 percent show acceptable mechanical properties for rocket applications.

The use of three types of aluminum was found to have no adverse effect on the ballistic and mechanical properties of the propellant.

References

1. K. Klager and J.M. Wrightson, "Recent Advances in Solid Propellant Binder Chemistry" in AIAA Selected Reprint Series Ed. R.A. Gross, Volume X. Solid Propellant Technology Ed. F.A.Warren, New york, pp. 37-64, (1970).

2. (a) Y.V Frolov, P.F.Pokhil, V.S. Logachiv, "Ignition and Combustion of Powdered Aluminum in High Temperature Gaseous Media and in a Combustion of Heterogeneous Condensed Systems", Combustion, Explosion and Shock Waves, 18, 213-236 (976); (b) J.L. Prentice, "Aluminum Droplet Combustion", Naval Weapons Center, Report TP 5569, April 1974; (c) R.L. Geisler, "Summary Report on 1977 JANNAF Aluminum Combustion Workshop", Proceedings of 14th JANNAF Combustion Meeting, Vol.1, Chemical Propulsion Information Agency, Laurel, MD, CPIA Pub. 292, December 1977; (d) R.R. Miller, M.M.

Donohue, R.A.Young, J.R. Martin, "Control of Solids Distribution in HTPB Propellants", AFRPL TR-78-14, April 1978; (e) E.N. Cohen, "Combustion of Highly Loaded Composite Propellants: Study of Pressure Exponents", Combustion Science and Technology, 14, 75-84 (1976).

3. A.L. Leu,R.J. Wu, "Formulation Effects on the Burning Rate of Aluminized Solid Propellants" J. Propulsion, 4, 22-26 (1988).

4. S. Gordon, B.J. McBride, "Computer Program for Calculation of Complex Chemical Equilibrium Compositions", Rocket Performance, Incident and Reflected Shocks, and Chapman-Jouguet Detonations, NASA SP-273 interim Revision N78-17724, March 1976.

5. M. Barrere, A. Jaumette, B.F. Veubeke, J.Vandenkerckhove "Rocket Propulsion": Chp. 4, pp. 193-199, Elsevier Publishing Company, New York, 1960.

6. S. N. Asthana, R.B. Mundada, P.A. Phawade, P.G. Shrotri, "Combustion Behaviour of Advanced Solid propellants", Defence Science Journal, Vol. 43, pp. 269-273, (1993).

7. W.P. Killian, "Loading Composite Solid Propellant Rockets Current Technology" in the proceedings of sixty fourth national meeting, American Institute of Chemical Engineers, May 19-22, 1968.

8. R.F. Gould, "Propellants Manufacture, Hazards and Testing", Advances in Chemistry Series 88, Chemical Society, Washington D.C., pp. 160-162 (1969).

Table 1. Variations in the mechanical and balistic properties of propellant samples with the aluminum content (BDH) at room temperature

Al (%)	Density (g/cm^3)	Heat of explosion (cal/g)	Stress at peak load (kg/mm^2)	Elongation at peak load (%)	Elastic modulus (kg/mm^2)	Burning rate at 100 bar (cm/s)	Pressure exponent n	Isp (s)
0	1.6565	1306.22	0.0651	21.575	0.537	1.461	0.5365	249.7
5	1.7183	1376.59	0.1100	48.920	0.396	1.397	0.5139	255.4
9	1.7313	1421.26	0.089	34.662	0.545	1.350	0.4762	259.2
11	1.7328	1444	0.0825	45.772	0.431	1.309	0.4559	260.7
12	1.7392	1450.55	0.0930	46.618	0.491	1.304	0.4630	261.3
13	1.7414	1462.87	0.0849	42.22	0.408	1.280	0.4552	261.9
14	1.7455	1473.91	0.0835	42.951	0.430	1.270	0.4355	262.4
16	1.7628	1482.67	0.0794	28.345	0.483	1.246	0.4365	263.1
18	1.7672	1506.38	0.0762	30.920	0.360	1.207	0.4227	263.3
20	1.7716	1468.84	0.0804	23.255	0.451	1.194	0.4048	262.7

Table 2. Effect of of three types of aluminum on mechanical and ballistic properties of the propellant containing 5 % aluminum.

Aluminum type	Average particle size (μm)	Viscosity at 65°C (poise)	Density (g/cm^3)	Heat of explosion (cal/g)	Stress at peak load (kg/mm^2)	Elongation at peak load (%)	Elastic modulus (kg/mm^2)	Burning rate at 100 bar (cm/s)	Pressure exponent n
BDH	25	384	1.7183	1376.59	0.1100	48.920	0.396	1.398	0.5139
ALCAN-TOYO	7.9	256	1.7104	1388.38	0.0944	55.481	0.459	1.432	0.4826
STAN CHEMICAL	10	486	1.7153	1397.02	0.0698	60.770	0.349	1.459	0.4813

Table 3. Variations in the composition of combustion products with the aluminum content (%) calculated by using the computer program OPHELIE.

Combustion products	0 % Al	5 % Al	9 % Al	11 % Al	12 % Al	13 % Al	14 % Al	16 % Al	18 % Al	20 % Al
Al_2O_3	0	0.024	0.0435	0.0534	0.0584	0.0633	0.0683	0.0784	0.0884	0.0982
CO	0.1065	0.1666	0.2077	0.2252	0.2331	0.2405	0.2472	0.2597	0.2695	0.2774
CO_2	0.1632	0.1067	0.0675	0.051	0.0436	0.0368	0.0305	0.0195	0.0106	0.0037
HCl	0.1864	0.1765	0.1689	0.165	0.1631	0.1611	0.1591	0.155	0.1507	0.1448
H_2	0.1216	0.1674	0.2091	0.2334	0.2465	0.2602	0.2746	0.3052	0.3379	0.372
H_2O	0.3289	0.2702	0.2184	0.189	0.1733	0.1569	0.1399	0.1033	0.0652	0.0259
Cl_2	0	0	0	0	0	0	0	0	0	0
N_2	0.0932	0.0882	0.0825	0.0825	0.0815	0.0806	0.0796	0.0776	0.0756	0.0736
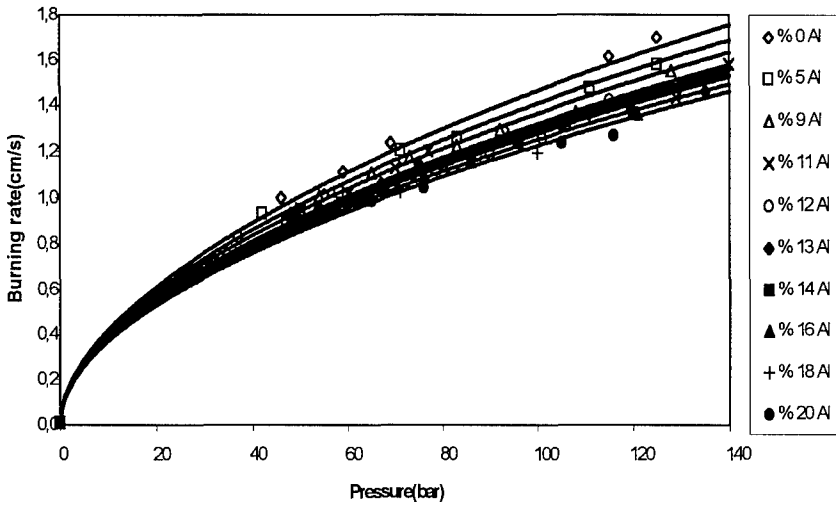
Figure 1 Variations in the burning rate with pressure for propellant samples of ten different aluminum contents.
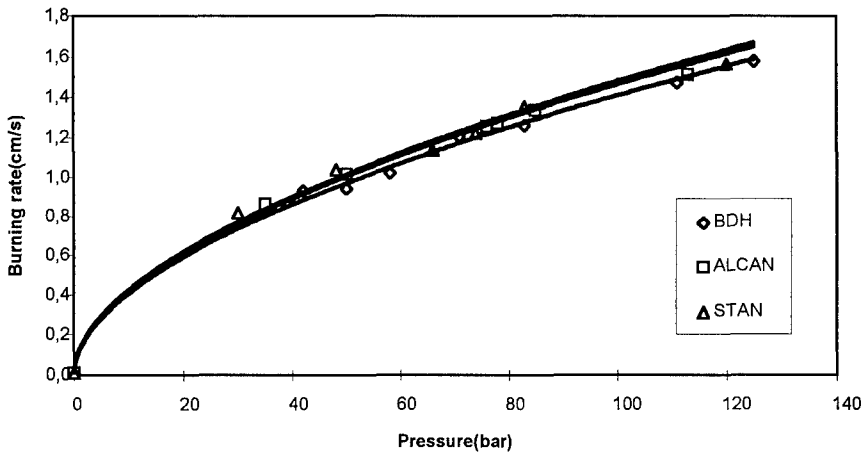
Figure 2. Variations in the burning rate with pressure for the propellant samples with 5 % aluminum of three types.
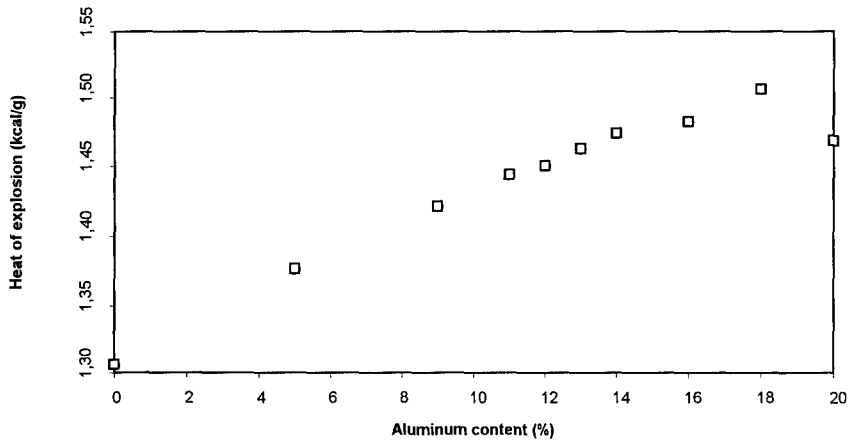
Figure 3. Variations in the heat of explosion with aluminum content of the propellant samples.

MODELING AND RHEOLOGY OF HTPB BASED SOLID PROPELLANTS

Cevat Erişken,[a] Ahmet Göçmez,[a] Ülkü Yılmazer,[b] Saim Özkar,[c] Fikret Pekel[a]

[a] Defense Industries Research and Development Institute, TÜBİTAK, P.K. 16 Mamak, 06261 Ankara, TURKEY
[b] Department of Chemical Engineering, Middle East Technical University, 06531 Ankara, TURKEY
[c] Department of Chemistry, Middle East Technical University, 06531 Ankara, TURKEY

ABSTRACT

Achievement of high density and specific impulse has been the ultimate goal of propellant development. Without changing the design of the motor the only way to get this is to increase the solid content of the propellant. Increasing the solid content, however, causes variations in the rheological as well as mechanical properties of the propellant. For a defect free casting, a propellant with minimum viscosity is required. The propellant with minimum viscosity can be obtained by choosing the proper fractions of solid component sizes leading to maximum packing density. In this study, Furnas' model is used to predict the particulate composition for the maximum packing density. Components with certain size dispersions are combined to yield a size distribution which is closest to the optimum one given by Furnas for maximum packing. The closeness of the calculated size distribution to the optimum one is tested by using the least square technique. The results obtained in this way are experimentally confirmed by rheological characterization of uncured propellants the solid part of which is prepared accordingly. Aluminum powder (volumetric mean particle diameter of 10.4µ) and ammonium perchlorate with four different sizes (the volumetric mean particle diameters: 9.22 µ, 31.4 µ, 171 µ, and 323 µ) are used in the preparation of a series of propellants having trimodal solid part and HTPB binder. In all of these propellants, the aluminum content of the solid part is kept constant for ballistic purposes. The propellant composition having maximum fluidity is determined by measuring viscosities of uncured propellants using a Brookfield Viscometer with T-spindle. The experimental measurements show that the compositions for the minimum viscosity are in good agreement with those predicted by using the model for maximum packing.

INTRODUCTION

Obtaining high levels of specific impulse and density is always the ultimate goal of propellant development, because these are the major factors affecting the performance of the rocket. As the solid content of the propellant is increased, its density increases resulting in an increase in the specific impulse and range. Previous studies have shown that a ten percent increase in ammonium perchlorate (AP) content (from 70% to 80% by weight) increases the specific impulse (I_{sp}) from 185 to 225 sec.[1] Further increase in AP content causes I_{sp} to reach a maximum value and beyond this particular value it shows a decreasing trend. Having an increase in the I_{sp} by increasing the solid content causes variations in the rheological and mechanical properties of the propellant. It is

well known that an increase in the solid content results in an increase in the viscosity of the uncured propellant and a decrease in the percent elongation of the cured propellant, hence causing a difficulty in the processing and failure in the absorption of the stresses in the rocket motor, respectively. Therefore the solid loading should be increased to such a level that propellant still remains processable and the other properties are still satisfactory.

Uncured solid propellants generally exhibit non-Newtonian flow behavior, i.e., viscosity is a function of the applied shear rate. This non-Newtonian behavior of propellant is attributed to the amount of solids contained in the propellant, because the polymer matrix itself shows a Newtonian flow behavior. Clearly, the rheology of the propellant dispersion is important in the manufacturing process.

One way to increase the solid content with a minimal change in the rheological and mechanical properties is to use the concept of packing density, the fraction of volume occupied by solid particles in a bed. Theory of particle packing is based on the selection of proper sizes and proportions of particulate material, so that the large voids are filled with particles of matching size, and the new small voids created are in turn filled with smaller particles, and so on. The packing density obviously depends on the particle sizes. In studies with concentrated suspensions, it is found that fluidity of the suspension decreases with an increase in the solid content, but increases with an increase in the packing density at a specified solid content. The aim is to pack as much AP and aluminum particles as possible within a unit volume of propellant.

In studies of uncured propellant rheology, the aim is always to have a propellant with minimum viscosity so that, a defect free propellant casting can be achieved. Developing a model that gives the composition of particulate leading to maximum packing density will therefore be very helpful in obtaining a propellant with minimum viscosity. An optimum size distribution leading to maximum packing density was obtained previously for discrete particle sizes[2]. In the development of the present model, it is assumed that this optimum size distribution is applicable for aluminum and AP particles. Based on this assumption, the model estimates the fraction of each solid component that yields a size distribution which is closest to the optimum distribution. The idea here is to minimize the deviation between the optimum size distribution and the size distribution obtained by the model. Mathematically, this idea can be expressed by a differential equation, and solution to this equation gives the fractions of components. The results predicted by the developed model were tested by viscosity measurements.

MODELING FOR OBTAINING THE FRACTIONS FOR MAXIMUM PACKING

One of the problems in packing of particles is the determination of optimum size distribution for maximum packing density. The early studies were largely focused on the development of optimum size distribution, without paying much attention to the determination of the fractions of multicomponent mixture. The first theoretical approach for the development of optimum size distribution is due to Furnas[2]. His work is valid for multicomponent mixtures with continuous size distribution. The following expression is given by Furnas for the calculation of the ratio, r, (large to small) of the amount of materials on two consecutive screens.

$$r^{(\frac{m-1}{n-1})} = \frac{1}{V} \qquad \text{or} \qquad r = \frac{1}{V^{(\frac{n-1}{m-1})}} \tag{1}$$

where   n: number of component sizes
m: number of screens with size ratio of 1.21
V: compositional average of the void fractions of component sizes

It is clear that the void fraction of each component size should be determined experimentally before beginning to develop the optimum size distribution for maximum packing density. In the studies of packing of multicomponent mixtures, Furnas' work is not the only one giving the optimum size distribution for maximum packing. Yu and Standish[3] proposed a method which was initiated by Fuller and Thompson[4]. This method yields an empirically optimum cumulative particle size distribution for maximum packing. Since it is valid for particles having diameters of tens of millimeters, this method was decided to be improper for the present study.

Determination of fractional volumes of components with different sizes

Furnas' method is a good way of approaching the maximum packing value and optimum size distribution, yet it does not explain how to prepare a mixture that will yield maximum packing. It is all right if one is planning to use 'm' number of fractions and all the fractions have particles which are uniform in size. If this were the case one would take the amounts determined by the ratio 'r' and mix them for a sufficient period of time to get the maximum attainable packing.

When the number of component sizes is not equal to 'm' and they are distributed over a range, however, preparation of mixture becomes somewhat difficult.

Referring to Table 1, 'm' is the number of screens with size ratio of 1.21, 'n' is the number of fractions, and 'O(D)' is the optimum cumulative distribution function.

Table 1 Size analysis of components

Particle diameter	Size distribution of components (cumulative percent undersize)					Optimum size distribution	Size distribution of the model
(D)	$F_1(D)$	$F_2(D)$	$F_3(D)$	$F_4(D)$	$F_n(D)$	O(D)	F(D)
D_1	$F_1(D_1)$	$F_2(D_1)$	$F_3(D_1)$	$F_4(D_1)$	$F_n(D_1)$	$O(D_1)$	$F(D_1)$
D_2	$F_1(D_2)$	$F_2(D_2)$	$F_3(D_2)$	$F_4(D_2)$	$F_n(D_2)$	$O(D_2)$	$F(D_2)$
.		.	.	.	.	.	.
D_m	$F_1(D_m)$	$F_2(D_m)$	$F_3(D_m)$	$F_4(D_m)$	$F_n(D_m)$	$O(D_m)$	$F(D_m)$

For any given number of fractions, x_n (n=1,2,3), there is a corresponding cumulative percent distribution of the mixture which can be written as

$$F(D) = \sum_{n=1}^{3} x_n F_n(D) \tag{2}$$

where $F_n(D)$ is the cumulative size distribution of component 'n' under particle size D (See Table 1). Equation (2) gives the model cumulative percent undersize corresponding to the same screen number in the optimum case. Equation (2) should be equal to $O(D_1)$ for the first screen, to $O(D_2)$ for the second and so on, if there is no deviation from the optimum size distribution. It is clear that the model particle size distribution should be as close to the optimum one as possible for the packing density to have the maximum attainable value. Thus, the difference between the optimum and the model cumulative size distributions corresponding to each screen or, for mathematical purposes, the square of the difference should be determined. Mathematically this can be expressed as

$$S = \sum_{1}^{m} \left[F(D_m) - O(D_m) \right]^2 \tag{3}$$

This equation contains, for this particular situation, three unknowns x_1, x_2, and x_3 which are the fractional volumes to be combined. It is, in general, valid for any number of fractions. To solve Equation (3) for values of x_n's that make the deviation from the optimum size distribution minimum, it is necessary to differentiate the equation with respect to x_n's and set it equal to zero, that is,

$$\frac{\partial S}{\partial x_1} = 0 \; ; \qquad \frac{\partial S}{\partial x_2} = 0 \; ; \qquad \frac{\partial S}{\partial x_3} = 0 \tag{4}$$

Fractional volumes can be obtained by simultaneous solution of the above differential equations with simple mathematical tools.

EXPERIMENTAL

The solid particles used in the experiments are the same as those used in manufacturing of solid propellants. These are aluminum particles and ammonium perchlorate particles with different mean diameters. All particles used in the experiments were purchased from various suppliers. The specifications of the materials are given in Table 2.

Malvern Mastersizer Model MSX was used for particle size measurement. This instrument is able to measure the particle sizes in the range 0.1-600 μ with an accuracy of $\pm$ 2% with respect to volume median diameter. In the determination of void fractions of the solid particles, Heinz Janetzki K.-G. T-5 Centrifuge was used for compressing the particles. The centrifuge has four cylindrical sample units. This centrifuge can be operated at three different rotational speeds of 1000, 3000, and 5500 rpm.

Table 2 Solid materials' specifications

Solid material	Density (gr/cm^3)	Volume mean diameter (micron)	Specific surface area (m^2/gr)	Manufactured by
Aluminum	2.7	10.4	not available	Alcan Toyo
AP	1.95	31.4	0.330	SNPE France
		171	0.140	
		323	0.088	

The void fractions of samples are determined by compressing the particles in the centrifuge. Solid particles to be analyzed are first dried in the oven at 110°C before measurements are taken. Eighty grams of dried sample from one selected size is transferred into the tubes in equal amounts and the top surfaces of the samples are smoothed for the ease of leveling. The tubes are then rotated with a speed of 5500 rpm for 15 minutes. Then apparent volume of particles is determined.

Mixing process is carried out in a 1 gallon Baker Perkins vertical propellant mixer. Control of temperature is critical during the process due to reactions taking place. Hot water is circulated through the jacket of the mixer so that the suspension is kept at a temperature of 65±1°C. First the liquids are mixed to obtain uniform concentration throughout the mixture. Then aluminum and ammonium perchlorate particles are added and mixed for sufficient period of time. Finally the curative is added. When mixing is complete, a sample of propellant slurry is taken for viscosity measurements and the rest is cast for analyzing other properties.

The measuring instrument is a rotational type digital Brookfield Viscometer Model HBTDV-II. T-A spindle is the most suitable one for analyzing the rheology of propellants because other type of spindles does not give accurate results due to shear thinning effect observed around the spindle. For this type of viscometers, the recommended sample container is a 600 ml low form Griffin beaker.

For measuring the viscosity, a 500 ml sample of uncured propellant slurry at 65 °C is transferred into the beaker and put in the water bath which is at 65 °C. The spindle which is previously conditioned at 65 °C is attached to the viscometer. The spindle should be centered in the test fluid and immersed to a marked level of the T spindle (T spindles do not have definite immersion levels marked by producer). The rotational speed is adjusted to the slowest value of 0.5 rpm. Approximately five minutes are allowed for the propellant slurry to reach steady state that is disturbed earlier during the spindle attachment. Viscosity measurements were carried out according to ASTM Standards Designation: D2196-81.

RESULTS AND DISCUSSIONS
Calculation of void fractions

Calculation of void fractions is based on the measured apparent volumes of the component sizes. In the previous studies, method of mechanical packing was very often used[5,6,7]. Method

of centrifugation is employed in this work, because it yields low fraction of voids. To test the repeatability of the method, four measurements are taken for each component size. Standard deviation of the results of the measurements are calculated and given in Table 3.

Void fraction is determined by,

$$V_f = 1 - \frac{\rho_{app}}{\rho_p}$$ (5)

where ρ_{app} and ρ_p are apparent and particle densities, respectively.

Table 3 Void fractions of component sizes

Average Diameter (μ)	Weight (gr)	Vol. (cm^3)	Apparent density (gr/cm^3)	Particle density (gr/cm^3)	Average void fraction	Standard deviation of void fractions
323	20	16.40	1.22	1.95	0.3742	0.0187
171	20	17.35	1.153	1.95	0.4088	0.0044
31.4	20	17.6	1.136	1.95	0.4172	0.0047
10.4	20	13.2	1.520	2.7	0.4382	0.0213
9.22	20	24.83	0.606	1.95	0.5868	0.0067

Calculation of the fractions of the solid component sizes

Using the void fractions of solid components from Table 3, the optimum size distribution can be obtained. The smallest screen size is 0.48μ and the succeeding screens have the sizes 1.21 times that of the preceding screen size. The largest screen size is 683μ and the total number of screens is 39. The number of the solid component sizes for all mixtures is 3. When Equation (3) is differentiated with respect to x_n's, the fractions of the solid component sizes can be determined. Solutions to this equation for different mixtures are given in Table 4. The fractions of the solid components obtained by the model are inserted in Equation (2) and the resulting size distribution (model distribution) for each set is plotted in the same graph with the corresponding optimum size distribution. The graphs for the each set are given in Appendix-A. The deviation from the optimum size distribution can be easily visualized from these graphs. For set No.1, there exists a gap for the particle diameters between 25μ and 150μ indicating that some particles of sizes in this range should be removed to increase the packing density of the mixture. Similar gaps are also present for the other sets. For the sets 2 and 4, some of the particles having sizes between 200μ

and 550μ should be taken out of the mixture. While some particles are to be removed from the mixtures of these sets, some sets require the addition of particles in certain range for maximum packing. Set numbers 3 and 6 are the examples for such a case. The least deviation from the optimum size distribution is observed for set No 5. From the plots of the size distributions for the all mixtures, it can be said that among the available sets, set No 5 contains the particles which are most suitable for maximum packing density. The packing densities for the remaining sets can be ordered in decreasing order as: No 3, No 2, No 4, No 1, and No 6. The most deviation is observed for the sets 1 and 6. For this reason, these sets were not prepared for rheological measurements, since they would exhibit high viscosities.

Table 4 Model results for the fractions of the solid components

Set	Volume fractions of sizes				
No	9.22μ	10.4μ(Al)	31.4μ	171μ	323μ
1	0.01	0.14	0.85	-	-
2	0.22	0.14	-	0.64	-
3	0.32	0.14	-	-	0.54
4	-	0.14	0.27	0.59	-
5	-	0.14	0.38	-	0.48
6	-	0.14	-	0.86	0.00

Results of rheological measurements

The thixotropic behavior of the propellant is best analyzed when the measurements are taken at 0.5 rpm, because the duration of the experiment is longer at this value. Figure 1 shows the thixotropic behavior of the propellant slurry with 75% vol. total solid content. Muthiah et al.[8] observed the same oscillatory behavior as in Figure 1 for the time range between 160 and 200 min. but the overall effect was to increase the viscosity with time which is caused by cure. The oscillatory behavior of Figure 1 may be attributed to the break down of the agglomerates by the effect of shear.

The last readings taken at each speed for all propellants are tabulated in Table 5. Among the results given in this table, those which are recorded at 2.5 rpm are used to compare the viscosities. It is known that best characterization of flow behavior is made with the results obtained at low shear rates[9]. Another restriction here is that the applied torque which is
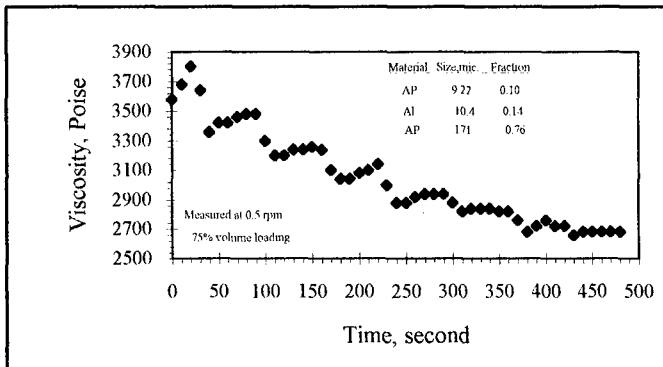
Figure 1 Time dependency of the propellant slurry viscosity

Table 5 The results of the viscosity measurements of the propellant slurries at different rpm's

Set No	Size comp.	Fraction of fine AP	Viscosity (Poise)									
			0.5rp	Torque	1rpm	Torque	2.5rpm	Torque	5rpm	Torque	10rpm	Torque
	Al	0.10	2680	8.4	2160	23.4	1810	28	1660	51.5	1590	97.7
2	9.22μ	0.24	864	2.7	800	5	776	12	768	24.1	784	48.8
	171μ	0.40	1380	4.3	1260	7.8	1230	19.2	1290	40.2	1410	87.8
	Al	0.04	1250	3.7	1010	6.2	824	12.9	720	22.6	685	41.5
3	9.22μ	0.15	704	2.1	640	3.9	564	8.9	540	17.1	523	32.8
	323μ	0.33	704	2.1	656	4.1	648	10	668	20.9	694	43.4
		0.50	1470	4.5	1380	8.6	1350	21.1	1430	44.5	1540	96.2
	Al	0.10	3520	9.7	2590	16.5	1760	26.6	1260	36.3	832	48.8
4	31.4μ	0.27	1180	3.7	1090	6.8	1000	15.6	966	30.2	928	58.2
	171μ	0.40	1060	3.3	992	6.2	960	15	950	29.7	936	58.8
		0.52	1220	3.8	1170		1150	18	1160	36.4	1170	73
	Al	0.15	608	1.9	512	3.3	472	7.4	448	14.2	429	27.1
5	31.4μ	0.30	544	1.7	480	3	448	7	442	13.9	438	27.2
	323μ	0.55	832	2.6	816	5.1	824	13	832	26.1	848	53.3
		0.40	544		528		504		506		507	

proportional to the applied shear stress should be around 10% for the Brookfield Viscometers to be used efficiently[9]. Approximately 10% torque is observed at the 2.5 rpm for all propellants (see Table 5) and this rpm value was used for comparison.

Effect of fractional variations of components

The change in the viscosity of a slurry with respect to the changes in the fractions of the components in the total solids is better understood by using the concept of packing fraction. For this, the relation derived by Maron and Pierce as given by Gupta[10] is used.

$$\eta_r = (1 - \frac{\varphi}{\varphi_p})^{-2} \qquad\qquad (6)$$

In Equation 6, η_r is the relative viscosity defined as the ratio of the suspension viscosity to the suspending medium viscosity, φ is the total volume fraction of solids in the slurry, and φ_p is the maximum packing fraction of the system at a specified total solid content. According to this equation, viscosity is a function of the total volume fraction of the solids and the maximum packing fraction at this loading level, i.e., $\eta_r = f(\varphi/\varphi_p)$. The relative viscosity is expected to decrease with the increasing maximum packing fraction of the system the loading level being constant.

Figure 2 Effect of fraction of the fines in the total solids on the viscosity of the propellant slurry (set numbers are given in Table 5)

Figure 2 shows the effect of compositional variation on the relative viscosity of the propellant slurry. It is seen that the relative viscosities of both propellant slurries first decrease with increasing concentration of the fines and then increase with further increase in the fines concentration showing minima. A second order polynomial trendline was inserted to determine this minimum viscosity clearly. It can be deduced from the Figure 2 that packing fraction (φ_p) of the solids mixture (set No 2) increases until the concentration of the fines (9.22μ) becomes 0.28. The viscosity of the slurry containing these particles decreases because (φ/φ_p) decreases. At the point where the fraction of the fines is 0.28, the packing fraction of the system reaches its maximum attainable value and (φ/φ_p) becomes minimum. At this point φ_p is equal to φ_{max}. After this point, φ_p begins to decrease with further increase in the fraction of fines. The relative viscosity at maximum packing condition is equal to 12 for set number 2.
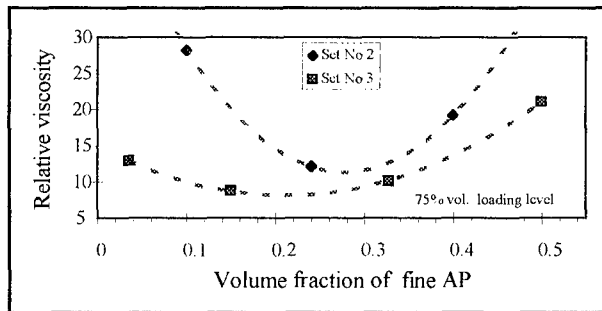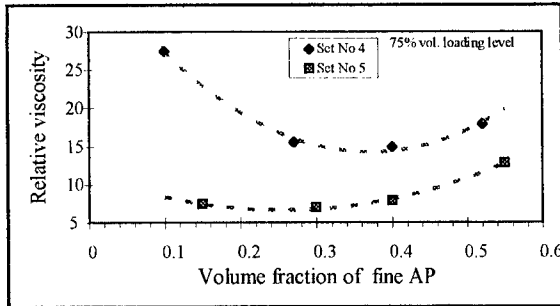
Figure 3 Effect of fraction of the fines in the total solids on the viscosity of the propellant slurry (set numbers are given in Table 5)

At maximum packing condition, the fractions of the solid components and the corresponding minimum viscosities can be determined for the other propellant slurries similarly. For the other propellants, the variation in the viscosity with respect to the concentration of fine AP is given in Figures 2 and 3. The minimum relative viscosities for the propellants for sets No 3, No 4, and No 5 are 8.8, 15, and 7, respectively. All of these are the minimum viscosities of each set. Among these, the propellant with minimum viscosity, that is, the minimum of the minimums is selected as the most processable one. The propellant consisting of 31.4μ and 323μ AP particles and 10.4μ aluminum particles was found to have maximum fluidity (minimum viscosity) at the fines fraction of 0.3.

COMPARISON OF MODEL AND EXPERIMENTAL RESULTS

Volume fractions of the solid components, for maximum packing, determined by modeling and by viscosity measurements (experimental) are given in Table 6. The last column shows the deviation of the model from the experimental results. The deviation was calculated with respect to the fractions of the coarse AP particles of the minimum viscosity propellant, considering that the experimental results are correct. A maximum of 18% deviation from the experimental results was observed. Although this is acceptable in engineering applications, the reasons should be clarified from a scientific point of view.

The solid particles used in propellant manufacturing have irregular shapes except for the aluminum powder. However, Furnas' method that gives the optimum particle size distribution was developed for spherical particles. This can be considered as one of the possible reasons.

Table 6 Comparison of the model results with the experimental findings

Set No	Volume fractions of sizes										Percent deviation of model
	9.22µ		10.4µ		31.4µ		171µ		323µ		
	Model	Exp	Model	Exp	Model	Exp	Model	Exp	Model	Exp	
2	0.22	0.28	0.14	0.14	-	-	0.64	0.58	-	-	10
3	0.32	0.2	0.14	0.14	-	-	-	-	0.54	0.66	18
4	-	-	0.14	0.14	0.27	0.36	0.59	0.50	-	-	18
5	-	-	0.14	0.14	0.38	0.30	-	-	0.48	0.56	14

The void fractions which are the inputs for the optimum size distribution were determined by dry mixing of the particulate. Dry mixing may yield inaccurate void fraction measurements, since the solid particles can not be perfectly mixed in dry conditions[5]. The particles were also mixed in a liquid (n-Heptane) in which the particles are insoluble, but this method gave higher void fraction than that obtained by dry mixing due to bridging that formed during the drying of n-Heptane. Therefore this method is not suitable for the determination of void fractions for this study.

Similar studies for maximum packing were performed using particles with very large diameters as compared to the particles used in this study[3,5]. Furnas' method was previously tested[11] only for the particles with large diameters (in the order millimeters), such as sand, aggregates, etc. On the other hand, the maximum particle diameter in this study is only 600µ. Although no restriction was given by Furnas in terms of particle diameter, the deviation of the model may also be due to this reason.

The diameter ratio (large to small) of the two consecutive sizes for the optimum distribution was taken as 1.41 by Furnas. In this study, it was taken as 1.21. Use of this ratio simplifies the calculations because the particle diameter measuring instrument gives the distribution according to this ratio. Different values of this ratio could be tested to see its effect on the deviation of the model. This requires a parametric study and is out of the scope of this study.

CONCLUSIONS

The method of centrifugation is a good way of determining the void fraction, because it yields repeatable results. The standard deviations of the measurements obtained by this method are given in Table 3.

The HTPB based uncured propellants showed time dependent (thixotropic) behavior. The time dependency of the uncured propellants showed an oscillatory behavior due to the breakdown of agglomerates.

Among the four candidate propellants, the one consisting of particles with mean diameters of 10.4μ, 31.4μ and 323μ was found to yield minimum viscosity. This minimum viscosity was observed when the fraction of the sizes with respect to total solids is 0.1412, 0.300 and 0.5588 respectively.

The results obtained by the model showed a maximum of 18% deviation calculated with respect to the fraction of the coarse AP of the minimum viscosity propellant. This deviation is acceptable in engineering applications.

REFERENCES

1 . Kuo K.K., Summerfield, M, Fundamentals of Solid-Propellant Combustion., Progress in Astronautics and Aeronautics, vol. 90, AIAA, New York, (1984).

2 . Furnas, C.C., "Grading Aggregates I-Mathematical Relations for Beds of Broken Solids of Maximum Density", Industrial and Engineering Chemistry, 23, 1052, (1931).

3 . Yu, A.B., Standish, N. A., "Study of the Packing of Particles with a Mixture Size Distribution", Powder Technology, 76, 113, (1993).

4 . Fuller, W.B., Thompson, S.E., Trans. Am. Soc. Civ. Eng., 59, 67, (1907), cited in Yu and Standish (1993).

5 Messing, C.L., Onada, G.Y., "Inhomogeneity- Packing Density relations in Binary Powders-Experimental Studies", Journal of the American Ceramic Society, 61(7-8), 363, (1978).

6 McGeary, R.K., "Mechanical Packing of Spherical Particles", Journal of the American Ceramic Society, 44(10), 513, (1961).

7 Sohn, H.Y., Moreland, C., "The Effect of Particle Size Distribution on Packing Density", The Canadian Journal of Chemical Engineering, 46, 162, (1968).

8 . Muthiah, R.M., Manjari R., Krishnamurthy, V.N., Gupta, B.R., "Effect of Temperature on the Rheological Behavior of HTPB Propellant Slurry", Polymer Engineering and Science, 31(2), 61, (1991).

9 Manual of Brookfield Viscometer, Manual No. M/92-161-E593

10 . Gupta, R.K., Seshadri, S.G., "Maximum Loading Levels in Filled Liquid Systems", Journal of Rheology, 30(3), 503, (1986).

11 Anderegg, F.O., "Grading Aggregates II-The Application of Mathematical Formulas to Mortars", Ind. Eng. Chem., 23, 1058, (1931).
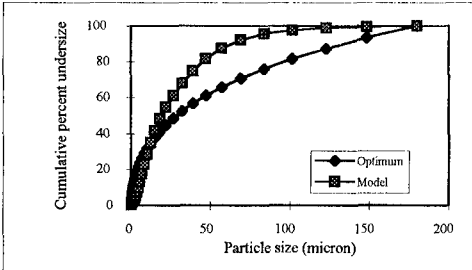
Figure A.1. Comparison of model and optimum
distributions for Set No 1
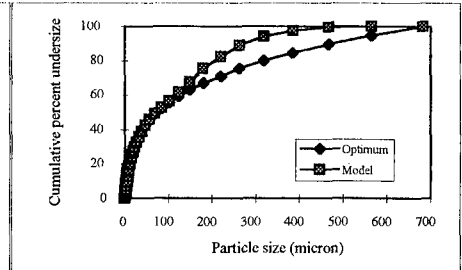
Figure A.4. Comparison of model and optimum
distributions for Set No 4
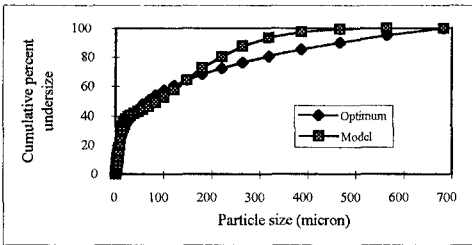
Figure A.2. Comparison of model and optimum
distributions for Set No 2
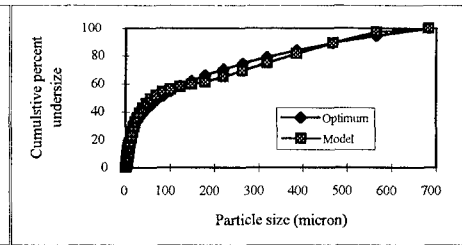
Figure A.5. Comparison of model and optimum
distributions for Set No 5
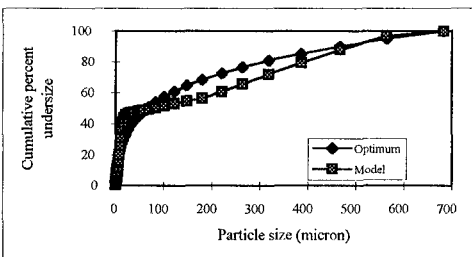
Figure A.3. Comparison of model and optimum
distributions for Set No 3
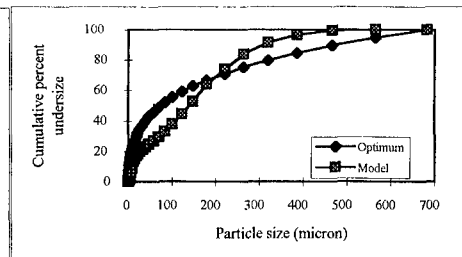
Figure A.6. Comparison of model and optimum
distributions for Set No 6

INFLUENCE OF N,N' —DINITROPIPERAZINE ON CHARACTERISTICS OF COMPOSITE MODIFIED DOUBLE BASE PROPELLANT

Pan Wenda, Chang Jingxiang

XI'AN Modern Chemistry Research Institute

P.O.Box 18 XI'AN 710061 P.R. CHINA

Abstract

In this paper formulations and manufacture of the composite modified double base propellant (CMDBP) containing N,N'-Dinitropiperazine(DNP) were described. Influence of DNP on specific impulse, burning rate, pressure exponent etc. of CMDBP were researched. It is shown that when DNP is added in the propellant, the specific impulse almost does not change or only dropped a little, the burning rate is decreased and the pressure exponent of burning rate is improved.

Symbol

NC---Nitrocellulose

NG---Nitroglycerine

DINA---Diethanolnitramine dinitrate

C_2---Methyl centralite

V---Vaseline

DNP---N,N'-Dinitropiperazine

RDX---Cyclotrimethylenetrinitramine

Is---Specific impulse (N · s / Kg)

Tc---Flame temperature at constant pressure (K)

α---Oxygen coefficient

ω---Specific gas (L / Kg)

u---Burning rate (mm / s)

n---Pressure exponent of burning rate

δ---Pressure range of plateau and mesa burning

n_m---Pressure exponent of burning rate at mesa burning zone

1. Introduction

It is important task for the propellant researcher that improving the combustion characteristics of propellant.In order to reduce the burning rate of double base (DB)and composite modified double base (CMDB) propellants the inert material is usually used and for the purpose of improving the pressure exponent of burning rate the catalyst is generally used . Because the inert material and the catalyst are non—energetic materials, the energy of propellantused them is greatly decreased . In this paper DNP which is energetic material, is used for decreasing the burning rate and improving the pressure exponent of burning rate of DB and CMDB propellants.

2. Properties of DNP

The properties of DNP are arranged in table 1. Because there are two-N —NO$_2$in molecule of DNP, it is energetic material. It can be observed from the table 2 that theoretical specific impulse of DNP at 9.8MPa is 1969.2N • s / Kg, specific gas of DNP is 1267.3L / Kg, impact and friction sensitivities of DNP are notably small, its stability of heat is good,and it is insolvable in water. Because of above properties of DNP, DNP is suitable for DB and CMDB propellants manufactured by solventless extruded processing.

3. Formulations and manufacture of propellant

It can be observed from the table 2 that there are three types of propellant formulations in this paper. The first type is No.1～No.6 in which the content of DNP is increased gradually, but the total content of NC and DINA is decreased gradually and for the sake of manufacture solvent ratio of formulation (NG+DINA+C$_2$/ NC) is increasedgradually .The second type is No.11～ No.15 in which DNPis substituted gradually for RDX. The third type is No.21～ No.26 in which DNP is substituted gradually for NC.

A solventless process is used to manufacture the propellants.

4. Measured method of burning rate and results

The burning rate of propellants is measured with a chimeney type strand burner which is pressurized with nitrogen. The size of the propellant samples is 5mm in diameter and 150mm in length.

The samples are coated by polyvinyl alcohol solusion in water.

Measured burning rates are drawn in figure 1 ~ 3 and exponent formulas of burning rate are calculated by mean square regression and are listed in table 3.

5. Discussion

5.1 Influence of DNP on energy of propellant

The theoretical energy properties of propellants were calculated by minimum free energy method and were show in table 2.

It can be observed from No.21 ~ No.26 in table 2 that theoretical specific impulse almost does not change when DNP is substituted for NC.

When 1% DNP is substituted for 1% RDX (see No.11 ~ No.15 in table 2), theoretical specific impulse only dropped 0.25% (6.1N • s / Kg) on an average.

When 1% DNP is added in DB propellant which has higher energy (see No.1 ~ No.6 in table 2), theretical specific impulse only dropped 0.1% (2.2N • s / Kg) on an average.

Hence it appears clear that influence of DNP on energy of DB and CMDB propellant is small.

In addition the flame tempreture is reduced and the specific gas is raised (see table 2) due to using DNP.

5.2 Influence of DNP on burning rate

It can be observed from the figure 1.2 and 3 that the burning rate of propellant is reduced due to adding DNP and the more the content of DNP, the lower the burning rate of propellant.

5.3 Influence of DNP on pressure exponent of burning rate

The pressure exponent of burning rate of propellants which do not contain DNP (see No.1, No.11 and No.21 in the figure 1,2 and 3) is approximately equal to zero in some pressure zone and the mesa burning ($n < 0$) is not obvious. But the pressure exponent of burning rate of the propellants containing DNP is negative in some pressure zone and the mesa burning is obvious (see figure 1,2,3 and table 3).

It can be observed from table 3 that the pressure range of plateau and mesa burning (representing by δ) is expanded due to adding DNP. For example δ of No.1 which does not contain DNP is 6MPa (10 ~ 16MPa), and δ of the No.3 containing 10% DNP is ex-

panded into 10.5MPa (10~20.5MPa).

It can also be observed from table 3 that when the content of DNP is smallerthan 20% or equal to 20%, the pressure exponent of burning rate of propellant at mesa burning zone (representing by n_m) is reduced with increasing the contentof DNP in the propellant. For example, for No.1 which does not contain DNP. $n_m$is equal to -0.03, for No.3 containing 10% DNP, $n_m$is equal to -0.20. for No.4 containing 15% DNP, $n_m$is equal to -0.37 and for No.5 containing 20% DNP, $n_m$is equal to -0.41.

Because the oxygen coefficient of DNP is only equal to 0.3333 (see table 2),during combustion of propellant contained DNP a great number of carbon black which is catalyst of plateau and mesa burning are produced. This factor is possibe reason of improving pressure exponent of burning rate of propellants containing DNP.

6. Conclusion

From above calculation, experimental result and discussion fol-low conclusion are abtained:

1) When DNP is added in DB and CMDB propellants, the flame temperature is decreased. the specific gas is increased and the specific impulse almost does not change or only dropped a little.

2) The burning rate is decreased and the pressure exponent is improved when DNP is added in DB and CMDB propellant.

Reference
1. Xi'an Modern Chemistry Research Institute. Propellant and Explosive Handbook 1987.4.(Chinese)

Table 1. Properties of DNP [1]

Molecular formula	$C_4H_8N_4O_4$
Structure formula	$O_2N-N{\Large\langle}\!\!\begin{array}{l}CH_2-CH_2\\CH_2-CH_2\end{array}\!\!{\Large\rangle}N-NO_2$
Molecular weight	176
Character	White crystal, solvable easy in nitric acid and sulphuric acid. Solvable in acetone, ethanol acetate and dioxane, insolvable in water, ethanol, chloroform, benzene and dichlorine ethane
Density	$1.63g / mm^3$
Melting point	$217.5 \sim 218.5℃$
PH	$5 \sim 6$
Combustion heat	$-15188KJ / Kg$
Formation heat	$\triangle H_f = -313.8KJ / Kg$ $= -55.2KJ / mol$
Activate energy of decompose	$E = 109.4KJ / mol$ $A = 108.47 / s$
Impact sensitivity	0% (hammer 10Kg, high 25cm)
friction sensitivity	0% (angle 90 ° at 3.9MPa)
Stability of heat	1)differential thermal analysis: endothermic peak at 216℃, maximum exothermic peak at 253℃ 2) no change for the weight at 100℃ ,96h

Table 2 Compositions and specific impulse at 9.8MPa

NO	NC	NC	DINA	C_z	V	DNP	RDX	other*	I_s (N.S/kg)	T_c (K)	α	ω L/kg
No1	57.2	26.5	10.5	1.5	0.5	0	0	3.8	2329.1	2641.0	0.6375	897.1
No2	53.2	26.5	9.5	1.5	0.5	5	0	3.8	2319.3	2586.5	0.6203	913.9
No3	49.2	26.5	8.5	1.5	0.5	10	0	3.8	2309.5	2532.5	0.6035	930.5
No4	45.5	26.5	7.2	1.5	0.5	15	0	3.8	2298.7	2476.6	0.5868	947.3
No5	42.0	26.5	5.7	1.5	0.5	20	0	3.8	2285.9	2419.7	0.5703	964.1
No6	38.5	26.5	4.2	1.5	0.5	25	0	3.8	2273.2	2363.5	0.5541	980.9
No11	42.0	26.5	5.7	1.5	0.5	0	20	3.8	2408.5	2823.9	0.6473	893.0
No12	42.0	26.5	5.7	1.5	0.5	5	15	3.8	2379.1	2724.2	0.6265	910.5
No13	42.0	26.5	5.7	1.5	0.5	10	10	3.8	2349.7	2622.9	0.6068	928.2
No14	42.0	26.5	5.7	1.5	0.5	15	5	3.8	2318.3	2493.4	0.5830	991.0
No15	42.0	26.5	5.7	1.5	0.5	20	0	3.8	2285.9	2419.7	0.5703	964.1
No21	38.5	26.5	4.7	1.5	0.5	0	25	3.3	2435.0	2881.6	0.6524	892.8
No22	37.5	26.5	4.7	1.5	0.5	1	25	3.3	2434.0	2872.8	0.6488	896.0
No23	36.5	26.5	4.7	1.5	0.5	2	25	3.3	2434.0	2864.0	0.6452	899.3
No24	35.5	26.5	4.7	1.5	0.5	3	25	3.3	2433.0	2855.2	0.6416	902.7
No25	34.5	26.5	4.7	1.5	0.5	4	25	3.3	2432.0	2846.3	0.6380	905.8
No26	33.5	26.5	4.7	1.5	0.5	5	25	3.3	2331.1	2837.5	0.6344	909.2
DNP	0	0	0	0	0	100	0	0	1969.2	1529.6	0.3333	1267.3

* Catalyst and burning stabilizer

Table 3 Burning rate formula

No	Burning rate formula		Pressure for n≤0 MPa
	for n≈0	for n<0	
1	$u=19.21\ P^{0.0003}$ (10~16MPa)	$u=20.96P^{-0.03}$ (11.5~14.5MPa)	10~16
3	$u=16.05\ P^{0.05}$ (10~13MPa)	$u=30.97P^{-0.20}$ (13~20.5MPa)	10~20.5
4	$u=15.11\ P^{0.07}$ (10~11.5MPa)	$u=45.28P^{-0.37}$ (11.5~22MPa)	8~22
5	$u=15.38\ P^{0.02}$ (10~14.5MPa)	$u=50.03P^{-0.41}$ (14.5~22MPa)	10~22
6	$u=13.28\ P^{0.04}$ (11.5~16MPa)	$u=37.49P^{-0.32}$ (17.5~22MPa) $u=89.94P^{-0.61}$ (20.5~22MPa)	11.5~22
11	$u=18.00\ P^{0.03}$ (11.5~14.5MPa)		11.5~14.5
13	$u=17.32\ P^{0.01}$ (11.5~14.5MPa)	$u=34.39P^{-0.25}$ (14.5~20.5MPa)	11.5~20.5
15	$u=15.76\ P^{0.01}$ (10~16MPa)	$u=59.74P^{-0.47}$ (16~22MPa)	10~22
21	$u=15.48\ P^{0.04}$ (11.5~13MPa)		11.5~13
23	$u=13.46\ P^{0.008}$ (8~10MPa)	$u=20.06P^{-0.09}$ (10~13MPa)	8~14.5
76	$u=14.03\ P^{-0.05}$ (8~11.5MPa)	$u=70.58P^{-0.11}$ (11.5~14.5MPa)	8~16
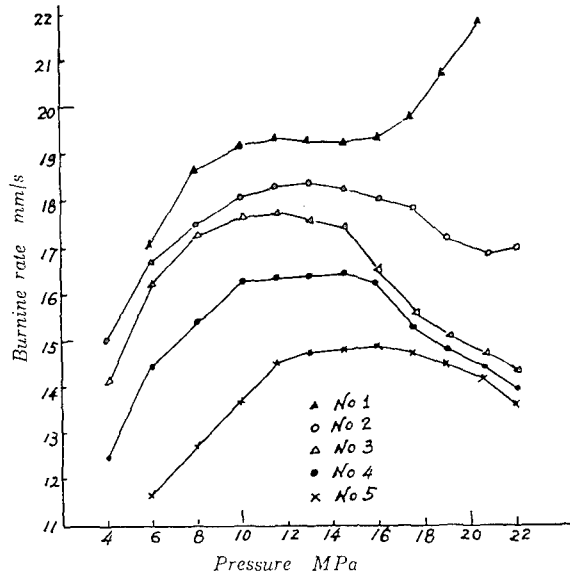
Figure 1 Influence of DNP on the burning rate
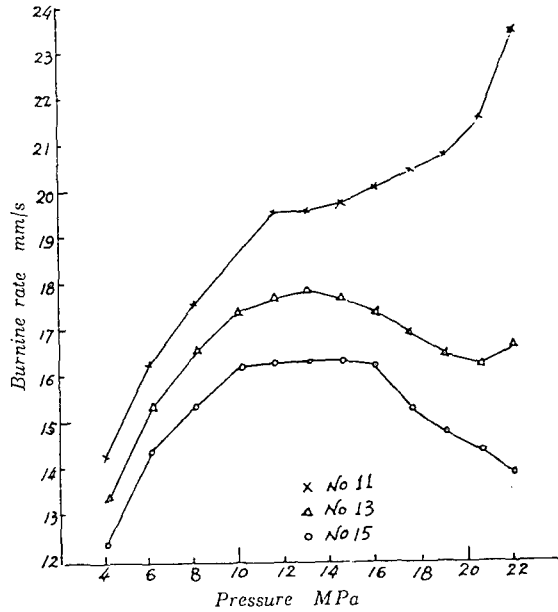
Figure 2 Influence of substitution of DNP for RDX on the burning rate
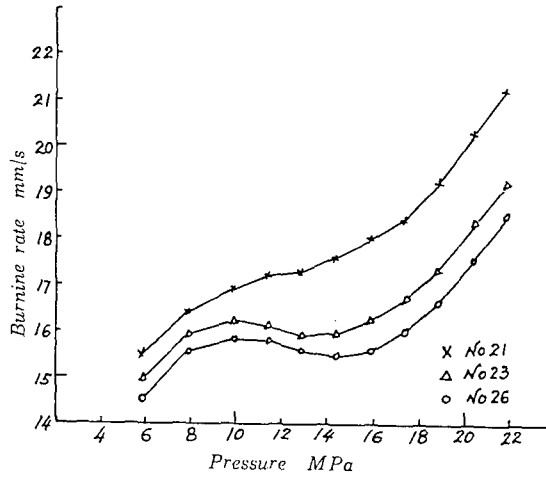
Figure 3 Influence of substitution of DNP for NC on the burning rate

PRELIMINARY STUDY OF BUNENA GUN PROPELLANTS

Lu An–fang   Shen Qiong–hua   Liao Xin   Bao Guan–ling
Xian Modern Chemistry Research Institute
P.O. Box 18, Xian, 710065, P.R.China

Abstract

BuNENA is an excellent liquid nitrocellulose plasticizer which has good physicochemical characteristics. Therefore BuNENA used as ingredient of propellants may overcome the problems that RDX and DINA can't be incorporated into propellant formulations in a large quantity because of decreasing mechanical performance and / or tendency to crystallize out of colloided nitrocellulose matrixes of propellants. Furthermore, RDX and HMX added into propellant formulations may result in exponent shifts of burning rate.

The purpose of this paper is to demonstrate some performances of BuNENA gun propellants by theoretical calculation, technological processes, experimental measurement as well as the firing in the gun.

These results indicate that BuNENA can formulate a variety of gun propellants in combination with conventional propellant ingredients. BuNENA is especially suitable for formulation of gun propellants with low temperature and high impetus and for the use as deterrent.

Introduction

DINA was an excellent NC plasticizer and was sealed up for use in a Navy flashless gun propellant known as Albanite in the United States of America during World War II (ref. 1).

In 1960s, DINA was also scaled up for use in some rocket propellants in China. However it didn't fit for the application in gun propellants because of tendency to slowly crystallize out of colloided NC matrixes of gun propellants during storage or after manufacture. This tendency greatly affected the mechanical and combustion performances of the propellants unless the content of DINA was less than 10%. Similarly, both HMX and RDX had good thermochemical characteristic as well and could be used to formulate various gun propellants with low flame temperature and high impe-

tus. However solid filler (RDX or HMX) can't be enoumously incorporated into propellant formulations because of decreasing mechanical performance. In addition, the propellants with RDX or HMX have high pressure exponent of burning rate and / or pressure exponent shifts over pressure region encountered in the gun.

NENAs contain both a nitrato group and a nitramino group, and remain their good thermochemical and excellent plastic characteristics for NC. For this reason, the interest of the military community in NENAs compounds in recent years has greatly increased [ref. 2, 3].

From the view point of energy, MeNENA is the best compound among the RNENA family, because it has high proportion of H / C and O / C as well as high nitrogen content, however the melt point or freeze point of MeNENA and EtNENA are $38\sim$ $40°C$ and $4\sim5.5°C$ respectively. They have still probability of the tendency to crystallize out of propellant matrixes.

As judged by molecular structure, the longer the carbon chain in the alkyl, the lower the corresponding melt or freeze point. Previous literatures [ref. 4] have indicated that BuNENA is a pale yellow oil with $-27\sim-24°C$ of freeze point and $-74.25°C$ of glass transition temperature, and an excellent NC plasticizer. While the neat BuNENA is noticeably more volatile than NG, however once mixed with NC, the volatility drops to half that of the NG mixture. Impact, friction and electrostatic sensitivities of BuNENA and the propellant mixtures containing 60 and 70% RDX are characterized as excellent. The thermal stability of unstabilized BuNENA was also determined to greatly exceed that of NG stabilized with 1% 2-nitrodiphenylamine at temperatures up to $70°C$. Therefore, on the basis of aforementioned analysis the BuNENA may be predicated about the best member among RNENA family when they are used as energetic plasticizer in neat form in combination with conventional propellant ingredients.

In order to demonstrate their performance and feasibility of BuNENA propellant, the BuNENA propellants have been prepared by various type of processes and some of their performances have been measured.

Results and Discussion

For the sake of understanding the action of BuNENA as ingredient in the formulation of propellants, the following gun propellants fitted in requirements for

different guns have been formulated. Some performances of these propellants have been theoretically calculated and experimentally measured.

1. The propellants with low flame temperature or erosiveness

Most mortar propellant charges were made up of double base propellants containing NG (at concentrations about 40%), because they worked under the low pressure and in the short gun barrels. The processability of these propellants had shortcoming, since fire or combustion was ready to happen during rolling process, especially during solventless rolling process.

The flakes of powder were sticked each other at higher temperature, but the flakes were too fragile at low temperature. It was probable that the minus rounds were produced at high temperature and disastrous pressures appeared in the bore of gun at low temperature, while they were fired in the mortar. On the meanwhile the temperatures of barrel well rose sharply during firing, so that the fire rate was greatly limited to increase, because the flame temperatures of these double base propellants were too high. Therefore the development of the propellants with low temperature for mortar gun was tried abroad in order to increase the firing rate.

The theoretical calculation shows that BuNENA is an energetic plasticizer with low temperature and larg gas volume, and can significantly decrease adiabatic flame temperature without marked decreasing of it's energy if NG is replaced partially by BuNENA in the S—11 mortar propellant (see Table 1).

The Table 2 shows the compositions and some performance of Bu—1 and Bu—2 propellants in which BuNENA partially replaces NG in SF—13 and S—11 conventional propellants respectively. As compared with the S—11 mortar propellant, after replacement for NG not only the Bu—2 propellant has markedly improved machanical performance but is superior to the SF—13 propellant. Although the burning rate of the Bu—2 propellant is decreased a little and the exponent is increased slightly, it doesn't exceed 1.0. The problem about that the BuNENA propellant burns out in the bore of mortar may be resolved by decreasing the web of grain because of the apparently enhanced NC plasticization of BuNENA as compared to NG. After replacement of DNT and DBP in SF—13 propellant by BuNENA, the energy of obtained Bu—1 propellant is increased markedly. As contrasted with above—mentioned situation, the burning rate is increased and the exponent is decreased.

The data of chemical stability measured by 120℃ pressure method point out that the turning point and the slope of the Bu−2 propellant is 210 min and 0.39 mmHg / min respectively. It's markedly superior to the S−11 propellant (>150 min and < 0.60 mmHg / min) and corresponding to the SF−13 propellant (>220 min and < 0.5 mmHg / min).

The American Navy has developed and equipped the NACO and NOSOL318 propellants with low flame temperature one after another in 1950s and 1970s respectively. While BuNENA plasticizer replaces expensive TMETN, not only the cost of the propellant can be greatly decreased but the increment over 5% of the impetus can be obtained at the equivalent flame temperature. Therefore these BuNENA propellants with low erosiveness fit into the use of high firing rate gun (see Table 3).

2. The propellants with high impetus and low flame temperature

Since 1970s the propellants which have same energy as M30 propellant and same mechanical performance as conventional double base propellants have been exploring abroad. Though the nitramine propellants were probable to meet this requirement, but there was a problem about the pressure exponent shifts over the pressure region encountered in the gun.

Therefore three kinds of propellants processed by the solventless procedure have been formulated. The composition and some observed performance of these propellants are shown in Tables 4 and 5. The results confirm that the propellants which are made of the mixture with BuNENA and NG as NC plasticizer can meet above−mentioned requirements. The impact strength of the propellant at −40℃ can compare with that of SF−13 propellant at higher impetus than M30 propellant (1128 J / g) and the pressure exponent shifts aren't observed. The erosiveness of these propellants can compare with the M30 propellant and are greatly superior to the TG115 mixed nitroester propellant with the equivalent energy.

3. The propellants deterred with BuNENA

It was recommended that BuNENA was used as a deterrent of propellants abrosd as early as 1980s. In order to inspect the characteristics of propellants deterred with BuNENA, 4 / 7 single base propellant as blank has been deterred with different amounts of BuNENA and some performances of the deterred propellants have been calculated and measured. The data shown in Table 6 indicate that with fundamentally

same impetus there will be less flame temperature with more amount of deterrent. This relationship is the same as that between calculated flame temperature and erosiveness. However, erosive amount isn't proportional to calculated flame temperature. It's possible for the reason that calculated flame temperature only characterizes an average effect but doesn't characterize the effect on the surface of grain. The results also show that these deterred propellants are difficult to ignite and their delay times (t_{20}) are extended simultaneously. Initial burning rates become so slow that pressure exponents of burning rate are increased obviously. These results conform to the characteristics of the deterred propellents clearly.

In order to understanding of interior ballistic performance and their stability, the firings in the 14.5 mm gun have been performed. The results shown in Table 7 point out that the muzzle velocity of 4 / 7 propellant deterred with 5% BuNENA is 13.1 m / s (1.37%) more than one for the 4 / 7 propellant as blank while bore pressure is slightly decreased. In addition, when the amount of propellant deterred with 5% BuNENA is 3.0 g (9.4%) less than the amount of 5 / 7 service propellant, the muzzle velocity of service round can be reached fundmentally as well. On the understanding that amounts of deterrent and deterred propellant are extended to 7% and 31 g respectively, muzzle velocity of projectile has the increment of 19 m / s (2%) as compared to one with 5% and 29 g. Though the amount of deterrent is expanded to 9%, more increment of velocity can't be obtained through an increment of powder amount because more amount of powder are unable to contain in the cartridge case of 14.5 mm gun due to expanded volume of grain after deterring.

As compared with 5 / 7 propellant of service round when firing of 4 / 7 propellant deterred with 7% BuNENA, under the condition of less powder amount, it's possible to that interior ballistic characteristic of service propellant is reached or excessed probably. The results shown in Table 7 point out that maximum increment of muzzle velocity can reach up to over 22 m / s.

If selected web of grain and deterrent amount are optimized then propellant deterred with BuNENA is able to markedly increase muzzle velocity of conventional 14.5 mm cartridge.

In order to inspect stability of deterred propellants, same lot of propellants deterred with 7% BuNENA had been stored under natural environment for half an year and their firings had been performed in the same gun. The results point out that ballistic performance for the propellant deterred with 7% BuNENA isn't changed obviously

after storage and the problem on physical stability has not been found. As contrasted with the propellant deterred with 7% BuNENA the propellant deterred with 9% BuNENA is indicative of instability, because ascension of bore pressure and fall of muzzle velocity arise evidently after storage.

Conclusion

Based on above preliminary study of gun propellants containing BuNENA, the following conclusions are made.

1. Calculated and experimental performances of propellants containing BuNENA have proved that the BuNENA is an excellent ingredient and provides a low risk route to higher energy in combination with conventional ingredient;

2. BuNENA is able to produce low combustion gas molecular weight products. The propellants formulated with BuNENA have this characteristic made higher energy and lower flame temperature level possible, and specially fitted into use in high firing rate gun;

3. Due to BuNENA readily plasticizes NC and other cellulosic polymer as compared with conventional plasticizer, therefore it is probable to be potentially an energetic deterrent. Experimental results verify that the propellants deterred with BuNENA clearly decrease flame temperature, specially the flame temperature during initial combustion of grain under condition that the level of original energy is remained fundamentally. Under optimal condition deterred propellants which replace conventional propellant can distinctly increase muzzle velocity of the 14.5 mm projectile, at least can obtain an increment $2\sim3\%$ of velocity;

4. The firing results after storage for six months show that the propellants deterred with BuNENA have good stability of ballistics. When the deterrent amount is in excess, not only the amount of propellant can't be increased in cartridge case further, but the ballistic performances become to bad and the problem of instability begins to happen. So far as 4 / 7 propellant as blank is concerned, the amount of BuNENA deterrent must not exceed 7% of total propellant amount.

Reference

1. Dupont Report, "Flashless Powder for Navy Cannon", NDRC / OSRD Report 3726, June 3, 1944.
2. Dr. R. A. Johnson and Dr. John J. Mullay, "Stability and Performance Characteristics of NENA Materials and Formulations", Joint International Symposium on Energetic Material Technology, New Orleans, Louisianausa, October 5–7, 1992, pp.116–121.
3. R. L. Simmons, "Thermochemistry of NENA Plasticizers", 25th Annual ICT Conference, Karlsruhe, Germany, June, 1994, pp.10–1～10–10.
4. P. A. Silver, et al, "BuNENA Gun Propellant", 1981 JANNAF Propulsion Meeting Vol. 2, pp.515–530.

Glossary

Term	Definition
BuNENA	Butyl nitrato ethylnitramine
DBP	Dibutyl phthalate
DINA	1,5–Dinitrate–3–nitrazapentane
DNT	Dinitrotoluene
% N	% Nitrogen
NC	Nitrocellulose
NENAs	Nitrato ethyl nitramines
NG	Nitro glycerine
NGu	Nitroguanidine
RNENA	Alkyl nitrato ethylnitramine
RDX	Trinitrotrimethylenetriamine
TEGDN	Triethylene glycol dinitrate
TMETN	Trimethylolethanetrinitrate
2#	Methyl centralite
f	Impetus in J / g
K	Average specific heat ratio of combustion product
MW	Average molecular weight of combustion gases in g / mole
n	Pressure exponent
P_m	Average maximum pressure or bore pressure in MPa
$\triangle P_m$	Maximum difference of maximum bore pressure in MPa
Q	Heat of explosion in J / g
T_v	Isochoric flame temperature in K

t	temperature of propellant in °C
t_{20}	Delay time in ms
U_1	Coefficient of burning rate in cm / s / MPa
V	Average muzzle velocity in m / s
$\triangle V$	Maximum difference of muzzle velocity in m / s
W	Volume of combustion gases in L / kg
ω	Amount of powder in g
ω_c	Erosive amount in mg
ω_e	Relative erosive amount in mg / g
α	Covolume in dm^3 / kg
$\sigma(t)$	Compression strength at temperature(t) in MPa
$\tau(t)$	Impact strength at temperature(t) in kJ / m^2
$\varepsilon(t)$	Compressibility at temperature(t) in %

Table 1   Calculated performance of the improved mortar propellants

NC (12.0 %N)	58.5	—	58.5	—	58.5	—	58.5	—	58.5	58.5	58.5	—
NC (12.6 %N)	—	58.5	—	58.5	—	58.5	—	58.5	—	—	—	58.5
NG	40	40	30	30	25	25	20	20	15	10	0	0
BuNENA	—	—	10	10	15	15	20	20	25	30	40	40
f (J / g)	1171	1194	1123	1152	1093	1124	1057	1091	1020	973	870	914
T (K)	3671	3820	3214	3357	2995	3136	2782	2920	2574	2370	1971	2101
Q (J / g)	4920	5121	4289	4491	3974	4176	3659	3860	3344	3029	2399	2601
K	1.210	1.206	1.229	1.225	1.238	1.234	1.248	1.243	1.257	1.267	1.288	1.282
W (L / kg)	859.5	842.4	941.8	924.7	983.1	965.9	1024	1007	1065	1107	1189	1172
MW (g / mol)	26.07	26.60	23.79	24.23	22.80	23.20	21.88	22.25	21.03	20.25	18.85	19.12

Table 2　The composition and some performance of SF—13, S—11 and the improved propellants

Propellant	Bu—2	S—11	Bu—1	SF—13
NC	57.5	58.5	56.4	56.0
% N	12.0	12.0	12.6	12.0
NG	20.0	40.0	26.1	26.5
BuNENA	20.5	——	16.0	——
2#	1.5	0.8	1.5	3.0
remnant	0.5	0.7	——	14.5
f (J / g)	1048	1171	1130	981.7
T (K)	2727	3671	3152	2579
Q (J / g)	3561	4920	4186	3171
W (L / kg)	1036	860	966	1026
σ (50℃)(MPa)	*	——	——	14.6
τ (−40℃) (kJ / m^2)	12.5	——	——	4.11
Combustion performance:	(the constant pressure method in closed bomb)			
Region of pressure	27.5~394.5	50~390	17~404	30~410
n	0.9833	0.9311	0.9452	1.005
u_1 (cm / s / MPa)	0.06588	0.1704	0.09905	0.04776

Note: * No fracture.

Table 3　The composition and calculated performance of propellants containing BuNENA with low flame temperature

Propellant	LTB—1	LTB—2	NACO(C)	NACO(D)	NOSOL 318
NC	45.0	45.0	91.7	89.3	46.0
% N	13.0	13.0	12.0	12.0	12.0
TMETN	——	——	——	——	38.5
TEGDN	——	——	——	——	3.0
BuNENA	33.5	28.5	——	——	——
centralite	1.5	1.5	1.0	1.0	2.0
NGu	20.0	25.0	——	——	——
remnant	0	0	7.3	9.7	10.5
f (J / g)	931	941	844	828	894
T_v (K)	2173	2238	2210	2184	2260
Q (J / g)	2704	2800	2765	2745	3138
W (J / kg)	1154	1132	1029	1022	1067

Table 4 The composition and thermodynamic performance of the propellants containing BuNENA

Propellant	BQ	BD	BR
NC (13.0 % N)	54.0	57.0	54.5
NG	20.0	14.5	17.0
BuNENA	20.0	18.0	21.0
NGu	5.0	——	——
DINA	——	9.0	——
RDX	——	——	6.0
2# centralite	1.0	1.5	1.5
f (J / g) (calcd)	1117	1117	1123
(obs.)	1127	1113	1104
T_v (K) (calcd)	3025	3026	3007
Q (J / g) (calcd)	4010	3998	3964
(obs.)	4088	4216	4066
W (L / kg) (clacd)	995.5	995.0	1006

Table 5 The measured performances of the propellants containing BuNENA

Propellant	M30	BQ	BD	BR	TG115	SF−13
σ (50℃) (MPa)	——	6.22	6.66	5.82	48.2	14.6
ε (50℃) (%)	——	65.7	70.3	65.2	78.6	——
τ (−40℃)(kJ / m^2)	——	1.96	4.61	2.35	9.90	4.11
erosiveness (the erosive tube method)						
T_v (K)	3040	3025	3026	3007	3340	2579
P_m (MPa)	226	217	218	214	239	239
ω_c (mg / g)	14.52	14.83	17.97	14.5	22.85	10.38
f (J / g)	1088	1117	1117	1123	1125	981.7
combustion performance (the constant pressure method in closed bomb)						
n	——	1.08	1.02	1.06	——	1.00
u_1 (cm / s / MPa)	——	0.0722	0.0721	0.0694	——	0.053

Table 6   Some characteristics of single base propellants deterred with BuNENA

Propellant	4 / 7	4 / 7+5% BuNENA	4 / 7+7% BuNENA	4 / 7+9% BuNENA
f (J / g) (calcd)	1046	1040	1037	1034
(obs.)	1054	1059	1090	1051
T_v (K) (calcd)	3080	2967	2925	2886
α (dm^3 / kg)(obs.)	0.93	0.92	---	0.98
n	0.57	0.67	---	0.96
t_{20} (ms)	0.7	1.3	1.25	1.3
erosiveness (the erosive tube method)				
P_m (MPa)	185.7	---	181.2	178.2
ω_c (mg)	0.7423	---	0.4503	0.5183

Table 7   The interior ballistic characteristic of the single base propellants deterred with BuNENA in 14.5 mm gun

firing date	t(℃)	propellant	ω (g)	P_m(MPa)	$\triangle P / P_m$(%)	V (m / s)	$\triangle$V(m / s)
89.12.29	15	5 / 7(critical)	32	258.6	---	963.9	5.9
89.12.29	15	4 / 7	27	282.2	---	955.7	7.8
89.12.29	15	4 / 7+5% BuNENA	29	276.4	---	968.8	6.4
90.1.17	15	5 / 7(critical)	32	257.6	---	953.2	13.4
90.1.17	15	4 / 7+7% BuNENA	31	272.8	---	987.8	19.4
90.1.17	15	4 / 7+9% BuNENA	31	258.8	---	947.8	16.4
90.2.27	15.5	5 / 7(critical)	32	278.8	---	986.1	8.4
90.2.27	15.5	4 / 7+7% BuNENA	30	286.7	---	986.2	7.1
90.2.27	50	4 / 7+7% BuNENA	30	331.9	+15.8	1014.7	11.2
90.2.27	−40	4 / 7+7% BuNENA	30	246.8	−13.9	926.3	10.3
90.7.17	15	5 / 7(critical)	32	264.3	---	969.5	13.5
90.7.17	15	4 / 7+7% BuNENA	31	262.9	---	991.6	11.0
90.7.17	15	4 / 7+9% BuNENA	31	288.8	---	925.7	13.1

HIGH ENERGY OXETANE/HNIW GUN PROPELLANTS

Robert B. Wardle, Paul C. Braithwaite, Andrew C. Haaland,
James A.Hartwell, Roger R. Hendrickson, Val Lott,
Ingvar A. Wallace, Charles B. Zisette

Thiokol Corporation
P.O. Box 707
Brigham City, Utah 84302-0707
U.S.A.

An attractive approach to high energy, low sensitivity propellants involves the use of energetic oxetane prepolymers. These binders act as energy partitioning agents by allowing an energetic formulation to maintain a constant energy level at a lower solids percentage. Partitioning a portion of the energy of the formulation into the binder phase is predicted to result in significant improvements in the formulation. The lower solids is predicted to result in improved processing, mechanical properties, and reduced friability. A high energy binder based on a random copolymer of 3,3-bis(azidomethyl)oxetane and 3-azidomethyl-3-methyloxetane (BAMO/AMMO) was examined to determine whether the postulated improvements suggest for this binder were possible in gun and rocket propellants.

As with several other energetic polymers of current interest and similar energy, there are there were problems with the producibility and reproducibility of polyoxetanes that give consistently good propellant properties. Therefore, the projected payoffs of these materials had not been realized. Our approach to this problem was to investigate an alternative polymerization of energetic oxetanes that we have shown has distinct advantages over the methods previously used in order to provide consistent materials with excellent functionality and molecular weight control. Using the activated monomer polymerization of energetic oxetanes, consistent BAMO/AMMO and thermoplastic elastomers based on BAMO and AMMO with controlled physical characteristics were obtained.

Formulation of the BAMO/AMMO with HNIW (CL-20), RDX and combinations of the two has afforded potentially attractive, high energy TPE gun propellants. Results of early formulation efforts, mechanical and safety properties, thermal characteristics, and ballistic performance are reported on the following pages.

ENERGETIC MATERIALS TECHNOLOGY

OBJECTIVE:

Develop novel energetic materials and formulations that will meet the future needs of the propellant, explosive and pyrotechnic communities.

- Clean, agile manufacturing processes and materials to reduce life cycle costs of formulation

- Target materials that reach performance goals unattainable with current materials

- Utilize a multidisciplinary team for rapid product development and demonstration

SCIENCE AND ENGINEERING

THIOKOL
SPACE · DEFENSE · FASTENING SYSTEMS

WHY AN ENERGETIC THERMOPLASTIC ELASTOMER?

What is a TPE?

Will flow - viscosity dependant on MW, miscibility of blocks, etc.

Will not flow - rubbery, much greater than 100% usable strain

ADVANTAGES	DISADVANTAGES
• Increased energy	• Initially expensive ingredients
• Energy Partitioning	• Less available
• Ballistic enhancements	• Limited TPE experience base
• Elastomeric properties	- but not non-existent
• Low cost thermal processing	
• Recoverable/recyclable	

SCIENCE AND ENGINEERING

THIOKOL
SPACE · DEFENSE · FASTENING SYSTEMS

ENERGETICS OF OXETANES

- **Structures allow tailoring of molecular formula**

  - nitrate esters provide oxygen
  - azides provide high heat of formation

- **BAMO/AMMO - AP - Al has same Isp x density OF 91% solids HTPB**

- **7.5 sec Isp gain when replacing PEG/NG in minimum smoke**

- **Gun propellants with RDX >1300 J/g; with CL-20 >1400 J/g**
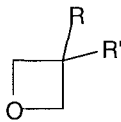
BAMO: $R=R'= CH_2N_3$

BEMO: $R=R'= CH_2OCH_2CH_3$

NMMO: $R= CH_3 \ R'=CH_2ONO_2$

AMMO: $R= CH_3 \ R'=CH_2N_3$

SCIENCE AND ENGINEERING

THIOKOL

SPACE · DEFENSE · FASTENING SYSTEMS

ACTIVATED MONOMER OXETANE POLYMERIZATION

PROPAGATION STEP OF OXETANE POLYMERIZATION:

STANDARD POLYMERIZATION:

ACTIVATED MONOMER POLYMERIZATION:

- Dramatic change in mechanism
- Very well behaved system at low molecular weights
- Moisture and kinetic concerns at high M.W.
- Described as activated monomer by Penczek
    REF:JPS-A **1991**, *29*, 619-28
- Similar work done by Sogah with non-energetic oxetanes using a silicon-based catalyst
    REF: SOGAH, POLYMER DIVISION, ACS MEETING 1988, TORONTO

SCIENCE AND ENGINEERING

THIOKOL

SPACE · DEFENSE · FASTENING SYSTEMS

(AB)n BLOCK COPOLYMERS (TPEs) MADE BY ISOCYANATE LINKING

• Schematic representation:

HO-A-OH $\xrightarrow{\text{TDI}}$ OCN-A-NCO

HO-B-OH $\xrightarrow{\text{TDI}}$ OCN-B-NCO
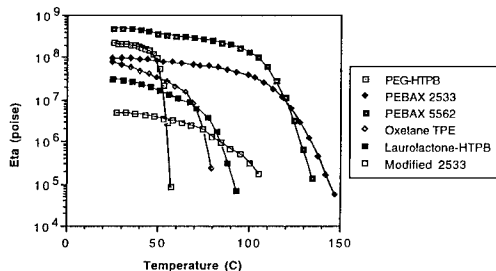
$\xrightarrow{\text{DIOL}}$ (AB)$_n$
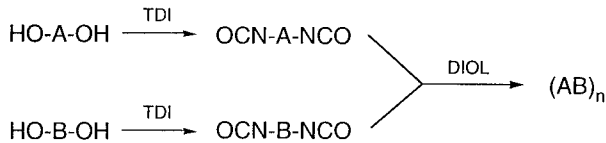
• Works with any oxetanes

• Allows easy tailoring of properties

• Simple, well-precedented chemistry

• Can use a variety of molecular weights of blocks

• Much improved mechanical properties

THIOKOL
SPACE · DEFENSE · FASTENING SYSTEMS

PROPERTIES OF OXETANE (AB)n BLOCK COPOLYMERS (TPEs) ATTRACTIVE

• Melting behavior critical to energetic materials processing
  • need narrow transition from hard to processible
  • m.p. too low and won't survive environment
  • m.p. too high and CL-20 or RDX can't be processed safely
  • RDS data show attractiveness of crystalline hard block oxetane TPE

Legend:
□ PEG-HTPB
♦ PEBAX 2533
■ PEBAX 5562
◊ Oxetane TPE
■ Laurolactone-HTPB
□ Modified 2533

Axes: Eta (poise) vs Temperature (C)

• Typical uniaxial mechanical properties of unfilled BAMO-AMMO TPE:
  • Modulus: 2-3 MPa (300-500 psi)
  • Strain at maximum stress: 300+%
  • Maximum stress: 850+ kPa (125+ psi)
  • Shore A hardness: 40-60

THIOKOL
SPACE · DEFENSE · FASTENING SYSTEMS

CL-20 CHARACTERISTICS

- **CL-20 is related to HMX and RDX**
  - Significantly higher density and energy than HMX
  - Material safety properties similar
- **Original synthesis by Nielsen at NAWC under ONR funding**
  - Thiokol improved and simplified synthesis
  - Scale-up at U.S. Army's MUSALL HMX pilot plant

CL-20   HMX
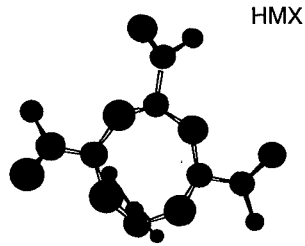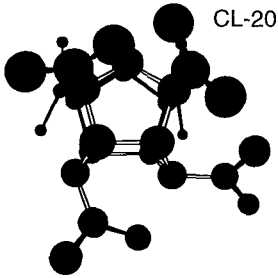
THIOKOL
SPACE·DEFENSE·FASTENING SYSTEMS

BAMO-AMMO TPE SYSTEMS WITH CL-20

CL-20/BAMO/AMMO
Flame Temperature

CL20/BAMO/AMMO
Impetus
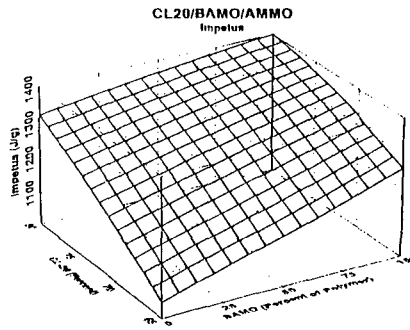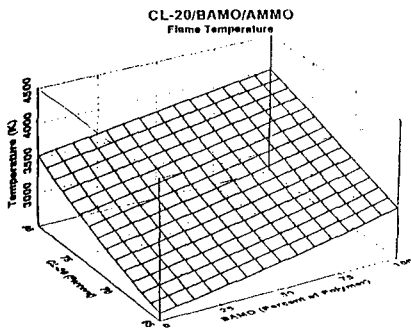
- Wide range of energy, temperature and, perhaps, burn rate
- Tailorability to meet specific needs possible
- Effects on vulnerability and mechanical properties to be determined

THIOKOL
SPACE·DEFENSE·FASTENING SYSTEMS

PROCESSING OF BAMO-AMMO / CL-20
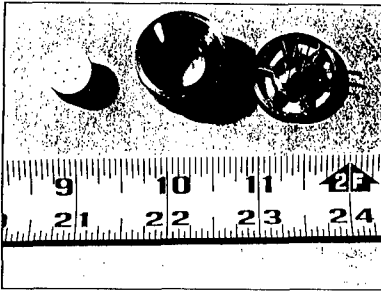
Extrusion Die & 1/2 inch diameter,
1.2 L/D 7 perforation gun propellant grain

Molding Powder & 1/8 inch diameter,
1, 5, L/D, 7
perforation gun propellant grains

- Multiple grain sizes and configuration available
- Coated polymer on CL-20 and ram extruded grains
- Demonstrated low scrap rate due to recycle (<0.5%)

SCIENCE AND ENGINEERING

THIOKOL
SPACE·DEFENSE·FASTENING SYSTEMS

PROPERTIES OF BAMO-AMMO / CL-20
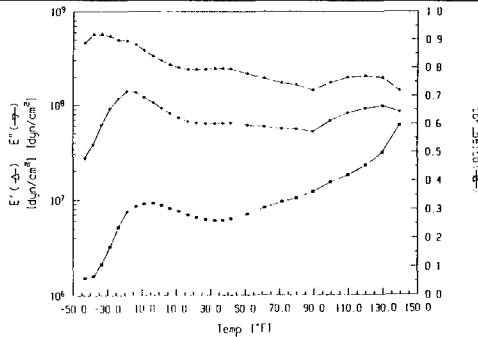
- RDS data consistent with gumstock properties
  - Tg and m.p. did not shift significantly
- Mechanical properties by compressive loading at 50 cm/min
  - Modulus: 41.0 MPa (5950 psi)
  - Strain at maximum stress: 49.7%
  - Maximum stress: 12.2 MPa (1780 psi)
    - Values are average of 15 samples
- Safety properties of coated CL-20 well within acceptable range
  - Indirect impact, sliding friction and electrostatic discharge

SCIENCE AND ENGINEERING

THIOKOL
SPACE DEFENSE FASTENING SYSTEMS

CL-20/OXETANE PREPARED AND COMPARED

	RDX/Ox	CL-20/Ox
Impetus (J/g)	1182	1297
Flame Temp (°K)	2827	3412
Gamma	1.268	1.277
Density (g/ml)	1.64	1.771
Energy Density (J/ml)	7233	8295
[Imp*den/(gamma-1)]		
Burn rate (ips)		
11 kpsi	1.52	4.52
26 kpsi	4.32	11.8

• Formulations with 76% solids, burn rate on small strands
• Inherently fast burn rate in CL-20 formulation suggests extra flexibility in grain design and energy management

SCIENCE AND ENGINEERING   **THIOKOL**
                                                    SPACE·DEFENSE·FASTENING SYSTEMS

CONCLUSIONS

• **Processing advantages of TPE demonstrated**
  • uniformity of sample
  • low scrap rate
  • recycling

• **Favorable properties obtained**
  • mechanical at low and high rates
  • ballistic properties allow extra tailoring
  • high ballistic energy inherent in formulation

• **Development as a gun propellant proceeding well**

SCIENCE AND ENGINEERING   **THIOKOL**
                                                    SPACE·DEFENSE·FASTENING SYSTEMS

EFFECT OF PLASTICIZER ON PERFORMANCE OF XM-39 LOVA

R. L. Simmons
Naval Surface Warfare Center - Indian Head Division
Indian Head, MD 20640
301-743-4635
FAX 301-743-4683

Abstract

Acetyl triethyl citrate (ATEC) was the plasticizer in the original XM-39 LOVA gun propellant formulation. However in considering ways to increase the impetus with minimal effect on the vulnerability properties, the substitution of an energetic plasticizer appears to be quite plausible. The best candidates appear to be TEGDN, a blend of methyl and ethyl NENA, and DANPE. Not only will impetus be increased significantly, but the density and burning rate as well. It is also expected that the mechanical properties will be enhanced because of the better colloiding and gelatinizing powers of TEGDN the NENAs, and DANPE. The TEGDN route is now being evaluated at Bofors Explosives.

Introduction

Acetyl triethyl citrate (ATEC) was the plasticizer of choice in the original XM-39 LOVA gun propellant formulation developed in the early 1980s. ATEC is an excellent plasticizer and colloiding agent for NC and CAB, and imparts desirable vulnerability properties. However, it also is a very inert plasticizer with a negative (endothermic) heat of explosion, meaning it contributes very little to the overall impetus or energy level of the propellant.

Since the development of the original XM-39 formulation, there has been an emphasis to increase the impetus level of LOVA propellants (to approximately 1200 joules/g), with minimal or no effect on LOVA vulnerability properties (References 1 and 2). In considering the possibilities, it was thought that perhaps the easiest and least risky route was to simply replace the plasticizer (present at a concentration of 7.6% by weight) with one of higher energy --- leaving the remainder of the formulation unchanged, which is as follows:

NC	4.0%
CAB	12.0%
Plasticizer	7.6%
EC (stabilizer)	0.4%
RDX	76.0%

There were many energetic plasticizers to choose from, and for this study, eight alternates were considered, as listed in Table 1. Four of these are NENAs (methyl, ethyl, propyl, and butyl), two are azides (GAP and DANPE - see references 3, 4 and 5), and two are nitrate esters (TMETN and TEGDN). Since TMETN alone is a poor plasticizer for NC (the behavior with CAB was unknown), a 1:1 blend of TMETN and TEGDN (which is an excellent plasticizer for NC) was included.

The theoretical propellant performance was calculated via Blake computer code, with the results shown in Table 2. As expected, the most energetic plasticizers gave the highest propellant impetus --- with GAP (at 1159 joules/g) being substantially better than ATEC (at 1069 joules/g) --- and MeNENA and DANPE the best (at 1206 and 1210 joules/g, respectively). A 1:1 blend of MeNENA and EtNENA (previously commercially available from ICI) was only very slightly less (at 1200 joules/g) to MeNENA (reference 6).

Three recommendations resulted from this study:

1) Replace ATEC with TEGDN for slightly higher performance. This will increase the impetus by slightly more than 10% (from 1069 to 1179 joules/g), and increase the density by 1.6% (from 1.631 to 1.658 g/cc). It will also burn faster simply because TEGDN has a high heat of explosion than ATEC, and will therefore burn faster. This propellant known as IHGP-101 is now being evaluated by Bofors Explosives in Karlskoga, Sweden for twin-screw processing (reference 7). BuNENA is also a possible alternate plasticizer for TEGDN (depending on availability).

2) Replace ATEC with the 1:1 blend of MeNENA and EtNENA for even higher performance. This will increase the impetus by more than 12% (to 1200 joules/g), and increase the density by 2.0% (to 1.664 g/cc) --- and burn even faster than with TEGDN (due to presence of nitramine moiety in the NENA). This possibility is now being considered at Bofors --- depending on the availability of NENA plasticizers in Europe.

3) Consider replacing ATEC with DANPE not only to gain slightly more impetus than with MeNENA/EtNENA blend, but more for the change in mechanical properties (due to better colloiding with DANPE), plus the increase in burning rate that occurs because of the azide moieties in DANPE (reference 8).

Conclusions

The replacement of ATEC with TEGDN, a NENA, or DANPE offers several advantages over the present XM-39 LOVA formulation --- in increased impetus, density, linear burning rate, and probably mechanical properties as well. Though the tests have not been conducted, it is expected that the vulnerability properties will be largely unaffected.

References

1. A. J. Beardell, *"LOVA Propellants - An Overview"*, Third International Gun Propellant Symposium, Picatinny Arsenal, NJ, October 30, 1984.

2. J. J. Rochio, *"Low Vulnerability Ammunition Propellant Technology"*, NATO-AGARD Meeting on Interior Ballistics on Guns, Florence, Ital, September 9-11, 1985.

3. M. B. Frankel and J. E. Flanagan, US Patent 4,268,450, *"Hydroxy-terminated azide polymer GAP"*, May 19, 1981.

4. R. L. Simmons and H. L. Young, US Patent 4,450,110, *"1,5-Diazido-3-nitrazapentane - DIANP"*, May 22, 1984.

5. J. E. Flanagan, E. R. Wilson, and M. B. Frankel, US Patent 5,013,856, *"1,5-Diazido-3-nitrazapentane - DANPE"*, May 7, 1991.

6. R. A. Johnson and J. J. Mullay, *"Stability and Performance Characteristics of NENA Materials"*, ADPA International Symposium on Energetics, New Orleans, LA, October 5-7, 1992.

7. A. Hafstrand and J. Sandstroem, *"Continuous Production of LOVA Propellant at Bofors Explosives"*, Sixth International Gun Propellant Symposium, Parsippany, NJ, November 14-17, 1994.

8. R. L. Simmons, *"Effect of Molecular Structure on Burning Rate"*, 26th International ICT Conference, Karlsruhe, Germany, July 4-7, 1995.

Glossary

Term	Definition
ATEC	Acetyl triethyl citrate
BuNENA	Butyl nitrato ethyl nitramine
CAB	Cellulose acetate butyrate
DANPE	1,5-diazido-3-nitrazapentane
EC	Ethyl centralite
EtNENA	Ethyl nitrato ethyl nitramine
GAP	Glycidyl azide plasticizer/polymer
MeNENA	Methyl nitrato ethyl nitramine
NENA	Alkyl nitrato ethyl nitramine
ProNENA	Propyl nitrato ethyl nitramine
TEGDN	Triethylene glycol dinitrate
TMETN	Trimethylol trinitrate

Table 1

Thermochemistry of Selected Plasticizers
For Use in XM-39 LOVA

Plasticizer	Formula	ΔHf - cal/mole
ATEC	$C_{14} H_{22} O_8$	-415,600
GAP	$C_3 H_5 N_2$	+33,000
BuNENA	$C_6 H_{13} O_5 N_3$	-46,000
TEGDN	$C_6 H_{12} O_8 N_2$	-145,400
ProNENA	$C_5 H_{11} O_5 N_3$	-42,603
EtNENA	$C_4 H_9 O_5 N_3$	-39,204
TMETN	$C_5 H_9 O_9 N_3$	-105,800
MeNENA	$C_3 H_7 O_5 N_3$	-35,800
DANPE	$C_4 H_8 O_2 N_8$	+163,316

Table 2

XM-39 LOVA Variations
(listed by increasing propellant impetus)

Plasticizer	Impetus	Tv - °K	Gas MW	Qex cal/g
ATEC	1069	2671	20.78	796
GAP	1159	2927	21.01	886
BuNENA	1173	2975	21.10	919
TEGDN	1179	3054	21.54	949
ProNENA	1183	3025	21.27	938
1:1 TMETN:TEGDN	1191	3113	21.72	970
EtNENA	1193	3083	21.48	959
1:1 MeNENA:EtNENA	1200	3122	21.62	974
TMETN	1203	3172	21.92	991
MeNENA	1206	3150	21.73	984
DANPE	1210	3107	21.34	953

PERKUSSIONS-ZÜNDELEMENT
MIT SCHADSTOFFARMEM ZÜNDSATZ
FÜR HANDFEUERWAFFEN

Jörg Kutzli, Walter Rauber, Markus Tobler
SM Schweizerische Munitionsunternehmung, Allmendstrasse 74, CH-3602 Thun

Abstract

A nontoxic primer mixture consisting of PETN, manganese dioxide, potassium nitrate, zirconium powder and AEROSIL® is presented by the Swiss Munition Enterprise.

It's main features are

- Increased handling safety
- Conventional mixing
- Readily available components

It can be wetloaded in Boxer and Berdan primers as well as in rimfire cartridges.

Because of it's shock dominated initiation mechanism, primers should be positioned in a non positive way and without deformation at the bottom of their housing.

Surface treatment is required for brass metal sheet parts in direct contact with the mixture to avoid stress corrosion cracking.

Einleitung

Seit über 15 Jahren bestehen Bestrebungen, die an den Schadstoffemissionen beim Schiessbetrieb beteiligten konventionellen Initialsprengstoffe, sowie die schwermetallhaltigen Redoxsysteme der Zündelemente durch weniger toxische Stoffe zu ersetzen.

Weitaus der grösste Teil der heute technisch vorgeschlagenen und patentierten Lösungen basiert auf dem organischen Initialsprengstoff 2,4 Dinitro-6-diazophenol. Auch bekannt unter dem Trivialnamen DINOL; DIAZOL [1-6].
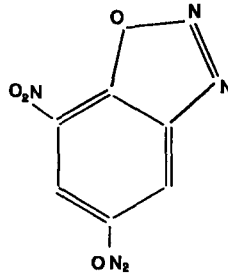
2,4 Dinitro - 6 - diazophenol

Die Synthese dieses Stoffes ist jedoch im Vergleich zu den einfachen Fällungsreaktionen der Schwermetallazide bzw. -styphnate als schwierig zu bezeichnen. Zudem ist die Substanz in ihrer unzersetzten Form karzinogen [7]. Alternativvorschläge auf der Basis Titan / Kaliumperchlorat [8], oder Zirkon / Kaliumchlorat [9] sind ebenfalls publiziert, wobei chlorhaltige Substanzen waffenseitig zu Korrosionsproblemen führen können.

Der hier vorgestellte Zündsatz basiert auf PETN und einem Redoxsystem bestehend aus Zirkon, Mangandioxid und Kaliumnitrat.

Zusammensetzung

Zirkonpulver CX	17 - 23 % (Gewichts%)
Mangandioxid	40 - 50 %
PETN	13 - 17 %
Kaliumnitrat	17 - 23 %
Aerosil®	0,4 - 0,6 %

Herstellung und Laborierung

Der Mischprozess der Komponenten erfolgt absolut konventionell in feuchtem Milieu auf herkömmlichen Betriebsmitteln. Der dem Mischer entnommene wasserfeuchte Teig kann direkt in die Dosierbrillen eingestrichen und in die Kapselhülsen gedrückt werden. Der Pressdruck beträgt ca. 280 - 300 MPa.

Als für die Empfindlichkeit des Zündelementes vorteilhaft hat sich das Mischen und Einstreichen unter Isopropanol erwiesen. Dies bedingt jedoch in der Produktion ein entsprechendes Lösungsmittelmanagement mit angepassten Sicherheitsmassnahmen.

Sicherheitskenndaten

Die für den vorliegenden Zündsatz ermittelten Sicherheitskenndaten seien zum Vergleich denjenigen eines verbreiteten Zündsatzes auf Basis Bleitrizinat, Calciumsilizid, Bariumnitrat, Antimontrisulfid, Tetrazen gegenübergestellt.

| | schadstofffrei | | konventionell |
| | Zündsatz trocken | Zündsatz feucht | |
	Fallhammer 2 kg		Fallhammer 1 kg
Schlagempfindlichkeit			
erste Reaktion	50 cm	bis 100 cm Fallhöhe keine Reaktion	30 cm
100 % Reaktion	80 cm	bis 100 cm Fallhöhe keine Reaktion	70 cm
Reibempfindlichkeit			
im Apparat nach Peters in kg			
erste Reaktion	11.2 kg	19.2 kg	0.6 kg
100 % Reaktion	19.2 kg	bis 36 kg Belastung nicht feststellbar	2.0 kg
Elektrostatische Empfindlichkeit			
erste Reaktion	3.3 mJ	0.68 J	0.22 mJ
100 % Reaktion	22 mJ	bis 1.0 J Zündleistung nicht feststellbar	1.50 mJ

Tab. 1 Sicherheitskenndaten des SM schadstofffreien Zündsatzes im Vergleich zu einem konventionellen Satz

Empfindlichkeit im Zündelement

Nachfolgend sind die Empfindlichkeiten von drei Standardboxer-Zündelementen im Run-down-Test verglichen. Das mit «konventionell» bezeichnete Zündelement enthält den vor-gängig mit den Sicherheitskenndaten vorgestellten Bleitrizinatzündsatz und das Diazolhal-tige stammt aus der Serienproduktion eines europäischen Herstellers.

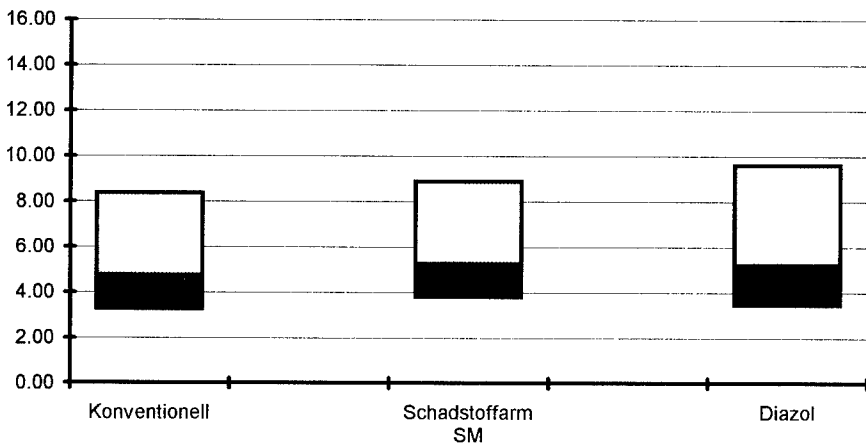| Benennung	Mw +5s	Mittelwert Mw	Mw - 2s
Konventionell	08.37	4.72	3.26
Schadstoffarm SM	08.89	5.24	3.78
Diazol	09.60	5.20	3.44

Abb. 1 Empfindlichkeit von drei Zündelementtypen im Rundown-Test, lose im Ring

Gestützt auf die Sicherheitskenndaten der Zündsätze kann der Zündmechanismus des kon-ventionellen wie auch des diazolhaltigen Satzes auf interne Reibung zurückgeführt werden. Dies wird in der Regel beabsichtigt durch das Beimischen von Reibungsadditiven, z.B. Calciumsilicid.

Beim SM Zündsatz bewirkt der Zusatz solcher Substanzen keine Empfindlichkeitssteigerung. Als dominierender Zündmechanismus kommt in diesem Fall Schlaginitiierung in Frage.

Diese Vermutung wird durch den signifikanten Einfluss der Satzdicke zwischen Amboss und Kapselhülsenboden erhärtet. Zu hohe Satzdicken führen zu einer Abdämpfung des Schlag-impulses und einer damit verbundenen Empfindlichkeitsabnahme. Dies zeigt ein Bruceton-test an Elementen mit zunehmender Satzdicke.
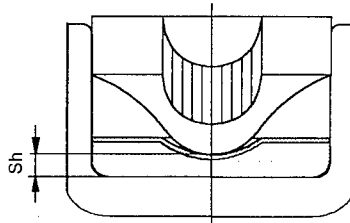
Abb. 2 Prinzipskizze zur Definition der Satzdicke Sh

Satzdicke Sh (mm)		mittlere Fallhöhe (cm)	«all fire» (cm)	«no fire» (cm)
	s	$\overline{x}$	$\overline{x}$	$\overline{x}$
0.67	0.019	40.6	46.2	35.7
0.72	0.020	43.1	49.2	37.7
0.83	0.021	49.2	56.2	43.1
0.95	0.028	61.5	73.8	51.2

n pro Satzhöhe = 50; Fallmasse 29 g

Tab. 2 Einfluss der Satzhöhe Sh auf die Empfindlichkeit

Die bei den heutigen Zündelementen übliche Abdeckung hat ebenfalls phlegmatisierende Wirkungen. Bei konventionellen, initialsprengstoffhaltigen Elementen ist dies aus Gründen der Handhabungssicherheit sogar erwünscht. Im Falle einer reinen Schlaginitiierung muss der Materialwahl der Abdeckung besondere Aufmerksamkeit geschenkt werden.
Wo Montage- und Verträglichkeitsverhältnisse es gestatten, kann auf eine Abdeckung verzichtet werden.

Ballistische Eigenschaften

Die ballistische Leistung eines Zündelementes kann am besten in einer Anzünddruckbombe bestimmt werden.

Die nachfolgenden Druckverläufe sind charakteristisch für die Anzündleistung der drei im Rundown-Test vorgestellten Zündelemente. Beim angezündeten Pulver handelt es sich um ein Kugelpulver, das standardmässig in 5,56 mm Gewehrmunition eingesetzt wird.
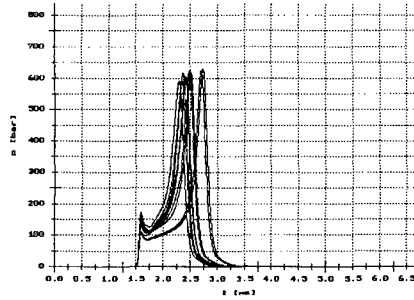
Abb. 3 Anzünddruckkurve des schadstoffarmen Zündsatzes
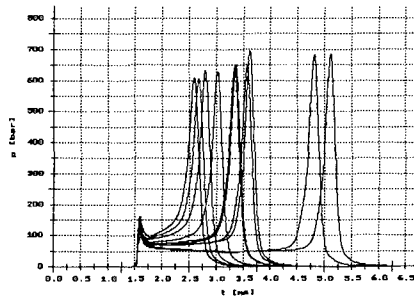
Abb. 4 Anzünddruckkurve des konventionellen Zündsatzes
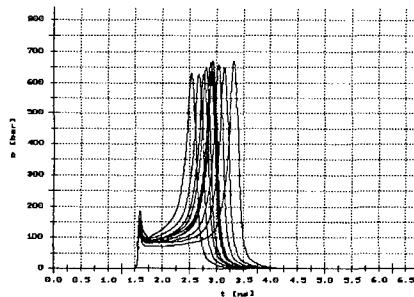
Abb. 5 Anzünddruckkurve des Diazol-Zündsatzes

Die in Abb. 4 ersichtlichen Zündverzögerungen sind als nichttypisch zu beurteilen.

Im Einsatz auf Systemebene (9 mm Parabellum; 5,56 Nato Standard) erfüllen alle drei Zündelementtypen die Anforderungen bezüglich Präzision und V_0-Streuung.

Chemische Eigenschaften

Entsprechend der Zusammensetzung ist der Satz gegenüber thermischen Einflüssen äusserst stabil. Im Gegensatz zu Chloraten wird der Nitratester PETN durch Mangandioxid nicht zersetzt. 14tägige Lagerung des feuchten Satzteigs und anschliessende Laborierung hat auf die Funktion des Zündelementes keinen Einfluss.

Ebenfalls Feuchtlagerung von unabgedeckten Zündelementen während 8 Tagen bei 60 °C und 80 % relativer Feuchtigkeit hat nur geringen Einfluss, dies obschon bei einigen Zündelementen die in der Feuchtigkeit bekannte Kaliumnitratmigration auftrat.

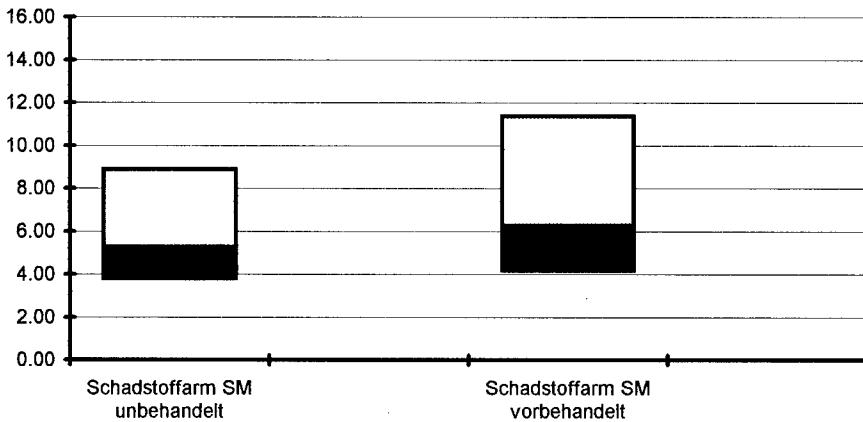| Benennung	Mw +5s	Mittelwert Mw	Mw - 2s
Schadstoffarm SM unbehandelt	08.89	5.24	3.78
Schadstoffarm SM vorbehandelt	11.38	6.23	4.17

Abb. 6 Rundown-Tests von frisch produzierten und während 8 Tagen bei +60 °C und 80 % rF gelagerten Zündelementen
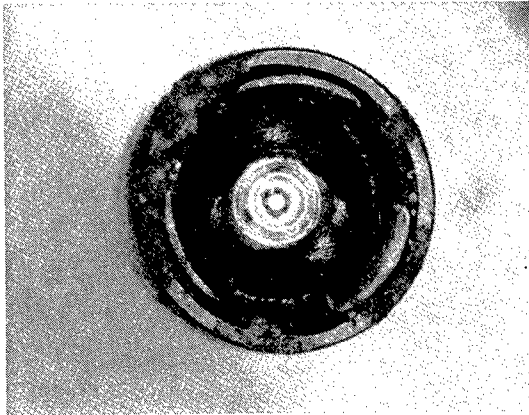

Abb.7   Kaliumnitratmigration infolge Feuchtigkeitseinfluss; ohne Einfluss auf die Funktion

Verträglichkeit mit Komponenten

Ausgehend von der Annahme, dass Zündelemente in der Patrone in sich geschlossene Baugruppen bilden, müssen vor allem Wechselwirkungen des Zündsatzes mit dem verwendeten Kapselmaterial untersucht werden. Hier ist in der Kombination des verwendeten Messings mit dem Substanzpaar Kaliumnitrat / Mangandioxid in der Literatur bisher nicht beschriebene Spannungsrisskorrosionen aufgetreten.

Bei ca. 5 - 7 % der gefertigten Elemente konnte bereits kurze Zeit nach der Herstellung Spannungsrisskorrosion an der Hülse oder am Amboss festgestellt werden.
Bei Feuchtlagerung verstärkte sich diese an den bereits befallenen Elementen, trat aber bei den übrigen nicht auf. Dies kann dadurch erklärt werden, dass der Umformvorgang der metallischen Komponenten auf einer Station nicht optimal verlief. In Anbetracht des hohen Kaltverformungsgrades und der sehr hohen Fertigungsrate muss mit solchen Erscheinungen gerechnet werden.

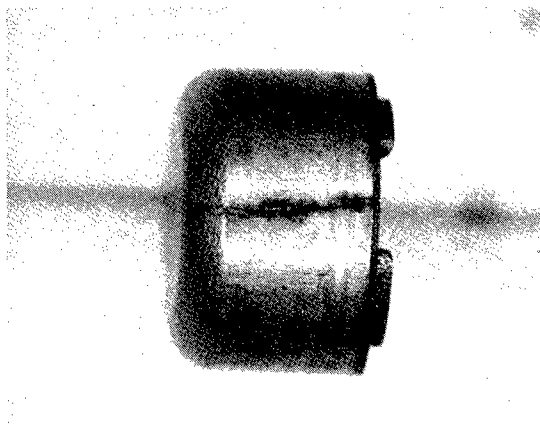Abb. 8 Spannungsrisskorrosion an der Kapselhülse aus Messing

Durch entsprechende Oberflächenbehandlung der Kapselhülse und des Ambosses kann das Problem jedoch behoben werden.

Erfahrungen im Einsatz auf Systemebene

Die bereits beschriebene dominierende Schlaginitiierung und der sie beeinflussenden Faktoren haben einen direkten Einfluss auf den Einbau des Zündelementes in der Patronenhülse:

- Kapsel- und Kapsellagerdurchmesser müssen gegenseitig so toleriert werden, dass beim Einsetzen des Zündelementes eine Zerstörung des im Zündelement eingepressten Satzbettes vermieden wird. Zündsätze, die durch Reibung initiiert werden, sind in dieser Beziehung weniger empfindlich.

- Der Einsetztiefe der Kapsel kommt primäre Bedeutung zu. Der Amboss muss kraftschlüssig auf dem Kapsellagerboden aufliegen. Ist dies nicht der Fall, wird ein Teil der Zündstiftenergie zum Verschieben der Kapsel aufgewendet. Dies hat Empfindlichkeitseinbussen zur Folge.

Benennung	Mw +5s	Mittelwert Mw	Mw - 2s
Lose im Ring	08.89	5.24	3.78
Nicht kraftschlüssig eingesetzt	14.16	7.00	4.15

Abb. 9 Empfindlichkeitsvergleich im Rundown-Test lose im Ring und nicht kraftschlüssig eingesetzt.

- Forciertes Einsetzen auf Anschlag kann aber auch die Zerstörung des Satzbettes mit den entsprechenden Auswirkungen zur Folge haben.

Die Erfahrung hat gezeigt, dass diese Anforderungen auf modernen, automatisierten Produktionsmitteln erfüllt werden können.

Schlussfolgerung

Der vorgestellte diazol- und chlorfreie Zündsatz zeichnet sich aus durch einfache Herstellung und leicht zugängliche Komponenten.

Gegenüber bisher bekannten Zündsätzen besitzt er eine bedeutend erhöhte Handhabungssicherheit.

Konventionell nasslaborierbar ist er geeignet zur Verwendung in Boxer- und Berdanzündsystemen aber auch in Randfeuerpatronen.

Er erfordert eine erhöhte Präzision in der Positionierung des Zündelementes, sowie eine Oberflächenbehandlung der mit ihm in Kontakt stehenden Messingteile.

Es ist vorgesehen, ihn für die Verwendung in Zündelementen der Kleinkalibermunition der SM Schweizerische Munitionsunternehmung zu qualifizieren.

Literatur

[1]   E-Patentschrift EP 02908 Priorität 18.6.83
        Veröffentlichung 5.84
[2]   US-Patenschrift US 4608102 Priorität 14.11.84
        Veröffentlichung 8.86
[3]   US-Patentschrift US 4674409 Priorität 2.6.86
        Veröffentlichung 6.87
[4]   FR-Patentschrift FR 2628735 Priorität 3.3.88
        Veröffentlichung 9.89
[5]   US-Patentschrift US 4963201 Priorität 10.1.90
        Veröffentlichung 10.90
[6]   WO-Patentschrift WO 9515298 Priorität 1.12.93
        Veröffentlichung 8.6.95
[7]   Römpp   Chemielexikon Band 2 8. Erweiterte Auflage 1981 Seite 932
                  Frankh'sche Verlagshandlung Stuttgart
[8]   Conkling   John A. Chemistry of Pyrotechnics
                     Marcel Dekker Inc New York and Basel 1985
[9]   E-Patentschrift EP 0159122 Priorität 3.3.84
        Veröffentlichung 10.85

SOME RULES FOR THE DESIGN OF HIGH SOLID LOADING COMPOSITE SOLID PROPELLANTS AND EXPLOSIVES

P. Carvalheira and **J. Campos**

Laboratório de Energética e Detónica, Departamento de Engenharia Mecânica, Faculdade de Ciências e Tecnologia da Universidade de Coimbra, Pólo II, Pinhal de Marrocos, P-3030 Coimbra, Portugal

G. M. H. J. L. Gadiot

TNO Prins Maurits Laboratorium, Lange Kleiweg 137, Postbus 45, 2280 AA Rijswijk, The Netherlands

ABSTRACT

This work presents rules to design composite solid propellants and explosives with solid particles of spherical shape, specifying the relations between the diameters of the particles, the number of particles of each particle size, the volume fraction occupied by each particle size and the solid mass fraction relative to each particle size based on geometric and volumetric relations and on the density of each particle used and of the polymeric binder, to obtain formulations with high total particle volume fraction and high solid mass fraction. The viscosity of the formulation is determined based on the viscosity of the binder system, the solids volume fraction and the modal character of the formulation.

Three examples are presented where the concepts are applied to the design of new propellant formulations. The first example concerns formulations of the type AN/HTPB-IPDI having solid particles of one type of oxidizer, Ammonium Nitrate (AN), and as binder the Hydroxyl Terminated Polybutadiene - Isophorone Diisocyanate (HTPB-IPDI) polymer system. The second example involves one formulation of the type AN/SN/HTPB-IPDI that have solid particles of two different oxidizers, Ammonium Nitrate (AN), and Sodium Nitrate (SN) and as binder the HTPB-IPDI polymer system. The third example involves one formulation of the type HNF/Al/GAP that have solid particles of one type of oxidizer, Hydrazinum NitroFormate (HNF), of one type of solid fuel, Aluminium (Al), and as binder the energetic polymer system of Glycidyl Azide Polymer (GAP) cured with Desmodur N100 (GAP-N100). It is seen the evolution of solid particles mass fraction of propellants as monomodal, bimodal, trimodal, tetramodal and 5-modal formulations are considered pursuing our objectives of obtaining castable compositions with high specific impulse and low pollutant emissions.

One example is presented of application of the concept to the design of explosive formulations of the type HMX/HTPB-IPDI with cyclotetramethylene tetranitramine (HMX) as oxidizer solid particles, and HTPB-IPDI polymer system as binder. The evolution of density, Chapman-Jouguet detonation velocity and pressure, and isentropic pressure exponent as a function of HMX solid particles mass fraction is also discussed as unimodal, bimodal, trimodal, tetramodal and 5-modal formulations are selected.

1. INTRODUCTION

Interest in the manufacture of high solids mass fraction castable and extrudable composite solid propellants and explosives comes from the following facts: The polymeric binder has a density lower than the oxidizer and by increasing the solids mass fraction, the density and the energy per unit volume of the composite solid propellant is increasing; For the same reason in explosives by increasing the solids mass fraction and consequently density, the energy per unit volume, the detonation velocity and pressure are increased; In some propellant and explosive formulations by increasing the solids mass fraction stoichiometric conditions are approached obtaining higher specific impulse and lower pollutant emissions in propellant deflagration and lower pollutant emissions in explosive detonation.

The objective of this paper is to discuss some simple rules to design high solids mass fraction composite solid propellants and explosives. Special attention is called to the manufacturers of solid particles of these new oxidizers (and old oxidizers) to develop particles of spherical shape or at least of smooth surface and with criteriously chosen particle sizes. The motivation for this work was the observation in the literature that attention is often paid to the solids mass fraction in propellants when is the volume fraction and density of ingredients the parameters to work with to attain high solids mass fraction. The other observation is that many authors present formulations of multimodal propellants to obtain high solids mass fraction in propellants without stating clearly the rational basis beyond the choice of the particle sizes and its mass fraction. The third reason is related to the time we live now were new oxidizers and energetic binders become available and where the effort to develop high solids mass fraction propellants or explosives could be reduced if we use some rational and simple rules to design the new propellants and explosives that use these new oxidizers and energetic binders.

2. RULES FOR THE DESIGN

2.1. Spherical particles

The first rule for the design of composite propellants or explosives with high solids mass fraction is to use spherical solid particles for its manufacture. Spherical particles reduce the

viscosity of propellants during casting for the same solids mass fraction when compared to particles with nonregular shape. This is more important for the particles of the larger size used in a propellant due to the fact that they use the larger volume fraction. In the following development it is assumed that all solid particles are spherical.

2.2. Particle size

We consider a closest-packed structure for the largest particles. The two possible structures are the face-centered cubic and the hexagonal closest-packed (Mahan, 1975). Any of these structures has three types of interstices. The first type is the octahedral interstice, the second type is the tetrahedral interstice (Mahan, 1975) and the third type is the triangular interstice. Assuming that the larger particles have a diameter D_1 we will have in consequence of geometrical relations.

An octahedral interstice will accommodate a spherical particle of diameter D_2, Eq. (1).

$$D_2 = \left(\sqrt{2} - 1\right)D_1 = 0.41421\, D_1 \tag{1}$$

A tetrahedral interstice will accommodate a spherical particle of diameter D_3, Eq. (2).

$$D_3 = \left(\frac{1}{\cos 35.2644} - 1\right)D_1 = 0.22474\, D_1 \tag{2}$$

A triangular interstice will accommodate a spherical particle of diameter D_4, Eq. (3).

$$D_4 = \left(\frac{1}{\cos 30} - 1\right)D_1 = 0.15470\, D_1 \tag{3}$$

For each particle of the largest diameter there is one octahedral interstice, two tetrahedral interstices (Mahan, 1975) and five triangular interstices.

The maximum volume fraction of the total volume occupied by the particles of the largest diameter is $\dfrac{V_{1,\max}}{V}$, Eq. (4).

$$\frac{V_{1,max}}{V} = \frac{\dfrac{\pi\,D_1^{\,3}}{6}}{D_1^{\,3}\,\sin 54.7356\ \cos 30} = 0.74048 \tag{4}$$

The maximum volume fraction of the total volume occupied by the particles in the octahedral interstice is $\dfrac{V_{2,max}}{V}$, Eq. (5).

$$\frac{V_{2,max}}{V} = \frac{\dfrac{\pi\,((\sqrt{2}-1)D_1)^{3}}{6}}{D_1^{\,3}\,\sin 54.7356\ \cos 30} = \frac{\pi\,(\sqrt{2}-1)^{3}}{6\ \sin 54.7356\ \cos 30} = 5.2624E-2 \tag{5}$$

The maximum volume fraction of the total volume occupied by the particles in the two tetrahedral interstices is $\dfrac{V_{3,max}}{V}$, Eq. (6).

$$\frac{V_{3,max}}{V} = 2\frac{\dfrac{\pi\,(0.22474\,D_1)^{3}}{6}}{D_1^{\,3}\,\sin 54.7356\ \cos 30} = 2\ \frac{\pi\,(0.22474)^{3}}{6\ \sin 54.7356\ \cos 30} = 1.6811E-2 \tag{6}$$

The maximum volume fraction of the total volume occupied by the particles in the five triangular interstices is $\dfrac{V_{4,max}}{V}$, Eq. (7).

$$\frac{V_{4,max}}{V} = 5\frac{\dfrac{\pi\,(0.15470\,D_1)^{3}}{6}}{D_1^{\,3}\,\sin 54.7356\ \cos 30} = 5\ \frac{\pi\,(0.15470)^{3}}{6\ \sin 54.7356\ \cos 30} = 1.3707E-2 \tag{7}$$

A fraction of the remaining volume that would be occupied by the binder can still be filled with particles of smaller size. To have this volume fraction as high as possible it is necessary that the particles be much smaller than the smallest size of the other particles. In this approach we have considered $D_5 = 0.1\ D_4 = 0.01547\ D_1$. The theoretical maximum fraction of the remainder volume that would be occupied with just one additional particle size would be $f_{v5,\,max}$ = 0.74 but its exact value is much more difficult to calculate than the previous volume

fractions. We have considered for the calculations of $\dfrac{V_{5,\max}}{V}$ two more conservative values,

that are more probable to attain in practice, $f_{v5} = 0.49$ and $f_{v5} = 0.25$. $\dfrac{V_{5,\max}}{V}$ is given by Eq. (8).

$$\frac{V_{5,\max}}{V} = f_{v5}\,(1 - (\frac{V_{1,\max}}{V} + \frac{V_{2,\max}}{V} + \frac{V_{3,\max}}{V} + \frac{V_{4,\max}}{V}))$$ (8)

The total volume fraction $\dfrac{V_j}{V}$ for particles of solid particle ingredient j is the sum of

volume fractions $\dfrac{V_{ij}}{V}$ occupied by particles of size D_i of solid ingredient j, Eq. (9). $\dfrac{V_{ij}}{V}$ must be

less than or equal to $\dfrac{V_{i,\max}}{V}$. For a z-modal formulation $n = z$.

$$\frac{V_j}{V} = \sum_{i=1}^{n} \frac{V_{ij}}{V}$$ (9)

The total volume fraction $\dfrac{V_p}{V}$ occupied by particles of all sizes is the sum of the volume

fraction occupied by particles of each size D_i and ingredient j, $\dfrac{V_{ij}}{V}$, Eq. (10).

$$\frac{V_p}{V} = \sum_{i=1}^{n} \sum_{j=i}^{m} \frac{V_{ij}}{V}$$ (10)

The volume fraction of the binder $\dfrac{V_b}{V}$ is given by Eq. (11).

$$\frac{V_b}{V} = 1 - \frac{V_p}{V}$$ (11)

The density of the propellant or explosive, ρ_p, is the sum of the products of volume fraction

occupied by an ingredient by its density and is given by Eq. (12).

$$\rho_p = \rho_b \frac{V_b}{V} + \sum_{j=1}^{m} \rho_j \sum_{i=1}^{n} \frac{V_{ij}}{V} \tag{12}$$

The mass fraction of particles of size D_i and ingredient j, x_{ij}, is given by Eq. (13).

$$x_{ij} = \frac{\rho_j \dfrac{V_{ij}}{V}}{\rho_p} \tag{13}$$

The mass fraction of particles of ingredient j, x_j, is given by Eq. (14).

$$x_j = \sum_{i=1}^{n} x_{ij} \tag{14}$$

The mass fraction of particles, x_p, is given by Eq. (15).

$$x_p = \sum_{i=1}^{n} \sum_{j=1}^{m} x_{ij} \tag{15}$$

The mass fraction of binder, x_b, is given by Eq. (16).

$$x_b = \frac{\rho_b \dfrac{V_b}{V}}{\rho_p} \tag{16}$$

2.3. Viscosity of binder and uncured composite propellant or explosive

The viscosity of the binder should be as low as possible. In general it is accepted that a composite solid propellant or explosive is no more castable when its viscosity is higher than 1500-2000 Pa.s (Davenas et al., 1989; Wanninger, 1990). The ratio between the viscosity of the propellant, η_p, and the viscosity of the binder, η_b, for a given ratio between the solids volume fraction, V_s, and maximum solids volume fraction, $V_{s,max}$, for a given particle size distribution can be given by Eq. (17) proposed by Krieger and Dougherty (1959). For spherical particles $K = 2.5$ which leads to Eq. (18). A graph of the evolution of this ratio of viscosities as a function of the volume fraction of solid particles for optimal monomodal and plurimodal distributions can be seen in Davenas et al. (1989).

$$\frac{\eta_p}{\eta_b} = \exp\left(-KV_{s,\max}\ln(1-\frac{V_s}{V_{s,\max}})\right) \qquad (17)$$

$$\frac{\eta_p}{\eta_b} = \exp\left(-2.5\,V_{s,\max}\ln(1-\frac{V_s}{V_{s,\max}})\right) \qquad (18)$$

Table 1
Viscosity of prepolymers and binder systems for composite solid propellant and explosives.

Ingredient	Viscosity at 20 °C /Pa.s	Viscosity at 40 °C /Pa.s	Viscosity at 60 °C /Pa.s	Reference
HTPB[a]	10.0	3.0	1.0	Atochem, 1990
HTPB-IDP[b]	2.2	0.85	0.4	Meulenbrugge and Sabel, 1988
GAP[c]	12-17[d]		3.0[e]	Manzara et al., 1994
GAP[f]	0.1-0.2			Manzara et al., 1994

[a] HTPB R45 HT
[b] HTPB R45 HT + 25 % of IDP (isodecylpelargonate) Plasticizer
[c] 3M GAP 5527 Polyol
[d] at 23 °C
[e] estimated
[f] 3M GAP Plasticizer L-12616

3. EXAMPLES OF APPLICATION

Table 2
Composition, enthalpy of formation and density of propellant and explosive ingredients.

Ingredient	Chemical Composition	$\Delta H^{\circ}_{f\,298.15}$ /(kcal/mol)	Density /(kg/m^3)	Reference
AN	$H_4N_2O_3$	-87.27	1725	Volk and Bathelt, 1994
SN	$NaNO_3$	-111.82	2261	Volk and Bathelt, 1994
HMX	$C_4H_8N_8O_8$	17.93	1902	Volk and Bathelt, 1994
HNF	$C_1H_5N_5O_6$	-17.20	1910	Gadiot et al., 1993
Al	Al	0	2702	Chase et al., 1985
HTPB	$C_{10}H_{15.6160}N_{0.2030}O_{0.1960}$	-10.90	901	Volk and Bathelt, 1994
IPDI	$C_{12}H_{18}N_2O_2$	-111.40	1061	Volk and Bathelt, 1994
GAP	$C_3H_5N_3O_1$	27.91	1300	Volk and Bathelt, 1994
HTPB-IPDI[a]			921.4[b]	This work
GAP-N100[c]			1.27 x 10^3	Stacer et al.,

[a] HTPB-IPDI cured with mass ratio 92.32-7.68 %
[b] measurement made with an Helium picnometer
[c] curative eq. ratio in weight is 1.05

Table 3
Maximum volume fraction of each spherical particle size and of the binder.

D_i/D	1.0000	0.41421	0.22474	0.15470	0.01547	--------	
	$\dfrac{V_1}{V}/(\%)$	$\dfrac{V_2}{V}/(\%)$	$\dfrac{V_3}{V}/(\%)$	$\dfrac{V_4}{V}/(\%)$	$\dfrac{V_5}{V}/(\%)$	$\dfrac{V_b}{V}/(\%)$	$\dfrac{V_s}{V}/(\%)$
Monomodal	74.048	0	0	0	0	25.952	74.048
Bimodal	74.048	5.262	0	0	0	20.690	79.310
Trimodal	74.048	5.262	1.681	0	0	19.009	80.991
Tetramodal	74.048	5.262	1.681	1.371	0	17.638	82.362
5-modal (f_{v5} = 0.25)	74.048	5.262	1.681	1.371	4.409	13.229	86.771
5-modal (f_{v5} = 0.49)	74.048	5.262	1.681	1.371	8.643	8.995	91.005
5-modal (f_{v5} = 0.74)	74.048	5.262	1.681	1.371	13.052	4.586	95.414

3.1. AN/HTPB-IPDI

Table 4 presents the maximum mass fraction of AN that is possible to obtain with unimodal, bimodal, trimodal, tetramodal and 5-modal propellants of the type proposed in this work. The predicted flame temperature and specific impulse calculated using the NASA Lewis CET89 (1971; 1989) computer code for a chamber pressure of 7.0 MPa, a pressure ratio of 70 and assuming equilibrium flow downstream of the combustion chamber and expansion into normal atmospheric pressure (0.1 MPa) can be interpolated from the data presented by Carvalheira (1995).

Table 4
Propellant formulations AN/HTPB-IPDI.

Ingredient	AN	AN	AN	AN	AN	HTPB-IPDI	
d_p /μm	60.0	24.85	13.48	9.28	0.93	--------	
	x_1 /(wt. %)	x_2 /(wt. %)	x_3 /(wt. %)	x_4 /(wt.%)	x_5 /(wt.%)	x_b /(wt.%)	ρ_p /(kg/m^3)
Monomodal	84.232	0	0	0	0	15.768	1516.5
Bimodal	81.946	5.824	0	0	0	12.230	1558.7
Trimodal	81.242	5.774	1.844	0	0	11.140	1572.3
Tetramodal	80.677	5.733	1.832	1.494	0	10.265	1583.3
5-modal (f_{v5} = 0.25)	78.911	5.608	1.792	1.461	4.699	7.530	1618.7
5-modal (f_{v5} = 0.49)	77.287	5.493	1.755	1.431	9.021	5.015	1652.7
5-modal (f_{v5} = 0.74)	75.665	5.377	1.718	1.401	13.337	2.503	1688.2

Assuming the viscosity of the system HTPB-IDP-IPDI at 40 °C equal to 0.85 Pa.s (Table 1) and a value for the propellant viscosity in the limit of castability equal to 1500 Pa.s (Davenas *et al.*, 1989) we can obtain for the ratio of $\dfrac{V_s}{V_{s,max}}$ a value given by Eq. (19).

$$\frac{\eta_p}{\eta_b} = \exp\left(-2.5\, V_{s,max}\, \ln(1 - \frac{V_s}{V_{s,max}})\right) = \frac{1500\ \text{Pa.s}}{0.85\ \text{Pa.s}} = 1765 \Rightarrow \frac{V_s}{V_{s,max}} = 0.96813 \tag{19}$$

Taking as example the propellant 5-modal ($f_{v5} = 0.25$) we can conclude that is feasible to make a propellant of this type with AN volume fraction 0.96813 x 86.771 % = 84.006 % maintaining the relative volume relations for each solid particle size and consequently with AN mass fraction equal to 90.768 % and with density equal to 1596.5 kg/m^3.

3.2. AN/SN/HTPB-IPDI

Table 5
Propellant formulations AN/SN/HTPB-IPDI.

Ingredient	AN	SN	SN	SN	SN	SN	HTPB-IPDI	
d_p /μm	60.0	60.0	24.85	13.48	9.28	0.93	--------	
	$x_{1,1}$ /(wt.%)	$x_{1,2}$ /(wt.%)	x_2 /(wt.%)	x_3 /(wt.%)	x_4 /(wt.%)	x_5 /(wt.%)	x_b /(wt.%)	ρ_p /(kg/m^3)
Monomodal	42.918	42.918	0	0	0	0	14.164	1688.2
Bimodal	44.531	37.703	6.827	0	0	0	10.939	1742.7
Trimodal	45.025	36.105	6.760	2.160	0	0	9.951	1760.1
Tetramodal	45.420	34.826	6.706	2.142	1.747	0	9.159	1774.3
5-modal ($f_{v5} = 0.25$)	46.651	30.845	6.538	2.088	1.703	5.478	6.697	1820.0
5-modal ($f_{v5} = 0.49$)	47.777	27.206	6.384	2.039	1.663	10.484	4.447	1863.8
5-modal ($f_{v5} = 0.74$)	48.894	23.594	6.231	1.991	1.623	15.454	2.213	1909.5

Beckstead (1989) calculated the flame temperature of the primary flame of formulations AN/HTPB and SN/HTPB with HTPB content varying in the range 0-40 wt. % in steps of 5

wt.% at 1000 psi (6.89 MPa), with CO_2 suppressed. The results of these calculations indicate that the maximum flame temperature of the primary flame at 1000 psi (6.89 MPa), with CO_2 suppressed, of formulations containing equal mass fraction of AN and SN seems to be obtained for a formulation AN/SN/HTPB-IPDI (43.5/43.5/13 wt. %). In the development of formulations presented in Table 5 the mass fraction of AN is kept equal to the mass fraction of SN. SN is added in several particle sizes to investigate if it is possible to attain the desired goal of SN mass fraction and AN mass fraction equal to 43.500 %. Results presented in Table 5 and example viscosity calculations made for AN/HTPB-IPDI propellant allow to give a positive answer to this question about the possibility to produce this propellant.

3.3. HNF/Al/GAP-N100

Gadiot *et al.* (1993) calculated the theoretical vacuum specific impulse of formulations HNF/Al/GAP with GAP content varying in the range 10-20 wt. % in steps of 2 wt.% and aluminium content varying in the range 0-25 wt. % in steps of 5 wt. %. The maximum vacuum specific impulse seems to be obtained for a formulation HNF/Al/GAP (62/20/18 wt. %). Theoretical calculations were performed using the NASA SP-273 computer code for a chamber pressure of 10 MPa, an area ratio of 100 and assuming equilibrium flow downstream of the combustion chamber and expansion into vacuum. Table 6 presents propellant formulations HNF/Al/GAP-N100 of the type proposed in this work with mass ratio HNF/Al equal to 62/20.

Assuming the viscosity of GAP at 60 °C equal to 3.0 Pa.s (Table 1) and a value for the propellant viscosity in the limit of castability equal to 1500 Pa.s (Davenas *et al.*, 1989) we can obtain for the ratio of $\dfrac{V_s}{V_{s,max}}$ a value given by Eq. (20).

$$\frac{\eta_p}{\eta_b} = \exp\left(-2.5\, V_{s,max}\, \ln(1 - \frac{V_s}{V_{s,max}})\right) = \frac{1500\,Pa.s}{3.0\,Pa.s} = 500 \Rightarrow \frac{V_s}{V_{s,max}} = 0.94301 \qquad (20)$$

Considering a 5-modal propellant ($f_{v5} = 0.25$) we can conclude that is feasible to make a propellant of this type with solids volume fraction 0.94301 x 86.771 % = 81.825 %

maintaining the relative volume relations for each solid particle size and maintaing the relative mass relation HNF/Al = 62/20 = 3.1. Consequently the solids mass fraction is equal to 91.398 % and the density is equal to 1953.0 kg/m³, which clearly exceeds the required solids mass fraction of 82.000 %. This analysis gives results that allow to give a positive answer to the question about the possibility to manufacture this propellant formulation. The use of GAP plasticizer presented in Table 1 can reduce the viscosity of GAP to lower values.

Table 6
Propellant formulations HNF/Al/GAP-N100.

Ingredient	HNF	Al	HNF	HNF	HNF	HNF	GAP-N100	
d_p /μm	20.0	20.0	8.28	4.49	3.09	0.309	--------	
	$x_{1,1}$ /(wt.%)	$x_{1,2}$ /(wt.%)	x_2 /(wt.%)	x_3 /(wt.%)	x_4 /(wt.%)	x_5 /(wt.%)	x_b /(wt.%)	ρ_p /(kg/m³)
Monomodal	62.160	20.052	0	0	0	0	17.789	1852.8
Bimodal	59.815	21.007	5.306	0	0	0	13.872	1894.2
Trimodal	59.088	21.303	5.269	1.683	0	0	12.656	1907.5
Tetramodal	58.502	21.542	5.240	1.674	1.365	0	11.677	1918.2
5-modal (f_{v5} = 0.25)	56.662	22.292	5.147	1.644	1.341	4.312	8.602	1953.0
5-modal (f_{v5} = 0.49)	54.955	22.987	5.060	1.617	1.318	8.311	5.752	1986.3
5-modal (f_{v5} = 0.74)	53.238	23.687	4.973	1.589	1.296	12.335	2.882	2021.0

3.4. HMX/HTPB-IPDI

Table 7 presents the maximum mass fraction of HMX that is possible to obtain with monomodal, bimodal, trimodal, tetramodal and 5-modal propellants and explosives of the type proposed in this work. Table 8 presents the results for the Chapman-Jouguet detonation velocity, D_{CJ}, and detonation pressure, p_{CJ}, isentropic pressure exponent, Γ, and the pollutant mole fraction in the detonation products of explosive formulations HMX/HTPB-IPDI, using the thermochemical equilibrium code that exist in our Laboratory based in the work of Heuzé (1985), with the BKW equation of state. The results show that both the Chapman-Jouguet detonation velocity and detonation pressure increase monotonically with the increase in mass fraction of HMX, that both the isentropic pressure exponent and the mole fraction of CO in the products of detonation decrease monotonically with the increase in mass fraction of HMX.

Both the increase in D_{CJ} and the decrease in Γ with the increase in mass fraction of HMX contribute to an increase of the specific detonation energy of the explosive, E, (Défourneaux, 1994).

Table 7
Explosive formulations HMX/HTPB-IPDI.

Ingredient	HMX	HMX	HMX	HMX	HMX	HTPB-IPDI	
d_p /μm	20.0	8.28	4.49	3.09	0.309	--------	
	x_1 /(wt.%)	x_2 /(wt.%)	x_3 /(wt.%)	x_4 /(wt.%)	x_5 /(wt.%)	x_b /(wt.%)	ρ_p /(kg/m^3)
Monomodal	85.486	0	0	0	0	14.514	1647.5
Bimodal	82.890	5.891	0	0	0	11.220	1699.1
Trimodal	82.093	5.834	1.864	0	0	10.209	1715.6
Tetramodal	81.455	5.789	1.849	1.508	0	9.399	1729.0
5-modal (f_{v5} = 0.25)	79.468	5.648	1.804	1.471	4.732	6.877	1772.3
5-modal (f_{v5} = 0.49)	77.649	5.518	1.763	1.437	9.063	4.570	1813.8
5-modal (f_{v5} = 0.74)	75.841	5.390	1.722	1.404	13.368	2.275	1857.0

Table 8
D_{CJ}, p_{CJ}, Γ and pollutants mole fraction in detonation products for explosive formulations HMX/HTPB-IPDI

	HMX /(wt.%)	HTPB-IPDI /(wt.%)	ρ_p /(kg/m^3)	D_{CJ} /(m/s)	p_{CJ} /(GPa)	Γ	x_{CO} /%
Monomodal	85.486	14.514	1647.5	8504.2	29.267	3.061	4.3489
Bimodal	88.780	11.220	1699.1	8591.6	30.930	3.046	3.0045
Trimodal	89.791	10.209	1715.6	8620.4	31.470	3.043	2.8817
Tetramodal	90.601	9.399	1729.0	8643.8	31.906	3.040	2.8198
5-modal (f_{v5} = 0.25)	93.123	6.877	1772.3	8718.4	33.353	3.034	2.7390
5-modal (f_{v5} = 0.49)	95.430	4.570	1813.8	8788.8	34.748	3.028	2.7470
5-modal (f_{v5} = 0.74)	97.725	2.275	1857.0	8860.8	36.226	3.023	2.7837

4. CONCLUSIONS

The presented rules allow to guide the design of composite solid propellants with high solids mass fraction and to answer the question if some of them whose calculated values of specific impulse and flame temperature are interesting, are feasible to be manufactured or not.

Three examples are presented of application of the concepts to the design of propellant formulations. The first concerns formulations of the type AN/HTPB-IPDI. The second involves formulation of the type AN/SN/HTPB-IPDI. The third example involves formulations of the type HNF/Al/GAP. The application of the concepts to the design of explosive formulations of the type HMX/HTPB-IPDI is also presented and discussed. The evolution of density, Chapman-Jouguet detonation velocity and pressure, and isentropic pressure exponent as a function of HMX solid particles mass fraction was evaluated.

REFERENCES

1. Mahan, Bruce H., *University Chemistry*, 3rd ed., Addison - Wesley Publishing Company, 1975.

2. Davenas, A. *et al.*, *Technologie des Propergols Solides*, Masson, Paris, 1989.

3. Wanninger, P., 'Influence of Raw Materials on Quality and Performance of HE Charges", 21st International Annual Conference of ICT, Karlsruhe, Germany, pp. 1-1, 1990.

4. Krieger, I. M., and Dougherty, T. J., *Trans. Soc. Rheol.*, 3: 137-152, 1959.

5. Atochem, Elf Aquitaine, 'Hydroxyl Terminated Poly Bd Resins Functional Liquid Polymers in Urethane Elastomers", October 1990.

6. Meulenbrugge, J. J., and Sabel, H. W. R., 'Castable Plastic-Bonded Explosives", TNO Prins Maurits Laboratory, Diverse and Dynamic, 37 Examples of Research, TNO Prins Maurits Laboratory, P.O. Box 45, 2280 AA, Rijswijk, The Netherlands, edited by Groothuizen, Th. M., pp. 144-154, 1988.

7. Manzara, A. P., Johannessen, B., and Denenholz, I. M., 'Characterization of GAP Polyol and Plasticizer", 25th International Annual Conference of ICT, Karlsruhe, Germany, pp. 73-1, 1994.

8. Volk, F., and Bathelt, H., *ICT Thermochemical Data Base*, Karlsruhe, Germany, June 15, 1994.

9. Gadiot, G. M. H. J. L., Mul, J. M., Meulenbrugge, J. J., Korting, P. A. O. G., Schnorkh, A. J., and Schöyer, H. F. R., 'New Solid Propellants Based on Energetic Binders and HNF", *Acta Astronautica*, 29(10/11): 771-779, 1993.

10. Chase, M. W., Jr. *et al.* (eds.), "JANAF Thermochemical Tables", Third Edition, *J. Phys. Chem. Ref. Data*, 14 (Suppl. 1), 1985.

11. Stacer, R. G., Eisele, S., and Eisenreich, N., "Polymeric Binder and the Combustion of Solid Propellants", 21st International Annual Conference of ICT, Karlsruhe, Germany, pp. 80-1, 1990.

12. Gordon, S. and McBride, B. J., "Computer Program for Calculation of Complex Chemical Equilibrium Compositions, Rocket Performance, Incident and Reflected Shocks, and Chapman-Jouguet Detonations", NASA SP-273, NASA Lewis Research Center, 1971.

13. McBride, B. J., "CET89 - Chemical Equilibrium with Transport Properties, 1989", LEW-15113 Program, Cosmic Software, The University of Georgia, Athens, U.S.A, 1989.

14. Beckstead, M. W., "Temperature Sensitivity Verification, Volume III, Computer User's Manual", AFAL-TR-88-109, Astronautics Laboratory, Air Force Space Technology Center, Space Division, Air Force Systems Command, Edwards Air Force Base, California 93523-5000, 1988.

15. Carvalheira, P., "Calculation of the Equilibrium Thermodynamic Properties of the Isobaric Adiabatic Combustion Products of AN/HTPB-IPDI Propellants at 7.0 MPa", 26th International Annual Conference of ICT, Karlsruhe, Germany, pp. 27-1, 1995.

16. Kubota, N., "Survey of Rocket Propellants and Their Combustion Characteristics" in *Fundamentals of Solid-Propellant Combustion.* Kuo, K. K. and Summerfield, M. (eds.), Progress in Astronautics and Aeronautics, 90: 1-52, 1984.

17. Heuzé, O., "Contribution au Calcul des Caractéristiques de Détonation de Substances Explosives Gazeuses ou Condensés", Thése presenté à L'U.E.R. - E.N.S.M.A., pour Obtenir le Grade de Docteur de l'Université de Poitiers, 24 Juin 1985.

18. Déforneaux, M., "About the Misuse of the Detonation Velocity to the Characterization of High Explosives", 25th International Annual Conference of ICT, Karlsruhe, Germany, pp. 2-1, 1994.

AQUEOUS EMULSION EXPLOSIVE WITH TNT

M. Mendonça, J. Campos, J.C. Gois and C. Moutinho*

Laboratory of Energetics and Detonics
Dep. of Mech. Engineering - Faculty of Sciences and Technology,
University of Coimbra, Pinhal de Marrocos P-3030 COIMBRA
*Sociedade Portuguesa de Explosivos - SPEL, Lisboa, PORTUGAL

ABSTRACT

Emulsion explosives are made of an aqueous solution of ammonium, sodium and calcium nitrates, emulsified with a solution of oils, wax and emulsifiers, and sensitised with hollow glass microballoons. The demilitarisation process origins large amounts of trinitrotoluene (TNT). This explosive is candidate to be used in civil industry, introduced melted in the solution of oil, wax and emulsifiers, and emulsifying this mixture with the aqueous solution of nitrates. The scope of the present work is to evaluate the contribution of 1 to 5% of TNT in the emulsion matrix, sensitised with 1 and 3% of GMB.
The experimental emulsifying equipment is composed by two vessels, keeping a constant stirring level, containing respectively the aqueous solution of nitrates and the mixture of oils, wax and emulsifiers. This second vessel contains TNT in the case of emulsions with TNT. Two peristaltic pumps ensures mass flow and flow control of components. A micrograph of emulsion explosive matrix with 5% of TNT, shows clearly the dispersion of TNT in emulsion matrix, as very thin sheets or flakes.
The global detonation velocity of emulsion explosives are presented, as a function of density, proving the non ideal detonation behaviour of this kind of explosives. The contribution of the addition of TNT to the emulsion explosive is discussed. It is observed detonation regime, for emulsion explosive with TNT, for densities where the corresponding emulsion explosive, without TNT, presents failure. The evaluation of expansion work of detonation products, of emulsion explosive with and without TNT, are performed using plate dent test experiments. The addition of TNT, increasing the displacement volume and the deepness of formed crater, also contributes to the expansion work of base emulsion explosive.

1. Introduction

The most common industrial explosives in Portugal are ammonium nitrate - fuel oil compositions (ANFO) and dynamite explosives, representing an annual production of 10000 tonnes for open air and underground mines applications. Emulsion explosives are more and more used in these applications. ANFO is an ammonium nitrate - fuel oil composition, with 6 % (weight) of fuel oil, with initial density 870 kg/m^3 and

detonation velocity 3300 m/s. Dynamite explosive is formed by 30 % of nitroglycerine, 6 % of DNT, 60 % of ammonium nitrate and 4 % of amidon, with density 1400 kg/m^3 and detonation velocity 5900 m/s.

Emulsion explosives are generally cited as water explosives, because they are made of an aqueous solution of ammonium, sodium and calcium nitrates, emulsified with a hydrocarbon solution of oils, wax and emulsifiers. Combustible materials such as aluminium, urea, sugar or glycol are often mixed with these solutions. An emulsion explosive in made of a matrix (the water-in-oil emulsion itself) sensitised by air bubbles from a gasifying agent, or from the introduction by hollow glass microballoons (GMB) or plastic hollow spheres. It is very known the influence of these GMB on the sensitisation of a homogeneous explosive - research studies (Gois, 1995) have been developed in our laboratory to understand the contribution of GMB on the initiation and detonation of mixtures of nitromethane-polymethilmetacrylate (NM-PMMA). A small percentage by weight of particles suspended in NM has been found to decrease abruptly the critical diameter and the minimum energy to initiation (Engelke, 1979; Engelke and Bdzil, 1983). Glass microballoons (GMB) were used with success to sensitise emulsion explosives (Yoshida et al., 1985, and Tanaka et al. 1987). Because emulsion are neither gelled nor cross-linked their life is relatively short. Its base composition is an aqueous solution of 10 % of water, 72 % of ammonium nitrate and 10 % of sodium nitrates, emulsified with oils, wax and emulsifiers (5.5%) and sensitised with hollow glass microballoons (2.5 %), having an initial density of 1170 kg/m^3. The life time of these emulsion explosives have being increased correcting their *ph* with calcium nitrate and using very specified emulsifying agents.

The demilitarisation process (Demilitarisation Technology, 1991) origins large amounts of trinitrotoluene (TNT), explosive candidate to be used in civil applications. Its direct utilisation generates many formal or environmental problems. Nevertheless, its high power and energy, associates with a very good knowledge of its detonation properties, suggests the use as energetic additive in industrial explosives. In order to obtain an effective contribution in the detonation regime of the base explosive, the additive material must be divided in a very fine dispersion inside the base explosive material, in order to have reaction inside the detonation zone. This question can be solved introducing melted TNT in the solution of oil, wax and emulsifiers, and

emulsifying this mixture with the aqueous solution of nitrates. This process can be possible because TNT is not miscible with any emulsion phases (aqueous oxidant phase or oil, wax and surfant mixture) and have a melting point lower than the formation temperature of emulsion matrix. Consequently introducing the TNT in the emulsifying process of matrix formation, it is possible to produce a very dispersion TNT in the emulsion matrix media.

The scope of the present work is to evaluate the contribution of 1 to 5% of TNT in the emulsion matrix, sensitised with 1 and 3% of GMB.

2. Emulsion components and characteristics

The matrix of emulsion explosive is obtained by an aqueous solution of ammonium and sodium nitrates, emulsified with oil, wax and emulsifiers, of global characteristics presented on Table 1. The compositions are presented in Table 2. The final density is controlled by the quantity of GMB (Table 2). In the case of the existing of TNT, it is dependent by the quantity of TNT.

Table 1. Components and characteristics

NAME	COM. NAME	REF.	GLOBAL FORM.	DENS. [g/cm3]		COLOUR	PHYS. STATE
				Bulk	Effective		
Ammonium Nitrate	Porous Ammoni Nitrate	AN	NH_4NO_3	0.69-0.74	1.725	white	solid
Sodium Nitrate	Industr. Sodium Nitrate	SN	$NaNO_3$	1.2-1.3	2.261	white	solid
Calcium Nitrate	Indust. Calcium Nitrate	CaN	$Ca(NO_3)$	1.18	2.504	white	solid
Oil	Galp Diesel SAE 30	Oil SAE 30	-		0.9	yellow	liquid
Microcristal Wax	Galp P1	Galp P1	-	-	-	white	solid
Paraffin Wax	Guerow. -70	Guerow. -70	-	-	-	yellow	solid
Sorbitan Monooleate	Span 80	Span 80	-	-	-	yellow	liquid
Sorbitan Sesquioleate	Arlacel 83	Arlacel 83	-	-	-	yellow	liquid
Hollow Glass Microballons	Q-CEL 400	Q-CEL 400	-	0.11	0.21	white	solid

Used GMB in preliminary work were Q-Cel 400 (AKZO). They were substituted by Q-Cel 520 FPS (supplied also by AKZO), with a mean diameter of 45 μm and with a granulometric curve from 16<d_p<79 μm.

Table 1. Composition of the emulsion explosive.

Material	Mass fraction (%)
Ammonium nitrate	71.36
Sodium nitrate	9.78
Water	10.75
Oil	2.05
Paraffin wax	1.03
Microcristalin wax	1.03
Sorbitan monooleate	1.41
Sorbitan sesquioleate	0.15
Glass microballoons	2.44

Differents compositions were produced (Table 3), showing very well the contribution of GMB and TNT on final attained density.

Table 3. Composition and density of final emulsion explosives.

Explosive charge composition	Density (g.cm^{-3})
Emulsion matrix	1.41
+ 1% GMB	1.32
+ 3% GMB	1.15
Emulsion matrix + 1% TNT	1.42
+ 1 % GMB	1.40
+ 3 % GMB	1.21
Emulsion matrix + 5% TNT	1.44
+ 1 % GMB	1.42
+ 3 % GMB	1.32

3. Theoretical prediction of detonation products composition and properties

Theoretical predictions of detonation velocity D_{CJ} and pressure P_{CJ} and products composition were performed using THOR code, based on theoretical work of Heuzé *et al*. ,1895 ,1989, later modified by Campos ,1991, and Durães *et al*. ,1995.

The selection of components are dependent of atomic initial composition. For a classical CHNO system it is assumed an equilibrium composition of CO_2, CO, H_2O, N_2, O_2, H_2, OH, NO, H, N, O, HCN, NH_3, NO_2, N_2O, CH_4 gases and two kinds of

solid carbon (graphite and diamond). Reported data are from JANAF Thermochemical Tables, 1971, and polynomial expressions of Gordon and McBride ,1971.
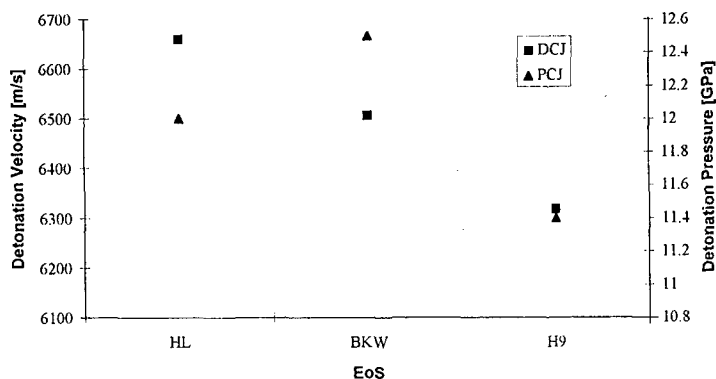

Figure 1. Theoretical detonation velocity D_{CJ} and pressure P_{CJ} of final emulsion explosive for BKW, H9 and HL EoS.
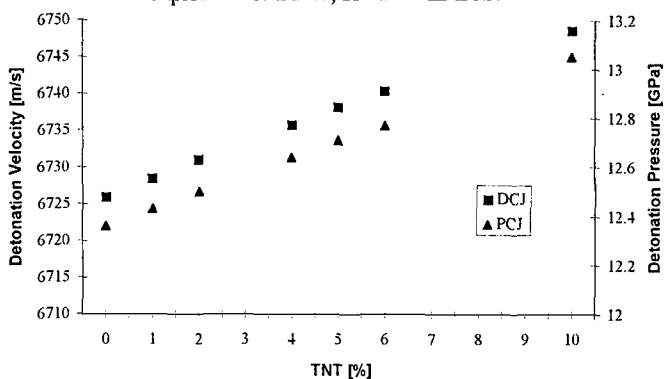

Figure 2. Theoretical detonation velocity and pressure as a function of TNT mass fraction for HL EoS.

The solution of composition problems involves simultaneously:

- the thermodynamic equilibrium (thermal, mechanical and chemical equilibria), obtained with the mass and species balance, and the equilibrium condition $G=G_{min}$ (P,T,x_i), applying to the condensed phase the model proposed by Tanaka, 1983,

- the thermal equation of state (EoS),

- the energetic equation of state, related to the internal energy $E = \Sigma\ x_i e_i(T) + \Delta e$, $e_i(T)$ being calculated from JANAF Thermochemical Tables, 1971, and polynomial expressions of Gordon and McBride, 1971,

- the detonation regime, being Chapman-Jouguet conditions, $D=a_o+U_p$, being a_o the sound velocity and U_p the particular velocity.

Three different EoS, HL, BKW and H9, can be used (Campos, 1991; Durães et al., 1995), assuming the preceding Chapman-Jouguet model of detonation and thermodynamical equilibrium of solid and gas detonation products. Theoretical predictions of detonation velocity D_{CJ} and pressure P_{CJ} and products composition are respectively presented in Figures 1, 2 and 3.
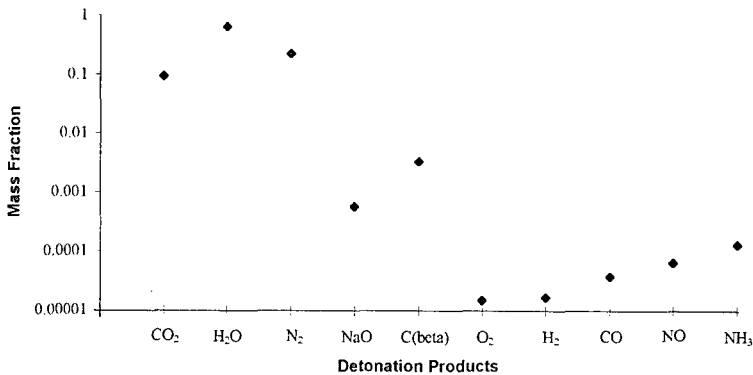
Figure 3. Theoretical detonation products composition.

4. Experimental emulsifying equipment

The emulsifying process, described in Figure 4, is according to the usual industrial procedures. The experimental emulsifying equipment, where is produced the emulsion matrix, is shown in Figure 5. It is composed by two vessels, keeping a constant stirring level, containing respectively the aqueous solution of nitrates and the mixture of oils, wax and emulsifiers. This second vessel can contain TNT, in the case of emulsions with TNT. Two peristaltic pumps ensures mass flow and flow control of components.

The two vessels are also provided with an heating system, controlled by thermocouples, for a constant temperature level of mixtures. The aqueous nitrates solution is obtained by heating, first, the water until 80 °C, and then adding progressively the nitrates. Final temperature is 92 °C. The vessel of oils, wax and emulsifiers is kept constant at 90°C, temperature enough to melt TNT (melting point is 80.9 °C). When the operational temperatures of the mixtures are achieved, the

pumping is initialised using the peristaltic pumps. The pumping chamber of this pumps, made in rubber tube, do not have significant heat loss. The pump mass flow are intermittent controlled by switches. The connection tubes of feeding circuit, made in rubber, are heated by evolved coaxial large tubes, with a steam flow at atmospheric pressure (Figure 5)
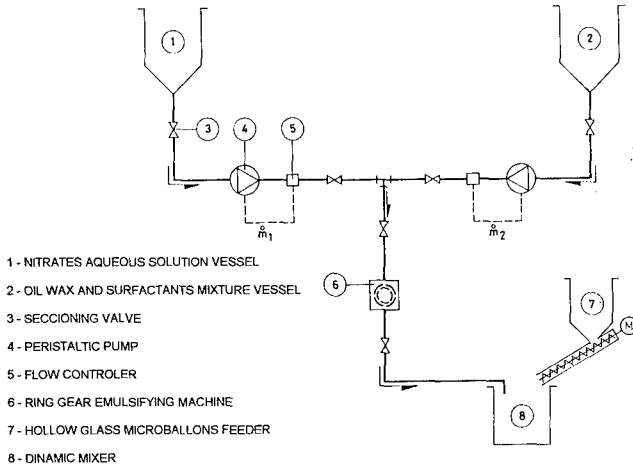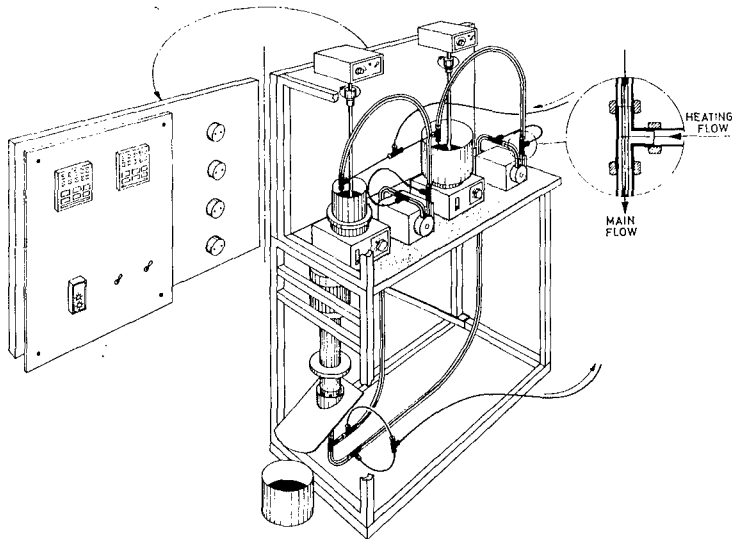

1 - NITRATES AQUEOUS SOLUTION VESSEL
2 - OIL WAX AND SURFACTANTS MIXTURE VESSEL
3 - SECCIONING VALVE
4 - PERISTALTIC PUMP
5 - FLOW CONTROLER
6 - RING GEAR EMULSIFYING MACHINE
7 - HOLLOW GLASS MICROBALLONS FEEDER
8 - DINAMIC MIXER

Figure 4. Emulsifying process.

Figure 5. Emulsifying equipment set-up.

The fluids are premixed by a simple static mixing device, immediately before its introduction into the emulsifying device. This equipment use a ring-gear dispersing machine, made with slotted rotor and stator. The emulsifying principle is based in combined shear stress and flow induced by rotor movement (Figure 6). Consequently high turbulence occurs in gap, between the rotor and stator, which leads to the emulsifying and dispersion of mixtures.
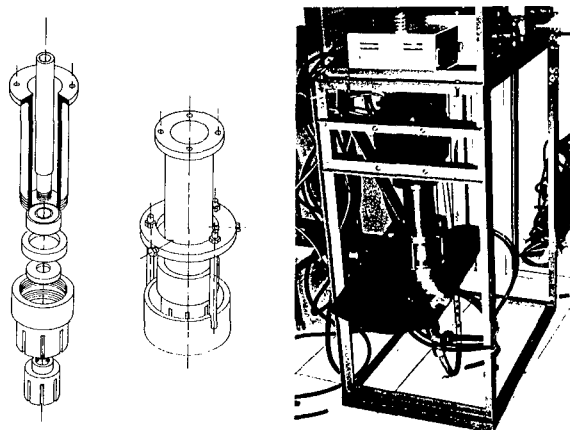

Figure 6. Emulsifying device.

The optical microscopy was used to evaluate the particle size of dispersed phase and the thickness of continuos phase in matrix. The micrograph of the emulsion matrix, produced by this experimental equipment, is shown in Figure 7. The particle size of dispersed phase seems to be lower than 5 μm. A micrograph of emulsion explosive matrix with 5% of TNT (Figure 8) shows clearly the dispersion of TNT in emulsion matrix as very thin sheets or flakes, as long as its initial structure allows.
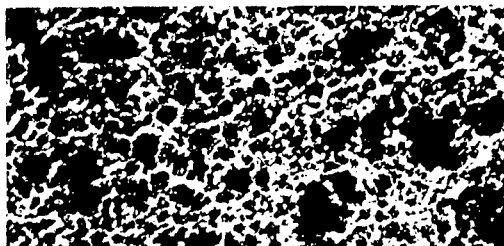

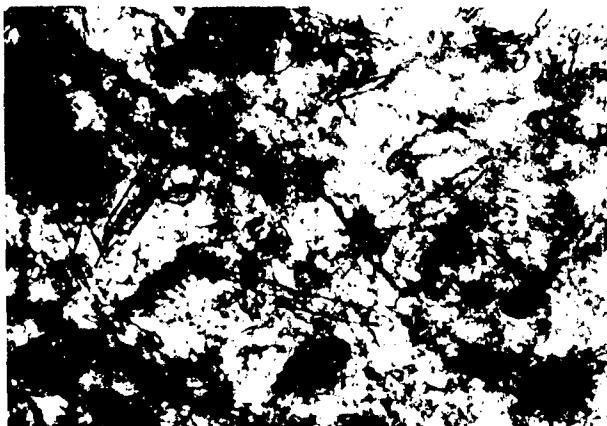Figure 7. Micrograph of emulsion matrix.

Figure 8. Micrograph of emulsion matrix with 5% of TNT.

Emulsion matrix needs the addition of a small amount of GMB to be sensitised. The very high viscosity of emulsion requires a classic mixer, operating under low rotation speed (Figure 4).

4. Experimental results and discussion

4.1. Detonation velocity and pressure

The experimental cylindrical charge (Mendes et al., 1993) has four contact probes formed by a very thin insulated electrical wire, short-circuited with the metal confinement by shock wave. These short-circuits actuate electronic time counters (1 ns resolution) and allow, changing distances between probes, the measurement of local mean velocity of detonation.

Preliminary detonation results of emulsion explosive without TNT, with different mass fraction of GMB (Figure 9) were performed in brass tube (internal diameter of 25.5 mm and 200 mm long) with an initiation by a detonator n° 8, being L is the distance measured from initiation section. They show detonation velocity become stable in a relatively short distance, proving the influence of GMB in sensitisation of emulsion matrix.

Experimental maximum $D_\infty = 5400$ ms^{-1}, obtained plotting measured D as a function of inverse charge diameter (Mendes et al., 1993), shows lower values than those predicted theoretically. It proves the non ideal behaviour of detonation in these kind of

heterogeneous explosives. In the present particular case, a plastic explosive booster was used to initiate the emulsion mixture charges in order to measure the detonation velocity (for 25.5 mm charge diameter and brass confinement). The detonation or failure of emulsion explosives, with and without TNT, are shown in Table 3.
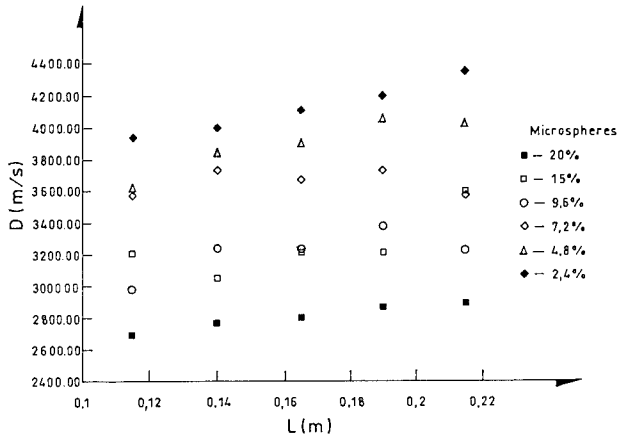

Figure 9. Experimental detonation velocity results of emulsion explosives with different mass concentration of GMB.

Table 3. Detonation results of emulsion explosive with and without TNT.

Explosive charge composition		Density (g.cm^{-3})	Detonation velocity (m.s^{-1})
Emulsion matrix		1.41	Failure
	+ 1% GMB	1.32	3967
	+ 3% GMB	1.15	5421
Emulsion matrix + 1% TNT		1.42	Failure
	+ 1 % GMB	1.40	Failure
	+ 3 % GMB	1.21	5183
Emulsion matrix + 5% TNT		1.44	
	+ 1 % GMB	1.42	5231
	+ 3 % GMB	1.32	5076

The global detonation velocity results of emulsion explosives are represented as a function of density in Figure 10. It shows clearly the contribution of the addition of TNT to the emulsion explosive, as it was predicted by theoretical calculation. An interesting result is to observe existing detonation, for an emulsion with TNT, for densities where emulsion explosives, without TNT, present failure.
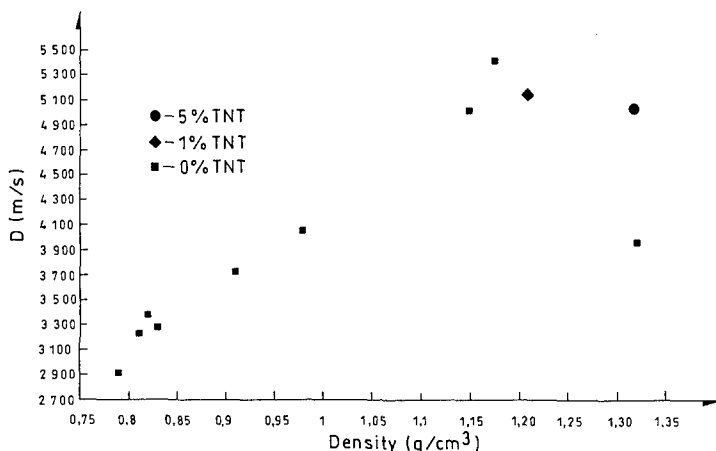
Figure 10. Experimental detonation velocity of emulsion explosives with and without TNT, as a function of density.

Detonation pressure of explosives were measured with shock induced polarisation (SIP), on 1 mm thickness PMMA plate (Mendes et al., 1993). Acoustical approach, applied to the difference of shock impedance of PMMA and explosive detonation products (Fisson, 1976), allows to obtain experimental detonation pressure. The measured experimental detonation pressure, for emulsion explosive without TNT is 12.1 GPa, a lower value than the predicted theoretically.

4.2. Detonation expansion work - plate dent test experiments

The evaluation of expansion work of detonation products, related with detonation pressure, of emulsion explosive with and without TNT are performed using a plate dent test experiment (Mader, 1979). An aluminium cylinder with 100 mm of diameter and 100 mm long was used to test explosive charge dimensions described below. The crater displacement volume and deepness induced by detonation products are presented in Table 4. They shows the contribution of the addition of TNT, increasing the displacement volume and the deepness of formed crater.

Table 4. Crater displacement volume and deepness for emulsion explosives with and without TNT.

Crater	Matrix + 3% GMB	99% (matrix +5 % TNT) + 1% GMB	97% (matrix +5 % TNT) + 3% GMB
Displacement volume x10^{-6} (m^3)	19.5	21.5	28
Deepness (mm)	11.8	13.6	12.4

5. Conclusions

Emulsion explosive matrix with 5% of TNT, shows clearly the dispersion of TNT in emulsion matrix as very thin sheets or flakes. The global detonation velocity of emulsion explosives are presented, as a function of density, proving the non ideal detonation behaviour of this kind of explosives. The contribution of the addition of TNT to the emulsion explosive is discussed. It is observed detonation regime, for emulsion explosive with TNT, for densities where the corresponding emulsion explosive, without TNT, presents failure. The evaluation of expansion work of detonation products, of emulsion explosive with and without TNT, are performed using plate dent test experiments. The addition of TNT, increasing the displacement volume and the deepness of formed crater, also contributes to the expansion work of base emulsion explosive.

References

Campos, J., 1991. "Thermodynamic calculation of solid and gas combustion pollutants using different equations of state", Proc. of *First International Conference on Combustion Technologies for a Clean Environment*, Vilamoura, Algarve, Portugal.

Demilitarisation Technology, 1991. *International Seminar on Demilitarisation Technology for Explosives and Explosive Ordnance*, Royal Military College of Science and Directorate of Land Services Ammunition, Oxfordshire, U.K. .

Durães, L., Campos, J., Gois, J. C., 1995. "Deflagration and detonation predictions using a new equation of state", in *Proc. of the 26th International Annual Conference of ICT*, pp. 67.1-67.13.

Engelke, R ,1979. Effect of a physical inhomogeneity on steady-state detonation velocity. In *Phys. Fluids*, vol. 22, n° 9, pp. 1623-1630.

Engelke R ,1983. Effect of the number density of heterogeneities on the critical diameter of condensed explosives. In *Phys. Fluids*, vol. 26 n° 9, pp. 2420-2424.

Fisson, F. ,1976. " *Étude de grandeurs caracteristiques de la détonation d'explosifs liquides*", Thesis, E.N.S.M.A, Poitiers, France.

Gois, J. C. ,1995. "*Influência das micro esferas ocas de vidro na detonação da mistura nitrometano-polimetilmetacrilato*", PhD Thesis, University of Coimbra, Portugal

Gordon, S., Mc Bride, B.J. ,1971. *Computer Program For Calculation of complex Chemical Equilibrium Compositions, Rocket Performance Incident and Reflected Shocks and Chapman-Jouguet Detonations.* Report NASA SP 273, NASA Lewis Research Center.

Heuzé, O., 1989. *Cálculo Numérico das Propriedades das Misturas Gasosas em Equilíbrio Termodinâmico*, Universidade de Coimbra, Portugal.

Heuzé, O., Bauer, P, Presles, H. N. and Brochet, C. ,1985. The equations of state of detonation products and their incorporation into the quatuor code. *Proceedings of the Eighth Symposium (International) on Detonation*, pp. 762 - 769, Albuquerque Conventional Center, New Mexico.

JANAF, 1971. *Thermochemical Tables* - 2nd Edition. National Bureau of Standards, Washington D.C.

Mader, C.L. ,1979. *Numerical Modeling of Detonations.* University of California Press, Berkeley, CA.

Mendes R, Campos J, Gois JC, Moutinho C ,1993. Shock initiation and detonation stability of industrial explosives. In *Proceedings of the 24th International Conference of ICT*, Karlsruhe, Germany, pp. 29.1-29.13.

Tanaka K, Yoshida M, Ilda M, Fujiwara S ,1987. Detonation properties of water gels. In *Proceedings of the Symposium International on Pyrotechnics and Explosives*, China Academic Publishers, Beijing, pp. 328-332.

Tanaka, K. ,1983. *Detonation Properties of Condensed Explosives Computed Using the Kihara-Hikita-Tanaka Equation of State.* Report from National Chemical Laboratory for Industry, Ibaraki, Japan.

Yoshida M., Ilda M., Tanaka, K., Fujiwara, S., Kusakabe, M. and Shiino, K. ,1985. "Detonation behaviour of emulsion explosives containing glass microballoons" *Proceedings of 8th Int. Symposium on Detonation*, pp. 993-1000.

PBX MANUFACTURING AND TESTING
WITH MODIFIED PETN PARTICLES

C. Moutinho*, J. Campos**, J. C. Góis** and M. Figueiredo***

Laboratory of Energetics and Detonics
*Soc. Port. de Explosivos - SPEL,**Dep. of Mech. Eng. and *** Chem. Engineering
Faculty of Sciences and Technology, Univ. of Coimbra - 3000 COIMBRA, Portugal

ABSTRACT
The development of non primary explosive detonators leads to study new plastic bonded explosives (PBX) based in pentaerythritol tetranitrate (PETN), chosen because is a nitroester sensible to shock initiation. A PBX explosive with PETN as filler and HTPB/IPDI/DOS as binder has been manufactured with two different concentrations of PETN: 95 and 80 % (weight). The shape of PETN particles, its particle size and specific area are also important in the sensitivity properties of this kind of explosive. In order to modify the particle shape and size, the original PETN particles were submerged in binary mixtures of ethyl acetate solutions and water, changing not only its solvent concentrations from 2 to 20 %, but also the submerged time, keeping constant the stirring level. The obtained results show the changement of particle shape, agglomeration tendency and granulometric particle size distribution. Thermal stability, infrared spectra and differential scanning calorimetry (DSC) of PETN prove its quality and purity and shows the relatively small influence of binder in this reactive system, comparing with the DSC of manufactured PBX. Obtained densities of PBX explosive are respectively ~0.92 and ~1.105 for PETN concentrations of 95 and 80%. Detonation velocity, performed with cylindrical charges of 10 mm diameter, is respectively 6000 and 5540 m/s, as a function of PETN concentration. Initiation experiments were performed with gap test configurations, having as donor a cylindrical charge of 32 mm diameter of NM-PMMA, with 4% of PMMA, and hollow glass microbaloons (GMB) final concentrations of 6 %, in order to have a very low intensity shock generator. Gap material was also PMMA, changing its thickness from 3 to 60 mm. The shock initiations gap test show initiation pressures values between 0.30GPa and 0.41GPa for PBX of 95% of PETN, and between 0.44GPa and 0.57Gpa for PBX of 80% of PETN. An interesting result was obtained for an induced pressure of 0.22 GPa, showing melted material of PBX without initiation. Detonation velocity is in a good agreement with literature for this kind of PBX explosive.

1. Introduction

The development of a non primary explosive detonator leads to study new plastic bonded explosive (PBX) based in a secondary explosive as filler. There are three families of explosives candidates to be used in this application: the nitric esters, the nitramines and the nitroaromatics. Thermal stability and shock sensitivity to initiation

were the parameters generally used to select the explosive. Nitric esters ($O-NO_2$ configuration) present higher sensitivity to initiation than nitramines ($C-NO_2$ configuration). There are two explosives candidates cited in bibliography: the pentaerythritol tetranitrate (PETN), a nitric ester, and hexanitrostilbene (HNS). The selection of HNS was not considered, because the manufacture of this explosive is not easy and its cost is higher than PETN. The shape of PETN particles, its particle size diameter and specific area are very important in the sensitivity properties. In order to modify the particle shape and size diameter the original PETN particles were submerged in binary mixtures of ethyl acetate solutions and water, changing not only its solvent concentrations from 2 to 20 %, but also the submerged time, keeping constant the stirring level. The selected binder system for PBX was a polyurethane based on HTPB and IPDI. Binder properties and final density of PBX are very important to have acceptable rheological properties. However, the energy of shock initiation is a function of initial density of explosive. A PBX explosive with PETN as filler and HTPB/IPDI/DOS as binder has been manufactured with two different concentrations of PETN: 80 and 95 mass percent (%). Detonation velocity experiments were performed with cylindrical charges. Initiation experiments were performed with gap test configurations, having as donor a cylindrical charge of 32 mm diameter of NM-PMMA, with 4% of PMMA, and hollow glass microbaloons (GMB) of final concentrations of 6 %, in order to have a very low intensity shock generator. Gap material was also PMMA, changing its thickness from 3 to 60 mm.

2. PBX characterisation

2.1 PETN (filler) characterisation

Pentaerythritol tetranitrate, usually designated by PETN, of chemical formula $C(CH_2NO_2)_4$ is a white solid and non hygroscopic substance. It fundamental crystal structure is tetragonal. Its chemical properties are presented on table 1.

Table 1 - Chemical properties

Explosive name	Global formula	Molecular Weight (g)	Theoretical Density (g/cm3)	Melting Point (°C)	ΔH_f (kcal/mol)
PETN	C5H8N4O12	316.2	1.78	140.5	-128.7

Infrared spectroscopy was used to identify the characteristical absorption bands of PETN, using a spectrometer equipment (Nicolet FTIR Spectrometer, model 740) with a global source, a DTGS detector and potassium bromide cells. The infrared spectra was obtained at room temperature and recorded in the region 400-4000cm^{-1} (vd. figure 1). In infrared spectra it can be identified the characteristical frequencies of nitric esters. The asymmetric stretching of NO$_2$ at 1647cm^{-1} and symmetric stretching at 1271cm^{-1}. At 1002cm^{-1} it has been identified absorption band of stretching of CO, and at 847cm^{-1} the stretching of NO. This results are in agreement with the values obtained by other authors.
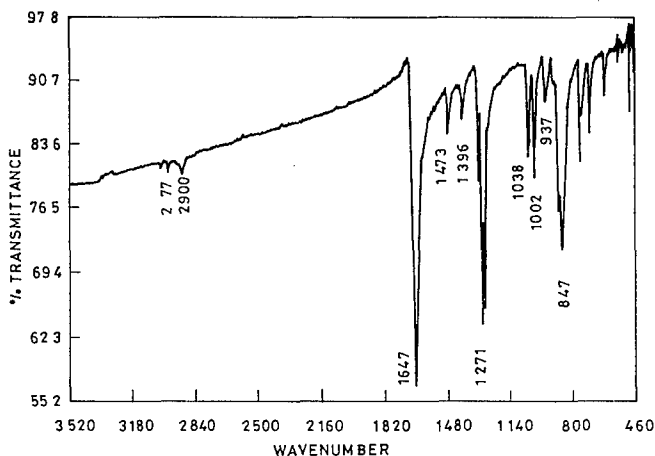

Figure 1 - PETN infrared spectra

In order to know the safety working temperature range of PETN it was evaluated its thermal evolution by two different techniques: vacuum stability test and differential scanning calorimetry (DSC). Vacuum stability test is a well known technical procedure based on the measured volume of gas, from the heating sample on a vacuum heated chamber. The tests were performed (German Specification, TL-1376-800) keeping the samples at 100°C during 40 hours. The obtained result was 0.375ml of generated gas. According the thermal stability evaluation criteria (American Military specification MIL-STD-1234) it can be concluded that PETN at 100°C is not reactive. Differential scanning calorimetry analysis was performed (Shimadzu DSC 50 equipment) under operative conditions of table 2.

Table 2 - Operative conditions
Temperature Programme:
Initial temperature - 25 °C
Final temperature - 250 °C
Heat Velocity: 5°C/min
Sampling time: 1s
Sample weight: 2.13mg

The obtained PETN thermogram is shown in figure 2. The measured melting point is 140.47°C and the initial decomposition temperature is 179.16°C. These results allow to conclude that PETN is thermally stable for PBX manufacture.
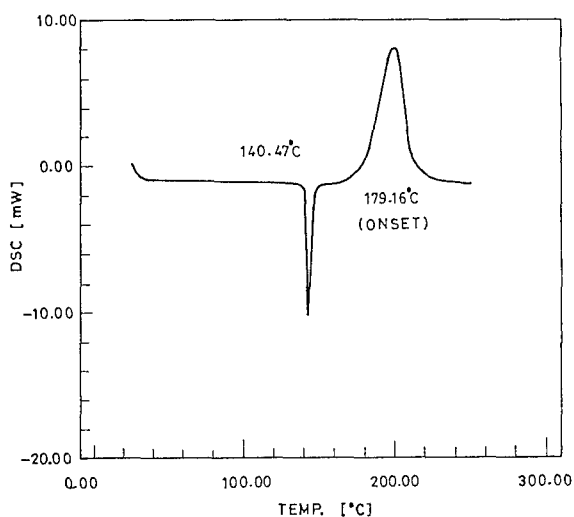

Figure 2 - PETN thermogram

2.2. PETN crystals modification procedures and results

PETN particle shape and size diameter were modified submerging in binary mixtures of aqueous ethyl acetate solutions with differents concentrations, from 2 to 20% (in weight), during 1 hour, keeping a constant stirring level. At the end of this time, the suspension was washed with distilated water and filtrated. The solids were then dried in an oven at 60°C. The evolution of the particle size diameter and particle shape was measured by Laser diffraction (Malvern model 2600C) and evaluated by optical microscopy. The surface area was also analysed by adsorption gas technique.

Before particle size analysis, PETN aqueous suspensions with dispersant were desaglomerated by ultra-sounds, during 3 minutes. During analysis the stirred system was mechanical. The obtained results are presented under cumulative frequence curves (undersize) mass base form (vd. figure 3). Table 3 shows the mean value of 10 experiments, allowing the evaluation of particle size diameter of PETN as a function of used concentrations of aqueous ethyl acetate solutions. The distributions were characterised by the mean value (d_{50}) and ratio $(d_{90} - d_{10})/d_{50}$.
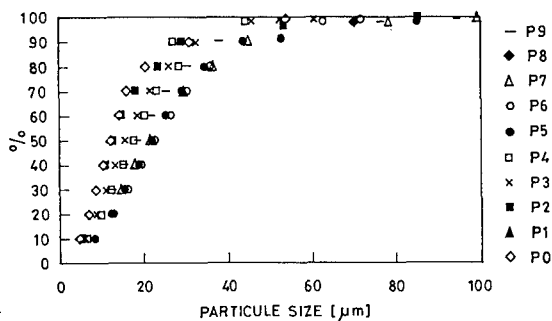

Figure 3 - Cumulative distribution curves of PETN by Laser diffraction

Table 3 - Characteristical parameters of cumulative frequence curves.

Sample	d_{50}	d_{90}	d_{10}	$(d_{90} - d_{10})/d_{50}$
P1	12.65±0.05μm	29.5±3.7μm	4.97±0.05μm	1.94
P2	13.02±0.4μm	30.10±0.9μm	5.27±0.09μm	1.91
P3	12.70±0.3μm	28.55±0.5μm	5.03±0.05μm	1.85
P4	16.10±0.7μm	32.93±2μm	6.13±0.2μm	1.66
P5	17.88±0.6μm	33.48±0.05μm	6.93±0.2μm	1.48
P6	22.48±0.7μm	45.48±5μm	8.56±0.1μm	1.64
P7	22.98±1μm	44.92±3μm	8.54±0.4μm	1.58
P8	20.70±0μm	38.70±0.3μm	7.90±0μm	1.49
P9	22.20±0μm	42.45±0.05μm	8.4±0μm	1.53
P10	19.03±0.8μm	38.97±1.8μm	4.30±2.69μm	1.82

PETN particles were observed by microscopy (Olympus BH2 microscope connected to a system of image analysis CUE-2, Olympus), in order to evaluate its shape as a function of solvent cpncentration. Figure 4 represents two examples of PETN samples.
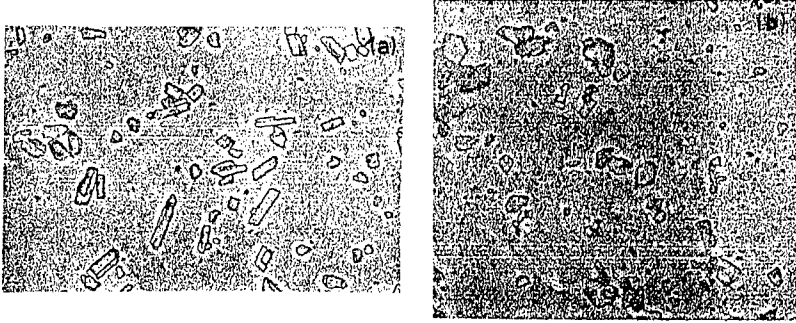
Figure 4 - Microscope image of PETN particles without solvent action (a) and with solvent (12%)action (b).

The particle shape was modified, from a long particle into a round shape. The calculated shape factor is 0.7.

The surface area was evaluated by physical adsorption gas technique (ASAP2000 Accelerated Surface Area and Porosimetry) using Krypton as adsorber gas. The specific surfaces of differents PETN granulometic classes were calculated from BET curves. The results are presented on table 4.

Table 4 -Specific surface values for PETN particles

Sample	d_{50}	Specific surface (m^2/g)
S1	12.65μm	0.515
S2	13.02 μm	0.400
S3	12.70μm	0.373
S4	16.10μm	0.356
S5	17.88μm	0.309
S6	22.48μm	0.266
S7	22.98μm	0.269
S8	20.70μm	0.264
S9	22.20μm	0.226
S10	19.03μm	0.252

The granulometric class of PETN particles, modified by the solution with 8% of solvent, was selected for manufacture of explosive compositions. This kind of PETN particles had presented lower sensitivity (7.9J for impact sensibility with fal hammer BAM test and 8kgf for friction sensibility; original PETN particles needs 6J for

impact and 5,4/kgf for friction). The chosen particles have its mean particle size (17.88µm) with a small deviation from the original 12.65µm.

2.3 Binder system characterisation

The selected binder system is a polyurethane compound, composed by isophorane disocianate (IPDI), a hydroxil terminated polybutadiene (HTPB) and a plasticizer dioctyl sebacate (DOS). The NCO and OH contents, initial density and viscosity have been verified in the polymer components. The chemical compatibility between PETN and all the binder components was tested by two procedures: vacuum compatibility test and differential scanning calorimetry (DSC). The vacuum chemical compatibility test was performed in a similar way to the previous vacuum stability test. The operative conditions were the same. Experimental results between PETN and polymers (HTPB, DOS, IPDI) are presented on tables 5, 6 and 7. The reactivity values are summarised on table 8.

Table 5 - Experimental compatibility results (PETN/DOS).

Sample	Generated volume gas (ml)
PETN	0.404
DOS	0.262
PETN+DOS	0.122

Table 6 - Experimental compatibility results (PETN/IPDI).

Sample	Generated volume gas (ml)
PETN	0.404
IPDI	1.098
PETN+IPDI	8.555

Table 7 - Experimental compatibility results (PETN/HTPB).

Sample	Generated volume gas (ml)
PETN	0.507
HTPB	0.157
PETN+HTPB	-0.092

Table 8 - Experimental reactivity results.

Mixture	Reactivity (ml)
PETN+HTPB	0
DOS	-0.088
PETN+DOS	-0.544

According the thermal stability evaluation criteria (American Militar specification MIL-STD-1234) it can be concluded that PETN is compatible with all the polymeric

components. Differential scanning calorimetry confirms these results by thermogram analysis of PETN and polymeric components (vd. figures 5a, 5b, 5c). Consequently, the concentration of polymeric components are on table 9.
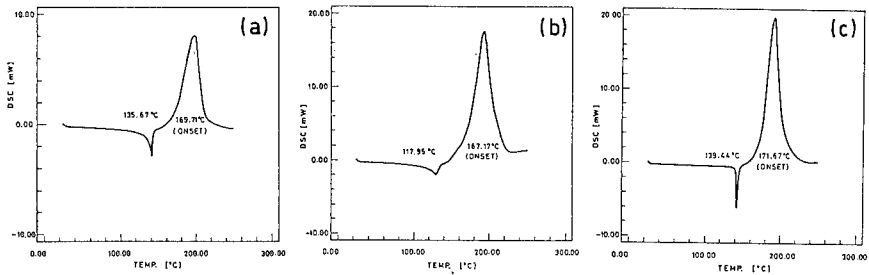

Figure 5 - DOS+PETN thermogram (a), IPDI+PETN thermogram (b), HTPB+PETN thermogram (c).

Table 9 - Compositions

Binder system		
HTPB (%)	IPDI (%)	DOS (%)
69,8	6,96	23,24

2.4 PBX Explosive compositions - PBXC8020 AND PBXC9505

Two explosive compositions were manufactured, designated by PBXC8020 and PBXC9505, with filler PETN concentration of 80% and 95% (in weight) respectively. PBX compositions was prepared in four steps:

- first, it was prepared   the binder solution, HTPB, DOS and a solvent (chloroform).
- second, it was added the explosive filler to the binder solution, and the mixture was stirred during 30 minutes.
- third, it was removed the solvent by vacuum technique.
- at last, it was additioned the isocyanate (IPDI).

The cure of the mixture was developed inside of brass cylindrical charges at room temperature. The density of two explosive compositions, was less than TMD:

- TMD of PBXC8020 is 1508kg/m^3, experimental value obtained was 1108kg/m^3 (73%),
- TMD of PBXC9505 is 1699kg/m^3 and obtained experimental value was 932kg/m^3(55%).

3. Detonation velocity assembly and results

Detonation velocity experiments were performed with brass cylindrical charges of 10mm diameter. The densities of PBXC8020 and PBXC9505 are respectively 1108kg/m^3 and 932 kg/m^3. The mean detonation velocity was measured by four contact probes (vd. figure 6) from a very thin insulated electrical wire, short-circuited with the metal confinement by the shock and expansion of detonation products (Mendes et al., 1973).
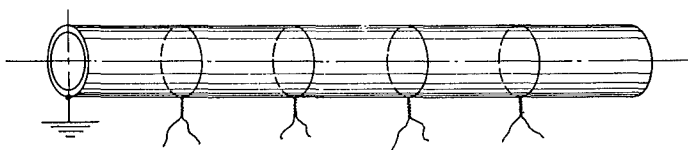

Figure 6 - Detonation velocity experimental assembly.

The obtained values, as a function of PETN concentration, show to be stable and greater than the expected predicted values, calculated with THOR code (Durães et al, 1995) with H9 equations of state (vd. Table 10).

Table 10 - Detonation velocity of PBX

PBX composition	ρ (Kg/m3)	Calculated D_{CJ} (m/s)	Experimental D (m/s)
PBXC8020	1108	5103	5539
PBXC9505	932	5565	6002

4. Initiation experiments

Shock initiation experiments (vd. figure 7) were performed with gap test configurations (Mendes et al, 1993), having as donor a brass cylindrical charge of 32mm diameter with an explosive mixture composed by nitromethane with 4% of PMMA and 6% of hollow glass microbaloons (GMB) in order to have a low intensity shock generator (Gois, 1995). Gap material was PMMA, changing its thickness from 3 to 60mm. The acceptor explosive charge (PBXC8020 and PBXC9505) was confined in brass cylindrical tubes (10x60mm).
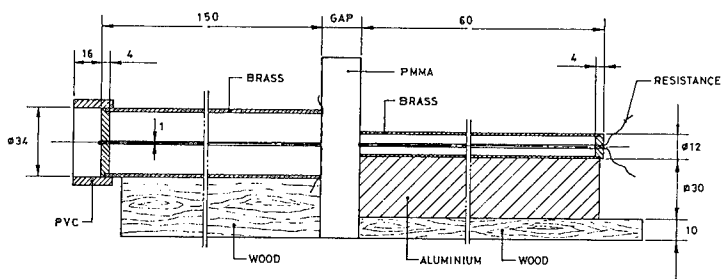
Figure 7 - Shock initiation experimental assembly.

The shock intensity in explosive acceptor (PBXC8020 and PBXC9505) is lower than the minimum value to be experimentally measured with manganin gauges. It is obtained, measuring the shock intensity of donor (8.72GPa) and taking in account the absorption law at PMMA gap material (eq. 1), taking by X the thickness value of the gap. (Sanchidrian, 1993).

$$LnP=2.17-0.0597X \tag{1}$$

The obtained results (vd. Table 11) show the initiation of PBXC8020 for critical gap thickness between 36 mm and 40 mm. Initiation of PBXC9505 was observed for a critical gap thickness between 40 mm and 45mm. The shock wave pressure between PMMA gap and explosive charge has calculated by equation 1. The obtained results are presented on Table 12.

Table 11 - Experimental results.

| Experimental n°	PBX Composition	"gap" thickness (mm)	Result
7	PBXC9505	3	detonation
1	PBXC9505	26	detonation
3	PBXC9505	40	detonation
8	PBXC9505	45	failure
5	PBXC9505	50	failure
4	PBX9505	60	failure
19	PBXC8020	3	detonation
13	PBXC8020	3	detonation
17	PBXC8020	31	detonation
11	PBXC8020	31	detonation
18	PBXC8020	36	detonation
15	PBXC8020	36	detonation
12	PBXC8020	40	detonation
14	PBXC8020	40	detonation
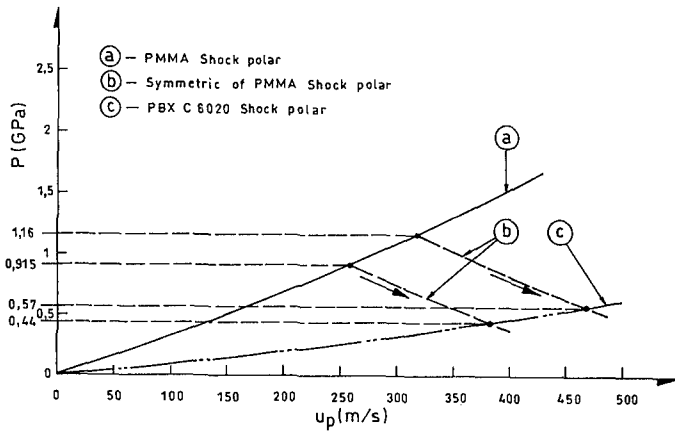
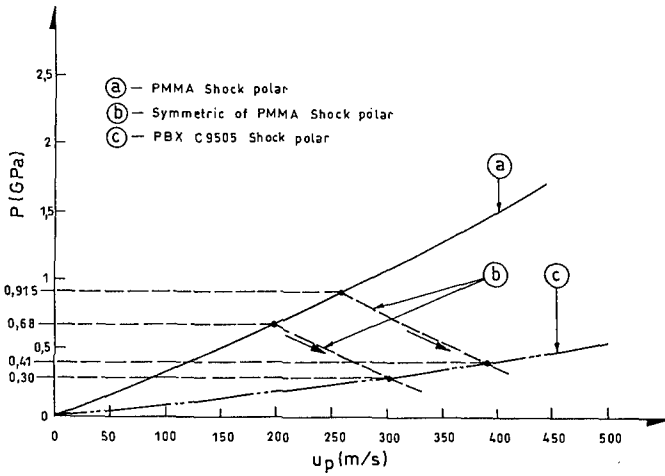Figure 8- Shock polar curves.

Figure 9- Shock polar curves.

Figure 10 - Melted PBXC8020 material after shock

Table 12 - Induced shock pressure values.

Compositions	Gap of PMMA (mm)	Shock wave pressure (LnP=2.17-0.0597*x) (GPa)
PBXC8020	36	1.16
	40	0.915
PBXC9505	40	0.915
	45	0.68

Shock polar of PMMA (eq. 2) and of explosives compositions PBXC8020 and PBXC9505 (eqs. 3 and 4) allow to calculate, by accoustical approach (Fisson, 1976), the induced pressure on explosive acceptor, from different gap thickness (vd. figures 8 and 9).

$$P_{PMMA}=1.798*10^{-6}\ u_p^2+3.08*10^{-3}u_p \tag{2}$$

$$P_{PBXC8020}=0.795*10^{-6}*u_p^2+0.840*10^{-3}*u_p \tag{3}$$

$$P_{PBXC9505}=0.689*10^{-6}*u_p^2+0.778*10^{-3}*u_p \tag{4}$$

The obtained results allow to conclude the initiation pression for PBXC8020 composition (between 0.44GPa and 0.57GPa) and for PBXC9505 (between 0.30GPa and 0.41GPa).

The gap test shows also a very interesting result for a gap thickness of 50mm, melting the PBX material without initiation (vd. figure 10), for a calculated induced pressure of 0.22GPa. Theoretical and bibliographical information show higher initiation pressure than the experimental values here presented.

5. Conclusions

Two plastic explosive compositions PBXC8020 and PBXC9505 were manufactured with an explosive filler of PETN. PETN particles were modified by a solvent action. These particles are less sensibles to initiation, proved by impact and friction tests. The shock initiations gap test shows initiation pressures values between 0.44GPa and 0.57Gpa for PBXC8020, and between 0.30GPa and 0.41GPa for PBXC9505. An interesting result was obtained for an induced pressure of 0.22 GPa, showing melted material of PBX without initiation. Detonation velocity values were in a good agreement with literature for this kind of PBX explosive.

References

Durães, L., Campos, J., Gois, J. C., (1995), "Deflagration and detonation predictions using a new equation of state", in *Proc. of the 26th International Annual Conference of ICT,* pp. 67.1-67.13.

Fisson, F. (1976), "*Étude de grandeurs caracteristiques de la détonation d'explosifs liquides*", Thesis, E.N.S.M.A, Poitiers, France.

Gois, J. C. (1995) "*Influência das micro esferas ocas de vidro na detonação da mistura nitrometano-polimetilmetacrilato*", PhD Thesis, University of Coimbra, Portugal

Mendes, R., J. Campos, J. C. Gois and C. Moutinho, (1973), "Shock initiation and detonation stability of industrial explosives", in *Proc. of the 23th International Annual Conference of ICT,* pp.29-1 29-13

Sanchidrián, J. A. (1973) - "Analytical and numerical study of the shock pressure in the gap test", *Propellants Explosives Technology Division*, Florida.

EVALUATING THE ABILITY
TO DO WORK OF PBX

Hua Pinghuan

(Institute of Chemical Materials, CAEP, Chengdu 513, 610003, CHINA)

ABSTRACT

Energy depression coefficients of TATB and other components were determined by using the data of cylinder test. The evaluated values of explosive energy by Dobratz's method can fairly agree with the experimental results, if the rectified energy depression coefficients given by this paper were adopted.

INTRODUCTION

There are a lot of methods to evaluate the ability to do work of plastic-bonded explosives (PBX).

Although the plate dent test is an old and quite simple method, the results of which are very valuable. In this test, the detonation products of the explosive sample stricks on a steel block, the depth of the dent formed on which is used as the measure of explosive brisnce, and there is an relationship between the dent depth and the ability to do work of explosives[1,2].

The flying plate test is widely used to determine the ability to do work. In this test, a metal plate is driven by the detonation products, a part of the chemical energy of explosive is converted into kinetic energy of the flying plate[1~4].

In Russia, Eremenko et al. take the relative impulse (I_{rel}) as the measure of explosive brisance. They measure the I_{rel} by a impulse

meter,which is similar to Kast brisance meter[5].

Among the methods to evaluate the ability to do work of explosives,the cylinder test is the best,it has been widely adopted in the world. It is regarded as the standard test to evaluate the ability to do work of explosives. Researchers attempted to relate the results of the cylinder test to that of other tests[2,3,5].

To evaluate the results of cylinder test,some empirical formulae have been postulated,one of them is the Dobratz method[6,7]. These formulae are based on the experimental data,so that the calculated values by them can agree with the experimental data to some extent. The coefficients in these empirical formulae, however,must be rectified to fit the data produced recently and to evaluate the energy of PBX more accurately.

DOBRATZ'S METHOD

The percent($v_i\%$) of a component i in a formulation can be calculated as follows:

$$V_i\% = W_i\%\rho/\rho_i \qquad (1)$$

$$V_a\% = 100 - \Sigma V_i\% \qquad (2)$$

where, ρ——practical density of PBX charge, g/cm³; $W_i\%$——percent by weight of component i in the formulation, %; ρ_i——theoretical maximum density of component i, g/cm³; $V_a\%$——volume percent of air in the charge, %.

The relative energy, i. e the energy relative to the energy of HMX, $E_{rel}\%$ can be calculated by formula (3).

$$E_{rel}\% = 100 - \Sigma S_i V_i\% - S_a V_a\% \qquad (3)$$

Table 2　Comparison between calculated E_{19} according to S, given by Dobratz and the experimental values

explosive	9159	9003	4748	RX-26-AW	RX-26-AF	569	RX-03-BB	9502	TATB
TATB wt. %/(%)	0	7	47	47.1	47.5	56	92.5	95	100
$E_{rel}/(\%)$	93.5	88.1	67.2	67.4	68.1	63.7	52.8	45.9	46.8
E_{19}cal. /(kJ/g)	1.631	1.535	1.171	1.175	1.188	1.111	0.921	0.800	0.816
E_{19}exp. /(kJ/g)	1.651	1.558	1.312	1.304[a]	1.328[a]	1.246[a]	1.072[a]	1.031[a]	1.045[a]
$\Delta E_{19}/E_{19}$exp. /(%)	−1.2	−1.5	−10.7	−9.9	−10.5	−10.8	−14.1	−22.4	−21.9

Table 3　Comparison between calculated E_{19} according to the rectified S_i and the experimental values

explosive	9159	9003	4748	RX-26-AW	RX-26-AF	569	RX-03-BB	9502	TATB
TATB wt. %/(%)	0	7	47	47.1	47.5	56	92.5	95	100
$E_{rel}/(\%)$	94.1	89.2	73.9	74.1	75.0	71.8	58.9	59.8	61.2
E_{19}cal. /(kJ/g)	1.640	1.556	1.289	1.291	1.307	1.252	1.026	1.040	1.067

where, S_i—— energy depression coefficient of component i；
S_a——energy depression coefficient of air.
The energy of a explosive, E, i. e the specific kinetic energy at R
$-R_0=19$mm in cylinder test, can be calculated as follows：

$$E = E_{HMX} \cdot E_{rel} \% /100 \qquad (4)$$

where, E_{HMX}—— detonation energy of HMX at its TMD (1.
905g/cm^3). The specific kinetic energy at $R-R_0=19$mm is de-
termined at a practical density, based on the experimental data,
the specific kinetic energy at TMD of HMX, 1. 743 kJ/g, can be
derivered, that is the E_{HMX}.
Some energy depression coefficients relative to HMX, S_i, given
by Dobratz are listed in Table 1.

Table 1 Some energy depression coefficients given by Dobratz

Components	TATB	TNT	NC	Kel-F	Viton	Wax	Air
S_i	0. 5	0. 5	0. 75	1. 0	1. 0	1. 3	1. 3

EVALUATING EXPLOSIVE ENERGY WITH ENERGY DEPRESSION COEFFICIENTS GIVEN BY DOBRATZ

Using the energy depression coefficients listed in Table 1, the
energy of some explosives has been calculated. The results are
listed in Table 2.
It can be seen from Table 2 that there is an obvious diffrence be-
tween the evaluated values and the experimental values. The av-
erage relative deviation is $\pm 11.4\%$, and the maximum relative
deviation may up to 22. 4%(PBX 9502). The difference between

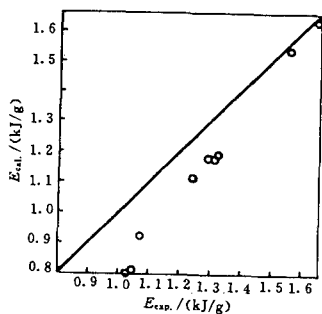calculated values and the experimental values are shown in Fig. 1.

Fig. 1   Comparison of the results calculated with
S_i given by Dobratz and the experimental values

EVALUATING EXPLOSIVE ENERGY WITH RECTIFIED ENERGY DEPRESSION COEFFICIENTS

The calculated values with energy depression coefficients given by Dobratz are far from the experimental values, since some energy depression coefficients given by Dobratz have not been examined by experiments and just are empirical ones, as remarked by Dobratz in his book. For this reason, we rectified the energy depression coefficients of TATB and other components according to the results of cylinder test. The energy listed in Table 2 are re-calculated with rectified coefficients and the results are listed in Table 3.

It can be seen from Table 3 and Fig. 2, that the evaluated values are fairly agree with that obtained from experiments. The average relative deviation is only $\pm 1.4\%$.
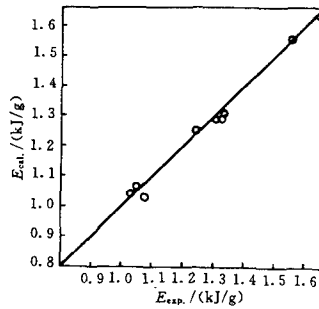

Fig. 2   Comparison of the results calculated with rectified S_i and the experimental values

DISCUSSION

It can be seen by comparing the data of Table 2 and Table 3, that the calculated results with rectified coefficients are better than that with the coefficients given by Dobratz. Therefore it is necessary to rectify these coefficients for Dobratz's method can be used efectively in practice.

To determine S_i, the data of cylinder test is necessary. If a formulation contains only one component, the formula (3) can be simplyfied as formula (5)

$$E_{rel}\% = 100 - S_i V_i\% - S_a V_a\% \qquad (5)$$

hence the S_i of that component can be obtained from the $E_{rel}\%$ determined experimentally. For example, the calculated wall velocities v_{19} at $R-R_0=19$mm in cylinder test using various S_i, for component TATB, are listed in Table 4 and Table 5.

Table 4　Calculated wall velocities based on various S_i for TATB at density 1. 856g/cm³

S_i	0. 35	0. 36	0. 37	0. 50	experimental
v_{19}/(km/s)	1. 461	1. 449	1. 438	1. 278	1. 446[9]

Table 5　Calculated wall velocities based on various S_i for TATB at density 1. 854g/cm³

S_i	0. 34	0. 35	0. 36	0. 50	experimental
v_{19}/(km/s)	1. 469	1. 457	1. 446	1. 274	1. 469[10]

From the data listed in Table 4 it can be seen, that the calculated value can fairly agree with experimental value if 0. 36 is taken as S_i. However, 0. 34 is the best value as S_i from Table 5. Summarizing the data in Table 4 and Table 5, considering the calculated results of some formulations containing TATB, 0. 35 is taken as the energy depression coefficient of TATB.

For TNT at density 1. 680g/m³, $v_{19}=1$. 4km/s is provided by reference[9] and $E_{19}=0$. 97kJ/g is provided by reference[7]. According to these data, the energy depression coefficient of TNT will be 0. 425 and 0. 428 respectively. The result of Octol(HMX/ TNT　78/22) is also given by [7]: $E_{19}=1$. 535kJ/g at density 1. 813g/cm³. Accordingly, the energy depression coefficientof

TNT ought to be 0.40. Summarizing these data, we take 0.41 as the energy depression coefficient of TNT.

The energy depression coefficients used in our calculation are listed in Table 6.

Table 6   Rectified energy depression coefficients

components	TATB	TNT	NC	Kel-F	Viton	Wax	Air
S_i	0.35	0.41	0.38	1.0	1.0	1.3	1.3
components	RDX	NQ	G	Estane	F	Ms	As
S_i	0.08	0.35	1.3	1.3	1.0	1.3	1.3

Among the 9 explosives listed in Table 3 there are 5 explosives whose cylinder tests are carried out by Hornig using various ID copper tube, and there are 4 explosives whose cylinder tests are carried out by us. All of these results can be estimated satisfactorily by the rectified energy depression coefficients listed in Table 6. Among the explosives listed in Table 3, there are two explosives (RX-25-AF and RX-03-BB) whose cylinder tests are carried out by Hornig using $\varnothing$50.8mm copper tube[8], however, their results and the results of $\varnothing$25.4mm cylinder tests of other formulations can be estimated with the same formulae. This fact indicates that the rectified energy depression coefficients are reliable in practical use. It also indicates that the scaling law can be used for HMX-TATB based formulations.

REFERENCES

[1] Hornberg H, Volk F. The Cylinder Test in the Context of Physical Detonation Measurement Methods. Propellants, Explosives, Pyrotechnics, 1989, 14(5):199~211

[2] Hua Pinghuan, Xia Shuigen. Determination of Detonation Performance of Explosives with Small Scale Cylinder Test. Proc. of the 18th ICT International Conference, Germany: 1987.

[3] Hua Pinghuan. Prediction of Plate Flyer Velocity. Proc. of the Int. Symp. on Pyrotechnics and Explosives (ISPE). Beijing: 1987.

[4] Mala J, Souletis J. Comparison of Cast PBX Ballistic Properties from Cylinder and Flyer Plate Tests. Proc. of the Int. Symp. on Pyrotechnics and Explosives (ISPE). Beijing: 1987.

[5] Eremenko L T, Nesterenko D A. Relationship between Brisance of Explosivesand their Molecular-Atomic Structures. Propellants, Explosives, Pyrotechnics, 1989, 14(5):181~186

[6] Dohery R M, Short J M and Kamlet M J. The Chmistry of Detonations. X. Prediction of Cylinder Test Energies of Usual and Non-usual Explosives. Proc. of the Int. Symp. on Pyrotechnics and Explosives. Beijing: 1987.

[7] Dobratz B M. Properties of Chemical Explosives and Explosive Simulants. UCRL—51319.

[8] Hornig H C, McGuire R R. Preliminary Development and Characterization of A TATB/HMX Plastic-bonded Explosive. UCID-18534.

[9] Gibbs T R, Popolato A. LASL Explosive Property Data. Berkeley and Los Angeles, California: University of California Press, 1980.

[10] UCRL-52997.

DETONATION OF MIXTURES ON BASE OF THE STRONG NITRIC ACID

V.M.Raikova, B.N.Kondrikov, G.D.Kozak
Mendeleev University of Chemical Technology
9 Miusskaya Sq., Moscow 125047, Russia

Mixtures of organic substanses with nitric acid (NA) are formed at nitrocompounds (RDX, HMX, NTO, etc.) production. They are used also as the rocket propellants and sometimes as the commercial high explosives. Some of them have very high energetic and detonation parameters, and are characterized by the high explosion hazard. The main purpose of this work is evaluation of relative reaction ability and explosion safety of that kind of energetic materials.

Nitromethane (NM), ethileneglycoldinitrate (NGL), diethylene-glycoldinitrate (DGDN), dinitrotoluene (DNT), trinitrotoluene (TNT), dichloroethane (DCE), and acetic anhydride (ACA) were used as the combustible components of the mixtures on base of NA (conc. of 94-100%). The experiments were carried out in the wide range of the components concentrations. Failure diameter of detonation d_f was measured in the cylinder tubes by go-no-go method. SFR-2 streak camera was employed for detonation velocity D measurements.

Minimum d_f of the mixtures NA/(NM, DNT, TNT) are very small, considerably less than 1 mm, values and correspond approximately to the compositions having zero oxygen balance (A=0). Minimum d_f values of NA-DCE and NA-ACA mixtures (2 and 3 mm, corr.) shift to the compositions having A < 0 (A=-6 and A=-12%, corr.). NGL (at A=0) and mixtures NA-NGL, containing less than 20% of NA (0<A<13%) have about the same d_f (~2 mm), higher than that of NA-DGDN mixture at A=O (~1mm).

Thermodynamic and detonation parameters of all the mixtures studied were calculated by means of developed in our Laboratory SD Computer Code, and were compared with the experimental results obtained. Maximum value of explosion heat (Q_v^m) of all the mixtures corresponds to A=0. Q_v^m of NA-nitrocompounds solutions (6.2 MJ/kg) is smaller than Q_v of NGL (6.7 MJ/kg). Q_v^m of NA-DCE and NA-ACA mixtures (4.4 and 4.2 MJ/kg, corr.) is close to Q_v of neat DNT (4.5 MJ/kg).

The calculation results carried out in frames of Dremin d_f theory show that the mixtures of NA with NM, DNT, and TNT have much higher reaction rates in detonation wave than those of pure nitric esters (NGL, DGDN) and mixtures of them with NA at corresponding content of the last. Oxygen contained in NA is more active chemically than oxygen in ONO_2-groups of the nitric esters.

Experiments with NA/(RDX, NTO, hexamethylenetetramine) mixtures, and with the real reaction masses of RDX production , particularly in form of porous, foamed solutions and suspensions, were also performed.

On the New Method of Brisance Specification of High Explosives

Jiří Vágenknecht[*], Aleš Vojtěch[*] and Jiří Pšenčík[**]

  * Department of Theory and Technology of Explosives,
    University of Pardubice, CZ - 532 10 Pardubice, The Czech Republic
 ** Military Institute for Weapon and Ammunition Technology
    CZ - 763 21 Slavičín, The Czech Republic

ABSTRACT

A new method of brisance specification is presented. The method is based on a deformation of testifying material by cumulative effect of the holle charge and this is use to five common high explosives testing, By means of results obtained, better applicability of the method is supported against the Plate Denting Test.

INTRODUCTION

The ability of explosives to break the objects in close contact with the source of explosion referred to as their *brisance* represents a very important and carefully monitored characteristic. Several methods have been developed for determining this characteristic. The most widespread and well-known involve indirect tests based on deformation. Out of them, the test by Hess[11] is often used. In spite of giving some information on the quality of the explosive, this test rather serves as a check of uniformity of quality in the production of industrial explosives.

Although the *brisance* represents an almost determining characteristic of high explosives, it is not usually provided as an isolated quantity. As a rule, the resultant „work ability" of the explosive is evaluated, e.g., directly in the ammunition object. Such tests, which evaluate, e.g., formation of splinters or the stab depth of cumulative ammunition, have a large information content and provide a precise picture of practical applicability and efficiency of the explosives tested. On the other hand, however, these tests are relatively demanding both economically and from the point of view of safety, which excessively increases the demands on research and development of the ammunition. Therefore it is very desirable to develop and verify some less demanding tests giving universal information.

The term *brisance* cannot unequivocally be defined physically. Therefore, the attempts[2] have appeared to replace this phenomenon by a more exact one, viz. the »detonation pressure«. The detonation pressure correlates relatively precisely with the performance of the explosive (defined, e.g., by the stab depth of a standard cumulative charge[3]). However, advantages of the detonation pressure are not quite unequivocal. Its experimental determination is considerably demanding and, moreover, the results obtained distinctly depend on the method[4] of the corresponding measurement. Therewith, the above-mentioned necessity is connected with introduction of a simple and inexpensive test for determination of *brisance* of highly efficient pressed or plastic explosives.

Such a test has been investigated at the Department of Theory and Technology of Explosives, University of Pardubice[5], and is presented in this communication. It is based on a comparison of relative effect of detonation of a hollow charge of given parameters upon a chosen standard material.

EXPERIMENTAL

The principle of the test is based on a directed action of gaseous products of detonation in the sense of known rules of cumulation of compressible media[6]. The detonation of hollow charge produces a cumulative beam with intensified parameters of products similar to that in the usual cumulation by *metal liner*. The revolving beam of gaseous products produces a crater in the standard material, the parameters of the crater correlating with properties of the deforming beam. When using the same standard material, identical parameters of the charge, the same way of initiation, and unchanged *standoff*, the properties of the crater depend exclusively on the qualitative characteristics of the explosives tested (i.e. the detonation pressure, detonation velocity, initial density, properties of products).

For the tests we selected a cumulative charge of 32 mm diameter and 37 mm height with a cavity of the vertex angle of 50°, without a *metal liner* (Fig. 1). A reliable initiation was secured by a donor composition of a small Gap test with booster tablets [7]. The priming was carried out with a standard detonator No. 8 placed in a centering ring (Fig. 2).
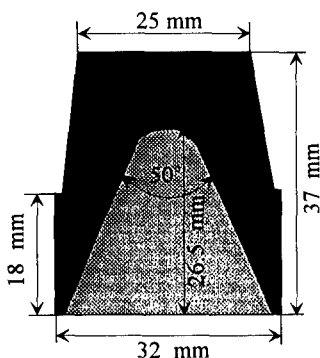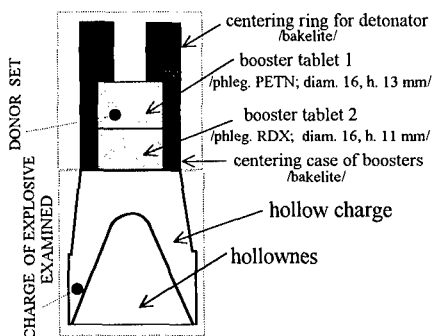
Fig. 1   Scheme of hollow charge
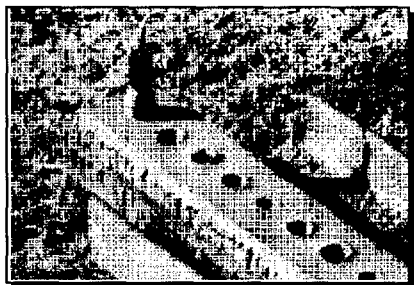

Fig. 2   Scheme of test's set

Fig. 3   Arangement of test

For the standard material we used the gauge armour of 900 MPa strength and 40 mm thickness. The whole arrangement of test is very simple (Fig. 3). The assembly needs no fixation and there is no danger of splinters bursting over the neighbourhood. The most highly demanding operation consists in handling relatively heavy armour plates.

The tests were carried out with a series of five selected currer⁺ʰ ⁻ᵈ pressed explosives adopting twelve samples for each of them. The explosives selected (viz. TNT, phlegmatized RDX with 5% w/w wax, phlegmatized RDX with 4% wax + 17% Al, pentolite with 10% TNT, and phlegmatized HMX with 3% wax) approximately cover the scale of brisance of available high explosives. TNT was used as a common standard to which the test results were referenced.

The explosives were given the required form by compression with a pressure of 1600 kp/cm² into a press mould with removable pressing mandrel. The resulting density of the pressed pieces is given in Table 1.

Tab. 1

EXPLOSIVE	TNT	phleg. RDX	phleg. RDX + Al	phleg. HMX	PENTOLITE
DENSITY [kg . m^{-3}]	1 556	1 652	1 777	1 744	1 674

The craters formed were evaluated primarily on the basis of relative volumes (the volume for TNT = 100%). It was just this volume where the greatest differences between individual explosives were observed. Less distinct differences were observed in the relative depth and inlet diameter of the craters (see Tab. 2). The absolute volume of the individual craters was determined by adding water with wetting agent from a burette until reaching the level height corresponding to the original surface. The necessary amount of water was determined with the accuracy of 0.05 cm^3.
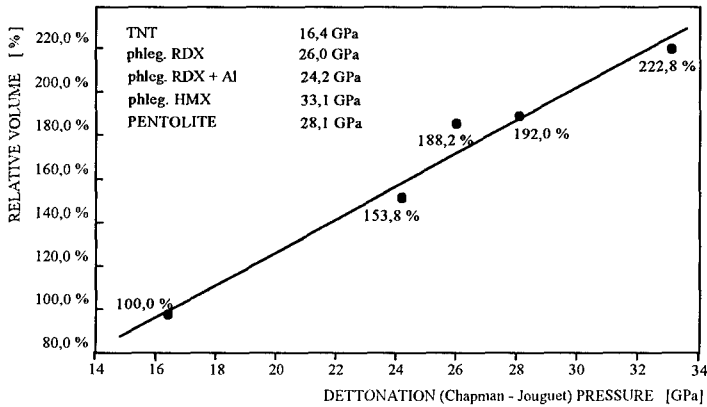
RESULTS AND DISCUSSION

Fig. 4   Dependence of relative cavity volumes on detonation pressure

Figure 4 shows an approximately linear dependence between the average values of relative cavity volumes and the detonation pressure. The values of detonation pressures of the individual explosives were determined by one of the authors [8]. The value of relative volume for RDX + Al slightly deviates from the said linear dependence. It can be presumed that a certain increase in specific mass of products formed from this explosive could not compensate for the overall decrease in

its inner energy. The lower inner energy is due to the presence of a larger amount of non-explosive admixture (aluminium in this case). This fact led us to avoid the application of the method developed to prediction of detonation pressures of high explosives. The method suggested, however, provides a certain information on the detonation pressure of pure or low-phlegmatized explosives.

The spread of results for an explosive at a given density is considerably lower than that in the Plate Denting Test. The dependence depicted in Fig. 5 (taken from ref.[9] and modified) clearly shows the spread of values of *dents* at identil densities of charges - typically for the density of 1.62 cm g^{-3}.
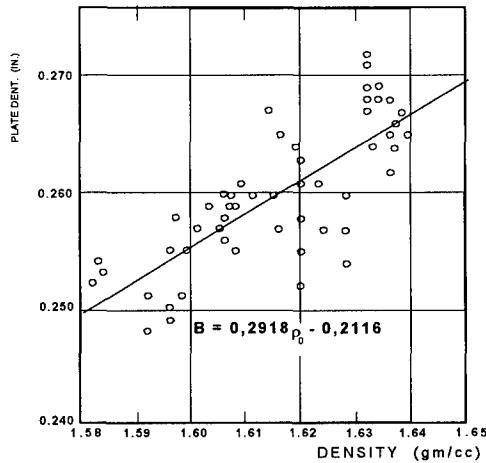

Fig. 5   Plate dent vs density, pressed TNT
(taken from paper [9])

As a result of use of cumulative effect, i.e. by the influence of more intensive action of products, the resulting deformations of materials are greater in the test presented by us. This eliminates - to a considerable extent - possible errors and inaccuracy of the individual experiments. The choice of another evaluation parameter of deformation against PDT (volume in our case) results in an unequivocally better resolving power (see Tab. 2 for illustration).

Tab. 2   Parameters of cavity

PARAMETER EXPLOSIVE	mean * volume [cm³]	mean * depth [mm]	mean * inlet diam. [mm]	relative** volume [cm³]	relative** depth [mm]	relative** inlet diam. [mm]
TNT	2,154	10,550	18,758	100,0%	100,0%	100,0%
standard deviation; n	0.0582;12	0.2576; 12	0.2575;12			
minimum value	2,05	10,00	18,50			
maximum value	2,25	10,80	19,20			
phleg. RDX	4,054	13,242	22,142	188,2%	125,5%	118,0%
standard deviation; n	0,0498; 12	0,0996; 12	0,3056; 12			
minimum value	3,95	13,10	21,80			
maximum value	4,10	13,40	22,80			
phleg. RDX + Al	3,314	12,533	20,133	153,8%	118,8%	107,3%
standard deviation; n	0,1325; 11	0,2387; 12	0,4658; 12			
minimum value	3,15	12,00	19,40			
maximum value	3,55	12,80	20,80			
phleg. HMX	4,800	14,158	22,920	222,8%	134,2%	122,2%
standard deviation; n	0,0000; 2	0,1782; 12	0,3994; 10			
minimum value	4,80	13,90	22,30			
maximum value	4,80	14,40	23,50			
PENTOLITE	4,135	13,183	22,383	192,0%	125,0%	119,3%
standard deviation; n	0,2003; 10	0,1337; 12	0,2290; 12			
minimum value	4,05	12,90	22,10			
maximum value	4,45	13,30	22,80			

n   - number of data evaluated in a set
*   - the mean value is the arithmetic mean of the correct parameters
**   - the relative value refers to the respective mean parameter
       of cavity produced by the TNT charge

CONCLUSION

The results obtained from evaluation of brisance by means of hollow charges indicate that this is a promising test of *brisance* of high explosives. Further research in this area can improve the test especially with respect to its evaluation part. The procedure could also be made cheaper by examining other standard materials (a cheaper construction steel).

REFERENCES:

[1] Hess, Mitt. Art. u. Geniewessen, 10, p.139 /1879/

[2] Taffanel, Dautriche. Commptes Rendus, 155, p.1595 /1912/

[3] Lavrentěv M. A., Shaped charge and principles of its work (Rus.),
U.M.N. SSSR, 12, 4, p.41; Moskva /1957/

[4] J.Majzlík, personal communication /1994 -5/

[5] J. Vágenknecht, Shaped charge effect classification, Thesis, Pardubice /1995/

[6] Stanjukovič K. P., Physics of explosion (Rus.); Nauka, Moskva /1975/

[7] Brebera S., Solnický L., Sensitivity of explosives towards compression wave
(gap - test); internal symposium, VÚPCH Pardubice - Semtín. /1965/

[8] J. Pšenčík, personal communication /1995/

[9] L. C. Smith, On Brisance, and a Plate-Denting Test for the Estimation
of Detonation Presure; Explosivstoffe Nr. 5 p. 108 /1967/

EIDS HIGH EXPLOSIVES FOR 1.6. MUNITIONS

Alain BECUWE - Alain DELCLOS - Jean ISLER
S.N.P.E. - Centre de Recherches du Bouchet
91710 VERT LE PETIT - FRANCE
☎   (33) (1) 64.99.14.06
Fax   (33) (1) 64.99.15.90

Abstract

The safety regulations for transportation and storage are now taking into account the new class/division 1.6 with the requirement that all high explosives contained in a 1.6 munition must be EIDS (Extremely Insensitive Detonating Substance).

The paper will present SNPE new formulations adapted to be able, while still being EIDS, to be used in different kinds of ammunitions (missiles warheads, GP bombs, shaped charges,...).

1. INTRODUCTION

The increasing efforts to improve platforms survivability has led to look for less sensitive munitions, which means munitions with reduced severity of damage when hit or in case of accident.

Although these requirements were adapted, at the starting point, rather to "crisis time" scenarios, it is obvious that the corresponding solutions should also provide benefits for "peace time" situations (storage and transportation).

This is the origin of the new C/D 1.6 : extremely insensitive articles which do not have a mass explosion hazard. This division comprises articles which contain only Extremely Insensitive Detonating Substances (EIDS), according to the UN test series 7 [1, 2, 3], described on table 1.

TEST NUMBER	NAME OF TEST	FAILURE CRITERIA
TESTS ON SUBSTANCES		
7(a)	EIDS CAP TEST	Detonation of any sample
7 (b)	EIDS GAP TEST	Detonation at gap of 70 mm
7 (c) (i)	SUSAN TEST	P > 27 kPA @ v = 333 m/s
7 (c) (ii)	FRIABILITY TEST	dp/dt > 15 MPa/ms for v = 150 m/s
7 (d) (i)	EIDS BULLET IMPACT TEST	Explosion/Detonation
7 (d) (ii)	FRIABILITY TEST	dp/dt > 15 MPa/ms for v = 150 m/s
7 (d) (e)	EIDS EXTERNAL FIRE TEST	Detonation, fragment throw > 15 m
7 (f)	EIDS SLOW COOK-OFF TEST	Detonation, > 3 fragments
TESTS ON ARTICLES		
7 (g)	1.6. EXTERNAL FIRE TEST	C/D. 1.1, 1.2, or 1.3 response.
7 (h)	1.6 ARTICLE SLOW COOK-OFF TEST	Reaction > burning
7 (j)	1.6 ARTICLE BULLET IMPACT TEST	Detonation
7 (k)	1.6 ARTICLE STACK TEST	Propagation

TABLE 1 : UN TEST SERIES 7

At this time, the C/D 1.6. has been officially adopted in several regulations, with more of less quantified benefits [5, 6, 7, 8, 9].

As an example, the US DOD Ammunition and Explosives Safety Standards [4] is indicating Q/D rules for 1.6 ammunitions, which are close to the 1.3 rules in the general case, and may offer lower Q/D under special conditions (for example when 1.6 items are packed in non flammable pallets and stored in earth-covered steel or concrete arch magazines : IBD and PTR -- 100 ft).

The aim of this paper, after having described the current position of in service high explosives versus the EIDS requirements, is to demonstrate that EIDS solutions are now available for most of the warheads.

2. CURRENT SITUATION

The current situation of in service high explosives can be described from the results known to the EIDS tests. For this analysis, the high explosives have been separated in two main families ;

- melt cast high explosives and pressed PBX (table 2)
- first generation cast-cured PBX (table 3)

2.1. Melt cast high explosives and pressed PBX : the knowledge of the position of melt cast and pressed high explosives is available for the most classical formulations.

TEST	MELT CASE HIGH EXPLOSIVES						PRESSED PBX		
	TNT [10,11]	Compo. B [1,10,11]	Octol [10,11]	Tritonal 85/15 [10,11]	HBX1	HBX3 [10]	HMX [10]	HMX/TATB 50/50 [10]	TATB [1]
EIDS Cap test : 7a)	-	+	[+]	[-]	[+]	[-]	[+]	+	-
EIDS Gap test : 7b)	+	+	+	+	[+]	[+]	[+]	[+]	-
Friability test :7c-d)	-	+	+	-	[+]	-	+	-	-
Susan test : 7c) (1)	-	+	+	+	?	[-]	[+]	[-]	-
EIDS Bullet impact test : 7d) (1)	-	+	+	-	[+]	[-]	[+]	[-]	-
EIDS external Fire test : 7e)	+	+	+	-	[+]	-	[+]	[-]	-
EIDS Slow cook off test : 7f	+	+	+	[-]	[+]	?	[+]	+	-
EIDS	*No*	*No*	*No*	*No*	*No*	*No*	*No*	*No*	*Yes*

TABLE 2 : EIDS TEST RESULTS FOR MELT CAST HIGH EXPLOSIVES AND PRESSED PBX

[ ] expected result   - : acceptance criteria is met
(1) alternative methods to friability test   + : acceptance criteria is not met

These results show clearly that classical TNT based melt cast high explosives don't meet most of the EIDS criteria. Concerning the pressed PBX, it seems that only those without HMX can pass the EIDS criteria.

When HMX is introduced with the proportion of 50 % of the filler, the shock sensivity and the behaviour to SCO are compromised at an acceptable level. More information are still needed to identify the maximum ratio of HMX leading to pass those two tests.

2.2. First generation cast cured PBX

One of the most promising way to replace the classical melt cast or pressed high explosives has been the use of cast cured PBX, with basic properties similar to those of the rocket motor propellants :

- good mechanical properties,
- no more exsudation,
- good thermal stability,
- good processability.

SNPE started to work in this way twenty years ago, with as a first result the introduction on service of cast cured PBX in the 80's. The position of these first generation PBX is described on the next table.

TEST	INERT BINDER		ENERGETIC BINDER		
	HMX [10]	RDX [10]	HMX [10]		HMX/Al [10]
EIDS CAP test : 7a)	+	-	+	+	+
EIDS Gap test : 7b)	+	+	+	+	+
Friability test : 7c-d)	-	+	+	?	-
Susan test : 7c) (1)	-	?	?	+	?
EIDS Bullet impact test : 7d) (1)	-	-	-	-	-
EIDS External fire test : 7e)	-	-	-	+	-
EIDS Slow cook off test : 7f)	-	-	-	+	-
EIDS	No (2)	No (3)	No (4)	No (5)	No (6)

TABLE 3 : EIDS TEST RESULTS CAST CURED PBX

[ ] expected result   + : acceptance criteria is not met
                             - : acceptance criteria is met

(1) Alternative methods to friability test   (4) Based on SNPE composition B 3.014 (HMX)
(2) Based on SNPE composition ORA 86 (HMX-PU)   (5) Based on ARC composition AFX 235 (HMX)
(3) Based on SNPE composition HEXABU (RDX-HTPB)   (6) Based on SNPE composition B 3108 (HMX-Al)

These results show that although the behaviour to some stimuli has been quite improved with these first generation cast cured PBX (friability, FCO, SCO), their shock sensitivity remains a major obstacle for being EIDS. That's the reason why SNPE developed new formulations, still cast cured, but with new energetic materials which allowed to meet the EIDS criteria.

3. E I D S

As the shock sensitivity is brought by the nitramine, the only mean to lower it is to replace a part of this nitramine by a less sensitive energetic component. Depending on the application, two kinds of energetic insensitive components have to be considered.

When the aim is only to project fragments (like in a missile warhead) or a metallic liner (in shaped charges for instance), the main part of the energy has to be delivered in the shock front. That means that the reaction rate of the additive has to be so fast that it has to be a high explosive. The choice of this insensitive high explosive made by SNPE was NTO which seemed to be the best compromise between energy, insensitivity, availability and cost [12, 13] .

Since we are looking for the highest energetic content while being EIDS we first plot curves representing the shock sensitivity = f (% HMX) for a given amount of binder in a PBX binder - HMX-NTO.

The fig 1 hereafter is an example of such a curve where the binder is HTPB, and the shock sensitivity is expressed in terms of PMMA thickness leading to a NO GO at the ELSGT (Expanded Large Scale Gap Test).
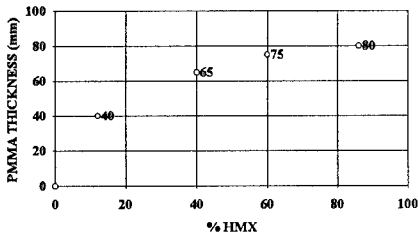

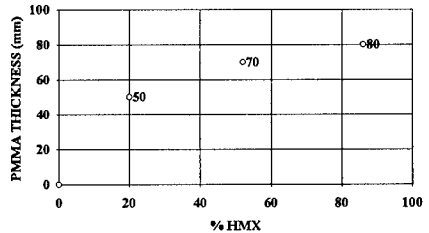*Fig 1* :

Shock sensitivity of a HMX-NTO PBX

Fig. 2 :

Shock sensitivity of a HMX-AP-Al PBX

The use of such a curve allows you to design either a just EIDS PBX (ie with a shock sensitivity just below 70 mm of PMMA) or a PBX with a given shock sensitivity able to avoid any sympathetic detonation in a given ammunition.

When the aim is also or only to develop a blast or a bubble effect it is well know that a part of the energy can be released far behind the shock front. That means a part of the nitramine can be replaced by a mixture of an oxidizer and a fuel (ie AP and Al).

In this case it is also possible to plot a curve representing the shock sensitivity = f (% HMX) for a given amount binder and ratio AP/Al. Figure 2 is an example of such a curve.

Again this kind of curve can help to design a PBX having the needed shock sensitivity.

From this type of curves, SNPE designed PBX for different applications, all of them being EIDS.
- GP bombs B 2214
- Penetrators B 2214-B 2211
- Mines or torpedoes B 2211 - B2245
- Missile warheads B 2248 - B 2237
- Shaped charges B 3021

The table 4 below summarizes some characteristics of these PBXs and their responses to UN test series 7. On the table 5 you will find for some of these PBXs results on articles.

PBX	B 2211	B2214	B2237	B2245	B 2248	B 3021
Ingredients	HTPB/RDX AP/Al	HTPB/HMX NTO	HTPB/HMX AP/Al	HTPB/RDX NTO/AP/Al	HTPB/HMX NTO	Energetic binder HMX/NTO
ρ g/cm^3	1,803	1,63	1,71	1,81	1,685	1,765
D m/s	5500	7495	7330	5150	8050	8100
Cap Test 7a	-	-	-	-	-	-
Gap Test 7b	-	-	-	-	-	-
Friability 7 c.d	-	-	-	-	-	-
Bullet impact 7d	-	-	-	-	-	-
External fire 7e	-	-	-	-	-	-
SCO 7f	-	-	-	-	-	-
EIDS	Yes	Yes	Yes	Yes	Yes	Yes

TABLE 4 : EIDS TEST RESULTS OF INSENSITIVE PBX

+ : acceptance criterion is not met   - : acceptance criterion is met

Composition	B3021	B2214
Article	Shaped charge ⌀ 100	250 KG GP bomb
BI 850 m/s	No reaction	Type V (generic unit)
FCO	Type V	Type V (generic unit)
SD in container	No reaction	/
SD in stock pile	/	No propagation

TABLE 5 : SOME RESULTS ON ARTICLES

CONCLUSION

It has been shown in this presentation that entering the C/D 1.6 can give an advantage at least in terms of storage. It was also shown that SNPE, using her wide knowledge of the cast cured PBX technology, is now able to design, for any application, an EIDS with good energetic properties.

Moreover it is possible to adjust the sensitivity of a PBX to insure the invulnerability to fragment attack and sympathetic detonation of most of the existing ammunitions. Of course in these cases the insensivity to bullet impact, FCO and SCO guaranteed by PBXs is kept.

REFERENCES

[1]   UN Recommendations on the transport of dangerous goods, tests and criteria ST/SG/AC.10/11/rev. 1, 1990.

[2]   J. WARD, "Hazard class/division 1.6 test protocol" 24 th Defence Explosives Safety Seminar, St-Louis, August 28-30, 1990.

[3]   M. SWISDAK " Hazard class/division 1.6. : articles containing extremely insensitive detonating substances, NSWC TR 89-356, NSWC, December 1, 1989.

[4]   DOD ammunition and explosives safety standards, DOD 6055.9-STD, October 1992.

[5]   Recommendations on the transport of dangerous goods, eighth revised edition 1994.

[6]   49 CFR - Parts 106, 107, 110, 171-180, 397 - April 15, 1993.

[7]   AC 258 (TR) (WPC) IWP/2-91, Draft AASTP3, September 6, 1991.

[8]   AC 258 - D/425, May 1992.

[9]   J.C. BESSON "What Q/Ds for H.D. 1.6. 1.6 " 25 th Defence Explosives Safety Seminar, Anaheim, August 18-20, 1992.

[10] J. ISLER "Classification tests for assignment to hazard class division 1.6. : SNPE two years experience", 25 th Defence Explosives Safety Seminar, Anaheim, August 18-20, 1992.

[11] B.M. DOBRATZ, P.C. CRAWFORD, LLNL Explosives Handbook, UCRL-52997 Change 2, January 31, 1985

[12] A. BECUWE, A. DELCLOS "Use of oxynitrotriazole to prepare an insensitive high explosive". Ninth Symposium on Detonation". Portland August 28 - September 1, 1989.

[13] A. BECUWE , A. DELCLOS "Low sensitivity explosive compounds for low vulnerability warheads" Propellants, Explosives, Pyrotechnics 18, 1-10 (1993)

ENTWICKLUNG EINES GALVANISCH LEITENDEN HOCHLEISTUNGSSPRENGSTOFFES

J. Mathieu[1], F. Lebet[2], H.R. Bircher[1]

[1] GR Gruppe Rüstung, Fachabteilung Waffensysteme und Munition, Feuerwerkerstrasse 39, CH-3600 Thun 2

[2] SM Schweizerische Munitionsunternehmung, Allmendstrasse 74, CH-3600 Thun

ABSTRACT

A new galvanic conductive high explosive was developped. The main application of this conductive high explosive is for shaped charges working to the principle of double domed ignition. The incorporation of a core-piece consisting of this conductive high explosive results in constructive simplification of the shaped charge. The galvanic conductivity is achieved by coating explosive crystals with metal powder. The resulting reduction of the detonation velocity in comparison with other high explosives, e.g. Octastit VIII, is 2.5 % only. Safety data, thermal behaviour and long term stability of this thermal conductive high explosive are comparable with other high explosives already in service.

SM produced some shaped charges with conductive core-pieces by means of isostatic pressing and final machining by leathe. These charges were successfully tested for basic function and safety.

A Swiss and US patent for the manufacture of this galvanic conductive high explosive and its application has been granted. A Europatent has been applied for.

1. EINLEITUNG

Im Rahmen einer Machbarkeitsstudie zur Vereinfachung der Hohlladungskonstruktion wurde gemeinsam mit der Schweizerischen Munitionsunternehmung (SM) ein galvanisch leitender Hochleistungssprengstoff entwickelt.

Bei elektrisch gezündeten Wirkladungen mit Doppelhaubenzündung muß im Innern der Ladung eine konstruktiv aufwendige Leiterbahn angebracht werden, welche sich störend auf die Symmetrie und somit auf die Leistung der Hohlladung auswirken kann.

Durch den Einsatz eines Herzstücks aus elektrisch leitendem Sprengstoff kann diese Leiterbahn ersetzt werden (siehe Anhang 1).

Bekannte Hochleistungssprengstoffe, wie z.B. Oktastit VIII und LX 14 sind Isolatoren. Durch Zugabe von Graphit kann die Ableitung von elektrostatischen Ladungen erzielt werden; jedoch weisen auch diese Sprengstofftypen einen hohen elektrischen Widerstand auf. Damit ein Sprengstoff bereits mit möglichst wenig Inertstoffanteil elektrisch leitend wird, müssen dünne Schichten leitender Metalle auf die Oberfläche der Sprengstoffkristalle aufgebracht werden.

2. BESCHICHTUNGSVERFAHREN

In die Untersuchung zur Bestimmung einer adequaten Beschichtungstechnik für Oktogenkristalloberflächen wurden drei verschiedene Methoden mit einbezogen, nämlich das Ausfällen von Metallen durch die chemische Reduktion von Metallnitratsalzen in wäßrigen Lösungen, die Metallbedampfung im Hochvakuum und die Einbettung eines Metallpulvers in den Sprengstoffbinder. Dabei zeigt sich, daß mit der chemischen Methode keine zusammenhängenden leitenden Schichten erzeugt werden konnten. Mittels der Hochvakuumbedampfung konnten wohl homogene metallische Schichten von 1-2µm Dicke auf die Oberfläche der Oktogenkristalle aufgebracht werden. Wie sich jedoch herausstellte, ist die mechanische Festigkeit solcher Schichten zu schwach um der Weiterverarbeitung des Sprengstoffs (Aufbringen des Binders) standzuhalten.

Als sehr effiziente und einfache Methode erwies sich die Einbindung von Metallpulvern in den Binderfilm. Dabei wurde dieses homogen in die wäßrige Oktastit VIII -Bindersuspension

eingemischt und die Sprengstoffkristalle mit dieser Mischung beschichtet. Durch Trocknen wurde der Binder verfestigt und es kam zur Ausbildung von dünnen, fest haftenden Metall-schichten auf der Sprengstoffoberfläche. Dieses Sprengstoffgranulat ist jedoch noch nicht lei-tend. Erst durch den Pressvorgang bildet sich ein zuverlässig elektrisch leitendes Gefüge (vgl. Anhang 2), welches auch durch mechanische Bearbeitung, wie z.B. Abdrehen auf einer Dreh-bank, erhalten bleibt. Dies ist für die vorgesehene Applikation, als leitendes Herzstück einer Hohlladung, von zentraler Bedeutung.

3. METALLPULVER

Von all den getesteten Metallpulvern führten nur Silber (Ag) und Gold (Au) bei einem Volu-menanteil von < 2 % zu elektrisch leitenden Sprengstoffen (Kriterium: < 3 Ohm/cm bei 5 mm^2 Querschnittsfläche).

Gold ist ein hervorragender Leiter und chemisch sehr stabil (spez. elektrischer Widerstand 2.35x10^{-6} Ωcm). Der hohe Preis läßt jedoch die Anwendung dieses Edelmetalls zur Herstel-lung von elektrisch leitendem Sprengstoff nicht zu.

Silber ist bedeutend billiger als Gold und darüber hinaus ein ebenso guter elektrischer Leiter (spez. elektrischer Widerstand 1.59x10^{-6} Ωcm). Zudem hat es gegenüber anderen Metallen den Vorteil, daß sein Oxidationsprodukt Silberoxid ebenfalls elektrisch leitend ist, was insbe-sondere dazu führt, daß seine Leitfähigkeit während der Lagerung über mehrere Jahrzehnte erhalten bleibt.

4. METALLANTEIL, LEISTUNG UND WIDERSTAND

Nachfolgende Graphik zeigt den elektrischen Widerstand und die Detonationsgeschwindigkeit eines Sprengstoffs auf der Basis von Oktastit VIII in Abhängigkeit des Silbergehalts. Die Messaufbauten für die Geschwindigkeits- und die Widerstandsmessung sind im Anhang 3 schematisch dargestellt.

Wie erwartet nimmt der elektrische Widerstand mit steigendem Silbergehalt ab. Bei zirka 1.2 % Volumen sinkt der Widerstand unter 3 Ohm. Die Detonationsgeschwindigkeit nimmt im dargestellten Bereich mit steigendem Silbergehalt linear ab.
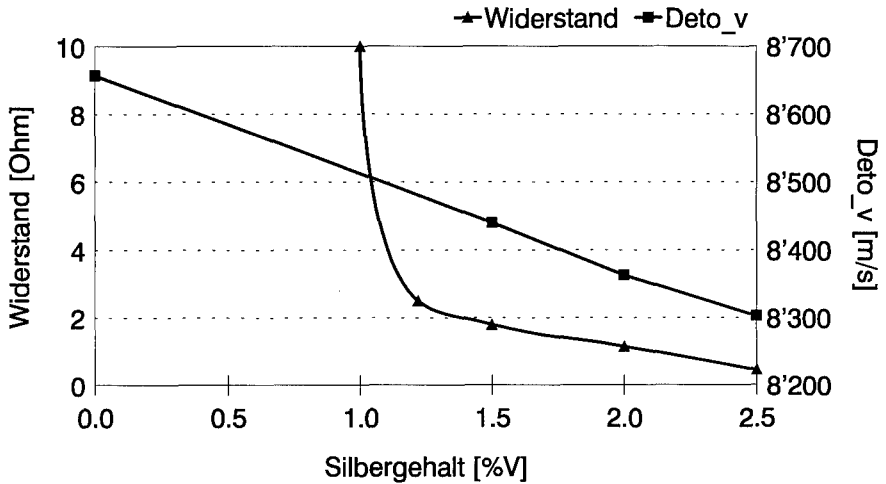
Bei einem Silbergehalt von 1.6 % Volumen ist einerseits, selbst bei kleinen Schwankungen des Silbergehalts, ein Widerstand von < 3 Ohm garantiert, andererseits liegt die erreichte Detonationsgeschwindigkeit von 8440 m/s nur 2.5 % unter derjenigen des Hochleistungssprengstoffs Oktastit VIII (8660 m/s).

5. HANDHABUNGSSICHERHEIT

Schlagempfindlichkeit:
(Methode: „BAM", 2 kg Hammer, 10 mm^3 Probe, ohne Verdämmungsring)

leitender Sprengstoff (1.6 % Vol. Ag)	4 J	erstes Ereignis
Oktastit VIII	3 J	erstes Ereignis

Reibempfindlichkeit (Methode: „Julius Peters"):

leitender Sprengstoff (1.6 % Vol. Ag)	12.0 kg	erstes Ereignis
Oktastit VIII	8.0 kg	erstes Ereignis

Empfindlichkeit gegenüber elektrostatischer Entladung:

leitender Sprengstoff (1.6 % Vol. Ag)   560   mJ   erstes Ereignis
Oktastit VIII   bis 1000   mJ   kein Ereignis

Sowohl Schlag- wie auch Reibempfindlichkeit sind für den leitenden Sprengstoff (1.6 % Vol. Silber) mit denjenigen der ursprünglichen Formulierung, Oktastit VIII, vergleichbar. Im Vergleich mit Oktastit VIII weist der leitende Sprengstoff eine erhöhte Empfindlichkeit gegenüber elektrostatischer Entladung auf. Mit 560 mJ ist diese jedoch weit über der kritischen Schwelle von 56 mJ (max. Entladungsenergie des Menschen).

6. THERMISCHE STABILITÄT

Die thermische Stabilität des leitenden Sprengstoffs wurde im Hinblick auf den Beginn seiner chemischen Zersetzung und im Bezug auf den Erhalt seiner Leitfähigkeit untersucht.

6.1 Thermische Zersetzung

„Differencial Scanning Calorimetry/Thermo Gravimetry" (DSC/TG)-Messungen zeigen (vgl. Anhang 4), daß sich die elektrisch leitende Oktastit VIII-Variante mit 2 % (Vol.) Silbergehalt in ihrem thermischen Verhalten kaum von der Originalformulierung unterscheidet. Der Beginn der exothermen Zersetzungsreaktion liegt bei einer Heizrate von 5 °C/Min bei 271.9 °C (leitende Variante) bzw. 272.8 °C (Oktastit VIII).
Da der Anteil des Silbers als Feststoff in Tiegel zurückbleibt, sind in der Thermogravimetrie Unterschiede im Bezug auf die Gewichtsabnahme feststellbar. Die thermische Zersetzung des Oktogens wird jedoch durch den Zusatz von 2% (Vol.) Silber nicht beeinflußt.

6.2 Elektrische Leitfähigkeit

Da die Wärmeausdehnungskoeffizienten, der zur Herstellung leitender Sprengstoffpresskörper verwendeten Materialien, unterschiedlich sind, war der Einfluß der Temperatur auf die Leitfähigkeit zu untersuchen.

Dazu wurde an einem Presskörper aus leitendem Sprengstoff (1.6 % Volumen Ag) die Widerstandsänderung während zwei Temperaturzyklen zwischen -35 °C und +65 °C kontinuierlich gemessen und in Funktion der Temperatur aufgezeichnet. Eine schematische Darstellung des Messaufbaus befindet sich im Anhang 5.
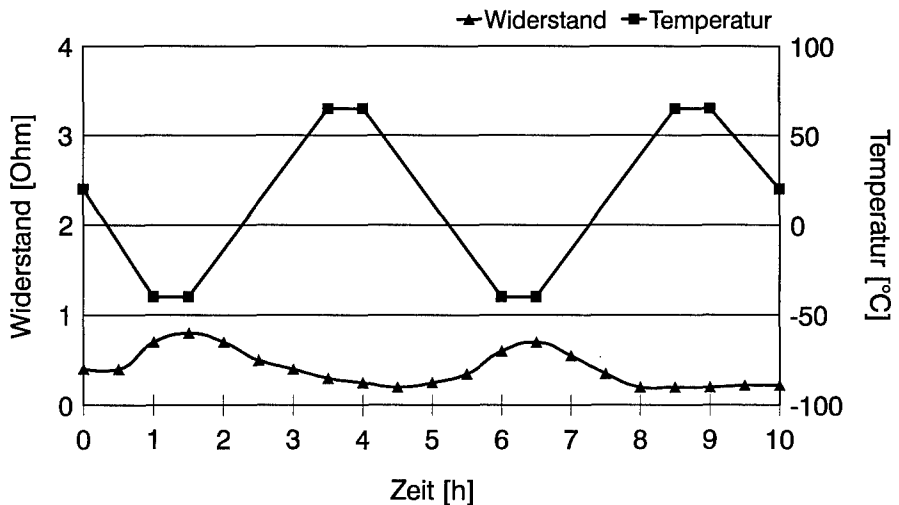
Im Temperaturbereich zwischen -35 °C und +65 °C tritt maximal eine Widerstandsänderung von 0.8 Ohm ein. Erwähnenswert ist dabei, daß beim zweiten Durchlauf des Temperaturzyklus sowohl die Schwankung, wie auch der Widerstand selbst, kleiner wird. Dies kann auf eine verbesserte Homogenisierung des Presskörpergefüges und der damit einhergehenden Optimierung der Brückenbildung (vgl. Anhang 2) leitender Teile erklärt werden.

Die geforderte Leitfähigkeit von < 3 Ohm/cm (Kontaktfläche 5 mm^2) ist somit über den militärischen Einsatzbereich von -35 °C bis +65 °C gegeben.

7. LANGZEITSTABILITÄT

Die chemische Verträglichkeit von Oktogen, Binder und Silberpartikeln wurde mit Hilfe der Mikrokalorimetrie während einer Messdauer von 15 Tagen bei 80 °C untersucht.
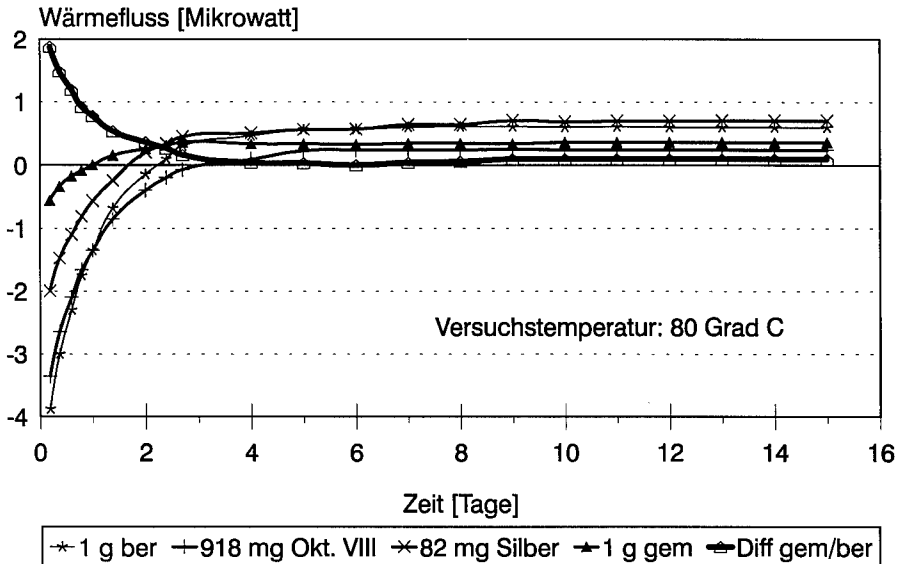
Dabei lag die maximale, auf ein Gramm Substanz bezogene, Differenz von gemessenem und aus den Komponenten berechnetem Wärmefluss weit unterhalb den geforderten ±30 µW. Somit kann von einer Lebensdauer von mindestens 20 Jahren bei Normaltemperatur ausgegangen werden.

Auch die Leitfähigkeit bleibt bei Presskörpern (1.6 % Vol. Ag), welche bei 65 °C während eines Jahres eingelagert wurden, erhalten, sofern diese in Plastiksäcken luftdicht verpackt werden. Nach dem temperaturbedingten Rückgang des Widerstands pendelt sich dieser für einen Presskörper von 20 mm Durchmesser und 16 mm Höhe bei 0.7 Ohm ein.

Presskörper: d=20mm; h=16mm; 1.6 % (Vol) Ag; Pressdruck: 2t/cm2
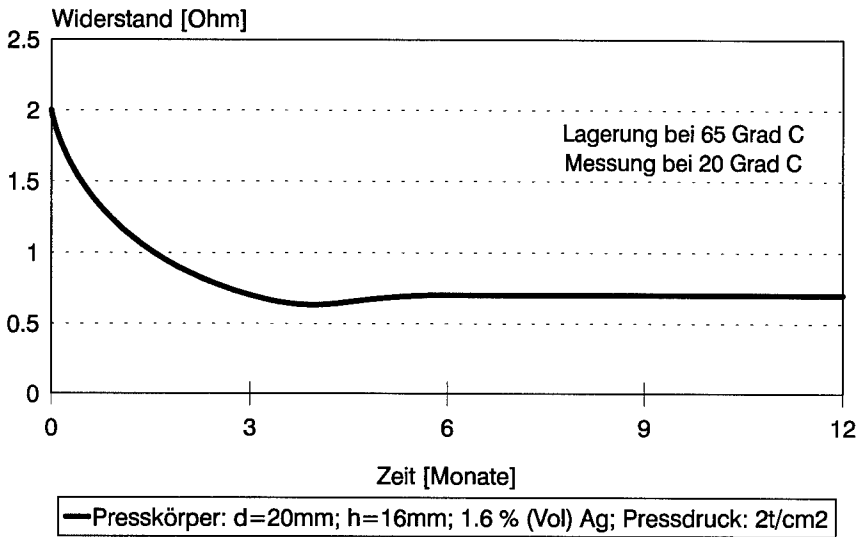
8. HOHLLADUNGSLEISTUNG

Der Vergleich der Leistung von Hohlladungen mit und ohne leitende Sprengstoffseele wurde aufgrund der resultierenden Bohrtiefe von Sprengungen gegen das Vollblockziel T1 ermittelt.

Kaliber [mm]	Abstand [CD]	Oktastit VIII	+ 1.6 % (VOL) Ag
40	6.25	256 ± 10 mm	246 ± 5 mm
40	12.5	–	193 ± 42 mm
50	8.0	228 ± 6 mm	252 mm
50	20.0	140 ± 57 mm	118 mm
Cu-Konus (Kegel, 60°), Ladung isostatisch gepreßt			

Die Anwendung des leitenden Sprengstoffs als Herzstück einer Hohlladung scheint die Leistung bei kurzem und mittlerem „Stand-off" nicht zu beeinträchtigen. Bei großen Sprengabständen ist jedoch eine größere Streuung zu erwarten.

9. SCHLUSSFOLGERUNGEN

Das Beschichten von Oktogenkristallen durch Beimengen von Metallpulvern in eine bestehende Binderrezeptur stellt eine einfache und kostengünstige Methode zur Erzeugung galvanisch leitender Sprengstoffe dar. Die geringe Menge metallischen Anteils (z.B. Silber) garantiert bei geringem Widerstand, im Vergleich mit der Ursprungsformulierung, eine gute Leistung. Die ausgezeichnete chemische Verträglichkeit von Oktogen und Silber resultiert bei einem geeigneten Binder sowohl in einer mit der ursprünglichen Rezeptur vergleichbaren thermischen Stabilität, wie auch in einem günstigen Alterungsverhalten. Daher ist diese Technik zur Herstellung galvanisch leitender Sprengstoffe grundsätzlich auch auf andere Sprengstoffe übertragbar. Durch den Einsatz von galvanisch leitenden Sprengstoffen kann die Hohlladungskonstruktion ohne nennenswerte Leistungseinbusse vereinfacht werden.

Anhang 1

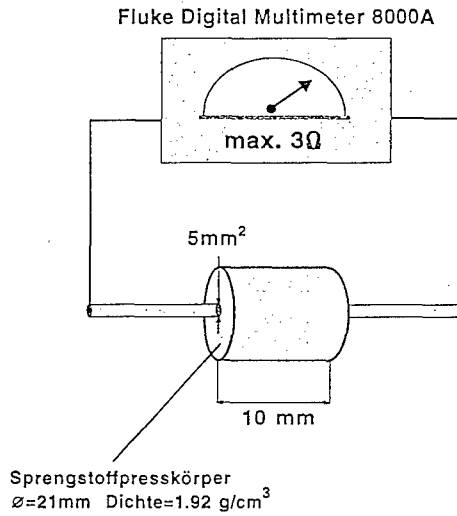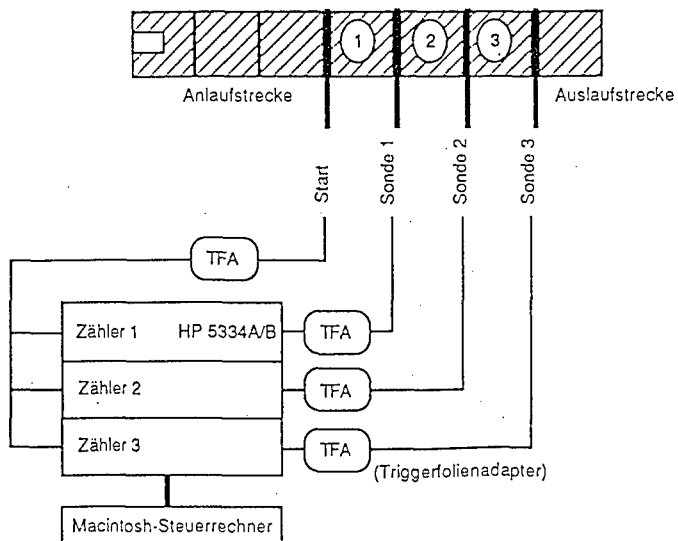# Hohlladung mit leitender Sprengstoffseele

Phase

Nullleiter

Sprengstoff (Isolation)

Herzstück (leitender Sprengstoff)

Inertlinse (metallbeschichtet)

Booster
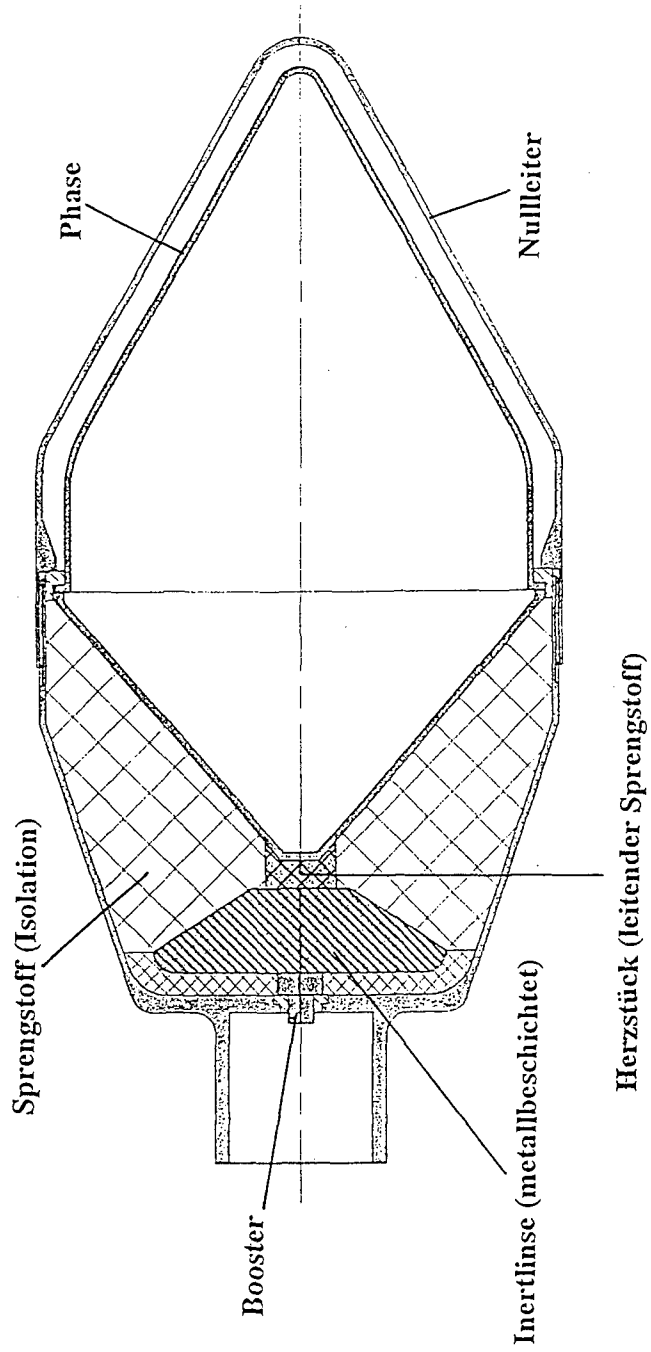
Anhang 2

Leitende Brücken im Presskörper
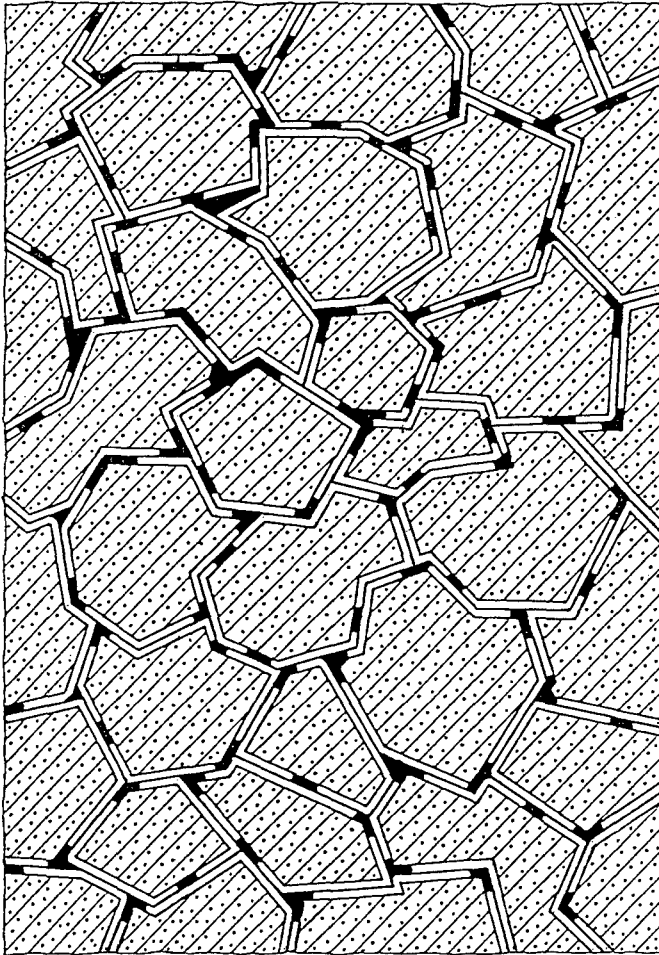
Anhang 3

Messaufbau: Widerstandsmessung

Fluke Digital Multimeter 8000A

max. 3Ω

5mm^2

10 mm

Sprengstoffpresskörper
∅=21mm Dichte=1.92 g/cm^3

Messaufbau: Detonationsgeschwindigkeit

Anlaufstrecke   Auslaufstrecke

Start
Sonde 1
Sonde 2
Sonde 3

TFA

Zähler 1   HP 5334A/B   TFA

Zähler 2   TFA

Zähler 3   TFA
                                    (Triggerfolienadapter)

Macintosh-Steuerrechner

Anhang 4

Messaufbau: Widerstand in Funktion der Temperatur

verschraubbares Kunststoff-
gehäuse

Sprengstoffpresskörper
⌀=21mm h=16mm 1.92g/cm³

National Digital Miliohm-
meter VP-2811

BBC 6 Kanal-Schreiber
SE 460

Fe/CuNi Thermoelement

Kontaktflächen Messing
80mm² je Seite; eine
Seite mit Feder

Anhang 5

Oktastit L 2% V Ag   File: 00142.001 DSC   METTLER   24-Jun-92
2.570 mg   Rate: 5.0 °C/min   Ident: 1.0   An

TG

Gewichtsverlust 86 %

20. mW

Oktastit VIII mit 2 % (Vol.) Silber

Onset   271.9°C

DSC

50.   100.   150.   200.   250.   300.   °C

Okt. VIII Ch. 5/89 Anf.   T. 2x perf.   File: 00063.001 DSC   METTLER   30-Jul-90
5.020 mg   Rate: 5.0 °C/min   Ident: 1.0   An

TG

Gewichtsverlust 96 %

50. mW

Oktastit VIII

Onset   272.8°C

DSC

50.   100.   150.   200.   250.   °C

EFFECT OF MICROSTRUCTURE ON EROSIVE COMBUSTION OF ENERGETIC MATERIALS

Yury I.DIMITRIENKO

R&D Corporation "NPO Mashinostroenia"
Gagarina, 33a, Reutov, Moscow region, 143952, RUSSIA
FAX: 7(095)302-20-01
E-mail: dimit@nw.math.msu.su

Abstract

In the present paper a new model of erosive combustion of energetic materials is developed, that, unlike classical models reducing erosive combustion only to turbulent one, takes account also of the phenomenon of mechanical erosion (dispersing) of a combustion surface in a high-speed hot flow. Conducted theoretical investigations determine the effect of microstructural parameters, for example, of a content of inert fillers, on a rate of erosive combustion of energetic materials. Experimental investigations of erosive combustion are also conducted that verify a validity of the suggested model.

1. Introduction

The phenomenon of increasing a linear rate of surface combustion D with growing velocity v_e of an overrunning external hot flow is usually called erosive combustion of solid combustible materials [1, 2]. In first theoretical investigations of this phenomenon there appears a hypothesis on the origination of turbulence in the boundary layer at critical Reynolds numbers Re that leads to increasing the heat flux to the material surface and, hence, to growing the combustion rate D. Therefore, now this phenomenon is often called turbulent combustion [1, 2].

Thus, the explanation of the discovered physical phenomenon on mechanical dispersion of particles of the burning material surface under the action of an overruning flow is reduced only to analyzing a heat and gas-dynamical character of the overruning flow. However, as it was known from the theory on ablative materials differing from combustible materials, in principle, only by an exothermical character of physico-chemical processes at the surface, that even for small Reynolds numbers Re, when a character of a hot flow is certainly laminar, increasing the flow velocity leads to growing the ablation rate. In this case a physical character of carrying-over the material surface corresponds just to erosive character of destruction, i.e. due to mechanical dispersion of particles. Theoretical description of this phenomenon was presented for the first time in [3, 4], and to describe a rate of erosion (or thermomechanical) ablation the model on coupled thermochemical and mechanical destruction of material was suggested.

The aim of the present paper is:
- to develop a theoretical model of erosive combustion of energetic materials based on the

phenomenon of mechanical destruction of the material surface (dispersing);
- to conduct experimental invetsigations of the phenomenon of erosive combustion of combustible solid materials in the zone of laminar flow of hot gases and to estimate the accuracy of the suggested model;
- to apply the developed model to estimate the effect of different parameters of energetic material microstructure (mainly, content of filler-oxidizer or inert filler) on the erosive combustion rate.

2. A Physical Model of Erosion Combustion.

The erosive combustion model is based on the following main physical assumptions.

A) In erosive combustion of solid energetic materials there are three independent physical phenomena simultaneously, namely
- free combustion (gasification) of the material surface without any external actions;
- internal erosive combustion (dispersing) or self-erosion of the materail surface under the action only of internal pore pressure of a gasified part of the material;
- external erosive combustion (dispersing) of the material surface under the action only of an external overruning hot gas flow.

A total linear rate of combustion of solid material D is a sum of three rates described above D_f, D_i, D_e:

$$D = D_f + D_i + D_e. \tag{1}$$

Increasing the combustion rate D under the action of external hot gas flow means that the following condition is satisfied:

$$\epsilon = \frac{D}{D_f + D_i} \geq 1, \tag{2}$$

where ϵ is the coefficient of erosive combustion.

B) Combustion rates D_f, D_i and D_e depend on parameters of the surrounding medium (perturbed or quiescent), as these parameters we can choose three main parameters describing interaction of solid materials with gas flows: p_0 - statical pressure of the quiescent gas; $p_0' = \rho_e v_e^2$ - pressure head of the overruning hot gas flow; q_e -heat flux to the burning surface of the energetic material. Here ρ_e is the gas density, v_e is the tangential component to the material surface of the flow velocity.

$$D_f = D_f(p_0, q_e), \qquad D_i = D_i(p_0, q_e), \qquad D_e = D_e(p_0', q_e). \tag{3}$$

C) Turbulent combustion is also described by this model, as the appearance of turbulence of an overruning flow means that flow characteristics q_e and p_0' change.

3. A Mathematical Model of Erosive Combustion.

3.1. A RATE OF FREE COMBUSTION

Free combustion means gasification of solid energetic material at its external surface. This scheme involves combustion of both mixed and ballistic energetic materials. Free combustion rate D_f is determined from thermodynamical relations at the solid and gas phase interface and has the form:

$$D_f = D_f^0 \frac{E^{-\frac{E_a \mu}{R_a \theta_w}}}{\sqrt{\theta_w / \theta_0}} \left(\frac{p_0}{p_a}\right)^{1/2} \left(1 - \frac{p_0}{p_a} e^{-\frac{2E_a \mu}{R_a \theta_w}}\right)^{1/2}; \qquad D_f^0 = \frac{p_a}{\rho \sqrt{R_a \theta_0 / \mu}}, \qquad (4)$$

where p_a is the standard pressure of quiescent gas medium, R_a is the gas constant, θ_0 is the initial temperature; and there are characteristics of the energetic material: ρ - density, μ - molecular mass, E_a - activation energy.

The surface temperature θ_w is determined from the solution of the heat-conductivity equation with the boundary condition:

$$\frac{\partial \theta}{\partial t} = \frac{k}{\rho c} \frac{\partial^2 \theta}{\partial x^2}; \qquad x \geq x_D, \qquad (5)$$

$$-k \frac{\partial \theta}{\partial x} = q_e - \varepsilon \sigma_{SB} \theta_w^4 - D_f \rho \Delta l^*, \qquad x = x_D,$$

where k is the heat-conductivity coefficient, c - heat capacity, Δl^* - heat of gasification of the energetic material, σ_{SB} - the Stefan- Boltsman constant, ε - blackness degree, and $x = x_D$ - location of the combustion surface in the Ox coordinates, t - time.

From equation (4) we find θ_w as a function of q_e and also k, ρ, c, ε and Δe^*. Approximate solution can be found in the form:

$$\theta_w(q_e) = \left(\frac{q_e - D_f \rho \Delta e^*}{\varepsilon \sigma_{SB}}\right)^{1/4}. \qquad (6)$$

On substituting expression (5) for θ_w into (4) the rate D_f is found in form (3) of function of p_0 and q_e.

3.2. A RATE OF INTERNAL EROSIVE COMBUSTION D_i.

Free combustion is an idealized scheme of combustion of real materials. Energetic materials even of the ballistic type are heterogeneous: at unheated state there are cristallic zones in them with higher thermo-resistance than resistance of the main part of the substance being in amorphic state. Therefore, gasification occurs in a volume (pyrolise process) in heating, and as a result there appear pores filled in by gaseous pyrolise products. A part of gas is filtrated to the external surface, however, this process is kinetic, therefore, in fast heating gases have no time to pass to the surroundings and create intrapore pressure p_g. The pore pressure level can be very high [3] and can reach $p_g \approx 250$ B. The pore pressure p_g reaches its maximum within a very thin surface layer. Under the action of the pore gas pressure a thin unstrength external layer of the material destructs and is carried out to the surroundings

where there occurs afterburning the dispersed particles. Destruction rate of a surface layer of energetic material under the action of pore pressure is combustion rate D_i.

Expression for rate D_i is determined on the basis of joint solving the heat-cunductivity, filtration equations and kinetic equation describing the pyrolise process in quasistatic approximation and has the form:

$$D_i = D_i^0 \left(\frac{p_0}{p_a}\right)^{1/2} \left(\frac{R\theta_w}{\mu E_a}\right) e^{-\frac{E\mu}{R\theta_w}};$$

$$D_i^0 = \frac{36 p_a k}{\rho^2 c K \sigma_0 \sqrt{T\theta_0/\mu}}, \tag{7}$$

where K is the coefficient of gas-permeability and σ_0 is the strength of the energetic material in tension.

Temperature θ_w can be evaluated approximately by formula (6), and to find its more precise value the heat-conductivity equation (5) should be resolved, and coordinate x_D should be determined from the equation:

$$x_D = \int_0^t (D_i + D_f) d\tau. \tag{8}$$

3.3. A RATE OF EXTERNAL EROSIVE COMBUSTION D_e.

Unlike internal erosive combustion when material particles at the surface destruct under the action of internal forces (intrapore pressure), combustion surface particles' destruction (erosion) at the presence of an external high-speed flow occurs due to the action of local pressure $p_0' = \rho_e u_e^2$ onto bulging parts of the combustion surface. An idealized scheme of a stress state of each the bulge of the burning surface can be represented as cantilever bending of a beam by uniform pressure p_0'. When the bending stress exceeds the strength limit of the energetic material in tension, there occurs breaking-off a surface particle and its carrying-off to the gas flow, wherein the particle burns completely.

The considered idealized model of erosion assumes that at each the elementary destruction a shape of a dispersed particle and a shape of the residual combustion surface remain self-similar.

Rate of external erosive combustion D_e is determined as D_i on the basis of joint solving the heat-conductivity equation and kinetic equation of pyrolise in quasistatic approximation and has the form:

$$D_e = D_e^0 f(p_0') \left(\frac{p_0}{p_a}\right)^{1/4} \left(\frac{R\theta_w}{\mu E_a}\right)^{1/2} e^{-\frac{E_a\mu}{2R\theta_w}}; \tag{9}$$

$$D_e^0 = \frac{1}{\rho} \left(\frac{6 p_a \lambda}{c l_0}\right)^{1/2} \cdot \left(\frac{\mu}{R\theta_0}\right)^{1/4};$$

$$f(p_0') = \left(-\ln\left(1 - \left(1 + \left(\frac{6 p_0'}{\sigma_0}\right)^{1/2}\right)^{-3}\right)\right)^{-1},$$

where l_0 is the characteristic dimension of roughness of the combustion surface that can be assumed equal to a characteristic size of pores in the initial energetic material.

Temperature θ_w can be also determined by formula (6), if heat flux q_e to the combustion surface is known. Numerical evaluation of the temperature θ_w on the basis of solution of heat-conductivity equation (5) should take account of the condition:

$$x_D = \int_0^t (D_i + D_f + D_e)d\tau. \tag{10}$$

Formula (9) together with (6) takes account of the dependence of combustion rate D_e on all the main parameters: static pressure p_0, pressure head p_0' and heat flux q_e, the last depends, in its turn, on streamlining conditions of the surface by the external hot flow, namely Reynolds number Re, velocity u_e, gas density ρ_e etc.

One of possible approximate analytical expressions for heat flux q_e has the form:

$$q_e = \left(\frac{\alpha}{c_p}\right)(I_e - c_w\theta_w), \tag{11}$$

where

$$I_e = Q^0 + c_e\theta_e + \frac{u_e^2}{2}, \tag{12}$$

- enthalpy of the overrunning flow, Q^0 - the total heat of combustion of gaseous products of the energetic material, θ_e - temperature of the external flow before the ignition time, c_e - heat capacity of the gas phase.

Coefficient of heat transfer (α/c_p) is expressed by formula:

$$\left(\frac{\alpha}{c_p}\right) = 0.425\frac{\rho_e u_e}{\sqrt{\text{Re}}} \tag{13}$$

for laminar flow;

$$\left(\frac{\alpha}{c_p}\right) = 0.038\frac{\rho_e u_e}{(\text{Re})^{0.2}} \tag{14}$$

for turbulent regime of the hot flow.

4. Experimental Investigations

4.1. DESCRIPTION OF EXPERIMENTS

To test an accuracy of determination of the rate of erosive combustion with the help of the model described above, experiments on combustion of solid combustible materialsin a high-speed hot flow were conducted.

Combustible polysiloxane rabber contained an inert filler with ratio 1.5:1 was chosen for investigations. In pyrolise of synthetical rubber besides such compounds as CO_2, vapour H_2O there also appear combustible compounds CH_4, CO, H_2 etc. Their oxidizer is oxygen contained in the external overrunning flow, a main mass of which is combustion products of kerosene.

A scheme of the experimental equipment is shown in Fig.1. Experimental specimen of material 3 was installed onto the cooled metallic slab 2 and was subjected to the action of high-sooed hot gas flow 1 with parameters q_e, p_0', u_e. In order to obtain a dependence of the
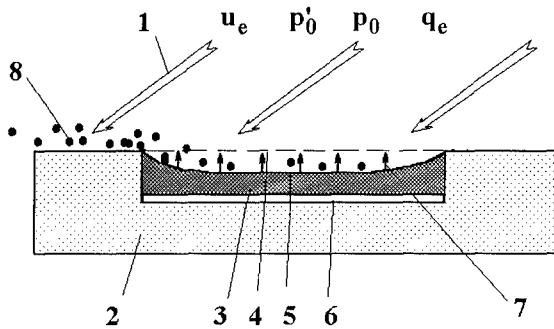
Fig.1.
A scheme of erosive combustion of a specimen of combustible material tested in a high-speed gas flow: 1 - gasodynamical flow; 2 - colled metallic slab; 3 - specimen of combustible material; 4 - initial location of the combustion surface; 5 - current location of the combustion surface; 6 - heat insulation; 7 - erosive destruction of the material; 8 - dispersed particles of the material.

rate D on the pressure head p_0' and q_e, three series of testing were conducted for different values of p_0', u_e, Re and the same value of heat flux q_e:

series 1:   series 2:

pressure head $p_0' \approx 0.05 - 0.1$ Bar,	pressure head $p_0' \approx 0.4 - 0.6$ Bar
heat flux $q_e \approx 0.1 - 1.5$ MW/m^2,	heat flux $q_e \approx 0.5 - 1.5$ MW/m^2
flow velocity $u_e \approx 30 - 80$ m/s,	flow velocity $u_e \approx 150 - 200$ m/s
number Re $\approx 10^5$,	number Re $\approx 3 \cdot 10^5$
test time $t \approx 100$ s,	test time $t \approx 20$ s

series 3:

pressure head $p_0' \approx 0.8 - 1.0$ Bar

heat flux $q_e \approx 0.7 - 2.0$ MW/m^2

flow velocity $u_e \approx 200 - 290$ m/s

Reynolds number Re $\approx 7 \cdot 10^5$

test time $t \approx 10$ s

In all the three series the overrunning flow was subsonic and laminar. This choice of testing regimes allowed us to estimate the effect of the flow velocity u_e and pressure head p_0' on the rate of erosive combustion at the fixed values of heat fluxes.

4.2. EXPERIMENTAL RESULTS

Testing results obtained in the three series of experiments are shown in Fig.2 for three values of heat fluxes $q_e = 0.75$, 1.0 and 1.5 MW/m^2.
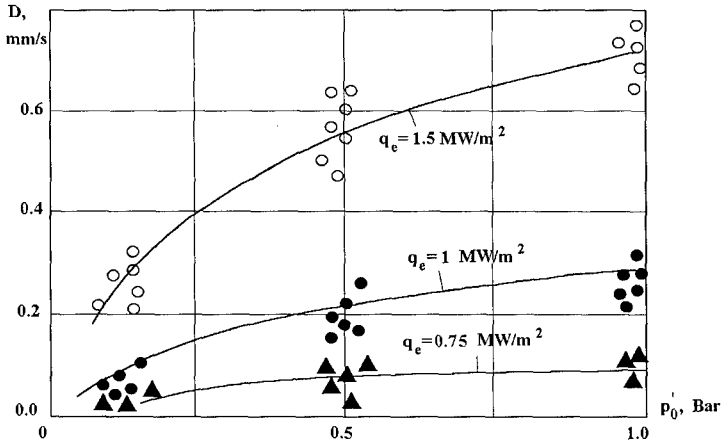
Fig.2.
Dependence of erosive combustion rate D on pressure head p_0' at three different values of heat flux q_e for the combustible material based on polysiloxane.
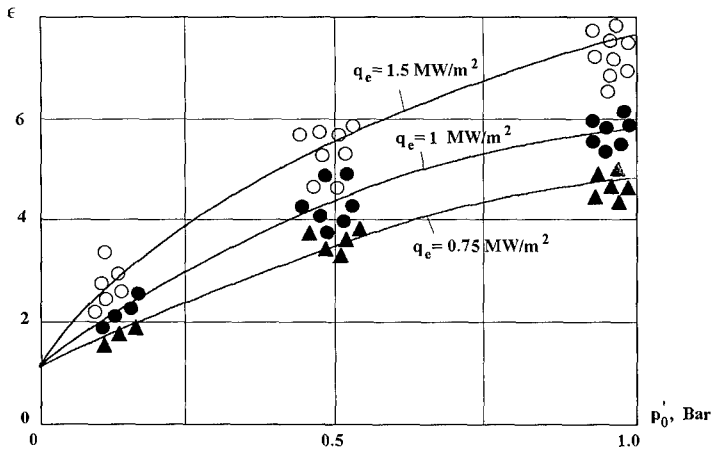

Fig.3.
Dependence of erosion coefficient ϵ on pressure head p_0' at three different values of heat flux q_e for the combustible material based on polysiloxane.

In the first series of testing the heat flux grew to its maximum value in step-way, and ignition of the material occured when q_e reached the certain value, and then combustion continued during the experiment, and erosional carrying-away the material specimen surface was also detected after testing.

In the second and third series of testing a heat flux increased to its maximum value for very short time and remained at this level during 10 - 20 s. Ignition of pyrolise products of the material occured practically immediately and continued during all the experiment. Considerable erosional carrying-away the material was discovered after completion of the experiment.

As seen from Fig.2, the pressure head p_0' of the overrunning flow has an essential effect on the rate of combustion of the material for all three values of heat flux q_e. This effect can be illustrated clearer in coordinates (ϵ, p_0') (Fig.3). Increasing the rate of material combustion at the expense of erosion of the material surface under the action of external flow is of 5 - 8 times at $p_0' \approx 1$ Bar. Maximum value $\epsilon \approx 8$ corresponds, as it was expected, to the maximum heat flux $q_e = 1.5$ MW/m^2 of the above considered ones, and minimum $\epsilon \approx 5$ corresponds to minimum $q_e = 0.75$ MW/m^2.

4.3. COMPARISON WITH THEORETICAL RESULTS

Theoretical calculations of the combustion rate D and its parts D_e, D_i and D_0 were conducted. In these computations the following characteristics of combustible material based on polysiloxane rubber were given:

$$\rho = 600 \text{ kg/m}^3, \quad c = 0.8 \text{ kJ/kg} \cdot \text{K}, \quad \lambda = 0.17 \text{ W/m} \cdot \text{K}, \quad E_a/R_a = 8.5 \cdot 10^3 \text{ K}^{-1},$$

$$\sigma = 5 \text{ MPa}, \quad K = 1 \text{ s}, \quad \Delta e^* = 2.8 \text{ MJ/kg}, \quad \epsilon = 0.5, \quad p_a = 1 \text{ Bar}.$$

Computed results of D and ϵ are shown in Fig. 2 and 3 by solid curves. As seen from these figures, the agreement of computed and experimental results is sufficiently good with taking into consideration that the scatter of experimental points is rather great that is typical for such gasodynamic testing.

5. Effect of Microstructure on Rate of Erosive Combustion

The analytical expresiions (4), (7) and (9) obtained above for the rate of erosive combustion D give us the possibility for optimum selection of a content of the energetic material in computational way. For this, it is necessary to obtain a relationship between macrocharacteristics of the energetic material ρ, c, K, σ, E_a, Δe^* (on which the combustion rate D depends) and microcharacteristics of phases of the material ρ_i, c_i, σ_i, E_{ai}, Δe_i^* and content of the phases.
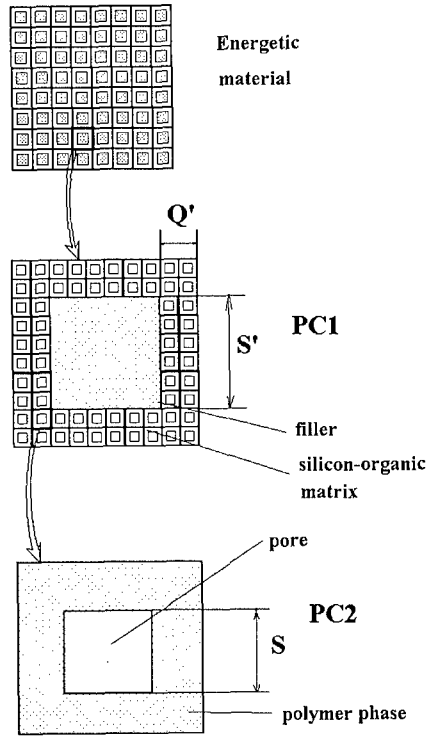
Fig.4.
A scheme of internal two-level structure of energetic material.

5.1. A MODEL OF STRUCTURE OF ENERGETIC MATERIAL

Let us consider a model wherein energetic material consists of three phases: phase 1 - polymer being a mixed propellant (it contains both fuel and oxidizer), phase 2 - inert filler that is introduced to regulate heat-physical features of the energetic material, phase 3 - pores filled in with gaseous pyrolise products of the phase 1 in heating.

Energetic material is modelled in the form of a multilevel structure with a two-level hierarchy (Figure 4). At the first structural level an energetic material consists of periodic cells of the first type (PC1). Each PC1 consists of two components: component 1 is a matrix, being a collection of 2nd and 3rd phases, and component 2 is filler (phase 1). The filler is modelled by a cube, and the matrix is also modelled in the form of a cube surrounding the filler (Figure 4).

Finally, the polymer matrix itself is a collection of periodic cells of the second level. PC2 is a hollow cube of a solid polymer (phase 2). The cavity of this cube is represented as a pore filled with gaseous products of polymer pyrolise (phase 3). Such a model of a energetic material structure permits to evaluate all the main characteristics of the material: elasticity modulus, strength in tension, heat-conductivity, density, ablation rate.

5.2. ELASTICITY MODULUS

The elasticity modulus of energetic material according to the multilevel structure described above is determined by the formula:

$$E = E_2^0 a',$$

(15)

where

$$a' = (1 - S'^2)\widetilde{a} + S'^2 a'_Q; \quad a'_Q = \left(\frac{1 - S'}{\widetilde{a}} + \frac{S'h_c}{\kappa} + \frac{S'(1 - h_c)}{\kappa h_c(2 - h_c)}\right)^{-1};$$

$$\widetilde{a} = \left(\frac{S'}{a_p} + \frac{1 - S'}{a_0}\right)^{-1}; \quad a_p = (1 - S^2)a_0;$$

(16)

$$a_0 = \exp\left(-a(\Delta\theta + P \int_0^t \exp\left(-Q(t - \tau)\right)\Delta\theta d\tau)^4\right).$$

Here E_2^0 is the elasticity modulus of the polymer phase at temperature θ_0; a' is the coefficient describing the effect of filler on the elasticity modulus of the material; $\widetilde{a}$ is the coefficient describing a change of elasticity modulus of the matrix on heating up to pyrolysis temperatures; a_0 is the coefficient describing a reversible change of elasticity modulus of polymer phase under relatively low temperatures before the pyrolysis commences; h_c is the geometrical parameter; κ is a ratio of elasticity moduli of filler and polymer phase $\kappa = E_1/E_2^0$; P and Q are universal constants. Functions S, S' are connected to the volumetric concentrations of phases φ_1, φ_2, φ_3 by the relations:

$$S = \left(1 - \frac{\varphi_2}{1 - \varphi_1}\right)^{1/3}; \quad S' = \varphi_1^{1/3}; \quad \varphi_1 + \varphi_2 + \varphi_3 = 1.$$

(17)

Let us introduce mass contents of phases y_i, $i = 1, 2$, which are connected to volumetric phase concentrations φ_i by the relations:

$$\varphi_2^0 = \frac{1 - \varphi_4^0}{1 + \frac{\rho_2}{\rho_1}\frac{y_1}{y_2}(1 - \varphi_4^0)};$$

(18)

$$\varphi_1 = 1 - \varphi_2^0 - \varphi_4^0; \quad y_1 + y_2 = 1,$$

5.3. STRENGTH IN TENSION

The strength of energetic material in tension in accordance with the multilevel structure described above is determined by the formula:

$$\sigma = \sigma_2^0 B, \tag{19}$$

where σ_2^0 is the strength of polymer phase in tension at temperature θ_0; B is the coefficient describing the effect of filler on the strength of the material

$$B = \frac{a'}{a_{Q'}} \cdot \frac{a_p}{a_0}. \tag{20}$$

Destruction of material reinforced with dispersed filler, which can be described by the formula (19), occurs due to destruction of polymer phase of its matrix in the vicinity of the filler in zone Q' of PC1 (Figure 4).

5.4. HEAT CONDUCTIVITY

The heat conductivity of energetic material in accordance with the multilevel structure described above is determined by the formula:

$$\lambda = \lambda_2^0 b', \tag{21}$$

where

$$b' = (1 - S'^2)\widetilde{b} + S'^2 b'_Q; \tag{22}$$

$$b'_Q = \left(\frac{1 - S'}{\widetilde{b}} + \frac{S'h_c}{\omega} + \frac{S'(1 - h_c)}{\omega h_c(2 - h_c)} \right)^{-1}; \qquad \widetilde{b} = \frac{1 - S}{S'}.$$

Herein λ_2^0 is the heat conductivity coefficient of the polymer phase at temperature θ_0; b' is a coefficient describing the effect of filler on heat conductivity of the energetic material; $\widetilde{b}$ is a coefficient describing a change of heat conductivity of the matrix in heating up to pyrolysis temperatures; ω is the ratio of heat conductivities of filler and polymer phase $\omega = \lambda_1/\lambda_2^0$.

5.5. DENSITY AND HEAT CAPACITY

The density and heat capacity of energetic material are determined by the formulae:

$$\rho = \rho_c\varphi_1 + \rho_2\varphi_2 + \rho_3\varphi_3, \tag{23}$$

$$c = \frac{1}{\rho}\left(c_1\varphi_1\rho_c + c_2\varphi_2\rho_2 + c_3\varphi_3\rho_3 \right),$$

where c_i - heat capacities of phases.

5.6. GAS PERMEABILITY

The gas permeability coefficient K of porous energetic material is determined by the porosity coefficient φ_g [1]:

$$K = K_0\exp\left(S\varphi_g^{1/3} \right), \tag{24}$$

where K_0 and S are universal constants, independent of the material type and the presence of fillers in the material.

6. Numerical Results

Numerical calculations of characteristics of energetic material according to the model developed above were conducted with the following values of component characteristics:

polymer phase:

$$E_2^0 = 8 \text{ MPa}, \quad \sigma_2^0 = 5 \text{ MPa}, \quad \lambda_2 = 0.17 \text{ W} \cdot \text{kg}^{-1} \cdot \text{K}^{-1}, \quad c_2 = 0.8 \text{ kJ} \cdot \text{kg}^{-1} \cdot \text{K}^{-1},$$

$$\rho_2 = 1100 \text{ kg} \cdot \text{m}^{-3}, \quad J_2^0 = 3 \cdot 10^5 \text{ kg} \cdot \text{m}^{-3} \cdot \text{s}^{-1}, \quad E_{a2}/R = 8.5 \cdot 10^3 \text{ K}^{-1};$$

filler:

$$E_1^0 = 7 \cdot 10^4 \text{ MPa}, \quad \sigma_1^0 = 100 \text{ MPa}, \quad \lambda_1 = 0.74 \text{ W} \cdot \text{kg}^{-1} \cdot \text{K}^{-1},$$

$$c_1 = 0.8 \text{ kJ} \cdot \text{kg}^{-1} \cdot \text{K}^{-1}, \quad \rho_1 = 250 \text{ kg} \cdot \text{m}^{-3}, \quad J_1^0 = 0;$$

and

$$K_0 = 1.76 \cdot 10^{-23} \text{ s}, \qquad S = 50.$$
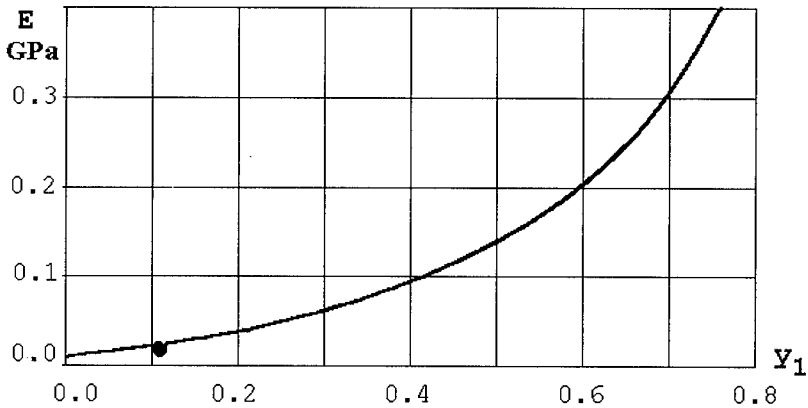
Fig.5.
Dependence of elasticity modulus E of the energetic material on concentration of inert filler y_1, points correspond to experimental data.
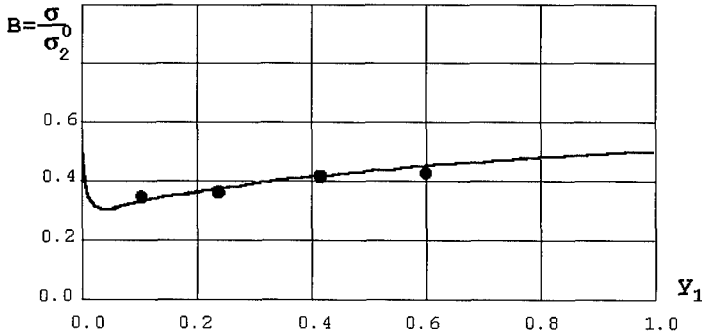
Fig.6.

Dependence of relative strength B in tension of the energetic material on concentration of inert filler y_1, points correspond to experimental data.
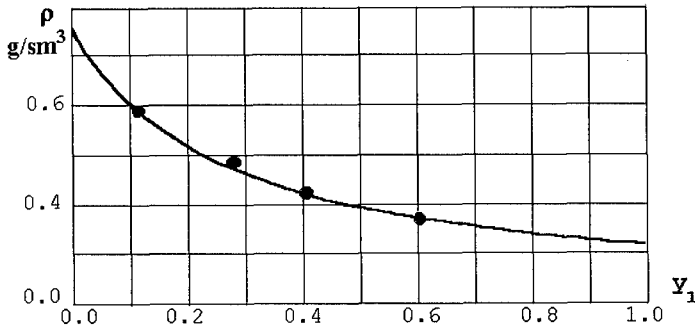

Fig.7.

Dependence of density ρ of the energetic material on concentration of inert filler y_1, points correspond to experimental data.
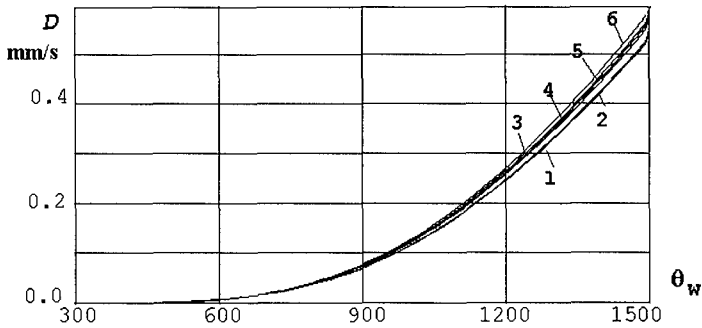

Fig.8.

Dependence of erosive combustion rate D of the energetic material on temperature of its surface for different values of content y_1 of filler 2: 1 - 5 %; 2 - 10 %; 3 - 20 %; 4 - 30 %; 5 - 40 %; 6 - 50 %.

Figure 5 shows the relationship between the elasticity modulus of the energetic material and the content of filler in it. With increasing filler content the elasticity modulus of the material grows sharply. As the strength of the material with filler decreases, then ultimate strain of the material also decreases rapidly, i.e. the material becomes embrittled.

Figure 6 exhibits the relationship between the relative strength $B = \sigma/\sigma_2^0$ of the material and the content of fillers 1 and 2 in the material. With increasing filler content, the relative strength decreases sharply at first, and then grows. The minimum strength value is 0.3 for filler 1 and 0.6 for filler 2.

Figure 7 shows the relationship between the density ρ of the material and filler content in the material at temperature θ_0. With increasing filler content the material density decreases.

Figure 8 shows the relationship between the of rate of erosion combustion D_e of the material and surface temperature for different values of content of filler in the material. Pressure head $p' = 0.01$ Bar. As seen from this figure, the filler content has practically no effect on rate of erosion combustion. This phenomenon is connected to the fact that, as seen from the formula (19), the erosion rate decreases with decreasing heat conductivity and grows with decreasing density and increasing filler content. These two processes compensate each other, and, on the whole, rate D is practically independent of the filler content.

7. Conclusions

The model on erosive combustion of energetic materials has been developed in the present paper, that describes, in essence, the effect of erosion destruction of the surface on the combustion rate of material in a high-speed flow. This model complements the known models of erosion combustion being, in fact, schemes of turbulent combustion.

Comparison of the model with experimental results on erosion combustion of combustible polysiloxane rubber showed a validity of the model.

The model describing an effect of microstructure of energetic materials on erosive combustion rate has been developed. Computed results showed that combustion rate D_e is practically independent of introducing inert fillers while density, heat conductivity and elasticity essentially change. This gives us the possibility to select an optimum structure of energetic materials, for example, with the aim to provide a minimum mass at the same energetical characteristics.

REFERENCES

1. Vandenkerkhove J. Erosive combustion of colloidal solid peopellants. *Problems on Rocket Engineering.* N 3 (1959) (in Russian).

2. Green L. Erosive combustion of several solid explosive substances. *Problems on Rocket Engineering.* N 2 (1959) (in Russian).

3. Dimitrienko Yu.I. Thermal stresses and heat-mass-transfer in ablating composite materials, *Journal of Heat Mass Transfer*, **38**, N 1, 139-146 (1995).

4. Dimitrienko Yu.I. Mathematical Modelling of Ceramic Composite Processing Based on Combustion, *Journ. Math. Comput. Modelling*, **21**, N 8, 69-83 (1995).

PRESSABLE TPE-BASED EXPLOSIVES
FOR METAL ACCELERATING APPLICATIONS

R E Hollands, T H Jordan*, C J Leach* and I E P Murray

British Aerospace Defence Limited, Defence Research Agency,*
Royal Ordnance Division,   Fort Halstead,
Glascoed,   Sevenoaks, Kent, TN14 7BP.
Usk, Gwent, NP5 1XL.   UK.
UK.

ABSTRACT

Polymer-Bonded Explosives (PBXs) possess a number of advantages over traditional explosives based on TNT, such as reduced vulnerability, improved mechanical properties and enhanced survivability in the operational environment. Simplified processing is also possible if the binder system utilised in the PBX is based on a thermoplastic elastomer (TPE).

This study examined the pressing behaviour of TPE-bonded HMX-based moulding powders. This type of formulation finds extensive use as main charge filling for metal accelerating applications such as shaped charges. The processability of moulding powders and their compaction characteristics are major considerations in achieving the high levels of homogeneity and density required for precision warheads.

As a means of identifying optimum conditions for producing full scale explosive billets, small scale trials were conducted to evaluate the use of dry lubricants and assess the effect of pressing parameters such as dwell time, vacuum level, temperature and press load.

1. **INTRODUCTION**

The work described in this report was part of a development program on pressed shaped charges carried out by Royal Ordnance in collaboration with the Defence Research Agency (DRA). The programme addressed the formulation, processing and characterisation of thermoplastic elastomer (TPE)-based explosive moulding powders. Highly nitramine loaded compositions containing, in this case, 95% by mass of HMX are required to meet the extreme metal moving demands required by high performance warheads. A velocity of detonation value of 8704 ms^{-1} and a detonation pressure value of 34.4GPa at TMD has been predicted using a proprietary computer program[1]. The pressing behaviour of the candidate compositions and evaluation of the pressed explosives with respect to hazard, performance, physical properties and ageing was then examined. The pressing behaviour of the candidate composition was firstly evaluated on the small scale, producing right cylindrical pellets. This enabled optimum pressing conditions to be isolated from a wide range of variables. Preferred conditions were thus identified for commencing full scale pressing trials on cylindrical and profiled billets.

2. **AIMS**

The overall aims of the study were as follows:

(a)   to develop a TPE binder system
(b)   to develop an HMX-based TPE-bonded moulding powder
(c)   to assess pellet pressing characteristics
(d)   to assess the performance and hazard parameters on test samples
(e)   to press full scale charges and assess their performance.

The present study covers the comparison of moulding powders and the assessment of pellet pressing characteristics in small scale trials.

3. **FORMULATIONS**

Binder Compositions

Three binder compositions based on a di-(2-ethylhexyl)sebacate plasticised styrene-ethylene/butylene styrene polymer and designated XBS 6000, XBS 6001 and XBS 6005 were prepared by methods which included hot melt, compounding and solvent lacquering techniques. The development of these TPE binder systems has been reported elsewhere[2].

Moulding Powders

The TPE formulations investigated are listed in Table 1. Moulding powders based on the TPE bonded systems were assessed using the following methods:

DSC
Vacuum Stability
Particle Size Distribution
Bulk Density and Tapped Density
Powder Flow Characteristics
Hazard Assessment [Rotter Impact (SCC Test No 1A) and mallet friction (SCC Test No 2)[3]]
Binder Coating Efficiency (Scanning Electron Microscopy and Optical Microscopy)

Processing Results

Moulding Powders using XBS 6000

Preparation of an initial formulation, composed of HMX Type A/XBS 6000 95/5 $\%^m/_m$
and designated RF-42-01/1 was attempted in an anchor stirrer type mixer with a jacket
temperature of approximately 105°C. Unfortunately, the dried product had discrete lumps of
binder interspersed with uncoated HMX, indicating that the mixer action was not vigorous
enough to induce coating. To improve phlegmatisation an identical mix, RF-42-01/2, was
conducted using a high shear mixer at a temperature of 95°C. This method produced a very
soft sticky granular powder.

Moulding Powders using XBS 6001

Formulations employing XBS 6001, a high styrene-ethylene/butylene styrene content binder
system, were manufactured by compounding at elevated temperature in a high shear
incorporator. The initial mix, designated RF-42-02/1, contained HMX Type A/XBS 6001
95/5 $\%^m/_m$. Once a homogeneous mix had formed the water was driven off by heating and the
product cooled. Visual inspection showed that the HMX was not effectively coated.

A second mix, RF-42-02/2, using the same ingredients in the same ratios was performed.
This time the binder ingredients were added individually in an attempt to compound all the
materials simultaneously. Powder sensitiveness testing gave a low Rotter impact value of 66
and microscopy revealed poor coating with loose binder present. These results suggest poor
phlegmatisation of the HMX.

A third mix, RF-42-02/3, using the same ingredients in the same ratios was performed. In this
case the product was promptly removed from the mixer at the end of the heating stage and
prior to the forced cooling stage. No improvement in the coating process was evident.

Moulding Powders using XBS 6005

Formulation RF-42-03/1 containing XBS 6005 binder loaded with 95% HMX Type A was
prepared in a incorporator using the hot melt technique adopted for the RF-42-01 variants.
The product was a sticky granulate possessing an F of I value of 78. A bimodal version of the
formulation, RF-42-03/2 containing HMX Type A and Type B was then prepared in the same
manner. The F of I value of 69 for this product was relatively low so a modified procedure
was used to manufacture another bimodal formulation, designated RF-42-03/3, which had an
F of I value of 74.

Powder Characterisation

Thermal Stability

DSC analysis and vacuum stability results were consistent and acceptable for all three variants.

Physical Properties

Bulk density values ranging from 0.633 to 0.852 $Mg.m^{-3}$ were obtained for the RF-42-01, -02 and -03 variants. RF-42-03/3 recorded a tapped density value of 0.852 $Mg.m^{-3}$ which gives a ratio of tap density to bulk density of 1.16. This high value suggested poor flow properties which were confirmed by the poor response in the flow time and slip angle tests.

Hazard Assessment

Rotter impact values ranging from 66 to 78 were recorded which indicates some desensitisation relative to HMX which has a Rotter impact value of 60.

Binder Coating Efficiency

Optical microscopy coupled with polarised top lighting dispersion staining techniques revealed some partially coated surfaces. Scanning electron microscopy showed areas of differing contrast highlighting where the TPE coating was thin or non-existent.

Conclusions

The most promising moulding powder formulation designated RF-42-03/3, containing 95% m/m HMX and 5% m/m XBS 6005, was selected for assessment in pressing studies. Unfortunately this composition was found to have unacceptably high pellet ejection loads. To reduce the pellet ejection forces three dry lubricants were assessed.

4. PRESSING STUDIES

Equipment

The initial work was performed using a 5 ton hand operated hydraulic press and a 12.6mm diameter die set. Statimeters were used to measure the applied load and the maximum force required to eject the pellet from the die set. A sketch of the equipment is shown in Figure 5. The latter work was carried out using a 20 ton downstroking hydraulic press and a nominal 25.4mm diameter die set. Vacuum pressing was carried out in a specially constructed chamber designed to take the standard Royal Ordnance die sets. The use of a hot oil circulator allowed pressing operations at elevated temperatures. A sketch of the apparatus is shown in Figure 6.

Assessment Methods

Pellet Ejection Forces and the use of Dry Lubricants

Pellets were pressed at various pressures between 2 and 15tsi [*31-233MPa*] at ambient temperatures with a dwell time of 15 seconds and at length to diameter ratios of 1:1 and 2:1.

Initial pressing load versus pellet density determinations were attempted with formulation RF-42-03/3 at an L to D ratio of 2:1 but the pellet ejection forces were considered to be too high. Pellet ejection forces were over 75% of the compaction load (see Table 3). Therefore, 0.5% of the binder was replaced in experimental formulations by a dry lubricant to reduce pellet ejection forces. RF-42-04/1 contained graphite, RF-42-06/1 contained Zinc stearate and RF-42-07/1 contained PTFE. Pellets having a 2:1 L to D ratio were pressed using these three formulations at a nominal pressure of 6tsi [*93MPa*] and the pellet ejection loads were recorded. The results for those pellets pressed with the formulation RF-42-03/3 which contained no lubricant are listed in Table 2. Graphite was the most successful of the three lubricants at the 0.5% level but ejection forces were still considered to be too high. Therefore the effectiveness of 1% graphite in reducing pellet ejection forces was investigated in formulation RF-42-05/1. This resulted in a further reduction in ejection forces to an acceptable level.
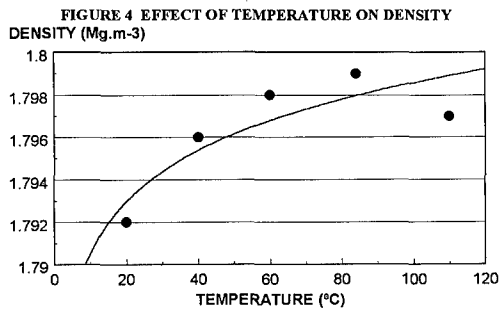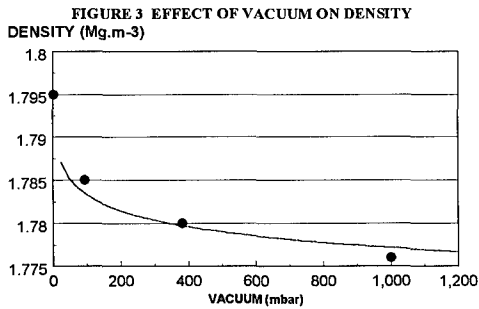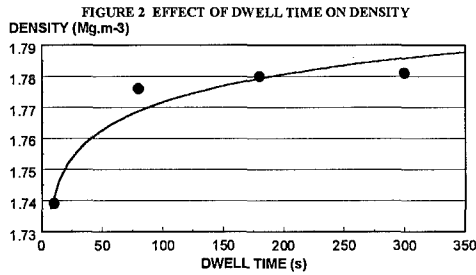
Pellet Ejection Forces and Pressing Load versus Pellet Density

Pellets were pressed using RF-42-05/1 at 2:1 and 1:1 L to D ratios at a range of pressing loads (see Table 4 and Figure 1). Pellets formed at pressures as low as 2tsi [*31MPa*] at an L to D ratio of 2:1 and densities of 93% of TMD were recorded (TMD 1.823Mg.m^{-3}). At the other extreme the density/load curve plateaued above 12tsi [*186MPa*] and pellets pressed at 15tsi [*233MPa*] with an L to D ratio of 1:1 had densities of 97.7% of TMD.

FIGURE 1 EFFECT OF PRESS LOAD ON DENSITY
[RF-42-05/1]
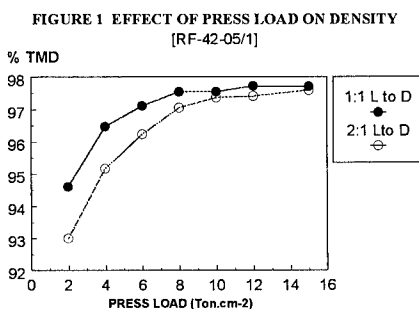
The method of manufacture for RF-42-05 was revised to incorporate a dry graphiting step. This formulation was redesignated RF-42-08 and mixes were made for subsequent pressing studies and for the determination of powder explosive and physical properties. The moulding powders were manufactured in high-shear mixers at a 0.5 kg minimum scale which was scaled up to 6 kg.

In the second part of the pressing study the effect of dwell time, vacuum level and temperature on pellet density was determined. The pellet density of the TPE formulation RF-42-08 increased steeply with respect to dwell time to 1.776 Mg.m^{-3} at 80 seconds and thereafter plateaued (see Figure 2). With respect to vacuum the pellet density increases rapidly as the vacuum level hardened to 1mbar at which point a density of 1.795 Mg.m^{-3} was achieved (see Figure 3). The density of the RF-42-08 formulation increased steadily with temperature from 1.792 Mg.m^{-3} at 20°C to 1.799 Mg.m^{-3} at 84°C (see Figure 4).

FIGURE 2 EFFECT OF DWELL TIME ON DENSITY

FIGURE 3 EFFECT OF VACUUM ON DENSITY

FIGURE 4 EFFECT OF TEMPERATURE ON DENSITY

Reassertion of the RF-42-08 pellets, air pressed, was relatively large (0.28%) whilst the vacuum pressed pellets had reasserted to less than half this value (0.12%). More representative reassertion values were later obtained in the large scale study.

Pellets pressed under optimum conditions had an average density of 1.812 $Mg.m^{-3}$ which is 99.37% of TMD. The final pellet diameter at ambient temperature was 25.34 mm compared to a mould diameter of 25.36 mm which is a shrinkage of 0.08%. The optimum pressing conditions are listed in Table 5.

Conclusions

The substitution of 1% graphite in the binder produced a composition which had relatively high but acceptable ejection loads and which could be pressed to a high percentage of its TMD (99.37%) with vacuum and heat applied.

5.   REFERENCES

1   Explosive Performance Theoretics (EXPERT) Computer Program, V1.1,
        Royal Ordnance.

2   TPE Binders for Pressable Explosives Formulations, TH Jordan, RE Hollands and
        AS Cumming, Insensitive Munitions Technology Symposium, June 1994

3   SCC Manual of Tests, DRA Fort Halstead

6.   ACKNOWLEDGEMENTS

TABLE 1: <u>NOMINAL FORMULATIONS</u>

TPE Formulations used to determine the effectiveness of dry lubricants

	TPE FORMULATIONS					
Ingredients	RF-42-03/3[a]	RF-42-04/1	RF-42-05/1[b]	RF-42-06/1	RF-42-07/1	RF-42-08/1
HMX	95	95	95	95	95	95
XBS 6005 binder	5	4.5	4	4.5	4.5	4
Graphite		0.5	1			1
Zinc stearate				0.5		
PTFE					0.5	

[a] Formulation recommended in Phase III containing no additives
[b] RF-42-05 and RF-42-08 have the same composition. RF-42-08 was
developed from RF-42-05

TABLE 2: EFFECT OF PRESS LOAD ON DENSITY AND EJECTION PRESSURE

MOULD   Ø12.6mm   L to D ratio   2:1
DWELL TIME   15s   Nominal pellet mass   5g
FORMULATION   RF-42-03/3

Pressure		No pellet	Max Ejection Pressure		Density	% TMD (TMD 1.802)
tsi	*MPa*		tsi	*MPa*	Mg.m^{-3}	
2	*31*	1	2.1	*33*	1.691	93.84
4.03	*62*		3.4	*53*	1.714	95.12
6.17	*96*		5.2	*81*	1.727	95.84
8.29	*128*		6.4	*99*	1.731	96.06

TABLE 3: EFFECT OF LUBRICANTS ON EJECTION LOAD

MOULD   Ø12.6mm   L to D ratio   2:1   Nominal Press Load 6 tsi
DWELL TIME   15s   Nominal pellet mass   5g

	Lubricant - Type and Percentage Present				
Lubricant	**None**	**Graphite**	**Graphite**	**Zinc stearate**	**PTFE**
Lubricant (% m/m)	0	0.5	1	0.5	0.5
Mix code RF-42-xx/x	**03/3**	**04/1**	**05/1**	**06/1**	**07/1**
Ejection pressure(psi)	5.2	4.2	3.2	4.8	4.8
Ejection pressure (MPa)	*80.6*	*65.1*	*49.6*	*74.4*	*74.4*
Pellet Density (Mg.m^{-3})	1.727	1.741	1.739	1.73	1.739
Pellet Density (%TMD)	95.84	95.98	95.97	96	95.97
Press pressure (psi)	6.2	6.1	6	6.1	6.1
Press pressure (MPa)	*96.1*	*94.6*	*93*	*94.6*	*94.6*

TABLE 4: PEAK EJECTION PRESSURES AND EFFECT OF PRESSING LOAD ON PELLET DENSITY [RF-42-05/1]

MOULD   Ø12.6mm   DWELL TIME   15s   TMD   1.823 g.cm^{-3}

L to D ratio	Pressure			No.	Peak Ejection Pressure			Average Density	%TMD
	tsi	ton.cm^{-2}	MPa		tsi	ton.cm^{-2}	MPa	Mg.m^{-3}	
1:1	2.03	0.31	31	3	0.28	0.04	4.3	1.725	94.61
	4.06	0.63	62.8	3	0.69	0.11	10.7	1.759	96.47
	6.03	0.93	94.4	3	0.92	0.14	14.3	1.771	97.11
	8.11	1.26	125.2	3	1.04	0.16	16.1	1.777	97.55
	10.11	1.57	157.3	3	0.94	0.15	14.6	1.777	97.55
	12.16	1.88	188.2	3	0.92	0.14	14.3	1.782	97.73
	15.08	2.34	235.6	3	0.94	0.15	14.6	1.781	97.71
2:1	2.04	0.32	31	3	1.04	0.16	16.1	1.695	93.01
	4.05	0.63	62.8	3	2.19	0.34	33.9	1.735	95.17
	6	0.93	93.2	3	3.10	0.48	48.0	1.754	96.23
	8.06	1.25	125.7	3	3.52	0.55	54.6	1.769	97.05
	10.18	1.59	158.6	3	3.64	0.56	56.4	1.775	97.36
	12.17	1.89	189.7	3	4.04	0.63	62.6	1.776	97.41
	15.08	2.34	234.5	3	3.68	0.57	57	1.779	97.59

TABLE 5: PELLET DENSITIES UNDER OPTIMISED PRESSING CONDITIONS [RF-42-08]

PARAMETERS		VALUES
PELLET SIZE	(mm)	Ø25.4 x 25.4
Av. DIAMETER	(mm)	25.34
PRESSING LOAD	(tsi)	15
DWELL TIME	(secs)	200
VACUUM	(mbar)	1
TEMPERATURE	(°C)	66
DENSITY	(Mg.m^{-3})	1.812
	(%TMD)	99.37

FIGURE 5

PRESS AND PRESSING TOOL SET UP

Top Drift

Die Body

Moulding
Powder

Bottom
Drift

Statimeter

Hydraulic
Ram
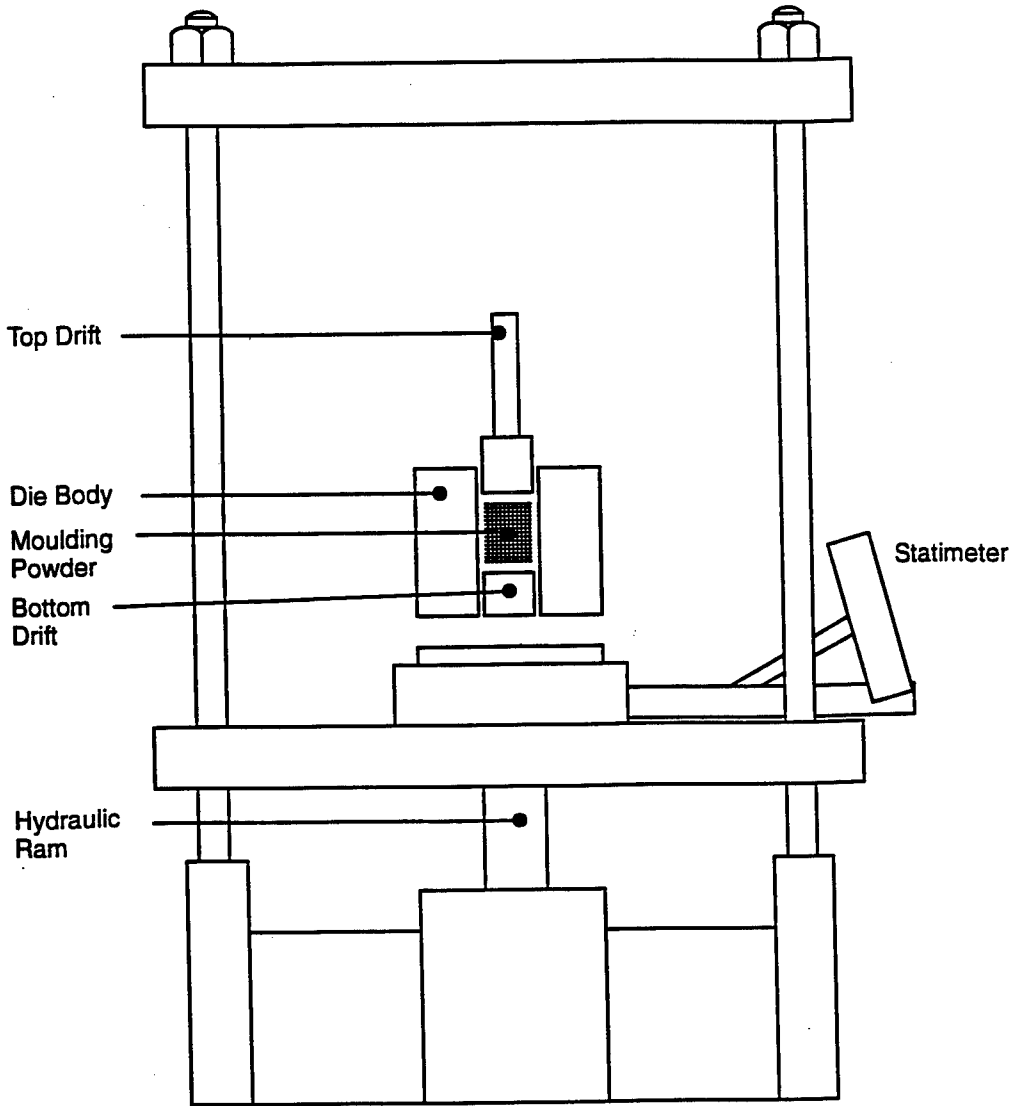
5 Ton Upstroking Press

FIGURE 6

EVACUABLE HEATING JACKET
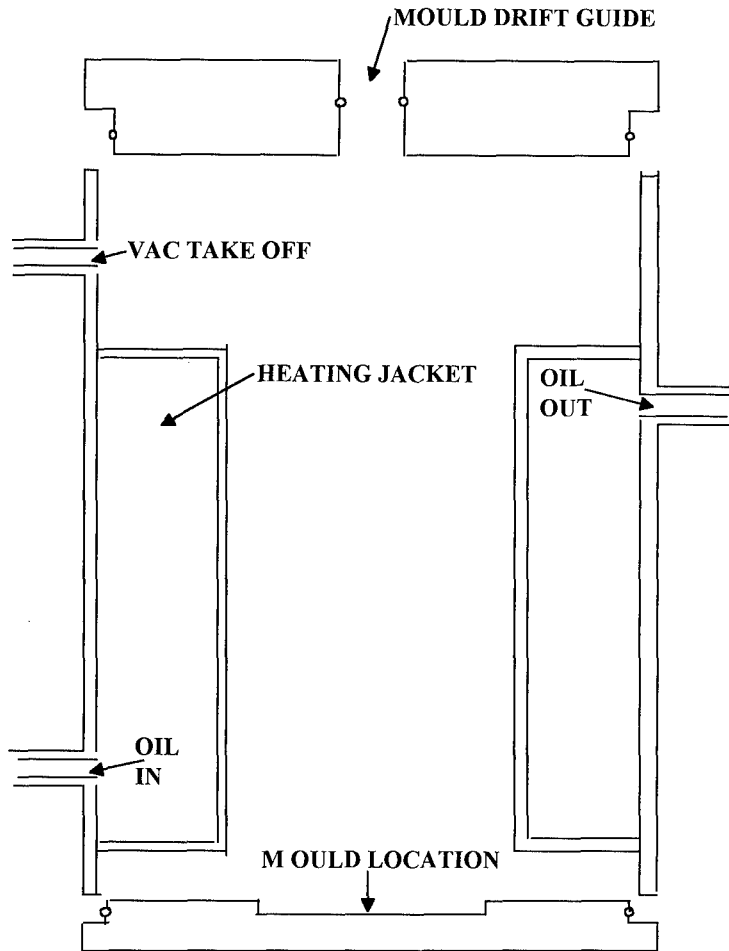
DEVELOPMENT OF THE HIGH PERFORMANCE, METAL ACCELERATING EXPLOSIVE, PBXW-11

Louis J. Montesi, Kim E. Alexander

Naval Surface Warfare Center
Indian Head Division, White Oak Detachment
Silver Spring, MD 20903

ABSTRACT

One of the objectives of the Navy Insensitive Munitions Advanced Development Program, High Explosives Project (IMAD HE) is the development of high performance metal accelerating explosives with superior vulnerability characteristics to those of current in-service formulations. Specifically, it is desirable to reproduce the performance properties of LX-14 and OCTOL 85/15 for use in shaped charges and other metal driving applications while improving upon their IM characteristics. The pressed, plastic bonded explosive (PBX) composition, PBXW-11 was developed at the White Oak Laboratory in the early 1990s and was Qualified for in-service use in October of 1995. The effort followed from the formulation of another Navy explosive, PBXN-9, which is composed of the following: 92% of the nitramine HMX, 2% HYTEMP acrylate binder and 6% dioctyl adipate (DOA) plasticizer. While PBXN-9 was shown to exhibit exemplary vulnerability characteristics, it did not produce the output required to replace most currently used metal accelerating explosives when substituted on a one-to-one basis. In an effort to enhance output, a similar formulation was developed (designated PBXW-11) in which the HMX content was increased to 96% while the plasticizer to binder ratio was maintained at 3:1.

PBXW-11 DEVELOPMENT AND EVALUATION

The advanced development of PBXW-11 was completed in mid FY 95. As part of a comprehensive evaluation performed upon PBXW-11 to qualify the material for fleet use, such properties as shock sensitivity, cookoff behavior and sensitivity to bullet impact were measured and found to either meet or exceed the acceptable requirements for use in Navy weapons systems (1). Measurements of detonation pressure, metal accelerating ability and armor penetration have shown that the composition demonstrates performance comparable to that of other high performance main charge explosives. Approximately 1,500 pounds of PBXW-11 was successfully manufactured at Holston Army Ammunition Plant (HAAP) to demonstrate the ability to scale-up processing of the material to production size batches. Table 1 summarizes the sensitivity data available for PBXW-11. The nominal densities cited are those at which small scale safety, performance and vulnerability testing were conducted unless otherwise noted. Additional test results for OCTOL 85/15, PBXN-9 and LX-14 are also included for comparison.

Table 1. Small Scale Safety Properties of PBXW-11

	PBXW-11	OCTOL 85/15	LX-14	PBXN-9
Formulation	96% HMX 3% Dioctyl Adipate 1% HYTEMP	85% HMX 15% TNT —	95.5% HMX 4.5% Estane —	92% HMX 6% Dioctyl Adipate 3% HYTEMP
Theoretical Max. Density (g/cc)	1.83	1.86	1.85	1.76
Nominal Density (g/cc)	1.80	1.86	1.82	1.73
Impact (cm)	25	25	26	34
ABL Friction (psig)	315	315	750	420
ESD (J)	4.20	0.25	12.5	8.75
Vacuum Thermal Stability (ml/g)	0.12	0.14	0.21	0.13
Large Scale Gap Test (cards)	205 (ρ = 1.80 g/cc)	236 (ρ = 1.81 g/cc)	199 (ρ = 1.80 g/cc)	201 (ρ = 1.73 g/cc)

SENSITIVITY

Basic small scale properties were determined for PBXW-11 as part of the requirement for the qualification of main-charge explosives. Results of impact sensitivity, friction sensitivity, electrostatic sensitivity, vacuum thermal stability and large scale gap testing were all within the acceptable range for Navy qualification. A comparison of the results with those of OCTOL 85/15 and LX-14 shows PBXW-11 exhibits overall improved sensitivity characteristics, with significant improvements evident in the electrostatic discharge and LSGT values over those shown by OCTOL 85/15. A series of laboratory tests was performed to support predictions that for a given geometry and size, the time to explosion for PBXW-11 at 82°C exceeds 500-days. Assuming the geometry and size of a general purpose bomb, the predicted isothermal 500-day cookoff temperature was determined to be 135°C, thus satisfying the qualification requirement.

VULNERABILITY

Vulnerability testing of PBXW-11 was conducted in the IMAD 3.2-inch generic shaped charge test unit (GSCTU) shown in Figure 1. The GSCTU assemblies used in these tests were equipped with inert detonators and booster pellets to evaluate the effects of only the main charge fill. With the exception of Variable Confinement Cookoff Test, vulnerability tests of PBXW-11 were performed in accordance with Reference (2) in conjuction with several other candidate shaped charge explosives, among them PBXN-9, OCTOL 85/15 and LX-14. A summary of test results is given in Table 2.

Slow Cookoff Testing

Slow cookoff tests were conducted in duplicate where the explosive-loaded 3.2-inch GSCTU was placed in an electric oven and heated at a slow cookoff rate of 3.3°C per hour until reaction occurred. Temperatures in the oven's air stream and on the external surface of the test unit were continuously measured by thermocouples. PBXW-11 demonstrated burning reactions in both tests in which there was no resultant damage to the test hardware. In comparison, slow cookoff testing of both OCTOL 85/15 and LX-14 resulted in detonations.
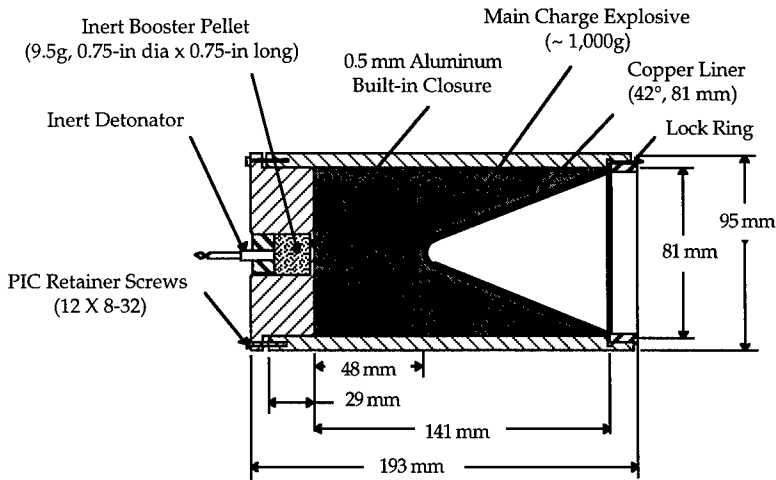
Figure 1. IMAD 3.2-Inch Generic Shaped Charge Test Unit

Fast Cookoff Testing

Two fast cookoff tests were performed on PBXW-11 loaded 3.2-inch GSCTUs in which the units were subjected to an enveloping flame produced by burning JP-5 fuel. Testing continued until the fuel was consumed. Post-test inspection of the test GSCTUs showed both tests resulted in burning. Burning reactions were also noted for LX-14 loaded units. Burning in two tests and partial detonation in a third were exhibited by OCTOL 85/15.

Table 2. Vulnerability Test Results for PBXW-11

Test	PBXW-11	OCTOL 85/15*	LX-14*	PBXN-9*
Slow Cookoff	Burn (2 Tests)	Detonation (2 Tests)	Detonation (2 Tests)	Burn (2 Tests)
Fast Cookoff	Burn (2 Tests)	Burn (2 Tests) Part. Detonation (1 Test)	Burn (2 Tests)	Burn (2 Tests)
Multiple Bullet Impact	Burn (1 Test) Deflagration (1 Test)	Deflagration (1 Test) Detonation (1 Test)	Deflagration (2 Tests)	Burn (2 Tests)
Variable Confinement Cookoff (in)	0.075	0.015 (OCTOL 75/25)	0.015	0.090**

*Data source is reference (3).
**PBXN-9 did not achieve failure in the VCCT. Reported value is the highest level at which the explosive was tested.

Multiple Bullet Impact (MBI) Testing

Duplicate multiple bullet impact tests were performed upon PBXW-11, LX-14 and OCTOL 85/15 in GSCTU hardware. Using the test configuration shown in Figure 2, three 50-caliber armor-piercing bullets impacted the test unit at velocities of 2,800 ± 200 ft/sec at intervals of 50 ± 10 ms. Bullet velocity was measured

using electronic velocity screens positioned between the guns and the test unit. Air blast gauges and high speed photographic coverage were used in the assessment of explosive response.
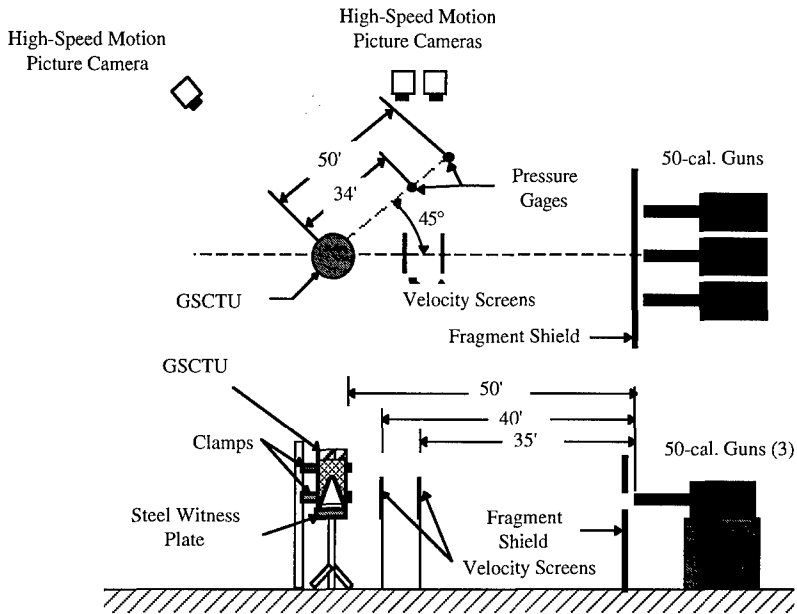
Figure 2. Multiple Bullet Impact Test Configuration

Testing of PBXW-11 resulted in burning in one test and deflagration in the second. It should be noted that no overpressure was detected by the air blast gauges in the test resulting in deflagration and a significant amount of unreacted explosive fill was recovered. Only the fact that two sections of the warhead case were propelled beyond the designated 50-foot allowable safe radius required for MBI testing with a force greater than 58 ft-pounds led to the classification of this reaction as a deflagration. It has been suggested in Reference (4), that the confinement of the 3.2-inch GSCTU is such that the explosive does not vent sufficiently and enough pressure may be generated to rupture the case and propel it long distances. A comparison of the results of MBI testing of PBXW-11 with those of the OCTOL 85/15 and LX-14 loaded units shows significant improvement was demonstrated by PBXW-11.

Variable Confinement Cookoff Test (VCCT)

Slow cookoff characteristics of PBXW-11 were evaluated in the Variable Confinement Cookoff Test depicted in Figure 3. Three PBXW-11 pellets (1.0-inch diameter by 0.833-inch long) were placed inside an aluminum thermal sleeve which was in turn centered within a steel sleeve of variable thickness and assembled into the test configuration as shown. Heating of the assembled test unit was achieved using two 1-inch

diameter, 110-volt, 125-watt mica heating bands. A slow cookoff rate of 3.3°C per hour was maintained until reaction occurred. The thickness of the confinement sleeve was varied from 0.015-inch to 0.120-inch in increments of 0.015-inch. Hydrostatically determined internal burst pressures for steel sleeves ranging in thickness from 0.015-inch to 0.075-inch are tabulated in Table 3.

Thermocouple (0.045" Diameter)

Witness Plates
(Steel, 3/8" or 1/2" Thick)

Retaining Bolts (4 Places)

Mica Heating Bands (2 - 125 Watt)

Explosive Sample ~ 50 Grams
(1.0" Diameter X 2.5" Long)

Aluminum Thermocouple Sleeve
(0.12" Wall)

Steel Confinement Sleeve
(Variable Thickness)
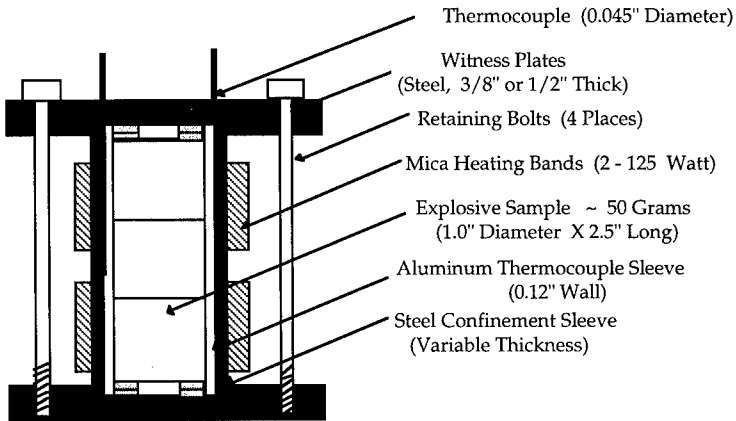
Figure 3. Variable Confinement Cookoff Test Configuration

The severity of the explosive reaction in the VCCT was determined through qualitative analysis of the resultant damage to the test hardware. Failing reactions in VCCT are considered as those more violent than a pressure rupture. Results are reported in terms of the thinnest steel confinement sleeve thickness at which a failing response first occurs.

Table 3. Measured VCCT Hydrostatic Burst Pressures

Steel Wall Thickness (in)	Burst Pressure (psi)
0.000	1,200*
0.015	2,350
0.030	5,230
0.045	7,725
0.060	10,000
0.075	12,700
0.090	15,300**
0.105	17,634**
0.120	19,963**

* Aluminum sleeve without steel confinement sleeve
** Calculated

VCCT testing of PBXW-11 at a pressed density of 1.80 g/cc demonstrated the first incidence of a violent reaction at a steel confinement sleeve thickness of 0.075-inches (corresponding to an hydrostatically determined internal burst pressure of 12,700 psi). In comparison, both OCTOL 85/15 and LX-14 failed at the minimum confinement sleeve thickness of 0.015-inch (2,350 psi).

PERFORMANCE

Detonation Pressure

The detonation pressure of PBXW-11 was calculated as a function of density from measured detonation velocity values using the Kamlet-Jacobs method (5). Using the following equations,

$$(1) \qquad D \ (mm/\mu sec) = 1.01 \ (\phi)^{0.5}(1 + 1.3\rho)$$

$$(2) \qquad P \ (kbar) = 15.58 \ \phi \ \rho^2$$

calculated detonation pressures were determined for PBXW-11 and are given in Table 4 with additional data for PBXN-9, LX-14 and OCTOL 85/15. It is clearly seen from the data presented, that PBXW-11 has theoretical detonation output comparable to that of the baseline explosives, LX-14 and OCTOL 85/15.

Table 4 . Calculated Detonation Pressures For PBXW-11

Explosive	Density (g/cc)	% TMD	Detonation Velocity (mm/μsec)	Detonation Pressure (kbar)
PBXW-11	1.55	84.7	7.70	243
	1.65	90.2	8.03	276
	1.72	94.0	8.48	316
	1.75	95.6	8.49	321
	1.79	97.8	8.80	350
	1.80	98.4	8.82	354
LX-14*	1.80	97.3	8.68	334
	1.82	98.4	8.83	351
PBXN-9**	1.73	98.3	8.43	310
OCTOL 85/15***	1.86	100	8.34	315

* Data sources are References (6) and (7).
**Data source is Reference (8)
***Data source is Reference (9)

To verify the theoretical values generated, detonation pressure testing was performed on PBXW-11 at the following densities: 1.55 g/cc, 1.75 g/cc, 1.79 g/cc and 1.80 g/cc using the Aquarium technique (10). Results are tabulated in Table 5 where measured detonation pressure values for PBXN-9, OCTOL 85/15 and LX-14 are also included. It is evident that good agreement exists between the calculated and empirical values of detonation pressure for PBXW-11 at the lower densities tested. At densities of 1.79 g/cc and 1.80 g/cc, however, a disparity is evident between the two values which is believed to be due to low detonation velocities read from the streak camera film used in the Aquarium test. Significantly higher detonation velocities (approximately 8.80 mm/μsec and 8.82 mm/μsec, respectively for densities of 1.79 g/cc and 1.80 g/cc) have been observed using the more commonly used ionization-probe method. If one were to redetermine detonation pressures for PBXW-11 at 1.79 g/cc and 1.80 g/cc using these higher detonation velocities, an increase in output is evident as shown in Table 5. One further aquarium test was performed upon PBXW-11 at a density of 1.80 g/cc where the detonation velocity was determined using both ionization probes and streak camera record with

increased magnification over the explosive-water interface. Good agreement between these velocities was shown to exist (the streak record yielded a velocity of 8.88 mm/μsec). The resultant detonation pressure was consistent with that previously determined at this density where a velocity of 8.80 mm/μsec was used.

For most metal accelerating applications, a density of 1.80 g/cc for PBXW-11 would typically be used. In comparing the measured detonation pressure of PBXW-11 with other explosive compositions at the same percentage of TMD, it is clear that PBXW-11 has performance which exceeds PBXN-9 and approaches that of OCTOL 77.6/22.4 (data was not available for OCTOL 85/15). It should be noted that the method by which the detonation pressures were obtained for LX-14 and OCTOL 77.6/22.4 were unavailable to the authors.

Table 5. Measured Detonation Pressures For PBXW-11

Explosive	Density (g/cc)	% TMD	Detonation Velocity (mm/μsec)	Detonation Pressure (kbar)
PBXW-11	1.55	84.7	7.88	235
	1.75	95.6	8.54	318
	1.79	97.8	8.50	316 (324†)
	1.80	98.4	8.61	320 (326†)
	1.80	98.4	8.88	327
LX-14*	1.84	99.5	N/A	370
PBXN-9**	1.73	98.3	8.49	296
OCTOL 77.6/22.4*	1.82	100.0	N/A	342

*Data source is Reference (7)
** Data source is Reference (8)
†Value obtained using a detonation velocity of 8.80 mm/μsec

Cylinder Expansion (CYLEX) Testing

The cylinder expansion test is a standard means of measuring the transfer of energy from an explosive to a metal case upon detonation. A relatively thin-walled metal cylinder is filled with explosive, and the mass of the explosive-filled cylinder is measured carefully. When the explosive is detonated, both the detonation velocity and the velocity of the expanding metal are measured. With this information, the JWL equation of state of the explosive can be determined (11,12). CYLEX testing was performed on PBXW-11 at a densities of 1.79 g/cc and 1.80 g/cc. The detonation velocity of the explosive, measured cylinder wall velocities (Gurney velocities) at 5 mm and 19 mm of expansion and the associated Gurney energies are given in Table 6 for each charge tested.

Table 6. Results of CYLEX Tests for PBXW-11

Density (g/cc)	Detonation Velocity (mm/μsec)	Gurney Velocity (5 mm) (mm/μsec)	Gurney Velocity (19 mm) (mm/μsec)	Gurney Energy (5mm) (MJ/kg)	Gurney Energy (19 mm) (MJ/kg)
1.80	8.75	1.56	1.79	1.22	1.60
1.79	8.75	1.57	1.78	1.23	1.58

Table 7 compares the ability of several explosives, including those of PBXW-11, to deliver energy to metal both head-on (at 5 mm) and tangentially (at 19 mm). Results indicate a favorable comparison exists in the metal-driving characteristics of PBXW-11 and the baseline composition LX-14. No cylinder expansion data is available for OCTOL 85/15.

Table 7. Comparison of Relative Metal Accelerating Abilities

Explosive	Density (g/cc)	Gurney Energy (5 mm) (MJ/kg)	Gurney Energy (19 mm) (MJ/kg)
PBXW-11	1.79	1.23	1.58
	1.80	1.22	1.60
PBXN-9*	1.73	1.20	1.51
OCTOL 78/22**	1.81	1.22	1.54
LX-14**	1.84	0.99	0.99

*Data source is Reference (8).
**Data source is Reference (7).

Armor Penetration

GSCTU shaped-charge jet penetration into a stack of rolled homogeneous armor (RHA) plates was used to provide a measurement of the performance of PBXW-11 relative to other metal driving explosive compositions. Figure 4 presents a typical test configuration.
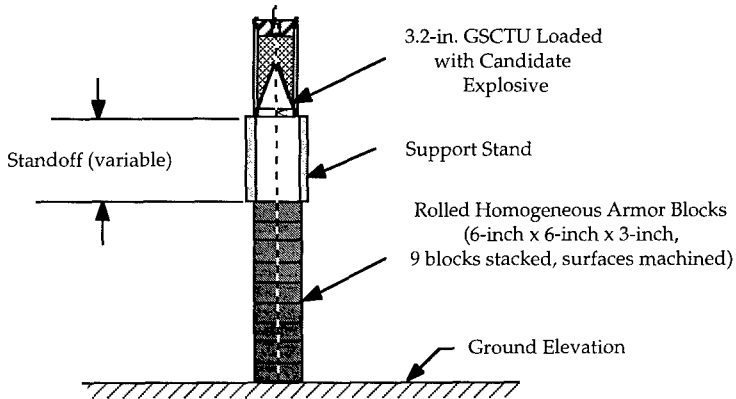
Figure 4. Armor Penetration Test Configuration

The 3.2-inch GSCTUs used for the armor penetration tests utilized a cold-formed copper liner rather than a low-cost, deep-drawn liner used for vulnerability tests. Tests were conducted at standoffs of two, five, seven and nine CDs (where the charge diameter equals 3.2-inches) from the RHA stack. The depth of pentration into RHA was measured. Table 8 provides a summary of armor penetration test results for PBXW-11, OCTOL 85/15, LX-14 and PBXN-9. The armor penetrating performance of PBXW-11 was much the same as that

of LX-14 which was not surprising in light of the similarity of the density and detonation velocities of the two formulations. A notable improvement was evidenced over PBXN-9 performance.

Table 8. Average Penetration Data For PBXW-11

Explosive	Average Penetration Depth (mm)			
	2 CD Standoff	5 CD Standoff	7 CD Standoff	9 CD Standoff
PBXW-11	475	539	594	575
OCTOL 85/15*	478	583	525	628
LX-14*	473	562	580	606
PBXN-9*	467	552	560	539

*Data source is Reference (3).

CONCLUSIONS AND DISCUSSION

Results of characterization testing of the pressed explosive, PBXW-11, have shown that the composition exhibits relatively insensitive behavior with performance nearly equal to that of the baseline explosives with which it was compared. The material exhibits overall sensitivity characteristics which are superior to OCTOL 85/15 and comparable to LX-14. PBXW-11 proved to be significantly less shock sensitive than OCTOL 85/15 in LSGT evaluation. In vulnerability testing in the 3.2-inch generic shaped charge test unit, PBXW-11 outperformed both materials, demonstrating exceptional cookoff properties. With the exception of one questionable deflagration reaction in multiple bullet impact testing, PBXW-11 met the criteria of MIL-STD-2105B for in-service use.

Detonation pressure testing of PBXW-11 at a pressed density of 1.80 g/cc has shown that the formulation demonstrates performance similar to OCTOL 77.6/22.4 when compared at 98 percent of theoretical maximum density. PBXW-11 possesses armor penetration ability similar to LX-14, especially at standoffs of 7 and 9 charge diameters. Results of cylinder expansion testing yield metal accelerating properties which exceed those of both LX-14 and PBXN-9.

REFERENCES

1.   NAVSEA INST 8020.5B, Ser 06,630 of May 1988, Subj: Qualification and Final (Type) Qualification Procedures for Navy Explosives (High Explosives, Propellants, and Pyrotechnics).

2.   MIL-STD-2105B (NAVY), Hazard Assessment Tests of Non-Nuclear Munitions, 12 January 1994.

3.   Collignon, S., Burgess, W., Davie, L., IMAD HE Project - Evaluation of Candidate Shaped Charge Explosives, NSWCDD TR 94-158, 31 July 1995.

4.   NSWCDD ltr 8800 G64: JSF of 03 February 1995, Subj: 3.2 Inch Shaped Charge Warhead Test Results.

5.   Kamlet, M.J. and Jacobs, S.J., Chemistry of Detonations I, A Simple Method of Calculation of Detonation Properties of C-H-N-O Explosives, J. Chem. Phys., Vol. 48, 1968, p. 23.

6.   Montesi, L.J., Baudler, B.A., Qualification Test Results of LX-14 Explosive, NSWC TR 88-296, August 1990.

7.   Dobratz, B.M., LLNL Explosives Handbook - Properties of Chemical Explosives and Explosives Simulants, UCRL-52997, 16 Mar 1981.

8.   Baudler, B., Hutcheson, R., Gallant, M., Leahy, J., Characterization of PBXW-9, NSWC TR 86-334, 1 August 1989.

9.   Montesi, L.J., unpublished data.

10.   Holton, W.C., The Detonation Pressure in Explosives as Measured by Transmitted Shocks Into Water, NAVORD Report 3968, 1 December 1954.

11.   Lee, E.L., Hornig, H.C., and Kury, J.W., Adiabatic Expansion of High Explosive Detonation Products, UCRL-50422, 1968, Lawrence Livermore National Laboratory, Livermore CA.

12.   Jacobs, S.J., Gurney Formula - Variations on a Theme by Lagrange, NOLTR 74-86, 12 September 1974, NOL (now NSWC), Silver Spring, MD.

MINIATURE INSENSITIVE SILVER CUTTING CORDS.

T. ROGERS and M. WASKO
Defence Research Agency
Fort Halstead, Sevenoaks,
Kent TN14 7BP. UK.

Abstract

Miniature explosive linear cutting cords, better known as Charge Linear Cutting (CLC) or Linear Cutting Charge (LCC) has been used for many years by both military and civilian industry. Explosive cords allow a wide range of metallic and non-metallic materials to be cut, usually in circumstances in which more conventional cutting techniques are for one reason or another unsuitable.

Until recently, explosive cords have consisted of a RDX based explosive filling enclosed in a lead sheath. Modern weapon applications require an explosive cord that is more efficient in the terms of cutting ability and that is also lighter, smaller and mechanically stronger. Other requirements are for an explosive filling with an improved thermal stability and lower shock sensitivity.

This paper investigates the advantages of changing the explosive filling to Hexanitrostilbene (HNS) or BX4 and the sheathing to silver. These explosives are two of the new generation of insensitive materials, they both have advantages over RDX, in particularly HNS is useful in high temperature applications and BX4 is good for its low explosiveness when ignited by a variety of ignition and cook-off stimuli.

Silver is an attractive alternative sheathing to lead as it can give up to a 30% increase in cutting ability compared to a similar width of lead cord. Silver cord is both lighter and

stronger than lead cord of similar dimensions. Results of the performance of cords with different silver sheath thickness and cord cross section are presented and discussed.

Introduction

Background

Lead sheathed cords have been in Service in the United Kingdom for over 25 years. They are shaped into a chevron section so that initiation of the explosive filling collapses the liner and produces a linear cutting jet. The cords are available in a wide range of sizes, from those containing 3 g explosive per metre, used in the air crew escape system or missile command break-up units, to those containing 250 gm^{-1} of explosive which are used as demolition charges.

Lead, as a sheathing material has many advantages for the manufacture of explosive cords. It is very ductile metal and is therefore easily drawn to a wide range of diameters. It can also be readily rolled to the required cross section shape and easily formed into the geometry of any specific application. The high density of lead provides an effective charge cutting jet against most target materials, however, the resulting high mass per unit length of the cord has resulted in a restriction in its use in some applications. Another disadvantage of lead sheathing is that it is mechanically weak and has to be well supported in most applications. The use of lead as a sheathing material for cutting cords has also given problems as regards health and environmental issues.

The main explosive filling used in associated with lead sheathed cords has been RDX based explosives, but the thermal stability of RDX (melting point of approximately 200°C) has limited its use in certain applications, additionally it does not meet insensitive munitions requirements.

Aim

This paper reports work which investigated the advantages of changing the sheathing from lead to silver and the explosive filling from RDX to Hexanitrostilbene (HNS) or BX4 (a mixture of TATB, RDX and PTFE).

Materials

Explosives

Three types of explosives were compared in this work. RHA consisting of 95% RDX and 5% HMX recrystallized from hot acetone (specification TS667), BX4, and Hexanitrostilbene (HNS2) a high temperature explosive manufactured by Swedish Ordnance.

General description of explosive cord manufacture.

The manufacture of miniature linear cutting cords is based upon the process of filling a metallic tube with explosive powder and then reducing the diameter of the tube by a wire drawing process. This is carried out using a hydraulic draw bench, which pulls the tube at a controlled rate through a series of dies, each die reducing the diameter by a precise amount. As the tube reduces in diameter and increases in length, the explosive core is also reduced in diameter and the density of the filling increases. At the required diameter, the drawing process is concluded and the explosive cord is then finished by rolling it between shaped rollers to produce the chevron section explosive cord. The use of different rollers enables the cross sectional geometry to be changed. The shape of the chevron section and the stand-off distance control the cutting efficiency of the cord.

Manufacture of lead explosive cord.

Lead alloy tubes with an internal diameter of 9.4mm and a wall thickness of 2.0mm were filled. The tubes were cleaned with acetone and allowed to dry. The

bottom of the tube was sealed with a plug of RD 1284 (black lutin sealing compound) and then weighed. The tube was attached to a compressed air vibrating rig, which allowed the tube to be vibrated continually whilst being filled with the explosive powder. The explosive powder was manually fed into the tube using a scoop and funnel. This vibration technique ensured that the explosive was filled to a consistent density, and that small air pockets or voids would not form in the filling. Once the tube was almost full a plug of RD 1284 was inserted into the remaining volume to retain the explosive powder during the subsequent processing. The tube was again weighed before being drawn to 6.25mm or 4.0mm diameter and shaped.

Manufacture of silver explosive cord

In general the thin walled silver tube was used but in one series of experiments with BX4 a tube with a thick wall tube was used. This was to allow the effect of wall thickness on the cords performance to be investigated.

All the silver sheathed cord was manufactured using a similar process to that described above for the lead sheathed cord.

Measurement of the explosive core loading (ECL) and weight of explosive cord.

In order to measure the explosive content of the cord, two samples were taken, one from each end of cord. The samples were accurately measured and weighed. The explosive was then dissolved or softened by boiling the cord samples in Dimethylformaldeyde for the cords filled with HNS and acetone for those cords filled with BX4 and RDX. The explosive BX4 was only softened not dissolved by the acetone so the softened explosive was carefully removed by hand. The empty sheaths were re-weighed and the mean explosive core loading (ECL) in grams per metre of the explosive cord calculated. The weight of the filled samples was used to calculate the total weight per metre of each type of cord.

3.   Velocity of detonation.

The velocity of detonation (VOD) of RHA and HNS has been measured in silver and lead cords with a similar explosive core loading (ECL) of around 9gm^{-1} For BX4 explosive the VOD was measured in silver sheaths using two different wall thicknesses but with the same ECL of around 9 gm^{-1} . The VOD of all six types of explosive cord was measured at ambient temperature (18°C.) For these experiments the cord samples were cut into 250mm lengths and four lengths of each type were fired and the mean velocity calculated. The measurements were made using an explosive timing system, which enables accurate measurement of the rate of propagation in energetic materials contained in all types of explosive cord.

The system is controlled by a computer which is interfaced to a Hewlett Packard 54112 oscilloscope. The oscilloscope is linked to an optical receiving unit to which are connected plastic fibre optic sensors. The fibre optics detect the light from the explosive reaction zone as it passes through the cord. The time taken for the reaction zone to reach each sensor is recorded and the velocity of the reaction is calculated by the computer. the ends of the fibre optic sensors are destroyed by the explosive, but the fibre is relatively inexpensive and by cutting off approximately 50mm from the damaged end, the sensor is ready to use again.

The optical receiving unit converts the light pulses transmitted by the fibre optics into electronic signals which are fed directly into the digitising oscilloscope. This scope is triggered by the initial signal pulse from the fibre which is close to the detonator and then proceeds to sample the remaining channel for the stop pulse.

Evaluation of explosive cutting performance

The cutting performance of all types of linear cutting cords varies greatly with stand-off distance. This is the distance between the base of the cord and the target surface to be cut. It was necessary to test the performance of each cord over a range of stand-off distances (0 to 6mm) in order to determine the optimum stand-off.

The target material selected for the explosive cutting evaluation of the cords was the aluminium alloy 6082 (HP TF 30). This relatively soft material is easy to cut, and therefore small changes in cutting performance could be easily measured. The material is also readily available in a wide range of thicknesses. When explosive cord cuts completely through a target plate, 70% of the thickness is cut by the penetration of the explosive cutting jet and the remaining 30% results from shear forces due to the shock pressure. Therefore in the tests carried out for this evaluation the target plate selected was of sufficient thickness so that the cutting cord failed to sever it completely. This enables the depth of penetration of the jet into the aluminium to be measured accurately.

The target plates were prepared by attaching to them, two thin walled aluminium tubes with cyanoacrylate adhesive, this ensured the explosive cord was at the correct stand off distance when fired. The explosive cord was secured at right angles to the stand-off pieces with small strips of tape.

For the firing test, the target plate with the explosive cord sample attached was positioned on a 25mm thick steel block. A number 3 flat base detonator manufactured by ICI was aligned and held in contact with the end of the explosive cord by adhesive lead tape.

After detonation of the explosive cord, the target plates were cooled for 30 minutes, in a freezer to approximately -80°C. The temperature of the plates was then further reduced

by placing them into a bath of liquid nitrogen (-200°C). The frozen test plates were then clamped in a vice and fractured along the cutting jet line using a sharp blow. This technique ensured that the metal fractured cleanly without bending, exposing the depth of cut produced by the explosive cutting jet. A vernier calliper was then used to measure the penetration of the cutting jet. Five readings were taken on each plate and the average depth of cut calculated.

Results and Discussions

Velocity of detonation.

The results of the VOD determinations are shown in Table 1. The velocity of detonation for all three explosive was found to be greater when the explosives were filled into silver tube rather than lead tube. For HNS explosive filled into silver the velocity of detonation was 19% greater than that of the lead sheathed HNS. The reason for the increase in detonation velocity when silver cord is used is not fully understood and requires further investigation.

Table 1: Mean velocities of detonation of silver and lead cord

Cord type	ECL gm^{-1}	Mean Velocity of detonation m/s^{-1}
4.0mm Silver/RHA	9.50	8500
4.0mm Silver/BX4 Thick wall	8.70	7600
4.0mm Silver/BX4 Thin wall	8.50	7500
6.25mm Lead/RHA	9.40	7420
4.0mm Silver/HNS	9.70	7350
6.25mm Lead/HNS	9.30	6160

Cutting Trials

The mean depth of penetration of the cutting jet into the target plate for each cord manufactured is given in table 2 below. These are shown at the seven different stand-offs (0 to 6mm) for each of the cords. The table also gives the total weight of the cord per metre and the ECL.

Table 2: Results of mean depth of penetration in relation to stand-off distance.

Size / type of cord combination	Stand-off (mm)							CLC gm^{-1}	ECL gm^{-1}
	0	1	2	3	4	5	6		
4 mm Silver/RHA	3.60	4.30	5.20	5.70	6.30	6.70	5.40	52.60	9.50
4 mm Silver/HNS	3.00	3.40	4.20	4.30	4.50	4.30	4.00	52.80	9.70
4 mm Silver/BX4 thick wall	3.30	4.20	4.90	5.60	6.10	5.80	5.30	57.20	8.75
4 mm Silver/BX4 thin wall	3.20	4.10	6.00	6.80	5.90	6.35	5.00	51.60	8.50
4 mm Lead/RHA	2.80	3.10	3.90	4.60	4.00	3.50	3.30	76.90	4.10
4 mm Lead/HNS	2.00	2.20	2.70	3.50	3.60	3.00	2.40	77.60	4.80
6.25mm Pb/RHA	4.10	4.70	5.30	5.80	5.90	5.30	5.20	191.00	9.40
6.25 mmPb/HNS	3.60	4.10	4.50	4.80	5.00	4.60	4.20	190.00	9.30

Figure 1 illustrates the cutting performance of the 4mm wide silver cord filled with HNS, BX4 and RHA and compares them with 4mm lead filled with HNS and RHA. The graph clearly shows the difference in performance between 4.0mm silver and 4.0mm lead sheathed cord. The lead cords poor performance was partly due to their lower ECL caused by its greater wall thickness.

Silver sheathed BX4 gives an increase of over 100% in the jet cutting depth in aluminium alloy compared to 4.0mm HNS filled lead cord.

The cutting efficiency of both silver and lead cord was found to improve as the stand-off distance increased, to approximately 4.0mm beyond this distance the performance began

to decrease. The optimum stand off distance was found to vary depending on the type of explosive, the sheath thickness and the sheath material.

Tests using BX4 and the thicker walled silver tube, indicates that the thicker walled cord performs better at the higher stand offs whilst the thin walled BX4 cord performed better at stand offs between 1mm and 3mm. The performance of both silver/BX4 cords was very similar to thin walled silver/RHA cord at 2, 4 and 6mm stand offs.

Figure 2. compares the performance of silver cord filled with HNS, RHA and BX4 with lead cord filled with RHA and HNS; all cords had a similar ECL. This was achieved by using 6.25mm wide lead cords, and 4.0mm silver cords. The graph highlights that with similar ECL the difference in performance was now governed more by the type of explosive, than the sheath material. Cords filled with HNS gave the lowest depths of cut, with silver cord found to be inferior to lead.

Table 2 shows that silver sheathed cord is considerably lighter than the cords sheathed in lead. For example, the silver cord of 4.00mm width is over 30% lighter (51.6 to 76.9 grams) than the equivalent lead cord. The silver cord is almost 3.5 times lighter than a lead cord of similar ECL (52.6 grams silver, 190 grams lead). Further weight savings can be achieved by selecting a smaller size of silver cord because of its enhanced cutting performance.

7.0   Conclusions

A manufacturing process for a range of miniature silver sheathed linear cutting cords has been defined which produces a silver sheathed cord that is considerably lighter and physically stronger than cord sheathed in lead.. Measurements of the explosive cutting performance established that for the same 4.0mm wide cord the silver cord was

found to produce a much greater depth of cut than the lead cord, due in part to the increased weigh of explosive. This increase in weight of explosive is due to a number of reasons including, a reduction in wall thickness giving increased volume and an increase in density of the explosive. Of all the combinations tested, thin-walled silver/BX4 cord gave the greatest depth of cut.

The improved thermal stability of BX4 and HNS explosive will enable these silver sheathed cords to be used in high environmental temperature applications. Preliminary tests have indicated that successful functioning can be achieved with cords filled with HNS after conditioning at temperatures of up to 260°C for short periods (up to 1 hour).

This research has confirmed that smaller, lighter and stronger cords with improved cutting performance can be manufactured using silver as the sheathing material. Significant improvements to the thermal stability of these cords can be achieved by using an HNS explosive filling. These improvements over lead cords will make silver sheathed CLC, attractive for applications such as rocket motor mitigation devices and other aerospace requirements.

Although the cost of the silver sheathing is greater than for lead, due to the relatively small quantities of silver used in these miniature cords, the overall cost penalty is not great.

Future work will study how the thickness of the silver sheath, which forms the chevron liner, and the shape of the chevron section influence the cutting performance of the cords. Improved filling techniques aimed at achieving an increase in the density of the explosive filling will also be studied.

Figure 1

COMPARISON OF 4.0mm WIDE LEAD AND SILVER CLCs FILLED WITH HNS, BX4 OR RHA CUTTING INTO ALUMINIUM PLATES

DEPTH OF CUT mm

STAND OFF mm

—■— THIN SILVER/RHA, 9.5g/m   —♦— THIN SILVER/HNS, 9.7g/m   —▲— THIN SILVER/BX4, 8.5g/m

—□— LEAD/RHA, 4.1g/m   —◇— LEAD/HNS, 4.8g/m   —△— THICK SILVER/BX4, 8.7g/m
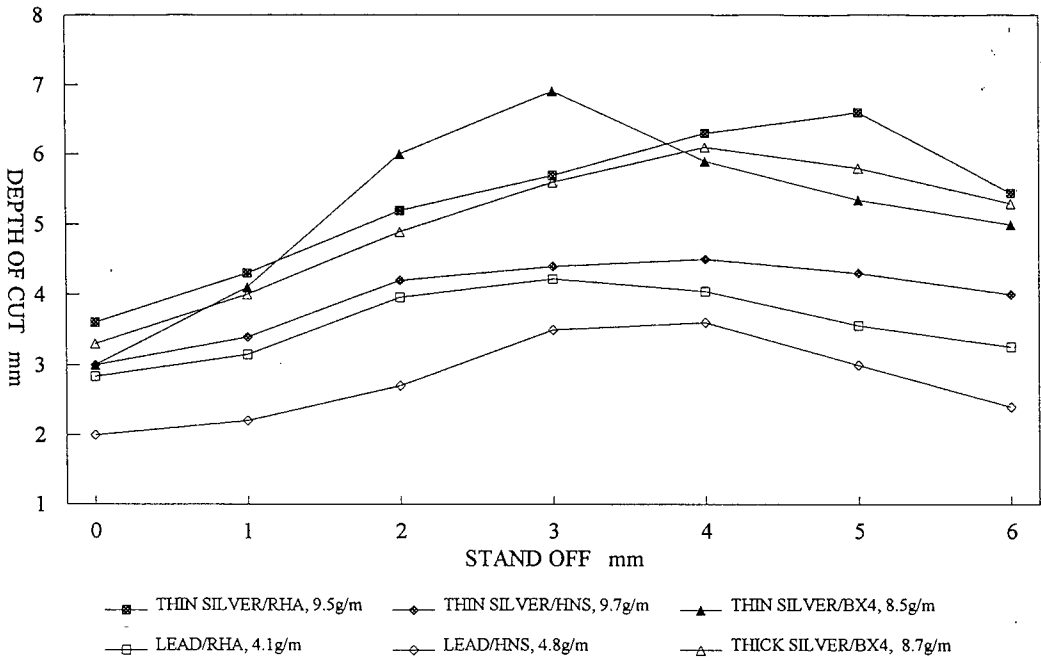
Figure 2

COMPARISON OF LEAD AND SILVER SHEATHED CLCs WITH SIMILAR EXPLOSIVE LOADING FILLED WITH HNS, BX4 OR RHA EXPLOSIVE. CUTTING INTO ALUMINIUM PLATES

DEPTH OF CUT mm

STAND OFF mm

—■— THIN SILVER/RHA, 9.5g/m   —♦— THIN SILVER/HNS, 9.7g/m   —▲— THIN SILVER/BX4, 8.5g/m

—□— LEAD/RHA, 9.4g/m   —◇— LEAD/HNS, 9.3g/m   —△— THICK SILVER/BX4, 8.7g/m
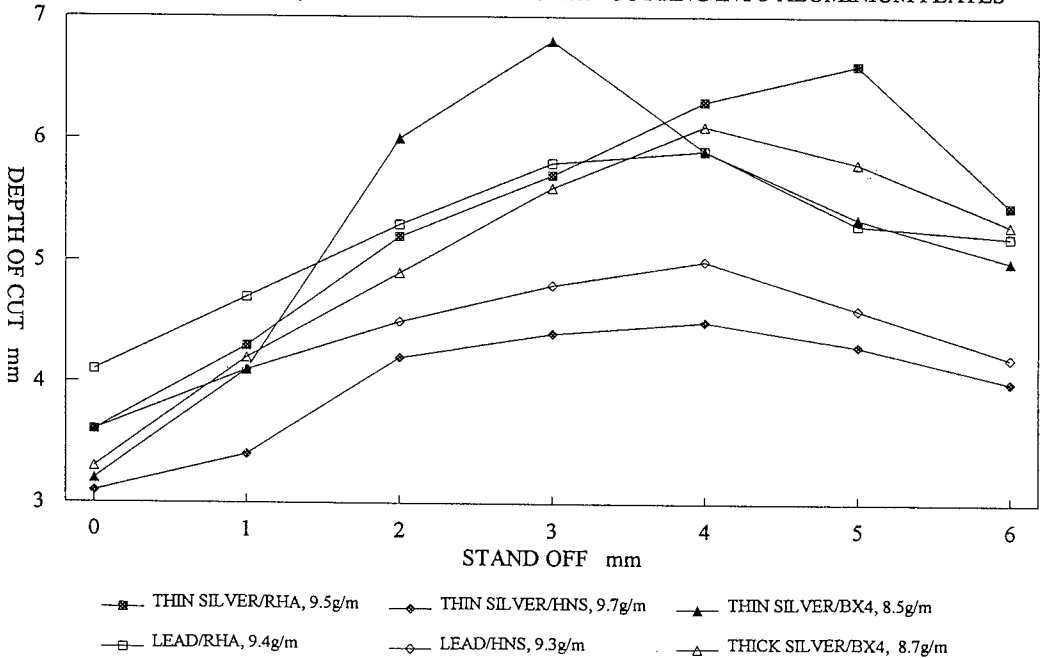
The effect of additives (HNS) in explosives filling on the structural integrity of TNT based columns and finally the terminal performance of the shells

F A Venter and F C Fouche

(Naschem (Division of DENEL) Private bag X1254, Potchefstroom,2520 South Africa)

Summary.

The structural integrity of TNT-based explosives filling, with and without the addition of HNS, was evaluated experimentally. Tests which were performed include 1,5 m drop test on a steel plate, radiographic tests and shell ramming. Visual inspection was done on the crystallisation characteristics of the explosives fillings by using split casings and sectioning of filled items. HNS in TNT-based fillings showed significant improvement in the structural integrity of various artillery HE shells. The advantages and disadvantages of TNT-based fillings with and without HNS are discussed with reference to thermal shock, crystal structure and radial sectioning of filled shells.

The terminal effectiveness of these shells were evaluated by means of static arena and fragmentation pit tests. By taking into account the fragment velocity, spread angle and mass distribution the dynamic performance of the shells were evaluated by means of computer simulation. The results of this study are discussed and the advantages and disadvantages of the addition of HNS in high explosives fillings are pointed out.

1   Introduction

With the trend in requiring less sensitive explosives as filling of ammunition in general but with special emphasis on those warheads, launched under high setback conditions, this study was conducted with the objective to quantify the influence of an additive such as HNS, with reference to structural integrity, as well as terminal performance.

2   Structural Integrity

The anchoring capability of fillings with and without thermal cycling treatment was evaluated by visual inspection of sectioned shells.   The filled shells were sectioned at the positions as indicated in **FIGURE 1.**
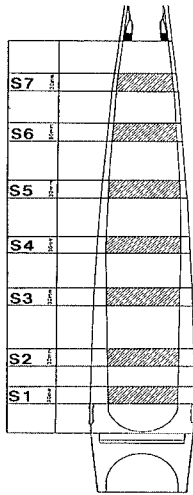
Figure 1
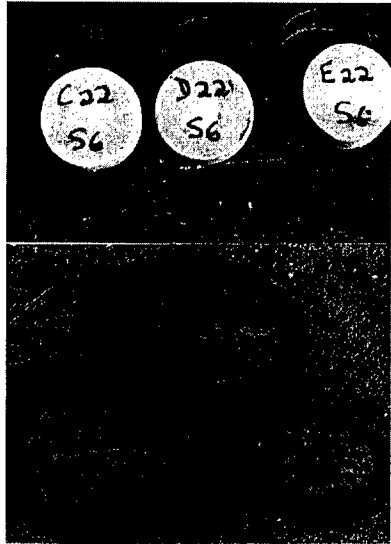
The filling of the shell presented in **FIGURE 2** was from a freshly filled shell, without thermal cycling, compared to the filling anchored to the shell after thermal cycling as presented in **FIGURE 3.**   The advantage of thermal cycling was found to be of greater importance in the case where the explosives filling does not contain **HNS**.   This is now explained by pointing out the difference in crystal growth as observed in sectioning of fillings recovered by means of split casings.   **FIGURE 4** shows the very distinct radial oriented crystal growth pattern.   **FIGURE 5** shows significantly less orientated crystal growth, and finally with **0,5% HNS** in the **RDX/TNT 60/40** mixture, 'complete' randomness in direction of crystal growth is seen from **FIGURE 6.**

These differences in crystal structure as observed visually have a significant influence on the filling integrity during rough handling. Drop tests (1,5m on steel plate) showed no cracks when filling contains HNS. The same observation was made from shell ramming tests. For both drop tests and shell ramming tests, the shells were radiographically examined in order to
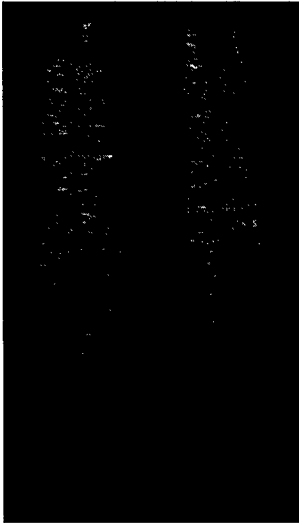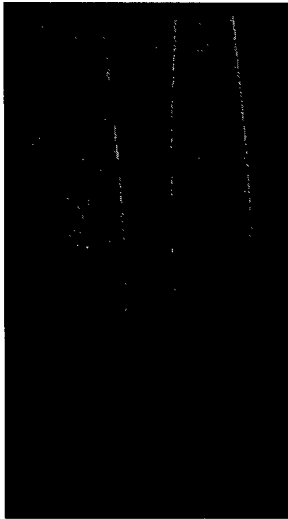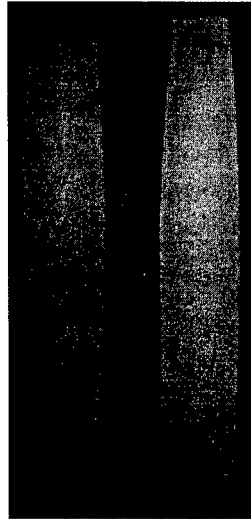
Figure 4   **Figure 5**   **Figure 6**

draw the conclusions made above. The improvement of filling integrity is explained by the crystal structure. In the case of TNT based explosives without the addition of HNS, the crystals are highly oriented. This causes pronounced cleavage planes along the outer surfaces of single crystals, with the reduced bonding strength between crystals. The presence of HNS, increases crystal growth errors. The hypothesis was that the crystal lattice energy, which is

$$U = \frac{N\,M\,z_i\,z_j\,e^2}{r}\,(1 - 1/n)^a$$

given by:

Where:

N Avogadro's number

z_i and z_j		Integral charges on the ions in the units of the electronic charge
M		Madelung constant
r		Shortest distance between action-anion pairs in cm
n		The Born exponent

was increased with the overall reduction of crystal orientation. Without going into detail which is not well understood at this stage, the effect of difference in explosives formulations and crystal structure of the filling was tested by evaluation of the terminal performance of the shells filled with these different fillings

3   Effectiveness of Warheads

Large calibre gun launched ammunition were respectively filled with **RDX/TNT** (50/50), **TNT, TNH** (TNT with 0,5% HNS) and **RTH** (RDX/TNT with 0,5% HNS). These warheads were detonated statically to obtain fragment mass distributions as well as fragment flux angle and fragment velocity.

It was found that the fragment velocities measured for these warheads filled by either of the above mentioned fillings, were not statistically significantly different to one another. In order to evaluate the terminal effectiveness of these warheads, the fragment flux angle, velocity and most important of all, the fragment mass distributions were simultaneously taken into account.

The sensitivity of this method for evaluating the effect of different fillings were reported by the same author at the **8th International Symposium on Ballistics (Orlando), 1984.**

FRAGMENT MASS DISTRIBUTIONS

Fragment Mass Distributions
Influence of HNS in filling

Legend: RT(50/50)   TNT   TNH   RTH(50/50)

TERMINAL EFFECTIVENESS

TNT (Flux)
Fragment flux 2.0 fragments/m^2
Covered area 1180. square meter

TNT (Lethality)
Both: perforation of 1.6 & Flux 2.0 /m^2
Covered area 1086. square meter

TNH (Flux)
Fragment flux 2.0 fragments/m^2
Covered area 1363. square meter

TNH (Lethality)
Both: perforation of 1.6 & Flux 2.0 /m^2
Covered area 1251. square meter
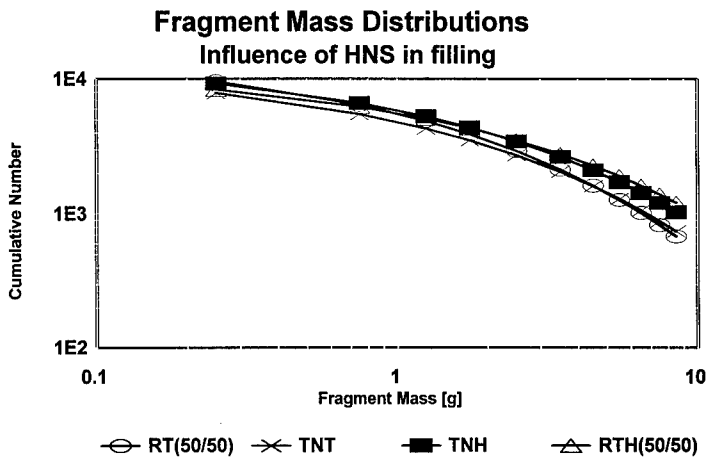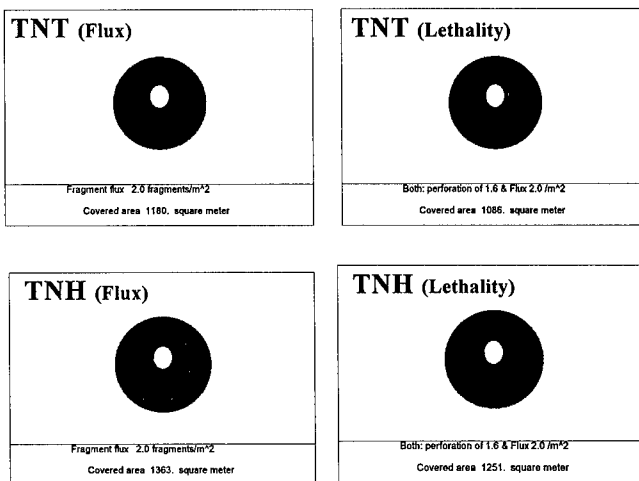
The effect on terminal effectiveness for **TNT** fillings with and without **HNS**.

RDX/TNT 50/50 (Flux)	RDX/TNT 50/50
	Lethality
Fragment flux 2.0 fragments/m^2	Both: perforation of 1.6 & Flux 2.0 /m^2
Covered area 1394. square meter	Covered area 1281. square meter

RTH 50/50 (Flux)	RTH 50/50
	Lethality
Fragment flux 2.0 fragments/m^2	Both: perforation of 1.6 & Flux 2.0 /m^2
Covered area 1315. square meter	Covered area 1212. square meter
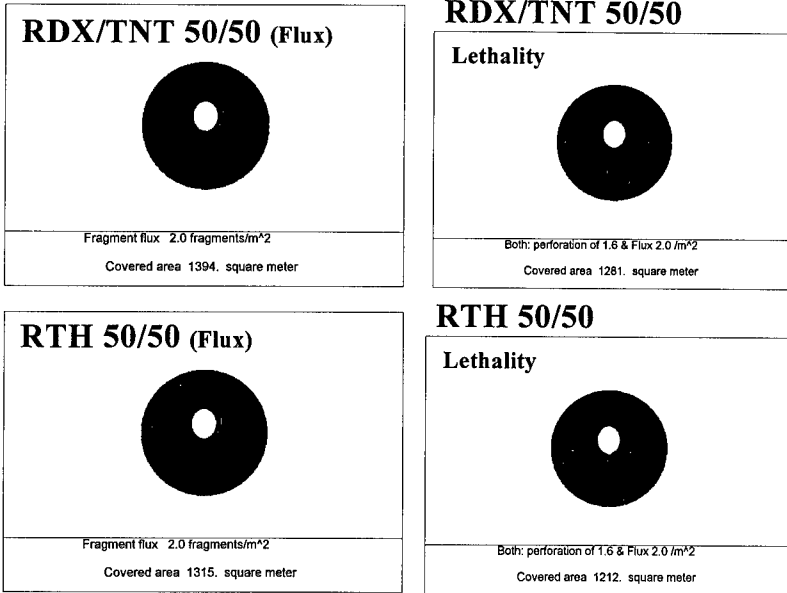
The terminal effectiveness of the same large calibre shells as used above, are now compared for mixtures of **RDX** and **TNT** with and without **HNS**.

The comparison of the terminal effectiveness is summarised in **TABLE 1** below.

	Fragment Flux density @ 2fragments per m^2 **[Area Covered in m^2]**	**Flux density of 2 m^{-2} and perforation of 1,6 mm mild steel plate.** **[Area Covered in m^2]**
TNT	1180	1086
TNT with HNS (0,5%)	1363 1032 average: 1197	1251 946 average: 1098
RDX\TNT 50/50	1394	1281
RTH 50/50	1315	1212

CONCLUSION

The addition of **HNS** in explosives fillings as used in large calibre shells has little influence on the terminal effectiveness in general. Taking into account the normal statistical fluctuations observed from round to round, it could safely be concluded at this stage that no significant influence with reference to terminal effectiveness was caused by the addition of **HNS**. From the summarised results listed in **TABLE 1**, it could be stated that only a slight improvement in terminal effectiveness was on average (two tests) observed in the case of **TNH**, compared to **TNT**. Similar tests are being done with smaller calibre warheads to confirm these preliminary conclusions.

The main advantage of the addition of **HNS** in explosives fillings is seen in the significant improvement of the structural integrity of the filling during exposure to high setback forces.

TNT-BASED INSENSITIVE MUNITIONS

Francois C Fouché[1] and Gideon C van Schalkwyk[2]

1 NASCHEM (Division of Denel, Private Bag X1254, POTCHEFSTROOM, 2520, RSA)
2 SOMCHEM (Division of Denel, Box 187, SOMERSET WEST, 7130 RSA)

ABSTRACT

The synthesis, recrystallisation and various chemical and physical characterization tests of NTO are described. The manufacture and characterization of various RDX/TNT, NTO/TNT and RDX/NTO/TNT formulations are described. The incorporation of NTO and/or fine RDX in TNT-fillings showed a significant improvement on sensitivity, mechanical properties and hence structural integrity of explosive columns in ammunition rounds. Special treatment: Thermal cycling. Tests: • Drop test on steel plate, • Fuel fire, • Bullet impact, • Static functioning. Analysis: • Radiographic examination of shells.

Conclusion: • Improved mechanical properties of TNT-based columns observed by incorporation of NTO and/or fine RDX. Tested shells filled with NTO/TNT 40/60 proved to be relatively insensitive to Bullet Impact and Fuel Fire tests. • The presence of NTO in TNT-fillings improved the fragmentation performance. • The incorporation of NTO and RDX (fine) in TNT-fillings showed a significant improvement in the sensitivity, mechanical properties and hence structural integrity of explosive columns in ammunition. • NTO/TNT (40/60) and RDX/NTO/TNT (25/25/50) could be considered as a safe and reliable main charge filling for application in various calibre shells.

1.   INTRODUCTION

The main objective with this project was to develop a less sensitive filling mixture to be used in high setback gun systems.

NTO (3 - Nitro - 1,2,4 - Triazol - 5 - one) was previously identified as a relatively insensitive explosive with a calculated performance near that of RDX[1-5]. NTO was manufactured, recrystallized and incorporated into NTO/TNT and RDX/NTO/TNT-mixtures. Various chemical and physical characteristics of these mixtures as such, as well as in ammunition, were determined.

2.   SYNTHESIS AND RECRYSTALLISATION OF NTO, AS WELL AS THE CHEMICAL AND PHYSICAL CHARACTERIZATION TESTS OF NTO/TNT FORMULATIONS

The synthesis of NTO involves three stages based on commercially available products.

STAGE 1: MANUFACTURING OF SEMICARBAZIDE HYDROCHLORIDE (Sc-HCl)

$$\underset{\substack{\text{UREA}}}{NH_2\overset{\overset{\displaystyle O}{\|}}{C}NH_2} + \underset{\substack{\text{HYDRAZINE}\\\text{HYDRATE}}}{N_2H_4O_2} \longrightarrow \underset{\substack{\text{SEMICARBAZIDE}\\(Sc)}}{NH_2\overset{\overset{\displaystyle O}{\|}}{C}NH\,NH_2} + H_2O + NH_3\uparrow$$

$$\underset{\substack{\text{SEMICARBAZIDE}\\(Sc)}}{NH_2\overset{\overset{\displaystyle O}{\|}}{C}NH\,NH_2} + HCl\ (32\%) \longrightarrow \underset{\substack{\text{SEMICARBAZIDE HYDROCHLORIDE}\\(Sc\cdot HCl)}}{NH_2\overset{\overset{\displaystyle O}{\|}}{C}NH\,NH_2\cdot HCl}$$
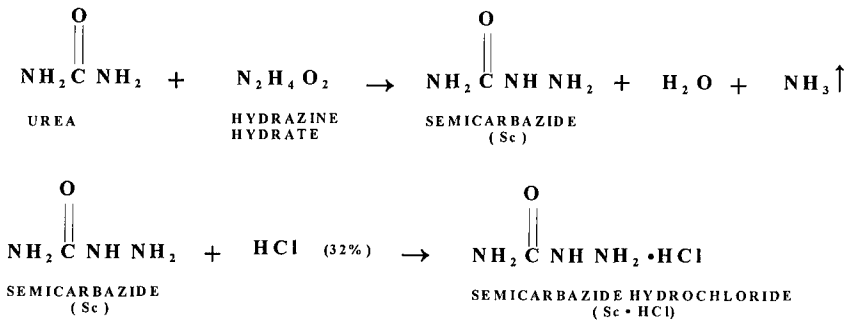
A mixture of urea and hydrazine hydrate (1:1,1 mole ratio) are refluxed between 110°C - 120°C. Excess hydrazine and water are stripped by vacuum distillation. The semicarbazide is purified in methanol, precipitated and acidified with hydrochloric acid.

STAGE 2: MANUFACTURING OF 1,2,4 - TRIAZOL - 5 - ONE (TO)

$$\underset{\substack{\text{Sc}\cdot\text{HCl}}}{NH_2\overset{\overset{\displaystyle O}{\|}}{C}NH\,NH_2\,HCl} + \underset{\substack{\text{Formic}\\\text{Acid}}}{HCO_2H} \longrightarrow \underset{\text{TO}}{\text{(ring structure)}} + 2H_2O + HCl\uparrow$$
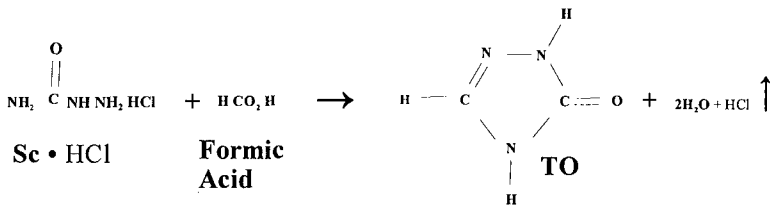
A mixture of Sc.HCl and formic acid (1:2,3 mole ratio) is refluxed until HCl stops being released.   Water and excess formic acid are stripped by vacuum distillation. The TO is washed with water and distilled again to remove residual formic acid. The TO is finally washed with water (yield ~ 80%).

STAGE 3: MANUFACTURING OF 3-NITRO - 1,2,4 - TRIAZOL - 5 - ONE (NTO)

$$\underset{\text{TO}}{\text{(ring structure)}} + \underset{\substack{\text{Nitric}\\\text{Acid}}}{HNO_3} \longrightarrow \text{(NO}_2\text{ ring structure)} + H_2O$$
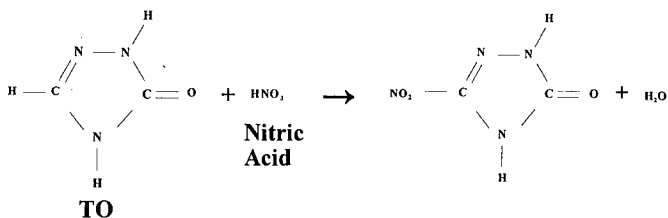
TO is nitrated with 80% HNO_3 at 60 - 70°C by adding the TO to the nitric acid.

After addition of all the TO, the mixture is aged at 75°C for 30 minutes. After ageing the mixture is filtered and washed with cold water (1°C) (yield 75 - 85%).

RECRYSTALLIZATION OF NTO

NTO may be recrystallized from water, 10% ethanol in water and ethanol, depending on the crystal size required.

Crystallization from water is a salting out process of a saturated solution of NTO in water. Cooling of the solution is as fast as possible from 100°C to 10°C (~ 20 minutes).

Crystallization from 10% ethanol in water required slow cooling of a saturated solution over an 8 hour period.

Crystallization from ethanol is similar to that from water i.e. a salting out process of a saturated solution of NTO in ethanol.

The average particle sizes obtained are shown in **TABLE 1.**

TABLE 1: Average Crystal Sizes Of NTO Crystallized From Different Solvents/Mixtures.

SOLVENT/MIXTURE	AVERAGE CRYSTAL SIZE (µm)
Water	160
10% Ethanol/Water	400
Ethanol	60

The NTO crystallized was throughout of a good quality with a melting point between 260 - 270°C, a single DTA exotherm at >236°C.

FORMULATION OF TNT-BASED MIXTURES FOR CHARACTERIZATION

- **RDX/TNT** 50/50 (RDX = 120 µm average crystal size)
- **NTO/TNT** 40/60 (NTO = 60 - 80 µm average crystal size)
- **RDX/NTO/TNT** 25/25/50 (RDX/NTO crystal sizes as above)
- **RDX/TNT 40/60** (RDX = 22 µm average crystal size)

CHARACTERISATION OF TNT-BASED COMPOSITIONS

CHEMICAL CHARACTERISTICS

- **Vacuum Thermal Stability (VTS)**

Vacuum thermal stability tests were performed according to NAVORD-OD-44811[7]. (**TABLE 2.**)

TABLE 2:   Vacuum Thermal Stability Of The Different Compositions

COMPOSITION	VTS (cm^3/g)
RDX/TNT 50/50	0,04
NTO/TNT 40/60	0,08 - 0,10
RDX/NTO/TNT 25/25/50	0,07
RDX/TNT 40/60	0,08

The gas generation for all the compositions are insignificant, i.e. <2cm^3/g after 48 hours at 100°C.

• **Chemical Compatibility**

A standard chemical compatibility test was performed on the different elements that constituted the different compositions. The tests are performed at 90°C for 40 hours and gas generation <1cm^3/g is insignificant. The results obtained are shown in TABLE 3.

TABLE 3:   Chemical Compatibility of the components of the different compositions.

COMPONENTS	COMPATIBILITY (cm^3/g)
NTO/TNT 50/50	+0,3
RDX/NTO 50/50	-0,33
RDX/NTO/TNT 25/25/50	-0,1

All the components of the different compositions are chemical compatible (<1cm^3/g).

PHYSICAL CHARACTERISTICS

• **Rheological Characteristics**

The rheological characteristics of a mixture describe the extent to which a certain mixture can be prepared and finally be used as a filling in an ammunition round.
The effluent viscosities[8] obtained are shown in **TABLE 4**.

TABLE 4:   Effluent viscosities of the different compositions

COMPOSITION	EFFLUENT VISCOSITY (S)
RDX/TNT 50/50	2,1
NTO/TNT 40/60	2,3
RDX/NTO/TNT 25/25/50	2,8
RDX/TNT 40/60	2,9

The effluent viscosities of all the compositions are « 5 seconds which make it easy to prepare.
The results with respect to sedimentation[9] are shown in **TABLE 5.**

TABLE 5: **Sedimentation of the different compositions**.

COMPOSITION	SEDIMENTATION (%/h)
RDX/TNT 50/50	22,6%
NTO/TNT 40/60	3,6%
RDX/NTO/TNT 25/25/50	6,0%
RDX/TNT 40/60	1,5%

The sedimentation of the different compositions is much less than that of normal RDX/TNT (22,6%), which means that they are quite processable in ammunition rounds.

● **Mechanical Integrity**

Compressibility tests were performed on 25mm Ø x 25mm long cast samples of the different compositions on an Instron Apparatus. The results are shown in **TABLE 6**.

TABLE 6: **Compressibility tests of the different compositions**.

COMPOSITION	STRESS AT MAX LOAD (MPa)
RDX/TNT 50/50	10,71
NTO/TNT 40/60	26,2
RDX/NTO/TNT 25/25/50	15,5
RDX/TNT 40/60	24,5

The results of the mechanical compressibility tests show that the NTO/TNT 40/60 composition has a much greater mechanical strength than the normal RDX/TNT 50/50, but that the enhanced compressibility is probably owed to the smaller crystal size of the NTO (compare with RDX/TNT 40/60 with small crystal size RDX).

● **Sensitivity of the different TNT-based compositions.**

The impact sensitivity (Julius Peters Apparatus, BAM standard), friction sensitivity (Julius Peters Friction sensitivity Apparatus, BAM standard) and electrostatic sensitivity of the different compositions as well as RDX, NTO and TNT were determined. The results are shown in TABLE 7.

TABLE 7: Sensitivity of the Different Compositions.

COMPOSITION (% m/m)	IMPACT SENSITIVITY *(F of I)	FRICTION SENSITIVITY	ELECTROSTATIC SENSITIVITY
RDX/TNT 50/50	158	36,0kg = Reaction	160 mJ
NTO/TNT 40/60	276	36,0kg = No reaction	170 mJ
RDX/NTO/TNT 25/25/50	186	36,0kg = No reaction	170 mJ
RDX/TNT 40/60	-	-	-
RDX	100	25,2kg = Reaction	225 mJ
NTO	316	36,0kg = No reaction	15 J
TNT	221	36,0kg = No reaction	138 mJ

*   F of I = Figure of Insensitivity; RDX = 100

The sensitivity results show that NTO as such is extremely insensitive and that compositions there-of are also less sensitive than normal RDX/TNT 50/50.

- **Detonative properties of different TNT-based compositions.**

The velocity of detonation (VOD) of 38mm Ø x 150mm long cast samples of the different compositions were determined. Shock sensitivity according to the large scale gap test (LSGT) was also determined with a nr. 6 detonator and 109g CH_6 donor. The results are shown in TABLE 8.

TABLE 8: VOD and Shock Sensitivity of the Different Compositions.

COMPOSITION (% m/m)	VOD (m/s)	VOD (BKW, m/s)	SHOCK SENS. (LSGT, mm)
RDX/TNT 50/50	7900	7759	30,5 - 33,5
NTO/TNT 40/60	7380	7418	18,95
RDX/NTO/TNT 25/25/50	7454	7662	29,24
RDX/TNT 40/60	-	-	28,95

The results show that the TNT-based NTO-compositions have a VOD marginally lower than standard RDX/TNT 50/50 (6-8%) and a significant lower shock sensitivity (NTO/TNT 40/60). The shock sensitivity of RDX/TNT 40/60 is only marginally lower than RDX/TNT 50/50.

3. EVALUATION OF VARIOUS TNT-BASED FORMULATIONS IN AMMUNITION

FILLING OF SHELLS

A series of shells were filled with the following explosive formulations:

- **NTO/TNT** 40/60
- **RDX/NTO/TNT** 25/25/50
- **RDX/TNT** 40/60 (Fine RDX)
- **RDX/TNT** 60/40 (Coarse RDX)

THERMAL CYCLING OF FILLED SHELLS

The filled shells were subjected to artificial thermal cycling and also radially sectioned prior, during and after thermal cycling. The obtained explosive segments were evaluated and exhibit a very interesting phenomenon viz.: Freshly filled shells show a loose filling with no anchoring of the explosive core to the shell wall. Refer to **FIGURE 1**. The explosive exhibits a soft and waxy structure as depicted in **FIGURE 2**. After thermal cycling the explosive column proved to be well anchored to the shell wall. The explosive exhibits a hard and brittle structure. Refer to **FIGURES 3 and 4.**

DROP TESTS ON A STEEL PLATE

TNT and TNT-based compositions show a cumulative permanent and irreversible expansion on thermal cycling and it has a vast improvement on the structural integrity of the explosive column. After 1,5 metre drop test on steel plate, (Nose, base and side-drops) cracks and separations were observed in 100% of those shells not subjected to any temperature cycling. However, excellent results were obtained with those shells where the explosive columns proved to be well anchored to the shell walls.

LOVA CHARACTERISATION TESTS

The following LOVA characterisation tests were carried out on 76mm shells filled with the various explosive formulations viz.:

- **Fuel Fire**
- **Bullet impact**

Fuel Fire

The test consists of engulfing the ordnance for at least fifteen minutes in a fuel fire and recording its reaction as a function of time.

The test facility is constructed from a 200 litre drum, designed to provide a heat source which completely engulfs the test item at the specified flame temperature for the duration of the test.

The fuel used, is similar to JP-5 aircraft fuel and the quantity fuel is sufficient to ensure a fire that engulfs the entire ordnance unit for at least fifteen minutes. The test item was located with its horizontal centre line 0,95m above the fuel surface.

The fuel was ignited and the temperature rise recorded with a thermocouple located 10 cm outside the ordnance skin for each item tested. According to the specification, the flame temperature must reach 538°C within thirty seconds after ignition. An average flame temperature of at least 871°C, as measured by the thermocouple at the test item, without contribution of the burning ordnance, will be considered a valid test. This temperature is determined by averaging the temperature from the time the flame reaches 538°C until all ordnance reactions are completed or until fifteen minutes has elapsed.

Typical flame temperatures obtained during the test at **NASCHEM,** are depicted in **FIGURE 5**.

Fuel Fire Test
Typical Flame Temperatures measured
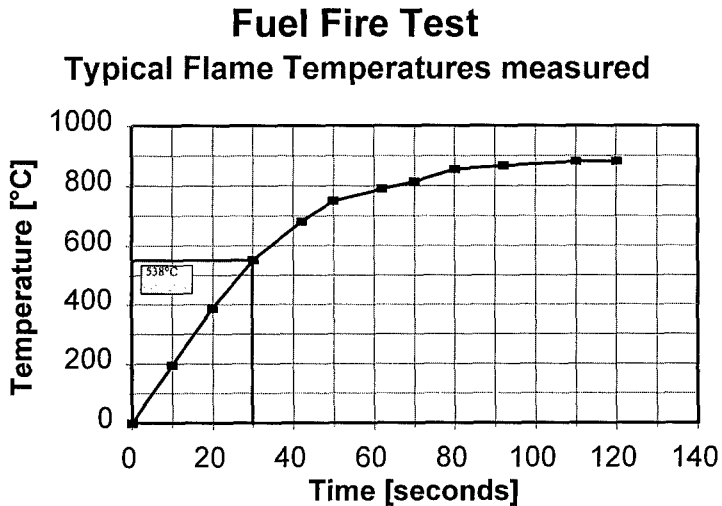
Figure 5

TEST RESULTS

All the reactions were observed visually and the results reported as one of the following

1. Burning   2.   Deflagration 3.   Propulsion
4. Partial detonation   5.   Detonation

NOTE: The severity of the reactions increases from 1 to 5 as indicated in the above categories. The test results obtained in these tests are summarised in TABLE 9. For detail of test results, refer to FIGURES 6 to10

TABLE 9:   FUEL FIRE TESTS

EXPLOSIVE	TIME TO OBSERVED REACTIONS	DESCRIPTION CF REACTIONS OBSERVED
NTO/TNT 40/60	2 minutes 10 seconds	• Steel plug was forced out. • No damage to round. • Propulsion effect.
RDX/NTO/TNT 25/25/50	2 minutes 30 seconds	• Pressure rupture • Deflagration
RDX/TNT 40/60 (Fine RDX)	2 minutes 25 seconds	• Low order detonation
RDX/TNT 60/40 (Coarse RDX)	2 minutes	• High order detonation

Bullet Impact Tests

The test items were medium calibre shells filled with **NTO/TNT** 40/60 **RDX/NTO/TNT** 25/25/50 and **RDX/TNT** 40/60.

These shells were fitted with steel plugs as depicted in **Figure 11.**

All the reactions were visually observed and the results reported as one of the following categories.   • Burning • Deflagration • Pressure rupture • Partial detonation • Low order detonation • High order detonation.

The test results obtained in these tests, are summarised in **TABLE 10**. (See also **FIGURES 12 to 14**).

TABLE 10:   BULLET IMPACT TESTS

EXPLOSIVE TYPE	DISTANCE	CALIBRE OF BULLET	DESCRIPTION OF REACTIONS OBSERVED
NTO/TNT 40/60	70 metre	20mm Ball Velocity : 800m/s	• Steel plug was forced out. • Burning reaction.
	70 metre	12,7mm AP Velocity: 1000 m/s	• Steel plug was forced out. • Burning reaction.
RDX/NTO/TNT 25/25/50 (Fine RDX)	70 metre	20mm Ball. Velocity: 800 m/s	• Burning reaction. • Pressure rupture.
	70 metre	12,7mm AP Velocity: 1000 m/s	• Deflagration reaction
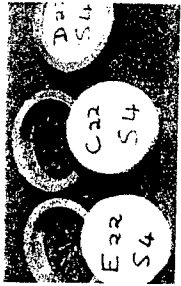
Figure 4
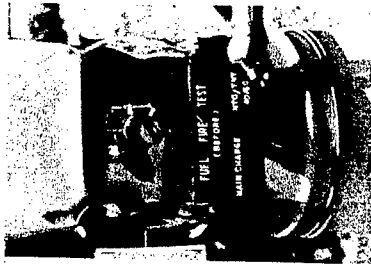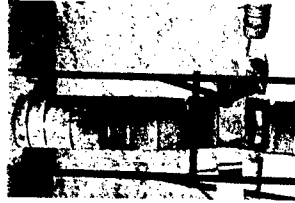
Figure 10

Figure 16

Figure 3

Figure 9

Figure 15

Figure 2

Figure 8

FUEL FIRE TEST (AFTER) MAIN CHARGE. NTO/TNT
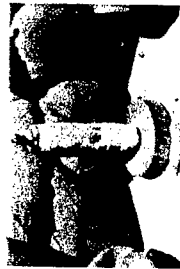
Figure 7

Figure 12

Figure 14
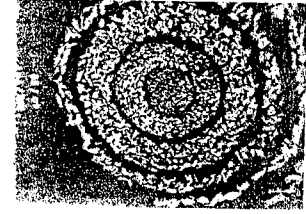
Figure 1

Figure 6

Figure 11

Figure 13

TABLE 10(cont): BULLET IMPACT TESTS

EXPLOSIVE TYPE	DISTANCE	CALIBRE OF BULLET	DESCRIPTION OF REACTIONS OBSERVED
RDX/TNT 40/60 (Fine RDX)	70 metre	2Omm Ball Velocity: 800 m/s	• Deflagration.
	70 metre	12,7mm AP Velocity: 1000 m/s	• Pressure rupture. • Burning.
RDX/TNT 60/40 (Coarse RDX)	70 metre	20mm Ball. Velocity: 800 m/s	• High order detonation.
	70 metre	12,7mm AP Velocity: 1000 m/s	• High order detohation

STATIC TESTS

Fragmentation pit tests were carried out on shells filled with **NTO/TNT** 40/60 and **RDX/TNT** 40/60.

The obtained fragments show a very similar pattern for both formulations. For more detail regarding the fragments, refer to **FIGURES 15 and 16.**

4.   CONCLUSIONS

- Good quality NTO was manufactured and recrystallized.
- TNT-based compositions containing NTO are significantly less sensitive than normal RDX/TNT compositions with marginally less performance. Crystal size has a significant effect on mechanical integrity.
- Shells filled with NTO/TNT 40/60 proved to be relative insensitive towards bullet impact and fuel fire tests.
- Improved mechanical properties of TNT-based explosives were obtained by the incorporation of NTO and/or fine RDX.
- Thermal cycling of TNT-based explosives has a vast improvement on the anchoring of the high explosive charge in the shell and hence the mechanical properties of the high explosive charge within ammunition.
- NTO/TNT 40/60 and RDX/NTO/TNT 25/25/50 could be considered as a safe and reliable main charge filling for universal application in various calibre shells.

5. ACKNOWLEDGEMENTS

6. BIBLIOGRAPHY

1. CHAPMAN LB, "NTO development at Los Alamos", Los Alamos National Laboratory, Los Alamos, New Mexico, USA. The Ninth Symposium on Detonation Aug. 28 - Sept. 1 1989, Portland, USA, Paper no. 160.

2. LEE KIEN-YIN & COBURN MO, "3-Nitro-1,2,4, Triazol-5-One, a less sensitive explosive", USA Patent No. 4733610, March 1988.

3. SPEAR RJ, ET AL, "A Preliminary assessment of NTO as an Insensitive high explosive", Material Research Technical Report 89-18, Australia.

4. LEE KIEN-YIN & COBURN MO "3-Nitro-1,2,4 - Triazol-5-one, a less sensitive explosive", Journal of Energetic Materials, Volume 5 p27-33, 1987.

5. BECUWE A & DELCLOS A, "Low-sensitivity Explosive compounds for low Vulnerability Warheads", Propellants, Explosives, Pyrotechnics 18, 1-10, 1993.

6. MARCHOCT & NOLL, (ANNATEN, 343, 24)

7. NAVORD OD 44811, "Safety and performance tests for qualification of Explosives".

8. PARRY MA & BILLON MH, "The viscosity of (molten) RDX/TNT Suspension material", Reseach Laboratory, Australia.

9. BOSWORTH, RCL; "The kinetics of collective sedimentation", Journal of colloid Science, 2, 1956.

Detonation Behaviour of HMX-based Explosives Containing Magnesium and Polytetrafluoroethylen

Stanisław Cudziło, Waldemar Trzciński, and Andrzej Maranda

Military University of Technology

Kaliskiego 2, 00-908 Warsaw, POLAND

Abstract

HMX-based compositions containing powdered magnesium (Mg) or polytetrafluoroethylen (PTFE) or mixture of Mg/PTFE were investigated. Experimental checking on the possibility of ignition and development of exothermic reactions in a detonation wave between Mg, PTFE, and detonation products was the main goal of this work. The detonation velocity and duration of an emission activity of the explosion cloud in the spectral range of $0.4 \div 1.1$ μm were measured for all mixtures tested. X-ray recording of a process of driving a copper cylinder was performed for chosen mixtures. The experimental detonation velocities were compared with those obtained theoretically from calculations by the assuming chemical activity or inertia of the admixtures. The results of numerical modelling the process of driving a cylindrical liner by the detonation products were confronted with X-ray records. On the basis of experimental and theoretical results the stages of explosion process, in which the predicted reactions proceed, are determined and the effects of the type and content of additive on detonation parameters are established.

1. Introduction

Introduction of powdered pyrophoric metals to an explosive is one of the widely used methods of increasing the energy effectiveness of explosives [1÷5]. If only metal is added then the combustion process runs mainly owing to oxygen from explosive. Too small quantity of oxygen causes incomplete oxidation of metal. That is why, some oxygen carriers or substances being able to react with metals are proposed to include in the explosive mixtures. Authors of the patent specification [6] suggest that an increase in the energetic efficiency of explosives can be achieved by including the thermite systems like Al/Fe_2O_3, Zr/B_2O_3, Li/WO_3, Be/V_2O_5, and others. Moreover, the explosive mixture containing powders of metals, which can create intermetallic combinations like Ti/B, Zr/B, Hf/B, Nb/B, are proposed in the patent [7]. A detonation wave propagating in a such mixture causes initiation of the exothermic self-propagating high-temperature synthesis reaction in the additive.

In this paper polytetrafluoroethylen is proposed as additional oxidizer for the explosive mixtures containing metal. The advantages of PTFE are, besides the ability to high exothermic reaction with metals [8, 9], an influence on explosive by increasing its mechanical resistance and acting as phlegmatizing agent. This paper is devoted to the experimental and theoretical verification of a hypothesis about reactions between Mg, PTFE, and the detonation products during detonation of mixtures containing Mg or PTFE. To this end, two component mixtures containing HMX and Mg, or HMX and PTFE, and a three component mixture of HMX, Mg, and PTFE were tested. On the basis of the measurement of the detonation velocity, the registration of the process of driving a copper tube, the results of measuring the duration of combustion of the additives in an explosion cloud, and the results of calculations of some detonation parameters, an attempt is made to determine the stage of the process, in which predicted reactions proceed, and the influence of these reactions on the detonation parameters of the mixtures tested is established.

2. Characteristic of the explosive mixtures tested

In our investigations explosive mixtures were used, in which octogen is the main component. These mixtures contained 20, 30, 40, or 50 wt % of powdered magnesium , PTFE, or the Mg/PTFE 50/50 system. To prepare the mixtures commercial HMX with 5 wt % wax, powder of Mg with purity beyond 98,5 % and grain size within a range of $60 \div 300$ μm, and powdered PTFE were used. Mixtures of HMX and additives in required proportions were prepared by long-duration rubbing in a porcelain mortar. The product obtained was pressed in three blocks of 33 g weight and 30 mm diameter each. The mean density of the charges prepared was approximately the same 1600 ± 50 kg/m^3.

3. The measurement and calculation of the detonation velocity

Charges used in measurements of the mean value of the detonation velocity, D_e, by the method of short-circuit sensors located on two measurement courses were prepared by sticking three pressed blocks of the explosive mixture, detonator and the final block made of pressed pure HMX; the set-up is shown in Fig. 1.
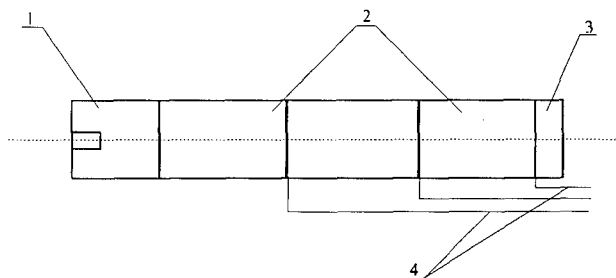
Fig. 1. Diagram of the system for measuring D_e. 1- detonator (HMX), 2 - blocks of the mixture tested, 3 - final block (HMX), 4 - short-circuit sensors.

The results of measuring the detonation velocity are presented in Fig. 2 (solid lines). In all cases considered the introduction of an additive results in a decrease of the detonation velocity as compared with the detonation velocity, 8050 m/s, for pure HMX. The highest fall of D_e with increasing the content of an additive, η, is observed for the HMX/PTFE mixture and the lowest one for the HMX/Mg mixture. This relation follows from differences in the density and compressibility of Mg and PTFE.
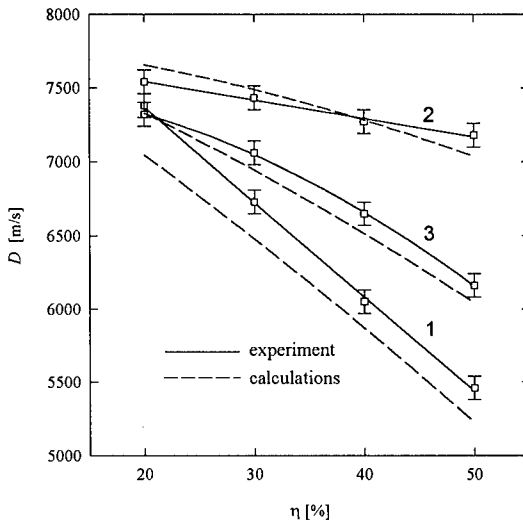
Fig. 2. Dependence of the detonation velocity on the type and content of an additive in the explosive: 1 - HMX and PTFE, 2 - HMX and Mg, 3 - HMX, Mg, and PTFE

Theoretical calculations of the detonation parameters of the mixtures investigated were performed first by means of the program for thermochemical calculations TIGER - [10] with the set of parameters in the BKW equation of state recommended in Ref. [11]: $\alpha = 0.50$, $\beta = 0.176$, $\kappa = 11.80$, $\theta = 1850$. The thermodynamical data for Mg, PTFE, and their compounds were taken from the tables JANAF -[12]. The detonation velocities of the explosive mixtures were calculated by assuming the chemical activity of the additives in the chemical reaction zone. The results of calculations of the detonation velocity, D_{calt}, are presented in Tables 1 to 3.

The detonation velocity of the explosive mixtures tested were also calculated by assuming an inertness of the additives. From the analysis made in Ref. [13] of the detonation process of explosives containing grains of an inert admixture it follows that in the reaction zone the temperature between components of the mixture, that is the detonation products and inert additive, is not equalised for grains greater than $1 \div 2$ μm in diameter. That is why the detonation velocity of the mixtures tested was calculated by the method described in Ref. [13] under the assumption of no heat exchange between the components. In this method the mixture of explosive and additives was described by a model of

multicomponent, multiphase medium. Additivity of specific volume and internal energy of components, and complete mechanical equilibrium were assumed. The thermodynamic properties of the detonation products were described by the JWL (Jones - Wilkins - Lee [14]) equation of state. As regards the additives and unreacted explosive the Grüneisen equation of state, obtained on the grounds of shock adiabate [15], was used. Empirical data for shock adiabate were taken from Refs. [2], [16], [17], and coefficients in the JWL equation were taken from Ref. [18]. The calculated values of the detonation velocity, D_{cal2}, are presented in Tables 1 to 3.

TABLE 1

Experimental and calculated detonation velocity for HMX/Mg charges

η_{Mg}, %	ρ_0, g/cm^3	D_e, m/s	D_{cal1}, m/s	D_{cal2}, m/s
20	1.60	7540 ± 110	7100	7650
30	1.60	7430 ± 120	6410	7500
40	1.60	7270 ± 100	5340	7270
50	1.60	7180 ± 110	5190	7040

TABLE 2

Experimental and calculated detonation velocity for HMX/PTFE charges

η_{PTFE}, %	ρ_0, g/cm^3	D_e, m/s	D_{cal1}, m/s	D_{cal2}, m/s
20	1.61	7380 ± 100	7480	7050
30	1.61	6780 ± 90	7120	6470
40	1.60	6050 ± 90	6770	5880
50	1.60	5460 ± 90	6410	5220

TABLE 3

Experimental and calculated detonation velocity for HMX/Mg/PTFE charges

η_{Mg}, %	η_{PTFE}, %	ρ_0, g/cm^3	D_e, m/s	D_{cal1}, m/s	D_{cal2}, m/s
10	10	1.60	7320 ± 90	7380	7330
15	15	1.61	7060 ± 100	6980	6940
20	20	1.61	6650 ± 90	6570	6520
25	25	1.61	6120 ± 90	6070	6040

From the Table 1 it follows that the detonation velocities obtained by assuming chemical activity of Mg in the reaction zone are considerably smaller than those calculated by assuming the chemical inertia of Mg. This is an unexpected result bearing in mind the additional heat releasing during the reaction between magnesium and oxygen. However the fact should be taken into account that the product of this reaction, magnesium oxide, occurs as a condensed phase and it not influences the pressure of the detonation products. Furthermore, magnesium fixes oxygen from HMX preventing this way a part of carbon from the reaction into gaseous carbon oxides. The increase in pressure of the detonation products owing to the heat of exothermic reactions with Mg is smaller than the fall of that pressure resulting from the smaller number of gaseous moles in the detonation products. This fact

causes that the detonation velocity of the explosive mixture calculated by assuming the activity of Mg is smaller than that for inert Mg. The reverse effect takes place in the case of the explosive mixtures with PTFE. The chemical decomposition of PTFE is endothermic but it results in an occurrence of additional gaseous products. This fact influences the calculated detonation velocity as it is shown in Table 2.

From the Table 3 it follows that the detonation velocities for the HMX-based mixtures with Mg and PTFE, calculated by using both the methods, are similar. This fact can be easily explained on the basis of the analysis made above for the mixtures with pure Mg or PTFE (Tables 1 and 2). The effect of the reaction of Mg is recompensed by that of the decomposition of PTFE.

The results presented in Tables 1 to 3 show that better agreement between the experiment results and those calculated is obtained when a neutrality of the additives is assumed in the reaction zone. The calculated detonation velocities for this case are presented in Fig. 2 (dashed lines). The analysis of the results as yet discussed enable us to draw a conclusion that magnesium behaves as an inert additive but PTFE decomposes partially in the reaction zone. Comparatively low temperature of decomposition (850 K) is conducive for such behaviour of PTFE. The degree of its decomposition can not be exactly appraised due to the assumptions of the model used for calculations, which idealises the real processes in the detonation products and additives. In particular, these assumptions concern no heat exchange between the components.

4. Recording and modelling the process of driving a copper cylinder

The analysis of the results presented in the previous section leads to the conclusion that possible reactions between the additives may take place in further phases of the explosion process. To determine the moment, in which the influence of those reactions on scattering the detonation products begins, the X-ray registrations of the process of driving a copper tube by the detonation products of the compositions containing 30 wt % of additive were performed. Comparison of the records of the tube shapes and the profiles obtained from calculations enable us to find a time correlation between these reactions and the detonation products expansion [19].
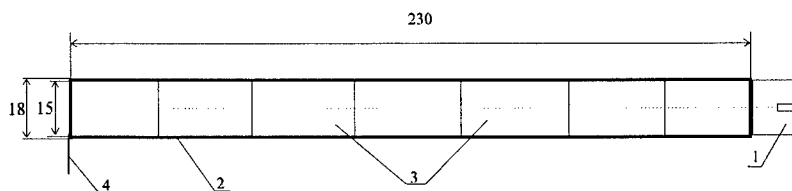
Fig. 3. Diagram of the system for X-ray recording the process of driving a tube: 1- detonator, 2 - copper tube, 3 - blocks of the explosive tested, 4 - short-circuit sensors.

The diagram of the set-up for driving the copper tube by the detonation products is shown in Fig. 3. The registration of the driving process was performed by X-ray apparatus of XR450 model. The X-ray photographs were made at the moment, when the detonation wave achieved the end of the last

charge. Thus, the process of scattering the detonation products could be observed during the time period of about 20 to 30 μs before the detonation process ended. Simultaneously with the X-ray registration the measurement of the detonation velocity was performed. The values of the detonation velocity obtained in such a set-up are presented in Table 4. They are about 200-300 m/s lower than those obtained for no sectional charges of 30 mm in diameter (Fig. 2).

TABLE 4

Results of measurement of the detonation velocity for charges used in the copper tube

.	Composition [wt %]	D_e [m/s]
1.	HMX - 100	7780 ± 110
2.	HMX - 70, Mg - 30	7300 ± 110
3.	HMX - 70, PTFE - 30	6480 ± 90
4.	HMX - 70, Mg - 15, PTFE - 15	6740 ± 100
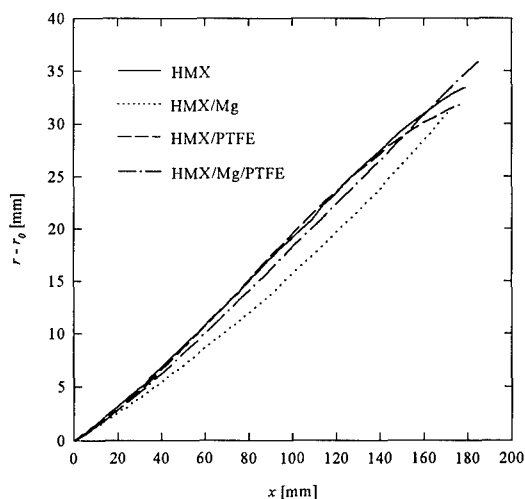
Fig. 4. Shapes of the external surface of copper tubes at the moment, when the end of charges was achieved by the detonation wave.

The results of registration of driving the copper tubes are presented in Fig. 4 in the form of shapes of the external boundary of tubes. The dependencies of radius position of the external boundaries on time are presented in Fig. 5. The time, t, is estimated from the relation $t = x/D_e$, where x denotes axial co-ordinate, by assuming that the expansion process of detonation products is stationary in a reference frame connected with the detonation wave. In reality, the process becomes stationary after a path of a few times the explosive diameter has been passed by the detonation wave. The effects of the development of detonation as well as the rarefaction waves propagating in a direction opposite to

the detonation wave on the driving process appear as a bend on the tube profile towards an axis of the set-up for large values of x. There are bends on the profiles obtained from the experiments with the HMX or HMX/PTFE charges (Fig. 4). The lack of such a bend on profiles for other charges will be explained in the further part of this paper.
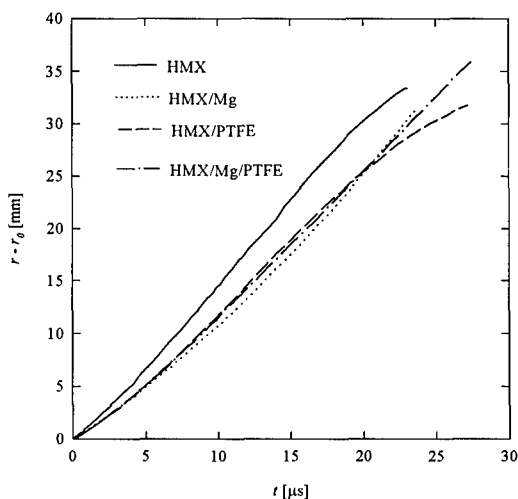
Fig. 5. Time dependence of the position of an external surface of copper tubes.

From Fig. 5 it follows that the charge of pure HMX brings the highest velocity of the tube about. The detonation products of HMX-based charges with the additives drive the copper tube much slower. The acceleration of the tube in the first stage of its motion depends mainly on the pressure of the detonation products in the C-J plane. From the appraisal of detonation parameters of the explosive mixtures by the method proposed in Ref. [13] it follows that the C-J pressure of pure HMX (24.8 GPa) is much higher than those of HMX-based explosives with Mg (18.6 GPa), or PTFE (15.6 GPa), or Mg and PTFE (17.7 GPa).

An isentropic exponent is one of the parameters describing the behaviour of the detonation products. The exponent value, changing during the expansion process, characterises a decay of the pressure with increasing the volume of the detonation products. The so-called effective exponent of isentrope is sometimes used in literature [2], [20]. Its value is determined by replacing the real isentrope with the energetically equivalent Poisson isentrope with the constant exponent. In the Ref. [21] the method is proposed to estimate the effective exponent of isentrope by comparison of the experimental profile of the copper tube with that obtained from numerical modelling the process of driving the tube by the detonation products described by a politropic gas equation with a constant exponent.
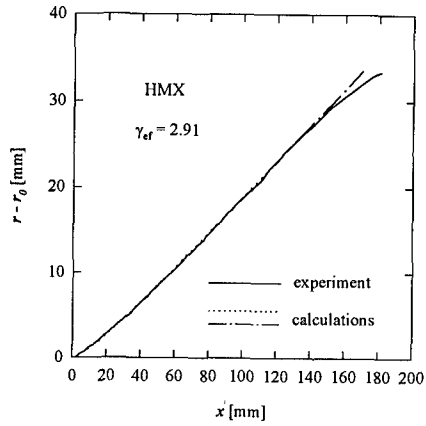
Fig. 6. Experimental and calculated profiles of the external surface of the copper tube driven by the detonation products of HMX.
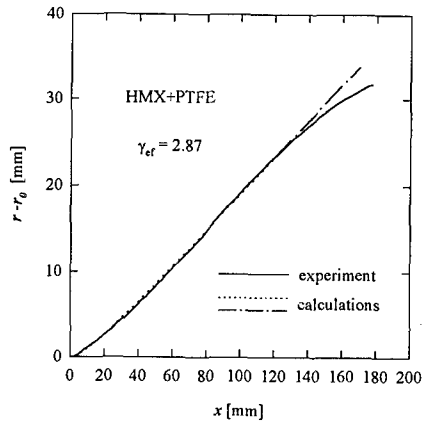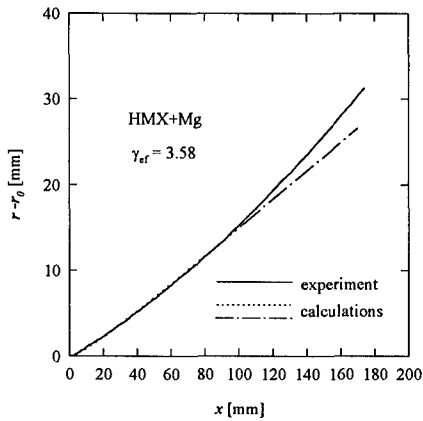

Fig. 7. Experimental and calculated profiles of the external surface of the copper tube driven by the detonation products of the HMX and PTFE mixture.

The method described in Ref. [21] was used to estimate the effective exponent of isentrope for the detonation products of the explosives tested. The tube material was modelled by a barotropic medium described by the equation of state obtained from the shock adiabate of copper. The results of calculations and the values of effective exponent obtained are presented in Figs. 6 ÷ 9. The experimental diagrams of radius position of the external boundary of tube are shown by the solid lines. The dotted and dashed lines denote the diagrams obtained from modelling the process of driving the tube by the

products being characterised by the constant polytropic exponent γ_{ef}. The range of axis co-ordinate used in the appraisal of the value of γ_{ef} is fixed by the dotted line.

Fig. 8. Experimental and calculated profiles of the external surface of a copper tube driven by the detonation products of the HMX and Mg mixture.
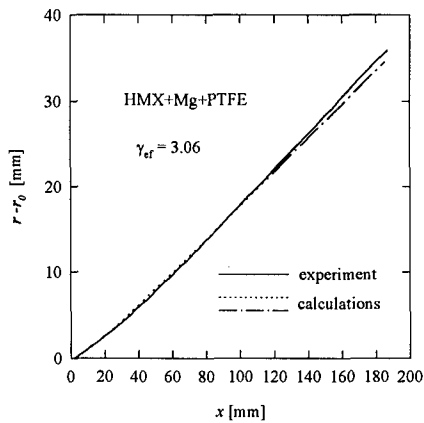
Fig. 9. Experimental and calculated profiles of the external surface of a copper tube driven by the detonation products of the HMX, PTFE, and Mg mixture.

The lowest value of the isentropic exponent of the detonation products was obtained for the mixture of HMX and PTFE. This means that for this mixture the fall of the pressure of explosion gases behind the detonation wave is the smallest one. This fact explains why the profiles of the tubes

driven by the detonation products of pure HMX and the HMX/PTFE mixture lie closely each other despite of great differences in the detonation velocities and the C-J pressures for these charges.

For large values of x the experimental tube profiles for the charges of HMX and HMX/PTFE bend down to the axis of set-up. It has been mentioned earlier that this fact can be connected with acting of the rarefaction waves on the detonation products. These waves are neglected in the model used. Similar shape of the experimental tube profiles obtained for pure HMX and the HMX/PTFE mixture means that neither an additional heat release nor a gaseous product increase take place during the driving process. Bearing in mind the conclusions drawn from the analysis of the results of measurement and calculation the detonation velocity presented in the previous section it can be inferred that the decomposition process of PTFE starts in the reaction zone and it ends just behind this zone. Further expansion of the detonation products containing gases from gasification of PTFE proceeds without a clear increase in their ability to accelerate metal.

The second of additives tested, magnesium, behaves like an inert additive in the first stage of expansion of the detonation products. Taking into account only the initial part of profiles (Figs. 8 and 9) we obtained the high values of the effective isentropic exponent for the detonation products of mixtures of HMX/Mg or HMX/Mg/PTFE. This means the large fall of the pressure and the low metal acceleration ability of the detonation products. However, in the further stage of the driving process the experimental tube profile bends up as regards the theoretical one obtained by assuming the constant value of γ_{ef}. This means that at some distance behind the detonation wave the acceleration metal ability of the detonation products increases due to the additional moles of gases occuring or the energy releasing. In the case of the MHX/Mg mixture only the latter influences the acceleration metal ability of the detonation products because the main reaction products of Mg, magnesium oxide, is solid. In the HMX/Mg/PTFE composition magnesium can react also with the decomposition products of PTFE. The analysis of curves in Figs. 8 and 9, and in Fig. 5 leads to the conclusion that the exothermic reactions with releasing the additional heat begin about $12 \div 14$ μs behind the detonation wave.

5. Measurement of the combustion time of the additives

The total time of combustion of the additives during scattering the detonation products was determined by measuring a period of an emission activity of the explosive cloud in the spectral range of $0.4 \div 1.1$ mm. The silicon photodiode working like a photoelement shorted by the resistance of 250 Ω was used as a radiation detector. The voltage drop across the resistor as a function of time was recorded on an digital oscilloscope. Diagram of the set-up is shown in Fig 10.

The charges used in all tests have the mass of 130 g and the same dimension. The courses of voltage generated by the photodiode are shown in Fig. 11. These courses correspond with the time variations of the power of radiation emitted by the explosion clouds in the spectral range of $0.4 \div 1.1$ μm.
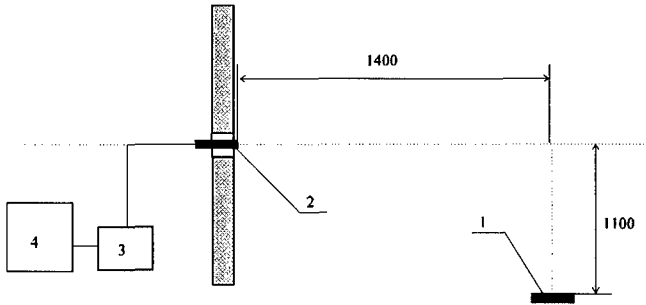
Fig. 10. Schematic diagram of the set-up for measuring a time period of the emission activity of the explosion clouds: 1 - charge of explosive, 2 - photodiode, 3 - oscilloscope, 4 - plotter.
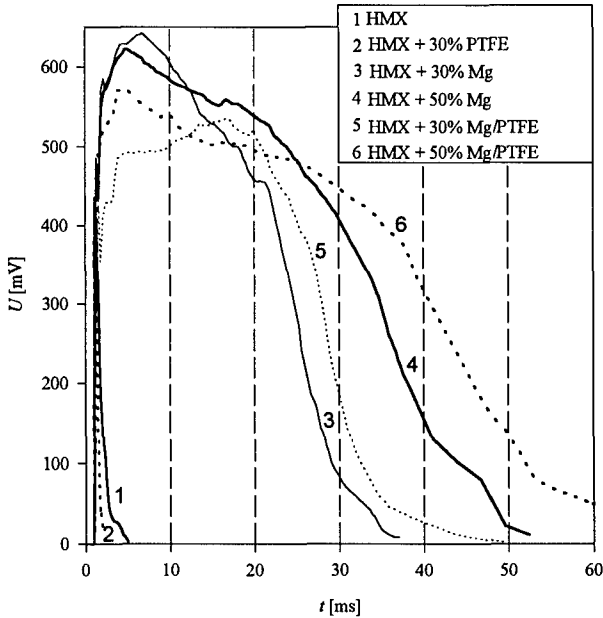

Fig. 11. Radiation power of the explosion clouds versus time.

The duration of the emission activity of the explosion products for pure HMX and the HMX/PTFE mixture are very short of the order of 2-3 ms (curves 1 and 2 in Fig. 11). The explosion clouds of the compositions containing Mg are active in more longer time: 30-40 ms for the mixtures with 30 wt % of additives (curves 3 and 5), and 50-60 ms for those with 50 wt % of additives (curves 4 and 6). The considerable increase in duration of the emission activity for these mixtures can be explained by the slow high-exothermic combustion reactions of the magnesium grains taking place in gaseous oxidiz-

ers. The grains of Mg heated by the detonation wave are dispersed in the surrounding gaseous medium. They burn either in the detonation product or in air as well. The combustion process is running in time of the order of tens milliseconds. The maximum power of radiation emission in the clouds is achieved in a few milliseconds after the detonation process ended. This facts enable us to draw conclusions that a velocity of combustion is limited by the diffusion process of oxidizers.

Summing up the results of measurement of the emission activity we can state than the main part of magnesium burns in the late stages of the explosion process and oxygen from air participates chiefly in reaction with Mg. The investigation methods used in this work do not answer to a question which part of magnesium reacts with the products of PTFE decomposition, which with oxygen from HMX, and which with oxygen from air. The phase composition analysis of the solid and gaseous products of detonation of the mixture in a bomb calorimeter can give an answer to that question.

6. Summary

1. Comparison of measured and computed values of the detonation velocity of the mixtures tested shows that magnesium is chemically inert in the reaction zone, but PTFE partially decomposes in the gasification process.
2. From the comparison of the experimental and calculated profiles of the copper tube it follows that the decomposition of PTFE, which has started in the reaction zone, is running during the first stage of expansion of the detonation products. Magnesium behaves like an inert additive during the time-period of about $12 \div 14$ μs after passage of the detonation wave. After that time, the heat of the exothermic reactions with Mg in the detonation products affects clearly the tube driving process.
3. The duration of the emission activity of the explosion products for pure HMX and the HMX/PTFE mixtures is very short of order of $2 \div 3$ ms. Radiation activity of the explosion clouds of the compositions containing Mg is going on up to 60 ms. This means, that the main part of magnesium burns during the late stages of the expansion process when the grains of Mg react with oxygen from air.
4. On the basis of the experimental and theoretical investigations of the detonation velocity it can be inferred that magnesium do not react with PTFE in the reaction zone of the detonation wave propagating in the HMX-based explosive. The method used in this work do not answer to a question which part of Mg reacts with the products of PTFE decomposition, which with oxygen from HMX, and which with oxygen from air.

Literature

[1]   K. P. Stanyukovitch, *Physics of explosion* (in Russian), Nauka, Moscow, 1975.
[2]   L. W. Dubnov, N. S. Bacharievitchz, A. I. Romanov, *Industrial explosives* (in Russian), Niedra, Moscow, 1988.

[3]   K.K. Shvedov, *Some questions of detonation of explosive mixtures* (in Russian), Tcherno-golovka, 1981.

[4]   A. I. Aniskin, *The influence of aluminium on a profile of the detonation wave in high-dispersed heksogen* (in Russian), Tchernogolovka, 1981.

[5]   V. Ju. Davydov, M. A. Grishkin, I. I. Fiedoboritov, *Experimental and theoretical investigation into oxidation of aluminium in the detonation wave* (in Russian), Fiz. Gor. Vzr., **28**, 5, 1992.

[6]   S. Hoffman, US Patent, 3297503, 01.01.1967..

[7]   M. M. West, US Patent, 4331080, 25.05.1982.

[8]   T. Kuwahara, S. Matsuo, N. Shinozaki, *Combustion and sensitivity characteristics of Mg/TF pyrolants*, EUROPYRO 1995, Tours, France, 1995.

[9]   S. Cudziło, W. Trzciński, *Investigation of the combustion process of metal and polytetrafluoroethylen* (in Polish), **45**, 3, 1996.

[10] Ch. L. Mader, *Numerical modelling of detonations*, University of California Press, 1979.

[11] P. Crawford, *Getting started with TIGER*, Lawrence Livermore National Laboratory, 1986.

[12] D. R. Stull, H. Prophet, *JANAF thermochemical tables*, II edition, National Bureau of Standards, Washington.

[13] R. Trębiński, W. Trzciński, E. Włodarczyk, *A method for determining detonation adiabates of explosives with admixture of inert additions*, J. Tech. Phys., **31**, 1, 1990.

[14] E. L. Lee, H. C. Horning, J. W. Kury, Lawrence Livermore Laboratory Report UCRL-50422, 1988..

[15] R. C. Queen, S. P. Marsh, J. W. Taylor, J. N. Fritz, W. J. Carter, *On equation of state of solids, High-velocity impact phenomena*, Academic Press, New York-London, 1970.

[16] S. P. Marsh, *LASL shock Hugoniot data*, University of California Press, 1980.

[17] M. A. Meyers, L. E. Murr, *Shock waves and high-strain-rate phenomena in metals*, Plenum Press, New York-London, 1980.

[18] H. Hornberg, *Determination of fume state parameters from expansion measurement of metal tube*, Propellants, Explosives, Pyrotechnics, **11**, 23-31, 1986.

[19] P. Gimenez, S. Lecume, J. Groux, *A study of explosive compositions containing ammonium perchlorate*, Propellants, Explosives, Pyrotechnics, **19**, 1-8, 1994.

[20] E. Włodarczyk, *Modification of the JWL equation of state - the W equation of state*, J. Tech. Phys., **34**, 3, 1993.

[21] R. Trębiński, W. Trzciński, *A method for determining an effective exponent of isentrope for the detonation products of condensed explosives* (in Polish), Biul. WAT, **45**, 3, 1996.

SULFURIC ACID INFLUENCE ON POLYNITROCOMPOUNDS
SLOW DECOMPOSITION AND DETONATION REACTIONS

Boris N.Kondrikov, Georgy D.Kozak, Vlada M.Raikova

Mendeleev University of Chemical Technology

9 Miusskaya Sq., Moscow 125047, Russia

Fax: (095)200-4204

e-mail: kondrikov@mhti.msk.su

Abstract

The slow decomposition and detonation reactions of the nitrocompounds/sulfuric acid (SA) solutions are investigated, and it is shown that in many cases SA affects drastically on the decomposition rate and explosion characteristics of the substances studied. Interaction of aromatic polynitrocompounds (DNT, TNT, TNB) with SA and nitrosylsulfuric acid (NSA) is examined by thermokinetic method at 200-400 $^{\circ}$C. The quantitative treatment of the results is implemented, and the overall reaction mechanism is established. The effective kinetic parameters of leading chemical reactions in the mixtures of nitrocompounds, SA and NSA are estimated. The detonation failure diameter d_f and detonation velocity D of SA/[DNT, TNT and TNB] solutions are measured in the wide range of concentrations. It has been shown that d_f depends strongly on SA concentration. The relative influence of NSA on detonation reactions rate is negligible small as compared to the slow decomposition NSA effect.

1.Introduction

Sulfuric acid (SA) of high concentration is widely used as a medium at manufacturing of different nitrocompounds, including some of the LOVA explosives. In this work the slow decomposition and detonation reactions of the nitrocompounds/SA solutions are investigated.

Interaction of aromatic polynitrocompounds (DNT, TNT, TNB) with SA and nitrosylsulfuric acid (NSA) have been examined by thermokinetic method at 200-400 $^{\circ}$C. Detonation failure diameter d_f and detonation velocity D of SA/[DNT, TNT and TNB] solutions have been also measured in the wide range of concentrations. The results of the investigations are used for development of the overall model of the safety level of the nitrocompounds manufacturing process evaluation.

2. Experimental

The experiments were carried out using the commercial grade TNT (freezing point, $T_f=80.2^O$C), and DNT ($T_f=68.9-69.2^O$C). TNB was produced in the laboratory and purified by recristallization from nitric acid ($T_f=122.8^O$C). The commercial-grade sulfuric acid (94% concentration) and oleum containing 60% "free" sulfuric anhydride were used to prepare the solutions containing up to 108.2% H_2SO_4. The H_2SO_4 concentration was determined by titration. The solution of nitosylsulfuric acid in anhydrous sulfuric acid was prepared by absorption of nitrogen oxides which in turn had been obtained by reaction of sulfuric acid with potassium nitrite.

Interaction of aromatic polynitrocompounds with SA and NSA was investigated by the thermokinetic method [1,2]. Sulfuric acid or the solution of NSA in sulfuric acid were poured into cylindrical glass reactor (diameter 37, height 140 mm) with a jacket (diameter 62 mm). The acid was heated by the hot air passing through the jacket. When temperature of the liquid reached the necessary value, usually in the limits of $T_O=180-240^O$C, heating was being regulated by such a way that temperature was being constant during about 15 min. Then liquid nitrocompound, which had been heated to the same temperature previously, was added into reactor and was mixed quickly with acid by the propeller link mixer. Temperature of the mixture at first decreased ($\Delta T \approx 5-7^O$C) and then began to rise. The moment of $T=T_O$ achievement was assumed to be a starting zero-point of a process. The temperatures of reacting mixture, and of hot air both before inlet and after outlet of the jacket were registered by three chromel-copel thermocouples and potentiometer. The heat-transfer constant of the reactor $\alpha=25\pm6$ Wt/m^2K was defined by measuring cooling rate of H_2SO_4.

Mixtures consisted of SA-DNT-TNT after decomposition were analyzed on NSA content. The probe of the reacting mixture was sampled by means of the small fluoropolymer tube connected with vacuum line. It was dissolved in SA and was treated by excess of ammonium persulphate to transform NO^+ to NO_2^+. The mixture obtained was titrated by solution of $FeSO_4$ in SA. The content of NSA was hold up in the limits of 0.25-1.2% during decomposition.

The detonation failure diameter d_f was measured in the glass tubes (wall thickness is 1.5 mm) by the method go-no-go.

The measurements were made mainly under the initial temperature T_O=85-86°C for TNT and DNT solutions, and 110°C for TNB solutions (except the cases where the effect of initial temperature was investigated).

The detonation velocity D was measured in the steel tubes (d= 10 mm, δ=13 mm, l=180-250 mm). The detonation process luminosity was registered by the streak camera SFR-2 through the radial holes (d=1.5-2.0 mm), drilled in the wall of the tube at distance of 15 mm one from another. The holes as well as the bottom of the tube were closed by the glass plates, adhered by the acid persistent glue.

3. Results

Decomposition.

The main result of an experiment was the time-temperature of the reacting mass dependence. Influence of T_O on the time-temperature dependence of decomposition is represented in Fig.1 for mixtures of SA with TNT, at TNT concentration being equal to 22%. The curves have the autocatalytic character. There is a small section of constant temperature (300-320°C) on curves, which is connected probably with SA boiling. The maximum temperature in experiments T_m reaches 350-370°C. Decomposition of the reaction mixtures containing more than 15% TNT is accompanied by intense foaming and by throwing out the content of the reactor. This process proceeds in pulsating regime at the final stage of the sharp temperature rise. The black-brown tar remains in the reactor after decomposition. Increasing of TNT content up to 44% does not change the period of maximum temperature reaching however the quantity of the mass throwing out increases significantly.

Curves T(t) for mixtures SA with DNT are not distinguished essentially from these with TNT. They appear a slower temperature rise in the beginning of the process, and more fast decomposition at the final stage of the reaction. Comparison of the curves for mixtures TNT-SA and DNT-SA is demonstrated in Fig.2 .

Addition of NSA to the solution of TNT in SA accelerates the temperature rise of the reaction mass (curves 1 and 2, Fig.3). Decomposition of the solution at 220°C in presence of $NOHSO_4$ proceeds 2-2.5 times faster.

It has been found previously that solutions of NSA in SA
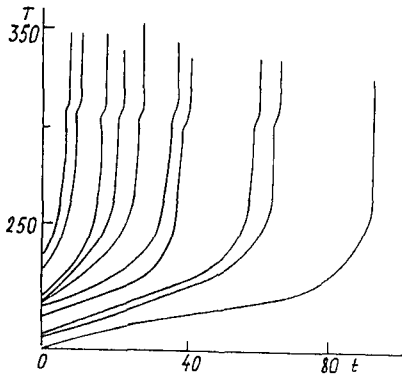
Fig.1. Influence of initial
temperature on T(t) dependencies
for TNT solutions (22%) in SA.
SA initial concentration is 98.6%.
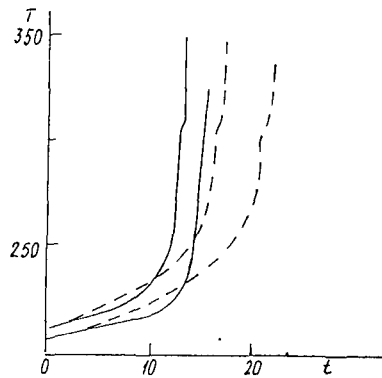
Fig.2. The comparison of T(t)
dependencies for DNT (solid
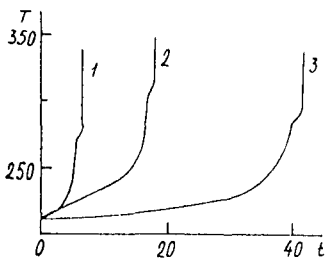lines) and TNT (dashed lines)
solutions in SA.

$(T, {}^{o}C; t, min)$

Fig.3. T(t) dependencies
for TNT (22%) solutions in
SA in presence of NSA (17%) (1)
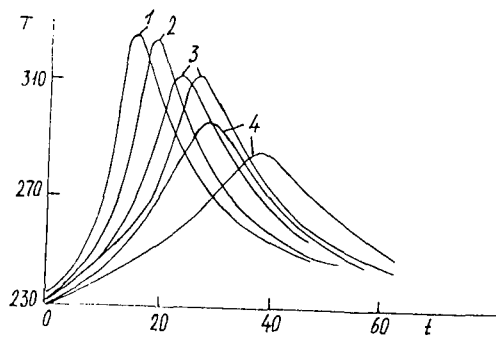and in SA of various concentrations:
2 - 98.6%, 3 - 94.8%.

Fig.4. Influence of TNT content
in the mixture with SA on T(t)
dependencies. Content of TNT,%:
1 - 6.3,   2 - 6.2,
3 - 5.6,   4 - 5.2.

(concentration $NOHSO_4$ up to 30%) are stable at 230-240°C, and do not change the concentration at least during two hours of heating.

Influence of NSA on decomposition of TNB solutions in SA is more pronounced. In absence of NSA there is no exothermic selfheating of TNB (22%) solution in SA during one hour at 220-240°C. In presence of NSA (17%) exothermic process begins at 200°C, the rate of decomposition though is lower than that in the case of TNT and DNT solutions. It was estimated analytically that NSA concentration in the course of constant temperature part of $T(t)$ curve remains almost constant, but during the period of the sharp rise of temperature it decreases quickly.

Addition of water (and corresponding reduction of SA concentration) significantly decreases the rate of TNT with SA interaction (curve 3, Fig.3).

Influence of TNT content (C_n) on character of $T(t)$ curves is represented in Fig.4. The dependence of temperature increment ($\Delta T = T_m - T_o$) on C_n is represented in Fig.5. The heats of decomposition reactions were calculated according to equation:

$$Q_r = M_n/m_n \ (Q_1 - Q_2) = M_n/m_n \ [m \ \overline{C}_p(T_m - T_o) + \alpha \ F \int_{t_o}^{t_m} (T - \overline{T}_o) \ dt$$

Q_1 is the heat expenditure at heating of the mixture to T_m, Q_2 is the heat loss into surroundings, M_n is the molecular mass of nitrocompound, m_n is the mass of mixture, C_p is the average specific heat at constant pressure, T_o is the average temperature of the hot air in the jacket of the reactor, F is the surface of heat exchange, α is the heat transfer constant of the reactor.

The experimental data (T_o, T_m) and results of calculations (Q_1, Q_2, and Q_r) are collected in the Table 1. They show that heat of interaction of TNT with SA is 25% higher than that of mixtures DNT-SA, in presence of NSA Q_r increases by the factor of 1.5.

The composition of gaseous products of the reaction was estimated by the methods [1,2]. The results are represented in the Table 2. They show that the main products of interaction of nitrocompounds with SA and NSA are CO_2, SO_2, and N_2. At small content of TNT or DNT in the mixture the low quantity of CO and N_2O are generated, at high (18%) content of TNT in mixture the quantity of carbon oxide increases and
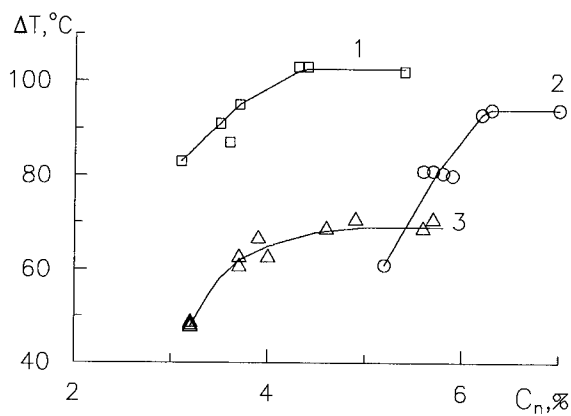
Fig.5. The temperature increment during interaction
versus the nitrocompound content.
1 - TNT+SA+NSA, 2 - TNT+SA, 3 - DNT+SA.

<div align="right">Table 1</div>

The experimental results of the heats of reactions   measurements

Mixture	c_n,%	T_o,C	T_m,C	Q_1, kJ	Q_2,kJ	Q_r,kJ/mol
TNT+SA	5.2	233	294	8.65	7.41	793
	5.7	231	312	12.02	6.73	838
	5.7	230	311	12.17	7.42	863
	5.8	228	309	12.08	6.9	816
	5.9	234	314	11.95	6.9	808
DNT+SA	3.2	235	284	7.25	2.89	652
	3.2	236	284	7.05	3.1	657
	3.2	237	286	7.18	2.76	639
	3.7	228	289	8.62	3.12	668
	3.7	230	293	8.98	2.85	677
	4	232	299	10.05	2.27	626
TNT+SA+ NSA	3.1	222	263	6.25	8.82	1180
	3.1	228	311	12.7	3.7	1270
	3.5	231	322	13.0	4.0	1353
	3.6	232	319	12.8	4.0	1173

of carbon dioxide decreases significantly.

Detonation

TNT: Oleum of concentration (S,% H_2SO_4) 100.6, 101.7, 103.8, and 108.2 was used to obtain TNT solutions. The results of the measurements of failure diameter of the solutions are represented in Fig.6. Curves at different oleum concentrations are similar to each other: as the oleum content c_S in mixture increases, detonation failure diameter reduces to the minimum value and then rises. Minimum critical diameter d_f^m (mm) depends on S(%):

$$\log_{10}(d_f^m) = 1.2 \ 10^7 \ \exp(-0.1619 \cdot S)$$

The minimum value of d_f for TNT diluted by oleum, S=108.2%, is about 2 mm, i.e. 30 times less, than that for neat melted TNT. It is practically equal to the detonation failure diameter of nitroglycerin. The influence of oleum content on detonation velocity of TNT, TNB, and DNT is shown in Fig.7. The velocity of detonation (D) is almost constant up to c_S=50%. Further growth of oleum content results in the considerable decrease of the D value leading to extinguishment of detonation. Influence of nitric acid on detonation of TNT solutions in oleum is of the obvious practical interest. Solubility of nitrocompounds in the sulfuric-nitric acids mixture is far less, than in oleum or sulfuric acid alone. One can admix without loss of solubility to the mixture containing 40/60 TNT/oleum (S=103.8%) no more than 4% of nitric acid. Experiments carried out with such solution at concentrations of nitric acid 2.5 and 4% show that d_f remains constant (11-12 mm). Introducing of extra quantity of nitric acid results in emulsion formation, experiments in this concentration region were not carried out.

DNT: The detonation failure diameter of pure melted DNT up to now is not estimated. In the steel tubes (d=10 mm, d=13 mm) the detonation extinguished even at 190°C. However, the steady-state detonation of the DNT solutions in oleum at S=103.8%, c_S=50 and 60% (T_o=85°C) was observed. The mean detonation velocity of the solutions was equal to 5.5 mm/ms (Fig.7).

TNB: The experiments with TNB solutions were carried out at the oleum concentration S=103.5%. At 110° C one can get the solutions
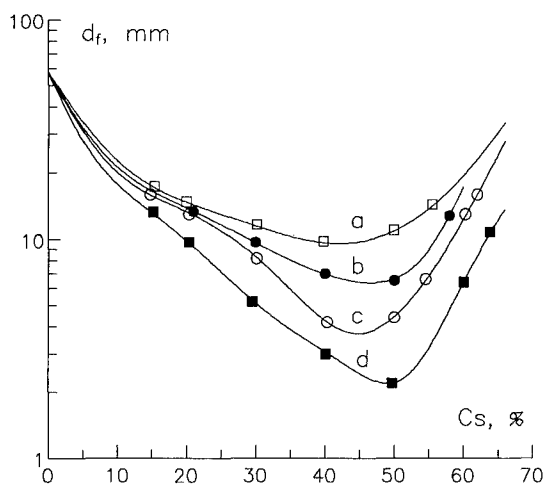
Fig.6. The detonation failure diameter of the mixtures of TNT with oleum versus its content in the solution. Oleum concentration S,%: a - 100.6, b - 101.7, c - 103.8, d - 108.2. The points are the mean experimental values; the solid lines are calculated for TNT mixtures using the kinetic scheme suggested in [3].
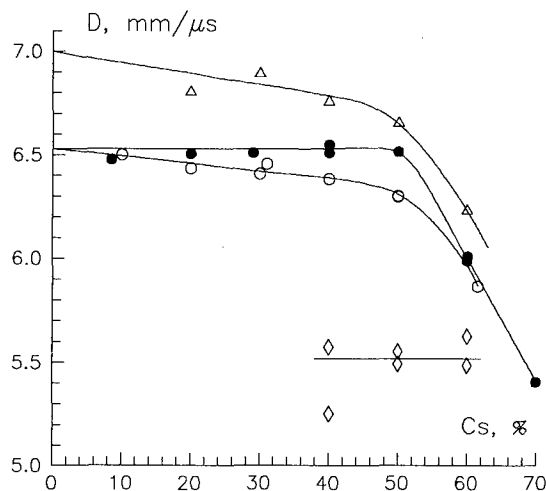

Fig.7. The results of detonation velocity measurements of the mixtures of nitrocompounds and oleum: Δ - TNB/oleum (S=103.5%, T_O=110°C), ● - TNT/oleum (S=103.8%, T_O=85-86°C), O - TNT/oleum (S=101.6%, T_O=85-86°C), ◊ - DNT/oleum (S=103.8%, T_O=85°C).

containing up to 80% of TNB. The curves $d_f(C_s)$ for TNT and TNB solutions are not only similar to each other, but even the values of d_f^m for TNT and TNB are almost exactly the same. However, to reach the same d_f values in the case of TNB the higher temperature is required.

Effect of initial temperature: $d_f(T_o)$ dependencies were determined for 50/50 mixtures of H_2SO_4 with TNT (at S=103.0%), and TNB (S=103.5%). As for number of other explosives, the straight lines

$$\log_{10} d_f = A + B/T_o$$

were obtained (TNB: A=-0.898, B=675, T_o=358-383 K; TNT: A=-2.176, B=1041, T_o=336-370 K).

4. Discussion

The composition of gaseous products represented in the Table.2 allows to obtain the stoichiometric coefficients of overall reaction:

$$TNT \ (DNT) + a_i \ H_2SO_4 \ (NOHSO_4) \rightarrow \qquad (1)$$
$$\rightarrow \ b_i CO_2 + \ c_i SO_2 + d_i N_2 + c_i H_2O + f_i H_2SO_4 + C_c H_h N_n$$
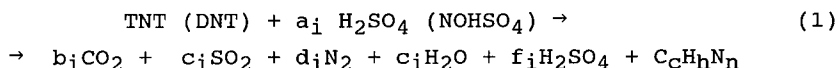
The stoichiometric coefficients of the reactions of the type (1) calculated by means of examination of the Table 2 data are presented in Table 3. In the Table 3 the indexes of the equation (1) are noted as follows: i=1 for reaction TNT+SA, i=2 for reaction DNT+SA, i=3 for reaction TNT+NSA, $C_c H_h N_n$ - condensed organic residue, $f_1=f_3=0$.

The rate of monomolecular decomposition of TNT in the temperature interval investigated is very low (for DNT and TNB it is even much lower) and can be neglected. At the same time ionization of TNT at interaction with SA may take place [4]. The degree of TNT ionization is regulated by the constant of equilibrium K_c

$$[(C_7H_5(NO_2)_3)H^+] \ = \ K_c \ [TNT] \ [SA] \qquad (2)$$
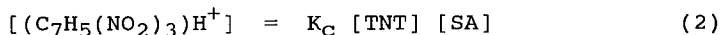
The results of analyses of reaction mixtures during the experiment have shown that NSA appeared at the initial stage of the reaction. NSA might be formed and disappeared according to reactions:

Table 2.

The relative concentrations of gases at interaction
of nitrocompounds with SA

Mixture	c_n,%	Gaseous products, %				
		CO_2	SO_2	N_2	CO	N_2O
TNT+SA	1.1 - 3.2 18.3 - 18.5	61-58 49-52	34-37 28-30	4.6-6.1 10	0.6 12	0.1 0.1
DNT+SA	1.6 - 3.3	52-43	45-52	2.4-3.8	0.5	0.05
DNT+SA+NSA	1.4 - 3.6	56-49	16-11	27-35	3.3	0.2

Table 3

The stoichiometric coefficients of the reaction (1)

Mixture	The stoichiometric coefficients					
	i	a	b	c	d	e
TNT+SA	1	2.5	4.2	2.5	0.5	2.6
DNT+SA	2	4	3.5	4	0.5	5
TNT+SA+NSA	3	5.5	7	1.7	4.2	1.4

Table 4

The Arrhenius constants K_{ef}, B_{ef}, and E_{ef} of the reactions
SA (98.6%) and NSA with nitrocompounds

Mixture	$K_{ef} \cdot 10^6$ at $200^\circ C$, $l \cdot mol^{-1} \cdot s^{-1}$	E_{ef}, $kJ \cdot mol^{-1}$	B_{ef} $l \cdot mol^{-1} \cdot s^{-1}$
DNT+SA	2.23	118 ± 6.0	$2.4 \cdot 10^7$
TNT+SA	1.43	110 ± 7.4	$2.0 \cdot 10^6$
TNT+SA[x)]	0.42	162 ± 8.3	$3.3 \cdot 10^{11}$
DNT+SA+NSA	30.6	136 ± 4.5	$3.2 \cdot 10^{10}$
TNT+SA+NSA	12.3	125.5±7.4	$8.9 \cdot 10^8$
TNB+SA+NSA	1.56	140 ±10	$4.5 \cdot 10^9$

[x)] concentration of SA is 94.8%.

$$C_7H_5(NO_2)_3 + H_2SO_4 \xrightarrow{K_1} a_1 \ NOHSO_4 + \ldots \qquad (3)$$

$$[C_7H_5(NO_2)_3H^+][HSO^-_4] \xrightarrow{K_2} a_2 \ NOHSO_4 + \ldots \qquad (4)$$

$$C_7H_5(NO_2)_3 + NOHSO_4 \xrightarrow{K_3} products \qquad (5)$$
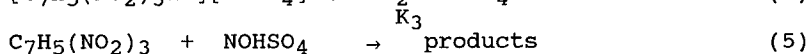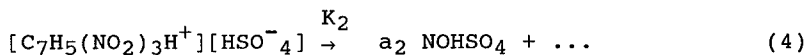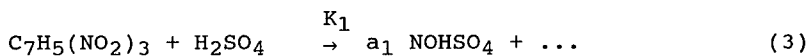
where K_1, K_2, and K_3 are the rate constants of the corresponding reactions, a_1, a_2 are the stoichiometric coefficients. On the initial step of $T(t)$ curve the concentration of NSA remains approximately constant, i.e.:

$$d[NSA]/dt = a_1 \ K_1[TNT][SA] + a_2K_cK_2 \ [TNT][SA] - K_3[TNT][NSA] = 0 \quad (6)$$

where $[TNT], [SA]$, and $[NSA]$ are the concentrations of the corresponding reagents (mol/l). Bearing in mind the equations (2),(3), and (5) the rate of TNT decomposition can be estimated:

$$d[TNT]/dt = [(1 + a_1)K_1 + a_2K_2K_c] \cdot [TNT] \cdot [SA] = K_{ef}[TNT] \cdot [SA] \qquad (7)$$

We have the equation of the second order, where the effective rate constant K_{ef} is the function of the individual rate constants, of the stoichiometric coefficients of the reactions (3),(4), and of the equilibrium constant K_c.

The effective value of the energy of activation and preexponential factor in Arrhenius low was found by treatment of curves $T(t)$, obtained at different initial temperatures in the framework of the usual equation for induction period (t_a) of adiabatic heat explosion for the reactions of the second order:

$$t_a = \frac{RT_oC_p}{E_{ef}Q_r} \frac{[TNT]}{W_o} = \frac{RT_oC_p}{E_{ef}Q_r} \frac{exp(E_{ef}/RT_o)}{[SA] \ B_{ef}} \qquad (8)$$

W_{ef} is the rate of reaction, Q_r is the heat of reaction, C_p is the specific heat at constant pressure.

For the mixtures containing NSA the reaction between nitrocompounds and NSA was supposed to be essential, and calculations concentration of NSA was inserted into solution (8) instead of [SA].

To calculate the effective parameters of equation (8) the results

of experiments were presented in co-ordinates $1/T_O$ - $\ln(t_m/T_O^2)$. The value of t_m was supposed to be equal to t_a.

The rate constants of the reactions at $200^O C$ and parameters of Arrhenius equation for all mixtures are collected in Table 4. K_{ef} for mixtures DNT and TNT with SA are appreciably lower than these for mixtures containing NSA. The effective rate constants at $200^O C$ for mixtures TNB-SA-NSA is close to K_{ef} for mixtures TNT-SA.

The quantitative treatment of results on detonation of mixtures on base of TNT, had been presented in [3]. Dremin theory of detonation failure diameter was used to treat the results [5,6]. The values of t_3 and T_3 of the theory calculated for mixture (50/50) TNT/H_2SO_4 (S=103.0%) at different initial temperatures are placed along the line:

$$\log_{10}(t_3/T_3^2) = - a + b/T_3$$

The activation energy of the reaction is changed correspondingly in the range of 100-120 kJ/mol. The activation energy of TNT detonation reaction calculated in [7], is equal to 109 kJ/mol, i.e. it corresponds to the middle of the interval obtained in [3].

The sequence of kinetic equations of the main reactions occured at detonation of TNT/ H_2SO_4/SO_3 mixtures is decomposition of TNT and sulfuric acid complex:

$$W_1 = k_1[TNT], \qquad (9)$$
$$W_2 = k_2[TNT \cdot nH2SO4] , \qquad (10)$$
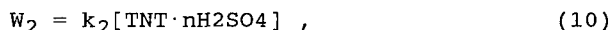
The possibility of the formation of such complex follows from the data on solubility of TNT in sulfuric acid [8]. The relative number of H_2SO_4 molecules in the complex n has to be determined from the best correlation of the calculation results with the experimental data. The considerable influence of "free" SO_3 shows, that a reaction with sulfuric anhydride also exists. One can suppose, that this reaction proceeds between the complex (10) and SO_3

$$W_3 = k_3[TNT \cdot nH_2SO_4] \cdot [SO_3] \qquad (11)$$
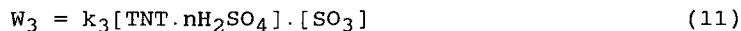
One can suggest also, that the intermediate stage of transition of the reagents, entering into reaction (9), to its products is the

formation of a complex with pyrosulfuric acid ($H_2S_2O_7$):

$$[TNT \cdot nH_2SO_4] + SO_3 \xrightarrow{k_3} \{[TNT \cdot (n-1)H_2SO_4] \cdot H_2S_2O_7\} \xrightarrow{k_4} \text{products,}$$
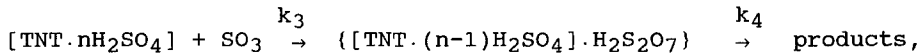
where $k_4 \gg k_3[SO_3]$.

Taking into account the reactions (9-11), the value of k_0 in the equation for the quasi first order reaction rate can be represented in the form of

$$k_0 = \frac{k_{01}[TNT] + k_{02}[TNT \cdot nH_2SO_4] + k_{03}[TNT \cdot nH_2SO_4] \cdot [SO_3]}{[TNT]_0}$$

The values of the preexponential factors k_{01}, k_{02}, and k_{03} for the reactions (7), (8), and (9), as well as the coefficient n have to be defined from the experimental data. The calculations were carried out at $E_a = 109$ kJ/mol. Using the obtained ignition delay t_3, the value of k_0 was calculated as

$$k_0 = \frac{C_v \, \rho \, RT_3^2}{Q_v \, M_{TNT} \, [TNT]_0 \, E_a t_3 \, \exp(E_a/RT_3)}$$

where C_v is the specific heat of the mixture, Q_v is the heat of TNT decomposition. The pre-exponential factor k_{01} corresponds to the decomposition of TNT remained after interaction with sulfuric acid:

$$[TNT] = [TNT]_0 - [TNT \, nH_2SO_4]$$

The values of k_{01}, k_{02} and k_{03} obtained by optimization, are equal to $1.42 \cdot 10^{10}$ s^{-1}, $2.2 \cdot 10^{11}$ s^{-1}, and $1.2 \cdot 10^{11}$ $1\text{-mol}^{-1} \cdot s^{-1}$, respectively, n=2.

The results obtained on detonation failure diameter prove a formation in TNT/oleum mixtures at high temperature and pressure (about 1000 K and 10 GPa) of the complexes of the nitrocompounds with sulfuric acid having the composition of $[TNT \cdot 2H_2SO_4]$. The TNT complex decomposes 15 times faster than the pure TNT. This complex reacts with SO_3 in oleum. The reaction rate at the maximum concentration of SO_3 ($C_S = 64\%$, $S = 108.2\%$) is 4 times higher, than the decomposition rate of the complex, and, hence, 60 times higher, than the decomposition rate of TNT itself.

REFERENCES

1. Vegera Ya.S., Kondrikov B.N., Raikova V.M. Sov. J.Prykl. Khim. (Russ.). 1992, v.65, N9, pp.2097-2101.

2. Raikova V.M., Vegera Ya.S., Kondrikov B.N. Ibid. 1993, v.66, N2, pp.376-381.

3. Gamezo V.N., Khoroshev S.M.,Kondrikov B.N.,Kozak G.D. J. de Physique IV, Coll.C4, supplement au J.de Physique III, v.5, mai 1995 pp.395-405.

4. Brand J.C.D.et al. J.Chem.Soc. 1952, pp.1374-1383.

5. Dremin A.N. DAN SSSR, v.147, 1962, pp. 870-873.

6. Dremin A.N., Trofimov V.S. PMTF, 1964, No 1, pp.126-131.

7. Enig J.W., Petrone F.J. Proc. of The 5th Symposium (Int.) on Detonation, Pasadena, Ca, Aug. 18-21, 1970, Office of Naval Research, Arlington, Va. ACR-184, pp. 99-104.

8. Khoroshev S.M., Kondrikov B.N., Kozak G.D., et al. Explosive materials and pyrotechnics. Problems of explosion safety of chemical workshops. (Russ. Ed. by B.N.Kondrikov), CNIINTIKPK, Moscow, 1992, N 3(218), pp.14-20.

A NEW APPROACH TO DETERMINATION OF THE DANGER OF DEFLAGRATION–TO–EXPLOSION TRANSITION IN EXPLOSIVE MATERIALS.

A.Sulimov, B.Ermolaev, V.Foteenkov, B.Khasainov, S.Malinin.
N.Semenov Institute of Chemical Physics,
Russian Academy of Sciences, Moscow.

Deflagration-to-explosion transition (DET) is an actual problem of safety at manufacture and handling of explosive materials (EM). A new approach consists in detailed examination of behavior of an initial burning kernel generated in the depth of EM. Unlike conventional tests on the deflagration-to-detonation transition conducted in closed strong tubes, in the suggested method the pressure build up at the burning kernel can be released by scattering of the EM surrounding it.

A vertical column of the tested EM is placed into a thin-walled cylindrical steel vessel with open upper end and ignited by a hot wire located (together with a pressure gauge) centrally at the bottom of the EM column.

Experiments revealed the existence of a critical height (H_{cr}): below it burning resulted in ejection of the EM column from the vessel and its quiet burn-out without explosion, while above it explosion took place. The critical height (H_{cr}) and the critical pressure (P_{cr}- maximal pressure in kernel at column height equal to the H_{cr}) could be used as reliable measures of propensity of EM large masses to DET under emergency conditions.

The values of H_{cr} and P_{cr} for granulated HMX, RDX, single-base and double-base propellants were studied. The effect of vessel diameter (up to 100 sm) on critical conditions were examined.

The typical dependence of H_{cr} on the vessel diameter has two regions: at small diameters (up to 30-40 sm) the H_{cr} rises sharply; at the large diameters (above 40 sm) the dependence is levels off. Besides, the effects of grain size, presence of inhibitor, bagging were studied.

An onedimentional mathematical model of the process is developed. It considers the transition from layer-by-layer burning to convective burning and the effects of discharging of the burning kernel due to scattering of EM.

The calculation and experimental results show good agreement. The H_{cr} is used to estimate a mass of EM explosion-safe in handling, and the P_{cr} is recommended use for designing explosion-preventing technological equipment and transport containers.

THERMAL BEHAVIOR AND REACTION MECHANISM OF SOME ENERGETIC MATERIALS WITH NYLON 6/12

Zhang Xiaoyi, Chen xuelin, Wang Xiaochuan and Zhou Jianhua

Institute of Chemical Materials,CAEP

P.O.BOX 513-105, Chengdu 610003,

P.R.CHINA

ABSTRACT: The thermal behavior and reaction mechanism of pentaerythrityl tetranitrate(PETN), trinitrotriazacyclohexane (RDX) and glycidyl azide polymer (GAP) with Nylon 6/12 were studied, respectively, by means of combined thermal- and IR-TGA in-line analysis at the temperature between 100℃—350℃. The experimental results indicated that the mixture containing different energetic compound with different reactive group shows different behavior at high temperature, which implies different chemical reaction mechanism caused by the different electronegativity of the reative group in the above said energetic compounds. The sequence of interreactivity of the three compounds with Nylon 6/12 is PETN>RDX>GAP. Among these mixtures GAP-Nylon seemed hardly to interreact.

The phenomena above are related with the electro-donation of the substituents in the energetic material molecules . It is known that nylon 6/12 decomposition products is reductive in some cases, so when it is mixed with GAP containing electro-donative substituents, no reaction occurs; While mixed with PETN and RDX containing electro-attracting substituents and the temperaure is high enough, the chemical reactions of the system will become easier . On the other hand, the results of IR-TGA in-line indentification also confirmed the conclusion about chemical reaction mechanism.

GREAT INFLUENCE OF ADDING WAY OF CARBON BLACK ON THE CATALYTIC COMBUSTION OF NITROAMINE–CMDB PROPELLANTS

Lei Liangfang, Ma Xieqi, Zhang Guodong,

Sun Tiegang, Shan Wengang

Xi'an Modern Chemistry Research Institute

P.O. Box.18

Xi'an, Post Code 710061, People's Republic of China

ABSTRACT

The nitroamine composite modified double base propellants are prepared by conventional slurry casting technology. The carbon black (C.B) is added in the propellant with three ways: the first way is that C.B is directly mixed in the solid composition of casting; the second way is that C.B and Pb–Cu catalyst are well distributed with nitrocellulose microspheres to form a composition of solid casting materials; the third way is that Pb–Cu catalyst is distributed with C.B in a superfine microcrystal form to make a kind of well–distributed substance, then the substance is added into the propellant as we do in the second way. The second way is much better than the first way, but the third way is the best way of all. The third way doubly increases the burning rate, tremendously decreases the pressure index, and results in plateau combustion. The datum of the burning rate and pressure index for two groups of propellants (one containing 30%wt. HMX, another containing 40%wt. RDX) are pro-

vided. The explanation of this wonderful phenomenon is discussed, and the further research direction is also put forward.
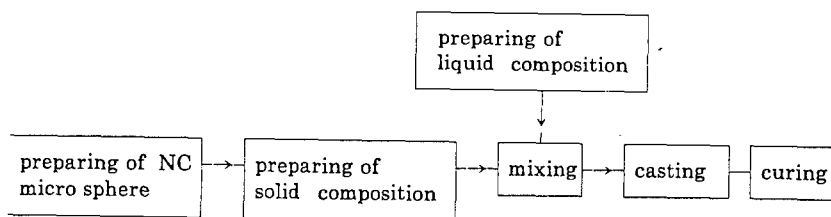
INTRODUCTION

The development history of solid rocket propellant has passed through double base propellant, composite propellant, composite double base (CMDB) propellant, cross—linking modified double base propellant and NEPE propellant. The GAP is a new kind of propellant with high energy, low sensitivity and low signature. It must be stressed that the combustion performance is always a key problem for every kind of propellant. It has been proved that organic and inorganic metal salts, expecially a composite catalyst in which lead and copper salts act as main catalyst and carbon black (C.B) acts as auxiliary catalyst, is able to increase the burning rate of DB and CMDB propellants up to 30—40 mm ∕ s and realize favorable or mesa combustion.

To increase the power of weapons and the range of fire, as well as to prevent the weapons from sudden attack and exposure, Propellants with high energy and low signature shall be a research focal point in the future twenty years. The U.S.A. and other developed countries put a lot of money into the research on high energy and desity materials (HEDM). Among a great deal of HEDM, RDX and HMX are the only mass production and high explosives, they

are inexpensive and have been extensively applied in DB and CMDB propellants. The combustion products of RDX and HMX do not include Cl and HCl, and the exhaust of rocket is clean, smokeless and non—erosive. Now RDX and HMX are extensively used to re-place Al or AP partly or wholely. The content of RDX and HMX raises from 10% to 50–80%. It is generally recognized that the high-er the content of RDX and HMX are, the lower the burning rate and the pressure index achieve, which brings about the trouble of the reguration of the burning rate [1,2,3,] .

EXPERIMENT

The main components of experimental propellants are com-posed of nitrocellulose (NC), RDX (or HMX), casting solvent, a composite catalyst made up of lead and copper salts and C.B. The test propellants are prepared by conventional slurry casting techriol-ogy shown as following diagram:

```
                           ┌─────────────────┐
                           │ preparing of    │
                           │ liquid composition │
                           └─────────────────┘
                                    │
                                    ▼
┌─────────────────┐   ┌─────────────────┐   ┌────────┐   ┌─────────┐   ┌─────────┐
│ preparing of NC │──▶│ preparing of    │──▶│ mixing │──▶│ casting │   │ curing  │
│ micro sphere    │   │ solid composition │  └────────┘   └─────────┘   └─────────┘
└─────────────────┘   └─────────────────┘
```

The auxiliary catalyst C.B is added into the propellants by the following three ways:

a) C.B is directly added into the solid casting composition according to the content of C.B in the propellant.

b) Process the measured C.B、 Pb—Cu salts and NC as a homogeneous dispersion before the preparation of casting slurry, then prepare a solid composition for casting from above dispersion and other solid components.

c) Prepare a superfine microcrystal of Pb—Cu salt firstly, prepare a homogeneous dispersion from above superfine microcrystal and C.B, then prepare a new homogeneous dispersion system from above dispersion and NC micro sphere, finally prepare a solid composition for casting from above new dispersion and other solid components.

The above solid composition and liquid composition are mixed thoroughly, then casted and cured. Cut the prepared propellants into cure strands with $100 \times 5 \times 5$ mm size. Measure the burning rate of the propellant strand samples in a Crawford bomb at different pressure, then calculate the pressure index. The experimental results are shown in table 1—2. It is obvious that the burning rate and pressure index for the three propellants have great difference which means the catalyzation of the three adding ways of C.B has remarkable difference.

RESULTS AND DISCUSSION

1.) Pb ∕ Cu ∕ C.B composite catalyst is still effective in RDX (or HMX) —CMDB propellant as in other DB propellant.

In order to raise the operating stability and reliability of rocket motor at various pressure and environmental temperature, it is agreed that lower pressure index and controllable burning rate for propellants are the favorable performances. Nevertheless it has been well known that it is very difficult to increase the burning rate and decrease the pressure index.

As well known, Pb / Cu / C.B composite catalysts can bring about plateau or mesa combustion in DB propellants, but this phenomenon is not very obvious in our experiments as shown in Table 1. The most important difference between DB and CMDB propellants is the addition of RDX (or HMX) in CMDB propellants. It has demonstrated that only at very low pressure the catalyzed HMX monopropellant shows plateau and mesa combustion [4]. Pb—Cu catalyst has no catalytic effect on the combustion of HMX (or RDX) at normal operating pressure of rocket motor. The combustion of HMX (or RDX) takes place in the luminous flame zone which is far from the combustion surface. The heat of HMX (or RDX) combustion has no influence on the burning rate of the propellant. RDX and HMX only act as an inert additive. Furthermore, crystal form transition (from β form to δ form) and melt of RDX (or HMX) before thermal decomposition absorb heat from combustion surface, which uses up the heat conducted from fizz zone to combustion surface. It is logical that RDX or HMX can be considered as a coolant for the combustion of propellant.

However, many experiments have proved that the structure of combustion wave for RDX (or HMX)—CMDB propellant is

basically the same as that for DB propellant, which means adding RDX (or HMX) into CMDB propellant does not break the structure of combustion wave for DB propellant. The combustion wave of DB propellant includes subsurface—surface zone, fizz zone, dark zone and luminous flame zone. The addition of Pb / Cu / C.B composite catalyst can accelerate the heat—release reaction in fizz zone and increase the heat conducted from fizz zone to combustion surface. The addition of C.B also increases the heat conducted from luminous flame zone to fizz zone and shortens the thickness of dark zone, thus the cooperation of Pb / Cu / C.B still has catalytic action on the combustion of RDX (or HMX)—CMBD propellants, but the catalysis is not so desirable as that in DB propellants. The datum of table 1 accord with above discussion.

Table 1   The catalytic effect of Pb / Cu / C.B composite catalyst

HMX %	CT %	burning rate at different pressure (mm / s)					Pressure index
		4MPa	7MPa	9MPa	11MPa	13MPa	
30	−	6.55	10.96	13.75	16.52	19.18	0.91
30	CT_1 3	14.53	18.40	20.70	22.55	24.35	0.44
30	CT_2 3	13.58	16.81	18.45	19.86	20.96	0.37

Note: CT_1 or CT_2 is a Pb / Cu / C.B composite catalyst

2.)   The mutual dispersion of C.B and Pb / Cu affects the combustion catalysis

It is shown from our experiments that Pb / Cu / C.B composite

catalyst is still effective in RDX (or HMX)−CMDB propellants, but the catalytic action is weaker than that in DB propellants. How to increase the catalysis of Pb／Cu／C.B composite catalyst in RDX (or HMX)−CMDB propellants is a very intresting problem. Now let us see the mutual dispersion of catalyts.

In adding way a), C.B is directly added into the solid casting composition, C.B and Pb／Cu catalysts are only mechanically mixed, so that the catalysis is not quite good. In adding way b), the mutual dispersion of C.B and Pb／Cu catalysts are much better than that in adding way a), at the same time, the composite catalyst is dispersed in the propellant homogeneously, as a result, the catalysis is enhanced a lot. In adding way c), the superfine microcrystals of Pb／Cu catalysts are dispersed in C.B, they are almost a quasimolecular dispersion and the specific surface is much bigger than that in adding way a) and b). Table 2 shows that the burning rate for adding way c) at 5 MPa pressure is doubled as that for adding way a), and the pressure index decreases from 0.596 to 0.140. Plateau combustion is almost gained in adding way c). The pressure index for adding way c) is only half of that for b). So the adding way of C.B plays an important part in the reguration of the combustion performance.

Table2   Influence of the C.B addition method on the buring rate and pressure index

RDX %	C.B adding way	burning rate (mm／s)			Pressure index
		5MPa	7MPa	10MPa	
40	2 a)	8.6	10.59	13.00	0.596
40	2 b)	12.59	14.17	15.03	0.256
40	2 c)	16.81	17.28	18.55	0.14

CONCLUSIONS

From above experiments and discussions, following conclusions can be drawn:

1) C.B—Pb—Cu composite catalyst is a quite effective catalyst for RDX (or HMX) —CMDB propellants as for DB propellants. Therefore these composite catalysts can increase the burning rate and decrease the pressure index, and result in supper—plateau combustion for RDX (or HMX)—CMDB propellants.

2) Not only the kinds of catalysts, but also the preparation method of catalysts are the important factors for the combustion performance of catalyzed solid propellants.

3) The adding way of C.B or composite catalyst is also as important as the composition of composite catalyst. Adding way c) leads to the supper—fine microcrystal which uniformly disperses in C.B and in solid propellants.

4) Every method which can prepare the fine catalyst crystal and result in homogeneous dispersion of C.B and Pb—Cu catalysts in the propellants is worth researching consistently.

5) Molecular dispersion or quasi—molecular dispersion for C.B— Pb— Cu catalyst should be the most favorable composite catalyst for RDX (or HMX)—CMDB propellants.

REFERENCES

1. Propellants, Explosives, Pyrotechnics 11, 1—5 (1986).

2. Propellants, Explosives, Pyrotechnics 10, 192—196 (1985).

3. Propellants, Explosives, Pyrotechnics 14, 6—11 (1989).

4. Ma Xieqi etal "the Flame Structure and Combustion Mechanism of Nitroamine Monopropellant" 18th International ICT Conference, 68, 11PP, 1987.

LOW-TOXIC BURNING RATE CATALYSTS
FOR DOUBLE BASE PROPELLANTS

Anatoly P. Denisjuk, Yury G. Shepelev, Babken M. Balojan, Larisa A. Demidova
D. Mendeleev University of Chemical Technology of Russia, 9, Miusskaya sq.,
Moscow, A-47, 125047
Dzerzhinsky Municipal Research Centre for Ecology Safety, "Centre-Ecology",
Dzerzhinsky, A/B-253, 140056

Various derivatives of lead are known to obtain the highest catalyzing influence on burning of medium and high-energy double base propellants [1...5][*]. Dependingly on their content, the derivatives increase the burning rate of the propellant and decrease the burning rate dependence on pressure and initial temperature of the charge in specific temperature intervals.

The influence of lead derivatives on the burning rate largely increases if being added into a composition combined with copper derivatives [6...8] or soot [5,9,10]. Until now, it is not clear if such a high effectivity of influence is restricted solely to the lead derivatives or other metals derivatives can also demonstrate similar catalyst properties during double base propellant burning. The investigation of this question is of a great scientific importance for researching of mechanism of catalysis of burning and is of a great practical importance because of possible wide use of double base propellants for peaceful purposes, as lead and it's derivatives are very ecologycally dangerous and so their use is highly undesirable.

The purpose of the present work is finding of effective burning rate catalysts among substances ecologycally more safety than lead ones. In accordance with this purpose, it was interesting to use bismuth derivatives, being on the one hand good catalysts of chemical reactions with the participation of nitrogen oxides [11,12] and because of that having some catalyst influence on propellant burning and, on the other hand they are ecologycally more safety than lead derivatives. For example, for bismuth derivatives the value of maximum permited concentration (MPC) in the working area air is 0.5 mg/cub.m [13], that is 50 times higher than that for lead derivatives (0.01 mg/cub.m) [14]. However, it must be notified that the influence of Bi-derivatives was not investigated systematically and it is possible that earlier found weak influence of bismuth derivatives was because of their unsufficient dispersivity and improper for burning rate catalysis propellant formulation.

Therefore, in the present work the investigations were carried out with propellants of various formulations (table 1) and high-dispersed bismuth derivatives.

The propelant samples were prepared according to the general laboratory methodology. Catalysts were introduced before rolling into dried at room temperature propellant mass. The roling temperature was 90°C, the clearance between rolles was ~ 0.5 mm. The received rolled sheet was extruded into 7 mm diameter graines that were then used for burning rate research. The burning of the samples coated with the transparent PVH tube was investigated in a constant pressure device (bomb) in nitrogen atmosphere with photo-registration.

Catalysts effectivity was estimated by value $Z = U_k/U_o$, where U_k - was the burning rate of catalyzed samples; U_o - the was burning rate of noncatalyzed samples. Burning rate dependence on pressure was expressed by formula $U = Bp^n$.

---

[*] For the first time it was shown in Prof. K.K.Andreev's works in Moscow Mendeleev Institute of Chemical Technology in early 1940-th.

To estimate catalyst properties of high-disperse bismuth derivatives, researches were previously made with propellant N the burning rate catalysis of which had been well investigated. Bi_2O_5 with particle size less than 1 μm was used as a catalyst.

Table 1

Formulations and Some Characteristics of Propellants

Formu-lation	Components content, %							T, K	U, mm/s under 4 MPa	ν
	NC	NG	DNT	DBP	RDX	DPA	Techno-logical additives			
N	57	28	11	-	-	-	4	2276	5.6	0.70
I	56	38	3.8	-	-	1.2	1	2759	7.2	0.77
II	53	40.7	4.1	-	-	1.2	1	2803	7.5	0.78
III	56	35.8	6.0	-	-	1.2	1	2674	6.8	0.77
IV	55	30.1	5.0	2.1	-	0.5	1.5	2457	5.6	0.72
V	37	33.0	-	-	28	-	2	3013	6.3	0.63

It is seen from table 2, that 1.5% of Bi_2O_5 has the same infuence on propellant N burning as high-disperse lead dioxide does. These additives are characterized by decreasing of Z-value with pressure increasing that results in a substantial (about 2.5...3 times) decrease of v-value (table 2).

Table 2

Bismuth and Lead Oxides Influence on Propellant N Burning

Additive	Z-value under pressure, MPa			v-value in 2...10 MPa pressure interval
	2	4	8	
Without additives	1.0	1.0	1.0	0.7
1.5% of PbO_2	2.2	1.4	1.0	0.2
1.5% of Bi_2O_5	2.2	1.46	1.0	0.3

Then, the investigations were done with more energetic propellants (table 1) containing various additional plastisizers in different quantities and 1.2% of promoting catalyst action diphenylamine (DPA). Bi_2O_4 (Bi_2O_3 + Bi_2O_5 mixture with particle size~ 5 μm) was used as a catalyst.

Table 3 shows the influence of various amount of Bi_2O_4 on propellant I burning rate. It is obvious, that under pressure 4 MPa the propellant burning rate increases from 7.2 to 10...12.4 mm/s as the content of Bi_2O_4 increases from 0 to 3 and 5%,

Table 3

Various Bi_2O_4 Content Influence on Propellant I Burning

Content of Bi_2O_4, %	U, mm/s under 4 MPa	Z	v-value (in interval of P, MPa)
0	7.2	1.00	0.77(2 - 10)
3	10.0	1.39	0.74(2 - 4) 0.50(4 - 10)
4	11.2	1.56	0.74(2 - 4) 0.40(4 - 10)
5	12.4	1.72	0.80(2 - 4) 0.37(4 - 10)
6	11.7	1.63	0.74(2 - 4) 0.40(4 - 10)

correspondingly. Futher increasing of catalyst content up to 6% brings up decreasing of its influence. Z-value decreases as pressure increases (fig. 1), that results in decrease of v-value from 0.77 to 0.5...0.4 under pressure above 4 MPa. Bi_2O_4 - catalyst has a similar but less strong influence on propellant II and propellant III burning as it is with propellant I (fig. 1).
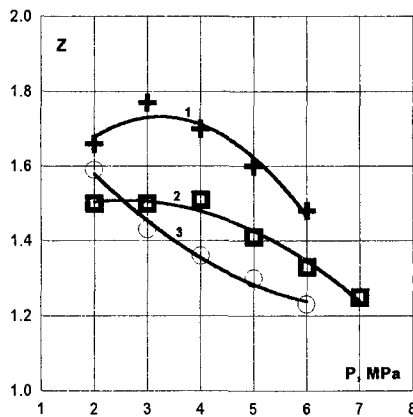
Fig.1. 5% Bi_2O_4 effectivity dependence on pressure for various propellant burning: 1-propellant I;2-propellant III;3-propellantII.

Thus, the experiments have shown that Bi_2O_4 is quite an effective burning rate catalyst for high-energy propellants with additional plastisizers and its influence is similar with that of lead-containing additives. At this basis, it could be understood that the effectivity of bismuth oxides influence as of lead-containing catalysts will increase if soot and copper-containing additives present in the composition.

It is obvious from fig. 2, that soot presence even in a small amount (0.2%) increases effectivity of Bi_2O_4. For example, under 2 MPa when 1% of soot is added Z-value is increased from 1.35 approximately to 2 for propellant I, while the function U (p) for all the catalyzed samples changes slightly, independingly soot presence.
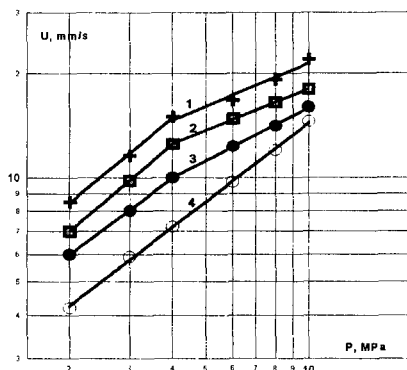
Fig.2. Burning rate dependence on pressure for the propellant I containing additives:1 - 3% Bi_2O_4 +1%Soot ; 2 - 3% Bi_2O_4 + 0.2% Soot; 3 - 3% Bi_2O_4; 4 - without additives.

Organic salts of bismuth in combination with soot have the similar influence (e.g. 5% of $Bi_2(C_2O_4)_3$ + 1% of soot).

In the following series of tests, the investigations were done with RDX-containing high-energetic propellant V without additional plasticizers (table1). As it was in case of lead-containing catalysts, Bi_2O_5 and $Bi(OH)_3$ do not practically effect the burning process of this propellant (fig. 3, 4). But in soot presence, the mentioned additives have a high influence on the burning rate of this propellant, including higher pressure cases; for example, for the sample with 1.5% of $Bi(OH)_3$ + 0.7% of soot Z-value under pressures 2 and 12 MPa is 2.7 and 2.1, correspondingly. As in the case of lead-containing additives [10], Z(% soot) dependence has its extremum (fig. 3, 4). Besides increasing of the burning rate, combined catalysts highly decrease v-value in some pressure intervals.

In the present work particle size 1...2 μm copper oxalate was used as a copper-containing additive. First of all, it was needed to investigate the influence of combined catalyst components ratio on effectivity of its influence for this ratio was found to be very important for early-known combined additives [15].

The investigations were done with propellant II, the total content of additives was constant and equal to 5% (above 100%). From fig. 5 it is seen, that copper oxalate introduction instead of a part of Bi_2O_4 results in burning rate increasing in lower pressure interval (80...100% under 2 MPa) and its decreasing above 6 MPa. As a result, v-value is significantly decreased (fig. 6). It must be underlined, that copper oxalate itself slightly decreases propelant burning rate.
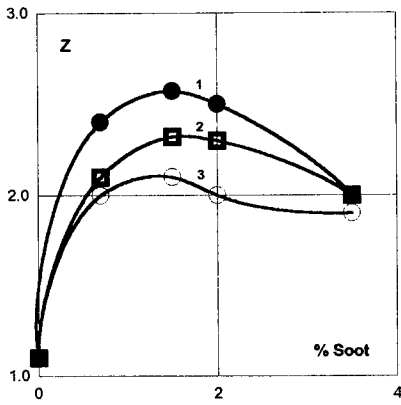
Fig.3. Soot influence on 1.5% Bi_2O_5 effectivity in RDX-containing propellant propellant burning under different pressures: 1 - 2 MPa; 2 - 10 MPa; 3 - 12 MPa.
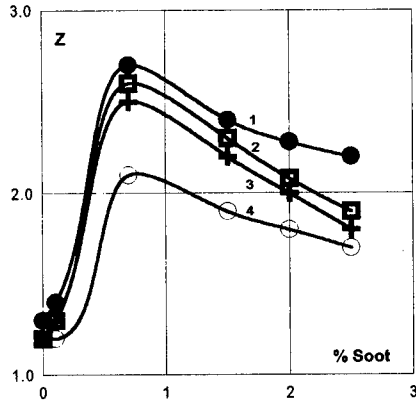
Fig.4. Soot influence on 1.5% $Bi(OH)_3$ effectivity in RDX-containing burning under different pressures: 1 - 2 MPa; 2 - 6 MPa; 3 - 8 MPa; 4 - 12 MPa.
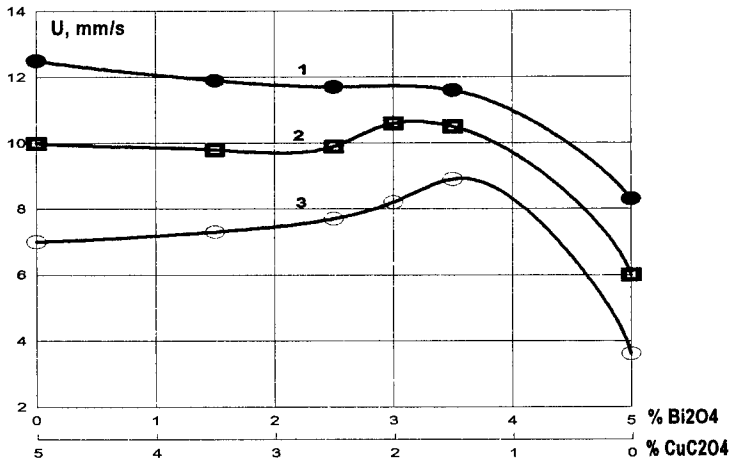

Fig.5. Combined catalyst components ratio influence on the burning rate of propellant II under pressures:1 - 6 MPa; 2 - 4 MPa; 3 - 2 MPa.
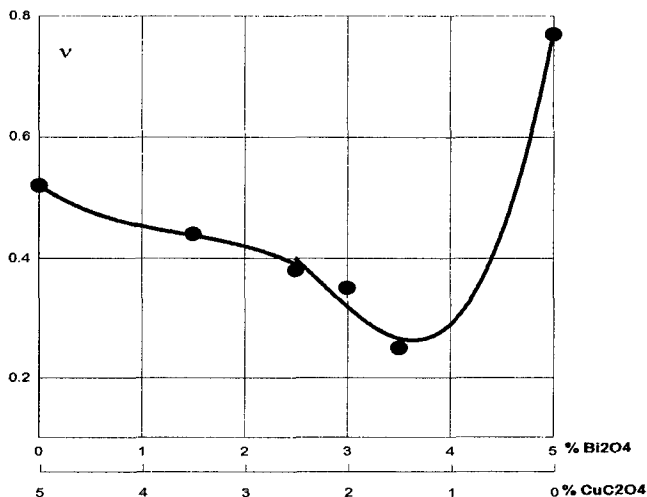
Fig.6. Propellant II combined catalyst components ratio influence on the n-value, within pressure interval 2 - 8 MPa.

The similar results were obtained with propellant IV.

It is obvious from table 4, that 5% Bi_2O_4 increases propellant burning rate within all pressure range investigated (2...10 MPa) and substantially decreases the value of v (up to 0.4). Addition into composition of copper oxalate results in some burning rate decreasing.

Table 4

Combined Catalyst Components Ratio Influence on Propellant IV Burning Rate

Additive	U-value, mm/s under P, MPa						v-value in P interval	
	P = 2		P = 4		P = 10			
	U	Z	U	Z	U	Z	v	P, MPa
Without additives	3.4	1.00	5.6	1.00	10.7	1.00	0.72	2 -10
5% Bi_2O_4	5.8	1.71	9.6	1.71	13.3	1.24	0.41	3 - 8
3% Bi_2O_4 + + 2% CuC_2O_4	7.7	2.26	10.7	1.91	13.5	1.26	0.26	4 - 10
2% Bi_2O_4 + + 3% CuC_2O_4	7.7	2.26	10.7	1.91	12.2	1.14	0.50 0.10	2 - 4 4 - 12
1.5% Bi_2O_4 + + 3.5% CuC_2O_4	7.2	2.10	10.0	1.79	12.0	1.12	0.50 0	2 - 6 6 - 12
5% CuC_2O_4	2.8	0.82	4.7	0.83	8.5	0.80	0.72	2 - 10

The combined introduction of Bi_2O_4 and copper oxalate mixture of a specific ratio into propellant results in large increasing of the burning rate in a small pressure range (fig. 7). For example, the burning rate increases from 3.4 to 7.1...7.7 mm/s under 2 MPa. For the sample with 1.5% of Bi_2O_4 and 3.5% of CuC_2O_4 a plateau-effect (n = 0) is observed beginning from the pressure of 6 MPa. Zone of a weak dependence U(p) starts from 4 MPa for a propellant containing 2% of Bi_2O_4 (table 5). High effectivity of catalyst influence is observed within all investigated pressure range, when total amount of catalyst is decreased to 3% and the ratio is 2:3.
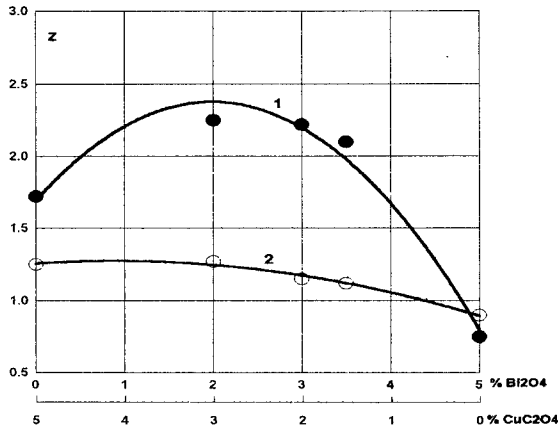
Fig.8. Propellant IV combined catalyst components ratio influence on its effectivity under pressures: 1 - 2 MPa; 2 - 10 MPa.

Table 5

Soot Influence on Effectivity of 1.5% of Bi_2O_5 and $Bi(OH)_3$ during Burning of RDX-Containing Propellant without Addition Plasticizers

Additives	Soot content, %	Z-value, under P, MPa			v-value in interval 8...16 MPa
		2	6	12	
Bi_2O_5	0	1.1	1.1	1.1	0.67
	0.7	2.4	2.3	2.0	0.4
	2.0	2.5	2.5	2.0	0.1
	3.5	2.0	2.1	1.9	0.4
$Bi(OH)_3$	0	1.3	1.2	1.2	0.63
	0.7	2.7	2.6	2.1	0.23
	1.5	2.4	2.3	1.9	0.30
	2.5	2.2	1.9	1.7	0.51

Conclusion

It is shown by experiments, that various bismuth derivatives are quite effective burning rate catalysts for a large range of propellant compositions. Their influence is much stronger than that previously mentioned. Probably, it may be explained by the high dispersivity of the additives used in the present work.

The influence of bismuth derivatives is very much alike with lead-containing catalysts influence. Both catalyst systems considerably accelerate burning of propellants with not less than 3...5% content of additional plasticizers (dinitrotolyene, dibutylphtalate and so on) and considerably decrease burning rate dependence on pressure in some pressure range.

As in case of lead-containing catalysts, bismuth derivatives influence on burning rate of above mentioned propellants, highly increases if being introduced combined with copper derivatives which are less ecologycally dangerous. Thus, MPC for copper and it's derivatives is 100...10 times higher than that for lead compounds [14].

Bismuth derivatives as lead ones almost do not effect the burning rate of high-energy propellants containing no additional plasticizers. However, being added into these propelants combined with soot bismuth derivatives effect the burning rate and the effectivity of their influence is an extremum function depending on soot content, as it has been observed for lead-containing additives [10].

Thus, high-dispersed bismuth derivatives can successfully replace ecologycally dangerous lead-containing burning rate catalysts for double base propellants.

References

1. Crawford B.L., Huggett C., Brady J.J. The mechanism of the burning of double based propellants // J. Phys. and Colloid. Chem. 1950. V. 54, No. 6. P. 854-862.

2. Preckel R.F. Gas producing propellant for jet propelled devices. U.S. patent 3033715. 1962.

3. Preckel R.F. Gas producing propellant for jet propelled devices. U.S. patent 3033716. 1962.

4. Preckel R.F. Gas producing propellant for jet propelled devices. U.S. patent 3033717. 1962.

5. Hewkin D.J., Hicks J.A., Powling J., Watts S.H. The combustion of nitric ester-based propellants: ballistic modification by lead compounds // Combust. Sci. and Technology. 1971. V. 2, No. 5-6. P. 307-327.

6. Camp A.T., rescenzo F.G. Copper and lead burning rate modifiers for double base propellants containing aluminum. U.S. patent 3138499. 1964.

7. Denisyuk A.P., Fogel`zang A.E. Temperature Profiles in Burning of Double Base Propellants with Abnormal Burning Rate Dependence on Pressure // Izv. VUZov SSSR. Himia i himicheskaia tehnologia. 1971. V. XIV, No. 6. P. 861-863 (in Russian).

8. Kubota N., Ohlemiller T.J., Caveny L.H., Summerfield M. Site and Mode of Action of Plationizers in Double Base Propellant // AIAA Journal. 1974. V. 12, No. 12. P. 1709-1714.

9. Preckel R.F. Plateau ballistics in nitrocellulose propellants // AJAA Journal. 1965. V. 3, No. 2. P. 346-347.

10. Denisyuk A.P., Kozyreva T.M., Khubaev V.G. Effect of a Ratuo between PbO and Carbon on the Combustion of a Double based Propellant // Fizika goreniya i vzriva. 1975. V. 11, No. 2. P. 315-318 (in Russian).

11. Catalist Properties of Substances. Reference Book / Editor Roiter V.A. Kiev: Naukova dumka, 1968 (in Russian).

12. Margolis L.Ya. Heterogeneous Catalyst Oxidation of Hydrocarbons. Leningrad: Himia, 1967 (in Russian).

13. Dangerous Chemical Substances. Reference Book. Inorganic Substances of Elements of V - VIII groups / Editor Filov V.A. and others. Leningrad.: Himia, 1988 (in Russian).

14. Dangerous Chemical Substances. Reference Book. Inorganic Substances of Elements of I - IV groups / Editor Filov V.A. and others. Leningrad.: Himia, 1988 (in Russian).

15. Androsov A.S., Denisyuk A.P., Tokarev N.P. Some Pecularities of Effect of Lead-Copper Catalysts on the Burning Rate of Propellants // Fizika goreniya i vzriva. 1976. V. 12, No. 5. P. 780-782 (in Russian).

COMBUSTION BEHAVIOUR OF RADIATION CURED ENERGETIC COMPOSITES

V.G.Dedgaonkar

Department of chemistry, University of Pune. Pune 411 007. India

P.B. Navle and P.G. Shrotri

High Energy Materials Research Laboratory, Pune 411 021, India.

ABSTRACT

Composite rocket propellants containing basically ammonium perchlorate (AP) and hydroxyl terminated polybutadiene (HTPB) have been prepared following gamma radiation treatment for curing. A ^{60}Co gamma source was employed (dose rate : 60 kGy d^{-1}) for this cold curing process. Influence of radiation dose was studied over the range of 0 - 600 kGy. Irradiation of conventional formulations containing toluene di-isocynate (TDI) and ferric acetyl acetonate (FAA) indicated that burning rate of such composites is a function of radiation dose. Similar trend was shown by the irradiated products without containing FAA and also by the products without FAA and TDI. The trend is attributed to the observed reduction in density caused by radiation induced interphase reactions at the surface of AP particles. Such processes cause increase in porosity. The calorimetric values in all the cases, however, remain practically constant around 800 cal g^{-1}. Over the high dose region some systems show a decrease in burning rate with increasing dose. even though there is an appreciable loss in density. This is attributed to the occurence of extensive crosslinking of polybutadiene segments. The burning rate data obey the Vieille's law, $r_b = ap^n$, and the GDF formula, $1/r_b = a'/p + b/p^{1/3}$. Attempt is made to interpret the variation observed in the emperical constants (a, n, a' and b) with respect to radiation dose and binder composition.

INTRODUCTION

Radiation is known[1-4] to alter the burning rate of composite propellant containing different binders such as polyurethane, polybutadiene, polyvinyl chloride, polysulphide, etc. In a few cases the rate is reported to be independent of dose and yet the dose influencing the mechanical properties. An appreciable change in burning rate has been reported even when irradiated ammonium prechlorate was used in preparing the propellants. Our earlier work[5-9] deals with radiation effects on cure characteristics and mechanical properties of the conventional HTPB-base binder systems and their composites when curing was done by means of gamma radiation treatment. The data reported here deal with burning rate of such simpler composite systems which do not contain additives other than TDI and FAA.

EXPERIMENTAL

The method of preparation of different composites and the procedure followed for their curing under the influence of gamma radiation has been discussed elsewhere[10]. The sample that contains HTPB alone as the binder (25%) for AP (75%) is denoted as A; composite B contains TDI (NCO:OH=1) as a curing agent in A while composite C consists of sample B and the curing catalyst FAA (~ 0.01%). The cured composites were evaluated for burning rate using a standard strand burner system coupled to an acoustic unit. Calorimetric values were determined with the help of a julius peter adiabatic bomb calorimeter.

the changes in n and a with dose follow the trends $S_{n_A} < S_{n_B} < S_{n_C}$ and $S_{a_C} < S_{a_B} < S_{a_A}$.

Since composite A contains crosslinkages among polybutandiene segments and the degree of crosslinking increases with increase in dose, pyrolysis of the binder during combustion requires high energy for breaking the rigid structure. Such materials should show the tendency of incomplete pyrolysis; the rate of combustion of the binder lags behind the rate of combustion of the oxidiser. Such situation causes a drop[14] in the pressure index as has been observed in the present system.

The values of a' and b obtained on the basis of GDF model: $1/r_b = a'/p + b/p^{1/3}$ are plotted for different composites against radiation dose in Fig. 4a and 4b respectively. Slopes $S_{a'}$ and S_b of these straight line plots as given in Table 1 indicate the dependance on composition as: $S_{a'_A} < S_{a'_B} < S_{a'_C}$ and $S_{b_C} < S_{b_B} < S_{b_A}$. The model further considers the diffusion parameter b to be a function of particle size of AP. Since the particle size and amount of AP in all the formulations under consideration are the same, the observed dose dependence of b should arise from the radiation induced processes that occur in the polymer binder. It is known[6] that upon irradiation the binder undergoes crosslinking. Variation in the degree of crosslinking probably cause variation in the size of the vapour pockets. Besides, the crosslinking should alter the rate of vapourisation of the binder, it should correspondingly alter the size of the pockets. The constant a' is a function of kinetics of combustion reactions and the variation in it is a consequence of allylic hydrogen reactivity of the binder containing HTPB[15]. With the progressive increase in dose, allylic hydrogen is lost as a result of either crosslinking among polybutadiene segments or due to loss of unsaturation during irradiation. This would lead to delaying of reactions between fuel products with the oxidising species. Thus extensive crosslinking induced by radiation in the binder is responsible for change in values of both a' and b. Both values decrease in the case of radiationally crosslinked composite A. It is noteworthy that the composites that exhibited very low pressure index have values of kinetic parameter close to zero.

RESULTS AND DISCUSSION

Effect of radiation treatment on burning rate (r_b) at different pressures (p) can be seen from the plot of r_b versus radiation dose. Slopes of these straight line plots are recorded in Table 1. In all the cases the rate increases with dose upto a certain limit; beyond that, composites A and C show a fall while composite B yields a continued increasing trend. For all these compositions, decreasing density with increasing dose has been observed[10]. These data are in conformity with the general observation that the burning rate is an inverse function of density of the material. The decrease in burning rate beyond certain dose (~500 kGy) is attributed to the radiation induced crosslinking process which further continues as the dose increases. In the case of excessive crosslinking, a large amount of energy is required to break[11] the bonds during burning and this probably causes slowing down the rate. Besides, penetration of the flame through the heavily cross-linked material also becomes more difficult under this situation. Thus the observed burning rate is the resultant of two opposing factors, namely, density and degree of crosslinking. For any pressure and at all doses burning rate for the composites under investigation shows the order: $r_{b_A} > r_{b_C} > r_{b_B}$. The same order is indicated by the slopes over the initial period of Figs. 1 and 2, viz. $S_A > S_C > S_B$. These trends seem to be set by the porosity introduced by radiation.

In order to understand the relationship between the observed burning rate of the irradiated material and the composition of the binder, the data were analysed on the basis of Vieille's law[12] and also on the GDF model[13]. All the irradiated formulations showed that burning rates at different pressures obey Vieille's law : $r_b = ap^n$. The plot of log r_b versus log p (at a constant dose) gave a straight line, the intercept and slope containing the constants a and n. Behaviour of these constants could be understood from the plots given in Fig. 3a and 3b. Interestingly, there is a linear dependance of n and a values on dose within certain ranges. Slopes of these plots are recorded in Table 1. It is to be noted that a decrease in n is associated with an increase in a and vice - versa. In general,

The TDI containing composites B and C, which were cured either by radiation treatment below 240 kGy or by standard thermal treatment, showed comparable burning rates observable over a wide range of pressure. These rates are lower than those obtained upon radiation curing over the higher (> 240 kGy) dose region. The latter results have been attributed to the lowering in density that results from radiation-induced microporosity. It is noteworthy that the values for Vieille's and GDF constants obtained upon thermal curing lie in between the widely varying values for radiationally cured composites over a wide range of dose.

Notwithstanding radiation is expected to produce gases particularly due to the decomposition of AP, data presented in Fig. 5 show practically no change in the cal-val. which is around 820 cal g^{-1}. One may therefore consider that the weight change due to loss of radiolysed products escaping to the atmosphere is not negligible. Radiation induced interphase reactions occuring between products of AP and of binder might be preventing to some extent the escape of gaseous products.

CONCLUSION

Exposure of AP/HTPB - base energetic formulations to ionising radiation alters the combustion behaviour of the product as a result of radiation induced crosslinking reactions The data convey that different burning rates can be obtained by varying the radiation treatment to a single formulation and that much higher rates can be obtained this way as compared to that which is achieved by means of the conventional thermal treatment. The radiation tool can be much more effective if the binder composition is properly selected. As a result of high degree of crosslinking over the high dose region the binder pyrolysis can be suppressed and hence pressure index can be brought down considerably.

REFERENCES.

1. R.E. Gardner J.Am. Rocket Soc. 32, 1050 (1962)

2. J. Flanagan and J.C. Gray. J. Spacecraft & Rockets. 3,135 (1966).

3. R.F. McAlevy and S.Y. Lee, "Heterogenous Combustion", AIAA progress in Astronautics and Aeronautics Academic Press. New York 15, 583 (1964).

4. M.R. Kurup, M.K. Venkitakrishnan and M.C. Uttam. Proc. Chem. Symp. 2nd Dept. Atomic. Energy, Barc, Bombay. 2, 43 (1990).

5. V.G. Dedgaonkar, P.B. Navle and P.G. Shrotri, J. Radional. Nucl. Chem. Letts. 176. 77 (1993).

6. V.G. Dedgaonkar. P.B. Navle and P.G Shrotri, J. Radional. Nucl. Chem. Letts. 176, 153 (1993).

7. V.G. Dedgaonkar, P.B. Navle and P.G. Shrotri, J. Radional. Nucl. Chem. Letts. 187. 1 (1994).

8. V.G. Dedgaonkar, P.B. Navle and P.G. Shrotri, 5th Internat. Symp. on Explosives Technology, Nat. Inst. Explos. Technol (NIXT) Pretoria. 451 (1994).

9. V.G. Dedgaonkar, P.B. Navle and P.G. Shrotri, Radiat. Phys. Chem. (in press).

10. V.G. Dedgaonkar, P.B. Navle and P.G. Shrotri, Propell. Explos. Pyrotech. - Communicated.

11. T.E. Krishnan, T.L. Varghese, L.Ramachandran, S.S Rao and K.N. Ninan, 7th Nat. Sem. on High Energy Materials. V.S.S.C. Thiruvananthapuram, 113 (1994).

12. N.Kubota. "Fundamentals of Solid propellant combustion",AIAA progress in Astronautics and Aeronautics, 90, 1, (1984).

13. K.N.R. Ramohalli; "Fundamentals of Solid propellant combustion", AIAA progress in Astronautics and Aeronautics Academic Press. New York. 90, 409 (1984).

14. K.Kishore and V. Gayathri, "Fundamentals of Solid propellant combustion". AIAA progress in Astronautics and Aeronautics Academic Press. New York. 90, 53 (1984).

15. J.M. Hitner and R. Reed Jr., Proc. Joint Internat. Symp. on Compatibility of plastics and other materials with explos. propell. pyrotech. and processing of Explos. Propell. and ingredients, California. 478 (1991).

Table 1 : Effect of binder composition on the change of combustion characteristics with dose.

Parameter	Composite		
	A	B	C
Burning rate			
r_c / dose X 10^2 (mm s^{-1} / kGy)			
at 3.4 MPa	3.75* -0.33**	0.17	2.00* -0.50**
6.8 MPa	3.75* -0.42**	0.97	0.42
10.2 MPa	7.58* -3.12**	1.07	3.52* -2.21**
13.2 MPa	5.09 -1.09**	1.15	3.33* 2.92**
Vieille's Constants			
a / dose X 10^2 (kGy^{-1})	4.00* 1.56**	-0.3	3.67* -1.00**
n / dose X 10^3 (kGy^{-1})	-0.83	0.28	-2.50* 1.50**
GDF Constants			
a' / dose X 10^4 (kGy^{-1})	-1.67	0.12	2.33
b / dose X 10^4 (kGy^{-1})	-0.07	-0.73	-1.25

*   Over the low - dose region
**   Over the high - dose region
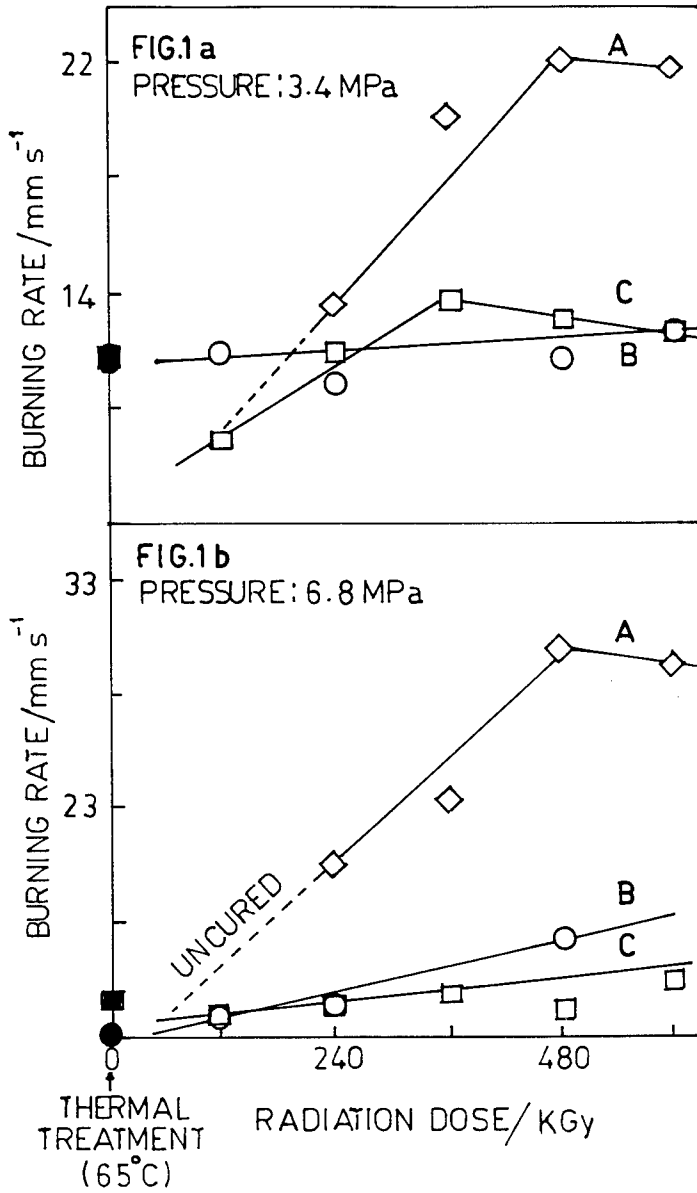
EFFECT OF BINDER COMPOSITION ON BURNING
RATE AT 3·4 MPA (FIG.1 a) AND 6·8 MPA
(FIG.1 b) AT DIFFERENT RADIATION DOSES.

FIG. 2a
PRESSURE: 10·2 MPa

FIG. 2b
PRESSURE: 13·2 MPa

UNCURED

0
THERMAL
TREATMENT
(65°C)

RADIATION DOSE/KGy
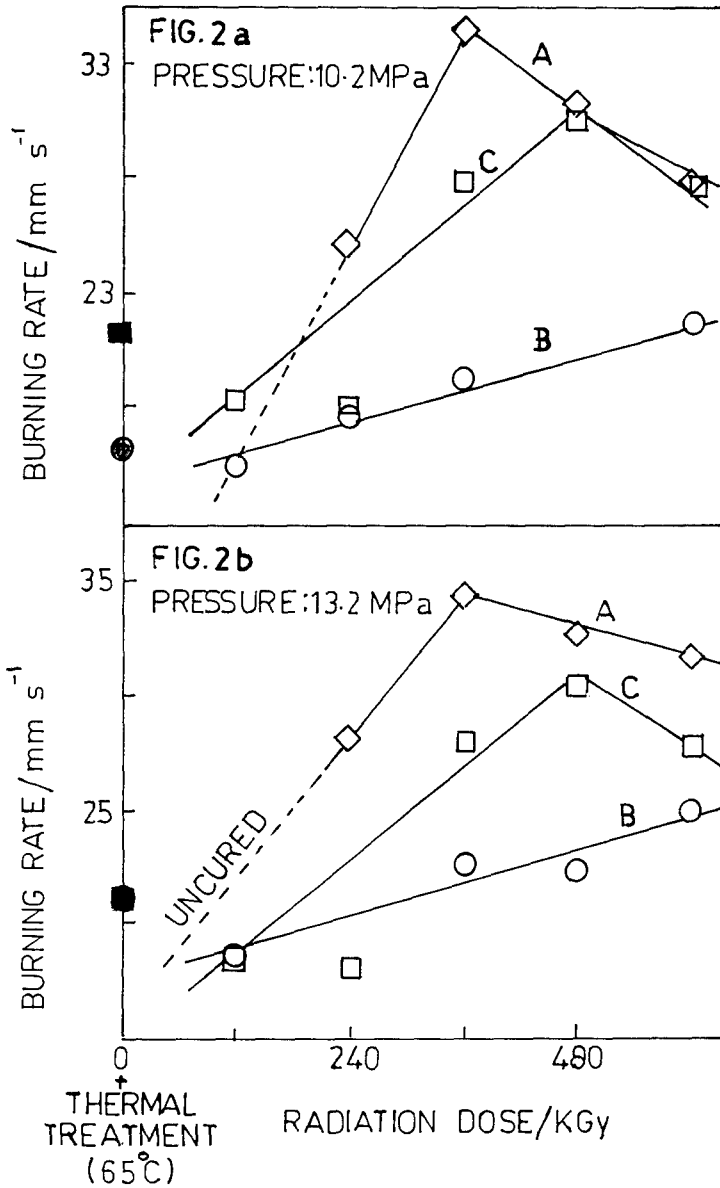
BURNING RATE/mm s^{-1}

EFFECT OF BINDER COMPOSITION ON BURNING
RATE AT 10·2 MPA (FIG. 2a) AND 13·2 MPA
(FIG. 2b) AT DIFFERENT RADIATION DOSES.
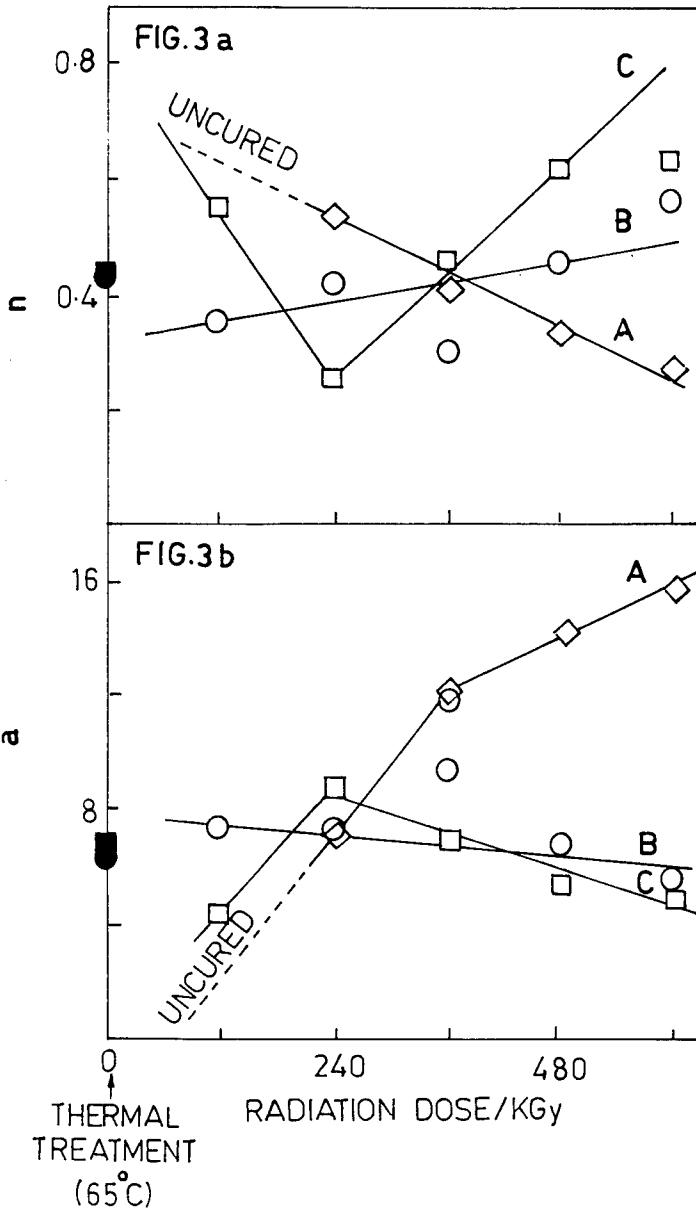
EFFECT OF BINDER COMPOSITION ON VIEILLE'S
CONSTANTS, n (FIG.3 a) AND a (FIG.3b) AT
DIFFERENT RADIATION DOSES.
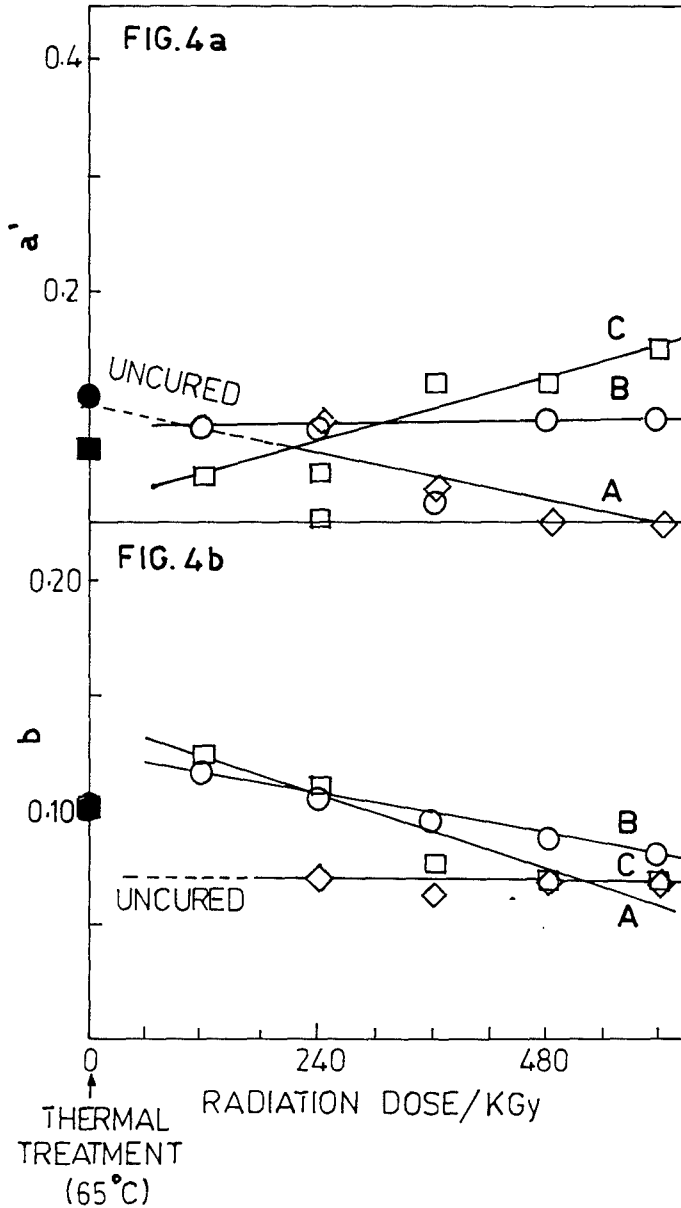
EFFECT OF BINDER COMPOSITION ON THE GDF
CONSTANTS, a'(FIG.4a) AND b(FIG.4b) AT
DIFFERENT RADIATION DOSES.
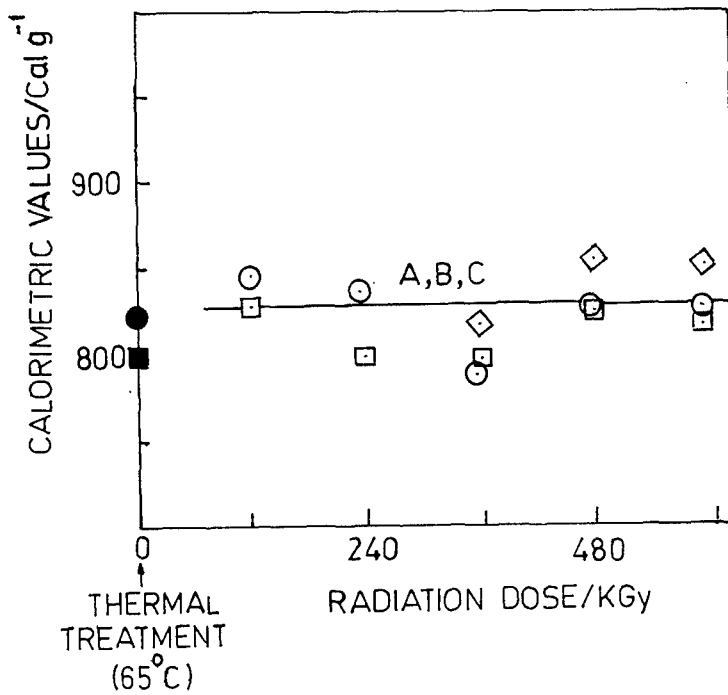
FIG.5 — EFFECT OF BINDER COMPOSITION ON
CAL VAL AT DIFFERENT RADIATION DOSES.

THE CHANGE OF COMBUSTION PERCOLATION MECHANISM BY THE ACTION OF TEMPERATURE AND CATALYSTS

Valentin Klyucharev

Institute of New Chemical Problems, Russian Academy of Sciences, Chernogolovka, Moscow region, 142432, Russia.

The effect of temperature and chemical additives on changes in the combustion mechanism as well as the thermal nature of multicenter and layered quasi-adiabatic self-propagating processes has been discussed.

The percolation mechanism of combustion was previously discussed [1-6], where the self-propagating chemical processes in heterogeneous condensed systems was involved. In many cases [1, 2], synthesis of ceramics and intermetallides in a wave of self-propagating high-temperature synthesis (SHS) becomes possible when volume fraction of one component is close to 0.16. This is close to the Sher-Zallen percolation criterion [7]. The authors of [3, 4] showed that the ignition surface constructed by means of cellular automata qualitatively well reproduces certain features of actual SHS waves. The results of [1-6] prompt a consideration of combustion in terms of percolation processes.

Previously it was noticed that thermochemical boundaries of combustion can be determined with the account of specific features of formation of quasi-adiabatic cells in a combustion wave [8]. Let us illustrate this on the example of a pyrotechnic system comprising magnesium, nickel oxide, sodium perchlorate, and sodium superoxide.

The studies were performed using differential thermal analysis (DTA) [9] in alundum crucibles with the heating rate of 10 $^{\circ}$C/min and by burning cylindrical samples 28 mm in diameter and 50-60 mm high; the density of the material was 1.8-1.9 g/cm^3. The sample was ignited with a 14-mm-diameter and 3-mm-thick pellet of Mg, Li_2O_2,

and Fe_2O_3 which secured heating to 700-750°C. The reaction was initiated by an electrically heated nichrom spiral. To promote ignition, the outer surface of the ignition pellet was covered by a thin (3 mm) layer of mixture of $Zr-BaO_2$ (1 : 1 molar).

The initial $NaClO_4$ was that of pure grade. It was prepared for experiments according to [10-12]; the particles size was 65-100 mcm. $LiClO_4$ (pure grade) was prepared by A.P. Razumova according to the [13]. Nickel oxide of extra pure grade was calcined in air during three hours at 600°C, the particles size of NiO was 30-50 mcm. The preparation of sodium superoxide was a yellowish powder containing 87 wt.% of NaO_2 and 11 wt.% of Na_2O_2 [13]; the preparation also contained traces of Na_2CO_3. The particles size was not controlled. Upon heating with the rate of 10°C/min, the preparation completely loss the superoxide oxygen below 285°C according to the reaction $2NaO_2 = Na_2O_2 + O_2$.

The DTA was performed on mixtures where metal magnesium was a powder with the particles size varied within 2 to 160 mcm. The pyrotechnical charges contained magnesium with the particles size 65-100 and 100-160 mcm. The fractions used in the charges were sifted from commercial MPF-4 powder.

In four-component mixture comprising Mg, $NaClO_4$, Na_2O_2, and NiO, there occurs rapid cooperative process of metal oxidation and oxygen release which resembles that previously described for the $NaClO_4-Mg-CaO_2$, $KClO_4-Mg-CaO_2$ [9], and $KClO_4-Mg-Fe_2O_3$ [14] systems. As a result of this reaction, the initial substances completely transform into the products: MgO, NaCl, Na_2O_2, NiO, and O_2. The ignition occurs at Tc = 290 ± 10°C (measured by the temperature jump in DTA).

Suppose that combustion is a quasi-adiabatic self-propagating process (QSP). In this case a node of percolation cluster can be associated with a quasi-adiabatic cell (QC), i.e., with a spatial domain where chemical reactions proceed so fast that heat loss from the cell can be neglected.

For stationary QSP and isotropic QC, twofold increase in the time of chemical transformation causes twofold increase in the radius of the cell and eightfold, in its volume. Therefore, if the process is quasi-adiabatic one, a QC must release amount of heat sufficient to heating to the same temperature T_c the products within already reacted sphere of radius R1 = 1 and virgin unreacted mixture within the spherical layer in between of R1 = 1 and R2 = 2.

If the sizes of the cells capable and incapable of burning are close in their volume, then, according to the Sher-Zallen criterion, the volume fraction of active centers must be close to 0.16 [7]. In this case, the above described model allows us to estimate the limits where chemical compounds are capable of stationary combustion from the following equation

$$Q = K * \int_{T_o}^{T_c} (7 * C_i + C_k) dT \quad (1); \quad Q = Q_r + K * \int_{T_o}^{T_c} (7 * C_i + C_k) dT \quad (2)$$

In equation (1) and (2) Q is the calorific value of mixture containing N initial substances at a rate of n_i mole of i component and forming M end products at a rate of m_k mole of k component; Q_r is the calorific value of the medium comprising the QC, K is Sher-Zallen coefficient, T_o is the initial temperature of the mixture, C_i, C_k are the summary isobaric molar heat capacity of the initial mixture (C_i) and the reaction products (C_k)

$$C_i = \sum_i (n_i * c_{pi}) \quad (3); \quad C_k = \sum_k (m_k * c_{pk}) \quad (4)$$

where c_{pi} is isobaric molar heat capacity of i initial substance, c_{pk} is isobaric molar heat capacity of k end product.

Let us consider the mixture containing 1 g-mol of $NaClO_4$, x g-mol of Mg, 0.16 g-mol of NaO_2, 0.03 g-mol of NiO. In the case, the initial components: sodium perchlorate metal magnesium, nickel oxide are stable up to ignition temperature ($300^\circ C$) and sodium superoxide is decomposed to form sodium peroxide and oxygen.

Consequently, the outer shell of two-layer QC contains 7 g-mol $NaClO_4$, 7*x g-mol Mg, 0.21 g-mol NiO, and in terms of the reaction 2 NaO_2 = Na_2O_2 + O_2, 0.56 g-mol Na_2O_2 and 0.56 g-mol O_2. This amount of initial components is present in QC, when after chemical reactions in first, inner shell the products 1 g-mol NaCl, x g-mol MgO, 0.08 g-mol Na_2O_2, 2.08 g-mol O_2 are formed and 0.03 g-mol NiO remains intact. The amount of reagents and products founding in QC takes account of equation (5) that is to say the cooperative process of magnesium oxidation and oxidizer decomposition.

$$NaClO_4 + x\ Mg + 0.16\ NaO_2 = NaCl + x\ MgO + $$
$$+ (4.16 - x)/2\ O_2 \qquad (5)$$
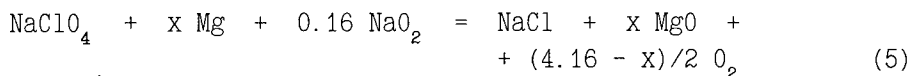
By summing over all components one can obtain the composition of QC which incorporates 7 g-mol $NaClO_4$, 1 g-mol NaCl, 0.24 g-mol NiO, 0.64 g-mol Na_2O_2, 7*x g-mol Mg, x g-mol MgO, (5.28-x)/2 g-mol O_2.

Taking into account the composition of QC and conditions (1-4), we can determine the minimum content of magnesium for which the mixture is combustible. The standard enthalpies of formation and heat capacities for the all compounds in the temperature range of interested are known [15-20]. In this work, we used the values of thermochemical and thermophysical functions summarized in Table 1.

The calculations showed that at ignition temperature of 290-300°C, the calculated minimum magnesium content corresponds to the molar ratio of $Mg/NaClO_4$ = 0.095-0.1. The value determined in experiments on ignition of pyrotechnical charges was 0.098-0.1. Similar good agreement of experimental and calculated values was obtained for pyrotechnical mixtures with different oxidant composition, with the $NaO_2/NaClO_4$ ratio within 0.1-0.25.

Not every combustible contains high calorific value components that would satisfy conditions (1) or (2), i.e., to make up a percolation cluster of QCs. In this case, formation of quasi-adiabatic layer (QL) may be preferable, since in the latter case, to sustain combustion is sufficient to heat to temperature T_c only a volume equivalent to that burnt [8]

$$Q = K * \int_{T_o}^{T_c} (C_i + C_k) dT \tag{6}$$

Consider the two-component system of $LiClO_4$-Na_2O_2. These reactants interact according to the exchange reaction (7) which might be employed as a heat source in oxygen-generating pyrotechnical compounds [13]

$$2 \; LiClO_4 + Na_2O_2 = 2 \; NaClO_4 + Li_2O + 0.5 \; O_2 + 92.32 \; kJ \tag{7}$$
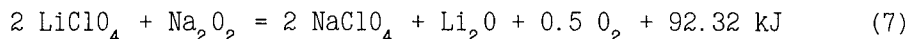
However, the energy released after all the reactions being completed

$$2 \; LiClO_4 + Na_2O_2 = 2 \; NaCl + Li_2O + 4.5 \; O_2 + 148.43 \; kJ \tag{8}$$
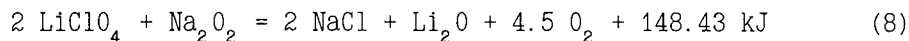
is much less than that releases in magnesium oxidation: $Mg + 0.5 \; O_2$ = MgO + 602.13 kJ. For this reason, it is impossible to achieve QC in compliance with (1) and (2) despite reaction (7) proceeding fast already at 203-220°C [13], which is substantially lower than ignition temperature for magnesium in Mg-$NaClO_4$-CaO_2 system (420-430°C) or in dry oxygen (570-600°C) [9].

Nevertheless, owing to the heat released in reaction (8) the QL can be heated to 203-206°C, i.e., to the point where reaction (7) transits to quasi-adiabatic regime, if initial temperature of the mixture is 20°C and composition corresponds to the molar ratio of $LiClO_4$: Na_2O_2 = 1: 0.58. In this case excess Na_2O_2 is necessary to reduce the temperature of subsequent decomposition of NaClO4 formed in reaction (7) to 300-320°C.

Experiment showed that in the cases when initial temperature of pressed pyrotechnical compound containing 1 g-mol of anhydrous $LiClO_4$ and 0.58 g-mol of Na_2O_2 exceeded 20-30°C, combustion with total oxygen release took place and the temperature of 440-460°C was produced. This virtually coincides with the calculated adiabatic temperature, T_{ad} [21].

The obtained result indicates that above considerations on thermodynamics of QC and QL provide means for accurate calculations of the limits of QSPs. The equations (1), (2), and (6), reflecting the thermal nature of various types of combustion, allow to establish the thermodynamic interrelations between multicenter and layered quasi-adiabatic self-propagating process and, thus, in many cases, to calculate possible effect of temperature and chemical additives on changes in the combustion mechanism.

For example, one of the results of such calculations is that with reduced difference between the initial temperature of the mixture and the temperature of ignition, owing either to preliminary heating or a catalyst, can result in appearance of isolated QCs within QL. A comparison of (1), (2), and (6) shows that percolation combustion requires less energy than the layered one. This is related to the factor $K = 0.16$ in equations (2) and (3). As a result, transition to a system with excess energy can result in spontaneous increase in the rate of QSP, owing to enhanced preheating zone due to onset of the conditions for development of percolation combustion.

At the same time, in many cases, enhancement of initial temperature of the mixture or reduction of the ignition temperature caused by chemical agents can transfer a combustion system to the layered combustion from the percolation one. This is the case, when calorific value of the system as a whole (Q) exceeds certain critical value sufficient to satisfy condition (6), while high calorific value of QC is preserved (integrand in (1) and (2)). This case was observed in binary mixtures of $Mg-CaO_2$.

One more consequence of (1), (2), and (6) is that it is possible to achieve a self-propagating process in the mixtures whose T_{ad} is below the ignition temperature. This possibility appears when initial temperature of combustible mixture is increases. The combustion can proceed by burnout of separate clusters [2].

A review given above allows us that conditions (1-6) must be taken into account when assessing safety of handling energetic materials.

References.

1. Yu.V.Frolov, A.N.Pivkina, B.E.Nikolskii. Fiz. Gor. i Vzryva, **1988**, 24, (5), 95.
2. Yu.V.Frolov, B.E.Nikolskii, Dokl. Ac. Sci USSR, **1989**, 305, 386.
3. S.A.Astapchik,   A.G.Merzhanov,   E.P.Podvojskii,   B.M.Khusid,
 + I.S.Chebotko, Dokl. Ac. Sci. USSR, **1991**, 318, 609.
4. V.V.Aleshin, Yu.V.Frolov, Proc. 21st Int. Pyrotech. Seminar, Moscow, **1995**, 1.
5. Yu.V.Frolov, A.N.Pivkina, Proc. of the 23rd Int. Conf. of Fraunhofer Inst. Chem. Technol., Karlsruhe, **1992**,
6. A.N.Pivkina, Fractal Structure and Characteristics of Heterogeneous Condensed Systems Combustion, Moscow: Inst. of Chem. Physics, **1994**.
7. B.I.Shklovskii, A.L.Efros, Electronic Properties of Alloyed Semiconductors, Moscow: Nauka, **1979**.
8. V.V.Klyucharev, in the 21st Int. Pyrotechnic Seminar, Moscow, **1995**, Pp. 414-416.
9. V.V.Klyucharev, S.M.Sinelnikov, A.P.Razumova, V.D.Sasnovskaya, Proc. of the 26th Int. Conf. of Fraunhofer Inst. Chem. Technol., Karlsruhe, **1995**, 64-1/64-11.
10. V.V.Klyucharev, S.M.Sinelnikov, A.P.Razumova, V.D.Sasnovskaya, Proc. of the 26th Int. Conf. of Fraunhofer Inst. Chem. Technol., Karlsruhe, **1995**, 65-1/65-12.
11. V.V.Klyucharev, in the 21st Int. Pyrotechnic Seminar, Moscow, **1995**, Pp. 417-434.
12. V.V.Klyucharev, S.M.Sinelnikov, A.P.Razumova, V.D.Sasnovskaya, Russ. Chem. Bull., **1996**, (1) 33.
13. V.Ya.Rosolovskii, Z.K.Nikitina, S.M.Sinelnikov, Zh. Inorg. Chem., **1995**, 40, 6.
14. V.V.Klyucharev, Abstr. of the 2nd Int. Conf. "Modern Trends in Chemical Kinetics and Catalysis", Part 3, Novosibirsk, **1995**. Pp. 520-521.

15. Thermodynamic Properties of Individual Substances. V.4. Ed. V.P.Glushko, Moscow: Nauka, **1982**.
16. Thermodynamic Properties of Inorganic Substances. Ed. A.P.Zefirov, Moscow: Nauka, **1965**.
17. G.B.Naumov, B.N.Ryzhenko, I.L.Khodakovskii, The Handbook of Thermodynamic Data, Moscow: Atomizdat, **1971**.
18. N.E.Shmidt, L.N.Golushina, G.A.Sharpataya, V.P.Babaeva, Zh. Phys. Chem., **1984**, 58, 2928.
19. N.E.Shmidt, L.N.Golushina, G.A.Sharpataya, D.G.Lemesheva, Zh. Phys. Chem., **1983**, 57, 2678.
20. Thermal Constants of Substances. V.10. Ed. V.P.Glushko, Moscow: VINITI, **1981**.
21. N.P.Novikov, I.P.Borovinskaya, A.G.Merzhanov, in: Combustion Processes in Chemical Technology and Metallurgy, Ed. A.G.Merzhanov, Chernogolovka: Inst. of Chem. Phys., **1975**, Pp. 174-188.

Table 1.

Thermochemical and Thermophysical Properties of Initial Reagents and Products.

Substance	Standard Enthalpy of Formation (kJ/mol)		The Molar Isobaric Heat Capacity as a Function of Temperature $Cp = a + b*10-3*T + c*10-5*T2 + d*105*T-1$ (J/mol*K)				
	$\triangle Hfo$		a	b	c	d	
LiClO4	-381.02	[19]	29.39	284	-10.94	---	[19]
NaClO4	-383.7	[13]	324.11	-1336.3	213.5	---	[18]
Mg	0	[17]	20.81	12.73	---	-0.167	[17]
NaO2	-261.0	[15]	---	---	---	---	--
NiO	---	--	57.32	3.475	---	---	[16]
NaCl	-411.8	[17]	45.97	16.329	---	---	[17]
MgO	-602.1	[17]	42.62	7.285	---	6.197	[17]
Na2O2	-512.0	[17]	59.75	117.24	-5.946	---	[15]
Li2O	-14.045	[17]	14.939	6.08	3.38	---	[17]
O2	0	[17]	29.99	4.187	---	1.675	[17]

Features of the solid propellant combustion in conditions of variable overload.

Dr. prof. V.I. Petrenko
Dr.-ing. V.L. Popov
Dr.-ing. prof. A.M. Rusak.

Experimental researches at the solid rocket propellant combustion under variable overload were fulfilled, said overload was varied by it's value and direction. Centrifugal test benches which allowed to attain value of "g" up to 100 units were used, the mass of charge tested was no more than 5 kg.

The condition of the combustion surface was researched on the faded charges. It was shown that for the mixed SP overload applied by different axels renders sufficient influence on combustion surface appearance. The homogeneous compounds are less sensitive to overload.

Gail G. Gubaidullin | Phone: 007/3472/53-44-32
Ufa State Aviation Technical University | Fax: 007/3472/22-99-09
Department of Technical Cybernetics | E-mail: gubai@tc.uaicnit.
Ufa, Russia | bashkiria.su

INCINERATION OF EXPLOSIVES IN A FLUIDISED BED

A. Pires, J. Campos, L. Durães* and S. Almada

Lab. of Energetics and Detonics

Dep. of Mech. and *Chem. Engineering - Fac. of Sciences and Technology

University of Coimbra, Pólo II, Pinhal de Marrocos, P-3030 Coimbra - PORTUGAL

ABSTRACT

The proposed method of environmentally responsible disposal of energetic substances is their incineration using an original fluidised bed combustion system. It was designed and built in order to incinerate the most common used explosives, ANFO, emulsion and dynamite, based in ammonium nitrate compositions. It is composed by a fluidised bed, warmed by the combustion of a propane-air mixture as fluidising gas. A wet scrubber and an exhaust gas system close the combustion cycle. The gas products composition and incineration regime can be predicted by THOR computer code. There are two regimes of incineration: the warming transient regime and constant incineration regime. Obtained temperatures show to be stable near 770 K, in a good agreement with theoretical predictions. This incineration system proves to be safe and reliable for the most used industrial explosives.

1. Introduction

Recycling or converting explosives, propellants and other chemical components is highly desirable, for environmental reasons. This is an old problem, that appears now with new dimension, as a consequence of the large quantities involved in demilitarisation and the recognition of the existence of important environmental problems. The potential classic strategies to the disposal of military explosives are based in storage in a secure site, or in stabilisation and storage, or recovering them to be used in a future civil or any other military use. The technological options can be their thermal destruction, controlled explosion, chemical and electrochemical oxidation, chemical transformation and, more recently, biodegradation (vd. Jupp, 1991, Demilitarisation Technology, 1991). It is also necessary to remain that cutting and opening up munitions generate large quantities of explosive-water slurries. These slurries and all the other kind of explosives that can not be integrated, as components, in industrial civil explosives, must

be incinerated. There are many different kinds of energetic materials included in this case (single and double base propellants, TNT, other rocket propellants, black powders, metallic oxides) generating pollutants in their gaseous exhaust products (NO_x, CO, HCl, HF, SO_2, H_2S - vd. Folk, 1990).

A reference of threshold values for gaseous exhaust products in Portugal (vd. Portaria, 1993) concerning the unlimited professional exposure has been published and accepted for industrial proposes. The relatively modest dimension of Portuguese Armed Forces, having insufficient quantities to stabilish a large national demilitarisation programme, the difficulties in locating suitable storage sites and the national policy of developing clean combustion and incineration technologies (vd. Campos et al., 1993) have led us to select two of all the possible disposal procedures of explosives and propellants:

  – the access and segregation of the energetic material, out from its metallic confinement,
  – the clean incineration of not recovered energetic material.

An original fluidised bed combustion system has been designed and built in order to incinerate explosive and other energetic substances. It is composed by a fluidised bed, previously warmed by the combustion of a propane-air mixture as fluidising gas. The energetic materials (explosives or pyrotechnic compositions) are pre-mixed with silica sand particles and injected into bed by a twin screw extruder. A wet scrubber and an exhaust gas system close the combustion cycle. An acquisition and safety data system controls all the combustion.

This method has some advantages over other processes of combustion:– security related to a better temperature homogeneity of bed;– easy control of temperature, pressure and equivalent ratio of mixture;– better heat transfer which means lower combustion temperatures and consequently a reduction of emission of polluting gases;– higher density power involved. The great disadvantage of a fluidised bed combustion equipment comes not only from its ignition and security, during initial working period, but also from the necessity of keeping the fluidised bed warmed before introduction of energetic substances.

In order to test and optimise the incineration equipment it has been selected the three most common industrial explosives used in Portugal: ANFO, emulsion explosive and dynamite.

2. Selected industrial explosives based in ammonium nitrate compositions

The most common industrial explosives in Portugal are ammonium nitrate derived compositions. The most simple is an ammonium nitrate-fuel oil composition (ANFO) and the most complex is the dynamite explosive, representing an annual production of 10000 tonnes for open air and underground mines applications. Recently, ammonium nitrate based emulsion explosives are also used in those industrial applications. In this study three types of explosives were selected:

– one composition of ANFO, an ammonium nitrate - fuel oil composition, with 6 % (in weight) of fuel oil, with initial density 870 kg/m^3 and detonation velocity 3300 m/s,

– one composition of emulsion explosive, formed by an aqueous solution of 10 % of water, of ammonium and sodium nitrates, respectively 72 and 10 %, emulsified with oils, wax and emulsifiers, 5.5 %, with hollow glass spheres as sensitizer, 2.5 %, with density 1170 kg/m^3 and detonation velocity 5340 m/s,

– one composition of dynamite explosive, formed by 30 % of nitro-glycerine, 6 % of DNT, 60 % of ammonium nitrate and 4 % of amidon, with density 1400 kg/ m^3 and detonation velocity 5900 m/s.

Pure ammonium nitrate undergoes a number of decomposition processes at elevated temperatures. The following are significant:

- endothermic dissociation above 169 °C : $NH_4NO_3 \rightarrow HNO_3 + NH_3$

-exothermic elimination of N_2O on careful heating at 200 ° C: $NH_4NO_3 \rightarrow N_2O + 2 H_2O$

- exothermic elimination of N_2 and NO_2 above 230 °C: $4 NH_4NO_3 \rightarrow 3 N_2 + 2 NO_2 + 8 H_2O$

- exothermic elimination of nitrogen and oxygen, sometimes accompanied by detonation: $NH_4NO_3 \rightarrow N_2 + 1/2 O_2 + 2 H_2O$
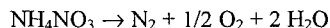
Consequently during incineration the temperatures and the quantity of ammonium nitrate must be controlled, in order to reach a stable regime.

The reactive system are a mixture of the selected explosives and silica sand, with a mass contents of 3%, 5%, 10%, 20%, in order to avoid unexpected ignition or increasing combustion rates. The incinerator uses inert silica sand (vd. Figure 1) as the bed material having a size range of 21.9 μm to 564 μm (d_{50}=377.7 μm).
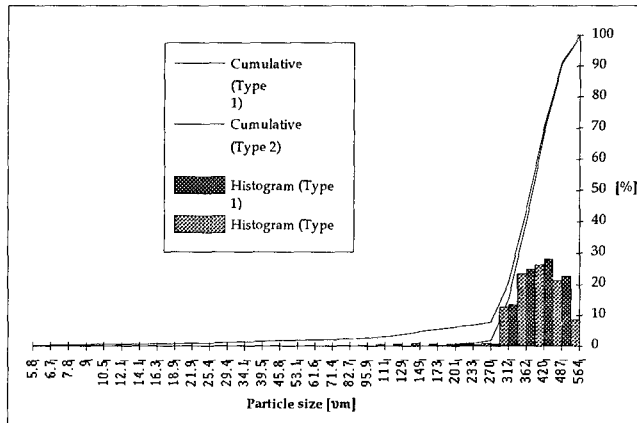
Figure 1 - Cumulative curve of used two types of sand.

3. Theoretical prediction of incinerating regime and gas products composition

The theoretical prediction of incineration products has been performed using THOR code, based on theoretical work of Heuzé et al. ,1985, 1989, and later modified by Campos, 1991. Several kinds of equations of state can be used, namely BKW, Boltzmann, JCZ3 and H9. This THOR code uses now a new EoS (Durães et al., 1995) with the same assumptions of a Boltzmann EoS, but based now on physical intermolecular potential of gas components instead of correlations from final experimental results.

The selection of product components are dependent of atomic initial composition. For a classical CHNO system it is assumed an equilibrium composition of CO_2, CO, H_2O, N_2, O_2, H_2, OH, NO, H, N, O, HCN, NH_3, NO_2, N_2O, CH_4 gases and two kinds of solid carbon (graphite and diamond). Reported data are from JANAF Thermochemical Tables, 1971 and polynomial expressions of Gordon and McBride, 1971. The solution of composition problems involves simultaneously:

- the thermodynamic equilibrium (thermal, mechanical and chemical equilibria), obtained with the mass and species balance, and the equilibrium condition $G=G_{min}$ (P,T,x_i), applying to the condensed phase the model proposed by Tanaka , 1983,

- the thermal equation of state (EoS),

- the energetic equation of state, related to the internal energy $E = \Sigma x_i e_i(T) + \Delta e$, $e_i(T)$ being calculated from JANAF Thermochemical Tables, 1971, and polynomial expressions of Gordon and McBride, 1971,

- the combustion regime, being P constant for the isobar adiabatic combustion (equal initial and final total enthalpy $H_b^{Tb} = H_o^{To}$).

The proposed equation of state is based on the same assumptions of $H\alpha$ EoS, proposed by Heuzé et al. , 1985, taking the general expression

$$\frac{P\ V}{n\ R\ T} = \sigma\left(V,\ T,\ X_i\right) \tag{1}$$

where V represents the volume, T the temperature and X_i the mass fraction. The second term, σ, represents a fifth order polynome derived from a Boltzmann EoS, traducing very well the behaviour of gaseous mixtures at high temperatures and pressures:

$$\sigma\left(V,T,X_i\right) = 1 + x + 0.625 x^2 + \\ + 0.287 x^3 - 0.093 x^4 + 0.014 x^5 \tag{2}$$

with

$$x\left(V,\ T,\ X_i\right) = \frac{\Omega}{V\ T^{3/\alpha}} \qquad (3) \qquad\qquad \Omega = \sum_{i=1}^{n} X_i\ \omega_i \qquad (4)$$

The α represents the exponent of the intermolecular potential. Heuzé et al., 1985, has proposed for α the values 9 and 12, based on theoretical and experimental final correlations. The values of ω_i are also dependent of each gas component. Their values are independent of the chosen α constant. The H_L EoS takes to α the value of 13.5 (Durães et al., 1995).

This THOR code allow to predict the influence of the decomposition mechanism of endothermic dissociation of ammonium nitrate $NH_4NO_3 \rightarrow HNO_3 + NH_3$, in the incineration regime, calculating the combustion temperatures and Gibbs free energy, as a function of concentration of formed NH_4NO_3/ HNO_3 (vd. Figure 2).

The influence of products concentration is shown in Figure 3, proving the influence of transient products composition as a function of obtained incineration temperature. Consequently the transition incineration temperature is near 800 K.
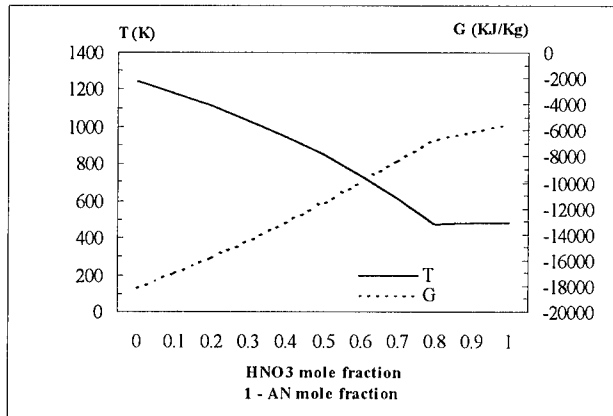
Figure 2. Calculated comb. temp. and Gibbs free energy, as a function of concentration of formed NH_4NO_3/ HNO_3.
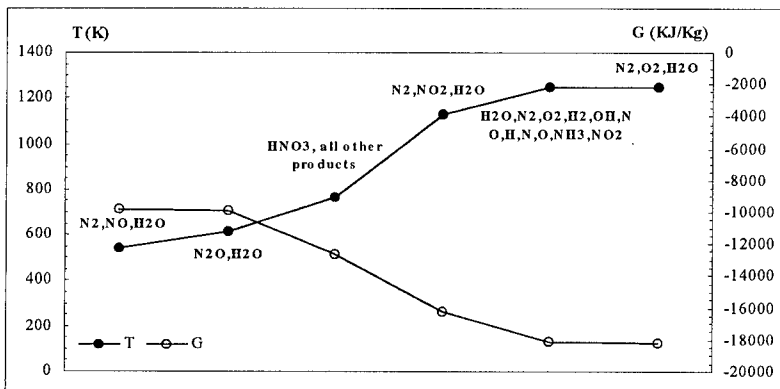

Figure 3. The influence of products concentration as a function of obtained incineration temperature and Gibbs free energy value.

The combustion composition of the combustion products of each explosive is almost the same independently of EoS used (vd. Campos, 1991). The calculated temperatures are 1994, 2241 and 2459 K respectively for emulsion, ANFO and dynamite explosives. The CO and NO emission levels are higher than those calculated for detonation regime, in good agreement with theoretical predictions (vd. Campos, 1991).

4. Incineration fluidised bed equipment and results

4.1. Fluidised bed equipment

An original fluidised bed combustion system was designed and built to incinerate selected explosives. It has a nominal power of 750 kW and it is composed by (vd. Figure 4):

    – a fluidised bed of constant height;

    – a slurry feeding twin screw system;

    – a pressure and temperature control with a real time data acquisition system;

    – a separation and filtration system for the gas combustion products;

    - a wet scrubber and an exhaust gas system close the combustion cycle.

The combustion chamber made of stainless steel is composed of four parts: a fluidised bed incineration chamber, outlet tubes for the solids, a TDH (transport disengaging height) chamber and an outlet conduct system for the combustion gases. The incineration chamber consists of an elutriator of internal diameter of 266 mm and is 300 mm high, which is wrapped by a water cooled liner. The fluidised bed combustion system is permanently warmed by the injection of a propane-air mixture as fluidising gas. Three thermocouples measure the temperature inside the bed. There is another thermocouple placed in the freeboard. Four tubes, for the discharge of sand and solid products, keep the height of fluidised bed constant. These tubes will be linked to the slurry feed system in a close circuit.

A chimney for the exhaust of the combustion gases is placed in the upper part of the chamber over the TDH chamber. The TDH chamber, made of stainless steel, has an internal diameter of 266 mm and is 735 mm high. It is also wrapped by a water cooled liner. Finally the exhaust gas system is composed by a cyclone, a mechanical filter and a wet scrubber. Dräger tubes were used in the preliminar analyses of NOx, CO and CO_2.

The energetic material feeding system is formed by a twin screw extruder for solids. To avoid the formation of slurry dunes in the connection tube, between the extruder outlet and the incineration chamber inlet, an entry of air was connected to the part of extruder outlet. Two sonic flow meters ensure the rigorous control of air and propane flows.
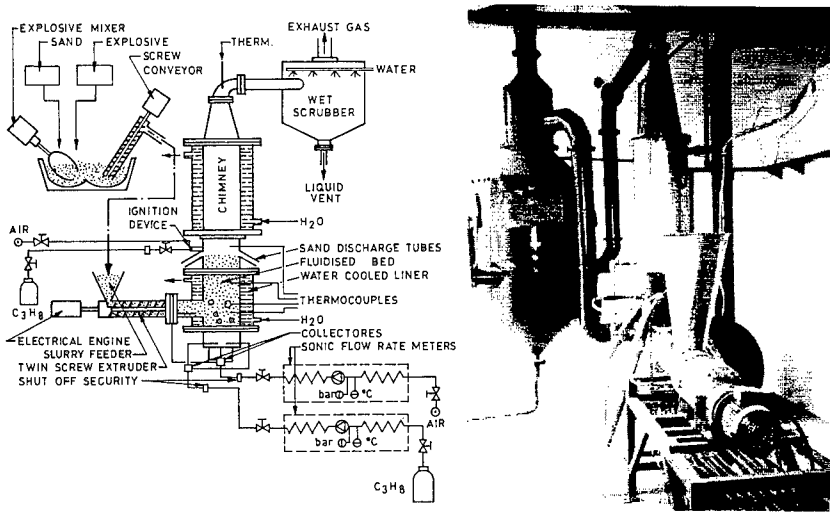
Figure 4 - Fluidised bed incinerator equipment.

The control and safety systems of the incinerator are composed by (vd. Figure 5):

     – a real time data acquisition temperature system, composed by a analogue digital converter (IBM GPIS 3D equipment) and a personal computer;

     – velocity control of the extruder changing rotating speed of driving motor;

     – ignition device composed by a vortice propane/air flame;

     – water cooling system;

     – opening outlet tubes.

The design values and calibration curves have been presented in a previous work (vd. Pires and Campos, 1993). The theoretical velocity for used mean particle of 350 μm is about 0.12 m/s and the theoretical superficial gas velocity is about 0.41 m/s. The design values of the chamber are presented in the next Table 1.

Figure 5 - Control systems

Table 1. - Design values

Superficial gas velocity, U [m/s]	0.413
Terminal velocity, U_t [m/s]	11.800
Minimum fluidization velocity, U_{mf} [m/s]	0.12
Bed height at incipient fluidization, H_{mf} [m]	0.3
Bubble diameter, D_b [mm]	147.3
Number of bubbles rising the top of the bed, per second, N	9.8
Bubble velocity, U_b [m/s]	0.303
Pressure drop across fluidized bed, ΔP [mm H_2O]	477.340
Residence time [min]	~ 15

4.2. Experimental conditions and results of incineration of ammonium nitrate base explosives

Experimental bubble diameter, at the surface of bed, measured between 0.9 and 0.12 m, which shows a good agreement with the theoretical value (d ≈ 0.15 m). The experimental combustion conditions are shown in Table 2.

Table 2. - Experimental combustion conditions

Static bed height, [mm]	300
Diameter of the bed[mm]	266
TDH chamber [mm]	735
Average silica sand size, d_{50} [µm]	377.7

There are two phases in a normal operation – the transient warming regime at the beginning and a permanent regime during its effective work. In the transient regime the aim is to heat the sand bed. The combustion of the mixture of the fluidising gas (air and C_3H_8) heats the sand bed while the refrigeration circuit protects the chamber from any possible overheating. Throughout all tests the sand bed was initially heated above 520 K. The freeboard temperature was kept between 680 K and 880 K (vd. Figure 6).
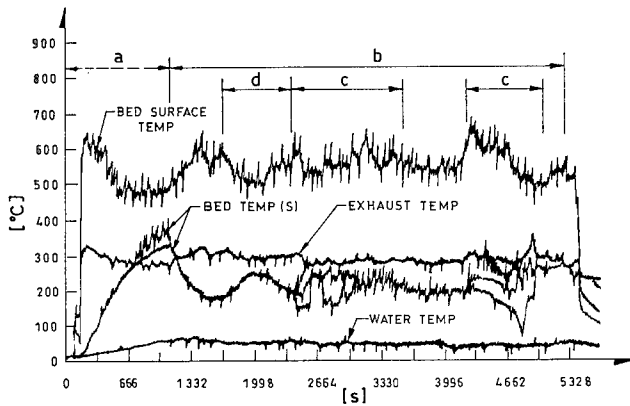
Figure 6 - Fluidised bed combustion temperature as a function of time (Emulsion explosive incineration).

When nominal designed temperatures are attained (vd. Figure 6,–a–), inside the chamber, the extruder gradually begins to send a mixture of sand and emulsion explosive (vd. Figure 6,–b–), while the flowing of C_3H_8 is being gradually reduced. It is necessary to take a special care with slurry mass flow feed in order to avoid the formation of big aggregates inside the fluidised bed (vd. Figure 6,–c–). Comparing the incineration of emulsion explosive and ANFO, it is possible to observe in the second case, the total homogeneity temperature inside the bed (vd. Figs. 6, –b–and 7, –b–). Meanwhile the sand that fills the chamber is expelled through the discharge tubes. Then the energetic material feeds the combustion chamber and the permanent regime is attained. When the incineration of energetic material starts the temperature inside the chamber rises (vd. Figure 6,–d–).

When the incineration is finished we must feed the combustion chamber with clean sand to avoid any pack aggregated slurry.
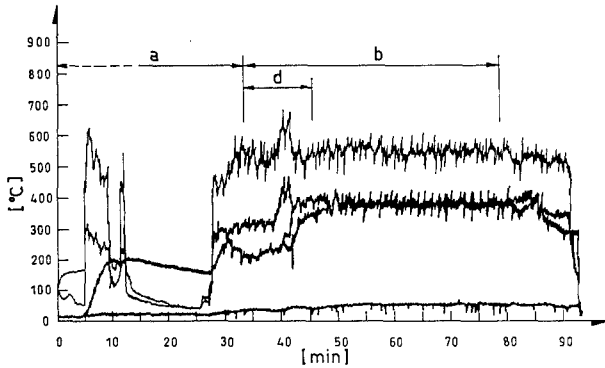
Figure 7 - Fluidised bed combustion temperature as a function of time (ANFO explosive incineration).

During the incineration of ANFO the freeboard temperature is slightly above the bed temperature ($100 - 150°C$). However during the incineration explosive emulsion, the temperature in the freeboard is about 300 K higher than the bed temperature. It reveals the importance of the water content in emulsion.

The water concentration in explosive emulsions causes two phenomena: one is the decreasing of the bed temperature; the other is the formation of big aggregates inside the fluidised bed. The incineration process for ammonium nitrate based explosives is possible only at temperatures above 520 K, because its decomposition only happens at high temperatures. For that reason it is necessary to reduce drastically the mass flow feed of explosive emulsion.

In the chimney the emission of nitrogen oxides is about 20 ppm for explosive emulsion (3%) and more than 100 ppm for ANFO (15%). The reason why there is a big concentration of nitrogen oxides during the incineration of ANFO is related with the dominant source of NO_x – the "fuel" nitrogen. Other reasons for that are the high mass flow feed and the high rate of destruction of ANFO. The CO emissions are about 75 ppm for explosive emulsion (3%) and more than 275 ppm for ANFO (15%). The emissions can be reduced with the perfect control of the air excess.

Measured products concentration of NO_x, CO and CO_2, of same tests, are presented in Figure 8.
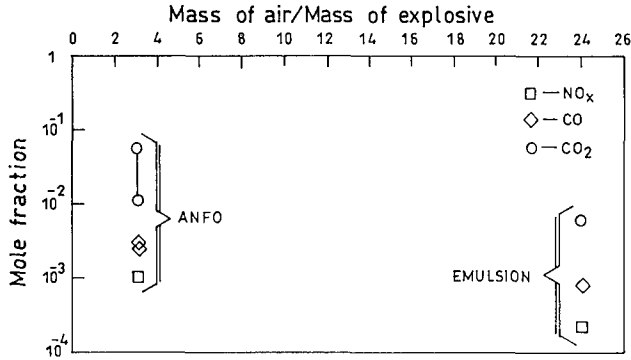
Figure 8 - Measured concentrations of NO_x, CO and CO_2

The analysis of the sand after the combustion reveals a complete decomposition for all the explosive tested; in the explosive emulsion, however, the ammonium nitrate is not entirely decomposed.

5. Conclusions

An original fluidised bed combustion system has been designed and built in order to incinerate the most common used explosives, based in ammonium nitrate compositions. It is composed by a fluidised bed, warmed by the combustion of a propane-air mixture as fluidising gas. A wet scrubber and an exhaust gas system close the combustion cycle. The gas products composition and incineration regime can be predicted by THOR computer code. There are two regimes of incineration: the warming transient regime and constant incineration regime. Obtain real temperatures are stable near 770 K in a good agreement with theoretical predictions. This equipment proves to be a safe and programmable incineration system for industrial explosives.

References

Campos, J., (1991). Thermodynamic Calculation of Solid and Gas Combustion Pollutants using Different Equations of State, *First International Conference on Combustion Technologies for a Clean Environment*, Vilamoura, Portugal

Campos, J., Pires, A., Gois, J. C., Portugal, A., (1993). Gas Pollutants from Detonation and Combustion of Industrial Explosives, *Second International Conference on Combustion Technologies for a Clean Environment*, Vilamoura, Portugal.

Demilitarisation Technology, (1991). *International Seminar on Demilitarisation Technology for Explosives and Explosive Ordnance,* Royal Military College of Science and Directorate of Land Services Ammunition, Oxfordshire, U.K. .

Durães, L., Campos, J., Gois, J. C., (1995), "Deflagration and detonation predictions using a new equation of state", in *Proc. of the 26th International Annual Conference of ICT,* pp. 67.1-67.13.

Folk, F., (1990). Analysis of Reaction Products of Propellants and High Explosives, *Chemistry and physics of energetic materials,* Nato ASI Series, Kluwer Academic Press.

Gordon, S., Mc Bride, B.J. (1971). *Computer Program For Calculation of complex Chemical Equilibrium Compositions, Rocket Performance Incident and Reflected Shocks and Chapman-Jouguet Detonations.* Report NASA SP 273, NASA Lewis Research Center.

Heuzé, O., (1989). *Cálculo Numérico das Propriedades das Misturas Gasosas em Equilíbrio Termodinâmico,* Universidade de Coimbra, Portugal.

Heuzé, O., Presles, H. N., Bauer, P., (1985). Computation of Chemical Equilibrium, *J. Chem. Phys.*, n°83 (9), pp.4734-4735.

JANAF, (1971). *Thermochemical Tables* - 2nd Edition. National Bureau of Standards, Washington D.C.

Jupp, M. F., (1991). An Assessment of the European Demilitarisation Scene, *International Seminar on Demilitarisation Technology for Explosives and Explosive Ordnance,* Royal Military College of Science and Directorate of Land Services Ammunition, Oxfordshire, U.K..

Pires, A. and Campos, J., (1993). Clean Combustion of Energetic Materials in a Fluidised Bed, *Second International Conference on Combustion Technologies for a Clean Environment*, Lisboa, Portugal.

Portaria (1993), nº 286/93 de 12 de Março, Portugal.

Tanaka, K. (1983). *Detonation Properties of Condensed Explosives Computed Using the Kihara-Hikita-Tanaka Equation of State*. Report from National Chemical Laboratory for Industry, Ibaraki, Japan.

COMBINED METHODS FOR DIAGNOSTICS OF BURNING PRODUCTS COMPOSITION IN FLAME

Sergey A. Korotkov, Victor P. Samsonov

Chuvash State Pedagogical Institute, K.Marx st.38
428000, Cheboksary, RUSSIA

The methods have been developed to study a flame structure and an incomplete combustion of gases and gasified solid fuels when the complex structural flows were forming in the flame.

Two diagnostics methods are proposed. One of them is the combination of the spectrometric method and the method of the convective precipitation of the burning products on the cold surface. It consists in spectrometric studying of the sediments of the flame trace on the heat-conducting (ceramic) surface where chemical reaction freesing occurs. The way of taking of small samples of the burning products (sediments) is developed for subsequent entering them into an electric arc of an spectrometer illuminator. The resolving power of the method is limited by the two-dimensional scale of the sample.

The second method consists in studying of an electrostatic field of the trace and measuring of electric conductivity of separated regions of the trace. All the measurements are made by the method of the current in a low conducting medium. A metal needle is used as a sonde. The dimensional resolving power of this method is limited by a diameter of a sonde. If the electrical properties of the products forming in the chemical reaction are known, it is possible to find out its existance and calculate its concentration in the corresponding zone of the flame. The measured values of a trace region conductivity are integral

and those are due to existance of the several components. The algorithm of the transition from the integral values of conductivity to the differential ones and then to the concentration of substance is proposed.

Both these methods complement the hydrodynamical method of the convective precipitation of burning products from gase phase on the surface in those cases when the thickness of the layer is too great and an interference pattern cannot be obtained.

These methods were tested in the cases of the diffusion propane flames and the model mixed solid fuel flames when the sequence of the "brutto-reactions" is assumed to be known.

The hydrodynamical method of the convective precipitation of the combustion products on the heat conducting wall formes the basis of some other combined method for diagnostics of the flame structure. If the speed of the burning products is not great and heat capacity of the wall is great enough freezing of the chemical reactions occurs on the wall [1]. The flame trace on the wall can have a great resolving power. The example of such a trace is shown in Fig.1. It is possible to separate several zones on the flame trace, those correspond to various stages of the chemical transformation if the velocity field is known. The further investigation of the chemical reactions process can be made by analysis of the burning products composition applying other physical methods.

The main aim of the spectrometric tests is the indentification of the expected chemical compounds and the measurement of their concentration in the studied soot layer. The basic problem of the spectral analysis is the question about the sensitivity limit of the identification method [2]. When studying the absorption spectrum the light sources having

Fig.1

the continuous spectrums or monochromatic light sources are usually used. The frequency change must be performed over as wide range as possible. The sensitivity of the method is defined by proportion of the radient ehergy absorbed in some spectral interval: $\Delta = (I_o - I_1)/I_o$. Here I_o and I_1 are the intensities of incindent light and light passed through the absorbing layer. The scheme of the experimental installation is shown in Fig.2. The experimental installation contains the following basic elements: 1 - the micrometric table, which can be rotated relatively studied sample 2 in the angle interval $0 \div 2\pi$; 3 - the light source connected with the micrometric table; 4 - the control unit; 5 - the detector; 6 - the registering block; The advantage of such a scheme is the possibility to study the scattering spectrum simultaneously with the absorption spectrum and the following simulation of the surface shape of the studied soot trace. The relative disposition of the light source and detector is controled by the computer program.

The thickness of the soot trace layer was so small that
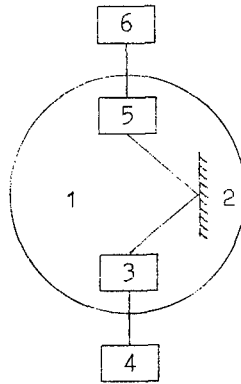
Fig.2

the number of the studied substance molecules was very few and that is why the value Δ was also small. At this reason the scheme of the experiment can be complicated to obtain light passing repeated many times. Then it is possible to record the absorption spectrums for definition of the expected elements of substance.

The decisive factor determinating the sensitivity limit of the spectrometric identification method based on the emission spectrum is the sensitivity of the device detecting the radiation. At present this problem is decided for many ranges of the infrared, visual and ultraviolet radiation [3]. The scheme of the installation that allows to obtain the emission spectrums is presented in Fig.3. Here the thin sonde 1 (electrode) is installed on the micrometric table. It can be moved over the studied trace 2 of burning products The installation can be located inside a vacuum chamber at the pressure about 10^{-5} Torr. The discharge is initiated in a location place. The type of the discharge (spark one,
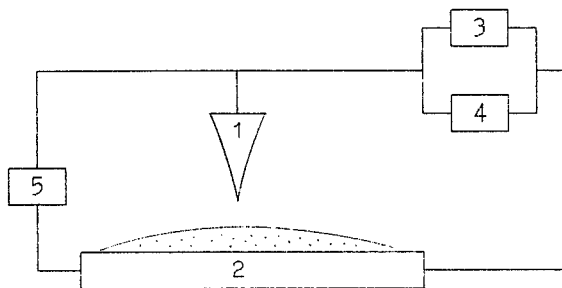
Fig.3

glow one or arcover) and the conditions determining the dis-
charge are controled by the computer.

The various types of the discharges can be controled by
circulation through the discharge area of the different
inert gases. A count of the radiated quantums does not offer
any scope to define the absolute concentration of any subs-
tances. It is possible only to evaluate the concentration of
the excited substance molecules. The discharge fashion rea-
lizes the high degree of the molecules excitation factor and
supplies obtaining of the concentration distributions for
the expected substances in the soot trace.

The precipitation of the burning products was carried
out on the flat ceramic plate to realize the method of elec-
trostatic field. The soot trace is badly electric conductive
medium. Retaining standard electrodes against the soot trace
we obtain some electrostatic cell. The investigation of the
potential distribution in the electrostatic field has shown
that the force lines configuration substantially differs

from the standard one at uniform electric conducting medium.
It is due to nonuniformity of the soot trace. The trace is
nonhomogeneous in the thickness and physical properties in
the separate zones. The nonuniformity is due to the non-
equilibrium soot formation process in the flame. The soot
particles are formed as a result of a complex process inclu-
ding the embrio formation, particle growth and agglomeration
of the particles. At this reason the electric conductivity
of the separate sections of the trace is defined by charac-
ter of the chemical reaction run at the combustion. In this
case the potential of an electrostatic field is not similar
to a current field. Really, the conditions for the current
density $\vec{j}$ on the badly electric conducting surface can be
written as follows

$$div \ \vec{j} = 0, \qquad \vec{j} = \sigma \cdot \vec{E}$$

Here $\sigma = \sigma(x,y)$ is the electric conductivity of the
trace. It is the function of the coordinates. Then we can
write

$$div\vec{j} = div(\sigma \cdot grad \ \varphi) = (grad \ \sigma \cdot grad \ \varphi) + \sigma \cdot \Delta\varphi = 0$$

The further information about the character of the che-
mical transformation in the flame can be obtained by measu-
ring of the electric conductivity of the separate sections
of the soot trace.

In this work the measured parameter was the current
between two sondes. The dependence of the current on the
distance from the diffusion propane flame front was investi-
gated. The sondes were two copper needles installed in the
dielectric holder. The diameter of the needle was 1 mm. The
distance between the soundes was 10 mm. The results of
measurements are presented in Fig.4.

The coordinate x was measured as a distance from the
flame front along the symmetry axis of the soot trace. The
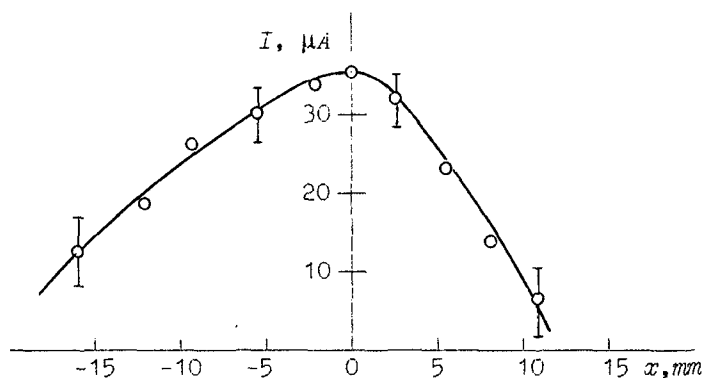sign of minus corresponds to the point inside the flame

Fig.4

cone.

If the electric conductivity of substance is known it is possible to find out its existance in studied point of the trace.

REFERENCES

1. Samsonov V. The hydrodynamical method to analyse the combustion products composition, concentration and temperature fields of the pyrotechnical fuel flame. 26th International Conference of ICT, Karlsruhe, 1995.

2. Malishev V.I. Introduction to experimental spectroscopy. Moscow, Nauka, 1979. (In Russian).

3. Skokov I.V. Optical spectral devices. Moscow, Mashinostroenie, 1984. (In Russian).

Temperature Profiles and Burning Rates of Pool Fires

V. Weiser; I.Franchin; N. Eisenreich

Fraunhofer-Institut für Chemische Technologie (ICT)
P.O.Box 1240, D-76318 Pfinztal 1 (Berghausen), Germany

Abstract

The heat transfer is the dominant mechanism of pool fire burning. For its modelling a one dimensional approach was applied which successfully described the comparable problem of solid propellants. In order to obtain the heat flows by radiation and conduction the fuel consumption rate and the temperatures profiles were measured, simultaneously. The fuels on investigations were methanol, nitromethan, 2-propanol, isooktane. The rate of the fuel consumption increases linearly with time due to the heating up of the pool. A least squares fit of the calculated temperature profiles to the measured curves indicates a continuous grow of the ratio of heat radiated to conducted heat.

Introduction

Chemical industry transports and stores large quantities of liquid fuels and chemicals. Accidents can lead to large fuel fires which endanger the environment by direct impact, the heat radiation and the emission of combustion and pyrolysis products [6].

Flames above liquids are sustained by the balance of evaporated, burning fuels and the heat feedback [4]. In addition, the energy transferred by conduction, convection and radiation heats up the fuel pool and increases the evaporated masses which is, in turn, feed to the flame [3, 5]. Overheating of the fuel leads to the ejection of flame balls which further form burning hotspots [1]. These effects prevent or hinder at least fire extinguishing. A pool heated above the flash point can only be quenched by air displacement with additional cooling of the pool.

The investigation described in the following aim at measuring the effects of pool heat up by heat feedback from the flame and the increase of the fuel consumption rate. The experimental data are discussed on the basis of an simplified model of the heat transfer of the flame and the pool.

Quasi-static energy balance in the fuel

Pool fires show a complicated structure which fluctuates strongly [9]. The diffusion flame above the surface also reduced to simplest shapes is rotational symmetry. The feedback of radiation to the pool can be assumed to be emitted from a disk [8] which transfer heat with approximated constant distribution near the pool centre.The fluctuations are fast enough (ca 5-10 Hz) to assume stationary condition with respect to the heat conduction within the pool. So being aware of the strong simplification a one-dimensional heat transfer within the pool is studied:

$$\Lambda\frac{\partial^2 T}{\partial x^2}+\left(c_p+h_v\delta\Delta T\right)\rho\frac{\partial T}{\partial t}=Q$$

The Dirac's delta function δ accounts for the enthalpy of evaporation taking place at a certain temperature at the phase boundary [2]. Q represents a general heat source. A quasi-static temperature profile $T(,x,t)=T(x)$ and surface regression rate r provided which means the heat up is slow with respect to the building of the temperature profile allows to substitute $\frac{\partial T}{\partial t}$ by $r\frac{\partial T}{\partial x}$. The indepth absorption of radiated heat is taken into account by an averaged absorption coefficient b of the liquid and an intensity q_R.

$$\Lambda\frac{\partial^2 T}{\partial x^2}+r\rho\left(c_p+h_v\delta\Delta T\right)\frac{\partial T}{\partial x}=q_R be^{-bx}$$

Integrating once with respect to x delivers the enery balance:

$$\Lambda\frac{\partial T}{\partial x}+r\rho\left(c_p\left(T(x)-T_0\right)+h_v\right)-q_R e^{-bx}=0 \qquad \text{for } x=0 \text{ (at the surface)}$$

and

$$\Lambda\frac{\partial T}{\partial x}+r\rho c_p\left(T(x)-T_0\right)-q_R e^{-bx}=0 \qquad \text{for } x>0 \text{ (in the fuel)}$$

The boundary conditions assume that the surface is at boiling temperature T_b and the temperature gradient is given by the heat conducted heat q_L:

$$T(x=0)=T_b \qquad \text{und} \qquad \Lambda\frac{\partial T}{\partial x}\bigg|_{T=T_b}=q_L$$

The integration of the equations yields the temperature profile in the pool:

$$T(x)-T_0=\frac{q_L}{m''c_p\exp(\frac{m''c_p}{\Lambda}x)}+\left(\frac{1}{m''c_p-b\Lambda\exp(bx)}-\frac{\frac{b\Lambda}{m''c_p-b\Lambda}}{m''c_p\exp(\frac{m''c_p}{\Lambda}x)}\right)q_R \quad (1)$$

The first term is obtained also by omitting the heat flux by radiation q_R.

Experimental set up

The experiments were performed in a cylindrical pool (113 mm diameter, 40 mm height) using a automated fuel supply to substitute consumed fuel (fig. 1). The level of the liquid surface was kept constant by a Mariotte's bottle (diviation from its mean value < 0.5 mm) at a position 1 mm below the top of the pool container. The weight of the fuel reservoir was continuously measured (+/- 0.1 g) to obtain the fuel consumption and the burning rate using a PC based data acquisition unit. The fuel flow to the pool was low (0.2 ml/s) that it did not influence the temperature of the pool substantially. The fuel supply was placed in a distance of 20 mm from the positions of temperature measurement. An array of 8 thermocouples (NiCrNi, diameter 1 mm) recorded the axial temperature profiles at various positions below the pool surface. These positions were 1, 5, 10, 20, 25, 30 and 35 mm. The thermocouple array was scanned every second band the data stored in the data acquisition unit. Depending on the fuel type the time period for measurement was 10 to 30 min starting at room temperature. The experiment was stopped on the observation of bubbles indicating beginning boiling of the whole pool. At that event convection would play a significant role which is assumed to be of minor influence before as only little movements are observed within the pool.

The fuels on investigations were methanol, nitromethane, 2-propanol, isooktane physical and thermodynamic data of these fuels are listed in table 1.

Although the data do not differ within orders of magnitude the flames emit strongly different radiation spectra [7]. Methanol burns with a blue flame and emits mainly bands of water and carbon dioxide. The other fuels show additionally continuous spectra with increasing intensity from nitromethane to iso-octane. The continous radiation is emitted by the soot particles.

Results

Burning Rate

The mass related burning rate m'' (kg $s^{-1}m^{-2}$) is obtained from the weight loss curve of the fuel reservoir by differentiation and deviding by the surface area of pool. Fig. 2 and tab. 2 show the measured weight loss curves and the burning rates in dependence of the different fuels. The weight loss increases with time. Parabolic curves approximate closely the experimental data as found by a least squares fit. This means: the burning rate increases linearly with time. Deviations at the begin of the experiments are caused by the time lag of the fuel supply.

Heating of the Pool

Fig. 3 shows a temperature history of the pool heating for the fuel 2-propanol. Close to the surface (x = 1 mm) the temperature rises close to the boiling point within seconds after ignition. Near the bottom of the pool the temperature begins to rise after some minutes followed by fast grows which is lower towards the bottom of the pool. Till the end of the experiments the temperatures in the pool attend to the boiling temperature, assymptotically.

Temperature Profiles

The temperature profiles of the heating phase of the pool are plotted in fig. 4 at various times. After ignition the temperature profiles are of a linear shape. Later, when the fuel is partially heated up, they become sigmaoid form with a point of intersection. Qualitatively, this indicates that flame radiation dominates the energy transfer with respect to heat conduction. The progression of the heat up of the fuel flattens the temperature gradients so reducing the heat conduction.

The temperature profiles $T(x)-T_0$ described by Eq. 1 depend on c_p, Λ, m'', q_L, q_R, b. The values c_p and Λ are well known constants listed in tab. 1. The burning rate m'' was measured simultaneously. q_L and q_R are unknown and their independent measurement is difficult. The sum of both (the total heat transfer from the flame to the pool) can be found from a global energy balance and from the burning rate. The heat losses of the fuel to the container and the environment are neglected. The results of the estamated heat transfer are listed in tab. 3. The absorption coefficient b is an averaged value which has to be estimated from the overlap of flame emission $I_{fl}(\lambda)$ and absorption bands $b(\lambda)$ of the fuels. Only in the case of a dominant absorption band of the fuel or emission band of the flame, it can be clearly assigned to that wavelength. In principle the absorption of the radiation absorption in the pool can be described by:

$$q_R(x) = \int I_{fl}(\lambda) e^{-b(\lambda)x} d\lambda$$

In the following is assumed for simplicity that $b(\lambda)$ can be approximated by one value b.

The measured temperature profiles allow to obtain conducted and radiated energy as well as the averaged absorption coefficient by a leasts squares fit of (1) to the experimental data. q_L, q_R and b were used as fit parameters. The calculated curves with the best fit parameters are shown in fig. 4 (solid lines).

Discussion

The calculated curves agree with the experimental temperature profiles quite well. This indicates that the heat transfer model expressed by (1) and the related approximations describe the situation sufficiently correct. The values of q_L, q_R und b vary strongly depending on the fuels and on the time which is obvious from fig. 5. As expected, the heat transfer by conduction decrease close to zero till the end of the experiment because of the heat-up of the pool. Complementary, the heat transfer by radiation increases. The total heat flow remains constant or increases slightly. The sum of both energy transfers give the same order of magnitude as estimated from the energy balance and the burning rate (see tab. 3).

The dominance of the heat conduction at the beginning of the experiments is also confirmed by the values of b. b starts with a value expressing the fact that heat absorption direct on the surface cannot, in general, be distinguished from heat transfer by conduction, there. Later b falls to an asymtotic value. The continuous decrease could be explained by the increase of evaporated fuel with time. This higher amount of fuel absorbs more radiation (blockage effect) and can influence the averaged absorption coefficient. It should also be taken into account that at the beginning the temperature profiles are not as static as asumed in the model and experimental errors have more influence due to the time response of the thermocouples.

Literature

[1]   Bagster, D. F.; Pitblado, R. M.; Thermal hazards in the process industry; Chem. Eng. Prog., 85(7), 69-75 (1989)

[2]   Eisenreich, N.; Vergleich theoretischer und experimenteller Untersuchungen über die Anfangstemperaturabhängigkeit der Abbrandgeschwindigkeit von Festtreibstoffen; ICT-Bericht 8/77

[3]   Hamins, A.; Fischer, S. J.; Kashiwagi, T.; Klassen,Heat feedback to the fuel surface in pool fires; M. E.; Gore, J. P.; Combust. Sci. Technol. (1994), 97(1-3), 37-62, 2 plates CODEN: CBSTB9; ISSN: 0010-2202; English

[4]   Hertzberg, M.; The theory of free ambient fires. The convectively mixed combustion of fuel reservoirs; Combust. Flame 21, 195-209 (1973)

[5]   Nakakuki, A.; Heat transfer in small scale pool fires; Combust. Flame (1994), 96(3), 311-24

[6]   Schönbucher, Axel; Brötz, Walter; Balluff, Christoph; Goeck, Dietmar; Schieß, Norbert; Erforschung von Schadenfeuern flüssiger Kohlenwasserstoffe als Beitrag zur Sicherheit von Chemieanlagen; Chem.-Ing.-Tech., 57(10), 823-34 (1985)

[7]   Weiser, V.; Weindel, M.; Hoffmann, A.; Eckl, W.; Eisenreich, N.; Spectral Emission from Pool Fires of Various Fuels - Considering Transient Structures; 26th International Annual Conference of ICT, 1995, Karlsruhe, pp. 79-(1-9);

[8]   Weiser, V.; Eisenreich, N.; Heat Feedback in Model-Scaled Pool Fires; 8th International Symposium on Transport Phenomena in Combustion, 1995, San Francisco; p. 8-C-2

[9]   Eckl, W.; Eisenreich, N.; Weiser, V.; Schnelle Temperaturmessverfahren in pulsierenden Tankflammen; 24th Int. Ann. Conf. of ICT 1993, pp. 68-(1-14)

Table 1 Physical fuel properties

	Einheit	Methanol	Nitromethan	2-Propanol	Isooktan
Molecular weight	kg/mol	$32.042*10^{-3}$	$61.040*10^{-3}$	$60.096*10^{-3}$	$114.232*10^{-3}$
Density ρ	kg/m^3	787	1130	786	692
Heat conductivity Λ	W/(mK)	0.202	0.195	0.157	0.131
Boiling point T_b	K	337.8	374.5	355.5	372.5
Specific Heat c_p	J/(kg K)	$2.547*10^3$	$1.750*10^3$	$2.579*10^3$	$2.066*10^3$
Heat of vaporation h_v	J/kg	$1102*10^3$	$556.8*10^3$	$663.1*10^3$	$269.5*10^3$
Net calorific value h_c	J/kg	$22.75*10^6$	$11.62*10^6$	$33.46*10^6$	$47.77*10^6$

Table 2 Burning rates as linear function of time

$m_1 + m_2 t$		Methanol	Nitromethan	2-Propanol	Isooktan
m_1	10^{-3} kg s^{-1} m^{-2}	12.25	20.67	11.10	10.00
m_2	10^{-6} kg s^{-2} m^{-2}	0.351	2.905	1.173	7.00

Table 3 Approximation of heat flux transfered from flame to fuel

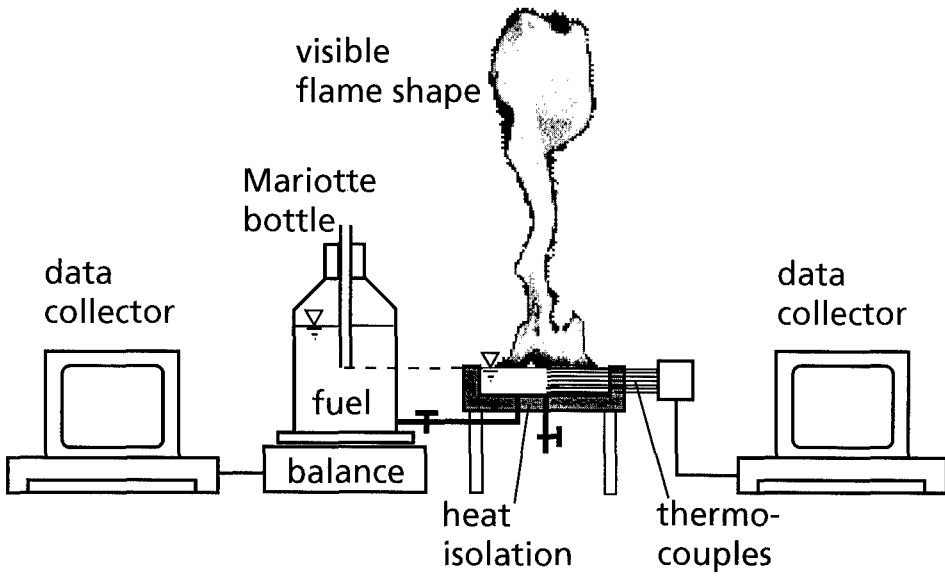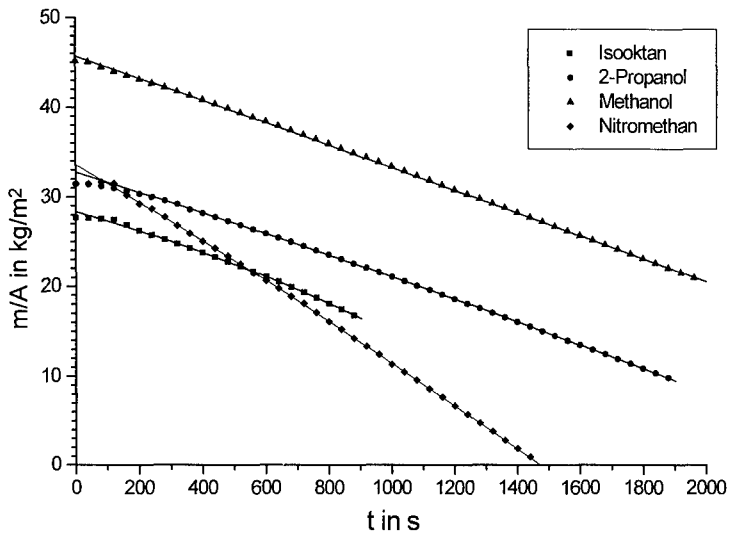| Symbol	Time	Unit	Methanol	Nitromethan	2-Propanol	Isooktan
Approximation by $q = m'' c_p dT_i/dt$						
q	300 s	W m^{-2}	2500	3500	2500	2500
q	600 s	W m^{-2}	1500	2000	1500	1500
Fit at axial temperature profil (Eq. 1)						
q_L	300 s	W m^{-2}	200	2100	500	800
q_R	300 s	W m^{-2}	1100	1600	1200	1300
$q_R + q_L$	300 s	W m^{-2}	1300	3200	1700	2100
$q_R + q_L$	600 s	W m^{-2}	1300	3300	1700	2500

Figure1 Experimental set-up

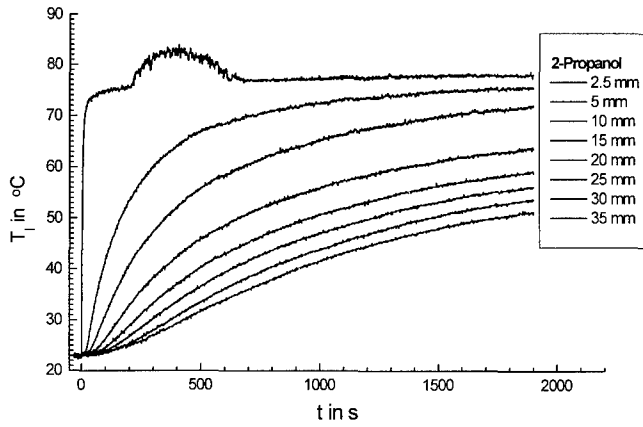Figure 2 Weight loss of fuel divided by surface area of pool

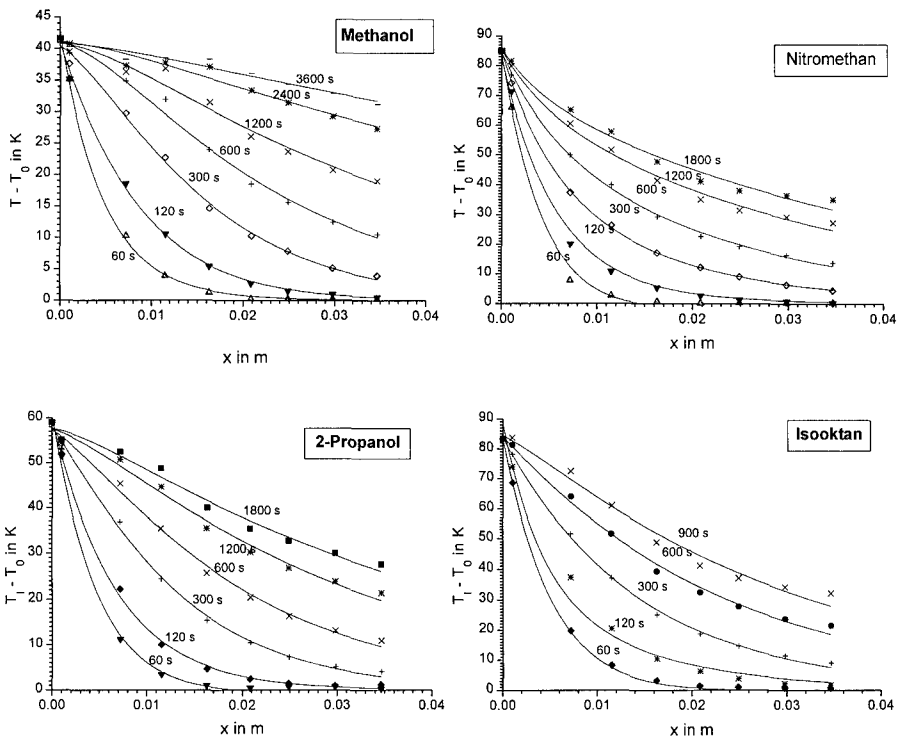Figure 3 Heat-up curves in the fuel at different axial positions (2-Propanol)

Figure 4 Temperature profiles in the fuel during the heating phase (points) and fit with eq. 1
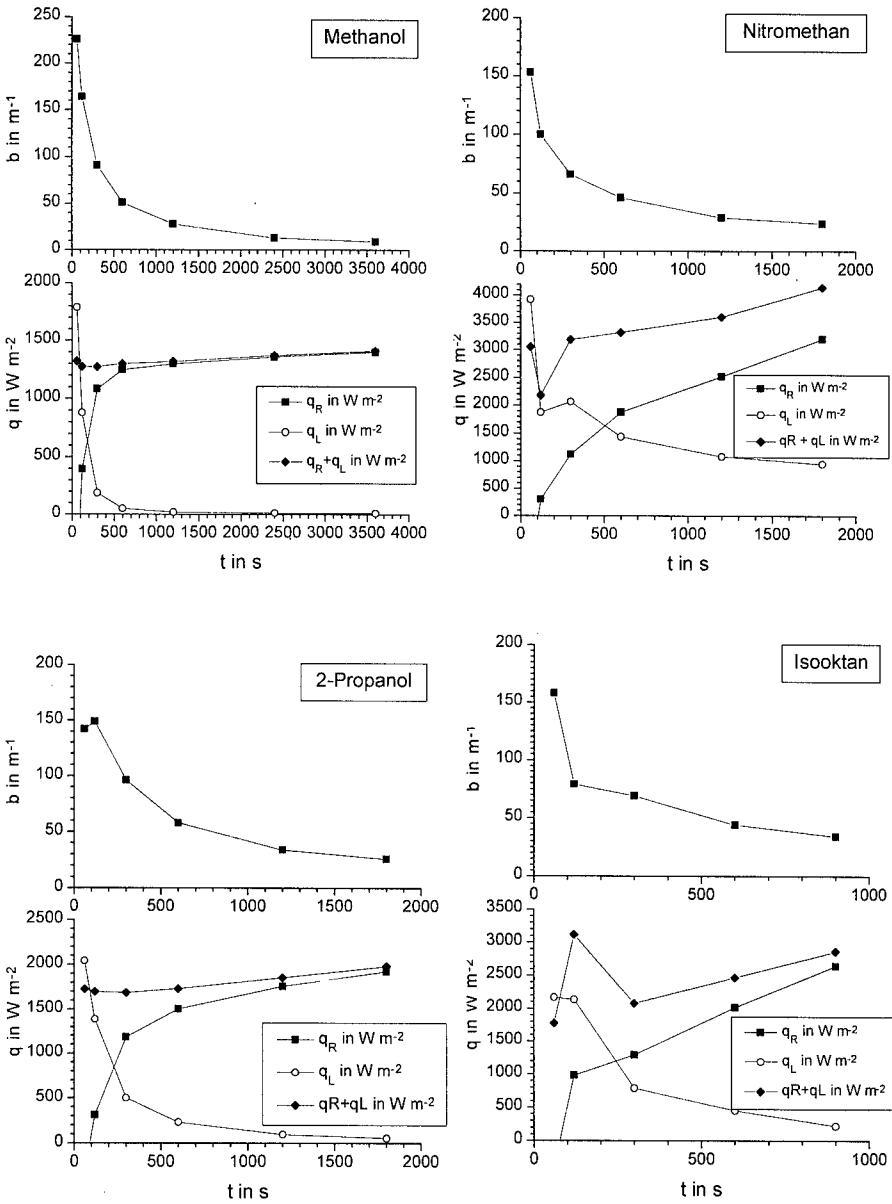
Figure 5 Best fit parameters

CHEMICAL KINETICS IN THE IGNITION DELAY OF AP/NSAN/INERT BINDER COMPOSITE PROPELLANTS

Octávia Frota

Laboratory of Energetics and Detonics, Av. Universidade de Coimbra

3150 Condeixa - Portugal

Luís Araújo

National Institute of Engineering and Industrial Technology - Combustion Technologies Dpt.

Az. dos Lameiros, Est. Paço do Lumiar - Ed. J1 - 1699 Lisboa, Codex - Portugal

Abstract

Partial substitution of ammonium perchlorate by non-stabilised ammonium nitrate as oxidiser component in composite propellants is an alternative solution for applications where a significant reduction of the emission of acid components is of concern, and high specific impulse is not a determinant parameter. This communication concerns the dependence of the ignition delay of AP/NSAN/Inert Binder solid composite propellants on temperature and weight content of ammonium nitrate. Several AP/HTPB and AP/Polyurethane (PU) based compositions, with increasing NSAN weight contents, were submitted to constant heating, until ignition occurred.

The results obtained, that confirmed the expected increment of the ignition delay when the temperature of the surrounding gas is decreased, also showed that in both types of propellants increasing weight contents of non-stabilised ammonium nitrate originate shorter values of $\tau_i(T)$.

The theoretical analysis of the ignition delays provided additional evidence of the existence of two alternative, temperature dependent, rate determining mechanisms of ignition, with different activation energy and β factor. The characteristic values of E, β and of the transition temperature were calculated, enlightening the fundamental role of the thermal degradation of NSAN in the ignition of this type of composite propellants.

Introduction

Significant efforts are been undertaken in the field of rocket propulsion aiming the development of a new generation of less polluting propellants, with low signature and reduced sensitivity to shock and thermal stimuli. In fact, the exhaust gases resulting of the combustion of composite AP based propellants include a large amount of hydrogen chloride, as well as some other chlorine components, which are the main source of high levels of toxicity for most living forms and equipment corrosion damages [1]. Furthermore, the formation of hydrochloric acid, by combination of hydrogen chloride with atmospheric water vapour, is the origin of visible and infrared optically dense secondary smoke, which is a major inconvenient for military applications [2].

Partial substitution of ammonium perchlorate by non-stabilised ammonium nitrate as oxidiser component in composite propellants is one of the possibilities under study for some time at the Laboratory of Energetics and Detonics [3 - 4]. The use of non-stabilised ammonium nitrate (NSAN) is not free of problems, namely the contribution to the depletion of the ozone layer by the formation of NO_x compounds, its high hygroscopicity, the existence of crystalline phase transitions with important volume changes and the low I_{sp} of NSAN/Inert Binder composite propellants. Nevertheless, one must consider that the absence of chlorine in NSAN composition and its low sensitivity to impact and friction make this component an attractive oxidiser candidate for those applications where increased insensibility and a significant reduction of the emissions of acid compounds, specially HCl, is of concern and high specific impulse is not a determinant parameter.

This work concerns the ignition characteristics of AP/NSAN/HTPB and AP/NSAN/PU composite propellants. Several compositions, with increasing NSAN weight contents, were submitted to constant heating, in ambient air and at atmospheric pressure, until ignition occurred.

The analysis of the ignition delays, in function of temperature and NSAN weight content, provided additional evidence of the existence of two alternative, temperature dependent, rate determining mechanisms, characterised by different E and β factor, which characteristic values were calculated, as well as the transition temperatures.

The results also enlightened the fundamental role of the thermal degradation of NSAN in the ignition of this type of propellants.

Experimental

Propellants test samples - Composition and Preparation

All the compositions were formulated with 80 % weight of solid oxidant charge and 20 % weight of bulk (pre polymer, plasticizer and curing agent) binder system. In both AP/NSAN/HTPB and AP/NSAN/PU propellants, the cases 0 %, 20 %, 40 % and 60 % of non-stabilised ammonium nitrate weight content, of the total solid oxidant charge, were studied (Table I).

PROPELLANT	COMPOSITION (% wt)	MOLAR COMPOSITION
B1	80 AP / 20 PU	0.681 AP + 0.2 (SIM + SFE)
B2	64 AP / 16 NSAN / 20 PU	0.544 AP + 0.199 NSAN + 0.2 (SIM + SFE)
B3	48 AP / 32 NSAN / 20 PU	0.408 AP + 0.399 NSAN + 0.2 (SIM + SFE)
B4	32 AP / 48 NSAN / 20 PU	0.272 AP + 0.599 NSAN + 0.2 (SIM + SFE)
C1	80 AP / 20 HTPB	0.681 AP + 0.2 (HTPB + IPDI + DOA)
C2	64 AP / 16 AN / 20 HTPB	0.544 AP + 0.199 NSAN + 0.2 (HTPB + IPDI + DOA)
C3	48 AP / 32 AN / 20 HTPB	0.408 AP + 0.399 NSAN + 0.2 (HTPB + IPDI + DOA)
C4	32 AP / 48 AN / 20 HTPB	0.272 AP + 0.599 NSAN + 0.2 (HTPB + IPDI + DOA)

Table I - Weight and molar composition of the propellants.

Compositions containing AP only were bimodal with a 50 % fine/coarse weight proportion of the AP particles, but in the formulations including NSAN the compositions used were trimodal, with the same fine/coarse AP weight composition.

AP fine	$45 < d_{AP} < 90 \ \mu m$
AP coarse	$106 < d_{AP} < 150 \ \mu m$
NSAN	$150 < d_{NSAN} < 180 \ \mu m$

Table II - Particle sizes used in the formulations.

The particle size distribution curves of both oxidisers were established by Laser Diffraction Spectrometry. The particle sizes presented in Table II were obtained by sieving and kept at 333 ± 5 K and 11 ± 2 % relative humidity for the propellants formulations. Two different polymers, HTPB R45, from France Elf Atochem, and PU, from CPB Portugal, were used as binders. The propellants were obtained by mixing under vacuum at 333 K in an anchor blade type mixer, casted in small boxes (50 mm×50 mm×30 mm) and cured at 333 K for 5 days. Slice-like strands were cut from the cured propellant blocks and its uniformity was verified by optical microscopy and bulk density measurements of the various strands. The test samples cut from the strands were circular

pellets of propellant 10 mm in diameter and 0.8 mm thick. In order to reduce the existence of ignition spots, that would increase data scatter, the surface of the samples was rubbed with fine emery paper and brushed to dust out any loose particles. The test samples were conditioned at 298 ± 2 K and 11 ± 2 % relative humidity before testing.

Experimental Set-up

Strong differences of opinion exist about the ideal set-up for ignition delay studies of solid propellants [5 - 6]. Nevertheless, the simplest and most reliable systems, like the hot plate and the electrical furnace, are still used in the majority of the large scale applications, even if the results obtained are often believed to be limited to comparative purposes. In fact, due to the good reproducibility of testing conditions, a large amount of information can be inferred from the results obtained.

The experimental apparatus (Fig. 1) used in this work for the measurement of ignition delays of the propellants, in ambient air and at atmospheric pressure, is essentially composed by an electrical furnace, a pneumatic system for rapid introduction of the propellant samples and peripheral devices allowing real time control of the process and data acquisition. The furnace, composed of a ceramic ignition chamber, cylindrical, 115 mm long and 65 mm in diameter, heated by a 650 Watt electrical element and externally isolated with ceramic fibber, has a maximum temperature of 1573 K. The temperature of the ignition chamber is controlled by an PID temperature controller associated with a Cromel-Alumel thermocouple.

The possibility of the non-uniformity of the superficial temperature of the test samples, due to natural convective flows and possible influence of the furnace end opening on radiation arriving at the upper surface of the pellet, was considered.

In previous studies [7], performed with a similar equipment and similar test samples, it has been demonstrated that, in what concerns natural convection, the heat transfer coefficient at a given pressure scarcely varies in approximately 200 K temperature intervals, and therefore the consideration of a global heat transfer and a mean surface temperature introduces very little error. The fact that the solid angle defined by the furnace end opening and the test pellet was very small led us to the assumption that the radiation losses could be assumed negligible in the total surface heating. Nevertheless, and in order to optimise the temperature uniformity, axial and radial measurements of the temperature

1 - Air pressure inlet
2 - Pressure control valve
3 - Pneumatic electric valve
4, 5, 6 - Pneumatic mechanical val
7 - Pneumatic cylinder
8 - Electrical switch
9 - Sample holder
10 - Measuring thermocouples
11 - Control thermocouple
12 - Furnace
13 - Electrical Transformer
14 - Relay
15 - Temperature controller
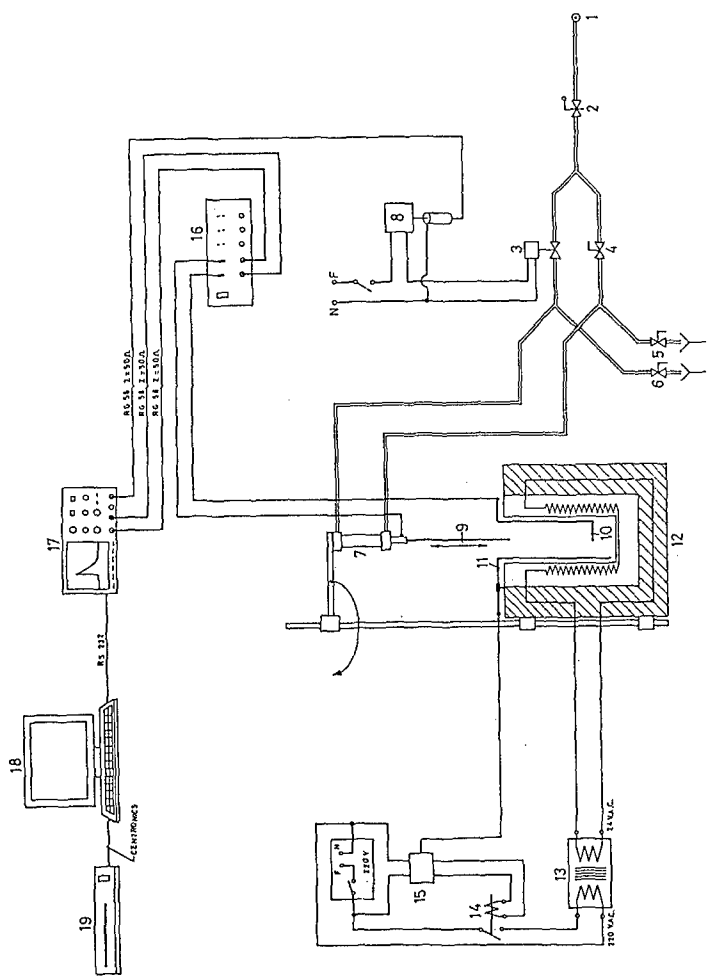16 - Thermocouple amplifier
17 - Oscilloscope
18 - PC
19 - Printer

Figure 1 - Experimental apparatus.

were made using a K type thermocouple that was displaced one millimetre between measurements.

The results of the calibration (Fig. 2) allowed the determination of a cylindrical test zone (10 mm high and 20 mm in diameter), were the maximum axial and radial temperature gradients proved to be always inferior to 0.05% of the pre-established temperature ($\Delta T_{rad\ max}$ = 3.5 K and $\Delta T_{ax\ max}$ = 2 K). During the ignition tests the temperature of the measuring zone was monitored by a shielded K type thermocouple perpendicular to its axis (Fig. 3).
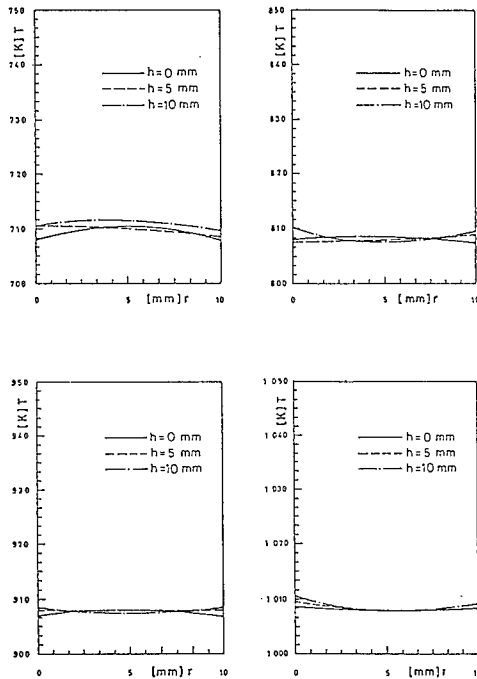
Figure 2 - Calibration results of the test zone.

A pneumatic cylinder was used for the rapid introduction of the propellant samples in the test zone. The pneumatic system is attached to a support that allows its axial and radial displacement away from the furnace entrance in order to avoid heating by convection of the propellant samples during the installation period and to enable the coaxial alignment of the injecting piston with the furnace axis, before injection. The test samples were fixed to the extremity of a thin wire isolated with Teflon, which is axially connected with the piston of the pneumatic cylinder. The length of the wire is such that at the piston maximum displacement the sample is positioned at the centre of the furnace measuring zone (Fig. 3).
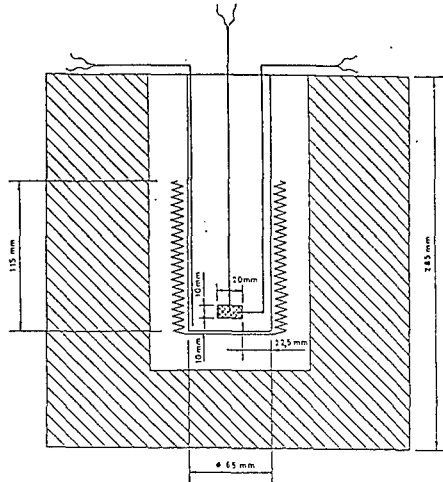
Figure 3 - Schematic representation of the furnace and location of the test zone.

The time evolution of the surface temperature of the sample was measured with a 78 μm K type thermocouple. Because ignition reactions of classic solid composite propellants always occur in a few microns distance from the surface of the propellants, and in order to optimise the accuracy of the measurements, the thermocouple was threaded up to the inferior side of the test pellet, in such a way that the sensitive junction, in a close contact with the solid phase by the characteristic elasticity of the propellant, was positioned as close as possible to its surface. A detailed view of the sample and thermocouple installation can be seen in Fig. 4.
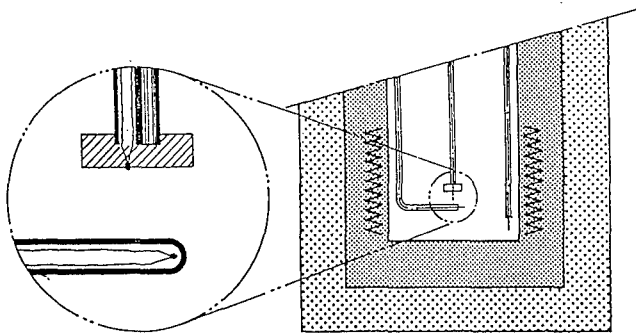

Figure 4 - Position of the thermocouple in the test sample.

The electrical output of the control and measuring thermocouples was amplified by an AD595AQ RS Data Control K type thermocouple amplifier, with cold junction compensation, and registered by a Tektronix 320 TDS oscilloscope which allows a maximum sample-rate of 500 MSamples/s. Specific software is used to transfer all the data to a personal computer for further analysis.

Time response of the equipment

Calibration tests were performed in order to measure the time response of the measuring equipment, Δt, that should be deducted from the experimental ignition delay measurements:

$$\Delta t = \delta t_1 + \delta t_2 \qquad [1]$$

δt_1 and δt_2 being, respectively:
- the mechanical time of injection of the test sample inside the furnace;
- the time delay characteristic of the measuring chain.

As the operation of the pneumatic system was made by actuation on an electric valve and the same input voltage was used to trigger the oscilloscope (Fig. 1), the calibration tests were executed injecting the thermocouple into several pure molten substances (paraffin, ammonium nitrate and lead) and boiling bi-distilled water. The moment of contact of the thermocouple with the free surface of the standard substances was clearly defined by a very sharp rise of the temperature measured by the thermocouple (Fig. 5).

Series of five runs were executed for each standard substance and the results obtained, with an acquisition rate of 500 samples/s, allowed the determination of the mechanical injection time $\delta t_1 = 38 \pm 2$ ms.

The time delay of the measuring chain, δt_2, was identified with the time interval between the moment of contact of the thermocouple with the free surface of the standard substances (t_0) and the moment when the temperature measured by the thermocouple was 95% of the characteristic phase change temperature of the substance (t_f), being the final value of δt_2 the arithmetic mean of the results obtained in each case (Fig. 6).

This procedure proved that the $\delta t_2(T)$ evolution was linear and could be represented by the equation:
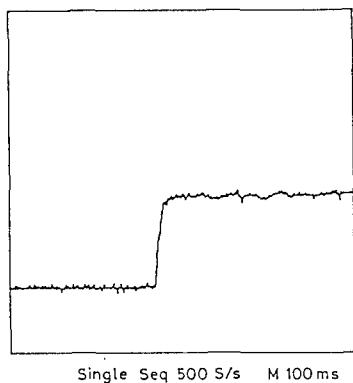
$$\delta t_2 = 53.189 - 0.049 \, T \quad (ms) \qquad [2]$$
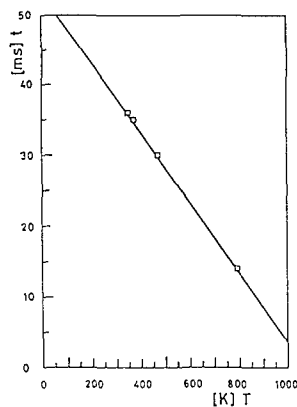
Figure 5 - Thermocouple output of a calibration test.

Figure 6 - Evolution of δt_2, in function of temperature.

Ignition tests

The measurement of the ignition delays of the formulations shown in Table I were made in the temperature range 600 K - 1100 K, with increments of 100 K. The procedure to obtain ignition delay data started with the radial displacement of the injection system, followed by the heating period of the ignition chamber up to the desired temperature. The measuring thermocouple was threaded trough the sample and the pellet was positioned on the support wire. Once thermal equilibrium inside the furnace was attained, the injection cylinder was displaced to the furnace axis and the propellant sample was injected into the measuring zone until ignition occurred. The obtained data was transferred to a personal computer for further analysis.

Definition of the instant of ignition

The occurrence of a very fast increment of the temperature of the propellant sample is a common criterion for the determination of the ignition delay when thermocouples are used as measuring device.

In this work a supplementary condition has been introduced, to increase the information concerning the influence of partial substitution of ammonium perchlorate by non-stabilised ammonium nitrate on the ignition delay of the composite propellants.

As the temperature of thermal degradation of NSAN (443 K) is significantly lower than the correspondent for AP (713 K), and in agreement with several authors [8] that refer to be the ignition delay of composite propellants controlled by the thermal degradation of the oxidiser, the ignition instant of the sample was determined by the simultaneous obtainment of a sharp rise of the output of the measuring thermocouple and a minimum surface temperature, T_s $\geq T_{m_{NSAN}}$, being $T_{m_{NSAN}}$ the melting temperature of NSAN.
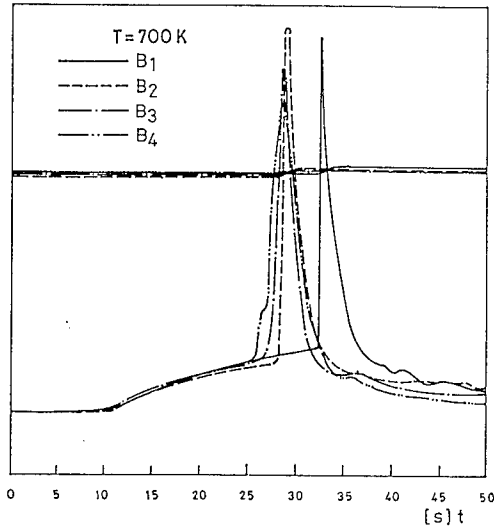

Figure 7 - Output of the measuring and control thermocouples.

Results Obtained and Theoretical Analysis

The ignition delay data obtained for the propellants is plotted in Fig. 8. The ignition delays, in function of temperature, were calculated using the equation:

$$\tau_i(T) = \Delta t_{exp}(T) - \delta t_1 - \delta t_2(T) \qquad [3]$$

where Δt_{exp} represents the time interval between the injection instant (t_0) and the moment of ignition (t_{fi}).

The results presented are the arithmetic mean of the 10 closest values obtained for each formulation, within ± 3 % reproducibility at each temperature level.